

**GALACTIC EXPLOSIONS, COSMIC DUST INVASIONS,
AND CLIMATIC CHANGE**

**by
Paul A. LaViolette**

**A dissertation submitted in partial fulfillment of the
requirements for the degree of**

**DOCTOR OF PHILOSOPHY
in
SYSTEMS SCIENCE**

Portland State University

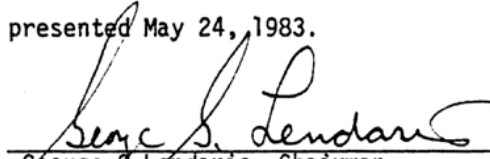
1983

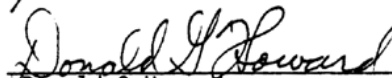
**© Feb. 2012 Paul LaViolette
Thirteenth edition ISBN 0-9642025-6-5**


Author contact: [Gravitics1 @ aol.com](mailto:Gravitics1@aol.com)

TO THE OFFICE OF GRADUATE STUDIES AND RESEARCH:

The members of the Committee approve the dissertation of
Paul A LaViolette presented May 24, 1983.

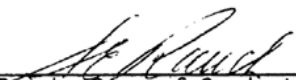

George S Lendaris, Chairman


Donald G Howard


Aslam Khalil


Alan P Marscher, Consultant

APPROVED:


Stanley E Rauch, Dean of Graduate Studies & Research



Paul A. LaViolette, Ph.D.
(Portland, Oregon, Summer 1983)

Abstract

Galactic Explosions, Cosmic Dust Invasions, and Climatic Change

by

Paul A. LaViolette

The hypothesis (Galactic Explosion Hypothesis, GEH) is put forth that about every 10,000 years or so the center of our Galaxy enters an explosive phase during which it generates an outburst of cosmic rays with total particle energies on the order of 10^{57} ergs or more. These outbursts or "superwaves," composed of highly relativistic electrons and positrons, would travel radially outward through the Galaxy at very close to the speed of light ($\sim 0.99999c$) with only moderate attenuation by the interstellar medium for the journey from the Galactic Center to the Sun). It is suggested that upon impacting the solar vicinity, the resulting thousand fold elevation in the ambient cosmic ray energy density would initiate a sequence of events which could profoundly influence the Earth's climate. For example, dust and gas vaporized from comets orbiting just outside of the Solar System would become transported into the Solar System which in turn would alter the radiation transmitting properties of the interplanetary medium and of the Earth's stratosphere. Upon accretion by the Sun, this nebular material would also alter the Sun's spectrum and could lead to the initiation of intense solar flare activity. It is proposed that, in various combinations, such effects could trigger the initiation and termination of ice ages, cause geomagnetic reversals, and indirectly bring about mass animal extinctions. It is proposed that the most recent major superwave passed through the solar vicinity beginning about 14,200 years ago and lasted about 2000 to 3000 years with a major peak occurring about 12,450 years ago.

Astronomical and terrestrial evidence are presented to support the Galactic Explosion Hypothesis. Also, the results of a critical Earth-based test of the hypothesis are presented. In particular, it is reported that the polar ice concentrations of iridium and nickel (both good indicators of extraterrestrial material) rose by one to two orders of magnitude close to the end of the Last Ice Age. These test results are consistent with the GEH prediction that cosmic dust deposition rates were significantly higher during the time when the 14,200 years BP superwave would have been passing through the solar vicinity.

FOREWORD

By its very definition, systems science entails interdisciplinary thinking. As such, a research project undertaken in the context of systems science is qualitatively different from one undertaken in a traditional discipline.

The Ph.D. is, generally speaking, a testimony of the candidate's ability to conduct original research. The faculty's criteria for approving such a testimony relate both to the research process and to the content of the dissertation. Usually, in single discipline research, an agreed upon research methodology has emerged and is taught to the student. In these situations, judgment of the dissertation's content takes the lead. In interdisciplinary research, however, the process is not so well defined. Thus, an important part of what the student demonstrates during his inquiry is his ability to delve into the literature and research of disparate disciplines. To understand that material at an appropriate depth, and to interrelate that knowledge in a way useful to the topic being researched.

An important question which emerges for this dissertation is as follows. If the candidate puts forth an hypothesis and develops a model and an array of evidence intended to support this hypothesis, must the Committee members (either individually or severally) be persuaded that the hypothesis is "true"? Or is it enough for them to testify that the candidate has demonstrated good procedures and appropriate depth of inquiry, has demonstrated originality and intellectual integrity, and has amassed corroborating evidence sufficient to submit the hypothesis to the scientific community for its judgment and interaction? A 'yes' answer to this latter question is assumed by the present Committee.

In particular, the hypothesis put forth here by the candidate is substantively different from currently accepted explanations of the phenomena treated. Nevertheless, one is impressed by the amount of data which the candidate has amassed which can be interpreted to be consistent with the hypothesis and model he advances. An important criterion in judging this dissertation is whether the data the candidate puts forth is represented honestly (allowing for possible differences in interpretation) and probably more importantly, to ask whether there is any body of data (though not necessarily interpretations of it) which contradicts the substance of the candidate's hypothesis--none has yet been found.

The signatures of the Committee members to this dissertation testify that the candidate has developed his intellectual skills and that he can fashion a research process appropriate to the rigors of an interdisciplinary inquiry. Further, the signatures testify that the model and corroborative evidence provided are, in the Committee's judgment, sufficient to submit the work to the scientific community for evaluation, modification and further development.

The candidate here places before the scientific community an *array* of new results, and if but half of these withstand the test of time and scrutiny, this will turn out to be a landmark dissertation.

George G. Lendaris
Professor of Systems Science
Chairman of Dissertation Committee
May 1983

ACKNOWLEDGMENTS

I would like to thank a number of people without whose help it would have been exceedingly difficult to complete this treatise: my father and mother, Fred and Irene LaViolette, who faithfully provided me with financial support at a time when money was hard to come by and who gave me consolation and encouragement during the past four years of conducting this research; my grandmother, Maria Voutsadakis, whose example of spiritual discipline and whose prayers helped me to find inner strength to continue this journey; my dissertation committee chairman, George Lendaris, who gave me continuous assistance and moral support in the face of the many difficulties and adverse circumstances which arose along the way and without whose active interest the birth of this work could not have taken place; my friend Loyd Murray, who continuously encouraged me and shared in the wonder of the scientific discoveries made along the way; and many other friends: Rona, Marion, John, Virginia, Larry, Dorothy, Denise, Susan, Gary, and Brent.

I would also like to thank Donald Howard (Portland State University), Aslam Khalil (Oregon Graduate Center), Alan Marscher (Boston University, Astronomy Department), Lonnie Thompson (Ohio State University, Institute of Polar Studies), Marvin Beeson (PSU, Geology Department), Larry Price (PSU, Geography Department), Victor Clube (Royal Observatory of Edinburgh), and Richard Lingenfelter (University of California) for their many helpful comments.

I would like to thank Lonnie Thompson for providing filtered glacial dust samples from the Camp Century and Byrd Station ice cores; Chester Langway of the State University of New York at Buffalo for sending three Camp Century ice core samples; David Fisher and Richard Koerner (Canadian Polar Continental Shelf Project) for sending seven bulk meltwater samples from the Agassiz (A77) ice core; Joann Loehr and John McCallum (PSU, Biology Department) for use of their biology laboratory facilities; Marvin Beeson (PSU, Geology Department) for use of the gamma ray spectrometer and geochemical laboratory facilities; Kenneth McDonald (Oregon Department of Environmental Quality) for use of the Kahn electrobalance; Allan Ryall (Oregon Graduate Center) for use of the OGC glass blowing facilities; David Roe (PSU, Chemistry Department) and Gary Baxter (Oregon Department of Geology and Mineral Industry) for supplying materials for elemental standards; the U.S. Government for a \$6,000 DOE grant supporting irradiation costs at Missouri University Research Reactor; James Carni (MURR) for his assistance in processing the activated samples; Michael Kay (Reed College) for the use of the Reed College Reactor; and Roman Schmidt (OSU) for the use of the Oregon State University Reactor Facility.

Also I would like to thank Hans Schraeder (OSU, Oceanography Dept.) for supplying samples from deep sea core #OSU 6609-7; John King and Herbert Wright (University of Minnesota Space Science Center) for supplying samples from the Elk Lake Core; Cesare Emiliani (University of Miami, School of Marine and Atmospheric Sciences) for supplying samples from the deep sea Caribbean core #P6304-7; and Charles Denham (Woods Hole Oceanographic Institution) for supplying samples from deep sea core #KN25-4.

Finally, I would like to thank Willi Dansgaard (University of Copenhagen, Geophysical Isotope Laboratory) for supplying oxygen isotope data for the Byrd and Camp Century ice cores; Anthony Gow (Cold Regions Research and Engineering Laboratory) for data on the Byrd core; and James Kennett (University of Rhode Island, Graduate School of Oceanography) and N. J. Shackleton (University of Cambridge, Subdepartment of Quaternary Research) for supplying data on Gulf of Mexico core K97.



Paul LaViolette at work on his dissertation in his living room in Portland, Oregon (summer 1982). Out of the seven years he spent in the Systems Science Ph.D. Program, this investigation took Paul four years to complete.



From left to right: Professor George Lendaris (Paul's dissertation committee chairman, who over the years had closely followed the progress of this research), Paul LaViolette, Irene and Fred LaViolette (Paul's two wonderful parents who faithfully supported his effort). (Portland, Oregon, summer 1982)

TABLE OF CONTENTS

| CHAPTER | PAGE |
|-----------------------|------|
| FOREWORD | vi |
| ACKNOWLEDGMENTS | vii |
| LIST OF TABLES | xv |
| LIST OF FIGURES | xvii |

PART I

INTRODUCTION AND MODEL DEVELOPMENT

| | |
|--|----|
| CHAPTER 1. INTRODUCTION | 2 |
| 1.1. THE GALACTIC EXPLOSION HYPOTHESIS | 2 |
| 1.2. DEFINITION OF A GALACTIC SUPERWAVE | 4 |
| 1.3. PROCEDURE OF INQUIRY | 4 |
| — Superwave Model Adjustments | 7 |
| 1.4. THE INTERDISCIPLINARY APPROACH | 8 |
| 1.5. DETAILED OVERVIEW OF THE REMAINDER OF THIS RESEARCH STUDY | 11 |
| CHAPTER 2. EXTRAGALACTIC EVIDENCE SUPPORTING THE SUPERWAVE MODEL: TOWARD A GENERAL THEORY OF GALACTIC OUTBURSTS .. | 21 |
| 2.1. EVIDENCE OF SUPERWAVE ACTIVITY IN ACTIVE GALACTIC NUCLEI | 21 |
| 2.1.1 Radiation Characteristics that Active Galactic Nuclei Share in Common. . | 21 |
| 2.1.2 Relativistic Radial Expansion of Cosmic Ray Outbursts from Active Nuclei | 24 |
| -- Incoherent Synchrotron Models | 25 |
| -- Ballistic/Relativistic-Beaming Models | 26 |
| -- Relativistic Blast Wave Models | 28 |
| -- The Superwave Model | 31 |
| 2.1.3 The Appearance of an Exploding Galaxy | 37 |
| 2.1.4 The Time Scale for Galactic Explosions | 46 |
| 2.2. EVIDENCE OF SUPERWAVE ACTIVITY IN INACTIVE SPIRAL GALAXIES | 47 |
| 2.2.1 The Origin of Galactic Cosmic Rays: Supernova Source or Nuclear Source? | 47 |
| -- Objections Against the Nuclear Source Hypothesis and Their Resolution | 48 |
| 2.2.2 Galactic Rings | 51 |

| CHAPTER | PAGE |
|--|-----------|
| CHAPTER 3. MODELING THE HYPOTHESIZED 14,200 B.P. SUPERWAVE | 62 |
| 3.1. GENERATION | 62 |
| 3.2. PROPAGATION | 66 |
| 3.3. ARRIVAL | 71 |
| 3.3.1 Superwave Cosmic Ray Electron Intensities Outside the Solar System, in the Inner Solar System, and at the Earth's Surface | 71 |
| -- The Effect of the Superwave Bow Shock Front and the Heliopause Sheath | 71 |
| -- The Screening Effect of the Geomagnetic Field | 76 |
| -- The Effect of the Earth's Atmosphere | 76 |
| 3.3.2 Cosmic Dust and Gas Influx into the Solar System and its Effect on the Transmission of Sunlight | 78 |
| -- The Circumsolar Nebula of Cometary Material | 79 |
| -- The Evolution of the Cometary Cloud and the Possible Role of the North Polar Spur | 79 |
| -- The Present Interplanetary Dust Cloud | 83 |
| -- Dust Purging Processes in the Solar System | 85 |
| -- The Effect of the 14,200 Years BP Superwave: Generation of the Nebular Cloud | 85 |
| -- Cosmic Dust Deposition on the Earth's Surface | 89 |
| -- The Interplanetary Hothouse Effect | 90 |
| -- Light Attenuation in the Earth's Vicinity | 92 |
| -- Nebular Material in the Inner Solar System and Its Effects on Light Transmission | 92 |
| -- The T Tauri Effect | 94 |
| 3.3.3 Geomagnetic Effects | 99 |
| 3.3.4 Cosmic-Dust-Induced Climatic Change | 102 |
| -- Climatic Consequences of a Change in the Earth's Radiation Budget | 103 |
| -- Climatic Consequences of a Change in the Albedo of the Upper Atmosphere | 103 |
| -- Solar Spectral Shift: Global Climatic Effects | 104 |
| -- Solar Spectral Shift: Alteration of the Arctic Thermal Regime | 109 |
| -- Glacial Growth and Recession | 113 |
| -- The Precession of the Equinoxes and the Production of Glacial Cycles | 114 |
| 3.3.5 Biological Effects | 115 |
| 3.3.6 The Possibility of Superwave Gamma Ray Pulses and Their Consequences for Present-Day Society | 119 |
| 3.4. PRESENT EFFECTS | 121 |
| 3.4.1 The Shape of the 14,200 BP Event Horizon | 122 |

PART II

ASTRONOMICAL EVIDENCE OF SUPERWAVE ACTIVITY IN OUR GALAXY

| | | |
|-------------------|--|------------|
| CHAPTER 4. | EVIDENCE OF RECENT ACTIVITY IN THE GALACTIC NUCLEUS AND DISK | 128 |
| 4.1. | THE INHOMOGENEOUS DISTRIBUTION OF HOT DUST AND IONIZED GAS WITHIN 6 LIGHT YEARS OF THE GALACTIC CENTER | 128 |
| 4.2. | EXPANDING CLOUDS OF IONIZED NEON AND THE PROPAGATING RING OF NEUTRAL OXYGEN GAS | 128 |
| 4.3. | THE RADIALY EXPANDING MOLECULAR RING CLOUD | 129 |
| 4.4. | NEUTRAL HYDROGEN ARM-LIKE EJECTIONS | 132 |
| 4.5. | THE VIOLENT INTERSTELLAR MEDIUM | 132 |
| 4.6. | THE INTERSTELLAR WIND | 133 |
| 4.7. | PLANETARY EVIDENCE | 135 |
| 4.7.1 | The Rings of Saturn | 135 |
| 4.7.2 | The Water Valleys of Mars | 139 |
| 4.7.3 | Lunar Evidence of Past Solar Activity | 139 |
| | -- The Remarkable Glazed Rock Patches on the Moon | 139 |
| | -- The Lunar Record of Past Solar Flare Activity | 140 |
| CHAPTER 5. | EVIDENCE OF THE PRESENCE OF THE 14,200 YEARS BP EVENT HORIZON | 147 |
| 5.1. | THE GALACTIC RADIO BACKGROUND RADIATION | 147 |
| 5.2. | THE DISTRIBUTION OF YOUNG SUPERNOVA REMNANTS | 154 |
| 5.2.1 | The Proximity of High Radio Surface Brightness SNRs to the 14,200 Years BP Event Horizon | 154 |
| 5.2.2 | Galactic Evidence that Superwaves May Trigger Supernovae | 160 |
| | -- A Possible Supernova Triggering Mechanism | 161 |
| 5.2.3 | The Proximity of Other Energetic Sources to the 14,200 BP Event Horizon | 162 |
| 5.3. | THE CRAB NEBULA | 163 |
| 5.3.1 | Arguments Against a Supernova Being the Source of the Relativistic Particles in the Crab Remnant | 163 |
| 5.3.2 | Difficulties with a Central Pulsar Being the Source of the Relativistic Particles in the Crab Remnant | 168 |
| 5.3.3 | Argument Supporting the Superwave Interpretation | 173 |
| 5.3.4 | The Luminous Front Activity | 175 |
| 5.4. | THE CASSEOPEIA A REMNANT | 181 |
| 5.5. | THE EXTRAGALACTIC SUPERNOVAE SN 1970g AND SN 1979c | 189 |

| CHAPTER | PAGE |
|---|------|
| CHAPTER 6. SUPERWAVE EVENT HORIZONS OF THE MIDDLE AND LATE HOLOCENE | 192 |
| 6.1. ENERGETIC ACTIVITY ON THE 6000 BP SUPERWAVE EVENT HORIZON | 192 |
| 6.1.1 The Cygnus Region | 193 |
| 6.1.2 The Carinae Nebula | 197 |
| 6.1.3 The Monoceros Region | 200 |
| 6.2. A 393 AD SUPERWAVE? | 202 |
| 6.2.1 SN 1006 | 202 |
| 6.2.2 The Vela XYZ and Cygnus Loop Remnants | 203 |
| 6.2.3 The Lupus Loop and North Polar Spur | 204 |
| 6.2.4 The Vanishing Nebula V-V 1-7 | 204 |
| 6.2.5 The Proximity to Two T Tauri Associations | 205 |
| <u>PART III</u> | |
| <u>TERRESTRIAL EVIDENCE COMPATIBLE WITH</u> | |
| <u>THE GALACTIC EXPLOSION HYPOTHESIS</u> | |
| CHAPTER 7. PALEOMAGNETIC EVIDENCE | 207 |
| 7.1. GEOMAGNETIC REVERSALS AND EXCURSIONS | 207 |
| 7.2. THE GOTHENBURG GEOMAGNETIC EXCURSION — 12,400 ± 100 varve years BP (14,200 cal yrs BP). | 207 |
| 7.3. GEOMAGNETIC EXCURSIONS OF THE CURRENT AND PREVIOUS INTERGLACIALS | 212 |
| 7.3.1 The 6000 BP Geomagnetic Intensity Decrease | 212 |
| 7.3.2 The Blake Event | 214 |
| CHAPTER 8. THE GLACIAL RECORD | 217 |
| 8.1. THE GLACIAL CLIMATIC RECORD | 217 |
| 8.2. DUST IN GLACIAL ICE | 219 |
| 8.3. COSMIC DUST IN GLACIAL ICE | 221 |
| 8.3.1 Compositionally Anomalous Layers in the Greenland Ice Sheet | 225 |
| 8.3.2 Possible Glaciological Evidence of Multiple Cosmic Events | 226 |
| 8.3.3 Anomalous Dust Sample #962-1 | 227 |
| 8.3.4 The Possible Cosmic Origin of Placer Gold Deposits | 230 |
| 8.4. COSMOGENIC BERYLLIUM VARIATIONS | 231 |
| 8.5. THE VOLCANIC ASH RECORD OF THE BYRD ICE CORE | 233 |

| CHAPTER | PAGE |
|--|------|
| CHAPTER 9. THE SEDIMENTARY RECORD | 245 |
| 9.1. CORRELATIONS OF THREE CLIMATIC PROFILES | 245 |
| 9.2. THE ABRUPT NATURE OF MAJOR CLIMATIC CHANGE | 247 |
| 9.2.1 The Terminal Pleistocene Interstadial | 248 |
| 9.2.2 Sudden Heating of the Ocean Surface at the Beginning of the Last Ice Age | 251 |
| 9.3. GLACIAL RETREAT AND THE TERMINAL PLEISTOCENE FLOOD | 253 |
| CHAPTER 10. THE TERMINAL PLEISTOCENE EXTINCTION EPISODE | 266 |
| 10.1. IN SEARCH OF A CAUSE | 266 |
| 10.2. THE DRIFT PHENOMENON | 269 |
| 10.2.1 The Permafrost Muck of the Arctic Regions | 270 |
| 10.3. THE GLACIER WAVE EFFECT | 277 |
| 10.4. DATING THE MEGAFUNAL EXTINCTIONS | 282 |
| CHAPTER 11. RECURRENT GALACTIC SUPERWAVES AND THE EVOLUTION OF LIFE | 315 |
| 11.1. QUANTUM SPECIATION | 315 |
| 11.2. EXTRATERRESTRIAL EXTINCTION HYPOTHESIS IN REVIEW | 318 |
| 11.2.1 The Cosmic-Ray/Extinction Hypothesis | 318 |
| 11.2.2 The Falling-Body/Extinction Hypothesis | 320 |
| <u>PART IV</u> <u>COSMIC DUST TESTS AND CONCLUSION</u> | |
| CHAPTER 12. TESTING THE GALACTIC EXPLOSION HYPOTHESIS | 323 |
| 12.1. NEUTRON ACTIVATION ANALYSIS OF DUST FROM GLACIAL ICE: CAMP CENTURY AND BYRD STATION DEEP ICE CORES..... | 323 |
| 12.1.1 Preliminary Reasoning | 323 |
| -- The Null Hypothesis | 323 |
| -- The Test | 324 |
| 12.1.2 First Irradiation: Experimental Procedure and Preliminary Findings | 328 |
| -- Sample Preparation | 328 |
| -- Irradiation and Counting | 328 |
| -- Preliminary Findings | 329 |
| 12.1.3 Second Irradiation: Experimental Procedure and Preliminary Findings..... | 331 |

| CHAPTER | PAGE |
|---|------------|
| -- Sample Preparation | 331 |
| -- Procedure Followed in Filtering Three Glacial Ice Dust Samples . . . | 331 |
| -- Irradiation and Counting | 332 |
| -- Preliminary Findings | 334 |
| 12.1.4 Overall Results | 334 |
| -- Camp Century Ice Core | 334 |
| -- Byrd Station Ice Core Dust Band | 341 |
| -- Elevated Cosmic Dust Deposition During the Late Wisconsin | 346 |
| 12.2. OTHER NEUTRON ACTIVATION ANALYSIS TESTS | 349 |
| 12.2.1 Analysis of Dust from the Agassiz Ice Core | 349 |
| -- Sample Preparation | 349 |
| -- Irradiation and Counting | 350 |
| -- Results | 350 |
| 12.2.2 Analysis of Ocean and Lake Bottom Sediments. | 350 |
| -- First Irradiation | 351 |
| -- Second Irradiation | 351 |
| -- Discussion | 351 |
| CHAPTER 13. CONCLUSION | 361 |
| BIBLIOGRAPHY | 371 |
| LIST OF SYMBOLS AND ABBREVIATIONS | 410 |
| APPENDICES | |
| APPENDIX A ESTIMATES OF THE QUANTITY OF COSMIC RAY ENERGY WHICH MUST IMPACT THE EARTH'S ATMOSPHERE IN ORDER TO DOUBLE THE TERRESTRIAL C-14 RESERVOIR | 413 |
| -- Cosmic Ray Protons | 413 |
| -- Cosmic Ray Electrons | 413 |
| -- Solar Flare Protons | 414 |
| APPENDIX B THE HELIOPAUSE SHEATH AND THE 3° K COSMIC BACKGROUND RADIATION | 415 |
| -- The Origin of the Dipole Anisotropy in the Microwave Radiation Field | 417 |
| APPENDIX C THE VELA SUPERNOVA | 421 |
| APPENDIX D A GRAVITATIONAL MECHANISM FOR TRIGGERING SUPERNOVAE EXPLOSIONS | 423 |

| CHAPTER | PAGE |
|--|------|
| D.1 TERRESTRIAL GRAVITY WAVE DETECTIONS | 423 |
| D.2 AN ALTERNATIVE VIEW OF GRAVITY | 424 |
| D.3 A MODEL OF A GRAVITY PULSE AND ITS EFFECTS ON CELESTIAL BODIES | 426 |
| -- Galactic Center Generation | 426 |
| -- Tidal Effects Induced on the Earth and on the Sun | 426 |
| APPENDIX E TIME SCALE CONSIDERATIONS | 430 |
| APPENDIX F SYNTHESIS OF HIGH RESOLUTION DUST CONCENTRATION PROFILES FOR THE BYRD STATION AND CAMP CENTURY GLACIAL ICE CORES | 432 |
| APPENDIX G NEUTRON ACTIVATION ANALYSIS RESULTS FOR GLACIAL ICE DUST SAMPLES: BYRD, CAMP CENTURY, AND AGASSIZ ICE CORES | 437 |
| APPENDIX H DETERMINING THE INTENSITY OF SUPERWAVE COSMIC RAYs IMPACTING THE EARTH AND SOLAR SYSTEM [Update]. | 448 |
| APPENDIX J THE CANYONS OF MARS [Update] | 454 |
| APPENDIX K CORRESPONDENCE AND NEWS ARTICLES [Update] | 465 |

LIST OF TABLES
(in original dissertation)

| TABLE | PAGE |
|-------|---|
| I | Early Predictions of the Galactic Explosion Hypothesis 6 |
| II | The 14,200 Years BP Superwave Model: Summary of Features 13 |
| III | The Energy Flux Histogram for the Proposed Cosmic Ray Outburst and the Effect of Heliopause Modulation 74 |
| IV | Determination of the Integral Number Flux of Secondary Electrons Reaching Sea Level 78 |
| V | Predominant Types of Emission from a Solar Flare 96 |
| VI | (Deleted) |
| VII | Hypothetical Brightness Temperature Profile for the 14,200 Years BP Event Horizon 149 |
| VIII | Supernova Remnant Data (a) 156 |
| IX | Supernova Remnant Data (b) 158 |
| X | Characteristics of Supernova SN 1970g 189 |
| XI | The Gothenburg Geomagnetic Excursion 210 |
| XII | Comparison of Dust Concentrations in Polar Ice for Ice Age and Post Ice Age Periods 220 |
| XIII | Comparison of Elemental Abundances in Certain Glacial Ice Dust Samples to Known Terrestrial and Cosmic Sources. 224 |
| XIV | Dust Band Occurrence Rate as a Function of Depth in the Byrd Station Ice Core 235 |
| XV | Cosmic Dust Accumulation Rates in Greenland 324 |
| XVI | Cosmic Dust Accumulation Rates in Antarctica 325 |
| XVII | Glacial Ice Dust Samples That Have Been Analyzed: Pertinent Information . . . 327 |
| XVIII | Specific Predictions Following from the GEH 364 |
| B-I | Determination of the Magnitude and Direction of the Dipole Anisotropy in the Cosmic Microwave Background Radiation 418 |
| E-I | A Classification of Dating Techniques (deleted) |
| E-II | Outline of How the CID Time Scale Was Derived (deleted) |
| E-III | Ice Core Correlation Features (deleted) |
| E-IV | Dates Adopted for Late Pleistocene Isotopic Stage Boundaries (deleted) |
| E-V | Radiocarbon Dates and Corrected Dates for the Laurentide Ice Sheet Movement Profile (deleted) |

| TABLE | PAGE |
|--|-----------|
| E-VI Key Features of the Grande Pile Peat Bog Pollen Profile and Their Dates According to the Ice Core Chronology | (deleted) |
| E-VII Radiocarbon Dates and Corrected Dates for the Wisconsin Section of the Grande Pile Peat Bog | (deleted) |
| E-VIII Rate of Linear Retreat of the Laurentide Glacier up the Hudson-Champlain Valley | (deleted) |
| E-IX Estimate of the Recession Rate for the Laurentide Ice Sheet | (deleted) |
| E-X Estimate of the Recession Rate for the Cordilleran Ice Sheet | (deleted) |
| F-I Dust Weight Concentrations in Polar Ice (Other authors) | 433 |
| F-II Microparticle Concentrations in Polar Ice | 435 |
| F-III Dust Weight Concentrations in Polar Ice (This work) | 436 |
| G-I-XV NAA Results for Glacial Ice Dust Samples from the Byrd Station, Camp Century, and Agassiz Ice Cores | |
| G-I Iridium (Ir) | 439 |
| G-II Gold (Au) | 440 |
| G-III Silver (Ag) | 440 |
| G-IV Iron (Fe) | 441 |
| G-V Cobalt (Co) | 442 |
| G-VI Nickel (Ni) | 442 |
| G-VII Barium (Ba) | 443 |
| G-VIII Antimony (Sb) | 443 |
| G-IX Tin (Sn) | 444 |
| G-X Scandium (Sc) | 444 |
| G-XI Hafnium (Hf) | 445 |
| G-XII Cesium (Cs) | 445 |
| G-XIII Lanthanum (La) | 446 |
| G-XIV Cerium (Ce) | 446 |
| G-XV Terbium (Tb) | 447 |

LIST OF FIGURES
(in original dissertation)

| FIGURE | PAGE |
|---|------|
| 1.1 Organizational Structure of the Dissertation | 5 |
| 1.2 The Variety of Disciplines Brought Together in the Study of the Galactic Explosion Hypothesis | 9 |
| 1.3 Schematic Illustration of a Paradigm Shift from a Set of Narrow, Isolated Interpretations of Observations to a Broad Interdisciplinary Perspective | 11 |
| 2.1 Monochromatic Fluxes in the Optical Range for the Spectrum of: Seyfert NGC 4151, Eta Carinae, Crab Nebula, Quasar 3C 48, and Quasar 3C 273 | 21 |
| 2.2 Spectral Power Distributions of the Galactic Center, Nebula W3, and the Nuclei of: Galaxy NGC 3034, Galaxy NGC 253, and Seyfert NGC 1068 | 22 |
| 2.3 Infrared Spectra of: a) Seyfert NGC 1068, b) Seyfert NGC 4151, c) Quasar 3C 273, and d) Quasar 3C 279 | 23 |
| 2.4 Radio Variations of: (a) Seyfert Galaxy 3C 120 and (b) Quasar 3C 273 | 24 |
| 2.5 Variation in the Radio Output of Blazar BL Lacertae During a Recent Flare | 25 |
| 2.6 Relativistic Ejection of Confined Beams of Synchrotron Radiating Plasma from the Nucleus of a Galaxy | 27 |
| 2.7 Composite Map of the Radio Galaxy NGC 315 | 30 |
| 2.8 Isotropic Radial Propagation of Cosmic Rays as Proposed in the Superwave Model | 33 |
| 2.9 The Formation of Double Compact Radio Sources with Superluminal Separation Velocities | 35 |
| 2.10 Absolute Magnitude Versus Redshift of Quasars, N-Type Radio Galaxies, Blue Compact Galaxies, Seyfert Galaxies, and Morgan N-type Galaxies | 38 |
| 2.11 U-B vs. B-V Color-Color Diagram for Galaxies with U-V Continuum and Broad Emission Lines | 39 |
| 2.12 How Viewing Angle Might Affect the Appearance of an Active Galaxy | 39 |
| 2.13 Phase Diagram for the Optical Appearance of a Spiral Galaxy | 41 |
| 2.14 Comparison of the Powers of Galactic Nuclei at 1415 MHz and at 10 μ | 42 |
| 2.15 Absolute Radio Magnitude of the Small Radio Components of a Galaxy Versus Total Photographic Absolute Magnitude | 42 |
| 2.16 NGC 5128 (SO Elliptical); NGC 4594 (Sa Spiral); NGC 4565 (Sb Spiral); NGC 4631 (Sc Spiral) | 43 |
| 2.17 Proportion of the Total Emission Which Is Due to the Small Radio Component for Galaxies of Different Structural Types | 43 |

| FIGURE | PAGE |
|---|------|
| 2.18 Schematic Diagram of the Radio, Optical, and X-Ray Emission from the Radio Galaxy Centaurus A (NGC 5128) | 44 |
| 2.19 Histogram Showing the Surface Density for the Occurrence of 78 Supernovae in a Spiral Galaxy as a Function of Galactocentric Distance | 47 |
| 2.20 Plot of the Monochromatic Luminosity of the Central Sources of Spiral Galaxies Against the Disk Average Brightness Temperature at 1415 MH. | 49 |
| 2.21 An Example of the Various Morphologies of Type-Sb Spirals in the Classification Scheme Developed by de Vaucouleurs | 52 |
| 2.22 The Andromeda Galaxy, M 31 | 53 |
| 2.23 The 408 MHz Map of M31 Superimposed on a Map of 688 Emission Nebulae | 54 |
| 2.24 X-Ray Source Positions in M 31 Detected with the Einstein Observatory Superimposed on an H I Map | 55 |
| 2.25 Ring Galaxies: a) NGC 3945, and b) NGC 1291 | 57 |
| 2.26 Ring Galaxy Lu 003-534 | 58 |
| 2.27 Peculiar Spiral Galaxy NGC 3646 | 59 |
| 2.28 Ring Galaxy VII Zw 466 | 59 |
| 2.29 Elliptical Galaxy NGC 3923 | 60 |
| 3.1 Stages in the Generation and Propagation of a Galactic Superwave | 62 |
| 3.2 Total Power in Cosmic Ray Electrons Radiated by the Galactic Center at the Time of Generation of the 14,200 BP Superwave | 63 |
| 3.3 Seyfert Galaxy NGC 4151 Shown in Negative Print | 65 |
| 3.4 A Comparison of the Radio Luminosities of the Nuclei of Various Kinds of Galaxies Normalized to the Radio Luminosity of the Galactic Center | 66 |
| 3.5 The Distribution of Faraday Rotation Measures for 543 Extragalactic Radio Sources and for a Collection of Galactic Pulsars | 69 |
| 3.6 The Polarization of Starlight in the Galaxy | 70 |
| 3.7 Differential Particle Number Intensity Spectra for the Cosmic Ray Electron Flux Proposed for the 14,200 BP Superwave Compared with the Current Cosmic Ray Flux in the Earth's Vicinity and Outside the Solar System | 72 |
| 3.8 Cosmic Ray Energy Flux Histograms for the 14,200 BP Superwave Outside the Bow Shock Front and in the Vicinity of the Earth | 74 |
| 3.9 The Total Number of Secondary Electrons of Energy Greater Than 100 Mev in a Shower Initiated by an Electron of Energy E_0 Plotted as a Function of Radiation Length X_0 | 77 |
| 3.10 Position of the North Polar Spur Supernova Remnant Relative to the Solar System | 81 |

| FIGURE | PAGE |
|--|------|
| 3.11 Location of the Nearby Interstellar Cloud Relative to the Solar System | 82 |
| 3.12 Cumulative Flux of Particles Reaching the Earth's Surface as a Function of Mass | 84 |
| 3.13 Normalized Mass Influx Rate to the Earth's Surface as a Function of Particle Mass | 84 |
| 3.14 The Heliopause Sheath Surrounding the Solar System and the Bow Shock Front That Would Be Formed as a Result of the Impact of Superwave Cosmic Rays | 86 |
| 3.15 The Heliopause Sheath and the Superwave Bow Shock Front Hypothetically Compressed by the Superwave Cosmic Ray Blast to a Position Just Outside the Orbit of Mars | 89 |
| 3.16 The Inner Solar System Congested with Nebular Material | 93 |
| 3.17 Continuum Spectra for the Sun, for an 1150° K Blackbody, and for the Dust-Obscured Infrared Star R Monocerotis | 95 |
| 3.18 A Model of a T Tauri Star | 98 |
| 3.19 The Inner Van Allen Radiation Belt and the Directions of Ring Current Particle Drift | 100 |
| 3.20 (a) Spectral Histogram for the Current Solar Continuum; (b) Spectral Histogram for a Dust-Obscured Sun; (c) Percentage of Solar Radiation Absorbed by the Circumsolar Dust Shell as a Function of Wavelength; (d) Percentage of Solar Radiation Absorbed by the Earth's Atmosphere as a Function of Wavelength | 106 |
| 3.21 Energy Balance Diagrams Depicting Average Annual Solar and Thermal Energy Exchanges for the Planet as a Whole: a) for the Present Climate, and b) for a Dust-Obscured Sun | 107 |
| 3.22 Energy Balance Diagrams Depicting Average Annual Solar and Thermal Energy Exchanges for the Central Arctic at the End of May: a) for the Present Climate, and b) for a Dust-Obscured Sun | 111 |
| 3.23 Annual March Air Temperature for an 80° N Latitude Location: a) Presently Observed, and b) for a Hypothetical Snow and Ice-Free Condition | 112 |
| 3.24 Meridional Temperature Gradients for the Northern and Southern Hemispheres as Presently Observed and for a 15° C Increase in the Average Annual Temperature of the Central Arctic | 112 |
| 3.25 Hypothetical Vertical Temperature Profiles for the Central Arctic Compared with an Observed Temperature Inversion Profile and with the Lapse Rate of Solar Radiation Absorbed in the Atmosphere for a Dust- Obscured Sun | 114 |
| 3.26 Ways in Which a Galactic Superwave Could Affect Living Organisms | 116 |
| 3.27 Solar Ultraviolet Flux on the Earth's Surface as a Function of Wavelength or Varying Degrees of Stratospheric Ozone Depletion and the Relative Harmfulness of Ultraviolet Radiation as a Function of Wavelength | 117 |

| FIGURE | PAGE |
|---|-----------|
| 3.28 The 14,200 Years BP Superwave Event Horizon for: a) Infinite Light Travel Time, and b) Finite Light Travel Time $v = c$, for a Superwave Velocity of c | 122 |
| 4.1 The Inner Region of the GC Mapped at a Radio Wavelength of 6 Centimeters | 128 |
| 4.2 The Distribution of Electromagnetic Radiation Around the Galactic Center (3.75 cm Radio Wavelength) | 132 |
| 4.3 Sky Map of the Heart of the Galaxy Showing the Galactic Center, the Location of the Upwind Direction of the Interstellar Wind, the Ecliptic Direction That is Orthogonal to the Large Scale Dipole Anisotropy in the Cosmic Microwave Background Radiation, and the Location of the Local Interstellar Dust Cloud | 136 |
| 4.4 Possible Trajectories for an Interstellar Wind Originating from the Galactic Center and Making an Angle of 3.6° to the Apparent Galactic Plane in the Solar Vicinity | (deleted) |
| 4.5 Solar Flare Track Production Rate as a Function of Time | 142 |
| 5.1 A Map of the Galactic Radio Background Radiation at 150 MHz | 147 |
| 5.2 Brightness Temperature Profiles Along the Galactic Equator: Observed Distribution at 150 MHz Compared to an Exponential Decrease Model and to the Distribution Projected by the 14,200 BP Superwave Model | 149 |
| 5.3 Histogram Showing the Percentage of Supernova Remnants in Each of 5 Surface Brightness Categories for a Sample of 125 Remnants | 155 |
| 5.4 The Current Position of the 14,200 BP Superwave Event Horizon Relative to 16 Young High Surface Brightness SNRs | 157 |
| 5.5 Elliptical Event Horizons Compared to the Locations of 49 Medium Surface Brightness SNRs ($0.1 < \epsilon < 1.0 \text{ f.u.}/(\text{arc}/\text{min})^2$) | 159 |
| 5.6 The Crab Nebula in Taurus, the Remnant of the Supernova of 1054 A.D | 164 |
| 5.7 Radio Luminosity Plotted Against Remnant Radius for a Dozen Extragalactic SNRs, Ages 20 - 75 Years | 166 |
| 5.8 Differential Energy Flux from the Crab Nebula and from the Pulsed Component of the Crab Pulsar | 170 |
| 5.9 An X-Ray Image of the Crab Nebula Taken with the Crab Pulsar in the "On" and in the "Off" State | 170 |
| 5.10 Top: A Contrast Enhanced Picture Showing the Optical Surface Brightness of the Central Region of the Crab Nebula. Bottom: The Degree of Optical Polarization and Electric Vector Orientation for This Central Region | 172 |
| 5.11 Electrodynamic Effects Generated by a Coherent Cosmic Ray Blast Propagating Through a Supernova Remnant | 175 |
| 5.12 Schematic Rendition of a Configuration of the Optical Wisps in the Central Region of the Crab Nebula | 176 |

| FIGURE | PAGE |
|--|-----------|
| 5.13 Observations of Wisp 1 Showing Its Excursion Following the Pulsar Glitch on September 20, 1970 | 178 |
| 5.14 Shock Front Profile for the Outer Surface of the Crab Nebula Facing the GC | 178 |
| 5.15 Radio Contour Map of Cassiopeia A (1410 MHz) Showing Also the Principal Optical Filaments | 182 |
| 5.16 Radio Contour Map of Cas A (2695 MHz) Showing the Asymmetry of the Remnant | 183 |
| 5.17 Spatial Distribution of the High Energy X-Ray Flux for the Cassiopeia A Supernova Remnant | 185 |
| 5.18 A 21 cm Radio Map of the Tycho Supernova Remnant | 188 |
| 5.19 Measurements Made of the Radio Emission from the Extragalactic Supernova SN 1970g and of the Adjacent H II Region NGC 5455 | 190 |
| 6.1 Positions of Several Point Sources Showing Unusual Energetic Activity and Their Location Relative to the 6000 BP Superwave Event Horizon | 192 |
| 6.2 X-Ray Intensity Map of the Cygnus Region in the 0.5 - 1.0 Kev Energy Band | 193 |
| 6.3 The Distribution of γ -Ray Flux with Respect to: a) Galactic Longitude and b) Galactic Latitude | 195 |
| 6.4 The Space Distribution of Luminous Supergiant Stars in the Carina-Centaurus Region | 198 |
| 6.5 Variations of the Apparent Visual Magnitude of Eta Carinae over the Period 1677 - 1979 | 199 |
| 6.6 The 393 A.D. Superwave Event Horizon and Its Proximity to Several Emission Sources | 203 |
| 7.1 The Time Scale for Geomagnetic Reversals over the Past 4.5 Million Years Based on Potassium-Argon Dating | 207 |
| 7.2 Recurrent Geomagnetic Excursions During the Brunhes Normal Epoch | 208 |
| 7.3 Paleomagnetic History of Core B 897 from Torsgarden, Sweden | 211 |
| 7.4 Correlation of Climate, Geomagnetic Field Intensity, and C-14 Production for the Holocene | 214 |
| 8.1 Oxygen Isotope and Dust Concentration Profiles for Three Polar Ice Cores | 218 |
| 8.2 Ice Core Time-Depth Relationship Adopted for: a) Dome C, b) Byrd Station, and c) Camp Century | (deleted) |
| 8.3 Extraterrestrial Dust Particles | 222 |

| FIGURE | PAGE |
|--|------|
| 8.4 (a) An Enstatite Crystal Platelet Selected from a Large Interplanetary Dust Particle Collected from the Stratosphere; (b) A Tin-Bearing Particle of Platelet-Type Morphology Selected From Core Tube #962 of the Camp Century Ice Core | 229 |
| 8.5 Beryllium-10 Concentration in the Dome C Ice Core | 232 |
| 9.1 (a) Pollen Profile for the Grande Pile Peat Bog; (b) Oxygen Isotope Profile for the North Atlantic Deep Sea Core Meteor #12392-1; (c) Graph of the Degree of Penetration of the Laurentide Ice Sheet to Southern Latitudes | 246 |
| 9.2 Average Summer Temperature Profile Reconstructed from Fossil Pollen Data from a Lake Core Penetrated in Alerce, Chile | 249 |
| 9.3 Variations in Average Summer Temperature in the Lowlands of Britain Based on Changes in the Abundance of Various Coleoptera Species | 250 |
| 9.4 Two Marine Sediment Paleotemperature Records of the Terminal Pleistocene Interstadial | 250 |
| 9.5 Change in Glacial Ice Sheet Volume and Mean Ocean Surface Temperature Registered in North Atlantic Core #V27-116 | 252 |
| 9.6 Comparison of the Relative Paleotemperature Index and the Oxygen Isotope Ratio for Core K97 from the Gulf of Mexico | 255 |
| 9.7 A Map Showing Glacial Lake Missoula (Western Montana) and the Channeled Scabland (Northern Idaho and Eastern Washington) | 257 |
| 10.1 Sea-Surface Temperatures, Ice Extent, Ice Elevation, and Continental Albedo for the Late Wisconsin Glacial Maximum Period | 270 |
| 10.2 A Glacier Wave Propagating Down the Surface of the Laurentide Ice Sheet | 278 |
| 10.3 Hydrograph for the 1934 and 1938 Grimsvothn Glacier Bursts | 279 |
| 10.4 Frequency Distribution of Megafaunal Extinctions in North America at the End of the Pleistocene | 282 |
| 10.5 Distribution of Michigan Mastodons and Other Extinct Pleistocene Genera in Comparison to the Location of the Port Huron Moranic System | 285 |
| 11.1 Phylogeny of the Order of Ammonoidea Showing the Rapid Appearance of New Families Following Events of Mass Extinction | 316 |
| 11.2 Fluctuations in the Number of Genera of Ammonites During the Mesozoic Period | 317 |
| 11.3 The Geologic Time Scale | 317 |
| 12.1 Elemental Concentrations Found in the Wisconsin Section of the Camp Century Ice Core: | |
| a) Ir, Au, Sb, Ag, Ni, Sn, Ba, and Fe. | 335 |
| b) Tb, Hf, Cs, Sc, La, Co, and Ce | 336 |

| FIGURE | PAGE |
|---|-----------|
| 12.2 Enhancement Factors Relative to the Earth's Crust for 15 Elements Found in Dust Samples Filtered from the Wisconsin Section of the Camp Century Ice Core | 339 |
| 12.3 Elemental Abundances Relative to C-1 Chondrites in the Anomalous Camp Century Ice Core Sample | 341 |
| 12.4 Microparticle Profile for a Section of Ice Taken from a Depth of 1585 Meters in the Byrd Ice Core | 342 |
| 12.5 Elemental Concentrations in Ice from the 1585 Meter Deep Byrd Ice Core Ash Band Normalized and Compared to Elemental Concentrations in Adjacent Ice . . . | 343 |
| 12.6 Elemental Enhancement Factors in Dust Filtered from the Analyzed Byrd Station Ice Core Ash Band Compared to Enhancement Factors in Adjacent Ice. . . | 344 |
| 12.7 Late Wisconsin and Holocene Cosmic Dust Deposition Rates at Camp Century, Greenland, Determined on the Basis of Iridium and Nickel Concentration | 347 |
| 12.8 Late Wisconsin and Holocene Cosmic Dust Deposition Rates at Byrd Station, Antarctica, Determined on the Basis of Iridium and Nickel Concentration | 348 |
| B-1 The Direction in Which the 3 K Microwave Background Radiation Field is the Warmest | 419 |
| B-2 Hypothetical Diffusion Trajectories Followed by Cosmic Ray Electrons Impacting the Heliopause Sheath | 420 |
| E.1 Pollen Diagram for the 120 Meter Philippi Peat Bog Core from Eastern Macedonia Compared with the Oxygen Isotope Profile for Core #V28-238 from the Equatorial Pacific | (deleted) |
| E.2 Relation for Converting Radiocarbon Dates into CID Dates | (deleted) |
| E.3 Illustration of How the Byrd Ice Core δO^{18} Profile and the Grande Pile Peat Bog Pollen Record Are Correlated to Establish a Correspondence Between CID and C-14 Chronologies | (deleted) |
| E.4 C-14 Age of Lake Jih Tan Sediment As a Function of the Accumulation of Noncombustible Sediment | (deleted) |
| E.5 Time-Distance Relationships for the Recession of the Hudson-Champlain Lobe of the Laurentide Ice Sheet | (deleted) |
| E.6 Historical Variations in Ice Sheet Recession Rate and in Meltwater Flow Rate: a) According to the C-14 Time Scale and b) According to the CID Time Scale | (deleted) |
| E.7 Global Sea Level Change During the Late Wisconsin and Holocene: a) According to the C-14 Time Scale and b) According to the CID Time Scale | (deleted) |

PART I
INTRODUCTION AND MODEL DEVELOPMENT

CHAPTER 1

INTRODUCTION

1.1. THE GALACTIC EXPLOSION HYPOTHESIS

This study puts forth, and supports with a substantial amount of observational data, an hypothesis that there exists an astronomical phenomenon which in the past may have caused profound changes in the Earth's climate and in its living species (and which, in turn, could pose a substantial future threat to life on our planet). This phenomenon is outlined by the following set of (sub)hypotheses which henceforth will be referred to as the "Galactic Center Explosion Hypothesis," or "Galactic Explosion Hypothesis" (GEH) for short:

- 1) Periodically the center (or core) of our Galaxy enters an explosive phase during which it generates an outburst of cosmic rays (in the form of highly relativistic electrons and positrons) with total particle energies on the order of 10^{57} ergs or more.
- 2) These outbursts recur on a time scale of about once every 10^4 years. The emission period may last anywhere from several hundred to a few thousand earth years and there may be considerable time-variability in the cosmic ray emission intensity over this period.
- 3) A cosmic ray blast, so generated, travels radially outward through the Galaxy at very close to the speed of light ($\sim 0.99999c$) with only moderate attenuation by the interstellar medium ($\sim 20\%$ loss of energy for the journey from the GC to the Sun).
- 4) Upon impacting the solar vicinity these cosmic rays would vaporize cometary material in the vicinity of the heliopause sheath and would transport the resulting nebular dust and gas into the solar system. Presence of this material in the solar system:
 - a) would cause the Sun's radiation continuum to vary in intensity and shift to the infrared, would back-scatter, absorb, and reradiate solar radiation producing an "interplanetary hothouse effect," and would increase the albedo of the Earth's upper atmosphere, all of which would in turn cause major changes in the Earth's climate with significant harmful side effects for life forms; and
 - b) would increase solar flare activity upon accretion by the Sun, which in turn could:
 - i) cause disturbances (and sometimes reversals of) the geomagnetic field,
 - ii) destroy the Earth's UV-protective ozone layer,
 - iii) produce accelerated mutational changes in terrestrial life forms, and
 - iv) produce temporary climatic changes.
- 5) If the cosmic ray outburst were sufficiently intense, upon impacting the Earth these Galactic cosmic rays could:
 - a) cause disturbances to (and sometimes reversals of) the geomagnetic field,
 - b) cause abrupt changes in the terrestrial climate,
 - c) destroy the Earth's UV-protective ozone layer,
 - d) produce an increased level of ionizing radiation capable of initiating major extinctions of fauna,
 - e) propel the heliopause sheath inward sufficiently that it could envelop the Earth, in which case all the effects described in a) through d) (above) would become briefly amplified.

- 6) Cosmic rays produced by a Galactic explosion passed through the solar vicinity beginning about 14,200 years ago and the event lasted about 2000–3000 years, with a major peak occurring about 12,450 years ago. Also another event of lesser magnitude peaked about 6000 years ago and lasted about 1000 years.

Galactic explosions are the most energetic natural phenomenon known to science. They take place in the centers of galactic nuclei, releasing enormous quantities of relativistic particles (cosmic rays). Such explosions, or cosmic ray outbursts, sometimes may involve total energies exceeding 10^{61} ergs released over a period of only years, as in the case of the radio galaxy CTA 102 (Burbidge, Jones, and O'Dell, 1974, pp. 51–53). To get an idea of the amount of energy involved, 10^{61} ergs is equivalent to the energy released from 10 billion of the most energetic kind of known supernovae (type II supernovae).

Suppose that such an explosion were to occur in the nucleus of our Galaxy, or even a more moderate explosion of say $\sim 10^{58}$ ergs radiated over a period of several hundred years. What impact would the cosmic ray component have on the Earth? This is a question which until now has not been seriously addressed in the geological literature, probably for three reasons. First, it has only been in the last 25 years or so that very much has been learned about galactic explosions—before the development of radio telescopes and infrared X-ray astronomy the phenomenon was essentially unknown.

Second, there is a belief among many astronomers that if a Galactic explosion did occur, the interstellar magnetic field would impede the radial propagation of particles such that the amount of energy in the form of cosmic rays reaching the Earth would be relatively insignificant. For example, Ginzburg and Syrovatskii (1964, p. 207) consider the effect of a "small size" cosmic ray blast of 3 to 10×10^{55} ergs emitted from the Galactic center (with a comparable amount of kinetic energy being transferred to the interstellar medium) and conclude that such an explosion would increase the cosmic ray densities in the Earth's vicinity by no more than a few percent.

Third, it has been commonly believed that these explosive events occur only about every 10^7 – 10^8 years, with each event lasting 10^6 years. Thus, noting that the Galactic center has maintained a relatively quiescent state during the recent decades in which modern astronomers have been gathering data, one is naturally led to infer that such a quiescence has probably persisted for millions of years and will perhaps continue to persist for a comparable length of time. Consequently, there has been little motivation to classify Galactic explosions as an important agency shaping the evolution of our planet.

However, as is demonstrated in Chapter 2, a number of phenomena observed in active and normal galaxies are more appropriately explained by a model which assumes that blasts of cosmic rays, periodically generated in the nucleus of a galaxy, propagate radially outward at close to the speed of light and *penetrate the entire extent of the galaxy*. Moreover as is demonstrated in Chapter 3, an outburst of $\sim 7 \times 10^{57}$ ergs, released over a 400 year period and experiencing a 20% interstellar attenuation would still have had sufficient intensity by the time it reached the solar vicinity to have elevated the cosmic ray background by about a thousand fold. This would not have been sufficiently intense to have produced the extreme effects described in Hypothesis #5, but it certainly would have been strong enough to propel nearby nebular dust and gas into the solar system and bring about the scenario outlined in Hypothesis #4. Finally, it is demonstrated in Subsection 2.1.4 that a time duration on the order of 10^2 – 10^3 years (rather than 10^6 years) and a recurrence time on the order of 10^4 years (rather than 10^7 – 10^8 years) is more compatible with existing astronomical observations. Consequently, not only is it justified to seek evidence on the Earth of past Galactic explosions, but in particular it makes sense to look for evidence of rather recent occurrences; i.e., those registered on the Earth sometime during the past 10^4 years or so.

1.2 DEFINITION OF A GALACTIC SUPERWAVE

A distinguishing feature of the galactic explosion model which I am proposing is that the effects of the outburst are propagated through a galaxy in the form of what I call a "*superwave*." A superwave may be described as being a shell-like disturbance that propagates radially outward from the center of a galaxy at approximately the speed of light, comprised of enhanced cosmic ray and electromagnetic radiation and (possibly) of sudden changes in the Galactic gravitational field potential. Specifically, the superwave begins as a relativistic radial expansion of a *brief* cosmic ray outburst. The overall thickness of the resulting relativistic shell is determined by the duration of the central outburst, and might typically be on the order of several hundred to a thousand light years in extent, small compared to the diameter of a typical spiral galaxy. As discussed in Subsection 2.1.2, this blast of particles would propagate outward through the nucleus and disk of a galaxy without significant attenuation. Moreover, the bulk of the electromagnetic radiation emitted by these cosmic rays would be produced throughout their passage through the galaxy, not just in the vicinity of the galactic center. Due to relativistic effects, continuum radiation generated by the particles would be beamed in the direction of particle propagation. Since the particle barrage would travel radially outward from the galactic center on a relatively straight-line course, this continuum radiation would also travel outward in this same direction in phase with the particle blast. Moreover, in the case of particles traveling very close to the speed of light ($\sim 0.9999999c$ for 1 GeV electrons), the continuum radiation generated by a given particle during its entire journey through the galaxy would be seen by the observer essentially simultaneously; see Subsection 2.1.3.

Two characteristics become apparent in regard to the observability of superwaves. First, an observer located in an active galaxy, even at the periphery of the galactic disk, would have little warning if a superwave was approaching since the cosmic rays would be traveling about as fast as the radiation they would be generating. Second, a superwave would become essentially invisible after it had passed by the observer, since the radiation it would generate would, for the most part, be beamed in its forward direction of travel.

1.3. PROCEDURE OF INQUIRY

The basic organization of this study is illustrated in Figure 1.1. To begin with, a hypothesis is formed: the Galactic Explosion Hypothesis. Then a (superwave) model of a particular Galactic explosion event is constructed and made compatible with available extra-galactic evidence. Next, the predictions of this model are checked out against Galactic and terrestrial evidence available in the literature. Finally, a critical test of the GEH is performed. The Galactic Explosion Hypothesis is stated in Section 1.1 of this chapter. The first three statements making up this hypothesis pertain to basic features characteristic of the Superwave Model. Although the statements refer to our Galaxy, they may be considered generically as being applicable to any spiral galaxy. The fourth, fifth, and sixth statements constituting the GEH refer more specifically to our own Galaxy, namely that superwaves are capable of periodically producing certain effects on the Earth and on the Sun, and that two of these superwaves passed the Earth at specific times in the past.

It is important to note that the initial formulation of the GEH was not based on a survey of astronomical and geological literature. The "data" upon which this hypothesis was originally based were derived from certain ancient records I have deciphered, records which appear to document that a major explosion occurred at the center of our Galaxy and that this event was experienced on the Earth beginning approximately 14,200 years ago. I realize that it is hazardous to rely on interpretations of archaeological or mythological

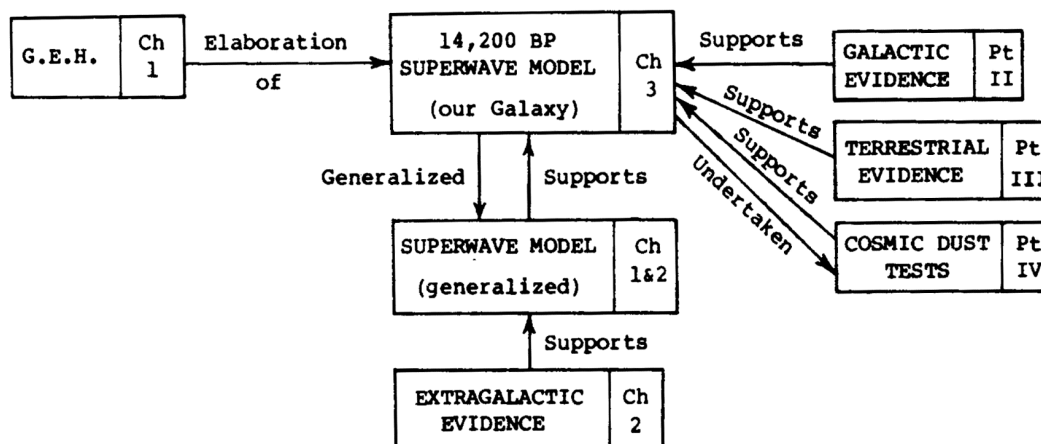


Figure 1.1. Organizational structure of this study. The supporting evidence given in Part I (Chapter 2) and Parts II through IV (Chapters 4 through 12) was gathered after the GEH had been formulated.

records in developing an argument or hypothesis of a scientific nature. Any idea that is inspired from such sources should receive most, or all, of its support from scientific (astrophysical, geophysical, geochemical, etc.) evidence, and it is with this understanding that I intend to proceed in the following study. I do not plan to rest any of my case on the claimed documentation. Rather, I have used this information source as a personal guide to give a clue as to the approximate time when this event may have passed the Earth, and as to where in the Galaxy this event horizon may now be located.

Thus, the whole purpose of the research undertaken for this study has been to accumulate convincing physical evidence to support the assertion that an explosion occurring at the center of the Galaxy affected our planet some 14,000 years ago. The astronomical and geological evidence I have gathered (Part I, Chapter 2, and Parts II and III,) and the results of the geochemical analysis I have performed (Part IV), in my opinion, support the contention that such an event actually took place. So my initial objective for this research study has been met. As a consequence, I can conclude that there is some degree of credence to the interpretation I have made regarding the aforementioned ancient documentation. In the near future I intend to do further research into that material and to write up those findings to supplement the present work. **[UPDATE:** This ancient documentation is an archeoastronomical record that I had discovered encoded within constellation lore and which served to initiate this scientific investigation. This material is now published in the book *Earth Under Fire* (Rochester, VT: Bear & Co., 1997, 2005). Also see dissertation proposal Appendix I for an early summary of these findings (LaViolette (1981).]

To test the GEH (see Figure 1.1, upper middle box), an idealized descriptive model of one of the hypothesized cosmic events, the "14,200 years BP superwave" has been constructed (Chapter 3). As much as possible, this model was designed to conform to what is known about galactic explosions. In particular, statements 1, 2, and 3 of the GEH, and the Superwave Model in general, find their support in the extragalactic evidence presented in Chapter 2. Although the GEH is basically qualitative in nature, it was necessary to make the 14,200 years BP superwave model quantitative in order to establish if such qualitative effects could indeed have been produced on the Earth and observed in other parts of the Galaxy. Wherever possible, these quantitative additions to the model (e.g., the total energy of the

outburst, and the average Lorentz factor of the particles) have been checked to ensure that they are consistent with available observations made of active extragalactic nuclei. Thus, the 14,200 years BP superwave model in particular and the Superwave Model in general are justified on the basis of extragalactic evidence. The only important hypothesis included in the 14,200 years BP superwave model that cannot be inferred from extragalactic evidence is the date at which the event horizon would have first passed the Earth, i.e., 14,200 years BP. As mentioned earlier, this was derived from what seems to be an ancient documentation of the event.

The 14,200 years BP superwave model predicts that there should be presently observable evidence of energetic phenomena taking place at certain locations in the Galaxy. Taking the date 14,200 years BP as the time when the superwave would have begun its arrival in the solar vicinity, the shape and location in the Galaxy of the radially propagating event horizon becomes uniquely specified. To an observer located within the perimeter of this superwave shell, the Galactic center and the region contained within the shell would appear relatively calm. However, slightly further out in the vicinity of the shell itself, a "cosmic storm" would be raging. The purpose of Chapter 5 is to review pertinent astronomical evidence available in the literature, and to show that it is compatible with the prediction that a superwave event horizon is present in the specified region of the Galaxy. In addition, to support the prediction that a superwave may have recently passed through the solar vicinity, evidence is presented (Chapter 4) of possible aftermath effects presently observable in the solar system. Also evidence is presented indicating that the Galactic center has been the site of recent explosive activity.

Part III reviews terrestrial evidence with the intention of determining whether the proposed superwave could have passed the Earth beginning about 14,200 years ago. In particular, this evidence is gathered in support of statements 4 and 6 of the GEH. In Part III the mode of inquiry changes from one of predominantly considering direct observations of related events currently taking place in the Galaxy, to one of piecing together past evidence registered in the Earth's sedimentary and glacial ice records.

The Galactic evidence presented in Part II and the geological evidence presented in Part III were gathered after the GEH had been formulated. To my knowledge, none of the evidence uncovered in the literature search contradicts the GEH in its present form. Rather, the evidence appears to be quite compatible with the hypothesis. Before the literature search was begun, a number of qualitative predictions were made on the basis of the GEH; see Table I. The resulting after-the-fact confirmation of these early predictions supports the credibility of the GEH. A list of additional predictions which have emerged as a consequence of conducting this study are presented in Chapter 13 (Table XVIII).

TABLE I
EARLY PREDICTIONS OF THE GALACTIC EXPLOSION HYPOTHESIS

-
- 1) There should be an "event horizon" which passed the Earth beginning about 11,000–14,000 years ago and which is presently traveling away from the Galactic center at close to the speed of light. Moreover, at the present location of this horizon, one should perceive highly energetic events taking place.
 - 2) About 11,000–14,000 years ago the Earth should have been exposed to elevated levels of cosmic ray radiation.
 - 3) There should have been an increased rate of deposition of cosmic dust around 11,000–14,000 years BP.
 - 4) There should have been a greater chance of extinction of animal life at this time.

Probably the strongest piece of evidence favoring the GEH comes from the results of an Earth-based test which was performed to check out one of the hypothesis' early predictions; see lower right-hand box in Figure 1.1. I reasoned that if a cosmic ray blast were to pass through the solar system, then it would probably transport particles of interstellar cosmic dust residing in the vicinity of the solar system and deposit them on the Earth. If a sufficient amount of cosmic dust were transported and deposited in the Earth's atmosphere, then an abnormally high concentration of extraterrestrial material could be expected to be deposited in glacial ice at that time. The GEH, therefore, predicts that elevated concentrations of cosmic dust should be observed during the interval 11,000–14,000 BP, and possibly at other dates in the glacial record, since it is proposed that superwaves are a recurrent phenomenon. Samples of glacial ice from Greenland and Antarctica were tested to determine if certain elements which are typically more abundant in cosmic material increased in relative abundance in atmospheric dust deposited around 14,200 BP. Details of the testing procedure and results are presented in Chapter 12. These tests, which were of an exploratory (rather than exhaustive) nature, confirm the prediction of the GEH that at certain times during the Wisconsin Ice Age cosmic dust was being deposited at an accelerated rate, a finding which represents a unique discovery on its own. As is discussed in Chapter 8 (p. 226) and Chapter 12 (p. 344) local solar system causes (e.g., asteroid impacts) can be ruled out. So, the results of the test constitute very strong evidence that the 14,200 years BP superwave event proposed herein may actually have taken place.

Superwave Model Adjustments. In the 3-1/2 years that have elapsed since the summer of 1979 when the GEH was first formulated, the 14,200 years BP superwave model has gone through various revisions, both in regard to the kind of cosmic ray particles assumed to compose the superwave, and in regard to the total intensity assumed for the cosmic ray blast. Though the ancient records which initially led me to formulate the GEH indicated only the approximate date when this cosmic event would have passed the Earth, they provided information that indicated the event was propagating at relativistic velocities from the direction of the Galactic center (GC). Details such as the intensity of the (supposed) cosmic ray blast and the kind of particles composing it were left unspecified. In specifying these factors for the 14,200 years BP superwave model, I have taken the approach that the choices I make should allow the model to be compatible with the existing body of astronomical and geological evidence. Consequently, as difficulties were consecutively encountered, the model was accordingly revised.

In the early stages of formulating the GEH, I proposed a very high cosmic ray intensity for the 14,200 years BP superwave model. I had noticed that the date of the cosmic event coincided closely with the end of the Last Ice Age. So, assuming that this was not merely due to chance, I supposed that the cosmic ray blast had been powerful enough to actually cause a change in the Earth's climate. I initially chose to set the total cosmic ray energy of the Galactic explosion at $\sim 2.5 \times 10^{61}$ ergs, comparable with the intensity of the most energetic of known extragalactic explosions. This scenario predicted a peak intensity in the solar vicinity of 6×10^5 ergs/cm²/s, equivalent to about half of the intensity of the solar radiation at the Earth's distance from the Sun. Such a high intensity maintained over a few hundred years would indeed have caused a warming of the Earth's climate, sufficient to melt a significant portion of the Earth's glacial ice sheet cover.

This initial model also proposed that the cosmic ray outburst consisted mainly of relativistic protons. This was a logical choice at the time since relativistic protons make up about 92% of the primary particle cosmic ray background radiation. However, it became evident that protons entering the Earth's atmosphere in such great quantities would produce inordinately high radiocarbon levels. For example, as is seen in Appendix A, an outburst from the GC of 2×10^{56} ergs of cosmic energy protons is sufficient to double the size of the

terrestrial C-14 reservoir (assuming no heliopause shielding). Thus a 2.5×10^{61} erg outburst would have increased the C-14 reservoir by $\sim 10^5$ fold, far too much. A study of the geologic record indicates that during the Late Wisconsin Period the atmospheric C-14 level probably increased no more than a factor of 2 in short term fluctuations; see Chapter 9, Subsection 9.1.1.

To circumvent this problem, a change in the model was made in the spring of 1981. The cosmic ray content of the outburst was changed from protons to a charge-balanced volley of cosmic ray electrons and positrons. I was under the impression at the time that cosmic ray electrons would produce only minimal amounts of C-14. However, I had underestimated the effectiveness of the γ -ray component generated in the Earth's atmosphere by photo-electron cascades. In the fall of 1982 I reevaluated the C-14 producing ability of cosmic ray electrons and to my disappointment found that electrons would be considerably more effective than I had supposed—perhaps 10% as effective as cosmic ray protons, but not much less; see Appendix A.

So, I was forced to confront the need to reduce the total energy of the outburst by several thousand fold to about 7×10^{57} ergs (or to $\sim 2.4 \times 10^{58}$ total, if the second outburst at 12,350 years BP is included). A reduction greater than this was hard to justify since it would require abandoning the model's ability to explain the unusual energetic phenomena observed in the Crab and Cassiopeia A supernova remnants which are currently positioned in the vicinity of the 14,200 BP Event Horizon; see Chapter 5 (Sections 5.3 and 5.4). Initially, it was with reluctance that I made this change, seeing that a superwave peak intensity of only $\sim 10^{-5}$ suns would have had an insignificant effect on the Earth's climate. Such a low intensity would not be able to provide the extra input of thermal energy needed to evaporate water at an accelerated rate to cause the Late Wisconsin stage ice sheet advances, nor could it have a significant impact on glacial melting to produce the rapid glacial ice sheet retreats at the end of the Wisconsin. Still, I firmly believed that there must be some sort of causal connection between the passage of the 14,200 years BP superwave and the sudden change of climate at the end of the Last Ice Age. I had accumulated far too much geological evidence at that point to discard such a connection.

The proposal that cosmic dust could have become transported into the solar system during the 14,200 years BP superwave event was an early prediction of the GEH, and this prediction was in fact subsequently verified with the author's discovery that glacial ice of this era contained high concentrations of iridium and nickel. Following the completion of the glacial dust analysis, I gave more serious attention to considering whether the implied amounts of cosmic dust played some major role in affecting the Earth's climate. The amount of cosmic dust which would have had to be present in the solar system to produce such high dust deposition rates on the Earth would have caused a considerable attenuation of sunlight at visual wavelengths. My thinking at that time was that this dust could have produced a cooling effect on the Earth's climate, supplementing the heating effect of the superwave cosmic rays (former model). But, with the model revision made in the fall of 1982 I became resigned to the fact that cosmic rays could not supply the necessary heat input.

Nevertheless, at the same time I realized that my earlier conclusion was only partially correct. Depending on the circumstances, the presence of dust in the solar system could produce a net cooling effect or a net *warming* effect on the Earth's climate. Thus, it became evident that the Earth's recent history of abrupt climatic change ($\Delta t < 50$ years) could be adequately accounted for by a mechanism solely involving the periodic influx of nebular material into the solar system. Having an additional atmospheric heating agent (e.g., superwave cosmic rays) was no longer required, and in fact was superfluous. Reducing the intensity of the cosmic ray blast not only met the objective of resolving the carbon-14 problem, but also satisfied the principle of Occam's razor. Nevertheless, in its revised form,

the cosmic ray volley of the superwave still performs a critical role. Namely, it is responsible for initially generating the gas and dust cloud from condensed nebular material lying close to the solar system and for transporting this material into the solar system; see Subsection 3.3.2. It is quite probable that without the mischievous action of the superwaves the Earth's past climate may have been much less eventful, and perhaps more pleasant. (Or, should the blame be put on the nebular material which appears to reside in the immediate vicinity of the solar system?)

It is important to note that despite the various revisions of the quantitative details of the 14,200 years BP superwave model, most of the basic tenets of the GEH remained unchanged. In particular, the proposal that cosmic dust would be swept into the solar system (if elevated dust concentrations were nearby) holds for a wide range of assumed superwave intensities and does not depend on the kind of cosmic ray particles that one chooses to assume for the blast. Thus the cosmic dust influx prediction, which was set up as a critical test of the GEH (and was subsequently verified), has remained invariant throughout the course of this research study. However, these test results and the recent quantitative revision of the 14,200 years BP superwave model have been a major source of feedback for the GEH. The realization that there would be significant solar-related effects brought about by the presence of elevated levels of interplanetary dust has prompted me to add items a) and b) under Hypothesis #4 (p. 2). Thus this portion of the GEH is much more recent than the main head statement of Hypothesis #4.

1.4. THE INTERDISCIPLINARY APPROACH

It has been necessary to employ an interdisciplinary approach in carrying out the present study. An example of the variety of disciplines brought to bear on the GEH in order to determine its tenability is shown in Figure 1.2.

In modern science there is a strong tendency to specialize when doing research. This

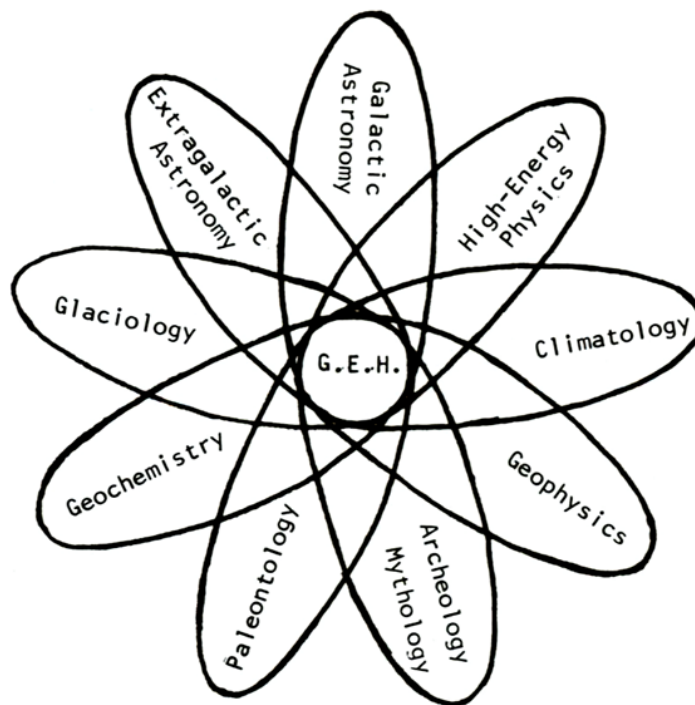


Figure 1.2. The variety of disciplines brought together in the study of the Galactic explosion hypothesis.

is often necessary if the researcher is to avoid becoming overwhelmed by the vast complexity of nature. For the sake of simplicity, there is often the desire to put a box around certain portions of a system or a phenomenon and to study that portion in isolation from everything else. However, in so doing, there is the accompanying danger of losing sight of the larger whole and of formulating models of natural phenomena which are unjustifiably narrow in scope. Scientific generalists continuously warn us that nature does not come as clean as we would like. And this warning applies equally well to the fields of geology and astronomy as it does to any other scientific field.

To some extent, the study of galactic explosions has already been an "interdisciplinary" venture. Scientists specializing in X-ray astronomy, infrared astronomy, radio astronomy, and optical astronomy have all been getting together to compare notes, with an awareness that observations made in any one portion of the electromagnetic spectrum only contain part of the story. In some cases, to induce nature to yield her secrets, international boundaries must be crossed in addition to disciplinary boundaries. An example of this is the development of very long baseline interferometry (VLBI) in which radio telescopes at different locations around the world become coordinated to simultaneously observe a particular galaxy, with the added advantage of significantly improved image resolution.

Even so, investigation into galactic explosion phenomena has been considerably specialized in other respects. For example, research has tended to focus on galaxies other than our own, and particularly on galaxies whose nuclei are in an active state. Such specialization is justified if it can be assumed that galactic explosions occur very rarely and that their effects are confined to the nucleus of a galaxy. However, according to evidence presented in Chapter 2, it may be that such assumptions are not justified. If instead it is acknowledged that the components of a galactic explosion are able to propagate relativistically through the entire disk of a spiral galaxy, then the modus operandi of how one goes about studying the galactic explosion phenomenon necessarily must change.

If this second, less restricted scenario is adopted, then it becomes apparent that much can be learned about galactic explosions by studying phenomena taking place in the disks and peripheral regions of galaxies as well as in galactic nuclei. Moreover, not only will active galaxies alone be the subject of investigation, but "normal" galaxies as well will be candidates for close study (i.e., galaxies whose nuclei appear to be in a quiescent state). For example, if it can be assumed that galactic explosions occur as frequently as every 10^4 years, then at any given time as many as 5 radially propagating event horizons might be expected to be contained within the boundary of a typical spiral galaxy whether or not its nucleus happens to be in an active state at the time of observation. It then becomes apparent that our own Galaxy, and in particular the Galactic disk, might be a prime candidate to search for evidence of such energetic phenomena.

Moreover, if it is true that outbursts of cosmic rays periodically pass the Earth and affect it in various ways, then it stands to reason that telltale evidence of such events ought to exist in the consecutive sedimentary strata of the Earth's crust and in the annual glacial ice layers accumulated in the Earth's polar regions. The Earth may be regarded as a delicate recording instrument providing an historical account of changes in its cosmic environment. Thus, much may be learned about Galactic explosions not only through the study of other distant spiral galaxies currently in their active phase, but by studying our own Galaxy and our own planet as well. Perhaps it will soon be realized that compared with the many extragalactic observations which have been painstakingly made over the years, data gathered by our geologists, geophysicists, glaciologists, and paleontologists may be of equal or even of greater importance to the understanding of galactic explosions.

An appreciation of the overall structure of the GEH and of the interrelation of its supporting evidence may not be realized at first, since by necessity the process of consideration and reinterpretation of the evidence must be done in a step-by-step fashion.

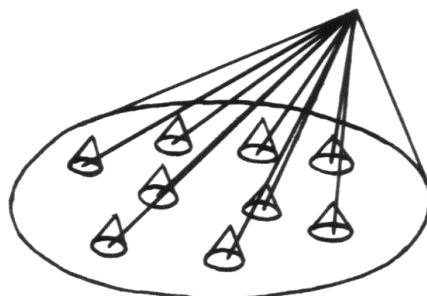


Figure 1.3. Schematic illustration of a paradigm shift from a set of narrow, isolated interpretations of observations to a broad interdisciplinary perspective such as that required by the Galactic Explosion Hypothesis.

Consider for example Figure 1.3. Suppose that the small cones represent interpretations of individual terrestrial or Galactic phenomena which have been reported in the literature, e.g., evidence accumulated in Parts II and III. These various interpretations are usually of relatively narrow scope and are often isolated from one another. In considering each of these phenomena, the reader will be asked to suspend judgment and consider the alternative explanation offered by the GEH, e.g., the solid line connecting each small cone to the apex of the large cone. In many cases the new interpretation will help to clear up problem areas left unexplained by the conventional interpretations. It is hoped that after this research study is read through carefully and completely the reader will be able to grasp a feeling for the whole and to visualize how the various pieces of evidence presented here relate to one another from the perspective offered by the GEH. It will be seen that the GEH offers a simpler and more unified base from which to explain these various phenomena.

It should be mentioned here that evidence is also presented that is very difficult to account for by any phenomenon other than the proposed 14,200 years BP superwave. The evidence presented in Chapter 12 falls into this category.

In a sense, the GEH constitutes a new *paradigm* for viewing Galactic and terrestrial phenomena. The difference between the "new" and "old" paradigms is that the new paradigm acknowledges the possibility that blasts of cosmic rays periodically sweep through the Galactic disk and could be responsible for producing effects on the Earth and on planets, stars, and interstellar gas throughout the extent of the Galaxy. It is hoped that the GEH and the Superwave Model concept will lead to the development of a new perspective on galactic explosion phenomena and to the formation of a closer relation between the astronomical and geological sciences.

1.5. DETAILED OVERVIEW OF THE REMAINDER OF THIS RESEARCH STUDY

As pointed out earlier, it has been necessary to bring together a vast amount of observational evidence from a variety of different fields in a coordinated fashion for the present study. In covering such a broad territory, it is easy to fall into the trap of treating each area in a superficial manner. I have as much as possible worked to avoid this. However, a consequence of thoroughness is bulk; Parts I, II, and III have become rather long. In reading through such a mass of material, it will be easy for one to lose sight of the "forest" and to see oneself surrounded only by "trees." To assist the reader in avoiding such a predicament, I offer an overview of this evidence and show how it all fits together in the context of the GEH.

Part I

Chapter 2 presents a survey of extragalactic evidence and demonstrates how this evidence supports several critical requirements of the Superwave Model. A synopsis of these requirements follows:

- 1) The nucleus of a spiral galaxy (like our own) periodically erupts, releasing large quantities of relativistic particles (e.g., electrons and positrons).
- 2) These particles travel radially and isotropically outward from the center of the galaxy at relativistic speeds.
- 3) This particle volley is capable of traveling through the entire extent of a galactic disk with only moderate attenuation.
- 4) These events are brief, lasting on the order of 10^2 – 10^4 years.
- 5) The events occur relatively frequently, about every 10^4 years.

In Section 2.1 it is shown that a variety of different kinds of galaxies, which astronomers consider to be in an explosive state, may all be spiral galaxies like our own, but whose nuclei are in an active phase (Subsection 2.1.3). It is suggested that apparent differences in these galaxies might be explained by: 1) differences in the intrinsic magnitude of each galaxy's outburst, 2) the resolution of the galaxy's optical image (which in turn depends on the galaxy's distance from the observer), 3) the angle at which the galaxy happens to be viewed, and 4) the galaxy's intrinsic morphology.

In Subsection 2.1.1 it is demonstrated that the electromagnetic continuum emission observed from the nuclei of these active galaxies is most probably generated by cosmic rays. Several cosmic ray propagation models seeking to explain the observed continuum emission are reviewed in Subsection 2.1.2. It is shown that the available evidence supports a model in which cosmic rays propagate *radially* outward from their source of generation in the galactic core and experience only *moderate attenuation* by the interstellar medium. In particular, the Superwave Model, which proposes that the radially propagating cosmic rays generate relativistically beamed radiation, is shown to be able to account for a wide variety of phenomena observed in active galactic nuclei. Finally, evidence presented in Subsection 2.1.4 supports the choice of a brief time scale for galactic outbursts.

Whereas Section 2.1 of Chapter 2 deals mainly with active galaxies, Section 2.2 concentrates on observations of spiral galaxies in which nuclear activity is either absent or subdued. Evidence presented in Subsection 2.2.1 supports the proposal that cosmic rays observed in the disks of spiral galaxies originate in the nuclei of these galaxies, rather than from supernova explosions in the galactic disk. Finally, evidence is presented (Subsection 2.2.2) indicating that the disks of spiral galaxies often contain concentric rings of ionized gas with unusually high concentrations of continuum-generating relativistic particles. The observation that such rings are found at considerable distances from the nucleus (sometimes over 100,000 light years) is compatible with the proposal (made here) that galaxies periodically emit from their nuclei blasts of cosmic rays capable of propagating through the galactic disk relatively unattenuated.

Chapter 3 presents a specific superwave model applied to our Galaxy, a superwave consisting of two cosmic ray outbursts generated at the Galactic center some 37,000 years ago and passing the Earth beginning about 14,200 years ago. Some of the quantitative features of this model (of the first of the two cosmic ray outbursts) are summarized in Table II. The initial conditions of the cosmic ray components of this superwave are specified in Section 3.1. The interactions which these cosmic rays would undergo as a result of their

TABLE II
THE 14,200 YEARS BP SUPERWAVE MODEL: SUMMARY OF FEATURES

1. GENERATION AT GALACTIC CENTER

| | |
|---|---|
| Duration of the event: | 200 years at peak flux; thereafter decays linearly over 200 years. |
| Frequency of the event: | About every 5000 – 10,000 years. |
| Type of cosmic rays: | Electrons and positrons (approximately equal numbers). |
| Total energy of the outburst: | 7×10^{57} ergs, $4000 M_{\odot} c^2$ (equivalent rest-mass energy) |
| Actual electron mass ejected: | $1.3 M_{\odot}$ |
| Differential particle number flux spectrum: | $N(E) \propto E^{-1.8}$ for $E < 1.5$ Gev, $N(E) \propto E^{-2.75}$ for $E > 1.5$ Gev |
| Particle energy flux at peak intensity for the entire outburst integrated over all energy | 7.5×10^{47} ergs/s |
| Particle number flux at peak intensity for the entire outburst integrated over all energy increments: | 10^{52} electrons/s |
| Particle energy density at peak intensity at 1 light year from the GC integrated over all energy increments | 2 erg/cm ³ (directed). 0.5 ergs/cm ³ (if isotropically distributed). 4000°K (equivalent equilibrium temperature). |
| Particle number density at peak intensity at 1 light year from the GC integrated over all energy increments | $10^4 - 10^5$ electrons/cm ³ |
| Particle kinetic energy: | Average for the outburst: 50 Mev; Lorentz factor = 100. At mode of differential energy flux spectrum: 1.5 Gev; Lorentz factor = 3000. |

2. PROPAGATION THROUGH GALACTIC DISK

| | |
|---|---|
| Kinetic energy transferred to the interstellar medium of the Galactic disk | 10^{56} ergs (about 7% of the total outburst energy) |
| Fractional loss of energy as a result of the journey to the solar vicinity: | 20% of the solid angle flux directed toward the solar system. |

3. ARRIVAL IN SOLAR VICINITY

a) Outside the Bow Shock Front.

| | |
|--|--|
| Particle energy flux at peak intensity integrated over all energy increments: | 90 ergs/cm ² /s; 10^{-4} suns. |
| Particle energy density at peak intensity integrated over all energy increments: | 3×10^{-9} ergs/cm ³ (directed) 7.5×10^{-10} ergs/cm ³ (if isotropically distributed). |
| Integral particle number density at peak intensity: | $10^{-6} - 10^{-5}$ electrons/cm ³ . |

b) Outside the Earth's Magnetopause.

| | |
|--|---|
| Particle energy flux at peak intensity integrated over all energy increments: | 9 ergs/cm ² /s; 10^{-5} suns. |
| Particle energy density at peak intensity integrated over all energy increments: | 7.5×10^{-11} ergs/cm ³ (if entirely isotropically distributed). 75 times the current cosmic ray proton background observed at solar minimum. |

c) At the Earth's Surface (sea level).

| | |
|--|---|
| Average integral number flux at peak superwave intensity | 0.16 electrons/cm ² /s/str. 80 times the current sea level flux |
| Ionizing radiation at peak superwave intensity: | 4 roentgens/year (average level) |

TABLE II (continued)

d) Influx of Cosmic Dust, Water Vapor, and Ice Grains

| | |
|--|--|
| Mean radius of dust and ice grains: | 0.1 microns (10^{-5} cm). |
| Concentration of cosmic dust in the Earth's vicinity: | 10^{-19} g/cm ³ ; ~15 times current interplanetary dust concentrations. |
| Concentration of nebular material in the Earth's vicinity: | 2×10^{-19} g/cm ³ for an H ₂ O: dust ratio of 1:1. |
| Optical depth of nebular material residing outside the Earth's orbit: | 0.14 |
| Backscattered radiation received: | $0.05 \times$ the solar constant. |
| Optical depth of nebular material in the Earth's upper atmosphere: | 0.15 |
| Earth/Sun optical depth of nebular materials: | 0.4 |
| Predominant spectral range where a dust-obscured Sun would radiate its energy: | 1 – 10 microns (equivalent blackbody temperature: 1150° K). |
| Mass accretion rate by the Sun: | 6×10^{-12} M _☉ /y r |
| Luminosity increase due to material infall: | 0.025% |

4. PRESENT CONFIGURATION OF EVENT HORIZON

| | |
|--|---|
| Geometry of the 14,200 years BP superwave, assuming a solar galactocentric distance of 7 kpc (22,800) light years: | Ellipsoid (as viewed from Earth). Semi-major axis: a = 5.68 kpc (18,500 l.y.) Semi-minor axis: b = 4.47 kpc (14,600 l.y.) |
| Distance from the solar system to the event horizon in the anticenter direction, $\ell = 180^\circ$: | 2.18 kpc (7100 light years). |

22,800 light-year (7 kpc) journey through the Galactic disk (the distance from the GC to the Earth)* are discussed in Section 3.2.

Section 3.3 speculates on the possible effects that this cosmic ray blast could have on the Earth and Sun, primarily through its ability to generate a nebular cloud of vaporized cometary material and to subsequently propel this material into the solar system. For example, it is shown that light backscattered from 0.2 micron diameter nebular dust grains lying outside of the Earth's orbit could have increased the solar constant in the Earth's vicinity by up to 5%. Also, upon entering the Earth's upper atmosphere, such material could have produced optical depths as high as $\tau \sim 0.14$, causing the Earth's albedo to increase by up to 1.5 percentage points. In addition, nebular material intervening between the Sun and Earth would have produced optical depths averaging $\tau \sim 0.4$. As much as 22% of the Sun's radiation would have been absorbed and reradiated in the infrared ($\lambda \sim 2\text{--}3$ microns) as a

* Estimates of the Sun's distance from the G.C. found in the scientific literature (circa 1983) range from 5.5 to 10 kpc. The value which is often quoted is 8.5 ± 1 kpc (28,000 \pm 3000 l.y.). The value assumed in this work is 7.0 kpc (22,800 l.y.) in accordance with the value quoted by Clube (1978). The discrepancy between this value and the 8.5 kpc figure is small enough that it should be of little consequence for the substance of the GEH.

[**UPDATE:** Year 2000 GC radial distance is usually quoted in the literature at 7.7 kpc]

result of the presence of this dust.. In combination, these effects would have produced a warming of the Earth's polar regions which, depending on the magnitude of this warming, would have caused the Wisconsin stage continental ice sheets to either advance or rapidly retreat. The accompanying climatic and hydrologic effects would have posed a severe threat to the survival of land life forms.

Accretion of nebular material by the Sun would have increased the Sun's luminosity by up to 0.6% from its present value and would have increased the level of solar flare activity by several orders of magnitude. The impact of charged particles (particularly solar flare cosmic rays) on the Earth's magnetosphere could cause major geomagnetic excursions and sometimes reversals of the Earth's magnetic field. Solar flare protons and superwave cosmic ray electrons, upon passing through the Earth's atmosphere would increase the production of oxides of nitrogen (NO_x) which would deteriorate the Earth's ozone layer and allow life-harming ultraviolet radiation to penetrate to ground level. Also, the penetration of these particles (particularly solar flare cosmic ray protons) could lead to accelerated mutational change, especially among land life forms.

Finally, it is possible that an energetic pulse of gamma ray radiation would be traveling at the forefront of the event horizon. At the end of the Last Ice Age this would not have had a significant effect on the Earth's climate or on its biosphere. However, such a pulse could possibly induce EMP (electromagnetic pulse) in the Earth's atmosphere. If this were to happen today, the consequences would be tragic for civilized society. The resulting high voltages generated in all unshielded metal conductors could cause widespread destruction of electrical and electronic equipment and possibly could even unwittingly trigger a global nuclear war.

Part II

The purpose of Part II (Chapters 4, 5, and 6) is to present evidence of an assortment of astronomical phenomena observed in our Galaxy and in the solar vicinity and to show that these are compatible with the model presented in Chapter 3.

Chapter 4 reviews evidence of recent activity in the Galactic Nucleus (Sections 4.1 – 4.4) and in the Galactic disk, with particular emphasis on the immediate solar vicinity and solar system (Sections 4.5 – 4.7). Regarding recent activity in the Galactic Nucleus, the asymmetric distribution of hot dust and ionized gas observed within 6 light years (l.y.) of the Galactic center and the presence in this region of 14 discrete clouds of ionized neon gas unhomogenized by cloud-cloud collisions both suggest that outbursts have taken place there within the last 10⁴ years. There is also abundant evidence of gas moving radially away from the Galactic center, e.g., the neutral oxygen gas at a galactocentric distance of $r = 10\text{--}20$ l.y., the molecular ring cloud at $r \sim 400\text{--}600$ l.y., the "arc" feature at $r \sim 80$ l.y., neutral hydrogen clouds at $r \sim 1000\text{--}2000$ l.y., and the inner spiral arms at $r \sim 10,000$ l.y. (Sections 4.2 – 4.4).

Section 4.5 cites evidence of recent energetic activity in the solar vicinity, indicated by the presence of million-degree interstellar gas lying within several hundred light years of the Sun. Also, there is evidence that the interstellar medium contains giant shells of gas, or "supershells." Their kinetic energies, which range up to 6×10^{53} ergs, are so high that it is unlikely that individual supernovae are responsible for their existence. However, energies of this magnitude would be available from Galactic superwaves. The general violent nature of the interstellar medium is also apparent from the presence of a shell of "high velocity" ($\sim 10^2$ km/s) neutral hydrogen gas distributed as a ring around the periphery of the Galactic disk.

Section 4.6 discusses the significance of the interstellar wind of neutral hydrogen and

helium that appears to be approaching the solar system from the direction of the Galactic center. It is pointed out that this steady flow of gas may be driven radially outward from the GC by the periodic passage of Galactic superwaves.

Section 4.7 discusses planetary evidence for recent heating of the solar system. For example, it is pointed out that the intricate grooved pattern composing Saturn's rings and the rapid radial motion of Saturn's C ring may be accounted for if Saturn's ring system is relatively young, i.e., if within the last 10^4 years its rings had become completely vaporized and reformed once again. Heating effects could also explain the unusual ice flow features observed on some of Saturn's moons, the outflow channel features observed on Mars, and the formation of glassy spherules observed on rocks recovered from the Moon. Such heating could have been caused by superwave cosmic waves trapped in the heliopause at times when the heliopause was being propelled through the solar system. Or, alternatively, these heating effects could have been due to a major enhancement of the solar wind associated with a T Tauri-like solar flare outburst.

Chapter 5 deals with phenomena currently taking place in the Galactic disk which may be specifically correlated with the present location of the 14,200 years BP superwave event horizon. One example concerns the Galactic radio background radiation, which is generally believed to be produced by cosmic rays propagating in the Galactic disk (Section 5.1). Models thus far proposed have been unable to adequately account for the longitudinal distribution of this emission, in particular its rapid increase in intensity at longitudes close to the Galactic center. The 14,200 years BP superwave model, on the other hand, predicts a radio intensity distribution which matches the general trend of the observed radio distribution very closely.

In Section 5.2 it is theorized that supernova remnants lying in the vicinity of the 14,200 years BP event horizon should have high radio surface brightnesses since these remnants would tend to trap superwave cosmic rays in synchrotron radiating orbits. To test this hypothesis, a subsample of 16 high surface brightness remnants was selected from a sample of 125 and plotted on a polar graph of the Galactic plane. The distribution of the remnants is found to be broadly consistent with the GEH. In particular, it was discovered that the Crab Nebula and Cassiopeia A, two young supernova remnants with the highest known radio surface brightness and whose distances from the Earth are among the most accurately known, both lie on the 14,200 BP Event Horizon. The positions and ages of these and certain other supernova remnants seem to indicate that the 14,200 years BP superwave is also active in *triggering* supernova explosions.

Section 5.3 is devoted exclusively to the Crab Nebula. This particular supernova remnant was chosen for in-depth study because of its close proximity to the 14,200 BP Event Horizon and because extensive investigations have been made of its unusual properties. The section begins by pointing out some of the difficulties of accounting for the nonthermal emission from the Crab in terms of an internal source of cosmic ray electrons, e.g., supernova explosion or central pulsar. As an alternative, it is shown that the Crab remnant would be able to intercept a sufficient flux of cosmic rays from the proposed 14,200 years BP superwave to explain the observed synchrotron radio and optical emission. Also, it is shown that the X-ray and γ -ray emission observed from the center of the remnant (which require a continuous and diffuse source of cosmic rays) can also be accounted for by the superwave. The elliptical shape and orientation of the Crab Nebula parallel to the Galactic equator, the acceleration in the nebula's rate of radial expansion, and the remnant's proper motion are all shown to be consistent with the expected electrodynamic effects associated with the superwave. The unique filled-center appearance of its optical and X-ray emission may also be accounted for. Finally, the continuous luminous front activity observed in the middle of the nebula may be produced by relativistic blasts of particles propagating toward

the Galactic anticenter and striking the outer shock front of the expanding nebular shell.

Section 5.4 reviews the characteristics of Cassiopeia A, another extensively studied supernova remnant, and as mentioned above, one which coincides with the 14,200 BP Event Horizon. It is shown that many not-well-understood features associated with this remnant may be explained if it is assumed that the remnant is being illuminated from its exterior by a blast of cosmic ray electrons. Such a model is able to account for the continuous powering of the X-ray emission observed from the remnant's shell and filaments. Also explainable is the asymmetrical distribution of the remnant's X-ray and radio emission, the region of more intense emission coming from the side positioned toward the GC, or from what may be a bow shock front formed between the remnant and the oncoming superwave. The observation of rapid variability in the radio flux at long wavelengths, comparable to the light travel time across the remnant, is consistent with a model in which electrons propagating relativistically across the surface of the remnant excite this emission. The rapid variation in the brightness of radio knot-like features observed in the shell and their unusually high proper motions (motions perpendicular to the line of sight) may also be accounted for by the 14,200 years BP superwave. Finally, it is demonstrated that the remnant could intercept an electron flux from the proposed superwave sufficient to explain its radio synchrotron and X-ray emission.

Section 5.5 discusses two very young extragalactic supernova remnants which are distinguished as being the only extragalactic remnants from which radio emission has been detected. The delayed appearance of the emission, its magnitude, and its final decline after 5 years (e.g., in SN 1970g) are all consistent with the Superwave Model. Moreover, the rapid variability of the radio emission, which is reminiscent of compact radio sources in active galactic nuclei, may also be accounted for.

Chapter 6 presents evidence for two smaller superwaves which may have passed the Earth ~6000 BP and 393 AD. In Section 6.1 a number of different unusually energetic objects are shown to coincide with the present location of the 6000 BP event horizon. A few of these nebulae and stars include: P Cygni, Cygnus X-1, MWC 349, NGC 7027, Eta Carinae, the Carina Nebula, NGC 2261, and A0620-00. By postulating the presence of the 6000 years BP superwave, the unusual behavior of these objects may be better understood. Extensive regions of diffuse X-ray and γ -ray emission are shown to be present in both the Cygnus and Carina regions in the vicinity of the 6000 BP Event Horizon. Also, it is shown that in the region where the Carina spiral arm crosses this horizon an unusually high density of luminous supergiant stars are found, again indicating the presence of energetic activity.

Astronomical evidence for the 393 AD superwave is discussed in Section 3.2. It is suggested that this superwave may be responsible for the strong radio and soft X-ray emission from the Vela XYZ and Cygnus supernova remnants, for powering the H_{α} emission from the Gum Nebula, for reheating the Lupus Loop and North Polar Spur remnants, and for stimulating the excess soft X-ray emission from SN 1006. The disappearance of the circumstellar nebula V-V 1-7 could also be accounted for with this scenario.

Part III

Part III discusses terrestrial evidence supporting the hypothesis that a superwave may have passed the Earth toward the end of the Last Ice Age (beginning about 14,200 years BP and reaching a peak about 12,450 years BP). Evidence for earlier superwaves is also discussed.

Chapter 7 reviews paleomagnetic evidence of geomagnetic excursions and polarity reversals occurring since the time of the Last Interglacial. An excursion occurring about

12,400 BP, which I have named the "Gothenburg/Erieau/ Laschamp Excursion" (or G/E/L Excursion), has had widespread detection around the globe. It is pointed out that this excursion occurred coincidentally with several other events: an abrupt climatic warming, a major acceleration in the rate of glacial melting, an episode of catastrophic, continental flooding in periglacial regions associated with the extinction of numerous genera of large land mammals. As is discussed in Chapter 10, the megafaunal extinction associated with this event was the most severe of the entire Pleistocene Epoch, one that rivals the extinction of the dinosaurs at the end of the Cretaceous Period.

Another interesting geomagnetic event is the Blake Event, which occurred during the second half of the Last Interglacial (oxygen isotope substage 5-d to 5-b). Although this is well before the time of the 14,200 years BP superwave, such an event could be attributed to earlier superwave passages. While glacial ice tests were not conducted for this period to check such an hypothesis, they could be done in the near future. Nevertheless, evidence is presented in this chapter of significant climatic changes occurring coincidentally with the boundaries of this event. Both at the time of the onset and at the time of termination of reversed polarity, a sudden global climatic cooling occurred. Each time, within less than 75 years, there was widespread destruction of forests in northeastern France followed by a several hundred year period during which steppe-type vegetation prevailed. These events occurred simultaneously with periods of considerable glacial growth in the Northern Hemisphere; see Chapter 9 (Sections 9.1 and 9.2) for pertinent correlations.

Chapter 8 reviews data regarding variations of oxygen isotope ratios, dust concentration, and dust composition contained in three glacial ice cores: the Dome C and Byrd Station ice cores from Antarctica and the Camp Century ice core from Greenland. Using the δO^{18} (oxygen isotope) ratio as an indicator of climate, it may be seen that a persistent climatic warming begins about 11,550 calendar years BP marking the termination of the Last Ice Age (Subsection 8.1).³ The closeness of this climatic transition to the time when the proposed 14,200 years BP superwave would have been passing through the solar system suggests that these events may be related.

Section 8.3 reviews some of the significant findings of the glacial ice dust tests conducted in this study, the results of which are described in greater detail in Chapter 12. For example, out of 8 Camp Century core glacial dust samples tested (spanning the period (35.3 k – 73.1 k calendar years BP), 6 were found to have significantly high levels of iridium (Subsection 8.3.1).^{*} These levels suggest that at certain times during the Late Wisconsin cosmic dust deposition rates exceeded current rates of extraterrestrial material influx by 5 to 50 times. In particular, high Ir values were found for one Camp Century core dust sample dated at 50.3 k calendar years BP and for one Byrd core dust sample dated at 28.4 k calendar years BP. Both of these positive results indicate an increase in the rate of cosmic dust influx. Asteroid or planetesimal impacts can be ruled out as the source of this iridium.

* Calendar dates given throughout this work report the best dates, presently known, for the particular ice core sample or climatic boundary being referred to, thereby correcting the dates given in original 1983 version of this dissertation. The ice core dates presented in the original dissertation were faulty due to reliance on inaccurate time-depth relationships that had been published for the Camp Century and Byrd Station ice cores. This flawed ice core chronology had also been used in the original dissertation to convert carbon-14 dates into calendar dates by correlating C-14 dated climate boundaries to ice core climate boundaries. These defective converted dates, which I had named composite ice core dates (CID) have been replaced with more accurate calendar dates derived by using the C-14 date-to-calendar date conversion scheme that uses the accurately dated Summit, Greenland GRIP ice core chronology (see Appendix E).

High Ir concentrations coinciding with dust peaks dated at 35.3 k calendar years BP, 54.6 kyrs BP, and at 73.1 kyrs BP] suggest that several other superwaves may have passed the Earth during the Last Ice Age. The discovery of high concentrations of Ir, Au, and Ag in sample #962-1 (50.3 k calendar years BP) along with large amounts of tin (already known to be present from Thompson's (1977b) microprobe analysis) implicates a cosmic origin for this dust and for samples at other depths reported to contain large amounts of tin (e.g., dust peak #1 and #10). A cosmic origin for dust peak #10 in the Camp Century core is particularly significant because this event immediately preceded a major period of glacial growth. Some authors have interpreted this portion of the ice core as marking the beginning of the Wisconsin Ice Age.

A Byrd core volcanic ash band was found to contain high concentrations of Ir, but this discovery is incidental to the main hypothesis tested in this study. However, it is still an interesting finding. It suggests that volcanic ash falls are able to accelerate the precipitation of cosmic dust grains present in the stratosphere; see Subsection 12.1.4 for a discussion.

Section 8.4 presents evidence that Be-10 concentrations in glacial ice were 2 – 3 times higher during the middle and late portions of the Last Ice Age as compared with average levels characteristic of the present interglacial.

Chapter 9 (Section 9.2) discusses evidence indicating the abruptness with which major coolings or warmings can take place in the Earth's climate. Of particular interest is the brief cooling episode toward the end of the Eemian Stage of the Last Interglacial. Also it is shown that toward the end of the Wisconsin, from 14.5 – 12.7 k calendar years BP, an abrupt global warming took place, an event which is here given the generic name "Terminal Pleistocene Interstadial." The finding that this event was of *global* proportions is an original and significant contribution of this study. It is shown (Section 9.3) that during this interstadial glacial melting and ice sheet recession rate were unusually high in both North America and Europe, reaching a peak at about 14.2 k calendar years BP. Most conventional climatic models have difficulty explaining how such a major worldwide climatic warming could have occurred at a time when the Earth was in a fully glaciated state. On the other hand, the GEH is able to successfully account for such a warming.

Chapter 10 (Section 10.1) discusses paleontological evidence of a major "worldwide" extinction episode occurring at the end of the Wisconsin, which primarily affected large land mammals, although many small mammals and several genera of birds also became extinct. Evidence that this extinction occurred in connection with widespread continental flooding is presented in Section 10.2. It is proposed (Section 10.3) that this continental flooding involved meltwater from rapidly melting glaciers. A mechanism is suggested by which large translating waves of glacial meltwater could form and propagate along the surface of an ice sheet, gaining in momentum as they traveled. This phenomenon, which is given the name "glacier wave effect," is presented here for the first time. Also new is the proposal that "glacier waves" were responsible for forming many of the observed alluvial deposits in periglacial regions and for being a main contributor to the Terminal Pleistocene Extinction. Continental flooding by glacier waves could also explain how the numerous carcasses of mammals could have become buried and sometimes frozen whole in the arctic tundra of Northern Siberia; see Subsection 10.2.1. Climatic warming, brought about by an interplanetary greenhouse effect due to the presence of nebular material immediately outside the Earth's orbit, is attributed as the immediate cause of this catastrophe, the ultimate cause being the passage of the 14,200 years BP superwave.

Chapter 11 discusses paleomagnetic evidence of numerous extinction episodes occurring throughout geological history. It is concluded that the abrupt nature of these

extinctions and their tendency to occur simultaneously with accelerated mutational changes could best be explained by an agent which repeatedly produces elevated levels of cosmic ray radiation in the Earth's vicinity. Galactic superwaves are chosen as the most likely candidate since supernovae that are sufficiently close to produce such an effect occur too infrequently. A cosmic ray mechanism could also explain why species with the highest extinction rate are also the ones with the highest rates of speciation. Also the coincidence of major extinction episodes with geomagnetic reversals could be accounted for.

Several other extraterrestrial extinction hypotheses that have been proposed in the literature are reviewed in Section 11.2, including those involving cosmic rays and those involving falling bodies such as asteroids or comets. It is concluded that the proposed phenomena either occur too infrequently or fail to adequately account for all facets of the extinction phenomenon.

Part IV

Chapter 12 covers in detail the procedure that was followed in conducting the NAA tests of glacial dust samples and ocean and lake bottom sediments and summarizes the results that were obtained. Section 12.1 covers glacial ice dust tests performed on samples from the Camp Century and Byrd Station ice cores. Section 12.2 covers glacial ice dust tests performed on the A 77 ice core penetrated in the Agassiz Ice Cap (Arctic Canada). And finally, Section 12.3 summarizes the procedure and results for tests performed on sediments from the Caribbean Ocean and from Elk Lake in Minnesota. Numerical data for the glacial ice dust tests are tabulated in Appendix G.

CHAPTER 2

EXTRAGALACTIC EVIDENCE SUPPORTING THE SUPERWAVE MODEL: TOWARD A GENERAL THEORY OF GALACTIC OUTBURSTS

2.1 EVIDENCE OF SUPERWAVE ACTIVITY IN ACTIVE GALAXIES

2.1.1 Radiation Characteristics that Active Galactic Nuclei Share in Common

Active galaxies, or "exploding galaxies," go by a variety of different names, such as: quasi stellar object (or quasar), B L Lacertae object (or blazar), N galaxy, Seyfert galaxy, Markarian object, Zwicky compact galaxy, and giant elliptical. As is discussed in Section 2.1.2, these different types may actually all be spiral galaxies (similar to our own) whose nuclei are in an active state, but which for various reasons have differing optical appearances. One indication that the same energetic phenomenon is involved in the nuclei of these variously classified objects is that their electromagnetic spectra share certain features in common. These include: a) strong nonthermal continuum radiation extending from the radio to the gamma ray region of the spectrum and coming from a region of small angular diameter coinciding with the center of the galaxy, b) erratic variability of the continuum, and c) strong emission lines, usually considerably broadened.

There is a general consensus that the continuum radiation is produced by *relativistic particles* (electrons or positrons) radiating from an "engine" (whose nature is currently not well understood) located at the very center of the galaxy (Burbidge, Burbidge, and Sandage, 1963; Weymann, 1969, p. 237; Fabian, 1979; Burbidge, 1970, pp. 424-430; Kellermann, 1978; and Burbidge, Jones, and O'Dell, 1974). Relativistic particles could generate the

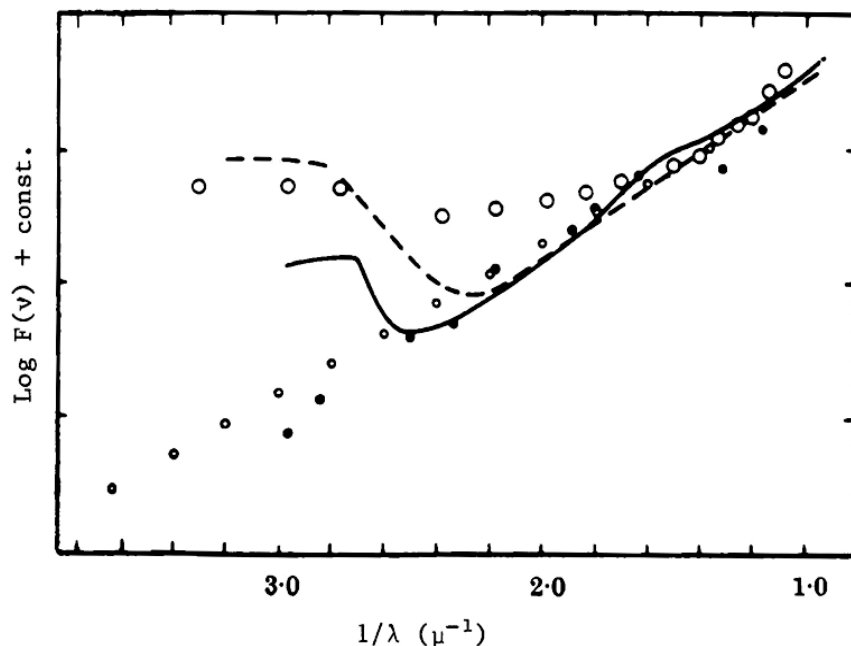


Figure 2.1. Monochromatic fluxes in the optical range for the spectrum of Seyfert NGC 4151 (full line), Carinae (dashed line), Crab Nebula (filled circles), quasar 3C 48 (small open circles) and quasar 3C 273 (large open circles) (Searle, Rodgers, and Sargent, 1965).

observed continuum radiation either by spiraling in magnetic fields (synchrotron mechanism), by colliding with photons (inverse Compton scattering mechanism), or by linearly decelerating (bremsstrahlung or Cerenkov mechanisms).

The nonthermal power-law character of the spectrum is one indicator that relativistic particles are involved. A second indicator is the observation that the continuum radiation is often polarized. Finally, several studies indicate that the intensity of the electromagnetic continua in different portions of the spectrum are correlated such that galaxies having greater optical continuum intensities would also have greater intensities in the radio, infrared, and X-ray spectral regions as well. A few of these correlation studies include: X-ray/optical (Ku, Helfand, and Lucy, 1980), X-ray/infrared (Kriss, Canizares, and Ricker, 1980), and radio/infrared (Rieke and Low, 1972; Van der Kruit, 1971a). Such spectral correlation is best explained if the entire continuum in each of the objects studied is generated in common by a flux of relativistic particles.

As further indication that a close relation exists between these variously classified objects, Searle, Rodgers, and Sargent (1965) have pointed out that Seyferts and quasars often have similar optical spectra. As seen in Figure 2.1, the spectra of Seyfert NGC 4151 and quasar 3C 48 closely follow each other at short wavelengths. The 3C 273, however, shows less similarity. They also point out that the spectra of these active galaxies are similar to the spectra for Eta Carinae and the Crab nebula. It is interesting to note that these two Galactic nebulae are located respectively in the vicinity of the proposed 6000 years BP and 14,200 years BP superwave event horizons.

Also, a strong similarity exists between the infrared continuum emitted from the nuclei

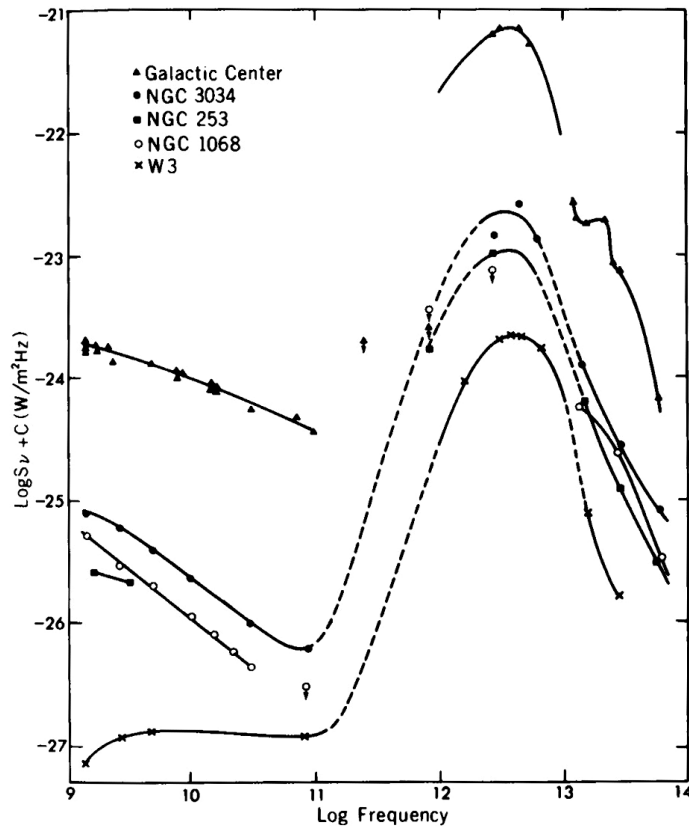


Figure 2.2. Spectral power distributions of the Galactic Center (triangles), the nebula W 3 (crosses), and the nuclei of: galaxy NGC 3034 (filled circles), galaxy NGC 253 (squares), and Seyfert NGC 1068 (open circles). (Harper and Low, 1973)

of Seyfert galaxies and from the nuclei of normal galaxies. The spectra of Seyfert nuclei appear to have a major hump in the 1 – 1000 micron range, indicating that over 80% of their power is radiated in the far-infrared (Low and Kleinmann, 1968). As seen in Figure 2.2 (Harper and Low, 1973), the Seyfert NGC 1068 shares this spectral feature in common with the nuclei of "normal" spiral galaxies such as M 82 and NGC 253, with our own Galactic Center, and with the Galactic infrared nebula W 3. Also, Low and Kleinmann (1968) have pointed out that the spectra of Seyfert NGC 1068 and the Planetary Nebula NGC 7027 increase in intensity in the infrared region in a similar manner. It is interesting to note that both W3 and NGC 7027 are located on superwave event horizons (14,200 years BP and 6000 years BP respectively); see Sections 5.3 and 6.1. Spectral similarities observed between Seyfert nuclei and Galactic infrared nebulae has led to the suggestion that the emission in both cases is due to thermal reradiation by dust grains (Jameson et al., 1974; Burbidge, 1970, pp. 424-430; Rieke and Lebofsky, 1979, pp. 493-499). I would extend this conclusion by proposing that the stars exciting such planetary nebulae and infrared nebulae are triggered into activity by the passage of a galactic superwave. The excessive brightness of this infrared continuum in active galaxies could be due to a photon shock effect described in (g) (p. 36). It should be noted, however, that some quasars such as 3C 273 and 3C 279 do not have this thermal continuum feature; see Figure 2.3 (Rieke and Liebofsky, 1979). In these objects the thermal emission phenomenon could be present, but not seen because the

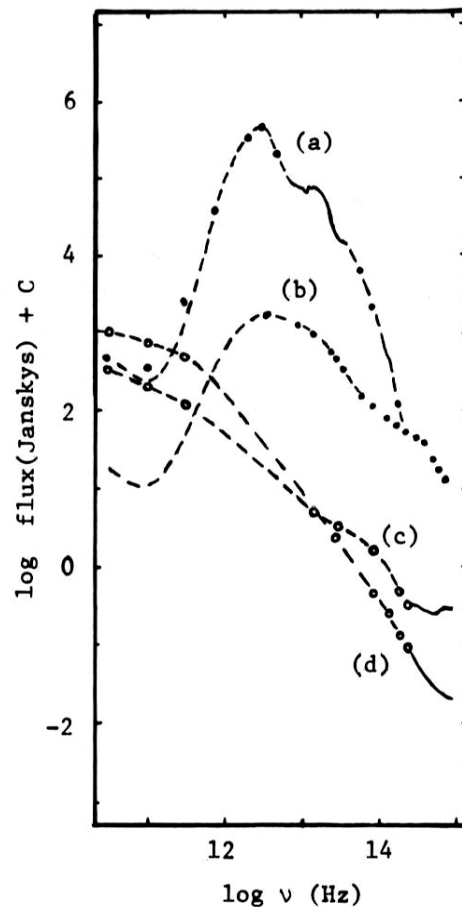


Figure 2.3. Infrared spectra of: (a) Seyfert NGC 1068 ($C = 3.7$), (b) Seyfert NGC 4151 ($C = 2.5$), (c) quasar 3C 273 ($C = 1$), and (d) quasar 3C 279 ($C = 2$) (adapted from Rieke and Lebofsky, 1979, Fig. 1).

thermal continuum is overpowered by the nonthermal continuum generated by the superwave cosmic rays.

Radio variability measurements have also shown that similar continuum generating processes may be at work in quasars, blazars, and Seyferts alike. For example, similarities may be seen by comparing Figure 2.4-a for Seyfert 3C 120, Figure 2.4-b for quasar 3C 273 (Kellermann and Pauliny-Toth, 1968), and Figure 2.5 for B L Lacertae (Mutel, Aller, and Phillips, 1981). Note that the time scale of the variation is roughly comparable. Sometimes the outbursts appear first at shorter wavelengths and then propagate to longer wavelengths with reduced amplitude, as seen in Figure 2.4-a and -b. However, often the amplitude of the outburst is nearly independent of wavelength with the outburst appearing simultaneously at different wavelengths.

If the spectra and energy continua of these variously classified active galaxies have so many characteristics in common, then why is it that the optical images of the galaxies appear so different? In Subsection 2.1.3, it is demonstrated that cosmic ray explosions issuing from the center of a spiral galaxy can generate such varied appearances, provided that it is assumed that these cosmic rays propagate radially at relativistic velocities through the entire extent of the galaxy (as the GEH proposes). But before discussing this, it is useful to first review evidence from the field of radio astronomy that confirms the existence of superwaves.

2.1.2 Relativistic Radial Expansion of Cosmic Ray Outbursts from Active Nuclei

A great deal may be learned about the behavior of relativistic particles in active galactic nuclei by studying the nature of the radio emission that they produce and in particular the

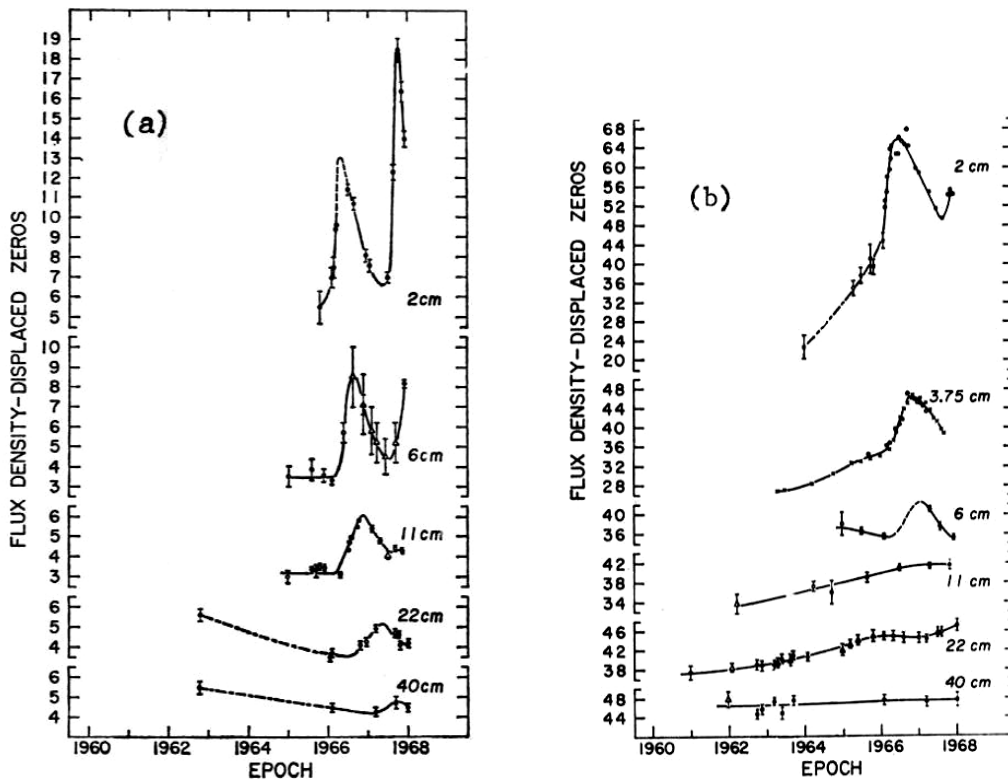


Figure 2.4 (a) Radio variations of Seyfert galaxy 3C 120. (b) Radio variations of quasar 3C 273. (Kellermann and Pauliny-Toth, 1968)

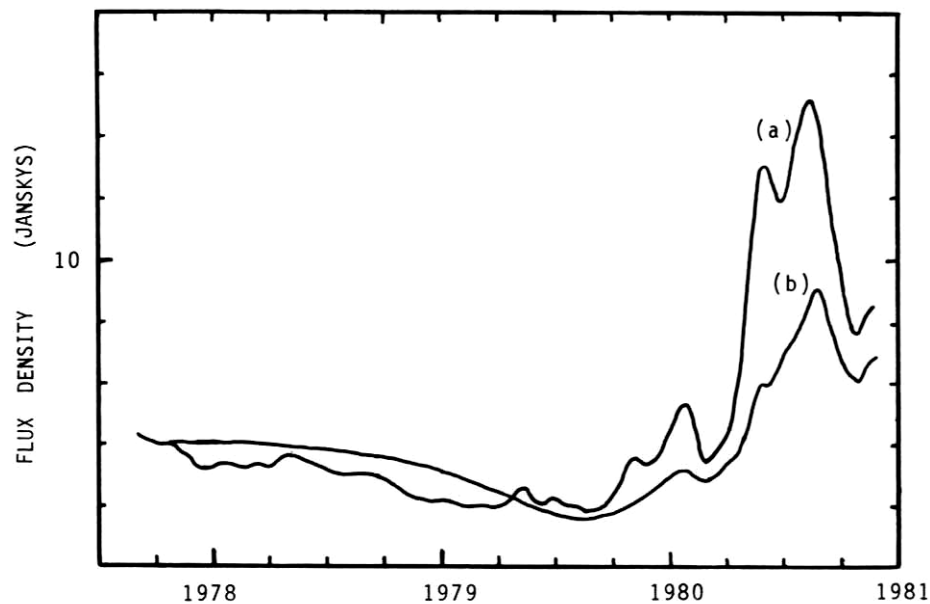


Figure 2.5. Variation in the radio output of blazar B L Lacertae during a recent flare: a) Flux density at 2 cm wavelength; b) Flux density at 6 cm wavelength. (after Mutel, Aller, and Phillips, 1981)

nature of the so called "compact radio sources" which are often present. These compact sources, which usually coincide with the nucleus of the galaxy, typically have dimensions on the order of milli-arcseconds or less at centimeter wavelengths and are characterized by rapid flux density variations on the order of months to years. Nearly all blazars, most quasars, and many radio galaxies contain compact radio sources (Kellermann and Pauliny-Toth, 1981). They are also found in a variety of other active galaxies which include: normal spirals (e.g., M81, NGC 4594), irregular galaxies (e.g., M82), giant elliptical galaxies (e.g., M87, NGC 5128), and Seyfert galaxies (e.g., NGC 1275, 3C 120). Despite this wide variety of galaxy types, no clear distinction can be made in the properties of their associated compact radio sources. However, those in blazars do show relatively high polarization and variability (Kellermann and Pauliny-Toth, 1981). It should also be mentioned that our own Galactic Center has a coincident compact radio source. But the very low intensity of this source (10^{33} ergs/s) places it at the extreme end of a luminosity distribution which typically ranges from 10^{38} to 10^{45} ergs/s (Kellerman, 1978); see Figure 3.4 (p. 66).

Incoherent Synchrotron Models. The emission observed from these compact radio sources may be modeled in a number of different ways depending upon the kind of radiation mechanism that is assumed to operate and depending upon the particular propagation geometry assumed for the relativistic particles generating this emission. According to one interpretation, the relativistic particles are confined to the immediate neighborhood of the nucleus and generate *incoherent* synchrotron radiation. The particles are assumed to spiral around magnetic field lines in a random fashion with each volume of the magnetically bound plasma radiating its continuum isotropically. The diameter of the emission region would then delineate the actual region in the nucleus to which these particles would be confined.

However, incoherent synchrotron models have several difficulties. For one thing, they lead to estimates of enormous bulk particle energy contents (Kellermann and Pauliny-Toth,

1968; Burbidge, Jones, and O'Dell, 1974). The critical factor is the angular size that is assumed for the diameter of the emitting region. From an estimation of the size and from observations of the intensity and spectrum of the radio continuum, synchrotron models may be developed and estimates may be derived of the total energy content of the source in the form of relativistic particles (e.g., electrons). When θ is determined from very long baseline radio interferometry (VLBI) measurements, compact sources are generally found to have total particle energies in the range $10^{52} - 10^{58}$ ergs, which is not unreasonably high. However, when smaller angular sizes are assumed for these sources, the particle energy content becomes inordinately large. And, smaller sizes are indeed implied by the rapid variability of the sources. For example, at radio wavelengths (e.g., $\lambda \sim 2$ cm) significant changes in source intensity sometimes take place in the space of a tenth of a year (see Figure 2.4), implying that the size of the emission region is less than 0.1 light years. That is, for an incoherent source, if the characteristic time scale of its variation is τ , then the size of the source should be smaller than $c\tau$, the distance that light would travel in this time.

Take, for example, the source 3C 273-B. Burbidge, Jones, and O'Dell (1974) have estimated its energy content at $U_e = 6 \times 10^{55}$ ergs based on an interferometry angular size $\theta \sim 0.011$ arcseconds. However, variability on a time scale of 0.1 years implies an angular size $\theta < c\tau/D = 6 \times 10^{-6}$ arcsec, for a distance to 3C 273 of $D = 3.1 \times 10^9$ light years. However, the estimated particle energy content for incoherent synchrotron sources scales according to the inverse sixth power of source angular size (Burbidge, Jones, and O'Dell, 1974);

$$U_e \sim \theta^{-6} \quad (1)$$

Thus this 1570 fold decrease in angular size translates into a 1.5×10^{19} fold increase in estimated particle energy, giving: $U_e \sim 10^{75}$ ergs. This is equivalent to a rest mass energy of $10^{20} M_\odot/c^2$. In other words, to power such a radio source the mass of one billion spiral galaxies would have to be converted into particle kinetic energy in the space of a tenth of a year!

Another problem with incoherent synchrotron models is that inverse Compton scattering between the relativistic electrons and the synchrotron photons would occur so frequently at these densities that the particles would be subject to catastrophic energy losses (Kellermann and Pauliny-Toth, 1968, pp. 439-441). So, the energy input required to explain the observed synchrotron radiation intensity would go up accordingly. Moreover, enormous fluxes of inverse Compton X-ray radiation would be expected to be radiated from such sources, and such outputs are not observed. Observations of active galactic nuclei at X-ray wavelengths indicate that X-ray fluxes are far below levels that are predicted by incoherent synchrotron models incorporating inverse Compton scattering (Jones, O'Dell and Stein, 1974; Burbidge, Jones, and O'Dell, 1974, p. 49; Marscher et al., 1979).

Ballistic/Relativistic-Beaming Models. Difficulties such as those described above have motivated astrophysicists to look at other alternatives. Particularly attractive are models which assume that the emission region does not remain stationary, but moves relativistically toward the observer. Investigation into such models has been rapidly increasing since the discovery in the early 70's that compact double radio sources exhibit superluminal behavior. That is, in some cases sources appear to be separating from one another at velocities typically around ten times the speed of light and in one case as high as 45c. This unusual phenomenon has been verified in quasars 3C 273, 3C 279, 3C 345, and 3C 179, and in the Seyfert galaxy 3C 120.

One group of relativistic models called "ballistic models" postulate *free expansion* of a relativistic synchrotron radiating plasma. In particular, they require that the ambient medium into which the plasma expands be extremely tenuous so that deceleration of the

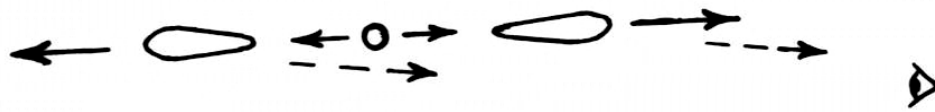


Figure 2.6. Relativistic ejection of confined beams of synchrotron radiating plasma from the nucleus of a galaxy.

relativistic component does not occur. The particles (e.g., electrons) are assumed to be in random motion and to emit synchrotron radiation as a result of their interactions with a "frozen-in" magnetic field. In the plasma reference frame this radiation would be emitted isotropically; however, in the observer's reference frame this radiation would appear to be beamed outward in the direction of bulk relativistic motion. For a plasma moving with a Lorentz factor $\gamma = (1 - (v/c)^2)^{-1/2}$, the radiation from a given emission region would be beamed into a conical region of aperture half-angle $\theta \sim \gamma^{-1}$ radians.

Rees (1966) was the first to propose such a model to account for the rapid flux density variations observed in compact radio sources. His model assumed *spherically symmetric* adiabatic expansion of the synchrotron radiating plasma. However, it was later shown (Terrell, 1977; Jones and Tobin, 1977) that a ballistic model of this sort would lead to the production of "superlight" flux variations only if the plasma was confined to a relativistically expanding shell.

Kellermann and Pauliny-Toth (1981) have reviewed a number of different models that have been proposed to account for the superluminal motion of compact radio sources and conclude that the *relativistic beaming model* constitutes the simplest interpretation. This model, which is a version of the ballistic model, proposes that the relativistic plasma is ejected linearly, rather than spherically, as a pair of confined beams or jets whose axis happens to be closely aligned with the observer (see Figure 2.6). Kellermann and Pauliny-Toth (p. 396) point out that for such a configuration the emission region moving toward the observer would appear to generate events whose time scale is shortened by a factor of γ^{-1} . Thus the angular size inferred from time-variability measurements should be increased by a factor of γ and the estimated particle energy content should accordingly be reduced by a factor of γ^6 .

Ballistic models reduce energy estimates in yet another way. Due to relativistic beaming effects, the radio emission seen by the observer would appear abnormally bright, and hence would lead to an overestimate of the particle energy content of the radiating plasma. For example, it can be shown that the apparent radio flux density S' (for beamed emission viewed head on) is given as:

$$S' \sim 8\gamma^3 S \quad (2)$$

where S is the flux density that the emission would have in the plasma rest frame (Kellermann and Pauliny-Toth, 1981). Moreover, since estimated total particle energy varies in proportion to the cube of flux density, relation (2) implies that actual bulk particle energy U_e in the plasma rest frame varies as:

$$U_e \sim \gamma^{-12} U_e' \quad (3)$$

where U_e' is the electron energy predicted with an incoherent synchrotron model. When this relativistic beaming effect is accounted for, the estimated bulk particle energy content drops accordingly.

Consider the example of radio source B seen in quasar 3C 273. Based on observations of apparent superluminal separation velocities of $v \sim 10 c$, it may be estimated that the emitting region is moving toward the observer with a velocity $v \sim 0.995 c$ and Lorentz factor $\gamma \sim 10$. The energy requirement for this compact source, earlier estimated to be 10^{75} ergs on the basis of an incoherent synchrotron model, would now have to be reduced by a factor of 10^6 to correct for time contraction (and underestimated θ) and by a factor of 10^{12} for overestimated flux density. Thus, the particle energy estimate for 3C 273-B now becomes reduced to the reasonable figure of 10^{57} ergs, delivered over a one-year period. This translates into a power requirement of $\sim 100 M_{\odot} c^2/\text{year}$. Hence the energy problem mentioned earlier is greatly reduced when relativistic motion of the radiating source toward the observer is assumed.

The relativistic beaming model would also help to resolve the "inverse Compton catastrophe" (Kellermann and Pauliny-Toth, 1981). The chances that inverse Compton scattering would take place between electrons and photons would be considerably reduced since the density of both electrons and photons would be lessened as implied by relations (2) and (3). Thus, both difficulties mentioned earlier in connection with the incoherent synchrotron model (i.e., excesses in energy content and in inverse Compton emission) would become partially resolved with ballistic models.

However, Kellermann and Pauliny-Toth (1981, pp. 399-400) point out a few areas in which ballistic/relativistic beaming models encounter potential difficulty. First there is a relatively small probability ($P \sim 1/2\gamma^2$) that the axis of beaming will be aligned toward the observer in such a way that superluminal effects would be seen. For example, for $\gamma \sim 10$ the probability would be less than 1%. Yet about half of all compact sources show evidence of superluminal motion or of rapid flux density variations implicating the presence of beaming. Some investigators (e.g., Scheuer and Readhead, 1979) have suggested that selection effects might be involved, components beamed toward the observer being the only ones observed. However Kellermann and Pauliny-Toth (pp. 401-402) point out several difficulties with the selection effect argument. Nevertheless, the orientation-probability problem may be alleviated if the cosmic ray component is assumed to propagate radially outward as a spherical shell. I propose such a configuration for the Superwave Model, to be discussed shortly.

A second difficulty with ballistic/relativistic beaming models involves the means by which a pair of invisible sources could be produced. For example, in the case of symmetrical component ejection, as shown in Figure 2.6, the receding confined beam would be expected to have a much lower flux density as compared to the approaching beam. For $\gamma \sim 10$ there should be a difference of $\sim 10^6$. However, such differences are not observed, and often the two components have comparable flux densities. This problem may be resolved by assuming that the receding jet remains invisible while the approaching jet creates a double source appearance. Blandford and Konigl (1979) have suggested such a model. They propose that one emission region could originate in the jet itself while the partner emission could come from radiative shock waves propagating in the jet relative to the jet. Nevertheless, such a model does not overcome the orientation-probability problem mentioned above.

Relativistic Blast Wave Models. One important way in which relativistic blast wave models differ from ballistic models is that the former assume that the interstellar medium in the galaxy is dense enough that it must be taken into account. Thus, the relativistic plasma is not treated as an isolated entity, as it is in the ballistic models, but rather as a component that strongly interacts with its environment. This interaction is usually described in terms of a *signal* interacting with a *screen*. In one formulation the signal is assumed to be in the form of a radially propagating pulse of energy, i.e., a spherical shell of magnetically bound plasma

expanding relativistically, and the screen is assumed to be in the form of a thin gaseous ring surrounding the source of the signal (cf. Marscher, 1978; Blandford, McKee, and Rees, 1977). The signal remains undetected by the observer until it strikes the screen. At this point a shock front is formed causing electrons in the screen to become accelerated and the ambient magnetic field to become compressed. The shocked plasma radiates efficiently by the synchrotron mechanism and the event is viewed by the outside observer as a radio outburst. As the signal strikes the screen, a blast wave develops and propagates in the direction of signal propagation. Since the signal consists of a magnetically bound plasma and since it ionizes, accelerates, and accumulates interstellar gas lying in its path, it is best visualized as an impermeable *fluid* plowing the encountered medium ahead of it; see Blandford and McKee (1976). Consequently, the blast wave remains relativistic only as long as the kinetic energy of the signal exceeds the rest mass energy of the intervening gas that is swept up. This condition may be expressed as:

$$E > (4/3)\pi r^3 \rho c^2, \quad (4)$$

where E is the energy of the signal, ρ is the average mass density of the interstellar medium, and r is the distance that the signal has covered in propagating from its source.

Marscher (1978) has developed a relativistic blast wave model which makes a relatively close fit to the flux density variations observed from blazar AO 0235+164 during its 1975 radio outburst. The model accounts for superlight radio flux variations, predicts the formation of double compact radio sources with superluminal separation velocities, eliminates the problem of excess inverse Compton emission, and reduces the bulk particle energy requirements to levels that are much lower than what would be obtainable with the use of ballistic models, though to use these effects this model requires a preferred viewing direction in which the gaseous ring is observed edge-on. The probability of this orientation is given as: $P \sim 1/\gamma$, which is considerably greater than the probability of viewing a relativistic beam head on. Blast wave models in which the signal is collimated as a jet (e.g., Blandford and Konigl, 1979), however, must reckon with the beam-orientation-probability problem mentioned earlier in connection with relativistic beaming models.

One difficulty which must be taken into account and circumvented in the design of blast wave models is the problem of rapid deceleration of the cosmic ray signal. For example, if the interstellar gas density in the vicinity of the outburst were 0.04 hydrogen atoms per cm^3 (as is found in the solar vicinity) and if the energy content of the signal were $\sim 3 \times 10^{57}$ ergs (as Marscher has assumed in his spherical shell blast wave model), then according to relation (4), a blast wave would be expected to propagate only about two hundred light years before becoming subrelativistic.

However, observational evidence is beginning to accumulate which indicates that these radially propagating cosmic ray outbursts actually do reach considerable distances from the nuclei of radio galaxies. For example, Perley and Johnston (1979) report radio telescope observations of 3 compact radio sources, one of which (quasar 3C 345) exhibits superluminal motion. They find diffuse emission extending (in projection) several seconds of arc away from these compact sources. In 3C 345, this would amount to a projected distance of $\sim 50,000$ light years, or to an actual deprojected distance of $\sim 400,000$ light years, assuming that this emission is beamed toward the observer at the same angle ($\theta \sim 8^\circ$) as the jet which forms the milli arcsecond compact source in 3C 345.

Moreover, Reich et al. (1980) report observations of 4 radio galaxies containing compact radio sources, two of which (quasars 3C 273 and 3C 345) are superluminal sources. They find that these galaxies have large scale radio emitting structures aligned with the compact sources and extending many megaparsecs away from the galactic core. For example, 3C 345 is found to have 3 radio hot spots aligned with the inner compact sources, the outermost emission regions lying on either side of the core at arc minute separations of

$\sim 25'$ and $\sim 29'$. This would correspond to projected distances of about 40 million l.y., or to deprojected distances of about 300 million l.y., assuming relativistic beaming toward the observer with a Lorentz factor of $\gamma \sim 7$ ($\theta \sim 8^\circ$), as inferred from the observed superluminal motion effects.

Finally, there is evidence that a substantial fraction of extended double lobe radio sources contain compact radio sources, these nuclear components usually being aligned in approximately the same direction as the axis joining the extended components. The radio galaxy NGC 315 provides a good example of this; see Figure 2.7 (Kellermann and Pauliny-Toth, 1981). Although superluminal motion, and hence relativistic beaming effects, have not yet been confirmed for this galaxy, such effects have been confirmed in the core of quasar 3C 179 which has a double lobed structure. This recent detection (Porcas, 1981) constitutes the fifth compact radio source found to exhibit apparent superluminal motion and is the first such source which also possesses a large scale double lobed radio structure. The fact that the central compact components appear to align very well with the outer extended components suggests that the outer double lobes, like the inner components, are tilted toward the observer and are powered by cosmic ray electrons propagating relativistically away from the galactic center (Porcas, 1981).

Attempts have been made to modify relativistic blast wave models to make possible long range propagation of the cosmic ray signal. For example, Shapiro (1980) has proposed a blast wave model in which the shock front accelerates, rather than decelerates. To accomplish this, he assumes that the density of the encountered medium decreases rapidly with increasing distance from the explosion center. His model is also able to obtain "coasting" behavior, i.e., constant velocity shock front advance, as a special case. Coasting behavior, though, is preferred to accelerating behavior for models of superluminal source motion, since in all documented cases superluminal sources have been found to separate at constant velocities. Accelerating or decelerating blast waves would instead predict time-varying source separation velocities. However, by postulating minimal levels of gas density,

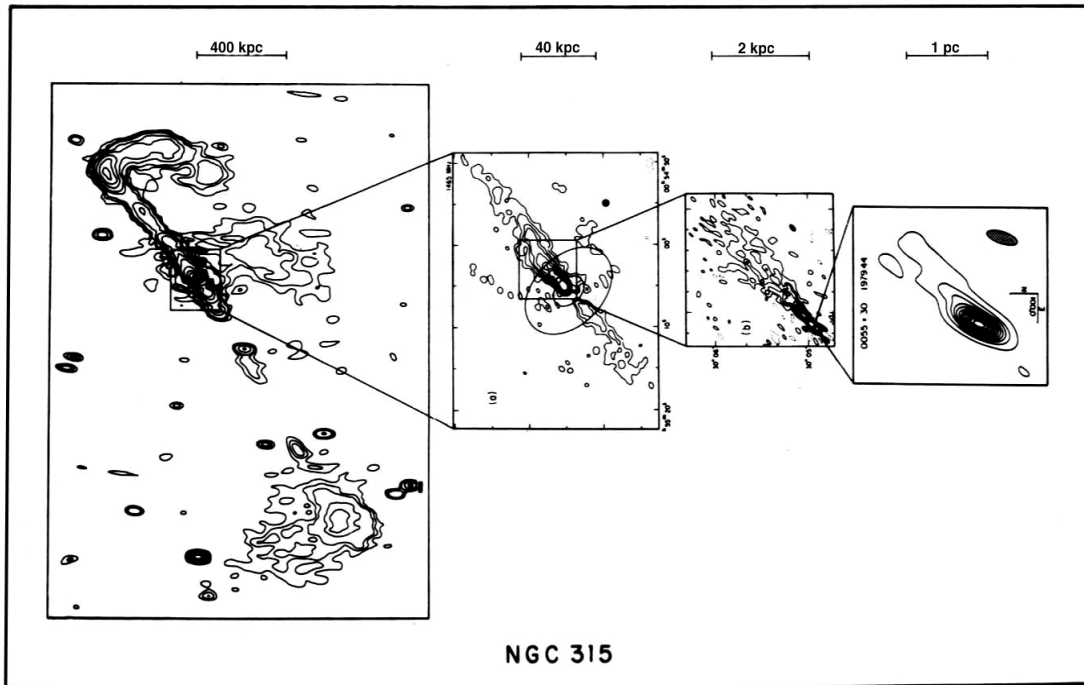


Figure 2.7. Composite map of the radio galaxy NGC 315 (Kellermann and Pauliny-Toth, 1981) reconstructed from data reported by Willis (1978), Bridle et al. (1979), and Linfield (1981).

far below levels found in most spiral galaxies, and by postulating that this gas density varies radially from the galactic center in just such a way that a cosmic ray outburst of a given arbitrary energy may attain a coasting condition, such modified relativistic blast wave models run the risk of being overly contrived.

Another potential area of difficulty which must be taken into account in designing blast wave models is the problem of the narrow optical emission lines emitted by HI regions close to the radio jets. If the emission from these excited gas clouds were being stimulated by the cosmic rays of the jet, then it must be assumed that these clouds lie in the path of the jet, in which case the clouds should be accelerated and their emission lines broadened (Kellermann and Pauliny-Toth, 1981, p. 399). For relativistic blast wave models to be compatible with the observation of narrow emission lines, it must be assumed that the relativistic particles of the propagating signal pass between these excited regions. Thus, if a spherical-shell-type blast wave model is proposed, it must be assumed that cosmic rays in the radially propagating shell are inhomogeneously distributed such that holes are present in the fabric of the signal. Alternatively, the assumption of shell homogeneity could be retained if some mechanism were conceived to allow cosmic rays to deflect around these excited clouds. In confined beam models (ballistic or relativistic blast wave) the emission-line problem would not be as severe since the assumption could be made that the beam is so directed that it misses the excited cloud regions.

The Superwave Model. Hypothesis #3 of the GEH (**p. 2**) proposes three basic features which are incorporated into the generic Superwave Model. These are: a) radial, shell-like propagation of cosmic rays from their point of generation, b) cosmic ray propagation at very close to the speed of light, and c) long range propagation of cosmic rays, i.e., passage through the extent of a galaxy with only minimal attenuation. The first two features are not proposed here for the first time, but rather as has been demonstrated above, are features often incorporated in models attempting to describe the behavior of compact radio sources. The third feature is supported by a number of observations that have been made of radio galaxies (see **p. 30**), and its importance in modeling radio galaxy phenomena cannot be ignored.

As was mentioned earlier, the ballistic and relativistic blast wave models require that magnetic field lines be transported at relativistic velocities along with the particles to form, on the one hand, a freely propagating, synchrotron-radiating plasmoid, or on the other hand, a synchrotron-radiating blast wave (preferably of the coasting variety). But because such magnetically bound plasmas behave as impermeable fluids, they necessarily interact strongly with any gas they encounter. Thus to insure nondecelerating movement and long range propagation with reasonable outburst energy contents, either the density of the ambient medium must be assumed to be negligibly small (as in ballistic models) or the density must be assumed to decrease radially in a certain defined manner (as in relativistic blast wave models). As an alternative to making these restricting assumptions about gas density, it might be assumed that the cosmic ray signal interacts *weakly* with the ambient gas medium, as the GEH suggests. Such a circumstance could be allowed if one were willing to abandon the assumption that the propagating cosmic rays are bound up with a relativistically propagating magnetic field.

Instead, a galactic magnetic field is postulated which *remains at rest* in the galaxy's frame of reference and which is disposed *radially* with respect to the galaxy's center. A cosmic ray outburst, itself free of an entangling magnetic field, would then be able to expand radially from the galactic center, parallel to the magnetic field lines without accelerating the galactic magnetic field relative to the interstellar medium. To some extent the magnetic field lines would tend to guide the individual particle trajectories, but at the same time the collective action of the particles would serve to keep the galactic magnetic field itself

disposed in a radial direction. A radial magnetic field configuration would be expected since the particle energy density would be much greater than the magnetic field energy density and hence would tend to control the field dynamics; e.g., see Section 3.2. The cosmic rays would most probably travel along helical pathways, spiraling around the magnetic field lines as they streamed outward at relativistic velocities. In so doing they would generate synchrotron radiation which they would relativistically beam radially outward from the galactic center. Since the cosmic ray outburst would be free of a relativistically propagating and entangling magnetic field, it would be more appropriate to speak of this as a *relativistic volley*, *barrage*, or *stream* of particles, rather than as a relativistic fluid (the term used in ballistic and in relativistic blast wave models).

In addition to synchrotron radiation, bremsstrahlung radiation might be produced as a result of cosmic ray collisions with interstellar electrons and gas molecules, or with nebular gas surrounding stars. Such radiation would tend to be a major contributor at X-ray and γ -ray frequencies.

Holman et al. (1979) have pointed out that in hot magnetized plasmas in which the ratio ζ of the plasma's thermal ion energy density (nkT) to its magnetic field energy density ($B^2/8\pi$) exceeds unity, relativistic electrons would be able to stream freely along the plasma's magnetic field lines at velocities approaching the speed of light. They point out that hydromagnetic waves in the plasma which might otherwise become amplified as a result of the streaming motion of the particles would become damped by the plasma's own thermal fluctuations. Hence, resonant scattering and mirroring of the streaming particles by Alfvén or magnetosonic waves would not occur. They note that this would be especially true for cases in which the streaming particles have an energy density exceeding that of the plasma's magnetic field. Cosmic ray outbursts from galactic nuclei not only would have the required high particle energy density, but the magnetized plasmas through which these cosmic rays travel are usually quite hot. For the solar vicinity $\zeta \sim 250$, given $T \sim 10^6$ K and $B \sim 3 \times 10^{-6}$ gauss. Verification that particles can stream parallel to field lines at velocities far in excess of the Alfvén velocity was demonstrated "experimentally" on July 9, 1962, by the Starfish nuclear detonation. As described by D'Arcy and Colgate (1965), beta particles from this northern hemisphere explosion began arriving in the Southern Hemisphere within seconds of detonation, implying a transit velocity of $\sim 0.01c$, a value consistent with the mean energy of the explosion. Thus, in view of the above, the proposal that superwaves are capable of long range relatively unattenuated propagation at close to the speed of light is reasonable.

Observations of active galactic nuclei indicate that outbursts may occur as frequently as once every few years. Consequently, such repetitive activity would be modeled as a sequence of radially propagating shells, formed either as a result of time variation in the rate of generation of cosmic rays by the central core, or as a result of instabilities which might develop in an initially uniform flow of cosmic rays. A given shell layer might have a thickness of the order of 20 – 30 l.y. Based on subhypothesis 2 of the GEH (p. 2), we may conclude that this sequence of shells would together have a thickness of several hundred to a few thousand light years. This clustering of shells would itself constitute a radially propagating shell-like region, or what is referred to here as a *superwave*, or *galactic superwave*; see Figure 2.8. Furthermore, according to the GEH, superwaves would be emitted from the center of a galaxy every 5000 – 10,000 years. This model does not necessarily conflict with the conventional view that regards the active phase of a galaxy as lasting 10^6 years, since a bunching of outburst activity at intervals of 10^4 years over the conventionally proposed 10^6 year period could be imagined. However, as is demonstrated later in this chapter, it is not necessary to assume such extended cycling times for galactic explosion activity.

The spherical shell-like outburst geometry adopted for the Superwave Model has an

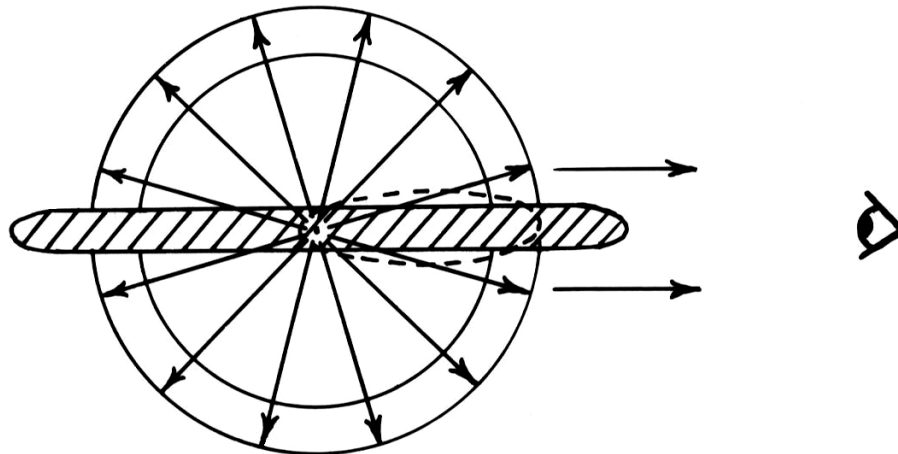


Figure 2.8. Isotropic radial propagation of cosmic rays as proposed in the superwave model. Cross-hatched region represents the galactic disk. This spherical shell would appear to an outside observer to be distorted into a prolate spheroid shape (dotted line) elongated toward the observer and having one of its foci coincident with the galactic center. The ratio of the semi-major to semi-minor axes of the spheroid would be equivalent to the Lorentz factor of expansion.

advantage over a linear beaming geometry in that the radially beamed radiation would have a greater chance of becoming aligned with the observer. Thus, the commonness of observing compact sources in active galaxies may be accounted for. Moreover, as is demonstrated in the next subsection, with a spherical shell cosmic ray propagation geometry, a model may be devised which is able to account for the diverse optical appearances which active galaxies produce. Finally, there is considerable observational evidence which indicates that explosive behavior in galactic nuclei occurs in an isotropic fashion; see Subsection 2.2.2.

The Superwave Model would be able to account for several features characteristic of galactic explosions: a) the ability for long range propagation of cosmic rays; b) the unusual brightness and small angular diameter of the compact radio sources and central star-like continuum emission region; c) the rapid time-variability of the continuum emission; d) the frequency dependence of time-variations in the continuum emission; e) the lack of excessive inverse Compton emission; and f) the formation of double compact radio sources and their superluminal motion. In addition, the Superwave Model is able to account for the strong emission-line radiation and infrared continuum observed in active galaxies in terms of a novel cosmic-laser-like, photon shock wave mechanism. This feature (labeled as (g)) and the other features a) – f) are discussed below in the order given.

Feature a): Long distance propagation would follow as a consequence of the fact that the cosmic ray volley interacts minimally with the ambient galactic medium, as has already been pointed out.

Feature b): The unusual brightness and small angular diameter of the continuum emission would be attributed to relativistic beaming effects. Following arguments similar to those employed in ballistic and relativistic blast wave models, it may be concluded that the continuum emission would be beamed into a narrow conical region of half-angle $\theta \sim \gamma^{-1}$ and that the observed intensity of this emission would be boosted by a factor of γ^3 . For 1 Gev electrons ($\gamma = 2000$) the emitted radiation would be beamed into a cone of half angle $\theta \sim 1.7$ minutes of arc and would be boosted in intensity by a factor of 10^{10} . Even if this radiation

were generated in a 100,000 l.y. diameter shell around the galactic nucleus, due to beaming it would appear to an outside observer to come from a region only 50 l.y. in diameter. By comparison, in the Seyfert galaxy NGC 1068 it has been determined that the bulk of the 2 micron infrared continuum emission comes from a region less than 60 l.y. in diameter (McCarthy et al., 1982).

One important consequence of the Superwave Model is that the observed radiation intensity produced by the radially propagating cosmic ray volley will depend on the amount of interstellar medium which the volley encounters along the observer's line of sight. Thus if an exploding galaxy has a spiral morphology, the beamed radiation will appear most intense when the galaxy happens to be viewed with its disk oriented edge-on to the observer. That is, cosmic rays passing through the entire extent of a galactic disk would have a greater probability of encountering gas clouds and shocked regions in the interstellar medium having transversely disposed magnetic fields which could cause the cosmic ray electrons to radiate their energy at a much greater rate. This geometric viewing-angle effect may help to account for the varied optical appearances of active galaxies; see the next subsection.

Feature c): Related to the relativistic Doppler (beaming) effect discussed in b), there is the effect of rapid time-variability of the continuum radiation. Relativistically expanding shells are able to produce such super-light flux variation effects (Jones and Tobin, 1977). As an illustration of how this could be produced, take for example a blast of relativistic electrons with $\gamma = 200$ ($E = 100$ Mev) propagating forward in a shell having a thickness of 10 AU and passing through a 100-l.y. diameter cloud lying in the line of sight. The radiation produced would be seen as a pulse lasting about three months, i.e., $\Delta t = 100 \text{ l.y.} \times (1-\beta)\gamma/c$, where $\beta = v/c = (1 - 1/\gamma^2)^{-1/2}$. With higher Lorentz factors, even greater time compression would be observed. For example, a signal of electrons with $\gamma = 2 \times 10^5$ ($E = 100$ Gev) would produce a radiation pulse lasting about 2 hours.

If it is assumed that the higher Lorentz factor particles tend to generate higher frequency radiation, then such a model might explain why outbursts observed at shorter wavelengths are variable on a much shorter time scale. For example, during the 1975 outburst blazar AO 0235+164 doubled its 2 cm radio flux density over a period of about 1 month, whereas at optical wavelengths this object has been known to vary its flux by 50% over a period of 1 day (Schendel, 1980). Variations at X-ray wavelengths are even more rapid. For example, the nucleus of Seyfert galaxy NGC 4151 has been observed to increase its X-ray intensity by a factor of 10 in 730 seconds (Tananbaum, 1978), and blazar H2155-304 has exhibited significant variations in X-ray flux in less than 2 seconds (Griffiths, 1979).

Feature d): The cosmic ray volley composing a superwave would be expected to exhibit time-of-flight dispersion effects as well. For example, after traveling a distance of $\Delta x = 1000$ l.y., 5 Mev electrons, ($\gamma = 10$) would lag behind the radiation event horizon by $\Delta t = (\Delta x/c) \times (1 - \beta) = 5$ years, whereas 1 Gev electrons would lag by only 1 hour. Thus, if the shorter wavelength radiation is assumed to be generated by the faster particles, and if time-of-flight separation has taken place, it would be expected that the shorter wavelength radiation would reach maximum intensity earlier than longer wavelength radiation. Such behavior is sometimes observed; recall Figures 2.4(a) and 2.4(b). This could also account for why galactic outbursts observed in the visible part of the spectrum do not necessarily coincide in time with the radio outbursts.

Feature e) As in the case of ballistic and relativistic blast wave models, the Superwave Model would predict low levels of inverse Compton X-ray emission. This would be due to two factors. First, the electromagnetic radiation produced by the propagating superwave would be generated within a much larger volume than is implied by the apparent size of the emission region. Thus the radiation density and, hence, the chance of photon/particle collisions would be greatly reduced. Second, the electromagnetic continuum radiation that

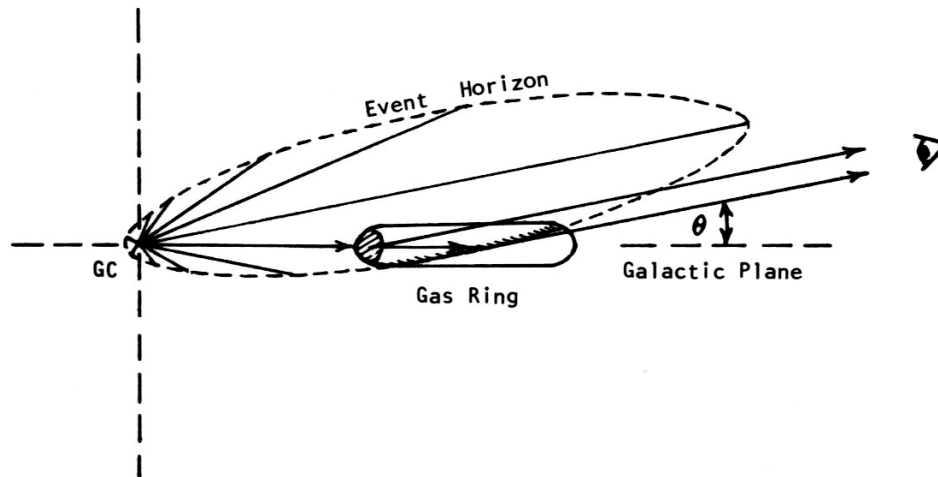


Figure 2.9. The formation of double compact radio sources with superluminal separation velocities. The diagram shows a cross-sectional view of the nuclear region of a spiral galaxy, the vertical and horizontal axes indicating the directions of the polar axis and galactic equator. "G.C." denotes the galactic center. The elongated shape denotes a concentric ring of gas viewed in cross section, whose inner side is shocked by the cosmic ray barrage and is a strong radio emitter. The barrage and is a strong radio emitter. The ellipse (of eccentricity $\epsilon \sim v/c$) denotes the event horizon for an outburst containing relativistic electrons with Lorentz factor $\gamma \sim \theta^{-1}$, where θ is the observer's viewing angle. The illusion of a superluminally separating emission region is created as the event horizon propagates outward through the ring.

is generated by these particles would be beamed in the same direction that the particles would be traveling; thus the chance that particle and photon paths would cross is greatly reduced. In fact, such a configuration would tend to encourage Compton scattering of forefront electrons by runner-up photons. Thus, photons would tend to lose, not gain energy.

Feature f): Finally, superwave models could be designed to account for the formation of double compact radio sources and their apparent superluminal motion. For example, suppose that the active galaxy being observed is a spiral galaxy and is oriented such that its disk is viewed nearly edge-on, as shown in Figure 2.9. Also, suppose that a stream of cosmic ray electrons radiates radially outward from the galactic center in an isotropic fashion and strikes a ring of gas which lies in the galactic plane concentric with the galactic center. Suppose this ring is positioned at a galactocentric radius of 100 l.y., has a breadth of 100 l.y., and a thickness of 20 l.y. A ring not very different from this is known to be present at the center of our own galaxy (Oort, 1977, p. 345; Sanders and Wrixon, 1974; also see Subsections 2.2.2 and 4.1.2). It is reasonable to suppose that the gas in the ring would be compressed to a higher density on the ring's inner side since this side would be shocked by the cosmic ray barrage. Thus the synchrotron emission from this inner region would be strongest. To an observer viewing this galaxy at an angle θ to its equatorial plane, this emission would appear as a single compact source. The emission that the observer would be seeing would come from particles having a Lorentz factor $\gamma \sim 1/\theta$, since the beamed emission cone created by particles of this particular Lorentz factor would most directly intersect the observer's line of sight.

Now suppose that a transitory increase occurs in the rate of generation of cosmic rays producing a pulse which propagates radially as a spherical shell having a thickness of 10 l.y.

As this pulse encounters the dense inner shocked region there would be an increase in the intensity of the observed compact source. But as the shell wave continued to propagate forward into the ring, the region of enhanced emission would propagate with it producing a second beamed compact source separating from the first. Due to beaming effects, this separation would appear to the observer to occur at a superluminal velocity of $v \sim \gamma c$. This same relation has been applied in a ballistic model description of the superluminal separation phenomenon; see Kellermann and Pauliny-Toth (1981, p. 398). Moreover the separation velocity would be expected to remain constant since the cosmic rays in the shell-like pulse would be able to pass through the gas cloud with a minimal amount of bulk deceleration.

Feature g): Broad emission lines observed in active galaxies have been interpreted as evidence that gas is being radially ejected from their nuclei at a high velocity (Burbidge, 1970). For example, the broadening of emission lines in Seyfert nuclei appear to indicate radial ejection velocities in the range of 500 to 5000 km/s. In the quasar PHL 5200, outflow velocities as high as 30,000 km/s (0.1 c) may be indicated (M. Burbidge, 1978). Superwaves could provide the mechanism for ionizing and propelling interstellar gas residing in the cores of these galaxies. However, the superwave model offers an additional way in which strong emission line spectra may be produced by processes occurring also in the disks of active galaxies. This photon "shock wave" effect may be described as follows.

In the vicinity of stars the relativistic electron volley of a superwave would be expected to become turbulent and become transformed into a blast wave. As a result, the superwave would couple strongly to the interstellar medium such that ionized gas and electrostatically charged interstellar dust grains would become propelled forward. Nebular material normally kept away from a star by the action of its stellar wind could now be propelled close enough so as to become accreted by the star. This could in turn activate the star's chromosphere initiating flare activity and T Tauri-like behavior; see Subsection 3.3.1. In addition, novae and supernovae could become triggered; see Subsection 5.2. These stellar chromospheres and supernova envelopes would adopt a strong emission-line spectrum exhibiting Doppler broadening. Emission lines having widths of ± 200 to 300 km/s are commonly seen in T Tauri stars, and widths of up to $\pm 10,000$ km/s are seen in supernova remnants. The region in which this enhanced emission-line activity would take place would coincide with the superwave shell and would propagate radially through the Galaxy, along with the superwave, at the speed of light. Consequently, emission-line photons traveling in the direction of superwave propagation would become recruited into a photon shock wave traveling in phase with the superwave.

At a certain level this process is analogous to the laser phenomenon except that instead of individual atoms, whole stars would become activated. Whereas in a laser only a single photon wavelength would become amplified, in this process an entire stellar continuum range would become enhanced. This photon shock wave effect would be strongest when a spiral galaxy was viewed edge on since an equatorial propagation path would offer the greatest opportunity for photon recruitment. As is discussed in Subsection 2.1.3, quasars may actually be spiral galaxies viewed edge-on during their active phase, in which case their high luminosity could be attributed to this photon shock wave effect. Perhaps this might be referred to as the *quaser effect*, where "quaser" is spelled instead with an "e" to signify the contraction of the words "quasar" and "laser".

The 100-micron infrared continuum peak, which is a common feature in the spectra of many active galaxies, may in a similar way be explained by a quaser effect. This infrared emission would come from nebulae in the galactic disk whose illuminating stars had become activated by the passage of a superwave. As noted earlier (p. 22), the continuum distributions of certain nebulae located on the 14,200 years BP and 6000 years BP superwave event

horizons in the Galaxy bear a strong resemblance to continua observed in active galaxies.

Many of the effects described above in a) through g) are possible only within the context of the Superwave Model. In particular, the viewing angle effect described in b) and g) is a distinguishing feature of this model. In summary, a shell-like volley of cosmic rays propagating radially outward from the galactic center parallel to magnetic field lines in the interstellar medium and beaming synchrotron radiation radially outward appears to be a promising mechanism for explaining many of the unusual phenomena observed in active galactic nuclei.

2.1.3 The Appearance of an Exploding Galaxy

Several factors together would determine how a galactic explosion would appear optically to an observer located outside the galaxy. One factor might be the *resolving power* of the observer's telescope. A second factor might be the *intensity* of the continuum emitted from the central portion of the galaxy. Both factors in combination cause imaging difficulties. For example, if the galaxy were located at a great distance such that its telescope image were unresolved or marginally resolved, the intense light from the galaxy's nucleus would make matters worse by tending to mask the subtle underlying differences of the galactic disk, if a disk were present. The optical luminosity of quasars can reach over 100 times the luminosity of an entire spiral galaxy (Morrison, 1973, p. 25), so it is understandable that such a masking effect could occur.

Although quasars are stellar in appearance, many investigators have come to the conclusion that they are actually the active nuclei of distant galaxies (Wyckoff and Wehinger, 1981; Wyckoff et al., 1980; Baldwin et al., 1980; Morrison, 1973; Kristian, 1973; Silk et al., 1973). For example, Tyson, Baum, and Kreidl (1982) have determined that quasar 3C 273 is surrounded by an elliptical nebulosity whose continuum resembles that of a giant elliptical galaxy. As will be demonstrated shortly, many giant ellipticals may actually be active spiral galaxies viewed from their edge.

Blazars, like quasars, are extremely bright and stellar in appearance. But in addition, their images are frequently surrounded by small, very faint nebulosities. These nebulosities have been interpreted as the images of underlying elliptical galaxies (Schendel, 1980; Miller et al., 1978). It may be that the image of the galactic disk is marginally detectable in blazars because objects of this classification are closer and, hence, more easily resolved. Indeed, optical images for blazars have diameters in the range of $\sim 20'' - 40''$, whereas the diameters of quasar images are typically in the range of $\sim 3'' - 4''$ (Wolfe, 1980).

At lower levels of continuum intensity and at better optical resolution we find the N-galaxies and similar designations such as Markarian objects and Zwicky compact galaxies. N-galaxies have been defined by Matthews, Morgan and Schmidt (1964) as "galaxies having brilliant star-like nuclei containing most of the luminosity of the system," with "a faint nebulous envelope of small visible extent."

Finally, the least luminous of the active galaxies are the Seyfert galaxies. Although the nucleus of a Seyfert is very bright, it is subdued enough that the spiral arms of the galaxy are distinctly visible. Thus, in proceeding from quasars and blazars to Seyferts, i.e., from objects with greater to objects with lesser central continuum emission, there is a tendency for the spiral arms of the underlying galaxy to become increasingly discernible.

The continuity of observed physical properties running through these various categories of objects has led many to conclude that there is an evolutionary sequence connecting them, i.e.,

quasar
blazar \rightarrow N-galaxy \rightarrow Seyfert galaxy

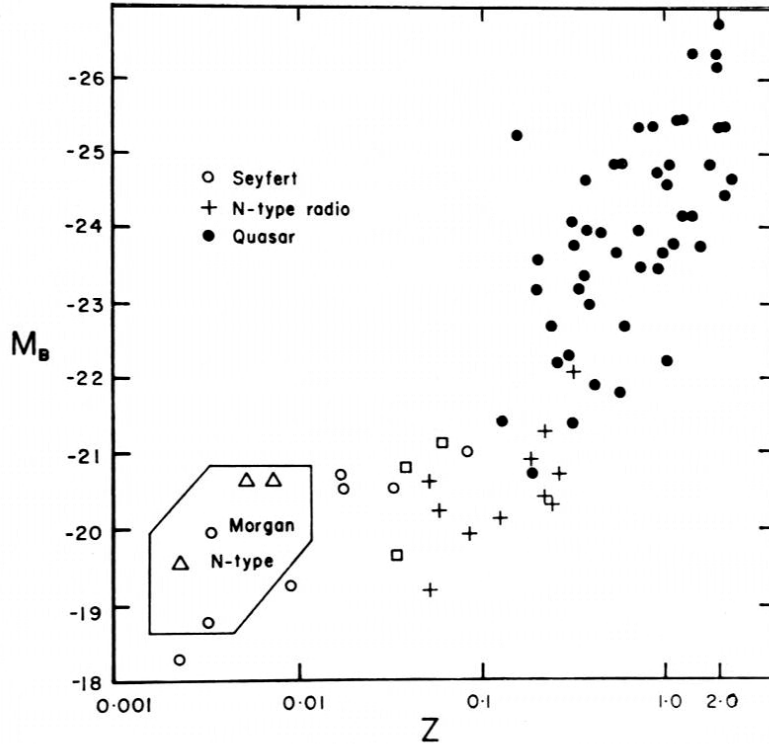


Figure 2.10. Absolute magnitude versus redshift of quasars (dots), N-type radio galaxies (crosses), blue compact galaxies (squares), Seyfert galaxies (open circles), and Morgan N-type galaxies (triangles) (Barnothy & Barnothy, 1968).

(Pacholczyk and Weymann, 1968, p. 841); Arp, 1968; Barnothy and Barnothy, 1968; Weymann, 1969, p. 238). For example, as seen in Figure 2.10 (Barnothy and Barnothy, 1968), the luminosity-redshift diagram for various types of active galaxies shows a continuous range of luminosities extending from quasars down to Seyferts. Also, in studying a sample of galaxies with a UV continuum and broad emission lines, Markarian (1977) has found that there is a general continuity from quasi-stellar types, through intermediate spheroidal types, to Seyfert-like galaxies. This continuity is evident when these galaxies are plotted on a color-color diagram such as that shown in Figure 2.11. Those which he designates as Type I galaxies (quasi-stellar and intermediate types) comprise about two-thirds of the sample and fall along the slanted line. Those which he designates as Type II galaxies (Seyfert-like having a low luminosity diffuse continuum) comprise about one-third of the sample and occupy the lower right hand corner of the diagram.

The Superwave Model projects that the continuum radiated outward from the plane of a spiral galaxy should be more intense than the continuum radiated at angles that are considerably inclined to the galactic plane; see items (b) and (g) (pp. 33 and 36). Thus in addition to outburst intensity, viewing angle should be an important factor determining the emission intensity observed from an active spiral galaxy. Radio-loud quasars (including their flat spectrum subclass the optically violent variable (OVV) quasars), blazars, and giant ellipticals may all be active spiral galaxies viewed edge-on, or at a slightly inclined angle; see Figure 2.12. Less luminous objects such as N-galaxies and Seyferts could be active spiral galaxies viewed at a steeper angle.

Ku, Helfand, and Lucy (1980) have classified optically selected quasars into two types. Type I quasars, those having estimated radio luminosities $L < 10^{41}$ ergs/s, they associate

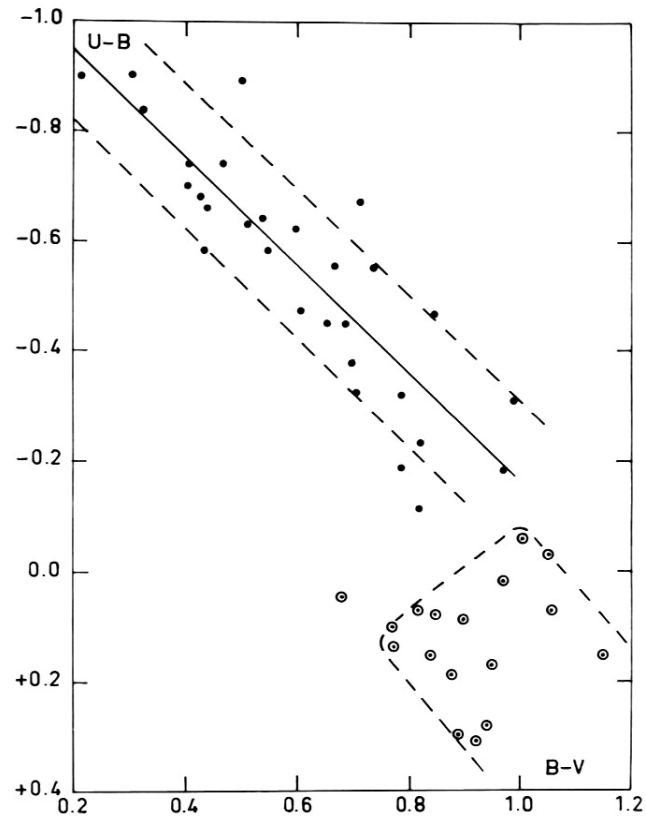


Figure 2.11. U-B vs. B-V color-color diagram for galaxies with UV continuum and broad emission lines. (Markarian, 1977)

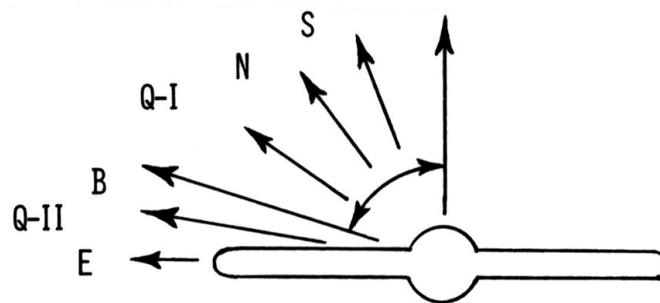


Figure 2.12. How viewing angle might affect the appearance of an active galaxy. Abbreviations include: S (Seyfert galaxy), N (N-galaxy), E (giant elliptical galaxy), Q-I (Type I quasar), Q-II (Type II quasar), and B (blazar).

with Seyfert galaxies; and Type II quasars, those having radio luminosities $L > 10^{41}$ ergs/s, are associated with blazars, N-galaxies, and giant ellipticals. I would suggest the Type I quasars are unresolved spiral galaxies viewed at a steep inclination angle, while Type II quasars are unresolved spiral galaxies viewed almost edge-on. Thus, according to this scheme, one would expect many more galaxies to fall in the Type I category. This is indeed observed to be the case. Ku et al. report that 90% of their optically selected quasar sample falls in the Type I category whereas only 10% falls in the Type II category. It may be

inferred, then, that Type II quasars are active spirals viewed within 6° of their galactic plane, assuming that there is an equal probability for viewing a galaxy at any arbitrary angle.

The viewing-angle scheme proposed for the Superwave Model is substantially different from the scheme proposed by Blandford and Rees (1978, p. 328). Their model involves an elliptically-shaped galaxy with an equatorial dust ring, cosmic rays being emitted from the poles of the galaxy as a pair of confined beams. According to their model, when this object is viewed from its poles in line with the beamed radiation, it appears as a blazar, with a strong continuum emission that overpowers the emission-line spectrum. When viewed along the equator, it appears as a radio quiet quasar with a strong emission-line spectrum supplementing the continuum emission. Hybrid objects such as radio loud quasars and OVV quasars would involve intermediate viewing angles.

The Blandford-Rees model involves a decrease in beaming effects with decreasing equatorial viewing angle. The scheme proposed for the Superwave Model instead involves *isotropic* cosmic ray beaming with increased continuum beaming at decreased equatorial viewing angles. Variations of continuum intensity with viewing angle in the Superwave Model depend on line-of-sight, *gas-column-density* variations and are explainable in terms of photon-recruiting effects (see [p. 36](#)), whereas variations of continuum intensity with viewing angle in the Blandford-Rees model are secured by postulating an anisotropic cosmic ray propagation geometry. By including a place for Seyferts, N-galaxies, and other intermediate spiral forms, the Superwave Model allows the incorporation of a wider variety of galactic classifications into a unified scheme.

In addition to optical resolution, cosmic ray outburst intensity, and viewing angle, a fourth factor influencing the appearance of an active galaxy would be the physical state of evolution of the galaxy, i.e., the extent to which its disk had become developed. Here I am assuming that galactic evolution proceeds from a dwarf elliptical stage to a spiral stage through a series of central explosions. According to the model proposed here, spirals having more extensive disks containing a greater quantity of gas in their equatorial plane would be expected to exhibit more intense equatorially beamed radiation. Hence the geometric, viewing-angle effect would be more pronounced for such galaxies.

An attempt to account for the varying appearances of an active spiral galaxy in terms of optical resolution, superwave intensity, and viewing angle is presented in Figure 2.13. The empty sector in the upper left hand corner of the cube is to be expected, since distant low-activity galaxies would be difficult to observe. If a spiral galaxy were to become active, its appearance would change by moving to classifications positioned toward the back of the cube. Depending on the observer's viewing angle and on the superwave intensity, the galaxy would take on the appearance of either a Seyfert or giant elliptical (SO or E). If poorly resolved, the galaxy would take on the appearance of a blazar or Type I or Type II quasar. At intermediate resolutions, a Seyfert galaxy might appear as an N-galaxy or related object (e.g., Markarian object, Zwicky compact galaxy). The Space Telescope scheduled for operation in 1985 is expected to have a resolving power about 50 times greater than earth-based telescopes. So if this scheme is correct, future observations should drop many active galaxy classifications from the blazar and quasar categories into the N-galaxy, Seyfert, and elliptical categories. Also, many galaxies classified as giant ellipticals should be expected to drop into the SO category.

The scheme shown in Figure 2.13 hypothesizes that once the active phase of a galaxy's nucleus has terminated, the galaxy acquires the appearance of a "normal" spiral. There is a substantial amount of evidence supporting the suggestion that there is a continuity of properties connecting active galaxies with normal galaxies. For example, Van der Kruit (1971a) has found that there is a continuous sequence of 21 cm radio luminosities running from quasars through radio galaxies through Seyferts and finally down to normal galaxies; see Figure 2.14. Also, Westurlund and Wall (1968) have found that quasars, N-galaxies,

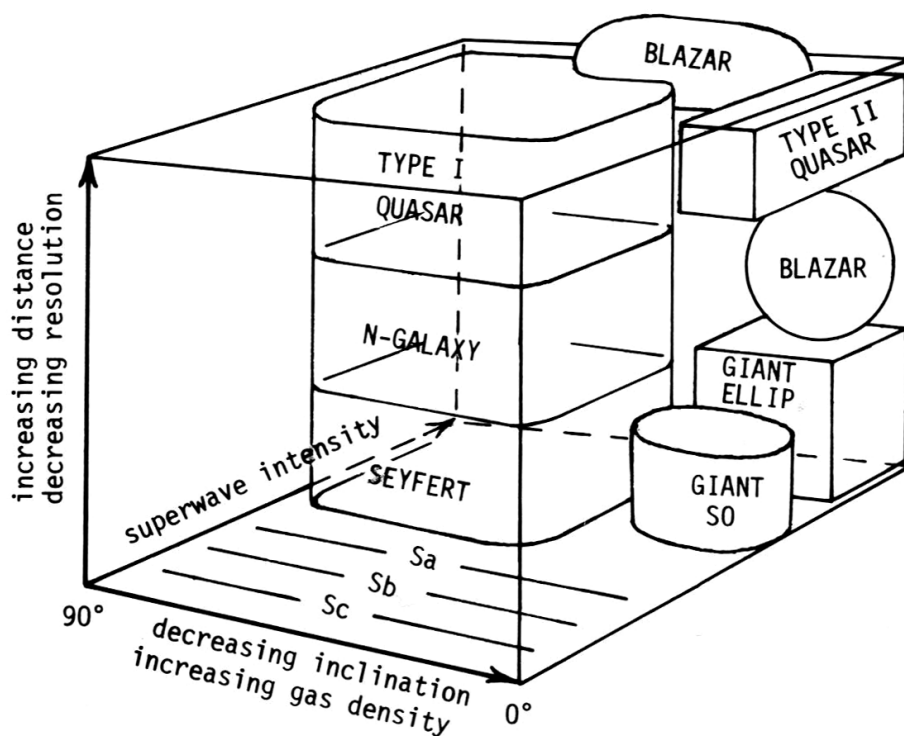


Figure 2.13. Phase diagram for the optical appearance of a spiral galaxy.

radio galaxies, and normal galaxies constitute a continuous sequence on a U-B/B-V color-color diagram. Wade (1968) has studied the 11 cm radio emission from various types of spiral galaxies and concludes that there is no clear separation between "normal" spirals and Seyferts. As seen in Figure 2.15, he found that Seyferts have the strongest nuclear radio components at a given optical luminosity. Hence they appear to define an upper boundary, rather than a distinct group.

A few Hubble-type designations (e.g., Sa, Sb, Sc) have been listed in Figure 2.13 as descriptors for the inactive or less active galaxies, the nuclear region of a galaxy being most prominent in the Sa-type and least prominent in the Sc-type. Note however that these same designations are often applied to Seyfert galaxies. A few normal edge-on spirals of type Sa, Sb, and Sc are displayed in Figure 2.16 for comparison to the giant elliptical (SO) galaxy NGC 5128. Some of the differences in appearance may be due to differences in galactic morphology (e.g., degree of spiral arm development). However, the presence of propagating superwaves, their intensity, and the quantity of coronal gas available for excitation might also be important factors. Emission-line radiation, being unbeamed, would still be detectable from the disk after the superwave event horizon had passed the observer.

There is a considerable amount of evidence which connects a galaxy's Hubble classification with the intensity of its nuclear activity. For example, Wade (1968) has found that galaxies, whose morphology places them earlier in the Hubble spiral sequence (Sa and Sb), have radio emission that is more concentrated to the nucleus; see Figure 2.17. Also, taking for example just the Seyfert galaxies plotted in Figure 2.15, it may be noted that in going from greater to lesser overall radio intensity there is a progressive change in galactic optical morphology from early to late Hubble type, e.g., NGC 7469 (Sa), NGC 1068 (Sb), NGC 4151 (Sb), NGC 3227 (Sb), NGC 4051 (Sbc).

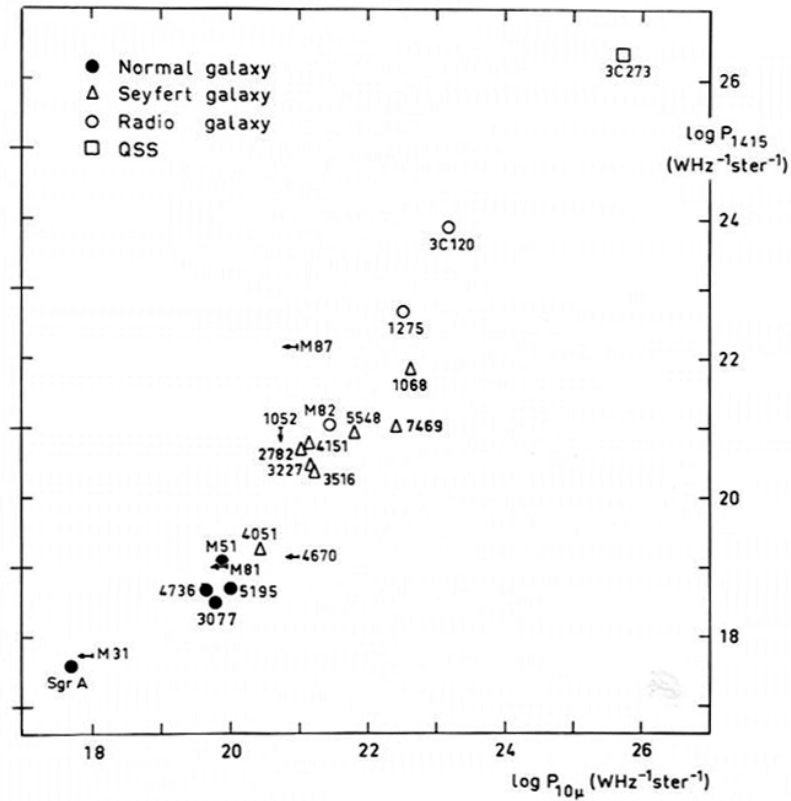


Figure 2.14. Comparison of the powers of galactic nuclei at 1415 MHz and at 10μ (after Van der Kruit, 1971a).

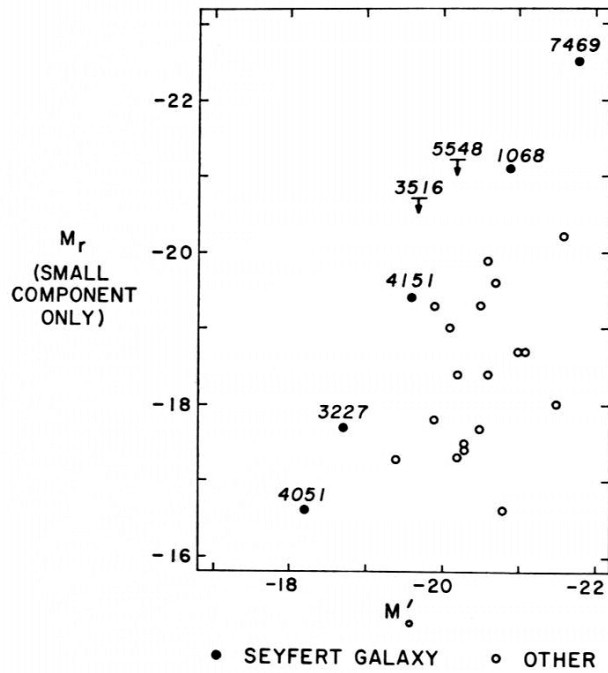


Figure 2.15. Absolute radio magnitude of the small radio components of a galaxy versus total photographic absolute magnitude (Wade, 1968).

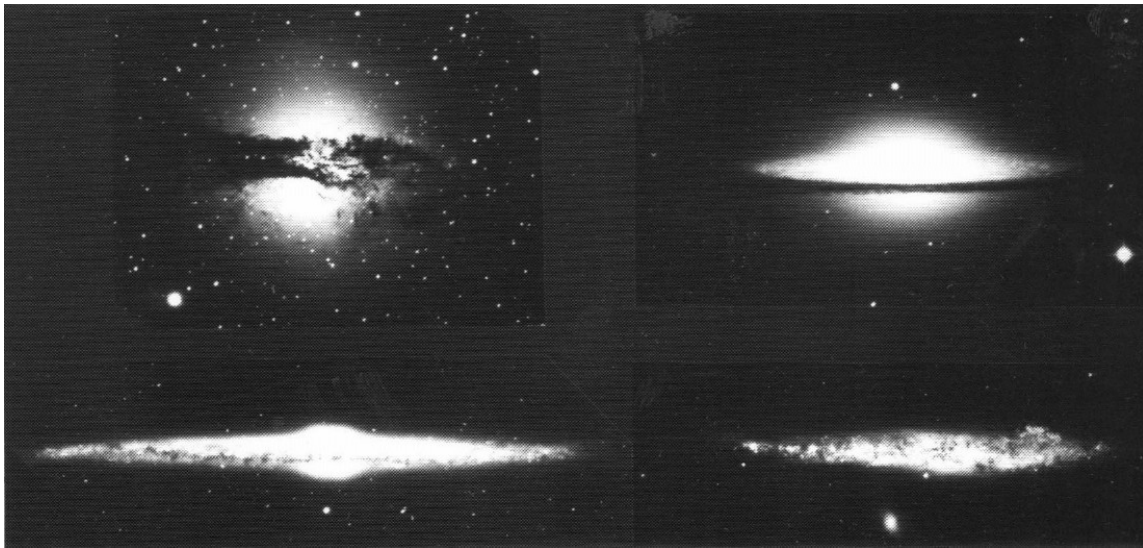


Figure 2.16. a) Upper left: NGC 5128 (SO elliptical); b) Upper right: NGC 4594 (Sa spiral); c) Lower left: NGC 4565 (Sb spiral); Lower right: NGC 4631 (Sc spiral) (Photos courtesy of Mt. Palomar Observatory).

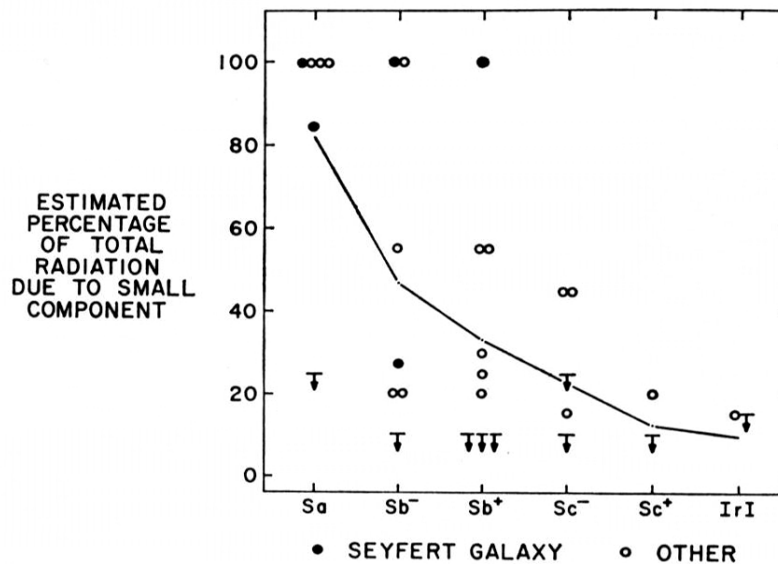


Figure 2.17. Proportion of the total emission which is due to the small radio component for galaxies of different structural types. Arrows denote upper limits (Wade, 1968).

Lequeux (1971a) also has found a connection between a galaxy's optical properties and its radio properties. Surveying 54 spiral and irregular galaxies, he notes there is a decreasing tendency for galaxies to show a radio nucleus in going from type-Sa to type-Sc spirals. In addition, the tendency for galaxies to show a radio disk appears to increase from type-Sa to type-Sc spiral. He observes that optically bright Sc galaxies have radio disks 2 or 3 times stronger than bright Sb galaxies. Also, he finds that bright Sb spirals seem more likely to have an associated strong nuclear source as compared with optically weaker

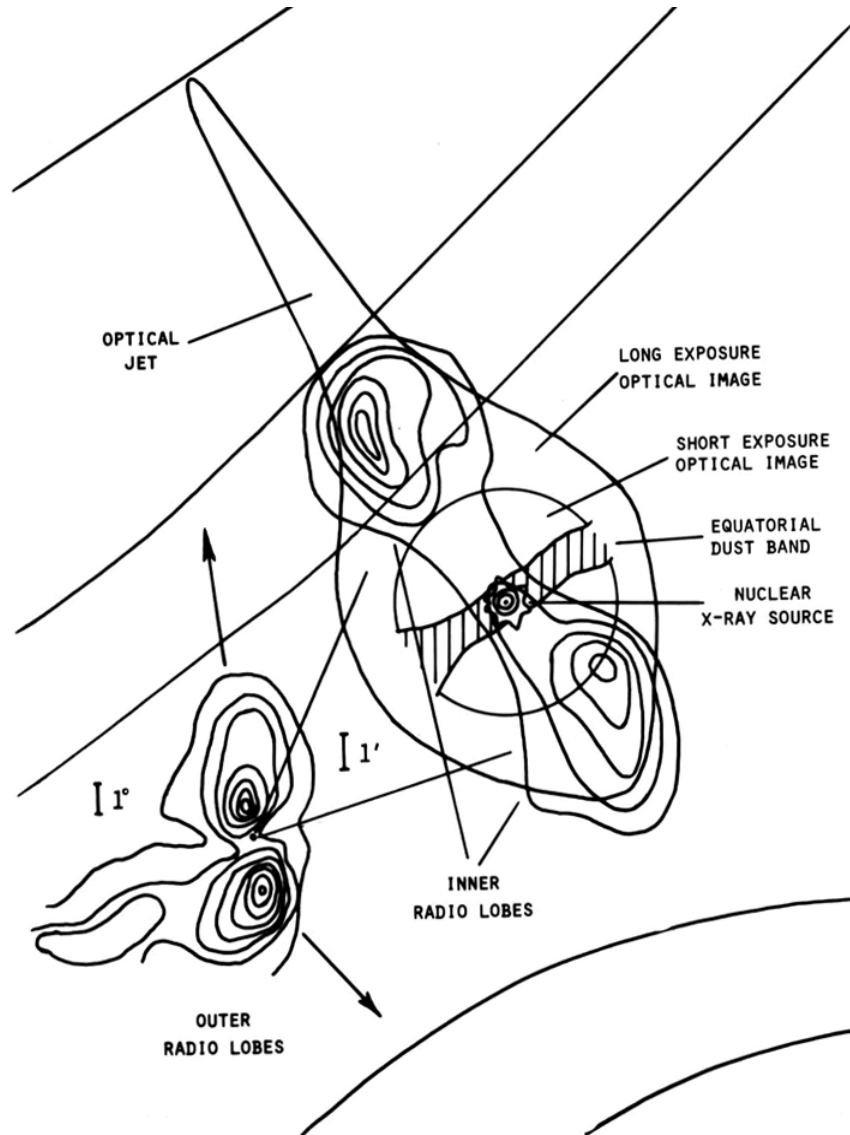


Figure 2.18. Schematic diagram of the radio, optical, and X-ray emission from the radio galaxy Centaurus A (NGC 5128). Inset at lower left, a 70 fold reduction of Centaurus A, shows the outer set of radio lobes which appear to extend millions of light years away from the galaxy (dot).

galaxies, and that disk radio emission is more common in the brighter Sb and Sc galaxies compared with the fainter ones.

A good example of a relatively nearby exploding galaxy is the radio galaxy Centaurus A (NGC 5128), represented schematically in Figure 2.18. It is the closest radio galaxy and one of the brightest extragalactic radio sources in the sky. It is classified as a giant elliptical or giant SO-type galaxy. But as may be seen by comparing the photographs shown in Figure 2.16, Centaurus A may actually be a spiral galaxy viewed from its edge, whose disk and corona are in a highly excited state.¹ This interpretation is supported by evidence that

¹ Other giant elliptical galaxies besides Cen A have been observed to possess dust lanes. These peculiar ellipticals differ from most elliptical galaxies in that they are prolate rather than oblate in shape, their bulges being elongated at right angles to their dust lanes (Bertola, 1981).

Centaurus A rotates about an axis that is perpendicular to the equatorial dust band (Burbidge and Burbidge, 1959).

The emission observed from Centaurus A may be summarized as follows; refer to Figure 2.18. Observations with the Einstein Observatory indicate that a very hard X-ray continuum is radiated within 1 minute of arc of the galaxy's center (Schreier et al., 1979). Also, in the direction of its nucleus a relatively strong, compact radio source is seen. Its size is about 1 to 10 milli-arcseconds and at millimeter wavelengths it is variable on time scales of about one day (Kellermann, 1974; Kellermann et al., 1975). A weak extended region of soft X-ray emission reaches out about 4' - 5' of arc from the nucleus and is elongated in a direction perpendicular to the orientation of the dust lane (Schreier et al., 1979). This X-ray emission region coincides with the optically visible portion of the galaxy. The circular optical image, as seen in Figure 2.16(a), has a diameter of about 5' of arc or ~28,000 l.y. for a distance to Centaurus A of 5 Mpc, and the dust band has a thickness of about 1' of arc or 4000 l.y. With longer exposure the optical image becomes larger and lemon-shaped and an optical jet appears jutting out from its north pole. Two compact inner radio lobes (Christensen et al., 1977) are found aligned with the apparent orientation of the polar axis of the galaxy and with the direction of elongation of the optical and soft X-ray emission. Their peak intensity lies about 4' of arc from the nucleus. Finally, two very large outer radio lobes, each extending over a span of several degrees of arc, are found to be reasonably aligned with the inner radio lobes, and in projection, with the galaxy's polar axis. Superluminal double compact sources have not yet been observed in the nucleus of Centaurus A, though if they were present, most probably they too would be aligned in a direction perpendicular to the equatorial dust band; recall Figure 2.10(b). This inference is supported by the observation that double compact radio sources and radio jets seen in active galactic nuclei are always found to be in fairly close alignment with the axis of the outer radio lobes.

The observed X-ray, optical, and radio emission from this galaxy could be evidence of a superwave propagating radially outward from the center of the galaxy, radiation being emitted nearly in line with the direction of particle propagation. Assuming an isotropic geometry for the cosmic ray component, regardless of the observer's viewing direction, a portion of this radiation would be beamed toward the observer. The axis of the observed radio and optical lobes would, therefore, extend toward the observer as has been inferred for the extended lobes of the radio quasar 3C 179.² The double structure of the inner and outer lobes could be due to absorption of relativistic particles (electrons) traveling radially through the disk. Our fortuitous edge-on viewing position, according to the Superwave Model, may be responsible for the unusual intensity of the continuum radiation and hence for the unusual appearance of this active (spiral) galaxy.

It is interesting to note that by assuming that the outer radio lobes are also produced as a result of relativistic beaming toward the observer, their generation may be accounted for

² The proposal that the radio lobes of Centaurus A and of other radio galaxies may be extending toward the observer was made by the author in the summer of 1981 in an earlier draft of this manuscript (sent out for review). At that time the generally accepted opinion was that such radio lobes instead extend out from the galaxy perpendicular to the observer's line of sight. It was several months later (November 5th) that the article by Porcas (1981) was published. As is mentioned in Subsection 2.1.2, Porcas's paper reports the observation that quasar 3C 179, a double-lobed radio galaxy, has a pair of compact radio sources that appear to be separating at a superluminal velocity. The alignment of these inner relativistic sources with the outer extended components strongly suggests that the outer, large-scale components are also relativistically beamed and are oriented toward the observer. Thus this identification provides the first clear evidence that the author's *a priori* proposal (an outgrowth of the Superwave Model) is correct.

by a cosmic ray blast of much shorter duration than has been previously assumed. For example, it becomes reasonable to assume that the lobes are closer to the observer than the parent galaxy. Hence the projected images of these radio lobes may be much smaller than previously thought, and the linear propagation distance for their cosmic rays much longer. The inner radio lobes may have been produced by the same cosmic ray blast while it was propagating through gas in the corona of Centaurus A. Millions of years later, the very same cosmic rays, upon reaching the gas surrounding our own Galaxy, would generate the outer lobes, which of course would appear larger to us. We see both the inner and outer lobes simultaneously because the cosmic rays travel to us nearly as fast as the radio radiation they produce.

2.1.4 The Time Scale for Galactic Explosions

One method which has been used to estimate the time duration of an outburst taking place in the nucleus of a Seyfert galaxy is to calculate the quantity $\Delta t = r/v$, r being the radius of the active region in the nucleus and v being the radial velocity of the ionized gas being expelled from this region. This gives the time taken for gas in the nucleus to travel from the center to the periphery of the region. Since r for a Seyfert galaxy is typically less than 50 parsecs and since v can reach as high as 5000 km/s, several investigators have concluded that the time scale for the activity in a Seyfert nucleus can only be about 10^4 years (Burbidge, Burbidge, and Sandage, 1963; Burbidge, 1968).

Two assumptions underlying this calculation are: a) The emission line broadening observed in the nucleus is interpreted as Doppler broadening due to gas being expelled from the nucleus; and b) the expelled gas is assumed to have originated at the galactic center and to have been traveling at the inferred Doppler shift velocity over its entire journey. According to the Galactic Superwave Model, on the other hand, a superwave traveling at the speed of light would be capable of accelerating gas residing at considerable distances from the nucleus. So, an estimate based on r/v should only be considered as a rough upper limit. Replacing v with c in this ratio gives much shorter durations, i.e., $t \sim 150$ years for $r = 50$ parsecs.

Evidence in favor of an outburst time on the order of 10^2 years comes from observations made on the Seyfert galaxy NGC 3516. Measurements made in 1967 show that the spectrum of this galaxy changed considerably over 25 years from the time Seyfert first observed it in 1943 (Andrillat, 1968). As a result, Souffrin (1968) has suggested that these spectral changes could be brought about by a brief outburst of relativistic electrons propagating through the ionized gas medium at close to the velocity of light.

Estimates of the fraction of time that a typical spiral galaxy spends in the active state range from 2% (de Vaucouleurs and de Vaucouleurs, 1968) to 10% (Oort, 1977, p. 317). Consequently, if the duration of an outburst is on the order of 500 to 1000 years, the time between successive outbursts should be on the order of 5×10^3 to 5×10^4 years. This is in the range assumed by the Galactic Explosion Hypothesis.

Often in the literature one finds values of $10^5 - 10^6$ years quoted for the duration of a typical outburst and $10^7 - 10^8$ years for the recurrence time of an outburst. These are usually based on observations of the extended radio emission lobes lying outside of radio galaxies such as Centaurus A. It is generally believed that relativistic particles generated in an explosion in the nucleus of the parent galaxy travel radially outward and generate the observed radio emission. Consequently, the time taken for a relativistic particle to traverse the length of the emission lobe is taken as the duration time of the outburst. Since these lobes are estimated in some cases to be up to several million light years in extent, comparable duration times are assumed for the associated galactic explosion. However, Burbidge, Burbidge, and Sandage (1963, p. 964) argue that the particles in these radio lobes

could just as well be supplied by a continuous series of outbursts each lasting on the order of $10^3 - 10^4$ years. Moreover as discussed in Subsection 2.1.2 (p. 27), the extended radio lobes of radio galaxies may actually be radio emission beamed toward the observer by approaching relativistic particles. If so, then it is misleading to use the length of the extended lobes as a measure of outburst duration. Due to travel-time effects, a brief outburst lasting for 10^3 years could conceivably produce a projected radio lobe image that was $10^6 - 10^8$ l.y. in size.

As a result of these ambiguities, it is best not to judge the duration of galactic outbursts on the basis of radio lobe observations. Shorter time estimates (i.e., $10^2 - 10^3$ years) inferred from optical observations of active nuclei should instead be used.

2.2. EVIDENCE OF SUPERWAVE ACTIVITY IN INACTIVE SPIRAL GALAXIES

2.2.1 The Origin of Galactic Cosmic Rays: Supernova Source or Nuclear Source?

There are two views concerning the origin of cosmic rays in spiral galaxies. One view (the more traditional of the two) suggests that cosmic rays originate in energetic activity taking place in the galactic disk; e.g., supernova explosions (Ginzburg, 1956; ter Haar, 1950). This will be referred to as the "supernova-source hypothesis." The other (more recent) view suggests that cosmic rays originate in energetic activity taking place in the galactic core; e.g., as a result of "galactic explosions" (Burbidge, Burbidge, and Sandage, 1963, p. 971; Ginzburg and Syrovatskii, 1964, p. 207). This will be referred to as the "nuclear-source hypothesis." Extragalactic evidence pro and con these two hypotheses is discussed below, and it is concluded that the nuclear source hypothesis is favored; also see Subsections 5.2 – 5.5. In particular, it is shown that several objections brought against the nuclear source hypothesis may be resolved if the GEH is adopted. Consider first the supernova source hypothesis.

Lequeux (1971b) has conducted radio observations of a number of spiral galaxies and has concluded that the nonthermal radio emission in the disks of spirals is produced by relativistic electrons accelerated in supernova explosions. He bases this conclusion on the observation that: a) the distribution of radio continuum disk diameters matches the galactocentric probability for the occurrence of supernovae, shown in Figure 2.19, b) the size,

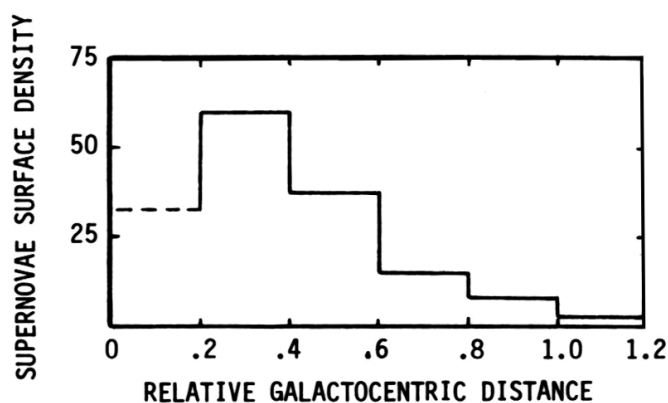


Figure 2.19. Histogram showing the surface density for the occurrence of 78 supernovae in a spiral galaxy as a function of galactocentric distance. Surface density is defined as: $\rho_n = n/2\pi r\Delta r$, where n is the number of supernovae occurring in an annular ring of mean radius r and width $\Delta r = 0.2r$. $r = 1.0$ is the radius of the galaxy (adapted from Johnson and MacLeod, 1963, Fig. 4).

shape, and position of radio disks makes a good match to the distribution of ionized hydrogen gas regions, and c) galaxies without conspicuous HII regions do not possess a radio disk.

However this data may be interpreted differently in the context of the Superwave Model. Namely, regions which exhibit high radio continuum emission and H II emission could be regions of enhanced interstellar gas density. If a superwave were to pass through such regions, scattered secondary relativistic electrons would be produced in greater numbers than in less dense regions. A certain fraction of these secondaries (and a fraction of the electron primaries carried by the superwave) would be expected to be captured by the local galactic magnetic field. These captured particles could both radiate a nonthermal radio continuum and also could ionize interstellar hydrogen gas. The particle enhanced regions would not partake of the relativistic motion of the superwave, and hence their radiation would be visible even when the galaxy had returned to an inactive state; also see the next subsection.

The observation that these ionized radio-emitting regions are more often found near the center of a galaxy is consistent with the Superwave Model, which requires that the cosmic ray density carried by a superwave decrease as the superwave propagates radially outward. The observation that the incidence of supernova explosions is also inversely correlated with increasing radial distance, on the one hand could be due to a fortuitously similar radial dependence in stars that are ready for their "supernova phase." Or on the other hand, as is suggested here, this could be evidence that supernovae are triggered by the passage of a superwave, and that such triggering is more probable near the center of a galaxy where the superwave is more intense. The low incidence of supernovae observed very close to the center of a galaxy (see Figure 2.19) is probably due to observational limitations since supernovae would be more difficult to detect against the continuum of a bright nucleus (Lequeux, 1971b; Johnson and MacLeod, 1963). This would especially be the case if the nucleus were in an active state at the time of triggering, as is suggested in the superwave scenario. Additional evidence that supernovae may be triggered by superwaves is presented in Chapter 5 (Subsection 5.2).

Van der Kruit and Allen (1976) point out several difficulties with the supernova model proposed by Lequeux. They note that if relativistic particles from supernovae were the cause of the disk radio emission, then one would expect this emission to match the distribution of neutral hydrogen gas in the galaxy. For it is from such dense HI associations that the extreme population I stars are supposedly formed, these being assumed to eventually give birth to the majority of supernovae. However Lequeux (1971b) himself found that the spatial distribution of the radio continuum disk is *not* correlated with the distribution of neutral hydrogen, and is generally of much smaller dimensions than the region of H I emission. Neither is the radio disk correlated with the distribution of stars which give most of the optical luminosity in these galaxies (Lequeux, 1971a). Second, Van der Kruit and Allen point out that the central regions of spiral galaxies are often devoid of H II regions, whereas the brightness of the radio disk generally *increases* with decreasing distance to the center. Finally, they tentatively point out that there appears to be a correlation between the luminosity of the central radio source of a spiral galaxy and the average radio brightness temperature of its disk. This may be seen in Figure 2.20 taken from Ekers (1975). Such a correlation would not be expected if disk supernovae were the sole generators of relativistic particles. Yet, this result and the observation that the radio continuum distribution has a radial dependence are both compatible with the Superwave Model which postulates that the galactic nucleus is the main source of relativistic particles.

Objections Against the Nuclear-Source Hypothesis and Their Resolution. Van der Kruit (1973) and Lequeux (1971b) have both brought up several objections to the nuclear-source hypothesis, to a large extent based on observations made within our own Galaxy. Some of

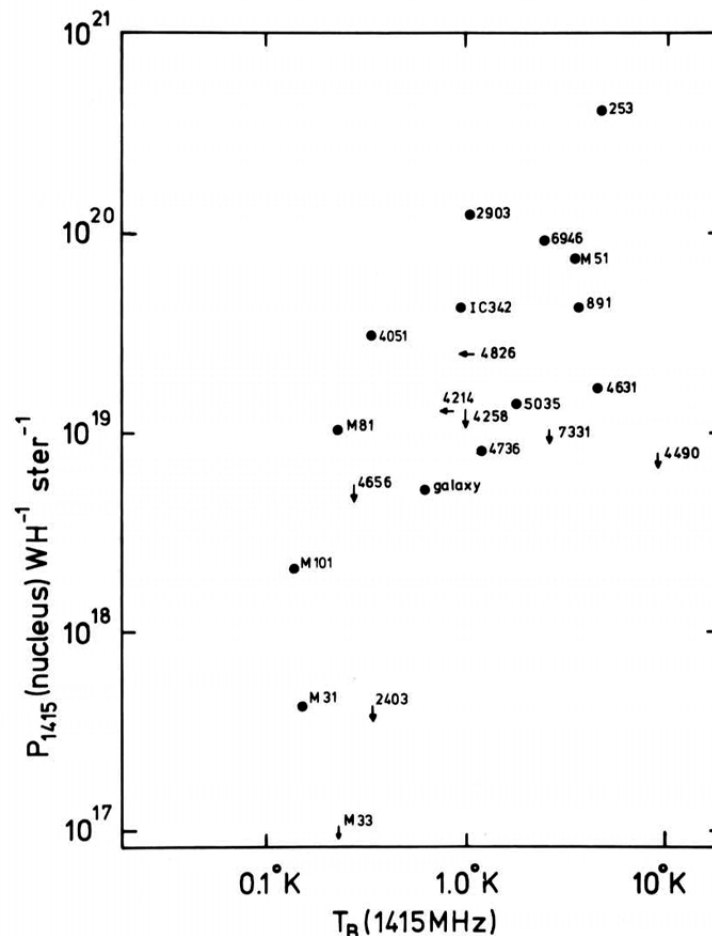


Figure 2.20. Plot of the monochromatic luminosity of the central sources of spiral galaxies against the disk average brightness temperature at 1415 MHz (Ekers, 1975).

these problems are listed below in a) through f). However, in each case (under "solution") the Superwave Model is shown to resolve the particular problem that they raise, thus vindicating the nuclear source hypothesis:

- a) **Problem:** It would take on the order of 10^8 years for a blast of cosmic ray electrons to diffuse from the center of our Galaxy to Earth (a distance of ~ 7 kpc). But cosmic ray electrons have a very short lifetime, $\sim 10^6$ years. So they would not be able to survive the journey. A similar argument would be true for other galaxies. (Lequeux, 1971b; Van der Kruit, 1973)

Solution: This objection is based on the assumption that cosmic rays do not travel directly to the Earth, but rather encounter galactic magnetic field lines disposed transverse to their radial propagation path, the energy density of this magnetic field being sufficient to resist being reoriented by the pressure of these cosmic rays. The particles, then, would be able to progress away from the galactic center only by diffusing across the field lines. The Superwave Model avoids this problem since it proposes that the galactic magnetic field lines are for the most part disposed *radially* with respect to the galactic center, allowing the cosmic ray blast to propagate outward relatively unimpeded.

- b) Problem: The abundance of heavy cosmic ray nuclei ($Z \geq 80$) in the solar neighborhood and the absence of a high-energy cut-off in the cosmic ray electron spectrum due to energy losses implies that the cosmic rays presently arriving in the Earth's vicinity were generated relatively recently. On the basis of the diffusion hypothesis one is led to conclude that these particles originate relatively close to our solar system, and hence that they were not produced in the Galactic Center. (Van der Kruit, 1973; after Meyer, 1969)

Solution: The Galactic Explosion Hypothesis proposes that the blasts of cosmic rays periodically passing the Solar System consist primarily of electrons and positrons. Thus, the origin of the heavy nuclei does not critically affect the Superwave Model. Moreover the majority of cosmic rays currently observed in the solar vicinity would not necessarily be related to the proposed blast, which by now would already have passed us. Hence any restrictions as to the origin of cosmic rays presently observed in the Earth's vicinity would not constrain the Superwave Model.

- c) Problem: The radio disk in our Galaxy is relatively uniform and not strongly concentrated toward the Galactic Center. Consequently, it does not seem likely that a central source was responsible for generating the relativistic electrons believed to power this emission. (Lequeux, 1971b)

Solution: The radio source at the Galactic Center (Sgr A) is relatively weak by comparison to the surrounding ring of nonthermal radio emission lying along the Galactic disk since we are now observing the Galactic Center during its quiescent state. I would suggest that the cosmic rays presently radiating in the disk were generated at the Galactic Center at an earlier time when the radio luminosity of Sgr A was considerably higher. Even so, contrary to Lequeux's claim, the radio disk in our Galaxy is not uniformly distributed, but rather *is significantly* concentrated in the direction of the Galactic Center. This evidence is reviewed in Section 5.1.

- d) Problem: The close correlation observed in several galaxies between disk radio emission and young population I, H II regions would not be expected if the cosmic rays generating this emission originated at the centers of these galaxies. (Lequeux, 1971b)

Solution: The Superwave Model does not contradict this observation, but rather anticipates it, since the same blast of cosmic rays would be expected not only to generate radio emission, but also to ionize intervening clouds of hydrogen gas.

- e) Problem: The classes of galaxies in which disk emission is frequently observed are those in which radio nuclei are less frequent. Consequently, observation suggests that the disk emission is not causally related to processes in the galactic nuclei. (Lequeux, 1971b)

Solution: Lequeux tacitly assumes here that if cosmic rays came from the nucleus, they would be emitted over a relatively long period of time, i.e., long compared with the flight time or diffusion time through the galactic disk. The Superwave Model, on the other hand, postulates a short outburst, lasting up to about 10^3 years, and radial unscattered propagation. Consequently, the fact that there are galaxies with either disk emission or nuclear emission, but not necessarily both, lends support to the brief outburst hypothesis. So, rather than refuting the Superwave Model, Lequeux's findings support it.

- f) Problem: Observations of radioactive isotopes in meteorites indicates that the cosmic ray density has remained relatively constant over the last several million years

(Balasubrahmanyam and McDonald, 1974; after Geiss, 1963), and that it has not changed by more than a factor of two over the last 10^9 years (Van der Kruit, 1971b; after Zahringer, 1964).

Solution: Superwave cosmic ray electrons, although less effective than cosmic ray protons in producing isotopic changes, would cause some degree of production. However, these periodic spurts would only be registered in meteorites in an integral manner. Isotopic constancy in meteorites would only indicate that the average rate of irradiation had not changed. Whether or not there were brief increases every 10^4 years, could not be easily determined by this method. A better technique, which would be sensitive to short-term fluctuations, would be the observation of changes in Be-10 or C-14 in the terrestrial stratigraphic record. Observational evidence that short-term variations actually do occur are discussed in Ch. 8, Sec. 8.4, and end-of-chapter update

In summary, it has been shown above that many of the objections normally brought forward in opposition to the nuclear source hypothesis for the origin of galactic cosmic rays are circumvented when the Superwave Model is adopted. In general, these extragalactic observations tend to support the view that cosmic ray outbursts occur in the nuclear region of galaxies and that the resulting cosmic rays propagate radially out into the disk of the galaxy.

2.2.2 Galactic Rings

Superwaves may be responsible for producing the ring-like emission regions found to surround many galactic nuclei. An emission ring may be a region in the disk of a galaxy where the direction of the interstellar magnetic field changes from a predominantly radial orientation to a predominantly transverse orientation. Superwave cosmic rays propagating through such a region would interact strongly with the interstellar medium and magnetic field and would become captured. These captured electrons in turn would be responsible for the synchrotron radiation and ionized gas observed in the rings. The observation that ring-like regions tend to be placed concentrically with respect to the Galaxy's nucleus suggests that they have been shaped by a series of explosive outbursts issuing from the galactic center, i.e., successive impacts from radially propagating superwaves. Hydromagnetic shock waves associated with a superwave could also be the driving force propelling the "density waves" that Lin and Shu (1964) have proposed in their theory of spiral arm formation.

Rings have been frequently observed in the closer Seyfert galaxies which are more easily resolved optically (e.g., NGC 474, NGC 1068, NGC 4151, NGC 4736, and NGC 7469). For example, there is evidence of an emission ring in NGC 1068 positioned at a distance of about 23,000 l.y. from the galaxy's center (Minkowski, 1968, Plate S-II). The active Sb spiral Markarian 10 also appears to have a ring feature surrounding its very bright and sharp nucleus (Khachikian, 1968, Plate S-XXI). For a distance to Markarian 10 of 174 Mpc, this ring would lie at a radius of about 40,000 l.y. From the observed high percentage of emission rings in Seyferts, Hodge (1968) has concluded that there is a connection between the explosive nature of certain galaxies and the presence of such ring features.

There is also abundant evidence for ring-like features in normal spiral galaxies. The galaxy classification schemes proposed by Sandage and by de Vaucouleurs both have distinctive categories reserved for galaxies with ring formations. For example, Figure 2.21 shows the pinwheel scheme developed by de Vaucouleurs in this case illustrating various types of Sb spirals (Menzel, Whipple, and de Vaucouleurs, 1970, p. 679). From the top going around the circle clockwise are the categories: (A) – ordinary spirals, (r) – those with ring

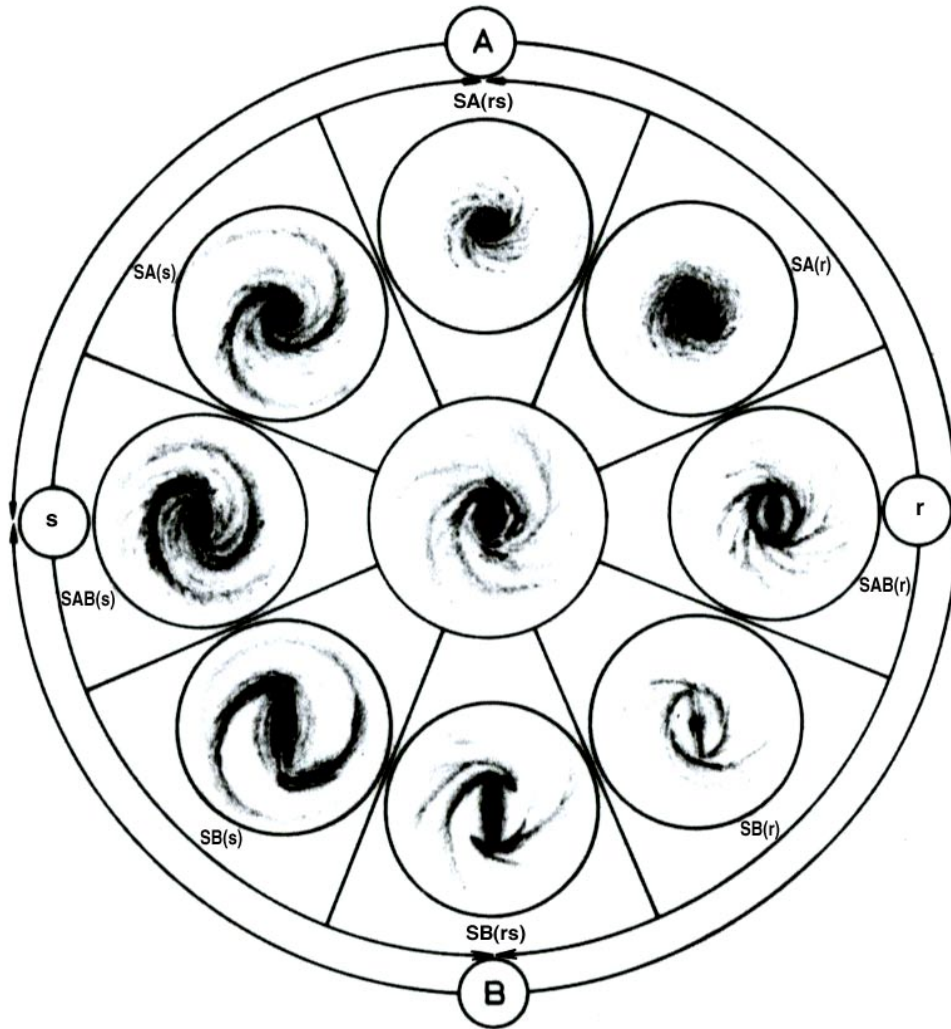


Figure 2.21. An example of the various morphologies of type-Sb spirals in the classification scheme developed by de Vaucouleurs (Menzel, Whipple, and de Vaucouleurs, 1970, p. 679).

structure, (B) – barred spirals, and (S) – s-shaped spirals without ring structure.

Kormendy (1979) has studied the morphology of 121 spiral galaxies regarding features such as bars, lenses, and inner and outer rings. He adopts the interpretation that the bar components projecting from the nucleus in barred spirals act as a gravitational mechanism for driving density waves, which in turn form inner rings and lenses. In galaxies where rings are present without bars he suggests that the bar has become dispersed after formation of the ring. Kormendy's findings, however, could be just as easily interpreted in terms of the Superwave Model. Bars, lenses, and rings could all be features produced by the periodic radial propagation of superwaves.

Quite often a galaxy may have ring features which are not apparent at optical wavelengths. Take for example the Andromeda galaxy (M 31). This galaxy, classified as an Sb spiral, is the closest spiral galaxy to our own Galaxy (~ 2 million l.y.), making possible relatively detailed observation of its structure. It has been classified by de Vaucouleurs as SA(s)b, i.e., an ordinary s-shaped spiral without rings; see Figure 2.22. However, when viewed at a radio frequency of 408 MHz, a distinctive ring of nonthermal emission is



Figure 2.22. The Andromeda galaxy, M 31.
(Photo courtesy of Mt. Palomar Observatory)

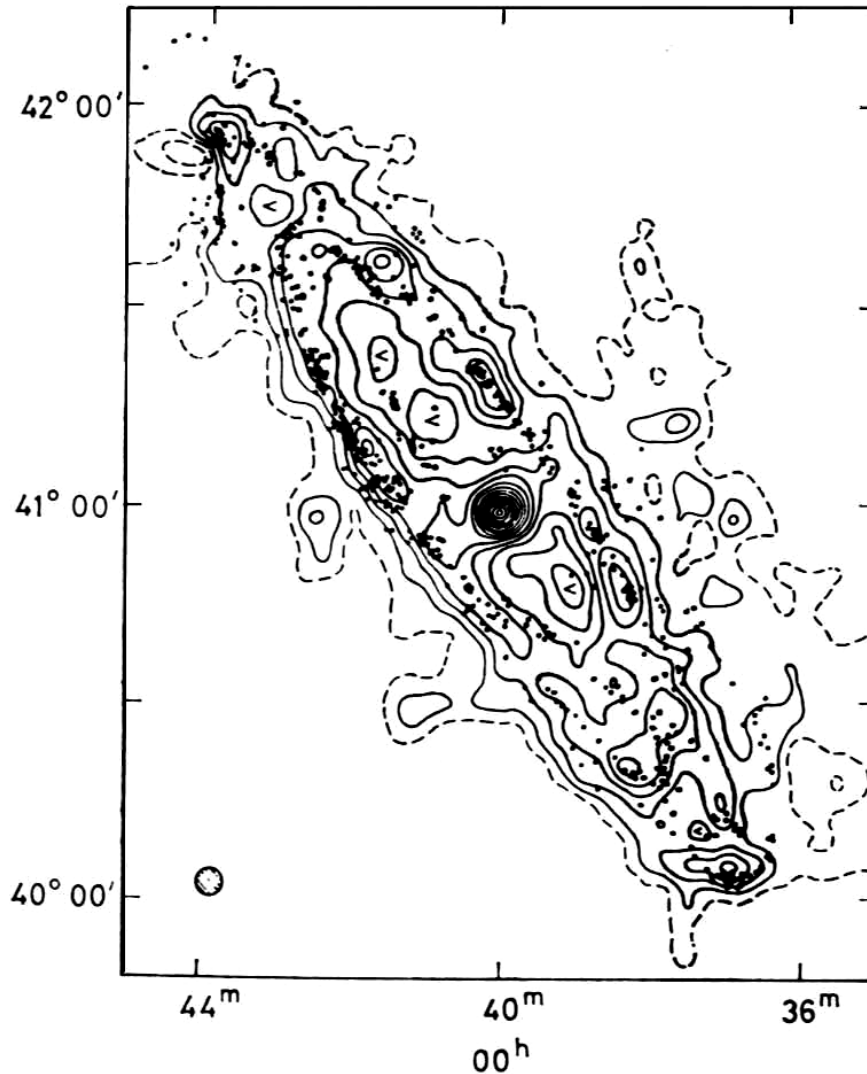


Figure 2.23. The 408 MHz map of M 31 made by Pooley (1969) superimposed on a map of 688 emission nebulae made by Baade and Arp (1964) (synthesis by Pooley, 1969).

observed; see Figure 2.23 (Pooley, 1969). This surrounds the nucleus which is also very bright at this frequency. This radio emission band is closely correlated with the distribution of H II emission nebulae also shown in Figure 2.23. Neutral hydrogen (H I) emission regions observed at a 21 cm wavelength (Guibert, 1973) and OB star associations (Van den Bergh, 1964; Richter, 1971) are also found to follow this same ring pattern. The location of these features suggests that there may actually be several rings, two inner rings lying at about 25,000 and 40,000 l.y. from the center (Pooley, 1969, p. 117) and an outer ring, marked by the presence of H I emission, lying at about 65,000 l.y. X-ray observations of M 31 with the Einstein observatory have revealed 69 point sources, one-third of which are contained in the galactic nucleus and two-thirds of which are contained in the disk (Van Speybroeck et al., 1979). This disk group shows a distinct correlation to the inner ring features; see Figure 2.24 (Van Speybroeck et al., 1979).

In speculating about the cause of the ring of nonthermal radio emission in Andromeda, Pooley (1969, p. 122) notes that this radiation could not come from the remnant shells of type II supernovae since there are few objects of this type that radiate with sufficient intensity.

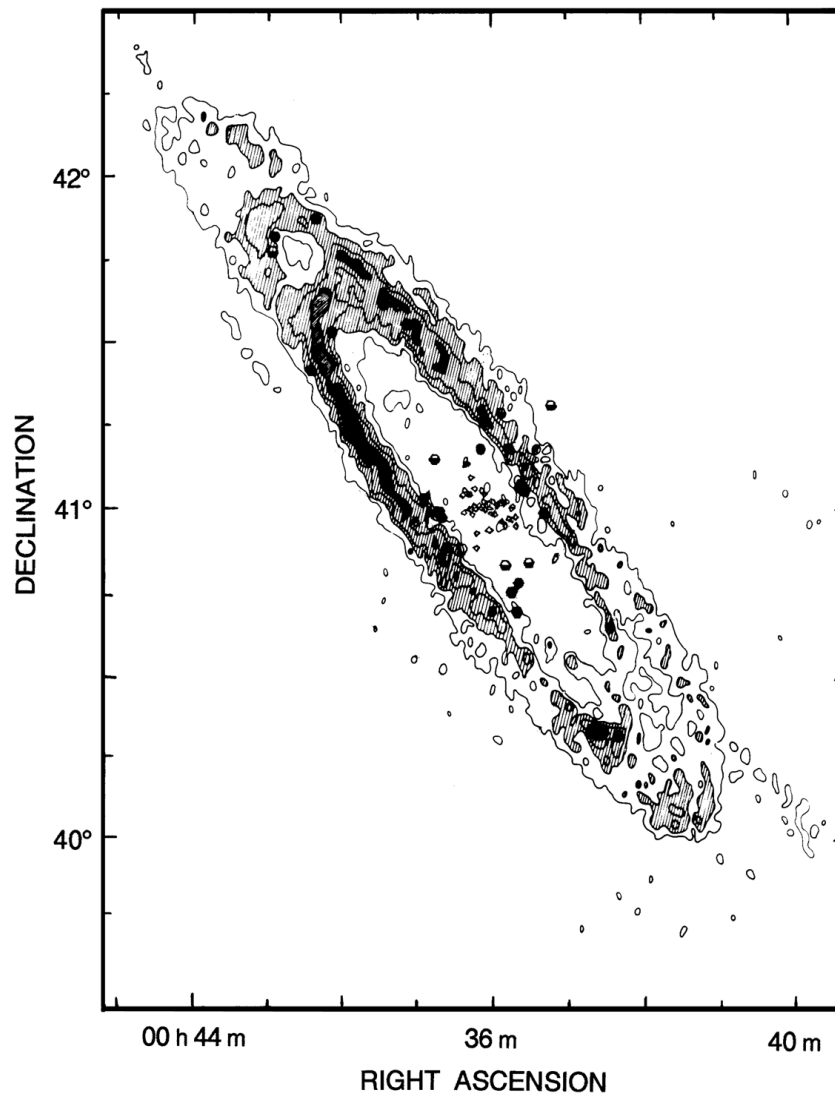


Figure 2.24. X-ray source positions detected in M 31 with the Einstein Observatory (filled, half-filled, and small open symbols) superimposed on an HI map made by Emerson (1976). (Van Speybroeck, 1979)

As an alternative he suggests that relativistic electrons accelerated in supernova explosions and confined to the spiral arms could in principle produce the observed nonthermal radiation through the synchrotron mechanism. He points out, however, that if this is the case one must explain why these magnetic fields and electrons are so highly concentrated in these particular ring-like regions. The inner two rings in general coincide with what is denoted as spiral arms #4 and #5 (Pooley, 1969, p. 117). However, as many as seven distinct spiral arms may be discerned. So the question remains, why do these other arms not have magnetically confined relativistic electrons also? According to Figure 2.19, the chance of supernova explosions should be even greater close to the nucleus. But emission is conspicuously absent between the nucleus and the ring. As a second possibility, Pooley suggests that a density wave propagating radially through Andromeda's disk at supersonic velocities could provide a mechanism both for the acceleration of particles and for increasing the strength of the interstellar magnetic field through compression. Thus, the

ring would simply mark the present location of a density wave.

As an alternative, I would suggest that the emission ring is a shocked region in which galactic magnetic field lines are oriented transverse to the direction of superwave propagation, causing a portion of the radially propagating superwave cosmic rays to become captured within the ring. These electrons would be responsible both for ionizing the interstellar medium and for generating the observed nonthermal radio continuum.

The emission ring should not itself be interpreted as indicating the location of a superwave event horizon. M 31 is viewed at an angle of $\sim 15^\circ$ to its galactic plane. Consequently, any superwaves intersecting the galactic plane would be expected to form highly eccentric open ellipses having one focus at the center of M 31 and the other focus at the observer's position. Such deviations from circularity are not observed.

Besides ring features, there is also evidence of nonthermal emission coming from an unusual 6000 l.y. diameter spherical region about half the size of Andromeda's nuclear bulge, and nearly concentric with its center. Hjellming and Smarr (1982) estimate that this region has an enhanced density of relativistic electrons, amounting to an energy total of about 2×10^{50} ergs. This radio emission region surrounds a 2500 l.y. diameter region in which Rubin and Ford (1971) find evidence of gas expanding radially at velocities of up to 100 km/s. This region, which contains less than 2% of the mass of M 31 is responsible for one-third of the X-ray emission observed from this galaxy (Van Speybroeck, 1979). Such radial gas motion and enhanced X-ray and radio emission could be interpreted as evidence that Andromeda's nucleus has recently undergone explosive activity. It is interesting to note that S Andromeda, a supernova observed in M 31 in 1865 and the only one observed in that galaxy to date, occurred in Andromeda's nucleus essentially coincident with its center (within 150 l.y.). It is interesting to speculate that this supernova was triggered by a superwave, and that the same superwave is responsible for producing the other energetic features observed in this region.

Rings are also observed in a class of peculiar galaxies called "ring galaxies." Generally, spiral arms are not visible in such galaxies. They often consist of a ring feature surrounding a nucleus; for example; see Figures 2.25(a) and (b) (Kormendy, 1979). Sometimes two rings are observed, such as those in the ring galaxy 1008-38 in Vela (Dennefeld, Laustsen, and Materne, 1979). The inner ring is estimated to lie at a distance of about 15,000 l.y. from the central nucleus and the outer ring at a distance of about 110,000 l.y. In both rings emission lines of hydrogen and nitrogen are detected. Dennefeld, Laustsen, and Materne interpret this system as a pair of colliding galaxies in which one galaxy has penetrated through the disk of the other, producing the two observed ring features. An alternative interpretation suggested here is that 1003-38 is a single spiral galaxy whose arms are not visible because they are unusually faint. The visible rings would then be produced by a series of radially propagating superwaves. Future observations with the Space Telescope should verify whether 1008-38 is indeed a spiral galaxy.

Another ring galaxy with two concentric emission rings is Lu 003-534, also known as the Cartwheel Galaxy, see Figure 2.26-a (Thieys and Spiegel, 1976). In this case spiral arms are visible as faint filaments extending between the rings. Hubble Space Telescope images which became available in 1994 show the spiral arms and inner ring more clearly; see Figures 2-26-b and 2-26-c (Struck, Appleton, Borne, Lucas, and NASA, 1994). Spiral arms are even more prominent in the peculiar Sc spiral NGC 3646; see Figure 2.27 (Burbidge, Burbidge, and Prendergast, 1961). For a distance to this galaxy of 82 Mpc, the inner ring would be located at a radius of 35,000 l.y. and the outer ring at a radius of about 100,000 l.y. Noncircular motions (i.e., radial motions) are detected in the outer ring. Colliding galaxy models would have trouble accounting for the double ring features in both spiral galaxies since a dynamic encounter of this sort would be expected to cause major disruption of the spiral arm pattern. But no such disruption is observed. As an alternative, the Superwave

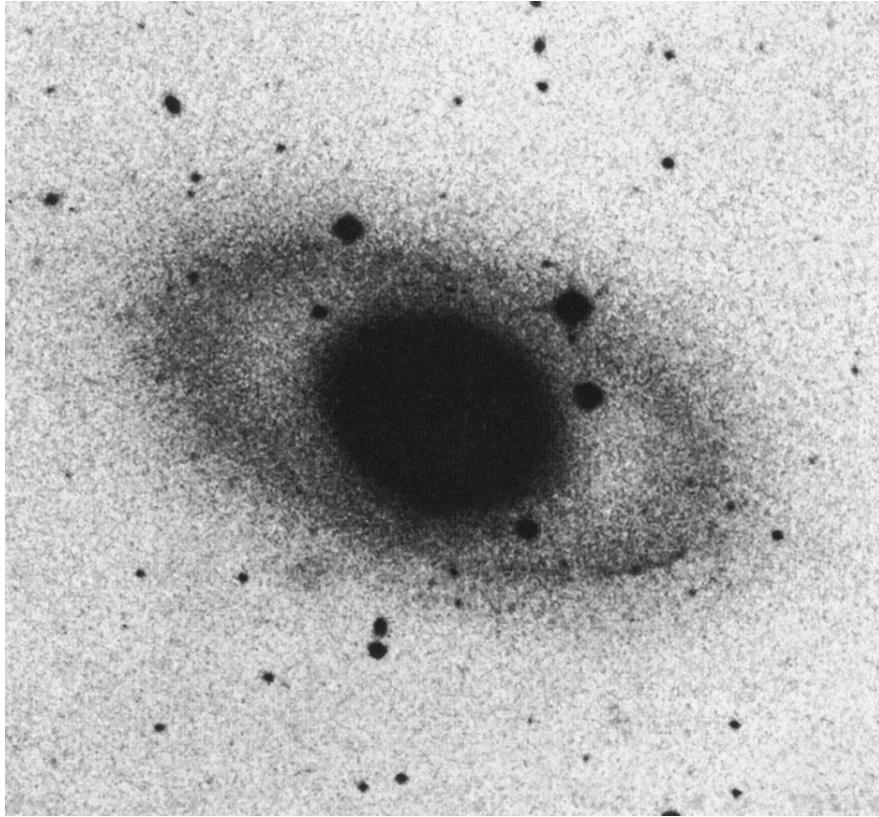
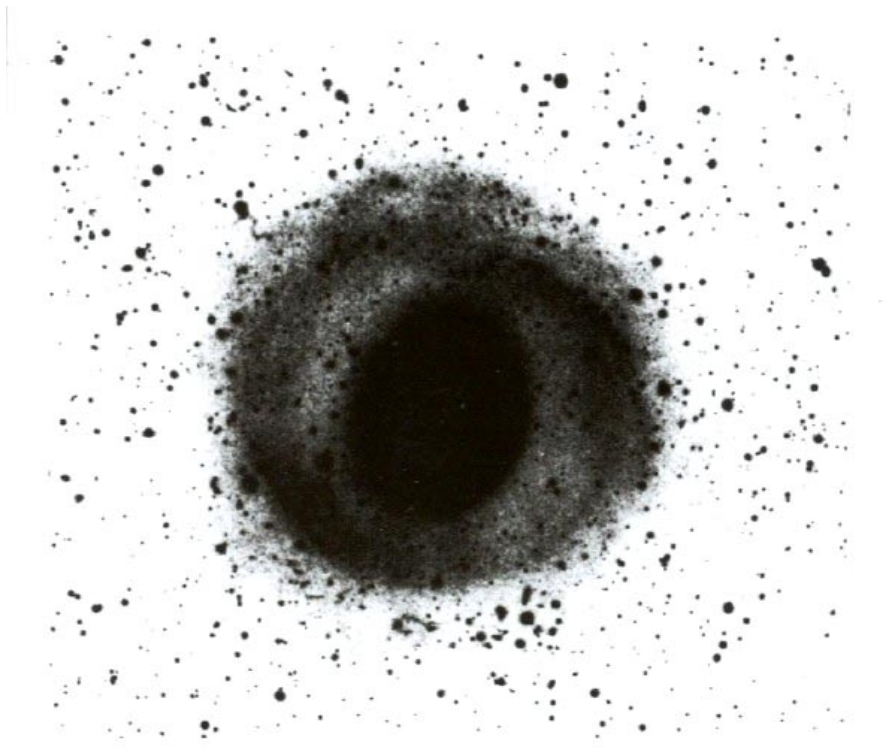
**(a)****(b)**

Figure 2.25. Ring galaxies: a) NGC 3945, b) NGC 1291. (Kormendy, 1979)

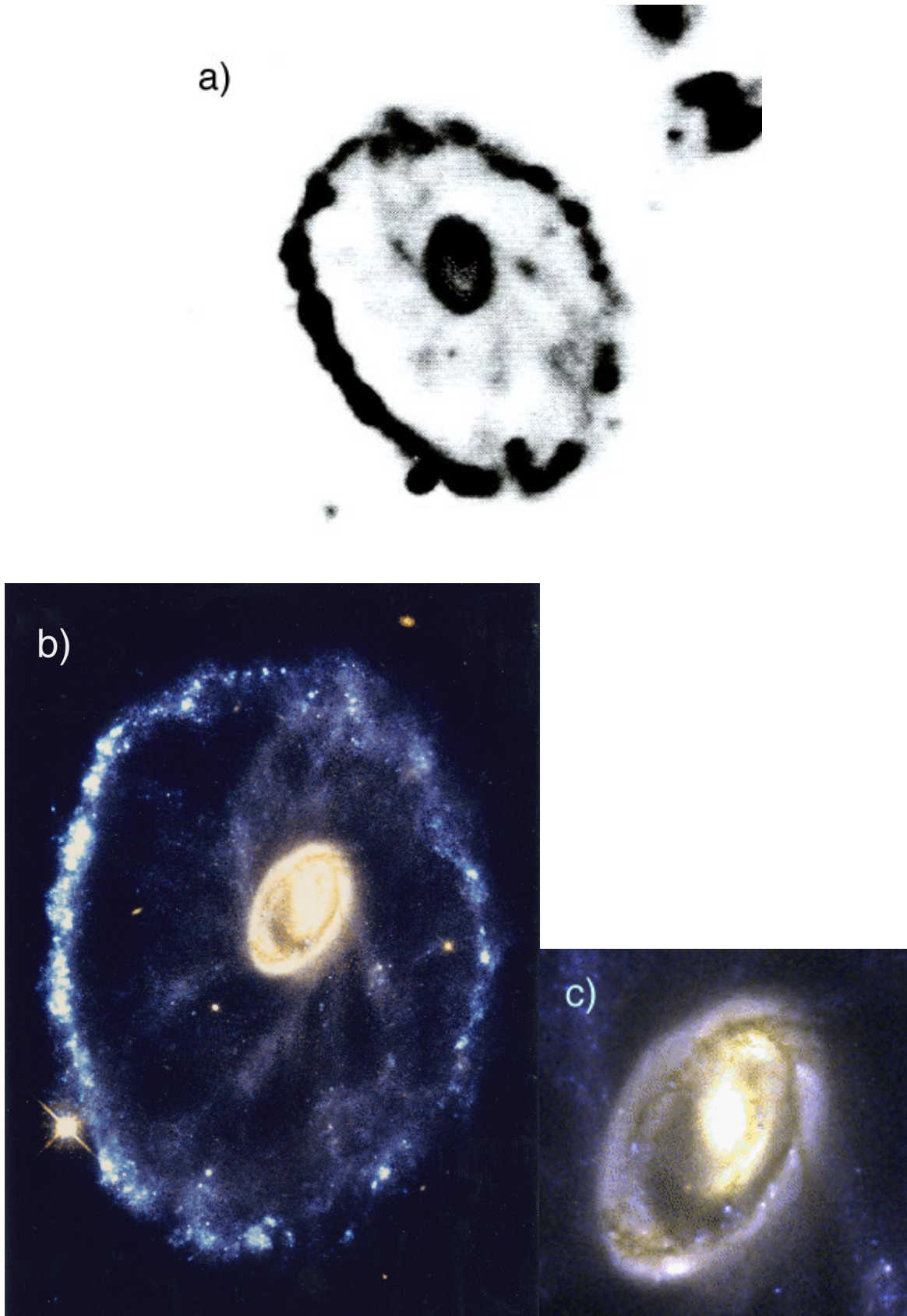


Figure 2.26. Cartwheel ring galaxy Lu 003-534. a) negative print from Thieys and Spiegel (1976), b) and c) recent Hubble Space Telescope shots (NASA 1994).



Figure 2.27. Peculiar spiral galaxy NGC 3646.
(Burbidge, Burbidge, and Prendergast, 1961)



Figure 2.28 (left). Ring galaxy VII Zw 466 (Freeman and de Vaucouleurs, 1974).

Model could provide an explanation for such ring structure.

Some ring galaxies appear as empty rings. One example is VII Zw 466, shown in Figure 2.28 (Freeman and de Vaucouleurs, 1974). One explanation could be that the nucleus was either ejected from the disk or blown apart by a very severe explosion.

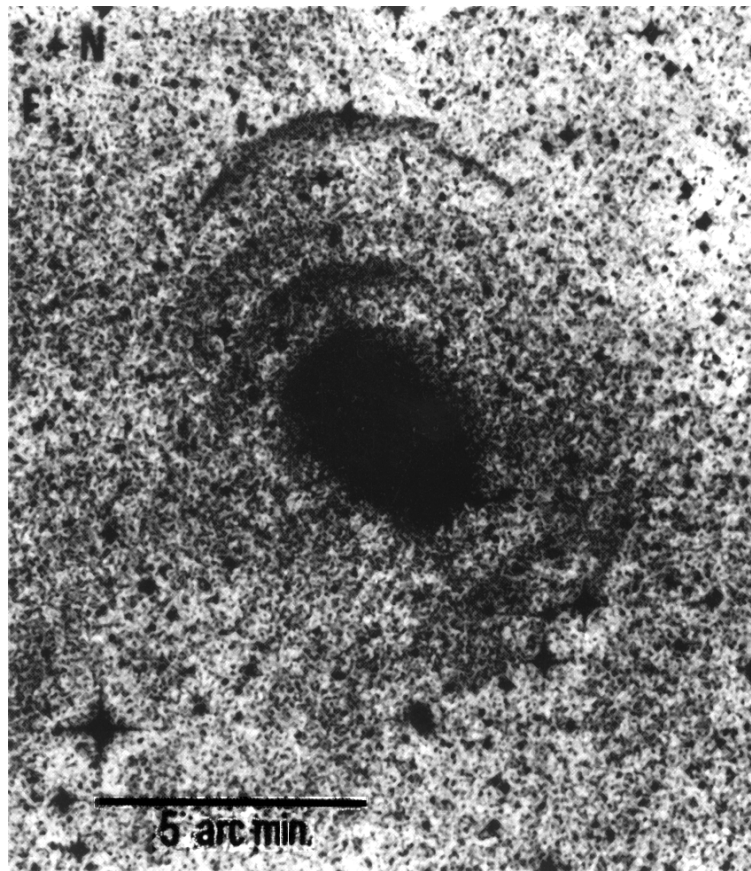


Figure 2.29 (right). Elliptical galaxy NGC 3923. Three inner shells are seen in this exposure (Malin and Carter, 1980).

Alternatively, it could be that galaxies with this morphology are simply spiral galaxies in which the nucleus and spiral arms are too faint to be visible in comparison to the emission ring. Again, observations with the Space Telescope should clear up this question.

Using special photographic techniques, it has been found that certain elliptical galaxies possess surrounding shells, e.g., M 89 (Malin, 1979), NGC 1316 (Schweizer, 1980), NGC 1344, NGC 1395, and NGC 3923 (Malin and Carter, 1980). NGC 3923, for example, has a shell at a radial distance of 580,000 l.y. and 3 concentric inner shells at distances of about 64,000, 96,000, and 170,000 l.y. respectively; see Figure 2.29. Malin and Carter (1980) suggest that these shells were formed as a result of explosive events taking place in the nuclei of these galaxies.

In summary, shells and rings found to surround the nuclei of many types of galaxies indicate that outbursts at the centers of these galaxies have effects on the interstellar medium at considerable distances from the nucleus. Galactic superwaves could be the vehicle by which these effects are transmitted.

UPDATE

Long-range Rectilinear Propagation of Galactic Cosmic Rays (p. 31): After completion of this dissertation, astronomical observations were announced which confirmed certain basic assumptions of the Superwave Model, namely that cosmic rays can propagate through the disk of our Galaxy following rectilinear trajectories at close to the speed of light.

For example, in 1985, astronomers discovered that Cygnus X-3, a strong cosmic ray source lying about as far away as the Galactic center (25,000 - 30,000 light years), was showering the Earth with high-energy particles. They found that despite the Galaxy's magnetic fields, these particles were able to reach the Earth at the speed of light following arrow-straight paths.⁽¹⁾ Several years later, scientists found that the Earth was also being showered by particles from the X-ray pulsar Hercules X-1.^(2, 3) The particles were found to come in bursts spaced by 1.2357 seconds, closely matching the pulsar's intrinsic period. Even though this source lay 12,000 light years away, the intervening interstellar medium had such a minor effect on the bursts that their pulsation period was constant to within 300 microseconds.

Also in 1997, a strong gamma ray pulse detected by satellite observatories was found to come from a galaxy billions of light years away having a redshift of 3.4. Mainstream media, such as *Sky & Telescope* magazine, suggested that this gamma ray pulse may have been accompanied by a volley of high energy cosmic ray particles traveling at very close to the speed of light along a rectilinear trajectory and that the gamma ray pulse is produced by the radial outward movement of this volley. In effect, they were restating the same Galactic superwave idea that I had proposed 14 years earlier.

Furthermore at the January 2000 American Astronomical Society meeting, radio astronomers announce that the synchrotron radio emission radiated from the Galactic center (Sgr A*) is circularly polarized.⁽⁴⁾ Scientists present at the meeting concurred with my suggestion that the circular polarization indicated that cosmic ray electrons were traveling radially away from the Galactic center along straight-line trajectories.

References to the Update

- 1) M. L. Marshak, et al. "Evidence for muon production by particles from Cygnus X-3," *Physical Review Letters* **54** (1985): 2079.
- 2) B. L. Dingus, et al. "High-energy pulsed emission from Hercules X-1 with anomalous air-shower muon production." *Physical Review Letters* **61** (1988): 1906.
- 3) B. Schwarzschild, "Are the ultra-energetic cosmic gammas really photons? *Physics Today* Nov (1988): 17.
- 4) G.C. Bower, H. Falcke, and D.C. Backer, "Circular Polarization in Sagittarius A*," (abs.) Session 62, 195th American Astronomical Society meeting, Atlanta, January 12, 2000. See Session 62 at <http://www.aas.org/meetings/aas195/program/index.html>

CHAPTER 3

MODELING THE HYPOTHESIZED 14,200 YEARS BP SUPERWAVE

This chapter presents a model of the propagating components of the proposed 14,200 years BP superwave and discusses some of the effects that these would create. The discussion of the cosmic ray component of the superwave is for convenience broken up into four sections, corresponding to the four stages shown in Figure 3.1. These are: 1) the generation of the outburst at the Galactic center (e.g., beginning 37,000 years BP), 2) its alteration as a result of its 22,800 l.y. (7 kiloparsec) propagation through the Galaxy (see Endnote 1 of Chapter 1), 3) its effects on the Earth upon arrival in the solar system (e.g., beginning 14,200 years BP), and 4) effects in the Galaxy which may be observed after the superwave has passed the Earth (i.e., effects presently detectable). Passage of the 14,200 years BP cosmic ray outburst through the solar system may have lasted for up to a few thousand years. Here this extended event will be referred to generally as the 14,200 years BP superwave. The minor outburst which is hypothesized to have passed the Earth ~6000 years BP is not modeled in this chapter. However, observational evidence indicating the existence of this and a more recent event horizon is presented in Chapter 6.

3.1 GENERATION

It is not the intent of this study to describe in detail the means by which the required outburst of cosmic rays is generated in the Galactic center; the necessary *initial conditions* may just as well be stated as an hypothesis. Such an approach is justified if it can be shown that the effects which the proposed components would manifest in the Galaxy and on the Earth are compatible with a wide variety of astronomical and geological evidence. The following section summarizes the initial conditions that I hypothesize for the cosmic ray component of the 14,200 years BP superwave event (generated ~37,000 years BP at the Galactic center). A model of the generation mechanism for the outburst will be left to future work.

I propose that around 37,000 years ago the Galactic center became active and began to radiate isotropically a flux of relativistic electrons and positrons *in approximately charge-balanced proportions*. Hereafter I will generically refer to these as "electrons," with the implication that they are of both plus and minus charge. The power-time profile for the 14,200 BP Galactic explosion may be modeled as follows; refer to Figure 3.2. For the first 200 years relativistic electrons (+ and -) are generated at the peak rate of 7.5×10^{47} ergs/s. For the following 200 years ($t = 200$ to 400 years) this generation rate decreases linearly to zero. Then about 1100 years later ($t = 1500$ years) the generation rate begins to rise linearly

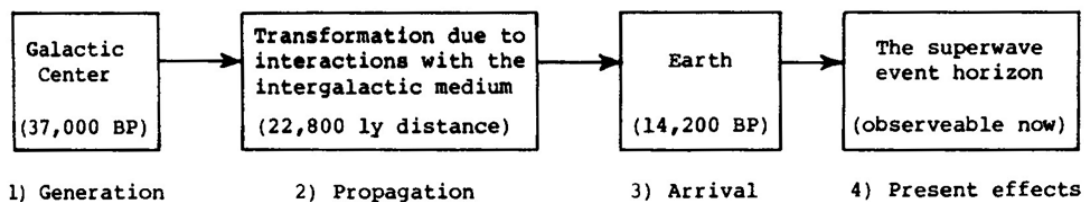


Figure 3.1. Stages in the generation and propagation of a Galactic superwave.

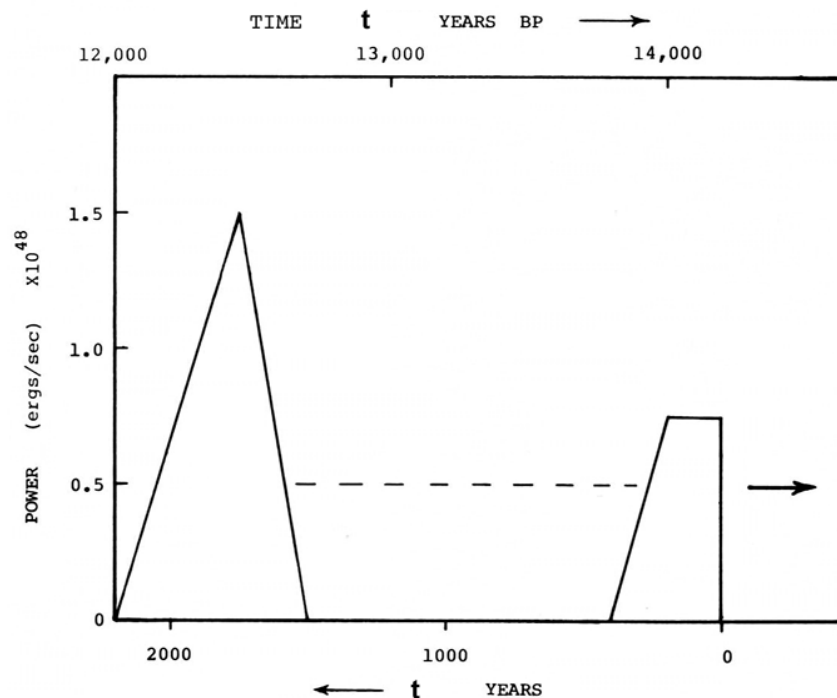


Figure 3.2. Total power in cosmic ray electrons radiated by the Galactic center at the time of generation of the 14,200 years BP superwave. Upper horizontal scale measures time from the moment the outburst becomes initiated at the Galactic center. Lower horizontal scale registers time of arrival in the solar vicinity in terms of years before present. Profile propagates from left to right over time.

reaching a peak of 1.5×10^{48} ergs/s at $t = 1750$ years, after which the generation rate declines linearly to zero at $t = 2200$ years.

The total integrated flux would come to about 7×10^{57} ergs for the first outburst and about 1.65×10^{58} ergs for the second outburst, giving a total of 2.4×10^{58} ergs for both outbursts. This is equivalent to a conversion of $\sim 10^4$ solar masses into kinetic energy. The total rest mass involved in the blast, however, would only come to about 4 solar masses, given that the electrons would have an average Lorentz factor of ~ 3000 . Note that in the next section it is proposed that about 20% of the superwave electrons become lost in the course of propagation to the solar system through the nucleus and disk of the Galaxy. Consequently, the values given above would have to be reduced accordingly for the purpose of calculating the effects of the superwave in the solar vicinity. For example, the "apparent" integral peak power radiated by the Galactic center for the two outbursts would be 6×10^{47} ergs/sec and 1.2×10^{48} ergs/s respectively, and the total apparent energies for each outburst would be equal to 5.5×10^{57} ergs and 1.3×10^{58} ergs respectively.

The energy requirements for these two outbursts may be compared with the quantity 3×10^{57} ergs that Marscher (1978) has proposed in his relativistic blastwave model of the 1975 radio outburst of AO 0235+164, a BL Lacertae object; see Chapter 2, **p. 29** for a brief discussion of his model. Given that outbursts of this size occur in this blazar about once a year, then Marscher's model would require a rest mass conversion rate of $\sim 10^3 M_{\odot}/\text{yr}$, 100 times higher than that proposed for the 14,200 years BP superwave. Among active galaxies AO 0235+164 is considered to be one of the more powerful sources, so by comparison the outbursts proposed here may be considered to be milder events.

The power-time profile shown in Figure 3.2 is admittedly highly simplified, but it is adequate as a starting point. The dotted line is intended to indicate an intermediary period during which cosmic rays may have been periodically generated at elevated rates. A more realistic profile would probably exhibit more detailed variations in cosmic ray production rate than are shown here; however, lack of sufficient data discourages construction of such a detailed model. The initial outburst is hypothesized to arrive in the solar vicinity beginning about 14,200 years BP with the second outburst peaking at about 12,450 years BP. The two events together are referred to as the 14,200 years BP superwave. But for simplicity of discussion most of the energy calculations in the following sections of this chapter will refer primarily to the first outburst ($t = 0$ to 400 years).

The differential particle number intensity spectrum for the proposed cosmic ray electron outburst is assumed to have a spectral index of $\Gamma = 2.75$, i.e., $N(E) \propto E^{-2.75}$, for $E > 1.5$ Gev, close to that of the high energy end ($E > 10$ Gev) of the solar modulated cosmic ray electron spectrum currently observed in the Earth's vicinity. For $E < 1.5$ Gev, a flattening of the spectral index to $\Gamma = 1.8$ is assumed; see Figure 3.7, curve (a) (p. 72). The proposed spectral index of $\Gamma = 1.8$ and the accompanying steepening at $E > 1.5$ Gev is consistent with the spectrum derived by Goldstein, Ramaty, and Fisk (1970) for the Galactic nonthermal radio background, a spectrum which these authors suggest is also representative of the unmodulated electron spectrum in the vicinity of the solar system. As noted in Chapter 5 (Section 5.1) the Galactic radio background is assumed to be produced by the 14,200 years BP superwave; consequently it is reasonable to use spectral data of this radio emission continuum as a guide in constructing the proposed superwave spectrum.

It is difficult to estimate how many orders of magnitude the current relativistic particle output from the Galactic center would have to increase in order to attain the peak intensity of the proposed outburst, since the present cosmic ray flux from the GC can only be guessed at. In Section 3.3.1 it is estimated that the proposed 14,200 years BP outburst would increase the average cosmic ray electron background energy density in the solar vicinity by about 3×10^4 fold at peak superwave intensity. However, caution should be exercised in associating the cosmic ray electron background intensity currently observed in the solar vicinity with the level of cosmic ray generation activity presently going on at the GC. For example, it is uncertain what percentage of the solar vicinity cosmic ray electron flux originates from the GC as opposed to coming from other sources in the Galaxy. Also, the particles responsible for the current radio luminosity of the GC might not travel to us radially from the GC nearly as fast as does this electromagnetic radiation. The particles currently observed in the solar vicinity may actually be post-outburst, quiescent-state particles that were able to propagate radially outward from the GC and traverse the Galactic disk "on the heels" of the last outburst.

The estimate that the cosmic ray generation activity of the Galactic center would increase by 3×10^4 fold at the time of the proposed outburst may be taken as a lower limit. An upper limit may be estimated as follows. Measurements of the 511 keV positron-electron annihilation line observed from the direction of the GC suggest that currently about 2×10^{43} positron/electron pairs are annihilated each second (Leventhal, MacCallum, and Stang, 1978). The rapid variability in intensity of this annihilation line on a time scale of 6 months suggests that the particles originate from a point source, most likely the GC itself (Leventhal, MacCallum, Hutters, and Stang, 1982). If it is assumed that electrons and positrons are radiated from the GC in charge-balanced proportions, then the total particle flux comes to $\sim 4 \times 10^{43}$ particles/s. Since the cross section for positron annihilation is greatest for positrons in the range of 0.1 – 10 MeV, the observed GC particle annihilation rate may be taken as a crude measure of the particle flux in this energy range. By comparison, at peak superwave intensity, electrons in this energy range would radiate from the GC at the rate of $\sim 10^{52}$ – 10^{53} particles/s or about 10^9 times the present inferred intensity. This peak flux estimate

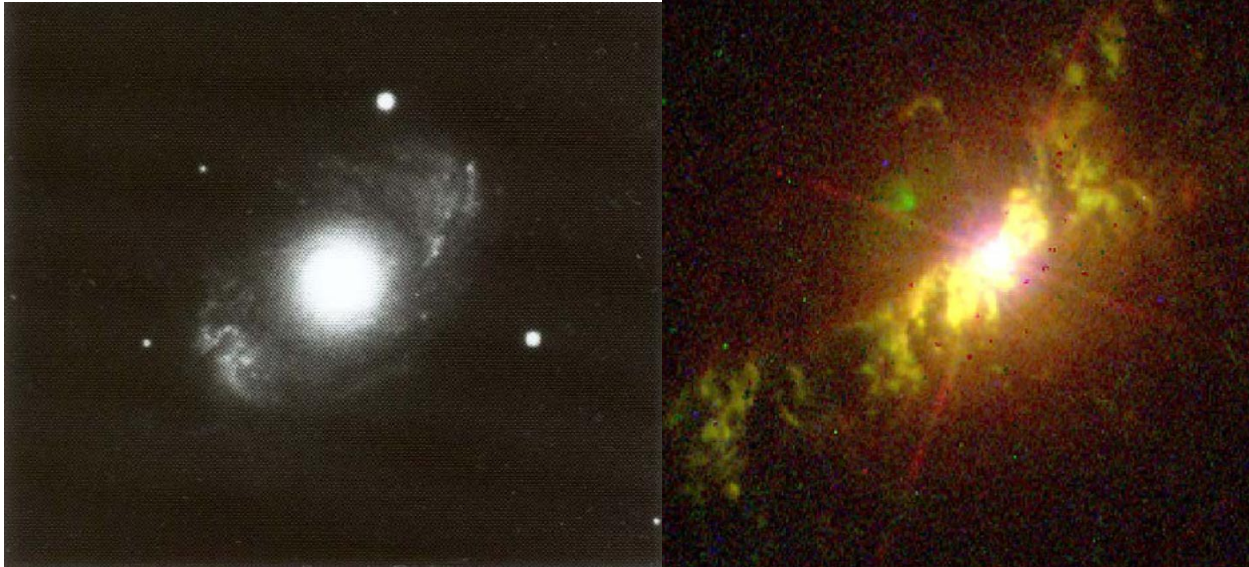


Figure 3.3. Left: Seyfert galaxy NGC 4151 (courtesy of Mt. Palomar Observatory). The large diameter of the central emission region is due to photographic overexposure caused by the brightness of the nucleus. Right (update): A close-up view of the central part of NGC 4151 made in 1997 with the Hubble Space Telescope, showing the region within 1000 light years of the luminous core (courtesy of J. Hutchings, B. Woodgate, M. B. Kaiser, S. Kraemer, and NASA). The gas clouds seen here are moving radially away from the core, propelled forward by the cosmic ray barrage.

presumes that in the vicinity of the GC the differential particle number intensity **spectrum** for the superwave would maintain a spectral index of 1.8 down to particle kinetic **energies** of a few tenths of an Mev; see Figure 3.7 (curve-a, dotted line, **p. 72**).

In view of the above limiting estimates I would expect that the magnitude of increase in the activity of the Galactic center would be in the range of $10^5 - 10^8$ fold. With an increase of this magnitude our Galaxy would probably adopt the appearance of a Seyfert galaxy such as NGC 4151; see Figure 3.3. Or, if viewed edge-on to the galactic plane, it might appear as a giant elliptical radio galaxy similar to Centaurus A (NGC 5128) shown in Figure 2.16(a) (**p. 43**). For comparison, the radio luminosities of the nuclei of several different kinds of galaxies are shown in Figure 3.4 normalized to the present radio luminosity of the GC ($\sim 10^{33}$ ergs/s). The luminosities recorded for these galaxies are accurate to the nearest order of magnitude (K.I. Kellermann, personal communication, 1982). It should be kept in mind that the cosmic ray luminosities of these various galaxies may not necessarily scale in proportion to their relative radio luminosities. For example, as is mentioned in Chapter 2 (**pp. 34-36, 40**), the amount of radiation beamed from the nucleus of an active galaxy may depend not only on the intensity of the cosmic ray outburst, but on the nature of the encountered interstellar medium as well. The column density of interstellar gas and the direction of the interstellar magnetic field lines intervening along the line of sight would be important variables since they would determine the degree to which the cosmic ray blast would become decelerated, i.e., the fraction of energy that would be converted into electromagnetic radiation.

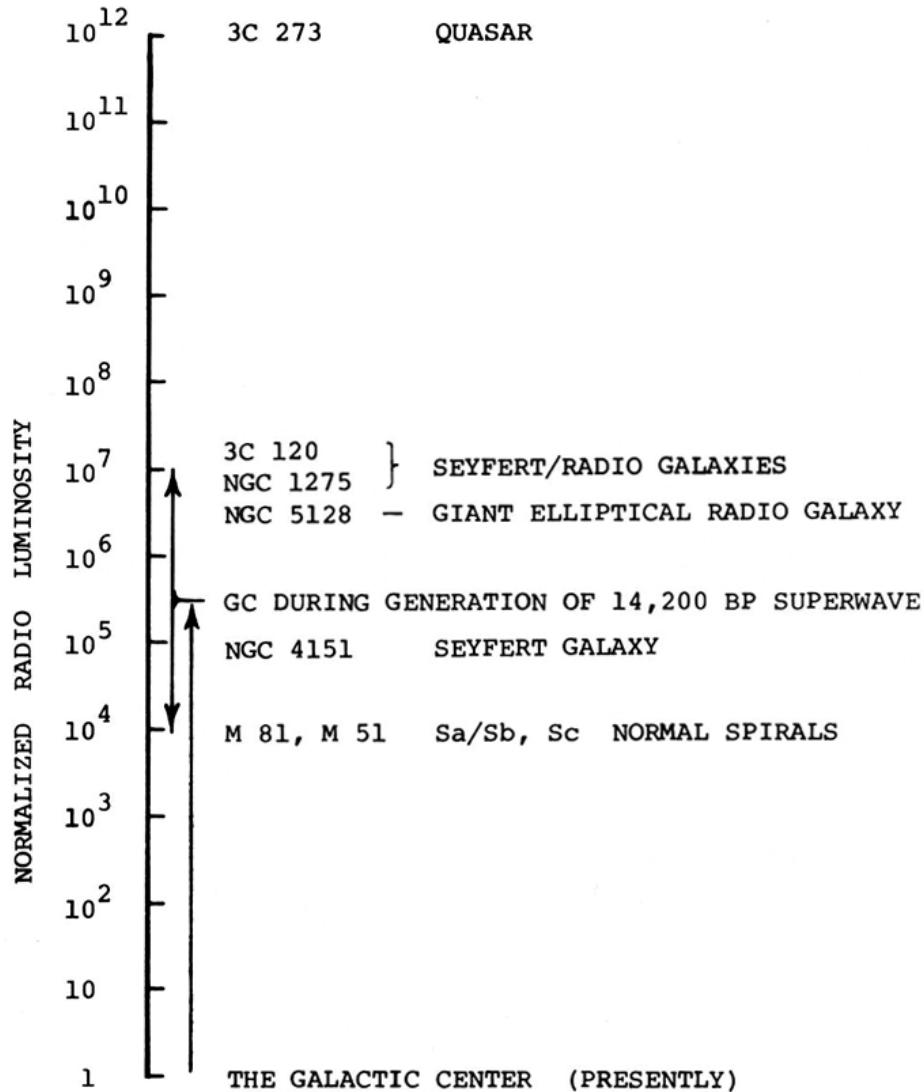


Figure 3.4. A comparison of the radio luminosities of the nuclei of various kinds of galaxies normalized to the radio luminosity of the Galactic center ($\sim 10^{33}$ ergs/s).

3.2 PROPAGATION

Next, it is necessary to consider what transformation, if any, occurs to the cosmic ray blast as a result of travelling 22,800 l.y. through the interstellar medium: Stage B as shown in Figure 3.1.

The differing travel times of the particles would not significantly disperse the blast since the particles are assumed to be travelling at velocities very close to the speed of light. For example, a 1 Gev electron would have a Lorentz factor $\gamma = E/m_0c^2 = 2000$; consequently, the amount of delay in its time of arrival (compared to that of a photon) would be one day, i.e., $t = 22,800(1 - \beta)$ years, where $\beta = v/c = (1 - 1/\gamma^2)^{-1/2}$. A 10 Mev electron having a γ of 20 would be delayed only 29 years. Since the bulk of the energy in the superwave would be conveyed by particles having kinetic energies greater than 10 Mev, the shape of the power-time profile shown in Figure 3.2 would be preserved almost unchanged during the journey from the Galactic center.

It is natural at this point to inquire whether the proposed blast would survive the journey through the Galaxy to the Earth, or would it become arrested due to interactions with the interstellar medium. Consider first a situation in which no magnetic field is present either in the relativistic particle outburst or in the interstellar medium through which it passes. Energy losses, then, would be primarily attributable to collisions and radiative interactions between cosmic ray particles and particles in the interstellar medium, e.g., electrons and protons (hydrogen nuclei). Under these circumstances, the amount of energy loss would be determined by the column density of the interstellar medium integrated over the line of sight between the Earth and the Galactic center. For example, cosmic ray electrons attenuate in hydrogen according to the relation:

$$E(x) = E_0 \exp(-x/138 \text{ g/cm}^2), \quad (5)$$

where x is the encountered column density of material in grams/cm^2 , and where 138 g/cm^2 is the *radiation length* for relativistic electrons in hydrogen (i.e., the distance over which the energy falls to $1/e$, or 0.368 of its original value). Given an interstellar hydrogen density of about $0.04 \text{ particles/cm}^3$, then over a distance of 22,800 l.y. the column density would amount to $\sim 10^{-3} \text{ g/cm}^2$. According to relation (5), the primary cosmic ray electrons would lose only $\sim 10^{-5}$ of their initial energy by the time they reached the Earth.

Consider now, at the other extreme, a situation in which the cosmic ray outburst is in the form of a relativistically propagating plasma containing a frozen-in magnetic field and where the outburst encounters an interstellar medium also having a magnetic field. As is discussed in Subsection 2.1.2, in such a plasma the particles would exhibit collective behavior forming an impermeable-fluid-like barrier to the encountered medium. Such a model would predict maximum interaction between the cosmic ray outburst signal and the interstellar medium, with the signal accelerating any encountered gas to its own bulk velocity. An outburst having a total energy of $\sim 10^{58}$ ergs (as proposed for the 14,200 years BP superwave Model) propagating outward as a spherical shell, would travel no more than a few tens of light years before being decelerated to subrelativistic velocities. To penetrate to the solar vicinity and to maintain relativistic speeds a total energy of 4×10^{63} ergs would have had to be expended, i.e., almost 10^6 times the amount of energy in the proposed outburst. Moreover, the present gas-congested state of the Galactic disk rules out the possibility that such a widespread sweeping-out of the Galaxy has recently taken place; nor is such behavior compatible with the observed morphology of other spiral galaxies.

The Superwave Model, adopted in the GEH, takes a more middle-of-the-road position. The cosmic ray barrage is assumed to be free of a magnetic field, as in the first case considered, and an interstellar magnetic field is assumed to be present in the Galaxy but oriented radially with respect to the GC. The energy density of the local interstellar magnetic field is given as: $u_m = B^2/8\pi = (3 \times 10^{-6} \text{ gauss})^2/8\pi = 3.6 \times 10^{-13} \text{ ergs/cm}^3$, and the energy density that the proposed particle blast would have in the solar vicinity at peak intensity is $u_e \sim 10^{-9} \text{ ergs/cm}^3$. So, even as far as the solar galactocentric distance, the particle barrage would have an energy density 10^4 fold greater than the energy density of the Galactic magnetic field, and hence would control the dynamics of the field. The radial orientation of the Galactic magnetic field would be maintained by periodic superwave passages. A residual interstellar wind periodically propelled by passing superwaves might also be effective in keeping the Galactic magnetic field combed out in a radial direction. Thus the bulk of the relativistic particle barrage would be expected to travel radially outward through the Galaxy relatively unimpeded.

With the assumption that the magnetic field is at rest in the Galaxy's frame of reference, rather than propagating through the disk relativistically, the problem of excessive energy loss to the interstellar medium is avoided; see Chapter 2, **p. 31**. Still, there would be

some regions in the Galaxy where the magnetic field would be oriented transverse to the direction of superwave propagation, and in such regions radial cosmic ray propagation would be impeded, e.g., in gas rings or in certain regions within spiral arms. Thus, some fraction of the particle energy would be expected to become transferred to the interstellar medium. As is discussed in Chapter 2, heating and radial propulsion of the interstellar medium to hundreds of kilometers per second is observed in the nuclei of many active spiral galaxies and in ring-like formations in the disks of spirals, in some cases located up to 100,000 l.y. from the nucleus. A model which assumes that no interaction takes place between the particle barrage and the interstellar medium would not be able to account for these features. Similarly, a model which assumes maximal interaction (e.g., relativistic blast wave models) also runs into difficulty because its effects necessarily would be confined to the interior nuclear region of the galaxy. On the other hand, by proposing moderate interaction with the interstellar medium, the Superwave Model can account for such features.

The cosmic ray volley would interact very strongly with the interstellar medium wherever young supernova remnants would be encountered. The remnant blastwave would be composed of a fluid-like, magnetically-bound plasma which would compress and reorient the interstellar magnetic field lines which it encountered into a transverse direction. The remnant would present a unified impermeable barrier to the superwave causing the cosmic ray trajectories to become bent from their straight line course and to ultimately spiral around magnetic lines of force both in the bow shock front surrounding the remnant and in the remnant itself. The consequences of the interaction between a superwave and a supernova remnant are discussed further in Chapter 5 (Subsections 5.3, 5.4, and 5.5). Magnetic field sheaths surrounding individual stars would be another region where the superwave cosmic rays would strongly interact and become captured into synchrotron radiating orbits; see **p. 87**.

It is not the objective of this study to develop a detailed quantitative model of how the proposed blast would interact with the interstellar medium, but rather to make qualitative statements in this regard and to show that they are supported by observational evidence. For the 14,200 years BP superwave it is assumed that about a 20% reduction of cosmic ray intensity occurs along the path between the Galactic center and the Sun, and that an average of 2% of the total energy of the superwave becomes transferred to the interstellar medium in the nucleus and disk of the Galaxy (when all propagation directions are averaged). This comes to about 5×10^{56} ergs for both outbursts associated with the 14,200 years BP superwave. By comparison, it has been suggested that the molecular ring cloud in the nucleus of the Galaxy required at least $10^{55} - 10^{56}$ ergs to reach its present position (Oort, 1977); also see Subsection 4.2. This amount of kinetic energy could be accounted for if ~0.1% of the superwave's total energy (10% of its "lost" energy) became coupled to this gas. It is assumed that the electrons that are lost from the superwave are primarily those having energies of less than 100 Mev. In particular, electrons having $E < 5$ Mev would be heavily attenuated during the journey through the Galactic disk since, as a result of their low velocity relative to the more energetic electrons, these would tend to lag behind the main blast and become more easily captured by interstellar magnetic fields.

Finally, a word about the configuration of the Galactic magnetic field and how the outbursts would affect it. Faraday rotation measurements of extragalactic radio sources provide one indication that the Galactic magnetic field is directed radially with respect to the GC. For example, as is seen in Figure 3.5(a) (Simard-Normandin and Kronberg, 1980), in the region close to the GC between $\ell = 0^\circ$ and $\ell = 45^\circ$ large positive rotation measures are found indicating the presence of a magnetic field component directed toward the Sun. Simard-Normandin and Kronberg (1980, p. 83) note that the high rotation measures in this region (50 to 300 rad/m²) suggest that this field orientation persists along the line of sight for a distance of ~3 kpc. Taking the Sun's galactocentric distance to be about 7 kpc, this

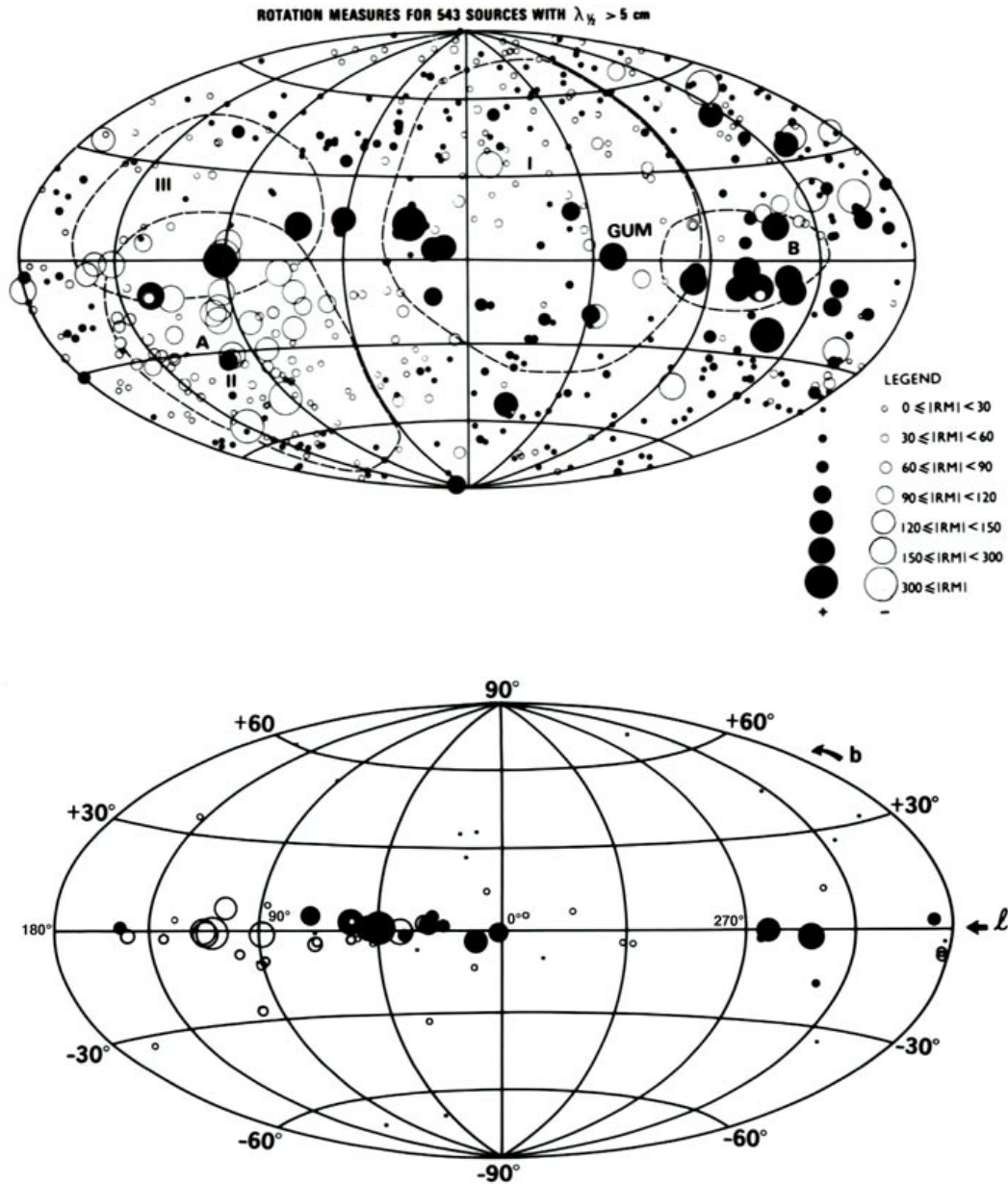


Figure 3.5. Top: The distribution of Faraday rotation measures for 543 extragalactic sources. Bottom: The distribution of rotation measures for a collection of Galactic pulsars (Simard-Normandin and Kronberg, 1980).

represents about 40% of the distance from the Sun to the GC. The map of rotation measures observed for pulsars found in our Galaxy also indicates the presence of a substantial component of the Galactic magnetic field directed toward the Sun from the direction of the GC; see Figure 3.5(b) (Simard-Normandin and Kronberg, 1980). A galactic-center-directed magnetic field would be consistent with the direction of the local interstellar wind (see Section 4.6) and with the direction of cosmic ray electron flow inferred from the anisotropy in the distribution of the microwave background radiation (see Appendix B).

Little is known about the orientation of the Galactic magnetic field in the Galactic Nucleus. However, in view of evidence that radial interstellar gas motions are found at of

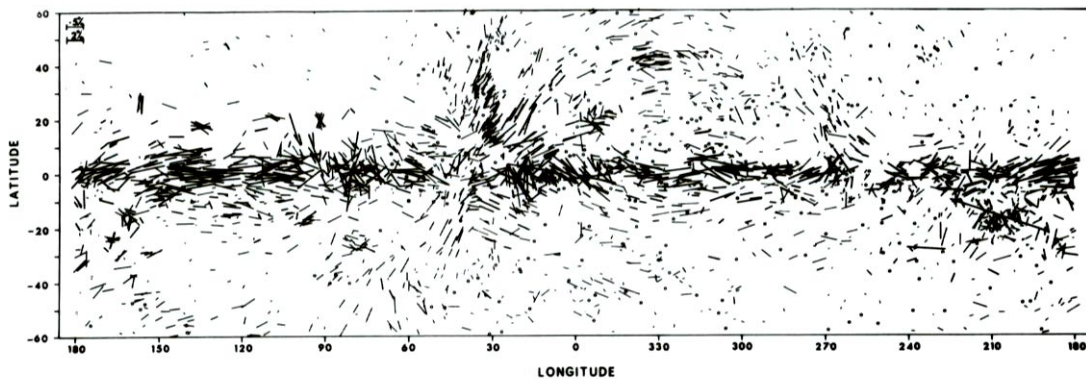


Figure 3.6. The polarization of starlight in the Galaxy. The data is plotted according to Galactic coordinates. The angle of each line indicates the direction of the electric vector for a given star. Small circles indicate a polarization $P < 0.08\%$, thin lines $P < 0.6\%$, and thick lines $P > 0.6\%$. Length of the lines is proportional to the percentage of polarization; see scale at top left (Mathewson and Ford, 1970).

up to 3 kpc from the GC (see Chapter 4, Sections 4.1 – 4.4) it is reasonable to conclude that in this inner region of the Galaxy the magnetic field also has a radial orientation. Together with the Faraday rotation observations discussed above it is reasonable to conclude that a considerable portion of the Galactic magnetic field extends radially all the way from the GC to the solar vicinity.

Observations of the direction of starlight polarization have been used as another means of inferring the direction of the Galactic magnetic field in the solar neighborhood ($d < 4$ kpc). As seen in Figure 3.6 (Mathewson and Ford, 1970), starlight is polarized parallel to the Galactic plane. There is, however, some ambiguity involved in interpreting whether the magnetic field is oriented parallel or perpendicular to the plane of starlight polarization. One mechanism, suggested by Spitzer and Tukey (1951), involves the alignment of ferromagnetic interstellar dust grains, or needle crystals, with their long axes parallel to a Galactic magnetic field that is itself oriented *perpendicular* to the Galactic plane. Such grains would preferentially absorb light vibrations oriented parallel to their long axis leaving the starlight polarized in a direction perpendicular to this axis. The properties of iron grains are discussed by Fick (1955) and Zimmermann (1957), and the formation of these grains is studied by Spitzer and Schatzman (1949). Iron filaments have strong polarizing properties (Hall and Serkowski, 1963, p. 307; van de Hulst, 1955) and are capable of producing not only linear, but circular polarization as well (Serkowski, 1960). Moreover, ferromagnetic elements such as Fe and Ni are among the most common of elements believed to be present in the interstellar medium.

Another mechanism suggested by Davis and Greenstein (1951) is that this effect is caused by elongated paramagnetic interstellar dust grains oriented perpendicular to the Galactic magnetic field which in this case would lie *parallel* to the Galactic plane. To account for this perpendicular orientation, they suggest that the grains are spinning about an axis that is parallel to the interstellar magnetic field which is oriented parallel to the Galactic plane. The spin axis of these particles would attain this preferred orientation through a process called "paramagnetic relaxation," in which the dynamic motion of the spinning particle sets up a field which interacts with the Galactic magnetic field. Though compared with ferromagnetic grains, paramagnetic grains would be much less efficient in polarizing light, in view of the amount of light extinction they would produce (van de Hulst,

1955). Also, Heiles (1976, pp. 19-20) reviews several reasons why it might be better to assume parallel alignment of dust grains, rather than perpendicular alignment. Regardless of which interpretation that one chooses, the presence of polarized starlight in the Galactic center direction ($330^\circ < l < 30^\circ$) and in the anticenter direction ($150^\circ < l < 210^\circ$) suggests that there is a component to the Galactic magnetic field which lies transverse to the line of sight. Such would be expected even for a field directed radially from the GC.

3.3 ARRIVAL

This section assesses the possible effects on the Earth (and on the Sun) due to the passage of the proposed superwave (Figure 3.1, box 3).

3.3.1 Superwave Cosmic Ray Electron Intensities Outside the Solar System, in the Inner Solar System, and at the Earth's Surface

The differential particle number flux spectrum of the 14,200 years BP superwave in the solar vicinity is represented by curve (a) (solid line) in Figure 3.7. The downward curvature of the spectrum at low energies $E < 100$ Mev is due to heavy losses of electrons in this spectral region as a result of the superwave's journey through the Galactic disk. The dotted line (spectral index $\Gamma = 1.8$) suggests how the spectrum would have appeared at the time of generation at the Galactic center.

The peak intensity of the 14,200 years BP superwave in the solar vicinity may be determined by dividing the total outburst power, reduced by $\sim 20\%$ to account for propagation losses, by the surface area of a sphere having a radius equal to the Sun's distance from the GC. Thus $I = P/\Sigma = (6 \times 10^{47} \text{ ergs/s}) / (6.5 \times 10^{45} \text{ cm}^2) \sim 90 \text{ ergs/cm}^2/\text{s}$ (for the first outburst). The *directed* energy density for this blast is given as $u_e = I/c = 3 \times 10^{-9} \text{ ergs/cm}^3$. The *average* energy density that a spherical surface would receive if these cosmic ray electrons were directionally modulated such that they propagated with equal probability in all directions, would be one-fourth of this amount or $u_e \sim 7.5 \times 10^{-10} \text{ ergs/cm}^3$. This is about 750 times higher than the solar modulated cosmic ray proton energy density ($10^{-12} \text{ ergs/cm}^3$) currently observed in the Earth's vicinity (spectrum shown as curve (e) in Figure 3.7), and is about 75,000 times higher than the presently observed cosmic ray electron energy density ($10^{-14} \text{ ergs/cm}^3$) presently observed in the Earth's vicinity (spectrum shown as curve (d) in Figure 3.7).

The cosmic ray electron spectrum that is inferred currently to be present near the solar system beyond the modulating effects of the solar wind and heliopause sheath is represented by curve (c) in Figure 3.7 ($\Gamma = 1.8$ for $E < 1.5$ Gev; $\Gamma = 2.75$ for $E > 1.5$ Gev). This is similar to the theoretical curve suggested by Goldstein, Ramaty, and Fisk (1970). At peak intensity the proposed superwave spectrum (curve a) would be $\sim 1.2 \times 10^5$ times more intense than the present unmodulated electron spectrum (curve c), when compared at 10 Gev. In terms of average *energy density* the magnitude of increase is one-fourth of this, or $\sim 3 \times 10^4$ fold higher.

Superwave cosmic ray electrons reaching the Earth's surface would be the survivors of three filtering agents: a) the superwave's bow shock front and the heliopause sheath, b) the geomagnetic field, and c) the Earth's atmosphere. Consider first the effect of cosmic ray modulation caused by the bow shock front and heliopause sheath.

The Effect of the Superwave Bow Shock Front and the Heliopause Sheath. The solar system is surrounded by a sheath-like region called the heliopause where the solar wind and

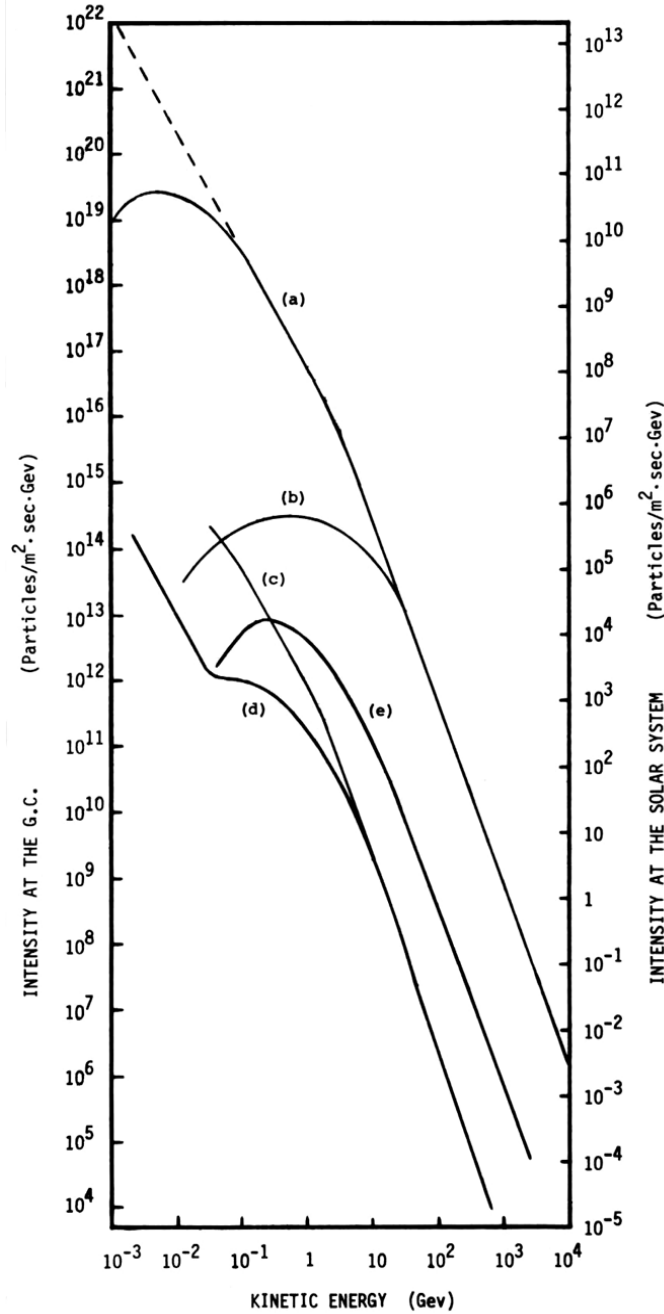


Figure 3.7. Differential particle number intensity spectra: a) for the cosmic ray electron flux proposed for the 14,200 years BP superwave at peak intensity, as it would appear at a galactocentric distance of one l.y. (left hand scale) and at a galactocentric distance of 22,800 l.y., the solar system distance (right hand scale); **b) for the 14,200 years BP superwave in the Earth's vicinity after modulation by the bow shock front and heliopause sheath;** c) proposed for the current cosmic ray electron flux in the vicinity of the solar system (unmodulated); d) for the current modulated cosmic ray electron background observed in the Earth's vicinity at solar minimum; and e) for the current modulated cosmic ray proton background observed in the Earth's vicinity at solar minimum. Curves d) and e) are based on data plotted in Figure III-15 of Ramaty (1974, p. 160).

interplanetary magnetic field confront the interstellar environment; see **p. 85**. Upon impacting the heliopause the proposed superwave would form a bow shock front behind which the interstellar magnetic field would become compressed; cf. **p. 89**. The turbulent magnetic field in the heliopause and behind the bow shock front would capture superwave electrons. Hence the cosmic ray intensity of the superwave would become reduced in the inner portion of the solar system and as a result the shape of the differential particle number flux spectrum would change; see curve (b) in Figure 3.7. This "modulated" differential particle number flux spectrum has been drawn to approximate that of the cosmic ray electron spectrum presently observed in the Earth's vicinity at solar maximum (cf. Urch and Gleeson, 1972), except that a greater degree of intensity reduction is assumed (e.g., about an order of magnitude greater at 1 Gev) and the modulation is assumed to begin taking its toll at 30 Gev rather than at 10 Gev. Both of these modifications are justified since the magnetic field lines in the heliopause sheath and behind its associated bow shock front would be considerably more compressed during the superwave event.

Curves (a) and (b) in Figure 3.7 were used to construct energy flux histograms for the superwave, before and after being modulated by the bow shock front and heliopause sheath; see Figure 3.8. The two histograms plot the fractional particle energy $\Delta Q_i/Q$ and $\Delta Q_i'/Q$ (before and after modulation) incident in a given particle energy range ΔE_i . The data entries for this diagram are listed in Table III, columns (6) and (9), and are derived as follows. To begin with, a series of energy intervals ΔE_i are selected (column 1). Corresponding to each of these intervals, average energies \bar{E}_i are calculated (column 2) along with the number of Mev channels n_i which they contain (column 3). Then the differential particle number flux dN_i and dN_i' (columns 4 and 7) for each interval is determined from Figure 3.7 (curves a and b; right hand scale), where the values tabulated reflect levels in the solar vicinity at peak superwave intensity. Next, the differential energy spectrum ΔQ_i and $\Delta Q_i'$ (columns 5 and 8) is calculated by multiplying $\Delta Q_i = \bar{E}_i \cdot dN_i \cdot n_i$. The resulting subtotal integral energy fluxes, $Q = 5.51 \times 10^8$ Gev/m²/s and $Q' = 5.92 \times 10^7$ Gev/m²/s, are then used to determine the fractional energy fluxes ($\Delta Q_i/Q$ and $\Delta Q_i'/Q$) which each interval represents (columns 6 and 9).

By comparing the two histograms shown in Figure 3.8, it is seen that the heliopause and the bow shock front produce about a tenfold reduction in the integral cosmic ray energy intensity, i.e., $I_{\text{before}} \sim 90$ ergs/cm²/s and $I_{\text{after}} \sim 9$ ergs/cm²/s. Also the mean particle energy becomes shifted upward about 10 to 20 fold from about 1 – 2 Gev to about 20 Gev, due to the fact that modulation is energy selective. For example, very energetic particles whose trajectories are bent only slightly by the magnetic fields in the shock front regions will be able to penetrate into the interior cavity of the heliopause relatively easily. On the other hand, less energetic particles whose trajectories would have a small radius of curvature compared to the thickness of the shocked region would either become captured in synchrotron radiating orbits or deflected around the sheath.

Whether or not a cosmic ray would be able to penetrate to the Earth's vicinity would depend on its magnetic rigidity, or alternatively on the particle's kinetic energy. Particles having a high magnetic rigidity or high kinetic energy would most easily penetrate. The magnetic rigidity of a particle, \overline{BR} , is an invariant quantity calculated by multiplying the ambient magnetic field strength B by the corresponding radius of curvature of the particles trajectory through this field R . The magnetic rigidity of an electron (expressed in gauss cm) may be determined from its kinetic energy E (expressed in electron volts) by the formula $\overline{BR} = E/300$. Thus, a 100 Gev electron would have a magnetic rigidity of $\overline{BR} = 3.3 \times 10^8$ gauss cm. If the magnetic field in the heliopause and bow shock front region had a strength $B \sim 10^{-4}$ gauss, then the trajectory of this particle would have a radius of curvature of $R = \overline{BR}/B = 3.3 \times 10^{12}$ cm ~ 0.2 AU. This is comparable with the thickness of the heliopause, as suggested by the sketch shown in Figure 3.14 (**p. 86**) and is probably much larger than the scale-size of inhomogeneities that would be present in the sheath's magnetic

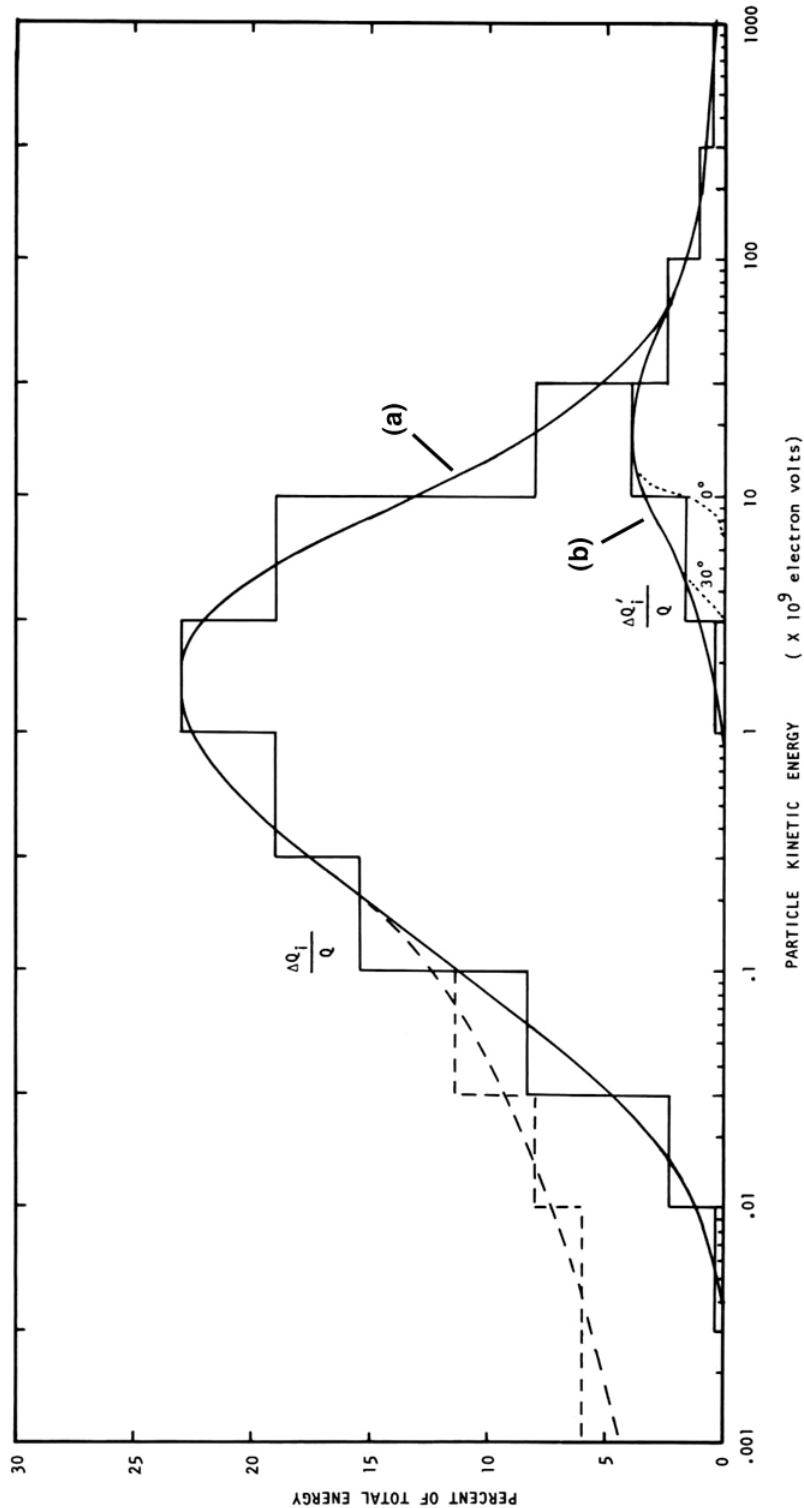


Figure 3.8. Cosmic ray energy flux histograms for the 14,200 years BP superwave: a) outside the bow shock front $\Delta Q_i/Q$, and b) in the vicinity of the Earth $\Delta Q'_i/Q$. The dashed line extension of curve a) illustrates how the profile might appear in the vicinity of the Galactic center. Dotted lines under curve b) illustrate the effects of geomagnetic modulation at geomagnetic latitudes $\lambda = 0^\circ$ and $\lambda = 30^\circ$.

TABLE III
THE ENERGY FLUX HISTOGRAM FOR THE PROPOSED COSMIC RAY
OUTBURST AND THE EFFECT OF HELIOPAUSE MODULATION

| (1) | (2) | (3) | (4) | (5) | (6) | (7) | (8) | (9) |
|----------------------------------|-------------------|-------------------|--|---|---------------------------------|---|--|------------------|
| ΔE_i (Gev) | E_i (Gev) | n_i | dN_i (part./m ² •s•Mev) | ΔQ_i (Gev/ m ² •s) | $\Delta Q_i/Q$ | dN_i' (part./m ² •s Mev) | $\Delta Q_i'$ (Gev/ m ² •s) | $\Delta Q_i'/Q$ |
| 10 ⁴ -10 ⁵ | 3×10 ⁴ | 9×10 ⁷ | 10 ⁻⁷ | 2.7 ×10 ⁵ | 0.0005 | 10 ⁻⁷ | 2.7 ×10 ⁵ | 0.0005 |
| 3000-10k | 5000 | 7×10 ⁶ | 10 ⁻⁵ | 3.5 ×10 ⁵ | 0.0006 | 10 ⁻⁵ | 3.5 ×10 ⁵ | 0.0006 |
| 1000-3000 | 1700 | 2×10 ⁶ | 3×10 ⁻⁴ | 1.02×10 ⁶ | 0.0018 | 3×10 ⁻⁴ | 1.02×10 ⁶ | 0.0018 |
| 300-1000 | 500 | 7×10 ⁵ | 8.1×10 ⁻³ | 2.84×10 ⁶ | 0.005 | 8×10 ⁻³ | 2.84×10 ⁶ | 0.005 |
| 100-300 | 170 | 2×10 ⁵ | 0.18 | 6.12×10 ⁶ | 0.011 | 0.18 | 6.12×10 ⁶ | 0.011 |
| 30-100 | 50 | 7×10 ⁴ | 4.5 | 1.58×10 ⁷ | 0.029 | 4.5 | 1.58×10 ⁷ | 0.029 |
| 10-30 | 17 | 2×10 ⁴ | 130 | 4.42×10 ⁷ | 0.080 | 64 | 2.18×10 ⁷ | 0.040 |
| 3-10 | 5 | 7×10 ³ | 3000 | 1.05×10 ⁸ | 0.190 | 260 | 9.10×10 ⁶ | 0.017 |
| 1-3 | 1.7 | 2×10 ³ | 3.7×10 ⁴ | 1.26×10 ⁸ | 0.229 | 640 | 2.18×10 ⁶ | 0.004 |
| 0.3-1 | 0.5 | 700 | 3.0×10 ⁵ | 1.05×10 ⁸ | 0.190 | 570 | 2.0 ×10 ⁵ | 0.0004 |
| 0.1-0.3 | 0.17 | 200 | 2.5×10 ⁶ | 8.5 ×10 ⁷ | 0.154 | 290 | 9.9 ×10 ³ | 10 ⁻⁵ |
| 0.03-0.1 | 0.05 | 70 | 1.3×10 ⁷ | 4.55×10 ⁷ | 0.083 | — | — | — |
| 0.01-0.03 | 0.017 | 20 | 3.7×10 ⁷ | 1.26×10 ⁷ | 0.023 | — | — | — |
| 0.003-0.01 | 0.005 | 7 | 5.3×10 ⁷ | 1.86×10 ⁶ | 0.003 | — | — | — |
| Q = 5.51×10 ⁸ total | | | | | Q' = 5.92×10 ⁷ total | | | |

field. Hence the majority of these particles would pass through the heliopause. For 1 Gev electrons, on the other hand, the trajectory would have a radius of curvature of only about 0.002 AU. Consequently, a large fraction of these particles would either become deflected or magnetically trapped in the heliopause. Those succeeding in entering the inner portion of the solar system would do so by a very slow process of diffusion through the sheath.

Besides reducing the intensity and changing the spectrum of the superwave blast, the bow shock front and heliopause sheath would also directionally modulate the incident cosmic rays, particularly those having a low magnetic rigidity. Particles having "low" kinetic energies ($E < 100$ Gev) would be made completely isotropic in their directional distribution. Hence they would impact the Earth uniformly from all directions. On the other hand, particles having high kinetic energies ($E > 1000$ Gev) would maintain their original straight line trajectories. Hence they would impact the Earth primarily from the direction of the Galactic center. Superwave cosmic rays of intermediate kinetic energy (100 Gev to 1000 Gev) would be anisotropically distributed to varying degrees depending on their respective magnetic rigidities.

At the superwave's peak intensity the Earth's magnetopause would be exposed to an average energy density of $\sim 7.5 \times 10^{-11}$ ergs/cm³ which is about 10% of the unmodulated average energy density of the superwave and about 75 times the present local energy density of the cosmic ray proton background radiation. At this peak intensity the 14,200 years BP superwave would cause only about a 10% increase in the terrestrial C-14 reservoir; see Appendix A. Thus the superwave cosmic ray intensity proposed to impact the

Earth is of reasonable magnitude. That is, the proposed superwave would not be expected to produce any large fluctuations in C-14 that might conflict with the geologic record.

The Screening Effect of the Geomagnetic Field. The geomagnetic field would have only a minor effect in further reducing the intensity of the superwave blast. Low energy cosmic rays, which the geomagnetic field would be effective in capturing and screening out, would already have been heavily filtered out by the bow shock front and heliopause sheath. Moreover, the high energy cosmic rays which would be capable of penetrating through the heliopause to the inner solar system would also easily penetrate the geomagnetic field. As a rough estimate, at a geomagnetic latitude of $\lambda = 0^\circ$, where the geomagnetic field is strongest, the total energy intensity of the cosmic ray blast penetrating to the Earth's upper atmosphere would be about 80% of the incident intensity, as a result of the elimination of cosmic rays having $E < 10$ Gev. At geomagnetic latitude $\lambda = 30^\circ$, about 90% of the total energy flux would survive since a larger fraction of cosmic rays in the 3 to 10 Gev energy range would be able to penetrate. The truncation of the differential energy spectrum produced by geomagnetic modulation at geomagnetic latitudes $\lambda = 0^\circ$ and $\lambda = 30^\circ$ is illustrated in Figure 3.8 by the dotted lines.

The Effect of the Earth's Atmosphere. As the incident cosmic ray electrons began to penetrate through the Earth's atmosphere, they would have initiated photon-electron cascades, single primary cosmic ray electrons giving rise to numerous secondary electrons. Such a *cascade process* was first proposed by Rossi (1952, Chapter 5) to account for the production of cosmic ray electron showers presently observed in the atmosphere. The process by which a single particle might induce a shower of multiple particles may be understood as follows. As a primary cosmic ray encounters air molecules in its trajectory, it becomes deflected, emitting electromagnetic (bremsstrahlung) radiation. The bremsstrahlung spectrum, being rather flat, contains most of its energy at the very high frequency end. Consequently, the majority of this wave energy is radiated in the form of γ -ray photons. A gamma ray generated by a parent primary electron, upon collision, would be able to generate two relativistic electrons (one plus and one minus) through the pair production process. These progeny in turn would each be able to generate at least one gamma ray bremsstrahlung photon apiece. So, with each photon/electron cycle a doubling would occur. Provided that electrons are generated through this self-reinforcing process faster than they are lost via ionization and atomic excitation, their population would tend to increase. At a certain point, however, the cascade would begin to become spent and consequently its population of electrons and gamma rays would plateau and finally decrease with increasing atmospheric depth.

Figure 3.9 illustrates how the population of secondary particles would vary as a function of atmospheric depth for an air shower initiated by a 10 Gev, 10^3 Gev, and 10^5 Gev electron primary (Rossi, 1952, Chapter 5, Figure 5.13.2). The ordinate plots the log of Π , the total number of secondary electrons in the shower having energies greater than $E = 100$ Mev, as a function of radiation length X_0 . The *radiation length* is the distance in grams per cm^2 of material traversed, over which a particle must travel for its energy to fall to $1/e$ (or 0.368) of its initial value. The radiation length for air is $X_0 \sim 38 \text{ g/cm}^2$ (Rossi, 1952, p. 295). As seen here, at an atmospheric depth of $X \sim 4X_0$ ($\sim 150 \text{ g/cm}^2$, or an altitude of $\sim 13 \text{ km}$) a 10 Gev electron would produce a maximum shower population of 15 secondary electrons having $E > 100$ Mev. However, there would only be about a 0.02% chance that any of the progeny of this shower would actually reach sea level at $27 X_0$ ($\sim 1033 \text{ g/cm}^2$). On the other hand, a 10^5 Gev electron would produce such a powerful cascade that at sea level 5000 secondary electrons would still be left in the shower. The value $E = 100$ Mev is chosen as a cutoff point in these estimates since this is close to the value of the critical energy, which for air is $\epsilon_0 =$

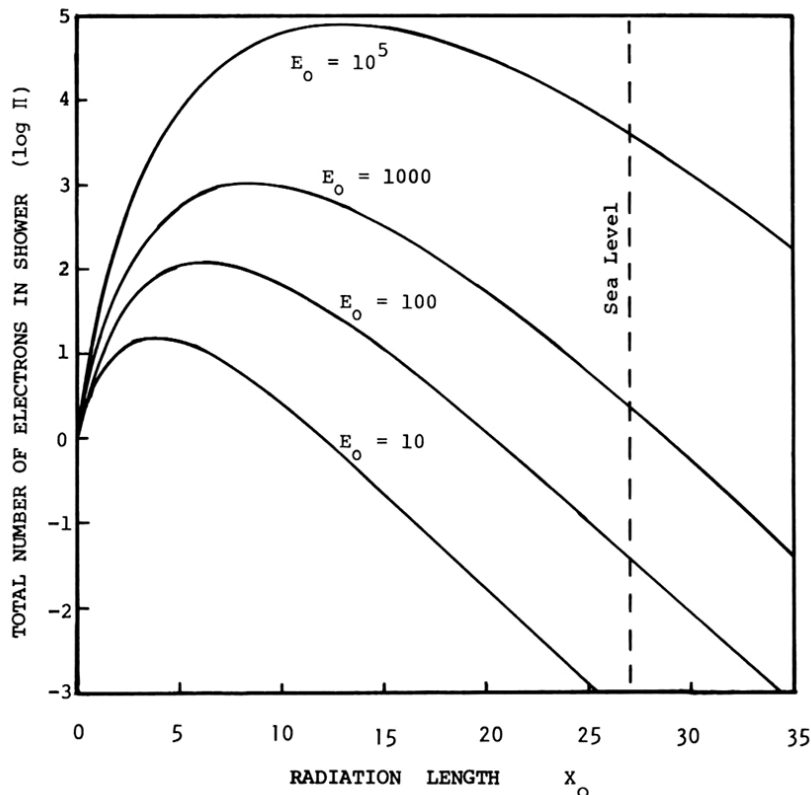


Figure 3.9. The total number of secondary electrons $\Pi(E_0, X_0)$ of energy greater than $E = 100$ Mev in a shower initiated by an electron of energy E_0 plotted as a function of radiation length X_0 (based on computations of Rossi, 1952, Chapter 5, Figure 5.13.2).

83 Mev. For $E > \epsilon_0$ techniques for computing Π become less accurate. The critical energy is the amount of energy that a particle gives up to the ambient medium as a result of ionization while traversing one radiation length.

The integral particle number flux that would reach sea level at geomagnetic latitudes $\lambda = 0^\circ$ and 30° , at the time when the superwave presented its peak intensity, may be estimated with the help of Table IV. Column 1 lists a series of 9 energy intervals ΔE_i ; cf. Table III, column 1 (p. 75). Column 2 lists the average energy \bar{E}_i corresponding to each of these 9 intervals. Column 3 lists ΔN_i , the total number flux (particles/m²/s) contained in each of these intervals; calculated from Table III (column 3 \times column 7). Column 4 gives the ratios $\bar{E}_i / 100$ Mev based on the values listed in column 2. Corresponding to the values listed in column 4, column 5 lists the Π_i values representing the number of secondary electrons reaching sea level (of energy greater than 100 Mev) that would be spawned by a primary electron in that energy interval. These Π_i estimates are based on the assumption that all of the particles reaching the Earth's upper atmosphere penetrate the atmosphere vertically. Column 6 lists for each energy interval the flux of particles that would be expected to reach sea level; e.g., column 6 = column 3 \times column 5.

As can be seen from the intensity distribution listed in column 6 of Table IV, 99% of the flux of secondary electrons at sea level is produced by electron primaries having energies $E > 10$ Gev. The geomagnetic field consequently would offer little protection, producing at most a 1% reduction in ground level flux. If all of the incident particles were to penetrate the atmosphere vertically, the flux at sea level would be about 2 electrons/cm²/s or about 1000 times higher than the current sea level radiation flux, which is estimated to be ~ 0.002 electrons/cm²/s/str. However, a more realistic estimate for a time-averaged flux would be

TABLE IV
DETERMINATION OF THE INTEGRAL NUMBER FLUX
OF SECONDARY ELECTRONS REACHING SEA LEVEL

| (1) | (2) | (3) | (4) | (5) | (6) |
|----------------------------------|-------------------|---------------------------|-----------------------------|------------------|---------------------------|
| ΔE_i | \bar{E}_i | ΔN_i | $\bar{E}_i/100 \text{ Mev}$ | Π_i | $\Delta \Phi_i$ |
| (Gev) | (Gev) | (part /m ² ·s) | | | (part /m ² ·s) |
| 10 ⁴ -10 ⁵ | 3×10 ⁴ | 9 | 3×10 ⁵ | 400 | 3600 |
| 3000-10,000 | 5000 | 70 | 5×10 ⁴ | 30 | 2100 |
| 1000-3000 | 1700 | 600 | 1.7×10 ⁴ | 5 | 3000 |
| 300-1000 | 500 | 5670 | 5000 | 0.7 | 3970 |
| 100-300 | 170 | 3.6 ×10 ⁴ | 1700 | 10 ⁻¹ | 3600 |
| 30-100 | 50 | 3.15×10 ⁵ | 5 00 | 10 ⁻² | 3150 |
| 10-30 | 17 | 1.28×10 ⁶ | 170 | 10 ⁻³ | 1280 |
| 3-10 | 5 | 1.82×10 ⁶ | 50 | 10 ⁻⁴ | 182 |
| 1-3 | 1.7 | 1.28×10 ⁶ | 17 | 10 ⁻⁵ | 13 |

total: $\Phi = 20,895$

1/4 π of this amount, i.e., ~0.16 electrons/cm²/s/str, or about 80 times the current average sea level cosmic ray electron flux. Thus the magnitude of the increase in the amount of ionizing radiation reaching the surface of the Earth would be comparable with the increase in the average cosmic ray density incident on the Earth.

3.3.2 Cosmic Dust and Gas Influx into the Solar System and Its Effect on the Transmission of Sunlight

Is it possible that this lash and chastisement are not given for our correction and amendment, but only for our total destruction and obliteration; that the sun will never more shine on us, but that we must remain in perpetual darkness and silence? . . . It is a sore thing to tell how we are all in darkness. . . . O Lord, . . . make an end of this smoke and fog. Quench also the burning and destroying fire of thine anger; let serenity come and clearness, let the small birds of thy people begin to sing and approach the sun.

(Prayer of the Aztecs addressed to the god Tezcatlipoca;
from Bancroft, 1874, p. 200)

If a superwave were to pass through the solar vicinity, then interstellar dust and gas and nearby nebular material would most likely become propelled into the inner part of the solar system. The present subsection constructs a reasonable model of the degree to which cosmic dust concentrations in the solar system might be expected to increase as a result of such an event and the effect that this would have on radiation transmission in interplanetary space and in the Earth's upper atmosphere. Also, an assessment is made of how the accretion of nebular material would affect the Sun's luminosity and level of solar flare activity. Resulting consequences to the Earth's climate are discussed in Subsection 3.3.4.

The Circumsolar Nebula of Cometary Material. To account for the frequent sightings of new comets with highly eccentric trajectories, Jan Oort (1950) has suggested that the solar system is surrounded by a huge cloud of comets extending from about 2×10^4 AU out to about 10^5 AU (1 l.y.) from the Sun. The comets in this so-called "Oort Cloud" would be gravitationally bound to the solar system, but from time to time, as a result of gravitational encounters with closely passing stars or gas clouds, a few of these would become nudged into highly eccentric orbits, and hence would make the journey to the inner part of the solar system where they would be observable. In the past it had been customary to place the inner boundary of the Oort Cloud at an heliocentric distance of about 2×10^4 AU. However, several authors (e.g., Whipple, 1975; Hills, 1982) have suggested that the circumsolar cometary cloud actually consists of an outer, observable portion (the traditional Oort Cloud inferred from observed cometary orbits) and an inner, much more massive unobservable portion, the "Inner Cometary Cloud." Thus the "inner edge" of the Oort Cloud would be due just to observational selection.

Whipple (1975) estimates that as much as $10^{-2} M_{\odot}$ may reside in the inner unobserved cometary cloud between an heliocentric distance of $50 \text{ AU} < r < 20,000 \text{ AU}$. Hills (1982) estimates that the observable Oort Cloud has a mass of about 0.15 earth masses (consisting of $\sim 2 \times 10^{11}$ cometary bodies), and that the Inner Cometary Cloud has a mass in the range of $10 - 10^4$ earth masses (about $100 - 10^5$ times the mass of the Oort Cloud). At the upper end of this mass range the Inner Cloud would have a total mass of approximately 3% of the Sun's mass, with more liberal (higher) mass estimates being possible. If the higher mass estimate of 20 – 30 solar masses is adopted for the Oort Cloud, such as that proposed by Napier and Clube (1979) and Clube and Napier (1982), then Hills's lower estimate for the mass of the Inner Cometary Cloud should be accordingly increased by 100 fold.

Hills suggests a median heliocentric distance for the Inner Cometary Cloud of about 3×10^3 AU, its inner edge possibly extending to within 50 – 100 AU from the Sun, just beyond the outer edge of the solar system. He estimates that the Inner Cometary Cloud may contain as much as $5 \times 10^{-3} M_{\odot}$ at an heliocentric distance of only about 100 AU, and points out that such a mass would be consistent with the observation that the orbits of many incoming comets (supposedly parabolic) appear to be perturbed toward hyperbolic trajectories. Also, Bailey (1983) shows that a simple extrapolation of the standard Oort Cloud theory to small heliocentric distances implies high cometary space densities on the order of 2×10^8 comets/AU³ at $r = 100$ AU. He notes that such a high-mass shell of unobservable cometary material located immediately outside of the solar system could be the source of the force perturbing the orbits of the outer planets.

In summary, according to the mass estimates quoted above, the average space density of cometary material in the immediate vicinity of the solar system may be as high as $10^{-3} - 10^{-4}$ earth masses per AU³, or as much as $10^{-14} - 10^{-16} \text{ g/cm}^3$ if this material were uniformly distributed. By comparison, this is about $10^5 - 10^7$ times higher than current interplanetary dust densities and about $10^3 - 10^5$ times higher than interplanetary dust densities required to account for the elevated cosmic dust deposition rates inferred for the end of the Wisconsin Ice Age; see text further on. Thus it may be concluded that sufficient cometary material exists in the immediate vicinity of the solar system in frozen form such that if at some time in the past a small fraction of this material ($\sim 10^{-5}$) had become vaporized and transported into the solar system by a passing superwave, a detectable increase in the cosmic dust deposition rate would very likely have been registered in the glacial record.

The Evolution of the Cometary Cloud and the Possible Role of the North Polar Spur.

There are at present two main schools of thought concerning the origin of the Circumsolar Cometary Cloud. One view (Oort, 1950; Cameron, 1975; Seargent, 1982, p. 102) suggests that the Cometary Cloud originated at the time that the solar system was being formed and

that it is a remnant of the primitive solar nebula. This "closed system" view assumes that the Cometary Cloud has had essentially no input from outside sources and that it has undergone relatively little change since the time of its formation, except for a possible depletion in the size of the initial cometary reservoir and a change of the orbital configurations. For example, Hills (1982) estimates that over a period of 4.5 billion years (the estimated age of the solar system) encounters with passing stars would have ejected about 3% of the total population of cometary bodies from the postulated Inner Cometary Cloud, a fraction of those ending up in the Oort halo.

The contesting view suggests that comets are primarily of interstellar origin. For example, Clube and Napier (1982) argue that close encounters with molecular clouds and with giant molecular clouds (GMCs), occurring about every few hundred million years, would have significantly perturbed the cometary population beyond an heliocentric distance of 1000 AU. They show that during a close approach a substantial number of cometary bodies formerly bound in heliocentric orbits would have been tidally stripped away by the passing GMC and would have been replaced (through gravitational capture by the Sun) by cometary bodies formerly residing in the GMC. According to this "open system" view, the composition of the Circumsolar Cometary Cloud would evolve over time, and most likely would be compositionally different from primitive solar system material.

The present study adopts an "open system" view of the Cometary Cloud, but in addition to close passages by stars and molecular clouds I would suggest that several other agents are responsible for the evolution of the cometary population, both in size and in composition. For example, the close passage of clouds of debris from nearby supernova explosions, *recurrent* T Tauri-like mass ejections from the Sun (as proposed further on), and recurrent superwave passages would all be major factors shaping the evolution of the Sun's Cometary Cloud. In regard to *recent* perturbations of the cometary population (i.e., $t < 1$ million years) it is interesting to consider the role played by the North Polar Spur remnant. Of all known supernova remnants, this is the closest one to the solar system. It is believed that the remnant is located about 420 ± 240 l.y. from the solar system and that it has a diameter of about 370 ± 230 l.y. (Spoelstra, 1972; Berkhuijsen, 1973). Based on these dimensions, Figure 3.10 illustrates the position of the North Polar Spur relative to the solar system, as viewed in projection onto the Galactic plane. Frisch (1981) suggests that the remnant's outer boundary has expanded to the point that it presently encompasses the solar system. In particular, she notes that "local gas" between the Sun and Alpha Ophiuchus (a star that is 60 l.y. away) is moving at about the same velocity as the local interstellar wind. (See Chapter 4, Section 4.6 for a discussion of the local interstellar wind.) Alpha Ophiuchus, whose position is shown in Figure 3.10, is unusual in that it is one of the few nearby stars which shows interstellar absorption lines in its spectrum.

Crutcher (1982) points out a number of interstellar clouds which may be in the immediate vicinity of the Sun and suggests that these may be part of the North Polar Spur remnant. Also, Bruhweiler and Kondo (1982) summarize several pieces of evidence indicating that the solar system is presently located *inside* an "interstellar cloud." They estimate an upper limit of ~ 10 l.y. for the cloud's diameter and a hydrogen density of $\sim 0.1 n_{\text{H}}/\text{cm}^3$ (hydrogen atoms per cm^3) dropping off to $\sim 0.01 n_{\text{H}}/\text{cm}^3$ outside of the cloud. Based on their observation of Doppler shifted UV absorption lines, they suggest that this enhanced local gas is moving through the Sun's vicinity from the general direction of the Galactic center, with about the same direction and velocity as the local interstellar wind. (See Chapter 4, Subsection 4.6, for a discussion of the local interstellar wind.) Their interpretation is that the cloud is of interstellar origin and passing through the solar system. It might be added that the inferred direction of motion for this cloud is consistent with a North Polar Spur origin.

The local interstellar cloud discussed by Vidal-Madjar, Laurent, Bruston, and Audouze

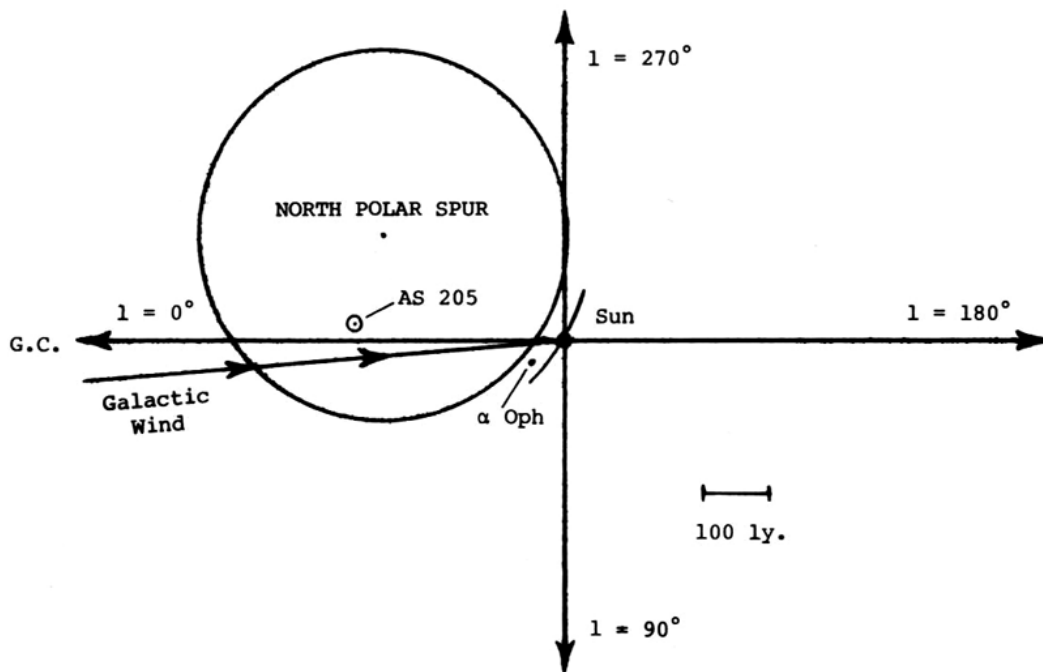


Figure 3.10. Position of the North Polar Spur supernova remnant relative to the solar system. A short arc has been drawn to indicate that the shell may actually be contacting the solar system. Arrow indicates direction of approach of the interstellar wind. Also shown is the position of AS 205, a T Tauri star, and the location of Alpha Ophiuchus, a spectral type A5 star.

(1978) may be another example of passing supernova ejecta. The authors, however, do not mention a supernova source origin, but rather infer that the cloud is one that just happened to be drifting by on a collision course with the solar system. They have determined that the cloud is about 40° in diameter and is centered between the stars Beta Scorpio and Sigma Scorpio ($\ell = 353^\circ$, $b = +20^\circ$). They tentatively place this cloud's position alarmingly close at a distance of ~ 0.1 l.y. from the solar system (see Figure 3.11), although their results indicate that it could be anywhere in the range of $0.03 - 6$ l.y. away. As seen in Figure 3.11, if the cloud were only 0.1 l.y. away, it would presently be located well inside the Inner Cometary Cloud, where it could substantially affect cometary orbits. Vidal-Majar et al. estimate that the cloud has a hydrogen column density of $\sim 10^{21}$ atoms/cm². Thus, for a cloud diameter of 10^{17} cm, a cloud hydrogen density of $\sim 10^{-20}$ g/cm³ ($\sim 10^4$ n_H/cm³) is derived. This suggests that the cloud has a mass of $\sim 10^{31}$ grams in the form of *diffuse* gas or a mass which is about the same order of magnitude as the mass of the entire Circumsolar Cometary Cloud. It might be added here that the location and inferred propagation direction of this cloud are consistent with a North Polar Spur origin. If the cloud is travelling at $15 - 20$ km/s, as Vidal-Madjar et al. propose, then the cloud will make its closest approach to the Sun about 3000 years from now. [**UPDATE:** Wood et al. (2000) report that the inner edge of the local interstellar cloud is located about 0.6 l.y. away.⁽¹⁾ Given that the cloud is moving towards the Sun at 26 km/s, they predict its inner edge will reach the solar system in 7400 years.]

If material ejected by the North Polar Spur supernova explosion were indeed passing through the solar vicinity, then one would expect to see evidence that the dynamics of the Cometary Cloud had been recently disturbed. The unrelaxed nature of the perihelion distribution of long-period comets, pointed out by Yabushita (1979), may be evidence of

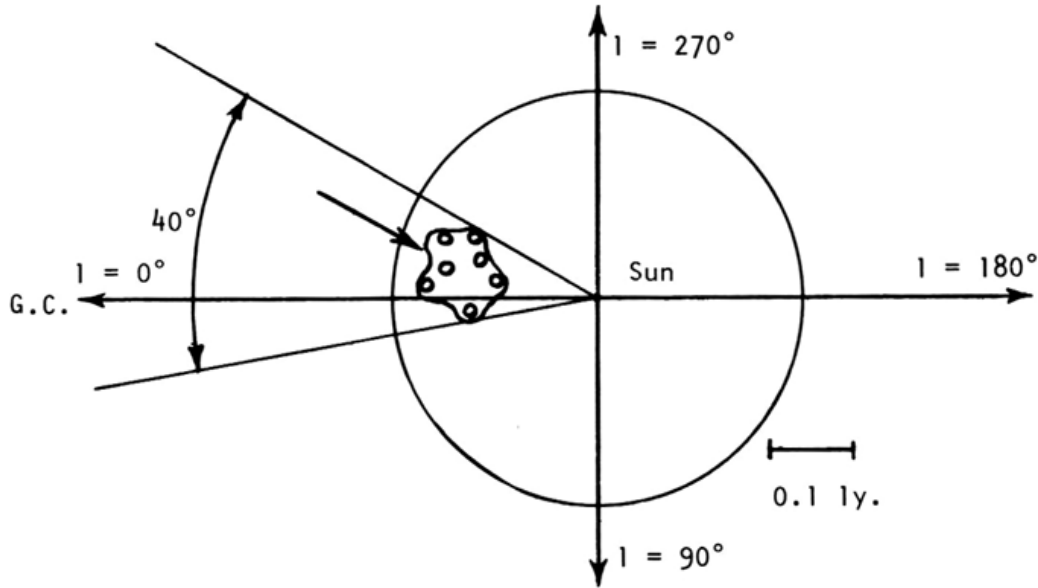


Figure 3.11. Location of the nearby interstellar cloud (proposed by Vidal-Madjar et al.) relative to the solar system; viewed in projection onto the Galactic plane. The irregular form indicates the boundary of the cloud corresponding to $n_{\text{H}} \sim 0.5$ particles/cm³ and the blobs within the cloud indicate regions of enhanced density containing most of the cloud's mass. The circle represents the cloud boundary at the Inner Cometary Cloud. The arrow indicates the direction that the invading cloud would be travelling if it originated in the North Polar Spur supernova explosion.

such recent disturbance. Clube and Napier (1982) interpret Yabushita's observation as indicative of a disturbance (possibly an encounter with a molecular cloud) occurring about 5 – 10 million years ago when the solar system was passing through Gould's Belt, a nearby extension of the Orion Spiral Arm. However, it is equally plausible that the encounter in question occurred more recently than this in connection with the close passage of a cloud (or clouds) of debris associated with the North Polar Spur supernova remnant.

A recent encounter of this second kind could have caused a portion of the cometary orbits to become more eccentric such that the comets would spend a fraction of their time in the vicinity of the heliopause sheath within the domain of the "vaporization zone" (to be discussed). In this critical region the comets would be subject to vaporization during the passage of a superwave, and if sufficient quantities of cometary bodies were present, a nebular cloud of substantial optical depth could be produced, causing the occurrence of terrestrial glaciation (as described further on). Thus it is interesting to speculate that the present "ice epoch" (sequence of glacial cycles) is connected with the current passage of the North Polar Spur remnant shell through the solar vicinity. [see **UPDATE: p. 123**]

The present Pleistocene ice epoch has lasted about 3 million K-Ar years (Shackleton and Opdyke, 1977). This time span is roughly comparable to the age of the North Polar Spur which is believed to have been created from a supernova explosion taking place about 10^6 years ago (Borken and Iwan, 1977). Assuming a supernova occurrence rate of one explosion every 50 years for the entire Galaxy, supernovae should occur about once every 500,000 years within 400 l.y. of the solar system. However, the chances would be much smaller that such a supernova would occur and that it would also project a sufficiently massive cloud of remnant material sufficiently close to the solar system to cause a perturbation of the Cometary Cloud. Such an event would happen perhaps once every billion

years or so. By comparison, 300 million years have elapsed since the time of the previous ice epoch. Thus passing supernova remnants should be considered as only one of several possible perturbing sources which are able to trigger the onset of an ice age sequence.

The Present Interplanetary Dust Cloud. The presence of interplanetary dust grains in the inner portion of the solar system is revealed by the light which they scatter from the Sun, the so-called "zodiacal light." It is believed that these particles gain entry into the solar system primarily by cometary transport, dust and gases being vaporized from cometary nuclei during close encounters with the Sun. Information on the particle size distribution of interplanetary dust has been obtained from satellite micrometeorite measurements and from visual observations of meteorite trails in the Earth's atmosphere. As seen in Figure 3.12, the integral dust particle number flux increases with decreasing particle size, at first steeply with a slope of $\sim 2.6 - 2.9$ on the $\log \phi - \log m$ graph, and then more gradually with a slope of ~ 1.55 ; cf. Hughes (1975, Figure 1). Frequency and size measurements of microcraters on lunar rock samples indicate that the upper branch of the integral particle flux curve extends at about the same slope down to particle masses of $\sim 10^{-18}$ grams ($r \sim 0.01\mu$); see Morrison and Zinner (1977). Based on the curve shown in Figure 3.12, it is possible to derive a particle mass distribution curve for the present interplanetary dust cloud. As seen in Figure 3.13, the particle mass distribution peaks at a particle mass of $\sim 10^{-6} - 10^{-4}$ grams, or at a particle radius of $\sim 100 - 200$ microns; cf. Hughes (1975, Figure 4).

Based on satellite data, the influx of extraterrestrial material to the Earth has been estimated to be about $3 \pm 2 \times 10^{-9}$ g/cm²/yr, or $\sim 10^4$ tons/yr over the entire surface of the Earth (Hughes, 1975). From this flux value the concentration of dust in the near Earth space environment has been estimated to be in the range of $1 - 4 \times 10^{-22}$ g/cm³ (Hughes, 1975; Millman, 1973). However, these estimates of terrestrial dust influx rate and interplanetary dust concentration appear to be on the low side. Cosmic dust deposition rates determined from Greenland and Antarctic ice cores suggest a cosmic dust deposition rate of $\sim 10^{-7}$ g/cm²/yr ($\sim 10^4 - 10^5$ tons/yr) for the present interglacial period, about 30 times higher than the satellite-determined values.

Based on upper atmosphere particle collections with balloon flights, Hemenway (1973, p. 219) estimates that extraterrestrial material is presently being deposited on the Earth's surface at an average rate of $\sim 3 \times 10^{-6}$ g/cm²/yr. This is three orders of magnitude higher than the value determined from satellite measurements and more than an order of magnitude above the glacial record estimates. Such a high value may be definitely ruled out on the basis of microparticle concentrations recorded in the Dome C ice core from East Antarctica; see Figure 8.1, curve-b. At present the concentration of particles in this core of size $> 0.6\mu$ is about 1.3×10^4 particles/0.5 ml (Thompson and Mosley-Thompson, 1981), which is equivalent to about 100 μ g/lit (see conversion factor for Byrd core, Appendix F). Given an ice accumulation rate of 3.7 cm/yr for the Dome C core, a total dust deposition rate of 3.6×10^{-7} g/cm²/yr is derived. Thus if the dust in the Dome C core were entirely of extraterrestrial origin, a comparable upper limit could be set on the cosmic dust influx rate.

In the present study the average glacial ice core value of $\sim 10^{-7}$ g/cm²/yr is adopted. Based on this influx rate, an ambient dust concentration of $\sim 6 \times 10^{-21}$ g/cm³ may be derived for an assumed geocentric dust velocity of ~ 15 km/s. This is about an order of magnitude higher than the satellite estimate quoted above. Note that the derived local interplanetary dust concentration value is about the same magnitude as the space density of cometary material postulated earlier to reside just outside the solar system.

For a near Earth concentration of 6×10^{-21} g/cm³ this interplanetary dust would present a column density of $\sim 5 \times 10^{-7}$ g/cm² between the Earth and the Sun. This would produce an insignificant amount of sunlight attenuation. For example, given that the cross section for 100 micron spherical particles (density ~ 1 g/cm³) is on the order of 100 cm²/g,

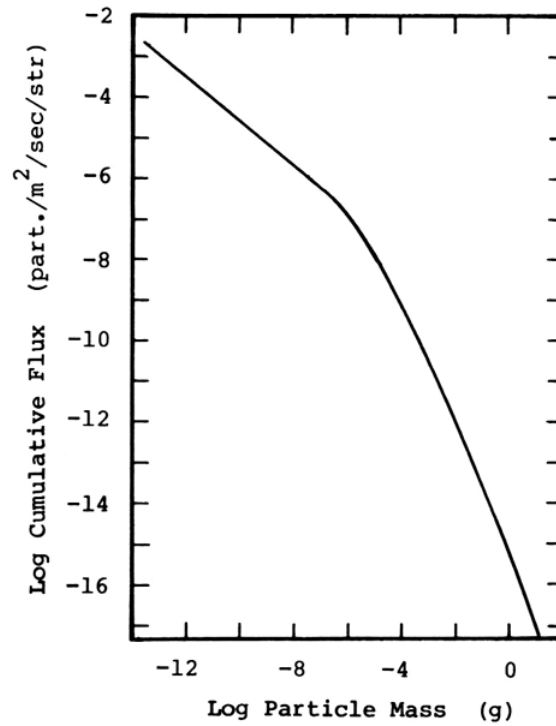


Figure 3.12. Cumulative flux of particles reaching the Earth's surface as a function of mass (or radius). Upper branch ($m < 10^{-6}$ g) based on satellite data, lower branch ($m > 10^{-2}$ g) based on visual data (after Hughes, 1975, Figure 1).

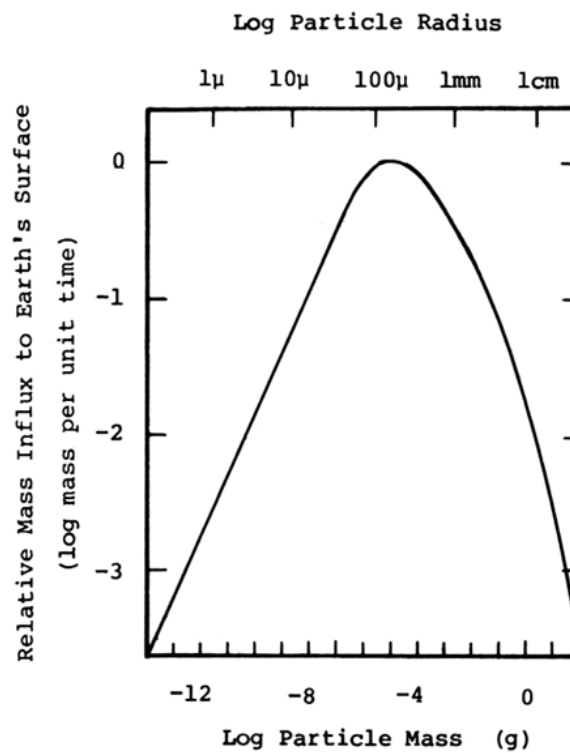


Figure 3.13. Normalized mass influx rate to the Earth's surface as a function of particle mass (based on Hughes, 1975, Figure 4).

the optical depth of this material would be $\tau \sim 5 \times 10^{-7} \text{ g/cm}^2 \times 100 \text{ cm}^2/\text{g} = 5 \times 10^{-5}$. Thus in the solar system's present "clean" state only about 10^{-4} of the sunlight reaching the Earth would become absorbed.

Dust Purging Processes in the Solar System. Several processes work together to keep the solar system in a gas-free and dust-free condition. First, the Sun's radiation pressure and the corpuscular pressure of the solar wind both serve to continuously sweep dust particles away from the Sun. Residence lifetimes for these particles have been estimated to range from 6000 years for 10μ particles, to 140 years for 0.1μ particles, to 2.4 years for $10^{-3}\mu$ particles (Schmidt and Elasser, 1967). In addition, abrasion of dust particles by solar wind protons, a process called "sputtering" progressively reduces the size of the particles. Brandt (1970, p. 158) estimates that the timescale for the complete destruction of a 1μ particle is in the range of $10^3 - 10^4$ years.

Shock fronts in the solar wind would also be effective in sweeping dust *and* gas out of the solar system. It is known that at regular intervals shock waves form in the solar wind plasma and propagate radially away from the Sun, transverse to the direction of the interplanetary magnetic field, the latter being frozen-in to the solar wind in the form of an Archimedes spiral. It is believed that such shocks, by their sweeping action, are responsible for the modulation of the Galactic cosmic ray intensity (cf. McKibben, Pyle, and Simpson, 1982). In a similar fashion, these propagating magnetic fields would be effective in continuously expelling from the solar system ionized gas and dust grains charged by solar ultraviolet radiation (through the photoelectric effect).

The *heliopause* would complement these other gas and dust expulsion processes by providing a barrier to the entry of ionized gas and charged dust particles. The heliopause is the shock region formed where the solar wind and its associated interplanetary magnetic field confront the local interstellar wind; see Figure 3.14. Recent measurements of the solar system's radial cosmic ray modulation gradient made with the Pioneer 10 and 11 spacecraft indicate that the heliopause is positioned at a radial distance of about 50 – 70 AU from the Sun (McKibben, Pyle, and Simpson, 1982). A distance of 60 ± 10 AU (10^{15} cm) and a sheath thickness of 20 AU are adopted here. Due to exposure to solar ultraviolet rays, interstellar dust particles would acquire charges and gas molecules would become ionized. Upon entering the heliopause sheath dust grains and gas molecules, charged by exposure to solar UV radiation, would become magnetically captured in spiral orbits. Hence their entry would be impeded. Neutral gas and dust particles, however, would be free to penetrate.

Finally, it is worth mentioning that the heavy planets, particularly Jupiter, would be important gas and dust scrubbers due to their gravitational sweeping action. In general, if left undisturbed the solar system should be able to maintain its interplanetary medium in a reasonably gas-free and dust-free state. However, this might not necessarily be the case in the event of a Galactic superwave passage. [see interstellar dust **UPDATE: p. 124**]

The Effect of the 14,200 Years BP Superwave: Generation of the Nebular Cloud. The heliopause sheath is believed to consist of a shocked, turbulent plasma bound together with a frozen-in interplanetary magnetic field. In this shock region incident cosmic rays become temporarily trapped by magnetic field lines. As a result, particle energy densities in the sheath should be much higher than in interstellar space. The charged particles filling the heliopause collectively constitute the solar system's "radiation belt" or "radiation zone."

Particle densities are found to be on the order of 10^4 fold greater than ambient densities in terrestrial radiation belts, and are observed to reach 10^7 fold enhancements in jovian belts. By comparison, let us suppose that under present conditions the cosmic ray integral energy density in the outer part of the heliopause reaches 10^5 fold above the ambient interstellar density; i.e., in the range of $u_p \sim 10^{-5} \text{ ergs/cm}^3$, or $I = c \cdot u_p = 3 \times 10^3 \text{ ergs/cm}^2/\text{s}$. If a

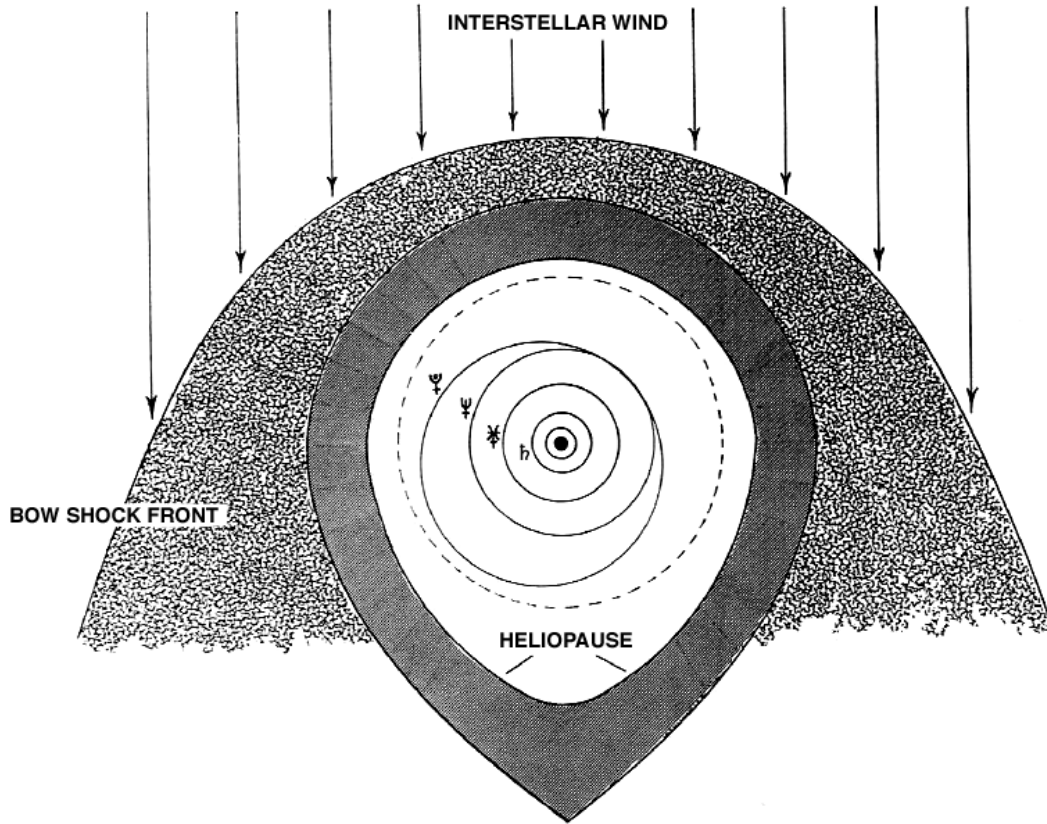


Figure 3.14. The heliopause sheath surrounding the solar system at its present heliocentric distance of about 70 AU. Also shown is the bow shock front that would be formed around the heliopause as a result of the impact of superwave cosmic rays. Dashed circle indicates the boundary outside of which a large number of cometary masses are likely to be orbiting the Sun. Shaded areas indicate regions of turbulent magnetic field.

cometary body were located in the heliopause and were exposed to this intensity it would become heated to an equilibrium temperature of $T = (I/\sigma)^{1/4} = 85^\circ \text{ K}$, where $\sigma = 5.67 \times 10^{-5} \text{ erg cm}^{-2} \cdot (\text{K})^{-4} \text{ s}^{-1}$ is the Stefan-Boltzmann constant. This is considerably below the sublimation point of water, which is believed to be the main constituent of cometary nuclei.

Consider now what would happen if the 14,200 years BP superwave were to pass through the solar vicinity. The heliopause sheath would present an impermeable barrier to the incident cosmic ray volley of the superwave in much the same fashion as would a young supernova remnant; see Chapter 5 (Section 5.3). Consequently, a bow shock front would become formed ahead of the heliopause boundary, similar to that believed to be formed around the heliopause by the present interstellar wind; see Figure 3.14. At the time of initial impact, if the heliopause were positioned at a radial distance of from 60 – 80 AU from the Sun, then it is reasonable to assume that a bow shock front would form on the order of 20 AU from the sheath's outer boundary, or about 100 AU from the Sun. The interstellar magnetic field would become highly compressed and disordered in the region between the outer surface of the bow shock front and the heliopause. Consequently, this shocked region, like the heliopause sheath, would be effective in trapping cosmic rays.

As a conservative estimate, suppose that cosmic ray energy densities rose by 10^5 fold in the outer portion of the bow shock front, comparable to the enhancement factor hypothesized for the outer portion of the heliopause sheath. Then, if the ambient cosmic ray

background were to increase 750 fold above present levels due to the passage of the 14,200 years BP superwave, particle energy densities in this portion of the bow shock front would increase to $u_p \sim 2 \times 10^6$ ergs/cm²/s (~ 2 suns; 1 sun = 10^6 ergs/cm²/s) and the equilibrium temperature would rise to $\sim 450^\circ$ K. At temperatures well below this the outer surface of a cometary mass would begin to vaporize, leaving behind a cloud of gas and dust. Exposed to those radiation intensities, the surface of a cometary mass would become vaporized at the rate of roughly 6 centimeters of depth per day.

Due to several unknown parameters, it is difficult to state precisely what space density of nebular material would result from this vaporization process. For example, unknown parameters would include: the space density of cometary bodies in the vicinity of the vaporization zone, the breadth of the vaporization zone, the rate of vaporization at the cometary surface (which in turn would depend on the superwave intensity and particle trapping efficiency of the bow shock front), and the rate at which this material would be propelled forward by superwave-driven hydromagnetic shock fronts. Here a reasonable model is constructed in an attempt to derive a local interplanetary dust density that is compatible with densities estimated on the basis of iridium concentrations which I have detected in Late Wisconsin ice; see Section 12.1 for a discussion of Ir results. The model is derived as follows.

First, it is assumed that most of the cometary body vaporization would take place at the outer surface of the bow shock front in a region about 1 AU thick. Assuming a magnetic field strength of $B \sim 10^{-4}$ for the bow shock front (see p. 73 of this chapter) and a trapped particle kinetic energy in the range of 0.5 – 5 Gev (see Figure 3.8, p. 74), then the radius of gyration of these particles would be in the range of 0.001 AU to 0.01 AU. Thus the vaporization zone thickness hypothesized above appears to be reasonable. It will also be assumed that the space density of comets in the vicinity of the bow shock front is 0.25% of Bailey's (1983) estimate of 2×10^8 comets/AU³ at a heliocentric distance of $r = 100$ AU; see p. 79. Thus a 0.1 AU³ region of the sheath would contain about 500 comets. If the mean diameter of the comets is assumed to be $d = 2$ km, then the total cometary surface area available for ice vaporization in this region of interest would be $A = 6.3 \times 10^{13}$ cm². If cometary material were to vaporize at the rate of 6 g/cm²/day as estimated above, then nebular material would be produced from this region at the rate of 4.4×10^9 g/s/(0.1 AU)³. A 1 cm² section of this vaporization sheath would be producing nebular material at the rate of 1.3×10^{-27} g/cm³/s $\times 1.5 \times 10^{12}$ cm = 2×10^{-15} g/cm²/s.

As the frozen cometary debris became vaporized, it would disperse to form a cloud of gas and ice-covered dust grains. In this dispersed state these constituents would be susceptible to being transported by the action of the superwave. Hydromagnetic shock fronts driven by the superwave would propagate through the cloud propelling forward gas and dust that had become ionized and charged by the cosmic rays and by solar UV radiation. If this material were being propelled forward at a velocity of ~ 4 km/s, then the resulting space density would be $\rho = (dm/dt)/v = (2 \times 10^{-15} \text{ g/cm}^2/\text{s})/(4 \times 10^5 \text{ cm/s}) = 5 \times 10^{-21} \text{ g/cm}^3$. As will be demonstrated shortly, this nebular concentration would be expected to increase about 1000 fold in the Earth's vicinity due to the funnelling effect of the Sun's gravitational field.

At any one given time, on the order of 10^9 cometary bodies would be present inside the vaporization zone. Any one given comet would spend about 2 – 6 months in the vaporization zone, during which time only about 5 – 10 meters of surface material would become vaporized. Thus for the majority of comets whose trajectories happened to intersect the bow shock front, only their outermost layers would be lost. In this way it could take several hundred superwave episodes to entirely vaporize a cometary population residing in the vicinity of the heliopause.

Normally, the heliopause would impede the entry of dust and gas into the solar system. However, if nebular concentrations were sufficiently high and if the material were driven at

a sufficiently high relative velocity, penetration would be possible. For example, suppose that at the outer boundary of the heliopause at ~ 70 AU the nebular material has a density of 5×10^{-21} g/cm³. If 4% of this material were to attain a velocity of 4 km/s, then a pressure of 1.6×10^{-11} dynes/cm² would be exerted on the heliopause, easily overpowering the opposing solar wind pressure which would be only $\sim 10^{-12}$ dynes/cm².

Under normal conditions the sweeping and eroding action of the solar wind and the pressure of the Sun's radiation are adequate for maintaining the solar system in a relatively dust free condition. However if dust were to enter the solar system at rates as high as 8×10^{-17} g/cm²/s (i.e., 5×10^{-21} g/cm³ $\times 0.04 \times 4 \times 10^5$ cm/s), these expulsion processes would become swamped. In addition, the solar wind's limited ability to expel particles and gas would itself become hampered since the heliopause sheath would become compressed by the incident cosmic ray blast to a position much closer to the Sun. This would allow nebular gas and dust to advance much closer to the Sun, and deeper within the Sun's gravitational field of influence, before becoming subjected to the solar wind.

The equilibrium position attained by the heliopause may be estimated as follows. The solar wind blows at an average velocity of ~ 500 km/s and has an average ion density of ~ 5 ions/cm³ at the Earth's distance from the Sun (Brandt, 1970, p. 150), and hence exerts an outward pressure of $\sim 10^{-8}$ dynes/cm². Assuming that $\sim 90\%$ of the energy intensity carried by the superwave ($\sim 2.7 \times 10^{-9}$ dynes/cm²) were able to exert a back pressure on the heliopause sheath, at equilibrium the sheath would become propelled inward to an heliocentric distance of ~ 1.9 AU where this "galactic wind" pressure would just counterbalance the outward pressure of the solar wind. (Solar wind pressure varies according to the inverse square of heliocentric distance.) Thus the heliopause sheath would become compressed to a position just outside the orbit of Mars; see Figure 3.15. Although the solar wind fluctuates in intensity the position of the heliopause would not deviate appreciably from this average position, due to its own inertia.

The rate at which the heliopause sheath would become accelerated by the cosmic ray blast would depend on the amount of charged dust and ionized gas trapped in its magnetic web. If the mass column density of the heliopause sheath were on the order of 10^{-5} g/cm² then under a pressure of 3×10^{-9} dynes/cm² presented by the superwave, it would be able to accelerate at a rate of $\sim 3 \times 10^{-4}$ cm/s², covering the distance from its former position at 70 AU to its equilibrium position at 1.9 AU in about 80 years. However, if the mass column density (and hence inertia) of the heliopause were considerably higher than the value assumed above, then it is conceivable that the movement of the heliopause would be so slow that it would never attain its equilibrium position.

As this gas and dust advanced forward, it would become drawn radially toward the Sun under the influence of the Sun's gravitational field. Hence the concentration of this material would accordingly increase. At the Earth's distance from the Sun, a 1000 fold increase could be expected, giving a density of $\sim 2 \times 10^{-19}$ g/cm³. This assumes that in going from 100 AU to 1 AU the radial velocity of this material increases from ~ 4 km/s to ~ 40 km/s. Suppose that 50% of the vaporized cometary material is in the form of dust (mostly submicron-sized grains), the remainder consisting primarily of water and including traces of other volatile substances such as CO₂, NH₃, CH₄, and C₂H₂. Then the density of the dust fraction in the Earth's vicinity would be on the order of 10^{-19} g/cm³. This would be about 15 times higher than present interplanetary dust densities.

It should also be mentioned that, besides gas vapors and finely divided dust particles, the comet vaporization process would also produce ice chunks of varying sizes. Explosive ejection would cause a large fraction of this coarse debris to become propelled into the solar system where it would bombard the Earth and other planets. To make a crude estimate of the earth-impact frequency for such material, suppose that 0.1% of the vaporized material were ejected in the form of 1-meter diameter ice chunks following orbital trajectories

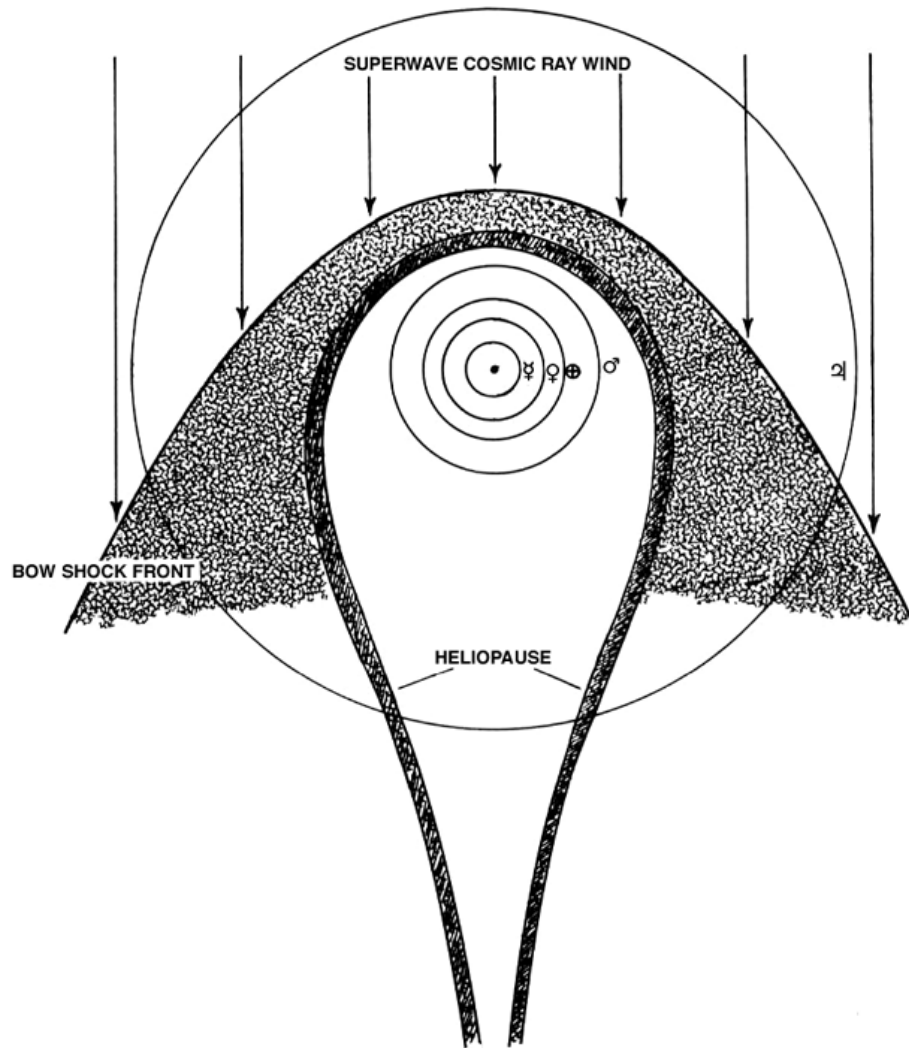


Figure 3.15. The heliopause sheath and the superwave bow shock front hypothetically compressed by the superwave cosmic ray blast to a position just outside the orbit of Mars. Shaded areas indicate regions of turbulent magnetic field.

carrying them inside the periphery of the Earth's orbit. Given that there would be a 10^{-9} chance of any given chunk hitting the Earth, then a flux of $10^3 - 10^4$ earth impacts per day could be expected. Chunks of this size would not do any physical damage since they would completely disintegrate before striking the ground. Kilometer-sized objects, however, would be capable of producing impact craters on the Earth's surface, but objects this large would probably be encountered very rarely.

Cosmic Dust Deposition on the Earth's Surface. As a result of increased ambient dust concentrations prevailing during the passage of a superwave, the rate of cosmic dust influx to the Earth's surface would be expected to increase. The rate of cosmic dust influx to the Earth's surface in the presence of a directed nebular flow of relative velocity v and space concentration ρ is given approximately as:

$$\phi = 0.25 \cdot \rho \cdot v \cdot (1 + (11.1/v)^2). \quad (6)$$



Figure 3-A. Artists depiction of the influx of nebular material into the inner solar system (© 1998 P. LaViolette).

The coefficient 0.25 is the ratio of the Earth's cross sectional area to its surface area, and 11.1 is the escape velocity from the Earth in km/s. A dust concentration of $\rho = 10^{-19} \text{ g/cm}^3$ and a relative velocity of 40 km/s would yield a dust deposition rate of $\sim 3\mu\text{g/cm}^2/\text{yr}$. Some of the cosmic dust deposition rates that have been determined in this study through neutron activation analysis of Wisconsin glacial dust samples are of comparable magnitude (see Chapter 12, Tables XV and XVI), and hence substantiate the deposition rate estimate made above. But more importantly, these experimental findings provide substantive grounds for believing that *toward the end of the Last Ice Age the radiation transmission properties in the inner portion of the solar system had become drastically altered*. Several ways in which the intensity of solar radiation reaching the Earth would be attenuated or enhanced are discussed in the remainder of this Subsection. Effects on the Earth's climate are discussed in Subsection 3.3.4.

The Interplanetary Hothouse Effect. The nebular dust and ice grains entering the solar system are assumed to have a radius of $\sim 0.1\mu$, i.e., a size of 0.2 microns. O'Dell (1971) has determined that the optical and infrared emission observed from three comets is produced by dust grains of about this size. Also, Hoyle and Wickramasinghe (1969) have suggested a similar size for interstellar dust grains. Moreover, dust grains of these dimensions are found to be a main constituent of large porous aggregate-type interplanetary dust particles (Millman, 1973, p. 197; Brownlee, 1977, 1738). Such aggregates, variously referred to as "fluffy," "chondritic porous," or "Type III" particles, are believed to be of cometary origin. They have been collected from the stratosphere and are usually found to range in size from 5 - 25 microns with their ice component long since evaporated. One collected specimen is shown in Figure 8.3(a) (p. 222). Smith, Adams, and Khan (1974) estimate that these low density particles make up about 70% (by weight) of the interplanetary dust particle population.

If cometary masses were to become vaporized as was suggested earlier, then most probably these large porous aggregate-type particles making up the cometary dust residue would become broken down into their submicron constituents. As a result, the peak of the particle mass distribution curve shown in Figure 3.13 would shift from about 10^{-5} grams mean particle mass ($r \sim 100 - 200\mu$) to about 10^{-14} grams ($r \sim 0.1\mu$). It is important to note that while the total mass concentration of interplanetary dust in the Earth's vicinity would increase by only about 15 fold from present levels, during the proposed Galactic superwave event, the space number density of 0.1μ particles would increase by about 10^5 times as a result of this mass-distribution-shift effect. In particular, these are the particles which are most effective in attenuating the intensity of visible light.

Nebular material in the outer portion of the solar system would present a considerable optical depth to the Sun's radiation. Dust particles and ice-covered dust nuclei residing outside the Earth's orbit would scatter solar radiation, returning a portion of the outgoing radiation flux to the inner part of the solar system creating a sort of "interplanetary hothouse effect." The magnitude of the hothouse effect produced by the dust component may be estimated as follows. Suppose that the dust concentration varies with heliocentric distance r according to the relation $\rho = \rho_0 r^{-1.5}$, where $\rho_0 = 10^{-19}$ g/cm³ is the dust concentration in the Earth's vicinity and where r is given in astronomical units. This increase of concentration with decreasing r is more gradual than an inverse square relation since the heliocentric velocity of the gravitating material would increase according to $r^{0.5}$. The column density of this material over the path from $r = a$ to b would be given as:

$$\chi = \int_a^b \rho r dr = -2\rho_0 [r^{-0.5}]_a^b.$$

Consequently, between the Earth ($a = 1$ AU) and a point distant from the solar system (e.g., $b = 100$ AU), there would be a column density of $\chi = 2.7 \times 10^{-6}$ g/cm², 85% of which would be encountered between a distance of 1 and 3 AU.

Suppose that these 0.2μ diameter dust grains have an extinction efficiency of $Q_{\text{ext}} \sim 2$ for the solar spectrum, similar to iron particles; cf. Wickramasinghe, 1973, p. 493. The optical opacity of these particles may then be determined to be $\alpha_v = 3 Q_{\text{ext}}/4 \cdot \rho \cdot r = 5 \times 10^4$ cm²/g for a particle density of $\rho = 3$ g/cm³ and a particle radius of $r = 10^{-5}$ cm. Consequently, a column density of $\chi = 2.7 \times 10^{-6}$ g/cm² would present an optical depth of $\tau = \chi \cdot \alpha_v = 0.14$, giving an attenuation of 13% of the direct solar beam. It has been estimated (O'Dell, 1971) that cometary dust grains scatter about $30 \pm 15\%$ of the light that they attenuate and absorb the remaining $70 \pm 15\%$. Consequently, about 4% of the direct solar beam would be scattered, of which $\sim 20\%$, or 0.8% of the direct beam, would be backscattered, 80% being scattered into the forward hemisphere. In addition, about 9% of the direct solar beam would be absorbed, of which half, or 4.5%, would be radiated into the rear hemisphere. Thus, a total of about 5.3% of the outgoing solar radiation would be returned to the inner solar system as a result of infrared reradiation and backscattering.

If the invading dust approached the Sun in a spherically symmetric manner, then the solar constant in the Earth's vicinity would increase by 5.3%. However, if the dust tended to concentrate toward the plane of the ecliptic forming an accretion disk, then the solar constant would be made to increase by a much smaller amount. For example, suppose that the encroaching dust adopts a configuration similar to that of the zodiacal dust cloud. Price (1980) estimates that in the antisolar direction the zodiacal cloud extends above and below the ecliptic by 40° of arc (full width at half maximum). With such a configuration only about 40% of the Sun's radiation would be intercepted, in which case the solar constant in the Earth's vicinity would increase by only about 2%.

In summary, depending on the geometry of the dust cloud formed by the invading nebular material, the solar constant in the Earth's vicinity would be made to increase by

between 2 – 5%. See Subsection 3.3.4 (p. 102) for resulting climatological effects.

Light Attenuation in the Earth's Vicinity. There are several ways in which high concentrations of submicron particles in the solar system could have attenuated sunlight reaching the Earth's surface. Particles of dust settling in the Earth's upper atmosphere would have constituted one source of obscurity. For example, suppose that cosmic dust was being deposited on the Earth at the average rate of $3 \mu\text{g}/\text{cm}^2/\text{yr}$, consistent with the findings in Chapter 12. Since particles less than 1 micron in size can take several years to settle to the ground through the mesosphere and stratosphere, a column density of dust sufficient to cause appreciable sunlight attenuation could build up. For example, an upper atmosphere column density of $\sim 3 \mu\text{g}/\text{cm}^2$ consisting of 0.2μ diameter cosmic dust grains having an optical opacity of $\alpha_v = 5 \times 10^4 \text{ cm}^2/\text{g}$ would produce an optical depth of $\tau \sim 0.15$. By comparison, the optical depth of the polar mesospheric cloud layer found at an altitude of 84 km is on the order of $\tau \sim 10^{-4}$ (Donahue et al., 1972). Also, the optical depth of the stratosphere is normally $\tau \sim 0.01$ increasing to $\tau \sim 0.1$ during volcanic eruptions (Toon and Pollack, 1982, p. 131). Or this may be compared to $\tau \sim 0.125$, the optical depth of the Earth's troposphere (Toon and Pollack, 1982, p. 134).

An optical depth of 0.15 would attenuate the direct solar beam by about 14%. About 70% of this, or 10% of the direct beam, would be absorbed by the aerosol and reradiated as infrared radiation, of which half would be lost into space. About 6% of the attenuated 14%, or about 0.8% of the incident radiation, would be backscattered. The net effect of aerosol absorption and backscattering would be to produce a $1\frac{1}{2}$ percentage point increase in the mean planetary albedo. In the Earth's polar regions, the presence of this dust would produce a climatic warming instead of a climatic cooling; see this chapter p. 104.

A circumterrestrial dust sheath positioned at a distance of several earth radii from the planet could also have caused a significant amount of light attenuation. Such a sheath would have formed out of charged interplanetary dust grains that had become captured by the geomagnetic field. Along similar lines, O'Keefe (1980) has proposed the formation of a circumterrestrial ring of lunar dust as a possible explanation for the temperature anomaly observed at the end of the Eocene (~ 34 million years BP) However, in the present scenario it is unlikely that such a ring system would have been stable. The dust particles, being of micron size, would have been easily purged from such a ring by the prevailing interplanetary weather.

Nebular Material in the Inner Solar System and Its Effects on Light Transmission. According to O'Dell (1971) the low infrared-to-optical emissivity ratio for cometary dust grains suggests that they attain temperatures about 50% greater than those found for blackbodies in the same radiation field. Becklin and Westphal (1966) have come to the same conclusion for dust particles observed in the tail of comet Ikeya-Seki. Consequently, it is estimated that the dust would be able to approach to within 0.08 AU (~ 16 solar radii) of the Sun before vaporizing at a temperature of $\sim 1500^\circ \text{K}$. As a result, a dust-free cavity would form around the sun. Figure 3.16 illustrates the size of this inner vaporization zone relative to the orbits of the inner planets.

The column density of nebular material that would have intervened between the Sun and Earth is estimated to be $\chi = -2 \rho_o [r^{-0.5}]_a^b = 7.9 \times 10^{-6} \text{ g}/\text{cm}^2$ for $\rho_o = 10^{-19} \text{ g}/\text{cm}^3$, $a = 1 \text{ AU}$, and $b = 0.08 \text{ AU}$. Consequently, given that the dust grains have an optical opacity of $5 \times 10^4 \text{ cm}^2/\text{g}$ for the solar spectrum, this dust would present an optical depth of $\tau \sim 0.39$ and would reduce the direct solar beam by about 32%. Given that 70% of the attenuated radiation would be absorbed, about $70\% \times 32\% = 22\%$ of the direct solar beam would be absorbed and reradiated in the infrared. The remaining 10% would emerge as scattered light, about 80% of which would be forward scattered.

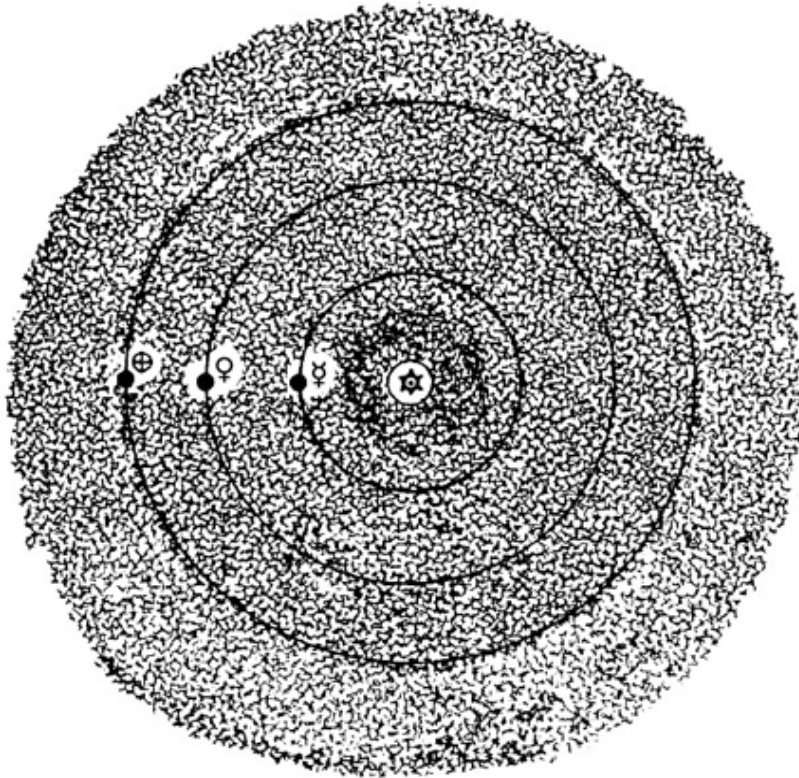


Figure 3.16. The inner solar system congested with nebular material. The blank area around the Sun indicates the region in which the dust would vaporize.

It is reasonable to expect that the interplanetary nebula would have contained concentration inhomogeneities. Enhanced concentration regions, i.e., "clouds," would periodically pass between the Earth and Sun causing their shadow to fall upon the Earth. Consider a 0.3 AU diameter cloud having a nebular particle mass concentration that was 20 times that of the ambient concentration in the Earth's vicinity, e.g., $2 \times 10^{-18} \text{ g/cm}^3$. This cloud would have presented a column density $\chi = 9.3 \times 10^{-6} \text{ g/cm}^2$ and would have had an effective optical depth of $\tau \sim 0.47$. It would have intercepted about 37% of the Sun's radiation, and of this, about half would have been scattered or reradiated away from the Earth. Hence, during the time that this cloud was eclipsing the Sun, the solar constant in the Earth's vicinity would have decreased by up to 20%. On the other hand, if the cloud were to have passed on the other side of the Earth such that the Earth was positioned between the cloud and the Sun, then the reflected light from the cloud would cause the solar constant in the Earth's vicinity instead to *increase* by a comparable amount. In summary, interplanetary weather prevailing in the inner solar system would have had a profound effect on the amount of solar flux that the Earth received at any given moment.

For simplicity, suppose that the main part of the dust intervening between the Earth and the Sun is concentrated in the form of a sheath positioned at a heliocentric distance of about 0.14 AU, where the equilibrium temperature would be $T \sim 1150^\circ \text{ K}$. The resulting continuum spectrum may be approximated by a blackbody radiation curve peaking at a wavelength of $\lambda = 2.5 \text{ microns}$. Figure 3.17 compares the present solar spectrum ($T = 5800^\circ \text{ K}$) with this dust reradiation curve. The irradiance ($\text{ergs/cm}^2/\text{s}/\mu$) for each curve is shown normalized to its peak irradiance value. For the above example, the net spectrum [(unscattered + scattered + absorbed)/reradiated light] as seen from the Earth would be bimodal, consisting of the original unaltered solar continuum at 78% of its normal intensity

complemented by an 1150° K blackbody infrared continuum making up the other 22%.

If the dust density assumed for this dust accretion model were to be increased by 10 fold ($\tau \sim 3$), then about 95% of the Sun's energy would be radiated in the infrared. In such a case continuum bimodality would disappear and the 1150° K blackbody curve would more appropriately represent the Sun's energy distribution. If viewed from a distance, the Sun would probably resemble an optically thick "infrared star." One example of an infrared star is R Monocerotis, which is embedded in Hubble's variable nebula. This is an appropriate example since Hubble's Variable Nebula lies on the 6000 years BP superwave event horizon; see [p. 201](#). (Refer to: Low et al. (1970), Geisel (1970), Allen (1975), and Cohen and Kuhl (1979b) for other examples of infrared stars, infrared nebulae, and stars having infrared excesses.)

The spectrum of R Mon is shown in Figure 3.17 where it is compared with that of the Sun. However, in making this comparison keep in mind that R Mon has a luminosity about 700 times greater than the Sun, and hence if it were unobscured and lying on the stellar main sequence it would appear as a type-B star peaking in the ultraviolet at about 900 Å (0.09μ). Hubble's Variable Nebula is believed to be a member of a class of nebulae called *bipolar nebulae* (Canto, Rodriguez, Barral, and Carral, 1981) in which gas is observed to be ejected in opposite directions from the embedded star. The current view is that in such objects a dense disk of dust and gas surrounds the star and impedes its stellar wind in equatorial directions causing the outward gas flow to emerge at the poles of the accretion disk.

T Tauri stars also constitute good candidates for comparison to a dust-congested solar system. Cohen and Kuhl (1979, p. 786, 792) report that half of the T Tauri stars that they surveyed show infrared excesses which may be interpreted as thermal emission from hot dust grains (800 – 1500° K). As in bipolar nebulae, the dust surrounding T Tauri stars may also be in the form of a disk or torus. For example, Cohen and Schmidt (1981) present evidence suggesting that the T Tauri star HL Tauri is being viewed edge-on through a disk of dust which is responsible for attenuating its visual continuum by 100 fold. Cohen (personal communication, 1982) suggests that this model of HL Tauri may be typical of T Tauri stars in general. While the majority of T Tauri stars are relatively unobscured, this may be due to the fact that we happen to be viewing these stars at a high inclination to their disks. As pointed out in Chapter 6 ([p. 201](#)), a considerable number of T Tauri stars lie in the vicinity of a superwave event horizon.

The T Tauri Effect. Hoyle and Lyttleton (1950) have proposed that the passage of the solar system through an interstellar dust cloud could cause significant brightening of the Sun, which in turn could initiate an ice age on the Earth. McCrea (1975, 1981) reviews this accretion theory and suggests that such cloud capture episodes would most likely take place at times when the solar system was passing through a spiral arm of the Galaxy, or through a great molecular cloud. In this scenario gas and dust from the interstellar cloud would become captured in the Sun's gravitational field and the kinetic energy of its infall onto the surface of the Sun would become converted into thermal energy, primarily emitted in the ultraviolet region of the spectrum. In an illustrative example Hoyle and Lyttleton (1950) show that a cloud having a density of $\sim 10^{-21}$ g/cm³ and passing the Sun at 1 km/sec could contribute material at a sufficiently fast rate that the Sun would experience a 10% increase in its luminosity. In addition, they point out that with higher dust cloud densities or slower relative velocities even higher luminosities are theoretically achievable.

The Galactic Explosion Hypothesis complements the Hoyle and Lyttleton accretion scenario. Namely, in addition to periods when interstellar dust clouds were transiting the solar system, dust influx could occur also at times when superwaves were passing by. Times when the remnant of a nearby supernova explosion ($d < 50$ l.y.) was passing through the

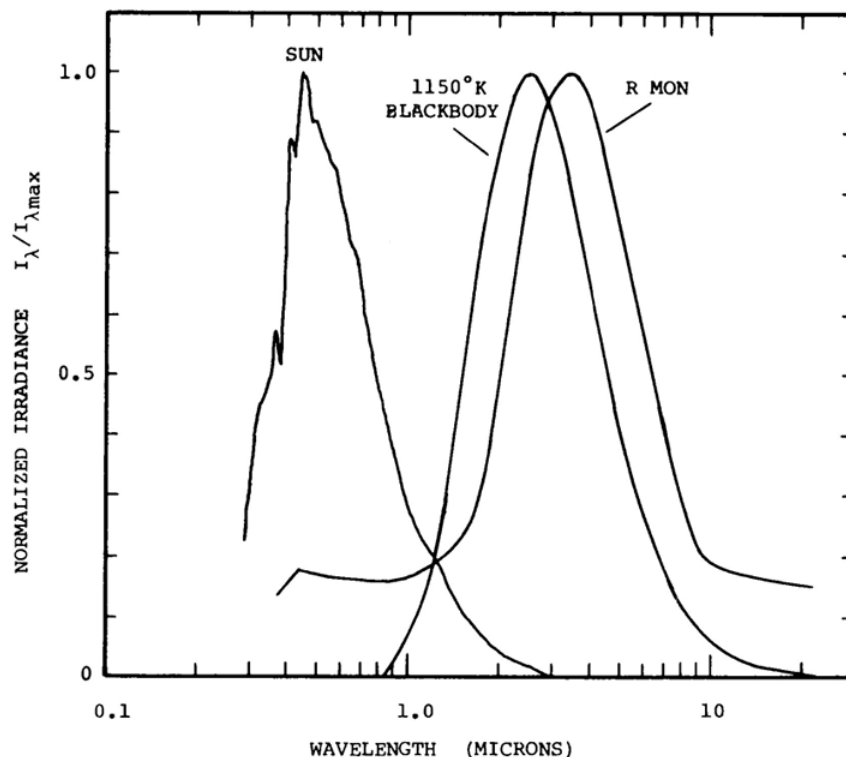


Figure 3.17. Continuum spectra for the Sun (Pierce and Allen, 1977), for a 1150° K blackbody, and for the dust-obscured infrared star R Monocerotis (Low et al., 1970). Spectra are given in units of $\text{ergs/cm}^2/\text{s}/\mu$ normalized to their respective peak irradiance values.

solar vicinity should also be included. become captured in the Sun's gravitational field and the kinetic energy of its infall onto the surface of the Sun would become converted into thermal energy, primarily emitted in the ultraviolet region of the spectrum. In an illustrative example Hoyle and Lyttleton (1950) show that a cloud having a density of $\sim 10^{-21} \text{ g/cm}^3$ and passing the Sun at 1 km/sec could contribute material at a sufficiently fast rate that the Sun would experience a 10% increase in its luminosity. In addition, they point out that with higher dust cloud densities or slower relative velocities even higher luminosities are theoretically achievable.

The Galactic Explosion Hypothesis complements the Hoyle and Lyttleton accretion scenario. Namely, in addition to periods when interstellar dust clouds were transiting the solar system, dust influx could occur also at times when superwaves were passing by. Times when the remnant of a nearby supernova explosion ($d < 50 \text{ l.y.}$) was passing through the solar vicinity should also be included.

The amount by which the Sun's luminosity would increase as a result of the dust and gas accretion rate proposed earlier may be roughly estimated as follows. If nebular material were advancing at the rate of $8 \times 10^{-17} \text{ g/cm}^2/\text{s}$ over a circular region having a diameter of $\sim 160 \text{ AU}$ (cf. p. 88), then material would be brought under the influence of the Sun's gravitational field at the rate of:

$$dm/dt = (8 \times 10^{-17} \text{ g/cm}^2/\text{s}) \times (5 \times 10^{30} \text{ cm}^2) = 4 \times 10^{14} \text{ g/s.}$$

If this material were all ultimately accreted by the Sun, equivalent to an accretion rate of $6 \times 10^{-12} M_{\odot}/\text{yr}$, the amount of kinetic energy released as a result of its infall would be: $L = (G M_{\odot}/R_{\odot})(dm/dt) = 10^{30} \text{ ergs/s}$, where G is the gravitational constant, and M_{\odot} and R_{\odot} are the

TABLE V
 PREDOMINANT TYPES OF EMISSION FROM A SOLAR FLARE

| <u>Flare Effect</u> | <u>Energy (ergs)</u> |
|---------------------------------|----------------------|
| Optical chromospheric emission | |
| - H α line | 10 ³¹ |
| - Total line emission | 5 × 10 ³¹ |
| - Continuum emission | 8 × 10 ³¹ |
| Soft X-rays (1 – 20 Å) | 2 × 10 ³⁰ |
| Hard X-rays | 5 × 10 ³¹ |
| Energetic protons (< 10 Mev) | 2 × 10 ³¹ |
| Cosmic rays (1 – 30 Gev) | 3 × 10 ³¹ |
| Interplanetary solar wind blast | 2 × 10 ³² |

mass and radius of the Sun. This represents only a 0.025% increase in solar luminosity. However, if accretion rates of nebular material were on occasion 15 times higher, as the polar ice record seems to indicate (p. 351), then the Sun's luminosity could have increased by as much as 0.5%.

Since very high temperatures would be produced by this material (impacting the Sun at up to 400 km/s), most of this luminosity increase would be generated at ultraviolet wavelengths, as Hoyle and Lyttleton (1950) have suggested. In addition, material falling into the Sun would be expected to trigger major solar flare activity, on a scale much larger than is currently observed. Currently, solar flares, or "chromospheric flares" as they are sometimes called, may last anywhere from 10 minutes to several hours depending on the size of the flare. Flare energies is typically run about 10³² ergs, with most of this energy appearing in the form of optical and ultraviolet emission, hard X-ray emission, and hot solar wind particles. Also, solar flares release a substantial amount of energy in the form of cosmic rays (protons and electrons) and nonthermal electromagnetic radiation ranging from the radio to the γ -ray region of the spectrum. Energies for some of these types of emission are given in Table V (after Piddington, 1969, p. 90).

Hyder (1968) suggests that solar flares are produced in the chromosphere and are powered by the kinetic energy of material falling out of the solar corona into the chromosphere. He (1967a and b) has studied a sample of 52 of the larger chromospheric flares and has found that of these about 38 (73%) were preceded by the infall of material, as indicated by red-shifted absorption features in their spectra. He infers densities for this infalling material in the range of $10^9 \leq n_o \leq 10^{11.5}$ particles/cm³. By comparison, for an accretion rate of 10¹⁶ g/s ($\sim 10^{-10}$ M $_{\odot}$ /yr), which could have occurred during the Last Ice Age, material infall densities of $n_o \sim 10^{10}$ particles/cm³ ($\rho \sim 10^{-14}$ g/cm³) would prevail over the entire surface of the Sun. Thus, Hypothesis #4-b (p. 2), which proposes that nebular material accretion by the Sun would increase solar flare activity, appears to be reasonable. Solar flare activity might be expected to increase by 100 to 1000 fold above its present solar-cycle-average level, with major solar flares becoming hourly or daily events, rather than monthly or yearly events as they are at present.

Viewed from a distance of several hundred light years during such a phase, the Sun would probably appear very much like a T Tauri star. T Tauri stars are observed to have the following characteristics:

- 1) They are dwarf stars having masses in the range of 0.2 – 3 solar masses and

photospheric radii in the range of 3 ± 2 solar radii (Cohen and Kuhl, 1979a and 1979b).

- 2) They have luminosities comparable to that of the Sun. However, they are overluminous for their spectral type; i.e., they lie above the main sequence on the Hertzsprung-Russell diagram (Kuhl, 1964; Herbig, 1967). They are mostly of spectral-type K and M (Cohen and Kuhl, 1979a and 1979b), but earlier spectral types also occur. The Sun (at present) is a type G-2 star.
- 3) Their luminosity varies erratically. Intensity changes of 20 fold are common and can occur in as short a time as a few hours or a day or can take years to occur (Herbig, 1967; Cohen and Schwartz, 1976; Burnham, 1978, p. 1832).
- 4) A typical T Tauri star is modeled as having an inflated photosphere ($R_o \sim 3 \pm 2 R_{\odot}$) surrounded by an extended chromosphere $R_c \sim 3R_o$ (or $9 \pm 6 R_{\odot}$ which in turn is surrounded by a shell of light absorbing material (Kuhl, 1964, 1966; Cohen, 1973, Appendix B); see Figure 3.18.
- 5) T Tauri stars have very strong chromospheric emission lines. The emission is sometimes so strong that it masks the star's absorption-line spectrum, chromospheric energy output substantially exceeding the output of the underlying star, although emission-line intensities are observed to cover a wide range down to intensities typical of the Sun's present spectrum (Herbig, 1967; Kuhl, 1966).
- 6) They have abnormally broad emission and absorption lines which, if due to the Doppler effect, indicates that either the gas is in rapid motion about the star or is engaged in radial motion with respect to the star (Herbig, 1967).
- 7) Investigation of the relative displacement of sodium D absorption lines indicates that gas is falling into these stars (Ulrich and Knapp, 1979). In addition, some stars show evidence of a high rate of mass ejection, one example being V1057 Cygni, which may be ejecting material at a rate of $10^{-11} - 10^{-8} M_{\odot}/\text{yr}$ (Ulrich and Knapp, 1979). Gas ejection velocities may reach as high as 200 - 300 km/s (Kuhl, 1964).
- 8) T Tauri stars are almost always associated with regions of interstellar nebulosity (Kuhl, 1966). However, there are some exceptions to the rule, such as AS 205 and Lk H 345, both of which are accreting gas but are not associated with any dense interstellar clouds (Ulrich and Knapp, 1979).
- 9) About half of the T Tauri stars have strong infrared excesses indicating that the stars are closely surrounded by massive clouds of hot dust grains which have surface temperatures in the range of $800^{\circ} - 1500^{\circ} \text{K}$ (Cohen and Kuhl, 1979b, pp.786, 792). Also see Mendoza (1966, 1968) and Geisel (1970).
- 10) They often have strong ultraviolet excesses (Mendoza, 1966). For example, observations of RW Aurigae indicate that the ratio of the 3000 \AA UV to 5000 \AA visible intensity is twice as large as in the Sun and that the $2500 \text{ \AA} - 5000 \text{ \AA}$ ratio is 10 times as large as in the Sun (Imhoff and Giampapa, 1980).
- 11) It is found that T Tauri stars having strong UV excesses tend to have red-shifted absorption lines indicating infalling material (Walker, 1966; Mendoza, 1966).
- 12) T Tauri stars emit strongly at X-ray wavelengths. Their coronal spectra are similar to that of the quiet Sun, but 10^5 times stronger (Gahm, 1980).
- 13) The lithium content of their atmospheres is 80 - 400 times higher than that in the Sun's atmosphere (Herbig, 1966, 1967).

The currently held view is that T Tauri stars are young, pre-main-sequence stars in their contractive stage of evolution forming out of the dust clouds which surround them

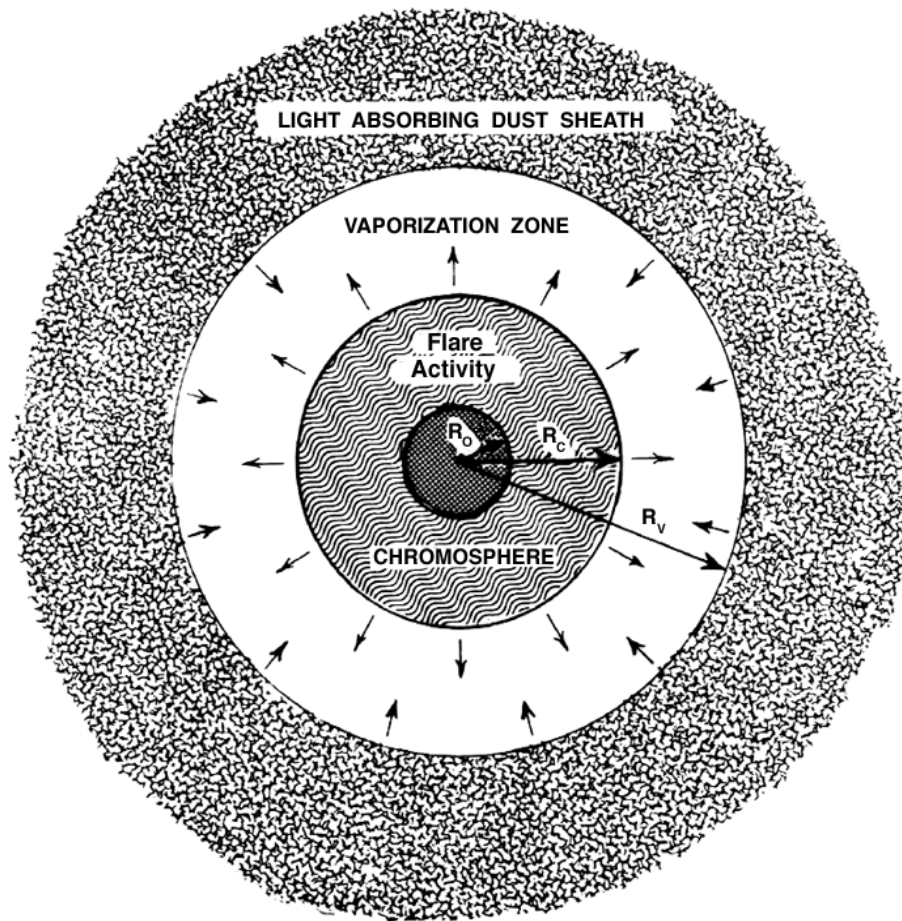


Figure 3.18. A model of a T Tauri star. R_0 = radius of the stellar photosphere, R_c = radius of the chromosphere, and R_v = radius of the vaporization zone boundary.

(Herbig, 1967). However, Aller (1956, p. 105) has suggested that T Tauri stars may be normal, middle-aged stars that happen to wander into regions where the interstellar medium is particularly dense. Their chromospheres would then become energized as they accreted material from their surroundings. This second interpretation is closer to the view adopted here. In addition, I would extend this "middle-aged-star" scenario by suggesting that superwaves (and supernova explosions) play an important role by making dust and gas available to the star for accretion when it otherwise might not be available. Superwaves would be instrumental both in generating the dust cloud by heating nearby condensed interstellar or cometary debris and for transporting this material toward the star against the pressure of the star's stellar wind. The influx of nebular material could account for the lithium overabundances observed in the spectra of T Tauri stars. For example, meteoritic material contains about 35 times more lithium than does the present solar atmosphere.

While a large fraction of T Tauri stars may indeed be young stars in their contractive stage of evolution, there are some such as AS 205 and Lk H 345, mentioned above in item #8, that have difficulty fitting in with this model due to the lack of a sufficiently large reservoir of surrounding nebular material. In fact, AS 205 may be a good star to study as an example of the kind of scenario proposed here for the Sun. It has a luminosity of $\sim 6 L_{\odot}$ for a distance of 100 pc, and as Ulrich and Knapp have suggested, the infalling material for this star may be coming from a dense cloud of cometary material similar to that believed to surround the Sun.

Moreover, since this star lies in the direction ($\ell = 355^\circ$, $b = +23^\circ$), it should lie within the domain of the North Polar Spur supernova remnant; see Figure 3.11. Perhaps AS 205 and the Sun are both victims of the aftermath of the passage of the North Polar Spur shock front, which together with cosmic rays periodically supplied by superwaves, could cause outlying cometary material to become vaporized and transported close to the star.

Several authors (e.g., Greenstein, 1950; Aller, 1956, p. 106; Kuhl, 1964; Gahm, 1980; and Worden et al., 1981) have suggested that solar-flare-like activity may be responsible for energizing the chromospheres of T Tauri stars. Kuhl (1964) has suggested that high-energy protons accelerated by a flare-type mechanism at the star's surface are responsible for ionizing the photospheric material and for producing the observed strong line emission. Worden et al. (1981) conclude that the short-period photometric fluctuations of T Tauri stars ($10^2 - 10^4$ seconds) can be understood as essentially continual flaring with the optical flare energy of individual events being on the order of 10^{34} ergs (about $10^2 - 10^3$ times more energetic than typical solar flares). Ulrich and Knapp (1979) interpret observations of sharp blue shifted Na D absorption lines as being discrete clouds of material ejected from the parent star by flare-like activity. Gahm (1980) suggests that the high X-ray intensities observed in T Tauri stars are due to flare-like events. Cram, Giampapa, and Imhoff (1980) note that the energy needed to account for the UV emission lines of T Tauri stars is equivalent to that of a solar flare maintained permanently over the entire surface of the star. Finally, Greenstein (1950) has suggested that the highly excited spectra of T Tauri stars is due to flares on the stellar surface *triggered by the infall of material*. Greenstein's proposal is consistent both with the findings of Ulrich and Knapp (1979) that T Tauri stars are accreting material and with the findings of Hyder (1968) that solar flares are triggered by infalling material.

In summary, based on our current understanding of the processes taking place in T Tauri stars it is reasonable to conclude that if the Sun were to begin accreting nebular material at an appreciable rate, as proposed earlier, it would exhibit many of the characteristics of a T Tauri star. The suggestion that superwaves may be critically involved in producing T Tauri-like behavior is supported by the finding reported in Chapter 6 that a major fraction of T Tauri stars are found in the vicinity of proposed superwave event horizons. Future study of T Tauri stars and other dust accreting objects such as infrared stars and infrared nebulae should help to shed light on the Sun's role in initiating abrupt climatic changes on Earth.

3.3.3 Geomagnetic Effects

As was mentioned in the previous subsection, solar flares would have been more energetic and would have occurred with greater frequency during a superwave event due to the accretion of nebular material by the Sun. Increased solar flare activity in turn would have produced substantial disturbances of the Earth's magnetic field, possibly even causing geomagnetic excursions and reversals. The means by which this could occur may be understood as follows.

Geomagnetic storms are known to occur several days after the appearance of a large solar flare, at a time when low and high energy particles from the flare are arriving in the Earth's vicinity. The first phase of the storm usually involves a sudden increase in the strength of the geomagnetic field, a phenomenon known as *sudden commencement*. This event typically lasts about 5 minutes and involves about a 0.1% increase in field strength. This is believed to be due to compression of the Earth's magnetosphere by solar-flare hydromagnetic blast wave consisting of an enhanced density of solar wind particles (Piddington, 1969, pp. 105, 118). The Earth's magnetopause would become thrust forward

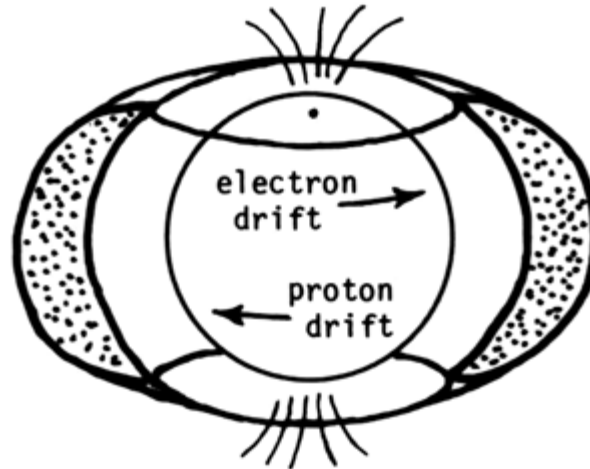


Figure 3.19. The inner Van Allen radiation belt. Arrows indicate the directions of particle drift which collectively constitute the ring current.

and compressed by the incident blast wave in much the same way that the heliopause sheath would become compressed by the arrival of a burst of Galactic cosmic ray electrons.

Sudden commencement is usually followed by a temporary decrease in geomagnetic field strength known as the *main phase decrease*. This period of decreased field strength, which may last for several days, is believed to be caused by solar flare cosmic rays trapped in spiral orbits around the Earth's magnetic field lines. These cosmic rays would form a *storm-time* radiation belt similar in nature to the Van Allen radiation belts which girdle our planet. Singer (1957) has suggested that such magnetically trapped particles would drift in an equatorial direction, westward for protons and eastward for electrons; see Figure 3.19. As a result, the motion of these particles would produce a *ring current* which in turn would generate a magnetic field *opposed* to the Earth's dipole field. The theory of this phenomenon has been more completely worked out by Dessler and Parker (1959) and others. Main phase decreases as large as 5×10^{-3} gauss (i.e., about 1% of the Earth's surface field intensity) are known to be produced by major solar flares, whose peak energy intensity can temporarily reach 100 times the intensity of the present cosmic ray background. It is believed that during such an event the Earth intercepts total cosmic ray energies in the range of $10^{22} - 10^{24}$ ergs, possibly supplied through the Earth's magnetotail plasma sheet (Piddington, 1969, pp. 180 - 181).

Suppose that during the proposed period of solar chromospheric activation a solar flare were to occur that was 100 times more intense than the most energetic solar flare observed during the past few decades, of a size typical of flares observed in T Tauri stars. Theoretical considerations show that the amplitude of the main phase decrease is proportional to the total particle energy in the radiation belt (Piddington, p. 180), and hence is roughly proportional to the initial magnitude of the solar flare. Thus ring current magnetic fields 100 times stronger than those thus far observed could conceivably occur, the applied opposed field reaching such a high intensity that it would essentially neutralize the Earth's dipole field.

It is difficult to say what would happen when the intensity of the ring current field exceeded that of the geomagnetic field. Very likely the ring current field lines would close to form a doughnut-shaped field configuration having a symmetry axis that passed through the Earth's geomagnetic axis. The net field at the Earth's surface would then be reduced in intensity or even reversed in direction by the dominant ring current field. Cosmic rays would have difficulty escaping from their toroidal magnetic bottle since to do so they would

have to slowly diffuse perpendicular to the direction of the field lines.

Such "field-reversed ion rings" have been created in the laboratory by using high-powered pulsed ion beams to inject large quantities of charged particles into an applied magnetic field (Golden et al., 1981). It is found that when the self-field generated by the ions exceeds the intensity of the applied magnetic field, a toroidal field-reversed configuration develops with a net reversed field in the interior of the particle ring. Field reversed ion rings are currently being researched as a means of confining plasmas for use in thermonuclear fusion reactors. However, they may also provide useful insights into the behavior of planetary fields during episodes of intense solar flare ion bombardment.

Whether the proposed ring current field was actually able to reverse the magnetic dynamo hypothesized to be present at the Earth's core would depend on a number of factors, such as the viscosity of the Earth's liquid interior and the momentum tied up in its motion. Under frictionless conditions a change in the dynamo's alignment would ultimately occur provided that sufficient time were allowed for the dynamo's inertia to be overcome.

The trajectory that the net magnetic field (ring current field) plus geomagnetic dynamo field) would follow is another question that must be considered. It is very likely that the local interplanetary field would play an important role. For example, the interplanetary magnetic field is known to reach peak strengths of 4×10^{-4} gauss during solar flare events (Brandt, 1970, p. 131). During mega-solar-flares associated with a solar T Tauri phase, temporary field strengths in the range of $10^{-3} - 10^{-2}$ gauss could be expected. The interplanetary field is observed to be oriented in the plane of the ecliptic in a spiral pattern. Consequently, if this ambient field were to cause a reorientation of the net field pattern, the virtual geomagnetic pole would probably drift to within $\pm 23^\circ$ of the Earth's equator. Such an orientation appears to have temporarily occurred around 14,100 cal years BP; see Chapter 7, Subsection 7.2.3.

As the intensity of the storm time radiation belts decreased and the ring current field subsided, the geomagnetic poles would be free to drift away from their metastable equatorial position, taking either their former orientation, or a reversed polarity position. If the reversed position were attained, then the geomagnetic field would have to wait for another solar-cosmic event for an opportunity to reverse once again and attain normal polarity.

Uffen (1963) has proposed that the Earth's core dynamo is inherently unstable and subject to spontaneous reversals. Thus he seeks a purely terrestrial explanation for this phenomenon. However, there are those who point out that the Earth's core dynamo would not be able to self-reverse, but would require the assistance of a sudden external disturbance (Bucha, 1973; after Bullard, 1971). I would add that since the hypothesized dynamo mechanism is not well understood, attempts to attribute flips to instabilities in this not-well-understood mechanism should be regarded as being speculative. Moreover, such a mechanism alone would not be able to account for the observation that geomagnetic flips coincide with extinction episodes; see Chapter 11 (Subsection 11.2.1).

The theory of radiation belt currents, on the other hand, is well developed (Singer, 1957; Dessler and Parker, 1959) and the proposal that cosmic ray outbursts (e.g., from the Sun) cause disturbances to the Earth's magnetic field is well established on observational grounds. My proposal that large solar flare outbursts associated with the passage of a superwave would cause disturbances to the Earth's magnetic field simply involves a quantitative scaling up of a phenomenon that is already well understood. The possibility that a ring current magnetic field could be responsible for causing geomagnetic polarity reversals though, to my knowledge, has not been previously suggested. Consequently, this may be regarded as an original contribution of this study.

It is also possible that a passing energetic superwave, a transit of the heliopause sheath, or a nearby supernova explosion could also supply sufficiently large quantities of cosmic rays to the radiation belts to cause a field reversal. While these may be reasonable mechanisms for explaining many of the reversals in the sedimentary record, they must be

ruled out as causes for the Late Pleistocene reversals since they would have produced an inordinately large increase in terrestrial C-14 levels, which is not observed.

[See **UPDATE:** p. 124 for evidence confirming this geomagnetic mechanism.]

3.3.4 Cosmic-Dust-Induced Climatic Change

When a world-cycle perishes by fire, there arises in the beginning a cycle-destroying great cloud, and a great rain falls throughout one hundred thousand times ten million worlds. The people are delighted and overjoyed, and bring forth seed of all kinds and sow; but when the crops have grown large enough for cow-fodder, the clouds keep up a braying noise, but do not allow a drop to fall; all rain is utterly cut off . . . When now a long period has elapsed from the cessation of the rains, a second sun appears . . . there is no distinction of day and night; each sun rises when the other sets, and an incessant heat beats upon the world . . . After the lapse of another long period, a seventh sun appears, and the whole world breaks into flames; and just as this one, so also a hundred thousand times ten million worlds.

(from the Pali writings of Ceylon and Burma on world cycles,
in *Buddhism in Translation*, Warren, 1979, pp. 321-323)

By itself, the superwave cosmic ray blast would not have been able to significantly affect the Earth's climate. At a peak superwave intensity of ~ 9 ergs/cm²/s, the cosmic ray energy flux would have been less than 10^{-5} of the incident solar energy flux. On the other hand, major climatic changes could have occurred if the Earth were to have passed through the heliopause sheath where the cosmic ray intensities may have reached 10^6 times higher. However, the occurrence of such a transit during the last ice age may be ruled out on the basis of the terrestrial C-14 record. Thus, it appears that the climatic oscillations ending the Pleistocene Epoch could not have been due to direct cosmic ray heating of the Earth. It is more likely that these events were brought about as a result of *indirect* effects of the 14,200 years BP superwave, namely effects arising from the transport of cosmic dust into the solar system.

There are several ways in which high levels of interplanetary dust could have affected terrestrial climate:

- a) Cosmic dust particles entering the Earth's upper atmosphere would have simultaneously increased the atmosphere's albedo and its ability to absorb solar radiation (cooling or warming effect).
- b) A circumterrestrial dust sheath would have attenuated sunlight reaching the Earth (cooling effect).
- c) Clouds of nebular material passing close to the Earth could have temporarily enhanced or attenuated sunlight reaching the Earth (temporary warming or cooling effect).
- d) An interplanetary hothouse effect would have increased the amount of radiation incident on the Earth by up to 5% (warming effect).
- e) A dust-obscured Sun could have radiated a large portion of its energy in the infrared portion of the spectrum rather than at visible wavelengths (warming effect together with a redistribution of energy in the earth-atmosphere system).
- f) Under certain conditions, cosmic dust intervening between the Earth and Sun could have reduced the solar constant in the Earth's vicinity as a result of scattering and absorption of the direct solar beam. If the dust were concentrated toward the ecliptic, then radiation lost to high latitude regions of the solar system would not be compensated for by light scattering and reradiation taking place in those places (cooling effect).
- g) The kinetic energy released by the accretion of nebular dust and gas would have

caused the Sun's total radiation intensity to increase, at times by up to several tenths of a percent (warming effect).

- h) Radicals such as NO_x and NH_3 produced in the Earth's atmosphere by solar flare and superwave cosmic rays could have affected terrestrial climate by altering the radiation transmitting properties of the atmosphere (warming effect).

With the exception of (g), most of the above scenarios are proposed in this study for the first time; refer to Subsection 3.3.2. The climatic consequences of a few of these are discussed below.

Climatic Consequences of a Change in the Earth's Radiation Budget. Several authors have explored the climatic consequences of a change in the Sun's radiation output and conclude that glacial/interglacial climatic flips could occur if the solar constant were to vary from its present value by 1 - 10%; e.g., Budyko (1974, pp. 306 - 308), Oerlemans and van den Dool (1978), Oerlemans (1980). Of the effects listed above, (b), (c), (d), (f), and (g) would produce variations in the amount of radiation received by the Earth, and of these (b), (d), and (f) would be most likely to produce major long-term effects. Effect (c) would have produced only temporary changes lasting on the order of a week to several months, and hence would have been effective in producing major climatic change only through frequent recurrence.

In regard to effect (d), it should be noted that a 5.3% long-term increase in the radiation intensity incident on the Earth, by itself, would be capable of producing an 8° C increase in global temperature assuming that atmospheric albedo remained constant. This is based on Budyko's (1974, p. 249) estimate that a 1.5° C temperature increase would be produced for every percent increase in the solar constant. If not compensated for by other effects (e.g., the melting of the glacial ice cover, solar obscuration, increased planetary albedo), this added insolation would have increased the Earth's mean temperature from its Ice Age value of ~8° C (46° F) to ~16° C (61° F). This additional radiation influx to the Earth would have been isotropic, equally affecting all latitudes. Moreover, this radiation source would have been present day and night producing in effect an "endless day."

To estimate the impact of an interplanetary hothouse effect on glacial recession, consider the effect of an addition of a background intensity of 0.05 times the solar constant, together with an unobscured solar flux. At a 50° N latitude location (40° noon, spring solar elevation angle) the day-averaged rate of glacial surface melting would be given as:

$$r = \frac{1.4 \times 10^6 \text{ ergs} / \text{cm}^2 / \text{s} \times (\sin 40^\circ + 0.05) \times 0.25 \times 0.5 \times 8.64 \times 10^4 \text{ s} / \text{day}}{4.186 \times 10^7 \text{ ergs} / \text{cal} \times 80 \text{ cal} / \text{cm}^3} = 3.1 \text{ cm} / \text{day},$$

where 0.25 is the time averaging factor and where 0.5 is the fraction of this radiation that goes into melting ice. For a summer noon solar elevation angle of 63° this melting rate would increase to ~4 cm/day.

At a rate of 3 cm/day, 11 meters of ice could become melted in one year and 2000 meters in 180 years, provided that such a high level of solar insolation were to persist. The sedimentary record indicates that glacial recession at the end of the Last Ice Age took place over a period of about 7000 years, though an extended period of accelerated glacial recession and continental flooding did occur about 14,500 – 14,000 cal yrs BP during an unusually warm interval; see Section 9.3. This seemingly perplexing event, which occurred at a time when the Earth was in a maximally glaciated condition, could be accounted for by an increase in the Earth's radiation budget by the amount proposed above.

Climatic Consequences of a Change in the Albedo of the Upper Atmosphere. Scenario (a) could have differing climatic effects depending upon the albedo characteristics of the

particular region of concern. For example, over low albedo regions (e.g., regions of low light reflection such as cloud-free and ice-free ocean regions) any increase in upper atmosphere albedo due to the presence of stratospheric and mesospheric dust would have had a maximal effect in decreasing the amount of incoming energy and would have tended to produce a climatic cooling. On the other hand, over high albedo regions (e.g., snow and ice covered polar regions) where only a small percentage of the incident radiation would normally be absorbed by the earth-atmosphere system, an added increase in albedo resulting from a dust laden upper atmosphere would not have had much of a cooling effect. But if these dust particles were partially light absorbing, then the additional radiant heat input to the Earth's surface resulting from upper atmosphere absorption and reradiation would more than compensate for the loss due to any increase in albedo. In such a case a net climatic warming could result (Twomey, 1977, pp. 278 - 287). Such a polar warming could initiate an ice advance or ice recession depending on its magnitude; see **p. 113** (this chapter).

Earlier (**p. 92**) it was estimated that entry of nebular material into the Earth's atmosphere could increase the mean planetary albedo by up to 1.5 percentage points. If not countered by atmospheric warming effects (such as (d) and (e) listed on **p. 102**), this could result in a 2° C drop in the Earth's surface temperature.

Toon and Pollack (1982, p. 131) present evidence indicating that periods of increased volcanic activity, occurring during the past 5 centuries, correlate with times of glacial advance. In particular the nineteenth century, which was a period of unusually high volcanic activity and accelerated ice advance, was characterized by an abnormally high stratospheric aerosol optical depth averaging on the order of $\tau \sim 0.1$. Thus it seems reasonable to expect that the proposed prolonged influx of cosmic dust into the Earth's atmosphere could have similarly brought about a glacial advance.

Scenario (a) in some ways resembles the proposal of Hoyle and Wickramasinghe (1978). They suggest that an ice age might become suddenly initiated by the deposition in the Earth's atmosphere of large quantities of submicron-sized dust particles of cometary origin, e.g., as a result of the Earth's passage through the tail of a comet. They estimate that 10^{-5} g/cm² ($\sim 5 \times 10^{13}$ grams total) of 0.1 μ particles having a visual opacity of 3×10^5 cm²/g would be able to produce an optically thick aerosol layer (optical depth $\tau \sim 3$) capable of attenuating 95% or more of the direct beam of sunlight incident on the Earth. Their theory suggests that the resulting shading would create a 40° C land/ocean temperature differential in a matter of weeks, since land surfaces cool more rapidly than ocean bodies. This temperature gradient would then cause the emergence of 100 mph winds, ocean evaporation rates of several meters per year, and ice accumulation rates of up to 100 meters per year (Hoyle and Wickramasinghe, 1978; Butler and Hoyle, 1979).

In contrast to the Hoyle-Wickramasinghe (H-W) theory, scenario (a) involves long term changes in upper atmosphere opacity. Hence land/ocean temperature differentials with this scenario would not be expected to form in the same way. Rather, scenario (c), which can involve brief abrupt occultations of the Sun, might be more apt to produce the required disparate land/ocean cooling rates. However, it should be noted that ice accumulation rates in polar regions much higher than 1 meter per year would be difficult to justify on the basis of the glaciological record. The H-W theory requires such high accumulation rates in order to achieve any significant climatic impact, since the event that it proposes is brief, lasting only on the order of a few years. Scenario (c), on the other hand, proposes a recurrent phenomenon.

Solar Spectral Shift: Global Climatic Effects. The effect of a spectral shift in the Sun's energy continuum (e.g., caused by the presence of a circumsolar dust cloud) until now has remained an unexplored virgin territory, probably because it was not evident that such spectral variations could periodically occur. Yet, such a shift would have had a major long

term impact on the Earth's climate. Thus it is worthwhile spending some time here examining the consequences of this scenario ((e) of **p. 102**).

If the Sun's continuum were to partially shift to the infrared, the Earth's climate would be substantially affected in several ways. One effect would be that a greater fraction of the incident solar radiation would become absorbed in the atmosphere with a smaller fraction being left over to penetrate to the Earth's surface. For example, curve-a in Figure 3.20 illustrates the current distribution of the solar radiation intensity for a series of spectral channels; based on data from Coulson (1975, Appendix B). The spectrum outlined by curve-b (shaded region) represents an extreme case in which the Sun's visible light is totally absorbed by the surrounding dust sheath and reradiated at 1150° K; cf. subsection 3.3.2 (**p. 94**). This spectrum was calculated on the assumption that the transparency of the dust sheath would vary as a function of wavelength as shown in curve-c (dashed line shown at the bottom of Figure 3.20). Obviously if optical wavelengths were to be totally extinguished for long periods of time (e.g., in excess of a year) its effects would be catastrophic for plant life. However, over short time periods, on the order of weeks or months, total solar obscuration could occur with a minimal amount of long-term damage to terrestrial vegetation.

Curve-d of Figure 3.20 (bottom) illustrates the percentage of solar radiation absorbed by the Earth's atmosphere at various wavelengths, as measured at sea level for a 50° solar elevation and under most probable weather conditions for middle latitudes. As is evident, the bulk of the obscured-sun spectrum (curve-b) spans the wavelength range 1 – 10 microns where the atmosphere is considerably less transparent as compared with the region 0.3 – 1.0 micron spanned by the bulk of curve-a. Most of this absorption would occur in the troposphere below an altitude of 15 kilometers, although absorption due to ozone, which accounts for the loss of ~3% of the incident radiation, would occur primarily in the stratosphere at an altitude of ~50 km. The way in which such a spectral shift would affect the energy flows in the earth-atmosphere system may be seen diagrammatically with the aid of the crude energy balance models shown in Figure 3.21(a) and (b); general format taken from Riehl (1972, pp. 44 - 58) and Budyko (1974, p. 226). Changes in stratospheric optical depth due to the presence of nebular aerosols are not considered here, nor are changes in the solar constant. Let us begin with the model shown in Figure 3.21(a) which represents average conditions for the Earth as a whole with its present climate and no solar obscuration (case-1). Among the incoming arrows at the left, Q represents the intensity of the incident radiation, and $Q_1 = (1 - \alpha_1)Q$ represents the intensity of this radiation after accounting for light reflection from the atmosphere and cloud cover, α_1 being the atmospheric albedo with the assumption of a 50% cloud cover. Here $\alpha_1 = 28\%$, so $Q_1 = 0.72 Q$, or simply 72% where the percentage is understood to imply a percentage of Q . Next, about 30% of Q_1 must be subtracted to account for atmospheric absorption; i.e., $Q_2 = Q_1 - \beta Q_1$ where $\beta = 30\%$ is the fractional attenuation. Radiation reflected due to ground albedo must then be subtracted, $Q_3 = Q_2 - \alpha_2 Q_2$, where $\alpha_2 = 0.14$ is taken as the average planetary ground albedo; cf. Budyko (1974, p. 226). Thus about 43½% of the incident radiant energy is able to finally reach the ground. A fraction βQ_4 of the radiation Q_4 reflected from the ground must be subtracted to account for atmospheric absorption, leaving $(1 - \beta)Q_4 = \alpha_2(1 - \beta)^2 \cdot (1 - \alpha_1)Q$ to escape into space. The total mean planetary albedo is given as $\alpha = \alpha_1 + \alpha_2(1 - \beta)^2 \cdot (1 - \alpha_1) = 33\%$ in accordance with the value used by Budyko (1974, p. 225). [See albedo **UPDATE: p. 125**]

The outgoing thermal energy fluxes and thermal energy exchanges to and from the troposphere are illustrated by the system of arrows on the right side of the diagram. The percentages again read as % of Q . Since the Earth has a mean temperature of $T \sim 15^\circ \text{C} = 288^\circ \text{K}$, its blackbody radiation curve peaks at around 10½ microns for an emissivity of $\epsilon = 0.6$. In this region of the spectrum from about 5 – 100 microns the atmosphere is heavily light-absorbing (see Figure 3.20, curve-d). Thus only a small fraction of the outgoing flux,

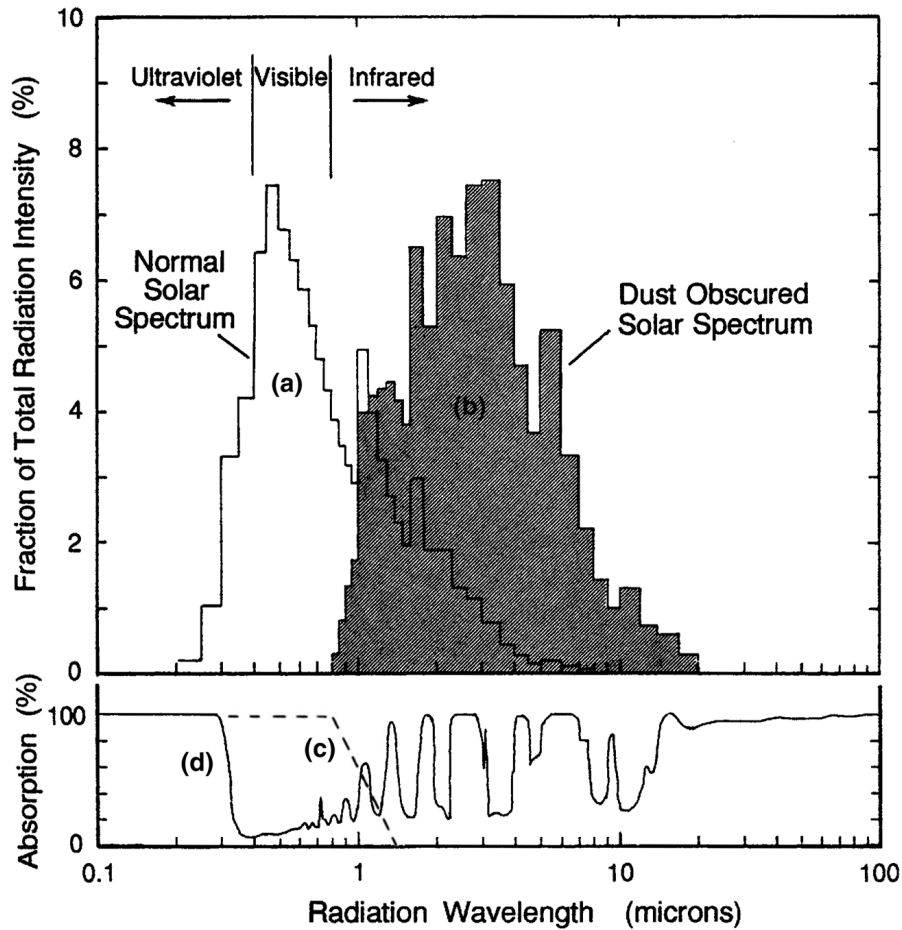


Figure 3.20. a) Current solar continuum spectral histogram ($T = 5800^\circ \text{K}$). Vertical axis plots radiation intensity in each spectral channel as a percentage of total intensity (units of $\text{ergs}/\text{cm}^2/\text{s}$), and the horizontal axis measures photon wavelength in microns. b) Solar spectral histogram for a dust obscured Sun, dust sheath radiating at $T = 1150^\circ \text{K}$. c) Percentage of solar radiation absorbed by the circumsolar dust shell as a function of wavelength. d) Percentage of solar radiation absorbed by the Earth's atmosphere as a function of wavelength (50° solar elevation angle).

about 13–14%, is able to escape into space, and this occurs primarily through the 10 micron window. The remaining 86–87% of the ground radiation is reabsorbed in the troposphere. As seen in Figure 3.21(a), I_1 represents the escaping radiation flux and I_2 the fraction that is absorbed by the troposphere. A comparable amount I_3 is returned from the troposphere to the ground and about half as much I_4 is radiated from the troposphere to space. Thus $I_2 \sim I_3 \sim \frac{1}{2}I_4$. Of the amount absorbed from the incident flux, $A = \beta(Q_1 + Q_4) = 23\frac{1}{2}\%$, about $A - 3\% = 20\frac{1}{2}\%$ must be figured into the energy balance of the troposphere, the remaining 3% being energy absorbed by ozone in the stratosphere. Thus for the troposphere we have a thermal flow input of $I_{\text{in}} = I_2 + A - 3\% = 118\frac{1}{2}\%$ and an output of $I_{\text{out}} = I_3 + I_4 = 147\%$. The troposphere energy balance therefore yields a deficit of $I = I_{\text{in}} - I_{\text{out}} = -28\frac{1}{2}\%$, as compared with an energy flow surplus from the ground of comparable magnitude; i.e., $R = Q_3 - I_1 = +28\frac{1}{2}\%$. Thus there would be a net transfer of thermal energy from the ground to

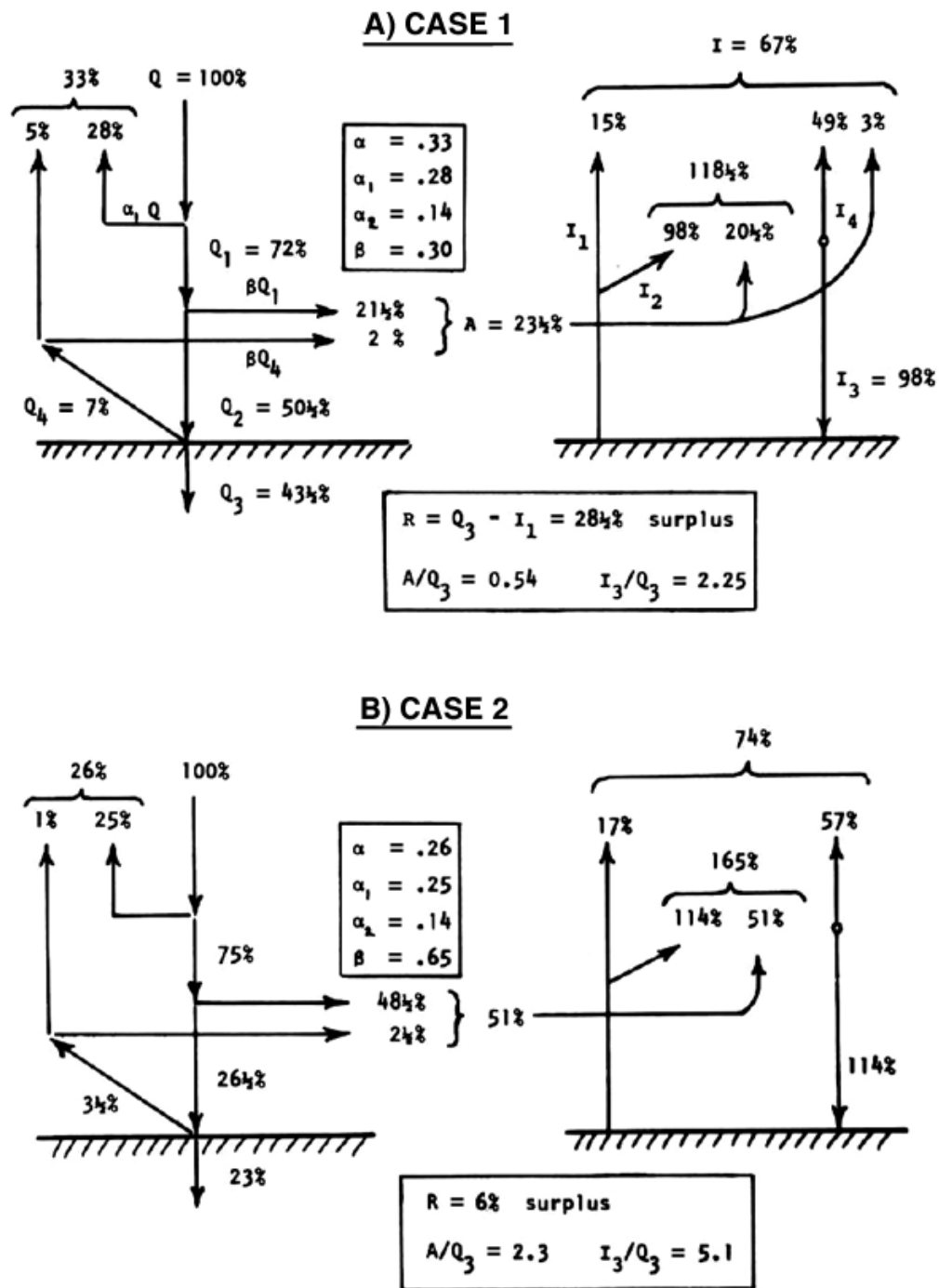


Figure 3.21. Energy balance diagrams depicting average annual solar and thermal energy exchanges for the planet as a whole; A) case 1: for the present climate, and B) case 2: for a dust-obscured Sun. Incoming solar radiation exchanges are shown on the left and outgoing infrared radiation exchanges are shown on the right.

[See **UPDATE:** p. 125 for cloud albedo revisions.]

the atmosphere which may be accomplished through the transfer of latent heat (through water evaporation) or sensible heat (through conductive heating of the air), latent heat transfer being the more important of the two. The various values in the above example for the albedo and fractional energy absorption of the atmosphere were chosen to be roughly consistent with values currently being used in energy balance models of the present climate (cf. Riehl (1972) and Budyko (1974)).

Now consider what would happen to the mean energy balance of the Earth if the solar intensity spectrum, which presently peaks at about 0.5 microns, were to shift to its maximally obscured form (curve-b) which peaks at about 3 microns (case-2). Figure 3.21(b) shows how the energy flows would become redistributed in such a case of extreme solar obscuration. First, let us assume a slightly lower atmospheric albedo of $\alpha_1 = 0.25$, neglecting for the moment the stratospheric aerosol contribution which undoubtedly would increase during dust congestion of the solar system. This 3% reduction in value is intended to account for the absence of Rayleigh scattering from gas molecules in the atmosphere which primarily affects short wavelengths. For example, blue light at 0.35 microns is 50% scattered, of which about half is scattered into space. For longer wavelengths the amount of scattering drops off rapidly according to λ^{-4} . In case-2 such scattering would be absent, thus Q would be 3% larger. In addition, the fractional attenuation due to atmospheric absorption would increase from $\beta \sim 30\%$ to $\beta \sim 65\%$ due to the fact that the Earth's atmosphere is more opaque at infrared wavelengths; see Figure 3.18 (curve-d). As a result of this greater degree of absorption, Q_2 would be far smaller than it was in case 1 and consequently the amount of radiation reflected by the ground $Q_4 = \alpha_2 Q_2$ would be proportionately smaller.

Comparing case-1 to case-2 it is seen that total albedo α drops by 7 percentage points from 33% to 26% due to a reduction in both Rayleigh scattering and ground reflection. If all other parameters were to remain constant (such as the fraction of cloud cover and stratospheric dust concentration), this would have the effect of producing a net warming of the terrestrial climate. According to Budyko (1974, p. 249), a 1% change in albedo would change the mean temperature of the Earth by 2.3° C. Thus a 7% drop in albedo should produce a 16° C increase in average global temperature. However, a portion of this reduction in albedo, or all of it, would most probably be cancelled by other effects. For example, earlier in this chapter (p. 104) it was shown that nebular particles entering the Earth's upper atmosphere would increase the planetary albedo.

Another effect of a displaced solar spectrum would be that direct solar radiation to the ground would become markedly decreased and the outgoing radiation from the ground slightly increased, thus reducing the energy balance of the ground from a surplus of 28½% in case-1 to a surplus of only 6% in case-2. It is very informative to compute the ratio A/Q_3 which compares the amount of incident solar energy absorbed in the atmosphere to the amount absorbed by the ground. For case-1 the ratio is 0.54, but for case-2 the ratio increases 4 fold to the value 2.3. Another informative quantity worth computing is the ratio I_3/Q_3 . It may be seen that in case-1 the ground receives on the average twice as much energy in the form of back-radiated thermal energy from the troposphere as compared with the amount it receives in the form of direct solar insolation. However, in case-2 this ratio would increase, with 5 times more energy reaching the ground in the form of tropospheric infrared as compared with direct solar infrared radiation. Thus it is apparent that there would be a major redistribution of thermal energy in the earth-atmosphere system.

For the present climate, air temperature is usually observed to decrease with increasing altitude since the ground is the principal absorber of radiant energy (case-1). However, under an obscured Sun (case-2), air temperature would be expected to remain roughly constant, or might even increase with increasing altitude, producing a temperature inversion. This would have the effect of increasing the vertical stability of the atmosphere and hence could lead to lower rates of heat loss from the oceans in tropical latitudes. However, counterbalancing this

effect, there would be a tendency toward greater heat loss due to a reduction in the atmospheric greenhouse effect. That is, since a larger fraction of the incident solar energy would be captured by the atmosphere at a relatively high altitude, less atmospheric thickness would be available to retain this captured heat.

In summary, several factors in combination would determine the degree to which the planetary temperature would be raised or lowered by the advent of an obscured Sun. These would include: a) the reduction in planetary albedo due to reduced Rayleigh scattering and reduced ground albedo contribution (warming effect), b) the increase in the tropospheric cloud cover fraction, hence an increase in planetary albedo (cooling effect), c) the increased vertical stability of the atmosphere (warming effect), and d) the decreased atmospheric greenhouse effect (cooling effect). These effects must be considered together with the possibility of an increase in albedo due to high stratospheric dust and moisture loadings (cooling effect), and an increase in background radiation back scattered from nebular material in the solar system (warming effect). Thus it is evident that determining the Earth's climatic response to a dust-congested solar system is a highly complex problem. Future studies using computer simulated models of the Earth's climate and of the radiative properties of the interplanetary environment would be very helpful in developing an understanding of this phenomenon.

Solar Spectral Shift: Alteration of the Arctic Thermal Regime. A shift of the Sun's continuum spectrum to the middle infrared would impact the Earth's climate most strongly at the polar regions. This would be due primarily to two factors. First, at high latitudes the Sun averages a much lower elevation in the sky and hence its radiation must pass through a greater quantity of the Earth's atmosphere before reaching the ground. For example, at a solar elevation of 20° typical of a 50° N latitude location in the winter or a Central Arctic location in the late spring, the path length is 2.9 times that of vertical penetration. Thus in the event of a spectral displacement of the Sun's continuum, changes in atmospheric radiation absorption would be considerably magnified at high latitudes.

The second factor applies specifically to snow or ice covered regions. Arctic snow has an albedo of about 0.8 in spring and autumn, decreasing to about 0.7 during the summer melting period. Thus for a Central Arctic location the effect of atmospheric absorption on total albedo (ground albedo + atmospheric albedo) would be considerably greater than in the global energy balance model considered earlier where the average ground albedo was taken to be 0.14. Consequently, the fractional increase in absorbed solar energy would be much greater in the Central Arctic. Such high latitude regions would therefore be expected to respond with a greater increase in their annual average temperature.

Energy balance diagrams for the Central Arctic are shown in Figure 3.22(a) and (b), presented in the same format as the global energy balance diagrams considered earlier. Here an 80° N latitude location is assumed, well within the southward extension of the present permanent ice cover which averages about 72° N. In addition, a solar elevation angle of 20° is assumed which would correspond to the average elevation typical of the end of May in the Central Arctic. The total albedo is taken as $\alpha = 0.62$, in accordance with the mean value based on satellite observations (cf. Raschke et al., 1968). The atmospheric albedo is taken as $\alpha_1 = 0.375$, which is $9\frac{1}{2}$ percentage points higher than the global average value used earlier. This is partly due to the higher than average cloud cover for an 80° N latitude location ($\sim 58\%$ as compared with $\sim 50\%$ for the global average) and because the cloud albedo would be slightly higher (50% rather than 45%) due to the low angle of the Sun; see Cess (1976) for a tabulation of pertinent data. Also more light will tend to be scattered by air molecules (Rayleigh scattering) and atmospheric aerosols (Mie scattering) due to the longer path length which light rays must follow in penetrating to the ground. For case-2 where the Sun's continuum is completely shifted to the middle infrared (extreme obscuration), an atmospheric

albedo of $\alpha_1 = 0.335$ has been assumed, 4 percentage points lower than that used in case-1, due to the absence of Rayleigh scattering. The ground albedo is assumed to remain unchanged at a value of $\alpha_2 = 0.8$, which is typical for snow cover. For radiation absorption by the atmosphere, an attenuation value of $\beta = 0.30$ is proposed for case-1, increasing to $\beta = 0.85$ for case-2. This β value is larger than the one proposed in the global energy balance diagram (case-2) since the Sun's rays would necessarily pass through a greater thickness of atmosphere before reaching the ground.

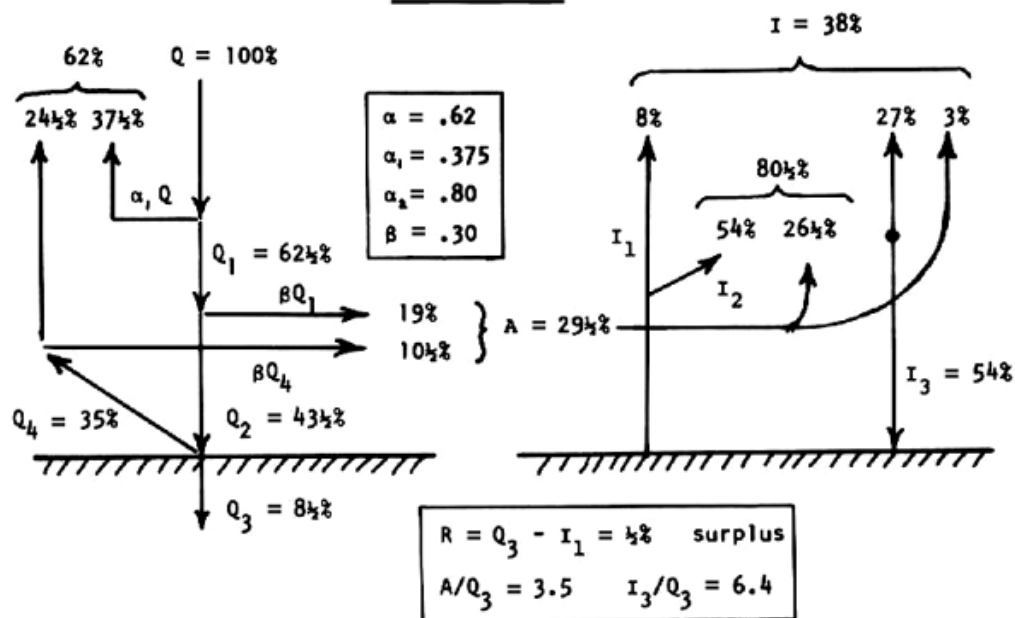
For case-1 it is seen (Figure 3.22(a)) that the Central Arctic at the end of May has a small positive radiation balance. In case-2 on the other hand (Figure 3.22(b)) a 14% radiation deficit is incurred at ground level. For ice free oceanic bodies of water this deficit would be made up by the flow of heat brought northward by ocean currents. Over land areas this negative energy balance would be made up by the transfer of latent heat from the atmosphere to the ground in the form of precipitation. Despite this ground level deficit, the total amount of radiation absorbed in the Central Arctic earth-atmosphere system would *increase* in case-2 due to a decrease in total planetary albedo from 62% to 34½%. The quantity A/Q_3 , representing the ratio of energy absorbed in the atmosphere to energy absorbed in the ground, would increase about 9 fold from 3.5 to 32. Also, the ratio I_3/Q_3 would increase about 8 fold from 6.4 to 50, indicating that in case-2 the ground would be receiving far more energy in the form of tropospheric reradiation as compared with direct solar insolation. Thus the proposed spectral shift of the solar continuum would have a major effect on the thermal energy structure of the Central Arctic earth-atmosphere system, the effects being more pronounced (relatively speaking) than those considered earlier in regard to the planet as a whole.

The proposed shift of the Sun's spectrum might affect the Arctic energy budget in a manner similar to the effect produced by totally removing the snow and ice cover of this region. Budyko (1974, Chapter IV, Section 2) has assessed an ice-free scenario for a Central Arctic location of 80° N latitude. He concludes that the decrease in planetary albedo from $\alpha = 0.62$ to $\alpha = 0.30$ resulting from ice-free conditions would raise the mean annual air temperature at this latitude by ~15° C. In view of Budyko's results (1974, p. 285), Figure 3.23 shows how the annual march of air temperature would increase as a result of snow and ice denudation. A similar change in temperature may be expected for a solar spectral shift (case-2) since the change in albedo would be of a comparable magnitude. For a low albedo Central Arctic, Budyko estimates an equilibrium temperature for the Arctic Ocean of ~4.3° C in the summer and -0.8° C in the winter, as compared to a water freezing point of -1.6° C. Thus, year around ice-free conditions would be insured in a region that is presently more than two-thirds covered by sea ice. Similar ice-free conditions could possibly exist during a period of extreme solar obscuration, provided that the resulting albedo reduction was not counteracted by other effects.

Elevated temperatures in the polar regions would also affect lower latitude regions of the globe causing an increase in their mean temperatures (Budyko, 1974, p. 286). Figure 3.24 illustrates the meridional temperature gradient presently observed in the Northern and Southern Hemisphere; cf. Cess (1976, p. 1833). The dashed line illustrates how a 15° C rise in mean annual air temperature at 80° N latitude might increase temperatures elsewhere in the Northern Hemisphere and reduce the meridional temperature gradient. A reduced meridional temperature gradient would be expected to form in a similar manner in the Southern Hemisphere. Thus it is evident that changes in polar climate brought about by a solar spectral shift would considerably alter the entire climate of the Earth.

A high concentration of stratospheric dust would (by itself) also tend to produce a climatic warming in polar regions. However, in this case solar radiation would become absorbed at a higher altitude where the atmospheric greenhouse effect would be lower and the climatic warming effect considerable reduced. Thus for a given amount of light

A) CASE 1



B) CASE 2

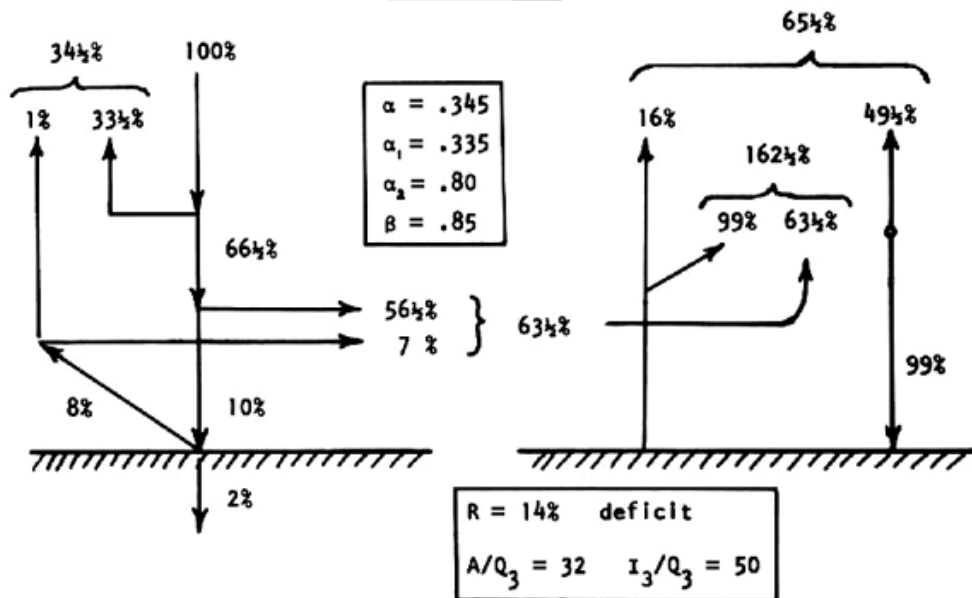


Figure 3.22. Energy balance diagrams depicting solar and thermal energy exchanges for the Central Arctic (80° N latitude location) at the end of May; A) case 1: for the present climate, and B) case 2: for a dust-obscured Sun. Incoming solar radiation exchanges are shown on the left and outgoing infrared radiation exchanges are shown on the right.

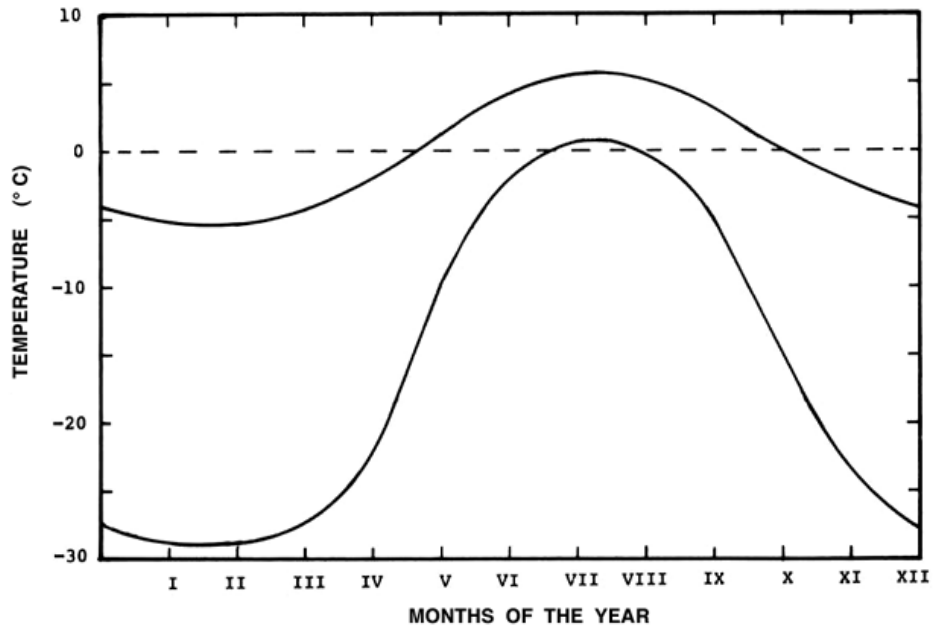


Figure 3.23. Annual march of air temperature for an 80° N latitude location: a) presently observed, and b) estimated for a hypothetical snow and ice-free condition (based on Budyko, 1974, Fig. 82 and Table 29).

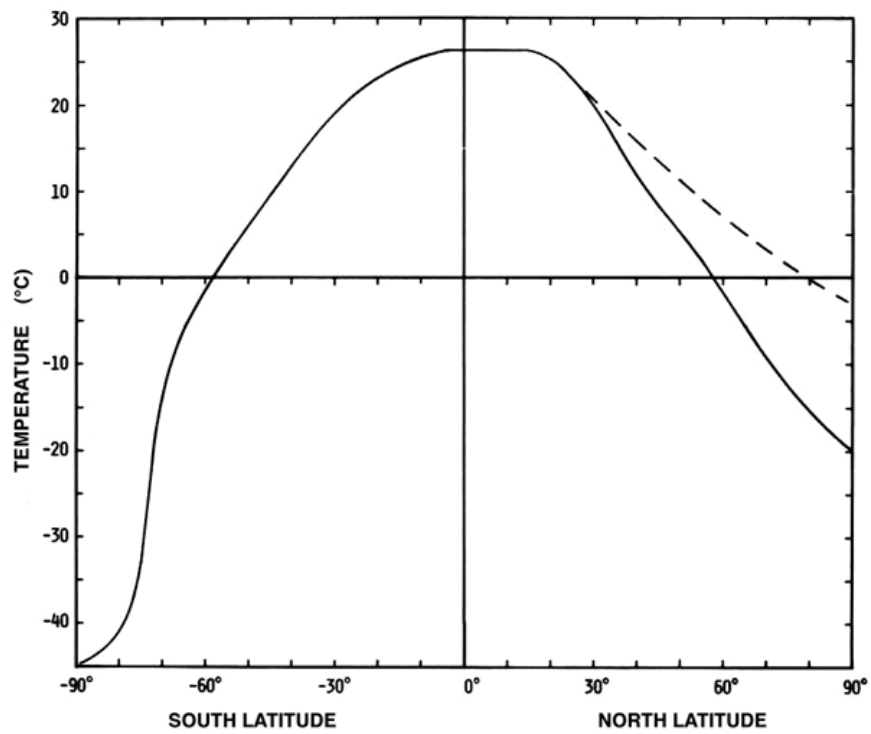


Figure 3.24. Meridional temperature gradients for the Northern and Southern Hemispheres as presently observed (solid line); data from Cess (1976, p. 1833). Dashed line indicates how the gradient might be altered if the average annual temperature of the Central Arctic (80° N) were to increase by 15° C.

absorption, less warming would be produced if this light were absorbed by stratospheric aerosols as opposed to being absorbed by the gas phase of the troposphere. Depending on the circumstances, the climatic effect of solar obscuration (and spectral shifting) and the climatic effect of stratospheric obscuration by nebular dust may be complementary or competitive. For low levels of solar obscuration, involving only a fractional shift of the Sun's radiation continuum to the infrared, atmospheric gas phase absorption would be more moderate, and hence there would be an opportunity for further reduction of the total albedo through the absorption of radiation by stratospheric aerosols. Thus the two effects would be complementary. However, for a heavily obscured Sun with a spectrum emitted almost totally in the infrared, the albedo would already be maximally reduced due to gas phase IR absorption effects. In this case the presence of stratospheric dust would instead produce a cooling effect due to its tendency to absorb radiation at a higher altitude. It is also possible that the stratospheric dust particles would be more reflective and less efficient absorbers at longer wavelengths, in which case the presence of such particles would be even more "parasitic" in the event of a solar spectral shift. Indeed, the plurality of variables involved and their interactive nature should present quite a challenge to future climatic modelers.

Glacial Growth and Recession. The cause of rapid glacial growth has long been a troublesome problem for theoreticians. Namely, if the Earth's climate were initially in a warm interglacial state, why should it suddenly become destabilized and thrown into a period of glacial advance, especially when such a climate had prevailed for many thousands of years. This problem is even more acute for episodes of glacial growth taking place during an ice age, when the temperature and absolute humidity of the atmosphere are significantly lower, thus reducing the rate of precipitation. Such an ice advance occurred at the beginning of the Late Wisconsin stage of the past ice age. The scenario proposed by the Galactic Explosion Hypothesis, however, is able to overcome many of these problems. First, it explains how a climatic state which has prevailed for a long time can become suddenly disturbed. The cause does not arise from within the terrestrial climatic system, but is forced upon it by sudden changes in its interplanetary environment. Second, the requirement of sudden initiation is met, since the passage of a superwave and injection of cosmic dust into the solar system would occur in an abrupt manner. Third, the altered radiation environment would produce climatic conditions ideal for glacial growth. For example, if the atmosphere were to heat up, as a result of a shift in the Sun's spectrum toward the infrared and as a result of light absorption by cosmic dust particles, then the absolute humidity of the atmosphere would increase, allowing more water vapor to become transported from the oceans. At the same time the ground and lower troposphere, being cooler than the atmosphere, would serve as a heat sink where water vapor could precipitate as sleet or freezing rain. Ground albedo, and hence the degree of terrestrial glaciation, would not be a critical factor determining the net energy balance since the above heating effects would depend primarily on the radiation absorption properties of the atmosphere.

Temperature inversion conditions would be most extreme at high latitudes where glacial growth would be most likely to take place. Figure 3.25 illustrates hypothetical vertical temperature profiles for a high latitude location (noon solar elevation of 50°) for: a) ice-free oceanic regions and b) inland regions. Curve-b may be compared to curve-c, which represents the temperature inversion profile observed over Portland, Maine, on the evening of January 6, 1962, during which time precipitation fell in the form of sleet and freezing rain (Riehl, 1972, p. 225). With warm air at high altitudes water vapor from oceanic regions could become transported inland a considerable distance before precipitating as sleet. As a result of the subzero temperatures prevailing at low altitudes sleet could accumulate on the ground and remain frozen over indefinitely long periods of time. In this way glacier formation could take place at an accelerated rate.

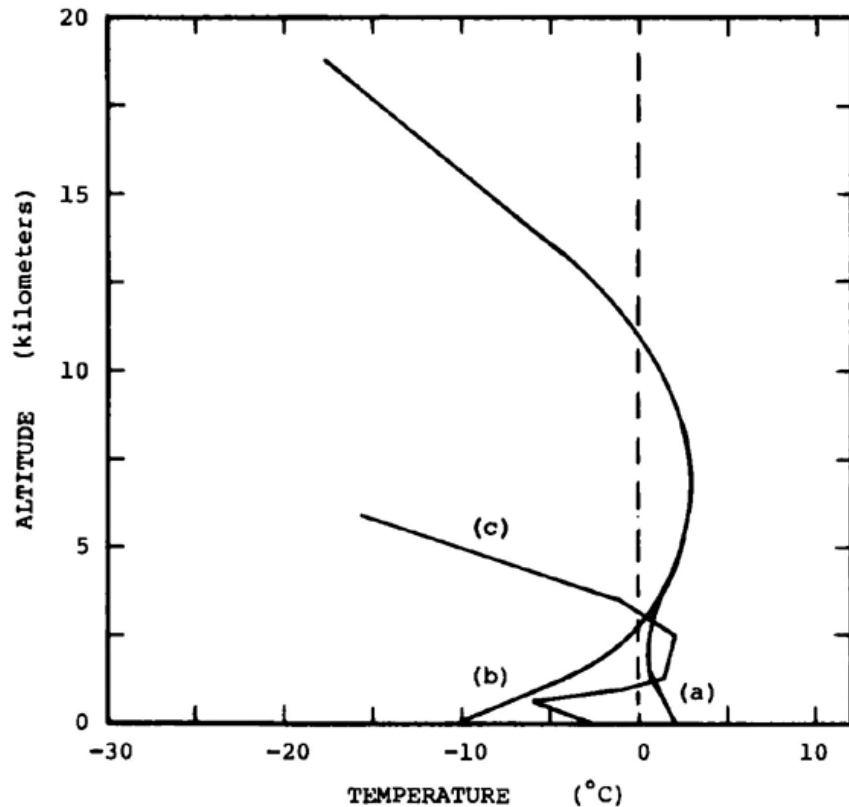


Figure 3.25. Hypothetical vertical temperature profiles for the Earth's atmosphere under a dust-obscured Sun for: a) ice-free oceanic regions (80° N latitude) and b) inland regions (80° N latitude) compared with c) a temperature inversion profile observed over Portland, Maine, in January, 1962.

If the warming at high latitudes were sufficient to maintain coastal bodies of water in an ice-free condition, this would have been another factor which would have led to enhanced precipitation rates in cooler inland areas. Free of ice, these bodies of water would be able to humidify and warm the atmosphere. The latent heat they would lose through evaporation would be replenished by warm water brought northward by ocean currents. Ruddiman et al. (1980) have emphasized that warm bodies of water adjacent to arctic regions are important prerequisites for rapid glacial build-up; see Chapter 9 (Section 9.2). Moreover, Fletcher (1966) has suggested that an ice-free Arctic Ocean would produce a high latitude climate characterized by cool summers and mild winters with abundant precipitation, conditions which could initiate the development of glaciation in high and mid latitudes.

Both glacial advance and recession may involve a common mechanism which depends on the degree of polar warming. For example, with moderate levels of high latitude warming, conditions would probably favor glacial advance. But with further warming, glacial advance would most likely be replaced by glacial recession due to accelerated melting of the ice or snow cover. Thus, cosmic dust invasions may serve as a triggering mechanism initiating and terminating ice ages. In addition, long-term variations in the Earth's orbital parameters would probably play an important role in biasing the Earth's climatic system toward one mode or the other.

The Precession of the Equinoxes and the Production of Glacial Cycles. It is interesting to speculate that the annual variation of the Earth's distance from the Sun due to the

eccentricity of the Earth's orbit may play an important role in determining whether an external perturbation of the terrestrial climate would result in ice sheet growth or recession. Presently the solar constant varies from a maximum of about 3.4% above its mean value at perihelion (closest approach to the Sun) on January 1 to about 3.4% below average at aphelion on July 1. Thus presently with perihelion occurring close to the winter solstice the Northern Hemisphere is having cool summers and mild winters, ideal conditions for the initiation of ice sheet growth. However, due to the precession of the equinoxes and other minor orbital effects the longitude of the perihelion changes through 360° over a period ranging from 20,000 – 25,000 years. Over the past cycle this period of variation has been close to 22,000 years. Using Berger's data (1977) to follow the variation of the longitude of the perihelion back in time, it is found that about 11,500 years BP perihelion coincided with the summer solstice, giving maximally hot summers and maximally cold winters in the Northern Hemisphere, ideal conditions for glacial retreat. Going further back in time, conditions would have been optimal for glacial growth around 22,000 years BP and for glacial recession around 33,000 years BP.

In summary, the following general model is proposed to account for the glacial-interglacial oscillations characteristic of the Pleistocene climate. The initiators of the abrupt climatic changes are ultimately astronomical in nature — superwaves that transport nebular material into the solar system. These particles of dust and ice would in turn cause changes in the Sun's continuum spectrum, in the intensity of solar radiation transmitted to the Earth, and in the Earth's atmospheric albedo. These external perturbations of the Earth's climate would occur in a random fashion, but they would have differing effects depending on the particular phase of planetary precession. Thus the regular variation of the longitude of the perihelion would introduce a cyclic character to the resulting climatic response, ice sheet growth being more probable during winter perihelion epochs and ice sheet recession being more probable during summer perihelion epochs. Following each brief destabilizing event, the Earth's climate would tend to enter a period of stabilization, the particular climatic state adopted being dependent on the extent of the glacial ice cover. If the supply of cometary debris residing near the heliopause were to gradually diminish, the amount of cosmic dust periodically injected into the solar system by passing superwaves would also diminish as would the severity of the induced climatic changes. Eventually, a point would be reached where superwaves of moderate intensity would be able to pass the Earth without producing significant climatic changes. However, even with dust-free conditions there is always the possibility that a superwave of high intensity could pass by and cause a major climatic perturbation.

3.3.5 Biological Effects

There are several ways in which the passage of a Galactic superwave could have affected living organisms, as seen in Figure 3.26. Consider first the direct effect of the superwave cosmic ray electrons. In Subsection 3.3.1 it was determined that at the superwave's peak intensity the sea level radiation intensity would have increased about 80 fold from its normal steady state level. Given that the current background flux of ionizing radiation measured at sea level at the geomagnetic equator is ~0.05 roentgens/year (r/yr) (Harrison, 1968), during peak superwave intensity a flux of ~4 r/yr would be present. Chronic exposure to such levels would not have serious consequences. This dosage rate is comparable to the maximum acceptable occupational dose rate for human beings (~100 mr/wk), although it is about 5 times the maximum acceptable occupational dose rate for pregnant women. At this exposure rate, a human being would accumulate about 100 r over the course of one generation, resulting in a doubling of the mutation rate (cf. Harrison, 1968; after Kato, Schull, and Neel, 1966; Glasstone, 1964).

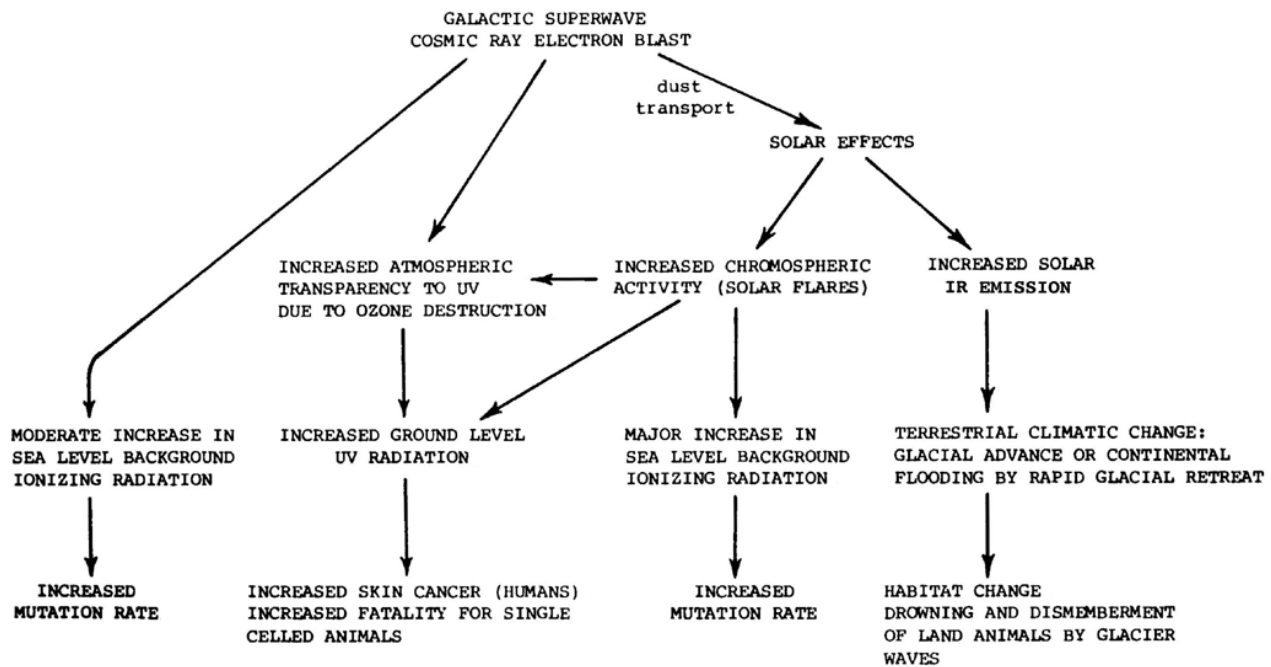


Figure 3.26. Ways in which a Galactic superwave could affect living organisms.

It is possible that at other times in geologic history there may have been superwaves having a much higher cosmic ray intensity than the levels postulated here for the 14,200 years BP event (perhaps even up to 1000 times higher), in which case the mutational and health effects would have been much more serious. However, radiation levels very much higher than the quoted level can be ruled out for the 14,200 years BP event, since higher cosmic ray intensities would have caused an excessive elevation in C-14 concentration in the terrestrial carbon reservoir.

The heliopause sheath would also have posed a substantial threat to planetary life. As was discussed in Subsection 3.3.2, the heliopause could have contained cosmic ray energy densities of the order of $10^{-4} - 10^{-3}$ ergs/cm³, or about $10^9 - 10^{10}$ fold greater than the current cosmic ray background levels. If the heliopause happened to contact the Earth during a period of peak superwave intensity, radiation levels on the order of 100 to 1000 r/min would have occurred at the Earth's surface. At these rates most unprotected life forms, both plants and animals, and surface dwelling sea creatures would have received the lethal dose within a matter of minutes. The planet would have become practically barren of life except for the lucky few which at the appointed time happened to be sheltered under a sufficient thickness of rock, soil, or water. However, for the 14,200 years BP superwave, exposure times longer than a few minutes at these high radiation rates can be ruled out on the basis of the Earth's C-14 record.

An increase in the cosmic ray electron background would also have affected life forms in an *indirect* manner. For example, the atmospheric photo-electron cascade produced by cosmic rays generates a considerable amount of atmospheric ionizations which in turn produces nitrous oxides (and other compounds) which in turn catalytically destroy atmospheric ozone. The ozone layer, which is found at an altitude of ~30 kilometers in the Earth's stratosphere is effective in screening out harmful solar UV radiation. Thus increased cosmic ray electron levels, by being involved in the destruction of the ozone layer, as a side effect would induce an increase in the level of UV radiation reaching the ground.

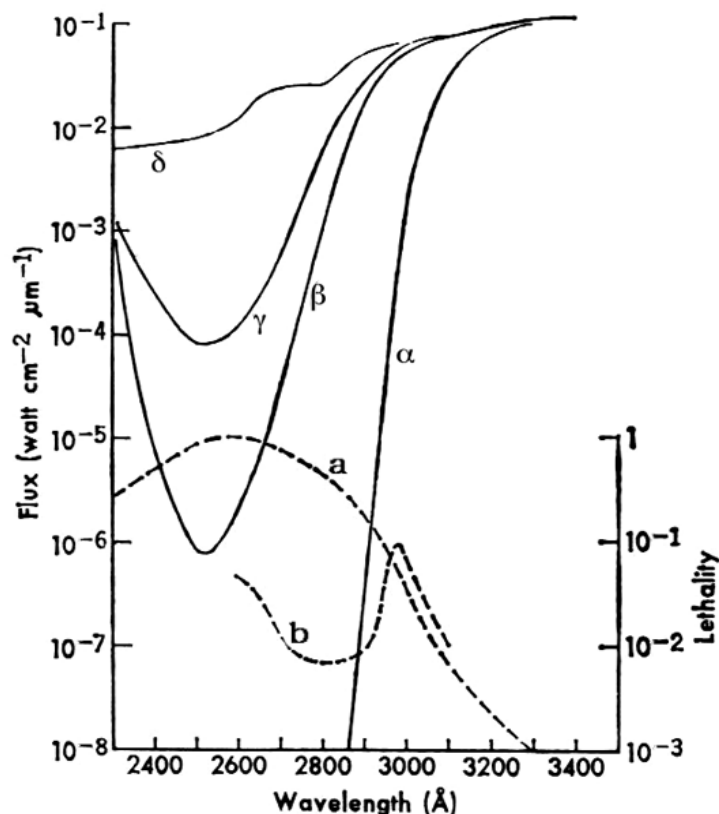


Figure 3.27. Solar ultraviolet flux on the Earth (vertical incidence): Curve α , after passing through a typical stratospheric ozone layer, Curve β , after passing through an O_3 layer depleted to 10% of its present concentration, Curve γ , after passing through a layer depleted to 6% of the present O_3 concentration, Curve δ , flux at the top of the atmosphere. Curve a, relative effectiveness of ultraviolet flux at various wavelengths in killing bacterial cells. Curve b, relative effectiveness of ultraviolet flux in producing erythema (sunburn) (reproduced from Ruderman, 1974). (Copyright 1974 by the American Association for the Advancement of Science.)

Ruderman (1974) estimates that a supernova explosion producing a hundredfold increase in cosmic ray intensity at the top of the atmosphere would cause a 2 – 50 fold increase in NO_x concentration, which in turn would produce a decrease in ozone concentration to a level that would be between 60 and 3 percent of its former value. These same figures would be equally applicable to the proposed superwave cosmic ray electron blast. At the hypothesized intensity the 14,200 years BP superwave would produce about a 75 fold increase in the cosmic ray flux reaching the top of the atmosphere.

Figure 3.27 (Ruderman, 1974) illustrates how varying degrees of ozone reduction would affect the level of UV radiation reaching sea level. Note that a 10 fold decrease in ozone (to 10% of its former level, curve β) would have drastic effects. At 3000 Å, the wavelength most effective in producing sunburn, there would be a hundredfold increase in UV intensity. However, at 2500 Å, the wavelength most harmful to single celled organisms, there would be a 10^{36} fold increase! At this wavelength the stratospheric ozone layer normally allows only 1 out of about 10^{40} photons to penetrate (Coulson, 1975, p. 144). A major increase in 2500 Å radiation could have serious consequences for phytoplankton which dwell near the ocean surface. Water is not a very good shield for UV radiation. It takes 5 meters of pure water to

attenuate 2900 Å wavelength radiation to 3% of its former intensity (Ruderman). For humans the main worry would be skin cancer, wavelengths in the 2000 – 3000 Å range being most biologically active (Coulson, p. 147). However, this would not be a problem for most mature land animals, since feathers, fur, or hide would offer suitable protection. But young animals would have to be sheltered.

There would have been several biologically significant effects arising as a result of the activation of the solar chromosphere. For example, if solar flare activity had become 10^3 times more intense as a result of nebular material falling into the Sun, cosmic ray proton intensities striking the Earth's atmosphere could have averaged 100 times higher than present background levels (i.e., assuming that solar cosmic rays currently contribute about 10% of the cosmic ray flux above 10 GeV). This would have produced an acceleration of the mutation rate comparable to that caused by the superwave cosmic ray electron flux. In addition, the UV flux from the Sun would have risen considerably. UV radiation would have been produced both from the ever-present solar flares and from heating of the solar chromosphere by infalling material; cf. Subsection 3.3.2. As an extreme example, if the Sun were to enter a T Tauri phase of activity and were to adopt a continuum similar to the star R W Aurigae, its UV emission in the 2500 Å band could conceivably increase 10 fold. However, at this wavelength a more dramatic change in the ground level UV flux would have come about as a result of deterioration of the stratospheric ozone layer.

Sudden climatic changes brought about as a result of a shifting of the solar spectrum to the infrared and changes of the solar constant would also have made a significant impact. Consequent increases in the amount of radiant energy absorbed by the Earth could have caused a considerable increase in the temperature of the Earth's atmosphere (and surface), particularly in low latitudes. This in turn could have induced death through hyperthermia, especially in the case of land animals. A very intense, but brief, heating episode associated with a major nova-like solar outburst (such as is considered in Section 4.7.3) could also have produced fatal results. In addition, glacier waves, forming as a result of accelerated glacial melting at high latitudes, would have been particularly hazardous through their ability to dismember and drown land animals; see Chapter 10, p. 277. Perhaps the greater portion of the Terminal Pleistocene fossil record owes its creation to the agency of such continental flooding episodes; see Chapter 10.

In general, the Galactic Explosion Hypothesis predicts that at the end of the Wisconsin Ice Age period (14,000 – 10,000 years BP) there would have been a greater chance for mass extinction. Large land mammals would have been at a particular disadvantage since they would have had greater difficulty in seeking shelter from the hazards of glacier waves and elevated levels of ionizing radiation. As is discussed in Chapter 10, a major extinction of large land animals, the worst of the Pleistocene, occurred between 14,500 and 12,700 calendar years BP, most likely in connection with a major episode of continental flooding of global extent.

If Galactic superwaves (and possibly associated solar effects) periodically produce very high radiation levels on the Earth, then the history of evolution should indicate the presence of periodic evolutionary spurts. That is, the reduction in population sizes brought about by the hazardous environmental conditions would have led to the formation of isolated animal communities. This isolation, together with the resulting acceleration in mutation rate, would have tended to foster speciation, i.e., the evolution of a parent species into a variety of daughter species. Thus over the space of a few centuries or less, a cosmic ray barrage could have terminated some species, while at the same time inducing the remainder to branch into a plurality of novel forms. As is discussed in Chapter 11, Section 11.1, the paleontological record indicates that, indeed, there appears to be a quantum, step-like character to evolution.

3.3.6 The Possibility of Superwave Gamma Ray Pulses and Their Consequences for Present-Day Society

By the power of God there issued from the essence of Brahma a being shaped like a boar, white and exceedingly small; this being, in the space of an hour, grew to the size of an elephant of the largest size, and remained in the air. . . . They were engaged in this conversation when that vara, or 'boar-form', suddenly uttered a sound like the loudest thunder, and the echo reverberated and shook all the quarters of the universe.

(The second Hindu "Avatar," quoted by Donnelly, 1883, p. 132
after Maurice, *Ancient History of Hindustan*, Vol. I, p. 304)

On the basis of theoretical considerations, it is estimated that about 1% to 50% of a supernova's energy is emitted as a brief pulse of gamma ray radiation lasting on the order of an hour or so (Gould and Burbidge, 1967). Supernova explosions typically have total energies in the range of 10^{49} – 10^{51} ergs, so gamma ray energies on the order of 10^{47} – 10^{50} ergs could be expected. In a similar fashion, a Galactic explosion might generate a pulse of gamma rays at the time of the initial outburst. Since Galactic explosions are a much larger scale phenomenon, the associated gamma ray pulse would also be more energetic. Since the initial outburst from a galactic core explosion has yet to be observed, it is uncertain if gamma ray pulses are indeed produced. The same could be said about supernova explosions. A superwave gamma ray pulse would have to be sufficiently intense (on the order of 10^4 ergs/cm²/s or about 100 times the peak cosmic ray electron intensity proposed for the 14,200 years BP superwave) and sufficiently brief (on the order of a few microseconds) in order to generate an electromagnetic pulse (EMP) in the Earth's atmosphere that would be hazardous to modern societies. For example, such a pulse was produced by the 1.4 megaton Starfish Prime hydrogen bomb test conducted at an altitude of 450 kilometers over the Pacific Ocean. The EMP resulting from the gamma ray burst from this nuclear explosion is known to have been responsible for serious electrical failures in nearby cities. For example, in Hawaii, 1500 km from the blast, street lights blew and power lines went dead. At the time of the Starfish Prime test this effect was totally unexpected. Since then the following explanation has been proposed. As the gamma rays from the airborne nuclear explosion struck the upper atmosphere they knocked electrons out of air molecules, and as these electrons twirled around lines of force of the Earth's magnetic field they radiated synchrotron radiation spanning the frequency range from 0 to 100 megahertz. This intense radio emission was then picked up by metallic objects on the ground (e.g., power lines, radio antennae, etc.) and became converted into very high voltages, on the order of 10^4 – 10^5 volts per meter of conductor length. This in turn caused widespread instances of electrical overloadings.

The dangerous effects of nuclear EMP has become a subject of great concern; see Broad (1983) for an overview. For example, a single nuclear warhead detonated above the U.S. would completely wipe out its satellite communication systems. In addition, ground-based telephone, radio, and television communication systems would become paralyzed as powerful electrical surges vaporized and permanently damaged the delicate semiconductor components of transmitting and receiving equipment. Any electrically powered unit plugged into the commercial power grid would be vulnerable to damage from lethal voltage surges conducted by power lines. Before protective fuses could operate countless appliances and machines, both in residential and industrial sectors, would become destroyed. Voltage regulators in automobile engines and trucks would similarly become damaged causing traffic everywhere to grind to a halt.

All of the above effects described for a nuclear explosion scenario might also occur in

the event of a Galactic explosion except that the event would be geographically more widespread and might transpire over a greater span of time. Moreover, like the threat of a nuclear attack, a superwave would come without warning since it would travel toward the Earth at the speed of light, conveyed at the forefront of the superwave event horizon. Within seconds of its arrival industrial societies around the globe would become thrown into a state of chaos. Virtually overnight societies would be forced to temporarily regress by 100 years into the pre-electrical, pre-automotive age. Industrialized societies would be most affected due to their extreme dependence on electrical equipment for the production and distribution of goods, for transportation and commerce, and especially for communication. Ironically, less developed countries of the third world would stand a better chance of recovery because such societies are not as dependent on automation.

A superwave EMP would cause some loss of life through electrocution, i.e. unfortunates who happened to be touching large metal objects at the time of pulse arrival. However, the greatest loss of life would occur in the days that followed as entire nations of people began to approach the point of starvation and as social chaos began to break out. Perhaps even more frightening is the threat that the arrival of the superwave could trigger a nuclear holocaust. Since to a local observer the effects of a superwave EMP would be virtually indistinguishable from those of an aerielly detonated atomic warhead, the unexpected arrival of a superwave could become simultaneously misinterpreted by military officials in various nations around the world as a nuclear attack. Moreover, with global and national communication systems knocked out there would be no opportunity for individual nations to check among themselves to determine if indeed a nuclear attack had been launched. In fact, commanders in charge of missile silos scattered around the world would not be able to contact their own headquarters to receive orders. Cut off from their superiors they might take matters into their own hands and independently order the firing of their cache of missiles. Within minutes an uncontrolled spasm of nuclear explosions and retaliations could become initiated. What would follow need not be detailed here. The tragic effects of nuclear annihilation are well understood and appreciated by a substantial segment of the informed world population. Moreover, the realization that plutonium-239, a biologically lethal by-product of nuclear fission, has a half-life of 24,400 years is itself a sobering fact.

[**UPDATE:** The danger of an EMP triggered global thermonuclear war has been significantly reduced since 1983 when this dissertation was first published. The former Soviet Union has been replaced by a group of republics and cold war tensions have ended for the most part. Nuclear missiles on both sides have been dismantled. Also the U.S. has made considerable progress in hardening its command center electronics and communications against EMP. In 1989, the Starburst Foundation conducted an international outreach to defense departments, world government representatives, and nongovernmental organizations that widely communicated the above recommendations to reduce the number of nuclear weapons and to EMP harden all critical military communications channels. Hopefully, this dissertation and outreach project contributed to the achievement of these goals. See Appendix K (pp. 473 – 476) for a few responding letters. However, the number of nations possessing nuclear weapons has increased since 1983 and the U.S. alone, as of this date, still has 7500 nuclear warheads, with 2500 of those being on alert status.]

The present world situation may be likened somewhat to a series of powerful spring-loaded traps whose jaws are cocked open, the superwave EMP being the feather or collection of feathers that unexpectedly happens to flutter down onto their sensitive hair triggers. Thus the worst effects of a superwave passage could be entirely avoided if the nations of the world would take proper precautions. We cannot predict exactly when a superwave EMP will arrive. However, on the assumption that Galactic explosions recur as frequently as once every 5000 years we can be sure that at least 4 or 5 such superwaves are already on their way toward the

Earth from their birthplace at the Galactic Center. The closest event horizon could arrive tomorrow, or it might arrive 2000 years from now. There is really no way of telling for sure.

The following steps should be taken both to reduce the threat of nuclear war and to make the social structure more resistant to the potential threat of a superwave gamma ray pulse.

- 1) Military strategists should become aware of the possibility that energetic gamma ray pulses could arrive without warning from astronomical sources in our Galaxy.
- 2) The use of nuclear arms should be abandoned by all nations. Until that time, EMP-proof communication channels should be developed. Not only should missile launching sites be securely linked to central defense headquarters, but also the defense headquarters of all nuclear-armed adversaries should be securely interlinked. This might involve setting up a relay network of infrared lasers, their beams being transmitted from EMP-proof apparatus on the ground and reflected back to Earth from large space mirrors positioned in geosynchronous orbits. Redundancy should be designed into the system.
- 3) Commercial communication systems should be completely redesigned. EMP-proof satellite communication systems should be designed perhaps employing laser technologies. Also, all critical telephone cables should be eliminated and replaced with fiber optic systems conducting modulated laser signals.
- 4) All commercial and industrial electrical appliances, electronic equipment, and machines should be equipped with high speed zener diodes capable of shorting out potential EMP surges.
- 5) The commercial power grid should become *decentralized*. Individual buildings should become energy self-sufficient, capable of generating their power needs through the use of zener-diode-protected photovoltaic cells.
- 6) The electrical components of all motor vehicles should be protected with fast-acting zener diodes.
- 7) A network of national and international emergency preparedness organizations should be set up for the purpose of coordinating repair operations and for hospitalizing accident victims should a global superwave disaster arise.

3.4 PRESENT EFFECTS

If a superwave event horizon did in fact depart from the Galactic Center about 37,000 years ago and pass the Earth about 14,200 years BP, its effects should be observable at present; see the right hand box in Figure 3.1. Wherever the relativistic electrons happened to encounter interstellar gas and magnetic fields, they would disclose their presence by the variety of electromagnetic radiation which they would produce ranging from the radio to the gamma ray portion of the spectrum. This radiation would be expected to be concentrated along the Galactic plane, since this is where stars and gas would be at their highest concentration. Evidence for such diffuse emission (the Galactic radio background) is discussed in Chapter 5, Section 5.1. Particularly, strong electromagnetic emission would be generated wherever superwave cosmic rays happened to encounter supernova remnants; see Section 5.2. In addition, superwave cosmic rays could serve as "catalysts" for initiating energetic stellar activity. For example, by propelling interstellar dust and gas close to stars, accretion processes could become initiated which in turn could promote stellar eruptions and in some cases could trigger supernova explosions; see Chapter 3 (Section 3.3.2) and Chapter 5 (Section 5.2.2).

3.4.1 The Shape of the 14,200 Years BP Event Horizon

If light (and information) were to travel instantaneously to us from any point in the Galaxy, then the superwave event horizon would appear as a perfectly spherical shell of radiation, or a perfect circle when projected onto the Galactic plane; see Figure 3.28(a). All points on the horizon would be equally distance from the Galactic Center at a radial distance of 37,000 l.y. Moreover, in the Galactic anticenter direction the horizon would be detected at 14,200 l.y. from the Earth.

However, since light travels at a fixed velocity, c , to observers on Earth this spherical geometry would become distorted into a prolate spheroid, or an ellipse when projected onto the Galactic plane; see Figure 3.28(b). One focus of the ellipse would be centered at the observer's location (Earth) and the other focus would be centered at the point of origin for the outburst (the GC). A straight line drawn from the GC to a point P on the ellipse (i.e., line \overline{OP}) would represent the superwave's travel distance (or travel time). Also, a straight line drawn from point P to the Earth (i.e., line \overline{PE}) would represent the distance that the induced radiation travelled to reach Earth. Since the superwave propagates uniformly in all directions at the speed of light, it must be true that for any point P on the ellipse $\overline{OP} + \overline{PE} = 37,000$ l.y. Thus, as an observer's line of sight to the ellipse swept toward the GC, he or she would be seeing the event horizon as it was positioned further and further back in time. The portion of the horizon that was closest to the Earth would be observed to lie in the Galactic anticenter direction at a distance of ~ 7100 l.y. (2.18 kpc). So even in this anticenter direction an observer would be looking quite a ways back in time.

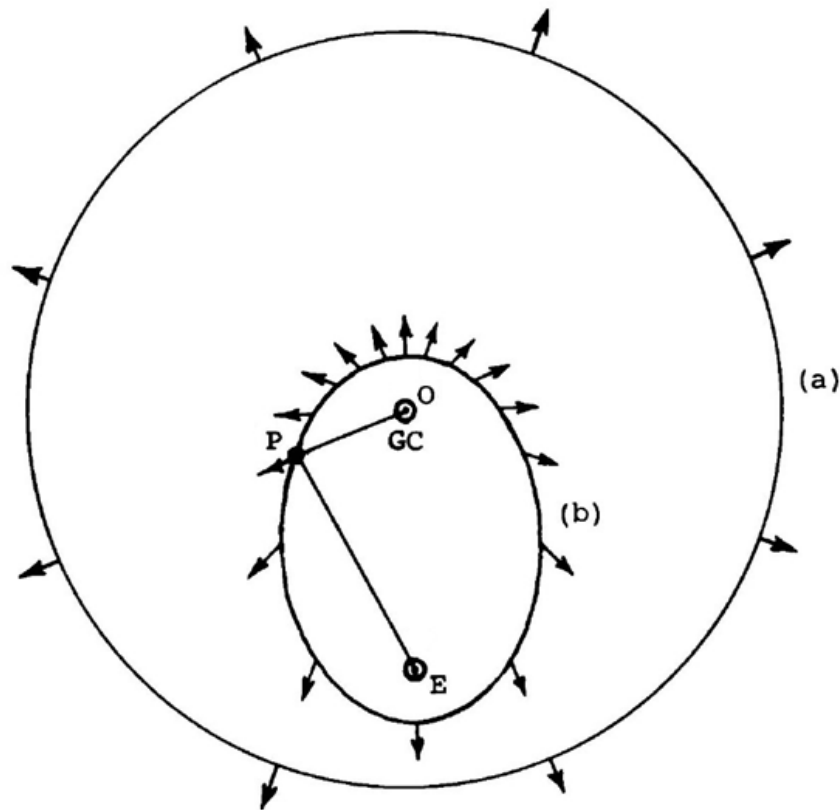


Figure 3.28. The 14,200 years BP superwave event horizon for a superwave velocity of c : (a) as would be seen if light from the event horizon were to travel to us instantaneously, and (b) as it actually appears due to the time required for light, travelling at the finite velocity $v = c$, to reach us from the event horizon.

The polar equation for an ellipse where the pole is at the center of one focus of the ellipse is given as:

$$d^2 = \frac{a^2 b^2}{a^2 \sin^2 \phi + b^2 \cos^2 \phi}$$

or,
$$d = b (\sin^2 \phi + (b/a)^2 \cos^2 \phi)^{-1/2}, \quad (7)$$

where a and b are the semi major and semi minor axes of the ellipse, and where ϕ is the angle between the major axis and an arbitrary ray drawn from the center to the periphery of the ellipse. It can be shown that the distance s from a focus of the ellipse to its major axis periphery is given as: $s = a - \frac{1}{2} \overline{OE}$, where \overline{OE} is the distance between the two foci. Consequently, if the distance from the GC to the Earth is given as $r_0 = \overline{OE} = 7$ kpc (22,800 l.y.), then the distance s that the superwave has appeared to travel since the time it passed the Earth is given as: $s = a - 3.5$ kpc. Given that $s = t/2$ l.y. = $t/6520$ (kiloparsecs), where t is the time that has elapsed since the event horizon passed the Earth, then $a = \frac{1}{2} r_0 + t/6520$ kpc = $3.5 + t/6520$ kpc. Moreover, based on geometrical considerations, b may be expressed in terms of a and r_0 with the relation: $b^2 = a^2 - (3.5)^2 = a^2 - 12.25$. Currently, $t = 14.2$ thousand years, so the semi major and semi minor axes may be calculated to be $a = 5.68$ kpc and $b = 4.47$ kpc. Thus relation (7) may be written as:

$$d = 4.47 (\sin^2 \Theta + 0.62 \cos^2 \Theta)^{-1/2}. \quad (8)$$

With this, the overview of the 14,200 years BP superwave model is completed. The chapters that follow, making up parts II and III of this study, will consider astronomical and geological evidence supporting the GEH.

UPDATE

Regarding the Presence of Interstellar Dust Near the Solar System (update to [p. 82](#)): At the time this dissertation was written, little was known about the presence of interstellar dust and debris in the immediate vicinity of the solar system. I went a bit out on a limb to presume that such material did exist in close proximity to the solar system and had been propelled into the inner solar system by an approaching superwave. Since that time, new discoveries have been made which substantiate that interstellar dust and frozen bodies are indeed present in the immediate vicinity of the solar system. For example, sky maps made with the IRAS satellite published in 1984 showed that the solar system is currently closely surrounded by wisps of infrared-emitting dust termed "infrared cirrus."^(2,3) Later in 1988, H. Aumann published infrared observations made with ground based telescopes which indicate that the Sun is enveloped in a thick sheath of dust 500 times denser than had previously been supposed and having a density similar to dust clouds seen to surround other nearby stars.^(4,5) Observations made at Mauna Kea observatory in the early 1990's and confirmed in 1995 with Hubble Space Telescope observations, indicated that the outer part of the solar system harbors a belt of cometary bodies, called the *Edgeworth-Kuiper belt*, that begins just beyond the orbit of Neptune and extends outward a hundred AU or more.⁽⁶⁾ This belt is estimated to contain a billion or more frozen dust-laden masses ranging up to 100 km in diameter and believed to be the source of the short period comets (orbital period < 200 years) currently entering the solar system. I suggest that the bodies forming this belt were recently captured due to the solar system's encounter with the North Polar Spur SNR and that they are not of primordial origin. This recent evidence strengthens my original hypothesis

that frozen debris resides in the immediate vicinity of the solar system which can act as source material for generating a nebular cloud that envelops and penetrates the solar system.

More recently, data from the Pioneer and Ulysses spacecrafts have shown that an ecliptic ring of interstellar dust orbits the Sun, its inner edge beginning just beyond the orbit of Saturn. The dust grains are typically larger than interstellar dust currently entering the solar system. They are present at a density of about $2 \times 10^{-17} \text{ g/cm}^3$, or at a space density about ten thousand times greater than that existing in the vicinity of the Earth. Markus Landgraf and his colleagues have concluded that this ring cannot be primordial since it would lose mass at the rate of $5 \times 10^4 \text{ g/s}$, because its dust grains would either gradually eject from the solar system or would coalesce into celestial bodies. But the origin of the dust has posed a problem since due to their large size it is unlikely that the grains are contributed by the present interstellar wind. Also they cannot come from comets since beyond Saturn's orbit comets remain frozen and shed little material. Landgraf et al. suggest that this dust belt is continually replenished as a result of particles being generated by collisions between the icy remnants of the Edgeworth-Kuiper belt. However in addition, it is suggested here that much of this dust was formed at the end of the last ice age during a time when cometary bodies (including debris in the Edgeworth-Kuiper belt) were being vaporized by the onslaught of Galactic superwave cosmic rays. Consequently, the presence of this outer solar system dust belt could also be evidence of a recent cosmic dust incursion event.

Interstellar Dust Particle Size and Purging (update to p. 85): Observations with the Ulysses spacecraft have shown that interstellar dust entering the solar system is deficient in small sized particles having masses in the range of 10^{-15} to 10^{-13} g (size ~ 0.1 to $0.4 \mu\text{m}$). Linde and Gombosi have proposed that this is due to the filtering effect of the heliopause shock region which captures this smaller fraction. Landgraf et al. report that this dust enters at the rate ranging from 5×10^{-9} to $2 \times 10^{-8} \text{ cm}^{-2} \text{ s}^{-1}$ and has a mean mass of $3 \times 10^{-13} \text{ g}$.⁽⁷⁾ This would amount to a mass flux of about 1.5 to $6 \times 10^{-21} \text{ g/cm}^2/\text{s}$ or about $10^{-13} \text{ g/cm}^2/\text{yr}$, more than a million times less than the current influx of extraterrestrial dust on the Earth's surface (see p. 83). Consequently, the extraterrestrial dust that currently falls on the Earth's surface is almost entirely interplanetary dust of cometary origin. Analysis of the Ulysses data showed that dust particles having a size below $0.4 \mu\text{m}$ were substantially depleted from the inner solar system at distances closer than 4 AU from the Sun, with particles in the size range of 0.1 to $0.2 \mu\text{m}$ being entirely absent.⁽⁸⁾ This was attributed to the repelling action of solar radiation pressure as well as the propelling action of the solar wind, the repelled fraction being theorized to deflect around this inner exclusion zone as the dust wind moves through the solar system. Larger-sized particles, however, are able to penetrate. These observations confirm the reasoning discussed above in the original 1983 edition of this dissertation, namely that the solar wind and solar radiation as well as the shielding effect of the heliopause have the effect of keeping light-scattering, submicron sized interstellar dust particles from entering the solar system.

Regarding "Geomagnetic Effects" (update to p. 100): At the time I proposed this theory of cosmic ray induced geomagnetic flipping, geophysicists believed that geomagnetic reversals and magnetic polarity flips were brought about by causes internal to the Earth, that they arose from instabilities in the inner rotation of the Earth's core magnetic dynamo. They believed that these field excursions took hundreds of years to occur due to the inherently slow movement of the core material.

However, in 1992 geophysicists discovered evidence of a very rapid geomagnetic reversal recorded in 16 million year old lava formations at Steens Mountain in southeastern Oregon.^(9, 10) These lavas were found to record a progressive change in direction of the geomagnetic pole that had occurred while the lavas were in the process of cooling. Based on

estimates for the lava cooling rate, researchers found that during this reversal the Earth's magnetic pole had changed direction as fast as 8 degrees per day. Subsequent data published in 1995 presented additional data indicating pole direction changing as fast as 6° per day.⁽¹¹⁾ This posed a serious problem for the conventional core dynamo theory view which was unable to account for such rapid changes. Correspondingly, these findings strongly supported the rapid solar-cosmic-ray induced flipping mechanism proposed in this dissertation almost a decade prior to the Steens Mountain discovery.

In 1995, two French geophysicists published a paper that sought to explain the Steens Mountain polarity reversal as being due to a solar cosmic ray cause.⁽¹²⁾ Their mechanism was essentially the same as the one I had proposed in my dissertation and subsequent publications.^(13, 14) They were apparently unaware of my previous work since they did not cite papers I had published on this. Nevertheless, their independent arrival at the same idea indicates a consensus that other researchers consider this to be a plausible theory.

Regarding "Cosmic-Dust-Induced Climatic Change" (update to p. 105): As of 1995, new data was published on planetary energy balance measurements which affects the estimates made in Figure 3.21. This new data indicates that cloud cover absorbs a greater fraction of incident radiation, 15% of the incident beam as opposed to earlier estimates of 4%. The data also assumes that cloud cover reflects 30% of the incident beam and that the atmosphere absorbs 16% of the incident beam. These figures would increase our estimate of β in Figure 3.21 (Case 1: present climate), raising it from 30% to 44%, increasing βQ_1 , the total atmospheric absorption (clouds included), from 21½% to 31%. Also the amount of cloud-reflected radiation would increase from 28% to 30%, and the amount of remaining radiation reaching the ground, Q_2 , would be reduced from 50½% to 39%.

The estimates shown in Figure 3.21 (Case 2: dust obscured Sun) would also change. The cloud reflected beam would increase from 25% to 27% and the atmospheric absorption fraction would increase from 48½% to 65%. This would leave a remainder of just 8% of the incident beam to reach the Earth's surface. Thus the new data would suggest that a dust obscured Sun would produce a more drastic drop in ground radiation, an almost 5 to 1 drop from 39% to 8%, as opposed to the 2 to 1 drop previously estimated.

References to the Update

- 1) B. E. Wood, J. L. Linsky, and G. P. Zank, "Heliospheric, astrospheric, and interstellar Lyman alpha absorption toward 36 Ophiuchi," *The Astrophysical Journal* **537** (2000): 304-311.
- 2) F. J. Low, et al. "Infrared cirrus: New components of the extended infrared mission," *Astrophysical Journal* **278** (1984): L19-L22.
- 3) M. G. Hauser et al., "IRAS observations of the diffuse infrared background," *Astrophysical Journal* **278** (1984): L15-L18.
- 4) H. H. Aumann, "Spectral class distribution of circumstellar material in main-sequence stars," *Astronomical Journal* **96** (1988): 1415-1419.
- 5) "Cold cloud may contain unseen solar dust." *Science News* **134** (1988): 246.
- 6) J. Horgan, "Beyond Neptune," *Scientific American* **273**, October 1995, pp. 24-26.
- 7) N. Altobelli, et al., "Cassini between Venus and Earth: Detection of interstellar dust." *Journal of Geophysical Research* **108** (A10) (2003): LIS 7-1.
- 8) M. Landgraf, H. Krüger, N. Altobelli, and E. Grün, "Penetration of the heliosphere by the interstellar dust stream during solar maximum." *Journal of Geophysical Research* **108** (A10) (2003): LIS 5-1.
- 9) T. Appenzeller, "A conundrum at Steens Mountain," *Science* **255** (1992): 31.
- 10) R. Lewin, "Earth's field flips flipping fast," *New Scientist*, January 25, 1992, p. 26.

- 11) R. S. Coe, et al; "New evidence for extraordinarily rapid change of the geomagnetic field during a reversal." *Nature* **374** (1995): 687.
- 12) P. Ulte-Guerard and J. Achache, "Core flow instabilities and geomagnetic storms during reversals--The Steens Mountain impulsive field variations revisited." *Earth and Planetary Science Letters* **135** (1995): 91-99.
- 13) P. A. LaViolette, "Cosmic ray volleys from the Galactic center and their recent impact on the Earth environment." *Earth, Moon, & Planets* **37** (1987): 241-286.
- 14) P. A. LaViolette, "Galactic core explosions and the evolution of life." *Anthropos* **12** (1990):239-255.

PART II

ASTRONOMICAL EVIDENCE OF SUPERWAVE ACTIVITY IN OUR GALAXY

CHAPTER 4

EVIDENCE OF RECENT ACTIVITY IN THE GALACTIC NUCLEUS AND DISK

4.1. THE INHOMOGENEOUS DISTRIBUTION OF HOT DUST AND IONIZED GAS WITHIN 6 LIGHT YEARS OF THE GALACTIC CENTER

If the Galactic center had been inactive for a long period of time, say for the last 20,000 years, then one would expect to find that the gas and dust in the inner few parsecs would be relatively homogeneously and symmetrically distributed around the dynamical center of the Galaxy. This is because any inhomogeneities that might otherwise have been present would have become smoothed out within a period comparable to the time taken for material to orbit the Galactic center (GC). Instead, radio and infrared observations of the emission from this inner region indicate that the gas and dust is quite inhomogeneously distributed. A considerable amount of asymmetrical structure is seen in the high resolution radio map of the Galactic center region (Sagittarius A) displayed in Figure 4.1 (Brown and Johnston, 1983). The extended radiation pattern is a combination of both thermal emission (the spiral-like structure) superimposed on a broader distribution of nonthermal emission (lowest 6 contours). The thermal emission is centrally peaked at a position that lies ~ 2 arc seconds south of the point nonthermal radio source Sgr A* which is believed to coincide with the GC.

[UPDATE: In the years that followed the publication of this dissertation, more detailed views of the Galactic center region became available using the VLA radio telescope and Hale Telescope fitted with an infrared CCD detector. These images are presented in **Figures 4-A** and **4-B**. Also **Figure 4-C** shows an X-ray telescope image of the Galactic center region.]

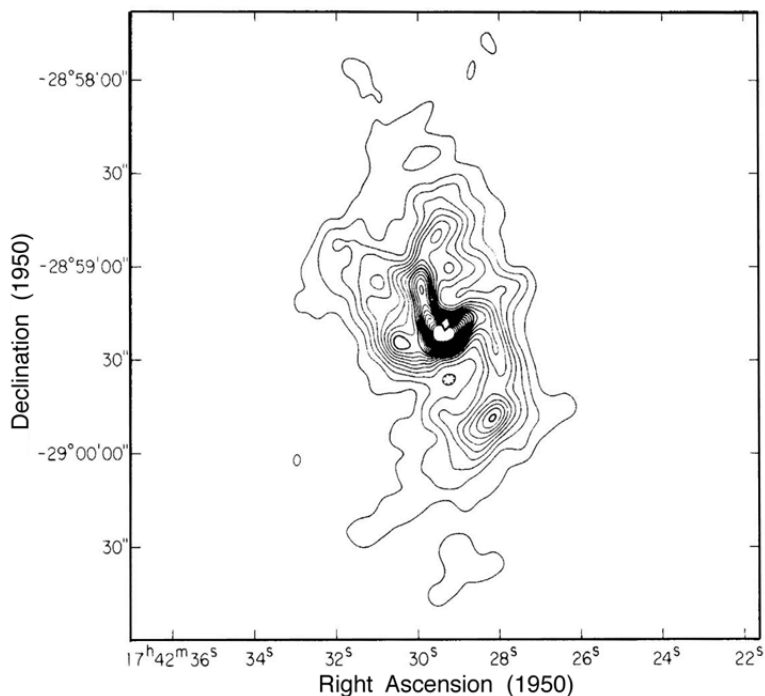


Figure 4.1. The inner region of the GC mapped at a radio wavelength of 6 centimeters (Brown and Johnston, 1983). The position of the compact radio source Sgr A* is indicated by the diamond just north of the central radio emission peak. ($10''$ of arc = 1 l.y.)

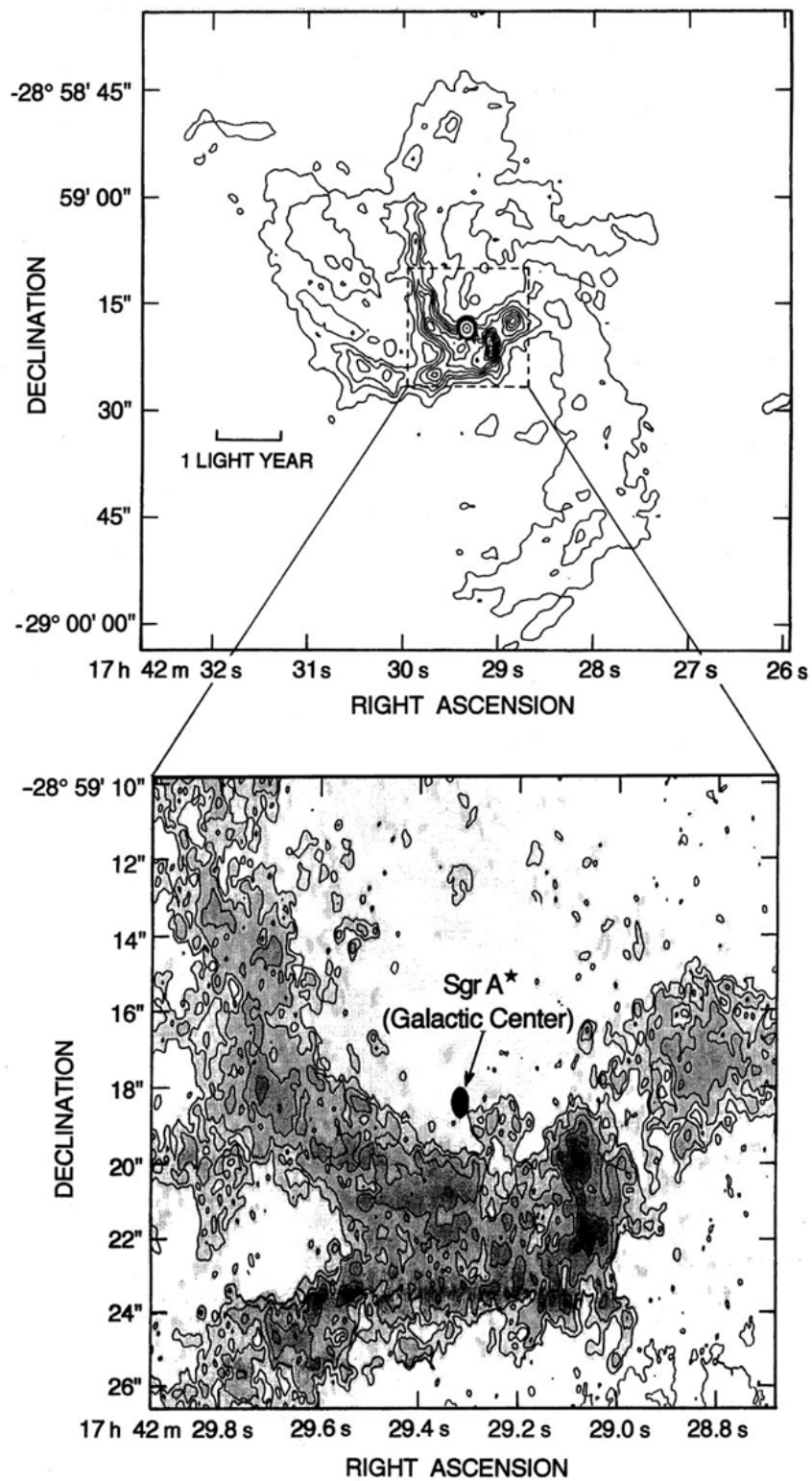


Figure 4-A. **UPDATE:** Top: The central part of Sagittarius A mapped at a 6 cm wavelength showing the same region as Figure 4.1, but in greater detail. Bottom: A close up of the central region mapped at a 2 cm wavelength (reproduced courtesy of NRAO, K. Lo, and J. Zhao [Lo and Claussen, *Nature* **306** (1983): 647-651; Zhao, et al., *Nature* **354** (1991): 46-48]).

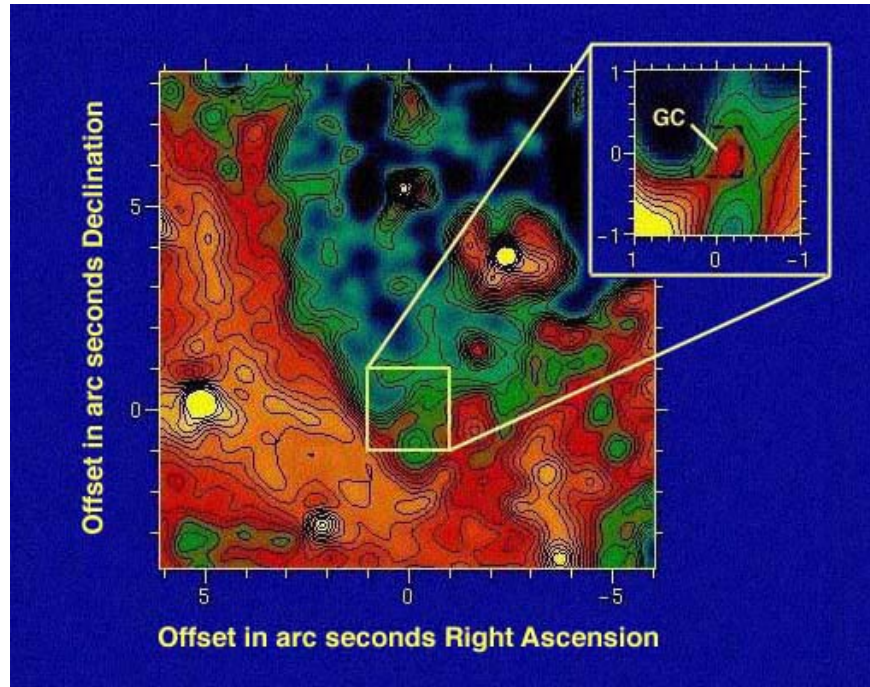


Figure 4-B. **UPDATE:** Infrared image of the Galactic center radio-emitting source Sgr A* seen in the infrared at a wavelength of 8.7 microns (red spot marked as GC). Taken with the Hale Telescope (courtesy of Stolovy, Hayward, and Herter [*Ap. J. Let.* **470** (1996): 45]).

Maps of the inner Galactic center region made in the infrared at wavelengths of 10 and 34 microns (Becklin et al., 1977; Gatley, 1982) show an arc-like emission distribution similar to that seen at radio wavelengths. However, Gatley (1982) reports that the region having the highest infrared surface brightness does not also have the highest temperature. Rather, the temperature peak in the map is found to be centered around the compact radio source and its $2.2\ \mu$ infrared counterpart IRS 16. Gatley suggests that it is this compact source at the GC that is responsible for heating the gas in this region. The fact that the region of highest gas density is displaced away from the GC suggests that this gas is an ejection which has become propelled some distance from the GC. Brown and Johnston (1983) conclude that we are observing a nonstationary transient phenomenon whose lifetime is only $\sim 7500 - 22,000$ years. It is interesting to note that the compact radio source has properties similar to those found in quasars and radio galaxies. Although it is presently weaker by many orders of magnitude, and relatively inactive except for fractional changes in its luminosity, its activity could be episodic. Hence at some earlier date during a period of intense activity it could have been involved in expelling this gas.

4.2 EXPANDING CLOUDS OF IONIZED NEON AND THE PROPAGATING RING OF NEUTRAL OXYGEN GAS

Additional evidence for recent activity at the GC comes from observations of the Ne II ($12.8\ \mu$) fine-structure line emission which suggests the presence of gas orbiting as well as radially expanding from the Galactic center (Wollman, 1976; Wollman et al., 1977). Oort (1977) has suggested that these radial motions have been produced by major eruptions from the GC on time scales of at most 10,000 years, each imparting to the gas a kinetic energy of $10^{49} - 10^{50}$ ergs. Spatial resolution of this neon line emission has revealed the presence of

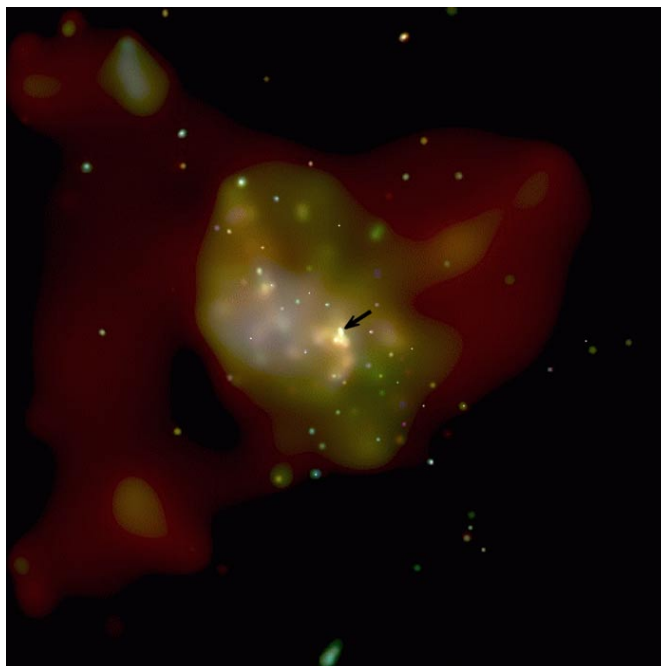


Figure 4-C. **UPDATE:** False-color image made with the Chandra X-ray Observatory showing the Galactic center region. The arrow indicates the location of the X-ray flare observed on October 26, 2000 which coincided with the Galactic core Sgr A* radio source. The image displays a region measuring about 55 light years square (8' X 8') (courtesy of NASA, MIT, and F. Baganoff et al.).

14 discrete clouds of ionized gas with masses ranging from $0.1 M_{\odot}$ to $10 M_{\odot}$ and positioned within 6 l.y. of the GC (Lacy et al., 1979; Lacy et al., 1980). An upper limit of $\sim 10^4$ years may be placed on the age of these clouds, which is comparable to the period of time in which such clouds would become disrupted through cloud-cloud collisions (Lacy et al., 1979). However, an even more stringent limit may be placed on their age. Line widths observed for the emission from these clouds indicate that the clouds are expanding at velocities of ~ 100 km/s. Given that the cloud diameters range from 0.3 – 1.5 l.y., ages in the range of 1000 – 8000 years are implied (see **pp. 371 and 374**). Since the largest, and hence oldest clouds **lie** furthest from the GC, the GC is implicated as their source of generation.

Further evidence of recent activity at the GC comes from observations of neutral oxygen emission that is primarily radiated from a region lying between 10 – 20 l.y. from the GC. The results of Genzel et al. (1982) indicate the presence of a ring of gas rotating about the GC, but also having substantial noncircular motions indicating the movement of material either into or out of the GC. Townes et al. (1983) estimate that such noncircular motions and the large scale inhomogeneities present in the gas could not have persisted longer than 5×10^4 years without having become damped by the ring's rotational motion. Thus the neutral oxygen observations, like the ionized neon observations, are consistent with the recent occurrence of explosive activity at the GC.

[UPDATE: Another indication of ongoing activity at the Galactic center comes from observations made with the Chandra X-ray Observatory which have shown that Sgr A* is a flaring X-ray source. On October 26, 2000, when it was being observed by Chandra for the second time, the X-ray emission from Sgr A* was seen to brighten 45 fold within the space of a few minutes and then decline to its preflare intensity over a period of 3 hours. The rapidity of this flare event indicates that it originated from a region smaller than 1 astronomical unit. X-ray observations should be a good way to monitor Galactic center activity in the future.]

4.3 THE RADIALLY EXPANDING MOLECULAR RING CLOUD

Oort (1977) suggests that the same mechanism responsible for the neon gas motion in the inner few light year region is also responsible for the expulsion of the ring-like molecular cloud which is estimated to lie at a radial distance of $\sim 400 - 600$ light years from the center. This molecular ring is presently expanding radially at a rate of about 150 km/s and has a mass of about $10^7 M_{\odot}$. Oort (1977, p. 345) estimates that $10^{55} - 10^{56}$ ergs would have been required to blow the gas in this ring out to its present radius from a radius of 65 light years. Much greater energies would have been required if this cloud had been directly expelled from the nucleus. It is unlikely that this expanding feature was produced by supernova explosions. For example, figuring at the most 10^{51} ergs per supernova, about 10^4 supernovae would have been required, and it is unlikely that these could have worked in a coordinated fashion over 180 as observed (Oort, 1977, p. 335). As an alternative Oort, (p. 343) considers the idea that this gas may have been expelled by an outburst of *radiation* and *relativistic particles* which issued from the nucleus in a manner comparable to what is observed in some radio galaxies. His suggestion is compatible with the superwave model which postulates that gas would be driven radially out from the GC by the successive generation and propagation of superwaves.

If the ring had maintained its present velocity over the entire 400 to 600 light year distance, it would have emerged from the GC about 1 million years ago. Though, a much

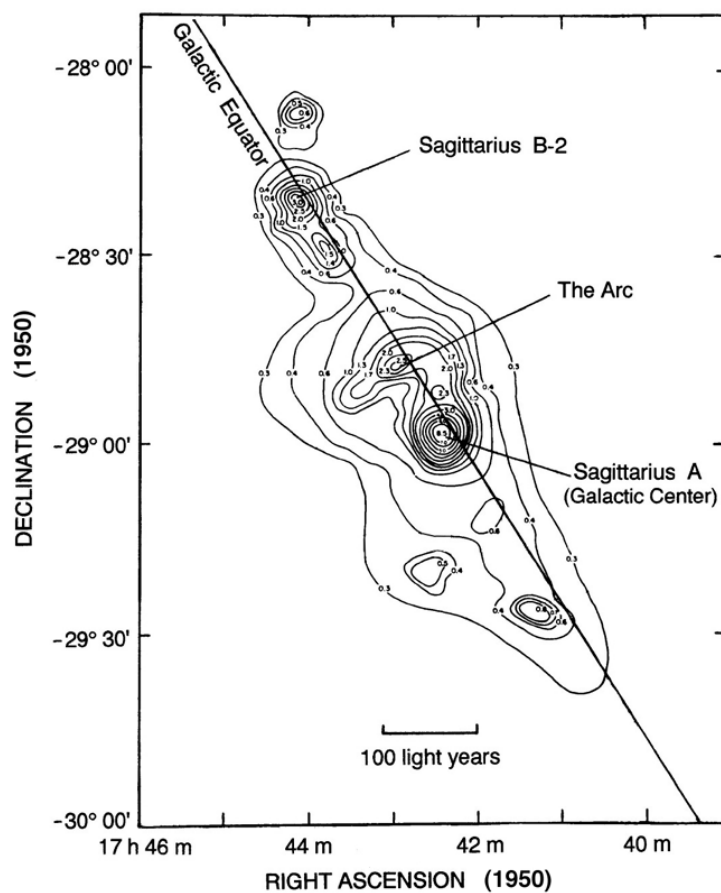


Figure 4.2. Distribution of electromagnetic radiation around the Galactic center. From a survey at a radio wavelength of 3.75 cm by Downes and Maxwell (1966) with the 120-ft Haystack antenna. Contours represent antenna temperature. (1° of arc ~ 400 l.y.)

more recent time of expulsion seems likely, since it is possible that the ring had higher radial velocities at earlier times. To assign its expulsion to the 14,200 years BP event would require that the ring had maintained an average radial velocity of 9000 to 13,000 km/s over this period of time, an unreasonably high value. It is more probable that it was expelled over a period of several hundred thousand years as a result of a series of explosive events. The arc-like feature, shown in the radio map in Figure 4.2 (Downes and Maxwell, 1966), is probably a more likely candidate for expulsion by the 14,200 year BP event. The "Arc," as it is called, lies along the Galactic equator at about 0.2° of arc or 80 light years from the GC. To have covered this distance in 14,200 years, the gas would have required an average velocity of about 1700 km/s. This is within the range of velocities assumed to exist in the nuclei of Seyfert galaxies, and comparable to ejection velocities observed in young supernova remnant shells.

[UPDATE: Close ups of Sagittarius A and the Arc made more recently with the VLA radio telescope are shown in Figures 4-D-a and 4-D-b. These images show that the Arc is composed of synchrotron radiating filaments that are oriented along its length. The "Sickle" filament and the additional filaments crossing the Arc and extending toward the Galactic center suggest that the Arc was formed by the compressive action of superwave cosmic rays issuing from the Galactic center. The authors who published these images failed to mention that the Arc may have been formed by a past core explosion. Conforming to the paradigm that regarded the Galactic core as presently being quiescent, they merely note that the Arc is a young feature ($<10^6$ years old) and that its geometry suggests that the Galaxy's magnetic field is poloidal in this core region.]

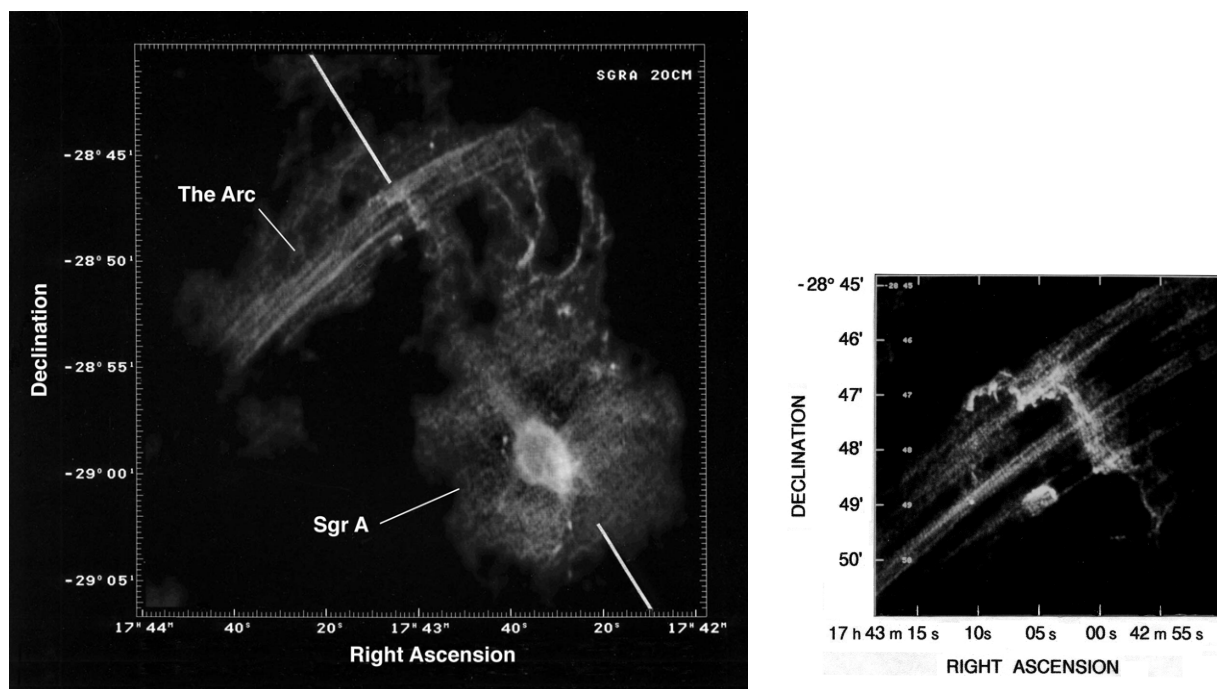


Figure 4-D-a. (left) **UPDATE:** The Galactic center radio source Sgr A* (lower right) and the Arc (upper left) seen on a map made with the VLA radio telescope. The line indicates the location of the galactic equator. Photo courtesy of NRAO/AVI and Farhad, Yusef-Zadeh (Yusef-Zadeh, Morris, and Chance, *Nature*, p. 558).

Figure 4-D-b. (right) **UPDATE:** A radio telescope image of a radio emission knot that runs crosswise to the Arc, a feature called "the Sickle." Photo courtesy of Yusef-Zadeh (Yusef-Zadeh and Morris, *Astronomical Journal*, plate 97).

4.4 NEUTRAL HYDROGEN ARM-LIKE EJECTIONS

Further out from the center of the Galaxy at distances of 1000-2000 light years from the Galactic plane, massive complexes of neutral hydrogen are observed, sometimes having an arm-like structure. Van der Kruit (1970) has suggested that these clouds, having radial velocities on the order of 100 km/s, were ejected in opposite directions from the Galactic nucleus. In another paper (1971b) he also suggests that the motion of the three-kiloparsec arm, located on the near side of the Galactic nucleus, and the arm receding from the LSR at +135 km/s, located on the far side of the Galactic nucleus, may be due to expulsion from the nucleus. He estimates that these neutral hydrogen arms emerged from the GC about 12 to 13 million years ago. His discussion of these gas motions assumes a single explosive event as the cause. However, it is equally likely that these features have been propelled over a comparable time by a series of explosive events. I suggest that superwaves may be the mechanism by which such interstellar gas may be radially propelled, even though these arm-like features may lie at considerable distances from the point of origin of the outbursts.

4.5 THE VIOLENT INTERSTELLAR MEDIUM

McCray and Snow (1979) point out that our conception of the interstellar medium (ISM) is in the process of undergoing a rapid change. It used to be thought that the ISM consisted of cool gas clouds ($T \sim 100^\circ \text{K}$) of partially ionized hydrogen. However, recent measurements of interstellar O VI emission lines with the Copernicus spacecraft and measurements of the soft X-ray background radiation indicate that the ISM actually consists of very hot gas ($T \sim 10^6 \text{K}$). Thus, although this interstellar gas is up to many light years away from stellar heat sources, it exhibits a temperature comparable to that of the coronal gas surrounding the Sun. While these observations pertain to the local ISM (within several hundred light years of the Sun), McCray and Snow suggest that they are an indication of more widespread conditions.

Hot "coronal" phase gas may retain its high temperature for millions of years (McCray and Snow, 1979; after Spitzer, 1956). This is because the extremely low density of this plasma makes it radiate very inefficiently by bremsstrahlung. Cool denser clouds, on the other hand, contain sufficient amounts of partially ionized matter that their atoms can radiate efficiently after being collisionally excited. Hence, these clouds are able to maintain lower temperatures. The GEH, which suggests that the cosmic ray electron background momentarily increases by a factor of 10^5 about every 10^4 years, unquestionably requires that an extremely hot interstellar medium should be observed. The fact that high temperatures are indeed observed reflects favorably on this hypothesis. Cox and Smith (1974) have suggested that the ISM coronal phase gas has been produced by a great many supernovae explosions occurring throughout the Galaxy. It is equally plausible, though, that superwaves cause this heating.

Another indicator that the interstellar medium has undergone violent agitation is the existence of vast shells of neutral hydrogen gas. Heiles (1979) reports 63 such shells in our Galaxy. The majority of these have kinetic energies of less than 3×10^{52} ergs, which means that they could have been produced by one or several supernovae. However, eleven of these objects, which have energies greater than this amount, must be attributed to other causes. Heiles calls these objects "supershells." Their individual kinetic energies range up to 6×10^{53} , hundreds of times the amount available from a single supernova. Multiple supernovae do not seem to be a likely cause because supershells are not found in association with extreme Population I stars. Heiles suggests that the agent responsible for the existence of supershells might be an extremely rare kind of astronomical object which

until now has gone unobserved. I suggest that this rare event or "astronomical object" might be a Galactic superwave.

Surveys at a radio wavelength of 21 cm also reveal the presence of a continuous shell of neutral hydrogen gas lying along the Galactic plane and forming a complete ring around the Galaxy. This gas exhibits the presence of very high velocities ranging from +120 km/s to -220 km/s. Dieter (1971) has proposed a model in which this gas is distributed in the form of a ring lying at a galactocentric distance of 40,000 to 50,000 light years and having a net inward velocity of 125 km/s. In the Galactic anticenter direction ($\ell = 180^\circ$) her model places the ring at about 10,000 light years from the Sun. However, De Noyer et al. (1977) present evidence that in the anticenter direction this ring lies less than 6500 light years from the solar system. If so, this would place it in the vicinity of the 14,200 year BP event horizon. One might speculate that this high velocity zone is in some way associated with the effects of a radially propagating superwave.

[**UPDATE:** see [p. 142](#) for evidence of a residual low energy galactic cosmic ray flux.]

4.6 THE INTERSTELLAR WIND

Ultraviolet observations of the interplanetary Lyman alpha background (1216 Å emission) indicate the presence of an interstellar wind of neutral hydrogen gas passing through our solar system from the general direction of the Galactic center. L_α sky maps indicate the upwind direction in celestial coordinates to be RA = 265° (17 h 40 m), $\delta = -23^\circ$ (Fahr, 1974). In Galactic coordinates this upwind direction would lie at $\ell = 4.6^\circ$, $b = +3.6^\circ$, within 6° of the GC; see (a) of Figure 4.3. Alternatively, based on observations of the 584 Å ionized helium line, Weller and Meier (1974) have proposed that the interstellar wind approaches from the direction RA = $252 \pm 3^\circ$, $\delta = -15 \pm 3^\circ$, or ($\ell = 4.5^\circ$, $b = +18^\circ$), when transformed to Galactic coordinates; see (c) of Figure 4.3. This higher latitude direction has been proposed more often in the literature; however, recently Bertaux et al. (1977) have suggested that the direction be revised to RA = $265 \pm 5^\circ$ in conformance with Fahr's determination (see Thomas, 1978).

[**UPDATE:** More accurate Ulysses spacecraft measurements published in 1993 determined that this helium wind approaches from the direction of RA = $250.9 \pm 2.4^\circ$, $\delta = -19.8 \pm 2.7^\circ$ at a velocity of 26 km/s; see point (d) in Figure 4.3.⁽¹⁾ It was determined that material in the Local Interstellar Cloud shares this same direction and velocity. It is remarkable how close this interstellar wind direction comes to the Galactic center direction. Translated into galactic coordinates, this wind would be approaching from $\ell = -0.2 \pm 2.5^\circ$, $b = +16.3 \pm 2.5^\circ$. To within the measurement accuracy, this coincides with the Galactic center longitude meridian. The 16° latitude deviation could arise if the solar system were moving towards the general direction of the galactic north pole in relation to this interstellar wind. For additional updated evidence see [p. 143](#).]

It is interesting to compare this local interstellar gas flow rate with the flow rate of gas observed from the GC. The GC emits a gas flow rate of about 1 – 2 M_\odot /year, propelled at a velocity of about 50 km/s (Rougoor and Oort, 1960; Arp, 1963). By comparison, Adams and Frisch (1977) have estimated the local interstellar wind velocity to be $v = 22 \pm 3$ km/s. Also, Ajello et al. (1979) have determined its particle density to be 0.04 cm^{-3} (for hydrogen) and 0.008 cm^{-3} (for helium), which totals to $\rho = 1.2 \times 10^{-25} \text{ g/cm}^3$. From these estimates the total mass flow of the wind at a galactocentric radius of $r = 22,800$ light years (7 kpc) may be determined as follows. Assume that this flow is taking place uniformly around the circumference of the Galaxy and through a band of area $A = 8.6 \times 10^{44} \text{ cm}^2$ (having a height of 6000 l.y. equal to the assumed thickness of the Galaxy, and a radius of 22,800 l.y.

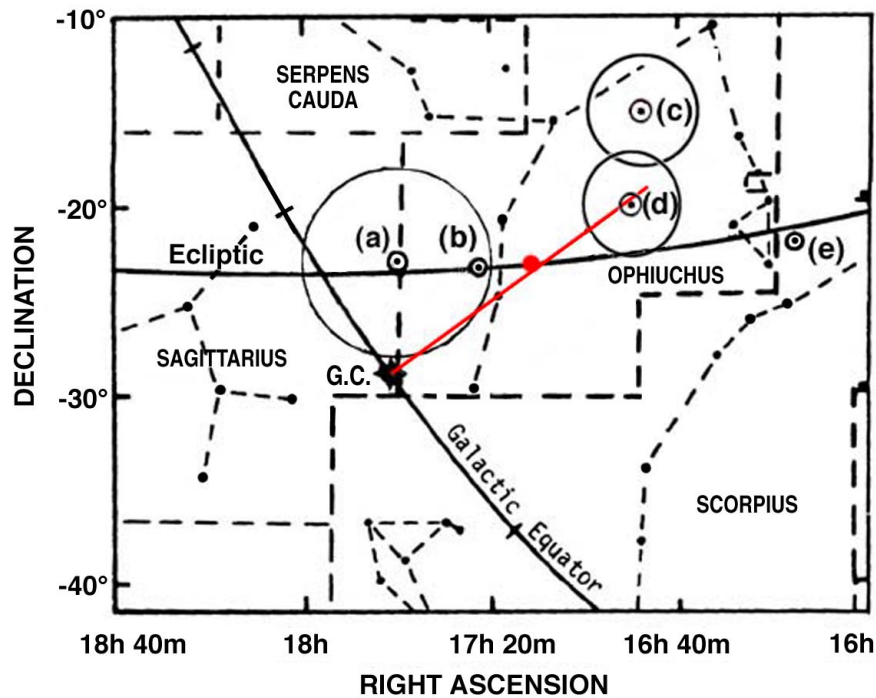


Figure 4.3. Sky map of the heart of the Galaxy showing: a) the position of the Lyman alpha maximum (interstellar wind upwind direction) as determined by Fahr (1974), b) the position of the ecliptic vector which lies orthogonal to the direction of the large scale dipole anisotropy in the cosmic microwave background radiation (see Appendix B), c) the position of the upwind direction for the interstellar helium wind as determined by Weller and Meier (1974), d) [UPDATE:] the 1993 Ulysses spacecraft determination of the interstellar helium wind radiant, and e) the location of the center of the local interstellar dust cloud which covers a 40° diameter region of the sky (see Chapter 3, p. 82). The Galactic center is marked as G.C. [UPDATE:] The red dot marks the location of the descending node of the zodiacal dust cloud; see update at end of chapter.]

equal to the solar-galactocentric distance. Then the total mass flow is given as: $M = \rho v A = (1.2 \times 10^{-25} \text{ g/cm}^3) \times (2.2 \pm 0.3 \times 10^6 \text{ cm/s}) \times (8.6 \times 10^{44} \text{ cm}^2) = 2.3 \pm 0.3 \times 10^{26} \text{ g/s} = 7.2 \pm 1 \times 10^{33} \text{ g/yr} = 3.6 \pm 0.5 M_\odot / \text{yr}$. This flow rate corresponds reasonably well to the flow rate observed near the GC. This observation together with the observation that the local interstellar wind comes from the direction of the GC strongly suggests that the local interstellar gas is part of a continuous flow extending all the way to the center of the Galaxy.

While a large fraction of the local interstellar wind gas undoubtedly originated from stellar nebula and supernova remnants in the Galactic disk, a comparably large fraction very likely could have originated from the GC itself, provided that some mechanism were present to periodically impart an outward momentum to this gas. Galactic superwaves could serve this purpose. As mentioned in Chapter 3, Subsection 2, a Galactic superwave would impart a fraction of its energy to the interstellar medium in the form of kinetic energy. Radial flow of ionized gas molecules in the interstellar medium could be induced by the cosmic ray volley through hydromagnetic interaction effects.

The magnitude of the energy flux required to drive the local interstellar wind may be estimated by calculating the wind's energy density. Using the values for the gas density and

velocity given earlier, the wind energy density is estimated to be: $E = \frac{1}{2}\rho v^2 = \frac{1}{2} \times 1.2 \times 10^{-25} \text{ g/cm}^3 \times (2.2 \times 10^6 \text{ cm/s})^2 = 2.9 \times 10^{-13} \text{ ergs/cm}^3$. This is almost an order of magnitude greater than the current energy density of the local cosmic ray electron background radiation, which is measured to be about $10^{-14} \text{ ergs/cm}^3$. So, even if it were hypothesized that the local cosmic ray electrons were impacting the solar system from the direction of the GC as a steady state wind, this still would not be sufficient to account for the energy source of the neutral hydrogen wind. However, at its peak intensity the proposed 14,200 years BP superwave would have had an energy density of $\sim 3 \times 10^{-9} \text{ ergs/cm}^3$ in the solar vicinity, or about 10^4 times greater than the present energy density of the local interstellar wind. So this could very well have been the energy source responsible for propelling this wind.

[UPDATE: Another possibility could be that the wind is a residual from a minor superwave that passed through the solar system around 5,300 years BP. Ice core data shows evidence of a brief cosmic ray event ($t < 600$ years) dating at around 5300 years BP. This more recent event would have been much less energetic than the 14,200 years BP superwave (judging from the absence of significant climatic change registered in the geologic record); however, it could also have contributed to the observed gas motion.]

It is argued in Appendix B that even at present there may be a directional anisotropy in the flux of cosmic ray electrons and that this flux is flowing primarily from a position ($\ell = 3.1^\circ$, $b = +5.6^\circ$) close to the upstream direction for the interstellar wind (see (b) of Figure 4.3). Such an anisotropic flow would be consistent with the suggestion made in the previous chapter (p. 67) that the present cosmic ray electron background observed in the Earth's vicinity is a residual flux remaining after a recent superwave passage. It might be pointed out here that, as yet, there is *no direct evidence* to indicate that electrons do not approach the solar system from the GC direction. A test of their anisotropy is difficult to perform since it requires elaborate equipment positioned above the Earth's atmosphere. Thus far, underground muon experiments have established only that the hard component of the cosmic ray background radiation (i.e., protons and heavier nuclei) is isotropically distributed.

4.7 PLANETARY EVIDENCE

4.7.1 The Rings of Saturn

Saturn's rings may be relatively recent creations. Measurements made with the Voyager I and II spacecraft indicate that there are actually hundreds of thousands of concentric rings resembling the grooves of a record (*Science*, 1981). The discovery that Saturn's rings have such intricate patterns ran contrary to expectation since over a long period of time such features should have become smoothed out as the contents of each ring element diffused to adjacent regions of lower concentration. The Voyager data stimulated considerable interest among scientists to conceive of active pattern-maintaining mechanisms which would counteract the process of entropy. However, the other alternative, which has not been given as much attention as it deserves, is that there are no patterning mechanisms and that we happen to have the privilege of seeing Saturn's rings in an inhomogeneous state simply because Saturn's rings are very young, i.e., $< 10^4$ years old. Napier and Clube (1979) have suggested that Saturn's rings may be a short-lived phenomenon, in existence for at most a few times 10^4 years, noting that Ring C has been spreading inwards at the rate of ~ 1.6 arc seconds per century ($\sim 10,000 \text{ km/century}$).

The GEH offers a relatively straightforward explanation for the apparent youth of Saturn's rings. Namely, during passage of the 14,200 years BP event horizon, the rings, if in existence at that time, would have become completely evaporated. This is a reasonable assumption since Voyager observations indicate that the present ring system is composed of

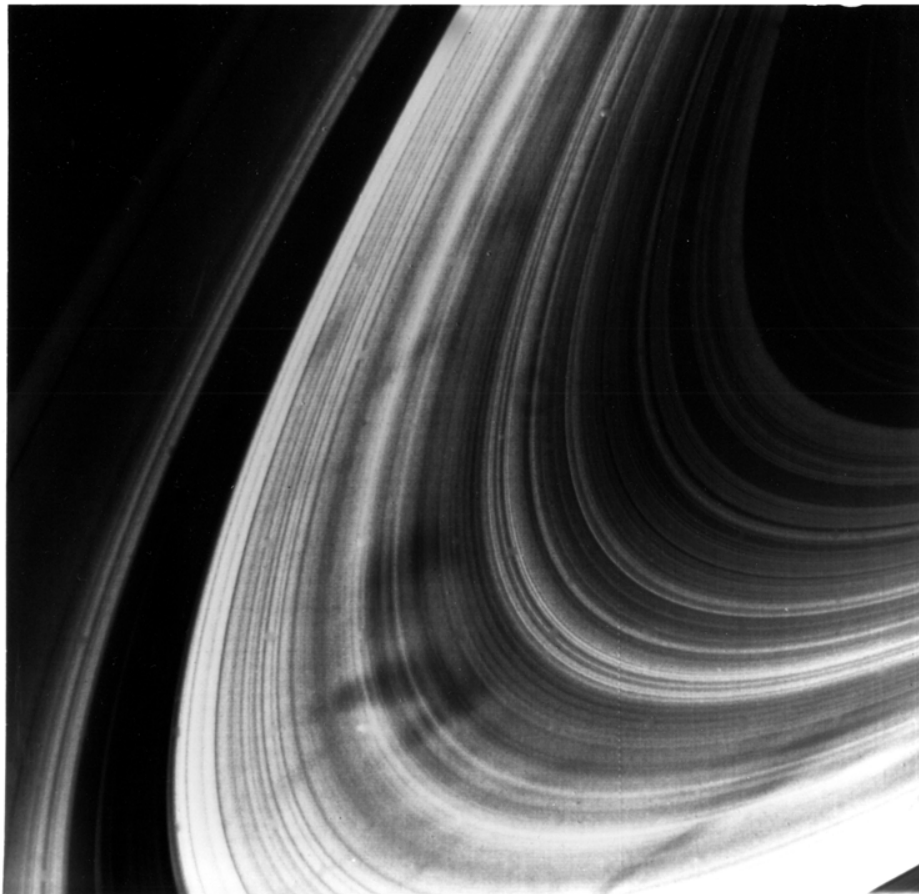


Figure 4-E. The rings of Saturn, as photographed by the Voyager 11 spacecraft (photo courtesy of NASA).

chunks of ice ranging in size from 1 to 100 meters. As is pointed out in Section 3.3.2, superwave cosmic ray electrons trapped in the heliopause sheath would have had a sufficiently high energy density to cause ice to evaporate at a rate of about $2\frac{1}{2}$ meters per day. As the heliopause sheath became propelled past Saturn, it would have caused Saturn's ring system to vaporize within a matter of a few weeks. After the cosmic ray blast had passed by and the heliopause sheath had returned to its former position, a new pattern of rings would have become formed, as water vapor in the vicinity of Saturn's orbit condensed on ice crystals orbiting in Saturn's gravitational field.

Closeup views of Saturn's moons made by Voyager I and II also support the hypothesis that ice melting has taken place, perhaps relatively recently. Voyager I found indications of fissuring and resurfacing on Dione, Rhea, and Tethys. On Enceladus Voyager II revealed the presence of fissures, canyons, corrugated terrain, and areas where cratered terrain had been eradicated by lava-like flows, possibly consisting of liquid water at the time of formation. These signs of melting on Enceladus are all the more difficult to account for on the basis of primordial heat reservoirs since Enceladus is only 490 kilometers in diameter. Tidal pumping has been suggested as a means for supplying heat to this tiny body, but this explanation remains at a speculative stage.

The GEH, however, could easily account for the observed signs of earlier melting. Since the radiation length for electrons traveling through ice water is about $X_0 \sim 37$ cm, most of the electron energy flux would be absorbed within a depth of 20 meters. Thus, a

large reservoir of liquid water could have been made available near the surface of these moons. Liquid water would not have been stable at the surface of the moons, but rather would have tended to evaporate rapidly into the vacuum of space. In so doing it is very likely that the rapid heat loss through evaporative cooling would have formed a surface ice crust. This surface barrier would have tended to preserve in a liquid state the water trapped underneath, and would have tended to insulate it from rapid heat loss. However, from time to time it is possible that this ice crust could rupture and spew out liquid water which could carve features in the surfaces of these moons.

4.7.2 The Water Valleys of Mars

The same superwave event possibly responsible for the vaporization of Saturn's rings and for surface features observed on Saturn's moons could have been responsible for the vaporization of the polar ice caps of Mars. This may explain why the polar caps appear to be among the youngest features of Mars. Satellite photographs indicate that the caps consist of layered ice deposits, about 1 to 2 km thick, that are almost entirely devoid of impact craters (Carr, 1980). This either indicates a very young age for the ice caps, or else that some mechanism must be at work to resurface the impacted areas.

It is unlikely that the fluvial features observed on Mars could have been directly connected with the vaporization of the ice caps. The so-called "outflow channels," which appear to be relatively young features cutting across cratered areas (Carr, 1980), are mostly

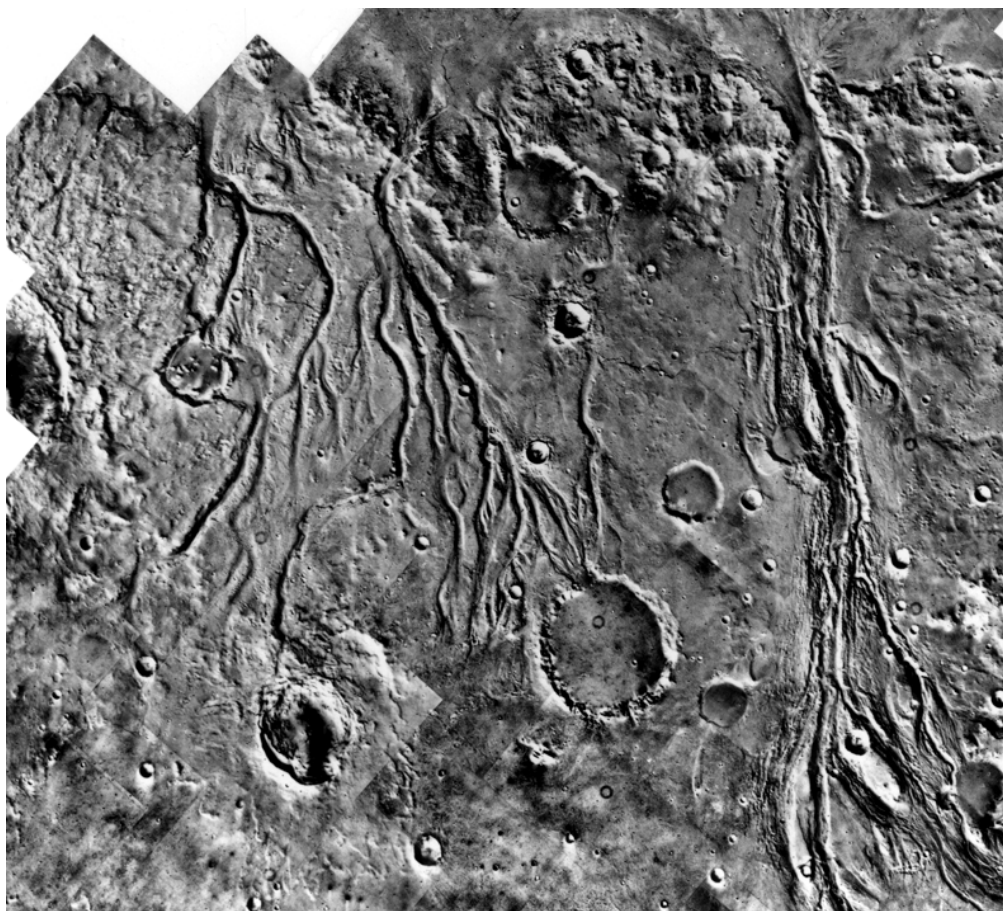


Figure 4-F. Outflow channels cut braided fluvial paths across the surface of Mars' cratered terrain (photo courtesy of NASA)

located near the equator ($\sim 20^\circ$ latitude), though it is possible that the polar caps might once have extended to lower latitudes. The form of these outflow channels strongly suggests that they were cut by catastrophic floods of water. Based on channel dimensions, Carr (1980) has estimated discharge rates ranging as high as $1 \text{ km}^3/\text{s}$. Baker (1978) points out that the martian channels are morphologically similar to the Channeled Scabland of eastern Washington. These terrestrial gorges are believed to have been produced by a catastrophic flood (the "Spokane Flood") occurring at the end of the Last Ice Age and connected with the recession of the continental ice sheet. For these channels, Baker estimates discharge flows as high as $0.02 \text{ km}^3/\text{s}$.

Explanations for the martian outflow channels include: icy comets striking the surface of the planet and melting suddenly in the process (Napier and Clube, 1979); the eruption of artesian water trapped about 1 km underground and possibly triggered by a seismic event (Carr, 1979); and volcanic melting of ice (Masursky et al., 1977). Two other possibilities are suggested here in the context of the GEH: temporary heating of subsurface martian permafrost either by an intense T Tauri-like solar outburst [coronal mass ejection] or by a transit of the heliopause sheath radiation zone.

4.7.3 Lunar Evidence of Past Solar Activity

The Remarkable Glazed Rock Patches on the Moon. One of the most amazing discoveries of the Apollo 11 manned landing on the Moon was that small lunar craters measuring between 20 cm and 1.5 meters across frequently contain at their bottoms lumps of soil whose upper surfaces are coated with a glassy glaze (Gold, 1969). The glassy patches that were photographed at close range by Apollo astronauts range in size from 0.5 to 10 mm. According to Gold (p. 1345):

The glazed areas are clearly concentrated toward the top surfaces of protuberances, although they exist also on some sides. Points and edges appear to be strongly favored for the glazing process. In some cases, droplets appear to have run down an inclined surface for a few millimeters and congealed there.

Eliminating a variety of possible alternate explanations, such as meteorite impacts, Gold concludes that these features were formed by intense radiative heating of the lunar surface by the Sun. Temperatures at crater bottoms typically being 10 – 20% higher than on flat ground, such regions would have been the first to melt. He points out that this event would have had to have occurred within the last 30,000 years in order to account for the absence of significant micrometeorite erosion. He estimates that the solar luminosity would have had to increase by 100 fold for 10 – 100 seconds in order to produce the observed glazing effects, and suggests that this luminosity increase may have occurred in the form of a very large solar flare or as a nova-like outburst. He proposes that either the Sun spontaneously engages in such outbursts on rare occasions (every few tens of thousands of years) or else something falling into the Sun happened to trigger the proposed eruption, e.g., the infall of a large cometary body having a mass of about 3×10^{21} grams and a diameter of about 100 km.

Gold's conclusion that the Sun has engaged in extremely energetic activity within the last 30,000 years parallels the conclusion that I have reached independently in this study on the basis of an entirely different set of data. As is suggested in Section 3.3.2, about 12,000 – 14,000 years ago the Sun temporarily may have become a T Tauri-like star due to the accretion of nebular material. Short-period flare-like outbursts lasting on the order of 10^2 – 10^4 seconds and having energies of the order of 10^{34} ergs are typical of T Tauri stars; see Section 3.3.2 (p. 99). However, for the outburst proposed by Gold, a total energy of $\sim 10^{37}$ ergs (1000 times greater) would be required. Such a large outburst would be more on the scale of a nova than a flare. T Tauri stars are observed to change their luminosity in an

erratic manner by 20 fold or more, but it is not certain whether this effect is due to variations in the optical depth of obscuring dust or to variations in the intrinsic output of the star.

Another possibility is that the Moon's surface was heated by solar wind particles, rather than by electromagnetic wave radiation. About half of the energy of a solar flare is normally emitted in the form of solar wind protons. If such a particle blast from a very large solar flare were to become magnetically trapped in the Earth's magnetopause tail, very high particle densities could become temporarily achieved. If then the Moon happened to be transiting through this energetic region, its surface could have become considerably scorched. Alternatively, it is also possible that both the Earth and Moon encountered a region of enhanced solar flare particle density, the remnant of a major prominence or "fireball" thrown out by the Sun [e.g., a coronal mass ejection]. In such a case the interplanetary magnetic field bound up with the particle blast wave could have acted as a magnetic bottle retarding the dispersal of this region of high particle density as it journeyed from the Sun.

Morgan, Laul, Ganapathy, and Anders (1971) have analyzed the glassy coating and crystalline interior of one lunar rock and find that the coating is enriched in a number of rare earth elements and alkali metals including Ir and Au. They conclude that the glass has been contaminated by a mixture of meteoric material with lunar soil. They suggest that the glassy material represents molten material splashed from a nearby meteoritic impact and that it was not produced by in situ melting due to radiative heating, as Gold has suggested.

However, the geochemical results reported by Morgan et al. could be interpreted differently. If at the time of radiative or solar wind heating the surface of the Moon had been covered by a fine deposit of micron and submicron-sized particles of cosmic dust, this material would have become fused into the underlying rock when melting occurred. This scenario is compatible with the proposal made earlier in this study (Chapter 3, Section 3.3.2) that the solar system was filled with unusually high concentrations of cosmic dust at the time of enhanced solar activity. In addition, the results of the glacial ice dust tests (Chapter 12) which indicate high cosmic dust deposition rates at the end of the Wisconsin ice age also support this interpretation.

The Lunar Record of Past Solar Flare Activity. Solar flare tracks left in the glassy surfaces of lunar micrometeorite craters provide a record of past solar flare activity. Assuming that the cratering rate has remained relatively constant for the past 2×10^4 years, Zook, Hartung, and Storzer (1977) conclude that solar flare activity must have been about 50 fold higher about 16,000 years ago. The activity curve which they have derived is shown in Figure 4.5. If the cratering rate was higher prior to 10,000 BP, as the GEH suggests, then the solar flare activity change presented in this diagram would be underestimated. The peak at 16,000 BP would then be expected to increase and shift to a more recent date. Thus this data would be compatible with the solar outburst date of ~12,950 years **b2k** established on the basis of geological evidence; see Part III. It is significant that the conclusion reached by Zook et al. on the basis of lunar rock studies parallels that which I independently arrived at on the basis of the analysis of glacial ice dust and theoretical considerations regarding the response of the Sun to the accretion of elevated amounts of nebular material. Zook et al. (1977, p. 120) speculate that the elevated solar flare activity around 16,000 years BP may somehow have been associated with the retreat of the continental ice sheets at the end of the last glaciation, although they are not able to suggest a mechanism by which terrestrial temperature would correlate with solar flare activity. The GEH suggests such a mechanism, namely the influx of nebular material into the solar system could have caused terrestrial heating through an interplanetary hothouse effect and spectral shift effect, and also by activating the Sun as a result of material accretion; see Section 3.3.2 (p. 90) and Subsection 3.3.4 (p. 102).

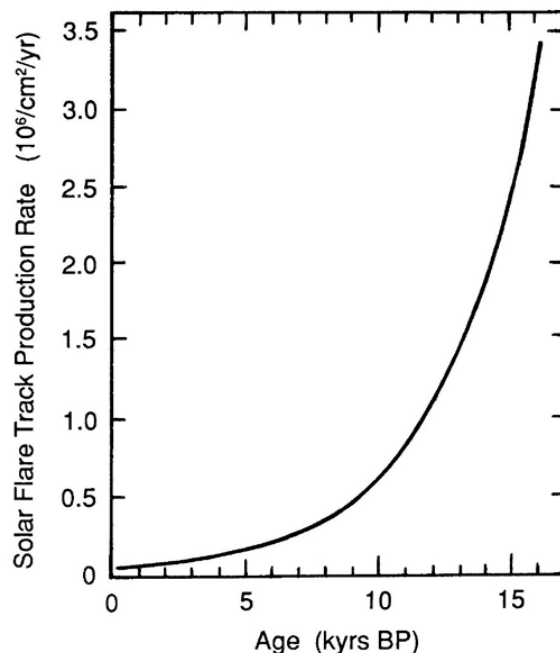


Figure 4.5. Solar flare track production rate (corrected for thermal annealing) as a function of time (adapted from Zook et al., 1977, Fig. 4).

It should be pointed out that the occurrence of a very brief, very intense heating of the lunar and terrestrial environment at the end of the Last Ice Age (either by a radiative outburst or by an outburst of solar wind particles) may be easily tested by conducting a detailed stratigraphic analysis of glacial ice cores. If this scenario is correct, a melt feature should be present in the ice cores discussed in Chapter 8. Such a feature would most easily be distinguished in Antarctic cores, where melt features are normally found to be quite rare. Also, if a major solar outburst had occurred, it would probably have left a signature such as a high nitrate concentration.

UPDATE

A Residual Low Energy Galactic Cosmic Ray Wind (update to [p. 134](#)): Ben McCall and his colleagues have observed nearby diffuse interstellar clouds and have detected the presence of H_3^+ ion at concentrations much higher than expected.⁽²⁾ They have suggested that these ionization levels are most likely accounted for by the presence of a low energy cosmic ray background flux that is 40 times greater than standard estimates have predicted. They theorize that this galactic wind is composed mainly of cosmic ray protons having energies of a few Mev (i.e., velocities of 2 to 4 percent of c). This unexpectedly high cosmic ray flux is expected on the basis of the superwave hypothesis which predicts episodic passages of Galactic core cosmic ray volleys. The low energy, low velocity component of the superwave cosmic ray volley would trail behind the main superwave front and become magnetically captured in the galactic disk where it would form an averaged out elevated low energy background flux. If these particles are protons they could be a lagging proton component of the superwave or could have been formed by superwave electrons Compton scattering off of interstellar hydrogen.

Interstellar Dust Coming from the Galactic Center Direction (update to p. 135): After this dissertation was published in 1983, several discoveries were made that supported its thesis that interstellar dust had recently entered the solar system from the direction of the Galactic center. In 1984 the IRAS (InfraRed Astronomy Satellite) scientific team reported observations of the solar system's zodiacal dust cloud, dust that orbits the Sun within the solar system.⁽³⁾ They noted that their findings confirmed earlier reports that this dust cloud is tilted about 3 degrees relative to the ecliptic with ascending and descending ecliptic nodes at ecliptic longitudes $\lambda = 87 \pm 4^\circ$ and $\lambda = 267 \pm 4^\circ$, but drew no conclusion as to why it had nodes at these particular positions.⁽⁴⁾ Noting that these nodes are aligned within one degree of the Galactic-center-anticenter direction (at ecliptic longitudes 86° and 266°), I concluded that the observed nodal alignment is just what one would expect if the dust forming the zodiacal cloud was interstellar dust that had recently entered the solar system from the Galactic center direction. This IRAS observation, therefore, was strong support for one of the key a priori predictions made in the present dissertation. I noted this confirming observation in a paper published in 1987 in the journal *Earth, Moon, and Planets*.⁽⁵⁾

This prediction of recent dust entry gained further support from a 1988 paper by Harold Aumann. He announced infrared observations which indicated that the Sun, like other nearby stars, is enveloped in a thick sheath of dust 500 times denser than previously supposed.⁽⁶⁾ However, more direct confirmation came some years later in 1993 when a NASA and European Space Agency team announced Ulysses spacecraft measurements which indicated that interstellar dust is currently entering the solar system from the Galactic center direction and that most of the dust outside the asteroid belt should be of interstellar origin.⁽⁷⁾ This directly confirmed my earlier 1983 and 1987 predictions for the recent entry of interstellar dust from the Galactic center direction, indicating that the present inflow may be a residual flow left behind by passage of the last superwave. That year in 1993 I published an article in *Eos* noting this confirmation.⁽⁸⁾

That same year, Witte et al. published the results of Ulysses measurements of the interstellar neutral helium wind determining that it was entering the solar system from ecliptic coordinate direction ($\lambda = 252^\circ$, $\beta = 2.5^\circ$) at a velocity of 26 km/s.⁽¹⁾ This direction, which is marked by point (d) in Figure 4.3, updates the earlier measurement of Weller and Meier. Then in 1994 Grün et al. announced their finding that the local interstellar dust wind enters the solar system with a mean velocity and direction consistent with this helium gas flow. They note that both gas and dust components are coming from the local interstellar cloud which is now blowing into our solar system.⁽⁹⁾ As noted earlier, this inflow direction translates into a galactic coordinate of ($\ell = -0.2 \pm 0.5^\circ$, $b = +16.3 \pm 0.5^\circ$) which lies along the Galactic center 0° longitude meridian (red line in Figure 4.3), thereby implicating Galactic superwaves as the periodic driving force behind this wind.

Evidence that interstellar dust is currently entering the solar system was further corroborated in 1996 with the announcement that the AMOR radar in New Zealand had detected a strong flux of interstellar meteoroid particles, measuring 15 to 40 microns in size, entering the solar system from the Galactic center direction.⁽¹⁰⁾

In 1998, the DIRBE (Diffuse Infrared Background Experiment) on board the COBE satellite made measurements that allowed more accurate modeling of the zodiacal dust cloud coordinates indicating that the slightly inclined zodiacal cloud has nodes positioned at ecliptic longitudes $77.7 \pm 0.6^\circ$ and $257.7 \pm 0.6^\circ$, or in galactic coordinates at ($\ell = 0.5 \pm 0.6^\circ$, $b = +10 \pm 0.6^\circ$).⁽¹¹⁾ This ecliptic position, indicated in Figure 4.3 by the added red dot, is also seen to coincide with the Galactic center zero degree longitude meridian indicating that the zodiacal dust cloud has been built up from an interstellar dust wind coming from the Galactic center direction and most likely propelled by cosmic ray volleys coming from the Galactic center. The finding that the interstellar helium wind and interstellar dust wind also

lie along this same zero degree longitude meridian (as noted above) further confirms what I had suggested in my *Eos* paper.

Coronal Mass Ejection Conflagrations (update to p. 141): Zook reviews evidence of elevated radiocarbon levels in the surfaces of lunar rocks and concludes that the Moon was exposed to solar cosmic ray levels 30 times higher than present levels over a period of 5000 years, this exposure occurring prior to 12,000 years BP and beginning as early as 2×10^4 years ago.⁽¹²⁾

As a possible explanation for the glazed moon rocks, I suggested above (p. 140) that thousands of years ago the Earth and Moon may have become engulfed by a "remnant of a major prominence or 'fireball' thrown out by the Sun." Although I did not specifically use the term *coronal mass ejection*, this is essentially what I was referring to. At the time this dissertation was being completed, coronal mass ejections had been observed leaving the Sun. However, at that time there was no way to track their outward trajectory once they left the Sun's immediate vicinity, to know whether they could reach as far as the Earth's orbit. Consequently, the idea that the Earth and Moon may have been affected in the past by the arrival of a giant solar coronal mass ejection was a theory that was advanced for the first time in this dissertation. Only in the late 1990's did we have the ability to track the progress of coronal mass ejections through the solar system using satellite imaging. Such observations did establish that these expanding balls of coronal plasma were able to travel beyond the Earth's orbit. This lent credence to my theory that a large coronal plasma "fireball" thrown off by an immense solar flare may have reached the Earth and Moon to scorch their surfaces.

Figure 4-G shows a large coronal mass ejection that was imaged on February 27, 2000. Figure 4-H shows an artist's conception of a coronal mass ejection and its subsequent impact on the Earth's magnetosphere. Figure 4-I shows a sequence of solar coronagraph images showing an event that took place on June 6, 2000 in which two consecutively emitted coronal mass ejections fused in space to form a giant outwardly traveling coronal mass ejection. This process whereby a high speed trailing coronal mass ejection overtakes a slower leading coronal mass ejection and engulfs it has been termed coronal mass ejection cannibalism. Scientists acknowledge that a cannibalized CME (or fused CME) would produce a more protracted geomagnetic storm when it envelops the Earth. This cannibalism mechanism could explain how our Sun, during its late ice age T Tauri phase, could have produced coronal mass ejections sufficiently large and intense to have glazed lunar rocks. Since the Sun's surface would have been covered with simultaneously erupting flares, not only would these have individually been more powerful ejections, but also the increased frequency of these eruptions would have allowed as many as 5 or more CMEs to fuse to form a single very intense plasma fire ball. A super large CME of this sort, upon impact, could have produced a ring current strong enough to neutralize the Earth's magnetic field and allowed the coronal plasma to contact the Earth's surface. Such a coronal plasma contact event could explain the radiation effects seen on Paleolithic artifacts dating from the end of the ice age; see Chapter 10 (update).

In 1975, astronomer A. Lovell suggested that sun-like stars occasionally produce flares of up to 10^{37} ergs, 30,000 times more energetic than the largest solar flare of modern times. In 1999, astronomers announced that they had observed large explosive outbursts from the surfaces of nearby "normal" sunlike stars. These "superflares" were observed to range from 100 to 10 million times the energy of the largest flare observed on the Sun in modern times and were estimated to occur about once every hundred years. This confirmed the Lovell hypothesis and increased the plausibility of my suggestion that the Sun was producing mega solar flares and intense coronal mass ejections at the end of the last ice age.

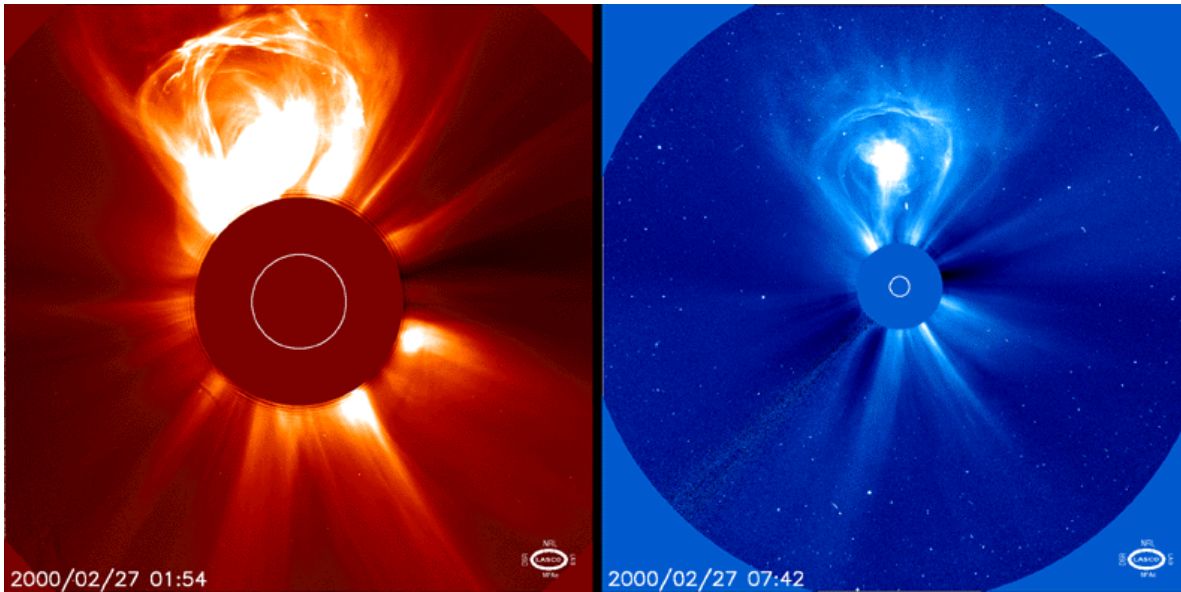


Figure 4-G. A lightbulb-shaped coronal mass ejection that blasted away from the Sun on February 27, 2000. The two shots taken 6 hours apart show its expansion and outward progress (courtesy of the LASCO project and NASA). Click on the above pictures to run them as movies. The white circle inside the coronagraph mask indicates the actual size of the visible solar disk.

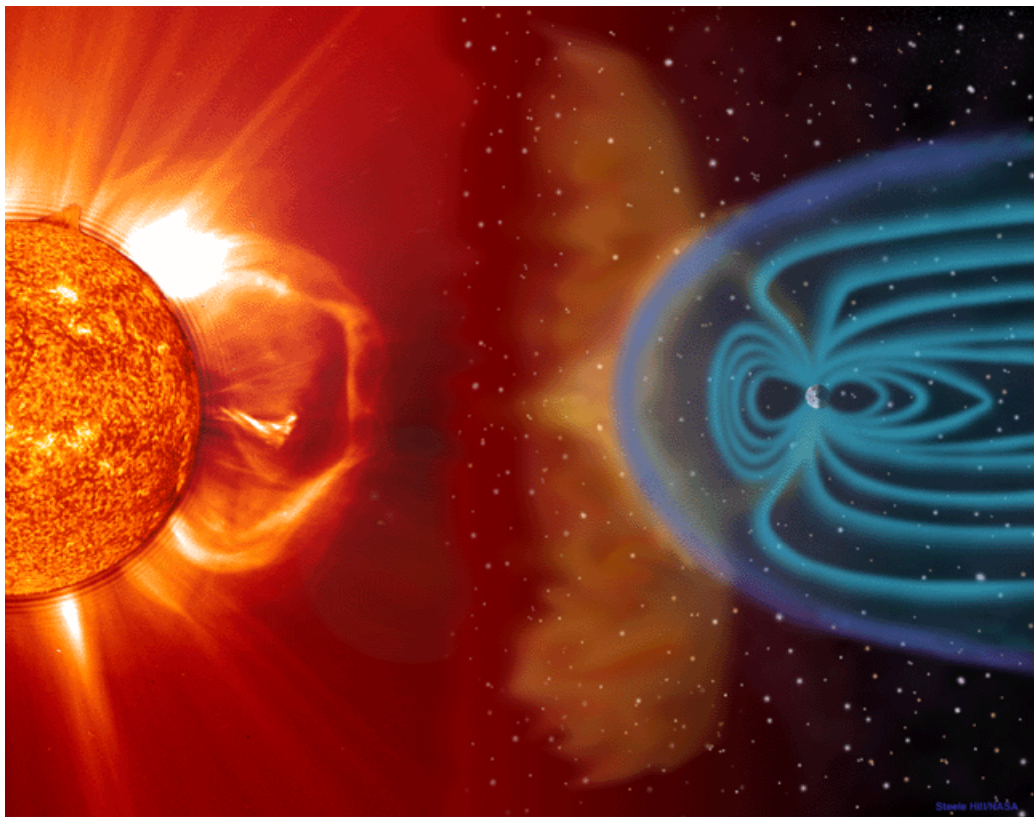


Figure 4-H. Illustration showing a coronal mass ejection blasting off the Sun's surface in the direction of Earth. This left portion is composed of an EIT 304 image superimposed on a LASCO C2 coronagraph. Two to four days later, the CME cloud is shown striking and beginning to be deflected around the Earth's magnetosphere. Objects in the illustration are not drawn to scale (courtesy of the LASCO project and NASA).

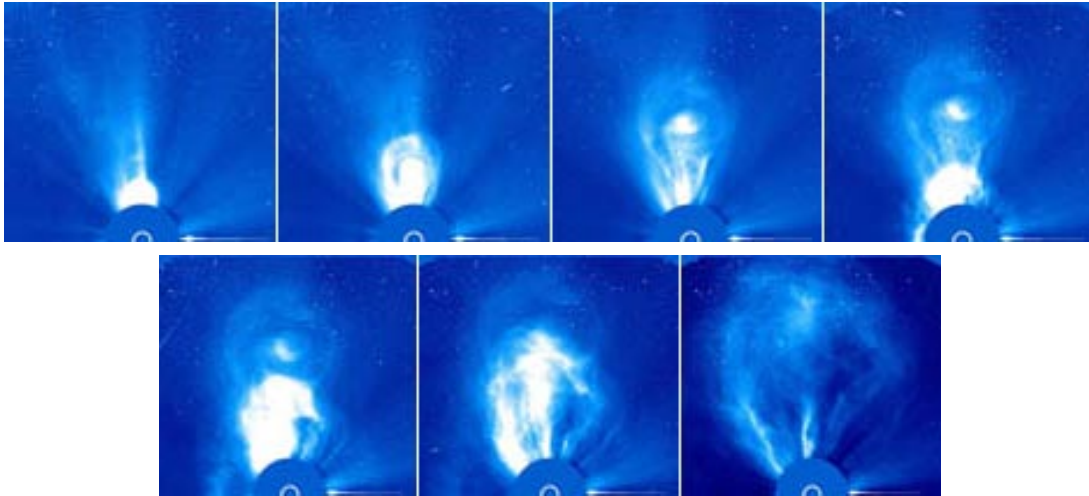


Figure 4-I. A sequence of images showing the phenomenon of coronal mass ejection cannibalism. This was observed on June 6, 2000 with a coronagraph on board the ESA-NASA SOHO spacecraft. The second CME overtakes the first and the two merge to form a giant CME. The white circle inside the coronagraph mask indicates the actual size of the visible solar disk. In the last frame, the CME has grown to 13 solar diameters.

References to the Update

- 1) M. Witte, H. Rosenbauer, M. Banaszekiewicz, H. Fahr, "The ULYSSES neutral gas experiment - Determination of the velocity and temperature of the interstellar neutral helium." *Advances in Space Research* **13**(6) (1993): 121-130.
- 2) B. McCall, et al., "An enhanced cosmic-ray flux towards zeta Persei inferred from a laboratory study of the $H_3^+ - e^-$ recombination rate." *Nature* **422** (2003): 500-502.
- 3) M. G. Hauser et al., "IRAS observations of the diffuse infrared background," *Astrophysical Journal* **278** (1984): L15-L18.
- 4) Leinert, C., M. Hanner, I. Richter, and E. Pitz "The plane of symmetry of interplanetary dust in the inner solar system." *Astron. Astrophys.* **82** (1980): 328 - 336.
- 5) P. A. LaViolette, "Cosmic-ray volleys from the Galactic Center and their recent impact on the Earth environment," *Earth Moon Planets* **37** (1987): 241 - 286
- 6) H. H. Aumann, "Spectral class distribution of circumstellar material in main sequence stars," *Astronomical Journal* **96** (1988): 1415 - 1419; also *Science News* **134** (1988): 246.
- 7) E. Grün et al. "Discovery of jovian dust streams and interstellar grains by the Ulysses spacecraft," *Nature* **362** (1993): 428 - 430.
- 8) P. A. LaViolette, "Anticipation of the Ulysses interstellar dust findings," *Eos* **74** (1993): 510-511.
- 9) E. Grün, et al., "Interstellar dust in the heliosphere." *Astronomy and Astrophysics* **286** (1994): 915-924.
- 10) A. D. Taylor, W. J. Baggaley, and D. I. Steel, "Discovery of interstellar dust entering the Earth's atmosphere," *Nature* **380** (1996): 323 - 325.
- 11) T. Kelsall, et al. "The COBE Diffuse Infrared Background Experiment search for the cosmic infrared background. II. Model of the interplanetary dust cloud." *The Astrophysical Journal* **508** (1998): 44 - 73.
- 12) H. Zook, "On lunar evidence for a possible large increase in solar flare activity $\sim 2 \times 10^4$ years ago." In *Proc. Conf. Ancient Sun*, edited by R. Peppin, J. Eddy, and R. Merrill, 1980, pp. 245-266.

CHAPTER 5

EVIDENCE OF THE PRESENCE OF THE 14,200 YEARS BP EVENT HORIZON

5.1 THE GALACTIC RADIO BACKGROUND RADIATION

At radio frequencies below about 800 MHz, a diffuse continuum radiation is observed from all directions of the sky. The nonthermal component of this radiation field is observed best at 150 MHz. As seen in the radio map in Figure 5.1 (Landecker and Wielebinski, 1970), there is a tendency for this emission to be concentrated in the Galactic plane and to be enhanced toward the Galactic center. The radial position of this encircling radiation with respect to the GC is not well known. However, it is certain that this zone extends behind the GC since H II clouds in the nuclear region appear in absorption against this radio background.

The spectral index of this radiation and the fact that the radiation is partially polarized, strongly suggest that it is synchrotron emission produced by relativistic electrons spiraling in magnetic fields (Ginzburg, 1956; Kraus, 1966, p. 377; Alexander and Clark, 1974). Alexander and Clark (1974) have modeled this nonthermal radiation by assuming that it is produced diffusely throughout the volume of the Galactic disk by electrons with spectral index 1.8 spiraling in a magnetic field of strength 3×10^{-6} gauss. Their model requires a higher electron density than is observed in the Earth's vicinity, e.g., 5 times higher for electrons in the 3 Gev energy range. Setti and Woltjer (1971) have also modeled the Galactic radio background, assuming an electron spectral index of 2.6 and a magnetic field strength of 3×10^{-6} gauss. Their model requires an electron density that is *10 times higher* than the solar vicinity level, for electrons in the 3 Gev range.

In view of the GEH it is reasonable to suppose that some fraction or perhaps all of the Galactic radio background is produced by cosmic ray electrons formerly carried by the 14,200 years BP superwave, but which have become trapped in the magnetic fields of the Galactic disk. Two possibilities may be suggested regarding the distribution of such

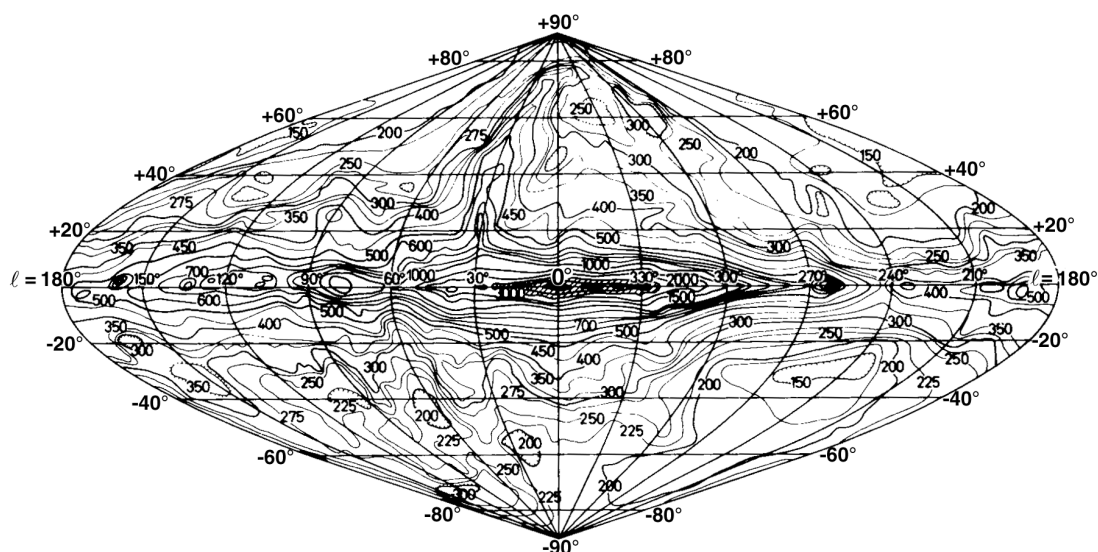


Figure 5.1. A map of the Galactic radio background radiation at 150 MHz in galactic coordinates (Landecker and Wielebinski, 1970).

electrons. According to one model they might be distributed throughout the Galactic disk within the elliptical region defined by the 14,200 years BP event horizon. According to another model, the electrons might be distributed within an elliptical shell coincident with the 14,200 years BP event horizon. In either case the density of these electrons would be expected to vary according to the inverse square of galactocentric distance, and the radio emission would be expected to be stronger in the vicinity of the Galactic disk than in regions above or below the disk where fewer superwave electrons would become captured. Although most models of the Galactic radio background assume that the radiating electrons are distributed throughout the Galactic disk, shell or sheet-like regions of enhanced electron density have also been considered; see Heiles (1976, p. 12).

Of the two electron distribution models suggested above, the shell model is considered below. First a rough estimate should be made to determine whether the 14,200 years BP superwave would have had sufficient energy to power the radio background emission. The values of Alexander and Clark, and Setti and Woltjer (quoted above) for the density of synchrotron radiating electrons should be boosted about 10 – 20 times to account for the fact that most of the observed radio emission is hypothesized to come from a shell-like region rather than from the whole disk. Thus electron densities averaging about 100 times the local interstellar density, $\sim 10^{-12} - 10^{-11}$ ergs/cm³, would be expected. If the perimeter of the shell is taken to be $\sim 10^5$ l.y., as defined by an ellipse having semi-major and semi-minor axes: $a = 18,500$ l.y. and $b = 14,600$ l.y., and if the height and depth of the shell are assumed to be $z = 4000$ l.y. and $r = 2500$ l.y., then the total volume of the shell would be: $V = 10^{12}$ l.y.³ = 10^{66} cm³. Consequently, the synchrotron radiating electrons in the shell would comprise a total energy of $10^{54} - 10^{55}$ ergs, or about 0.1 – 0.01% of the total superwave energy. By comparison, in Section 3.2 it was suggested that about 2% of the superwave's particle energy content would become captured by magnetic fields in the nucleus and disk of the Galaxy. Thus it is conceivable from an energetics standpoint that the 14,200 years BP superwave could be powering the Galactic radio back-ground emission.

The hypothesis that the Galactic radio background is primarily produced in the vicinity of the 14,200 years BP superwave Event Horizon may be checked by noting if the expected longitudinal variation in cosmic ray intensity along the superwave event horizon matches the observed longitudinal variation of radio brightness temperature. According to the Rayleigh-Jeans Law, the observed radio brightness temperature, T_b (°K), should be proportional to the observed radio brightness (in watts/m²/Hz/rad²), which in turn should be proportional to the ambient cosmic ray electron density (Kraus, 1966, p. 85). Moreover, according to the GEH, the ambient electron density in a given longitudinal increment of the elliptical event horizon should vary according to the inverse square of the distance of that increment from the center of the Galaxy. Thus, if synchrotron emission occurs along the event horizon it should be true that::

$$T_b \propto [r(\ell)]^{-2} \quad (12)$$

where $r(\ell)$ is the distance of the event horizon from the GC, this distance varying as a function of galactic longitude ℓ . However, an additional small correction of $1/\cos \theta$ should be made to the calculated brightness temperature where θ measures the angular deviation of the line of sight from an orientation orthogonal to the event horizon.

To determine $r(\ell)$ for various values of ℓ , the 14,200 years BP event horizon was plotted on a polar coordinate graph and the galactocentric distances were measured directly from this graph. An example of such a polar plot is shown in Figure 5.4. Table VII lists values of galactic longitude ℓ (column 1), galactocentric radius $r(\ell)$ (column 2), the inverse square relation $r(\ell)^{-2}$ (column 3), the angular deviation θ (column 4), and the correlation factor $1/\cos \theta$ (column 5). To synthesize the theoretical brightness temperature distribution (column 6), a temperature of $T_b = 5000^\circ$ K was arbitrarily assigned for $\ell = 0^\circ$ and the values

TABLE VII
 HYPOTHETICAL BRIGHTNESS TEMPERATURE PROFILE
 FOR THE 14,200 YEARS BP EVENT HORIZON

| (1) ℓ (deg) | (2) $r(\ell)$ (kpc) | (3) $r(\ell)^{-2}$ (kpc ⁻²) | (4) θ (deg) | (5) $1/\cos \theta$ | (6) T_b (°K) |
|------------------------|---------------------------|---|--------------------------|------------------------|----------------------|
| 0 | 2.178 | .2108 | 0 | 1.00 | 5000 |
| 2/358 | 2.180 | .2104 | 2 | 1.00 | 4990 |
| 5/355 | 2.22 | .2029 | 7 | 1.01 | 4880 |
| 10/350 | 2.38 | .1765 | 15 | 1.035 | 4330 |
| 15/345 | 2.67 | .1403 | 22 | 1.08 | 3590 |
| 20/340 | 3.02 | .1096 | 27 | 1.12 | 2910 |
| 40/320 | 4.75 | .0443 | 39 | 1.29 | 1360 |
| 60/300 | 6.30 | .0252 | 37 | 1.25 | 750 |
| 90/270 | 7.85 | .01623 | 32 | 1.18 | 450 |
| 120/240 | 8.65 | .01336 | 23 | 1.085 | 340 |
| 180 | 9.18 | .01187 | 0 | 1.00 | 280 |

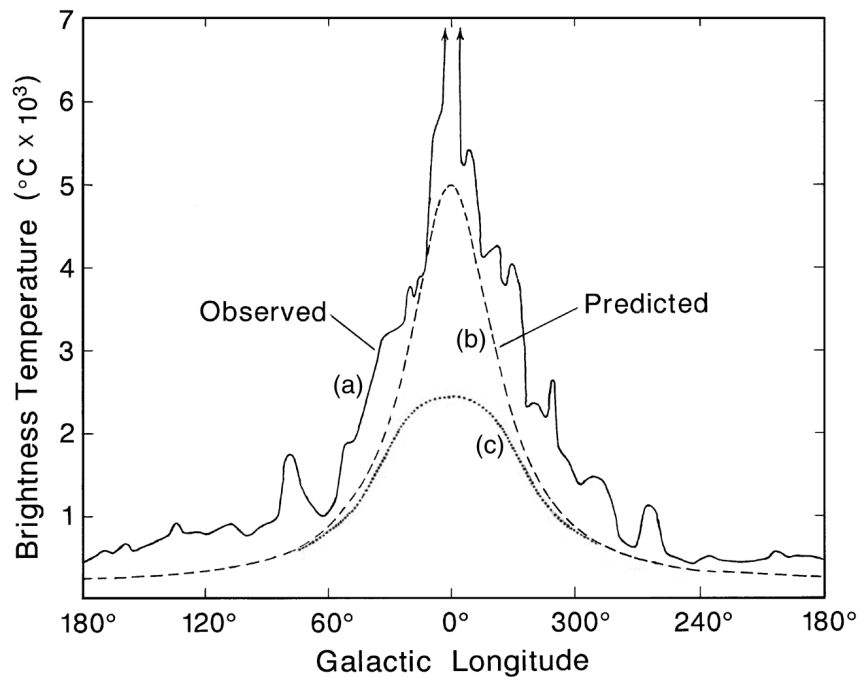


Figure 5.2. Brightness temperature profiles along the Galactic equator: a) observed distribution at 150 MHz (adapted from Price, 1974, Fig. 1); b) the distribution predicted by the 14,200 years BP superwave Model; c) exponential decrease model suggested by Price (Price 1974).

for the other longitudes were scaled according to the product of the values given in columns (3) and (5).

The theoretical brightness temperature curve has been plotted in Figure 5.2 (dashed

line) and is shown in comparison to the observed temperature distribution for 150 MHz radiation (solid line). The observed distribution was compiled and normalized by Price (1974) from data by Landecker and Wielebinski (1970), Wielebinski et al. (1968), and Hamilton and Haynes (1969). The profile represents a longitudinal scan of the Galaxy along the equator ($b = 0^\circ$) with an angular resolution of 3° . Price (1974) has fitted this observational distribution with a number of volume emissivity models. For example, the model plotted as the dotted line in Figure 5.2 assumes that cosmic rays occupy the entire disk and that their volume emissivity drops off with galactocentric radius according to the exponential form $e^{-r/6}$, where r is given in kiloparsecs. However, all of the models proposed in the past, including Price's exponential decrease version, fail to account for the sharp peak within $\pm 20^\circ$ of the GC. The 14,200 years BP superwave Model, on the other hand, makes a good fit to the data in this region.

It is important to note that the Superwave Model makes a highly rigid prediction. That is, given the date of occurrence of the outburst (e.g., 37,000 years BP at the GC), the shape of the predicted brightness temperature distribution becomes rigidly defined. The close correspondence between the theoretical superwave model distribution and the observed distribution is encouraging.

UPDATE

The Milky Way's Infrared, X-ray and Gamma Ray Background Emission

The Diffuse Infrared Emission : The 14,200 years BP superwave could also account for the origin of a portion of the galactic diffuse infrared background emission. As seen in Figure 5-A, this emission is concentrated toward the center of the Galaxy in a manner similar to the radio background.

The Diffuse X-Ray Emission Ridge: This superwave could also account for the diffuse hard X-ray emission observed to come from the galactic plane. The emission is found to be most concentrated in a 2° wide strip extending about 40° of longitude on either side of the GC. The X-ray intensity as a function of galactic longitude (from Warwick et al, 1985) is plotted in Figure 5-B where it is compared with how cosmic ray intensity would vary with longitude along the proposed superwave event horizon.^(1, 2)

Worrall et al. have shown that this emission may be modeled as synchrotron radiation produced by 10^{14} eV cosmic ray electrons.⁽³⁾ Since the lifetime of such particles is on the

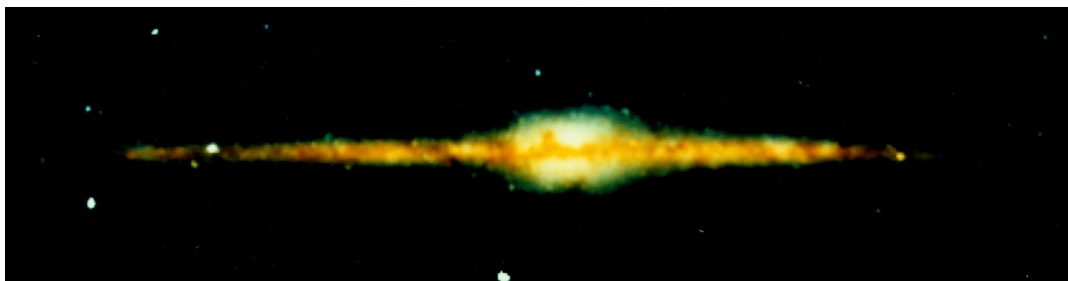


Figure 5-A. False color image showing the distribution of the galactic diffuse infrared background emission. The image made with data obtained by the Diffuse Infrared Background Experiment (DIRBE) on NASA's Cosmic Background Explorer satellite (COBE) combines data obtained at the near-infrared wavelengths of 1.2, 2.2, and 3.4 microns, represented respectively as blue, green, and red, and covers about 180° of galactic longitude (courtesy of NASA/Goddard Space Flight Center).

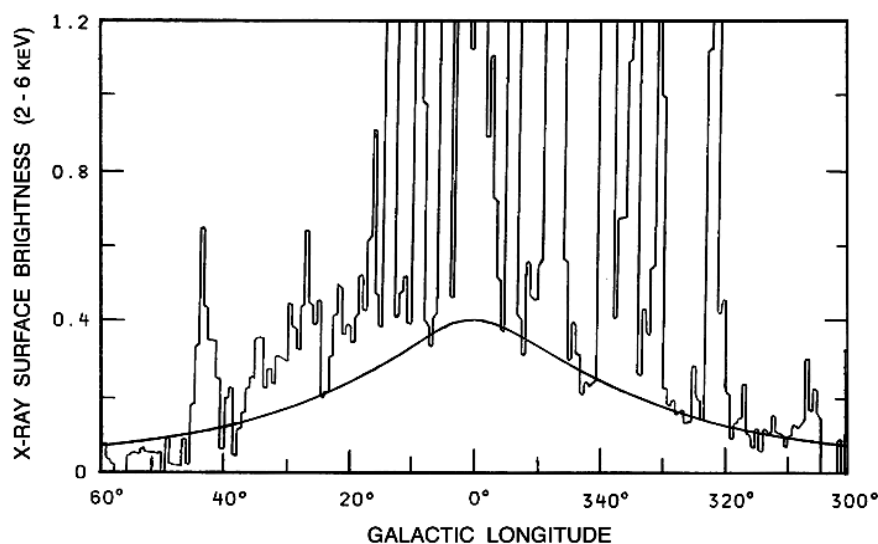


Figure 5-B. The intensity of the galactic X-ray emission ridge plotted as a function of galactic longitude (after Warwick et al., 1985). The emission profile expected from a superwave shell bounded by the 12,500 and 15,000 years BP superwave event horizons is shown for comparison (LaViolette, 1987). The profile was normalized to an intensity of 0.4 at $\ell = 0^\circ$.

order of 10^4 years, new particles would have to be supplied at the rate of 10^{48} ergs/yr to maintain this radiation at its observed intensity. This source of injection must itself be diffusely distributed since the particles are capable of diffusing only about 500 l.y. due to their short life span. A Galactic superwave would satisfy both the energy requirements and would provide a means of diffusely injecting particles over an extended region.

The Galaxy's Gamma Ray Halo: Gamma ray observations announced in November 1997 provided strong corroborating evidence for the existence of a superwave cosmic ray shell surrounding the Galaxy.⁽⁴⁾ The observations were made with the Energetic Gamma Ray Experiment Telescope (EGRET) orbiting on board NASA's Compton Gamma Ray Observatory. The data indicate the presence of a diffuse gamma ray glow or "halo" enveloping our entire Galaxy. Figure 5-C presents a galactic map showing the gamma ray intensity distribution over the whole sky for gamma rays ranging in energy from 30 Mev to ~20 Gev. Like the diffuse radio background emission (Figure 5.1), it is more concentrated toward the galactic plane and toward the center of the Galaxy, as predicted by the Galactic superwave model. Thus the gamma ray halo and the diffuse radio background radiation would both be produced by the same cosmic ray volley, the 14,200 years B.P. superwave. Figure 5-D is a computer-generated image of the EGRET data illustrating the excess high-energy gamma-ray emission that surrounds the Milky Way.

The EGRET observing team reported this discovery as an unexpected result since it was not possible to attribute the source of the gamma ray emission to discrete stellar sources scattered throughout the Galaxy; see news release in text box. As their leading explanation, they suggest a diffuse volley of cosmic rays originating from past activity of our Galaxy's core. This is exactly what the Galactic Explosion Hypothesis was predicting. Since the Galaxy's diffuse gamma ray emission was discovered 14 years after this dissertation was published, these gamma ray findings provide strong confirmation for the superwave theory.

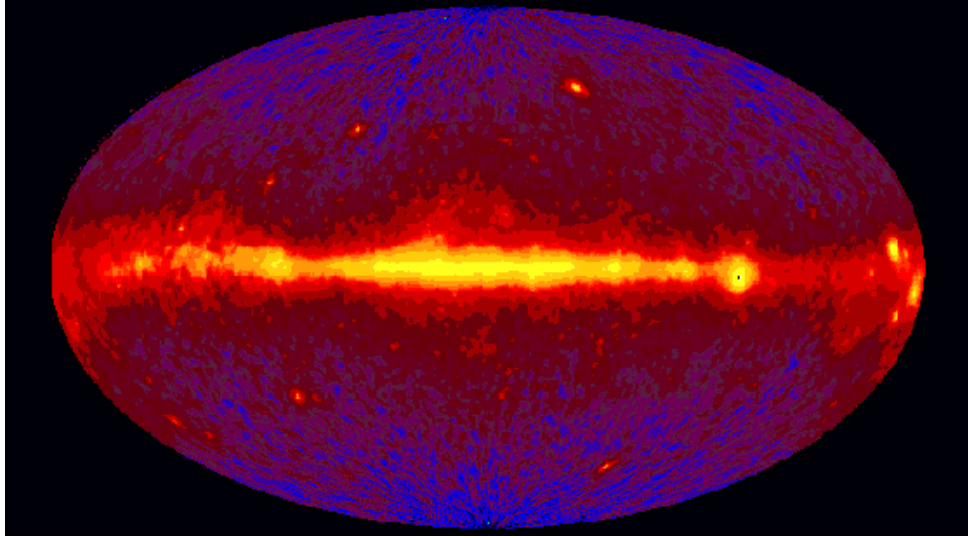


Figure 5-C. Galactic map of the diffuse gamma ray background radiation that surrounds our Galaxy (courtesy of D. Dixon, D. Hartmann, E. Kolaczyk, and NASA).

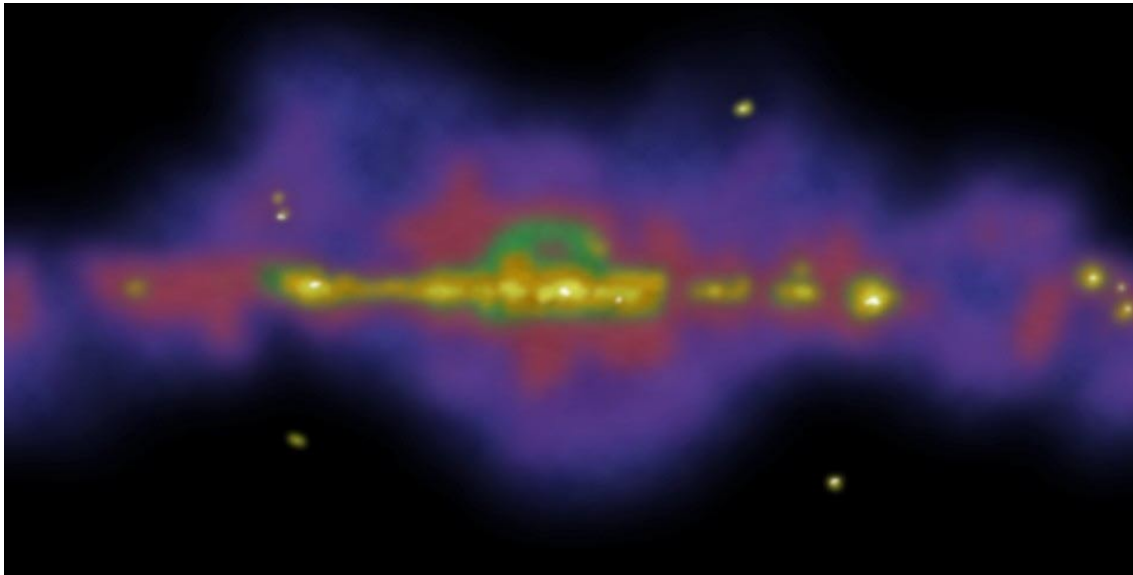


Figure 5-D. Computer-generated map of the Galaxy's gamma ray halo. Violet and blue portions represent the halo of gamma rays originating far off the galactic plane that cannot be accounted for by known celestial sources. The map excludes gamma rays that are predicted from the ordinary interaction of cosmic rays with light and matter in the Milky Way galaxy as well as those coming from a uniform gamma-ray "glow" which is thought to originate outside the Milky Way. The bright localized spots are discrete gamma-ray sources (courtesy of D. Dixon, D. Hartmann, E. Kolaczyk, and NASA).

Scientists Report Halo of Gamma Rays Surrounding Milky Way Galaxy

News release by K. Barton published in *New Astronomy* magazine, November 1998
(<http://tigre.ucr.edu/halo/halo.html>)

A huge cloud of high-energy gamma-rays forms a halo extending into outer space from the Milky Way, a phenomenon that cannot be accounted for by known celestial bodies, scientists reported today (Tuesday, Nov. 4).

The new, unexpected distribution of gamma rays, mapped by NASA's Compton Gamma Ray Observatory, forms an aurora many thousands of light years thick and possibly surrounding the entire Milky Way, the galaxy containing Earth, according to Dave Dixon, an assistant research physicist at UCR.

"Looking in any other wavelength, there is nothing out there that should be obviously making gamma rays. These gamma rays are providing the first evidence that some high energy process is occurring out there," said Dixon who made the discovery with Dieter Hartmann (Clemson University, and Eric Kolaczyk (University of Chicago).

The three scientists analyzed data collected by the Energetic Gamma-Ray Experiment Telescope (EGRET), one of four instruments aboard the Compton Gamma Ray Observatory, which is orbiting Earth on a satellite to measure and record invisible gamma rays which cannot be detected on the ground because Earth's atmosphere absorbs them. . .

What is so curious about the newly discovered gamma-ray cloud, Dixon said, is that the photons do not appear to be coming from any compact sources, like other galaxies or a black hole. "The reason this is interesting is that there isn't any obvious source for these gamma rays, based on astronomical observations in other wavelengths of light," Dixon said. "That is, as far as we can tell using other telescopes, the space around our galaxy is rather empty of the kinds of things which we would expect to generate gamma rays in the observed brightness distribution."

. . . The high-energy gamma rays seen in the halo could be the result of collisions of high-energy cosmic rays, in the form of electrons, traveling at near the speed of light and colliding with low energy photons they encounter in space, . . . a process called the "inverse Compton effect."

It has recently been reported that some other spiral galaxies that are similar to the Milky Way have a dim halo of infrared photons surrounding them, providing the "seed photons" that could be converted to gamma rays by interacting with high-energy cosmic rays. Some galaxies are also seen to be undergoing "starbursts" – rapid formation and destruction of massive stars in their centers. These massive stars are short-lived, and die in giant explosions called supernovae. The shock wave of energy from supernovae leads to even more star formation activity, making the center of such galaxies a caldron of violent activity. Such a starburst would generate massive amounts of cosmic rays, providing the high-energy electrons needed to generate gamma rays.

The cloud of gamma-rays detected may provide evidence that the Milky Way, too, was once a starburst galaxy, Dixon said. "That is sort of an open question right now," he said. "There seems to be unexplained evidence for such past activity in the center of the Milky Way."

References to the Update

- 1) Warwick, R. S., Turner, M. J. L., Watson, M. G., and Willingdale, R., *Nature* 317 (1985):218.
- 2) LaViolette, P. A. "Cosmic-ray volleys from the Galactic center and their recent impact on the Earth environment." *Earth, Moon, and Planets* 37 (1987):241–286.
- 3) Worall, D. M., Marshall, F. E., Boldt, E. A., and Swank, J. H. *Astrophysical Journal* 255 (1982): 111.
- 4) D. Dixon, D. Hartmann, E. Kolaczyk, paper presented at the High Energy Astrophysics Division of the American Astronomical Society, Estes Park, Colo, November 4, 1997.

5.2 THE DISTRIBUTION OF YOUNG SUPERNOVA REMNANTS

One of the early predictions of the GEH was that energetic events should be presently taking place on the proposed event horizons; see Table I (p. 6). In the previous subsection it was demonstrated that the 14,200 years BP event horizon might be the site of generation of the diffuse Galactic radio background radiation. It is also interesting to examine possible effects that the 14,200 years BP superwave would have on discrete objects lying on the event horizon. For example, if cosmic rays associated with the superwave were to encounter a young supernova remnant (SNR), it would be expected that the SNR would deflect these particles and temporarily trap them within the remnant; see Section 3.2. Consequently, a considerable amount of synchrotron emission would be expected to be radiated by such remnants. Indeed, synchrotron emission is detected in SNRs and it has been inferred that this emission is produced by relativistic electrons spiraling in magnetic fields within the remnants (Ginzburg, 1956).

However, the question which must be addressed is whether the relativistic particles producing the observed radiation always originate from within the remnant or would it be preferable in some cases to assume that these cosmic rays come from outside of the remnant from a rather inobvious source (e.g., a Galactic superwave). In the past, theorists had no reason to suppose that regions of enhanced cosmic ray density propagated relativistically through the Galactic disk at periodic intervals. Consequently, it was naturally assumed that the inferred relativistic particles were of *internal origin*, that is generated within the boundary of the supernova remnant, for example, as a byproduct of the supernova explosion (Ginzburg, 1956; ter Haar, 1950), as emission from a central star or pulsar (Baade, 1942; Gold, 1969), or at the remnant's boundary, e.g., due to convective instabilities (Gull, 1973), second order Fermi acceleration (Scott and Chevalier, 1975), or Rayleigh-Taylor instabilities (Shirkey, 1978). On the other hand, the GEH would project that in some cases these various internal sources of cosmic rays would be supplemented by cosmic rays of *external origin*, associated with a Galactic superwave.

The external origin hypothesis may be tested as follows. If cosmic ray electrons powering the nonthermal radio emission from supernova remnants were exclusively of internal origin, then there should be no particular correlation of the intrinsic brightness of a SNR to its location in the Galaxy. On the other hand, if the GEH is adopted, it would be expected that those remnants having the highest radio surface brightness would tend to be anisotropically distributed in the Galaxy, and in particular, would have a tendency to lie close to a superwave event horizon where the Galactic cosmic ray intensity would be most enhanced. The 14,200 years BP superwave event horizon would be a good choice as a candidate for a correlation study since a study of the terrestrial record indicates that this "Terminal Pleistocene Event" may have been the most severe event of the last several glacial-interglacial cycles.

5.2.1 The Proximity of High Radio Surface Brightness SNRs to the 14,200 Years BP Event Horizon

To test this prediction of the GEH, the locations of SNR having a high radio surface brightness were studied to see if they fell near the current position of the 14,200 years BP superwave. Out of a sample of 125 supernova remnants reported by Milne (1979), 16 were selected which had surface brightnesses greater than 1 flux unit/(arc min)². As is seen in Figure 5.3, the subsample of SNRs that was considered constituted about 13% of the total sample. Since the remnants with the highest surface brightness should also be those that

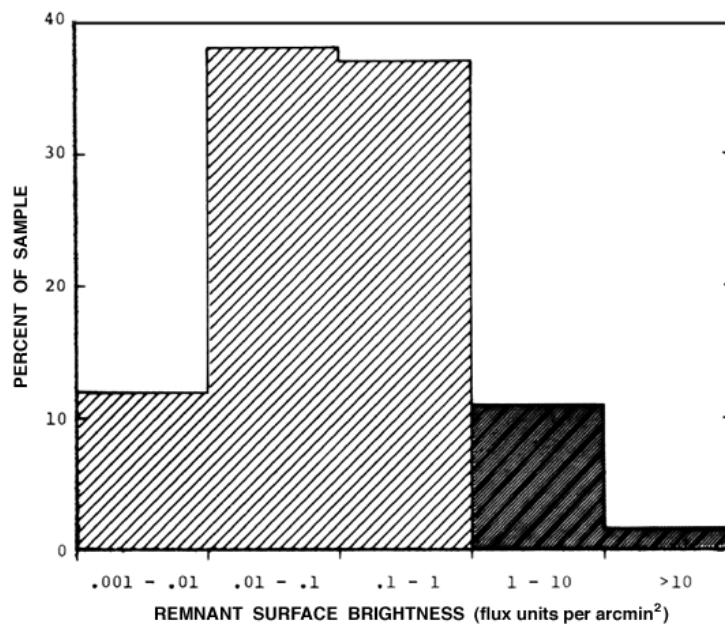


Figure 5.3. Histogram showing the percentage of supernova remnants in each of 5 surface brightness categories, for a sample of 125 remnants published by Milne (1979).

are most easily distinguishable, there is a minimum of sample bias introduced in selecting this subset. Remnant surface brightness measures the intrinsic radio luminosity, a parameter that is independent of distance to the SNR.

Relevant data for this sample is listed in Table VIII (rows 1 – 16), where ℓ and b are the galactic coordinates of the remnant center (columns 2 and 3), ϕ is the angular diameter of the shell in arc minutes (column 4), S is the radio luminosity at 1 GHz in flux units (column 5), Σ is the radio surface brightness at 1 GHz in flux units per square arc minute (column 6), d is the geocentric distance in kpc (column 7), and t is the time that the explosion occurred, if known (column 8). Column 9 gives references for the distances listed in column 7. The inequalities in column 7 indicate distances that are based on line absorption measurements, and the distance quantities in parentheses are rough estimates determined on the basis of Milne's (1979) surface-brightness-diameter relationship corrected for remnant height above the galactic plane. These $\Sigma - D$ distances may be uncertain by a factor of two or more.

The (ℓ, d) locations of the 16 high surface brightness SNRs have been plotted in Figure 5.4 along with a number of proposed superwave event horizons. Within 5 kpc of the Earth only 3 high surface brightness remnants are found, all of which have historically recorded supernova dates. Of these, the Crab Nebula and Cassiopeia A (Cas A), whose distances are the best determined for the 16 SNRs, make an excellent fit to the 14,200 years BP event horizon. Tycho's distance is less certain; however, the range of distances quoted for this remnant does intersect the event horizon. The Crab and Cas A remnants are particularly noteworthy in that they both have the highest surface brightness of the sample. In fact, their surface brightnesses exceed the sample mean of $3.0 \pm 2.6 \text{ f.u./(')}^2$ by over an order of magnitude; see Table VIII. The possibility that the close association of the Crab and Cas A SNRs with the 14,200 years BP event horizon is just due to chance is negligibly small. Both of these unusual remnants are studied in greater detail in Subsection 5.3 and 5.4 of this chapter.

As for the remaining SNRs, most of which lie in the direction of the GC, a definite However, note in Figure 5.4 the relative absence of high surface brightness SNRs closer than 5 kpc in directions that lie within $\pm 60^\circ$ of the GC, whereas in the supplementary range $60^\circ -$

TABLE VIII
 SUPERNOVA REMNANT DATA (a)

| (1) | (2) | (3) | (4) | (5) | (6) | (7) | (8) | (9) |
|------------------------------|-----------------|------------|------------------|------------------------------|---|----------------------|-------------------|-------|
| Name | ℓ (deg) | b (deg) | ϕ (arc') | S_{IGHZ} (f.u.)* | Σ_{IGHZ} f.u./(') ² | d (kpc) | t (yrs) | ref** |
| 1 Kepler | 4.5 | +6.8 | 3.8 | 20 | 1.76 | 9 ± 5 | 378 | 2 |
| 2 G 11.2-0.3 | 11.2 | -0.3 | 4.2 | 22 | 1.59 | (11.9 ± 6) | | 2 |
| 3 G 21.5-0.9 | 21.5 | -0.9 | 1.0 | 6.5 | 8.3 | (15 ± 8) | | 2 |
| 4 4C-0.370 | 29.7 | -0.2 | 2.4 | 10 | 2.2 | (18.9 ± 9) | | 2 |
| 5 3C 391 | 31.9 | 0.0 | 4.2 | 22 | 1.6 | $11 \pm 2, (16)$ | | 2 |
| 6 3C 397 | 41.1 | -0.3 | 3.6 | 20 | 2.0 | $(12.8 \pm 6), 7.5$ | | 2 |
| 7 W 498 | 43.3 | -0.2 | 4.2 | 36 | 2.6 | $12 \pm 2, (11.6)$ | | 2 |
| 8 Cas A | 111.7 | -2.1 | 4.2 | 3400 | 245 | 2.8 ± 0.2 | 300 | 2 |
| 9 Tycho | 120.1 | +1.4 | 7.9 | 58 | 1.2 | 2.2 ± 4.3 | 420 | 3 |
| 10 Crab | 184.6 | -5.8 | 6x4 | 1000 | 53 | $2.0 \pm .1$ | 928 | 4 |
| 11 MSH 11-54 | 292.0 | +1.8 | 2.3 | 15 | 3.6 | (7.8 ± 4) | | 2 |
| 12 MSH 15-57 | 328.4 | +0.2 | 4.0 | 17 | 1.35 | (14 ± 7) | | 2 |
| 13 CTB 37A | 348.5 | +0.1 | 8.0 | 77 | 1.5 | $10.2 \pm 2, (8.0)$ | | 2 |
| 14 CTB 37B | 348.7 | +0.3 | 5.1 | 38 | 1.9 | $10.2 \pm 2, (9.9)$ | | 2 |
| 15 G349.7+0.2 | 349.7 | +0.2 | 1.7 | 21 | 9.3 | $18.3 \pm 2, (18.7)$ | | 2 |
| 16 MSH 17-39 | 357.7 | -0.1 | 4.3 | 38 | 2.6 | $(12.5 \pm 6), 6$ | | 2 |
| 17 Vela X,Y,Z | 263.9 | -3.3 | 256 | 1750 | 0.034 | 0.5 ± 0.1 | 12,000 | 2 |
| 18 Cygnus Loop 2 | 74.0 | -8.6 | 180 | 200 | 0.008 | 0.77 ± 0.2 | $1-2 \times 10^4$ | |
| 19 SN 1006 | 327.6 | +14.5 | 34 | 21 | 0.023 | 1.2 ± 0.3 | 976 | 5 |
| 20 3C58, SN 1181 2.6±0.2) | 130.7 801 | +3.1 6 | 6x10,4.5 | | 35 | $0.74-2.2$ | (| |

* f.u. (flux unit) = 10^{-26} watts/m²/Hz

** references: 1: van den Bergh and Kamper (1977); 2: Milne (1979); 3: Reid et al. (1982);
 4: Trimble (1968); 5: van den Bergh (1976); 6: Green & Gull (1982).

300°, three remnants are found, all relatively closely aligned with the 14,200 years BP event horizon. The absence of bright SNRs from the interior portion of this elliptical region is consistent with the GEH and with the suggestion that these high surface brightness remnants are supplied with cosmic rays from superwaves. For example, according to the terrestrial climatic record (see Part II, Chapters 8 and 9) the period from about 10,000 years BP to the present has been a relatively calm period free of major climatic excursions. Although other superwaves may have passed the Earth at ~6000 years BP and 393 AD, these events would have had to be much milder than the postulated 14,200 years BP event. Thus if the GEH is to be consistent with this geological evidence, a relatively "calm" region (and hence an absence of energetic SNRs) should occupy the interior of the 14,200 years BP event horizon, and this appears to be the case, in view of the SNR data.

The supernova remnant SN 1006 which lies in the interior of the 14,200 years BP event horizon region (see Figure 5.4) is not part of the 16 SNR subsample, since its surface

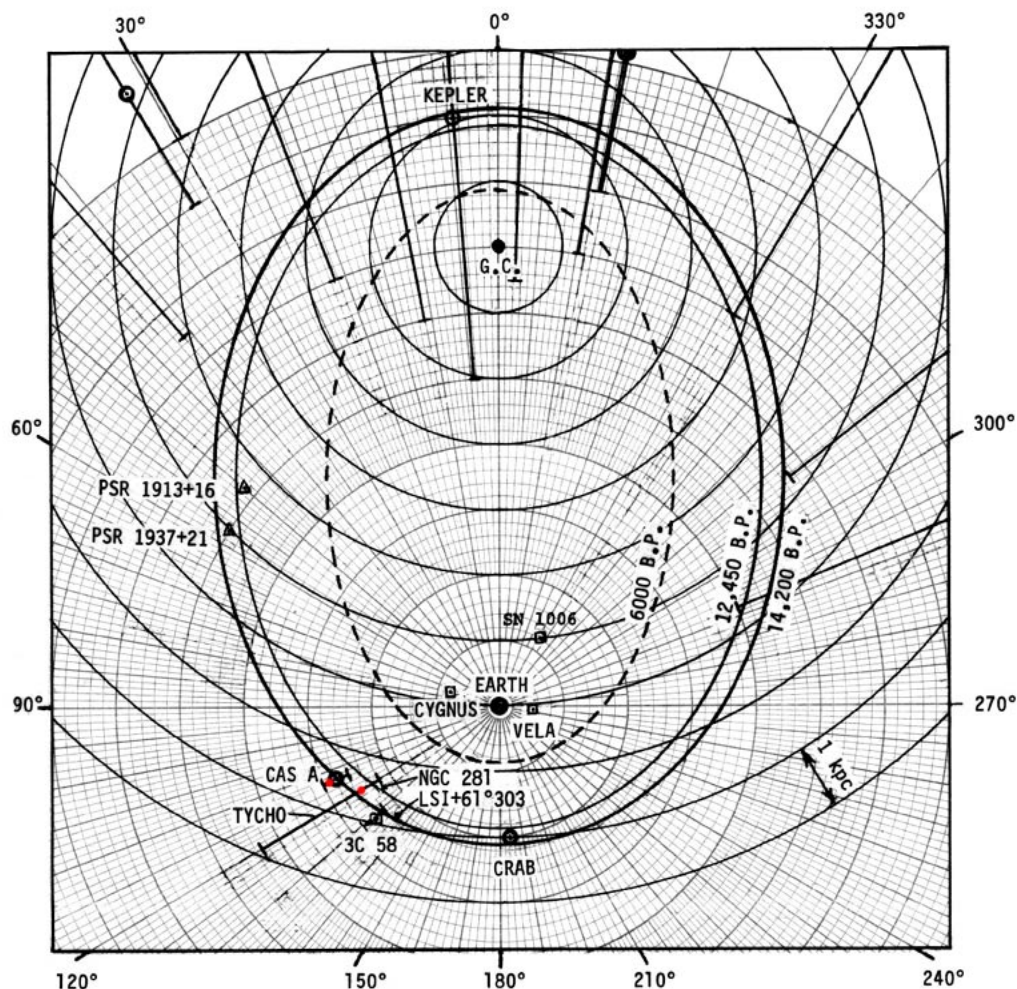


Figure 5.4. The current position of the 14,200 years BP superwave Event Horizon relative to 16 young, high surface brightness ($\Sigma \geq 1 \text{ fu}/(\text{°})^2$) SNRs (circles). Bars indicate the degree of positional uncertainty. Also shown are the 12,450 years BP and 6000 years BP event horizons. Open squares show the positions of the Cygnus Loop, Vela XYZ, 3C 58, and SN 1006. Open triangles indicate the estimated positions of two of the fastest-known pulsars: the Millisecond Pulsar (PSR 1937+21) and the Binary Pulsar (PSR 1913+16). Also shown are the estimated positions of the variable radio star LSI+61 303 and of the emission nebula NGC 281.

[Update: The red dots indicate more accurate positions for Cas A and Tycho.]

brightness is almost two orders of magnitude below the sample cut off; however, it is interesting to compare its 1 GHz surface brightness to that of the Crab Nebula. Both of these nebulae are approximately the same age and both have historically recorded supernova dates. Also both remnants are elliptical in shape and have power-law X-ray spectra (Becker et al., 1980). However, the Crab Nebula, which lies close to the 14,200 years BP event horizon, is over three orders of magnitude brighter; see Table VIII. SN 1006 lies close to a more recent event horizon belonging to the 393 AD Superwave; see Subsection 6.2.1. However, in view of the geological and historical records, this superwave must have been a much milder event.

Another remnant worthy of consideration is 3C 58, which is associated with the historically recorded supernova of 1181 AD. This remnant is not only about the same age as the Crab Nebula, but also it is elliptical in shape, has a filled-center (*plerionic*) emission

distribution and like the Crab lies close to the 14,200 years BP event horizon. Although its surface brightness is almost two orders of magnitude less than that of the Crab, it is quite bright when compared with the other SNR's in Milne's sample. In fact, if the 16 high surface brightness SNR sample were to be slightly expanded, 3C 58, which is presently on the borderline, would be the next inclusion. The fact that 3C 58 is relatively bright and that it lies close to the 14,200 years BP event horizon is additional evidence in favor of the hypothesis being tested.

For comparison to the 16 SNR subsample, 46 supernova remnants from Milne's sample having surface brightnesses in the range $0.1 \leq \Sigma \leq 1$ (see Table IX) have been plotted in Figure 5.5. Distance error bars would probably extend from $+d$ to $-d/2$ (at least), but these have been omitted for diagrammatic clarity. Although there is some degree of clustering among the remnant positions, there is no indication of a void being present within the boundary of the 14,200 years BP event horizon. In fact, about 30% of the SNRs in this subsample lie within this boundary. This differs remarkably from the high surface brightness subsample, and is consistent with the earlier suggestion that this portion of the galaxy has a

TABLE IX
SUPERNOVAE REMNANT DATA (b)*

| Name | ℓ (deg) | $\Sigma_{1\text{GHz}}$ f.u./(') ² | d (kpc) | Name | ℓ (deg) | $\Sigma_{1\text{GHz}}$ f.u./(') ² | d (kpc) |
|-----------------|-----------------|---|------------|-----------------|-----------------|---|------------|
| 1. G 2.4+1.4 | 2.4 | 0.28 | (7.2) | 24. Kes 17 | 304.6 | 0.40 | 9.4 |
| 2. Milne 56 | 5.3 | 0.20 | (5.0) | 25. G308.7+0.0 | 308.7 | 0.29 | (14.1) |
| 3. W 28 | 6.4 | 0.17 | (2.4) | 26. G311.5-0.3 | 311.5 | 0.31 | (16.9) |
| 4. G 11.4-0.1 | 11.4 | 0.16 | (15.2) | 27. MSH 14-57 | 316.3 | 0.11 | (7.7) |
| 5. G 12.0-0.1 | 12.0 | 0.15 | (19.1) | 28. RCW 89 | 320.4 | 0.12 | 4.2 |
| 6. G 15.9+0.2 | 15.9 | 0.24 | (16.5) | 29. Kes 24 | 322.3 | 0.19 | 20.0 |
| 7. MSH 18-18 | 18.9 | 0.17 | 9.5 | 30. MSH 15-56 | 326.3 | 0.14 | (2.4) |
| 8. MSH 18-113 | 21.8 | 0.17 | 6.3 | 31. G 330.2+1.0 | 330.2 | 0.12 | (7.8) |
| 9. W 41 | 23.3 | 0.17 | (5.0) | 32. MSH 16-51 | 332.4 | 0.19 | (8.2) |
| 10. G 23.6+0.3 | 23.6 | 0.19 | (11.9) | 33. RCW 103 | 332.4 | 0.36 | 3.3 |
| 11. Kes 73 | 27.4 | 0.19 | (25.7) | 34. CTB 33 | 337.0 | 0.42 | (11.3) |
| 12. G 33.6+0.1 | 33.6 | 0.24 | (10.8) | 35. G 337.2-0.7 | 337.2 | 0.18 | (13.3) |
| 13. W 44 | 34.6 | 0.40 | (3.1) | 36. Kes 40 | 337.3 | 0.14 | (6.2) |
| 14. G 35.6-0.4 | 35.6 | 0.25 | (8.1) | 37. Kes 41 | 337.8 | | 0.19 |
| | (10.0) | | | | | | |
| 15. 3C 396 | 39.2 | 0.58 | 11.3 | 38. G 338.3-0.1 | 338.3 | 0.13 | (13.7) |
| 16. W 51 | 49.2 | 0.29 | 4.1 | 39. G 338.5+0.1 | 338.5 | 0.22 | (8.3) |
| 17. CTB 87 | 74.9 | 0.30 | 12 | 40. G 340.4+0.4 | 340.4 | 0.18 | (12.1) |
| 18. Dr 4 | 78.1 | 0.11 | (1.6) | 41. G 340.6+0.3 | 340.6 | 0.27 | (14.7) |
| 19. IC 443 | 189.1 | 0.13 | 2.0 | 42. MSH 16-48 | 341.9 | 0.15 | (14.0) |
| 20. MSH 11-61A | 290.1 | 0.53 | (5.0) | 43. G 346.6-0.2 | 346.6 | 0.19 | (11.7) |
| 21. MSH 11-62 | 291.0 | 0.25 | (9.9) | 44. G 350.1-0.1 | 350.1 | 0.42 | (15.4) |
| 22. G 298.5-0.3 | 298.5 | 0.50 | (16.1) | 45. G 351.2+0.1 | 351.2 | 0.19 | (16.2) |
| 23. G 299.0+0.2 | 299.0 | 0.10 | (10.6) | 46. G 352.7-0.1 | 352.7 | 0.18 | (15.9) |

* after Milne (1979)

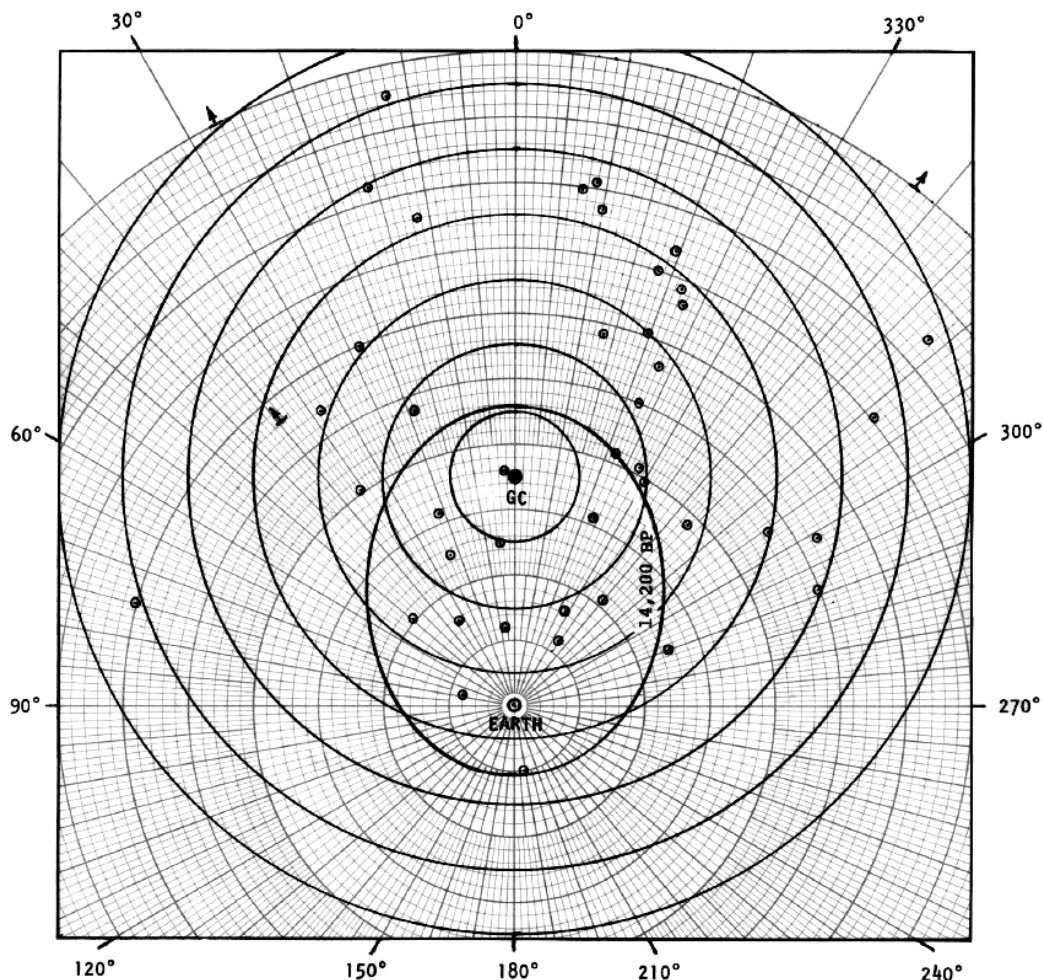


Figure 5.5. Elliptical event horizons compared to the locations of 49 medium surface brightness SNRs ($0.1 \leq \Sigma \leq 1.0 \text{ fu}/(\text{')}^2$). For purposes of visual clarity, bars indicating degree of uncertainty in distance have not been added.

much lower cosmic ray density than does the 14,200 years BP event horizon. Of course, any conclusions regarding the overall distribution of SNRs should be considered as tentative in view of the fact that the distances to most SNRs is not accurately known.

As a general rule, young supernovae remnants, those with small diameters, are found to be the ones with the highest radio surface brightness; although see Subsection 5.3.1 (p. 165) regarding very young SNRs (≤ 100 years old). The internal origin hypotheses would attribute the high luminosity of young remnants to factors such as: a) a pulsar that is still young and energetic, b) a remnant shell that still has a high kinetic energy of expansion and is able to effectively accelerate interstellar electrons and compress or modulate encountered magnetic fields, c) a remnant that has not had time to lose its reservoir of energetic particles through diffusion and synchrotron losses.

Alternatively, the GEH would also predict that young SNRs would be more luminous, but for different reasons. In young SNRs the remnant shell would be composed of a fresh, magnetically bound plasma and would present the superwave with a unified fabric capable of effectively absorbing cosmic rays (see Chapter 3, Section 3.2), whereas in older remnants in which the shell had become considerably expanded and decelerated by the interstellar medium, the magnetically bound plasma fabric would have lost its integrity and developed

holes. Thus the older remnants would be far less efficient in absorbing cosmic rays from a passing superwave. Even so, older remnants would be expected to radiate more intensely than they normally would if they happened to be in the presence of a superwave of sufficient intensity; see Subsections 6.2.1, 6.2.2, and 6.2.3.

5.2.2 Galactic Evidence that Superwaves May Trigger Supernovae*

An interesting question to consider is whether a Galactic superwave could play a role in triggering supernova explosions; recall Chapter 2, Subsection 2.1. The possibility that the 14,200 years BP superwave may have been active in triggering supernovae finds support in the young ages of the Crab and Cas A SNRs and their close proximity to the 14,200 years BP event horizon. Given the birth dates and positions of these two remnants, then if triggered by a superwave, Earth-passage dates of $14,000 \pm 700$ and $14,300 \pm 1200$ years BP respectively would be predicted, in excellent correspondence with the proposed date of 14,200 years BP.

The age and position of the nearby Vela XYZ supernova remnant would also support the triggering hypothesis. Although this remnant has a low radio surface brightness compared to the sample of 16 SNRs, it has been included in Table VIII and plotted in Figure 5.4 since its distance and age are fairly accurately known. Also, the Cygnus Loop, another nearby, low surface brightness SNR, has been plotted, although the distance to this remnant and its age are not as accurately known. For the Vela remnant, which lies only about 1600 ± 300 l.y. from the solar system, the supernova explosion would have been perceived on Earth about $12,250 \pm 450$ years BP, if triggered by the 14,200 years BP superwave. This date checks well with the age of $\sim 12,000$ years BP derived for Vela XYZ on the basis of observations of remnant expansion rate and deceleration rate estimates (Weiler & Panagia, 1980); also see Appdx C.**

For the Cygnus Loop, which is located about 2500 l.y. from the solar system, the supernova explosion would have been perceived on the Earth about $12,200 \pm 700$ years BP. By comparison, Tucker (1971) estimates an age for this remnant in the range 12,000 – 20,000 years assuming a shock velocity in the range of 400 – 600 km/s (on the basis of X-ray observations) and a distance to the SNR of 2500 l.y. Ilovaisky and Bowyer (1971) estimate an age of 18,000 years for a shock velocity of 440 km/s and a 2500 l.y. distance, and Ilovaisky and Lequeux (1972b) estimate an age of 14,000 years for a shock velocity of 560 km/s and a 2500 l.y. distance. Thus to the degree of accuracy of knowing the age of this remnant, it is feasible to consider that, like the Vela supernova, the Cygnus Loop supernova may also have been triggered at the time that the 14,200 years BP superwave passed by.

If the 14,200 years BP superwave is to be regarded as having a major influence on the probability of supernova occurrence, then an acceleration of the supernova occurrence rate would be expected, beginning about 14,200 years BP. There may be evidence of such acceleration. The date reported by Ilovaisky and Lequeux (1972a, pp. 174-175) indicate that within 2 kpc of the solar system there is a 3-fold deficiency of supernova remnants in the size range of 35 – 60 pc from expected levels. "Expected levels" here implies levels that would be expected if supernovae were assumed to occur in a random fashion and if the

* **UPDATE:** In his 1983 paper in *Astrophysical Journal* (vol. 265, pp. 719-721), Sidney van den Bergh noted that there is a 0.5 % probability of discovering a supernova such as S And so close to the nucleus of the Andromeda galaxy (< 16") in the course of 100 years of observation and suggested that the frequency of supernova in the nuclei of galaxies may be unusually high, which requires some sort of explanation.

** **UPDATE:** Recently the Vela remnant has been determined to lie 820 ± 100 light years from the solar system. If triggered by the 14,200 years BP superwave, the predicted age for the remnant would increase to 13,200 years, somewhat older than the estimated age.

probability of occurrence had not changed over time. Moreover, they report that when their sample is expanded to include a solar vicinity region of radius 6.3 kpc, a significant deficiency of remnants in the 30 - 60 pc size range is still found, even when size-limiting selection effects are accounted for. The Vela SNR, whose age is $\sim 12,000$, has a diameter of ~ 40 pc. So if the Vela SNR is typical, it appears that the number deficiency which Ilovaisky and Lequeux report is for remnants older than $\sim 10,000$ years. This is consistent with the hypothesis of triggering by the 14,200 years BP superwave, which predicts an acceleration in the rate of occurrence of Galactic supernovae beginning about 14,200 years ago.

When the above evidence is considered together with the proximity of the 14,200 years BP event horizon to the young Crab and Cassiopeia A remnants and at an earlier time to the older Vela and Cygnus remnants, it is reasonable to conclude that the 14,200 years BP superwave was (and still may be) instrumental in triggering supernovae. Caution should be exercised in generalizing from just a few SNR examples; however, it should be borne in mind that these few examples are among the supernovae that have been the most thoroughly studied and that we know the most about, e.g., regarding their age and location. Still, it would be incorrect to assert that *all* observed SNRs are due to supernovae triggered by this particular superwave. Some supernovae could have been triggered by other superwaves, or could have been brought about as a result of a star's own internal evolution (conventional explanation). One example of a young SNR that does not lie near the 14,200 years BP event horizon is SN 1006, discussed earlier. If SN 1006 were triggered by a superwave, its present location and distance would predict a superwave Earth-passage date of 350 ± 330 AD (1630 ± 330 years BP), which correlates very well with the date of the 393 AD Superwave; see Section 6.2.

A Possible Supernova Triggering Mechanism. As one possible triggering mechanism, the superwave could have been instrumental in transporting a large quantity of interstellar dust within reach of the gravitational pull of a white dwarf. The gravitational potential energy released by the resulting infall of this dust would have heated the surface of the star, and in the case of a marginally stable dwarf could have caused it to explode. See Appendix D for an alternate mechanism.

For example, consider a 4 solar mass white dwarf which in the course of its evolution was unable to generate a sufficiently high temperature to initiate carbon burning reactions, which typically require a temperature of ~ 600 million degrees. Also, suppose that as a result of continuous mass ejection the star has accumulated about itself a circumstellar shell of gas and dust having a radius of 20 AU, a thickness of 1 AU, and a density of 10^{-12} g/cm³ (a total mass of $0.01 M_{\odot}$). Suppose that on impacting this shell the 14,200 years BP superwave accelerates this material toward the white dwarf at a velocity of ~ 1 km/s. This is energetically feasible since the shell would present a column density of ~ 15 g/cm² and to achieve this velocity would require an energy input of 7.5×10^{10} ergs/cm², which could be supplied by the proposed superwave (at peak intensity) in the space of 25 years. However, as the dust shell approached closer to the star, higher velocities would be achieved due to the gravitational pull of the star.

Suppose now that the white dwarf were able to accrete about 1% of the advancing shell, i.e., a shell section having a diameter of 3 AU and a mass of $m = 10^{29}$ grams. Also suppose that this amount of matter were funneled onto a 1000 km diameter region at the pole of the star, funneling being assisted by the configuration of the star's magnetic field. The potential energy released is estimated to be $E = GMm/R = 10^{47}$ ergs, where $M = 8 \times 10^{33}$ grams and $R = 5 \times 10^8$ cm are the mass and radius of the white dwarf. If this energy went into heating a hemispherical region of the star having a radius of 500 km and containing about 5×10^{-4} of the star's mass, then this region would acquire about 3×10^{16} ergs/gram. If the specific heat of the stellar material is on the order of 0.1 cal/g°C, then the acquired energy density would

be capable of raising the temperature of this hemispherical region by 6 billion °C if heat loss to the rest of the star could be neglected. However, since conductive and radiative heat losses would be substantial, it must be assumed that a substantial fraction of the accreted material is acquired in a very short space of time, e.g., a few hours or a day.

Once carbon burning had become initiated, heating of the star would become self-sustaining and regions adjacent to the "hot spot" would ignite. Because of the electron degeneracy of the star and its consequent nonexpandable nature, its temperature would rapidly rise following carbon ignition. As a result, a runaway reaction would develop, the so-called "carbon flash," causing the star to ultimately explode as a supernova.

Some theorists have proposed an external triggering mechanism for supernovae explosions, applicable to regions where the stellar density is extremely high, as at the center of the Galaxy (e.g., Burbidge, 1961). According to this "domino theory," the shock wave from one supernova explosion would trigger an explosion in a nearby unstable star, whose shock wave would in turn trigger explosions in other unstable stars, etc. The suggestion that an intermediary external agent (e.g., a galactic superwave) might be effective in triggering supernovae in a coordinated fashion, with individual explosions separated from one another by up to *thousands* of light years, has until now not been suggested. The above theoretical treatment and the earlier presentation of supporting evidence, therefore, constitute original contributions of this research study.

5.2.3 The Proximity of Other Energetic Sources to the 14,200 Years BP Event Horizon

Besides supernova remnants, two unusual objects, LSI +61°303 and NGC 281 are found to lie close to the 14,200 years BP event horizon; see Figure 5.4. LSI +61°303 is a variable radio star which lies at $\ell = 136^\circ$, $b = +1^\circ$, and $d = 2.3$ kpc, near the 14,200 years BP event horizon. This B1 spectral-type star exhibits periodic variations in its radio output on a cycle of 26.5 days. It also has been found to be a high-energy gamma ray source and a relatively luminous X-ray source (Bignami et al., 1981). It is tempting to link the unusual energetic activity exhibited by LSI +61°303 with the high levels of cosmic radiation postulated by the GEH to be in its vicinity.

The emission nebula NGC 281 is located at $\ell = 123^\circ$, $b = -6^\circ$, and $d \sim 2.2$ kpc, which places it near the 12,450 years BP event horizon, close to Tycho. The nebula and its immediate surroundings exhibit a substantial amount of energetic activity. In addition to radio continuum emission, this region exhibits H II, H I, H₂, H₂O maser, and CO emission lines. Roger and Pedlar (1981), who have mapped the relative positions of these emission regions suggest that the star HD 5005, located in the center of NGC 281, is the main energy source. However, it is interesting to note that they find an extensive region of molecular hydrogen gas trailing off to one side of the nebula's H II emission region. In particular, the undissociated H₂ gas is found on the side of the nebula facing higher galactic longitudes. This observation is consistent with the GEH, which suggests that this region of the Galaxy is being exposed to a blast of cosmic rays propagating from the GC. That is, the H₂ gas could be interpreted as a region in the wake of the H II emission cloud that was protected from direct exposure to the superwave particle blast.

It is also interesting to see if pulsars that happen to be situated close to the 14,200 years BP event horizon have any unusual characteristics. Based on the (ℓ , d) coordinates published by Manchester and Taylor (1981) for a sample of 330 pulsars, it is determined here that 34, or $\sim 10\%$ of the sample, fall within 0.4 kpc of either the 14,200 or 12,450 years BP event horizons. This is about what would be expected if these positional coincidences were due to chance. However, consider the (ℓ , d) positions of three of the fastest pulsing pulsars: the recently discovered Millisecond Pulsar having a period of 1.558 ms ($\ell \sim 57.5^\circ$,

$d \sim 5$ kpc), the Crab Pulsar ($P = 33.1$ ms, $\ell \sim 184.6^\circ$, $d \sim 2.0$ kpc), and the Binary Pulsar ($P = 59.0$ ms, $\ell \sim 50.0^\circ$, $d \sim 5.2$ kpc). It is found that all three pulsars lie within 0.4 kpc of the 14,200 years BP event horizon.* Even taking into account that the distances to two of these pulsars are not accurately known, still the positional correlations are quite impressive and would be difficult to attribute to chance. Hence there appears to be a relation between short period pulsars and the 14,200 years BP superwave. Considering the position of the Vela Pulsar, which is also a fast pulsar ($P = 89.2$ ms, $\ell \sim 263.6^\circ$, $d \sim 0.5$ kpc), it is seen that the 14,200 years BP superwave would have been passing through this region about the time of this pulsar's birth, about 14,000 years ago. Thus the Vela Pulsar also appears to be positionally associated with the 14,200 years BP event horizon.

It is worth mentioning that the Crab and the Vela pulsars were instrumental in the initial stage of hypothesis formation. Certain attributes of these pulsars attracted my attention and led me to hypothesize that the Crab and Vela supernovae may have been triggered by a relativistically propagating superwave and that this phenomenon was associated with the sudden climatic change which occurred on the Earth about 14,200 years ago. As a result of these considerations (to be detailed in a subsequent publication), I had become quite seriously convinced of the existence of the 14,200 years BP event horizon.** It was after this that I thought of plotting the positions of the sample of young supernova remnants discussed earlier in this section. As has been demonstrated, the results of this test support the proposal that some disturbance (e.g., a superwave) passed the Earth about 14,200 years ago, and is presently in the process of propagating radially through the Galaxy at close to the speed of light.

5.3 THE CRAB NEBULA

The Crab Nebula (see Figure 5.6) is the most luminous and most unique of the 21 high surface brightness supernova remnants (SNRs) listed in Table VIII. It is also the closest and most thoroughly studied. It is elliptical in shape and measures about $6' \times 4'$, or about 12×8 light years for a distance to the remnant of 2 kpc. Its shell, which probably has a mass of $\sim 1 M_\odot$ and a kinetic energy of $\sim 2 \times 10^{49}$ ergs, is believed to be the product of a Type-I supernova (Woltjer, 1972). It is radiating nonthermal radiation at the rate of about 2×10^{34} ergs/s in the radio range, increasing to 2×10^{36} ergs/s in the optical range and to 6×10^{37} ergs/s in the X-ray and γ -ray region of the spectrum (Piddington, 1969, p. 234; Ling et al., 1979).

In 1953 Shklovsky proposed that the radio and optical continuum might be synchrotron radiation produced by relativistic electrons spiraling in a magnetic field; see also Ginzburg (1953). Later with the observation that this radiation is polarized, the synchrotron theory was confirmed. Ginzburg (1956) proposed that these cosmic ray electrons were produced in the Crab supernova explosion. However, with the discovery that the Crab Nebula radiates an enormous flux of X-ray and γ -ray radiation the concept of a supernova source for the particles had to be abandoned in favor of a mechanism which could *continuously* supply particles to the remnant. Radioactive decay was shown to fail by a factor of about 100 in meeting the X-ray and γ -ray requirement (Clayton and Craddock, 1965). However, in 1968 the Crab pulsar was discovered and not long after, this object was assigned the leading role of supplying the required relativistic electrons. However, as I demonstrate below, there are several difficulties with the suggestion that a centrally located pulsar is responsible for the relativistic particles.

* At the time of writing (1983), a second fast radio pulsar, PSR1953+29, has just been discovered ($P = 6.1337$ milliseconds, $\ell = 65.8^\circ$, $d = 3.5$ kpc) (Boriakoff et al., 1983).

** This "publication" is the now published book entitled *The Talk of the Galaxy* (Alexandria, VA: Starlane Publications, 2000).

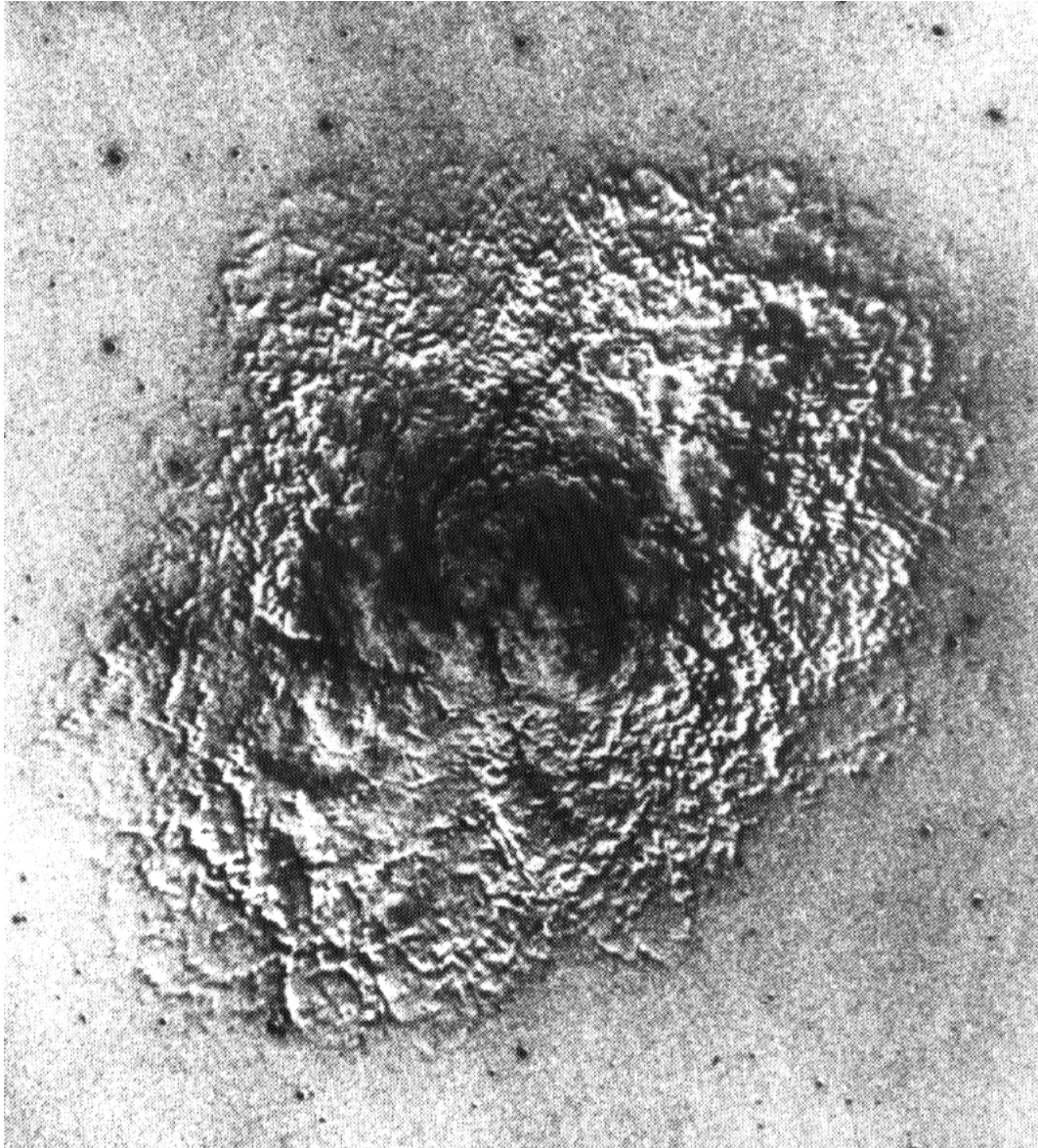


Figure 5.6. The Crab Nebula in Taurus is the remnant of the supernova of 1054 AD. This composite photograph, which shows the nebula's expansion over a 14 year period, was made by Guido Munch from a negative print he took in 1964 with the 200" Palomar telescope and from a positive print taken with the same telescope in 1950 by Baade (courtesy of *Scientific American*).

Many of the difficulties associated with "internal origin" hypotheses, such as those postulating a supernova source or a pulsar or neutron-star source, may be circumvented if it is postulated that a cosmic rays volley of sufficiently high intensity is impacting this remnant from the direction of the GC. Such an external origin for the Crab's electrons is compatible with the GEH since, as seen in Figure 5.4, the Crab lies directly on the 14,200 years BP event horizon. Moreover, the intensity proposed in Chapter 3 (Section 3.1) for the 14,200 years BP superwave is sufficient to account for the energetic phenomena observed in the Crab. As is shown further on, a large number of energetic phenomena observed in the Crab remnant may be accounted for in a simple manner when the 14,200 years BP superwave model is adopted.

I will begin by reviewing below some of the difficulties associated with the internal-origin hypotheses. Consider the first hypothesis of a supernova origin.

5.3.1 Arguments Against a Supernova Being the Source of the Relativistic Particles in the Crab Remnant

One problem concerns the required magnetic field strength. At present there is no direct way of measuring the field strength. However, it can be reasoned that if both particles and field originated from the supernova explosion, then the energy content of the magnetic field (U_m) would have had to be greater than or equal to the energy content of the relativistic particles (U_p) hypothesized to have been generated in the explosion (i.e., $U_m \leq U_p$). Otherwise, early in the explosion the relativistic particles would have rapidly escaped into space. Usually, approximate energy equipartition is assumed (i.e., $U_m \sim U_p$) in order to minimize the total energy requirements involved (Weekes, 1969, p. 18). With this assumption it is possible to construct a synchrotron model of the radio and optical continuum emission in which $U_p \sim U_m \sim 3 \times 10^{48}$ ergs (Weekes, 1969, p. 36). For a nebular diameter of 6×8 l.y., or a volume of $V \sim 10^{57}$ cm³, this would imply a magnetic field energy density of $\sim 3 \times 10^9$ ergs/cm³ and a magnetic field flux density of $B \sim 3 \times 10^{-4}$ gauss throughout the remnant. However, this is about 100 times greater than the strength of the ambient Galactic magnetic field. For a remnant radius of $R \sim 7$ l.y. this constitutes a total magnetic flux of: $\psi = B \cdot 4\pi R^2 \sim 10^{35}$ gauss·cm². But, as Piddington (1969, pp. 226, 236) points out, such an enormous magnetic field intensity could not have been initially contained in the original star prior to its explosion, the upper limit for the most massive stars being $\psi_{\max} \sim 10^{32}$ gauss·cm². Consequently, one is inevitably led to the conclusion that $E_p \gg E_m$, in which case the relativistic particles should have escaped soon after the explosion.

Another problem concerns the enormous amount of energy required for the relativistic particles. For example, the total energy requirement in the form of relativistic electrons and possibly even relativistic ions may far exceed 10^{49} ergs, which is more than the kinetic energy provided by the supernova explosion (Piddington, 1969, p. 235). Moreover, since particles radiating in the X-ray region have strong synchrotron losses, they would be expected to radiate away most of their energy within a very short time. For example, electrons responsible for generating high-energy X-rays (> 20 keV) would have life times on the order of months to a few years. So, the observed X-ray and γ -ray emission from the Crab demands a *continuous* input of relativistic particles over an extended period of time. Thus, sources other than the original supernova explosion must be sought as an explanation.

The notion that the relativistic particles responsible for the emission in supernova remnants are somehow internally generated by the supernova explosion also meets with difficulty in view of recent radio observations of extragalactic supernovae. Young supernovae whose remnant volumes are of very small size would be expected to have very high relativistic particle and magnetic field densities, given the assumption that these components would be generated in the initial explosion. Consequently, very high radio luminosities would be expected. However, no significant radio emission has been detected from such objects. For example, de Bruyn (1973) has searched for radio emission from 35 optically recorded supernovae in 22 extragalactic systems at 1.4 GHz. The supernovae ranged in age from 1 month to 86 years. But no emission was detected. Brown and Marscher (1978) obtained similar results in a survey of 46 optically detected supernovae in 26 galaxies, ages ranging from a few months to 79 years. Again, no emission was detected.

According to an *empirical* relation, mainly determined by *old* supernova remnants remnant luminosity is found to vary according to the inverse square of remnant diameter,

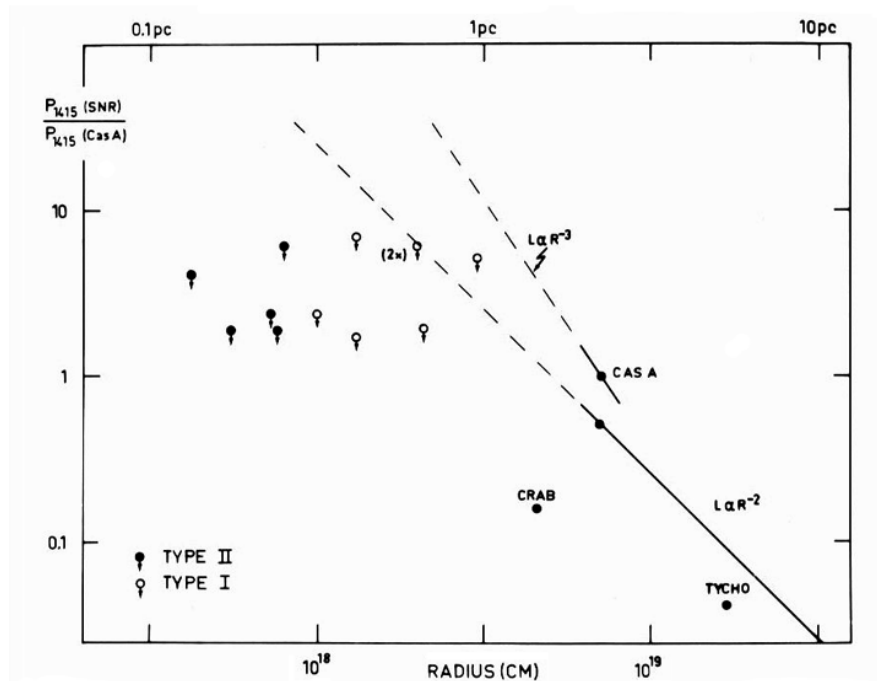


Figure 5.7. Radio luminosity ($\propto \Sigma R^2$) is plotted against remnant radius R for a dozen extragalactic SNRs, ages 20 to 75 years. The luminosities are upper limits which have been normalized to the spectral luminosity of Cas A at 1415 MHz. For comparison the Σ - D relation, $L \propto R^{-2}$ (Ilovaisky and Lequeux, 1972a), is shown along with the R^{-3} evolution law presently followed by Cas A (after de Bruyn, 1973).

i.e., $S \propto D^{-2}$ (Milne 1970; Ilovaisky and Lequeux, 1972a; Woltjer, 1972). Classical theories, which suggest that relativistic particles and magnetic fields are generated internally as a result of the supernova explosion, *would predict an even stronger exponential dependence* since both particle density and magnetic field density in *very young* SNR (< 100 years old) would be expected to vary according to the *inverse cube* of diameter. But even this modest inverse square S - D relation (luminosity vs. diameter relation) is found to significantly overestimate the radio fluxes observed for very young SNRs. As seen in Figure 5.7 (de Bruyn, 1973), a dozen of the most promising young remnants fall up to 10-100 times below the luminosity predicted by this relation. The upper limits set by the sensitivity of the de Bruyn instruments indicate that the luminosity of 12 of these SNR is less than 2 to 7 times the present radio luminosity of Cassiopeia A. Moreover, in the case of S Andromeda, the supernova observed in the Andromeda Galaxy in 1885, the radio telescope measurement sensitivity sets an upper limit for its remnant of less than 6% of the luminosity of Cas A (van der Kruit and Allen, 1976; Spencer and Burke, 1973). De Bruyn also points out that the three young SNRs in our own Galaxy, Cas A, Crab, and Tycho, also do not fit well to the S - D relation; see Figure 5.7.

[UPDATE: In 1987, following the completion of this dissertation, a supernova occurred 170,000 light years away in the Magellanic cloud, supernova 1987A. Daily radio telescope observations of the emission coming from its expanding shell have shown that this supernova also fits this same pattern of exhibiting little or no emission during its early stages. As seen in Figure 5-E, several days after the initial explosion, radio emission peaked at 130 mJy (0.01 Cas As) and within the following 10 days

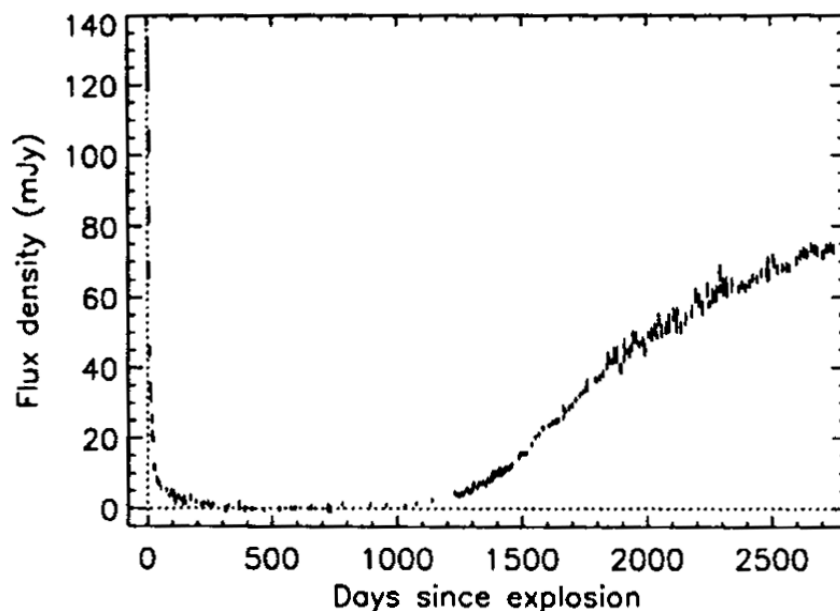


Figure 5-E. Evolution of the flux density from supernova 1987A at 843 MHz. over a period of 7.5 years (Ball, et al., 1995).⁽⁵⁾

declined to 20% of its peak intensity. This initial radio emission is associated with the initial fireball and not with the remnant, since optical emission followed a similar rise and decline. By six months its radio emission disappeared below background levels. Radio emission from the remnant became detectable above background levels about three years later, gradually rising and reaching about 60% of the fireball's peak intensity by mid 1994. The theory that the remnant's emission is generated by explosion-generated cosmic rays interacting with the residual stellar magnetic field would instead predict that radio emission should fall exponentially from a very high initial value, many orders of magnitude higher than was observed, eventually reaching present values. This detailed history of SN 1987A directly contradicts that theory's predictions.

Several mechanisms have been proposed to explain the absence of radio emission from young SNRs. One model proposed by Gull (1973) involves a time varying magnetic field generated by shearing motions in a convective region at the shock front where the ejected material contacts and sweeps up the surrounding medium. This model predicts essentially no radio emission in the first hundred years. However, the type II supernovae SN 1070g (observed in the galaxy M 101) and SN 1979c (observed in the galaxy M 100) do not fit this picture. Although delayed in appearance, radio emission at 6 cm wavelength was detected from SN 1979c about *one year* after maximum light at which time its radio spectral power was found to be 180 Cassiopeia A's! Considering that its shell size was no larger than $\sim 2.5 \times 10^{16}$ cm at that time, a luminosity two orders of magnitude less than the S-D relation is implied. In the case of supernova SN 1970g, radio emission began to be observed several months after maximum light and was found to peak at a luminosity of about 10 Cas A's.

[UPDATE: Also observations of SN 1987A have shown that remnant radio emission appeared three years after the explosion; see Figure 5-E.] Gull's model would not be

5) L. Ball, D. Campbell-Wilson, D. F. Crawford, and A. J. Turtle, "Radio observations of SN 1987A at 843 MHz." *Astrophysical Journal* 453 (1995):864- 872.

expected to generate sufficient relativistic electrons this early since an insufficient amount of interstellar material would have been swept up by the shock front to produce the required time-varying fields. Thus an additional mechanism would have to be introduced to account for the observed early emission, but this in turn would increase the complexity of the model.

Regarding the current status of our understanding of extragalactic supernovae, Van der Kruit and Allen (1976) in their review article conclude that *the origin of relativistic particles and magnetic fields in quantities and strengths sufficient to have produced the observed early radio emission by the synchrotron mechanism is still obscure*. However, as shown in Section 5.5, the Superwave Model may be able to account for the unusual behavior of very young extragalactic supernovae remnants.

5.3.2 Difficulties with a Central Pulsar Being the Source of the Relativistic Particles in the Crab Remnant

The X-ray and γ -ray emission from the Crab Nebula requires a continuous input of cosmic ray electrons amounting to more than 10^{38} ergs/s. As one solution to this particle energy problem, it has been suggested that a spinning neutron star (or *pulsar*) located within the remnant might provide the required continuous input of relativistic particles; see Gorenstein and Tucker (1971) for a review. According to classical theories of supernova explosions, it is thought that during a supernova the core of the exploding star would become compressed to very high densities leaving behind a remnant neutron star at the center of the expanding shell of gas. Rotational energy originally present in the parent star would then be stored in the neutron star as a rapid spinning motion. Various mechanisms have been suggested by which the mechanical energy stored in the rotary motion could be converted to accelerate subatomic particles away from the surface of the neutron star to relativistic velocities. These particles are then hypothesized to propagate out and illuminate the SNR. Also, the same particles, near the surface of the pulsar are assumed to interact with the pulsar's magnetic field (which could reach as high as 10^{13} gauss) generating a narrow beam of synchrotron emission. This beam is thought to sweep past the Earth periodically as the neutron star rotates producing brief pulses of broad band radiation. The Crab pulsar, for example, generates pulses repeating every 1/30 of a second, each pulse lasting about 2 milliseconds. The lighthouse model of pulsar emission, however, should be regarded only as a tentative hypothesis. While it offers an explanation for the regularly spaced pulses and their nonthermal, polarized character, it fails to account for the considerable complexity inherent in pulsar signals.

However, there are several areas of difficulty with the hypothesis that supernova remnants are powered by pulsars. For example, this hypothesis does not account for the high radio luminosity which was observed in SN 1979c only one year after peak light. To develop such a power output, a central pulsar would have to have been in existence several hundred to a thousand years to establish a suitable reservoir of relativistic particles (Weiler et al., 1981). Moreover as of 1983, of the 330 or more known pulsars and of the 125 or more known SNRs, only 4 pulsars are found to be associated with supernova remnants.* These are the Crab and Vela supernova remnant pulsars, pulsar 1930+22 associated with SNR G57.1+1.7, and a recently discovered X-ray pulsar found inside of the supernova remnant RCW 89. To appreciate this scarcity, picture a Venn diagram consisting of two circles. The

* Several other remnants have been observed to have energetic point sources at their centers, but in all cases the objects are not pulsars. These remnants include: RCW 103, W 50 which has the unusual binary system SS 433 at its center, G 74.9+1.2, G 127.1+0.5, the Cygnus Loop, and G321.9-0.3 which is associated with Circinus X-1 (Tuohy and Garmire, 1980; Margon, 1980; Weiler and Shaver, 1978).

area of one would represent the number of known pulsars and the area of the other would represent the number of known SNRs. The meager intersection of these circles, which would constitute less than 1% of the combined area of both circles, would represent the number of pulsar-SNR associations.

[UPDATE: As of 2001, over 1100 pulsars and 200 supernova remnants have been discovered and of these only 10 pulsars have thus far been found to be associated with supernova remnants. This is about the same association ratio as existed in 1983.]

To account for this lack of correlation between pulsars and SNRs, it was supposed that pulsars detected without remnants were older pulsars whose remnants had long since disappeared. Also, it was assumed that the several hundred remnants detected without pulsars contained neutron stars, but that they escaped detection because the pulsar radiation was being beamed in a direction that missed the Earth. However, such an explanation is no longer tenable. Measurements with the Einstein X-ray observatory indicate that neutron stars are conspicuously absent from SNRs (Murray et al., 1979; Giacconi, 1980; Tucker, 1980a). If they were there they should have been detected because their temperature even hundreds of years after the supernova explosion should have been above a million degrees, easily detectable in the X-ray region of the spectrum.

[UPDATE: In 1999, observations made with the Chandra X-ray Observatory revealed the presence of a compact X-ray source near the explosion center of the Cassiopeia A supernova remnant; see Figure 5-I (p. 184). However, compared with the bright emission from its surrounding remnant, the X-ray luminosity from this compact source is extremely low and hence cannot be the source of cosmic ray particle energy that is currently powering this remnant. Moreover, the lack of optical emission from this source rules out the possibility that it is either a neutron star or black hole powered by matter accretion.⁽⁶⁾]

In the case of the Crab nebula, where a pulsar is indeed found, studies of the pulsar's proper motion show that it did emerge from the 1054 AD explosion site (see Figure 5-H, p. 180). Hence it may be assumed to be the remnant core of the Crab's exploded progenitor star. However, substantial difficulties are encountered in demonstrating that this pulsar is the source of the illuminating cosmic rays. These may be enumerated as follows:

First, as seen in Figure 5.8 (Erickson et al., 1972), the spectrum of the Crab pulsar in the radio and optical range is significantly different from that of the nebula. This would imply that the differential energy spectrum for cosmic rays producing these two radiation spectra is substantially different. Thus, unless special circumstances are assumed, it would seem that the radio and optical radiation from the nebula is not produced by the same cosmic rays that produce the radio and optical radiation from the pulsar. Rather, the Crab's spectrum appears to more closely resemble that of active galactic nuclei; recall Figure 2.1.

Second, the Crab pulsar is located conspicuously off center from the nebula's X-ray emission peak; see Figure 5.9 (Harnden, 1983) and Figure 5-F. The majority of the X-ray emission comes from a region about 25×65 arc seconds (0.8×2 l.y.) in extent which is centered northwest of the pulsar by about 20 arc seconds (0.6 l.y.). As mentioned earlier, the X-ray and γ -ray region is the critical portion of the spectrum which demands that cosmic rays be *continuously* injected. So, the proximity of the X-ray emission region to the pulsar should be of critical importance. The fact that this emission is not centered on the pulsar strongly suggests that the pulsar is not the source of the inferred relativistic particles.

Third, the time taken for cosmic rays to hypothetically diffuse from the pulsar to the perimeter of this X-ray emission region also presents a problem. Even if the cosmic rays

6) D. Chakrabarty, et al., "The central x-ray point source in Cassiopeia A." American Astronomical Society meeting 195, session #112.13, 1999.

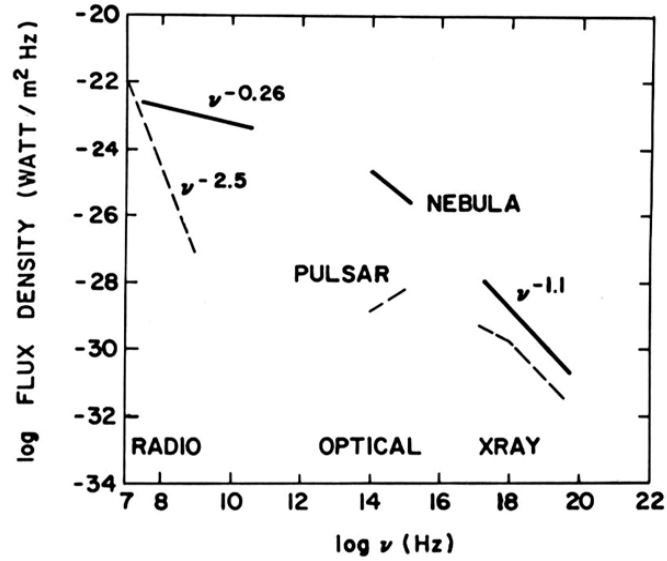


Figure 5.8. Differential energy flux from the Crab Nebula and from the pulsed component of the Crab pulsar (Erickson et al., 1972).

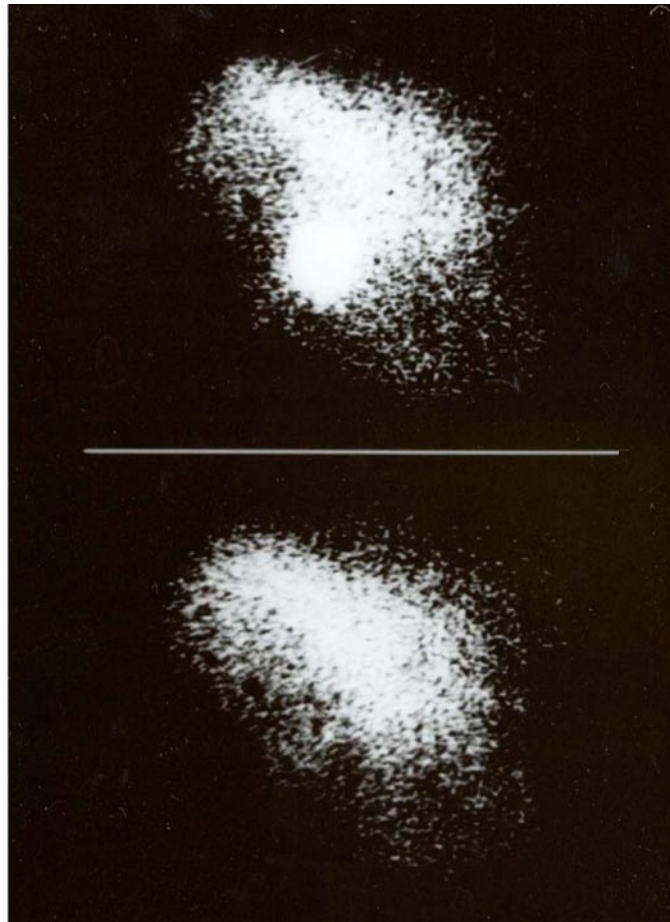


Figure 5.9. An X-ray image of the Crab Nebula detected by the Einstein satellite. The upper frame was exposed during the pulsar emission peak, the lower frame during the pulsar emission trough (courtesy of F. R. Harnden; also see Harnden, 1983).

UPDATE

Crab Nebula X-ray Image

The X-ray image of this same region taken with the Chandra X-ray Observatory is shown in Figure 5-F. The luminous region northwest of the pulsar appears to be in the form of an inclined ring situated about 0.6 light year away from the pulsar. Some have claimed that the southeastern plume is a jet from the pulsar that feeds particles into the surrounding ring. However, this is highly speculative considering that the plume appears to be aimed in the wrong direction and it is not certain that it is associated with the pulsar. Also see the third point made on page 167.

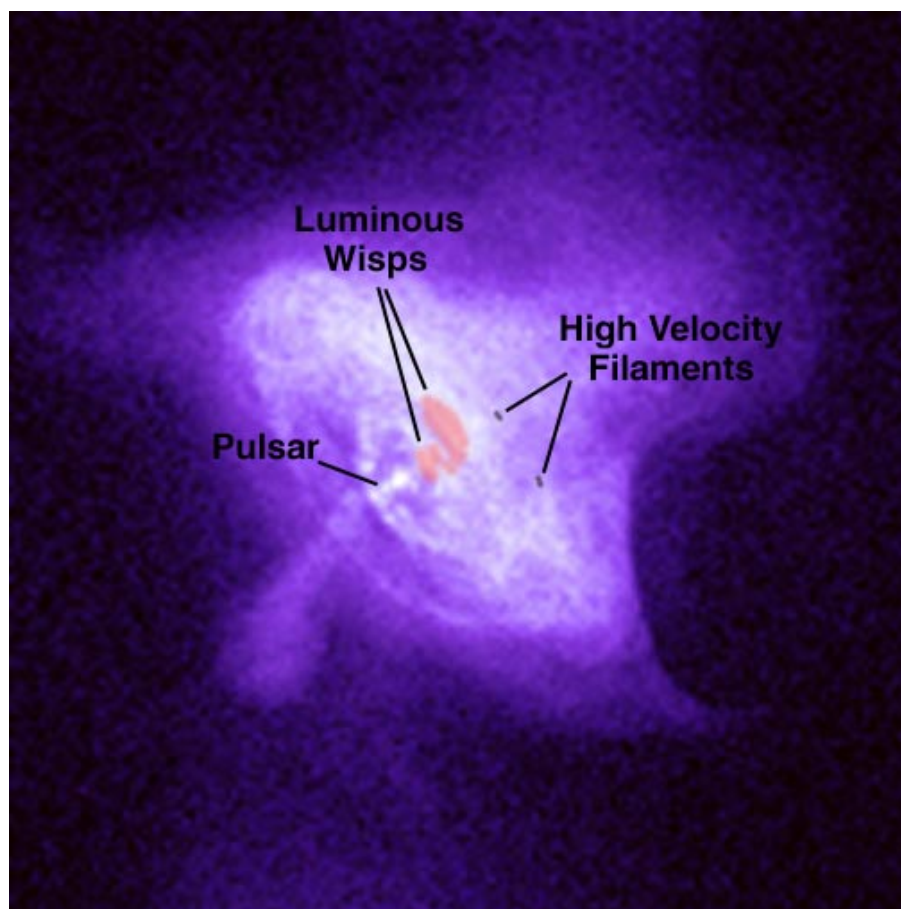


Figure 5-F. X-ray image of the central part of the Crab Nebula made with the Chandra X-ray Observatory displays this region in higher resolution (courtesy of NASA).

were to travel rectilinearly from the pulsar to the X-ray emitting region, required propagation times would be on the order of 1 year, as compared with the lifetime of the cosmic rays which is as short as a few months. So, one is inevitably led to the conclusion that the cosmic ray injection region must be *extended and of a size comparable to and coincident with the X-ray emitting region*. The pulsar model fails to meet this criterion.

Fourth, a model in which relativistic electrons diffuse away from a central pulsar also has difficulty accounting for the observed optical synchrotron emission in the nebula. For

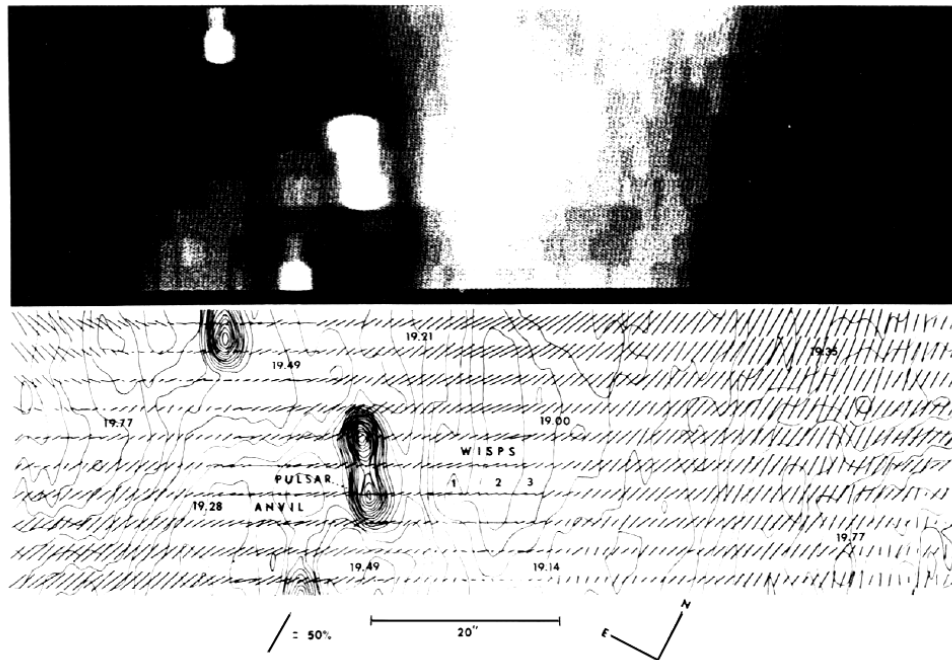


Figure 5.10. **Top:** A contrast enhanced picture of the central region of the Crab Nebula derived from observed optical surface brightness data. **Bottom:** The degree of optical polarization and electric vector orientation for this central region. Isophotal contours of the total flux are drawn at 0.07 magnitude intervals and are labeled in units of magnitude per arcsec² (Schmidt, Angel, and Beaver, 1979).

example, Schmidt, Angel, and Beaver (1979) point out that electron diffusion models require that the magnetic field be randomly oriented on a scale smaller than the electron mean free path in order to permit these particles to "random walk" away from their region of generation. They estimate that the mean free path in the Crab is of the order of $\sim 5''$ of arc (~ 0.15 l.y.). Even tighter constraints would be required if the electron plasma were considered to be collisionless. In this case for any diffusion to occur perpendicular to the field lines, magnetic inhomogeneities must be present on a scale comparable to or smaller than the synchrotron gyration radii of the particles which, for those emitting X-rays, would be on the order of ~ 0.03 l.y. (Scargle, 1969, p. 419). However, a study of the small scale optical polarization of the nebula's central region indicates that the magnetic field structure is extremely uniform and lacks significant structure on a scale below $20''$ of arc (~ 0.6 l.y.); see Figure 5.10 (Schmidt et al., 1979). Consequently, diffusion models would have great difficulty accounting for how energy is transported from the pulsar to the nebula.

Fifth, the small scale optical polarization data which Schmidt et al. have gathered do not seem to support the hypothesis that the nebular magnetic field originates in the pulsar. As seen in Figure 5.10, the polarization angle of the nebula remains extremely uniform in scans taken across the pulsar, and is oriented at an angle of 144° . Alternatively, Forman and Visvanathan (1971) find a slightly larger nebula polarization angle of 157° . In comparing the field orientation of the nebula to that of the pulsar, Cocke et al. (1970) find no simple relationship. They report that the light pulses from the Crab pulsar are on the whole polarized at about 90° , approximately 60° from the orientation of the nebular polarization. Moreover, the polarization angle of the Crab pulsar is observed to sweep through an angle of 360° with every pulse cycle, these pulses recurring at a frequency of about 30 Hz. Similar high frequency oscillations have not been observed in the surrounding nebula.

5.3.3 Arguments Supporting the Superwave Interpretation

Most of the features of the Crab Nebula that present problems for internal-origin models may be resolved when it is assumed that the illuminating cosmic rays originate from *outside* of the remnant and travel coherently as a blast propagating from the direction of the GC. For one thing the flux of relativistic particles which the 14,200 years BP superwave would be carrying would be sufficient to account for the observed nonthermal radio and optical emission. For example, at its present size the Crab remnant presents a cross-sectional area of $A \sim 75 \text{ l.y.}^2$, which at a galactocentric distance of 29,000 l.y. would intercept 7×10^{-9} of the total energy flux of the superwave. Assuming that the superwave carries a total electron energy of $U_e \sim 5.5 \times 10^{57}$ ergs, then if it is supposed for the moment that the Crab remnant had maintained its present size during the entire period of superwave passage, it would have been capable of intercepting a total cosmic ray energy of $\sim 4 \times 10^{49}$ ergs, about 13 times the amount required to explain the observed synchrotron and optical emission; c.f. the model proposed by Weekes (1969) discussed on **p. 165** of this chapter.

To realistically explain the Crab Nebula emission, the 14,200 years BP superwave model should also be able to account for the X-ray and γ -ray luminosity presently observed from the inner portion of the nebula. As mentioned earlier, particle lifetime considerations require that relativistic electrons are being continuously injected over the extent of this emission region.

The energy requirements to power this high energy emission may be estimated as follows. The central region from which hard X-ray radiation is observed has dimensions 0.8 by 2 l.y., which represents an area of $\sim 10^{36} \text{ cm}^2$. Given an X-ray and γ -ray luminosity of 6×10^{37} ergs/s, this represents an energy flux of $\sim 60 \text{ ergs/cm}^2/\text{s}$. This is comparable to the energy flux that would be carried by the 14,200 years BP superwave at the peak intensity of the first outburst. However, if it is assumed that the Crab supernova was triggered by the 14,200 years BP event horizon at point $t = 0$ in Figure 3.2 (**p. 63**), then the first outburst should have already passed by and the nebula should be encountering the intermediary portion of the superwave positioned at $t \sim 900$ years. Consequently, to account for the presently observed X-ray and γ -ray emission, elevated cosmic ray intensities would have to be postulated for this intermediary period, comparable to those proposed for the first outburst (over the period $t = 0 - 400$ years). If the power-time profile proposed in Section 3.1 were appropriately revised, the required particle energy could double the previously quoted estimate for the 14,200 years BP superwave.

If a superwave were continuously supplying particles to the remnant, then it would be expected that the outside of the remnant would be hotter than the inside, just the reverse from what would be expected if a centrally located pulsar were supplying the particles. Here too, observations tend to support the superwave model. Trimble (1970) has found that the nitrogen-hydrogen ionization line ratio (N_{II}/H_{α}) is larger near the surface of the nebula and smaller near its center. This indicates the presence of a thermal gradient with the surface being hotter than the center. Since radiative cooling is expected to be more efficient near the surface, the observed thermal gradient is strong evidence that energy is being supplied from outside of the nebula, rather than from the inside. Trimble's interpretation is that the heating is due to the expanding nebula collisionally interacting with the surrounding interstellar medium. She suggests that any deceleration would be counteracted by radiation pressure exerted from within the nebula. However, the same observations also support the interpretation that the nebula is being heated (and radially accelerated) by an exterior blast of cosmic rays.

In Chapter 3, Section 3.2, it was postulated that the cosmic rays associated with a superwave would be able to pass through a considerable portion of the Galactic disk with only

minimal interaction and minimal diversion from their straight-line course. However, young supernova remnants would be an exception to this rule. They consist of gas in a highly ionized and turbulent state having a frozen-in magnetic field. Moreover, the outer boundary of the remnant which is propagating through space at supersonic velocities would form a shock front. Upon passing through this shock boundary, cosmic rays from the superwave would become scattered from their straight-line course and captured within the remnant. Assuming that the remnant boundary is permeable to the relativistic electron volley, there should be little bulk motion of the remnant in the superwave's direction of propagation. At least, this must be assumed to be the case in order to account for the lack of observed radial motion of the remnant toward the Galactic anticenter. However, the trapped electrons would be expected to affect the dynamics of the remnant. The propagation directions of the relativistic electrons trapped within the remnant, being randomly oriented, would exert an outward pressure on the remnant shell causing its rate of expansion to accelerate.

Such an effect is actually observed. Trimble (1968) finds that when present filament velocities are extrapolated back in time, they yield a convergence date that is too early by ~ 86 years (1140 AD rather than 1054 AD, the date for the supernova recorded by Chinese astronomers). This gives a percentage velocity excess of $\Delta V/V = 8\%$ (a percentage similar to that estimated for the excess proper motion). This represents an average acceleration over the lifetime of the remnant of $\sim 5 \times 10^{-4} \text{ cm/s}^2$. Also, Baade (1942) has found a slightly larger acceleration of about $1.1 \times 10^{-3} \text{ cm/s}^2$ along the long axis of the nebula.

To account for these observations, Bodenheimer and Ostriker (1974) and Chevalier (1977) have suggested that the accelerating force is being applied symmetrically by a relativistic particle wind emanating from the Crab pulsar. Also, Kundt and Krottscheck (1980) have suggested that the accelerating force is due to the pressure from a 30 Hz wave field radiating from the Crab pulsar. The interpretation offered by the superwave model is essentially similar to the pulsar-cosmic-ray-wind hypothesis except that the particles are assumed to be externally injected into the remnant, rather than internally injected.

The accelerating force may be determined as follows. A trapped particle energy of $U_p \sim 3 \times 10^{48}$ ergs and a volume $V \sim 10^{58} \text{ cm}^3$ implies a particle energy density of $U_p/V \sim 3 \times 10^{-9} \text{ ergs/cm}^3$, or a pressure of $3 \times 10^{-9} \text{ dynes/cm}^2$. For a remnant surface area $\Sigma \sim 6 \times 10^{38} \text{ cm}^2$, this would exert a total outward force on the shell of $\sim 2 \times 10^{30}$ dynes. For a shell mass of $1 M_\odot$ this implies a shell acceleration of $\sim 10^{-3} \text{ cm/s}^2$, which is in the range of the observed acceleration.

If the 14,200 years BP superwave is passing through the Crab Nebula, then certain electrodynamic effects should also be observed, provided that the electron blast of the superwave is not completely charge-balanced. For example, polarimetric studies of the Crab Nebula (Woltjer, 1957) show that the magnetic field lines of the remnant are oriented perpendicular to the nebula's long axis; see schematic shown in Figure 5.11. The particle blast would impact the remnant perpendicular to these field lines and hence would tend to force them to spread apart in a direction at right angles to both the field orientation and direction of particle propagation; see Figure 5.11. This would give an added radial acceleration to the expanding nebula in a direction oriented preferably along the Galactic plane and perpendicular to the incident cosmic ray blast. Consequently, the expanding spherical SNR shell would become distorted into a prolate spheroid shape. Indeed, observations of filament velocities (Trimble, 1968) indicate that the Crab Nebula is very likely a prolate spheroid, i.e., cigar shaped. The length ratio of the major to minor axes is 1.5 – 1.6 and a similar ratio is found for the maximum proper motion in these respective directions. Moreover, the long axis of the nebula is found to be oriented along the Galactic plane in a direction perpendicular to the Galactic center-anticenter axis, as predicted by this electrodynamic model.

Munch (1958) was the first to point out that the nebula's major axis happens to be

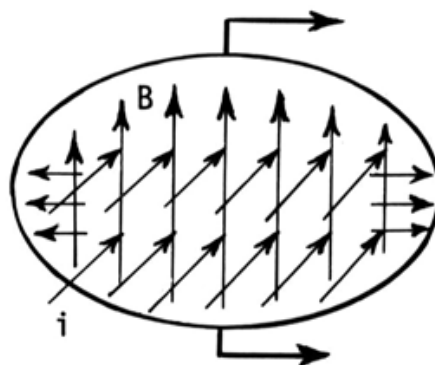


Figure 5.11. Electrodynamic effects generated by a coherent cosmic ray blast propagating through a supernova remnant.

oriented parallel to the Galactic equator. He has taken this as evidence that the expansion of the Crab envelope has been influenced by the interstellar magnetic field. Except, he has suggested that the interstellar field is oriented along the Galactic equator and that expansion occurred more freely along the direction of the field lines, i.e., parallel to the equator. However, as was discussed earlier, the polarization data for the Crab indicate that the magnetic field lines are instead oriented perpendicular to the Galactic equator. Rather, Munch's explanation seems to be better suited for 3C 58, a remnant which lies well beyond the 14,200 year BP horizon at $\ell = 131^\circ$, $d = 7.5$ kpc. Like the Crab, it has an elliptical shell whose long axis is oriented approximately parallel to the Galactic plane. Also, radio polarization measurements of 3C 58 indicate that its magnetic field, although regular is oriented parallel to the long axis of the nebula (Kundu and Velusamy, 1972).

5.3.4 The Luminous Front Activity

The central region of the Crab Nebula shows evidence of relativistically propagating fronts. As seen in Figure 5.12, there is a set of luminous structures which are separately referred to as "the Anvil," "the Thin Wisp," "Wisp 1" (or "the main wisp"), "Wisp 2," and "Wisp 3." These structures are observed to brighten and fade and change their positions relative to one another on time scales as short as a month (Scargle, 1969). The Thin Wisp, located just 1" (250 A.U.) from star S-1 (the Crab pulsar) brightens and fades, changes in shape, and wiggles its ends, but it does not move from its location. Wisp 1, on the other hand, about once every few years, is observed to propagate rapidly away from the Thin Wisp and return again to its initial position. The total extent of its excursion is $\sim 2''$ of arc (~ 0.06 l.y.) and velocities as high as $1/3$ of the speed of light are indicated (Scargle, 1969, p. 418). Oscillatory motion and brightening are also detected in Wisps 2 and 3, but these effects are of lesser magnitude. Scargle (1969, p. 422) suggests that the Thin Wisp lies close to the center of symmetry of the wisp structures with activity in the Anvil being complementary to wisps 1, 2, and 3.

No emission lines are present in the wisps. However, because their continuum emission is linearly polarized, it is believed that they radiate by the synchrotron mechanism, the magnetic field lines being oriented parallel to their long axis (Scargle, 1969). However, Kundt (1977) points out that the synchrotron mechanism cannot account for the observed circularly polarized radiation which constitutes about 1% of the polarized emission. Also, he notes that at optical frequencies, incoherent synchrotron emission can only account for $\sim 1\%$ of the luminosity of the wisp region. As an alternative, he suggests that the observed

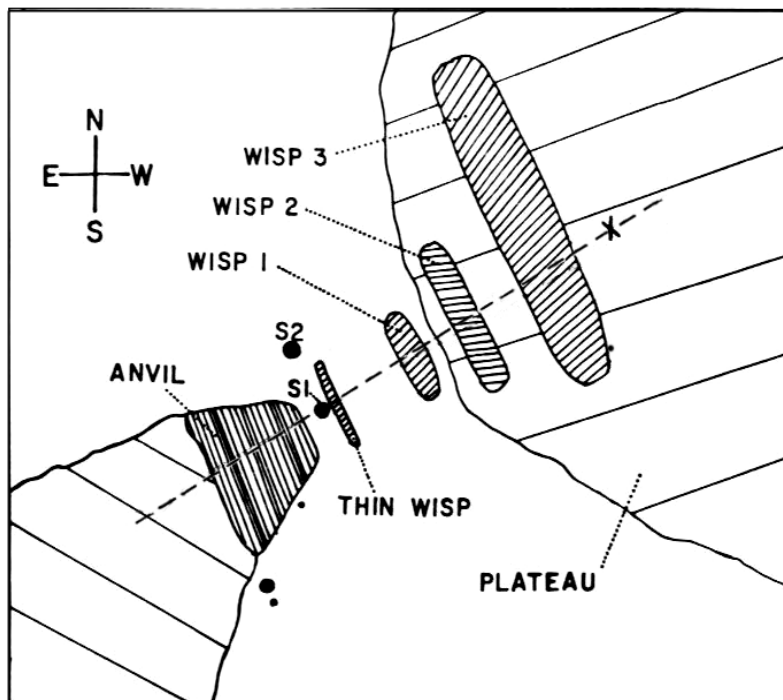


Figure 5.12. Schematic rendition of a configuration of the optical wisps in the central region of the Crab Nebula (after Scargle, 1969). The Crab pulsar PSR 0532 is marked as star S1. The cross added here marks the position of the high-velocity line-emitting filament #220 studied by Trimble (1968). The superimposed dotted line indicates the orientation of the hypothetical cross-sectional view displayed in Figure 5.14 (p. 178). The image views a region $\sim 52'' \times 45''$ (1.65×1.4 l.y.); see Figure 5-G (next page).

emission is stimulated synchro-Compton (laser) emission beamed toward the observer, generated by neutral sheets of relativistic particles emitted by the pulsar. I propose a slight modification of Kundt's mechanism in which the emission is powered by superwave cosmic rays; see p. 178.

Scargle and Pacini (1971) report that about 2 months after the September 1970 pulsar "glitch" (an event in which the frequency of the pulsar temporarily increased in an abrupt manner), Wisp 1 was observed to propagate away from the pulsar at a velocity of about $10''/\text{yr}$. This would be about $0.3 c$ for a distance to the Crab of 2 kpc. Wisp 1 moved out about $1''$ (~ 0.03 l.y.) and then returned to its initial position, whereupon Wisp 2 began to propagate outward also at about $0.3 c$. This sequence of events is shown in Figure 5.13 (Scargle and Pacini, 1971). They suggest that the pulsar glitch is accompanied by the release of a burst of relativistic plasma travelling outward from the pulsar at very close to the speed of light. They interpret Wisp 1 as a standing shock front formed where the relativistic wind from the pulsar impacts the surrounding nebula. Thus, they suggest that with the arrival of this relativistic pulse (dashed line shown in Figure 5.13), the shock front becomes propelled outward (solid line shown in Figure 5.13). The pressure exerted by the nebula subsequently returns Wisp 1 to its initial steady state position, while a magnetosonic wave generated by Wisp 1 (dotted line shown in Figure 5.13) causes the displacement of Wisp 2.

The 14,200 Years BP Superwave Model offers a different interpretation of this luminous front activity. For example, suppose that the cosmic rays which initiate this activity come, not from the pulsar, but from an exterior superwave blast travelling toward the nebula from

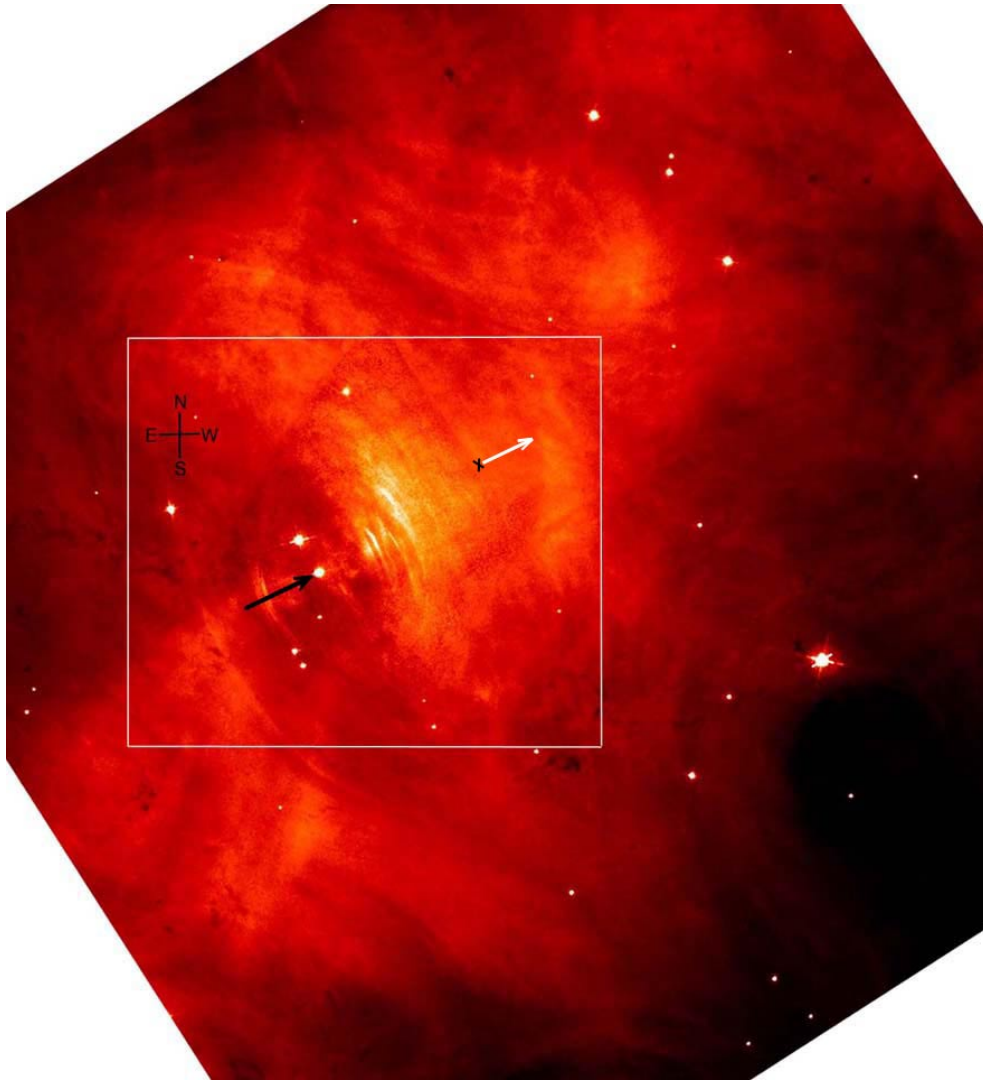


Figure 5-G. Optical image of the inner part of the Crab Nebula made in 1996 with the Hubble Space Telescope (courtesy of J. Hester, P. Scowen, and NASA). The added box marks the extent of the view shown in Figure 5.12. The black arrow shows the direction of the Crab Pulsar's proper motion and its displacement from the 1054 AD explosion site. The added cross indicates the position of high-velocity filament #220 and the direction of its proper motion.

To view a time lapse movie of the Crab Nebula's luminous wisp activity imaged with NASA's Hubble Telescope, [click here](#).

the GC. For example, suppose that the wisps are taken to be a shocked region formed between the outward expanding nebula and the incident cosmic ray blast, and suppose this region has a shape similar to that shown in Figure 5.14. This diagram might be thought of as a cross-sectional view where the x-axis plots the distance in light years along the dotted line shown in Figure 5.12, and where the y-axis plots the distance in light years measured toward the Galactic anticenter direction from the Crab pulsar (CP). The Thin Wisp (TW), which marks the leading edge of the shock region, is assumed to be at the same y-axis position as the pulsar, but 2" (~0.06 l.y.) to the right. However, with an exterior blast model the observational data are also compatible with the Thin Wisp being slightly behind the pulsar at a positive y position. The row of arrows indicates the direction in which the cosmic

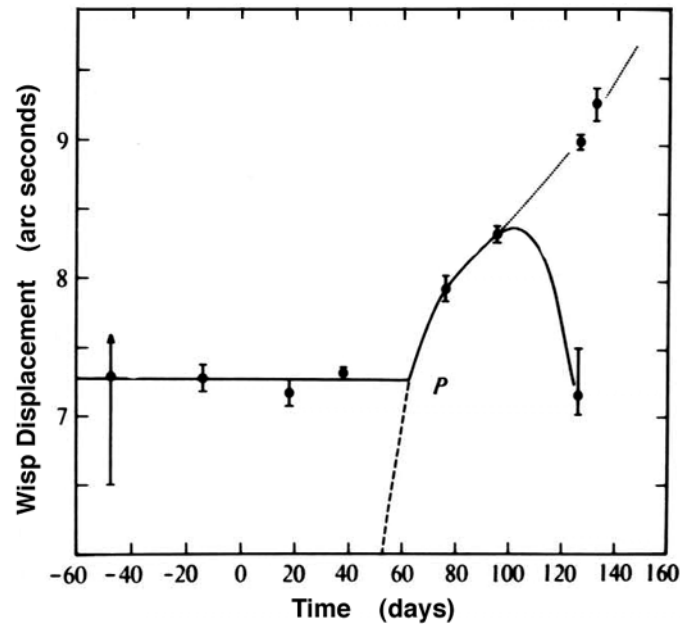


Figure 5.13. Observations of Wisp 1 showing its excursion following the pulsar glitch on September 20, 1970. The displacement of the wisp from the pulsar, in seconds or arc, is plotted against time in days relative to September 20th (Scargle and Pacini, 1971).

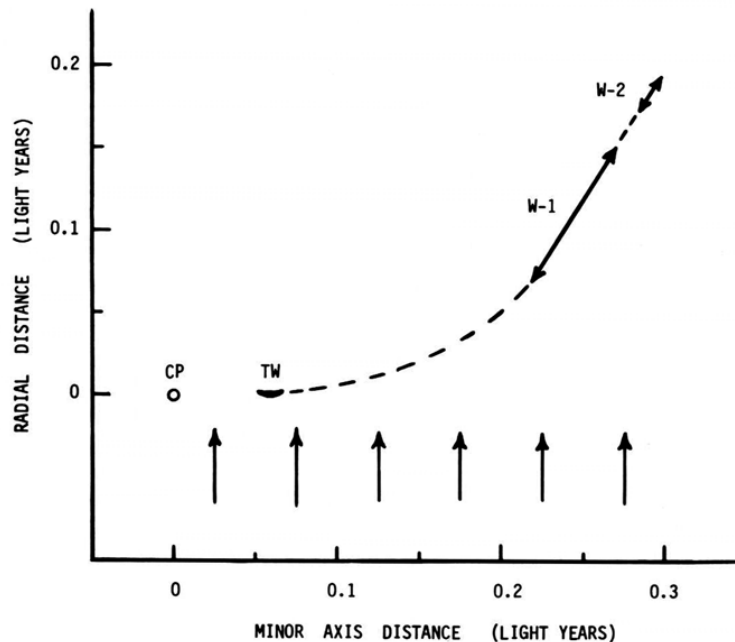


Figure 5.14. Shock front profile for the outer surface of the Crab Nebula (central portion on the side expanding toward the GC). CP = Crab pulsar, TW = Thin Wisp, W-1 = Wisp 1, W-2 = Wisp 2. A blast of cosmic rays associated with a superwave would be propagating at the speed of light in the direction indicated by the arrows. The arrows on the shock front indicate the degree of displacement in Wisps 1 and 2 after the September 1970 glitch event. An observer would see only the component of motion projected on the x-axis.

ray volley would propagate. The direction at which an Earth-based observer would view the nebula would deviate from this direction by about 6.6° , due to the fact that as viewed from Earth, the position of the Crab Nebula deviates from the Galactic anticenter position by this amount. However, for simplicity this deviation will be ignored and it will be assumed that the arrows also indicate the direction of viewing. Consequently, events triggered by the receding cosmic ray volley which are spaced by an amount of time, Δt , to the Earth-based observer will appear to be spaced by a time interval $\Delta t' = 2\Delta t$ due to light travel time effects.

To simulate the data shown in Figure 5.13, imagine that a pulse of cosmic rays, whose flux exceeds the level of the steady state cosmic ray flux, travels in the positive y direction (Figure 5.14) at the velocity of light. Also, suppose that at time $t = 0$ this volley encounters the pulsar and the Thin Wisp, initiating a glitch in the pulsar's emission pattern and causing a brightening of the Thin Wisp. About 0.07 years later (~ 25 days later, but 50 days later to the Earth-based observer) the blast would arrive at the Wisp 1 shock region displacing it along the trajectory shown by the solid line segment. The motion of Wisp 1, which to the observer appears to involve a recession of W-1 from TW at a velocity of $0.3c$, may be simulated by the proposed "signal-screen" model if the shock region trajectory (solid line) makes an angle of 32° to the observer's line of sight. The reciprocatory phase, in which Wisp 1 "snaps back" to its initial position, might begin after the relativistic pulse passes a field discontinuity in the shock front. Finally, about 0.1 years (~ 35 days or 70 days to the observer) after first encountering Wisp 1 the pulse encounters Wisp 2 and begins to displace it also. It might be assumed that a superwave contains a series of such relativistic blasts and that these periodically encounter this shock front region and produce the observed activity.

[UPDATE: Observations with the Hubble Telescope show features having a characteristic width of one arcsec (0.03 ly) in the outer parts of the nebula propagating outward toward the nebula's edge.⁽⁷⁾ Like the luminous wisp activity, this activity could similarly be explained by a superwave cosmic ray volley impacting the Crab nebula face on. As a galactic cosmic ray volley impacted the nebula shock front, emission would first be stimulated in the more inner regions of the nebula which would be closer to the Galactic center and, as this volley proceeded forward into the nebula, these emission regions would progressively move toward the outer nebular regions located further from the Galactic center.]

One piece of evidence which supports this model is the observation that the high velocity ionized filament #220 lies along this axis and is moving away from the 1054 AD explosion site in a direction similar to that of the Crab pulsar. Its position is marked by the cross shown in Figure 5.12. [Moreover the position of this filament coincides with the center of the ridge of maximum X-ray emission imaged with the Chandra X-ray Observatory (see **Figure 5-F**).] This filament has the highest radial velocity towards the Galactic center of any other filament of ionized gas observed in the Crab, the velocity being ~ 1480 km/s (Trimble, 1968). Consequently, it might be expected that if a cosmic ray blast were propagating through the nebula from the GC direction, an unusual amount of high energy activity would be observed in the vicinity of this filament. Both the X-ray emission and the optical Wisp emission coming from a region closer to the pulsar would be emission from a bow shock front that had formed around the nebula's high-velocity outer fringe on the side facing the Galactic center and was being excited by the oncoming superwave barrage. On the other hand, the pulsar-SNR model, which assumes that the pulsar and wisps are both located at the center of the nebula, would assign this positional proximity as being due to chance, i.e., a projection effect in the line of sight.

7) Scowen et al. "Dynamics and magnetic morphology of the outer Crab synchrotron nebula.." American Astronomical Society Meeting 188, Session #75.05 (1996)

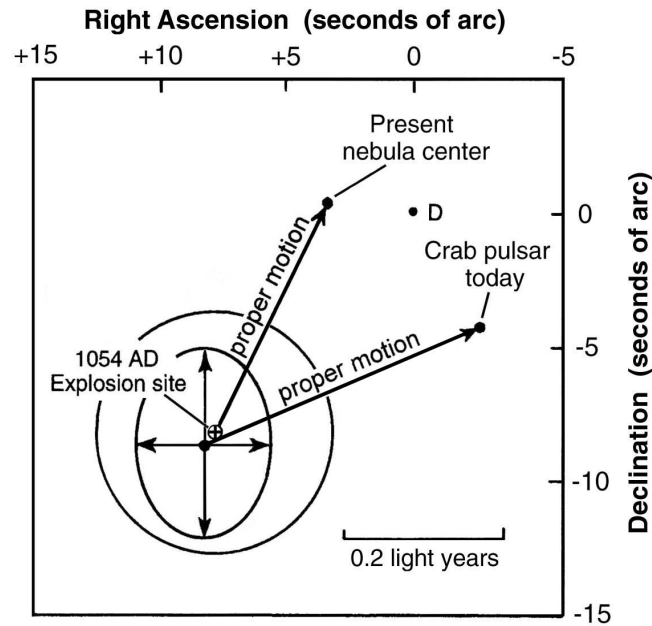


Figure 5-H. 1054 AD location and trajectory of the Crab pulsar as compared with the 1054 AD location and trajectory of the Crab remnant explosion center.

Further indication that the wisps and pulsar are on the outer surface of the nebula, rather than inside, comes from a study of the pulsar's proper motion. [Radio telescope data indicates that it has a proper motion of -12 ± 3 mas/yr in right ascension and $+5 \pm 4$ mas/yr in declination, giving it a velocity of 123 ± 40 km/s toward position angle $293 \pm 20^\circ$.⁽⁸⁾ This is about the same magnitude as the net space motion of the nebula (see Figure 5-H). Interestingly, the pulsar is receding from the vicinity of the nebula's expansion center in the same general [northwesterly] direction as filament #220 which is moving toward position angle $285 \pm 2^\circ$; see **Figure 5-G**. Also, compared with this filament, the pulsar is located about 40% of the distance to the explosion center and has about 40% as much proper motion, 123 km/s as compared with Trimble's measurement of 300 ± 50 km/s, for the proper motion of filament #220. Consequently, I would suggest that, like filament #220, the Crab pulsar is also propagating outward from the expansion center with a velocity of ~ 1500 km/s! This picture, indeed, contrasts strongly with the classical picture of a pulsar quietly drifting along inside the remnant. A definitive answer regarding the pulsar's true radial velocity cannot be obtained spectroscopically since no emission lines are present in the pulsar's continuum spectrum. The same is the case for the polarized emission from the luminous wisps. Nevertheless, the above dynamical argument strongly favors the view that the Crab pulsar and the wisp features are on the forefront of the Crab's shell, expanding toward the observer and toward the proposed superwave blast. To my knowledge the proposed placement of the Crab pulsar and luminous wisps is a novel idea, suggested here for the first time.

The intense X-ray emission centered in this wisp region may also be attributed to the interaction of this shock zone with the superwave blast. Perhaps a beaming mechanism is involved in which electrons in the advancing nebular plasma are relativistically accelerated toward the Galactic center direction by time-varying magnetic fields (e.g., the betatron mechanism). Since we are favorably positioned with respect to the Crab Nebula we happen

8) J. H. Taylor, R. N. Manchester, and A. G. Lyne, "Catalog of 558 pulsars." *Astrophysical Journal Supplement Series* 88 (1993):529 - 568.

to see this beamed radiation whereas in other young SNRs, such as Cas A, this radiation misses us. This may account for why the Crab is structurally unique with regards to its plethoric (filled center) optical and X-ray nonthermal emission. Also, it may explain why the bend in the nonthermal emission spectrum of the Crab occurs at optical wavelengths ($\sim 10^{13}$ Hz) whereas in other remnants, such as Cas A, it occurs at X-ray wavelengths ($\sim 10^{17}$ Hz).

[UPDATE: This beaming mechanism also accounts for Kundt's observation of circularly polarized radiation coming from the luminous wisps, circularly polarized radiation being produced only if the emitting cosmic rays are traveling toward the observer. This particle beam orientation rules out the pulsar as a candidate source for the particles since the particle trajectory from the pulsars to the offset wisps would necessarily present a substantial angle to our line of sight. Recall that circularly polarized emission has similarly been detected coming from Sgr A* (see update on page 61).]

In general, the superwave model coupled with the hypothesis that an event horizon is presently in the vicinity of the Crab Nebula helps to solve many of the difficult problems encountered by conventional SNR models. Not only does this one model alleviate many separate problems in the interpretation of the Crab Nebula, but it also simultaneously accounts for many other *seemingly* unrelated phenomena in other portions of the Galaxy and on the Earth.

5.4 THE CASSIOPEIA A REMNANT

Cassiopeia A, another well-studied SNR, is the youngest of the dated remnants and also one of the closest. It measures about $4\frac{1}{2}'$ in diameter, which is about 11 light years for a distance to the remnant of 2.8 kpc. Its shell probably has a mass of $\sim 10 M_{\odot}$ and a kinetic energy of $\sim 3 \times 10^{51}$ ergs, and is believed to be the product of a type-II supernova. Cas A is unusual in that it has the highest radio surface brightness of all known Galactic SNRs; recall Table VIII. Its radio emission spectrum is nonthermal, indicating that the shell of this SNR is populated by synchrotron generating relativistic electrons.

The proposal made here that Cas A is being impacted by a relativistic electron wind from the GC direction is supported by radio observations. For example, as seen in Figure 5.15, the radio emission distribution is highly asymmetrical in the east-west direction. The strongest radio emission is found on the western side of the remnant, which faces toward the GC, while a gap in the radio shell is found on the eastern side facing the anticenter direction. In fact, it is found that a line drawn from the western emission peak through the center of the eastern gap is precisely aligned with the Galactic equator! This asymmetry cannot be ascribed to large scale inhomogeneities in the distribution of filamentary material. For example, in the western region of high radio intensity such material is conspicuously absent, whereas in the eastern radio gap where one filament is found there is no associated radio emission. A relativistic particle blast directed from the GC, though, could account for the observed asymmetrical emission pattern, and in fact would predict that the radio emission peak should be located on the nebular shell precisely where it is found.

Dickel and Greisen (1979) have noted that the centroid of the radio emitting shell is displaced westward from the remnant's center of expansion, which is determined from the motion of the optical filaments. To illustrate this asymmetry on their 1976 radio contour diagram the authors have drawn two circular arcs of radius 1.3 pc and 1.7 pc centered on the point of expansion; see Figure 5.16. They interpret this discrepancy as arising either from an anisotropy in the initial supernova explosion, or from an inhomogeneity in the encountered interstellar medium, the ambient medium being hypothesized to be 3 to 4 times more dense on the eastern side as compared with the western side of the remnant. However, in the context of the Galactic Explosion Hypothesis a considerably different

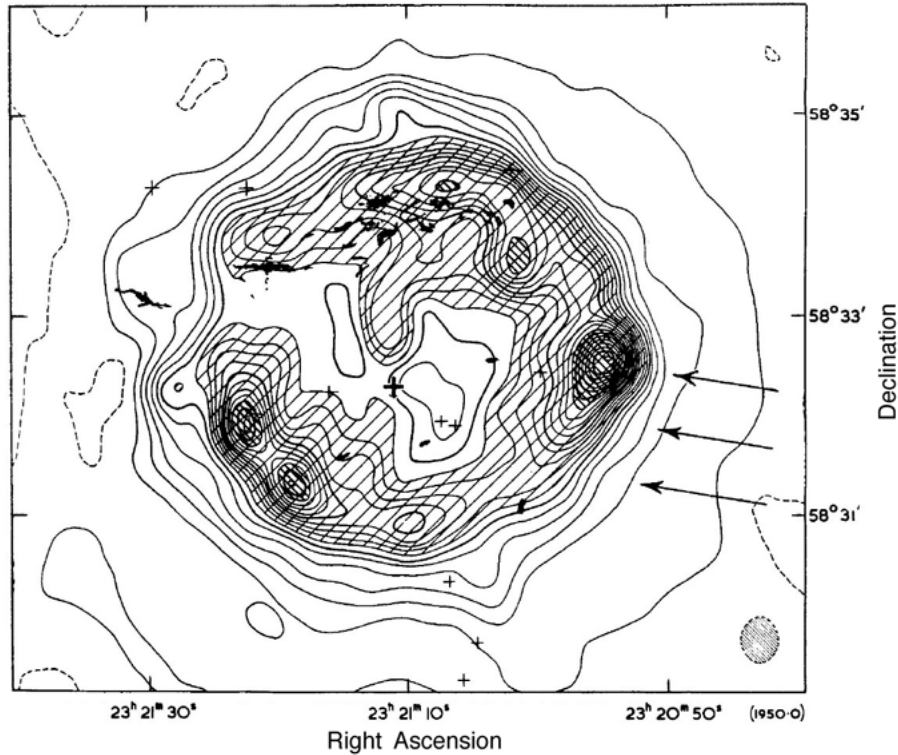


Figure 5.15. Radio contour map of Cassiopeia A (1410 MHz) showing also the principal optical filaments as dark patches (adapted from Ryle, Elsmore, and Neville, 1965). The contour interval is 3000 K. The small crosses indicate the positions of some of the brighter stars in the field of view. The large central cross indicates the remnant's dynamical center of expansion. Arrows have been added on the western side to indicate the direction of impact of the 14,200 years BP superwave.

interpretation is possible. The westward displaced emission arc may actually be outlining the contour of a *bow shock front* formed between the outward expanding SNR and the west-to-east impact of the incident electron volley; see Figure 5.16 (dashed line). In the vicinity of Cas A the 14,200 years BP superwave would be propagating in a direction inclined at about 60° of Galactic longitude from our direct line of sight to the remnant. Hence we would be viewing the shock profile in a slantwise manner.

It is interesting to note that the 3 quasi-stationary flocculi are discussed by van den Bergh (1983), lettered A, B, & C in Figure 5.16, lie at a position close to the proposed bow shock front. These features are highly unusual in that they lie *outside* of the remnant's radio shell and do not participate in the remnant's expanding motion. They have a mean outward velocity of ~ 150 km/s as compared with 4100 – 8500 km/s which characterizes most of the optically visible condensed material. Chevalier and Kirshner (1978) suggest that the quasi-stationary flocculi are interacting with a turbulent medium since a major part of their motion is randomly directed. They propose that the optical emission from these flocculi is due to heating by shock waves emanating from the remnant. The alternate interpretations offered by the GEH is that such shock fronts are propagating *transverse* to the remnant and that they derive their energy instead from the proposed incident blast of Galactic cosmic rays. Propagating shock fronts would be expected to form within the quasi-stationary bow shock front since in this region the interstellar magnetic field would become turbulent and would be susceptible to being propelled by the incident cosmic ray blast.

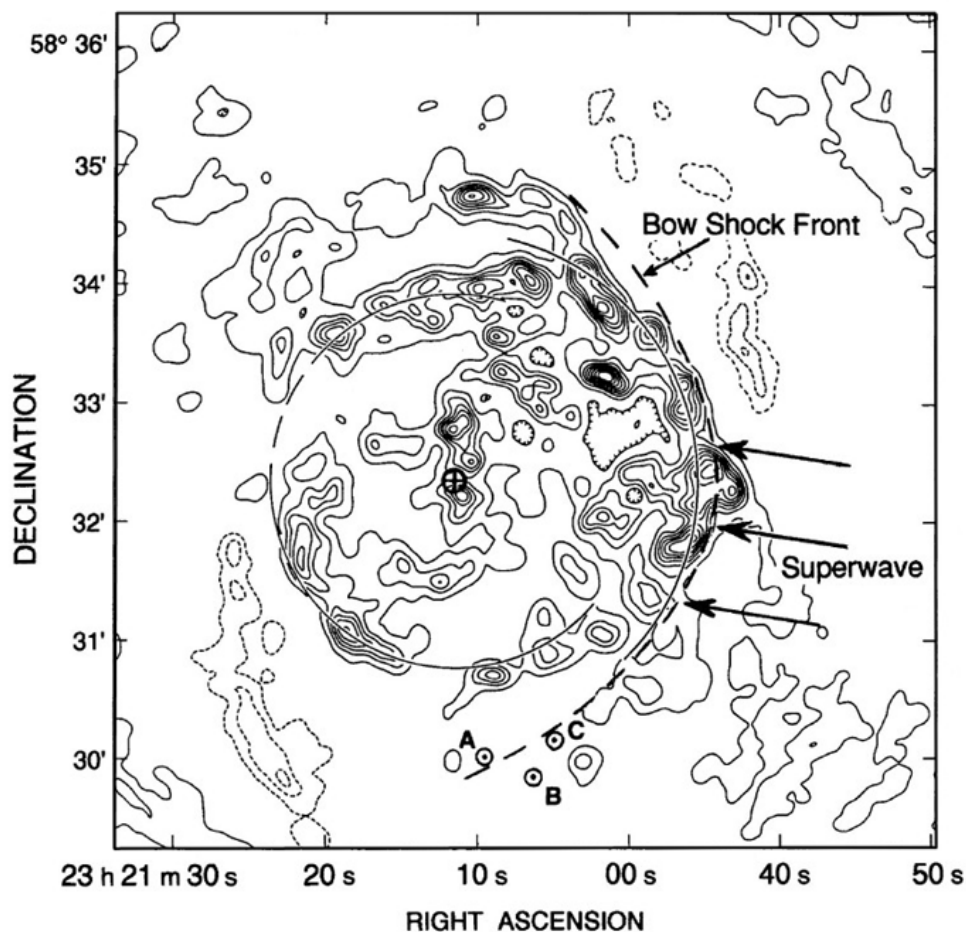


Figure 5.16. Radio contour map of Cas A (2695 MHz) made in 1976 with arc (solid lines) drawn to illustrate the asymmetry of the remnant (adapted from Dickel and Greisen, 1979). The central cross represents the position of the supernova explosion as determined from the motion of the optical filaments. The letters indicate the positions of 3 quasi-stationary flocculi. The added dashed line illustrates the position of the proposed bow shock front.

Dickel and Greisen (1979) have identified about 83 discrete compact radio emitting features in their 2695 MHz radio map of Cas A made in 1976; see Figure 5.16. They suggest that these "radio knots" which make up the radio shell do not participate in the nebular expansion. If they did, then it would be expected that the radial component (with respect to the center of expansion) of their projected motion should increase with increasing radial distance from the center, and that the tangential component of their projected motion should be zero. However, this is not observed. Instead, these knots are seen to have high-speed random motions. In their sample of 83 knots they found that the root mean square velocity was ~ 2600 km/s in the tangential direction and ~ 3000 km/s in the radial direction with component velocities in some cases reaching as high as 9000 km/s. They estimate that if a radial velocity gradient is present, it is probably of the order of 500 km/s/parsec, which would predict an outward velocity component of $\sim 700 - 800$ km/s at the edge of the radio emitting shell. This is considerably less than the value of 1600 km/s predicted for the case of adiabatic expansion of the remnant. They conclude that whatever causes the relativistic particle acceleration and/or magnetic field amplification responsible for these knots probably

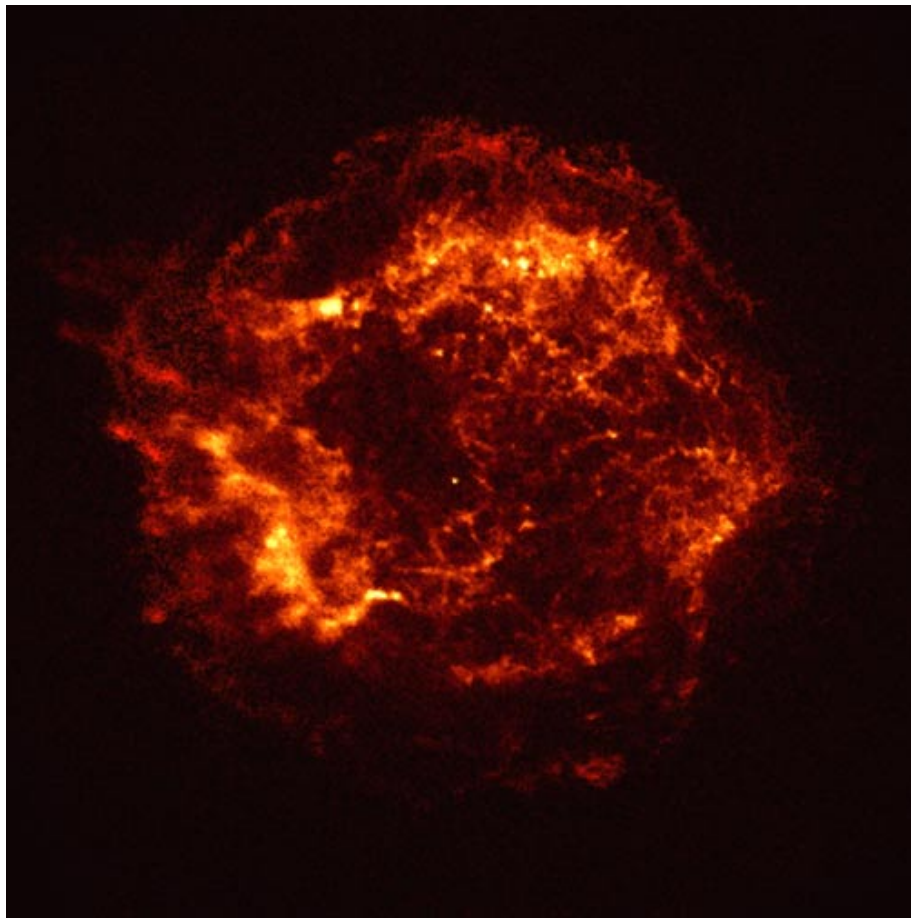


Figure 5-I. Update: Soft X-ray image of the Cassiopeia A supernova remnant made with the Chandra X-ray Telescope in 2000 (courtesy of NASA). The faint compact source evident at the center is unable to explain the strong X-ray emission of the surrounding remnant.

does not participate in the mean nebular motion.

Dickel and Greisen do not offer an explanation for the cause of the substantial, randomly directed velocities of the compact radio components. However, an explanation may be readily found in the context of the GEH. The compact radio sources may be interpreted as radio-emitting features embedded in the surface of the bow shock front. The power source responsible for diffusely exciting these features would be the cosmic ray volley of the proposed superwave. The large scale random motions would then be due to electrodynamic effects produced by the external impact of the cosmic ray wind. It might also be added that if the radio shell is interpreted as a quasi-stationary bow shock front surrounding the true remnant shell (as defined by the optical filaments), then its low expansion velocity ($v \sim 1000$ km/s) may be reconciled with its observed large diameter which would otherwise seem to imply a very high expansion velocity ($v \sim 10,000$ km/s).

The Cassiopeia A remnant is also found to be quite luminous in the X-ray region of the spectrum. Murray et al. (1979) report that Cas A radiates about 2×10^{35} erg/s in the 0.1 - 4 keV spectral range. This is about 20% of the power which this remnant radiates at radio frequencies. The presence of X-ray emission requires a mechanism for *continuously* supplying energy to the gas and particles making up the remnant; however, no central object is observed which could serve as a source of relativistic particles [see Figure 5-I update]. As will be discussed further on, the 14,200 years BP superwave would carry a

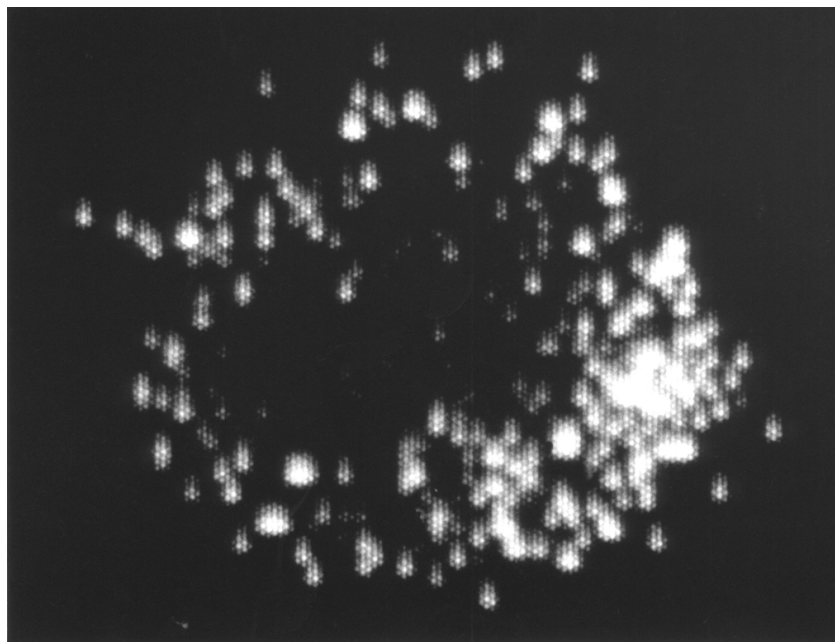


Figure 5.17. Spatial distribution of the high energy X-ray flux (normalized to total X-ray flux) for the Cassiopeia A supernova remnant (photo courtesy of S. Murray, Smithsonian Astrophysical Observatory).

sufficient amount of particle energy that it could reasonably power both the X-ray and radio emission observed from this remnant.

X-ray images obtained with the Einstein X-ray Observatory reveal a remnant morphology east-west asymmetry similar to that seen at radio wavelengths. For example, Figure 5.17 (photo courtesy of Stephen Murray, Smithsonian Institution Astrophysical Observatory) shows the distribution of the "hard" (high energy) X-ray flux (2.4 – 3.6 keV) normalized to total X-ray flux (0.1 – 4 keV), the light regions having a flux ratio greater than 0.25. Note that the west-southwest side of the remnant is unusually bright in hard X-rays as compared with the rest of the remnant. This bright region corresponds to the high intensity region observed on radio maps (compare with Figures 5.15 and 5.16) and is positioned about where a bow shock front would be expected to form if the nebula were being impacted by a cosmic ray blast travelling away from the GC.

Murray et al. point out that this western X-ray emission feature cannot be explained by shock heating models (i.e., heating arising from nebular motion relative to the interstellar medium) since optical observations reveal that this region is devoid of filamentary material. They suggest that this emission is nonthermal, possibly synchrotron emission from relativistic particles accelerated at the remnant's outer boundary by time-varying magnetic fields. Moreover they note that such relativistic particles must be injected continuously since in order to generate synchrotron emission at X-ray wavelengths the radiative lifetime of these particles would be relatively short (<10 years vs. 300 years for the age of Cas A). But if the accelerated particles were originating from within the remnant shell, as Murray et al. propose, then the observed asymmetrical distribution of this emission seems unexpected. Moreover the observed location of this energetic region on the remnant shell would have to be regarded as purely fortuitous. On the other hand, the GEH is able to simultaneously account for the *continuous* injection of relativistic particles, for the *asymmetrical* mode of their injection, and for the fact that this inject region *faces the GC*.

Murray et al. also report the detection of thermal X-ray radiation from an emission plateau surrounding the remnant which they interpret as a blast wave shock front interacting with the ambient interstellar medium. To explain the X-ray emission they require that the remnant be significantly decelerated with a ratio of swept up material to ejected material of >1.7 . However, Brecher and Wasserman (1980) call into question the shock heating scenario. They note that since the Cas A remnant has suffered little deceleration over its 300-year lifetime, the amount of interstellar material that its shell has swept up must be correspondingly small, on the order of 10% of the mass of the shell. The GEH, though, offers an exit from this bind. Namely, the observed X-ray emission could be powered by propagating shock fronts driven by the relativistic electron blast. Moreover, nonthermal emissions such as bremsstrahlung and synchrotron, are available as additional possibilities. Either of the above mechanisms would also be able to explain the X-ray emission detected from the high velocity optical knots as well as from the quasi-stationary flocculus.

According to theoretical considerations, the flux density of Cas A should be decreasing at the rate of $\sim 1\%$ per year since as the remnant expands there would be an adiabatic loss of energy of the trapped relativistic particles along with a decrease in the magnetic field strength (Dickel and Greisen, 1979; Shklovsky, 1968, Section 7). Observations confirm that there is a rate of decrease of about this magnitude; however, also a flattening of the radio spectrum is indicated. That is, the flux density of the lower frequency radio emission is observed to be decreasing faster than the flux density of the higher frequency radio emission. For example, the rate of decrease is observed to be $-0.86 \pm .02\%/yr$ at 1420 MHz, $-1.2 \pm .4\%/yr$ at 151 MHz, and $-1.9 \pm .5\%/yr$ at 38 MHz (Read, 1977). Dickel and Greisen (1979) note that spectral flattening is normally thought to be associated with acceleration processes, and suggest that some diffuse acceleration mechanism must be in operation in the remnant shell. They suggest that the energy for this particle acceleration is derived from the kinetic energy of the expanding shell. However, it is equally plausible to suppose that particles are being injected into the remnant from an external source, e.g., from the 14,200 years BP superwave.

Another unusual phenomenon, which may indicate that particle acceleration processes are coherently fluctuating over a large area of the remnant, is the "soft radio flare" reported by Erickson and Perley (1975) and confirmed by Read (1977). Between 1967 and 1975-76 the flux density of Cas A at 38 MHz was observed to increase by $\sim 8\%$ at a time when the trend line of previous measurements predicted that a decrease of 16% ($-1.9 \pm .5\%/yr$) should be taking place. The 1975-76 flux density measurements represent a 28% increase over the projected 1975 trend line value. Read points out that such a large increase cannot be accounted for by the brightening of single features due to their motion through the ambient medium. For example, a single filament moving at 6000 km/s in 7 years would sweep out an area of only $\sim 10^{-2}$ l.y.², or $\sim 10^{-4}$ of the cross-sectional area of the remnant; and as Read shows, the maximum increase in 38 MHz luminosity expected from a single compact component is only about a factor of two. Hence, the expected change in overall remnant luminosity would be $<0.01\%$. As one alternative, he suggests that the brightening may involve many radio knots or filaments functioning coherently, and that this brightening may be due to a certain stage reached simultaneously by many parts of the remnant as a result of its kinetic evolution. However, it is also possible that such coherent brightening at 38 MHz is produced by an enhanced density of low energy electrons ($\gamma \sim 80$) propagating *relativistically* across the surface of the remnant transverse to our line of sight.

Another interesting finding reported by Dickel and Greisen (1979) is that over the period of 9 years between 1967 and 1976 there have been significant changes in the brightness of most of the compact radio components. They find that 59 radio knots have been getting weaker at the mean rate of about $-3.5 \pm 1.5\%/yr$, while 24 knots have been

getting brighter at the mean rate of $+2.7 \pm 2.5\%/yr$. When all compact sources are averaged together a net decrease in flux density of $-1.7\%/yr$ is found. They note that the brightening features, which indicate regions where particle acceleration is taking place, are scattered around the remnant in a random manner. However, large regions still remain within which a net brightening or a net dimming is taking place, some of these regions extending over distances of as much as 8 l.y. (3 minutes of arc). It might be pointed out that such regional coherent behavior is difficult to explain in terms of local particle acceleration effects produced by random interactions of the remnant with the ambient medium. It is possible, though, that as in the case of the soft radio flare, these regions of coherent behavior constitute evidence that Cas A is being externally excited by a propagating blast of cosmic rays, a blast that varies its intensity over time.

In the future a series of high resolution VLBI radio maps should be made of Cas A, about once every year or maybe even as frequently as once every two months, to see if regions of enhanced radio surface brightness are observed to propagate at relativistic speeds in a west-to-east direction across the surface of the remnant. Special attention should be paid to the "bow shock front" region on the western side of the remnant which faces the GC. Since this side of the nebula would make a low angle of inclination to the plane of the hypothesized superwave front, superluminal motion of surface brightness changes could be observed in this region. Evidence of such coherent relativistic behavior would strongly favor the 14,200 years BP superwave model. Simultaneous sequential monitoring at optical wavelengths should also be carried out in view of the fact that the optical morphology of Cas A continues to change on a time scale of only a few years, as reported by van den Bergh and Kamper (1983).

A definite contrast may be seen in comparing Cassiopeia A to the Tycho SNR. While both remnants are of about the same age (300 years vs. 420 years) and in the same general part of the sky, Cas A has a surface brightness over two orders of magnitude greater. Moreover, as may be seen by comparing radio maps of Cas A (Figures 5.15 and 5.16) to the radio map of Tycho (Figure 5.18), the shape of the Tycho remnant is considerably smoother, more regular, and more symmetrical about its point of expansion. Radio knots such as those observed in Cas A are absent in Tycho. Dickel and Spangler (1979) attribute the differences between these two SNR to differences in the ambient medium surrounding each remnant. They suggest that Tycho is expanding adiabatically into a relatively uniform, low density interstellar medium, whereas Cas A is expanding into a medium that has been highly disturbed by the ejection of a presupernova shell. However, Chevalier, Krishner, and Raymond (1980) and Brecher and Wasserman (1980) come to the opposite conclusion. Chevalier et al. suggest that the Tycho remnant is *decelerating* and is in the blast wave stage of evolution with a ratio of ejected mass to swept-up mass of ~ 0.08 . Also, Brecher and Wasserman suggest that Cas A is still freely expanding with a ratio of ejected mass to swept-up mass of 8 to 10. Thus it appears that another reason must be found to explain the differences between these two remnants.

The superwave scenario would suggest that the differences between Cas A and Tycho are due to the positions of these remnants with respect to the 14,200 years BP event horizon. In the case of Cas A, whose position is well known, the proximity is very close. In the case of Tycho, there is some question as to its exact distance from the Earth. Thus it is quite possible that Tycho does not coincide with the horizon and instead is just beyond it in a region of low Galactic cosmic ray density. Tycho, like SN 1006, may be a good choice for studying the behavior of a young SNR in a region where the ambient cosmic ray environment has a minimal influence.

[**UPDATE:** Tycho's distance has now been determined to be $8,150 \pm 0.300$ l.y., placing it in the immediate vicinity of the 14,200 years BP superwave event horizon; see Figure 5.4.]

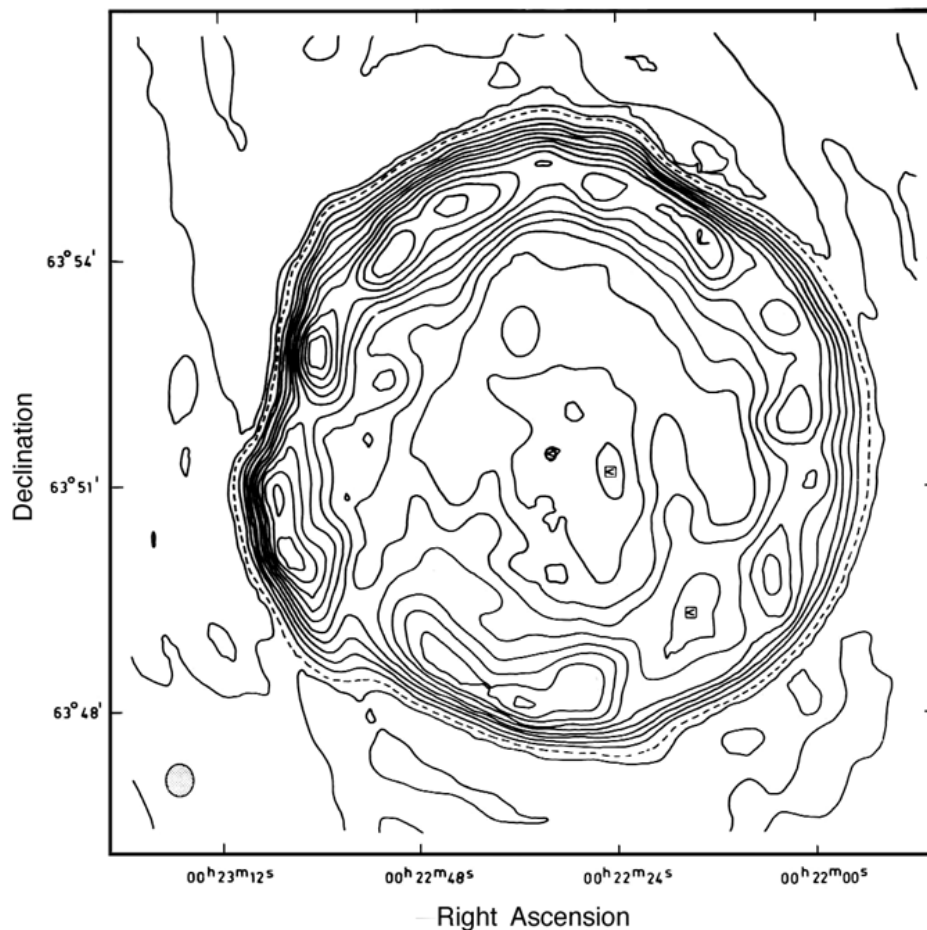


Figure 5.18. A 21 cm radio map of the Tycho supernova remnant (Strom and Duin, 1973).

The proposed 14,200 years BP superwave could account for the nonthermal radio emission from Cas A as follows. Woltjer (1972) has modeled the radio emission from Cas A with a synchrotron model having a field strength of $B \sim 3 \times 10^{-4}$ gauss and a total particle energy of $U_p \sim 3 \times 10^{48}$ ergs. The Cassiopeia A remnant presently has a cross-sectional area of ~ 100 l.y.² and hence at a galactocentric distance of 28,000 l.y. would intercept $\sim 10^{-8}$ of the total cosmic ray intensity projected by the superwave. If the cosmic ray intensity were at 50% of its peak value 300 years after the time of initial event horizon passage, the Cassiopeia remnant would be presently intercepting cosmic rays at the rate of $\sim 3.0 \times 10^{39}$ ergs/s. So, the required relativistic particle reservoir could be built up in the space of 30 years. Consequently, from an energetics standpoint, the 14,200 years BP superwave model is satisfactory.

The 14,200 years BP superwave could also account for the observed X-ray emission. For example, given that the X-ray luminosity of Cas A in the 0.1 to 4 keV energy band is 2.2×10^{35} ergs/s (Murray et al., 1979) and that the projected area of the remnant is $\sim 10^{38}$ cm², the required illuminating flux would be: $2.2 \times 10^{35} / 10^{38} \sim 2 \times 10^{-3}$ ergs/cm²/s. This is well within the energy requirements of the 14,200 years BP superwave, which as proposed would have an energy intensity about 10^4 -fold greater. In summary, the GEH opens up new possibilities in accounting for many puzzling features observed in Cassiopeia A.

5.5 THE EXTRAGALACTIC SUPERNOVAE SN 1970g AND SN 1979c.

The discussion of supernovae presented in Sections 5.2, 5.3, and 5.4 would not be complete without covering the subject of extragalactic supernovae. It is estimated that supernovae occur in our own Galaxy only about once every 50 years (Ilovaisky and Lequeux, 1972a). Those that have been historically recorded constitute even rarer events, seven having been observed in the last 1000 years, or about one observation every 140 years. None have been observed in our Galaxy since the era of modern astronomy began. Thus most of what we know about supernovae and very young supernovae remnants (< 100 years old) comes from observing such events in other galaxies. This section reviews the unusual radio behavior of two extragalactic supernovae SN 1970g and SN 1979c. As is demonstrated below, many of the properties of these very young remnants may be accounted for if we assume that a blast of relativistic electrons is propagating through interstellar space in the immediate environment of these remnants.

In the preceding sections (5.3 and 5.4) on the Crab and Cas A SNRs, it was suggested that the relativistic particle content of a supernova remnant increases as its cross-sectional area increases, allowing the remnant to absorb a greater energy flux from the passing superwave. Such a model could explain why the radio emission from supernovae 1970g and 1979c did not appear until a few months to a year after the explosion. However, note that the radio luminosity of these supernovae was not observed to increase with respect to time in a simple power-law manner, as might be expected with an expanding target exposed to a constant exterior particle flux. Take for example SN 1970g observed in galaxy M 101. In this particular supernova remnant the radio emission plateaued after the first year, varied erratically for about four years, and then on the fifth year disappeared below the threshold of detection; see items (1) and (2) of Table X and Figure 5.19. This unusual emission

TABLE X
CHARACTERISTICS OF SUPERNOVA SN 1970g

-
- 1) The radio emission appears at centimeter wavelengths about half a year to one year after maximum light. After 1.4 years the radio power spectral density at 21 cm reaches a value of about 10 Cas A's. It holds this level for 2 years and then declines to less than 4 Cas A's by an age of 4.2 years.
 - 2) The radio spectrum is nonthermal.
 - 3) The brightness temperature at a radio wavelength of 21 cm and a remnant age of 1.4 years is $>10^7$ °K (possibly $>10^8$ °K).
 - 4) At 1.5 years (for an expansion velocity of 10,000 km/s and a diameter of $\sim 10^{17}$ cm) the source may be modeled with an energy of a few times 10^{46} erg and a magnetic field of about 10^{-2} Gauss.
 - 5) The observed H_α luminosity indicates a free-free optical depth at 11 cm of at least 10^4 cm. Thus, either the radio emission is generated on the outside of the expanding shell (jeopardizing models in which the source of relativistic particles is internally generated), or else the main portion of the gas is in radially disposed filaments shielding only a small fraction of the radio emitting volume.
 - 6) The radio emission is highly variable, changing by a factor of $1\frac{1}{2}$ within a few months or by a factor of 2 to 3 over a year.
 - 7) The data give some indication that the peak arrives later and lasts longer at longer wavelengths.

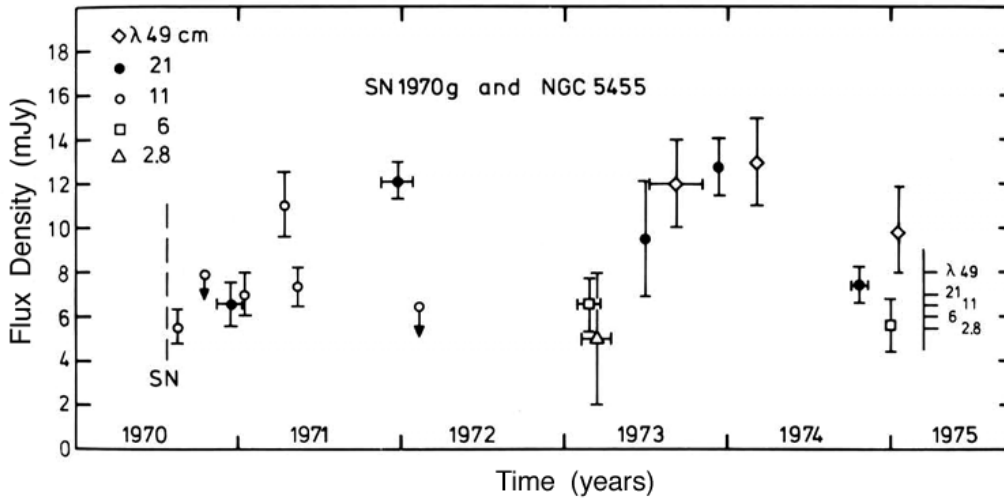


Figure 5.19. Measurements made of the radio emission of SN 1970g and of the adjacent H II region NGC 5455. The spatial resolution was such that the supernova emission could not be separated from the thermal radio background radiated by NGC 5455. So, the estimated steady-state emission level for NGS 5455 is given, for subtraction, by the scale to the right-hand side of the figure (Allen et al., 1976).

behavior, though, could be explained with a superwave model if it is assumed that the observed radio emission is primarily linear bremsstrahlung and/or Cerenkov radiation, rather than synchrotron radiation. With the former two mechanisms the observed amount of radiation would depend on: a) the size of the remnant (i.e., the amount of flux intercepted), b) on the intensity of the cosmic ray flux in the vicinity of the remnant at that time, and c) on the column density of the remnant.

Consider the following scenario for the temporal behavior of SN 1970g. Assuming that the remnant is expanding at $\sim 10^4$ km/s, and consists of 10_{\odot} of gas, then after 1 year the column density in the shell would be ~ 2 g/cm², and after 5 years it would have dropped to ~ 0.1 g/cm². If the radiation length for electrons travelling through the gas in the remnant shell is $X_0 \sim 40$ g/cm², then at $t = 1$ year an electron passing through the shell just once would encounter 2 g/cm²/ $X_0 = 0.05$ radiation lengths of matter, and at $t = 5$ years, 0.0025 radiation lengths of matter would be encountered. In either case, many passes through the shell ($10^2 - 10^4$) would be required for the kinetic energy of the injected cosmic rays to be converted entirely to radiant energy. But this would not be a problem if it can be assumed that the intercepted cosmic ray electrons are captured and held within the shell by the remnant's frozen-in magnetic field. While the amount of cosmic ray flux that the remnant intercepted would increase according to the square of the remnant radius, the column density of the shell would at the same time be decreasing according to the inverse square of the remnant's radius. Consequently, the rate at which the remnant produced radiation would probably plateau. The final drop in radio intensity from SN 1970g after 5 years could have been due to a drop in the intensity of the incident cosmic ray flux carried by the superwave.

As a demonstration that a superwave could account for the radio emission radiated from very young SNRs, consider the case of supernova SN 1979c observed in M 100. The radio emission from this supernova was far more intense than that from SN 1970g and hence serves as an extreme example. Assuming a perfectly flat radio spectrum, Weiler et al. estimate the radio luminosity of SN 1979c, integrated over the frequency range $10^7 - 10^{11}$ Htz to be $\sim 2 \times 10^{38}$ ergs/s, one year after maximum light (Weiler et al., 1981). This radio output, equivalent to ~ 180 times the radio output of Cassiopeia A, is about 20 times stronger

than that of SN 1970g. Assuming an expansion velocity of $\sim 10^4$ km/s, the size of the 1979c SNR shell would be $\sim 3 \times 10^{16}$ cm one year after peak light. Thus, SN 1979c would present a cross-sectional area to the hypothesized superwave of 7×10^{32} cm². So, for SN 1979c to be radiating at its observed radio luminosity, its shell would have to be absorbing an energy flux of at least 3×10^5 ergs/cm²/s. This figure would have to be inflated by probably several fold to account for energy radiated at shorter wavelengths. By comparison, the 14,200 years BP superwave proposed for our own Galaxy, at a distance of 30,000 l.y. would present a peak energy flux of ~ 50 ergs/cm²/s, about 10^4 -fold less. So, the unusually high radio luminosities observed in both SN 1970g and 1979c may be accounted for by a superwave model but would require a superwave of much greater intensity as compared with the 14,200 years BP superwave.

Several characteristics of SN 1970g reported by Allen et al. (1976) are listed in Table X. In particular, it is seen that the radio emission above background, identified with SN 1970g, lasted for about 4 years (see Figure 5.19). Also, the intensity of this radiation was observed to vary irregularly in intensity by a factor of as much as 3 over time periods ranging from a month to a year. Moreover, the emission peaks appeared to arrive later and last longer at longer wavelengths. Similar behavior is now being observed in SN 1979c (Sramek, 1981; personal communication). Such erratic behavior is difficult to explain with conventional models of SNRs. However, it is interesting to note that time-variable behavior of this sort is observed in the radio emission from active galactic nuclei; see Chapter 2, Section 2.1.1. The similarity between nonthermal radio emission outbursts in active galactic nuclei and in SNRs could be linked to a common cause: the interaction between a propagating blast of cosmic rays (of galactocentric origin) and intervening clouds of gas or supernova remnants. As mentioned in Section 2.1.2, longer wavelength radiation from a superwave would be expected to be generated by less energetic electrons lagging behind those with higher Lorentz factors. Compare statement (7) of Table X with the behavior shown in Figure 2.4 on **p. 24** and with item (d) on **p. 34**.

The time scale of the radio flux changes provides a clue which suggests that a coherent blast of relativistic particles may be responsible. For example, as seen in Figure 5.19, about 9 months after peak light the radio flux at 11 cm was observed to change by a factor of 3 over a period of a month. Given that the radial expansion velocity of the SNR was $\sim 10^4$ km/s, by 9 months the shell would have had a diameter of $\sim 5 \times 10^{16}$ cm. So for flux variations to occur in a coordinated fashion over the entire remnant in less than one month (i.e., $\sim 2.5 \times 10^6$ s) these effects would have to propagate through the remnant at a velocity of at least $v = d/t \sim 2 \times 10^{10}$ cm/s, or at about at least 2/3 of the speed of light. The radio flare observed in Cas A (discussed in the preceding section) may be a similar type of phenomenon.

It has been shown in this section that the superwave model can account for the unusual radio behavior of SN 1970g and 1979c. The arguments made earlier for the interpretation of the Crab Nebula and Cassiopeia A are, therefore, strengthened.

CHAPTER 6

SUPERWAVE EVENT HORIZONS OF THE MIDDLE AND LATE HOLOCENE

6.1 ENERGETIC ACTIVITY ON THE 6000 BP SUPERWAVE EVENT HORIZON

It appears that several superwaves more recent than the 14,200 years BP superwave, but of lesser magnitude, passed by the Earth during the Holocene Epoch. One such event appears to have passed the Earth about 6000 BP. The presence of this horizon was inferred partly from climatic and paleomagnetic evidence discussed in Subsection 7.3.1, and partly from astronomical evidence discussed below. In this section it is demonstrated that when the positions of certain highly energetic sources are plotted on a polar graph of the Galaxy, such as that shown in Figure 6.1, a strong correlation is found with the position of the 6000 BP event horizon. The discrete stellar objects and nebulae discussed below have been selected because published accounts consider them to be unusually peculiar in certain respects, and hence of particular astronomical interest. Of course, such appraisals have a strong subjective component and the distances to these objects are not accurately known. So, the evidence collected below should not be taken as a definitive proof that a one-to-one correlation exists between objects exhibiting "unusual" energetic activity and those having a close proximity to the 6000 BP event horizon.

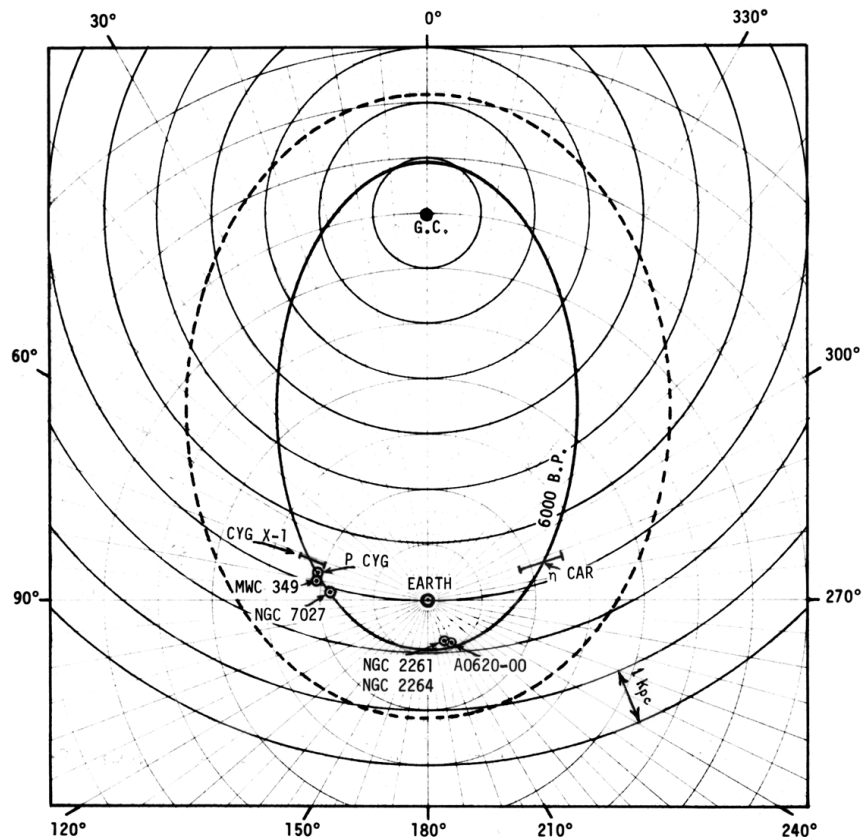


Figure 6.1. Positions of several point sources showing unusual energetic activity and their location relative to the 6000 years BP superwave event horizon.

6.1.1 The Cygnus Region

About 2 kpc from the Sun in the constellation of Cygnus a particularly energetic region is found, located about where the 6000 BP Event Horizon would cross the Carina-Cygnus spiral arm. A large region of diffuse soft X-ray emission has been discovered to extend from about $\ell = 65^\circ$ to $\ell = 90^\circ$, with a galactic latitude width of about $15 - 20^\circ$; see Figure 6.2. Cash et al. (1980) find that the emission spectrum from this region indicates the presence of interstellar gas heated to about 2 million $^\circ\text{K}$. The blank region in the midst of the X-ray emission, and which probably absorbs much of the radiation in its path is called the Great Rift of Cygnus. This massive dust lane is aligned with the Galactic equator and is about 600×1200 l.y. in extent. The Cygnus Rift is about 4500 l.y. away, so it has been estimated that the region of hot gas behind it lies at a distance of about 6000 l.y. (~ 2 kpc). Cash et al. (1980) estimate that about 10^{52} ergs (about 20 times the energy content of a typical supernova) are contained in this X-ray emitting gas. To explain such a large luminosity, they have proposed that this "superbubble" of hot gas was built up gradually from the energies of about 100 supernovae occurring in a coordinated fashion over a period of some 3 million years.

The superbubble interpretation places strong emphasis on the ring-like morphology of the large scale X-ray distribution. The ring shape, however, could be an artifact of the

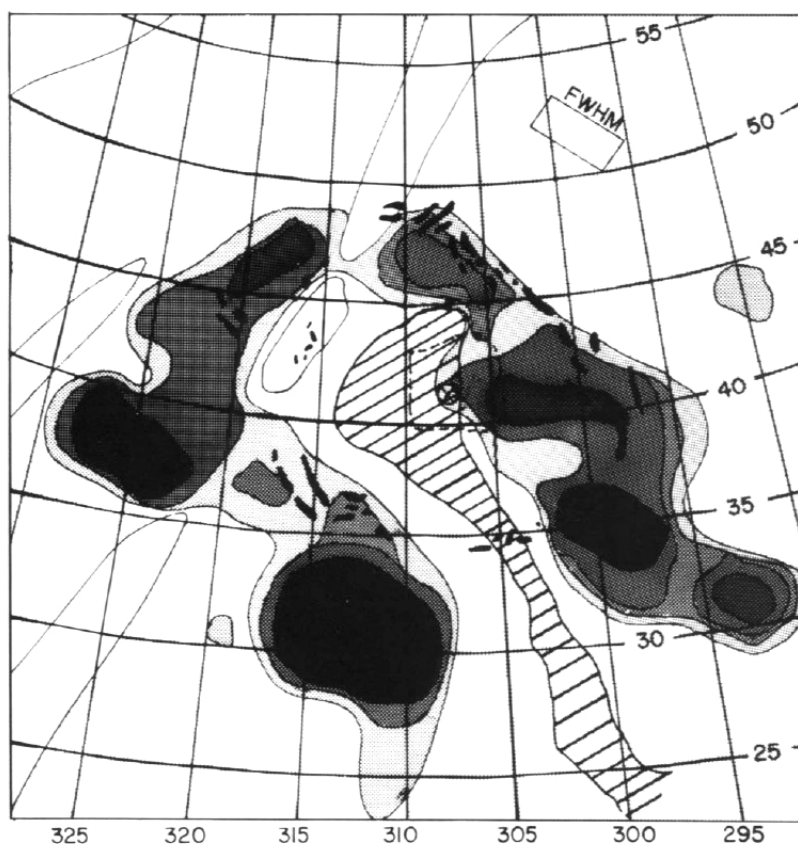


Figure 6.2. X-ray intensity map of the Cygnus region in the 0.5 – 1.0 keV energy band. Darkest contours represent regions with the highest counting rate. Small dark forms are $\text{H}\alpha$ filaments. The cross-hatched region marks the area of strongest optical extinction caused by the Great Rift of Cygnus. The circle at $\text{RA} = 308^\circ$, $\delta = +41^\circ$ ($\ell = 80^\circ$, $b = 0^\circ$) marks the position of the Cygnus OB2 association and the dashed line square surrounding it indicates the area covered by the Cygnus X radio source (Cash et al., 1980).

obscuring presence of the Cygnus Rift. Thus, were it not for this absorption, it is very likely that this entire region would be visible in soft X-ray emission. Indeed, uniform emission over this entire region is seen at γ -ray wavelengths and is actually strongest in the rift region; see Figure 6.3 (Protheroe, Strong, and Wolfendale, 1979). Protheroe et al. suggest that the γ -ray emission is due to Galactic cosmic rays of solar neighborhood concentration interacting with neutral and molecular hydrogen which exists in greater quantities in this region at distances of 1– 2 kpc. According to the GEH, on the other hand, at least a portion of this γ -ray enhancement would be primarily due to elevated levels of cosmic rays.

The Cygnus region is particularly active at longer wavelengths also. Campbell et al. (1980) report that this region has a particularly high concentration of far infrared sources. Also, the region centered around ($\ell = 79^\circ$, $b = 0^\circ$) is a strong source of CO emission (Protheroe et al.; after Cong, 1978). Weaver and Williams (1973) find an extensive region of equatorial neutral hydrogen emission centered at ($\ell = 75^\circ$, $b = +1^\circ$). Moreover, when photographed in H_α light, the whole Cygnus region reveals the presence of a substantial amount of ionized hydrogen gas (Cash and Charles, 1980). All of these observations are consistent with the suggestion that the entire Cygnus region is being energized by the 6000 years BP superwave.

NGC 7027. This compact H II region (diameter of ~ 0.34 l.y.) is located in the Cygnus region near the proposed 6000 BP Event Horizon (at $\ell = 85^\circ$, $d = 1.8$ kpc). It has the richest emission-line spectrum of all the planetary nebulae (Burnham, 1978, p. 749), and is also one of the most luminous, radiating at a rate of $2.3 \times 10^4 L_\odot$ mostly in the infrared in the 1 – 300 micron wavelength region (Telesco and Harper, 1977). Allen (1975, p. 190) has emphasized the unusual nature of NGC 7027, pointing out among other things that of all planetaries it is the brightest at 10 microns, and is also a very strong radio source. Low and Kleinman (1968) have pointed out that the infrared spectrum of this nebula is similar to that of the Seyfert galaxy NGC 1068.

It might be speculated that dust and gas propelled by the 6000 years BP superwave have activated a star embedded in the nebula and that this stellar source, in turn, powers the nebula's infrared emission. The energy flux from the nebula is about one to two orders of magnitude too high to itself be accounted for by the 6000 years BP superwave. However, superwave cosmic rays would be able to account for the strong ionization observed in the nebula, something which is difficult to explain otherwise since ultraviolet photons from an embedded stellar source would be heavily attenuated.

It should be added that there are other infrared planetary nebulae which are not aligned with a superwave event horizon, an example being NGC 6523 (M 8), which is found at $\ell = 7^\circ$, $d = 1.5 - 2$ kpc. But these do not share many of the unusual features of NGC 7027.

MWC 349. This is a particularly unusual and controversial object, located in the Cygnus region at $\ell = 80^\circ$, $d = 2.1$ kpc. It does not seem to fit most conventional stellar models. It consists of a central star surrounded by a nebula of diameter $\sim 10^4$ AU. The star has been classified as an early B-type star, although Ciatti, D'Odorico, and Mammano (1974) would put it in a special class designated BQ[]. This class includes hot stars having certain abnormalities in their spectra, e.g., a rich variety of very strong emission lines with some forbidden lines, CN absorption bands, and photometric variability. Based on their discovery of "winged" H_α spectral lines, Hartman, Jaffe, and Huchra (1980) have suggested that the central star is of the P Cygni variety and that it has a very low velocity stellar wind ($v \sim 50$ km/s) giving a mass loss rate of $\sim 3 \times 10^{-5} M_\odot$ /yr. In addition, MWC 349 exhibits a 300 °K thermal infrared continuum peaking at ~ 10 microns and a flat nonthermal spectrum extending from the radio to the far infrared, which has been attributed to bremsstrahlung emission from a hot, dense gas cloud (H II region) surrounding the central star (Harvey,

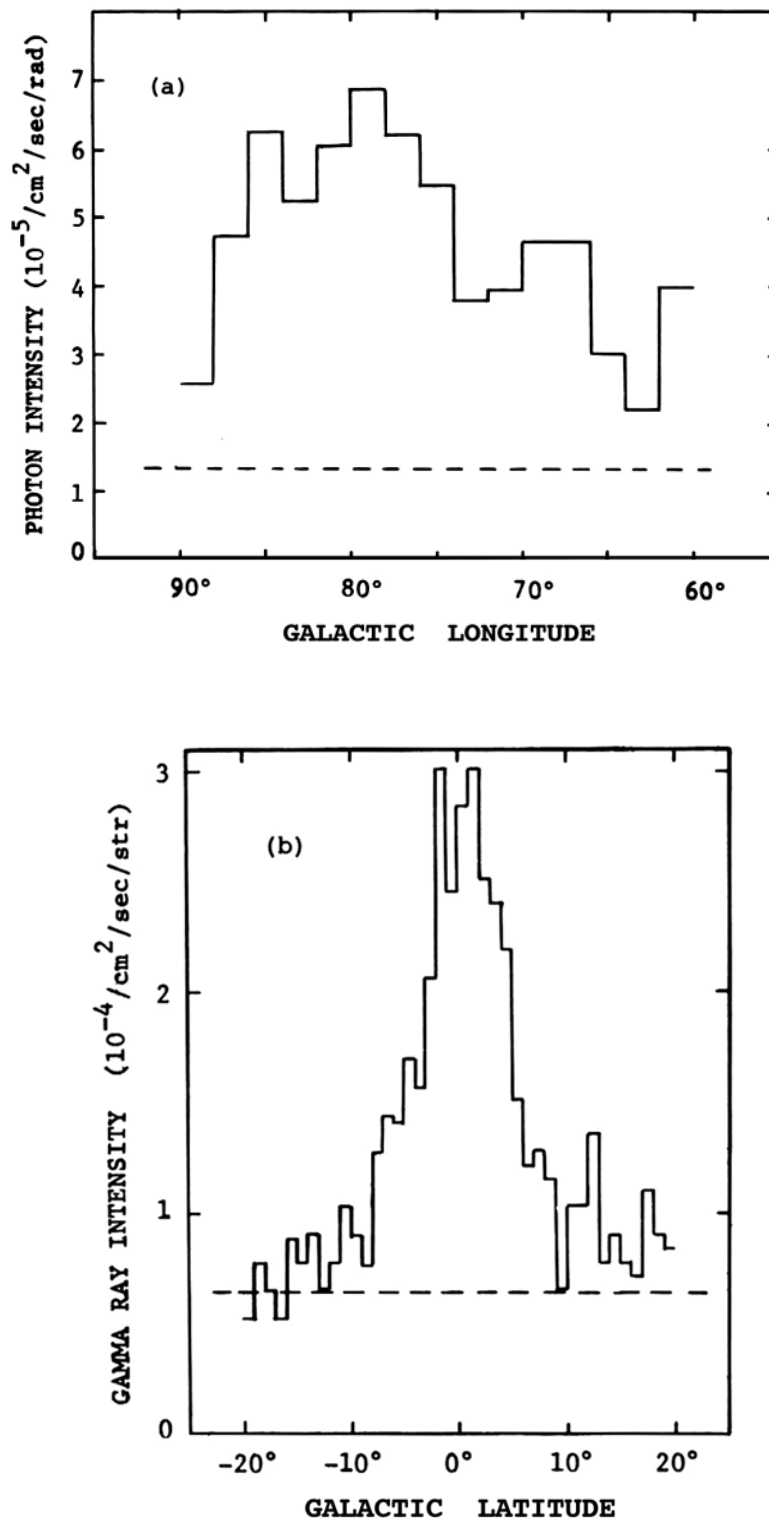


Figure 6.3. The distribution of γ -ray flux with respect to: a) galactic longitude, integrated over $|b| < 6^\circ$, and b) galactic latitude integrated over $60^\circ < \ell < 90^\circ$. The histograms give the observed flux ($E > 100$ Mev) after subtraction of the flux associated with the point sources CG64+0 and CG75+0. The dashed line indicates the adopted background level (adapted from Protheroe et al., 1979, Fig. 3 and 4).

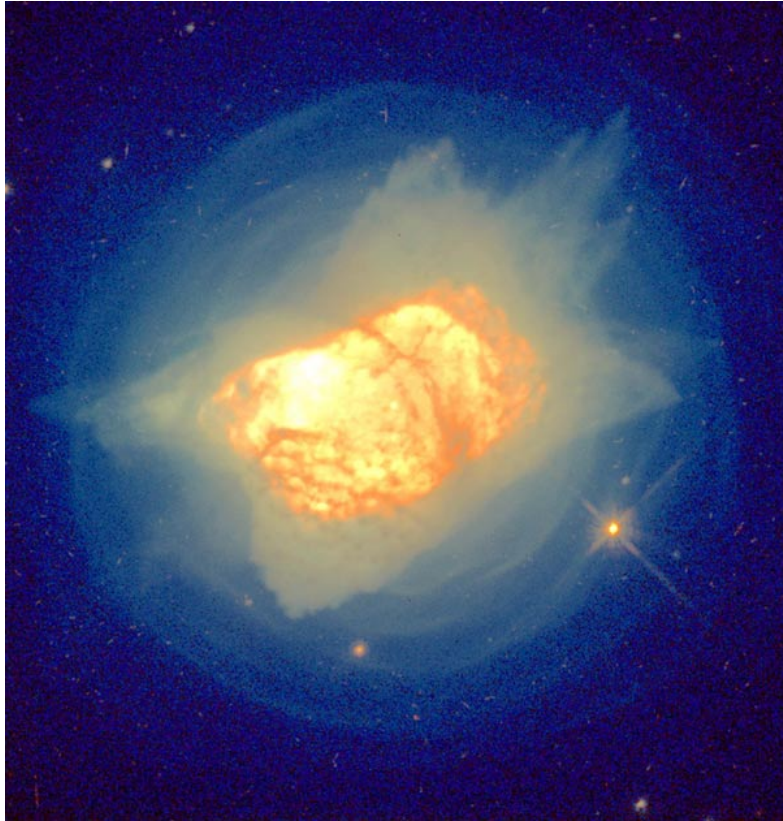


Figure 6-A. Planetary nebula NGC 7027 shown in a false color composite of two images made in 1996 with the Hubble Space Telescope in the visible and infrared spectral regions (courtesy of H. Bond and NASA).

Thronson, and Gatley, 1979). There is debate as to whether or not the circumstellar disk surrounding the central star contains dust (cf. R. Thompson et al., 1977; Harvey et al., 1979), and it is probably safe to say that the nature of this object is not well understood.

Other complications involve the rapid variability of MWC 349. For example, the hydrogen emission lines have been found to vary by a factor of 2 – 4 in a one day period (Greenstein, 1973). Also, the B magnitude (blue light) of MWC 349 has been observed to vary erratically, exhibiting as much as a factor of 4 change in luminosity on a timescale of months (Gottlieb and Liller, 1978). If the optical flux comes from a region of diameter 8×10^{16} cm (~ 0.08 l.y.) as inferred from 5 GHz radio measurements (Baldwin, Harris, and Ryle, 1973), then the short time scale of the B magnitude variations implies that relativistic effects may be involved. Perhaps the erratic variability of MWC 349 is associated with the passage of the 6000 years BP superwave through this region.

P Cygni. P Cygni, a star of spectral type B1, is located in the vicinity of the 6000 years BP event horizon at $\ell = 76^\circ$, $d \sim 2.1$ kpc (Burnham, 1978, p. 772). According to the summary presented by Burnham, P Cygni first appeared as a nova in 1600. Since that time it has varied considerably in intensity, twice disappearing from sight. Since 1715 it has stabilized at a luminosity of $\sim 10^{39}$ ergs/s ($\sim 3 \times 10^5 L_\odot$) which makes it one of the most luminous stars known in the Galaxy. Study of its spectrum reveals a set of broadened absorption lines possibly indicating the presence of three shells of gas travelling away from the star at velocities of -95 , -125 , and -210 km/s (de Groot, 1969). Because of its persistently

high luminosity and continued mass ejection, P Cygni has sometimes been called a "permanent nova," and has been compared to the infrared object η Carinae.

Cygnus X-1. Another puzzling astrophysical object is Cygnus X-1. It lies in the vicinity of the 6000 years BP event horizon at $\ell \sim 71^\circ$, $d \sim 2.0 - 2.5$ kpc (Burnham, 1978, p. 793). It is emitting X-rays at the rate of about 10^{37} ergs/s which makes it one of the brightest X-ray sources in the sky (Gursky and van den Heuvel, 1975). It has also been identified as a radio source. Since its X-ray output varies irregularly on time scales as short as 1 millisecond, it may be concluded that its emitting region is less than 1000 km in diameter. Cygnus X-1 has been optically identified with a binary star system in which one of the stars is invisible. This invisible component, which appears to have a mass of over 6 solar masses, is believed to be responsible for the X-ray emission. The inference that the emission region is very small has led to the proposal that this is a black hole.

6.1.2 The Carina Nebula

The Carina Nebula (NGC 3372) is the second brightest nebula in the sky, after M 42 in Orion; see Figure 6-B. This massive nebula covers $\sim 2^\circ$ of the sky and lies at $\ell \sim 288^\circ$ between 1.8 and 2.6 kpc from the Sun (Allen, 1979; Seward et al., 1979) in the midst of the Carina spiral arm. I have marked Carina's position in Figure 6.4, a diagram showing the positions of luminous supergiant stars which Humphreys (1972) has used to trace out the extent of the arm. Also, on this diagram the 6000 years BP event horizon has been superimposed for comparison.

The Carina Nebula contains large quantities of ionized hydrogen gas and many luminous early type stars. The Einstein X-ray observatory, detecting in the energy range 0.5 – 3.0 keV, has found a *diffuse* X-ray emission of about 6×10^{34} ergs/s coming from NGC



Figure 6-B. The Carina Nebula (or Keyhole Nebula) imaged in 2000 with the Hubble Space Telescope is over 200 light years in extent (courtesy of NASA).

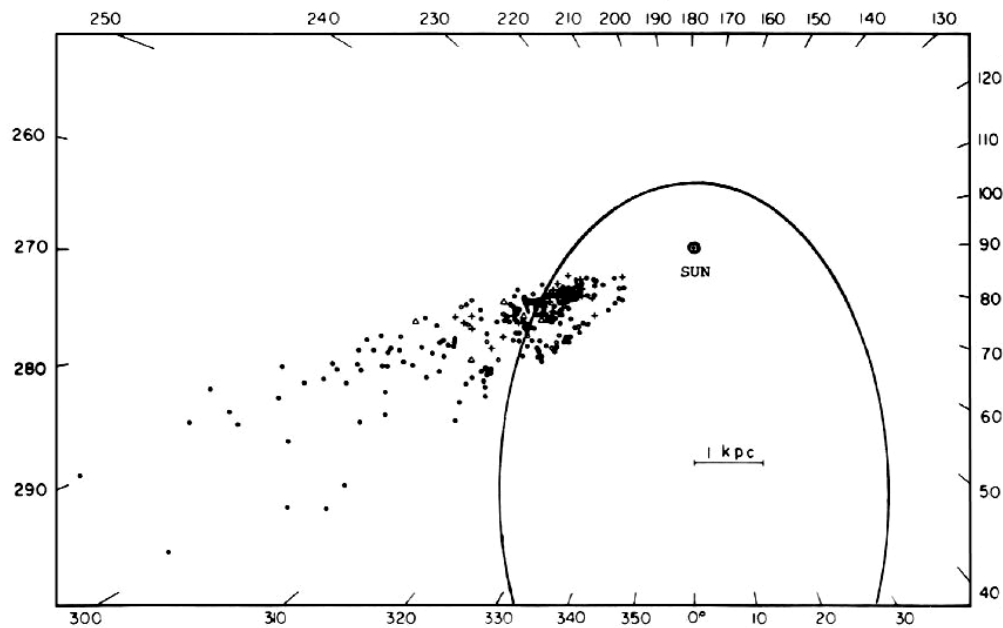


Figure 6.4. The space distribution of luminous supergiant stars in the Carina-Centaurus region $l = 282 - 305^\circ$ (O-B5, \bullet ; B5-A5, \cdot ; A5-K5, \circ ; and K5-M, $+$); the position of the Sun is indicated by \odot (Humphreys, 1972). The bar superimposed on Humphreys' diagram indicates the location of NGC 3372. Also, an ellipse has been added to illustrate the position of the 6000 BP event horizon.

3372 (Seward et al., 1979). Type O stars in the nebula were also found to be X-ray emitters, but together they only account for about one-fourth of the total emission from the nebula. Seward et al. suggest that the diffuse emission is most probably from very hot gas. They propose that this gas either comes from stellar winds of early type stars or was produced by supernova explosions which occurred within the last $10^6 - 10^7$ years. I would suggest the alternative that, as in the Cygnus counterpart, this gas is being heated by cosmic rays from the passage of a superwave. The same particles may also be responsible for producing much of the observed ionized gas. It is interesting to note that the Carina Nebula which subtends a projected area about 1% as large as the X-ray emitting region in Cygnus also is estimated to contain about 1% as much thermal energy, i.e., $\sim 10^{50}$ ergs. Thus, whether or not a region is unusually active may depend on how much gas is present to interact with the blast of cosmic rays. The Cygnus region may be a particularly high region of X-ray and γ -ray activity because the Cygnus spiral arm contains more gas than the Carina spiral arm. Indeed, optical measurements reveal that the extinction in the Cygnus region is quite high, whereas in the Carina-Centaurus region it is particularly low.

Eta Carinae. In the Carinae Nebula a very unusual object is found called *Eta Carinae*; see Figure 6-C. Its history has been very peculiar. It was first recorded in 1677 as a 4th magnitude star. But subsequent observations revealed that its luminosity was highly variable. It reached its apex of brightness in 1843 when it attained an apparent magnitude of -0.8 ; see Figure 6.5 (Tucker, 1980b). At this point it was brighter than every star in the sky except Sirius. During the 25 years that followed, it declined to one-thousandth of its peak luminosity. Since its decline in the late 1800's, it has remained variable at a low level of visual luminosity.

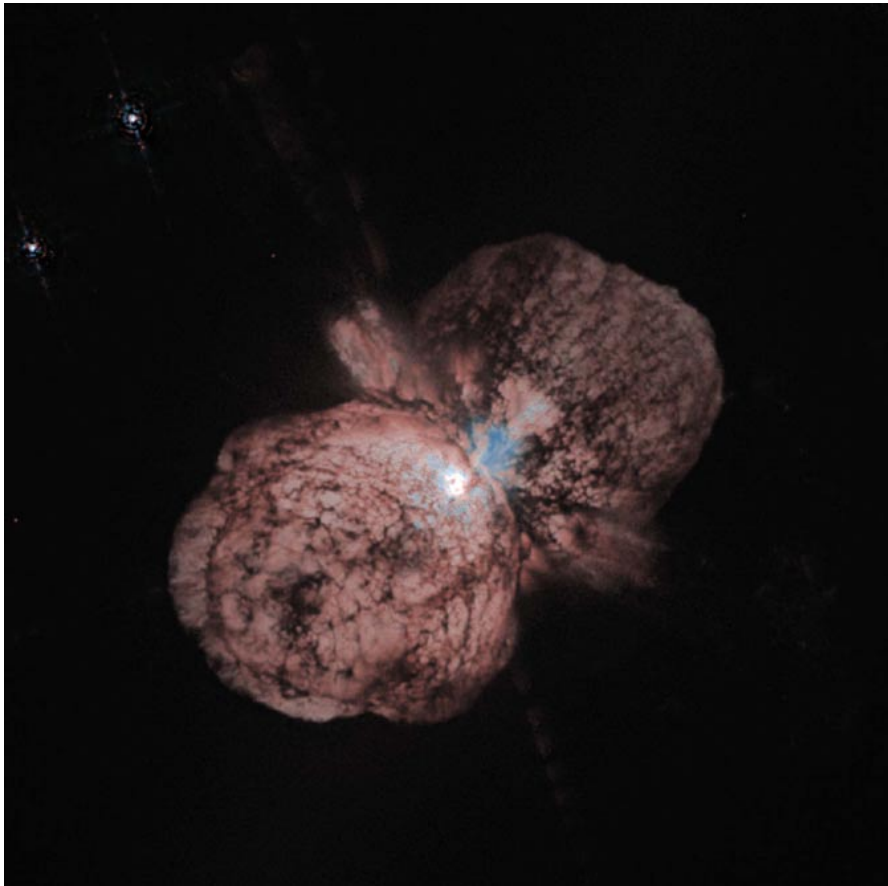


Figure 6-C. The star Eta Carinae and its nova generated nebula imaged by the Hubble Space Telescope in 1996 (courtesy of NASA).

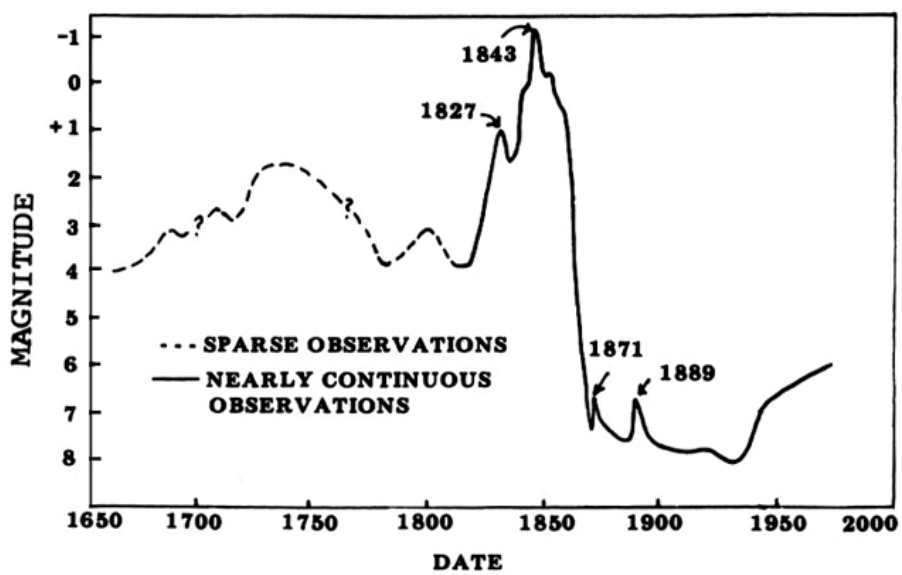


Figure 6.5. Variations of the apparent visual magnitude of eta Carinae over the period 1677 - 1979 (Tucker, 1980b).

It consists of a very bright *core* surrounded by a very bright, reddish-orange elliptical nebulosity called the homunculus, which in turn is surrounded by an elliptical *outer shell*. The homunculus is about $12'' \times 17''$ in extent (0.4×0.6 l.y. for a distance of 2.2 kpc). At 10 – 20 microns, it is the brightest infrared source in the sky, and of all objects has the strongest infrared excess. Measurements in the infrared indicate that it is presently radiating as intensely as it did at its visible peak in 1843. Taking its distance to be 1.8 kpc, Allen (1979) estimates a bolometric luminosity of $6 \times 10^6 L_{\odot}$. With the distance adopted here of 2.2 kpc this luminosity would have to be adjusted upward to $\sim 9 \times 10^6 L_{\odot}$. Thus far, no adequate model has been proposed for the energy output of the homunculus. Allen points out that if the observed illumination is due to a central star, it is very likely that this star would have exceeded its Eddington limit (the Eddington limit being the maximum allowable luminosity for which a star of a given mass remains stable.)

The outer shell of η Carinae has dimensions of $21'' \times 29''$ (0.73×1.0 l.y.) and its outermost condensations appear to be expanding away from the homunculus at a velocity of about 750 - 1000 km/s (Walborn, 1976). Burbidge (1962) has suggested that η Car is a presupernova, that is, a star undergoing expulsion of its envelope prior to its main supernova explosion. Yet, as Allen (1979) points out, since its outburst in 1843, Eta Carinae has released as much energy as some of the most energetic supernovae. For example, at a power output of 5×10^{40} ergs/s, it has released on the order of 2×10^{50} ergs. By comparison, type I supernovae are estimated to release on the order of 10^{47} - 10^{48} ergs, and type II on the order of 10^{51} - 10^{52} ergs. However, the nebula can be considered neither a typical supernova nor a typical nova. Its peak optical luminosity was several orders of magnitude greater than that observed for most novae and less than that of a type I or type II supernova. Moreover, most novae and supernovae ignite abruptly and diminish their luminosity within one year of peak light, whereas the main rise and fall of η Carinae's light curve spanned a period of almost 50 years. For this reason η Car is often referred to as a "slow nova."

Observations with the Einstein X-ray observatory reported by Seward et al. (1979) indicate that both the core and outer shell condensations of η Car are sources of intense X-ray emission, total output being estimated at 3.3×10^{33} ergs/s. They point out that the observed X-ray flux suggests a temperature greater than 10^8 °K, which is about an order of magnitude greater than what would be expected if the X-rays originate from an outgoing shock front. However, a Galactic superwave could be responsible for this emission. Given an outer shell area of 0.6 l.y.^2 the surface X-ray luminosity would be 6×10^{-3} ergs/cm²/s, which is four orders of magnitude less than the intensity proposed for the 14,200 years BP superwave.

6.1.3 The Monoceros Region

A0620-00. The transient X-ray source A0620-00 is one of the most unusual stars in the constellation of Monoceros. In galactic coordinates it is found at $\ell \sim 217^\circ$, $b \sim 7^\circ$, $d \sim 870 \pm 200$ pc (Oke, 1977), coincident with the 6000 years BP event horizon. In 1975 this object exhibited an energetic outburst that was observed at X-ray, optical, and radio regions of the spectrum. It is referred to as Nova Monocerotis 1975 and has been identified as a recurrent nova due to an eruption which occurred in 1917. However, Boley et al. (1976) report that the spectral behavior of the outburst does not resemble typical novae since for three weeks after its discovery no stellar absorption or emission lines were observed. Before the outburst, this star was observed to be a cool, faint K or M dwarf ($T \sim 3000 - 4000$ K). However, during the outburst its optical spectrum became very flat. Owen et al. (1976) also report that A0620-00 has a very flat spectrum at a radio frequency of around 1400 MHz, spectral index 0. They suggest that the emission is most probably *nonthermal*.

Oke (1977) and Oke and Greenstein (1977), though, have interpreted the optical emission with a thermal model and propose that it is produced by a hypothetical neutron star (optically invisible before the outburst) accreting gas from the K dwarf. However, there are several difficulties with this interpretation. First, as Oke points out, the neutron star would not be within the Roche Lobe of the K dwarf, so it would not be able to pull large quantities of material to its accretion disk by gravitational means. Moreover, the mass loss rate required to power the X-ray emission ($10^{-10} M_{\odot}/\text{yr.}$ to $10^{-7} M_{\odot}/\text{yr.}$) is many orders of magnitude greater than the mass loss rate expected from the stellar wind of normal K dwarf stars. As an alternative, Oke suggests that the K star might be ejecting gas to the neutron star in a manner similar to T Tauri ejection. However, the K star does not resemble a T Tauri star. Perhaps the 6000 years BP superwave hypothesized to be in this vicinity is the agent responsible for propelling nebular material onto the hypothesized neutron star.

NGC 2261. Hubble's Variable Nebula (NGC 2261), another unusual object in Monoceros, is located at $\ell \sim 204^{\circ}$, $d \sim 800$ pc, near the 6000 years BP event horizon. For a distance of 800 pc, the nebula would be about $1\frac{1}{2} \times 2\frac{1}{2}$ l.y. The nebula appears as if a strong wind is blowing it away from the star R Monoceros (R Mon) located in the nebula's southern tip. R Mon is highly variable in luminosity and has been observed to change its spectral appearance over the range A to late F (Burnham, 1978, p. 1205). It is heavily obscured by dust and consequently emits most of its energy (98%) in the infrared (Mendoza, 1968) at a luminosity of $\sim 700 L_{\odot}$. Its infrared continuum peaks in the vicinity of 3 microns, indicating a nebular temperature of ~ 1000 °K; see Figure 3.17 (p. 95). Canto, Rodriguez, Barral, and Carral (1981) have suggested that R Mon is a bipolar nebula whose stellar wind is focussed by a circumstellar disk of dust into two oppositely directed flows, one flow forming the visually observed conical nebula and the other flow being obscured by the circumstellar disk.

Photographs show that the outline of the nebula undergoes marked changes within a period of a few months, indicating velocities approaching the speed of light. Slipher has suggested that the nebula might be illuminated by reflected light from the embedded star and that variations in the output of this star are responsible for the nebula's brightness variations (Burnham, p. 1205). However, Bruck (1974) points out that the nebula is too large and too bright for R Mon to be the illuminating source. Stockton, Chesley, and Chesley (1975) attribute the emission lines in the nebula to S Monoceros, a luminous type O7 star which lies about 1° northwest of R Mon, i.e., at least 40 l.y. away.

Perhaps many of the unusual features of this nebula, such as its O II emission lines and its blue polarized optical continuum, are due to superwave cosmic ray electrons interacting with the nebular gas. The apparent relativistic motions in the nebula could be caused by blasts of cosmic rays propagating through the nebula in the anticenter direction. Thus the motion of NGC 2261 may involve a mechanism similar to that suggested for the propagating wisps observed in the Crab Nebula.

NGC 2264. This nebula in Monoceros ($\ell \sim 204^{\circ}$, $d \sim 0.8$ kpc) is distinguished as having the fourth largest collection of T Tauri stars, 37 according to the sample of Cohen and Kuhi (1979b). As discussed in Chapter 3, Section 3.3.2, some T Tauri stars may be normal dwarf stars in which nebular accretion has recently become initiated by the passage of a superwave. The conventional interpretation is that these are young stars in the process of being born. Other large concentrations of T Tauri stars are found in the Orion Nebula, Taurus-Auriga Complex, and NGC 7000/IC 5070 region. Of these, the last two associations appear to lie close to a more recent superwave event horizon discussed in Section 6.2. The Orion Nebula is a major region of energetic activity, but being at a distance of 0.5 kpc, it does not appear to lie on any of the proposed event horizons.

6.2 A 393 AD SUPERWAVE?

Chinese astronomers chronicled the appearance of a "guest star" in AD 393 which lasted for about eight months. This star-like object appeared in the asterism *Wei*, which corresponds to the tail of the celestial Dragon in Oriental astronomy or to the tail of the Scorpion in western constellations. Unfortunately, a more specific location for this event was not recorded. Stephenson (1979) suggests that this event may have been a supernova occurring at a distance of some 15,000 – 20,000 l.y. from the Earth, although it is also possible to interpret this event as a small scale Galactic explosion. An outburst from the Galactic Center would naturally have been catalogued in the asterism of *Wei* since this is the closest constellation to the GC.

The terrestrial record over the past 6000 years shows little evidence of any major climatic change. So if a superwave did pass the Earth about 393 AD, it would have had to have been a relatively minor event. However, the paleomagnetic record does indicate a reversal in the secular trend of the geomagnetic field intensity at about this time; see Figure 7.4(c) (p. 213). Also at about this time the Dome C ice core registered an increase in microparticle concentration beginning about 400 AD and reaching threefold higher by about 1400 AD (spanning 100 – 30 meters in log book depth); see Figure 8.1, curve-a, (p. 218). Whether these terrestrial effects can be attributed to an extraterrestrial cause such as the passage of a superwave cannot be stated with certainty at this time.

Another way to check for the presence of this superwave would be to plot the location of its event horizon and check whether it lies close to regions of unusual energetic activity. In particular, supernova remnants would serve as good indicators of the presence of superwaves because of their ability to temporarily trap relativistic particles into synchrotron radiating orbits. The locations of five well-studied supernova remnants (SN 1006, Vela XYZ, Cygnus Loop, Lupus Loop, and North Polar Spur) and the unusual circumstellar nebula V-V 1-7 are shown in Figure 6.6 together with the location of the 393 AD Event Horizon. The bar at $\ell \sim 140^\circ$ indicates the minimum and maximum distance limits to a shell of relativistic electrons which may be responsible for the polarized component of the diffuse Galactic radio background radiation (Heiles, 1976, p. 12). In the remainder of this subsection some unusual energetic features of the above mentioned nebulae are reviewed and the possibility is explored that a superwave may be responsible.

6.2.1 SN 1006

The remnant of the 1006 AD supernova is situated at $\ell \sim 328^\circ$, $b \sim 15^\circ$, and $d \sim 1.2$ kpc. Although presently the 393 AD event horizon lies about 600 ± 100 parsecs from this remnant, in 1006 AD at the time of the supernova explosion this event horizon would have been traversing through this location. It is possible that the passage of this proposed event horizon was instrumental in triggering this supernova; see discussion on p. 160. Note that this remnant is the only young remnant definitely known to lie in the interior of the region bounded by the 14,200 years BP event horizon.

Toor (1980) notes that thermal shock heating models have difficulty explaining the high X-ray flux observed in SN 1006, which amounts to $\sim 2 \times 10^{35}$ ergs/s in the 0.2 – 10 Kev range. He suggests that the X-ray emission is probably synchrotron radiation from relativistic electrons. However, since the lifetime of these electrons would be much shorter than the age of the remnant, a source of *continuous* particle injection is required. Toor suggests that such a source could be in the form of a rotating neutron star. However, there is no evidence for such an object since there is no apparent source of strong central X-ray emission. This problem, though, could be easily resolved by assuming that the tail end of the

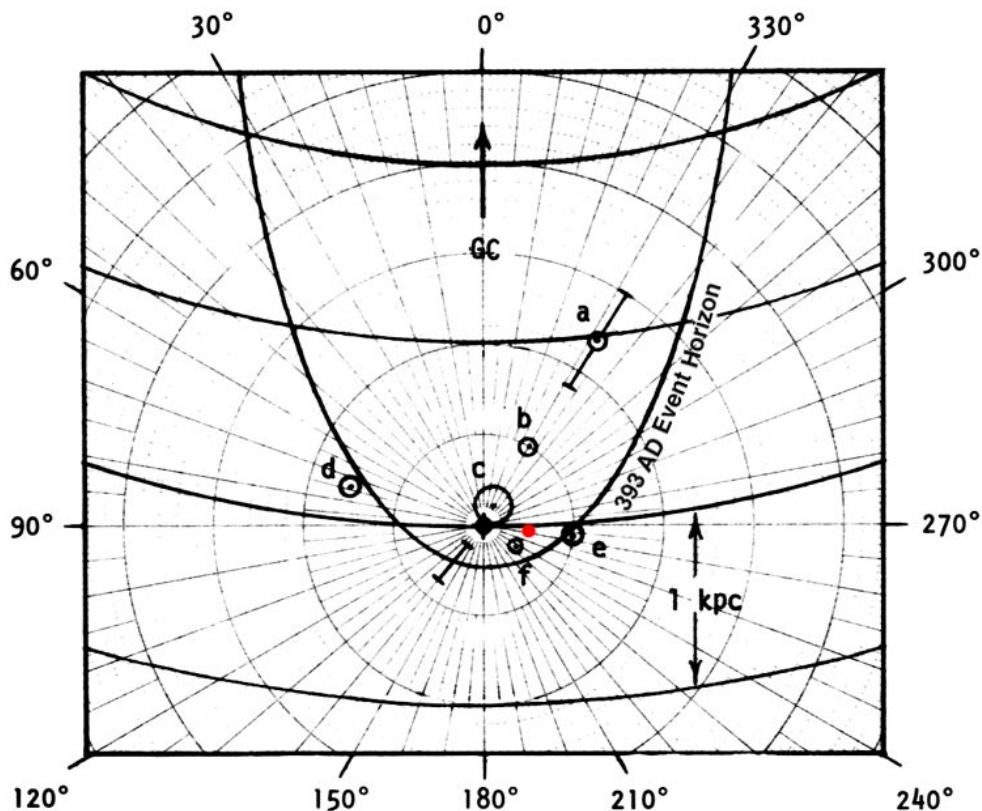


Figure 6.6. The 393 AD Superwave Event Horizon and its proximity to several emission sources: a) SN 1006, b) Lupus Loop, c) North Polar Spur, d) Cygnus Loop, e) Vela XYZ, and f) V-V 1-7. [The red dot indicates the revised location of the Vela XYZ remnant based on data published in 2000.]

393 AD Superwave is still propagating through this remnant and diffusely injecting cosmic rays. (Note that a similar "external source" mechanism has been suggested for the Crab and Casseopeia A remnants; see Sections 5.3 and 5.4.) SN 1006 exhibits an X-ray intensity of $\sim 3 \times 10^{-4}$ ergs/cm²/s, which is over 10^6 fold less than the intensity proposed for the 14,200 years BP superwave, and probably could easily be supplied by the 393 AD Superwave event.

6.2.2 The Vela XYZ and Cygnus Loop Remnants

The positions of both the Vela XYZ and Cygnus Loop supernova remnants coincide with the present position of the 393 AD event horizon. [**UPDATE:** As of 2000, the distance to the Vela XYZ remnant has been revised downward to 820 ± 100 l.y. (~ 250 pc). Consequently, it would not coincide with this event horizon.] Both of these remnants are relatively middle-aged, large-diameter remnants ($D \sim 40$ parsecs); however, both are also unusually strong sources of radio and soft X-ray emission. The soft X-ray emission has been interpreted as thermal emission from an optically thin plasma that has been heated to a temperature of $\sim 3 \times 10^6$ °K in Vela and $\sim 4 \times 10^6$ °K in Cygnus (Seward et al., 1971; Gorenstein et al., 1971). However, it has been pointed out that if the heating of the Cygnus Loop is due to interaction of this supernova remnant shell with the interstellar medium, then the required shock wave velocity would be on the order of 4 to 5 times greater than the observed velocity of the optical filaments (Tucker, 1971). This dilemma could be resolved if

this remnant were being heated externally by a superwave, rather than by the remnant's interaction with the ambient medium. A similar argument could be made for Vela XYZ.

A superwave could also account for the H_{α} emission from the Gum Nebula. This nebula is about 400 parsecs in diameter and its center is located about 460 parsecs from the solar system at a point very close to the location of Vela XYZ. Brandt et al. (1971) point out that the ultraviolet emission from stars in the interior of the Gum Nebula cannot account for the observed ionization and suggest instead that the Vela X supernova explosion, which occurred about 12,000 years ago, is responsible. An alternative explanation would be that cosmic rays associated with the 393 AD superwave are currently exciting this nebula. Earlier superwaves may have also been instrumental in exciting this nebula.

6.2.3 The Lupus Loop and North Polar Spur

The Lupus Loop, an old supernova remnant, is about 50 parsecs in diameter and is located about 500 pc from the solar system ($\ell \sim 330^{\circ}$) in the direction of SN 1006. The North Polar Spur, a very old supernova remnant, is about 230 ± 140 parsecs in diameter and is located about 130 ± 75 parsecs from the solar system in the direction of the Lupus Loop; see Section 3.3.2. Soft X-ray emission has also been detected from the Lupus Loop and North Polar Spur. On the basis of their soft X-ray spectra, temperatures of respectively 2.5×10^6 °K and $2 - 5 \times 10^6$ °K have been estimated for these two SNRs (Winkler et al., 1979; Borken and Iwan, 1977). To account for the observed X-ray emission the Lupus Loop has been modeled as a remnant in its adiabatic stage of evolution, in which blast-wave heating takes place as a result of the interaction of the expanding remnant with the interstellar medium. However, it is also possible that the high temperature of the Lupus Loop is a result of heating by the 393 AD superwave. Winkler et al. (1979) note that the spectrum of the Lupus Loop is similar to that of the Cygnus Loop, but that the flux is lower by a factor of 40. This reduced flux could be due to the fact that this superwave has passed out of the Lupus Loop vicinity several hundred years ago, whereas Cygnus is now at the frontier of the superwave.

The case for external heating is even stronger for the North Polar Spur remnant. Borken and Iwan (1977) suggest that this remnant is on the order of 10^6 years old and in its radiative stage of expansion. They point out that such an old remnant would not be able to generate the observed soft X-ray emission as a result of its own motion. For example, Cleary, Heiles, and Haslam (1979) report an H-I expansion velocity for the remnant of only ~ 3 km/s. expansion velocities of several hundred kilometers per second usually being required to produce soft X-ray emission. As a solution, Borken and Iwan suggest that the North Polar Spur has been *reheated*, since the time of its initial supernova explosion, by intersection with another, young SNR. In addition, Heiles et al. (1980) suggest that relativistic electrons accelerated within the remnant in shock fronts or in energetic stellar winds may account for the strong radio continuum emission observed from the North Polar Spur shell. As an alternative, it is possible that the 393 AD Superwave is responsible for both the heating of this remnant and for restocking it with relativistic particles. The superwave may have left this region only about 500 years ago.

It should be pointed out that if the 393 AD Superwave is the heating source for the five remnants mentioned above, it may be erroneous to estimate ages for these remnants on the basis of shell shock velocities inferred from soft X-ray spectra. It could be that several of these remnants are older than is presently thought.

6.2.4 The Vanishing Nebula V-V 1-7

A Palomar Observatory Sky Survey blue photo print taken in 1953 of the star HD 62001 (BD-18°1967) shows that it is surrounded by a 0.26 pc diameter nebula, given that the

distance to the star is ~ 213 pc (Kohoutek and Wehmeyer, 1975). However, between 1953 and 1979 when a second photographic plate was made of this star, the nebula mysteriously vanished (Mendez et al., 1980). HD 62001, a late-type B star at present is not bright enough to illuminate such a nebula. Mendez et al. suggest that V-V 1-7 was a "light echo" produced on nearby interstellar material by a nova outburst from the central star or from an unseen companion. However, it is also possible that in 1953 V-V 1-7 was being excited by cosmic rays from a passing superwave and that between 1953 and 1979 the ambient cosmic ray density in that vicinity dropped to a low level leaving the nebula invisible. For a galactic longitude of $\ell \sim 236^\circ$ and a distance of 213 pc, HD 62001 would be situated in the vicinity of the 393 AD event horizon; see Figure 6.6.

6.2.5 The Proximity to Two T Tauri Associations.

The 393 AD Superwave Event Horizon is presently in the midst of two major associations of T Tauri stars and related objects. One of these, the Taurus-Auriga complex is situated at $\ell \sim 172 \pm 2^\circ$, $d \sim 160$ pc, about 80 pc from the event horizon. Another, NGC 7000/IC 5070 is situated at $\ell \sim 85^\circ$, $d \sim 700$ pc coincident with the event horizon. Cohen and Kuhl (1979b) have studied 83 T Tauri stars in the Taurus-Auriga complex and 42 such objects in NGC 7000/IC 5070. It is significant that of the T Tauri stars and related objects in their sample (for which distances are listed), *half lie within 100 parsecs of either the 6000 years BP event horizon or the 393 AD event horizon.* As is discussed in Section 3.3.2, T Tauri stars may actually be normal dwarf stars that are going through an accretion phase triggered by the passage of a superwave.

UPDATE

Ice Core Evidence of a Superwave Passing Around 6000 Years BP (update to [p. 192](#)):
The ^{10}Be ice core data of Beer et al.⁽¹⁾ show no evidence of any ^{10}Be increase around 393 AD. So the existence of the 393 AD event horizon is at present tentative. However, ice core data do show that there was a small increase in ^{10}Be close to the 6,000 years BP date; see [p. 236](#).

1) J. Beer, et al. "The Camp Century ^{10}Be record: Implications for long-term variations of the geomagnetic dipole moment." *Nuclear Instruments and Methods in Physics Research* **B5** (1984): 380 – 384.

PART III

TERESTRIAL EVIDENCE COMPATIBLE WITH THE GALACTIC EXPLOSION HYPOTHESIS

CHAPTER 7

PALEOMAGNETIC EVIDENCE

7.1 GEOMAGNETIC REVERSALS AND EXCURSIONS

Currently, the Earth is in a period of normal magnetic polarity, its north magnetic pole being aligned approximately with its north geographic pole. However, the geologic record indicates that in the past this has not always been the case. Apparently the Earth's magnetic field has settled numerous times into positions of reversed polarity. The polarity reversal sequence for the past 4.5 million years (potassium-argon chronology) is illustrated in Figure 7.1 (Cox, 1969). For the sake of classification, this reversal sequence is usually divided into a series of polarity epochs to indicate periods during which the Earth's field has tended to remain predominantly normal or predominantly reversed. Currently, we are in the Brunhes

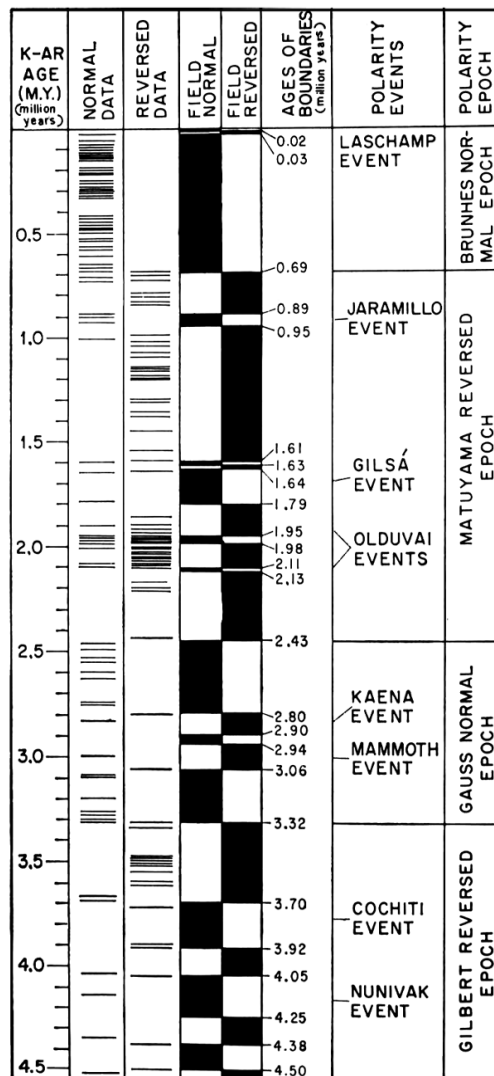


Figure 7.1. The time scale for geomagnetic reversals over the past 4.5 million years, based on potassium-argon dating (Cox, 1969). (© 1969, American Association for the Advancement of Science)

normal epoch which, according to the potassium-argon time scale began about 700,000 years ago.

While the Earth's magnetic field has consistently maintained a normal mode during the Brunhes epoch, there have been brief intervals during which it has become reversed. For example, as seen in Figure 7.2 (Nakajima et al., 1973), there may have been at least 5 times during the course of this epoch when the magnetic field became temporarily reversed. Unlike real reversals, however, these events are relatively brief and are generally not consistently recorded in sediments from different geographical locations. In fact, the paleomagnetic profile of these excursions may differ considerably even when adjacent cores are compared. Moreover, it is often found that during these events the geomagnetic pole attains an equatorial position, rather than a completely reversed position. For these reasons, such large scale fluctuations have been referred to variously as geomagnetic *excursions*, *events*, or *features*, rather than as geomagnetic *reversals*.

Verosub and Banerjee (1977, pp. 151-152) suggest that geomagnetic excursions of the Brunhes epoch may be due to a temporary decrease in the dipole component of the geomagnetic field together with a temporary increase in the nondipole components of the

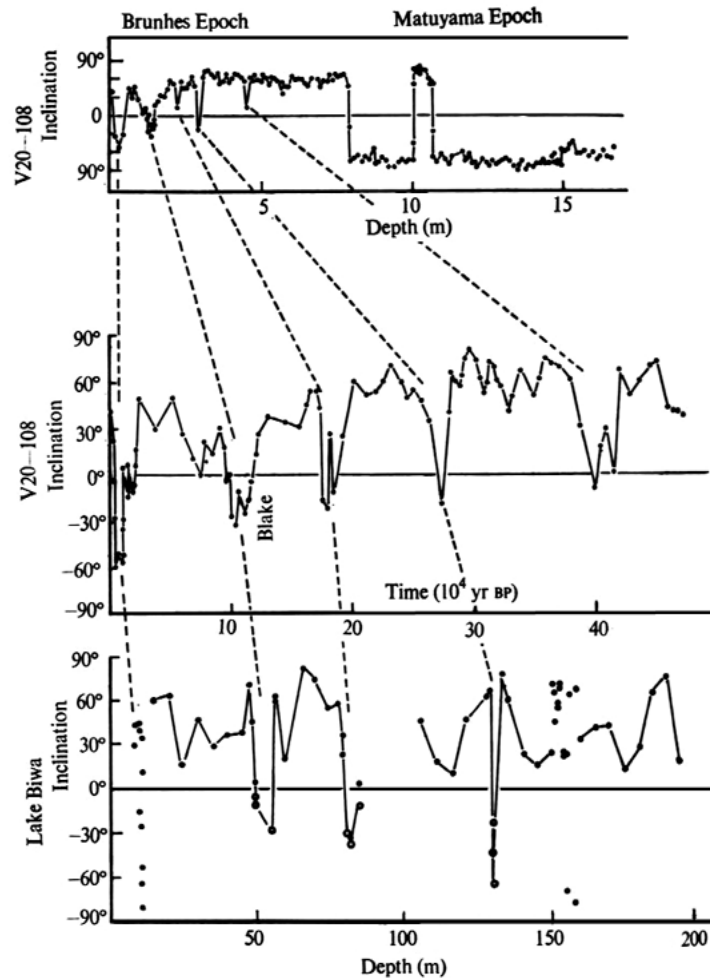


Figure 7.2. Recurrent geomagnetic excursions during the Brunhes normal epoch. The profiles from top to bottom include: magnetic inclination vs. depth in North Pacific core V20-108 (Ninkovich et al., 1966), magnetic inclination vs. time in core V20-108 (Wollin et al., 1971), and magnetic inclination vs. depth in a core from Lake Biwa-ko (Nakajima et al., 1973). Correlation scheme after Nakajima et al., 1973.

field. They point out that this could leave some areas with reversed polarity and others with normal polarity, thus explaining the recording inconsistencies. Such an explanation fits well with the scenario proposed in Subsection 3.3.3, which postulates a cancellation of the Earth's dipole field by an opposed ring current field generated by charged particles spiralling in the radiation belts. With the dipole field neutralized in this manner, only the non-dipole components would remain. Moreover, the field lines predominating at ground level would probably vary erratically in inclination, declination, and intensity due to magnetic disturbances imposed by the interplanetary magnetic field.

7.2 THE GOTHENBURG GEOMAGNETIC EXCURSION

The Galactic Explosion Hypothesis predicts that major disturbances of the Earth's magnetic field would have been more likely to occur close to the end of the Last Ice Age (at the end of the Wisconsin), about the time when the 14,200 years BP superwave would have been passing through the solar system; see Hypothesis #4-b and #6 (pp. 2-3). There is considerable evidence indicating that in fact a brief geomagnetic disturbance did occur during this period at about 14,100 calendar years BP along with two minor geomagnetic events at ~11,600 calendar years BP. Such excursions would most likely have been due to energetic solar flare activity resulting from the Sun's accretion of interstellar nebular material; see Subsections 3.3.2 and 3.3.3. Transits of the heliopause sheath and energetic Galactic superwaves may be ruled out since these would have produced inordinately high C-14 levels which are not observed in the geologic record.

Table XI lists dates and places for the "Gothenburg, Erieau, and Laschamp excursions. Of the dates listed in Table XI, those based on corrected varve chronologies may be assumed to be the most accurate. In southern Sweden this event has been named the "Gothenburg Magnetic Flip," appearing in varved sediment cores as a brief interval of reversed polarity (Mörner and Lanser, 1974; Mörner, 1977). Analysis of these cores indicates that during this event the virtual geomagnetic pole had attained an equatorial position in the mid Pacific Ocean at ~180° W longitude. Mörner (1977) reports that the Gothenburg Flip occurs within an unvarved sediment layer called the "Fjärås zone" (see Figure 7.3) which was deposited synchronously with the Fjärås moraine stage. Based on a version of the C-14 calibrated Scandinavian varve chronology, he has dated the Fjärås zone at 12,400 – 12,350 years BP [14,250 – 14,150 calendar years b2k]. Assuming that a constant sedimentation rate is maintained from varved to unvarved sections in the cores that he has studied, he has determined that the unvarved Fjärås layer was deposited over a period of about 50 years. Thus, a shorter duration of perhaps about 25 years is implied for the extent of the magnetic flip, which checks with the 26 varve year duration reported by Noël and Tarling (1975). Apparently the direction change at the beginning and end of the flip each time transpired within the space of a few years.

An interesting climatic correlation may be made to the Gothenburg Flip. Mörner (1977, p. 417) correlates the Fjärås zone with the formation of the Fjärås moraine which extends across the southern tip of Sweden. This moraine has been conventionally interpreted as a "stadial" or "standstill" period in the history of ice recession from Sweden and has been attributed to a temporary climatic cooling. However, the opposite conclusion may also be reached, namely that the Fjärås moraine was produced during a period of *accelerated* glacial melting associated with an unusually warm climate. Under such conditions the ice sheet margin could stand still or even readvance, a phenomenon which is referred to as *ice surging*; cf. Wright (1973, pp. 268 - 270). The Fjärås, which lasted 50 years or perhaps less, is flanked on either side by the Ågård and Bölling interstadials, each of which lasted about 500 and 450 years respectively, according to the varve chronology adopted by Mörner (1977). Moreover, Tauber (1970, p. 185) notes that at the time of the Fjärås standstill the Scandinavian ice sheet

TABLE XI
THE GOTHENBURG, ERIEAU, AND LASCHAMP GEOMAGNETIC EXCURSIONS

| LOCALITY | PUBLISHED AGE (years BP) | CORRECTED AGE (calendar years b2k)* | DATING METHOD | MATERIAL | REFERENCE |
|---|-----------------------------|--|---|------------------------|---|
| Gothenburg, Sweden | 12,350 - 12,400 | 14,150 - 14,250 | varves | varved clay | Mörner (1977) |
| Torsgarden, Sweden | " | " | " | " | " |
| Ågård, Sweden | " | " | " | " | " |
| Bjorkerods Mosse, Sweden | " | " | " | " | " |
| Baltic Sea, Southeast Sweden | " | " | " | " | " |
| Viby, Sweden | 12,400 | 14,100 | " | " | Ising (1942) |
| Blekinge, Sweden (Stilleryd and Starno Cores) | 12,077 - 12,103 | 13,800 | uncorrected varves | " | Nöel and Tarling (1975) |
| Laschamp and Olby, France | 20,000 | _____ | K/Ar | lavas | Bonhommet and Zahringer (1969) |
| Puy de Laschamp, France | 7,000 - 9,000 | 8,000 - 10,000 (too young) | C ¹⁴ | volcanic scoria | Bonhommet and Babkine (1967) |
| Lake Erie (Erieau, Ontario) | 13,000 - 13,800 | 15,500 - 17,100 | C ¹⁴ till horizon correlations | glaciolustrine clay | Creer et al. (1976) |
| Port Dover, Canada | 13,300 | 16,300 | C ¹⁴ till horizon correlations | glacial clays | Mörner (1977) |
| North Atlantic (core A179-15) | 12,350 - 12,400 | 14,150 - 14,250 | geomagnetic correlations and microfauna | marine sediments | Mörner and Lanser (1975) |
| North Island, New Zealand | 12,450 ± 340 | 14,300 ± 350 | C ¹⁴ | Okupata tephra | Mörner and Lanser (1974) after Topping (unpublished) |
| Czechoslovakia | 12,000 | 13,800 | C ¹⁴ | loess | Bucha (1973) |
| Maniana Pali I, Hawaii | 10,410 ± 310 | 12,250 ± 300 | C ¹⁴ | lava flow | Coe et al. (1978) |

* Update: Corrected ages have been revised using the new C-14 date conversion scheme presented in [Appdx E](#).

had been receding more rapidly than at any other time during the entire post glacial recessional period.

(Mörner, 1977, p. 417) notes that at the Fjärås pollen zone boundary in core B 896 there was an abrupt change in mollusk species from boreo-arctic to the cooler arctic species, followed by a change at the Fjärås/Bölling boundary from arctic to the warmer arctic/boreal species. However, rather than indicating a cooler climate for the Fjärås, I would suggest that this evidence actually indicates the presence of a *warm spell* during which glacial melting became accelerated. The sudden flourishing of arctic species during the Fjärås could have

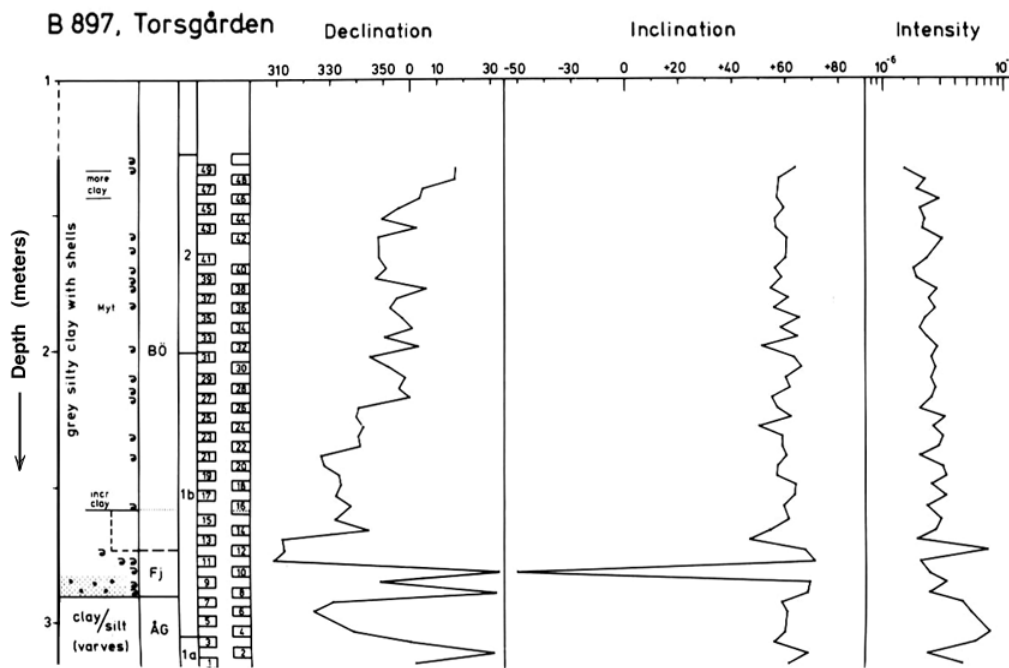


Figure 7.3. Paleomagnetic history of core B 897 from Torsgården, Sweden. Shown to the left are the Bölling (BO), Fjärås (FJ), and Ågård (AG) pollen zones. Sample 10 in the middle of the FJ zone exhibits a fully reversed inclination (Mörner, 1977).

been initiated by the abrupt influx of cold glacial meltwater. This conclusion is supported by Mörner's stated observation (1977, p. 416) that the Fjärås zone in nearby marine cores and local clay pits was formed by ice rafted material. Core B 896, for example, was taken from a site that would have been just 30 km from the Fjärås ice margin at the time that the Fjärås zone was deposited. Thus I postulate that a major climatic amelioration occurred coincidentally with the time of the Gothenburg Flip.

Creer et al. (1976) have studied two sediment cores taken from Lake Erie near Eriean, Ontario, and they report the presence of a geomagnetic feature which they call the "Eriean Excursion." They find reversed inclinations beginning in the upper portion of a till layer which they identify with the youngest portion of the Port Stanley Till and which they date at ~13,800 C-14 years BP [17,100 calendar years b2k]. The reversal continues up through glaciolacustrine clay (containing reddish clay inclusions) to a section of core dated in the vicinity of 13,000 C-14 years BP. After this, the magnetic inclination becomes more positive, wandering around a 0° inclination with reversed as well as normal orientations. This magnetically unstable period persists on up to about 10,500 years BP. For the lower portion of the Eriean Excursion I will adopt the date range of 13,800 – 13,000 C-14 years BP or 17,100 - 15,500 *calendar years b2k*, where the respective radiocarbon dates have been translated into calendar dates according to the ice core calibrated radiocarbon conversion scheme presented in Appendix E (p. 435). This excursion spans the Carey-Port Huron Interstade, a period of rapid ice sheet retreat in the Great Lakes Region; see p. 253.

Mörner (1977) reports the presence of a geomagnetic excursion in Canadian clays that were deposited immediately before the Paris/Galt moraines of the Port Huron readvance, i.e., during the Cary-Port Huron retreat. He dates this event, which he calls the "Port Dover Excursion," at 13,300 C-14 years BP [16,500 calendar years b2k] and notes that the position of the virtual geomagnetic pole (VGP) during the excursion was in the southeast Pacific not

far from the VGP position of the Gothenburg Flip. It appears that in both the Great Lakes Region and in Scandinavia, the glacial ice sheets at this time were retreating faster than at any other time in their retreat history; see Subsection 9.3.2. Consequently, I conclude that the Gothenburg Flip must have been associated with a period of intense climatic amelioration that took place on a global scale.

It is difficult to believe that the abrupt climatic warming that peaked at the time of the Gothenburg Flip was purely coincidental. Solar flare activity which may have produced the Gothenburg Flip could have simultaneously initiated a climatic warming by expelling interplanetary dust from the inner portion of the solar system. It would be interesting to do a detailed stratigraphic analysis of nitrate concentrations in ice core sections spanning this excursion to see if a major increase is registered. A positive finding would constitute strong evidence that this geomagnetic excursion was produced by an overloading of the radiation belts with charged particles.

Since it appears that excessive glacial recession and flooding took place at about the time of the Gothenburg Flip, it is very likely that in many locations around the world a disturbance would exist in the sedimentary record, obliterating any trace of this brief event. For example, Opdyke, Ninkovich, Lowrie, and Hays (1972) have done a detailed paleomagnetic study of core V10-58 from the Aegean Sea and found no trace of this event.

7.3 GEOMAGNETIC EXCURSIONS OF THE CURRENT AND PREVIOUS INTERGLACIALS

7.3.1 The 6000 Years BP Geomagnetic Intensity Change

Paleomagnetic data indicate that during the Holocene Epoch (the present interglacial) the Earth's magnetic field has undergone considerable change in intensity. Over the period 9000 – 6000 years BP the intensity of the geomagnetic field decreased, followed by an intensity increase over the period 6000 – 2000 years BP; see Figure 7.4(c) (Bucha et al., 1970). Wollin et al. (1971) have noted that, correlated with this intensity change, there was a change in the Earth's climate along with a variation in the atmospheric radiocarbon concentration. Four climatic profiles (Figures 7.4(a), (b), (e), and (f)) indicate that during the first part of the Holocene from about 10,000 years BP to about 6000 – 6500 years BP, there was a warming trend, which was subsequently followed by a cooling trend over the period 6000 - 3000 years BP. This climatic oscillation is a well-known feature of the Holocene called the climatic hypsithermal. Also, Figure 7.4(d) indicates that around 6000 years BP the radiocarbon concentration in the atmosphere was about 10% higher than at present.

Taken together these six profiles indicate that there is a direct correlation between more moderate climate, decreased magnetic field intensity, and increased radiocarbon production. This correlation cannot be explained by variations in orbital eccentricity, since over this period orbital eccentricity attained an almost constant value. The explanation that Wollin et al. (1971) suggest is that the geomagnetic field may modulate climate by shielding the Earth from solar corpuscular radiation. However, it is difficult to imagine how energy inputs of such small magnitude (as are available from solar flares) could significantly impact the Earth's climate.

Astronomical evidence, presented in Section 6.1, suggests that a Galactic superwave may have passed the Earth about 6000 years BP. The geologic record indicates that at about this time the Earth's climate had reached its hypsithermal peak. Also at this time a reversal occurred in the secular decrease of the geomagnetic field intensity. However, the GEH as it is currently structured has difficulty accounting for these correlations. Dust concentrations recorded in the Dome C ice core (Figure 8.1(a), **p. 218**) appear to be particularly low at this time, so if a superwave passed the solar system it would have had to have been a mild event.

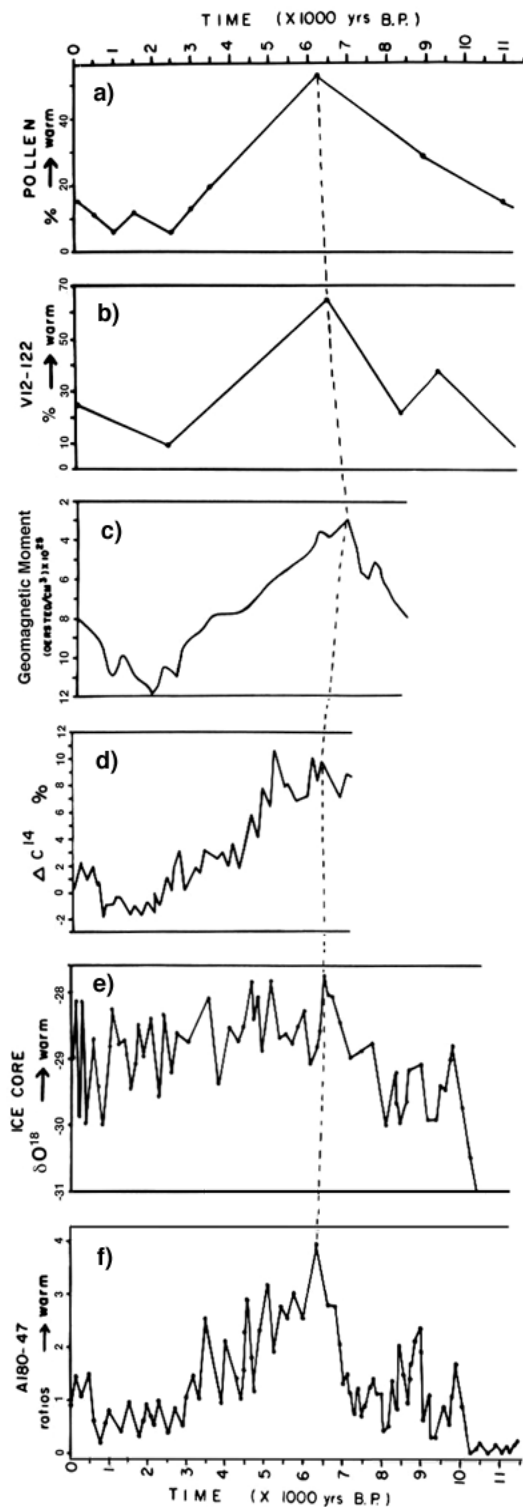


Figure 7.4. Correlation of climate, geomagnetic field intensity and C-14 production for the Holocene. The profiles from top to bottom include:

- a) a climate curve based on the pollen composition of peat in Germany (Bertsch, 1935);
 - b) a climate curve based on changes in coiling direction of *G. truncatulinoides* in deep-sea core V12-122;
 - c) the geomagnetic field intensity curve (Bucha et al., 1970);
 - d) the profile of variations in atmospheric radiocarbon activity (Suess, 1965);
 - e) the oxygen isotope climate curve for the Camp Century ice core (Dansgaard, 1969); and
 - f) the climate curve for deep-sea core A180-47 based on changes in *Globorotalia menardii*.
- (Overall scheme from Wollin et al., 1971)

Also, it is not clear why the decreasing trend in geomagnetic field intensity should have become suddenly reversed at the time of superwave passage.

7.3.2 The Blake Event of the Previous Interglacial

Since its discovery by Smith and Foster (1969), the Blake Event has been found in sediments in many places around the world (Wollin et al., 1971; Kukla and Koci, 1972; Eardley et al., 1973; Nakajima, 1973; and Denham, 1976). Kukla and Koci found the reversal in Czechoslovakian loess deposits and determined that it occurred at about the middle of the Sangamon (Last Interglacial) during a period that corresponds to the Barbados II Terrace climatic stage, equivalent to oxygen isotope substage 5-c. On the Grande Pile peat bog pollen diagram shown in Figure 9.1(a) (p. 246) this interval would correspond to the St. Germain I stage (substage 5-c). As seen in Figure 9.1(a) brief stadials occurred precisely at the time of initiation and termination of the reversed polarity period, substages 5-b and 5-d, i.e., when the polarity was in the process of reversing its direction. These dry, cold periods (Melisey I and Melisey II) each lasted for several hundred years and were marked by the widespread destruction of forests and the simultaneous expansion of herbal plants adapted to steppe conditions. Such a coincidence between climatic change and geomagnetic change may be accounted for by the Galactic Explosion Hypothesis. Namely, the passage of a superwave could have transported cosmic dust into the Earth's vicinity, temporarily reducing the amount of sunlight reaching the Earth's surface and initiating climatic cooling. Enhanced solar flare activity triggered by the Sun's accretion of this nebular material would then have been responsible for causing the observed geomagnetic reversals.

[UPDATE: As seen in Figure 8-B, cosmic ray levels were elevated during the times when the Blake geomagnetic excursions took place.]

UPDATE

Calendar Date for the Gothenburg Geomagnetic Flip (update to p. 209): At the time of writing this dissertation I had used an incorrect scheme for converting radiocarbon chronology to calendar dates by depending on an inaccurate ice core chronology developed by L. Thompson for the Camp Century and Byrd ice cores. As a result, the calendar date that I had erroneously assigned to the Gothenburg Flip fell close to the radiocarbon date for this event. Since that time, however, the Greenland ice core chronology has become more accurately dated, allowing radiocarbon dates to be accurately converted into calendar dates. According to this revised date conversion scheme presented in Appendix E, the Gothenburg Flip may have occurred between 14,150 to 14,250 calendar years b2k (in the case where the event is correlated with a radiocarbon date of 12,350 to 12,400 C-14 years BP). This coincides with a peak in ¹⁰Be concentration evident in the Vostok and Byrd ice cores (see update in Ch. 8) which indicates that the Gothenburg Flip occurred during a period when the Earth was being exposed to a high cosmic ray flux.

In the early 80's when this dissertation was written, I had relied on an incorrect radiocarbon date conversion scheme, which led me to incorrectly conclude that the Gothenburg, Eriau and Laschamp excursions occurred contemporaneously and were various names for the same event. However, based on a more accurate date conversion scheme, the Eriau excursion is seen to have occurred around 15,000 – 14,500 calendar years BP; i.e., prior to the Gothenburg event. Also the Laschamp event occurred much earlier, around 27 – 32 kyrs BP. Nevertheless the main point I had originally made was essentially correct, namely that geomagnetic disturbances were occurring around the time when the 14,200 years BP superwave would have been passing through the solar vicinity.

Other geomagnetic events and their correlation with Be-10 increases. Chapter 3 of this dissertation (pp. 99 - 101) proposed that geomagnetic excursions could be produced by giant solar storms occurring during periods of elevated solar activity, this being in turn triggered by a superwave passage.^(1,2) Also it was proposed in this chapter (p. 212) that the Gothenburg excursion which dates around 14.15 to 14.25 k calendar years b2k could be explained by such a mechanism. Data that has since been published shows that both ^{10}Be and ^{14}C increased sharply at this time coincident with the Younger Dryas (Fjåras) stadial, thereby confirming this prediction; see Figure 8-C (p. 237) and Figure 10-B (p. 287).

Data also came out establishing a ^{10}Be spike connection for earlier geomagnetic excursions as well. For example, McHargue, et al. found that changes in ^{10}Be concentration in a well-dated Gulf of California sediment core track changes in the dipole moment, higher ^{10}Be production rates (and atmospheric cosmic ray intensities) tending to occur at times of lower magnetic field intensity.^(3, 4) They found two ^{10}Be anomalies at 32 kyrs and 43 kyrs b2k, contemporaneous with the Mono Lake and Laschamp geomagnetic excursions which were of so large that they could not be explained by low geomagnetic field intensity alone. They concluded that they must have been produced by elevations in the background cosmic ray flux. Also Mangerud et al. found paleomagnetic excursions dated at 34kyrs and 41 kyrs b2k in Norwegian cave lake sediments which they identify with the Mono Lake and Laschamp excursions.⁽⁵⁾ Like Wagner et al.⁽⁶⁾, they correlate these events with times of peak ^{36}Cl deposition in the GRIP ice core, which indicates times when the background cosmic ray flux was elevated.

Lund et al. have found the Laschamp excursion registered in North Atlantic deep sea sediments dating at 41 kyrs b2k.⁽⁷⁾ They found that the excursion occurred during a 2000 year period when geomagnetic field intensity was 10% of its normal intensity. The solar cosmic ray model pioneered in the present dissertation predicts that geomagnetic field intensity should be low at the time of a geomagnetic excursion due to the ring current produced by magnetically trapped solar flare cosmic rays.

Hughen et al. have found that the period from 45 kyrs to 40 kyrs b2k was characterized by a very high rate of radiocarbon production which caused atmospheric radiocarbon levels to almost double.⁽⁸⁾ This indicates that the Earth was exposed to a very extended elevation of

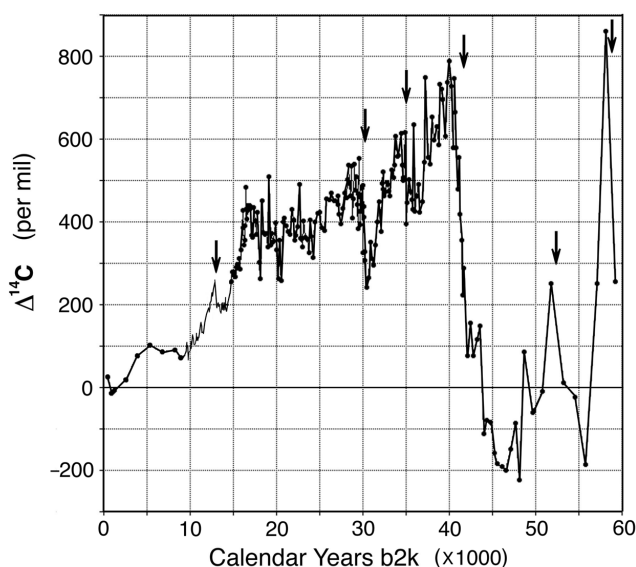


Figure 7-A. Radiocarbon abundance excess relative to trend line in a Carioca Basin sediment core (after Hughen, et al., 2004).

the solar cosmic ray flux during the time of the Laschamp excursion. They also found several other radiocarbon production peaks, one of which occurred around 35 kyrs b2k could correlate with the Mono Lake excursion. These findings confirm early predictions of the superwave theory that there should be a connection between ^{10}Be peaks and geomagnetic excursions via the induction of enhanced solar activity.

McHargue et al. were apparently unaware of these predictions, but nonetheless similarly sought a Galactic cosmic ray explanation, attributing the 32k and 43k ^{10}Be peaks to the occurrence of a nearby supernova explosion. In 1991, C. Sonett proposed a similar supernova explosion theory to account for the ^{10}Be peaks seen in the Vostok ice core record at 40k and 63k years b2k (see [p. 236](#)).⁽⁹⁾ Although the occurrence of the geomagnetic excursions coincident with these ^{10}Be anomalies remained for him a paradox, he speculated that these excursions might have been caused by high interplanetary magnetic field intensities accompanying supernova shock fronts that had impacted the heliosphere and Earth's magnetosphere. But their theories have the problem of explaining why supernova shock fronts would have passed the Earth so frequently. Alternatively, Sonett suggested that these cosmic ray anomalies may have occurred during a time of unprecedented long-term solar activity, in so doing alluding to the solar flare geomagnetic flip mechanism proposed in this dissertation and in subsequent publications. But he did not elaborate. In 1995 two other researchers published a more detailed discussion of a geomagnetic flip mechanism triggered by giant solar storms to explain the Steens Mountain geomagnetic reversal (see [p. 125](#)).

Update References:

- 1) P. A. LaViolette, "Cosmic ray volleys from the Galactic center and their recent impact on the Earth environment." *Earth, Moon, and Planets* **37** (1987): 241-286.
- 2) P. A. LaViolette, "Galactic core explosions and the evolution of life." *Anthropos* **12** (1990): 239 - 255.
- 3) L. R. McHargue, "A 50,000 year Beryllium-10 record from Gulf of California sediments." Ph.D. dissertation, University of Arizona, 1994.
- 4) L. R. McHargue, , Damon, P. E., Donahue, D. J. "Enhanced cosmic-ray production of Be-10 coincident with the Mono Lake and Laschamp geomagnetic excursions." *Geophys. Res. Let.* **22** (1995): 659-662.
- 5) J. Mangerud, et al. "Paleomagnetic correlations between scandinavian ice sheet fluctuations and greenland dansgaard-oeschger events, 45,000 - 25,000 yr B.P." *Quaternary Research* **59** (2003): 213-222.
- 6) G. Wagner, et al., "Chlorine-36 evidence for the Mono Lake event in the Summit GRIP ice core." *Earth Planetary Science Letters* **181** (2000): 1-6.
- 7) S. P. Lund, et al. "Deep-sea sediment records of the Laschamp geomagnetic field excursion (~41,000 calendar years before present)." *J. Geophysical Research* **110** (2005) B04101.
- 8) K. A. Hughen, et al. " ^{14}C Activity and global carbon cycle changes over the past 50,000 years." *Science* **303**, January 9, 2004.
- 9) C. P. Sonett, "A local supernova model shock ensemble using Antarctic Vostok ice core ^{10}Be radioactivity." December 1991 American Geophysical Union meeting, abstract in *Eos* **72** (1991): 72.

CHAPTER 8

THE GLACIAL RECORD

8.1 THE GLACIAL CLIMATIC RECORD

It has been discovered that polar ice contains a detailed record of the Earth's climate, possibly extending back as far as the interglacial period preceding the Last Ice Age (the Wisconsin, or Wurmian ice age). The manner in which the Earth's climate has become recorded in the ice may be described as follows. At times when the oceans are cooler water molecules containing "heavy oxygen" (^{18}O) are not as easily evaporated, their vapor pressure being $\sim 1\%$ lower than that of a typical water molecule. Consequently, water vapor derived from cool oceans will be relatively deficient in ^{18}O . Also, at times when the air is cooler water molecules containing heavy oxygen would tend to become condensed out of the air more easily, further reducing the $^{18}\text{O}/^{16}\text{O}$ ratio. Thus, during times of cool climate the ratio of oxygen isotope ^{18}O to oxygen isotope ^{16}O becomes measurably reduced in the snow precipitating at that time. In glacial regions where consecutive snow falls become preserved as firn and later (with compaction) as glacial ice, this isotopic ratio record becomes similarly preserved.

Variations in the isotopic ratio in glacial ice serve as a useful climatic indicator when they are referenced to the standard mean ocean water (SMOW) ratio according to the formula:

$$\delta(O^{18}) = \frac{(H_2O^{18} / H_2O^{16})_{\text{sample}}}{(H_2O^{18} / H_2O^{16})_{\text{SMOW}}} - 1, \quad 28$$

where $\delta(O^{18})$ is given in parts per thousand ($\%$) (Craig, 1961). A trend of this indicator to more negative values, then, would be correlated with a trend to cooler climate. However, other factors are important in determining the oxygen isotope ratio. These include the ocean surface altitude at the time of evaporation, the altitude where final precipitation occurred, and the isotopic ratio of the ocean water which itself depends on the extent of glacial ice cover. Curves (a), (c), and (f) of Figure 8.1 present oxygen isotope profiles for the 905 meter Dome C ice core from East Antarctica (74.65° S , 124.17° E), for the 2164 meter ice core drilled at Byrd Station, West Antarctica (80° S , 119.5° W), and for the 1387 meter ice core drilled at Camp Century, Greenland (77.2° N , 61.1° W).

It can be seen in Figure 8.1 that all three cores register the climatic amelioration (trend toward less negative δO^{18} values) which took place near the end of the Last Ice Age. The isotopic change of $\pm 8\%$, registered in the Byrd core at this time corresponds to a climatic warming of about $7 - 8^\circ \text{ C}$ (Epstein, Sharp, and Gow, 1970). By comparison, the atmospheric temperature increase was about 5° C at Alerce, Chile ($\sim 41^\circ \text{ S}$) and about 9° C in the British Isles ($\sim 52 \pm 2^\circ \text{ N}$); see Figures 9.2 and 9.3 (pp. 249 and 250). Also, the average ocean water temperature change at the end of the Last Ice Age has been determined to be about $+2.3^\circ \text{ C}$ (McIntyre et al., 1976).

The late, middle, and early Wisconsin glacial stages and the Sangamon Interglacial have been tentatively marked on the ice core δO^{18} profiles using the abbreviations LW, MW, EW, and S. Subdivisions of the Sangamon have been marked by numbers 5a – 5e, a number system which was originally developed to distinguish oxygen isotope climatic substages in ocean sediment cores. I have positioned these stages relative to the profiles in a manner that

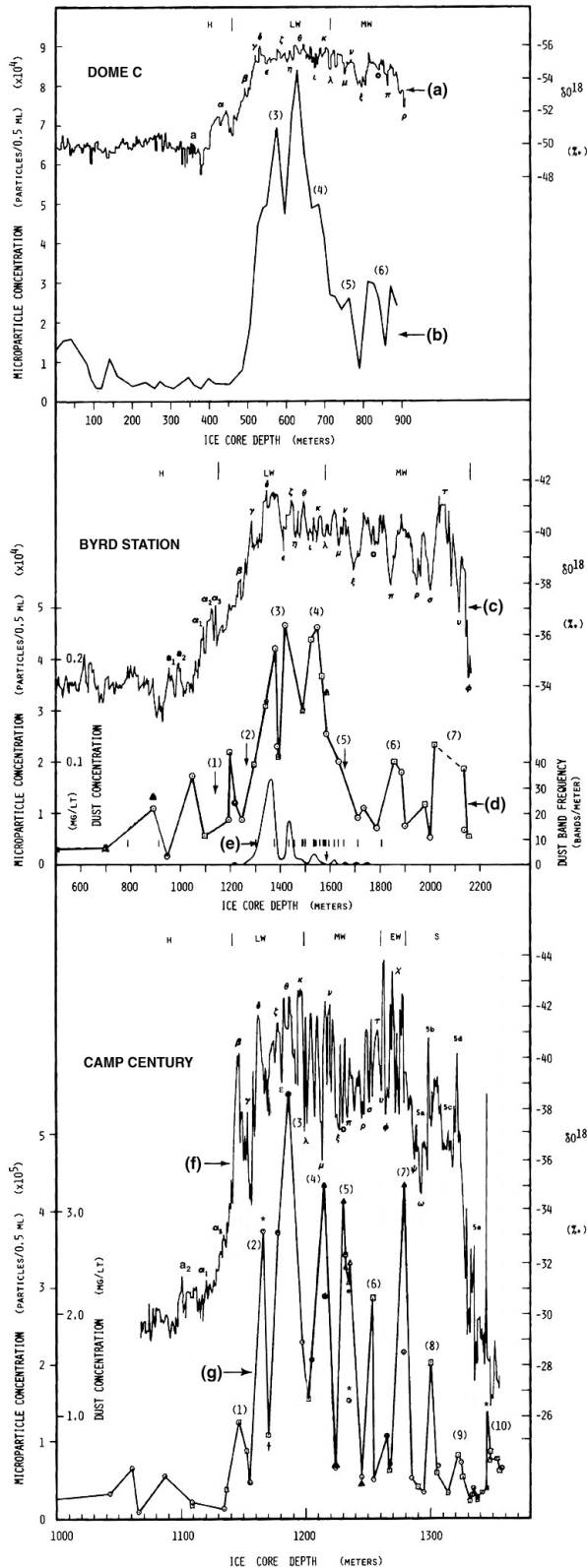


Figure 8.1. Oxygen isotope and dust concentration profiles for three polar ice cores.

a) $\delta^{18}O$ for Dome C, East Antarctica (adapted from Lorius et al., 1979).

b) Microparticle concentration for Dome C (adapted from Thompson and Mosley-Thompson, 1981).

c) $\delta^{18}O$ for Byrd Station, West Antarctica (plotted from data supplied courtesy of Dr. Dansgaard; also see Johnson, Dansgaard, Clausen, and Langway (1972).

d) Microparticle concentration and estimated dust weight concentration for Byrd Station (based on data from Thompson (1977b) and Cragin et al. (1977); see Appendix F).

e) Dust band frequency curve; vertical lines indicate the positions of ash bands (adapted from Gow and Williamson, 1971).

f) $\delta^{18}O$ for Camp Century, Greenland (plotted from data supplied courtesy of Dr. Dansgaard; also see Hammer et al. (1978).

g) Microparticle concentration and estimated dust weight concentration for Camp Century (based on data from this study and from Thompson (1977b) and Cragin et al. (1977); see Appendix F). Climatic periods marked on the diagrams include: Sangamon (S), Early Wisconsin (EW), Mid Wisconsin (MW), Late Wisconsin (LW), and Holocene (H).

is broadly consistent with stage assignments that have been employed in the past by other glaciologists. For example, by correlating the Camp Century and Dye 3 ice core δO^{18} profiles with a δO^{18} climatic profile developed for an ocean sediment core from the Indian Ocean, Dansgaard (1982) has set the interglacial/ glacial division (isotope stage 5/4 boundary) at a depth of about 1300 meters, consistent with that shown in Figure 8.1-f.

The less negative δO^{18} values found at the bottom of the Camp Century and Byrd cores have been interpreted by some authors (e.g., Johnsen et al., 1972; Epstein, Sharp, and Gow, 1970) as an indicator of the Last Interglacial. However, it is also possible that this change could have been caused by tectonic effects rather than climatic effects. For example, in the Byrd ice core, ground water having a less negative δO^{18} ratio could have become entrained in the base of the ice sheet as the ice advanced over the bedrock surface (L. Thompson, personal communication, 1982).

8.2 DUST IN GLACIAL ICE

During the latter part of the Wisconsin Ice Age, large quantities of dust were apparently present in the Earth's atmosphere. This dusting must have been global because corresponding portions of the Camp Century, Devon Island, Byrd, Dome C, and Agassiz cores all reveal substantial increases during the Late Wisconsin. Compare, for example, curves -b, -d, and -g, shown in Figure 8.1, for the Dome C, Byrd, and Camp Century ice cores, respectively.

To generalize, it may be said that dust levels were about an order of magnitude higher during the Late Wisconsin as compared with post glacial (Holocene) levels; see Table XII. Moreover, the degree of increase in atmospheric dustiness during the Late Wisconsin *relative* to other periods appears to have been about the same for both the Northern and Southern Hemispheres. Although dust concentrations are about an order of magnitude higher in Northern Hemisphere ice cores, this tendency is observed during all three geological periods. It should be noted that just on the basis of this observational evidence alone (i.e., the greater dustiness of Late Wisconsin ice) it may be concluded that during the Last Ice Age the optical depth of the atmosphere should have been at least tenfold greater than at present ($\tau \geq 1$).

In the context of the GEH, volcanism need not play a leading role in glacial initiation. Rather, the cooling effect of volcanic aerosols may be viewed as supplementing other more important climatic effects related to the presence of nebular material in the solar system. The coincidence of increased volcanism with times of major climatic change may involve a reverse causal relation in which isostatic shifts of the Earth's crust brought about by changes in global ice sheet volume trigger volcanic eruptions. Such a scenario is supported by paleoclimatological findings indicating that volcanic eruptions usually closely follow major climatic changes, rather than precede them; see Kennett and Huddlestun (1972) and Bray (1977).

The results of glacial ice core analyses strongly suggest that the Wisconsin (and particularly the Late Wisconsin) was characterized by high levels of windy weather. For example, elemental analysis of Camp Century ice indicates that the majority of this dust is typical of that derived from crustal rock and hence is most probably of windblown origin (Cragin et al., 1977). Thompson (1977a) estimates that fewer than 5% of the Wisconsin particles in the Camp Century core are of volcanic origin and interprets the high concentrations of dust as being of continental origin, deposited by an intense atmospheric circulation in the Northern Hemisphere. Volcanic activity may be considered to be the agent responsible for some of the dust features observed in the Byrd Station ice core, such as the "dust bands" and "ash bands" (p. 233). Also, Thompson (1977a) suggests that most of the Late Wisconsin particles in the Byrd ice core are of volcanic origin. However, Petit, Briat,

TABLE XII
COMPARISON OF DUST CONCENTRATIONS IN POLAR ICE
FOR ICE AGE AND POST ICE AGE PERIODS

| | (1) EARLY & MID WISC. | (2) LATE WISC. | (3) HOL. | (4) RATIO (col.2/col.1) | (5) RATIO (col.2/col.3) | REF. |
|---|-----------------------------|----------------------|-------------|-------------------------------|-------------------------------|-----------|
| <u>CAMP CENTURY, GREENLAND</u> | | | | | | |
| Microparticle concentration. (Number × 1000 >0.65μ per 0.5 ml) | 89±62 | 298±150 | 24±20 | 3.2±2 | 12.2±6 | (a) |
| Dust concentration (μg/lt) | 1250±880 | 880±210 | 216±244 | 0.7±1 | 4.1±3 | (b) |
| <u>AGASSIZ ICE CAP, ARCTIC, CANADA</u> | | | | | | |
| Dust concentration (μg/lt) | | 3960 | 530±300 | — | 7.5±4 | this work |
| <u>DEVON ISLAND, ARCTIC, CANADA</u> | | | | | | |
| Microparticle concentration. (Number × 1000 >10μ per ml) | 30 - 50 | 220 | 10 | 4 - 7 | 22 | (c) |
| <u>BYRD STATION, WEST ANTARCTICA</u> | | | | | | |
| Microparticle concentration. (Number × 1000 >0.65μ per 0.5 ml) | 13±7 | 24±14 | 9±5 | 1.9±2 | 2.8±2 | (a) |
| Dust concentration (μg/lt) | 72±30 | 157±50 | 20±6 | 2.2±1.5 | 7.9±3 | (b) |
| <u>DOME C, EAST ANTARCTICA</u> | | | | | | |
| Microparticle concentration. (Number × 1000 >0.65μ per 0.5 ml) | 23±7 | 44±24 | 6.7±4 | 1.9±1 | 6.5±4 | (d) |
| Microparticle concentration. (Number × 1000 >0.4μ per ml) | 23±22 | 87±30 | 7.2±3.3 | 3.8±2 | 12±4 | (e) |

(a) Thompson (1977b). (b) Estimate based on Si and Al concentration data of Cragin et al. (1977). (c) Fisher (1979). (d) Thompson and Mosley-Thompson (1981). (e) Petit, Briat, and Royer (1981).

and Royer (1981) present several pieces of evidence indicating that volcanism was *not* the cause of the Late Wisconsin dust maximum observed in the Dome C core and in other Antarctic ice cores. Instead, they suggest that the dust is primarily of windblown origin. They have concluded that wind speed was globally higher during the Late Wisconsin by as much as 1.5 – 1.8 times, pointing out that marine aerosol inputs to the Dome C site during the Late Wisconsin increased by a factor of ~5 over Holocene inputs, as judged by Na and Cl concentrations found in the ice. Also, they suggest that increased continental aridity was an important factor in addition to greater aeolian activity.

One advantage of assuming a wind-blown origin for the majority of glacial dust in both hemispheres is that the unusual dustiness of northern hemisphere ice may be accounted for. That is, for the same amount of wind activity in both hemispheres, air in the Northern Hemisphere would have a greater dust loading due to the greater prevalence of continental land masses. However, it appears that wind-blown continental dust is not the only major

constituent in glacial ice dust. As is discussed in Section 8.3, cosmic dust may constitute a sizeable fraction, especially in Antarctic ice.

Several questions may be raised at this point. First of all, if wind activity was a major factor producing the dusty atmospheric conditions at the end of the Wisconsin, then what was the cause of this windiness? And why did it occur when it did, particularly at the end of the ice age? It is known that there was a major ice advance during the first half of the Late Wisconsin stage. Could this glacial advance have been the causative factor? Probably not. If anything, the reverse would have been the case, i.e., the wind would have facilitated the glaciation process. Moreover, what relation does this dusty period bear to the termination of the Last Ice Age? That is, why did climatic warming and rapid glacial recession begin during this dusty period and continue after its termination? The glacial recession cannot be attributed to this windiness because otherwise why did glacial recession not cease when the windiness ended?

Many of these questions can be cleared up if it is hypothesized that the windiness was caused either by brief episodes of solar obscuration involving veils of cosmic dust transported through the solar system by superwave shock fronts or by brief variations in the atmospheric opacity brought about by changes in the stratospheric aerosol loading; see **p. 104**). In addition, such scenarios could account for the *abruptness* with which windiness varied in magnitude. For example, Thompson (1977b, p. 77) observes that the transition from the Wisconsin high to the Holocene low particle concentrations in the Camp Century core occurs in less than 100 years. Moreover, judging from the short term fluctuations in dust concentration which Thompson (1977b) has found in ice core sections taken from the Camp Century and Byrd Station cores, it appears that dustiness can be modulated on timescales as short as a few years, or perhaps as little as several weeks (as in the case of the Byrd core dust bands).

Evidence supporting the GEH and a cosmic cause for these dusty windy conditions is discussed in the next two sections of this chapter.

8.3 COSMIC DUST IN GLACIAL ICE

Micrometeorites (interplanetary dust) constitute the main source of extraterrestrial material falling on the Earth. As was mentioned in Subsection 3.3.2 (**p. 83**), most of the mass presently falling on the Earth enters in the form of particles that are a few hundred microns in size, with a whole range of sizes being present down to submicron size particles. Most of these particles are irregular in shape. The larger ones are most commonly low density, highly fragile aggregate-type particles, similar to the one shown in Figure 8.3(a); from Bradley, Brownlee, and Veblen (1983, *Nature* magazine cover picture). They are composed of submicron size cosmic dust grains embedded together with platelet-like or whisker-like crystals of larger size. Through neutron activation analysis (NAA) of individual particles, it has been determined that these aggregates have a composition similar to C-1 chondrites (Ganapathy and Brownlee, 1979), and hence they have been classified as "chondritic porous" or "CP" particles. Due to their large dimensions and fragile nature, CP interplanetary dust particles must be of recent origin to have remained intact in the interplanetary environment; hence it has been suggested that they are derived from *contemporary* comets (Bradley et al., 1983).

Spherically shaped particles are also part of the extraterrestrial fallout; see Figure 8.3(b); from Thompson (1977b, p. 137). Such extraterrestrial microspheres, because of their unique shape, are easily distinguishable under a microscope and hence have been reported to occur in ocean sediments, glacial ice, lunar soil, in the Earth's stratosphere, and inside chondritic meteorites (as "chondrules"). While spherules are the most common morphology among the

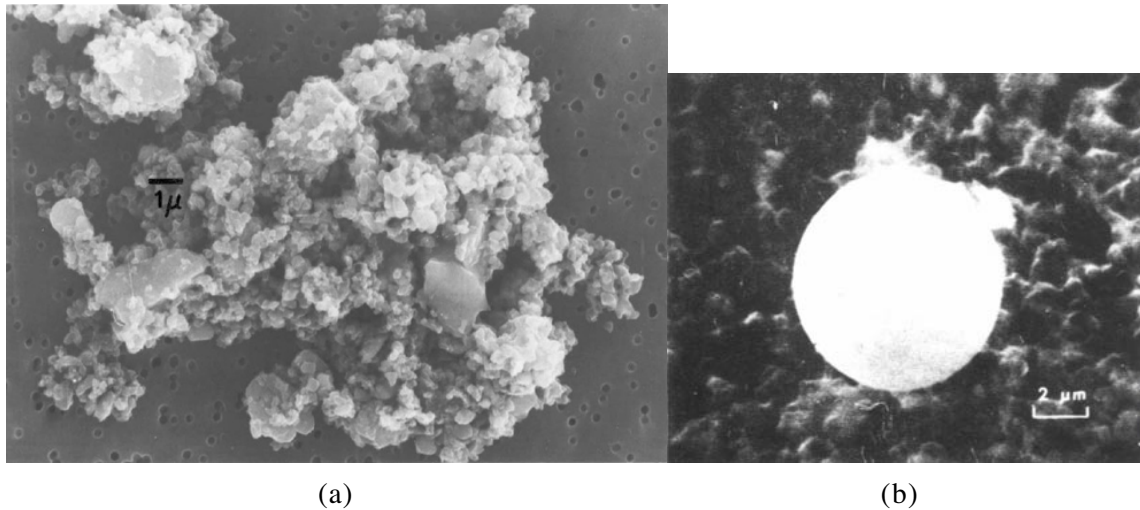


Figure 8.3. Extraterrestrial dust particles. a) A "chondritic porous" interplanetary dust particle collected from the Earth's stratosphere (Bradley, Brownlee, and Veblen, 1983; photo courtesy of D. E. Brownlee, University of Washington). b) An extraterrestrial microspherule retrieved from a depth of 566 meters in the Byrd Station ice core (Thompson, 1977b, p. 137).

smooth surface micrometeorites, odd morphologies such as tear drops, ovals, dumbbells, and rings have also been found in: ocean sediments (Glass and Heezen, 1967), polar ice (Langway, 1970), and in lunar soil (Mueller and Hinsch, 1970).

There is general agreement that these rounded particles must once have been heated to a molten state in order to attain their smooth shapes. One theory is that these were originally irregular micrometeorites that became heated during entry through the Earth's atmosphere. Whether a particle would melt into a spherule would depend on several factors such as the particle's melting point, density, entry velocity, angle of incidence, and diameter. Particles about 10 – 100 microns in size would be most likely candidates for melting; see Whipple (1951). However, this mechanism has difficulty accounting for airborne microspheres found at high altitudes (which have been shown to be non-rocket-exhaust in nature) and for spherules found on the Moon. Parkin, Sullivan, and Andrews (1977) have suggested that some cosmic spherules are already round before they enter the atmosphere. Consequently, some other agent besides air friction may be involved in the production of cosmic spherules. Perhaps these were interplanetary dust grains that were originally irregular in shape but that became abraded into a spherical form by solar wind bombardment. Another possibility would be an intense outburst of solar radiation such as that proposed by Mueller and Hinsch to account for the spherules found on the Moon; see Chapter 4 (Subsection 4.7.3).

Langway (1970) reports that the cosmic spherules he has found in Greenland ice were generally less than 100 microns in diameter, with about 75% - 85% being 5 – 25 microns in size. He has studied the concentration of cosmic spherules at a depth of 300 meters (~1250 A.D. ice) in a core drilled at Site 2, Greenland (77° N, 56.1° W) and at a depth of 6 meters (~1952 A.D. snow) at Camp Century, Greenland. He reports spherule concentrations at these locations of about 44 spherules per liter of ice, or weight concentrations ranging from 1.2 – 4.2 μg/lit of ice. Assuming Holocene dust concentrations of ~200 μg/lit of ice for Camp Century (see Table XII), this represents about 0.5 – 2% of the total dust weight deposited at these locations. Based on known rates of ice (or snow) accumulation at these two sites, it is estimated that cosmic spherules are deposited at the rate of about $0.4 - 1.3 \times 10^{-7}$ μg/cm²/yr, giving an integral influx of about $10^5 - 10^6$ tons of cosmic dust per year.

Thiel and Schmidt (1964) find cosmic spherule deposition rates for Antarctica that compare with Langway's findings for Greenland. They estimate a deposition rate of $3.6 \times 10^{-8} \mu\text{g}/\text{cm}^2/\text{yr}$ based on a study of cosmic spherules filtered from ice taken within 10 meters of the Antarctic glacier surface. Thompson (1977a) has noticed a rather constant occurrence of extraterrestrial microspheres throughout the entire length of both the Byrd and Camp Century cores. However, he has found levels one to two orders of magnitude lower than the levels reported by Thiel and Schmidt and by Langway. In Antarctic cores Thompson finds that the incidence of such particles range from 8 out of 5000 (0.16%) for the Byrd core down to 1 out of 9500 ($\sim 0.01\%$) for the Dome C core (personal communication, 1982).

The GEH proposes that toward the end of the Wisconsin Ice Age interplanetary dust concentrates (particularly particles of submicron size) became significantly elevated. If this were indeed the case, then a record of this event should have been preserved in glacial ice. That is, one would expect that glacial ice dating from this period would contain a higher concentration of extraterrestrial material as compared with present concentrations. Previous to the formulation of the GEH, the only report of cosmic materials in Wisconsin ice was that made by Thompson (1977a) of a relatively invariant occurrence of cosmic spherules. However, this easily identifiable fraction may not be a good indicator of the *total* concentrations of Wisconsin stage extraterrestrial material. For example, most dust particles, especially those under 10 microns in size would be expected to retain their original form in the course of their entry through the Earth's atmosphere. Hence, if originally irregular in size such cosmic particles would be difficult to distinguish from windblown continental dust of terrestrial origin. The total amount of extraterrestrial material is then better measured through the use of *geochemical analysis* of the gross sample, rather than through morphological observation of individual particles. It is the former technique, total sample analysis, that has been used in this study to check the GEH.

Iridium and nickel were chosen as cosmic dust indicators since these elements are enhanced by two to three orders of magnitude in meteorites as compared with typical terrestrial crustal material; see Table XIII. Platinum and osmium are also good indicators, but are difficult to measure with the neutron activation analysis (NAA) technique used in this study. Ganapathy, Brownlee, and Hodge (1978) using the NAA technique have analyzed three cosmic spherules retrieved from ocean sediments and found that 2 out of these 3 had high Ni concentrations (2.9% and 1.0%) and that all three had high Ir concentrations (35 ppb, 285 ppb, and 535 ppb). One of these particles was found to have elemental ratios (for 10 elements) similar to C-1 chondritic material, although 5 elements were depleted by over an order of magnitude from chondritic abundances. Also, Ganapathy and Brownlee, (1979) have analyzed two aggregate-type interplanetary dust particles collected from the stratosphere and have found that both particles have elemental compositions similar to C-1 chondritic material (for 7 elements tested), although two elements (Zn and Au) were exceptions, being enhanced by 2.8 ± 1 fold and 34 ± 11 fold respectively. Some of the elemental concentrations of both the 3 cosmic spherules and the two interplanetary dust particles are listed in Table XIII for comparison to terrestrial and extraterrestrial material.

It is concluded that Ir and Ni may be taken as reasonably good indicators of the presence of micrometeoritic material with the assumption that these materials are present in C-1 chondritic ratios (514 ± 25 ppb for Ir and 1.0% for Ni). However, as is discussed in the next subsection, some extraterrestrial material may be compositionally very different from C-1 chondritic meteoric material. Thus, Ir and Ni should only be considered as approximate indicators for the amount of cosmic material present in glacial ice.

TABLE XIII

COMPARISON OF ELEMENTAL ABUNDANCES IN ONE CAMP CENTURY ICE CORE
DUST SAMPLE TO KNOWN TERRESTRIAL AND COSMIC SOURCES

| Material | Ir (ppb) | Au (ppb) | Fe (%) | Ni (%) | Co (ppm) | Sn (ppm) | References |
|--|-----------|--------------|-----------|----------------|-----------|------------|--|
| Upper Continental Crust | 0.024 | 1.8 | | 0.0019 | 12 | | Shaw et al. (1976) |
| Columbia River Basalt (BCR-1 Standard) | 0.004 | 0.9 ± .4 | 10.7 ± .4 | 0.0012 ± .0001 | 42 ± 2 | < 3 | Flanagan (1976) |
| C-1 Chondrites | 514 ± 25 | 152 ± 27 | 17.1 | 1.03 | 483 | 1.05 ± .19 | Krahenbuhl et al. (1973); Mason (1971); Shima (1964) |
| Iron Meteorites | 10 - 2000 | 1200 ± 900 | 89 ± 2 | 9 ± 2 | | 0.1 - 7.7 | Wasson and Kimberlin (1967); Boyle (1979); Shima (1964); Ehmann (1963) |
| Three Cosmic Spherules | | | | | | | |
| #1 | 35 ± 1 | 1.8 ± 5.2 | 30.4 ± .3 | 2.9 ± .2 | 460 ± 5 | ----- | Ganapathy, Brownlee, and Hodge (1978) |
| #2 | 285 ± 10 | 1.4 ± 3.7 | 38.6 ± .4 | < .02 | 289 ± 3 | ----- | |
| #3 | 535 ± 4 | 7.6 ± 4.2 | 41.8 ± .4 | 1.0 ± .1 | 452 ± 4 | ----- | |
| Interplanetary Dust (two particles) | 530 ± 120 | 5200 ± 1700 | 19 ± 5 | 1.0 ± .3 | 390 ± 150 | ----- | Ganapathy and Brownlee (1979) |
| Anomalous Sn Sample from Camp Century Ice (1234.7 meter depth) | 37 ± 18 | 12600 ± 6300 | 1.6 ± .8 | 0.065 ± .01 | 22 ± 11 | (40 ± 20%) | This work |

8.3.1 Compositionally Anomalous Layers in the Greenland Ice Sheet

Prior to the present study, a stratigraphic analysis of the concentration of precious elements in deep ice cores had not been undertaken. Previous investigations have tended to study elements more commonly found in the Earth's crust. For example, Thompson (1977b) using the electron microprobe technique has analyzed individual dust particles from the Camp Century and Byrd deep ice cores to determine their concentrations of Mg, Al, Si, P, S, K, Ca, Fe, Ti, Sn, Cu, Zn, and Mo. Cragin et al. (1977) have spectrophotometrically analyzed the meltwater of glacial ice samples taken from the Camp Century and Byrd cores to determine their concentrations of Mg, Al, Si, Na, K, Ca, and SO₄. Finally, Petit et al. (1981) have used the neutron activation analysis technique and atomic absorption to detect Al, Na, Cl, V, Mn, and Zn in ice samples from the Dome C core.

Of particular interest is Thompson's finding that tin (Sn) and molybdenum (Mo) are present in significant quantities at certain depths in the Camp Century Core. For example, in dust that he had filtered from glacial ice sampled from a depth of 1230.5 meters (dating 50,500 calendar years b2k) he found that 6 out of 7 dust particles contained substantial amounts of tin (2 – 30%) and 4 out of 6 particles contained molybdenum (14 - 22%).* Further down in the core, at a depth of 1342.2 meters (125,000 cal. yrs b2k), 3 out of 5 particles were found to contain Sn and 1 out of 5 particles contained Mo.* In addition, at a depth of 1162 meters (~19,000 cal. yrs BP), Thompson found tin at a concentration of 45.5% in 1 particle out of the 8 particles that he sampled. These three compositionally anomalous sample sections are marked in Figure 8.1 (curve-g) with asterisks. Of the other 10 Camp Century ice core depths studied by Thompson, none of the analyzed particles showed any trace of Sn or Mo. Moreover, in an analysis of 15 locations in the Byrd core, tin was found in only 1 out of 8 particles in a single core sample section taken from a depth of 700 meters (~7400 years b2k). Molybdenum was not found in the Byrd core at all.

Thompson (1977b, p. 46) has suggested that the Sn and Mo particles became entrained into the ice from the bedrock, with the implication that the Greenland glacier in this region is moving over a deposit of cassiterite (SnO₂) mixed with molybdenite (MoS₂). However, the levels containing the anomalous particles are found at distances of 42 m, 152 m, and 221 m above the bedrock surface. Thus, it becomes difficult to imagine how bedrock scrapings could work themselves up to such heights. Moreover, if bedrock scrapings had become entrained in the ice, then particles greater than 1 mm in diameter would be expected. However, as Thompson reports in his study (1977, p. 12), almost all of the particles observed had diameters less than 30 microns.

The strongest evidence against a bedrock origin for these particles comes from the recent discovery that the δO¹⁸ curves for the Camp Century and Dye 3 deep ice cores are virtually identical at heights greater than 90 meters and 70 meters, respectively, above bedrock (Dansgaard et al., 1982). If these particles had been entrained in the ice due to glacier flow over mountain ranges then it would be expected that the Camp Century δO¹⁸ record would have become considerably distorted, especially its signature of short term fluctuations. In such a case a close correspondence with the Dye 3 δO¹⁸ profile would not be expected. Instead, the evidence suggests that the upper portion of both of these ice core records have had a relatively undisturbed tectonic history.

I first came in contact with Thompson's work in November of 1979, not long after having formulated the GEH. It was my opinion at the time that the Sn and Mo particles discovered by Thompson had been *airborne* prior to their deposition in the ice, and in particular that they were of *extraterrestrial* origin. A terrestrial origin for such airborne

* In his publications, Thompson gives the logbook depths of these three samples as 1234.7 m, 1345.4 and 1166 m respectively. Above I give their actual core depths as determined by S. Johnsen.

particles seemed to me to be unlikely since Sn and Mo are present in the ice at concentrations $\sim 10^5$ times higher than levels found for the average composition of the Earth's crust. This led me to suspect that the material in these atypical sections could be cosmic dust deposited on the Earth by the periodic passage of superwaves.

One thing that strengthened this view was the observation that in each case these sample sections fall close to boundaries of major climatic change. For example, the 1342 meter section ($\sim 125,000$ cal. years b2k) coincides with a period of climatic cooling, while the 1231.5 meter anomalous section (50,500 cal. years b2k) coincides with an interstadial (positive δO^{18} values) in the Camp Century record. The 1163 meter section ($\sim 17,000$ calendar years b2k) is immediately followed by a brief cold stadial... ; see peak δ in Figure 8.1, curve-f. Finally, it was noted that the Byrd ice core section containing the single anomalous tin particle, dates at 7500 years b2k close to the time when the proposed 6000 BP Superwave would have passed the Earth.

I hypothesized that in all cases superwaves had transported the tin particles as cosmic dust and deposited them on the Earth as they passed by. The δO^{18} excursions associated with each of these events could be interpreted as evidence that this cosmic dust was able to exert a major influence on the Earth's climate; e.g., through its effect on the solar radiation continuum.

8.3.2 Possible Glaciological Evidence of Multiple Cosmic Events.

To determine whether the anomalous layers in the Camp Century ice core were of extraterrestrial origin I requested from Dr. Thompson of Ohio State University a portion of the filter paper from which the 1231.5 meter depth anomalous dust particles had been selected. This sample (#962-1) was then subjected to neutron activation analysis (NAA) along with several other ice core dust samples including two from the Camp Century ice core: #949 (1212 meter depth) and #992 (1275 meter depth).* The results of this analysis are discussed in Subsection 12.1.4 of Chapter 12. All three Camp Century dust samples were found to contain unusually high levels of Ir; see **p. 339**. Moreover, combining these results with the results of a second irradiation that I performed on additional samples from the Camp Century core, it is seen that out of 8 Wisconsin stage dust samples tested, spanning the dates 78.5 k – 38.7 k cal. yrs b2k, 6 had high Ir levels. Also, it is found that the cosmic dust deposition rates, as indicated by the Ir concentrations in these 6 samples, were from 10 – 60 times higher than present average deposition rates of extraterrestrial material. The results of these glacial dust tests are discussed more completely in Subsection 12.1.4 of Chapter 12.

One other interesting finding is that ice samples with high Ir concentrations tend to correlate with those samples that have high dust concentrations. Although more geochemical analysis is needed to confirm this correlation, this finding suggests that in addition to dust peaks #4, #5, and #7, for which high Ir concentrations were found, other dust peaks not yet analyzed (e.g., #6, #8, #9, and #10) may also be connected with cosmic events.

Planetesimal impacts, of the sort suggested by Alvarez et al. (1980) or Clube and Napier (1982), may be ruled out as the source of this iridium-bearing material. For example, dust from the impact of an asteroid or comet would be airborne for no more than a few years, equivalent to the period spanned by a few centimeters of ice in the Wisconsin section of the Camp Century ice core. Hence, there would be a very small chance of sampling such an event. For 6 out of 8 glacial ice samples to register high cosmic dust deposition rates ($1 - 6 \times 10^{-6}$ g/cm²/yr), with most ice samples spanning time periods of 15 - 20 years, 10^{14} to 10^{15} gram impacts would have had to occur as frequently as once every 20 years. First, such a

* Thompson instead lists these samples as having logbook depths of 1215 m, 1234.7m, and 1279 m.

high impact frequency is highly improbable. Second, if such a bombardment were maintained over a period of 5500 years, at least 100 impact craters greater than 4 kilometers in size would have been produced. But there is no geological evidence of young craters of such large a size or occurring in such great numbers. A third difficulty is that the composition of the dust does not match a simple mixture of chondritic material with average terrestrial crustal material. This is especially apparent in the case of Sample #962-1 discussed below. Thus, impacts by asteroids or meteorites of solar system origin may be ruled out. Cometary bodies of anomalous interstellar origin, however, cannot be ruled out on the basis of this compositional evidence.

8.3.3 Anomalous Dust Sample #962-1.

The unusual composition of dust sample #962-1 was verified. My analysis indicates that it consists of about $60 \pm 15\%$ tin (see [p. 357](#)), giving it an enhancement factor of 286,000 relative to Earth crust abundance. Also it was found to contain substantial amounts of Ir, Au, Ag, and Sb, also at very high enhancements. Molybdenum, however, was not found to be present above the detection threshold of 14 ppm. Tin was also found to be present in dust filtered from an ice sample positioned one meter below this sample at a depth of [1231.5](#) meters, hence dating about 400 years earlier. This dust sample(#962-2) was filtered from Camp Century ice obtained for this study from the ice core storage facility in Buffalo, New York. Using this deeper sample as a reference, within just this depth of 1 meter, the concentration of Sn was found to jump by $>2.7 \times 10^4$ fold, Au went up by >21 fold, Ir by >74 fold, Ni by >17 fold, and Ag by >218 fold; see Figure 12.1(a) ([p. 339](#)). The full magnitude of this step-function jump could not be determined because the levels of Sn, Au, Ir, and Ag in sample #962-2 were either below the threshold of detection, or below the filter background levels.

As pointed out in Chapter 12 (see Figure 12.3, [p. 345](#)), Ir, Fe, Co, and Ni occur in Sample #962-1 in approximately the same relative ratios as found in C-1 chondrites. However, Sn, Sb, Au, and Ag occur at levels that are many orders of magnitude higher. Thus the elemental data for Sample #962-1 seem to indicate the presence of two main components: one being extraterrestrial dust of C-1 chondritic composition and making up about 7% of the sample, the other consisting of tin-bearing particles containing traces of antimony, gold, silver, and possibly other elements that are undetectable by the particular NAA technique employed in this study. In addition, a small amount of wind-blown continental dust is probably present in the sample. Gold is much more abundant in meteoritic material than it is in terrestrial material (Earth's crust average), so its presence encourages the choice of a cosmic origin for the tin. Also the presence of the Ir-Fe-Co-Ni C-1 chondrite signature, by association allows the inference of a cosmic origin for the tin. Finally, the fact that both Ir and Ni (both good indicators of extraterrestrial material) increased abruptly in conjunction with the increase in tin again leads to the inference of an extraterrestrial origin for the tin.

The tin cannot be attributed to a terrestrial source since the enhancement factor for Sn in this anomalous sample relative to crustal material is greater than 10^5 fold. But neither can its origin be attributed to the more familiar categories of meteoritic material, a few of which have been listed in Table XIII ([p. 224](#)) since the abundance of Sn in such substances is comparable to the abundance in the Earth's crust. Thus if this material is of extraterrestrial origin, its source must be different from that of the majority of meteoritic material. As one possibility, this dust could be derived from vaporized cometary masses of anomalous composition that at one time resided in the Oort cloud. Alternatively, this material could be of interstellar origin, i.e., derived from a nearby interstellar cloud or from a nearby supernova remnant (e.g., the North Polar Spur); see Chapter 3, Subsection 3.3.2.

Evidence has recently been accumulating which indicates that the composition of extraterrestrial dust falling on the Earth sometimes differs radically from the composition of stony or iron meteorites or of C-1 chondrites. A good source of information on anomalous particle compositions is the NASA Cosmic Dust Catalog, Volumes 1 - 3 (1982). This is a compilation of scanning electron microscope images and energy dispersive spectra of dust particles captured from the stratosphere with the aid of high altitude aircraft. Besides particles exhibiting a typical meteoritic elemental signature, this collection of particles commonly includes cosmic microspheres having the following anomalous elemental signatures: Al-Ca, Al-Si-Ca, Al-Fe, Al-Cu, Al-Si-Fe, Ti, and Al-Ti. Also sometimes a Mg-Si signature typical of stony meteorite material is present, but mixed with anomalously high amounts of Al and Ca. It is interesting to note that spherical inclusions containing very high concentrations of Ca, Al, and Ti have also been found in the Allende meteorite (Grossman, 1973). Perhaps these C-Al-Ti-rich microspheres found in the stratosphere were originally formed in a similar fashion. Manmade rocket-exhaust microspheres are also found to be present in the NASA collection, but they can be easily distinguished by their pure aluminum signature. In addition, Al, Ca, and Ti are also found to be present in irregularly shaped particles listed in the catalogue and these also may be identified as being of cosmic origin.

Hallgren and Hemenway (1976) have conducted an energy dispersive X-ray analysis of micrometeorite craters found on polished plates exposed in a Skylab experiment. The element most commonly detected was aluminum, which was found in about 70% of the 18 craters analyzed. By comparison, iron was found in only about 20% of the craters and nickel in 1 out of 18 craters. Also, Hemenway, Hallgren, and Schmalberger (1972) report the presence of unusually high concentrations of heavy elements in submicron cosmic dust particles collected by rocket from noctilucent clouds over Sweden. As a source for these particles they rule out the Moon, meteorites, asteroids, and comets, leaving the Sun and interstellar dust as possible candidates. While they suggest a solar origin, an interstellar origin is also quite probable. Finally, Brownlee (1983, personal communication) has found that deep sea sediments contain extraterrestrial microspheres composed of a metallic alloy of platinum, iridium, osmium, and ruthenium. Again, the composition of such particles deviates radically from the composition of the various classes of meteorites.

It should be pointed out that some of the large plate-like dust particles that Thompson (1977b) has found in the Camp Century ice core resemble the micron-sized crystal platelets that Bradley, Brownlee, and Veblen (1983) have found in aggregate-type interplanetary dust particles. Some of these platelets may be seen embedded in the "CP" particle shown in Figure 8.3(a). One particularly large and thick crystal (about 3 microns long) is shown magnified in Figure 8.4(a) (Bradley et al., 1983). This may be compared to the 30 micron tin-bearing particle shown in Figure 8.4(b) (Thompson, 1977b, p. 147) which was selected from core tube section #962 of the Camp Century core.

Bradley et al. have identified the interplanetary dust platelet as a crystal of enstatite (MgSiO_3) and also report the presence of enstatite crystals in the form of whiskers (rod and ribbon shapes). They conclude that such crystal morphologies were most probably formed by gas-to-particle condensation from a low-pressure hot vapor phase, as might exist in a nebular gas cloud. Donn and Sears (1963) have predicted that interplanetary dust particles derived from comets would very likely contain whiskers and platelets. The discovery of Bradley, Brownlee, and Veblen strongly supports this prediction and suggests that CP micrometeorite particles are derived from cometary material. In a similar manner the platelet-like tin-bearing particles found in Camp Century ice may also have been derived from a cometary mass. These particles may also be crystals (cassiterite?) which like the CP micrometeorite enstatite crystals may have originally formed through primary growth from a vapor phase. [**UPDATE:** After this dissertation was completed, some interplanetary dust particles were reported to contain monolithic grains of tin oxide (see [p. 359](#)).]

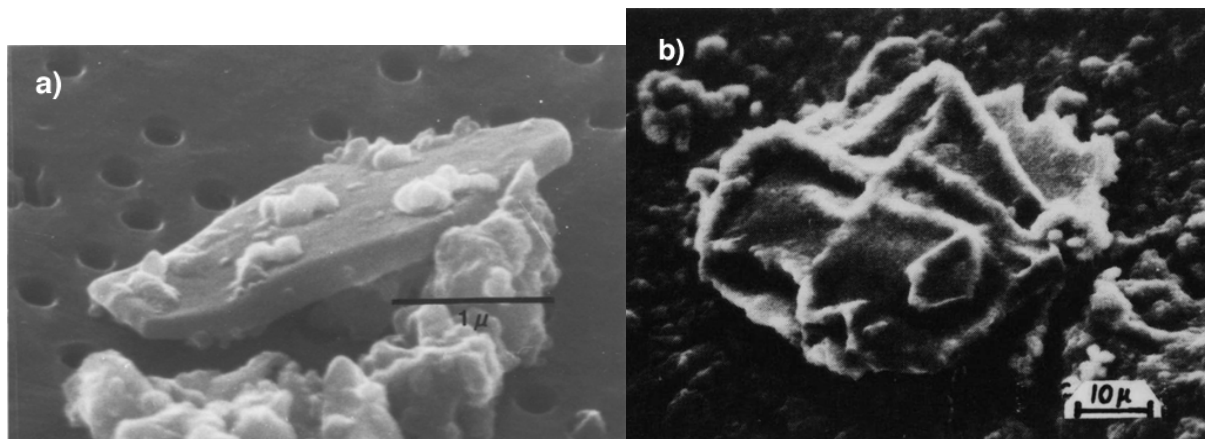


Figure 8.4. a) An enstatite crystal platelet selected from a large interplanetary dust particle collected from the stratosphere (Bradley, Brownlee, and Veblen, 1983; photo courtesy of D. E. Brownlee, University of Washington). b) A tin-bearing particle of platelet-type morphology selected from core tube section #962 of the Camp Century ice core (Thompson, 1977b, p. 147).

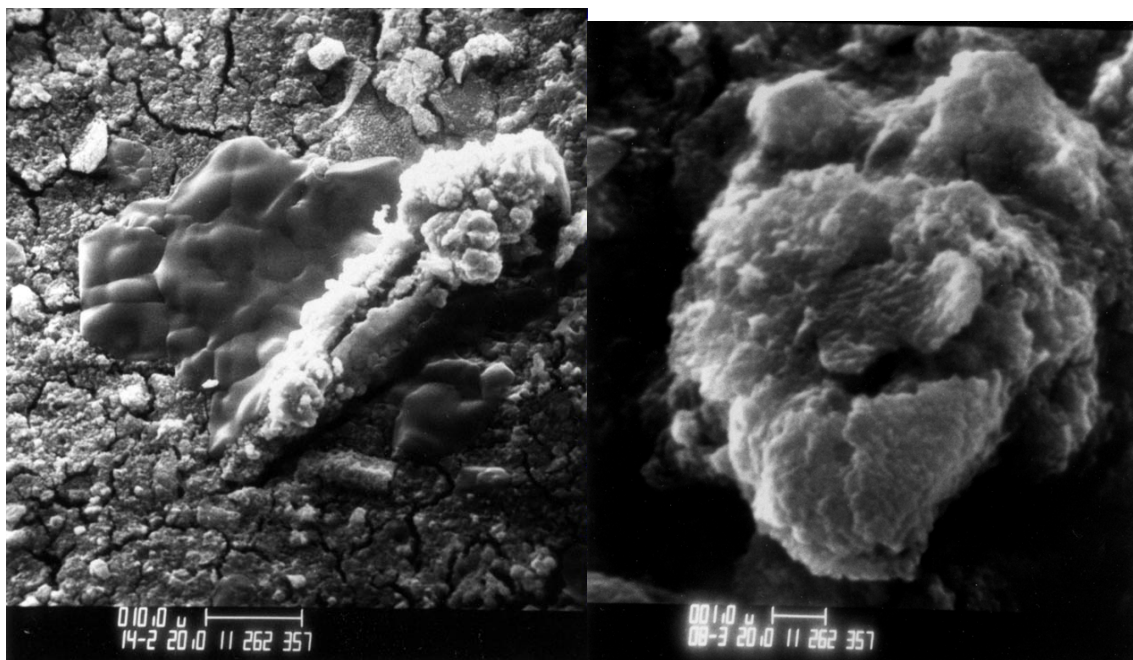


Figure 8-A. **UPDATE:** Scanning electron microscope photos imaged of another tin-bearing particle from Camp Century ice core tube section #962. The image at the right is a magnification of the upper right hand corner of the particle shown on the left (courtesy of E. Cerlin).

To ascertain the amount of extraterrestrial material present in the glacial ice dust sample, the composition of the source material must be known. If this material had come from outside of the solar system, then there is considerable uncertainty involved in estimating the amount of cosmic material (e.g., based on Ir and Ni concentrations) since little is known about the composition of such material. Even for material originating from within the solar system there is some uncertainty as to the precise composition. For example, C-1 carbonaceous chondrite meteorites contain 514 ± 25 ppb of Ir whereas for iron meteorites the concentrations of Ir may range from 10 ppb to 2 ppm. Also, nickel is 9 times more abundant in iron meteorites, being present in concentrations of $9 \pm 2\%$ as compared with $\sim 1\%$ for C-1 chondrites; see Table XIII. If the iridium content of Sample #962-1 is used as an indicator and the source material is assumed to have a C-1 chondritic abundance of 514 ppb, then only about 9% of the sample would be cosmically derived. On the other hand, if an extraterrestrial origin is assumed for the tin, then perhaps as much as 69% (by weight) of the dust deposited in the ice at that particular time would be cosmically derived.

In either case the sharp transient increase in cosmic dust deposition, suggested by the results shown in Figure 12.1(a) (p. 339), indicates that the concentration of interplanetary dust in the Earth's vicinity rose and fell in an abrupt manner. As seen in Figure 12.1(b), coincident with this tin event there is a decrease in the weight concentration in ice of elements typically found in terrestrial crustal material. This could have been caused by a temporary reduction in the atmospheric loading of continental dust (e.g., due to lower wind speeds), or more probably it could have been caused by an increase in the rate of ice accumulation.

It is interesting to note that at a depth of 1170 meters, just 4 meters below the Camp Century core sample section where Thompson has reported his discovery of a single tin-bearing particle, Cragin et al. (1977, p. 620) have observed an unusually high concentration of aluminum, many times higher than the highest concentrations found in their other samples; see core section marked with a dagger in Figure 8.1, curve-g. The other elements which they measured in the anomalous sample did not show a comparable enhancement. Consequently, they concluded that the sample had become contaminated with aluminum during the measuring procedure. However, it may be that the Al excess found at this depth is not due to laboratory contamination, but rather to the deposition of aeri ally borne particles. Since aluminum is one of the most abundant elements in the Earth's crust, second only to silicon and oxygen, it might be inferred on first impulse that this Al excess is terrestrially derived. However, the recent finding that aluminum occurs commonly in cosmic dust (see p. 228) also suggests the possibility that this anomaly may be of extraterrestrial origin. This is further supported by noting that this sample occurs close to the tin-bearing dust sample. However, to check whether this material is indeed of extraterrestrial origin, further elemental analysis of this core section should be done. As a further test of the hypothesis that the Sn particles found in the Camp Century core were deposited aeri ally over a large portion of the Earth's surface, an attempt should be made to locate this anomaly in an isochronous portion of another ice core.

8.3.4 The Possible Cosmic Origin of Placer Gold Deposits

The detection of high gold concentrations in the Camp Century ice core (Sample #962-1) raises an interesting question. Namely, if this gold were of cosmic origin, wouldn't its deposition be more widespread, and hence could some portion, or perhaps a large fraction of the gold observed in the Earth's sedimentary record also be of cosmic origin? In checking out this possibility in the literature, it was discovered that indeed gold is quite prevalent in Late Pleistocene deposits. Moreover, it was found that if the source of this gold were extraterrestrial, rather than terrestrial, then some of the problems raised in regard to its origin

could be resolved. For example, in his world survey of gold deposits, Boyle (1979, p. 381) notes that in many placer districts there are no large auriferous deposits that could have supplied particles of gold to the placers.

Further extending this scenario, it might be hypothesized that gold nuggets are a special class of meteorite, e.g., fragments of a common mass of native gold that once composed a portion of the core of a star and that had become dispersed into space as a result of a supernova explosion. Of course, at this stage such a suggestion must be viewed cautiously. While gold is found in meteorites, sometimes enhanced as much as 2000 times above crustal abundances, it is always found in combination with other metals such as iron and nickel, which are present in much greater abundance. No class of meteorites is known to consist almost entirely of native gold. Thus, if a meteoritic origin for gold nuggets were to be maintained, it would be necessary to concede that such objects would fall to the Earth very rarely. However, recently Donald Brownlee of the University of Washington (1983, personal communication) discovered that deep ocean sediments contain micrometeorite spherules composed of an alloy of platinum group metals. Gold, however, was not found to be present, which could be due to the fact that Au is more volatile. The discovery of the platinum alloy spherules was made 1½ years after the discovery reported here of high gold concentrations in glacial ice.

Another problem mentioned by Boyle (p. 382) is the question of how gold nuggets were formed. According to one theory, nuggets are formed by a chemical accretion process in which gold, originally in a solution or vapor state, crystallizes onto the surface of the nugget. According to another theory, nuggets are formed as detrital material eroded from primary gold veins. Boyle points out that there is no general agreement in the literature as to which of these mechanisms predominates. However, both of these theories have particular difficulty in accounting for the larger nuggets, which are known to reach sizes of 15 cm and weights on the order of 100 – 200 troy pounds. For nuggets this size to have formed by chemical accretion, inordinately long times would be required, especially in view of the fact that the surface-to-volume ratio of a nugget decreases in proportion to its size. On the other hand, if a nugget of this size were of detrital origin, from what vein could such a large nugget have come, and how did it become transported to its location of discovery in the placer deposit? Obviously, conventional theories of terrestrial nugget formation (i.e., by chemical or mechanical processes) would be at a distinct disadvantage in accounting for the presence of nuggets in places such as Northern Siberia or Alaska where the ground is usually frozen solid all year around.

It should be cautioned that the proposal that placer gold is of cosmic origin rests primarily on evidence of high gold concentration found in just one core section of just one particular ice core. For the present all that can be concluded is that the gold that has been discovered in Subsamples #962-1-a and #962-1-b appears to be in a finely divided form, since the ratio of gold to other elements such as Fe and Sn in these two subsamples is very similar. Whether this gold is in native form or alloyed with other elements enhanced in this sample, such as iridium or tin, cannot be said for sure. However, it is worth noting that placer gold is often found in nature in association with cassiterite (SnO₂) and sometimes with iridium and other platinum group metals. Clearly, further geochemical analysis should be done before definite conclusions are drawn. Other sections of Wisconsin ice from the Camp Century core and from other ice cores should be studied for their precious metal content.

8.4 COSMOGENIC BERYLLIUM VARIATIONS

A critical prediction of the GEH is that cosmic ray intensities should have increased at the end of the Wisconsin. One way of checking to see if such an increase in fact occurred would be to determine whether at these times there had been a corresponding increase in the

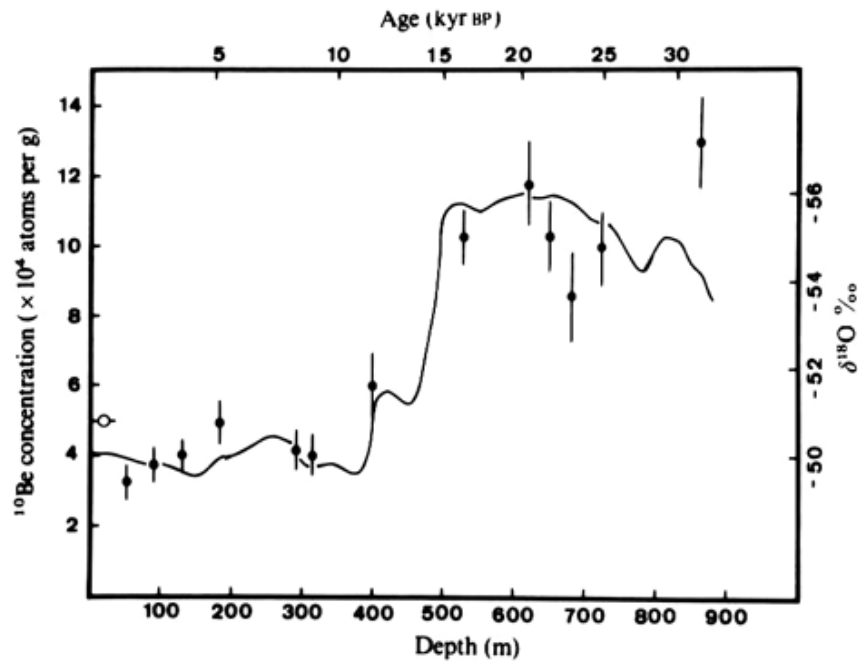


Figure 8.5. Beryllium-10 concentration in the Dome C ice core. Be-10 concentration is plotted as the data points (left-hand scale) and O^{18} is plotted as the solid line (right-hand scale). The horizontal scale is given in ice equivalent core depth. (Raisbeck et al., 1981)

deposition rate of the beryllium isotope Be-10. Be-10 is produced primarily in the stratosphere through collisions between cosmic ray nucleons and atmospheric nitrogen and oxygen nuclei. The beryllium then precipitates to the ground within a year of its formation. Cosmic ray protons and proton and neutron secondaries are currently the main producers of this isotope. Cosmic ray electrons, through the production of gamma rays, would also be able to produce Be-10, but not nearly as effectively as protons and neutrons.

There is strong evidence indicating that indeed the deposition rate of Be-10 was higher during the Wisconsin. Raisbeck et al. (1981) have found that the concentration of Be-10 in Dome C ice was 2 – 3 times higher during the Wisconsin as compared with the Holocene; see Figure 8.5. Also, Beer et al. (1982), testing ice samples from the Dye 3, Greenland ice core, have discovered that Be-10 concentrations in Wisconsin ice are 2.5 – 3 fold higher than in Holocene ice.

Several causes for the Be-10 increase have been suggested by Raisbeck et al. (1981). These include: a) a 2 – 3 fold decrease in the ice accumulation rate during the Wisconsin age, b) a change in the atmospheric circulation pattern resulting in more Be-10 being deposited in the Antarctic troposphere, and c) a reduction in solar activity (and hence in solar cosmic ray modulation) allowing the local cosmic ray background intensity to increase.

[UPDATE:] Their first suggested cause accounts for most of the increase since the ice accumulation rate at Dome C during the Late Wisconsin was only about half of the Holocene accumulation rate. However, some points are too high to be accounted for in this way. After carrying out additional work on this core, these researchers later established that a real ^{10}Be deposition rate peak existed around a depth of 850 meters. The second suggested cause might be a possibility if ^{10}Be were being deposited by a wet deposition process. But, recent data suggests that ^{10}Be is deposited in Antarctica by a dry deposition process.] Their third suggestion is unlikely since, as Beer et al. (1982) point out, the Be-10 results which Raisbeck

et al. (1981) have derived for the Maunder minimum indicate that Be-10 concentration would be increased at most by only 100% during periods of very low solar activity.

Either the cosmic ray background intensity in the solar vicinity was higher during the Wisconsin, or else solar cosmic rays were being produced at an unusually high rate due to enhanced solar flare activity. Both scenarios follow as a consequence of the GEH. More detailed stratigraphic analysis of the Be-10 profile is needed to distinguish between these alternatives, although at present I am inclined to interpret this long term increase as being due to an elevation of the Galactic cosmic ray flux associated with the passage of the 14,200 years BP superwave.

The model proposed in Subsection 3.3.1 (p. 75) suggests that, during the passage of the 14,200 years BP superwave, the local cosmic ray electron background intensity was up to 75 times higher than the current cosmic ray proton background. However, until a good estimate can be made of the effectiveness of γ -ray secondaries for producing Be-10, it would be difficult to say exactly how much of a Be-10 increase one could expect with this model; perhaps a 1 – 20 fold increase might be a good guess. Even so, it should be stressed that the values proposed for the peak superwave cosmic ray electron intensity outside the solar system and subsequently for the degree of modulation by the heliopause sheath and bow shock front are tentative. The GEH itself does not make precise quantitative estimates of these values due to the lack of sufficient information. However, the GEH does make the *qualitative* prediction that cosmic ray electron intensities should have been higher at the close of the Wisconsin Ice Age. The results of Raisbeck et al. and Beer et al. appear to confirm this prediction. It is interesting to note that this early prediction of the GEH (see Table I, p. 6) was formulated two years before the Be-10 results of Raisbeck et al. were published; e.g., LaViolette (1981). In fact, the author had completed early gamma ray counts on the first set of glacial ice dust samples just prior to the publication of these confirmatory data.

Another way to check the glacial ice record for evidence of elevated cosmic ray activity is to search for the presence of high nitrate concentrations. Gamma rays and secondary electrons associated with a superwave would ionize the atmosphere and produce large quantities of compounds such as ammonia and oxides of nitrogen. Supernova explosions and asteroid impacts would also be expected to produce large quantities of atmospheric nitrates. However, such events would appear in the ice record as a single concentration spike, rather than as a general increase in the background level. If increased levels of NO_x are found in Wisconsin ice it could be difficult to distinguish if these high levels were due to increased intensities of Galactic cosmic rays or to increased intensities of solar cosmic rays. However, both possibilities are embraced within the GEH.

8.5 THE VOLCANIC ASH RECORD OF THE BYRD ICE CORE

Studying the Byrd ice core, Gow and Williamson (1971) have found a series of about 2000 cloudy layers, called *dust bands*, and about 25 volcanic ash layers, referred to as *ash bands*. Dust bands and ash bands are generally on the order of 1 cm thick, but may vary in thickness from a few millimeters to several centimeters. Dust bands differ from ash bands in several respects. For example, the weight concentration of the debris found in dust bands is several orders of magnitude less than that found in ash bands (≤ 10 mg per lt of ice vs. up to about 1 gram per lt of ice for ash bands). Also, the mean particle size typical of a dust band is nearly two orders of magnitude smaller, 1 to 2 microns as compared with $\sim 50\mu$ for particles in the ash bands.

Gow and Williamson have conducted a petrographic examination of 15 of these ash bands and have found that 11 are predominantly composed of volcanic glass fragments, two are lithic (volcanic rock), and that two can be classified as crystal ashes. They believe that

these ash falls are local since Byrd Station is quite close to several recently active volcanoes. Confirming this proposal, Kyle and Jezek (1976) and Kyle et al. (1981) have studied 6 ash bands from the Byrd core and have found that these tephra layers have a peralkaline trachyte composition similar to volcanic rock taken from Mt. Takahe, a volcano about 350 km from Byrd Station.

While the origin of the ash bands is fairly well understood, much less is known about how the dust bands were formed. [See Chapter 12 of this dissertation for NAA results on a Byrd ice core dust band.] Gow and Williamson (1971) suggest that dust bands, like ash bands, might be of volcanic origin and that their finer particle sizing is due either to a change in the nature of the eruption producing the ash bands or to the onset of more distant eruptions. It is worth noting that dust bands and ash bands are not randomly intermixed. Their respective times of peak occurrence are separated in time by several thousand years. For example, as seen in Figure 8.1, ash bands (indicated by vertical lines near curve-e) appear in greatest numbers between depths of 1450 – 1650 meters (24 k – 35 k calendar years b2k). This may be compared to the dust band frequency curve (Figure 8.1, curve-e) which indicates that dust bands appear in greatest numbers between depths of 1300 – 1450 meters (16.5 k - 24 k calendar years b2k). Thus it appears that the dust bands are produced by a source different from that responsible for the ash bands.

The dust band frequency curve (after Gow and Williamson, 1971) is based on visual inspection of the Byrd ice core immediately after core drilling. Data were recorded for 1 out of 7 to 10 core tube sections, i.e., about every 10 to 15 meters. Estimates of dust band frequency (bands per meter of ice) have been derived from the original log book data made available courtesy of Anthony Gow. These values are presented in Table XIV along with their corresponding core depths (corrected for bore hole slanting).

If distant volcanic eruptions are claimed as the source of the bands, then one arrives at unusually high rates of volcanism for the Late Wisconsin. For example, of the 23 world wide ash falls that have occurred since 1750 AD only four have produced increases in microparticle concentration significantly above background levels prevailing in Antarctic ice. In an ice core penetrated at the South Pole, Mosley-Thompson and Thompson (1982) found microparticle concentration peaks in the range of 10^5 – 10^6 particles/ml at 1887 AD (Tarawera eruption, $38\frac{1}{2}^\circ$ S), at 1883 AD (Karakatoa eruption, 6° S), at 1815 AD (Tambora eruption, 8° S), and at 1767 AD (Mayon Luzon eruption, $13\frac{1}{2}^\circ$ N). By comparison, at a depth of about 1360 meters dust bands exhibiting particle concentrations in this same range occur as frequently as 30 per meter of ice core depth. This translates into a rate of about one band every two years, implying a volcanic eruption rate about 25 times higher than the current rate. Moreover, this rate of explosive eruptions would have had to have been sustained over periods of hundreds of years. Clearly, in the geologic past there have been periods of extensive volcanism, and it is known that the Late Wisconsin was a period of unusually high volcanic activity. But the question that must be asked here is whether such a high rate of volcanism is compatible with the geologic record.

UPDATE

Beryllium-10 Data (update to p. 232): The Galactic Explosion Hypothesis predicts that their were episodes during the last ice age when cosmic ray intensity was quite high. This was first stated in my 1980 dissertation proposal and restated in this dissertation in Chapter 1 (p. 6) and in Chapter 13 (p. 369). An attempt was made to check this prediction by citing the 1981 Dome C ice core beryllium-10 data shown in Figure 8.5. However, this graph plotted raw data that had not been adjusted for changes in ice accumulation rate or solar wind screening. Moreover its data points were not sufficiently close together to show evidence of

TABLE XIV
DUST BAND OCCURRENCE RATE AS A FUNCTION OF DEPTH
IN THE BYRD STATION ICE CORE

| Ice Core Tube No. | Log Book Depth (m) | Corrected Depth (m) | Date (cal. yrs BP) | Dust Band Frequency (No./meter) |
|----------------------|--------------------------|---------------------------|-----------------------|---------------------------------------|
| 756 | 1209.09 | 1201.63 | 14,200 | 0 |
| 766 | 1224.30 | 1216.50 | | 1 |
| 774 | 1236.09 | 1228.07 | | 0 |
| 782 | 1248.02 | 1239.78 | | 0 |
| 789 | 1258.36 | 1249.94 | | 1 |
| 797 | 1270.65 | 1262.03 | | 2 |
| 806 | 1284.22 | 1275.38 | | 2 |
| 813 | 1294.72 | 1285.72 | | 4 |
| 820 | 1304.72 | 1295.57 | | 4 |
| 827 | 1315.99 | 1306.68 | | 8 |
| 834 | 1326.08 | 1316.62 | 17,700 | many |
| 841 | 1336.17 | 1326.57 | | many |
| 847 | 1345.13 | 1335.39 | | 24 |
| 854 | 1355.61 | 1345.69 | | many |
| 863 | 1369.06 | 1358.90 | | many |
| 870 | 1379.61 | 1369.27 | 20,500 | 27-34 |
| 877 | 1389.82 | 1379.30 | | 20 |
| 884 | 1400.39 | 1389.61 | | 4 |
| 892 | 1412.24 | 1401.32 | | 2 |
| 898 | 1421.34 | 1410.29 | | 2 |
| 905 | 1431.84 | 1420.64 | | 8 |
| 912 | 1442.94 | 1431.56 | 23,800 | 16 |
| 920 | 1454.87 | 1443.31 | | 14 |
| 936 | 1478.48 | 1466.56 | | 2 |
| 943 | 1488.93 | 1476.85 | | 2 |
| 951 | 1500.87 | 1488.58 | | 2 |
| 957 | 1509.85 | 1497.39 | | 1 |
| 964 | 1520.39 | 1507.67 | | 0 |
| 971 | 1530.63 | 1517.78 | | 1 |
| 978 | 1541.48 | 1528.42 | | 4 |
| 987 | 1554.93 | 1541.62 | | 3 |
| 993 | 1563.98 | 1550.49 | | 1 |
| 1005 | 1581.99 | 1568.17 | | 0 |
| 1012 | 1592.84 | 1578.80 | | 0 |
| 1020 | 1604.96 | 1590.65 | | 1 |
| 1027 | 1615.65 | 1601.10 | | 0 |
| 1036 | 1629.17 | 1614.31 | | 2 |
| 1044 | 1641.19 | 1626.05 | | 0 |
| 1061 | 1667.28 | 1651.63 | | 0 |
| 1068 | 1677.76 | 1661.91 | | 1 |
| 1075 | 1688.24 | 1672.15 | | 0 |
| 1089 | 1709.63 | 1693.04 | | 0 |
| 1098 | 1723.19 | 1706.29 | | 1 |
| 1106 | 1735.19 | 1718.01 | | 0 |
| 1116 | 1750.15 | 1732.65 | | 0 |
| 1125 | 1763.88 | 1746.16 | | 1 |
| 1132 | 1774.54 | 1756.6 | 41,000 | 0 |

peaks. So definitive proof of the cosmic ray prediction did not come until later when more detailed ^{10}Be data became available. This more recent data, discussed below, confirms this key prediction.

Ice core beryllium-10 data that became available after this dissertation was published shows that cosmic ray radiation intensity impacting the solar system has indeed fluctuated dramatically over the past 140,000 years. This may be seen in Figure 8-B which charts relative cosmic ray intensity (lower profile) and climatic temperature change (upper profile) versus ice core depth (time) in the Vostok, East Antarctic ice core.⁽¹⁾ Distinct peaks are evident, some rising over 2 fold above the intensity of the present cosmic ray background, the highest cosmic ray levels correlating with glacial periods (stages 2 – 5d, and 6). In particular, high intensities are registered for the period 15,000 – 11,000 years b2k, spanning the time when the 14,200 years BP superwave would have been impacting the solar system. The cosmic ray intensity profile obtained for the Byrd Station, Antarctic ice core similarly shows high cosmic ray intensities at the end of the last ice age (15.9 – 12 kyrs b2k); see Figure 8-C.⁽¹⁾ The downward pointing arrows in both diagrams indicate a time of enhanced solar flare activity and increased screening of the incident galactic cosmic ray flux. The text box below describes how these cosmic ray profiles were generated.

Changes in geomagnetic field intensity cannot account for these peaks since near the

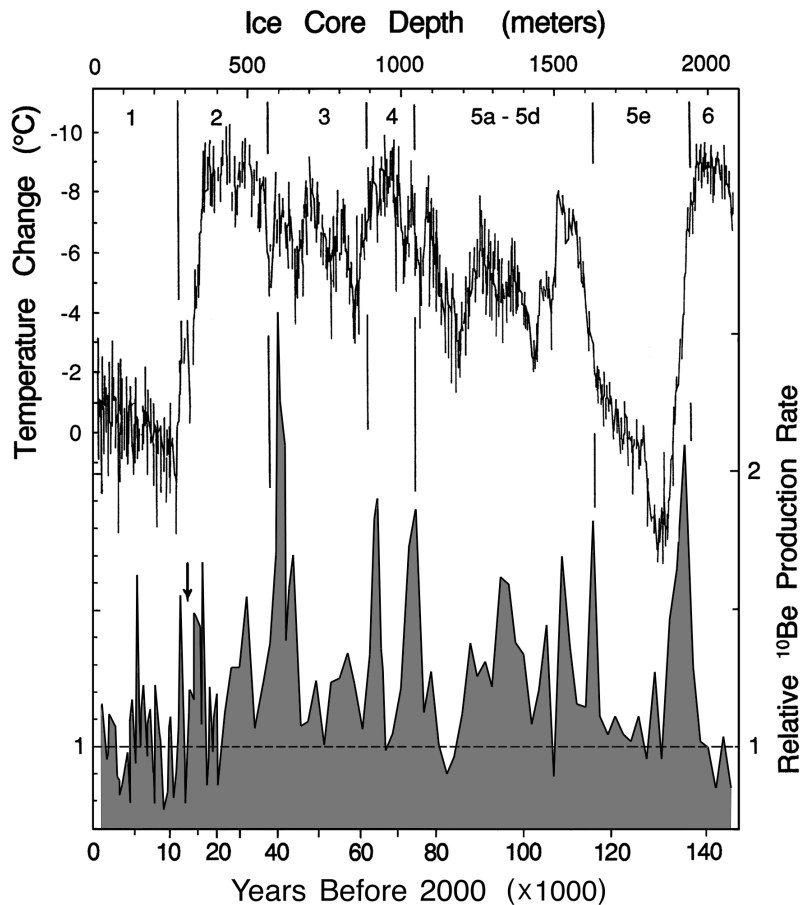


Figure 8-B. Lower profile: Cosmic ray intensity impacting the solar system (0 – 145 kyrs b2k) normalized to present levels (based on the Vostok, Antarctica ice core ^{10}Be concentration data of Raisbeck et al. [*The Last Deglaciation*, p. 130] and Raisbeck et al. [*Nature*, 1987], adjusted by P. LaViolette for changes in ice accumulation rate; see textbox below). Upper profile: Ambient air temperature, as indicated by the ice core's deuterium content (from Jouzel, *Nature*, p. 403).

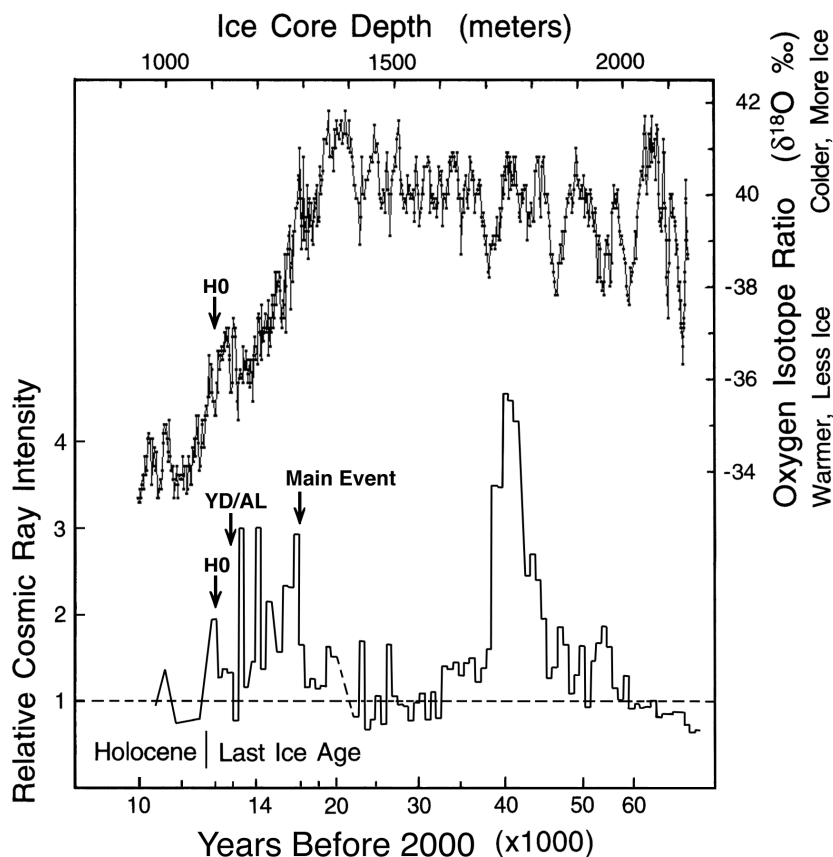


Figure 8-C. Lower profile: Cosmic ray intensity impacting the solar system (10 – 70 kyrs b2k) normalized to present levels. (Based on the Byrd Station ice core ^{10}Be concentration data of Beer et al. [*Nuc. Instrum. Meth. Phys. Res.*, p. 204, and *The Last Deglaciation*, p. 145], adjusted by P. LaViolette for changes in ice accumulation rate; see textbox below.) Upper profile: The ice core's oxygen isotope ratio, an indicator of ambient temperature and glacial ice sheet size (courtesy of T. Blunier, B. Staufer, and J. Chappellez, 1998, Antarctic and Greenland GRIP synchronization data.).

poles, where these cores are located, geomagnetic screening of the incident cosmic ray flux is minimal and hence has a minimal effect in reducing ^{10}Be production. Beer, et al. have concluded that the geomagnetic field has little effect on ^{10}Be concentrations in polar ice since such concentrations in the Camp Century ice core have remained constant over the past 5000 years despite the two fold change in geomagnetic field intensity.⁽²⁾

In addition, several cosmic ray peaks are evident at earlier times and are seen to coincide with boundaries of rapid climatic change. We find cosmic ray peaks at 32.1, 40.0, 43.7, 65, 75.6, 95, 105.6, 109.4, 117, and 132 kyrs b2k. The peak centered at around 40,000 years b2k is present in both the Vostok and Byrd ice core records. Liritzis and Grigori have performed a spectral analysis of the Vostok Be-10 record and find that it contains recurrence periods of 5.4 ± 0.3 k, 12.2 ± 1 k, 18.6 ± 1.4 k, 25.4 ± 2 k, and 40 ± 6 k years.⁽³⁾ Thus this confirms a key prediction of the Galactic Explosion Hypothesis that superwaves recur approximately every 10^4 years and have a significant impact on the Earth's climate.

Superwaves have tended to pass through our solar system at times when the Earth's precessing polar axis was near a Galactic center solstice inclined with the north pole leaning either toward or away from the Galactic center; see table 1 below. In 60% of the cases, a

Generation of Cosmic Ray Intensity Profiles from Ice Core ^{10}Be Data

The ^{10}Be concentration values published by Raisbeck et al.^(4, 5) for the Vostok ice core are multiplied by the ice accumulation rate (cm/yr) for the corresponding depth in the Vostok ice core; see Appendix H (p. 452). This calculates the rate of ^{10}Be deposition in the Antarctic region, which in turn serves as an indicator of the Galactic cosmic ray radiation intensity striking the Earth's atmosphere. This assumes that ^{10}Be deposition rate is not affected by changes in ice accumulation rate. These rate values have been normalized to the Holocene average to determine relative cosmic ray intensities (the sum of superwave cosmic ray flux plus the intergalactic cosmic ray background flux). To estimate the relative change in intensity outside the solar system, these relative intensities must further be adjusted to take into account solar wind screening. The little data we have on solar activity levels indicates that the period 10 - 16 kyrs b2k was one of particularly high solar activity. So, as far as reflecting cosmic ray intensities outside the solar system, the graph during that period would be underestimating the rise in intensity relative to the Holocene background intensity. The peak at 40 kyrs b2k would be another place where the intensity increase would be underestimated since the 5000 year rise in radiocarbon production leading up to that time implies an extended period of elevated solar flare activity. The peak at the end of the Penultimate glaciation (stage 6) may also underestimate the true rise in cosmic ray intensity outside the heliopause. A cosmic ray intensity profile was similarly developed based on the Byrd ice core ^{10}Be data of Beer et al.^(6,7)

Table 1. Polar Axis GC Solstice Dates Compared to Superwave Dates

| Pole orientation relative to GC | Date of pole orientation years b2k (x 1000) | Date of cosmic ray peak years b2k (x 1000) |
|---------------------------------|---|--|
| north toward | 13.1 | 15 - 11 large |
| north away | 26.0 | 25.5 small |
| north toward | 38.5 | 40.1 large |
| north away | 51.2 | 56.6 small |
| north toward | 63.9 | 63.5 large |
| north away | 77.1 | 75.5 large |
| north toward | 89.8 | none |
| north away | 102.5 | 97.0, 100.4, 105.5, 109.2 large |
| north toward | 115.6 | 117 large |
| north away | 128.5 | 133 large |

superwave occurred within 1600 years of a polar GC solstice; i.e. the pole was within $\pm 25^\circ$ of the solstice position. If this is not just a coincidence, it would seem to support the idea that superwaves carry a gravity wave component that is capable of producing tidal effects on planets and stars.⁽⁸⁾ A tidal force aligned in the direction of the Galactic center would have a maximal effect in torquing the Earth's spin and assisting its precession at times when the poles (and equatorial bulge) are maximally inclined relative to the Galactic center. The result would be entrainment of the polar precession cycle to the superwave cycle.

Castagnoli, et al. have shown that the 40 kyrs BP ^{10}Be peak was truly a global event.⁽⁹⁾ Analyzing samples in a well-dated Mediterranean sediment core spanning the last 60,000 years, they found the presence of a ^{10}Be peak dated at 34 ± 3 kyr BP. Consequently, their findings negate the suggestion that the ^{10}Be peaks in the Antarctic ice record may be due to changes in the latitudinal distribution of ^{10}Be atmospheric fallout.

C. P. Sonett has suggested that the ^{10}Be peaks which are dated here at 40,000 and 63,500

years b2k were produced by the arrival of shock fronts from the North Polar Spur supernova explosion whose explosion site is assumed to lie about 400 light years away.⁽¹⁰⁾ Their model requires that this explosion was unusually energetic and that it occurred only 75,000 years ago in a very rarefied interstellar medium. However, there are problems with this interpretation. As discussed in Chapter 6 (p. 204), observations suggest that the NPS remnant is a very old reheated remnant having an age of about 10^6 years, that it is presently expanding only at about 3 km/s and that it arose from a supernova explosion of average energy release occurring in a region of normal interstellar gas density. The blast wave from this explosion, then should have passed through our solar system hundreds of thousands of years earlier and hence its ^{10}Be signature would not be registered in the polar ice record.

Beryllium-10 Evidence for a Minor Superwave Between 5400 – 5200 Years b2k (update to p. 192): The cosmic ray intensity profile presented in Figure 8-B (p. 236), which is based on the Vostok ice core ^{10}Be data published by Raisbeck et al. in 1992, indicates that cosmic ray intensity rose 40% above background intensities at ice core depth 139.41 meters, an event which I have dated at around $5,300 \pm 200$ years b2k; see dating scheme on p. 453.^(11, 12) This same cosmic ray event is seen in the more detailed ^{10}Be record from the GISP 2 Greenland ice core published by Finkel and Nishiizumi; see Figure 8-D.⁽¹³⁾ Their graph shows that cosmic ray intensity rose 30% above background intensities on three occasions centered at 5590, 5450, and 5280 years b2k, the latter event being the more prominent of the three. They found that these events were correlated with increases in atmospheric ^{14}C as indicated in dendrochronology data also plotted in Figure 8-D. Increased ^{14}C concentrations suggest periods of increased solar flare activity and hence periods when the Galactic cosmic ray intensity would have been more strongly screened. Consequently, the heights of these ^{10}Be peaks may be somewhat underestimated.* Finkel and Nishiizumi are inconclusive as to the cause of these ^{10}Be peaks. However, as I have noted in several publications,^(14, 15) and in the 2003 third edition of this updated dissertation, these peaks may be evidence that a minor superwave passed through the solar system during the present interglacial. Hence this could be confirming the proposal discussed in Chapter 6 that a minor superwave may have passed the Earth close to 6,000 years BP. Atmospheric nitrate ion concentration, an indicator of incident cosmic ray intensity, is seen to rise five fold on 5,300 years b2k; see Figure 8-E.⁽¹⁶⁾

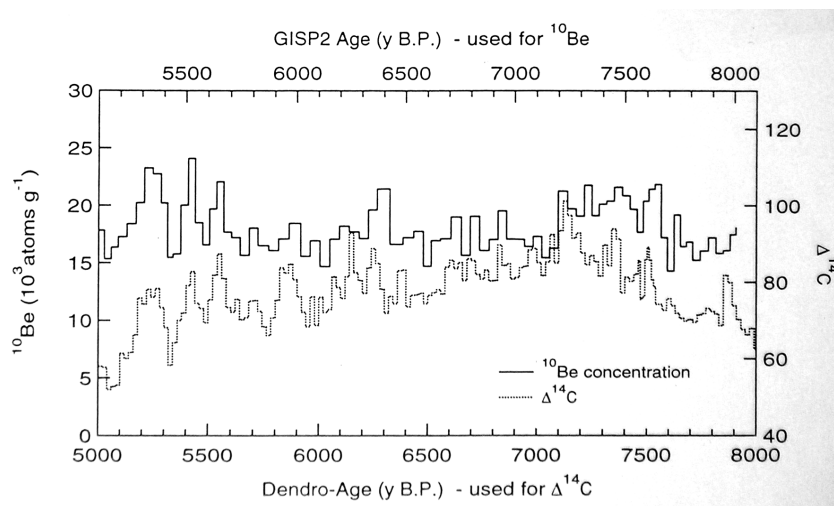


Figure 8-D. Beryllium 10 concentration in the GISP2 ice core compared with radiocarbon $\Delta^{14}\text{C}$ in tree ring data . (diagram from Finkel and Nishiizumi, 1997, Figure 3)

* Here we take the more reliable dendrochronological ages of these events which are about 100 years younger considering that the GISP2 chronology has an uncertainty of 2% or about 100 years at this core depth.

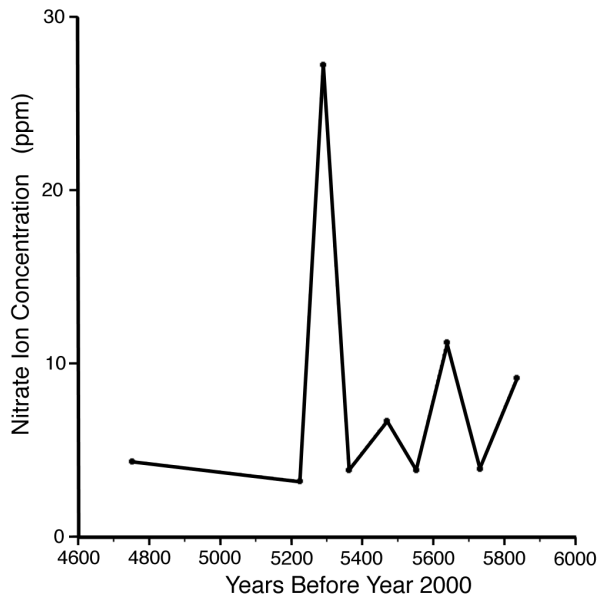


Figure 8-E. Nitrate ion concentration in the GRIP Summit Greenland ice core (data from Legrand, et al., 1993).⁽¹⁶⁾

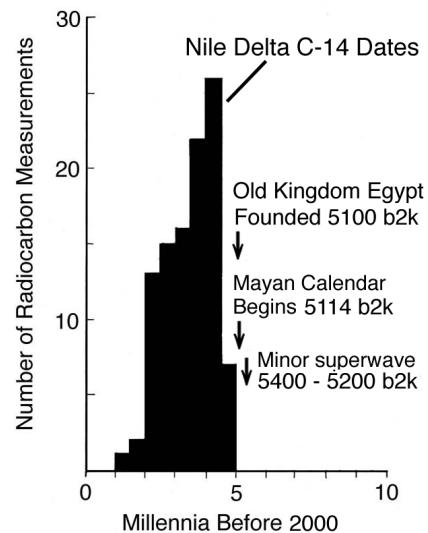


Figure 8-F. Histogram showing the number of published radiocarbon dates from the lower Nile valley for each of a series of calendar year increments (after Labeyrie, 1979).⁽¹⁷⁾

In several of these previous discussions I had noted that this 3,300 B.C. cosmic ray event coincided with the close of the Neolithic Period and preceded the rise of the Nile Delta civilization and the founding of Old Kingdom Egypt. Figure 8-F, for example, shows the sudden onset of civilization in the Nile Delta around 3,100 B.C. In other words, one may infer that prior to this event, the Earth's climate was more harsh and hence unfavorable to the development of civilization. Although this event was not intense enough to initiate an ice age, it nevertheless could have injected a sufficient amount of interstellar dust to have produced a serious climatic disturbance. Note also that the Mayan calendar for the present fourth world cycle began on 5114 b2k, about one century after the superwave event (5,350 - 5,250 years b2k) finished its passage. Also Fourier analysis of the Vostok ^{10}Be data discussed earlier indicates the presence of a $5,400 \pm 300$ year period in the data. This indicates that the Mayan calendar may be preserving knowledge of one of the recurrence periods characterizing our Galaxy's superwave cycle. Since the last superwave event began about 5,400 years ago, this implies that we are now due for the arrival of another superwave any time soon. So the Mayan prediction that a cataclysm would occur at the time of their fourth world cycle's end in 2012 takes on an even greater significance.

In November 2003 evidence emerged which indicated that a sudden climatic disturbance had in fact occurred during the time when the 5,300 years b2k superwave event was passing the solar system. Ohio State University glaciologist Lonnie Thompson announced that his team had discovered a wetland plant that had been remarkably preserved under the ice along the margin of the Quelccaya ice cap. Later testing determined the plant had been frozen 5,200 years ago. Thompson relates that this soft-bodied plant must have been captured by a very large snowfall occurring at that time, a snowfall and climate change that began very abruptly and was fast enough to capture a plant but not kill it.⁽¹⁸⁾ For example, the plant was so exceptionally preserved that the Ohio State group was able to obtain viable DNA from it. For a plant to be growing and then frozen rapidly enough to avoid being killed by frost, this event must have transpired in a matter of hours at a time when climate was relatively warm. Earlier, the Ohio State team had studied ice cores taken from Tanzania's Mount Kilimanjaro

ice fields which showed that a catastrophic drought had devastated the tropics around this same date. So this climatic change appears to have had a global effect and to have occurred very abruptly. The same climatic event may explain the fate of the "ice man" whose mummified remains were discovered in the Italian Alps in 1991. The relatively well preserved body has been dated to be 5,300 years old. The ice man appears to have died of hypothermia and to have been covered in a thick snow fall much like the plant found in the Peruvian ice cap. We may conceive of an accelerated aerosol induced blizzard scenario somewhat like that suggested by Hoyle and Wickramasinghe (p. 104).

My earlier suggestion that a minor superwave had passed through the solar system around $5,300 \pm 150$ years b2k and proposal that such superwaves can produce climatic disturbances of varying magnitudes, then appears to have been confirmed by a variety of discoveries. In the future it may be interesting to study polar ice core samples dating from this period to look for evidence of a possible increase in extraterrestrial dust influx. It is possible that the interstellar dust influx was sufficiently high to register an elevation in iridium or nickel concentration above the background levels produced by the normal influx of interplanetary dust. However, the extraterrestrial dust concentration peaks may not be found to be as high as those found in ice age polar ice.

High Atmospheric Dust Concentrations During the Last Ice Age (update to p. 219): Dust concentrations present in the Dye 3, Greenland ice core are presented in Figure 8-G.⁽¹⁹⁾ This data published in 1985 presents a more detailed record of dust concentration variations than the data shown in Figure 8.1. It is apparent that greater amounts of dust were transported to the polar regions during periods of cold climate. This suggests that climate was much windier during these cold climate periods.

Abrupt Changes in Atmospheric Dust Content and Climate (update to p. 221): The electrical conductivity profile for the Greenland Summit ice cores, published in 1993 presents excellent evidence of the rapidity with which climate and atmospheric dustiness were changing at the end of last ice age; see Figure 8-H.⁽²⁰⁾ This data indicates that major changes took place over time scales of less than 5 to 20 years, a phenomenon referred to as "climatic flickering."

A Prolonged Cosmic Dust Incurion Event: The 15,850 years b2k Ice Core Acidity Spike: Hammer et al. report the presence of regularly spaced acidity peaks (H^+ , F^- , Cl^-) in the Byrd Station, Antarctica ice core present between depths 1283.5 m and 1279.3 m. This spans a period of about 100 years and falls at the beginning of the deglacial warming; see Figures 8-I and 8-J.^(21, 22) If these depths are referenced to the isotope profile of Johnsen,

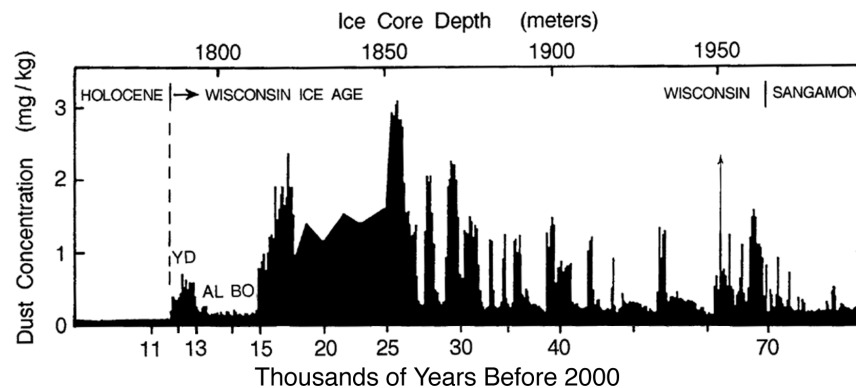


Figure 8-G. Dust concentration in the ice age portion of the Greenland Dye-3 ice core indicate that the Earth's climate was particularly windy during the late Wisconsin stage (Hammer, *Geophysics, Geochemistry, and the Environment*, figure 1).

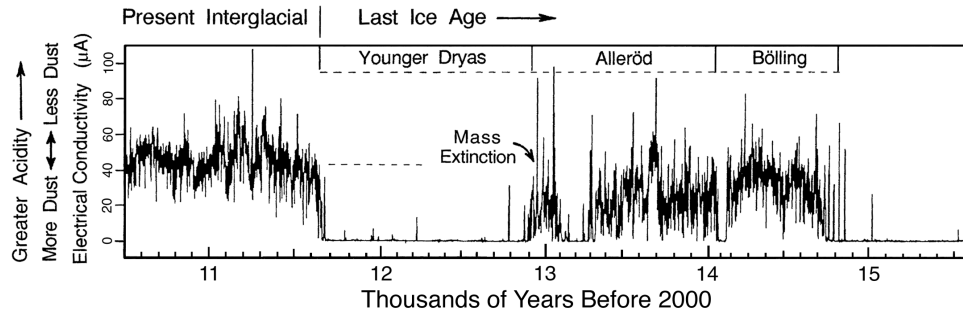


Figure 8-H. A record of ice acidity in the Greenland Summit ice core which charts changes in windiness at the close of the last ice age (adapted from Taylor, *Nature*, figure 2). High acidity may also be an indicator of elevated solar flare activity. The time scale shown here is based on climatic boundary dates given in Appendix E.

this feature dates at ~ 15.85 kyrs b2k, the event beginning around $15,885 \pm 500$ years b2k and tailing off around $15,785 \pm 500$ years b2k. (If referenced to the isotope profile of Blunier, the feature dates 185 years younger, spanning the period 15,700 to 15,600 years b2k.)

Since the total acid deposition of this event was over 20 fold greater than the largest known volcanic eruption, volcanism is an unlikely source. Moreover volcanic eruptions are not known to recur at regular intervals. In 2000 I discovered that the recurrence period of these peaks averages to 11.5 ± 2.4 years, which approximates the solar cycle period; see **solar cycle paper** reproduced on this CD.⁽²³⁾ Since these acids accumulate on the Earth's surface at a rate that varies with the phase of the Sun's activity cycle, it is very likely that they are of extraterrestrial origin. This layer is found in all West Antarctica radar studies, appearing as the strongest above bedrock echo.

In 2000, when I first discovered that these peaks have a solar cycle period, I had surmised that the Sun might be the source of this influx and that this was recording evidence of a substantially enhanced solar wind mass outflow during a period when the Sun had become particularly active. I had disregarded the possibility that these acids might be of interstellar origin because I did not imagine at that time that the solar wind could modulate interstellar dust influx to such a great extent.

However, in 2003 after hearing the latest news on data from the Ulysses spacecraft, I realized that my earlier hesitation was unwarranted. Markus Landgraf and his coworkers had found that during the past decade the interstellar dust influx observed by the Ulysses spacecraft has varied by a factor of three in phase with the solar cycle, with this cyclical variation possibly reaching as high as an order of magnitude.⁽²⁴⁾ The greatest rate of dust influx was found to occur at times of solar maximum, when the solar wind and its magnetic field was most turbulent and least able to screen the incoming dust wind. During times of solar minimum, when the Sun's magnetic field assumes an undisturbed dipole configuration, it is able to more effectively screen the interstellar wind and cause a decrease in its flux observed inside the solar system. Consequently, seeing that the six fold chlorine ion variation observed in the Byrd ice core falls in the expected range, I have now decided that it is best to interpret this chlorine and fluorine influx as being associated with the entry of interstellar dust. The question this leaves is whether vaporized cometary sources or a local interstellar cloud could have supplied this amount of chlorine and fluorine.

Just prior to this acid deposition event, within the span of less than 25 years, $\delta^{18}\text{O}$ became 1 mil more negative, indicating a climatic cooling of about 1°C . This is visible as the upward spike in Figure 8-I (A). The Main Event occurred as climate subsequently began to warm, with the commencement of the Pre-Bölling interstadial. At about this same time there was intense glacier wave flooding which produced Heinrich layer H1 seen in North Atlantic ocean cores; see update at the end of Chapter 10. Following the Main Event, climate

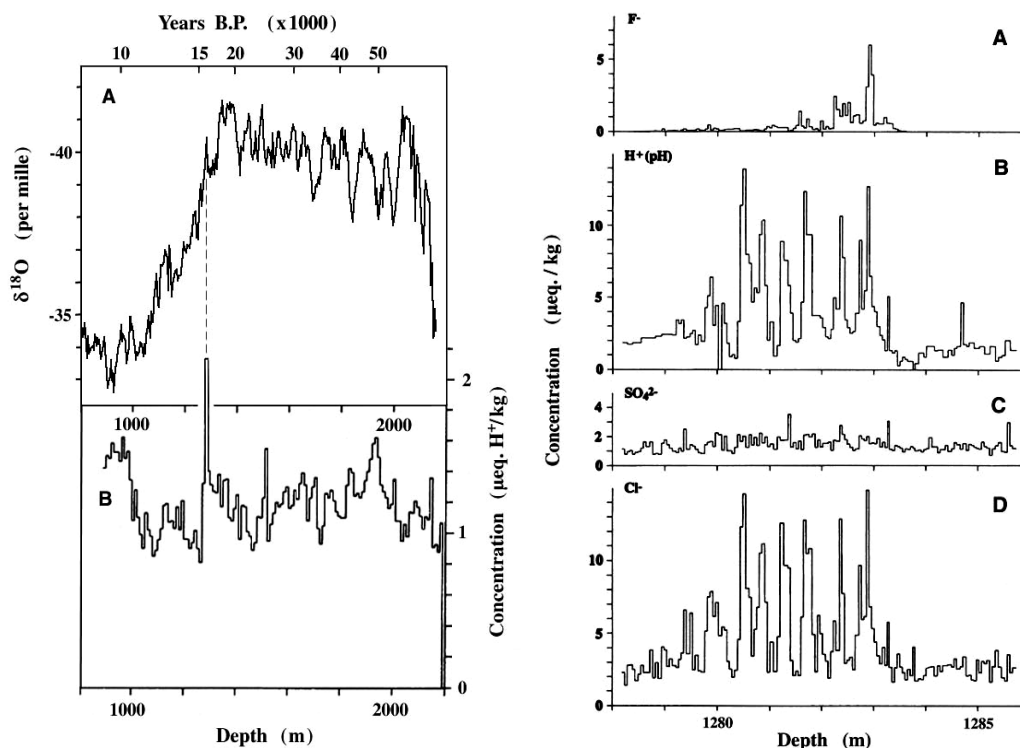


Figure 8-I. (Left) The 15,850 years b2k Byrd ice core acidity feature. The $\delta^{18}\text{O}$ and ECM acidity concentrations plotted versus depth for the Byrd Station deep ice core. (A) shows the $\delta^{18}\text{O}$ values in per mil plotted in 2 meter averages (Johnsen et al., 1972) and (B) shows the ECM levels in $\mu\text{eqH}^+/\text{kg}$ plotted in 10 meter averages (Hammer et al., 1997). The time scale at the top of (A) was developed by P. LaViolette.

Figure 8-J. (Right) Cyclical acidity peaks recurring approximately every 11 ± 2 years. Multiple chemical analyses made on laterally adjacent segments of the Byrd Station ice core from depths of 1278 m to 1286 m presenting the content of: (A) F^- , (B) H^+ by pH measurements, (C) SO_4^{2-} , and (D) Cl^- (Hammer et al., 1997). The data are plotted in 5 cm depth increments.

continued its deglacial warming with the onset of the Bölling and Alleröd interstadials. This global warming, would have been brought about both by the light scattering effects attributed to the presence of this interstellar dust in the solar system and to the activation of the Sun, the latter being brought about by the effect of this material falling into the Sun. As discussed in Chapter 4, the lunar rock findings of Zook et al. and Gold establish that during this deglacial warming the Sun was particularly active. This solar activity would have initially made the solar wind magnetic field increasingly turbulent, compromising its normal ability to deflect this interstellar wind and allowing the superwave to more easily inject its flow of interstellar dust and gas. The subsequent decline in influx of this acidic wind could indicate that this influx was brought into check by the progressive increase in the outgoing solar wind flux.

Consequently, this unparalleled inflow of acidic dust would have marked the beginning of a major superwave passage, the associated cosmic dust influx initiating the end of the last ice age. Based on the concentration of dust and acids found in the Byrd ice core in the first peak of the Main Event, this material would have been present in the Earth's vicinity at concentrations as high as $5 \times 10^{-20} \text{ g/cm}^3$. Assuming that this material had an average particle size of $0.2 \mu\text{m}$, this nebular material would have presented an optical depth between the Earth and the Sun of $\tau = 0.2$, indicating 18% absorption of the direct solar beam, hence would have had a substantial impact on the Earth's climate.⁽²³⁾ This is comparable to the optical depth originally estimated in this thesis; see Ch. 3 (p. 91). If this scenario is correct, chlorine found

in this part of the ice record should be expected to have an isotopic anomaly and to be associated with elevated concentrations of extraterrestrial indicators such as iridium and nickel.

References to Update

- 1) P. A. LaViolette, *The Talk of the Galaxy*. Schenectady, NY: Starlane Publications, 2000.
- 2) J. Beer, et al., "The Camp Century ¹⁰Be record: Implications for long-term variations of the geomagnetic dipole moment." *Nuclear Instruments and Methods in Physics Research* **B5** (1984): 380-384.
- 3) I. Liritzis, and E. Grigori, "Astronomical forcing in cosmogenic Be-10 variation from East Antarctica coast?" *J. Coastal Research* **14** (1998): 1065-1073.
- 4) G. M. Raisbeck, et al., "Evidence for two intervals of enhanced ¹⁰Be deposition in Antarctic ice during the last glacial period." *Nature* **326** (1987): 273-277.
- 5) G. M. Raisbeck, et al., "¹⁰Be deposition at Vostok, Antarctica during the last 50,000 years and its relationship to possible cosmogenic production variations during this period." In *The Last Deglaciation: Absolute and Radiocarbon Chronologies* (Proc. NATO ASI, vol. 12), edited by E. Bard and W. Broecker, pp. 127-139. Heidelberg: Springer-Verlag, 1992.
- 6) J. Beer, et al., "¹⁰Be measurements on polar ice: Comparison of Arctic and Antarctic records." *Nuclear Instruments and Methods in Physics Research*, **B29** (1987): 203-206.
- 7) J. Beer, et al., "¹⁰Be peaks as time markers in polar ice cores." In *The Last Deglaciation: Absolute and Radiocarbon Chronologies*, Proc. NATO ASI Series, vol. 12, 140-153. Heidelberg: Springer-Verlag, 1992.
- 8) P. A. LaViolette, *Earth Under Fire*. Rochester, VT, Bear & Co., 1997, 2005.
- 9) G. Castagnoli, et al. "Evidence for enhanced ¹⁰Be deposition in Mediterranean sediments 35 Kyr BP." *Geophysical Research Letters* **22** (1995): 707-710.
- 10) C. P. Sonett, "A local supernova model shock ensemble using Antarctic Vostok ice core ¹⁰Be radioactivity." December 1991 American Geophysical Union meeting, abstract in *Eos* **72** (1991): 72.
- 11) G. M. Raisbeck, et al., "¹⁰Be deposition at Vostok, Antarctica during the last 50,000 years and its relationship to possible cosmogenic production variations during this period." In *The Last Deglaciation: Absolute and Radiocarbon Chronologies* (Proc. NATO ASI Series, vol. 12), edited by E. Bard and W. Broecker, pp. 127-139. Heidelberg: Springer-Verlag, 1992.
- 12) G. M. Raisbeck, et al., "Evidence for two intervals of enhanced ¹⁰Be deposition in Antarctic ice during the last glacial period. *Nature* **326** (1987):273-277.
- 13) R. C. Finkel, and K. Nishiizumi, "Beryllium 10 concentration in the Greenland ice sheet Project 2 ice core from 3 - 40 ka." *J. Geophysical Research* **102** (1997):26,699 - 26,706.
- 14) P. A. LaViolette, *The Talk of the Galaxy*. Alexandria, VA: Starlane Publications, 2000, p. 55.
- 15) P. A. LaViolette, "A Galactic superwave hazard alert." *Nexus* March-April 2001, pp. 47-52; "A superonda Galáctica: Um alerta de perigo." *Frater* July 2002, pp. 4-5.
- 16) Legrand, M.R., M. De Angelis, and F. Maupetit. "Field investigation of major and minor ions along the Summit (central Greenland) ice cores using ion chromatography." *Journal of Chromatography* **640** (1993):251-258.
- 17) J. Labeyrie, "Sea level variations and the birth of the Egyptian civilization." In *Radiocarbon Dating*, edited by R. Berger and H. E. Suess, p. 33. Berkeley: University of California Press, 1979.
- 18) "Ice Cores May Yield Clues To 5,000-Year-Old Mystery." Ohio State University November 6, 2003 news release: <http://researchnews.osu.edu/archive/quelcoro.htm>.
- 19) C. U. Hammer, et al., "Continuous impurity analysis along the Dye 3 deep core." In *Geophysics, Geochemistry, and the Environment*, edited by C. C. Langway, Jr., et al. AGU Monograph **33**, 90-94. Washington, DC: American Geophysical Union, 1985.
- 20) K. C. Taylor, et al., "The 'flickering switch' of late Pleistocene climate change." *Nature* **361** (1993):432-436.
- 21) C. U. Hammer, H. B. Clausen, and C. C. Langway, Jr., "Electrical conductivity method (ECM) stratigraphic dating of the Byrd Station ice core, Antarctica." *Ann. Glaciol.* **20** (1994):115-120.
- 22) C. U. Hammer, H. B. Clausen, and C. C. Langway, Jr., "50,000 years of recorded global volcanism." *Climatic Change* **35** (1997):1-15.
- 23) LaViolette, P. A. "Solar cycle variations in ice acidity at the end of the last ice age: Possible marker of a climatically significant interstellar dust incursion." *Planetary & Space Science* **53** (2005): 385-393; preprint (reproduced on this CD) also see arXiv.org/physics/0502019.
- 24) M. Landgraf, H. Krüger, N. Altobelli, and E. Grün, "Penetration of the heliosphere by the interstellar dust stream during solar maximum." *Journal of Geophysical Research* **108** (A10) (2003): LIS 5-1.

CHAPTER 9

THE SEDIMENTARY RECORD

9.1 CORRELATIONS OF THREE CLIMATIC PROFILES

The effects of the Last Ice Age are also clearly registered in the Earth's sedimentary record. For example, the three climatic profiles presented in Figure 9.1 give: a) a history of local vegetational composition (northeastern France), b) global glacial ice volume, and c) local ice sheet size (Great Lakes Region). The profiles shown in Figure 9.1(a) and (b) extend back through the last glacial period, or Wisconsin (Weichselian, Devensian, Würm, or Lantern glaciation by European terminologies), through the Last Interglacial, or Sangamon Period (Eemian, Ipswichian, or Riss/Wurm in Europe), to include a portion of the previous glacial period, or Illinoian Period (Saalian, Wolstonian, Riss, or Linxert in Europe).

Figure 9.1(a) (after Woillard and Mook, 1982) is a pollen graph which Woillard has synthesized from cores I, X, XIV, and XVIII taken from the Grande Pile peat bog in northeastern France (47.7° N, 6.5° E). A greater percentage of nonarborescent pollen (higher ordinate value) indicates a cooler atmospheric climate. This may be compared to Figure 9.1(b) (after Thiede, 1977) which depicts the δO^{18} graph for an ocean sediment core (Meteor #12392-1) penetrated in the North Atlantic (25.2° N, 16.9° W). Oxygen isotope ratios were determined from the carbonate in planktonic shells found in the core stratigraphy. More *positive* δO^{18} values (higher ordinate value) reflect greater global ice volume build-up, and simultaneously lower sea level. Note that this profile tends to "mirror" the δO^{18} profiles presented in Figure 8.1(a), (c), and (e), since the δO^{18} ratio in oceans should become more positive at times when the δO^{18} ratio in glacial ice becomes more negative. That is, water molecules containing heavy oxygen would tend to become concentrated in the oceans as "lighter" water became preferentially evaporated and trapped in glaciers. Finally, both of these cores may be compared with the profile shown in Figure 9.1(c) which displays the degree of extension to southern latitudes of the Laurentide Ice Sheet during the Wisconsin (Dreimanis and Goldthwait, 1973).

The dotted lines correlating the three diagrams mark the boundaries of standard climatic stages used in interpreting oxygen isotope profiles. These isotope stages include: Stage 1: the Holocene Epoch or present interglacial; Stages 2, 3, and 4: The Late, Middle, and Early Wisconsin ice age stages; Stage 5: the Sangamon or Last Interglacial; and Stage 6: the Illinoian glacial period. The Sangamon is further divided into five substages, three periods of relatively warm climate (substages a, c, and e) separated by two brief periods of cold weather (substages b and d). Substages 5-a, -c, and -e may be correlated with the Barbados Island coral reef terraces: Barbados I, II, and III, respectively (Matthews 1972, 1973). Alternatively, using the Grande Pile classification system (Woillard, 1975, 1978) these substages correlate with the St. Germain II, St. Germain I, and Eemian temperate periods. Two brief cold stadials (5-b and 5-d) are designated in the Grande Pile terminology respectively as Melisey II and Melisey I. Note that stages 5-a through 5-d constitute a semi-glaciated interglacial stage in which the continental ice masses had attained about half of their Wisconsin size; see Figure 9.1(b).

[UPDATE: The timescale along the top of Figure 9.1 has been updated to conform to the presently accepted scheme for dating these climatic boundaries.]

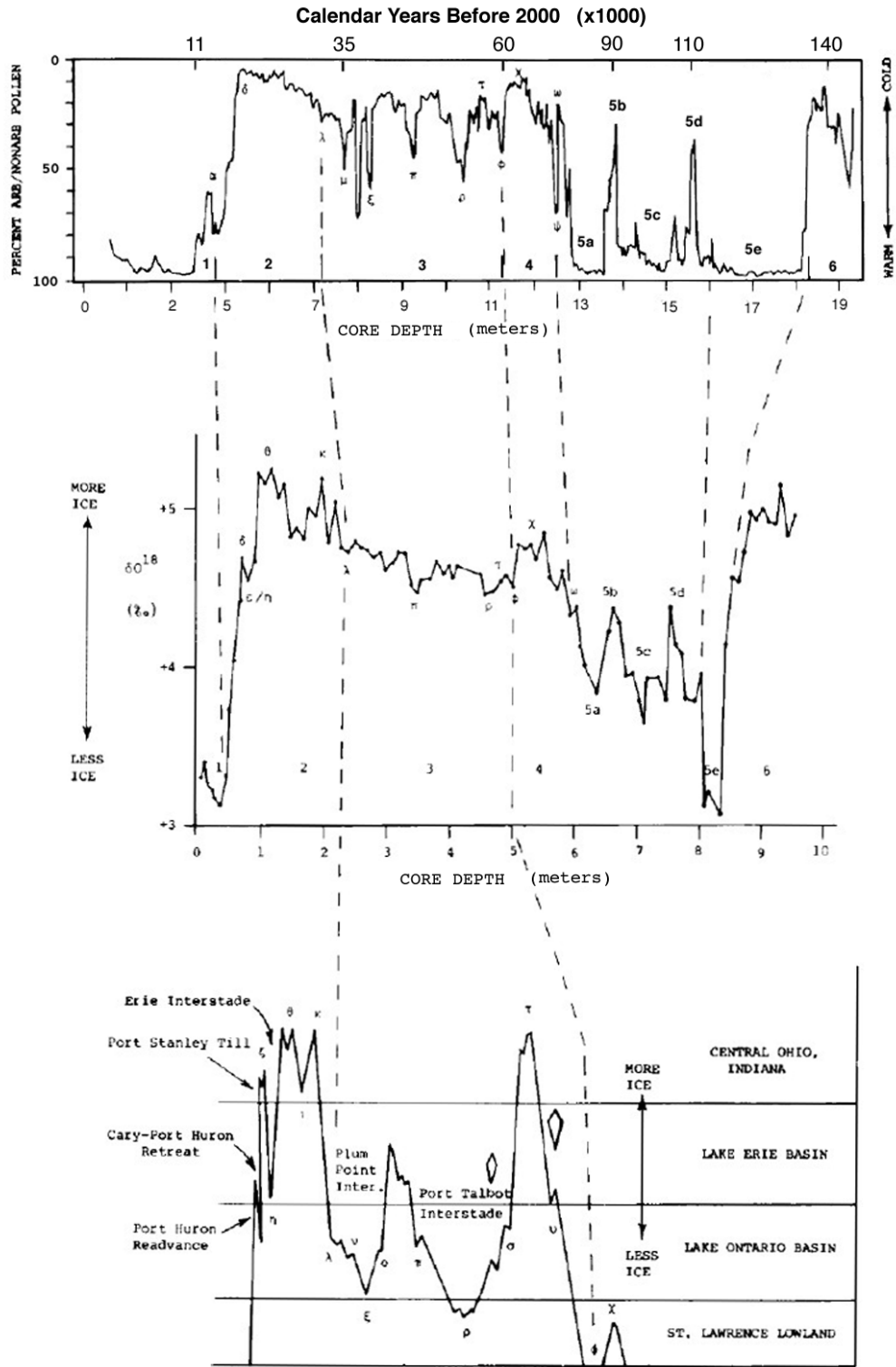


Figure 9.1. a) Pollen profile of the Grande Pile peat bog (adapted from Woillard and Mook, 1982, Fig. 1); b) Oxygen isotope profile for Meteor core #12392-1 penetrated in the North Atlantic (adapted from Thiede, 1977, Fig. 4); c) Graph of the degree of penetration of the Laurentide Ice Sheet to southern latitudes (adapted from Dreimanis and Goldthwait, 1973, Fig. 3).

9.2 THE ABRUPT NATURE OF MAJOR CLIMATIC CHANGE

The problem of abrupt intense coolings during an interglacial climate similar to the present climate resembles, to some extent, the Damocles' sword hanging high above the globe and its inhabitants. Because of its possible consequences for the human race, its study deserves a much higher priority.

(Hermann Flohn, 1979, p. 145)

One of the distinguishing features of global climatic changes is their abrupt nature. Major climatic alterations are found to take place within the space of 100 years or less. Swedish varved sediment records have revealed the presence of climatic changes as brief as 150 years at the end of the ice age, e.g., the Older Dryas Stadial. Moreover, as noted by Flohn (1979), Osborne's (1974) data on English beetle faunas indicates that the warming at the end of the Younger Dryas (11,650 calendar years b2k) transpired within a period of 50 to 150 years. **[UPDATE:** Isotope studies of the Summit, Greenland ice cores show that half of this warming occurred within a single 15-year period. Also see update on [p. 257](#).] The Grande Pile peat bog pollen profiles studied by Genevieve Woillard (1975, 1978, 1979) provide one of the best records registering the rapid climatic changes of the Late Pleistocene. For example, the beginning of the Wisconsin Ice Age involved a series of climatic oscillations which in core X (Woillard, 1978) make their respective excursions within the space of 2.5 - 5 cm (150 - 300 calendar years).

Thus far, investigators have not been able to adequately account for these abrupt warming and cooling events in terms of indigenous instabilities of the Earth's climatic system. However, it is quite possible that these excursions could be explained by an extraterrestrial phenomenon such as the passage of a Galactic superwave. Nebular material brought into the solar system and modifying the radiation transmission properties of interplanetary space could serve as an external forcing mechanism periodically destabilizing the Earth's climatic system. Such a phenomenon not only could bring about climatic changes in an abrupt manner, but it would also be capable of impacting the climatic system over an extended period of time.

The stadials of the Sangamon, denoted as substages 5-b and 5-d, were also apparently induced over an extremely short period of time. For example, the Melisey I and II stadials, which in Grande Pile core X each span depths of about 10 cm (1000 calendar years), register their most rapid climatic transition over an interval of 2.5 cm (250 years). Woillard (1978, p. 16) comments that these periods were so cold that the forests were completely destroyed and replaced by a very open landscape.

Any explanation proposing an Earth-based cause for the Melisey I and II stadials not only would have difficulty accounting for their abrupt nature, but also would have difficulty explaining the correlation of these two brief events with the initiation and termination of the Blake geomagnetic reversal. However, as mentioned in Chapter 7 (Subsection 7.3.2), a succession of two superwaves could have produced the Blake reversal, the first event causing a flip from normal to reversed polarity and the second event causing a flip from reversed to normal polarity. Each time the superwaves would have transported cosmic dust into the solar system inducing the temporary onset of glacial conditions. Perhaps the tin particles found at a depth of 1341.5 meters in the Camp Century ice core (Thompson, 1977b) are evidence of such cosmic dust. In the future this dust sample should be analyzed to determine if, like Sample #962-1, it too contains a high concentration of iridium.

Woillard (1979) has done a detailed stratigraphic pollen analysis of the climatic changes which occurred toward the end of the Eemian Interglacial (equivalent to oxygen isotope substage 5e). She found that within the space of just 150 ± 75 years (Eemian subzone 6b) the

prevailing hardwood temperate forest was gradually deteriorating in favor of a subarctic coniferous forest consisting of pine, spruce, and birch; i.e., a forest which today is found 15° further north from the Grande Pile location. More puzzling, she found that at the end of this 150-year "transitional period" (at the Eemian subzone 6b/7 boundary) this replacement became markedly accelerated with most of the observed vegetational shift taking place within the space of just 20 ± 10 years!

This abrupt shift at the Eemian 6b/7 subzone boundary may be the same event that produced the abrupt change in δO^{18} values recorded in the Camp Century ice core at a depth of ~1342 meters; see Figure 8.1, curve-f. Within just 15 cm of ice core depth, δO^{18} values were found to drop by more than 10% (~16° C) (Dansgaard, Johnsen, Clausen, Langway, 1972; Dansgaard et al., 1982, p. 1273). That is, within the space of only 100 calendar years the climate changed from being warmer than today into full glacial severity! The temperature in Greenland appears to have dropped as fast as 1.7° C per decade.

Sudden climatic changes also appear in records from earlier interglacial periods. For example, the temperate period of the Holstein Interglacial (the interglacial before the Last Interglacial) was interrupted by two brief subarctic periods. On the basis of annual lake varve counts Müller (1974, 1978) has determined that this interglacial lasted for about 15,000 to 16,000 years and that the two intervening stadials lasted about 300 and 400 years respectively. They occurred at about the middle of the interglacial period and were separated by some 2600 years or more. The commencement of the earlier of these two stadials was marked by the sudden destruction of a thermophilous forest which had been dominant at that time and its replacement with subarctic species (i.e., pine and birch). This transition occurred within the space of 100 years and perhaps in as short a time as 60 years (Müller, 1978). The Ruhme (or Cromerian) Interglacial (preceding the Holstein) lasted for about 30,000 years, according to varve counts by Müller (1965, 1978) and was interrupted suddenly at about its middle by a 400 year long expansion of pine and birch. Surprisingly, this cooling spell occurred between the two warmest periods of this particular interglacial. Reviewing the findings of Müller and others, Flohn (1979, p. 144) states:

Especially important, and indeed disquieting, is the evidence of abrupt coolings within warm (interglacial) periods, apparently as rare events with a recurrence time on the order of 10^4 yr. Apparently their intensity can surpass (with up to 5° C/50 yr) all climatic changes during the Holocene.

9.2.1 The Terminal Pleistocene Interstadial

One of the most unusual of abrupt climatic oscillations is the interstadial that occurred at the end of the Last Ice Age. In each case, previous authors had attributed this warming to local circumstances, and hence often named it after the region of its discovery. For example, this event has been referred to by the various names: Two Creekan Interstadial (Great Lakes Region), Windermere Interstadial (Great Britain), or as the Ågård/Bölling interstadial sequence (Scandinavia). Based on evidence collected here, it is suggested that this climatic warming was actually a *global event*, rather than a series of disconnected local phenomena. I will refer to this generically as the *Terminal Pleistocene Interstadial*. This interval extended from 14,750 to 12,950 calendar years b2k. [UPDATE: The original dissertation identified the Terminal Pleistocene Interstadial with just the Bölling. However, since then I have included the Alleröd interstadial as well so that this interstadial sequence would end with the beginning of the Younger Dryas stadial. The Ågård interstadial is today conventionally considered the early part of the Bölling.] The global nature of this climatic warming event may be seen from the fact that it is distinctly recorded in the δO^{18} profiles of both the Camp Century ice core from Greenland and in the Byrd Station ice core from Antarctica.

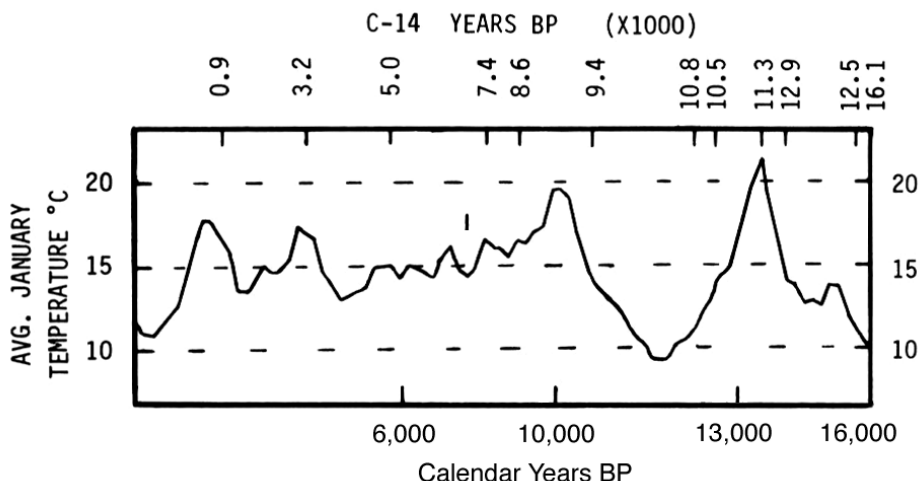


Figure 9.2. Average winter temperature profile (3 point moving average) reconstructed from fossil pollen data from a lake core penetrated in Alerce, Chile (modified drawing based on Heusser and Streater, 1980, Fig. 2). **[UPDATE:** I have added a calendar year timescale along the bottom of this profile to correspond to the C-14 dates of Heusser and Streater. Also Figure 9-A(d) (p. 259) gives a more detailed version of the earlier half of this profile.]

Studies of fossil pollen taxa in Alerce, Chile (41.4° S, 72.9° W) and of fossil beetle fauna (Coleoptera) in the southern and central British Isles ($\sim 52 \pm 2^{\circ}$ N) reveal that in *both* hemispheres there was a $9 - 10^{\circ}$ C warming followed by a cooling of comparable magnitude. The Alerce paleotemperature profile shown in Figure 9.2 (after Heusser and Streater, 1980) was derived on the basis of a regression analysis of 20 pollen taxa. The vertical scale indicates that a warming of about 11° C took place at this time with summer temperatures reaching 21° C ($\sim 70^{\circ}$ F), about 6° C warmer than the present summer mean of 15° C! The Coleoptera paleotemperature profile reported by Coope (1977) for the British Isles records two interstadials; see Figure 9.3. The more recent one Coope has named the "Windermere Interstadial." This warming period for Great Britain began about 13,500 - 13,000 C-14 years BP (17,000 - 15,450 calendar years b2k). Then shortly before 12,150 C-14 years BP (14,050 calendar years b2k) a sharp climatic deterioration began. This temperature drop plateaued for about 1000 years during a period that corresponds to the Alleröd Interstadial in Scandinavia. Finally, a cold peak was achieved about 10,200 C-14 years BP ($\sim 11,900$ calendar years b2k), a time which corresponds with [the end of] the Younger Dryas in Scandinavia. **[UPDATE:** See more recent profile in Fig. 9-A (a) (p. 259)]

The Terminal Pleistocene Interstadial is also recorded in several ocean sediment cores. For example, it appears in the North Atlantic core Meteor #12392-1 (25.2° N, 16.9° W); see feature marked as " ϵ/η " in Figure 9.1(b). It also appears 30° of latitude further north in core V 23-81 (54.2° N, 16.8° W) reported by Ruddiman, Sancetta, and McIntyre (1977); see Figure 9.4(a), 210 - 180 cm depth. Ruddiman et al. fix the lower boundary of this warming at 13,500 C-14 years BP (which is equivalent to $\sim 17,000$ calendar years b2k) and the cold peak at 10,200 C-14 years BP (equivalent to 11,900 calendar years b2k). Ruddiman et al. estimate that this climatic fluctuation represents a $7 - 8^{\circ}$ C warming (and cooling) of surface water temperature. They find this feature in several North Atlantic cores and attribute it to a local shift in the polar/subpolar water front. However, such a mechanism would not explain why a temperature oscillation of similar form is recorded at about the same time in surface waters of the Gulf of Mexico; see Figure 9.4(b) (Beard, 1973). Also, several cores drilled in

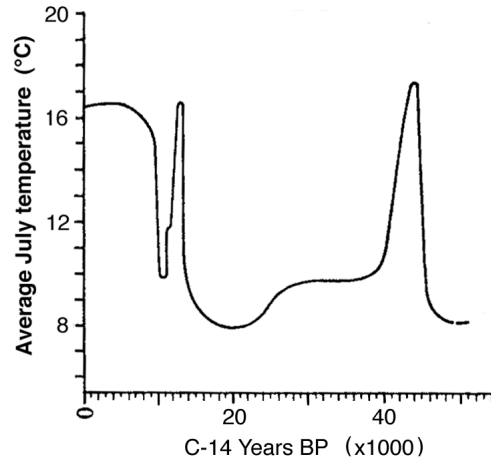


Figure 9.3. Variations in average summer temperature in the lowlands of Britain based on changes in the abundance of various Coleoptera species (after Coope, 1977, Fig. 2). [UPDATE: Figure 9-A(a) at the end of this chapter (p. 259) gives a more detailed version of the Terminal Pleistocene Interstadial recorded in this profile.]

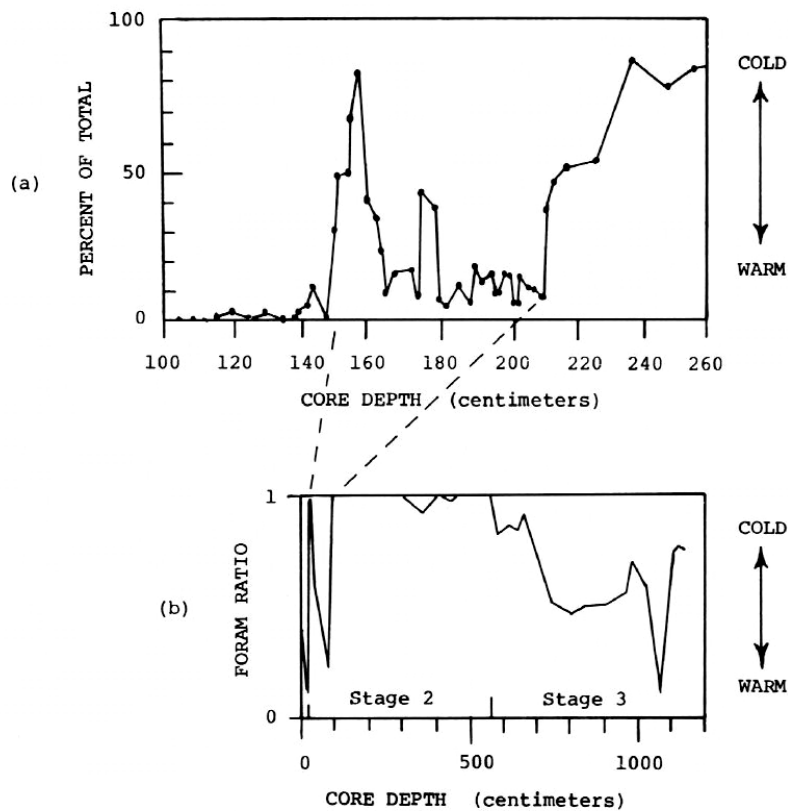


Figure 9.4. Two marine sediment paleotemperature records of the Terminal Pleistocene Interstadial: a) Core V 23-81 from the North Atlantic (54.2°N, 16.8°W) (adapted from Ruddiman, Sangetta, and McIntyre, 1977, Fig. 7). Profile is based on the abundance of *G. pachyderma* as a percent of total planktonic foraminifera. b) Core 64-A-9-42 from the Gulf of Mexico (21.0°N, 94.1°W) (adapted from Beard, 1973, Fig. 10). Profile is based on the frequency ratio of two planktonic foraminifera groups, *Globorotalia menardii* to *Globorotalia inflata*. [UPDATE: A more detailed profile for core V 23-81 is presented in Figure 10-S (p. 309). Also see climatic profiles in Figure 9-B (p. 260).]

the eastern Pacific off of the Oregon coast register this climatic oscillation, with warming being fully under way between 13,000 – 12,000 C-14 years BP (15,450 – 13,800 calendar years b2k); see Duncan, Fowler, and Kulm (1970). It appears that whatever caused the rapid change of ocean surface temperature in these various geographically separated regions was causing similar effects on a global scale.

Any theory attempting to explain the climatic changes of the Late Wisconsin must account for how an increase in air temperature by about 10° C could have simultaneously taken place in both hemispheres together with a general increase in ocean surface temperature of almost the same magnitude. Such a theory must be able to account for rates of warming on the order of 1.8° C/century at a time when the Earth was in a fully glaciated state with an overall high surface albedo. Major climatic warmings of this sort are possible within the context of the GEH; see pp. 103, 110. The detection of high cosmic dust levels in glacial ice deposited during this interstadial would constitute strong evidence in favor of linking this event to the passage of the proposed 14,200 years BP superwave.

9.2.2 Sudden Heating of the Ocean Surface at the Beginning of the Last Ice Age

The surface waters of the North Atlantic appear to have undergone a similar episode of heating at the *beginning* of the Wisconsin Ice Age when the Earth was in a *partially* glaciated state. Ruddiman et al. (1980) have studied 19 ocean sediment cores from the North Atlantic to determine the climatic conditions at the 5/4 isotope boundary. From shells of benthonic foraminifera (deep water dwelling protozoa) sampled from each core they have developed oxygen isotope profiles indicating the degree of global ice sheet growth. Also, for each core they have made counts of certain species of planktonic foraminifera (surface dwelling protozoa) to serve as indicators of sea-surface temperature. They have found that at the time of initiation of the Wisconsin glaciation, during the period of maximum ice sheet growth rate, the oceans actually became warmer! As one example, their findings for core #V27-116 (52.8° N, 30.3° W) are shown in Figure 9.5. The lower ordinate scale plots estimated winter and summer mean ocean surface temperature, while the upper ordinate scale plots δO^{18} . Core depth in meters is plotted along the horizontal scale with time advancing from right to left. As seen here, at a depth of 2.5 meters in the core, ocean surface temperature suddenly increases by ~5° C. This is coincident with a rapid rise in δO^{18} marking the onset of glacial advance at the beginning of the Wisconsin. After several thousand years, the surface water temperature began to decline, returning to its initial temperature. At this point the Earth's ice volume had reached its maximum value. Ruddiman et al. draw the following conclusion:

The entire subpolar North Atlantic between 40°N and 60°N remained in a warm ("interglacial") mode for at least the first half of ice accumulation during the isotopic stage 5/4 boundary. At the approximate midpoint of ice growth, sea-surface temperatures in many areas reached their highest values during the entire 5a/4 transition. At this time, the subpolar ocean was nearly as warm as today.

The process of rapid glacial ice sheet growth has in the past been difficult to explain. The problem may be stated as follows. If the Earth's climate were to cool off (e.g., due to a reduction in incident solar radiation), the rate of evaporation from the oceans would be expected to decrease causing a concomitant decrease in snow precipitation. The significant findings of Ruddiman et al. help to alleviate part of this mystery in that they have shown that at the time of most rapid ice accumulation the oceans were not cooler than normal, but rather *abnormally warm*. Taking core V27-116 as an example, an increase in average annual water temperature from 3° C to 8° C would increase the aqueous vapor pressure over the ocean surface from 5.7 mm Hg to 8.0 mm Hg, i.e., a 40% increase. Or, taking an extreme case, core

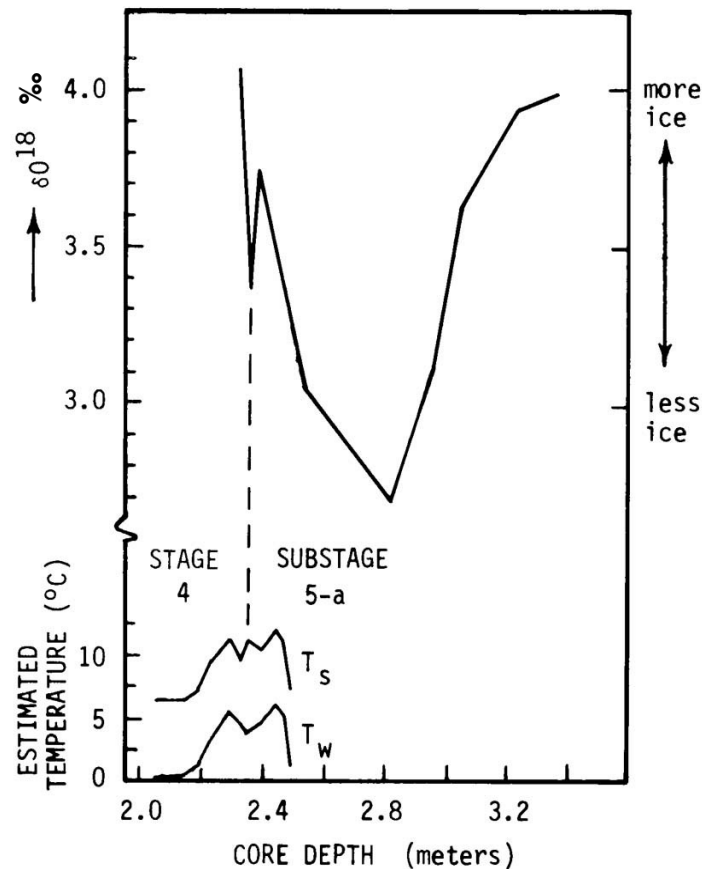


Figure 9.5. Change in glacial ice sheet volume (upper ordinate scale) as indicated by the δO^{18} ratio found in the shells of benthonic foraminifera in core #V27-116 from the North Atlantic. Change in mean ocean surface temperature (lower scale) for the winter (T_w) and summer (T_s) estimated from counts of planktonic foraminifera species found in the same core (adapted from Ruddiman et al., 1980, Fig. 5).

#CH-K-9 (41°45'N, 47°21'W) indicates that the average annual surface temperature rose from 4° to 12° C, implying a 70% increase in aqueous vapor pressure at the ocean's surface. This unusually humid air in the vicinity of the thermal gradient along the North American coast would have combined to efficiently deliver moisture to the Laurentide Ice Sheet (Ruddiman et al., 1980).

However, several questions remain unanswered: 1) Why did the North Atlantic warm up rather than cool off at the onset of glacial build up? 2) Why did this regional ocean surface warm-up occur so suddenly? 3) What energy source maintained these abnormally high ocean temperatures over a period of several thousand years, particularly at a time when continental temperatures were falling to ice age levels (as indicated by the Grande Pile pollen graphs)? That is, what energy source maintained these elevated ocean temperatures in the face of a 40 – 70% increase in evaporative heat loss? If wind activity were boosted at this time, which seems likely, it would be necessary to admit an even larger increase in heat loss from the ocean surface. 4) Why did ocean temperatures in the North Atlantic increase to and become maintained at almost present-day warmth at a time when for many thousands of years the Earth had been glaciated much more extensively than it is today?

Many of these questions have already been addressed in Subsection 3.3.4 (pp. 113 –

114). With some combination of the scenarios presented there, it should be possible to construct a model that predicts both warm oceans at high latitudes together with increased precipitation rates and glacial growth. For example, a shift in the solar spectrum to the infrared and/or a moderate high latitude radiation influx from an interplanetary greenhouse effect could have led to warming of the oceans at high latitudes, while at the same time maintaining subfreezing temperatures over northern continental regions.

9.3 GLACIAL RETREAT AND THE TERMINAL PLEISTOCENE FLOOD

As for those genealogies of yours which you just now recounted to us, Solon, they are no better than the tales of children. In the first place you remember a single deluge only, but there were many previous ones. . . . There have been, and will be again, many destructions of mankind arising out of many causes; the greatest have been brought about by the agencies of fire and water, and other lesser ones by innumerable other causes.

(Egyptian high priest to Solon of Athens; after Plato, *Timaeus*)

Around 13,500 – 12,800 C-14 years BP (17,000 – 14,900 calendar years b2k), the Ontario, Erie, and Huron glacial lobes of the Laurentide ice sheet retreated very rapidly, during a phase known as the Cary-Port Huron retreat. Dreimanis and Goldthwait (1973, p. 95) comment that during this phase ice was retreating at a rate of up to 500 meters per year, which is even faster than the maximum retreat rate during the final dissipation of the Laurentide ice sheet during the Holocene. This rapid glacial recession is reminiscent of the Bölling interstadial. As noted by Tauber (1970), immediately prior to and following the formation of the Fjärås moraine, the Scandinavian ice sheet was retreating at the rate of 350 meters per varve year, faster than at any other time during the entire glacial retreat in Sweden. Just as the rapid glacial retreat in Sweden was interrupted by the Fjärås stadial at about 12,400 – 12,350 varve years BP (14,250 – 14,150 calendar years BP), similarly the Cary-Port Huron retreat of the Laurentide ice sheet in the Great Lakes region was interrupted by the Port Huron/Lake Whittlesey readvance dated at about 13,000 ± 500 C-14 years BP (15,600 ± 500 calendar years b2k). Thus, one may conclude that, *climaxing at around 14,600 calendar years b2k, a major global climatic amelioration took place that affected glaciated areas in different parts of the world in a similar fashion*. This constitutes an independent check of the proposal made earlier regarding the global nature [of the Bölling portion] of the Terminal Pleistocene Interstadial, which took place between 14,750 – 14,200 calendar years b2k.

Data from the Hudson-Champlain area of New York similarly shows an accelerating glacial recession rate peaking at around 12,900 C-14 years BP (15,350 calendar years b2k). Till studies in the New England area also offer support for the proposal that there was a global climatic amelioration peaking around 13,000 C-14 years BP (15,600 calendar years b2k). For example, Borns (1973) concludes that a major climatic amelioration began prior to 14,200 C-14 years BP (17,400 calendar years b2k), resulting in the formation of numerous recessional moraines along the New England coast. In Maine, this general recession was interrupted by the Pineo Ridge readvance, dated at ~12,700 C-14 years BP (~14,900 calendar years b2k), which approximately correlates with the Port Huron readvance of the Great Lakes Region. However, by ~12,600 C-14 years BP the ice sheet had retreated northwestward almost to the St. Lawrence River, a distance of about 300 km. Even in terms of the C-14 timescale, this indicates a very rapid recession rate of several kilometers per year. Thus, just as in the case of the Port Stanley and Fjärås readvances, here too, at about the same time, a readvance (or ice surge) occurred in close association with a period of rapid glacial retreat.

During this period of rapid glacial retreat, the Connecticut River apparently became overburdened with meltwater. The water level of the river, which today seldom exceeds 20 – 30 feet, then rose 150 – 180 feet above its present level. Dana (1882, p. 367) has estimated that at that time the river was discharging about 1.2 cubic miles of water per year ($\sim 8 \text{ km}^3/\text{year}$). On the geology of the New Haven district, Dana (quoted in Howorth, 1893, p. 893) states:

When it is considered that the waters which leveled this plain were the same that distributed the sand and gravel of the drift formation then deposited, it is obvious that the waters, to have made such a slope over so wide a region, even to the shores of the bay, must have been those of a flood of no common magnitude.

If a major discharge of glacial meltwater actually did occur around 14,600 calendar years BP, then there should be evidence of a change in the salinity of the ocean surface waters at about this time. Indeed, Kennett and Shackleton (1975) report data which they interpret as evidence of such a salinity change, peaking at the end of the Last Ice Age. They have performed a detailed stratigraphic analysis of ocean sediment core K 97 taken from the Gulf of Mexico, determining oxygen isotope ratios recorded in a certain type of phytoplankton called *Globigerinoides sacculifer*. Their results are plotted in Figure 9.6(b).

Oxygen isotope ratios in ocean water may be reduced (made more negative) either by a reduction in water salinity or by an increase in water temperature. The isotopic change of 2.6‰ shown in Figure 9.6(b), if due to temperature alone, would translate into a surface water temperature increase of about 10° C (@ 4° C per δO^{18} ‰ change). Kennett and Shackleton conclude that a large portion of this isotopic change must have been caused by the formation of a low salinity surface layer over the Gulf, which they attribute to a massive inpouring of glacial meltwater into the Gulf of Mexico, the water being channeled from the Laurentide ice sheet via the Mississippi River.

Some portion of the observed isotopic change, however, must be due to a thermal effect, as can be seen by comparing the meltwater profile to the relative paleotemperature curve for core K 97 shown in Figure 9.6(a) (after Malmgren and Kennett, 1976). Note that the period of peak meltwater influx into the Gulf occurred during a temporary warm period (positive component ratio) which immediately preceded the glacial-to-interglacial climatic transition. This warm interval is here identified with the temporary global climatic amelioration which in Subsection 9.2.1 is designated at the Terminal Pleistocene Interstadial.

The dates which Kennett and Shackleton, and Malmgren and Kennett (KS/MK) have assigned to their data are based on the assumption of a constant core sedimentation rate of $\sim 27 \text{ cm}/1000 \text{ years}$. They base this rate on the accepted radiocarbon date of $11,000 \pm 500 \text{ C-14 years BP}$ for the Y-Z microfaunal boundary, which in core K 97 corresponds to a depth of 3 meters. However, in the present study a higher sedimentation rate is proposed for sediments laid down for core depths $>320 \text{ cm}$. We assume a date of 12,950 calendar years b2k (11,000 C-14 years BP) for core depth 320 cm, marking the Younger Dryas/Alleröd boundary and a constant sedimentation rate of $\sim 24 \text{ cm}/1000 \text{ calendar years}$ for core depths 0 – 310 cm. This is in essential agreement with the timescale of KS/MK. However, for core depths below 320 cm (dates earlier than 12,950 years b2k) this study adopts a sedimentation rate of $\sim 50 \text{ cm}/1000 \text{ years}$, two times higher than the rate proposed by KS/MK. This revision is adopted in order that the dates for the boundaries of the relative paleotemperature curve (Figure 9.6(a)) would conform with the calendar dates earlier assigned to the boundaries of the Terminal Pleistocene Interstadial. That is, the following time-depth correspondences are adopted: 3.2 meters = 12,950 calendar years b2k and 4.1 meters = 14,750 calendar years b2k, giving a sedimentation rate of 50 cm/1000 years for this warm interval.

The elevated sedimentation rate adopted here is acceptable. For example, Broecker,

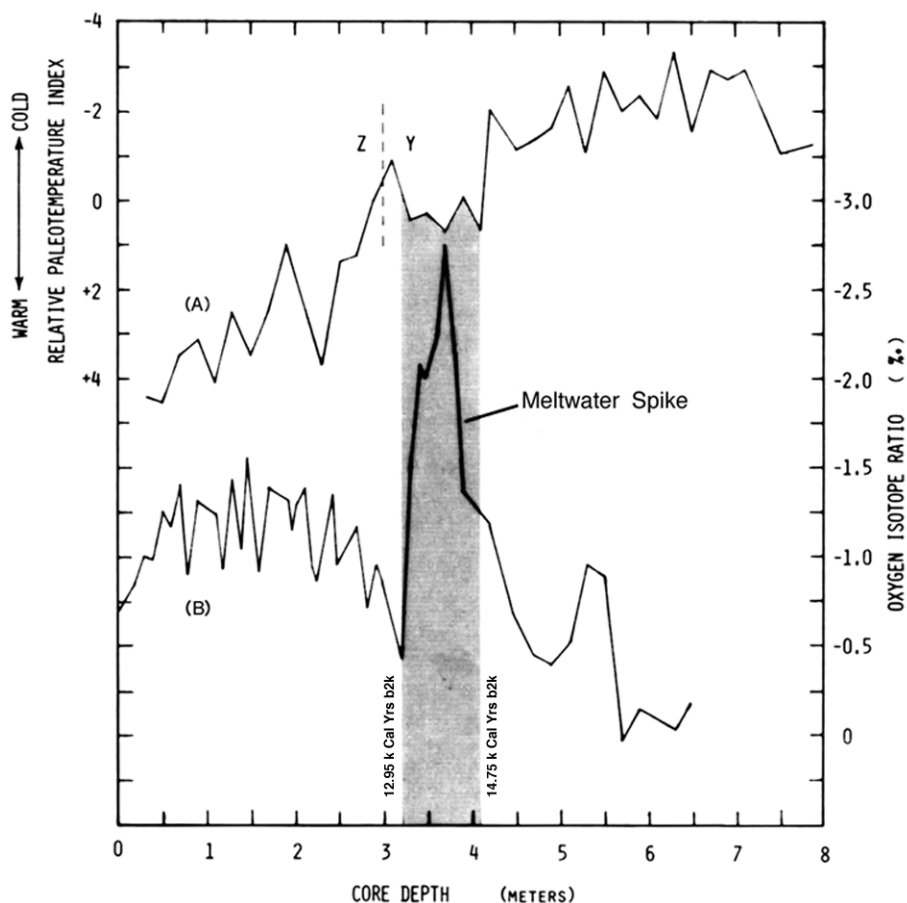


Figure 9.6. Comparison of the relative paleotemperature index (curve a) and the oxygen isotope ratio (curve b) for sediment core K 97 taken from the Gulf of Mexico (25.6°N, 93.2°W) (based on Malmgren and Kennett, 1976, Fig. 4; Kennett and Shackleton, 1975, Fig. 2). Shaded region indicates the Terminal Pleistocene Interstadial. [**UPDATE:** See more recent profile displayed in Figure 9-E (p. 263)]

Ewing, and Heezen (1960) present evidence that, compared with the Holocene, sedimentation rates during the Wisconsin in the equatorial mid-Atlantic were several times greater. Moreover, in the Gulf of Mexico elevated sedimentation rates would be expected, especially at the time of the glacial recession rate peak when large quantities of meltwater (laden with continental material) were apparently being discharged from the North American continent. Thus, the sedimentation rates for core K 97 which KS/MK derive as a linear extrapolation of the Holocene rate, should only be considered as a *lower limit*.

The meltwater peak shown in Figure 9.6(b) at 3.7 meters, which dates at 13,700 C-14 years BP according to the KS/MK uniform sedimentation rate assumption, adopts almost the same date of 13,900 calendar years BP when using the calendar date calibrations proposed here. The date for the meltwater discharge peak correlates: 1) with the time of the peak glacial recession rate observed in Scandinavia — 14,300 calendar years b2k (~12,400 C-14/varve years BP), 2) with a period of rapid glacial recession in North America dated at ~15,550 calendar years b2k (13,000 ± 500 C-14 years BP), and 3) with the peak of the Terminal Pleistocene Interstadial dated in the British Isles at 16,500 ± 300 calendar years b2k (13,300 ± 300 C-14 years BP). [**UPDATE:** Based on recent more accurate data, this peak period of peak warmth in the British Isles profile dates about 14,450 cal yrs b2k; see Figure

9-A(a) on p. 259.] Thus the evidence presented above is consistent with the hypothesis that a rapid glacial recession and considerably enhanced glacial meltwater discharge was occurring about $14,400 \pm 100$ calendar years b2k and that this was brought about by a major warming of the Earth's climate. As pointed out in Chapter 3 (p. 103), such a climatic warming could be brought about by an interplanetary greenhouse effect caused by enhanced concentrations of nebular material in the outer solar system. It is also interesting to note several other events which occurred at about this time, including: the Gothenburg Geomagnetic Excursion ($\sim 14,200$ calendar years b2k) and the peak in the megafaunal frequency curve $\sim 12,000 \pm 1000$ C-14 years b2k ($\sim 14,300$ to $12,500$ calendar years b2k).

Like the Terminal Pleistocene Interstadial, the $14,400 \pm 100$ calendar years b2k meltwater flooding event appears to have been global in scope. That is, besides the Gulf of Mexico data there is evidence of freshwater inflow into the Mediterranean occurring about the same time. For example, oxygen isotope measurements made by Rossignol-Strick et al. (1982) on core KS 52 from the eastern Mediterranean reveal the presence of two freshwater flooding episodes, a more recent one spanning $12,500 - 10,000$ calendar years b2k ($10,450 - 9000$ C-14 years BP), and an earlier one spanning the period $20,000 - 13,600$ calendar years b2k ($17,000 - 11,750$ C-14 years BP). The calendar dates for these two flooding periods match well with the two warm periods registered in the Alerce core. The lack of a second, more recent, meltwater peak in the Gulf of Mexico, correlative with the more recent peak in the eastern Mediterranean, could be due to the fact that, following $13,600$ calendar years b2k, meltwater from the Laurentide ice sheet was draining primarily via the St. Lawrence River into the North Atlantic.

Because of the observation of the $14,400$ calendar years b2k flooding peak in two widely separated geographic locations (both locations receiving meltwater from nearby continental ice sheets), this event may be regarded as resulting from a global condition (climatic warming) and is referred to here generically as the Terminal Pleistocene Flood; see Chapter 10.¹

It should be pointed out that the fresh water influx into the Mediterranean during these episodes may not have been entirely due to glacial melting alone. Pluvial runoff also could have been a major contributor. For example, at about $17,000$ calendar years b2k ($13,500$ C-14 years BP), close to the time of the earlier flooding peak, the silt wedge of the Nile River was cut through by an enormously high flow of water, at least 4 times the Nile's present discharge rate (Fairbridge, 1977). Rossignol-Strick et al. also reach this conclusion, suggesting that an unusually high fresh water input from the Nile, draining precipitation from equatorial Africa, was responsible for the more recent of the two meltwater peaks. Indeed, high lake levels are recorded in many parts of North and equatorial Africa at this time (Street and Grove, 1979).

Of the flooding and glacial surge events found to cluster near the $14,400$ calendar years b2k peak in glacial recession rate, particularly interesting is the Spokane Flood of eastern Washington, also known as the Scabland Flood or Missoula Flood. The geology of the Channeled Scablands of eastern Washington is best explained if the unusual land features found in this region were carved out by a vast, short-lived flood of water or a series of such floods. Baker (1978) estimates that the discharges at their maximum were as great as 21×10^6 m³/s (~ 1800 km³/day), with flow velocities as high as 30 m/s and a flow gradient of >10 m/km in flood water that was over 100 meters deep! It is currently believed that this flood occurred during the period of glacial recession at the end of the Last Ice Age and that it was

¹ This may be identified with the Great Deluge that is documented in myths from various parts of the world. Plato dates the time of "the sinking of Atlantis" at about 9000 years before the time of Solon, which would be about $11,600$ years b2k. This date approximates the date of $11,300 \pm 800$ calendar years b2k for the secondary global flood peak.

[Update: It also coincides with the date when the Holocene warming abruptly began.

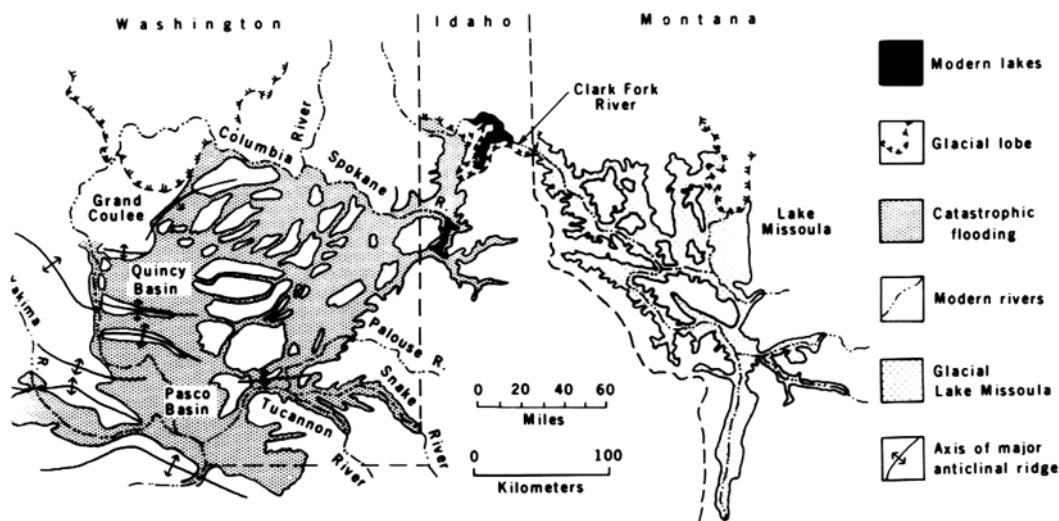


Figure 9.7. A map showing Glacial Lake Missoula (western Montana) and the Channeled Scabland (northern Idaho and eastern Washington (Baker, 1978) (copyright 1978 by the American Association for the Advancement of Science).

caused by the rupturing of an ice dam which allowed glacial meltwater accumulated in Glacial Lake Missoula to become suddenly released. As seen in Figure 9.7, Glacial Lake Missoula occupied a region in northern Montana west of the Rocky Mountain continental divide and east of the Montana-Idaho border. It is suggested that once the ice dam was breached a flood of water and ice surged onto the Scabland region of eastern Washington and finally drained into the Pacific Ocean via the Columbia River Gorge. Mullineaux et al. (1978) have dated deposits of this flood at $\sim 13,100 \pm 300$ C-14 years BP, which corresponds to $\sim 15,900 \pm 300$ calendar years b2k. **[Update: This coincides with the time of Heinrich Event H1; see p. 308.]**

It is interesting to note that the calendar date for the Spokane Flood falls close to the time of the beginning of a major meltwater influx into the Gulf of Mexico, with the peak of the Terminal Pleistocene Interstadial, and with the time of the Gothenburg geomagnetic polarity flip. Because of this coincidence of dates it is reasonable to speculate that the failure of the postulated Missoula Lake ice dam was triggered by this episode of accelerated glacial melting which appears to have taken place simultaneously on a global scale. If ice were to melt at the rate of 4 cm per day (see p. 103), then a $1000 \text{ km} \times 1000 \text{ km}$ ice sheet region could produce 40 km^3 of meltwater per day, which over a period of $1\frac{1}{2}$ months would equal the volume inferred for Glacial Lake Missoula. The resulting increase in hydrostatic pressure could have caused an ice dam to rupture. There is, on the other hand, an alternative possibility: the Spokane Flood could have been produced by the passage of a "continental glacier wave" of the sort postulated in Chapter 10 (Section 10.3).

UPDATE

Abrupt Climatic Change (update to p. 247): The 1993 Summit, Greenland electrical conductivity profile shown in the last chapter (Figure 8-H, p. 242) shows that major changes in climate were occurring within times shorter than 5 to 20 years. This indicates evidence of climate changing even more rapidly than the timescales cited in this chapter. Consequently, the new evidence presents an even more pressing need to find an alternative to the Milankovitch theory as the main trigger for climatic change. This further supports the

superwave cosmic dust incursion theory as being the means by which such rapid climatic change is brought about.

The Terminal Pleistocene Interstadial (update to p. 248): Data that appeared after this dissertation was published confirmed the proposal put forth here for the first time that the warming at the end of the last ice age was global in extent. For example, Figure 9-A (a) shows this warm period in a Coleopteran climate profile from the British Isles and correlates this with pollen climate profiles from (b) Columbia, (c) Central Brazil, and (d) Alerce, Chile. The correlated appearance of this warming and subsequent cooling in dated climate profiles from both the northern and southern hemispheres presents strong evidence that this Terminal Pleistocene Interstadial (TPI) climatic oscillation occurred in a globally synchronous manner further supporting the suggestion made in Chapter 3 that the ice age was ended by an extraterrestrial cause, one that changed the Earth's received solar energy flux. The Coleopteran profile shown in **Figure 9-A (a)**,⁽¹⁾ which is more recently published than the profile shown in Figure 9.3. Profiles (b) and (c) were published prior to the publication of my dissertation, but had not been included because at the time I was not aware of them.^(2, 3) Alerce profile (d) is from the same data as the smoothed version plotted in Figure 9.2. Subsequent to their presentation in this dissertation, these northern and southern hemisphere climate profile correlations have been described in several publications.⁽⁴⁻⁷⁾

The same widespread climatic correlation is evident in ocean core climate profiles from high and low latitude regions from a) the Norwegian Sea, b) the Gulf of Mexico, c) the southeast coast of Portugal, d) the Arabian Sea, e) the Sulu Sea off of the southern coast of China, and f) the Bay of Bengal; see **Figure 9-B**.⁽⁸⁻¹³⁾ The comparison of these various profiles dates from a paper I first wrote in 1993.⁽⁶⁾ Note that profile (b) in this figure is the same as that shown in **Figure 9.4 (b)**.

The various climatic oscillations at the end of the last ice age are clearly visible in the accurately dated GISP2 and GRIP ice core isotope climatic profiles which became available in 1993; see **Figure 9-C**.⁽¹⁴⁾ In 1998, Steig et al. published the results of their study which used changes in atmospheric methane concentrations as a way of correlating the Taylor Dome, Antarctica ice core climate profile with the GISP2 climate profile from Summit, Greenland; see upper two profiles in **Figure 9-D**.⁽¹⁵⁾ Although they also attempted to correlate these profiles with the Byrd Station and Vostok ice core profiles, their correlations with these particular profiles were improperly matched due to their use of faulty time-depth relationships for the Byrd and Vostok ice cores. Consequently, although they correctly concluded that there was a correlated warming between the northern and southern hemisphere, they incorrectly concluded that climate at the Byrd Station and Vostok locations of Antarctica did not synchronize with this warming. However, with the correct timescale, the Byrd and Vostok ice core climate profiles do synchronize with the Taylor Dome and GISP2 ice core profiles. The lower curve in Figure 9-D shows how the Byrd core profile matches up. The timescale used here, the same as the one used in **Figures 8-C** and **8-I**, was developed by correlating the Byrd and Camp Century, Greenland ice core records using ¹⁰Be peaks common to both records.⁽¹⁶⁾ Since the Camp Century record has in turn been correlated to the accurately dated Summit, Greenland ice core, this accurate Summit chronology may be transferred to the Byrd ice core; see Appendix H (**p. 454**). Consequently, ice core data shown in Figure 9-D corroborates the conclusions I had reached prior to the publication of the findings of Steig et al., namely that the Northern and Southern Hemispheres warmed and cooled in a synchronous manner.

Synchronized Glacial Retreat (update to p. 254): In 1989, several years after this dissertation was published, Broecker et al. published a Gulf of Mexico isotope salinity-change profile EN 32-PC4; see upper profile in Figure 9-E.⁽¹⁷⁾ This was more detailed and better

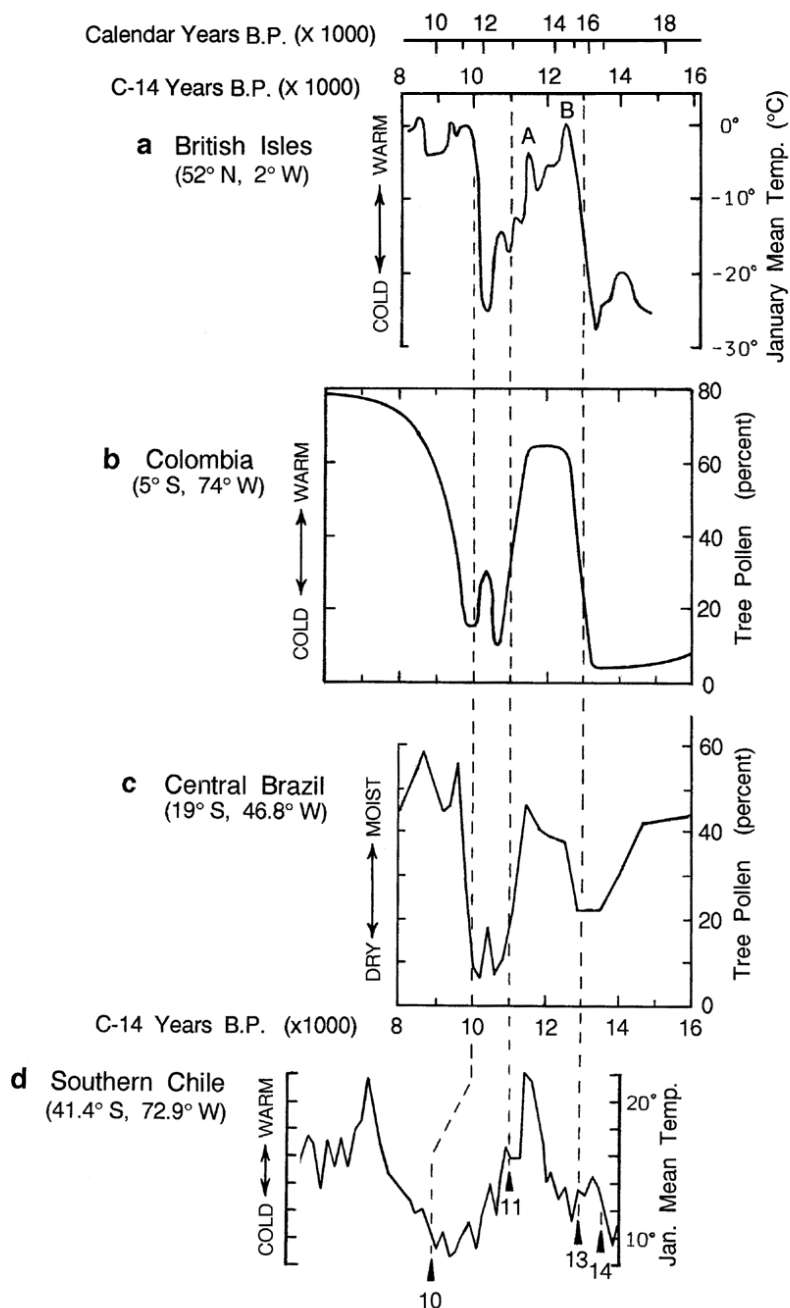


Figure 9-A. A comparison of radiocarbon-dated paleotemperature profiles from the Northern and Southern Hemispheres: a) the British Isles, b) the El Abra Corridor, Colombia, c) Central Brazil, and d) Alerce, Chile. Radiocarbon years may be converted to calendar years by reference to the uppermost timescale.

(After Atkinson et al., *Nature*, figure 2; Schreve-Brinkman, *Paleogeography, Paleoclimatology, Paleocology*, figure 15; Ledru, *Quaternary Research*, figure 4; and Heusser and Streeter, *Science*, figure 2)

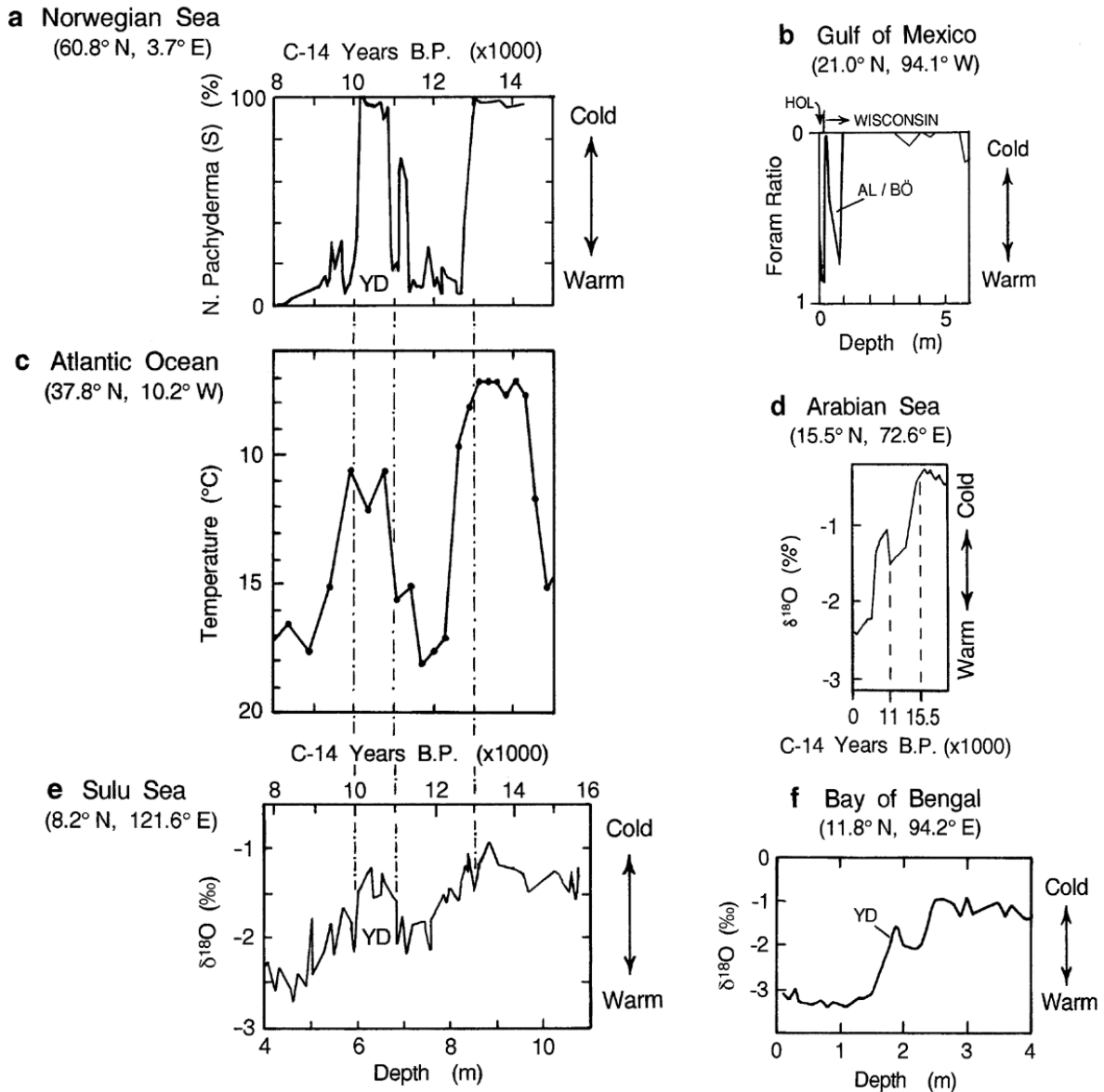


Figure 9-B. A comparison of ocean paleotemperature profile from various parts of the world: a) foraminifera abundance in Norwegian Sea core Troll 3.1 (Lehman and Keigwin, 1992), b) foraminifera ratio in Gulf of Mexico core 64-A-9-42 (Beard, 1973), c) foraminifera temperature profile SU 81-18 from the southeast coast of Portugal (Bard et al., 1989), d) $\delta^{18}\text{O}$ profile from Arabian Sea core MD 76-131 (Van Campo, 1986), e) $\delta^{18}\text{O}$ profile from Sulu Sea core SO49-82KL (Kudrass et al. 1991), and f) $\delta^{18}\text{O}$ profile from Bay of Bengal core MD 13-36 (Duplessy et al., 1981).

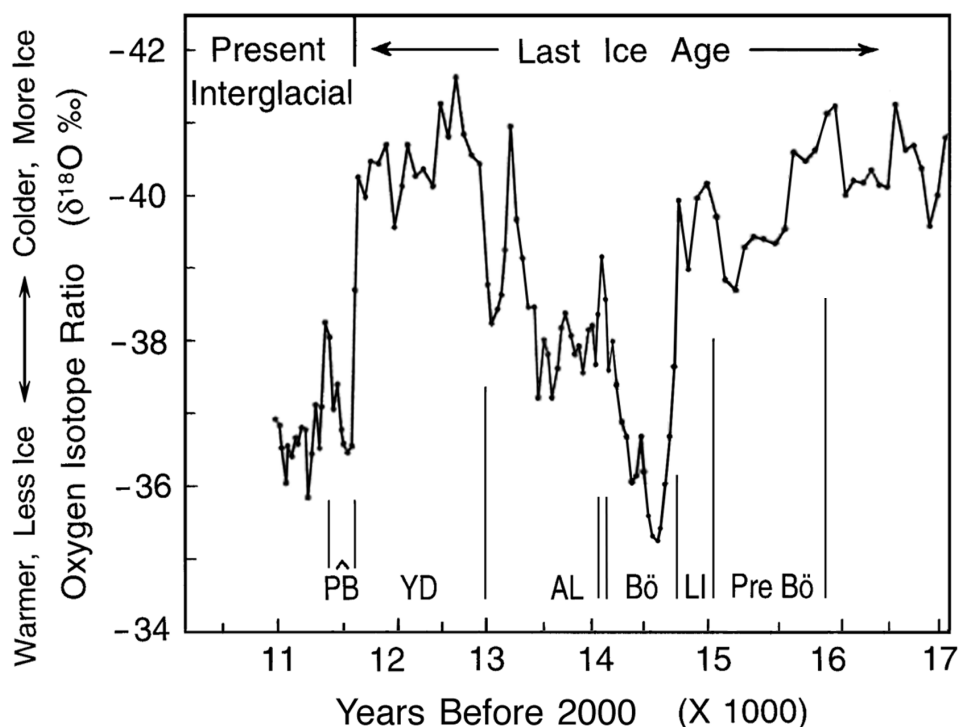


Figure 9-C. Climate profile charting oxygen isotope ratio in the GISP2 ice core as an indicator of air temperature over Summit, Greenland. Dating of the data points has been modified to conform to the GRIP Summit ice core chronology. Higher temperatures (and less glacial ice) plot downward. Climatic zones include: Pre-Bölling Interstadial (Pre Bö), Listerian Interstadial (LI), Bölling Interstadial (Bö), Alleröd Interstadial (AL), Younger Dryas Stadal (YD), and Preboreal warming (PB).

profile EN 32-PC4; see upper profile in Figure 9-E.⁽¹⁷⁾ This was more detailed and better dated than the K97 profile shown in Figure 9.6. It more accurately shows the glacial meltwater output from the Mississippi River as terminating with the onset of the cold Younger Dryas stadial. This indicates that climate in North America was synchronized with that in Europe, thus supporting the proposal of global climatic synchrony advanced in this dissertation. To illustrate this intercontinental correlation, I have plotted the rate of ice sheet recession in Scandinavia in Figure 9-E (lower profile) based on data published by Björck and Moller, and by Tauber adapted to the current GICC 05 ice core chronology.^(18, 19) As expected, periods of high ice sheet recession rate in Europe correlate with times of high meltwater output in North America.

This ice sheet recession rate profile also matches up with the glacial meltwater output curve derived from the rate of sea level rise; see Figure 9-F (upper profile).^(20, 21) As expected, times of high ice sheet recession rate correlate with periods when sea level was rising at its fastest rate due to the global influx of glacial meltwater.

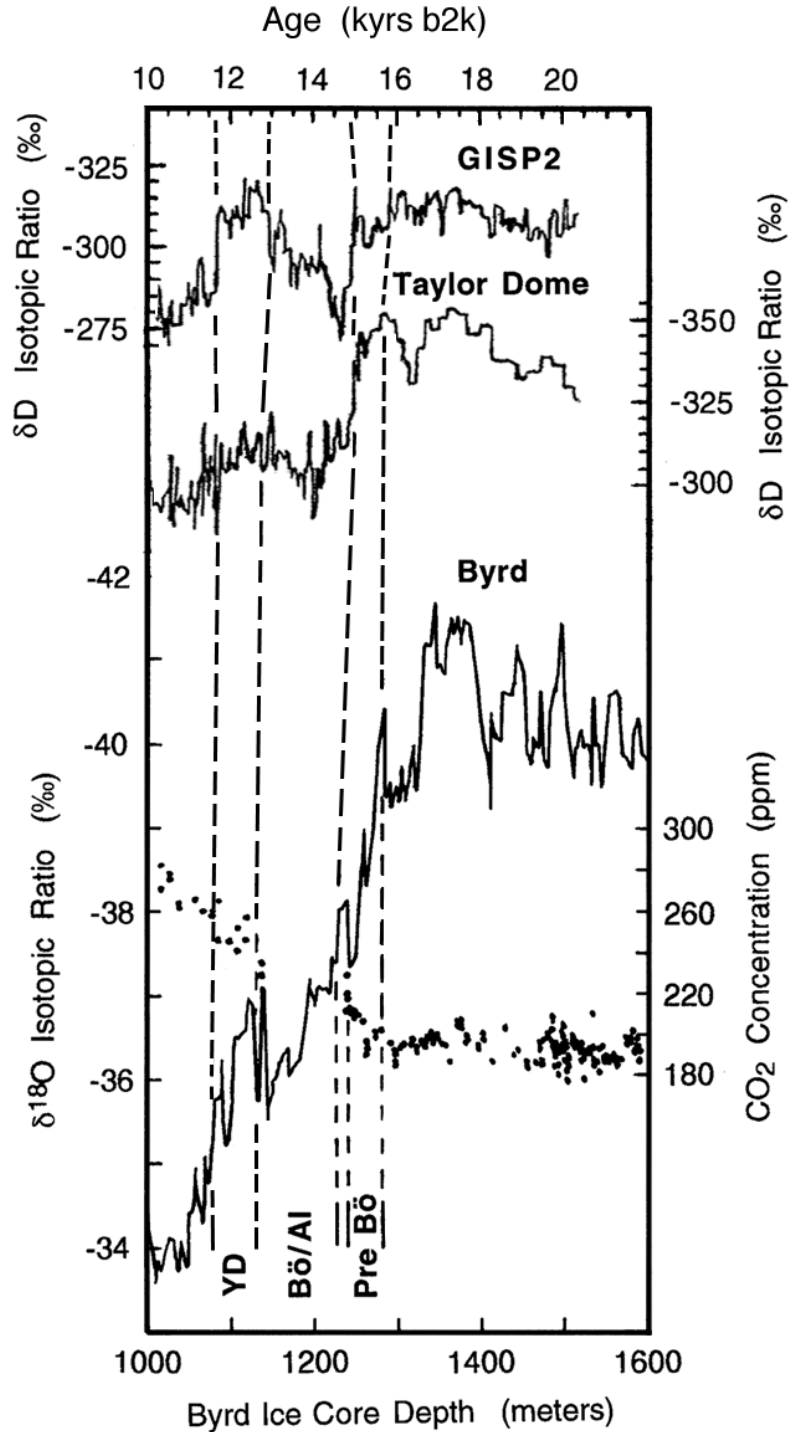


Figure 9-D. A comparison of Greenland and Antarctic ice core profiles showing climatic synchrony of the Bölling-Alleröd-Younger Dryas oscillation. Upper profiles: Summit, Greenland GISP2 deuterium profile correlated to the Taylor Dome, Antarctic deuterium profile using methane as an indicator (adapted from Steig et al., 1998). Lower profile: Byrd Station, Antarctica $\delta^{18}\text{O}$ profile (Johnsen et al., 1972) correlated to the Greenland ice record by means of Be-10 peaks (Beer et al., 1992); see Appendix H (p. 454) for a discussion. The CO_2 data is taken from Neftel et al. (1988).

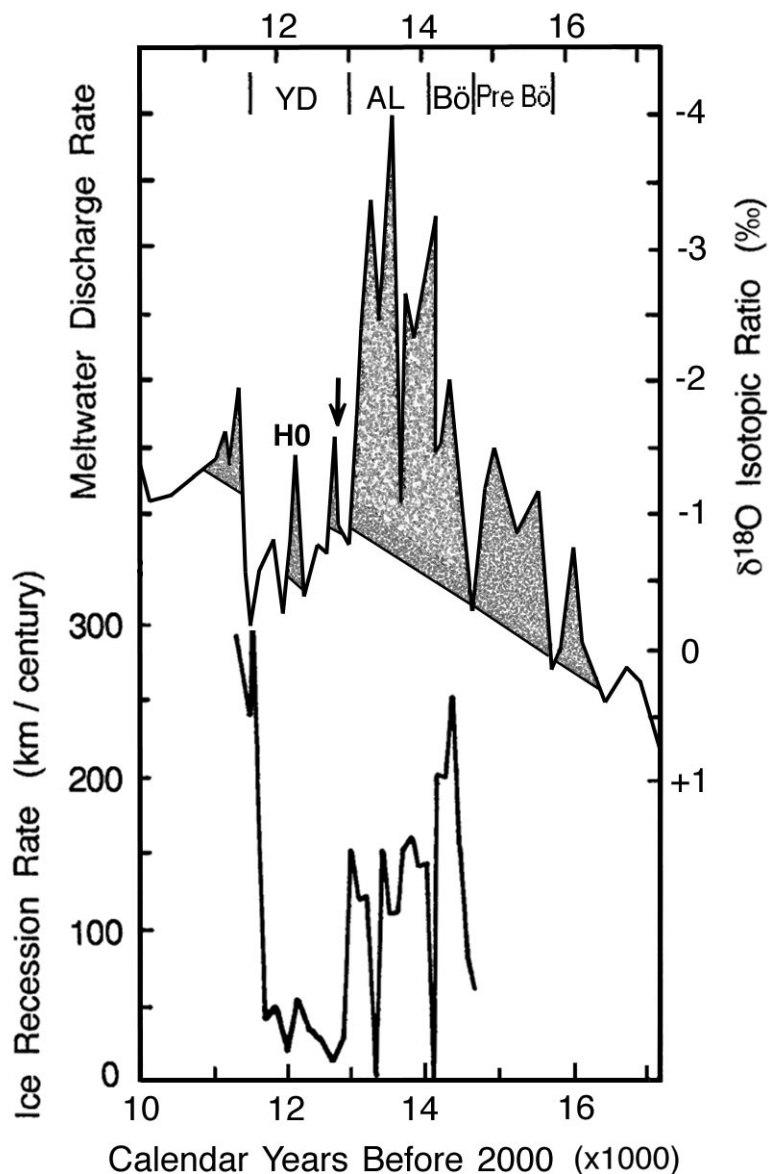


Figure 9-E. Upper profile: Rate of meltwater discharge by way of the Mississippi as indicated by the oxygen isotope profile for Gulf of Mexico core EN32-PC4 (after Broecker et al., *Nature*, figure 2; data courtesy of J. Kennett). Shaded portion charts the rate of glacial meltwater discharge. Lower profile: ice sheet recession rate in southern Sweden (data from Björck and Moller, *Quaternary Research*, figure 18; Tauber, *Radiocarbon Variations and Absolute Chronology*, table 3). Climatic zones include — YD: Younger Dryas, AL: Alleröd, BO: Bölling, and Pre Bö: Pre Bölling Interstad.

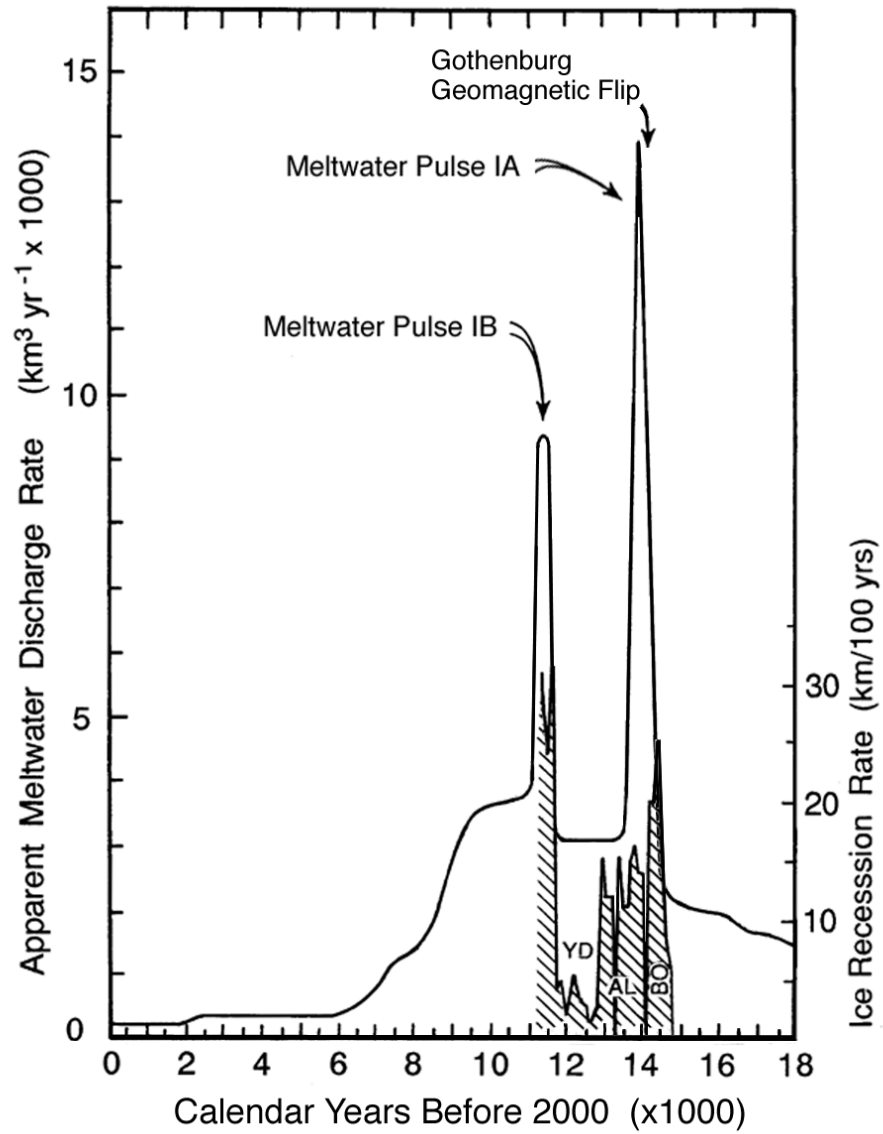


Figure 9-F. Upper profile: the rate of global glacial meltwater discharge into the oceans calculated from the rate of sea level change observed in the Barbados coral reef record (data from Bard et al., *Nature*, figure 1; Fairbanks, *Nature*, figure 3). Lower profile: ice sheet recession rate in southern Sweden.

References to the Update

- 1) T. C. Atkinson, K. R. Briffa, and G. R. Coope, "Seasonal temperatures in Britain during the past 22,000 years, reconstructed using beetle remains." *Nature* **325** (1987): 587 – 592.
- 2) E. J. Schreve-Brinkman, "A palynological study of the upper Quaternary sequence in the El Abra corridor and rock shelters (Colombia)." *Paleogeography Paleoclimatology Paleoecology* **25** (1978): 1 – 109.
- 3) M. P. Ledru, "Late Quaternary environmental and climatic changes in central Brazil." *Quaternary Research* **39** (1993): 90 – 98.
- 4) P. A. LaViolette, "Cosmic-ray volleys from the Galactic Center and their recent impact on the Earth environment." *Earth Moon Planets* **37** (1987): 241 – 286.
- 5) P. A. LaViolette, "Galactic core explosions and the evolution of life." *Anthropos* **12** (1990): 239 – 255.
- 6) P. A. LaViolette, "Global warming at the Termination I boundary and its possible extraterrestrial cause." 1993, 2007; Eprint at: arxiv.org/abs/physics/0503158.
- 7) P. A. LaViolette, *Earth Under Fire*. Rochester, VT, Bear & Co., 1997, 2005.
- 8) S. J. Lehman, and L. D. Keigwin, "Sudden changes in North Atlantic circulation during the last deglaciation." *Nature* **356** (1992): 757 – 762.
- 9) J. H. Beard, "Pleistocene-Holocene boundary and Wisconsin substages in the Gulf of Mexico." In: R.F. Black, R.P. Goldthwait, and H.B. Willman (Editors) *The Wisconsin Stage* (GSA Memoir 136). GSA, Boulder, CO, 1973, pp. 277– 297.
- 10) E. Bard, et al., "Sea-level estimates during the Last deglaciation based on $\delta^{18}\text{O}$ and accelerator mass spectrometry ^{14}C ages measured in *Globigerina bulloides*." *Quat. Res.* **31** (1989):381 – 391.
- 11) E. Van Campo, "Monsoon fluctuations in two 20,000-Yr B.P. oxygen-isotope pollen records off southwest India." *Quat. Res.* **26** (1986): 376 – 388.
- 12) H. R. Kudrass, H. Erienkeuser, R. Vollbrecht, and W. Weiss, "Global nature of the Younger Dryas cooling event inferred from oxygen isotope data from Sulu Sea cores." *Nature* **349** (1991): 406 – 409.
- 13) J. C., Duplessy, A. W. H. Bé, and P. L. Blanc, "Oxygen and carbon isotopic composition and biogeographic distribution of planktonic foraminifera in the Indian Ocean." *Paleogeogr. Paleoclimatol. Paleoecol.* **33** (1981): 9 – 46.
- 14) P. M. Grootes, et al. "Comparison of oxygen isotope records from the GISP2 and GRIP Greenland ice cores." *Nature* **366** (1993): 552 – 554.
- 15) E. J. Steig, et al., "Synchronous climate changes in Antarctica and the North Atlantic." *Science* **282** (1998): 92– 95.
- 16) J. Beer, et al., " ^{10}Be peaks as time markers in polar ice cores." In: E. Bard and W. Broecker (Editors) *The Last Deglaciation: Absolute and Radiocarbon Chronologies* (Proc. NATO ASI Series, vol. 12). Springer-Verlag, Heidelberg, 1992, pp. 140– 153.
- 17) W. S. Broecker, et al. "Routing of meltwater from the Laurentide Ice Sheet during the Younger Dryas cold episode." *Nature* **341** (1989): 318 – 321.
- 18) S. Björck and P. Moller, "Late Weichselian environmental history in southeastern Sweden during the deglaciation of the Scandinavian ice sheet." *Quaternary Research* **28** (1987): 1 – 37.
- 19) H. Tauber, "The Scandinavian varve chronology and ^{14}C dating." In *Radiocarbon Variations and Absolute Chronology*. Nobel Symp. 12, edited by I. Olsson. New York: John Wiley & Sons, 1970.
- 20) E. Bard, B. Hamelin, and R. G. Fairbanks, "U-Th ages obtained by mass spectrometry in corals from Barbados: Sea level during the past 130,000 years." *Nature* **346** (1990): 456 – 458.
- 21) R. G. Fairbanks, "A 17,000-year glacio-eustatic sea level record: Influence of glacial melting rates on the Younger Dryas event and deep-ocean circulation." *Nature* **342** (1989): 637 – 642.

CHAPTER 10

THE TERMINAL PLEISTOCENE EXTINCTION EPISODE

It is impossible to reflect on the changed state of the American continent without the deepest astonishment. Formerly it must have swarmed with great monsters; now we find mere pigmies, compared with the antecedent allied races . . . The greater number, if not all, of these extinct quadrupeds lived at a period and were the contemporaries of the existing sea-shells. Since they lived no very great change in the form of the land can have taken place. What, then, has exterminated so many species and whole genera? The mind at first is irresistibly hurried into the belief of some great catastrophe; but thus to destroy animals, both large and small, in Southern Patagonia, in Brazil, on the Cordillera of Peru, in North America, and up to the Bering Straits, we must shake the entire frame-work of the globe.

(Charles Darwin)

(quoted without reference by Henry Howorth, 1887, p. 351)

10.1 IN SEARCH OF A CAUSE

The Pleistocene Epoch, which lasted almost 2 million years (according to K-Ar radioisotope chronology) and which ended about 10^4 years ago with the termination of the Last Ice Age, is made up of a continuous sequence of glacial and interglacial intervals. A study of the fossil record reveals that at no time during the entire Pleistocene did faunal extinction proceed at a more rapid pace than at the terminal Pleistocene boundary, when at least 200 genera became extinct. As will be argued further on, this extinction involved a single relatively brief episode of global extent and occurred about $12,950 \pm 100$ calendar years b2k.

The anomalous nature of this event is made apparent by the observation that out of 22 genera of birds that became extinct in North America during the entire Pleistocene, as many as 10 (45%) became extinct at the end of this epoch (Grayson, 1977). A similar pattern is found in the extinction of the large land mammals (greater than 50 kg adult body weight). The data of Hibbard et al. (1965) indicate that in the United States over the course of two glacial cycles (before the last cycle) 8 large mammalian genera were lost: 4 at the end of the Kansan (glacial), 3 at the end of the Yarmouth (interglacial), none at the end of the Illinoian (glacial), and 1 at the end of the Sangamon (interglacial). However, by the end of the Wisconsin glacial period (which followed the Sangamon) 33 genera had become extinct! Some of these extinct mammalian megafauna include the mastodon, the mammoth, the ground sloth, the bison, the saber tooth tiger, and many others; e.g., see **p. 271**. The disappearance of Neanderthal Man also took place about this time (Fairbridge, 1977; after Kopper, 1976).

[Update: Actually, Neanderthal Man disappeared around 35 kyrs ago, most likely attributable to the 40 kyrs b2k superwave (LaViolette, 1997)]

Another distinctive feature of the Late Pleistocene extinction is its terminal nature. Following this event new genera did not replace extinct species either by immigration or by evolution (Martin, 1967, p. 78). This circumstance contrasts with the rest of the Pleistocene during which there was a more or less orderly replacement of the old by new genera. Guilday (1967, p. 122) compares the Late Pleistocene event with the extinction of the dinosaurs at the end of the Cretaceous:

True extinction (end of a phyletic lineage without phyletic replacement) has occurred throughout the history of life on earth. Among the terrestrial vertebrates, the fossil evidence suggests two striking episodes of extinction: one at the Mesozoic-Tertiary transition saw the extinction of the last of the dinosaurs, the other at the Pleistocene-

Pleistocene-Recent transition saw the sudden dramatic disappearance of large mammals in most but not all parts of the world.

The terminal Cretaceous event was by far the more severe of the two in that to some extent sea life was affected in addition to land fauna, e.g., extinction of the ammonoidea and of many genera of foraminifera and nannoplankton. The terminal Pleistocene event, on the other hand, left marine organisms including cetaceans (the largest mammals in the world) unaffected. However, both events produced *differential* extinctions, affecting primarily the large land animals (greater than 25–50 kg adult body weight) and leaving the smaller vertebrates and the plant kingdom in general relatively unaffected. Martin (1967) quotes Wallace (1876, p. 150) who comments:

We live in a zoologically impoverished world from which all the hugest, and fiercest, and strangest forms have recently disappeared . . . yet it is surely a marvelous fact, and one that has hardly been sufficiently dwelt upon, this sudden dying out of so many large Mammalia, not in one place only but over half the land surface of the globe.

According to one theory proposed by Wallace (1911) and developed further by Martin (1967), the Late Pleistocene extinction was due to the advent of a predator of unprecedented efficiency, primitive man. Martin suggests that prehistoric man had a carnivorous diet and hunted the large mammalia as "big game." However, there are objections to this "overkill hypothesis." For example, Grayson (1977) points out that it is very difficult to see how primitive hunters in North America could succeed in exterminating as many as 10 genera of birds and at the same time be responsible for killing off almost all of the megafauna. Moreover, Kowalski (1967, p. 354) points out that although man was present in Europe at the end of the Pleistocene, there is almost no evidence that he was involved in the extermination of animals. He states:

The hunting activity of primitive man, even over a very long period, does not necessarily bring the extinction of his prey. Extensive literature concerning the hunting habits of European Paleolithic man indicates that all large phytophagous mammals were hunted, but it is very difficult to judge the size of the human population and the degree to which hunting influenced the population of particular species. Reindeer, red deer, aurochs, wild horse—all extensively hunted—were able to survive, whereas some mammals, which were probably more difficult for primitive man to kill (mammoth, woolly rhinoceros, cave bear) or were of no interest to him (lion, hyena), became extinct. When the density of the prey dropped, man with his primitive weapons could not get enough game and began to hunt other animals, migrated, or finally died of hunger. (p. 349)

Also, Vereshchagin (1967) believes that the Late Pleistocene disappearance of the megafauna in the U.S.S.R. cannot be attributed to the hunting activities of paleolithic man alone, but rather involved changes in climate.

The accumulations of mammoth bones and carcasses of mammoth, rhinoceros, and bison found in frozen ground in Indigirka, Kolyma, and Novosibirsk islands bear no trace of hunting or activity of primitive man. (p. 388)

The descriptions of layers containing bones, skeletons, and carcasses of mammoth, rhinoceros, bison, and horse in the basins of the Indigirka, Vilui, Jana, and Kolyma rivers suggest that the animals died in winter, generally in great numbers and thus catastrophically. The corpses of herbivores were swept away with the floods into depressions. In summer these carcasses formed in boggy areas the so called "mammoth horizon," a thick layer consisting of bones, skulls, tusks, peat, and tree trunks interlocked by permafrost. (p. 392)

Slaughter (1967) also believes that climatic change was the main factor causing the Late Pleistocene extinctions. For example, he points out that the coincidence should not be overlooked that this major period of extinction took place at a time of rapid climatic change marking the termination of the Last Ice Age. He suggests a causal connection between the resulting temperature change and these extinctions. Guilday (1967, p. 121) suggests that the cause was due to a period of excessive dryness that immediately followed the Ice Age:

The fact that these late-Pleistocene extinctions were so widespread and geographically almost simultaneous does call for a major overlying cause . . . I suggest that the prime mover was post-Pleistocene desiccation. Evidence for such an episode is present on all continents, and its effects would have been both swift and lethal.

However, Edwards (1967, p. 150) points out that climatic change could not have accounted for these extinctions since abrupt changes have occurred in a cyclic manner throughout the Pleistocene without having any particularly pronounced effects on animal life. Mehringer (1967, p. 247), also opposed to climatic causes for the extinction episode, states:

The same types of habitat that are widespread today in the western United States were occupied by the late-Pleistocene megafauna. The arid regions of today were less widespread even after the major wave of extinction, which ended by 10,000 years ago. About 12,000 years ago some areas of the Southwest probably became marginal habitat, but there were no major barriers to migration into favorable regions . . .

Excluding nonclimatic factors, the period of rapid deglaciation should have resulted in the expansion and not the demise of the megafaunal populations. At the present time there is a greater area and probably a greater variety of habitats available to herbivores than existed in North America during the major Wisconsin ice advances. Large herbivore biomass should have increased, not declined, as the ice retreated.

Moreover, Mehringer points out that the extreme cold of the Wisconsin glacial climate could not have been a major cause of the extinctions since several of the megafauna that became extinct were already well adapted to live in cold climates, e.g., the mammoth and the woodland musk-ox, *Symbos*.

Almost a century ago, Henry Howorth, in his classic work *The Mammoth and the Flood*, effectively countered those old chestnuts: prehistoric overkill and climatic maladaptation. Regarding the North American extinctions, he states (p. 306):

We cannot assign the extinction of these animals to a change of climate in America, for the climate in large parts, and this where the remains most abound, has not virtually changed at all. The same plants and the same land-shells still thrive on the same ground. The fact that the animals found were apparently in robust health when they died, with their stomachs distended with food, and the further fact that remains of many very young animals have occurred, preclude the supposition that disease or want of food destroyed them. The same reasons adduced in the case of Asia, seem to point with even greater force in America to the impossibility of man having caused the destruction of the animals. The scattered tribes of Indians, using rude stone weapons, could hardly accomplish in the way of destroying life what their better armed and apparently more numerous successors who were found there when the Europeans discovered America, failed to accomplish with the animals which then surrounded them. If the modern Indian could barely cope with the bison and the grizzly bear, how did his ruder ancestor destroy the megatherium and the mastodon?

So, to what cause should we attribute this mass extinction? Based on the ideas developed in the present research, a plausible candidate is widespread continental flooding manifested in the form of translating waves of glacial meltwater. Evidence to this effect is

presented in Section 10.2. Also, in Section 10.3 a mechanism is proposed for the production of such "glacier meltwater waves" through a process of accelerated surface melting of glacial ice sheets, occurring during a period of climatic amelioration (e.g., during the Terminal Pleistocene Interstadial). If the vegetation in periglacial regions were destroyed by such floods, any surviving megafauna, both herbivores and their predators, would have been at a distinct disadvantage relative to smaller animals. That is, larger land animals would require a greater biomass for their sustenance and would require a much longer time to increase their population size. Continental flooding would also explain why this extinction happens to be correlated with a major climatic boundary, the ending of the Last Ice Age.

Moreover, such a mechanism could also explain why the severity of the extinction varied as it did with respect to geographical location. Paleontological evidence indicates that the cataclysm was most severe in North America where it is estimated that 95% of the megafauna became extinct (Slaughter, 1967); moderately severe in Northern Europe, Northern Siberia, South America, and Australia; and almost nonexistent in Africa and Southeast Asia where hardly any of the large land animals became extinct (Martin, 1967). A quick look at Figure 10.1 indicates why this would be so. North America had the largest glacial ice sheet while Southeast Asia had none and Africa had only a slight amount of coverage at its southernmost tip. Northern Europe, Northern Siberia, South America, and Australia had varying amounts of glacial coverage in between these extremes.

10.2 THE DRIFT PHENOMENON

Contemporary geologists, in suggesting various causative agents for the drift, have tended to avoid deluvial explanations mainly for two reasons. First, such proposals run counter to the uniformitarian paradigm which has characterized the history of geology as a science. Instead, gradual depositional processes (e.g., involving the action of wind, running water, lake-impounded water or glacial action) are generally considered more plausible and hence are usually proposed. Second, no adequate mechanism has been available in the past to explain how major floods of water could be produced over large geographic regions.

Both of these issues confronted Harlen Bretz when he first proposed his Spokane flood theory in a series of papers from 1923–1932; refer to the discussion of this flood on [pp. 256–257](#). It was not until 1942 that the flood-source problem was resolved with Pardee's proposal that Glacial Lake Missoula was the water source and that an ice dam failure was the cause of the flood. Today it is generally accepted that the Spokane flood actually did occur. However, this may be owed primarily to the efforts of Bretz who dedicated a good portion of his life to prove his flood hypothesis. An interesting historical review of the Spokane flood controversy may be found in a paper by Baker (1978).

The question which must now be asked is whether there are other Wisconsin age periglacial regions in which the terminal Pleistocene drift deposits may be better explained by catastrophic flooding. Explaining the origin of such deposits is not an easy matter. This can be seen, for example, in the wide variety of explanations that had been put forth in the course of the Spokane flood controversy to explain the features of the channeled Scablands of eastern Washington. Clearly it would be a big project to reexamine all of the geological literature on all of the terminal Pleistocene drift deposits around the world and to conduct reevaluation field trips to these various locations in order to decide if in each case catastrophic flooding might be a better explanation, as compared with explanations already offered. Such is not the intent of the present study. Instead I will attempt to concentrate on a few regions, e.g., central Alaska and Northern Siberia, making a cursory overview of some of the literature. The origin of the perennially frozen silt deposits found in these arctic regions has been a matter of controversy and hence there is considerable room here for

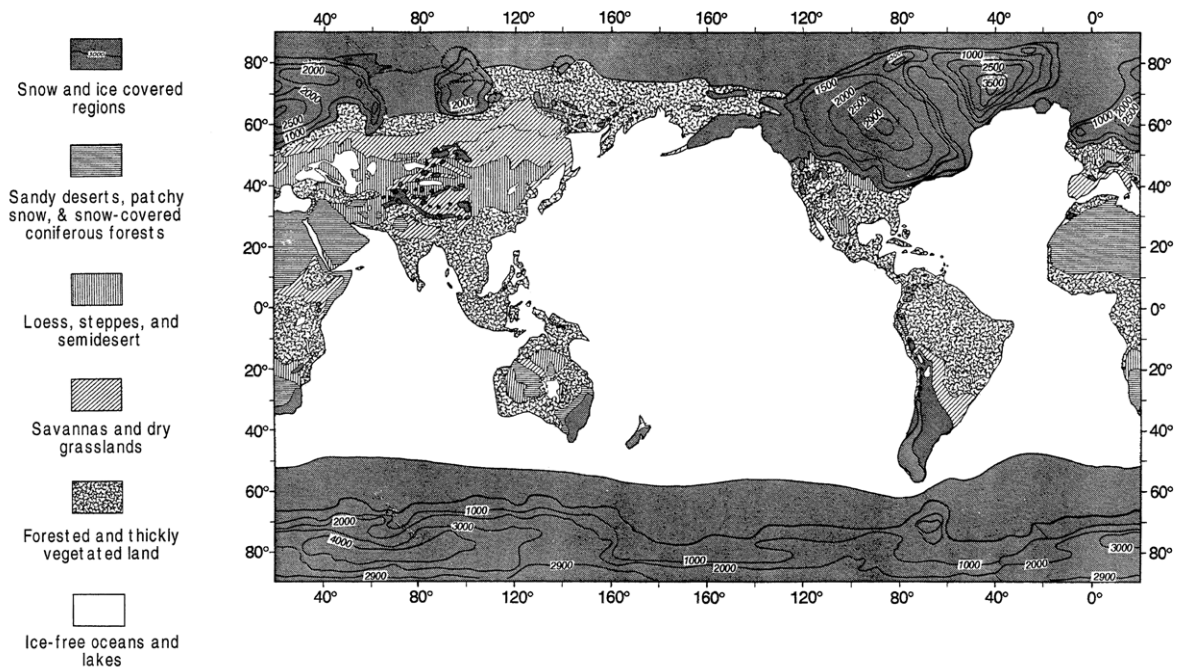


Figure 10.1. Sea-surface temperatures, ice extent, ice elevation, and continental albedo for the Lake Wisconsin glacial maximum period (month of August, 18,000 C-14 years BP). Contour intervals are 1° C for ocean isotherms, and 500 m for ice elevation. Continental outlines represent a sea-level lowering of 85 meters. Albedo levels given in the key are: A) over 40% (snow and ice); B) 30-39% (sandy deserts, patchy snow, and snow-covered dense coniferous forests); C) 25-29% (loess, steppes, and semideserts); D) 20-24% (savannas and dry grasslands); E) 15-18% (forested and thickly vegetated land); F) <10% (ice-free ocean and lakes). (CLIMAP Project Members, 1976; Copyright 1976 by the American Association for the Advancement of Science).

theories of a catastrophic nature. Also, in Section 10.3 a mechanism is presented which should solve the source problem of how large scale catastrophic floods might be generated. Namely, it is shown that given the presence of large continental ice sheets and enhanced surface melting of these glaciers such as might occur during a period of unusual climatic warmth, translating waves of glacial meltwater emerge as a distinct mechanism of meltwater transport. Such glacier waves would not be restricted to a particular locale, but could be produced wherever large continental ice sheets were present.

10.2.1 The Permafrost Silt Deposits of the Arctic Regions

Almost all areas of Alaska that lie below an altitude of 300-450 meters are covered with a loamy blanket of perennially frozen silt that ranges in thickness from a few millimeters to over 60 meters (Pewe, 1975a, p. 37). For at least 100 years there has been a controversy as to the origin of this material, referred to locally as "muck." Explanations in the geological literature have mostly included gradually acting processes, such as fluvial, lacustrine, marine, and eolian deposition mechanisms and weathering. Hibben (1943, p. 255–256) describes this silt as follows:

The outwash plains of the local glaciations are likely points of origin for this loess material. These muck deposits are from four to one hundred feet thick and are

especially well known in the vicinity of Fairbanks, Circle, and the other gold mining centers of the upper Yukon and the Tanana where the muck overlies auriferous gravels. Muck deposits of considerable thickness, however, are found in the lower reaches of the Yukon, on the Koyukuk River, on the Kuskokwim, and on several places along the Arctic Coast, and so may be considered to extend in greater or lesser thickness, over all unglaciated areas of the northern peninsula. The deposits are concentrated in creek or river valleys for the most part, and have been exposed in gold mining operations. In addition to amorphous bodies of loess material, the muck contains inter-bedded volcanic ash layers, lenses of clear ice and peat, and abundant animal and vegetal material, the whole frozen into a solid mass.

Several Alaskan silt formations have been distinguished, dating as far back as the Illinoian glaciation. Of these formations the Goldstream Formation is of particular interest. This is one of the most widespread formations in central Alaska and is believed to date from the latter portion of the Wisconsin Ice Age (Pewe, 1975b; Pewe et al., 1977). It is a valley-bottom accumulation which is present in almost all creek and small river valleys in central Alaska. The Goldstream Formation is regarded as the greatest depository of Pleistocene vertebrate remains in Alaska if not in North America (Pewe, 1975b). Most of these fossils are found in valley bottoms and the greatest concentrations occur where small tributaries join large creeks (Pewe, 1975a, p. 98). To get an idea of the quantity of these fossils, just in the Fairbanks area tens of thousands of specimens have been collected over a period of 30 years as a result of gold digging operations, with about 8000 specimens being collected in a typical year (Pewe, 1975a, p. 92). Pewe et al. (1977) note that the vertebrate remains found in the Goldstream Formation in Alaska are similar to those found in the Siberian "middle silt unit," with mammoth, bison, and horse being most abundant in both regions. However, actually a wide spectrum of animals, both large and small, has been found in Wisconsinian age silts. A list of mammalia found in the perennially frozen creek-valley deposits in the Fairbanks district of Alaska includes: shrew, bear, dire wolf, coyote, wolf, fox, badger, wolverine, saber-toothed tiger, lion, lynx, mammoth, mastodon, horse, camel, antelope, bison, caribou, moose, elk, giant elk, sheep, musk ox, bovid, ground sloth, beaver, ground squirrel, vole, lemming, collared lemming, porcupine, hare, and pika (Pewe, 1975a, p. 97).

Particularly unusual is the finding that the soft parts of animals (e.g., skin, hair, tissue, entire carcasses) are often found preserved in the frozen ground along with their hard parts (e.g., bones). Instances where entire carcasses of mammoths and rhinoceros have been found frozen in Northern Siberian silt deposits are particularly well known because of their sensational character.

Several investigators concur that these mammoths and rhinoceros died from asphyxia as might occur by drowning or by being buried alive in a mud flow (Farrand, 1961, p. 734; Tolmachoff, 1929, p. 57; Howorth, 1887, p. 184). However, Ferrand (1961) is probably incorrect in concluding that their deaths were individual, natural (noncatastrophic) occurrences, e.g., due to drowning as a result of breaking through river ice, becoming trapped in valleys filled with snow, or bogging down in a slowly moving stream of sticky mud. Crucial to Ferrand's argument is his assumption that only large animals (e.g., mammoths and rhinoceros) have been found in Siberia with their soft parts preserved, inferring from this that the deaths of these beasts were due to the peculiarity of their physique and inability to negotiate marshy ground and snow drifts. However, as Pewe (1975a) reports, besides the frozen partial carcasses of mammoths, carcasses of other smaller, more agile animals have also been found in Alaskan muck, including: bison, musk ox, moose, horse, lynx, caribou, and ground squirrel. Thus the megafaunal clumsiness argument appears itself to be treading on thin ice. Moreover, as Tolmachoff (1929) points out, the idea that mammoths had become enclosed within ice is untenable, and hence rules out two of Ferrand's entrapment scenarios. Tolamchoff states (p. 51):

Mammoth-bearing drift deposits sometimes have a thickness tens of feet, sometimes they are spread out in comparatively thin layers. In some localities, as in the one of Schmidt's mammoth, have been discovered, underneath these deposits, the sediments of the last Arctic transgression. In Northeastern Siberia they are usually underlain by layers of rock ice [solid transparent ice], and very often, in this case, are reduced to a thickness of only two or three feet. An inaccurate expression by Adams created the idea that his mammoth had been frozen within ice. But after the detailed consideration of this matter by Toll there is no more doubt that this mammoth like others had been frozen within the driftground underlain by rock ice. Theoretically, it is possible to imagine carcasses enclosed within ice, but as matter of fact, neither mammoth nor rhinoceros was ever found in such conditions, as Howorth has already emphasized.

Also, analysis of the vegetation frozen into the muck deposits confirms that at the time that this catastrophe occurred the climate in the arctic was much milder than it is today (Taber, 1943, pp. 1483–1484; Howorth, 1887, p. 71). A boreal forest grew at that time in regions that are today so cold that they are devoid of vegetation. A moderate northern latitude climate is also suggested in Figure 10.1, where it is seen that east of 60°E longitude and west of 140°W longitude boreal forests grew as far as 10° north of the arctic circle! Temperatures would have become particularly warm during the Terminal Pleistocene Interstadial judging from Figures 9.2 and 9.3 (pp. 249 - 251). It is then reasonable to conclude that during this interstadial these arctic regions were the habitat of the mammoth and of the other megafauna found in the drift. Whatever killed them must have overtaken them unawares while they were grazing, for food has been found between their teeth and in their stomachs undigested. A catastrophic flood would be a likely candidate. Not only would it have taken the beasts by surprise, but it would have buried them alive and in many cases would have prevented their carcasses from decaying. According to Howorth (1887, p. 96):

The facts compel us to admit that when the Mammoth was buried in Siberia the ground was soft and the climate therefore comparatively mild and genial, and that immediately afterwards the same ground became frozen, and the same climate became Arctic, and that they have remained so to this day, and this not gradually and in accordance with some slowly continuous astronomical or cosmical changes, but suddenly and *per saltum* . . . When we find such a series ranging so widely preserved in the same perfect way, and all evidencing a sudden change of climate from a comparatively mild temperature to one of great rigour, we cannot help concluding that they all bear witness to a common event. We cannot postulate a separate climatic cataclysm for each individual case and each individual locality, but we are forced to the conclusion that the now permanently frozen zone in Asia became frozen at the same time from the same causes.

However, Howorth may be exaggerating somewhat the rapidity with which freezing took place. For example, Taber (1943, p. 1489) mentions that quick internment in fine silts saturated with cold water, if left in a stagnant condition, would be sufficient to partially preserve animal soft parts for a considerable length of time until climatic change would have caused the ground in Alaska to become perennially frozen. Taber (p. 1490) considers glacial floods as a major cause of burial, although he does not seem to state that these floods would be of a catastrophic nature. However, other data that he presents are consistent with catastrophic depositional processes. For example, he notes (p. 1489) that only hard part remains (e.g., bones) are found in the gravel deposits, soft parts only being found in the overlying slits. He proposes that the gravel deposits were laid down at an earlier time and hence had a greater period of time in which to decay before freezing of the remains occurred. However, these results are much more easily explained if it is assumed that the

gravel and silts were deposited catastrophically in a common deluvial event. In such a circumstance bones stripped of flesh would have settled out first along with the coarse sedimentary fraction (e.g., gravel) and hence would have occupied the lower portion of the deposit. Carcasses, being much less dense than bones, would have settled out more slowly or possibly would have floated for some time, and hence would be found to occupy the upper portion of the deposit along with the finer silt fraction.

Taber's description of the fossil remains also implicates either catastrophic dismemberment prior to burial or a reworking of previously deposited remains. Suggesting the latter, he writes (pp. 1489–1490):

Fossil bones are astonishingly abundant in the frozen ground of Alaska, but articulated bones are scarce, and complete skeletons, except for rodents that died in their burrows, are almost unknown. Of several tons of bones of the larger mammals seen in 1935, four bison vertebrae were the only ones found in a position indicating original articulation. The dispersal of the bones is as striking as their abundance and indicates general destruction of soft parts prior to burial. However, occasional articulated bones indicate primary burials.

Hibben (1943, p. 256) emphasizes a catastrophic burial for at least some portion of the Alaskan silts stating:

Although the formation of the deposits of muck is not clear, there is ample evidence that at least portions of this material were deposited under catastrophic conditions. Mammal remains are for the most part dismembered and disarticulated, even though some fragments yet retain, in this frozen state, portions of ligaments, skin, hair, and flesh. Twisted and torn trees are piled in splintered masses concentrated in what must be regarded as ephemeral canyons or arroyo cuts.

In view of the evidence presented above it becomes difficult to defend a uniformitarian position such as that espoused by Pewe (1975, p. 98) who suggests that these vertebrates died of natural causes and their bones were gradually transported downslope to the valley bottoms where they are presently found.

Pewe (1975a, p. 37) is of the opinion that the muck composing the Goldstream Formation in Alaska was originally wind-blown material that had become *gradually* deposited through the action of glacial rivers. But such an interpretation would have difficulty accounting for why valley bottom slits are often found to overlie deposits of gold-bearing gravels, e.g., the Fox Gravel, the gold usually being found immediately above the bedrock surface. This stratigraphic placement of placer gold deposits has been construed by Boyle (1979) as an unresolved problem. He states (p. 381): "One would suspect on casual examination that gold would be rather evenly distributed throughout the gravels and sands rather than concentrated in well defined streaks." However, the flood scenario proposed here would resolve this problem. Under the action of turbulent water flowing at a high velocity catastrophic deposition would be expected, the densest and coarsest sedimentary components (e.g., gold and gravel) would be expected to settle out first, followed by the less dense and finer silt fraction. It might also be mentioned that auriferous gravels similarly underlie megafaunal-bearing drift deposits in other parts of North America, Northern Siberia, South America, and Australia (Howorth, 1887, pp. 318, 358, 372; Boyle, 1979, p. 369). Such evidence is consistent with a theory that proposes the occurrence of continental flooding on a rather widespread scale, as is proposed here.

The origin of the Alaskan upland silts presents an even greater challenge for theoreticians. Pewe (1955) reports that in the Fairbanks area (as one example) the silt ranges from 1 to 80 feet in thickness on the tops of low hills located 50–150 feet above the valley floor and thins out to a thickness of a few feet on ridges situated 800–2000 feet above the valley floor. Clearly, normal fluvial action, such as that proposed by some theoreticians

to explain the valley bottom deposits, has considerable difficulty accounting for deposits perched at such altitudes. Again, many theories have been put forth to account for the origin of the upland silt, ranging from an estuarine inundation of Central Alaska to high velocity winds as the transporting agent. Pewe (1955) reviews a number of these theories and concludes that an eolian mechanism best accounts for the upland silt. However, if wind were the transporting agent, then one might ask why should such "wind-blown" material often be found to overlie auriferous gravel deposits. For example, Pewe (p. 704) reports that on top of Gold Hill at an altitude of about 700 feet (250 feet above the flood plain) a bore hole revealed the presence of 150 feet of dry upland silt overlying auriferous gravels. The eolian hypothesis must attribute this to chance superposition, the deposition of wind-blown loess over a preexisting auriferous gravel substrate. The flood hypothesis, though, is able to not only account for the origin of the silt *and* the gravel, but also for their stratigraphic placement relative to one another.

Besides the unique stratigraphic placement of the placer gold, these upland silt deposits also bear a resemblance to the valley bottom deposits in that the silt is often found to overlie the remains of extinct megafauna; e.g., see Taber (1943, p. 1486) or Pewe (1955, p. 714). Pewe (1955, 1975a, 1975b) attempts to account for the upland silts in terms of eolian transport and for the valley bottom deposits (e.g., the Goldstream Formation) in terms of fluvial action. But if such completely different transport mechanisms were actually involved, then it becomes difficult to understand why these high and low altitude deposits are so strikingly similar. A major glacial meltwater flood, on the other hand, would be able to account for the formation of both the valley bottom deposits and the upland silts, and also would explain their similarity.

Of the various other proposals accounting for the origin of the Alaskan upland silts it is interesting to consider the lacustrine hypothesis as put forth by Eakin (1916, 1918). Eakin (1918, p. 44) states that the "mechanical analysis of the silt seems to indicate more strongly an aqueous rather than an eolian origin." Moreover, he cites several geomorphic features to support his argument. For example, he notes that the presence of plains standing at different elevations connected by steep scarps running for several miles in length could be produced only by aqueous erosion. He states (p. 45):

The most salient fact that is unmistakably indicated in the features described above is that the drainage level during the deposition of the uppermost silt beds was nearly 1000 feet above the present level of the Yukon at Ruby and still higher above the base-level that controlled the erosion of the preceding cycle. Transportation of detritus by wind is obviously incapable of producing such a result. Likewise the idea that such a change in the drainage level could be the result of overloading streams with material as fine as the silts is untenable. Through some agency apart from erosion itself the old base-level of erosion was eliminated and a new base-level was established at a much greater elevation. The change of base-level apparently involved extensive inundation of the old land surface, a fact indicated by the character, structure, distribution, and topographic expression of the unconsolidated deposits and the bedrock beneath them.

Eakin suggested that a 50,000 – 100,000 square mile region in central Alaska had temporarily impounded glacial meltwater to a height of 1200 feet, drainage to the sea being blocked by an ice dam. Pewe (1955, p. 716) offers several convincing criticisms of Eakin's hypothesis, such as the lack of evidence for the required drainage barrier, the lack of lacustrine varves, clay, or aquatic life in the silt deposits, and the finding that the silts do not have a definite upper limit in their altitude. However, while Pewe's criticisms correctly rule out the lacustrine scenario, they leave untouched Eakin's conclusions that the silts are of aquatic origin. In fact, many of Eakin's suggestions could be rescued from these criticisms if the glacial meltwater inundation of central Alaska were a temporary phenomenon

involving a translating wave of water. It is interesting to note that the divide between the Laurentide and Cordilleran ice sheets created a natural water course which emptied northward onto the central Alaskan plains. This geographic feature could have served to channel glacial meltwater to this region whether the meltwater originated from the ice sheet surface itself in the form of a glacier wave, or whether it involved (more conventionally) the sudden release of water impounded behind an ice jam such as may have occurred in the ice sheet divide.

The same depositional agent forming the Alaskan muck appears to also have been at work in Northern Siberia forming the so called "mammoth horizon" or "tundra horizon." Pewe, Journaux, and Stuckenrath (1977) call attention to the striking resemblance between the perennially frozen silt deposits in Central Alaska and those found in central Yakutia. They note that both areas consist of unglaciated rolling lowlands and river terraces surrounded by high mountains that were extensively glaciated in Pleistocene times. Thus they suggest that a similar depositional history for these geographically widely separated regions would not be surprising. In agreement with Pewe et al., I might add that a similarity of the deposits in these two regions would be expected especially if glacier waves were the depositional agents.

The islands of the Arctic Ocean to the north of Siberia offer the most striking evidence that the megafauna of this region perished in a widespread catastrophe. In regard to the Bear Islands, one explorer describes the soil as consisting of sand and ice containing mammoth bones "in such quantities that they seemed to form the chief substance of the island" (Howorth, 1887, p. 53). The Liachof Islands have been similarly described. Hedenstrom, who explored the New Siberian Islands in 1806, describes the scene as follows (after Wrangell, 1841, note to p. 173):

On the southern coast of New Siberia are found the remarkable wood hills. They are 30 fathoms [60 meters] high, and consist of horizontal strata of sandstone, alternating with strata of bituminous beams or trunks of trees. On ascending these hills, fossilized charcoal is everywhere met with, covered apparently with ashes; but on closer examination, this ash is also found to be a petrification, and so hard that it can scarcely be scraped off with a knife.

The German scientist Adolph Erman (1848, pp. 379-380) describes his impression of the New Siberia Islands as follows:

It is only in the lower strata of the New Siberian wood-hills that the trunks have that position which they would assume in swimming or sinking undisturbed. On the summit of the hills they lie flung upon one another in the wildest disorder, forced upright in spite of gravitation, and with their tops broken off or crushed as if they had been thrown with great violence from the south on a bank, and there heaped up . . . So it is clear that at the time when the elephants and trunks of trees were heaped up together, one flood extended from the centre of the continent to the furthest barrier existing in the sea as it now is. That flood may have poured down from the high mountains through the rocky valleys. The animals and trees which it carried off from above could sink but slowly in the muddy and rapid waves, but must have been thrown upon the older parts of Kotelnoi and New Siberia in the greatest number and with the greatest force, because these islands opposed the last bar to the diffusion of the waters.

The megafaunal deposits of the tundra regions are strikingly similar to the skeleton-bearing deposits found in Michigan and New York and in other more temperate regions of the globe, with the exception that in the arctic there are many places in which, in addition to skeletons, portions of carcasses or entire carcasses have become preserved from decay due to permafrost conditions. Regarding the mounds of skeletal remains found in New Siberia,

Erman (1948, pp. 377–378) states:

This is one of those phenomena which were formerly thought to be confined to a narrow locality, but are now found recurring in all parts of the globe. The attempt to explain them, however, is not thereby rendered more easy, for the explanations must apply equally to the coasts of the Polar Sea, the region of the Ohio, and, besides, to all the valleys in the plains of Europe, Northern Asia, and America, with hardly any exception.

Regarding the extinction of the mammoth in the Old World, Howorth (1887, pp. 183-184) writes:

However ingeniously and with whatever subtlety we may deal with our evidence, the facts constrain us therefore to one inevitable conclusion, namely, that the Mammoth and its companions perished by some wide-spread catastrophe which operated over a wide area and not through the slow processes of the ordinary struggle for existence, and that the greater portion of the remains we find in Siberia and Europe are not the result of gradual accumulation under normal causes for untold ages, but the result of one of Nature's hecatombs on a grand and widespread scale, when a vast fauna perished simultaneously.

We must next inquire what the nature of this catastrophe was . . . We want a cause that should kill the animals, and yet not break to pieces their bodies, or even mutilate them, a cause which would in some cases disintegrate the skeletons without weathering the bones. We want a cause that would not merely do this as a wide-spread murrain or plague might, but one which would bury the bodies as well as kill the animals, which could take up gravel and clay and lay them down again, and which could sweep together animals of different sizes and species, and mix them with trees and other debris of vegetation. What cause competent to do this is known to us, except rushing water on a great scale. Water would drown the animals, and yet would not mutilate the bodies. It would kill them all with complete impartiality, irrespective of their strength, age, or size. It would take up clay and earth, and cover the bodies with it. This is the very work it is doing daily on a small scale. Not only could it do this, but it is the only cause known to me capable of doing the work on a scale commensurate with the effects we see in Siberia.

Howorth (1887, p. 311) comments on the extinction of the megafauna in North America, saying:

In America, as in Europe, the number of the remains and their universal distribution, contrast notably with the scarcity and local character of the debris of mammals in other sub-aerial beds, on other geological horizons, and point, there, as here to their having been the victims of a catastrophe. The unweathered bones, the intact skeletons, the crowds of animals of different species found together, the similarity in condition of the remains, all converge upon one conclusion, namely, the existence of a great and sudden hecatomb . . . If we are to meet the facts, we need a cause which not only destroyed animals old and young, great and small, aggressive and helpless, in a common doom, and in many cases in herds or schools of Mammoths and mastodons, but also buried them deeply in such tough material as gravel and clay while still intact, and buried them occasionally very deeply . . . and buried them with shells, both land and fresh-water; and under deposits which form, like the Bluff beds"; continuous strata, unbroken and undisturbed, over many miles of country. It seems to me there is no other agency available to produce this result save a flood of water.

It is concluded here, in concurrence with Howorth, that the arctic drift deposits were formed in a similar fashion as the drift deposits found elsewhere, and that water was the agent responsible for this cataclysm. It is proposed that these floods occurred in connection

with major climatic warmings brought about by periods of excessive solar activity, the most recent of these major floods occurring about $12,700 \pm 100$ calendar years BP. Moreover, it is proposed that this flooding episode manifested as a sequence of large scale, high kinetic energy meltwater waves created as a consequence of accelerated ice sheet surface melting; see Section 10.3. As seen in Figure 10.1, continental ice sheets were present in portions of both Northern Siberia and Alaska. Moreover, most regions of Northern Siberia and Alaska were within 2000 km of the edge of the Laurentide ice sheet (Siberia by a polar route). In addition, Northern Siberia had alpine-type glaciers in the ice-sheet-free regions. Thus in the event of a sudden climatic amelioration, it is easy to see how flooding could take place on a widespread scale throughout these arctic regions.

A high kinetic energy, glacial meltwater wave, or "glacier wave," could simultaneously account for many of the puzzling features of the megafaunal extinctions in Northern Siberia and Alaska. The meltwater not only would have drown and buried the animals without warning, but it would have tended to preserve them as well. The icy contents of a glacier wave would have been close to 0° C and would probably have been composed of a slushy mixture of meltwater and ice chunks. Ice chunks mixed in with the alluvial deposits would have helped to refrigerate the carcasses preventing their decay. Meanwhile, long after the wave had passed, as the climate changed from boreal to arctic, the region would have become locked into a permanently frozen state.

10.3 THE GLACIER WAVE EFFECT

The idea that rapid melting of glacial ice sheets may have led to continental flooding on a grand scale is not new. One hundred years ago James Dana (1880) proposed this in his *Manual of Geology*. Except in his day, oxygen isotope analysis and radiocarbon dating were unknown. He came to this conclusion simply from studying the morphology of the landscape. He states (p. 553):

The fact that a flood vast beyond conception was the final event in the history of the glacier (i.e. of the great American ice sheet) is manifest in the peculiar stratification of the flood-made deposits, and in the spread of the stratified drift southward along the Mississippi Valley to the Gulf, as first made known by Hildyard. Only under the rapid contribution of immense amounts of sand and gravel, and of water from so unlimited a source could such deposits have been accumulated.

Howorth (1893, p. XX), however, came to a different conclusion regarding the Flood. He suggested that the flooding was produced by a marine incursion into the continental regions, an immense translational wave of water that was set in motion by the sudden upheaval of some of the world's largest mountain ranges (e.g., the Rocky Mountains, the South American Cordilleras). However, a marine incursion may be ruled out as a single causative agent of the Lake Wisconsin silt deposits in Alaska and Northern Siberia due to the scarcity of marine animals in the majority of the deposits, e.g., see Péwé, 1955. Nevertheless, for historical purposes it is interesting to note that Howorth was aware of Dana's glacial meltwater flooding scenario, but found difficulties with this mechanism. Howorth states (1893, pp. 814–815):

If the glacial climate was so severe that it was possible to accumulate enormous sheets of ice and ice caps, I cannot understand how the summer melting of this ice, on any great scale, can be admitted. . . . If . . . floods were due to the melting of the ice, at the close of the glacial age, the change of climate involved must have been very sudden, or very rapid, much more sudden and rapid than is consistent with any uniformitarian theory.

Again, it seems impossible by an appeal to the sub-glacial streams to explain the facts as we find them. The water flowing from a glacier either originates along its surface and is due to surface melting, or is due to the melting of the ice foot by friction. In either case, as we see it in the greatest glaciers, it runs from underneath the ice in separate streams. These separate streams could not deposit widespread sheets of debris in a continuous way, nor can we understand how they could be made to flow at the heights at which the stratified drift occurs.

Howorth makes a good point here. Even with the accelerated melting rate of ~ 4 cm of ice per day proposed in Subsection 3.3.4 (p. 103), the resulting flow of meltwater from the glacier's edge would not amount to much. For example, if meltwater were to flow off the surface of the Laurentide Ice Sheet at a constant rate of 5 m/s, it would take about 28 days to make the 12,000 km journey from the ice sheet's center to its edge. By the time this stream reached the edge, it would have accumulated a depth of only about 1 meter, i.e., ~ 4 cm/day \times 28 days = 112 cm.

However, it is possible to conceive of a mode of meltwater discharge quite different from that of continuous runoff. Consider a mechanism in which the meltwater accumulated on the glacier's surface becomes discharged in a manner appropriate to compose a self-amplifying travelling wave, an avalanche having enormous height, mass, and velocity, and consequently having great destructive force. I will call such a wave a "continental glacier meltwater wave," or for short a "glacier wave;" see Figure 10.2. How this wave amplification process might operate will be described shortly. But first it is useful to briefly review some of what is known about glaciers regarding their ability to store up and then suddenly release meltwater.

It is known that glaciers have the ability to store a considerable amount of meltwater, e.g., on their surface in the form of perched ponds or lakes, in caverns within their ice body, or in tributary channels backed up behind ice jams. Also, they can store a considerable amount of meltwater near their surface in the form of laterally percolating liquid runoff. Sudden releases of such stored water are referred to as *glacier floods* (Ward, 1978, p. 34) or *glacier bursts* (Thorarinsson, 1953). The hydrograph of two such bursts which took place in Grimsvotn, Iceland, in 1934 and 1938 are shown in Figure 10.3. (Thorarinsson, 1953). As is

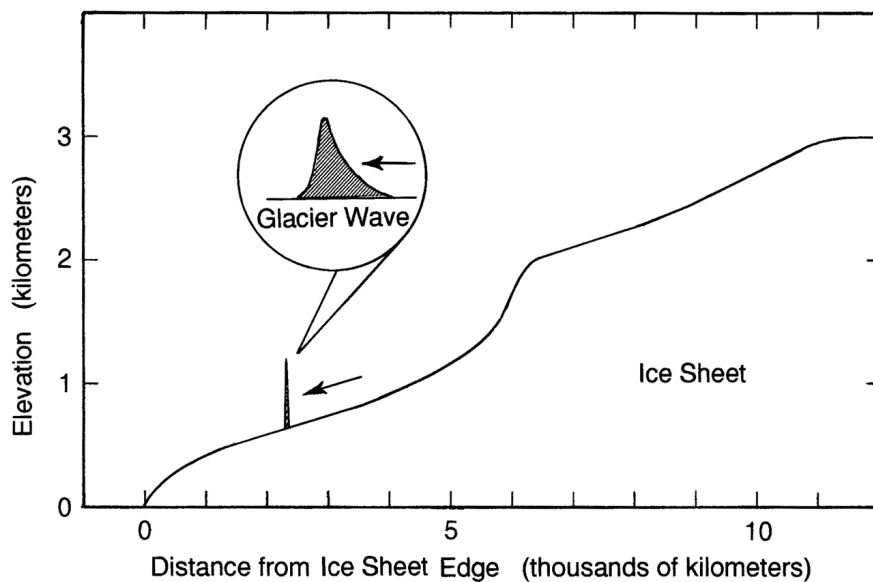


Figure 10.2. A glacier wave propagating down the surface of the Laurentide ice sheet. Ice sheet profile has been drawn with a vertical exaggeration of 2000:1.

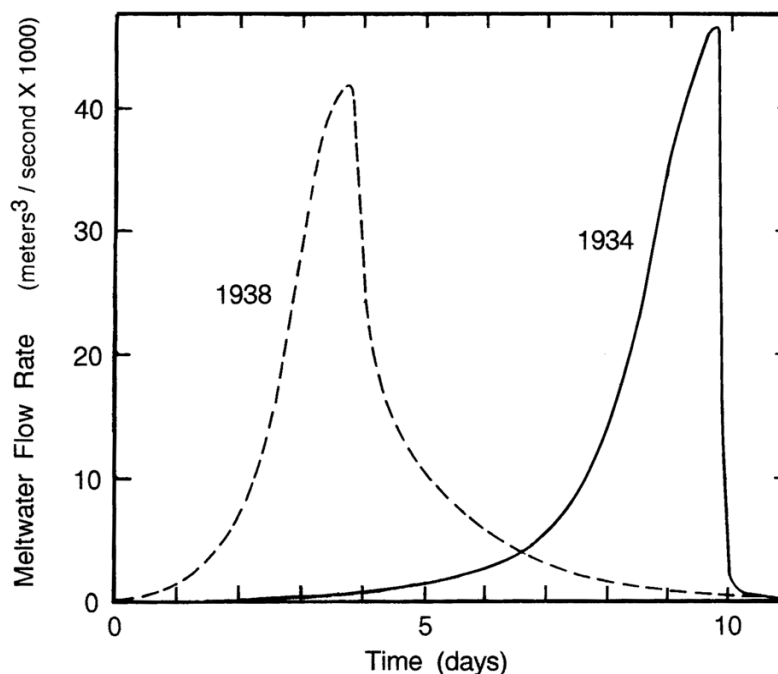


Figure 10.3. Hydrograph for the 1934 and 1938 Grimsvotn glacier burst (adapted from Thorarinsson, 1953).

seen here, about $7 - 8 \text{ km}^3$ of glacial meltwater became discharged in the space of just 1 to 2 days. The phenomenon at Grimsvotn appears to have a periodicity of about once per decade.

According to Thorarinsson, the floods issue from a large perched lake capable of impounding about 7.5 km^3 of glacial meltwater (~ 35 to 40 km^2 by 200 meters deep) at a height of ~ 1500 meters above sea level. The lake is about three-fourths of the way to the summit of the Vatnajokull glacier and is fed from a 300 km^2 region. The heat source for this high-altitude melting is geothermal heat, which continually issues from the active volcano underlying the glacier. The meltwater stored up in this lake becomes periodically released due to progressive failure of the cauldron walls when the stored capacity becomes excessive. Ward (1978, p. 36) notes that the exponential increase in discharge rate may be explained by a feedback process in which increased flood flow rate through the water transmitting channels progressively enlarges the channels which in turn progressively increases the flow rate. The sharp drop off in the 1934 glacier burst would signify abrupt exhaustion of the source reservoir, although there are instances in which glacier flood hydrographs have steep initial rises and gradual tail-offs, as in the case of the sudden release of impounded meltwater due to failure of an ice dam.

Returning now to the Laurentide Ice Sheet example, consider a case in which a glacial meltwater lake, retained near the center of the ice sheet by an ice dam and fed from surface meltwater runoff, is suddenly released as a result of dam failure. Suppose that the wave of water thus produced has a cross-sectional area of $25,000 \text{ m}^2$ (50 meters high by 500 meters wide), is 5 km long, and travels forward at a velocity of 10 m/s. Whether this 0.1 km^3 glacier wave will continue to grow in size as it travels down the ice sheet slope, or whether it becomes dissipated by the pools of water it encounters, depends on whether its continued forward motion results in a net energy gain or a net energy loss for the wave. The kinetic energy which the glacier wave imparts to the ambient meltwater medium to accelerate this medium to the wave's bulk velocity must necessarily come from the wave itself.

Moreover, the wave, in turn, must acquire its kinetic energy from its store of potential energy which is gradually released as the wave travels forward down the slope of the glacier. If the energy demand on the wave were to become so great that the rate of energy loss to the encountered medium exceeded the rate at which the wave acquired kinetic energy from its descent, the net kinetic energy of the wave would become reduced and the wave's velocity relative to the ambient medium would tend to diminish. On the other hand, if the rate of kinetic energy supply were to exceed the rate of kinetic energy demand, the net kinetic energy of the wave would tend to increase and the wave would be able to accelerate.

Consider the following idealized example. A 1 centimeter wide increment of the 50 meter high wave proposed above, travelling forward at a velocity of $v = 10$ m/s through an ambient medium of depth $d = 20$ cm would encounter water at the rate of: $\dot{m} = 1 \text{ cm} \times 20 \text{ cm} \times 1000 \text{ cm/s} \times 1 \text{ g/cm}^3 = 20,000 \text{ g/s}$. Suppose (in this idealized case) that the wave accelerates all of the water that it encounters to its own bulk velocity and that the accelerated meltwater is initially at rest relative to the ice sheet. In imparting a forward velocity of 10 m/s to this water, the wave would be losing kinetic energy at the rate of:

$$E_{\text{out}} = \frac{1}{2} \dot{m} v^2 = \frac{1}{2} (20,000 \text{ g/s}) \times (1000 \text{ cm/s})^2 = 10^{10} \text{ ergs/s.}$$

At the same time, as the wave advances at a velocity of 10 m/s down the glacier slope, which has an average gradient of $\kappa = 2.5 \times 10^{-4}$, the wave would be dropping in altitude at the rate of:

$$\dot{h} = \kappa v = 1000 \text{ cm/s} \times 2.5 \times 10^{-4} = 0.25 \text{ cm/s.}$$

As a result, the wave would be releasing potential energy at the rate of:

$$\dot{E}_m = M g h = 2.5 \times 10^8 \text{ cm}^3 \times 1 \text{ g/cm}^3 \times 980 \text{ cm/s}^2 \times 0.25 \text{ cm/s} = 6.1 \times 10^{10} \text{ ergs/s.}$$

Consequently, since $E_{\text{in}} > E_{\text{out}}$, the wave's store of forward kinetic energy would be able to increase, provided that a sufficient portion (i.e., >16%) of the released potential energy went into forward motion as opposed to turbulent motion or frictional losses.

For a glacier wave of a given mass M , travelling down a sloped ice sheet of a given gradient κ , and through a meltwater medium of a given depth d , there would be a unique upper limit to the wave's velocity which would be determined by the efficiency ε with which the wave is able to convert released potential energy into forward kinetic energy. This terminal velocity would be given by the relation:

$$v_T = \sqrt{2M\varepsilon\kappa g / d}$$

However, over a period of time the glacier wave would grow in size and mass, and hence would be able to release potential energy at a greater rate as it advanced. If the wave were to sweep up all of the meltwater encountered in its path, and if this meltwater were formerly stored on the surface of the ice sheet at an average depth of ~1 meter, then by the time the glacier wave had reached the edge of the ice sheet it would have a cross-sectional area of $\sim 1 \text{ m} \times 1.2 \times 10^7 \text{ m} = 12 \text{ km}^2$ (e.g., a height of ~600 meters and a width of ~40 kilometers). Thus a 1 cm wide increment would have a mass of $M = 1.2 \times 10^{11} \text{ g}$. If, at the bottom of the ice sheet, the wave were encountering ambient meltwater having an average depth of 200 cm, then the wave could theoretically attain a terminal velocity of 100 m/s (~200 mph), even with an efficiency as low as $\varepsilon = 10^{-4}$. With this mass and velocity, each meter length of the wave front, in cross section, would have a kinetic energy of 6×10^{20} ergs, equivalent to about 14,000 tons of TNT (or about 0.7 Hiroshima A-bombs).

The example discussed here, of course, is only a rough estimate made for the purpose of illustration. However, a more precise analysis would still render essentially the same results. Namely, in a nonequilibrium, low-friction regime such as would exist on the sloping

surface of a rapidly melting continental glacier, if a meltwater wave of sufficient size were spontaneously generated, this wave would grow in size through a "domino effect." Beyond a critical threshold of wave size, a growing glacier wave would become the dominant mechanism of meltwater transport since a glacier wave would be capable of *dissipating potential energy at a greater rate* as compared with homogeneous meltwater flow. The phenomenon of glacier wave formation and growth should be amenable to treatment using the tools of nonequilibrium thermodynamics.

Glacier wave growth would take place not only in the cross-sectional dimension, but along the length of the wave front as well. A dam failure beginning as a localized event near the summit of the ice sheet could grow into a semicircular extended wavefront, measuring perhaps thousands of kilometers in length by the time it had reached the ice sheet border.

Upon encountering proglacial lakes at the foot of the ice sheet, a wave of the magnitude estimated above would probably have enough force to jettison the entire lake over its retaining moraines or ice dam. For example, Proglacial Lake Missoula in northern Montana (see Figure 9.7, **p. 257**) is estimated to have contained about 2000 km³ of meltwater (Baker, 1978). By comparison, a 200 km long section of a glacier wave of the size proposed above would contain about 2400 km³ of meltwater (along with chunks of unmelted ice). If a wave of this size were to accelerate the entire lake to its own bulk velocity, the wave would suffer only a 50% drop in velocity (in an ideal encounter having minimal losses due to turbulence). Thus the flood features of the Channeled Scabland could just as well be attributed to the action of a major glacier wave or a series of such waves causing rapid discharge of Lake Missoula. Alternatively, a glacier wave may itself have been sufficient to cause such features.

A 600 meter high glacier wave consisting of water, unmelted ice chunks, and other debris travelling at, let us say, 50 m/s (100 mph) and having a cross-sectional area of 12 km² and a length of several thousand kilometers could probably have traversed thousands of kilometers over a continental land mass before becoming entirely dissipated. Upon entering the ocean, such a glacier wave would have caused a considerable volume displacement of the water mass, producing a tsunami. The resulting disturbance could have crossed thousands of kilometers of ocean and still had sufficient energy to produce considerable damage on the shores of another continent.

In conclusion, it is suggested here that the loam-like drift deposits observed in many areas of the world that were once periglacial regions during the Wisconsin Ice Age were produced by a series of such glacier waves issuing at about the same time from the continental ice sheets. The peak of this flooding activity would have occurred about 14,000 calendar years BP at the peak of the Terminal Pleistocene Interstadial. It is proposed here that both this climatic warming and the associated Terminal Pleistocene Flood were the result of an interplanetary greenhouse effect produced by elevated concentrations of nebular material located just beyond the Earth's orbit during a period when interplanetary dust concentrations between the Earth and Sun were at a particularly low level. However, glacier waves could be triggered by a number of other mechanisms capable of supplying a large quantity of thermal energy in a short period of time to an extended ice sheet area.

[UPDATE: For example, as mentioned on **p. 286**, energetic solar activity may have been a contributing factor. That is, accelerated glacial melting could have occurred during a period when the Sun was unusually luminous and active and especially at a time when the Earth may have suffered a solar cosmic ray induced conflagration while being engulfed by an unusually large solar coronal mass ejection. Evidence presented at the end of this chapter suggests that this latter phenomenon may have played a major role in the final stage of the Terminal Pleistocene Extinction, just prior to the onset of the Younger Dryas.]

10.4 DATING THE MEGAFUNA EXTINCTIONS

Meltzer and Mead (1983) have made an analysis of radiocarbon dates for 375 Late Pleistocene megafauna unearthed from 150 North American fossil sites. The frequency distribution which they found for a reduced set of 232 of these dates is shown in Figure 10.4. Note that this distribution has a bimodal peak centered between 11,000 – 12,500 C-14 years BP suggesting that extinction was proceeding at its highest rate between 12,700 – 14,200 calendar years BP. This initial rise of this peak precedes by about 1200 years the date derived in Chapter 9 for the Terminal Pleistocene Flood, i.e., ~14,400 calendar years b2k.

[**UPDATE:** When the C-14 dates composing this histogram are converted into calendar dates using the radiocarbon conversion relation given in Appendix E, the frequency distribution appears as shown in Figure 10-A (p. 283). Figure 10-A was plotted using more recent data from Meltzer and Mead (1985) and Martin (1987).^(1, 2) The date 12,950 years b2k (11,000 C-14 years BP), which corresponds to the beginning of the Younger Dryas stadial, marks the agreed upon termination boundary beyond which no surviving extinct Pleistocene mammals are found in most parts of the world. Radiocarbon dates younger than this boundary date are likely to be erroneous (gray bars). The correlation of the Terminal Pleistocene extinction boundary to this sudden global climatic reversal suggests that the extinction was associated to the same agent causing the rapid changes of climate at that time; i.e., the Sun. A solar cause to the extinction is also supported by the finding that the rise in the number of extinct mammals parallels the rise in glacial meltwater outflow and climatic warming of the Bölling/Alleröd which, as was suggested earlier, had a solar flare/cosmic dust incursion cause. More frequent flooding during this time could also explain the increasing number of megafaunal remains, these often being preserved from decay by being entombed in flood deposits. Also a comparison of Figure 10-A with the Be-10 profile of Figure 8-C shows that a Galactic superwave was passing through the solar system at the time]

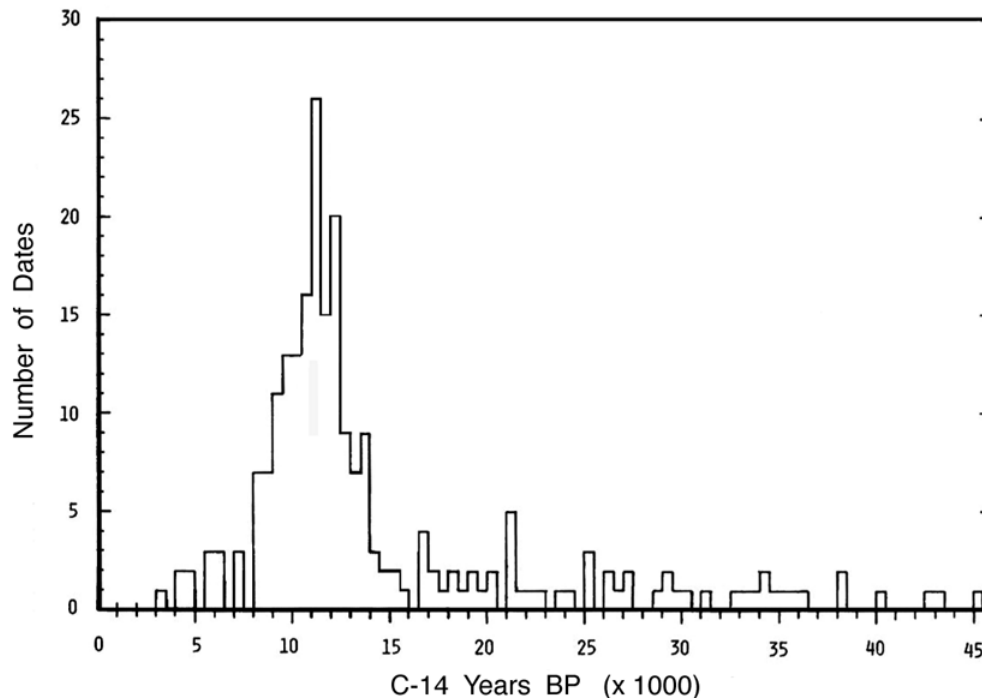


Figure 10.4. Frequency distribution of megafaunal extinctions in North America at the end of the Pleistocene. Shown here are the distribution of 232 unadjusted C-14 dates from 150 sites (adapted from Meltzer and Mead, 1983).

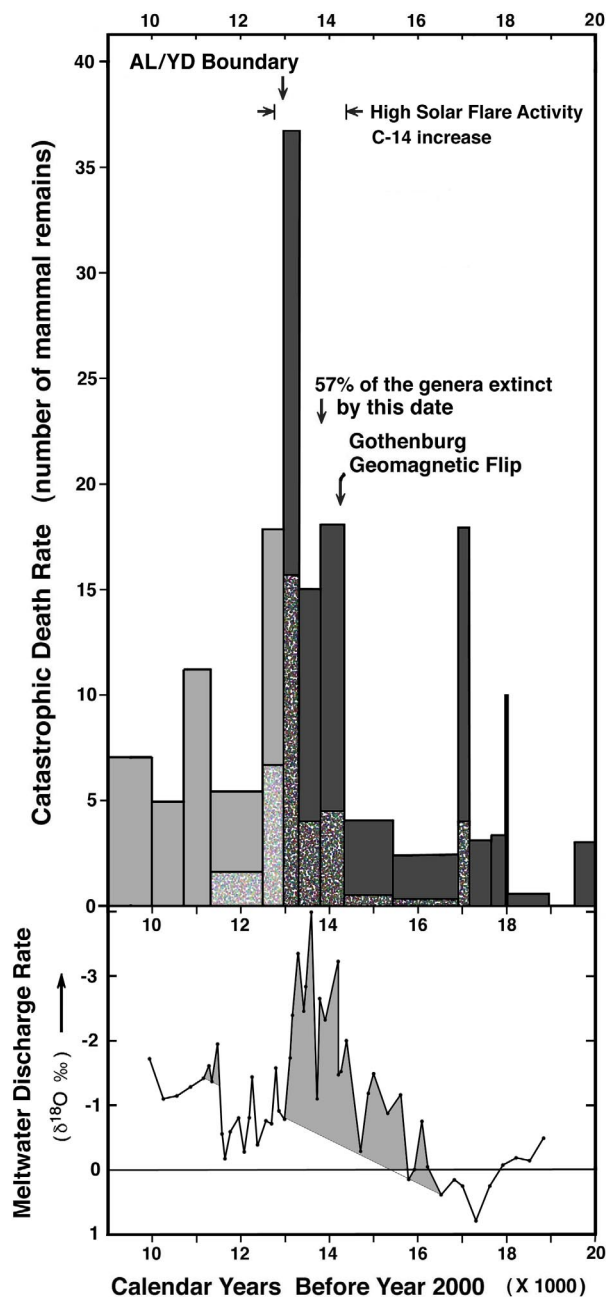


Figure 10-A. Upper bar graph: Chronological distribution of calendar dates on remains of extinct mammals from 163 localities in North America. Black bars indicate dates prior to 12.9 kyrs b2k. Pixilated bars indicate the subset of more reliable dates. Lower profile: The rate of meltwater discharge from the North American ice sheet (see Figure 9-E of Chapter 9). Upper graph based on data from Meltzer and Mead (1985) and Martin (1987) with their ^{14}C dates being converted to calendar dates.

The remainder of this section argues that the majority of the extinctions actually took place over a period of time shorter than what is indicated by the apparent temporal dispersion of dates, the dispersion being due to a number of causes. For example, excessively old dates may be due to contamination of the remains with old carbon or to the alluvial reworking of

older fossils from preexisting deposits. Excessively young dates may be due to contamination with young carbon or may reflect an unusually high ^{14}C content in the remains associated with a brief episode of intense cosmic ray bombardment. Martin (1967), for example, argues that many radiocarbon dates assigned to the remains of Pleistocene megafauna should not be trusted. He cites the problematically young date of $2,040 \pm 90$ ^{14}C years BP found for the terminal Pleistocene deposits in St. Petersburg, Florida and also questions the youth of several mastodon remains found in Michigan and dated at around 6000 ^{14}C years BP. Because of these few dates, which are in obvious error, he warns that all ^{14}C dates of mastodon remains may be in error to some degree. He states (p. 98):

Is it possible that all postglacial dates on mastodons are overshoots? No skeptical archaeologist would consider accepting a radiocarbon date of 6,000 to 8,000 years on an alleged Clovis site before subjecting it to the most minute excavation and examination, without demanding an effort at replication of the date on the critical beds, without considering carefully all the possibilities of intrusion, and without a field demonstration of the evidence to equally critical colleagues.

Variability in radiocarbon dates is also encountered in remains unearthed from the permafrost muck layer in Alaska and Siberia. In Alaska, dates on remains from essentially the same muck layer have been found to range from ~ 200 ^{14}C years BP for mammoth-bearing deposits from Sullivan Creek (Martin, 1967, p. 93) to $<30,000$ ^{14}C years BP for similar deposits near Fairbanks (Broecker, Kulp, and Tucek, 1956). In Siberia, dates on wood and animal remains from the mammoth horizon have ranged from 11,500 ^{14}C years BP (Taimyr Peninsula) to 30,000 ^{14}C years BP (Lena River); see Martin (1967). However, it would be incorrect to interpret this wide range of dates as being indicative of the span of time during which this silt layer was being deposited. As was pointed out in Section 10.2, there is substantial evidence to indicate that the mammoth horizon in Northern Siberia and the Late Wisconsin Goldstream Formation in Alaska were deposited in a short space of time by a flood (or by floods) of water.

[**UPDATE:** Radiocarbon dating of these strata indicates that they were both deposited around 11,000 ^{14}C years BP (12,950 calendar years b2k), the time of the final disappearance of the Pleistocene megafauna. Several studies indicate the presence of a radiocarbon anomaly at this date (see update at the end of this chapter).]

Unusually young radiocarbon dates may be accounted for within the context of the Galactic Explosion Hypothesis. For example, in Section 7.2 (p. 212) it is suggested that a period of unusually intense solar flare activity (or a T Tauri-like solar outburst) may have been involved in simultaneously producing the Gothenburg Geomagnetic Excursion and in clearing out dust from the inner portion of the solar system; also recall Figure 4.5 (p. 142). If so, such an event could temporarily have produced very high solar cosmic ray intensities which in turn would have produced abnormally high levels of ^{14}C in the atmosphere. Also, excess ^{14}C may also have been produced within the animal remains through the capture of secondary neutrons by nitrogen nuclei present in protein tissue such as collagen. Future measurements of ^{14}C and Be-10 in glacial ice dating from this period should help to determine if such an event actually occurred. If it did, then ^{14}C dates on organic matter deposited at this time should be mistrusted.

Schove (1977) warns, in agreement with the above conclusion, that ^{14}C dates from the mid-Bölling/Ågård Interstadial ($\sim 14,100 \pm 100$ calendar years BP) may be abnormally young. He notes that a geomagnetic excursion occurred about this time (i.e., the Gothenburg Excursion) and that during this time the Earth's magnetic field may have been abnormally weak allowing greater penetration of ^{14}C producing cosmic rays.

So, some way, other than ^{14}C dating, should be found to date organic remains

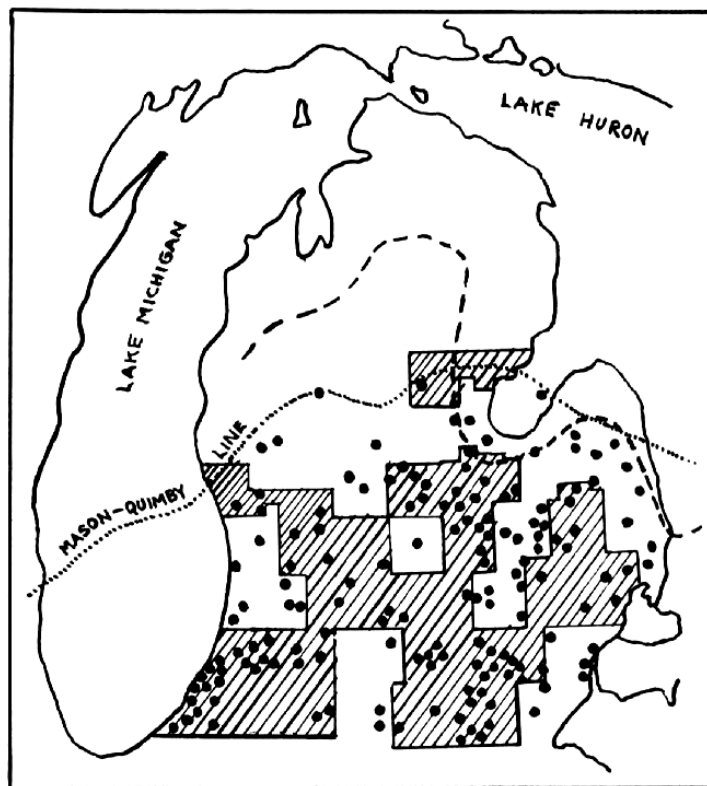


Figure 10.5. Distribution of Michigan mastodons (dots) and other extinct Pleistocene genera (shaded regions), in comparison to the location of the Port Huron morainic system (dashed line). Also shown is the location of the "Mason-Quimby line" north of which fluted projectile points are absent from deposits. (Modified drawing based on Martin, 1967, Fig. 2 and Dreimanis and Goldthwait, 1973, Fig. 1)

associated with the Terminal Pleistocene Extinction. One such method will now be presented. Consider Figure 10.5. Most of this diagram is taken from Martin (1967, p. 99). The dots (after Skeels, 1962) illustrate locations where mastodon remains have been found, and the shaded regions indicate the locations of extinct fauna other than mastodons. The dotted line shows the location of the "Mason-Quimby line" north of which fluted projectile points manufactured by paleolithic man are suddenly absent from alluvial deposits. Superimposed on this map I have drawn the approximate position of the Port Huron morainic system (dashed line) based on a map presented in Dreimanis and Goldthwait (1973, p. 73). The lack of fluted projectile points in regions further north could be due simply to the fact that these regions were still in a glaciated state at the time of the megafaunal demise. Note the relatively close correspondence between the Port Huron morainic system line and the northern boundary of faunal extinctions. The Port Huron /Lake Whittlesey readvance (or ice sheet margin) is dated at about $13,000 \pm 500$ ^{14}C years BP ($15,600 \pm 1100$ calendar years b2k); see Section 9.3. By comparison, the Powell/Union City moraines, dated at about $15,000$ ^{14}C years BP ($18,000$ calendar years b2k), pass through central Ohio and Indiana. Thus we may infer that the megafaunal extinction episode took place after $13,000$ ^{14}C years BP ($15,600 \pm 1100$ calendar years b2k).

The correspondence between the Mason-Quimby line and the faunal extinction boundary has been cited as evidence that early man was responsible for the extinctions of these animals; see Martin (1967). However, as was argued in Section 10.1, it is difficult to attribute this global extinction episode to human hunting activities. The lack of fluted

projectile points to the north could simply reflect the fact that after the extinction episode there were few animals left to hunt, and perhaps few hunters left to hunt them. Howorth (1887, Ch. 9 and 11) for example, presents considerable evidence suggesting that paleolithic man perished in the same cataclysmic plight as his animal contemporaries.

The same correlation technique that is proposed here for limiting the age of the mastodon remains in Michigan may be used in New York State with similar results. For example, a map of mastodon deposits for the eastern part of North America constructed by Dreimanis (1968) shows that in eastern New York mastodon deposits are found only in the lower portion of the Hudson River Valley. The deposits appear to terminate suddenly in the Orange County area near Albany. The ice sheet had receded to about this point by the time of the Luzerne readvance dated at about 13,000 ¹⁴C years BP (15,600 calendar years b2k).

[**UPDATE:** These ice margin dates precede by 1600 years the calendar date of the peak in the megafaunal remains histogram shown in Figure 10-A and by almost 2600 years the time of the final demise of the Pleistocene mammals. So this earlier flood-related demise may have been local to these regions. The animals apparently continued to survive until a subsequent tragedy finally extinguished them around 12,900 calendar years b2k. The existence of the Mason-Quimby line would suggest that these fluted projectile points are not contemporaneous with Paleo-Indian sites that have been dated to around 12,400 – 13,000 calendar yrs BP. Or, if they are, then some barrier other than the ice sheet margin, such as a northward extending proglacial lake, would have had to be present to account for the absence of artifacts and mastodon remains further north.]

In light of the material presented in Section 9.3, it may be argued that the extinction of the mammoths and other fauna found in association with them, and the deposition of the drift in which they are found, may be linked in common to the passage of one or a series of glacier waves. These waves would have reached their peak severity about 14,300±100 calendar years b2k in connection with a period of unusual climatic warmth during which time the continental ice sheets in all parts of the world were melting at an unusually high rate.

[**update:** An extended period of even more lethal glacier wave discharges also occurred towards the end of the Younger Dryas.] It may be argued that associated harsh environmental conditions were also a major cause of death; e.g., high temperatures prevailing in low latitude regions. It is suggested here that this climatic warming was brought about by the injection of nebular material into the solar system during the passage of the 14,200 years BP superwave. Energetic solar activity may also have been a contributing factor, e.g., see Subsection 4.7.3. Future determinations of ¹⁴C, ¹⁰Be, and cosmic dust concentrations in ice cores spanning this period should confirm this hypothesis.

UPDATE

Evidence of High Solar Activity During the Alleröd and Early Younger Dryas (update for [p. 141](#) and [p. 284](#)): I had suggested in section 10.4 that the anomalously young radiocarbon dates found in some megafaunal remains may have been produced by exposure of these animals to intense solar cosmic ray bombardment. This scenario seemed plausible in view of lunar rock evidence which indicated that solar activity was significantly enhanced at the end of the ice age. I had reasoned that the same immense coronal mass ejection event that scorched the moon rocks could have overpowered the Earth's magnetic field and exposed the Earth's surface to high levels of ionizing radiation close to the beginning of the Younger Dryas. This solar conflagration theory later gained strong evidenciary support after 1995 with the discovery that sediments dating from the Alleröd/Younger Dryas transition boundary contain a radiocarbon excess.⁽³⁻⁶⁾ In particular, measurements of radiocarbon levels in the

sediments of the varved Cariaco Basin core from Venezuela show that atmospheric ^{14}C had risen 7 percent over a period of 200 years during the cooling that marked the transition from the Alleröd to the Younger Dryas; see figure 10-B.⁽⁶⁾ It reached a peak about 12,810 yrs b2k, and then, after plateauing for about 120 years, declined through the Younger Dryas stadial and PreBoreal period after which it experienced a brief upturn.

Solar cosmic ray induced climatic cooling. The progressive 155 year-long cooling at the beginning of the Younger Dryas climatic transition (13,009 - 12,853 cal yrs b2k) could have been partly due to the high intensity cosmic ray bombardment that prevailed during the correlative ^{14}C rise phase. Increased cosmic ray intensities would have led to greater cloud formation in the upper atmosphere either through ion-induced formation of condensation nuclei⁽⁷⁾ or through the increased production of ice crystals resulting from an increase in the ionosphere-Earth electric current.⁽⁸⁾ This, in turn, would have increased atmospheric albedo and reduced ground surface temperature, producing a climatic cooling trend. Corroborating this, Svensmark and Friis-Christensen^(9, 10) have found that between 1980 and 1995 changes in the background cosmic ray flux correlated positively with changes in cloud cover, a 25% increase in cosmic ray flux translating into a 3% increase in cloud cover over the course of a solar half-cycle. The resulting increase in planetary albedo would have a cooling effect comparable to a 0.6% decrease in solar irradiance.⁽⁹⁾ During the onset of the YD, an elevated flux of solar cosmic rays, rather than of galactic cosmic rays most likely produced the required increased cloud cover.

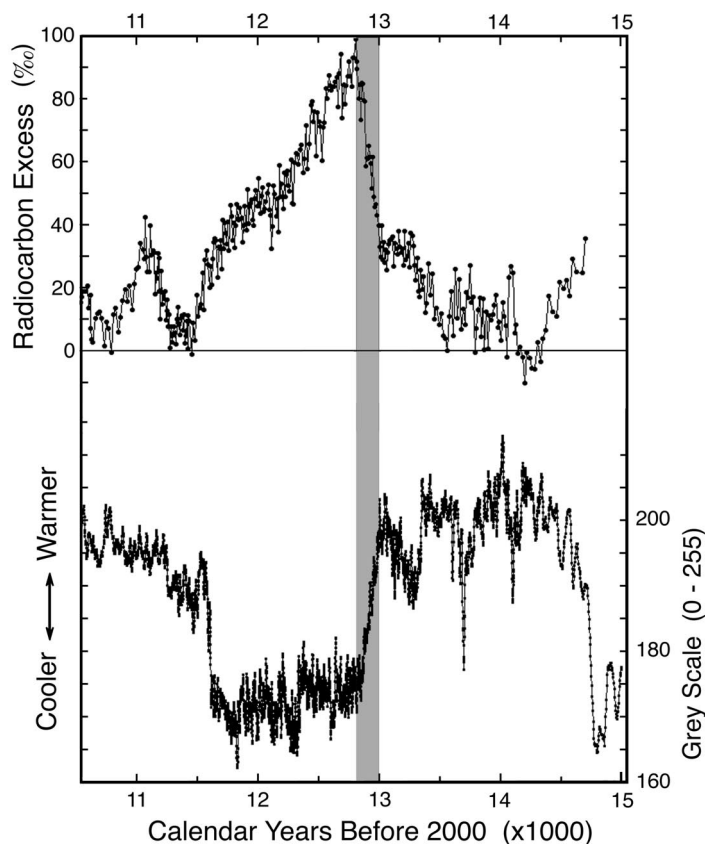


Figure 10-B. Upper profile: radiocarbon abundance excess relative to trend line as seen in a Cariaco Basin sediment core. Lower profile: Corresponding grey scale climatic profile for the Cariaco Basin. Higher values indicate warmer temperatures (after Hughen, et al. 2000).

Polar ice core studies have established that dust peaks during the ice age are modulated with the eleven year solar cycle period.⁽¹¹⁻¹³⁾ They suggested that during the solar cycle phase when solar activity was low, Galactic cosmic ray flux would increase and this, in turn, would produce increased cloud cover and climatic cooling leading to increased aridity and dustiness. I feel, however, that while Galactic cosmic rays may have a dominant cloud producing effect during periods of normal solar activity, that solar cosmic rays take over as the principal cloud nucleation agent during periods when the Sun is highly active, such as at the end of the last ice age. In such a case one would expect a direct correlation between solar activity and climatic cooling, as is seen in the Cariaco Basin record.

The discharge of cold low salinity meltwater into the North Atlantic and the cold temperatures induced by the cloudy weather during this early phase of the Younger Dryas would have reestablished the North Atlantic sea ice cover and helped to partially shut down the deep water ocean current conveyor transporting heat northward. There is evidence that the rate of meridional overturning circulation (MOC) at a Bermuda rise location partially decreased around 13 kyrs b2k (Cariaco Basin varve chronology) at the onset of the YD cooling.⁽¹⁴⁾ This decreased MOC could have helped to maintain the Earth's climate in its cold stadial phase through the end of the Younger Dryas even though the period of intense solar flaring subsided after 12,750 cal yrs b2k.

However, the suggestion that there is a causal connection between thermohaline circulation and climate may need to be reconsidered. The Bermuda rise record shows that MOC, which had been shut down through most of the Bölling interstadial, abruptly increased to modern levels around 14,200 cal yrs b2k. So, if there an MOC-climate connection exists, why did the increase in MOC follow, rather than precede, the onset of the Bölling warming, and why were these two changes separated in time by half a millennium. Meltwater discharge from the ice sheets was at a maximum around 14,200 cal yrs b2k and far higher than the meltwater influx rate prevailing at the time of the Younger Dryas.⁽¹⁵⁾ So, considering that thermohaline circulation increased at the time of the meltwater influx rate max, the suggestion that overturning rate would decrease in response to glacial meltwater influx occurring just before the onset of the YD appears inconsistent.

[The following four sections are based on findings published in the following paper: P. A. LaViolette, "Evidence for a solar flare cause of the Pleistocene mass extinction." *Radiocarbon* (June 2011): .]

More about the early YD radiocarbon increase and its likely solar cause. The upward trend in ¹⁴C concentration actually had an early phase that began prior to the Intra Alleröd Cold Peak, i.e., about 13,550 b2k. So we may conclude that period of elevated solar flare activity began even at this early date. If this is added to the increase that occurred during the Younger Dryas transition, then atmospheric ¹⁴C concentration would have in total risen by 10%. By comparison, during the Holocene, increases in ¹⁴C were no greater than about 2 - 3% above the average. Also ¹⁴C rose sharply about the middle of the Older Dryas, 14,100 calendar years b2k, shortly after the time of the Gothenburg geomagnetic excursion.

The radiocarbon excess seen in the floating Late Glacial Pine dendrochronology record,⁽¹⁶⁾ profile b) in Figure 10-C, also shows that the radiocarbon excess began rising as early as 14,000 cal yrs b2k. The ¹⁴C rise up through 13,200 cal yrs b2k correlates with the death rate peak at the climax of the extinction. The decline in ¹⁴C excess from 15,000 to 14,500 cal yrs b2k could be attributed to the major influx of radiocarbon-depleted glacial meltwater during this period which would have had the effect of diluting the radiocarbon content of the oceans during this period. This interpretation of the ¹⁴C record is resumed later in the update of this chapter where the correlation between Heinrich flooding events and Cariaco Basin record ¹⁴C is discussed.

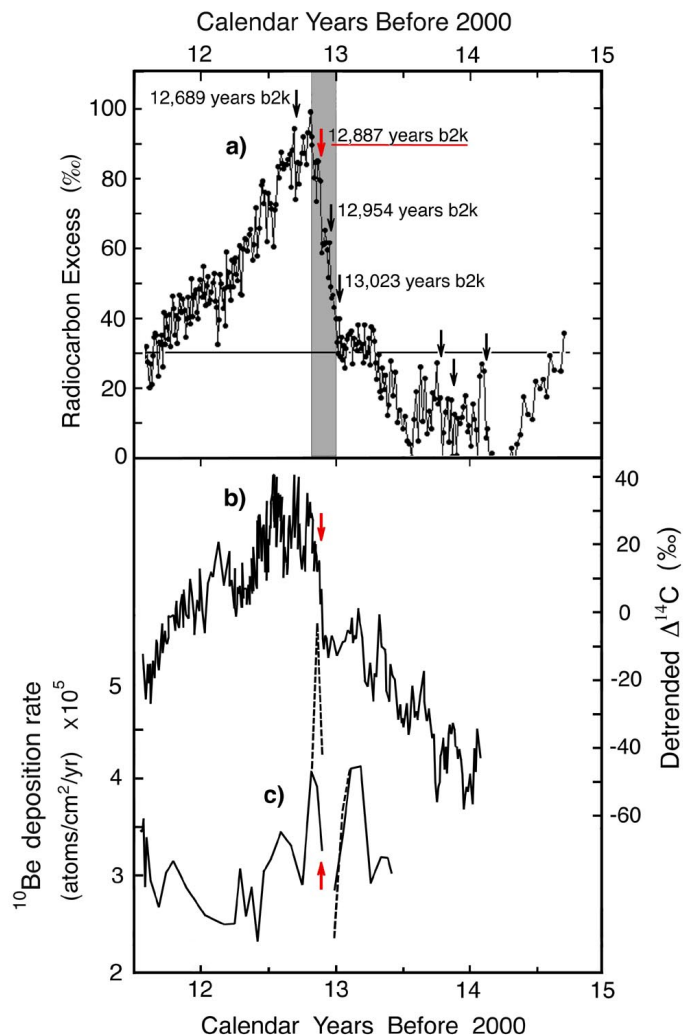


Figure 10-C. a) Radiocarbon abundance excess relative to trend line as seen in a Cariaco Basin sediment core. Arrows indicate times of four large spurts in ^{14}C production, as well as several smaller events all possibly registering major solar proton events. The largest increase is marked in red. (Data is from Hughen, et al. 2000.) b) Radiocarbon excess relative to trend line as seen in the floating Late Glacial Pine dendrochronology record (Hua, 2009) matched to the GISP2 ice core ^{10}Be deposition rate profile shown in (c). b) Beryllium-10 deposition rate based on the ^{10}Be concentration data of Finkel et al. (1997) adjusted using the ice accumulation rate data of Alley et al. (1997) and dated according to the Cariaco Basin chronology (solid line). Beryllium-10 deposition rate based on accumulation rates inferred from applying the Cariaco Basin chronology (dashed line).

Thus the Earth may have been exposed to hazardously high solar cosmic ray intensities on several occasions throughout the period from 14,100 to 12,800 cal yrs b2k which spans the entire period of elevated megafaunal mortality seen in Figure 10-A.. Thus intense solar flare activity is implicated as one of the primary causes for the demise of the Pleistocene megafauna. Such mega solar storms not only could have delivered lethal levels of ionizing radiation and UV to these megafauna, but also secondary cosmic rays produced during an atmosphere-contacting event could have ignited fires that destroyed their food supply.⁽¹⁷⁾

In a computer simulation of the YD $\Delta^{14}\text{C}$ rise, Stocker and Wright were able to attribute only half of the rise to a decrease in North Atlantic deep ocean ventilation.⁽¹⁸⁾ Muscheler et al. subsequently used beryllium-10 deposition rates determined from analysis of ice from the

GISP2 Greenland ice core to model atmospheric radiocarbon production rate at the end of the ice age.⁽¹⁹⁻²¹⁾ They concluded that the $\Delta^{14}\text{C}$ increase at the onset of the YD is partly due to the increased production of atmospheric radiocarbon and partly to a reduction in old carbon entering surface waters which they attribute to a 30% reduction in the diffusive carbon exchange in the ocean arising from a reduction in North Atlantic deep water formation.

Atmospheric ^{10}Be , like radiocarbon, is currently produced primarily by the intergalactic cosmic ray proton background radiation that strikes the Earth's atmosphere. As seen in the lower profile of Figure 10-C,^(20, 21) the ^{10}Be deposition rate at Summit, Greenland was generally elevated around the latter part of the Alleröd and early YD, although there was a 200-year lull period during the onset of the YD (13,075 to 12,880 cal yrs b2k).

To facilitate comparison, the ^{10}Be sample dates from the GISP2 ice core have been adjusted to conform to the Cariaco Basin varve chronology using the climatic match points presented in Table 10-1. These ^{10}Be and ^{14}C variations are unlikely due to changes in

Table 10-1.
Depth-Time Marker Horizons Used in Transferring the
Cariaco Basin Chronology to the Summit, Greenland
GISP2 and NGRIP Oxygen Isotope Profiles

| Climatic Boundaries | Cariaco Basin (years b2k) | GISP2 mid depth (meters) | NGRIP mid depth (meters) | GICC05 Chronology (years b2k) |
|----------------------------|-------------------------------------|---------------------------------------|---------------------------------------|---|
| PB ends | 11,514 | 1664.0 | | |
| YD ends | 11,593 | 1676.17 | 1490.44 | 11,660 |
| temp. min. | 11,597 | 1677.15 | 1491.45 | 11,680 |
| temp. min. | 11,619 | 1678.25 | 1492.15 | 11,696 |
| temp. min. | 11,833 | 1684.9 | | 11,927 |
| temp. max. | 12,211 | 1688.7 | | 12,048 |
| temp. max. | 12,500 | 1699.2 | | 12,417 |
| temp. max. | 12,645 | 1702.25 | | 12,520 |
| temp. min. | 12,820 | 1705.35 | | 12,641 |
| temp. min. | 12,853.5 | 1706.90 | 1520.45 | 12,695 |
| temp. max. | 12,881.5 | (1708.45) | 1521.98 | 12,746 |
| warming begins | 12,884 | (1708.55) | 1522.08 | 12,750 |
| acidity spike | 12,887 | 1708.65 | 1522.20 | 12,754 |
| temp. max. | 12,896 | 1708.8 | 1522.35 | 12,760 |
| temp. min. | 12,923 | 1709.55 | 1522.98 | 12,783 |
| temp. min. | 12,945 | 1710.35 | 1523.78 | 12,792 |
| temp. max. | 12,962 | 1711.25 | 1524.43 | 12,832 |
| YD begins | 13,007 | 1712.25 | 1526.9 | 12,906 |
| IACP ends | 13,183 | 1721.26 | | 13,089 |
| IACP begins | 13,350 | 1727.29 | | 13,253 |
| temp. min. | 13,703 | 1762.2 | | 13,098 |

geomagnetic screening since the average field intensity did not change appreciably across the Alleröd/Younger Dryas transition.⁽²²⁾ The minimum between the two ^{10}Be peaks could be attributed to enhanced solar wind screening of an elevated cosmic ray background flux, indicating a time when the Sun was more active than normal.

The Cariaco Basin varve chronology has been synchronized with the Holocene dendrochronology scale and is believed to be accurate to ± 10 years.⁽⁶⁾ It should provide a more reliable time indicator over the Younger Dryas interval than the Greenland ice core chronology since the ice sheet was subject to melting during particularly warm YD intervals. The Cariaco Basin chronology is here transferred to the GISP2 ice record by matching up major climatic excursions evident in the GISP2 oxygen isotope profile with similar excursions in the Cariaco Basin grey scale profile. Figure 10-D illustrates this matching over the early YD and late AL portion of the Cariaco Basin grey scale profile. Table 1 shows how associated Cariaco Basin varve dates correspond with ice core meter depths for these features seen in the GISP2 and NGRIP Greenland ice core records. The bracketed GISP2 depths are interpolations. The standard GICC05 Greenland ice core chronology (Rasmussen et al., 2008) is shown for comparison in the last column.

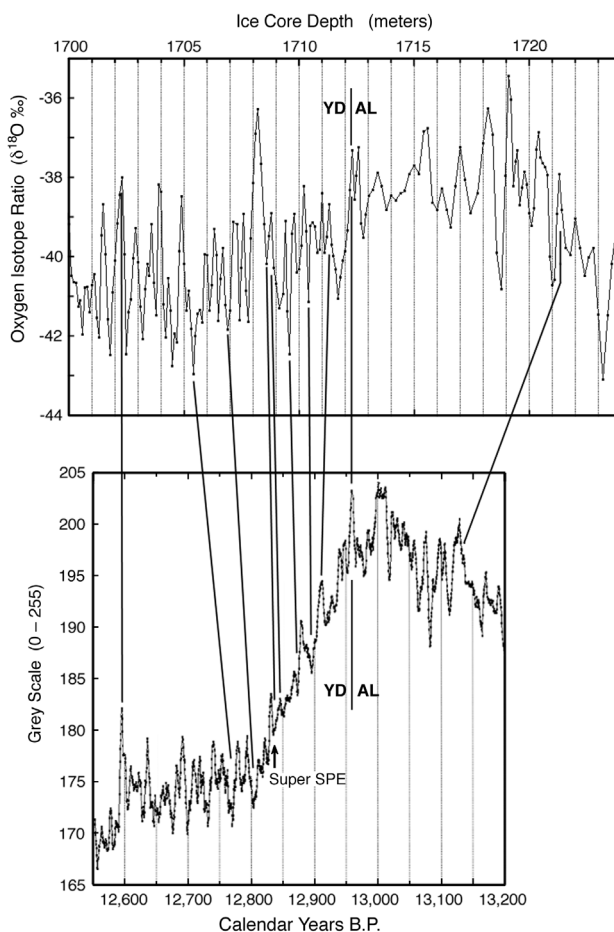


Figure 10-D. Correspondence between the Cariaco Basin grey scale climate profile (lower graph) and the GISP2 oxygen isotope profile (upper graph), allowing the Cariaco Basin varved chronology to be matched to GISP2 ice core depth scale. Data courtesy of Hughen, et al.⁽⁶⁾ and Stuiver and Grootes.⁽²³⁾

Varve dating of the Cariaco Basin grey scale profile shows the Younger Dryas as having lasted for a period of 1414 years, whereas the GISP2 ice core chronology of Alley,⁽²¹⁾ which is based on counts of annual layers in the ice, shows the Younger Dryas as having lasted only about 1281 years, or 1246 years in the GICC05 ice core chronology. The 156 and 168 year shortfalls in the Greenland chronologies may be attributed to a possible loss through melting of about 11 - 12% of the ice accumulated during the YD period. This could have occurred during the mid and late phase of the YD when the oxygen isotope ratio reached above the -38 per mille Alleröd level on numerous occasions, as seen in high resolution isotope profiles.

The Cariaco Basin chronology projects accumulation rates for the GISP2 ice core that differ from those published by Alley et al. during the early YD. When the ^{10}Be deposition rate values are recalculated using ice accumulation rates inferred from the Cariaco Basin chronology, they appear as shown with the dashed line profile in figure 10-C-(c) which has been adjusted so that both chronologies give the same ^{10}Be deposition rate value at a depth of 1717.4 meters (13.06 kyrs BP). This causes the ^{10}Be deposition rate peak at 12.81 kyrs BP to increase in magnitude and the ^{10}Be data point at 12.94 kyrs BP to decrease in magnitude. So, ^{10}Be deposition rate is now seen to rise more than 50% between the 12.94 kyrs BP sample and the 12.85 kyrs BP sample that spans the 12,837 years BP ^{14}C spurt, thus providing stronger support for the hypothesis that this part of the ice record registers the occurrence of a super SPE. The gap in the data between 12.87 and 12.91 kyrs BP is due to missing ^{10}Be data for the ice core depth range 1709.5 - 1711 meters.

It is proposed that the 12,837 yrs BP ^{14}C spurt evident in the Cariaco Basin ocean sediment record and this ^{10}Be deposition rate peak that closely follows it were both produced by one or more large magnitude SPEs. Finkel and Nishiizumi analyzed 1.6 meter ice core sections for their ^{10}Be data, which span relatively long intervals of 30 to 40 years. So any large increase in ^{10}Be influx rate from a discrete SPE event would average out to a much lower value in the existing ^{10}Be data. To properly represent this ^{10}Be rise, a more detailed stratigraphic analysis is needed in this part of the ice core.

The detrended $\Delta^{14}\text{C}$ profile for the floating Late Glacial Pine (LGP) dendrochronology record taken from the data of Hua, et al.,⁽¹⁶⁾ is compared in figure 10-C (b) with the detrended Cariaco Basin $\Delta^{14}\text{C}$ profile. The floating LGP profile is anchored to the Cariaco Basin chronology by correlating its sharp $\Delta^{14}\text{C}$ rise with the prominent ^{10}Be deposition rate peak plotted in profile (c).^{*} Comparing the two profiles, the LGP profile shows a smaller ^{14}C excess of about 40 per mille occurring at the beginning of the YD. But interestingly, its sharp rise in $\Delta^{14}\text{C}$ coincides in time with the sharp rise in ^{14}C excess evident in the Cariaco Basin record at 12,837 cal yrs BP. At the time of this event, $\Delta^{14}\text{C}$ in the LGP record increased 17 per mille within a 20 year time span, reaching an overall increase of 26 per mille after an additional 10 years. By comparison, in the Cariaco Basin profile $\Delta^{14}\text{C}$ increased 20 per mille within an 8 year time span and reached an overall increase of 26 per mille within the space of 25 years (three sampling intervals). A second $\Delta^{14}\text{C}$ peak is seen to follow this primary peak in the LGP record. This matches approximately with the date of the second major Cariaco Basin C-14 spurt at $12,639 \pm 10$ cal yrs BP. The more minor ^{14}C spurts evident in the Cariaco Basin record at $12,973 \pm 10$ and $12,904 \pm 10$ cal yrs BP do not correlate with any

^{*} Hua, et al.⁽¹⁶⁾ have also matched the detrended $\Delta^{14}\text{C}$ LGP profile to the same peak in the ^{10}Be deposition rate data of Finkel and Nishiizumi.⁽²⁰⁾ However they date their ^{10}Be profile using the GICC05 ice core chronology with an applied -65 year correction, which instead dates the YD onset at $\sim 12,810$ corrected years b2k. Nevertheless, their chronology shows the sharp rise in the LGP $\Delta^{14}\text{C}$ record as occurring ~ 125 years after the YD onset, which is consistent with the Cariaco Basin chronology which shows the 12,887 yrs b2k ^{14}C spurt in the Cariaco Basin record as similarly occurring 120 years after the YD onset.

significant ^{14}C rise in the LGP profile suggesting that the magnitude of those earlier spurts in the Cariaco Basin profile may have been exaggerated by a sudden reduction in old carbon entering ocean surface waters at the beginning of the YD.

Radiocarbon production spurts as evidence of supersized solar proton events. A study of the Cariaco Basin ^{14}C record indicates that the rise in ^{14}C was punctuated by several ^{14}C production spurts, suggesting that at times the solar cosmic ray influx was particularly strong. The four largest ^{14}C spurts occurred near the beginning of the Younger Dryas at $13,023 \pm 10$, $12,954 \pm 10$, $12,887 \pm 10$, and $12,689 \pm 10$ years b2k, as dated in the Cariaco Basin chronology; see Figure 10-C (upper profile). Not surprisingly, they are spaced from one another by multiples of the 22-year solar cycle period. That is, they are separated from one another by 69 ± 4 , 67 ± 4 , and 198 ± 4 years, or in other words by three, three, and nine 22.2-year Hale solar cycles. They most likely register the occurrence of very large solar proton events. The earliest of these events occurred about three decades prior to the beginning of the YD cooling trend, while the two most recent ^{14}C spurts occurred about one century and three centuries respectively after the beginning of the YD cooling. The 12,887 and 12,689 years b2k events were the largest ^{14}C production spurts in the entire 4000-year Cariaco Basin ^{14}C record. However, the event that delivered the final blow in the megafaunal extinction was likely the earlier of these, the 12,887 years b2k event, indicated in Figure 10-C by the red arrow. Any Pleistocene megafaunal population that happened to survive this particular solar event could have been finished off by the subsequent 12,689 years b2k event.

The finding that these ^{14}C spurts are separated by multiples of the solar cycle period is reported here for the first time. This is quite significant, for it establishes that the spurts are real solar-related events and not measurement artifacts. We are left to conclude that they register times when the Earth experienced very intense solar storms. The actual duration of the ^{14}C increases is currently not known, only that they occurred in a time shorter than the sample time width which spanned a period of 8 to 12 years. So, there is a strong possibility that these events were produced by solar proton event impacts of very large magnitude during which the Earth was being intensely bombarded by solar cosmic rays over a period of a week or so. Furthermore the 198-year interval between the 12,887 and 12,689 yrs b2k events is of particular interest because it approximates the Suess (de Vries) solar cycle of 205 ± 5 years. Also Wagner et al. have noted that the Suess cycle is present in ^{10}Be data from the GRIP ice core (25 to 50 kyrs BP).⁽²⁴⁾

The research team that originally reported the Cariaco Basin ^{14}C data had not previously recognized the significance of the ^{14}C spurts. For example, John Southon conveyed to me (personal communication, March 2008) that such sudden rises are likely artifacts of the radiocarbon measurement process and not real events. However, the discovery that they are spaced apart by multiples of the 22.2-year solar cycle indicates that they are indeed real events. The identification of these spurts as real events and the suggestion that they mark solar proton events produced by impacts of super-sized coronal mass ejections is a novel idea that is reported here for the first time.

Assessing the radiation hazard. The Cariaco Basin record registers a 2 percent rise in atmospheric ^{14}C concentration during both the 12,887 and 12,689 years b2k events. This is 5 times the ^{14}C increase produced during the course of a typical solar cycle in modern times. By comparison, the solar proton event (SPE) that impacted during the 1956 solar maximum, which was one of the largest in modern times, produced a ^{14}C increase of only 0.016 percent

(4% of the variation produced over the course of a typical solar cycle). So, we may infer that the 12,887 and 12,689 years b2k ^{14}C spurt events were 125 times more intense than this record breaking 1956 event. Since the 1956 solar proton event was able to produce a 1% decrease in the geomagnetic field, it stands to reason that these ice age events, which were 125 times stronger, would have entirely overpowered the Earth's field, allowing the full intensity of their solar cosmic ray barrage to contact the Earth's atmosphere.

Flares of such a large magnitude are not unusual from the astronomical perspective. For example, "superflares" ranging from 10^2 to 10^7 times the energy of the February 1956 solar flare have been observed to occur on nearby sun-like stars.⁽²⁵⁾ Currently, solar cosmic rays account for less than 1 percent of the ^{14}C production.⁽²⁶⁾ But a solar proton event two orders of magnitude larger than the February 1956 SPE could have produced a sufficient amount of radiocarbon to yield a net short-term rise in atmospheric ^{14}C concentration in spite of any increased galactic cosmic ray screening that would have prevailed.

If either of these ^{14}C increases occurred over a more extended period, say due to flaring activity spanning an entire half of a solar cycle, the cosmic ray flux at any given time would have been insufficient to overpower the Earth's magnetic field and produced a conflagration on the Earth's surface. Nevertheless, the discovery of an acidity spike in the GISP2 Greenland ice core correlating with the 12,887 years b2k event supports the contention that this event was very brief, lasting just a few weeks and hence strong enough to overpower the geomagnetic field. To know for sure, a detailed study should be performed on Cariaco Basin sediments spanning these candidate events. Each of these events should have produced brief geomagnetic excursions that should be present in sediments dating from this time.

Uffen has proposed that geomagnetic reversals could occur at times when the Earth's field is at minimum strength and that at such times cosmic rays and solar wind particles trapped in the radiation belts could spill onto the Earth causing a major increase in the mutation rate.⁽²⁷⁾ I have suggested the alternate possibility that these geomagnetic minima are solar flare induced.^(28, 29) Magnetopause collapse caused by the arrival of a super-sized coronal mass ejection would result in cosmic ray exposures many orders of magnitude higher than Uffen was considering and hence could induce mass extinctions rather than just a rise in mutation rate. This would explain why Earth's history shows a strong correlation between geomagnetic reversals and the extinction of foraminifera and radiolaria (see Ch. 11) The geomagnetic excursion produced by the proposed super-sized SPE would be difficult to detect in the sedimentary record due to its brevity. Nevertheless, a study of Lake Erie sediments does show that geomagnetic inclination was unstable during this period 13,000 to 10,500 ^{14}C years BP (15,500 to 12,600 cal yrs b2k); see Ch. 7.

The $12,887 \pm 10$ cal yrs b2k ^{14}C production spurt, one of the two largest spurts to occur over the entire Alleröd-Younger Dryas period, likely registers the occurrence of the solar proton event that was the final episode of the Pleistocene mass extinction, bringing its 1400 year-long climax phase to an end. The $10,900 \pm 50$ ^{14}C years b2k date that Haynes⁽³⁰⁾ gives for the Rancholabrean termination converts to $12,933 \pm 60$ cal yrs b2k in the Cariaco Basin varve chronology. This coincides with the 12,887 cal yrs b2k date to within the stated margin of error. Also, Jull, et al.⁽³¹⁾ have radiocarbon dated the black mat stratum at the Murray Springs site and find it has a base date that ranges from 10,600 to 10,200 ^{14}C yrs BP, hence between 12,800 and 11,900 Cariaco calendar years b2k. Based on all of the above boundary dates (Rancholabrean, Clovis, and black mat), it is reasonable to place the abrupt termination of the Pleistocene megafauna as having occurred sometime within the first 200 years of the YD onset, or somewhere in the range of 12,930 to 12,800 calendar years b2k in the Cariaco

Basin chronology. Hence from a chronological standpoint, the proposed 12,887 cal yrs b2k solar proton event proves to be a good candidate as being the final cause of the megafaunal demise. Any megafauna that happened to survive this event could have been finished off by the equally lethal 12,689 yrs b2k SPE.

The cosmic ray radiation from such an event would have been fatal to large animals that were not sheltered from exposure. High latitude regions would have been particularly susceptible. The February 1956 SPE, which had a relatively hard spectrum, was observed to produce a ground level particle enhancement at Leeds, UK that was 50 times that of the cosmic ray background. Foelsche estimates as an upper limit that this SPE would have delivered a radiation dose of 0.7 rads/hr at an altitude of 14 kilometers at 60° geomagnetic latitude.⁽³²⁾ This is equivalent to about 1.2 rem/hr or 12 milli Sieverts per hour, where 1 Sievert (Sv) = 100 rems. His radiation dose vs. altitude plot projects a lower value at ground level of about 0.5 mSv/hr (or ~0.25 mSv/hr for his lower limit estimate), the dose reduction being due to the shielding effects of the atmosphere. If it had a comparable spectral hardness, the 12,887 years b2k SPE would have delivered a dose rate about 125 fold larger than this, causing animals at sea level to accumulate as much as 3 Sv over a 50 hour period. Here we assume that the period of elevated cosmic ray exposure continued for at least two days as it did during the 1859 Carrington event. If it had suppressed the geomagnetic field, the 12,887 years b2k event would likely have delivered a ground-level dose of about 10 Sv over a two day period. Short duration exposure to radiation doses exceeding 3.5 Sv are known to be lethal to humans with 100% fatalities (LD-100) occurring at around 4 to 6 Sv.⁽³³⁾ LD-100 for most large mammals spans the range from 3 to 8 Sv. If the cosmic ray intensity had reached very high intensities in certain locations, this could explain why some megafaunal remains have anomalously young radiocarbon dates uncharacteristic of the strata age they are found in (see above).

A Solar Conflagration Possibly Recorded in Polar Ice. Specific depths in the Summit, Greenland ice core that correlate with these ¹⁴C spurts (or SPEs) may be located by transferring the Cariaco Basin chronology to this ice record. This may be done by correlating specific temperature excursions evident in the Younger Dryas portion of the Cariaco Basin grey scale climatic profile with similar features seen in the GISP2 ice core oxygen isotope profile (Table 10-1).

Checking the GISP2 ice core electrical conductivity measurement (ECM) record, we do see a solitary acidity spike at a depth of 1708.65 meters which dates at 12,887±10 cal yrs b2k using the transferred Cariaco Basin chronology. This same ECM event is found at depth of 1657.51 m in the GRIP ice core and at 1522.2 m depth in the NGRIP ice core. It is the second largest magnitude acidity spike to occur in the Younger Dryas period. A spike of similar magnitude is not seen in the record for hundreds of years. The largest ECM spike of the Younger Dryas occurred around 12,150 years b2k in coincidence with Heinrich event H0, a meltwater flood event to be discussed shortly. The presence of a very large magnitude acidity spike at 12,887 cal yrs b2k indicates that very acidic snows were being deposited around the time of the 12,887 cal yrs b2k ¹⁴C spurt. The snows falling at the time of this event were so highly acidic that they were able to increase the electrical conductivity of the ice 1900 fold compared with background conductivity levels prevailing before and after the event. Highly acidic snows would be an expected outcome if, as suggested earlier, the atmosphere had been exposed to a high flux of cosmic rays during a large-magnitude solar particle event. A high resolution ECM plot of this acidity spike is shown in Figure 10-E

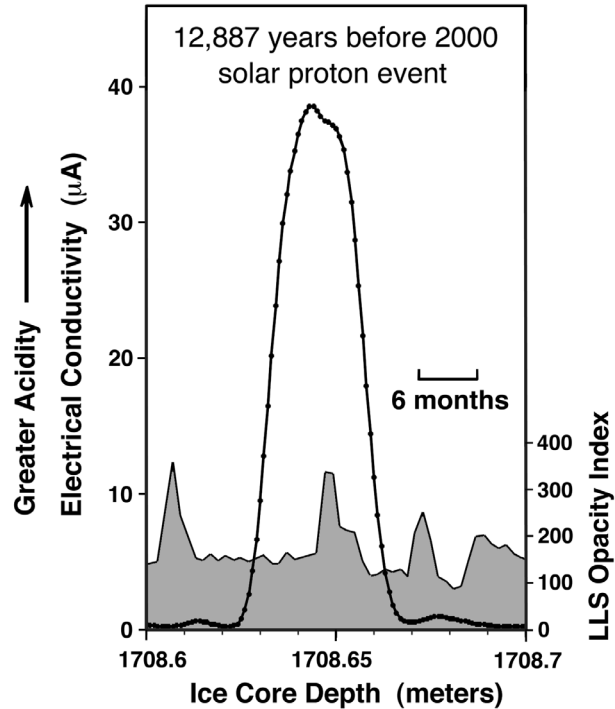


Figure 10-E. Ice core conductivity profile from the GISP2 Greenland ice core [data is from K. Taylor.⁽³⁴⁾] This period of high ice acidity is presumed here to register the occurrence of a super large sized solar proton event. The date for this event, arrived at by adjusting the GISP2 ice core chronology to the Cariaco Basin varve chronology, matches closely that of the $12,887 \pm 10$ years b2k ^{14}C production spurt which was one of the two largest such spurts to occur during the ice age termination period. Shaded profile below plots the light scattering index, an indicator of dust content [data from Ram, et al.⁽³⁵⁾].

plotted from the data of Taylor et al.⁽³⁴⁾

The laser light scattering (LLS) data for this section of the ice core shows that ice opacity, an indicator of ice dust content, underwent a 100% increase above background levels at the time of the ECM spike.⁽³⁵⁾ This relatively modest LLS peak, which spans about half a centimeter of ice, likely represents the true width of this acidity spike. The broader width of about 3 cm for the ECM peak may be attributed to the use of half-centimeter diameter electrodes for measuring ice core conductivity, which tend to blur discrete acidity spikes and make them look broader than they really are. Also some peak broadening may be due to the tendency for ions to gradually diffuse through the ice. Based on the annual layer thickness of 3.3 cm/yr estimated for this portion of the ice core on the basis of the Cariaco Basin chronology, this ECM event would span about 4 months. Such a duration is consistent with the duration of the ECM signals for historical solar proton events. For example, the ECM signal for the Carrington event is seen in one GISP2 core to have a duration of three months.⁽³⁶⁾

Nitrate ions are produced when the atmosphere is exposed to cosmic rays. Hence nitrate ion concentration spikes serve as good indicators of SPEs. McCracken et al.^(37, 38) have found that nitrate ion concentration spikes registered in the polar ice record during the period 1561 to 1950 correlate with major historical SPEs and that impulsive nitrate events serve as reliable indicators of large fluence SPEs. The 12,887 yrs b2k ECM spike is seen to be associated with high nitrate ion concentrations in the GISP2 ice record, where the nitrate values plot 10 cm sample increments; see dashed line in Figure 10-F. By one year after the event it had increased to 200 ppb, its highest level for the entire Younger Dryas period.⁽³⁹⁾ A continuous sampling for NO_3^- ion in the NGRIP Greenland ice core shows that this same

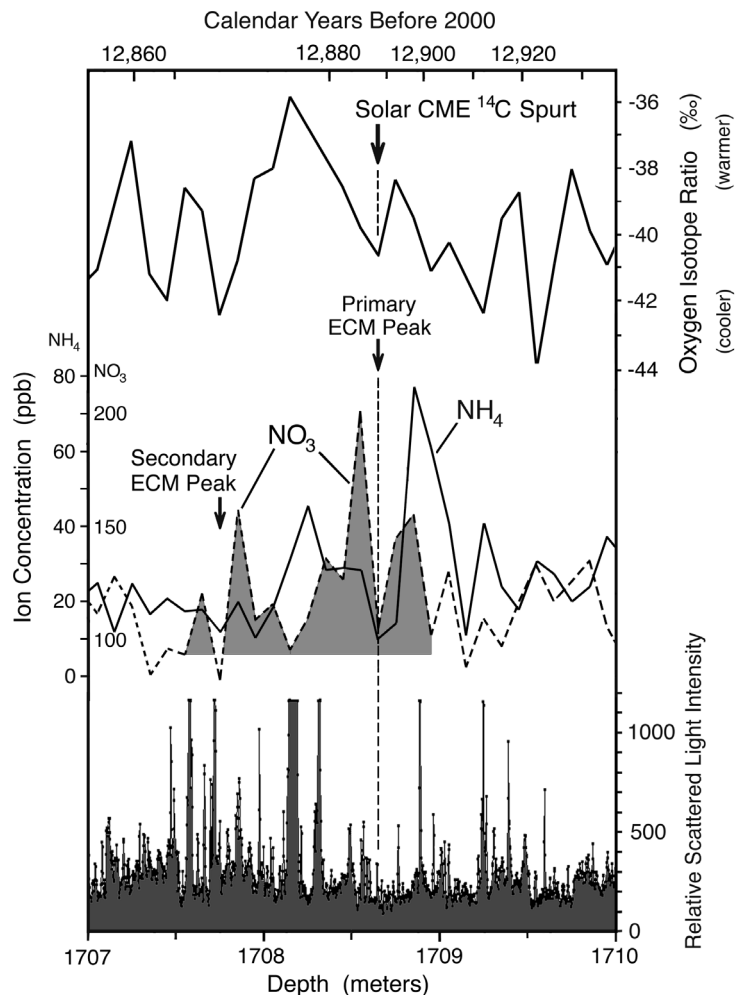


Figure 10-F. Nitrate and ammonium ion concentration in the GISP2 ice core (middle profile)^(40, 41) compared to oxygen isotope ratio (upper profile),⁽²³⁾ and relative scattered light intensity (lower shaded profile).⁽³⁵⁾ The plots are charted according to the Cariaco Basin varve chronology. Large arrows indicate the dates of the GISP2 ECM spike and the correlated 12,887±10 years b2k ¹⁴C spurt. Small arrow indicates the time of a subsequent small magnitude ECM spike.

NO_3^- peak reached as high as 400 ppb and lasted about two years.⁽⁴⁰⁾ Hence the nitrate evidence supports the suggestion that the 12,887 yrs b2k acidity peak records the occurrence of a very large magnitude cosmic ray event.

A small magnitude acidity spike measuring about 4% of the height of the 12,887 yrs b2k ECM spike is seen at a depth of 1707.75 meters, dating to around 12,869 cal yrs b2k. It too is seen to be associated with elevated nitrate ion concentrations, implicating that it also may mark the occurrence of a solar proton event. It correlates with the 6 per mil rise $\Delta^{14}\text{C}$ seen in the Cariaco Basin record to follow the 12,887 yrs b2k ¹⁴C spurt.

The high levels of nitrous and nitric ions that would have been present in the upper atmosphere at this time would have destroyed the Earth's ozone layer letting harmful UV penetrate to the Earth's surface (see Chapter 3, Section 3.3.5). The UV exposure danger would have been greatest during the occurrence of the 12,887 years b2k SPE. UV is known to photolytically dissociate nitrate ions deposited in surface snows.⁽⁴¹⁻⁴⁴⁾ Such a process would be particularly active during super proton events and could explain why nitrate ion is

depleted in coincidence with the occurrence of both ECM peaks seen in Figure 10-F.⁽⁴⁵⁾ If these register the occurrence of super SPE's, when nitrate ion production should have been at a peak, the occurrence of deep troughs at these times would suggest that both events were associated with high levels of UV due to ozone layer destruction.

The SPE that occurred on July 2000 (fluence $\sim 4 \times 10^9$ protons/cm² with energy >30 Mev) was found to eliminate 9% of the ozone in the upper stratosphere and up to 70% in the middle mesosphere over a period of several days in northern polar regions above 60° geomagnetic latitude.⁽⁴⁶⁾ The 12,887 yrs b2k super SPE, which is estimated to have had a fluence 30 times larger than this, would have been able to deplete the Earth's ozone layer to a much greater extent and over a much more extended period of time than has been observed for recent lower fluence SPEs. Given that these nitrate ion troughs each span a period of several years, we may infer that the ozone depletion persisted for a comparable period of time and created an ozone layer hole that reached even to mid latitudes.

A comet impact event of the sort suggested by Firestone, et al.^(47, 48) or a meteor swarm of 10⁴ Tunguska sized bodies of the sort suggested by Napier⁽⁴⁹⁾ may both be ruled out on the basis of the ice core data since these would have produced nitrate ion signals that were respectively 10⁵ and 10⁴ fold higher.⁽⁵⁰⁾

The 12,887 yrs b2k ECM spike also coincides with a two to three fold increase in chlorine and sulfate ion, which raises the question of whether the acidity peak may have been due to a volcanic eruption. However, no volcanic eruption is known to have occurred at this time. The Laacher eruption dated at 11,063±12 ¹⁴C years BP,⁽⁵¹⁾ or at 12,990 cal yrs b2k in the Cariaco Basin chronology, occurred one century prior to this event. Also ECM signatures of volcanic eruptions usually span a longer period of time, a few years. Considering the unique magnitude of this spike, its 10³ fold increase in acidity, and its proximity to the 12,887 years b2k ¹⁴C spurt, it seems more likely that it records the occurrence of a solar particle event. Such sulfate peaks have been observed in association with contemporary SPEs such as the one that occurred in February 1956 SPE.⁽⁵²⁾ The high concentrations of NO_x and OH radicals generated in the stratosphere by a SPE create condensation nuclei which attach to sulfate aerosols and accelerate their deposition through a scavenging process.^(53, 54)

Ammonium ion concentration, an indicator of biomass combustion, is also seen to peak around the time of the 12,887 years b2k ¹⁴C event, reaching its highest value for the Younger Dryas period; see solid line in Figure 10-F.⁽³⁹⁾ High concentrations were sustained over a period of about two decades with the exception of a decline around the time of the ECM spike. Concentrations of formate and oxylate ion, also indicators of biomass combustion, reached high levels around this time as well.⁽⁵⁵⁾ High ammonium concentrations occurred during the warm intervals that both preceded and followed the ECM spike; see Figure 10-G.⁽⁵⁶⁾ The arrows indicate periods when ammonium ion concentration reached peak values.⁽⁴⁰⁾ The discovery that biomass combustion occurred preferably during these periods of climatic warming is consistent with the findings of Marlon et al. who report that wildfires historically tend to occur at times of climatic warming possibly due to an associated increase in climatic aridity.⁽⁵⁷⁾

Since these two temperature maxima are spaced apart by about one solar cycle period, this raises the question of whether these warmings may have been due to an increase in the Sun's total energy output during this period. Current observations show that solar irradiance is 0.1% higher at solar maximum as compared with solar minimum, far too small to have any significant climatic effect. However, 10 to 20% of this irradiance variation is in the UV and UV output correlates positively with the level of solar flare activity. So if flare activity was a few orders of magnitude higher than current levels, the solar constant could have increased by as much as one percent which would have had a substantial impact on climate.

The LLS data for the GISP2 ice core registers a pair of very dark layers at about 12,881 to 12,883 years b2k (Figure 10-F).⁽³⁵⁾ These date about 4 to 6 years (35 to 50 centimeters of

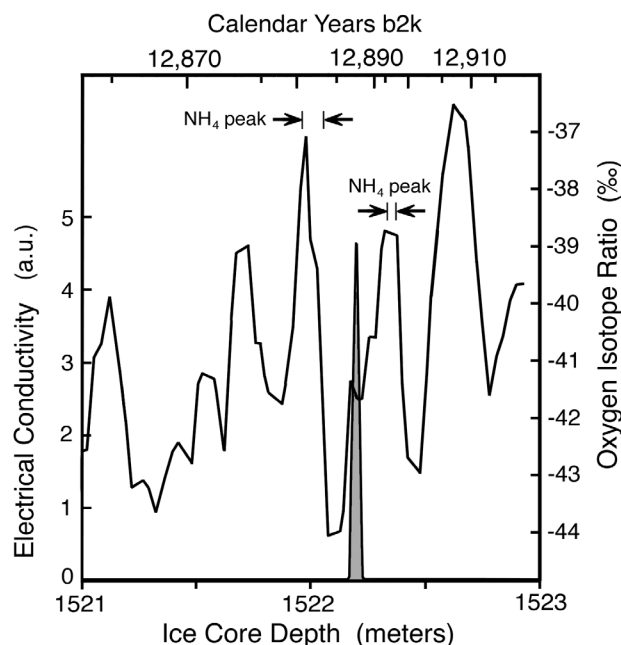


Figure 10-G. High resolution oxygen isotope profile for the NGRIP Summit Greenland ice core compared to relative ECM (shaded profile). Data is from Steffensen, et al. (2008). Dating is based on the Cariaco Basin varve chronology.

ice) after the 12,887 yrs b2k ECM spike. The bands are so dark that the LLS reading saturates at its maximum value. They are also quite thick. Two bands span 4 centimeters of ice (~0.5 years) and the band at 12,881 years b2k spans 7 centimeters of ice (~1 year). They occur at a time when ammonium ion concentration reached a peak value. They are followed by additional dark bands that together span a period of about 14 years. A narrower, one-centimeter-thick band of dark ice dating around 12,894 cal yrs b2k is seen to coincide with the ammonium peak that preceded the ECM spike. Because of their proximity to the elevated ammonium ion concentrations, it may be surmised that these bands contain high concentrations of soot generated during a period of widespread biomass combustion. Future analysis of these dark ice layers should show if this is the case.

The proximity of these dark layers to the 12,887 years b2k acidity spike and to the date of the large ^{14}C spurt seen in the Cariaco Basin record suggests that the wildfire interval associated with the YDB layer had a solar cause. If the atmosphere was so congested with particulate that sunlight was obscured at times for up to an entire year, as the LLS data appears to indicate, then even vegetation that had been spared from combustion would have withered from lack of light. Both effects together would have temporarily eradicated the food supply for herbivores. Along with the hazards of exposure to cosmic ray and UV radiation, food scarcity would have been another factor that contributed to the mammalian extinction.

I propose that the 12,887 cal yrs b2k acidity spike seen in Greenland ice marks the time of the legendary conflagration that is described in myths and legends from all over the world, a compendium of which may be found in my book *Earth Under Fire*.⁽¹⁷⁾ Evidence that a glacial meltwater flood occurred after this event is discussed toward the end of this chapter update.

The identification of this event in the ice record, reported here for the first time (June 2008), may be one of the most important discoveries in geology and paleontology considering the lethal effect it once had on the human race. It was possible to come about this discovery only by examining high-resolution ice core data charting oxygen isotope

values at 40 to 60 centimeter intervals, nitrate and ammonium ion at 10 centimeter intervals, and ECM values at millimeter intervals. This points to the importance of high resolution data in paleoclimatology studies, such solar proton events being so brief as to go unnoticed in coarser data averages.

The Usselo Horizon evidence of the 12.885 years b2k conflagration (update for [p. 141](#) and [p. 284](#)). The boundary between the Alleröd and Younger Dryas is marked by a blackened layer which appears in various parts of Europe, in the U.S. and in Canada. In Europe the layer was first discovered in the Netherlands at the township of Usselo, where it came to be called the Usselo horizon; see Figure 10-H. Figure 10-I shows this ten centimeter thick layer appearing also at a site in Ede, The Netherlands. It is also found in the UK, Belgium, France, Germany, Denmark, and Poland; see Figure 10-J, 10-K and 10-L for a few examples. Based on an analysis presented at the Schleswig Archaeology Museum, he maintains that this black layer consists of charcoal fragments, fine bleached sand particles, and soot. His opinion that black layers present in Alleröd/Younger Dryas sediments may be indicative of a global conflagration dates back to the late 1970's.⁽⁵⁸⁾ The evidence of the Usselo Horizon, as well as Kloosterman's independent conclusion that this ubiquitous black layer signifies the occurrence of a global conflagration close to the Alleröd/Younger Dryas boundary, together constitute strong evidence in favor of the coronal mass ejection scenario proposed by LaViolette in 1983 as well as a similar scenario proposed by William Topping which is discussed below. Kloosterman, though, also considered the possibility that this conflagration may have been produced by a cometary impact.⁽⁵⁹⁾

Firestone et al.^(47, 48) report the presence of soot and polycyclic aromatic hydrocarbons in an approximately 5 cm thick layer which they term the Younger Dryas Boundary (YDB) layer which they say overlies the last of the extinct Pleistocene megafauna as well as Clovis artifacts at certain southwestern U.S. Clovis sites. They state that this is found at the base of a dark stratum called the "black mat" which was previously studied by others.^(60, 61) Firestone et al. have suggested that these biomass combustion indicators indicate the occurrence of

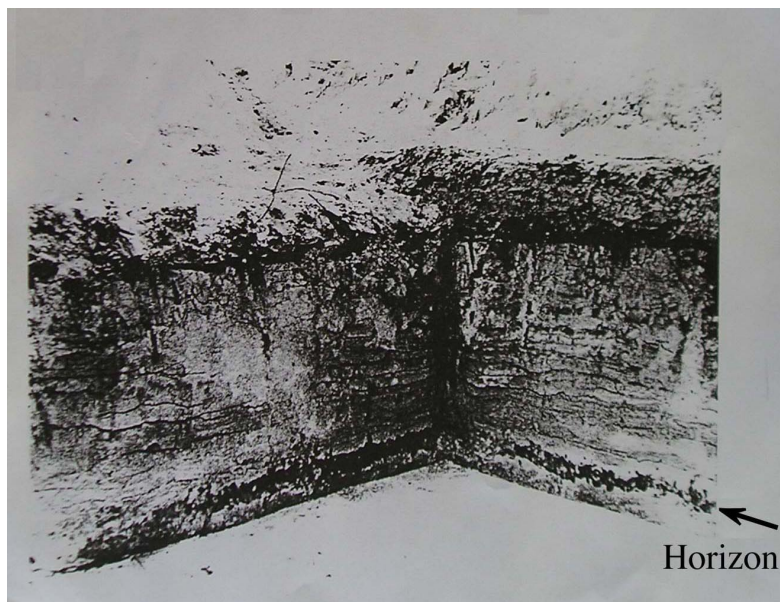


Figure 10-H. The Usselo Horizon (see arrow) is a blackened layer measuring approximately 10 cm thick. The pit is one meter deep. (1955, Twente Archief, Enschedé)



Figure 10-I. The Usselo Horizon in Ede, The Netherlands (1968).

[The above pictures were obtained from the photo-collection of Dr. J. B. (Han) Kloosterman, Amsterdam, The Netherlands, who has given permission for their publication.]

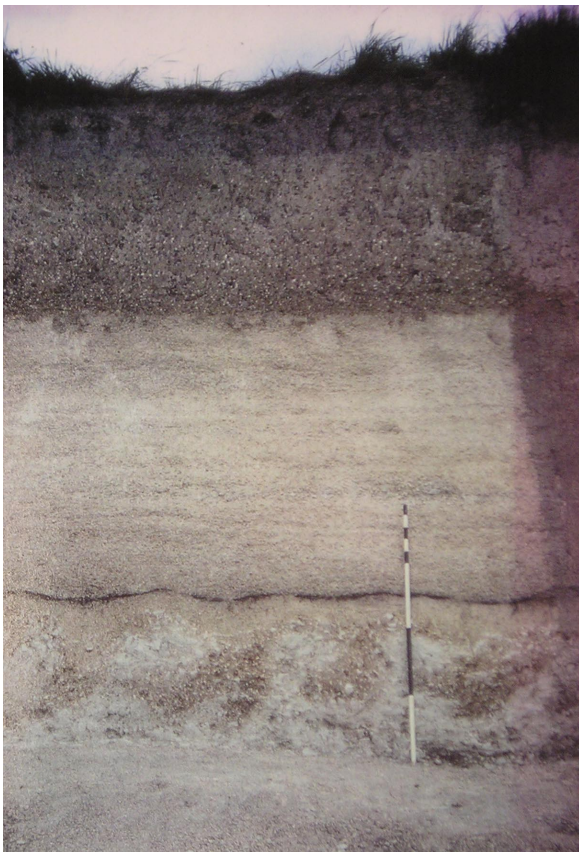


Figure 10-J. The Usselo Horizon seen in a section at Pitstone, Buckinghamshire, England. A two-meter scale is shown for comparison.
Photo by Dr. John Evans, Cardiff University, 1964.

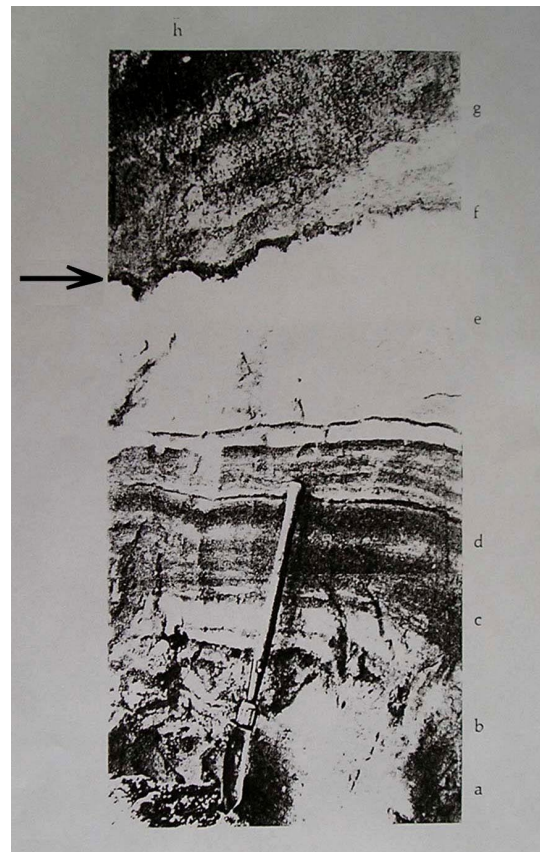


Figure 10-K. The Usselo Horizon near Hamburg, Germany. Photo by Karl Gripp.

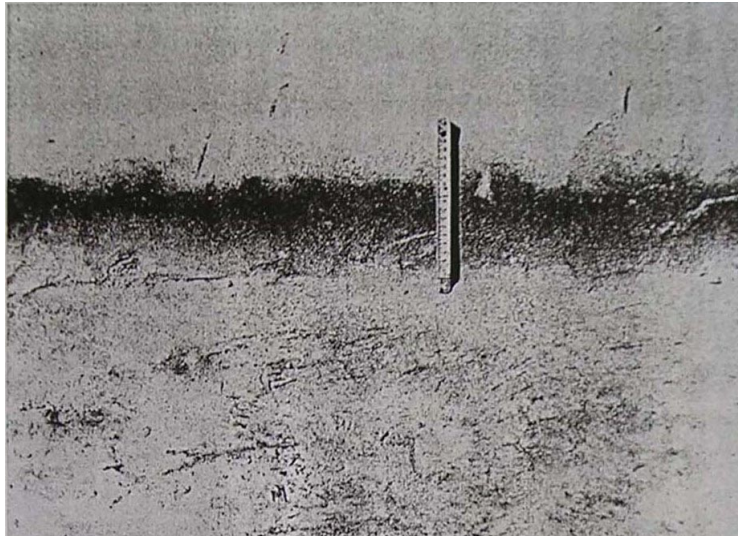


Figure 10-L. The Usselo Horizon in Poland. (Photo by Ronald Schild)

[The above pictures were obtained from the photo-collection of Dr. J. B. (Han) Kloosterman, Amsterdam, The Netherlands, who has given permission for their publication.]

widespread wildfires which they say were the cause of the rise of biomass combustion gasses (ammonium, formate, oxylate) found in Greenland ice near the beginning of the YD. These wildfire indicators do not appear higher up in the black mat layer. Haynes, however, concludes that vitreous carbon, vitrinite, and charcoal found at the base of the black mat at the Murray Springs Clovis site more likely originate from a local Clovis hearth.⁽⁶²⁾

Firestone, West, and others suggest that these wildfires were triggered by the fireball from a comet impact or explosion that occurred around 12,900 years b2k and was responsible both for forming the YDB layer and for triggering the onset of the YD climatic cooling.^(47, 48) However, Greenland ice core evidence does not support this comet-impact-climatic cooling scenario. The elevated ammonium ion concentrations marking this wildfire episode in GISP2 ice date between 12,880 and 12,900 cal yrs b2k using the Cariaco Basin chronology whereas the YD cooling began around $13,007 \pm 10$ cal yrs b2k in the Cariaco Basin grey scale record, hence about 110 to 130 years prior to the wildfire episode. A similar temporal offset is found for the date of the Rancholabrean termination ($12,933 \pm 60$ cal yrs b2k or $10,900$ ^{14}C years b2k),⁽³⁰⁾ which falls about 75 ± 60 years after the start of the YD cooling.

Hence biomass combustion, or debris injected into the atmosphere by a cometary explosion, cannot be pointed to as the cause of the YD cooling. The YD cooling was more likely induced by the elevated solar flare activity that was occurring during this time. As noted earlier, this progressive cooling paralleled the progressive build-up of atmospheric radiocarbon concentrations. This implies that the elevated solar cosmic ray flux that was showering the Earth during this time and was creating large quantities of atmospheric CN particles capable of seeding clouds that in turn had a climatic cooling effect due to their reflection of the incoming solar radiation. The climatic cooling at the beginning of the Younger Dryas should only be considered a factor that contributed to the extinction and not an effect associated with the final extermination of the megafauna.

Moreover various evidence favors a solar cause for this conflagration. First, there are the particle tracks in lunar rocks, as described in Chapter 4, which indicate that solar flare activity was very high at the end of the ice age. Second, there is the evidence that ^{14}C levels were rising during the Alleröd/Younger Dryas climatic transition which suggest that the Sun was particularly active at the time that the Usselo Horizon and YDB layer was formed. Third,

there is evidence presented here which directly links the YDB conflagration with the 12,887 years b2k solar proton event. Moreover, as discussed in chapter 12 (p. 362), the magnetic spherules and ET material indicators found in high concentrations in the YDB layer could be extraterrestrial material propelled onto the Earth by the impacting solar coronal mass ejection. In view of the close association of the YDB layer with the 12,887 years b2k ^{14}C spurt, ECM spike, and nitrate ion spike, we are led to believe that the ET indicators in this layer were implanted by a solar event and not a cometary impact/explosion.

Ice core samples from this conflagration horizon should be analyzed for their content of iridium, nickel and other ET indicators. High concentrations may be found between 1658.7 and 1657.7 meter depths in the GRIP ice core, between 1708 and 1710 meter depths in the GISP2 ice core, and between 1524 and 1522 meter depths in the North GRIP ice core.

Corroboration from the Paleo-Indian Artifact Findings of William Topping (update for p. 141 and p. 284): After seven years of research, archeologist William Topping came to the same conclusion that I had reached that a solar coronal mass ejection conflagration could explain the abnormally young radiocarbon dates found at ice age Paleo-Indian sites (actual dates circa 12,450 - 13,050 calendar yrs b2k).⁽⁶³⁾ He noted that charcoal from the Gainey Paleo-Indian site in the central part of lower Michigan, yielded a radiocarbon date of just 2930 ± 175 years b2k while a thermoluminescence date from this site gave a date of $12,410 \pm 1240$ years b2k. Other Paleo-Indian sites in the Great Lakes region similarly are found to yield abnormally young dates: 2936 ± 115 years b2k at the Leavitt site, 3430 years b25 at Zander in Ontario, 2170 years b2k at Thedford in Ontario, 3860 years b2k at Potts in New York, and 1910 years b2k at Alton in Indiana. At the Whipple site in New Hampshire, charcoal samples from a single feature yielded different radiocarbon dates that ranged from $11,480 \pm 395$ to 8290 ± 380 years b2k with samples from the lowest part of the feature yielding older radiocarbon dates. This suggests that whatever caused these date abnormalities had its strongest influence at the soil surface, as would solar cosmic ray radiation.

Topping proposed that these young dates could be explained if a major solar flare cosmic ray particle storm had caused in situ carbon-14 production from nitrogen in the organic remains of those strata. Topping notes that there would have been sufficient nitrogen in wood to yield the observed radiocarbon levels. For example, a piece of charcoal from the Meadowood artifacts site was found to contain 0.5 per mil nitrogen, or about one billion nitrogen atoms for every ^{14}C atom.

This ^{14}C production mechanism is similar to the in situ mechanism I had proposed 15 years earlier to explain the young dates for Pleistocene mammal remains dating from the same period. However, Topping's theory differs from my own in that he proposed that the ^{14}C was generated by primary thermal neutrons passing through the atmosphere.⁽⁶⁴⁾ I had instead proposed that the ^{14}C was produced by secondary neutrons generated in situ within the animal or plant tissue by an incident cosmic ray flux consisting chiefly of protons which is far less problematic. For example, in their critique of Firestone and Topping's article, Southon and Taylor note that if the atmosphere had been exposed to such a high neutron flux, it should have produced radiocarbon levels many orders of magnitude higher than are observed today.⁽⁶⁵⁾ The in situ ^{14}C production mechanism proposed in this chapter, however, avoids that problem since the neutrons are produced mainly in the animal remains or vegetation rather than in the atmosphere.

Topping's conclusion that the Paleo-Indian artifacts were exposed to heavy particle bombardment came in part from the finding that these artifacts were abnormally radioactive. For example, he reports that the Taylor Paleo-Indian flakes were found to be 41 percent more radioactive than controls. Sediments from the Paleo-Indian horizon at Gainey were also found to be "more active" than controls. Also he found that the artifacts were scored by



Figure 10-M. Particle pits found on the surface of a Chuska flake from the Folsom Paleo-Indian site in New Mexico.

particle tracks and micrometeorite craters. Figure 10-M shows impact pits marking the surface of a Chuska flake from the Folsom Paleo-Indian site in New Mexico (image size is not given).⁽⁶⁶⁾ Topping estimates that the pits have a density of approximately 10 to 20 thousand per cm² and were formed by hyper velocity particles having a diameter of about 10 microns. The pits appear only on one side of the artifact, presumably the side that was exposed to the sky at the time of the event.

Topping has concluded that the spalling evident on the Gainey artifacts is due to micrometeorite bombardment.⁽⁶⁷⁾ The thicker artifacts have spalling primarily on one side that is visible to the naked eye. The thin artifacts have a small spall (U-shaped pit) on one side and on the other side in opposition is a larger spall (V shaped pit), exactly like the fracture pattern in a piece of glass struck by a BB pellet. He says the spalls do not resemble those produced by heat-treatment..

Topping lists the following evidence for artifact pitting by a high-energy particle event at the time of this radiocarbon-date/radioactivity anomaly:⁽⁶⁸⁾

1. The presence of particle tracks, and particles, in Paleo-Indian artifacts, the tracks appearing preferentially on one side of artifacts;
2. The lack of such particle tracks, and particles, in artifacts from later cultures within the same geographic area;
3. Experiments which suggest the particles only could have entered the chert artifacts at a speed of about 335 meters/second which effectively "rules out" terrestrial events;
4. A density of particle tracks at the sites in Michigan, being about 70,000 per square centimeter, which "rules out" any sort of sediment process;
5. A "pattern" to the density of particle tracks and particles in which the artifacts from Michigan manifest the highest density but those artifacts from different latitudes and longitudes manifest a lower density;
6. Another "pattern" to the track configurations in which the entrance trajectories in artifacts from Michigan, Illinois, Indiana and New Mexico are essentially perpendicular to the flat surfaces of artifacts whereas the entrance trajectories on artifacts in Ontario and Pennsylvania are angled with the Ontario tracks being less angled than those from Pennsylvania;
7. The presence of spherules/chondrules on some of the particles embedded in artifacts;
8. A "spike" of magnetite/ilmenite particles in the sediments directly "on" (at depth) the Paleo-Indian horizon at the Gainey site in Michigan;
9. The presence of spherules/chondrules "on and in" some of the magnetite/ilmenite particles from the Paleo-Indian horizon at Gainey;
10. A "spike" of "spherules" directly "on" the Paleo-Indian horizon at the Gainey site;
11. Reddened artifacts, which could be from irradiation, at the Gainey site;
12. Larger "impact pits" in artifacts at the Gainey site;
15. The XRF analysis of the Gainey Paleo-Indian horizon sediments (silty, possibly from wind deposit) which shows elevated chromium and nickel which both could be construed as evidence of extraterrestrial matter "somehow" having been deposited.

As discussed in the update to Chapter 12, such micrometeorite bombardment could have

been due to the hypervelocity entry of debris from the circumterrestrial dust sheath, making it unnecessary to propose a comet explosion scenario.

Climatic Considerations. Another interesting finding reported here for the first time is that brief, but very large magnitude interstadial warmings occurred at the times of the larger of the Younger Dryas ^{14}C spurts. The proximity of these interstadial warmings to the ^{14}C spurts is best checked in the varve dated Cariaco Basin record in which climatic variation has been charted on semi-annual time intervals and where anomalous ^{14}C production has been determined in decadal intervals.⁽⁶⁾ Figure 10-N shows that the three largest solar proton events of the early Younger Dryas occurred close to brief climatic warmings. The two largest ^{14}C production events, a) and b), occurred just prior to or synchronous with a climatic warming trend which is consistent with the suggestion that the associated climatic warming was solar induced. This heat input could have come both from the solar cosmic rays that were showering through the Earth's atmosphere onto the Earth's surface as well as from the high output of soft X-ray and UV radiation that would have been coming from the Sun at that time. The 12,954 years b2k solar event, which produced a much smaller radiocarbon spurt, is seen in Figure 10-N (c) to coincide with the cooling trend that followed a climatic warming episode. The reason why this smaller solar event has this offset is not known.

At least 36 climatic warming episodes may be discerned over the course of the Younger

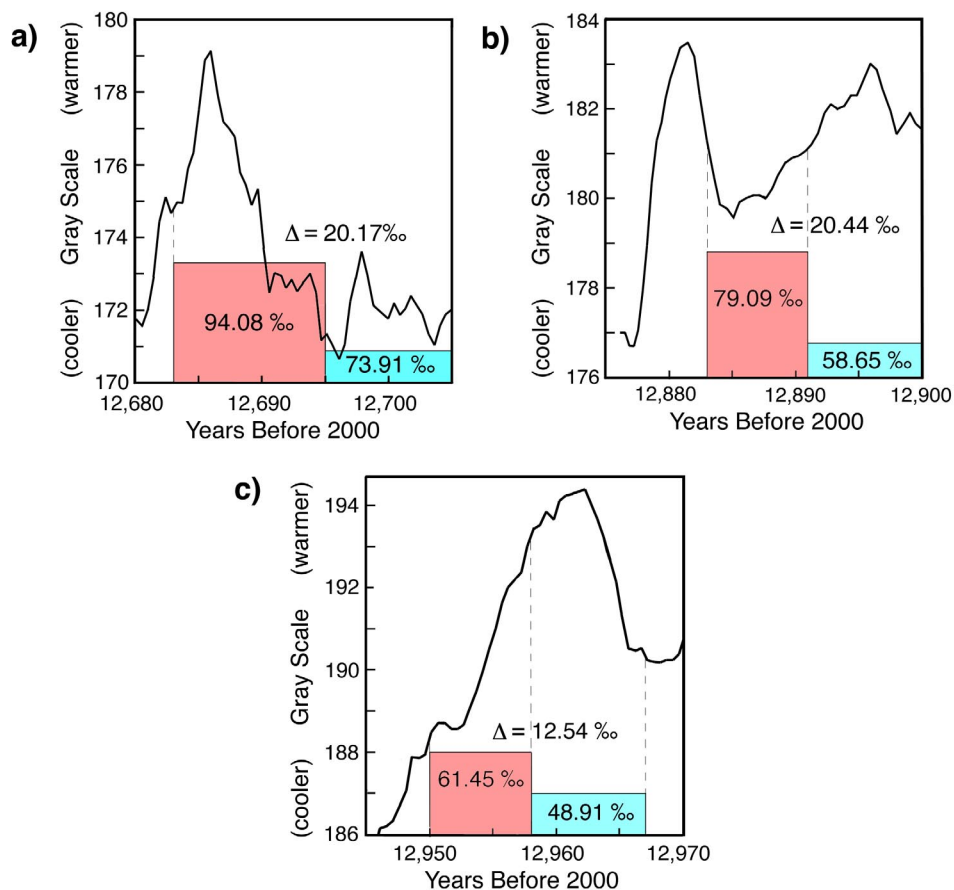


Figure 10-N. Comparison of climatic change (black solid line) to large incremental increases in atmospheric ^{14}C concentration (transition from blue to red) shown for three ^{14}C spurts: a) 12,689 years b2k, b) 12,887 years b2k, and c) 12,954 years b2k.

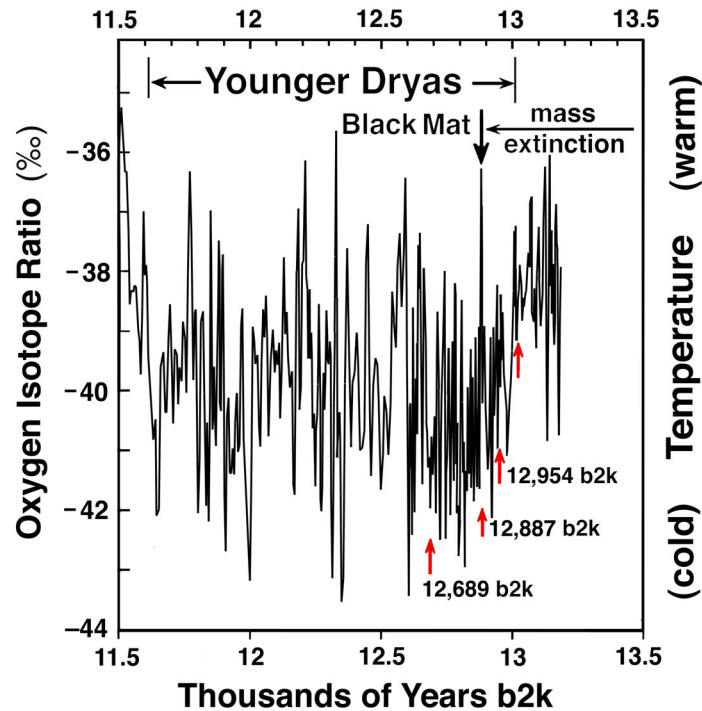


Figure 10-O. Oxygen isotope profile for the GISP2 Summit, Greenland ice core spanning the Younger Dryas (data courtesy of Johnsen et al. (1997)). The profile's chronology has been adjusted to correspond to the Cariaco Basin varved record. The red arrows indicate times of solar proton events as indicated by spurts in ^{14}C generation.

Dryas, as seen in the oxygen isotope record for the GRIP Summit, Greenland ice core; see Figure 10-O.⁽⁶⁹⁾ The shifts are so numerous as to make it difficult to attribute them to dramatic shifts of the North Atlantic polar front. It is possible that they are all solar induced arising at times of peak solar flare activity which would correlate with periods of elevated solar luminosity. The arrows indicate dates of the large ^{14}C spurts registered in the Cariaco Basin profile during the early Younger Dryas. Shortly after the 12,887 and 12,689 years b2k events temperatures warmed to interglacial values, as indicated by a 4 to 5 per mil change in the oxygen isotope ratio. Only three other of the 36 interstadial warming events (Dansgaard-Oeschger events) registered in the GRIP record for the Younger Dryas were of comparable magnitude. The interstad following the 12,887 years b2k event was unique in that of these major warmings it was the most rapid. Climate switched from glacial to full interstadial temperatures within just 3 years. Climate remained warm for about 15 years after which it returned to extremely cold glacial temperatures. Both instances, the associated climatic warming immediately followed the ^{14}C rise. A climatic warming episode also followed the more minor solar proton event that occurred at 13,023 years b2k. However, in the case of the minor 12,954 years b2k solar event the climatic warming is seen to have preceded the solar event. So the evidence suggests that the solar flare cosmic ray episodes producing the most prominent ^{14}C production spurts had a strong warming effect on the Earth's climate. In making the above comparison, the GRIP ice core isotope profile chronology was adjusted to correspond to the varve-dated Cariaco Basin chronology by correlating GRIP temperature minima and maxima with those evident in the Cariaco Basin grey scale profile (Table 10-1).

Corroboration of the Glacier Wave Theory by the Discovery of Heinrich Events (update for p.277): In 1988, five years after this dissertation was published, Hartmut Heinrich

reported discovering that North Atlantic sediments contain layers composed primarily of rock grains of continental origin and having unusually low concentrations of foraminifera plankton.⁽⁷⁰⁾ These so called "Heinrich layers," or "Heinrich events," provide confirming evidence for the existence of glacier waves described earlier in this chapter. The presence of these layers suggests that immense avalanches of glacial meltwater had discharged from the ice sheet surface during periods of climatic warming. Studies of these layers indicate that continental bedrock debris was somehow transported for distances of up to 3000 kilometers and deposited at these ocean locations. These layers appear in ice age sediments and recur at intervals of 5000 to 10,000 years. In particular, they appear at the beginnings and endings of ice ages and also precede the onset of Dansgaard-Oeschger events (interstadials) occurring within glaciated periods; see Figures 10-P, 10-Q, and 10-R.^(71, 72)

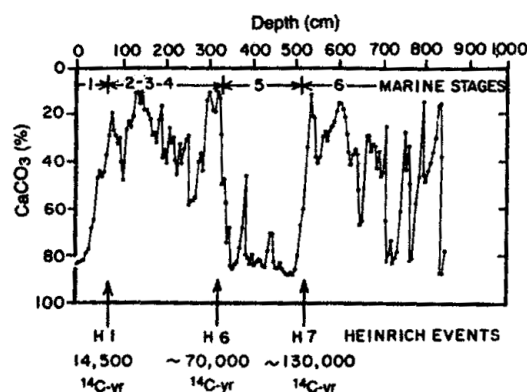


Figure 10-P. Climatic profile from the North Atlantic core V28-82 using percent foraminifera CaCO_3 as the climatic indicator. The arrows indicate Heinrich Events that coincide with the beginning and end of the last glaciation and with the end of the penultimate glaciation. Heinrich events H6 and H7 should actually be assigned higher numbers since the event labeled here as H6 corresponds to event H8 in Figure 10-Q.

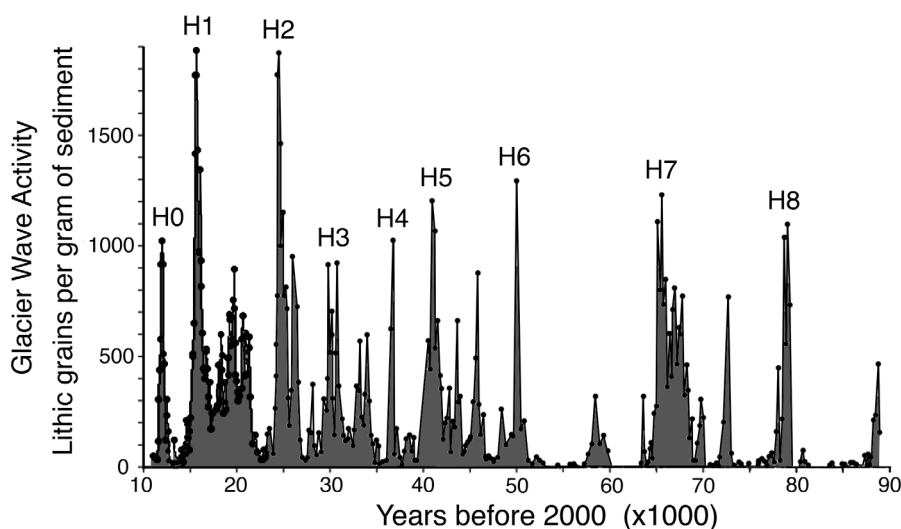


Figure 10-Q. Heinrich events over the last 90,000 years, as seen in North Atlantic sediment core V23-81. (Data courtesy of G. Bond)

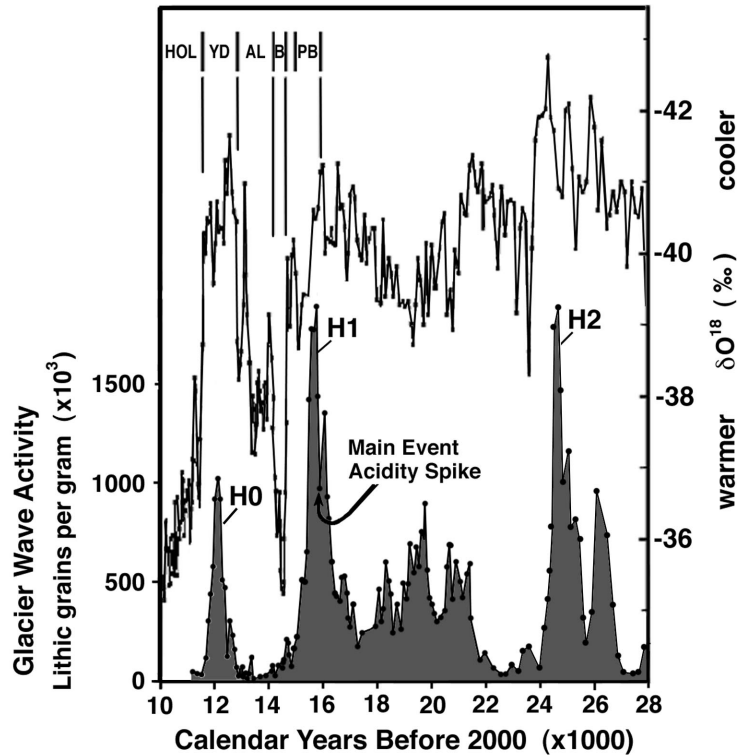


Figure 10-R. Dating of Heinrich layers compared with major climatic transitions. Upper profile: oxygen isotope climatic profile from the GISP2 Summit, Greenland ice core (lower values indicate warmer climate). Lower profile: Lithic grain abundance in sediments from North Atlantic core V23-81 (54.5°N, 17.5°W); data courtesy of G. Bond. A timescale for this core was developed as described in the text box below. Peaks designated as H0, H1, and H2 indicate Heinrich layers. Abbreviations designate the following climatic boundaries at the end of the ice age: Pre-Bölling Interstadial (PB), Bölling (B), Alleröd (AL), Younger Dryas (YD), and Holocene (Hol).

Timescale Adopted for Core V23-81

A timescale for dating the Heinrich events is developed as follows. Figure 10-S shows the foraminifera climate profile for core V23-81 published by Broecker et al.⁽⁷³⁾ The positions of Heinrich events H1 and H0 in this core (data from G. Bond) have been superimposed for comparison. A time depth chronology is developed for the core by correlating the climatic boundaries of this profile with corresponding climatic boundaries dated using the GICC05 ice core chronology adjusted to the Cariaco chronology (Appdx E); see table 10-2 below. Dates for intervening depths have been interpolated. For depths greater than 2.1 meters dating is based on radiocarbon dates for core V23-81 published by Vogelsang and Sarnthein.⁽⁷⁴⁾ which have been converted to calendar dates by using the radiocarbon conversions from INTCAL 09. The adopted time-depth model, displayed in Figure 10-T, gives a date of around 15.8 kyrs b2k for the peak of event H1. Other researchers have dated the H1 event as peaking 16.8 to 17 kyrs BP, hence over one thousand years earlier.^(71, 75) The radiocarbon dates of Vogelsang and Sarnthein in the depth range 2.1 - 2.4 m are here judged to be approximately 1200 years too old due to the influx of old carbon during the H1 meltwater discharge event. Similarly radiocarbon dates in the depth range of 3.7 - 4.0 m are judged to be 1000 - 2000 years too old due to old carbon influx associated with the H3 meltwater discharge event.

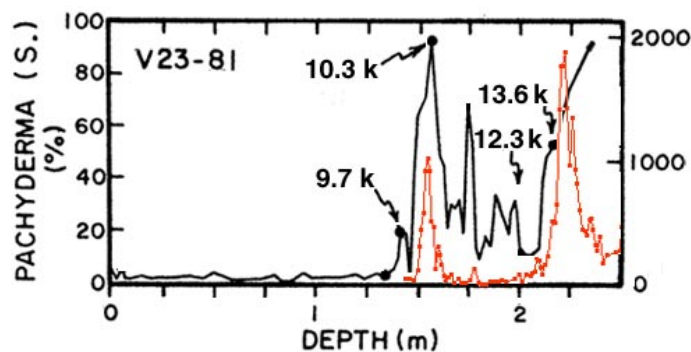


Figure 10-S. The positions of Heinrich events H0 and H1 compared to climatic boundaries. Black curve: foraminifera ratio climate profile for core V23-81 (from Broecker et al., 1988). Radiocarbon dates are indicated by arrows. Red curve lithic abundance data provided courtesy of G. Bond.

Table 10-2
Dating Core V23-81 (150 - 210 cm) using Climatic Boundaries

| Depth (cm) | Years b2k | Climatic zone |
|------------|-----------|-----------------------------|
| 148 | 11,600 | Holocene begins |
| 164 | 13,000 | Younger Dryas begins |
| 175 | 13,300 | Intra-Alleröd cold peak max |
| 200 | 14,180 | Older Dryas begins |
| 210 | 14,750 | Bölling begins |

Heinrich layer H1 is of particular interest since it peaks near the beginning of the Pre-Bölling interstadial (15.8 kyrs b2k), the warming trend that began the deglaciation which ended the ice age. This warming was global in extent since in Chile, mountain glaciers were rapidly retreating at this time.⁽⁷⁶⁾ Also the Alerce, Chile climatic profile and Byrd Station, Antarctica ice core show that a major deglacial warming trend began at this time; see Chapter 9, **Figures 9-A (d)** and **9-D**. The upsurge in H1 lithic grain deposition correlates with the time of the Main Event acidity peak found in Antarctic ice. Consequently, the warming that produced this Heinrich event and associated glacier wave activity occurred during a period of enhanced interstellar dust inflow described in the update to Chapter 8; see **Figure 8-H and I**. This suggests that enhanced solar activity and solar energy input to the Earth associated with cosmic dust invasions may ultimately be responsible for the production of Heinrich events.

A smaller continental debris event labeled as Heinrich Event H0 is seen to have culminated around 12.1 kyrs b2k. It correlates with a Younger Dryas interstadial warming evident in the Byrd Station, Antarctica and Summit, Greenland ice core climate profiles; see Figures 8-C and 10-R. A moderate rise in lithic grain deposition occurs at the beginning of this event around 12.6 kyrs b2k, or about 300 years after the terminal boundary for the Pleistocene megafaunal extinction. Consequently, event H0 was likely responsible for the formation of the permafrost glacier wave deposits found in Alaska and Siberia. This 12.6 kyrs b2k event coincides with a major D/O warming seen in the Greenland ice core record; see Figure 10-O. It may correspond to the occurrence of a super SPE whose ¹⁴C rise is masked in the Cariaco Basin record by the influx of old carbon due to enhanced meltwater discharge into the Gulf of Mexico. A radiocarbon increase around this date, however, is seen in the Floating Late Glacial Pine dendrochronology record; see Figure 10-C.

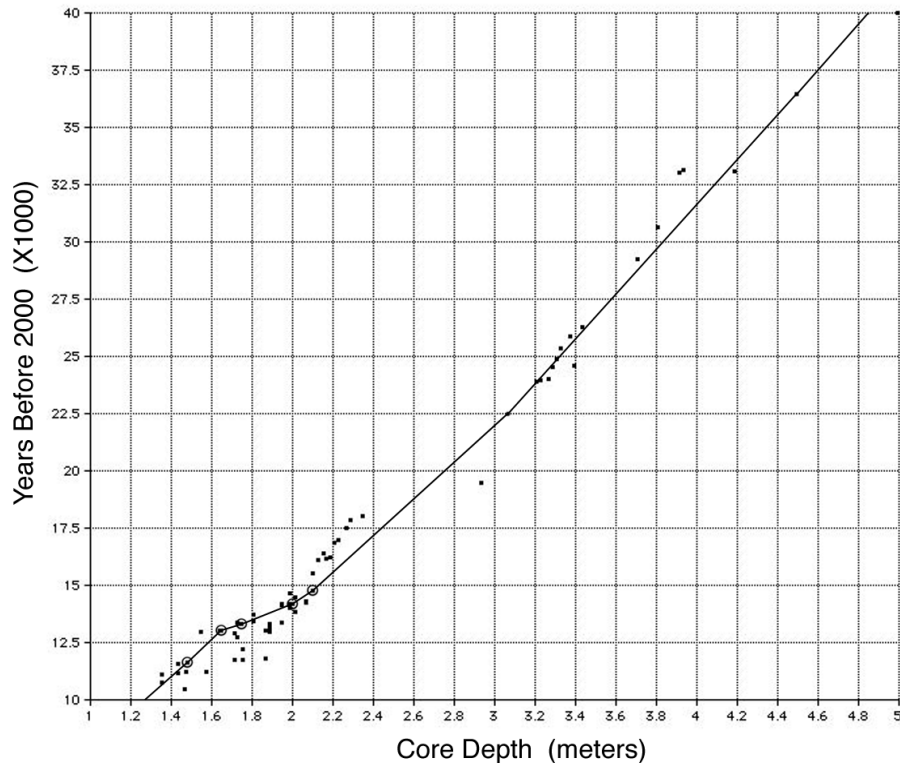


Figure 10-T. Time depth relationship adopted for core V23-81. Data points indicate radiocarbon dates of Vogelsand and Sarnthein converted to calendar dates. Conversion used the Cariaco Basin chronology for dates 10 - 12.55 k ^{14}C years BP and the INTCAL 09 chronology for dates 12.55 - 37 k ^{14}C years BP. For depths greater than 4.495 meters a sedimentation rate of 101 yrs/cm was assumed. Circled points indicate dates adopted through climatic boundary correlations.

Ocean core studies show that foraminifera population dropped markedly during the period when Heinrich layers were being formed, with arctic species being the only ones present.⁽⁷⁷⁾ Also isotopic studies show conspicuous decreases in planktonic $\delta^{18}\text{O}$ ratio, indicating colder water temperatures and lower surface salinity. Strata consisting primarily of lithic grains and nearly devoid of foraminifera are found within Heinrich layers. The almost total absence of foraminifera in these strata indicates that they were deposited very rapidly. It is also generally agreed that this material was being transported by outflow from the continental ice sheet, since Heinrich layers are found to be most prominent at the mouths of the Gulf of St. Lawrence, the Hudson Bay, and the Denmark Strait and also at other locations around the world where meltwater was discharging.

Core V23-81, whose Heinrich layer record is displayed in [Figures 10-Q](#) and [10-R](#) was taken from a location that would have been about 700 kilometers west of the edge of the European ice sheet and about 1500 kilometers south of the edge of the Greenland ice sheet. Core DSDP 609, which also registers Heinrich layers, was taken from an even more remote location that formerly was situated about 1500 kilometers west of the edge of the European ice sheet and about 2000 kilometers south of the Greenland ice sheet. So apparently, glacier waves are able to transport continental soil debris substantial distances into the ocean.

Heinrich proposed that the bedrock material making up Heinrich layers was transported by armadas of icebergs launched from the ice sheet. He suggested that, during their journey out to sea, the icebergs gradually melted and progressively released their trapped sediment.

However, these layers begin with a sharp boundary suggesting that they were deposited far more suddenly and catastrophically than can be explained by rapid increases in iceberg population. X-ray studies carried out by Manighetti, et al. show that this bottom-most layer was deposited so abruptly that it compressed the ocean bottom fluff layer, the thready surface zone produced by burrowing animals.⁽⁷⁸⁾ Normally, this surface fluff layer migrates upward as sediment gradually accumulates. But in this case deposition was so sudden that the layer had no time to migrate. Instead, it became pancaked and preserved beneath the Heinrich layer as would have occurred if large amounts of sediment were dumped in a matter of hours. Glacier waves, advancing at speeds of a few hundred miles per hour and passing in a matter of minutes would have produced such rapid deposition.

There is also evidence of stratification within the Heinrich layers, suggesting that this material was not deposited by a single event, but by clusters of events spanning hundreds of years. To explain these sharp boundaries and successive stratified layers a sudden depositional mechanism is needed, one capable of recurring at spaced intervals. Recurring glacier waves fit this requirement.

During this period of accelerated glacial melting, the ocean surface bordering the ice sheet would have been covered with a layer of meltwater, ice chunks, and icebergs of various sizes. This layer of meltwater and ice would have cooled the ocean surface waters and prevented their immediate warming by reflecting incident sunlight. Consequently, only arctic foraminifera species would have been able to survive during this period, as is observed. Many researchers, however, have mistakenly interpreted the presence of cold water foraminifera species as indicating a time when atmospheric climate had turned cold. However when properly dated, Heinrich layers are found instead to correlate with periods of transition from cold to warm climate, as seen in Figure 10-R. Such warmings would have promoted the generation of glacier waves.

Thinking that Heinrich events instead took place during periods of colder climate, researchers have been led to assume that climatic cooling caused the ice sheets to advance and that this increased the rate of ice calving and hence the rate of iceberg rafting of continental soil thereby producing Heinrich layers. But it is not clear how ice sheet advances or cooler climate would result in a dramatic increase in ice calving. One theory suggests a mechanical effect in which the ice sheet over the Hudson Bay, having reached a critical thickness and weight, sloughed down the Hudson Strait into the ocean. Similar ice surges in other parts of the ice sheet would be needed to explain the sediment transported from other straits. However, ocean core data indicates that Heinrich layers were produced by sediment transported in a synchronized fashion via geographically separated outflow channels. The ice sheet advance theory has difficulty explaining such synchronization since advancing ice sheets would not be expected to necessarily calve ice at the same time.

The geologic record, however, overwhelmingly supports the notion that Heinrich events occur when there is a rapid climatic warming, hence supporting the idea that they denote glacier wave flooding events. This is seen in Figure 10-R which correlates the timing of Heinrich events registered in core V23-61 with warmings registered in the GISP2 Greenland ice core oxygen isotope profile. It is even more dramatically illustrated in Figure 10-U which correlates the timing of Heinrich events in this same core with shifts in the GISP2 ice core $^{15}\text{N}/^{14}\text{N}$ isotope ratio, where higher $^{15}\text{N}/^{14}\text{N}$ values indicate warmer temperatures.⁽⁷⁹⁾ The correspondence appears quite close. The slight deviation for Heinrich event H1 may be attributed to dating inaccuracies for the V23-81 sediment core. In particular, considering that core sedimentation rate increases during Heinrich events due to the deposition of wave transported debris, peak H1 would span a shorter period of time than is indicated here and its onset would likely move to the left with an onset of ~16 kyrs b2k to bring it into coincidence

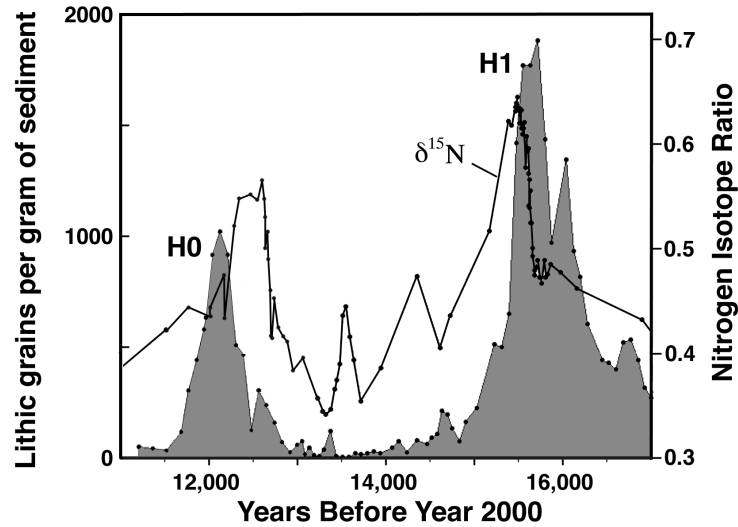


Figure 10-U. Isotopic nitrogen ratio in the GISP2 Greenland ice core (solid line) is compared to the timing of Heinrich Events in core V23-81 (shaded curve). Greater ^{15}N ratio indicates warmer climate.

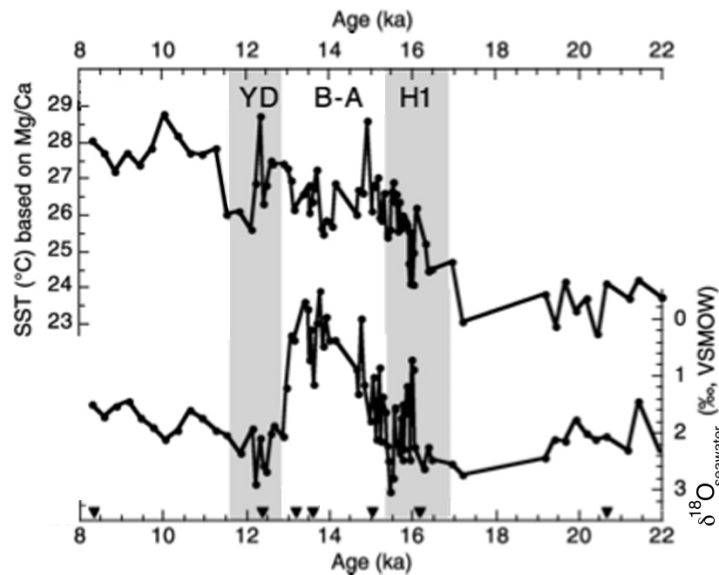


Figure 10-V. Upper profile: Orca Basin sea-surface temperatures based on Mg/Ca ratios from *G. ruber* in core EN32-PC6. Lower profile: Calculated $\delta^{18}\text{O}$ seawater values based on paired $\delta^{18}\text{O}$ values and Mg/Ca ratios. Data from paper by Flower et al.⁽⁸⁰⁾

with the warm interval indicated in the Greenland ice core isotope ratio record.

An early date for Heinrich event H1 is also indicated in sea salinity data from the Gulf of Mexico. Flower et al.⁽⁸⁰⁾ have measured Mg/Ca ratios and $\delta^{18}\text{O}$ ratios in foraminifera in Orca Basin core EN32-PC6 and find that seawater salinity declined during the interval 16.1 to 15.5 kyrs b2k, preceding the more prominent salinity decline dating between 15.2 - 13.0 kyrs b2k. They interpret both as an indication of an increased influx of glacial meltwater into the Gulf during this period. They note that the earlier meltwater influx event occurred during Heinrich Event H1 where they have marked the time position of H1 with a shaded band which is consistent with conventional dating for this event. However, in view of the

more recent onset of H1 indicated by the revised chronology used here for core V23-81 and based on the time correspondence of this event to the warming evident in the Greenland nitrogen isotope profile, it seems reasonable to conclude that the 16.1-15.5 kyrs b2k meltwater influx event in core EN32-PC6 marks the real temporal extent of Heinrich Event H1. The finding that H1 was associated with glacial melting and meltwater influx into the Gulf, in turn, supports the contention made earlier that Heinrich events are essentially powerful meltwater avalanches that discharge from the ice sheet during the onset of climatic warmings. A matching episode of meltwater discharge into the Gulf of Mexico is also evident in the salinity curve for core EN32-PC4 shown in Figure 9-E (p. 263).

The meltwater spike evident in the Younger Dryas portion of the Mg/Ca profile dates at around 12.6 kyrs b2k in the Cariaco Basin chronology (converting the 10.51 ± 0.16 kyrs BP ^{14}C control date using the Cariaco Basin radiocarbon conversion scale). This may correlate with the spike evident in the early part of Heinrich Event H0 discussed earlier and also likely correlates with the early meltwater influx spike evident in core EN32-PC4 marked by an arrow in Figure 9-E. Again, as mentioned earlier, this warming was likely associated with the super SPE event dating around that time.

Over eight major Heinrich events have occurred over the course of the past 80,000 years and the number reaches almost 20 when more moderate events are included; see Figure 10-Q. Comparing this record with the Cariaco Basin radiocarbon record shown in Figure 7-A (p. 215), it is seen that times of major Heinrich events correlate with downturns in the radiocarbon excess evident in Cariaco Basin sediments. For example, ^{14}C declines dating around 37,500, 32,000, and 15,000 years b2k correlate with the dates of Heinrich events H4, H3, and H1. These ^{14}C declines are easily explained if attributed to large amounts of radiocarbon-depleted glacial meltwater entering the oceans and thereby lowering the ocean's ^{14}C concentration. Thus these ^{14}C declines are further proof that Heinrich events arise from glacial melting and meltwater discharge rather than from glacial growth.

As seen in Figure 7-A, the period from 16,500 to 14,500 years b2k experienced a 190 ± 10 per mil decline in the ^{14}C excess, equivalent to a 13.6% drop in the $^{14}\text{C}/\text{C}$ ratio. Broecker and Barker suggest that this could be explained if radiocarbon-depleted meltwater had entered the ocean and mixed with surface waters, but they could not locate a reasonable source.⁽⁸¹⁾ They consider the possibility that the water may have come from an isolated high-salinity ocean bottom reservoir that subsequently mixed with surface waters, but conclude that the size of the abyssal reservoir is insufficient to explain the decline. They acknowledge that alpine glaciers were rapidly retreating during this time, suggestive of a major climatic warming, but did not consider the possibility that the ^{14}C decline was due to radiocarbon-depleted meltwater from these receding glaciers entering the oceans.

Broecker and Barker note that climatologists call this period the "Mystery Interval" since during this climatic warming unusually cold temperatures prevailed in the North Atlantic and western Mediterranean. But there is no mystery if one acknowledges that glacial meltwater entering the oceans at near 0° centigrade would have kept sea surface temperatures low even during a climatic warming period. They mention that this ^{14}C decline falls close to the time of Heinrich event H1, but make no connection between the two events. One reason is that they incorrectly date H1 as occurring about 17,500 years b2k, which would give it an end date prior to the beginning of the Mystery Interval. However, when core V28-32 is properly dated as per the method explained in the above text box, Heinrich event H1 is found to peak at 15.8 kyrs b2k spanning the bulk of the Mystery Interval ^{14}C decline. The sharp decline in ^{14}C evident in Figure 10-C around 12,750 to 12,700 calendar years b2k near the beginning of the Younger Dryas correlates with a brief interstadial evident in the GRIP ice core climatic profile around that time; see upper profile in Figure 10-K. So available data appears to

support the conclusion that ^{14}C declines in the Cariaco Basin radiocarbon record were due to the influx into the oceans of large amounts of glacial meltwater.

Research on Drumlins Corroborating the Glacier Wave Theory (update for p.277):

Large areas of land that once lay at the border of the North American ice sheet are covered with oval-shaped hills called drumlins (Figure 10-W). These measure about 60 to 100 feet in height, 1200 to 1800 feet in width and can range in length from less than half a mile to several miles. One such drumlin field in central-western New York is estimated to contain as many as 10,000 drumlins. In 1989, Canadian geologist John Shaw pointed out that drumlins were produced by forceful discharges of glacial meltwater hundreds of feet deep that originated from beneath the melting glaciers.⁽⁸²⁾ He estimates that meltwater shaping the Livinstone Lake drumlin field in northern Saskatchewan was discharging as fast as 60 million m^3/s .⁽⁸³⁾ Such evidence that forceful meltwater discharges once flooded large tracts of land at the end of the ice age confirms the glacier wave theory, which proposes that such discharges originated from the ice sheet surface.

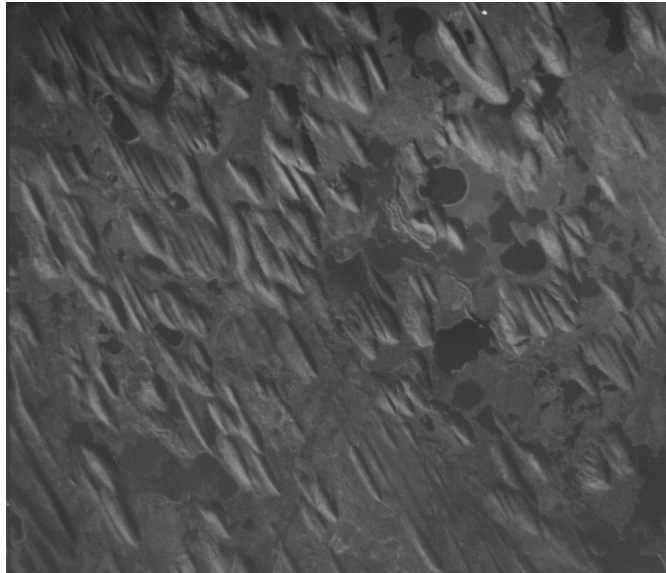


Figure 10-W. Aerial photograph of a drumlin field in southern Canada (courtesy of J. Shaw and the Canadian Air Photo Library)

References to the Update

- 1) D. J. Meltzer and J. I. Mead, Dating late Pleistocene extinctions: theoretical issues, analytical bias, and substantive results. In *Environment and Extinction: Man in Late Glacial North America*, edited by J. Mead and D. Meltzer, 145-173. Orono, Maine: Center for the Study of Early Man, University of Maine, 1985.
- 2) P. S. Martin, "Late Quaternary extinctions: The promise of TAMS ^{14}C dating." *Nuclear Instruments and Methods in Physics Research* **B29** (1987): 179 – 186.
- 3) T. Goslar, et al., "High concentration of atmospheric ^{14}C during the Younger Dryas cold episode." *Nature* **377** (1995): 414 – 417.
- 4) I. Hajdas, et al., "Cold reversal on Kodiak Island, Alaska, correlated with the European Younger Dryas by using variations of atmospheric ^{14}C content." *Geology* **26** (1998): 1047 – 1050.
- 5) K. A. Hughen, et al., "Deglacial changes in ocean circulation from an extended radiocarbon calibration." *Nature* **391** (1998): 65 – 68.

- 6) K. A. Hughen, J. R. Southon, S. Lehman, and J. Overpeck, "Synchronous radiocarbon and climate shifts during the last deglaciation." *Science* **290** (2000):1951-1954.
- 7) R. E. Dickinson, "Solar variability and the lower atmosphere." *Bull. Amer. Meteorol. Soc.* **56** (1975):1240-1248.
- 8) B. A. Tinsley, "Correlations of atmospheric dynamics with solar wind changes of air-earth current density into cloud tops." *J. Geophys. Res.-Atmospheres* **101** (1996): 29701.
- 9) H. Svensmark and E. Friis-Christensen, "Variation of cosmic ray flux and global cloud coverage: A missing link in solar-climate relationship." *J. Atmos. Sol. Terr. Phys.* **59** (1997):1225-1232.
- 10) E. Friis-Christensen and H. Svensmark, "What do we really know about the Sun-climate connection?" *Advances in Space Research* **20** (1997):913-921.
- 11) M. Ram, et al., "Eleven year cycle of dust concentration variability observed in the dust profile of the GISP2 ice core from Central Greenland: Possible solar cycle connection." *Geophysical Research Letters* **24** (1997): 2359-2362.
- 12) M. Ram and M. R. Stolz, "Possible solar influences on the dust profile of the GISP2 ice core from Central Greenland." *Geophysical Research Letters* **26** (1999): 1043-1046.
- 13) J. Donarummo, et al., "Sun/dust correlations and volcanic interference." *Geophysical Research Letters* **29** (2002): GL014858.
- 14) J. F. McManus, et al., "Collapse and rapid resumption of Atlantic meridional circulation linked to deglacial climate changes." *Nature* **428** (2004):834-837.
- 15) R. Fairbanks, "A 17,000-year glacio-eustatic sealevel record: influence of glacial melting rates on the Younger Dryas event and deep-ocean circulation." *Nature* **342** (1989):637-642.
- 16) Q. Hua, et al. Atmospheric ^{14}C variations derived from tree rings during the early Younger Dryas. *Quat. Sci. Rev.* **28** (2009): 2982-2990.
- 17) P. A. LaViolette, *Earth Under Fire*. Rochester, VT, Bear & Co., 1997, 2005.
- 18) T. F. Stocker and D. G. Wright, "Rapid changes in ocean circulation and atmospheric radiocarbon." *Paleoceanography* **11** (1996):773-795.
- 19) R. Muscheler, J. Beer, G. Wagner, and R. C. Finkel, "Changes in deep-water formation during the Younger Dryas event inferred from ^{10}Be and ^{14}C records." *Nature* **408** (2000):567-570.
- 20) R. C. Finkel and K. Nishizumi "Major features and forcing of high latitude northern hemisphere atmospheric circulation." *J Geophys Res* **102** (1997):26,699-26,706.
- 21) R. B. Alley, et al., "Visual-stratigraphic dating of the GISP2 ice core: basis, reproducibility, and application." *J Geophys Res* **102** (1997):26367-26381.
- 22) C. S. G. Gogorza, et al., "Holocene geomagnetic secular variations recorded by sediments from Escondido Lake (south Argentina)." *Earth Planets Space* **51** (1999):93-106.
- 23) M. Stuiver and P. M. Grootes, "GISP2 oxygen isotope ratios." *Quat. Res.* **53** (2000): 277-284.
- 24) G. Wagner, D.M. Livingstone, J. Masarik, R. Muscheler, J. Beer, "Some results relevant to the discussion of a possible link between cosmic rays and the Earth's climate." *Geophys Res Lett* **28** (2001):303-306.
- 25) B. E. Schaefer, J. R. King, C. P. Deliyannis, "Superflares on ordinary solar-type stars." *Ap J* **529** (2000):1026-1030.
- 26) J. Masarik and R. C. Reedy, "Terrestrial cosmogenic-nuclide production systematics calculated from numerical simulations." *Earth Planet Sci Let* **136** (1995):381-395.
- 27) R. J. Uffen, "Influence of the Earth's core on the origin and evolution of life." *Nature* **198** (1963):143-144.
- 28) P. A. LaViolette, "Cosmic ray volleys from the Galactic center and their recent impact on the Earth environment." *Earth, Moon, Planets* **37** (1987):241-286.

- 29) P. A. LaViolette, "Galactic core explosions and the evolution of life." *Anthropos* **12** (1990):239-255.
- 30) C. V. Haynes, Jr., "Younger Dryas "black mats" and the Rancholabrean termination in North America." *Proc Natl Acad Sci USA* **105** (2008):6520-6525.
- 31) A. J. T. Jull, et al., Radiocarbon ages at Murray Springs, Arizona and the influence of climate change on Clovis man. *Proc. 3rd Conf. on ¹⁴C and Archaeology*, Lyons, France, 1998.
- 32) T. Foelsche, "Estimates of radiation exposure from solar cosmic rays in SST altitudes." 1974. NASA TM X-71990.
- 33) S. Epelman and D. R. Hamilton, "Medical mitigation strategies for acute radiation exposure during spaceflight." *ASEM* **77** (2006):130-135.
- 34) K. C. Taylor, et al., "The flickering switch of Late Pleistocene climate change." *Nature* **361** (1993):432-436.
- 35) M. Ram, M. Stolz, and G. Koenig, "Eleven year cycle of dust concentration variability observed in the dust profiles of the GISP2 ice core from central Greenland." *Geophys Res Lett* **24** (1997):2359-2362.
- 36) G. A. M. Dreschhoff and E. J. Zeller, "415-year Greenland ice core record of solar proton events dated by volcanic eruptive episodes." *Inst. Tertiary-Quaternary Studies - TER-QUA Symposium Series 2* (1994):1-24.
- 37) K. G. McCracken, D. F. Smart, M. A. Shea, and A. M. Dreschhoff, "400 years of large fluence solar proton events." *Conf Pap Int Cosmic Ray Conf* **8** (2001): 3209-3212.
- 38) K. G. McCracken, et al., "Solar cosmic ray events for the period 1561 - 1994. 1. Identification in polar ice, 1561 - 1950." *J. Geophys. Res.* **106** (2001): 21,585-21,598.
- 39) Q. Yang, et al., "Global perspective of nitrate flux in ice cores." *Nature* **346** (1995):554-556.
- 40) J. P. Steffensen, 2008, personal communication (data of M. Bigler).
- 41) A. E. Jones, et al., "Speciation and rate of photochemical NO and NO₂ production in Antarctic snow." *Geophys. Res. Lett.* **27** (2000): 345-348.
- 42) A. E. Jones, et al., "Measurements of NO_x emissions from the Antarctic snowpack." *Geophys. Res. Lett.* **28** (2001): 1499-1502.
- 43) J. E. Dibb, et al., "Fast nitrogen oxide photochemistry in Summit, Greenland snow." *Atmospheric Environ.* **36** (2002): 2501-2511.
- 44) J. R. McCabe, et al., "Oxygen isotopic fractionation in the photochemistry of nitrate in water and ice." *J. Geophysical. Research* **110** (2005): D15310.
- 45) P. A. LaViolette, "Evidence for a solar flare cause of the Pleistocene mass extinction." *Radiocarbon* (June 2011): .
- 46) C. H. Jackman, et al., "Northern hemisphere atmospheric effects due to the July 2000 Solar Proton Event." *Geophys. Res. Lett.* **28** (2001): 2883-2886.
- 47) R. B. Firestone, et al., "Evidence for an extraterrestrial impact 12,900 years ago that contributed to the megafaunal extinctions and Younger Dryas cooling." *Proceedings of the National Academy of Sciences* **104**, October 9, 2007, 16016 -16,021.
- 48) R. B. Firestone, A. West, and S. Warwick-Smith, *The Cycle of Cosmic Catastrophes*. Rochester, VT, Bear & Co., 2006.
- 49) W. M. Napier, "Paleolithic extinctions and the Taurid complex." *MNRAS* **405** (2010): 1901-1906.
- 50) A. L. Melott, et al., "Cometary airbursts and atmospheric chemistry: Tunguska and a candidate Younger Dryas event." *Geology* **38** (2010): 355-358.
- 51) M. Baales, F. Bittmann, and B. Kromer, "Verkohlte Bäume im Traß der Laacher See-Tephra bei Kruft (Neuwieder Becken)." *Archäologisches Korrespondenzblatt* **28** (1999):191-204.

- 52) E. Isaksson, et al., "A new ice-core record from Lomonosovfonna, Svalbard: Viewing the 1920-97 data in relation to present climate and environmental conditions." *J. of Glaciology* **47** (2001): 335-345.
- 53) O. I. Shumilov, et al., "Enhancement of stratospheric aerosols after solar proton event." *Ann. Geophysicae* **14** (1996): 1119-1123.
- 54) K. C. Taylor, P. A. Mayewski, M. S. Twickler, S. I. Whitlow, "Biomass burning recorded in the GISP2 ice core: A record from eastern Canada?" *The Holocene* **6**(1) (1996):1-6.
- 55) M. R. Legrand, M. De Angelis, T. Staffelbach, A. Neftel, B. Stauffer, "Large perturbations of ammonium and organic acids content in the Summit-Greenland ice core. Fingerprint from forest fires?" *Geophys Res Lett* **19** (1992):473-475.
- 56) J. P. Steffensen, et al. "High-resolution Greenland ice core data show abrupt climate change happens in few years." *Science* **321** (2008):680-684.
- 57) J. R. Marlon, et al. "Wildfire responses to abrupt climate change in North America." *Proc Natl Acad Sci USA* **106** (2009):2519-2524.
- 58) J. B. Kloosterman, "An Alleröd conflagration? (Comments on Apophoreta-II). *Catastrophist Geology* **2-1** (1977): 13-15.
- 59) J. B. Kloosterman, "Correlation of the Late Pleistocene Usselo Horizon (Europe) and the Clovis Layer (North America)." Paper PP41A-02, May 2007 AGU Conference, Acapulco, Mexico. [http://www.agu.org/meetings/sm07/sm07-sessions/sm07_PP41A.htm]
- 60) S. Fiedel. "Clovis age in calendar years: 13,500 - 13,000 B.P." *Clovis and Beyond*, Santa Fe, 1999.
- 61) C. V. Haynes, Jr., "Younger Dryas "black mats" and the Rancholabrean termination in North America." *Proc Natl Acad Sci USA* **105** (2008):6520-6525.
- 62) C. V. Haynes, Jr. (2009) personal communication.
- 63) W. Topping, "Cosmogenic radiocarbon as a source of error at Paleo-Indian sites and evidence for a giant solar flare in prehistory." Paper posted on W. Topping's website, June 1998.
- 64) R. B. Firestone, and W. Topping, "Terrestrial evidence of a nuclear catastrophe in Paleoindian times." *Mammoth Trumpet* **16**(2) March 2001, pp. 9 - 16. [<http://abob.libs.uga.edu/bobk/nuclear.pdf>]
- 65) J. R. Southon and R. E. Taylor, "Brief comments on 'Terrestrial evidence of a nuclear catastrophe in Paleoindian times'," *Mammoth Trumpet* **17** (March 2002). [<http://www.centerfirstamericans.com/mt.php?a=61&h=firestone>]
- 66) W. Topping, "Topping's Photographs of Chuska Flakes from Folsom Site 34-2-13, Central New Mexico" Paper posted on W. Topping's website, January 1997.
- 67) W. Topping, "More evidence for micrometeoritic bombardment of the Gainey Paleo-Indian site in lower Michigan." Paper posted on W. Topping's website, June 1998.
- 68) W. Topping, "The evidence (some inferential) for a cosmic event in Paleo-Indian times." Paper posted on W. Topping's website, February 1999.
- 69) S. J. Johnsen, H. B. Clausen, W. Dansgaard, N. S. Gundestrup, C. U. Hammer, U. Andersen, K. K. Andersen, C. S. Hvidberg, D. Dahl-Jensen, J. P. Steffensen, H. Shoji, Á. E. Sveinbjörnsdóttir, J. White, J. Jouzel, and D. Fisher, "The $\delta^{18}\text{O}$ record along the Greenland Ice Core Project deep ice core and the problem of possible Eemian climatic instability." *Journal of Geophysical Research*, **102**(C12) (1997): 26397-26410.
- 70) H. Heinrich, "Origin and consequences of cyclic ice rafting in the northeast Atlantic Ocean during the past 130,000 years." *Quaternary Research* **29** (1988): 142 - 152.
- 71) W. Broecker, "Massive iceberg discharges as triggers for global climate change." *Nature* **372** (1994):421 - 424.
- 72) G. C. Bond and R. Lotti, "Iceberg discharges into the North Atlantic on millennial time scales during the last glaciation." *Science* **267** (1995): 1005 - 1010.

- 73) W. S. Broecker et al. "The chronology of the last deglaciation: Implications to the cause of the Younger Dryas event." *Paleoceanography* **3** (1988): 1 – 19.
- 74) E. Vogelsang and M. Sarnthein, "Age control of sediment core V23-81." *Pangaea* (2001), doi: 10.1594/PANGAEA.59872.
- 75) J. Adams, M. Maslin, and E. Thomas, "Sudden climatic transitions during the Quaternary." *Progress in Physical Geography* **23** (1999): 1-36.
- 76) T. V. Lowell, et al., "Interhemispheric correlation of late Pleistocene glacial events." *Science* **269** (1995): 1 541 – 1549.
- 77) G. Bond, et al., "Evidence for massive discharges of icebergs into the North Atlantic ocean during the last glacial period." *Nature* **360** (1992): 2 4 5 – 249.
- 78) B. Manighetti, et al. "Chronology for climate change: Developing age models for the biogeochemical ocean flux study cores." *Paleoceanography* **10** (1995):513 – 525.
- 79) J. P. Severinghaus and E. J. Brook, "Abrupt climate change at the end of the last glacial period inferred from trapped air in polar ice." *Science* **286** (1999):930– 934.
- 80) B. P. Flower, D. W. Hastings, H. W. Hill, T. M. Quinn, " Phasing of deglacial warming and Laurentide ice sheet meltwater in the Gulf of Mexico." *Geology* **32** (2004): 597-600.
- 81) W. Broecker and S. Barker, "A 190‰ drop in atmosphere's $\Delta^{14}\text{C}$ during the "Mystery Interval" (17.5 to 14.5 kyr)." *Earth and Planetary Science Letters* **256** (2007):90– 99.
- 82) J. Shaw, "Drumlins, subglacial meltwater floods, and ocean responses." *Geology* **17** (1989): 853–856.
- 83) J. Shaw, D. Kvill, and B. Rains, "Drumlins and catastrophic subglacial floods." *Sedimentary Geology*, **62** (1989): 177–202.

CHAPTER 11

RECURRENT GALACTIC SUPERWAVES AND THE EVOLUTION OF LIFE

11.1 QUANTUM SPECIATION

A considerable amount of evidence has been accumulating in recent years which indicates that biological evolution is not a process of gradual change, as was formerly thought. Rather, it appears that evolution proceeds in a step-like manner such that the majority of change in a species occurs at periodic intervals over a very short space of time. This punctual mode of evolution emerged primarily through the writings of Ernst Mayr (1942, 1954, 1963) who argued that most of the net evolutionary change in the history of life may be accounted for by rapid morphologic divergence at the species level. Verne Grant (1963) coined the term "quantum speciation" to refer to this phenomenon. Quantum speciation may be defined as evolutionary branching (marked morphologic divergence) at the species level, most of the evolution being concentrated: 1) within a small population and 2) during a time interval that is very brief with respect to the total longevity of the new lineage that is produced (Stanley, 1979, Chapters 2 and 6). The size of the germinal population may involve fewer than 10 individuals and the quantum jump may occur in a space of time spanning only a few generations (Stanley, 1979, p. 145).

Often these evolutionary quantum jumps occur at times when the parent species becomes decimated. Such a circumstance, whereby a population is destroyed leaving one or more localized genotypically distinctive populations, has been termed *catastrophic selection* (Lewis, 1962, 1966). Catastrophic selection is difficult to explain in terms of the Darwinian theory of natural selection since the latter suggests that major evolutionary changes should occur at times when the forces of competition and survival of the fittest are particularly acute, i.e., during times of overpopulation.

Another phenomenon related to quantum speciation is *adaptive radiation*, the rapid proliferation of new taxa from a single ancestral group. The branching points in Figure 11.1 clearly illustrate this phenomenon. As seen here, each extinction episode is immediately followed by an evolutionary burst in which many new kinds of organisms suddenly make their appearance. Extinction boundaries during the Mesozoic period are also clearly revealed in Figure 11.2, which shows how the number of genera in the family Ammonitidae has varied over time. Ammonitidae, one of several families of the Ammonoidea order, are a kind of spiral shelled cephalopod. Note that this family became completely extinct at the Cretaceous/Tertiary boundary 65 million years ago. The geologic time scale is represented in a more extended form in Figure 11.3.

Simpson (1944, 1953) and Stanley (1979, pp. 65, 170) suggest that most evolutionary change occurs during adaptive radiation and that this takes place in particular geographic regions where the ecological conditions allow the opportunity for diversification. Stanley (1979, p. 169) has coined the term *ecoinsular radiation* to refer to adaptive radiation which occurs within *ecological islands*. Ecological islands may be defined as isolated regions in which competition and predation are unusually weak making conditions generally more favorable to speciation. Stanley emphasizes the importance of this concept in considering the dynamics of evolution where mass extinction plays a dominant role. That is, extinction creates vacant ecologic islands made available for colonization. One good example is the extinction of the dinosaurs at the end of the Cretaceous period. This episode was

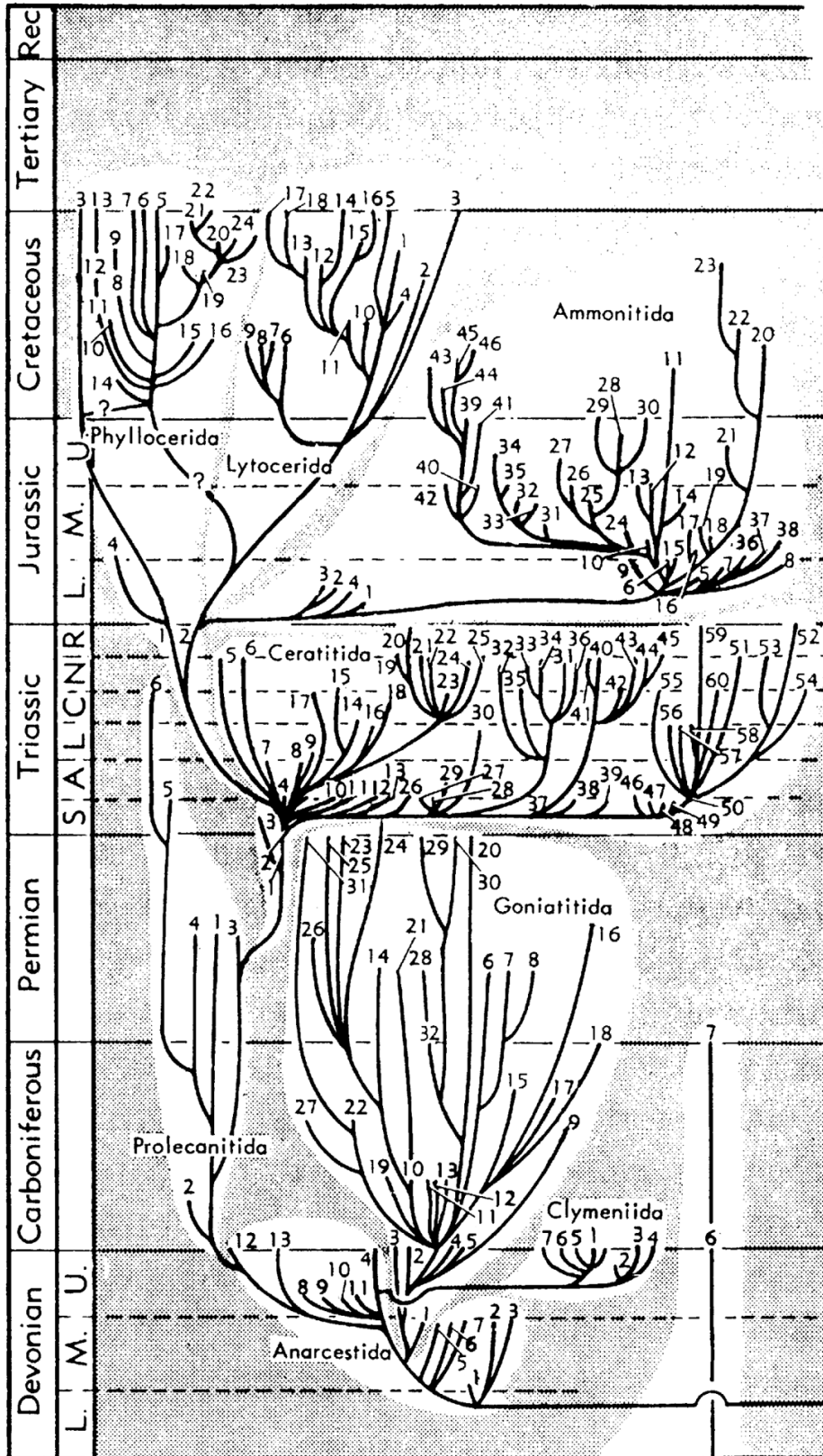


Figure 11.1. Phylogeny of the order of Ammonoida showing the rapid appearance of new families following events of mass extinction (Teichert, 1967).

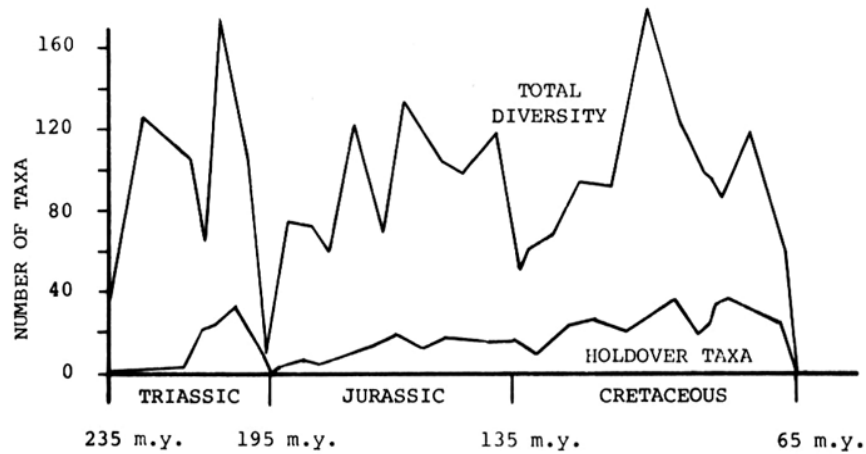


Figure 11.2. Fluctuations in the number of genera of ammonites during the Mesozoic period (Kennedy, 1977).

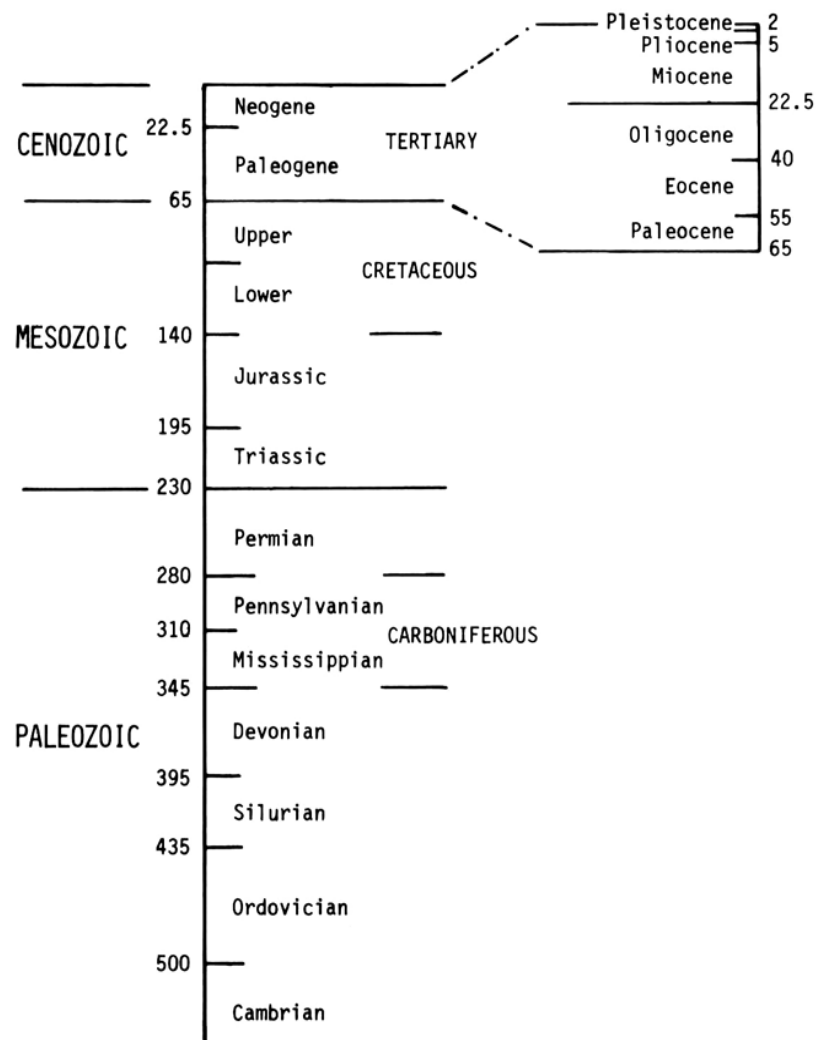


Figure 11.3. The geologic time scale. Ages are in millions of Potassium/Argon years.

immediately followed by a six fold increase in the number of mammalian families occurring in the Cenozoic period over about 25 million years.

The concepts of quantum speciation, catastrophic selection, and ecoinsular radiation are quite compatible with the Galactic Explosion Hypothesis. For example, background radiation levels could increase by as much as 10^5 times present levels during major superwave events or during transits of the heliopause sheath past the Earth; see Subhypotheses 5-d and 5-e (p. 2). Such high radiation levels could simultaneously cause populational decimation, species segregation, and mutational acceleration. This would take place over a wide geographical area and would act relatively indiscriminately over a wide variety of unrelated species occupying distinctly different ecological niches.

But if the GEH is correct, then differences in the rate of extinction among various species should depend on their relative degrees of vulnerability to radiation exposure. Moreover, if both extinction and mutation are produced by a common cause (e.g., cosmic radiation), then the rate of speciation and the rate of extinction for a given species should be positively correlated. Indeed, observational evidence supports both of these projections. For example, land taxa, which are more vulnerable to exposure to cosmic radiation, speciate much more rapidly than marine taxa; see Stanley (1979, p. 231). Also, Stanley finds that the rate of speciation in adaptive radiation and the rate of extinction are strongly correlated in the animal world. For example, species with high average duration, i.e., low rate of extinction E , also have low net rates of speciation R . As defined by Stanley (1979, pp. 104–108), the net rate of speciation is given by $R = S - E$ where S is speciation rate and E is the rate of termination of lineages.) A second related finding is that as the rate of extinction E increases across a spectrum of taxa, the rate of speciation S in adaptive radiation tends to increase proportionately (Stanley, 1979, p. 259). Thus, if E is twice as large for species B as for species A, then it is found that S (and R) is also twice as large.

However, if marine life forms are less susceptible to mutagenic radiation than land life forms, then why do sea creatures such as Graptoloids, Ammonites, and Trilobites (all now extinct) rank among the highest in R and E values? Perhaps this could be explained if part or in some cases all of their life cycle were spent either close to the ocean surface or in shallow water.

11.2 EXTRATERRESTRIAL EXTINCTION HYPOTHESES IN REVIEW

11.2.1 Cosmic-Ray Extinction Hypotheses

Loeblich and Tappan (1964) have put forth the proposal that the sudden extinctions of phytoplankton observed periodically in the geologic record were produced by an increased influx of cosmic radiation. They point out that local extinctions due to unfavorable environments could not have been significant in causing mass extinctions. This is because the short life span of plankton (as short as one week), coupled with their extreme abundance and rapid dispersal make it possible for them to quickly recolonize any such local region. Thus Loeblich and Tappan conclude that whatever caused the sudden extinction of entire groups of plankton, as for example occurred at the Cretaceous/Tertiary boundary, must have been due to "a cause that was effective world-wide not merely an accidental mutation in a single species." Moreover, they point out that the rapid turn over and rapid dispersal ability of foraminifera require that any such global effect if mutagenic must have occurred over a very short space of time. They also note that planktonic foraminifera of the open ocean were strongly affected by the terminal Cretaceous event, to the extent that few species survived into the early Tertiary period, whereas two-thirds of the deep water foraminiferal species living along the continental shelves were able to safely cross the Cretaceous/Tertiary boundary.

They rule out sea-level and strand-line changes as causal factors for the planktonic extinctions because these would be expected to affect primarily the deep water species, just the opposite of what is observed. On the other hand, they point out that mutational effects arising from excessive exposure to cosmic radiation would have affected surface dwelling foraminifera of the open ocean to a much greater extent as compared with deep water species.

Uffen (1963) has proposed that at times when the Earth's magnetic field is at minimum strength, i.e., at times of field reversals, cosmic rays trapped in the radiation belts and solar wind particles could spill onto the Earth causing a major increase in the mutation rate of organisms. He suggests that these geomagnetic minima last several thousand years and arise as a result of instabilities in the Earth's liquid metal core dynamo, believed to generate the Earth's magnetic field. However, contrary to the suggestion made by Uffen, Waddington (1967) argues that removal of the Earth's magnetic field sheath would have little effect on the evolution of organisms. He considers the effects that would be produced by the current cosmic ray background component, by periodic solar flares, and by possible dumping of the Earth's radiation belts, and concludes that removal of the Earth's magnetic shielding would increase the sea level radiation background by at most 16%. Arguing along the same lines as Waddington, Harrison (1968) estimates that human beings living at sea level at the equator would experience only an 0.6% increase in their mutation rate if the Earth's protective magnetic sheath were removed. For mammals with shorter life spans the increase would be even less.

However, Uffen (1964) and Simpson (1965) both present evidence that reversals of the Earth's magnetic field correlate with times of mass animal extinction and evolutionary spurts. Also, others have shown that there is a correlation between the extinction of certain types of microfauna (e.g., foraminifera and radiolaria) and magnetic field reversals (Harrison and Funnel, 1964; Opdyke et al., 1966; Hays and Opdyke, 1967; Hays et al., 1969; Hays, 1970 and 1971). For example, Hays (1971) demonstrates that during the past 2.5 million years eight species of radiolaria became extinct and six of these eight species disappeared close to magnetic reversals, although he points out that, besides cosmic radiation, other causes such as climatic change might be responsible for these extinctions. He cites a few cases in which climatic changes have been found to correlate with geomagnetic events.

At present, the general consensus is that past extinctions could not have been induced by the ambient cosmic ray flux, even at times of near zero magnetic field intensity, simply because the current background radiation is not strong enough. However, despite this, there is a considerable body of data to indicate that there is indeed a link between extinctions and geomagnetic reversals. Moreover, the pattern of these extinctions is such that cosmic radiation appears to be a prime candidate.

The objections that have been raised against Uffen's cosmic ray hypothesis may be avoided simply by admitting the possibility that the cosmic ray background becomes considerably enhanced specifically at times when magnetic field reversals occur. Such a scenario is proposed by the GEH. With this approach it is no longer necessary to invoke an independent means for generating field reversals since (as in shown in Subsection 3.3.3) the cosmic ray blast could serve as the reversing agent. The Earth's magnetic field, then, need no longer be regarded as the cause of extinctions; it merely serves as a marker indicating when these cosmic events take place.

The Galactic Explosion Hypothesis could also account for an interesting finding made by Simpson (1965). He notes that the evolutionary history of plants does not appear to make a good correlation to field reversals. Forest irradiation studies (Woodwell, 1967; Bhatt et al., 1960) indicate that, compared with animal life, vegetation is considerably more resistant to the effects of cosmic radiation. So if it is indeed the case that geomagnetic reversals are associated with cosmic ray outbursts, then it is to be expected that geomagnetic reversals would correlate better with the evolutionary history of animal life.

The GEH is not the first to involve a scenario in which extinctions are caused by large doses of cosmic radiation. For example, Terry and Tucker (1968) have proposed that supernova explosions occurring close to the solar system might sufficiently increase radiation levels in the Earth's vicinity so as to cause major extinctions of fauna. They show that 1000 roentgens of radiation delivered over a short period of time, i.e., over a few days, would surpass the LD(50) dose level for most animals. Lethal Dose (50) is the amount of acute exposure required for 50% of a population to succumb. They point out that elevated levels of cosmic radiation can account for why faunal groups were dramatically affected at extinction boundaries, while floral groups were relatively unaffected. However, they admit that their model does not propose intensities sufficient to account for the extinctions of marine organisms such as plankton and algae living at depths of 50 meters or more. Another disadvantage of their theory is the rarity of such events. They estimate that supernovae producing 10^3 roentgens would have a chance of occurring only about once every 150 million years. Thus, supernovae could not be linked to the numerous field reversals observed in the geologic record.

Another group, Wdowczyk and Wolfendale (1977), has proposed a theory of animal extinction based on the assumption of elevated levels of background radiation. They suggest that these catastrophes could be due to rare solar flare events that take place on scales much larger than those observed so far. They also suggest that γ -ray outbursts from the Galactic center could cause extinctions. However, they propose that these events would occur only about every 10^8 years and would be communicated to the solar system over a period of 10^6 years. Moreover, they propose an intensity of only $\sim 10^{-4}$ ergs/cm²/s (or $\sim 10^9$ ergs/cm² total), which would have an insignificant effect.

11.2.2 Falling-Body/Extinction Hypotheses

Brief mention should be made about a complementary set of theories that also propose extraterrestrial causes for extinctions. These will be referred to here as the "falling body hypotheses." These would be catastrophes due to the collision of the Earth with a planetesimal such as a comet or asteroid. To begin with, Urey (1957, 1962, 1963, 1973) has proposed that fields of tektites (meteoritic debris) found on the Earth were produced by periodic collisions with passing comets, and that these collisions terminated geological periods. He notes that tektite fields have been found coinciding with the termination of the Eocene, Miocene, and Pliocene periods (Urey, 1973). He lists several factors that could have caused the related extinctions at these boundaries, e.g., atmospheric heating, ocean heating, tidal waves, seismic activity, and volcanic eruptions.

More recently, Glass and Zwart (1977) have found an unusually high concentration of microtektites in a Caribbean deep sea core coincident with the extinction of several species of radiolaria dated at the end of the Eocene 34 million years ago. Microtektites are small glassy pieces of cosmic debris smaller than 1 mm in diameter and, like tektites, are believed to be formed in the atmosphere as ablation products from falling bodies, although such spherules may also be formed in space; see Section 8.3 (p. 222). The first such microtektite field, reported by Glass and Heezen (1967), was found in Indian Ocean sediments dated at about 700,000 years BP (K-Ar chronology). This event coincides with changes in fossil plankton and marks the time of extinction of Java man (*Homo erectus*), precursor of *Homo sapiens*. Observations of many deep-sea sediment cores taken from different parts of the Indian Ocean indicate that the cosmic debris from this event is strewn over an area 10,000 by 7000 kilometers in extent. Glass and Heezen estimate that the total mass of these microtektites approaches 2.5×10^{15} grams. If this mass were reconstituted as a single body with a density $\rho = 2.5 \text{ g/cm}^3$, its diameter would be ~ 1 km. Rubidium-strontium dating indicates that this

body, and the masses that apparently fell at the end of the Eocene and Miocene, came from the same parent body, which was formed about 400 million years ago. However, another object that apparently fell around 1.2 million years ago forming the Ivory Coast strewn field appears to have come from a different body that was created about 2 billion years ago.

Glass and Heezen note that at the time of the 700,000 years BP event the Earth's magnetic field reversed, heralding the beginning of the Brunhes magnetic epoch. Noting that the Ivory Coast tektite field also coincides with a magnetic reversal, they suggest that there must be a causal connection, cosmic encounters somehow causing a disturbance to the Earth's magnetohydrodynamic dynamo. More recently, Clube and Napier (1982) have expanded on this idea with calculations demonstrating that an impacting planetesimal would set up a shock wave that would propagate to the Earth's core. They suggest that this could cause a disturbance to the core dynamo that subsequently would be manifested as a field reversal. They suggest that even collisions with bodies as small as 10^{13} grams with impact energies equivalent to $10^{3\pm 1}$ megatons of TNT, arriving as frequently as every 10^4 years, might at times initiate field reversals. However, until more is known about the operation of the Earth's core dynamo and its degree of stability or instability, direct links between planetesimal impacts and geomagnetic reversals should be regarded with some reservation.

Nevertheless, the evidence that deposits of asteroid-like material coincide with certain extinction episodes is compelling. The possibility should be left open that besides superwave induced cosmic ray events, planetesimal collisions may constitute another means by which faunal extinctions are brought about.

Alvarez et al. (1979, 1980) have discovered a compositional anomaly at the Cretaceous/Tertiary boundary (~65 million years BP) which indicates the presence of a substantial amount of extraterrestrial chondritic matter. They suggest that an asteroid collided with the Earth and upon impact became pulverized, mixed in a 60 to 1 proportion with crustal material, and ejected into the stratosphere. Then, finally this material settled to form the presently observed anomalous boundary layer. They propose that this dust remained suspended in the stratosphere for several years where it totally blocked out sunlight, causing the death of vegetation, collapse of the food chain, and leading to mass extinctions of megafauna, e.g., the last of the dinosaurs.

Hickey (1981) has challenged this model, pointing out that the observed patterns of plant extinctions are not accounted for. Moreover, Kyte, Zhou, and Wasson (1980) point out that if an asteroid impact had occurred, the sunlight would have been blocked out for no more than a few months due to rapid coagulation of the suspended dust. More direct evidence is reported by Russell (1982, p. 63) who has studied a sediment exposure at Fort Peck Reservoir in northeastern Montana. His pollen studies indicate that there was no decrease in the abundance of plant life at the extinction boundary. Rather, a zone of "poor preservation" of pollen spores is encountered 5 meters above this horizon.

Kyte et al. (1980) note that if an asteroid of the type that Alvarez et al. propose had impacted the Earth's land surface, then the chondritic matter should have become diluted to a much greater extent than is observed. They point out that this would not be a problem if the assumption is made that the asteroid impact had occurred in the ocean and had ejected a minimal amount of material from the Earth's crust, though as one alternative to the asteroid impact hypothesis they suggest that the approaching body (i.e., a comet) broke up into a shower of small fragments near the Earth and became decelerated in passing through the Earth's atmosphere. As another alternative, they suggest that this dust could have been directly accreted from a nearby interstellar cloud, rather than supplied by a falling body. However, for this latter alternative they do not propose a mechanism for transporting this material to the inner parts of the solar system against the pressure of the solar wind. A Galactic superwave, though, could serve as an effective mechanism for transporting interstellar dust into the solar system. Moreover, a superwave could simultaneously account for the mass

extinction of the dinosaurs and the coincident occurrence of the geomagnetic polarity reversals found at the Cretaceous/Tertiary boundary, which otherwise would be difficult to explain.

[**UPDATE:** Following the publication of this dissertation, evidence of a 240 - 300 km diameter impact crater for the Cretaceous/Tertiary event was found in the Chixculub, Yukutan region of the Gulf of Mexico.⁽¹⁾ This indicated a water impact type of event, Kyte's first alternative mentioned above.]

It is reasonable to consider the possibility of asteroid impacts when seeking an explanation for the major terminal extinction events, which occur relatively infrequently. However, for the numerous extinction boundaries between the major boundaries (see Figure 11.1) appeals to such falling-body causes become less convincing. For example, Alvarez et al. (1980) estimate that the collision of the Earth with a $10^{17} - 10^{18}$ gram Apollo object (asteroid in elliptical orbit around the Sun) would occur only about once every 10^8 years. Bailey and Clube (1978), though, have suggested that the more minor events could be caused by smaller Apollo objects. Smaller objects, being more numerous, would have a higher probability of colliding with the Earth. However, it remains to be shown that objects as small as $10^{15} - 10^{16}$ grams arriving as frequently as $10^5 - 10^6$ years could account for the numerous global extinction episodes recorded throughout geologic history. Even greater difficulty would be encountered in proposing such a mechanism to account for the abrupt climatic changes of the Pleistocene, which appear to occur on a time scale of less than 10^4 years.

UPDATE

Further evidence supporting the prediction that mass extinctions may have a Galactic cause came in 1984. Rampino and Stothers, analyzing the data of Raup and Sepkoski, found that mass extinctions historically have recurred every 30 ± 1 million years, a period that approximates the intervals between times when the Sun crosses the Galactic plane.^(2, 3) This correlation is explained by the Galactic Explosion Hypothesis since the solar system would have a greater chance of encountering interstellar dust and gas at times when it crosses the Galactic plane, and as described in Chapter 3, such material would energize the Sun and its flaring activity when propelled into the solar system by a superwave.⁽⁴⁾

-
- 1) P. Claeys, W. Alvarez, J. Smit, A. Hildebrand, and A. Montanari, "KT boundary impact glasses from the Gulf of Mexico Region." *Lunar Planetary Science Conference, XXIV* (1993): 297 – 298.
 - 2) M. R. Rampino and R. B. Stothers, "Terrestrial mass extinctions, cometary impacts, and the Sun's motion perpendicular to the galactic plane." *Nature* **308** (1984): 709 – 712.
 - 3) D. M. Raup and J. J. Sepkoski, *Proc. National Academy of Science* **81** (1984): 844.
 - 4) P. A. LaViolette, "Galactic core explosions and the evolution of life." *Anthropos* **12** (1990): 239 – 255.

CHAPTER 12

TESTING THE GALACTIC EXPLOSION HYPOTHESIS

12.1 NEUTRON ACTIVATION ANALYSIS OF DUST FROM GLACIAL ICE: CAMP CENTURY AND BYRD STATION DEEP ICE CORES

12.1.1 Preliminary Reasoning

As mentioned in Chapter 1 (p. 7), an important test of the GEH would be to determine whether cosmic dust deposition rates had, in fact, increased at the end of the Wisconsin glacial period. Glacial ice would constitute an ideal medium to study time-variations in the rate of cosmic dust influx since in glacial ice there would be a minimal amount of dilution by terrestrial dust, as compared with, for example, an ocean sediment environment. Also, by determining the rate of ice accumulation, a time scale may be developed allowing ambient dust concentration rates to be directly converted into dust deposition rates. Finally, glacial ice contains a record of other important parameters such as ambient temperature, glacier altitude, and atmospheric gas composition.

The elements iridium (Ir) and Nickel (Ni) were chosen as cosmic dust concentration indicators since these elements are enhanced in extraterrestrial material, $10^2 - 10^4$ times for Ni, as compared with oceanic sediment abundance; see Table XIII (p. 224).

The Null Hypothesis. Before analyzing the glacial ice dust samples for Ir, Ni, and other elements, I formulated the null hypothesis that the deposition rate of cosmic dust had remained constant over time. This hypothesis is challenged by the Galactic Explosion Hypothesis which instead predicts that cosmic dust deposition rates should have increased toward the end of the Wisconsin Ice Age. Prior to the present study, there had been no analysis made of the cosmic dust content of Wisconsin ice. Most investigations of this sort involved the study of Holocene ice and, more specifically, ice accumulated within the last few hundred years. So the situation was ideal for making an *a priori* prediction regarding the concentration of cosmic dust in Late Wisconsin ice and for subsequently checking out that prediction.

For the Holocene Epoch a cosmic dust deposition rate baseline value of $\sim 10^{-7}$ g/cm²/yr ($1.3 \pm 0.9 \times 10^{-7}$) was chosen. This was based on the work of several investigators which suggest deposition rates in the range of $3 - 6 \times 10^{-8}$ g/cm²/yr for Antarctica and $0.4 - 4 \times 10^{-7}$ g/cm²/yr for Greenland; see Tables XV and XVI. For example, Thiel and Schmidt (1964) have studied the concentration of cosmic spherules in Antarctic firn; Langway (1970) has studied the concentration of cosmic spherules in firn and ice from Camp Century and Site 2, Greenland; McCorkell et al. (1967) have studied the concentration of dissolved Ni and Co in Camp Century ice; Davidson et al. (1981) have determined the concentration of Ni in fresh snow from Dye 3, Greenland; Hanappe et al. (1968) have studied the concentration of Ni in firn from Plateau Station, Antarctica, and at the South Pole. In addition, Takahashi et al. (1978), using neutron activation analysis (NAA) with radiochemical separation, have determined the concentration of Ir in Camp Century ice and in snow from Dome C, Antarctica. However, the findings of Takahashi et al. predict anomalously low deposition rates of $\sim 2 \times 10^{-9}$ g/cm²/yr for Antarctica and $\sim 3 \times 10^{-9}$ g/cm²/yr for Greenland, if an Ir concentration of 514 ppb is assumed for the cosmic dust fraction. At present the author

TABLE XV
COSMIC DUST ACCUMULATION RATES IN GREENLAND

A. Estimates Based on Nickel Concentrations

| (1) Sample | (2) Depth (m) | (3) Age (years b2k) | (4) Ni conc. ($\mu\text{g/l}$) | (5) Ice accum. rate (cm/yr) | (6) Cosmic dust accum. rate ¹ ($\mu\text{g/cm}^2/\text{yr}$) | (7) Reference |
|-----------------------------------|---------------------|---------------------------|--|--------------------------------------|--|--|
| Dye 3 65°N, 44°W | ---- | 4 | 0.05 | 50 | 0.25 | (Davidson et al., 1981) |
| Site 2 77°N, 56.1°W | 300 | 730 | ---- | -- | 0.04 ⁽²⁾ | (Langway, 1970) |
| Camp Century <u>77°N, 61°W</u> | 6.1-7.6 70 | 30 220 | ---- 0.11 | -- 35 | 0.13 ⁽²⁾ 0.35 | (Langway, 1970) (McCorkell et al., 1967) |
| #949 | 1212.0 | 38,650 | 0.53 | 17.5 | 0.85 ± 0.17 | This work |
| #955 | 1221.0 | 45,000 | <0.05 | " | <0.08 | " |
| #959 | 1226.2 | 49,000 | <0.13 | " | <0.21 | " |
| #960 | 1227.7 | 49,500 | 0.26 | " | 0.42 | " |
| #962-1a | 1230.5 | 50,500 | 1.50 | " | 2.4 ± 0.5 | " |
| #962-2 | 1231.5 | 51,300 | <0.09 | " | <0.14 | " |
| #969 | 1241.0 | 58,700 | 1.11 | " | 1.78 ± 0.36 | " |
| #992 | 1275.0 | 78,500 | 0.64 | " | 1.02 ± 0.2 | " |

B. Estimates Based on Iridium Concentrations

| (1) Sample | (2) Depth (m) | (3) Age (years b2k) | (4) Ir conc. (pg/l) | (5) Ice accum. rate (cm/yr) | (6) Cosmic dust accum. rate ³ ($\mu\text{g/cm}^2/\text{yr}$) | (7) Reference |
|---------------------|---------------------|---------------------------|---------------------------|--------------------------------------|--|-----------------------------|
| <u>Camp Century</u> | ---- | 220 | 0.017-0.07 | 35 | 0.001-0.004 | (Takahashi et al., 1978) |
| #949 | 1212.0 | 38,650 | 54 | 17.5 | 1.68 ± 0.34 | This work |
| #955 | 1221.0 | 45,000 | 14.6 | " | 0.46 ± 0.09 | " |
| #959 | 1226.2 | 49,000 | <0.91 | " | <0.03 | " |
| #960 | 1227.7 | 49,500 | 17.1 | " | 0.54 ± 0.11 | " |
| #962-1a | 1230.5 | 50,500 | 85 | " | 2.66 ± 0.5 | " |
| #962-2 | 1231.5 | 51,300 | <0.95 | " | <0.03 | " |
| #969 | 1241.0 | 58,700 | 31 | " | 0.97 ± 0.19 | " |
| #992 | 1275.0 | 78,500 | 20.5 | " | 0.64 ± 0.13 | " |

¹ For Ni, col. (6) = $0.1 \times 0.917 \times \text{col. (4) numeral} \times \text{col. (5) numeral}$. (Assume Ni = 1%)

² Estimate based on cosmic spherule counts.

³ For Ir, col. (6) = $1.95 \times 10^{-3} \times 0.917 \times \text{col. (4)} \times \text{col. (5)}$. (Assume Ir = 514 ppb)

TABLE XVI
COSMIC DUST ACCUMULATION RATES IN ANTARCTICA

A. Estimates Based on Nickel Concentrations

| (1) | (2) | (3) | (4) | (5) | (6) | (7) |
|---|--------------|--------------------|---------------------------------|--|---|----------------------------|
| Sample | Depth (m) | Age (years b2k) | Ni conc. ($\mu\text{g/l}$) | Ice accum. rate (cm/yr) | Cosmic dust accum. rate ¹ ($\mu\text{g/cm}^2/\text{yr}$) | Reference |
| Amundsen-Scott Station (South Pole) | 1 | 30 | 0.1 ± 0.06 | 6.0 | 0.06 ± 0.036 | (Hanappe et al., 1968) |
| Plateau Station 79°S, 40°E | 1 | 40 | 0.12 ± 0.06 | 2.8 | 0.034 ± 0.02 | " |
| Byrd Station, Antarctica <u>80°S, 119°W</u> | 10 | | | --- | $0.036^{(2)}$ | (Thiel & Schmidt, 1964) |
| #422 | 700.8 | 7,500 | 0.07 | 12.8 | <0.09 | This work |
| #552 | 897.5 | 9,600 | 0.12 | 12.8 | <0.15 | " |
| #1016 | 1585.0 | 31,000 | 0.25 | 7 | 0.18 ± 0.04 | " |
| #1016-B | 1585.15 | 31,000 | 9.7 | 7 | 6.8 ± 1.4 | " |
| #1016 plus #1016-B | } 1585.0 | 31,000 | 0.64 | 7 | 0.45 ± 0.09 | " |

B. Estimates Based on Iridium Concentrations

| (1) | (2) | (3) | (4) | (5) | (6) | (7) |
|------------------------------------|--------------|--------------------|-------------------------------|--|---|------------------------------|
| Sample | Depth (m) | Age (years b2k) | Ir conc. (pg/l) | Ice accum. rate (cm/yr) | Cosmic dust accum. rate ³ ($\mu\text{g/cm}^2/\text{yr}$) | Reference |
| Dome C 75 S, 124 W | ----- | 10 | 0.31 ± 0.12 | 3.6 | $0.0022 \pm .0008$ | (Takahashi, et al., 1978) |
| Byrd Station <u>80°S, 119°W</u> | | | | | | |
| #422 | 700.8 | 7,500 | 11.4 | 12.8 | 0.28 ± 0.05 | This work |
| #552 | 897.5 | 9,600 | 13.7 ± 3.4 | 12.8 | 0.34 ± 0.08 | " |
| #1016 | 1585.0 | 31,000 | 58 | 7 | 0.79 ± 0.16 | " |
| #1016-B | 1585.15 | 31,000 | 1100 | 7 | 15 ± 3 | " |
| #1016 plus #1016-B | 1585.0 | 31,000 | 100 | 7 | 1.5 ± 0.3 | " |

¹ For Ni, col. (6) = $0.1 \times \text{col. (4) numeral} \times \text{col. (5) numeral}$. (Assume Ni = 1%)

² Estimate based on cosmic spherule counts.

³ For Ir, col. (6) = $1.95 \times 10^{-3} \times \text{col. (4) numeral} \times \text{col. (5) numeral}$. (Assume Ir = 514 ppb)

knows of no explanation for this discrepancy of one to two orders of magnitude. Therefore a more "conservative" estimate derived from the results of the other investigators mentioned above has been adopted as a Holocene baseline.

The Test. To determine the concentration of cosmic dust in Wisconsin Period ice, a total of 12 samples of glacial dust were analyzed. Eight of these were filtered from ice samples from the Camp Century core, and four were filtered from ice samples from the Byrd Station core. All samples except for three were provided through the courtesy of Dr. Lonnie Thompson (Institute for Polar Studies, Ohio State University). These were dust samples that he had filtered in the course of an earlier study in which he stratigraphically determined microparticle concentrations in glacial ice spanning the Wisconsin and Holocene (Thompson, 1977b). The other 3 dust samples were prepared by the author from ice samples that were cut from the Camp Century ice core and were provided through the courtesy of the Department of Geological Sciences, State University of New York at Buffalo.

The NAA technique was used to analyze these ice dust samples for the following elements: Ir, Au, Ag, Fe, Co, Ni, Ba, Sb, Sn, Sc, Hf, Cs, La, Ce, and Tb. The results of these elemental evaluations pertain specifically to the insoluble dust fraction. Iridium, which is chosen here as a primary indicator of cosmic dust, is highly insoluble even in acidic solutions. Hence it is unlikely, even for the short time that the meltwater was in liquid form, that much Ir was lost.

Table XVII presents some vital statistics for these samples. The weights for samples 959, 960, and 962-2 were determined by weighing the filter papers before and after filtration using a Kahn electrobalance and following the procedure described in Subsection 12.1.3 below. The weights of the other Camp Century and Byrd core samples could not be determined in this way since the filter papers on which the samples resided had not been preweighed. Consequently, the weights of these samples had to be determined by an indirect method. For samples 422, 552, 1016, 1016-B, 949, 955, 969, and 992 the dust weights were estimated on the basis of the NAA iron weights determined for the samples. By making certain assumptions in regard to the percent concentration of Fe expected to be found in this sample, the total sample weight could then be derived. Justification for the choice of Fe concentration values is addressed in the footnotes to column (6) of Table G-IV in Appendix G.

For Sample #962-1 (subsamples a and b) the total sample dust weight was estimated from the weight of Sn in the sample, determined through NAA, and by assuming that the dust from this sample had a tin abundance of $60 \pm 15\%$ [see update on]. This Sn concentration is a bit high in comparison to concentration values which Thompson (1977b, Appendix D) found in individual microparticles chosen from the sample and which average to $16 \pm 11\%$ abundance for Sn. But the Fe concentration of $\sim 2.5 \pm 1.0\%$ here estimated for this sample falls in the range of the Fe abundance values that Thompson reported for selected microparticles, which average to $2.1 \pm 4.8\%$.

[UPDATE: Originally, I had estimated that tin was present at a concentration of $40 \pm 20\%$ in these samples. However, in 1984, one year after the dissertation was published, I had arranged to have energy dispersive X-ray analysis measurements performed on sample #962-1 and on the basis of these measurements determined that the Sn in this sample had an abundance of $60 \pm 15\%$; see update at the end of this chapter (p. 357). This new more accurate assessment of the Sn abundance resulted in a 50% increase of the originally estimated $40 \pm 20\%$ value. Since the total dust weight estimated for this sample became correspondingly revised downward by 50%, the abundances I had originally estimated for the other elements in this sample correspondingly increased by 50%.]

To determine the exact percentage of Sn in Sample 962-1, I had initially planned to obtain a sample of ice immediately adjacent to Thompson's sample, to then filter this ice and

TABLE XVII
GLACIAL ICE DUST SAMPLES THAT HAVE BEEN ANALYZED:
PERTINENT INFORMATION

| (1) | (2) | (3) | (4) | (5) | (6) | Analyzed Portion | | (9) | (10) |
|------------------------|----------------|-----------------|--------------------|------------|------------|------------------|-------------|---------------------|------|
| Core Tube Number | Depth (meters) | Age Years (b2k) | Filter.Irr by: run | Vol.. (ml) | Frac.. (%) | Vol. (ml) | Weight (µg) | Dust Concen. (µg/l) | |
| A. Byrd Station | | | | | | | | | |
| 442 | 700.80 | 7,500 | L.T. II | 267 | 2 | 66.75 | 1.15±0.4 | 17±5 | |
| 552 | 897.50 | 9,600 | L.T. II | 82 | 5 | 41.00 | 2.7±0.8 | 66±20 | |
| 1016 | 1585.00 | 31,000 | L.T. I | 214 | 10 | 214.00 | 80±20 | 370±90 | |
| 1016-B | 1585.15 | 31,000 | L.T. I | 19 | 5 | 9.50 | 410±60 | 4300±6k | |
| B. Camp Century | | | | | | | | | |
| 949 | 1212.0 | 38,650 | L.T. I | 144 | 50 | 72 | 235±50 | 3260±700 | |
| 955 | 1221.0 | 45,000 | L.T. II | 89 | 50 | 44.5 | 23.4±4.7 | 525±100 | |
| 959 | 1226.2 | 49,000 | P.L. II | 175 | 100 | 175 | 541±7 | 3090±40 | |
| 960 | 1227.7 | 49,500 | P.L. II | 228 | 80 | 182.4 | 449±7 | 2460±40 | |
| 962-1a | 1230.5 | 50,500 | L.T. I | 130 | 40 | 52 | 80±20 | 1530±380 | |
| 962-1b | " | " | L.T. II | " | 1.2 | 1.58 | 2.4±0.6 | " | |
| 962-2 | 1231.5 | 51,300 | P.L. II | 186 | 100 | 186 | 466±7 | 2510±40 | |
| 969 | 1241.0 | 58,700 | L.T. II | 39 | 50 | 19.5 | 6.7±1.3 | 345±70 | |
| 992 | 1275.0 | 78,500 | L.T. I | 81 | 50 | 40.5 | 132±26 | 3260±700 | |
| C. Agassiz | | | | | | | | | |
| 80 | 100.9-102.4 | 700 | ---- | -- | 825 | ---- | 825 | ---- | |
| 83 | 105.4-106.9 | 745 | ---- | -- | 798 | ---- | 798 | ---- | |
| 84 | 106.9-108.4 | 760 | ---- | -- | 829 | ---- | 829 | ---- | |
| 80+83+84 | ---- | ---- | P.L. I | 2452 | 100 | 2452 | 760±5 | 310±2 | |
| 85 | 108.4-109.9 | 775 | ---- | -- | 842 | ---- | 842 | ---- | |
| 86 | 109.9-111.4 | 790 | ---- | -- | 820 | ---- | 820 | ---- | |
| 87 | 111.4-112.9 | 810 | ---- | -- | 763 | ---- | 763 | ---- | |
| 85+86+87 | ---- | ---- | P.L. I | 2425 | 100 | 2425 | 1793±5 | 740±5 | |
| 225 | 313.1-314.6 | >10 k | P.L. I | 716 | 100 | 716 | 2838±5 | 3960±26 | |

Table Note: Column (1) of this table lists the ice core tube number from which each sample was taken. Column (2) gives the sample depth in meters. Formerly published logbook depths are here converted to corrected depths by subtracting 3 to 4 meters depending on the depth. Column (3) indicates the corresponding age of each sample based on the time-depth relationships given in Appendix E. Column (4) indicates who filtered the sample; "L.T." indicates that Thompson had filtered it some years ago for his microparticle study, while "P.L." indicates that it was filtered in this study. Column (5) indicates whether the dust sample was analyzed in the first or second irradiation run. Column (6) indicates the volume of ice core meltwater that was filtered onto each filter paper sample. Columns (7), (8), and (9) indicate the fraction of each filter paper that was analyzed (irradiated), the amount of meltwater which the analyzed fraction represents, and the weight of the analyzed sample. Column (10) gives the dust concentration in micrograms of dust per liter of ice.

gravitometrically determine the weight of its dust, and finally to analyze the resulting dust sample by NAA. However, such an ice sample was not made available by the ice core laboratory at Buffalo. Instead, a sample was mistakenly supplied (#962-2) that was 110 cm below Thompson's sample, and subsequent analysis conducted by the author revealed that this particular ice sample did not contain any tin.

Two batches of glacial ice dust samples, both containing samples from the Byrd and Camp Century ice cores, were analyzed with a sequence of two irradiations. The procedure followed in preparing and analyzing these samples is described below beginning with the first irradiation run.

12.1.2 First Irradiation: Experimental Procedure and Preliminary Findings

Sample Preparation. In the first irradiation five glacial ice dust samples were analyzed. Two were from the Late Wisconsin stage portion of the Byrd Station ice core, of which one was filtered from a 36 cm long section of ice core (from tube #1016) and the second was a 1.3 cm wide dust band filtered separately from the 36 cm section; see Figure 12.4 (p. 346). Also, there were three samples from the Late Wisconsin section of the Camp Century ice core: samples 949, 962-1a, and 992. All five were sent from the Institute of Polar Studies.

The filters were rolled up (dusty side inward) and each was inserted into a 4 mm ID high purity quartz irradiation vial. The vials were numbered with a tungsten carbide engraver. They were then put into a vacuum oven and were heated at 160 – 170° C at half of normal atmospheric pressure for 15 hours. In this way the filter papers became slowly carbonized without spontaneously combusting. This was done with the intention of preventing the carbonized remains from sticking to the vial walls. Subsequently, the open end of each vial was sealed shut with an oxy-hydrogen torch. This was done while the vial was maintained under a vacuum.

In addition, several quantities of USGS PCC-1 standard and several quantities of a mixture of a powder containing gold and iridium diluted in a silica base were weighed, inserted into quartz vials (in powder form), and sealed under a vacuum. Extreme precautions were taken to avoid possible contamination of the glacial dust samples by the standards.

Irradiation and Counting. The samples and standards were shipped to the Missouri University Research Reactor (MURR) for neutron activation analysis. Under the supervision of James Carni, they were irradiated for 1000 hours at a neutron flux of 6.8×10^{13} n/cm²/s. The irradiation period terminated on July 29, 1981.

During the 42 day period that they were in the reactor, the vials and their contents were made radioactive. A certain fraction of their atomic nuclei had become "activated" to unstable isotopic states through the absorption of a neutron. These unstable isotopes upon decay would release beta and gamma radiation at certain characteristic energies. Consequently, these neutron activated samples could each be analyzed for their chemical composition by studying their characteristic gamma ray spectra. Such spectra could be obtained by counting the numbers of gamma rays given off, over the range 50 – 2000 keV, in each of a series of ½ – 1 keV energy bins. Four days after removal from the reactor the quartz vials were counted at MURR. Each vial was counted for 5400 seconds at a distance of 14" from the face of a Ge-Li detector having a 1 keV energy resolution.

After this preliminary count, the samples were removed from their quartz vials and transferred into clean half-dram polyvials. This operation was done at MURR by James Carni. Working inside a glove box, each quartz vial was broken open and the bulk of its carbonized contents were transferred to a clean polyvial. Residual particles of carbon sticking to the walls of the quartz vial were removed with the assistance of disposable hypodermic needles. Following this, the inside of each quartz vial was rinsed with dilute nitric acid. This

solution was administered to and drawn from each quartz vial with the aid of a hypodermic syringe. The wash solution was then transferred to the appropriate polyvial to become mixed with its corresponding filter sample. The standards, which were in a powder form, were also transferred to clean polyvials. Sample transferral efficiency is estimated to have been greater than 95%.

About 6 – 7 days after irradiation, the dust samples and standards were again counted, this time without the interfering background of the irradiated quartz vials. Each polyvial was counted for 6000 seconds at a distance of 7" from the detector face. This "early count" was done mainly to detect short half-life elements such as Au and Mo. The samples and standards were then put into temporary storage for about 1 month to give the short half-life elements a chance to decay. Then the vials were sent to Portland State University (PSU) where they were received by the author on September 14, 1981.

On September 16, 1981, the samples were counted on the gamma ray spectrometer of the PSU Geochemistry Laboratory to determine the presence of long lived isotopes, such as iridium and some of the rare earths [see Figures 12-A and 12-B]. The samples were counted for a period of 6 hours to one day with the sample positioned from 1 to 3 cm from the detector face. The results of these measurements are presented in Tables G-I through G-XV of Appendix G together with the results of the second irradiation. Detailed discussion of both sets of results are presented in Subsection 12.1.4. However, the following general summary of the first irradiation is presented to indicate the basis for the decision to make a second irradiation of glacial ice dust samples.

Preliminary Findings. The first irradiation was exploratory in nature. It was not known in advance exactly what to expect since NAA had not previously been done on ice from the Wisconsin stage. However, it was expected that an unusual quantity of tin would be found in Sample #962-1, on the basis of Thompson's (1977b) earlier X-ray analysis of microparticles from the sample. Indeed, Sn was found in great abundance in this sample and in much lesser amounts in some of the other samples. Most surprising of all was the discovery that Sample #962-1a also contained a very high concentration of gold. This was interpreted as

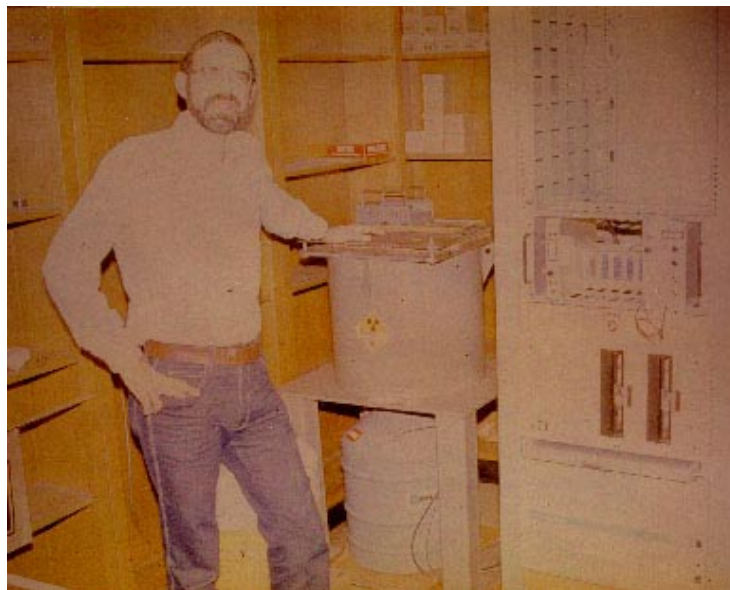


Figure 12-A. Paul LaViolette in the Portland State University Geology Department standing next to the Tracor-Northern gamma ray spectrometer used in this study.

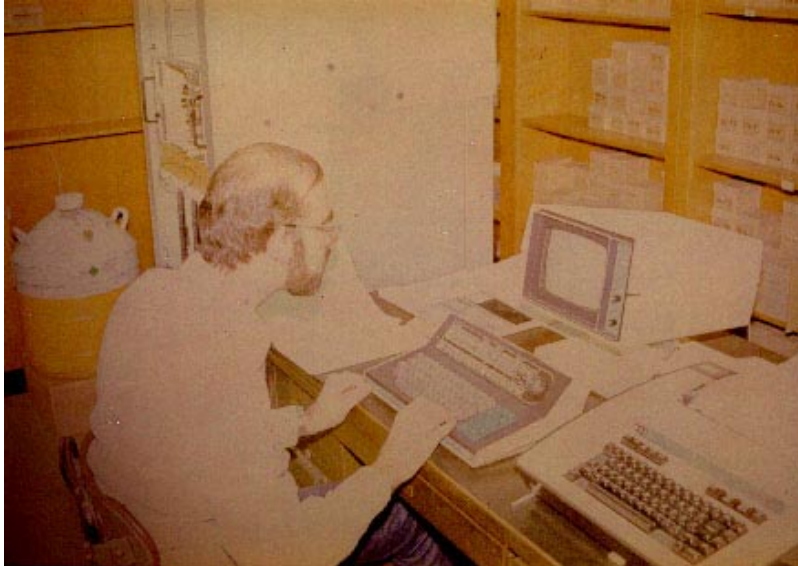


Figure 12-B. Paul LaViolette working at the Tracor-Northern computer terminal displaying NAA gamma ray spectra on the monitor.

an indication of the presence of an unusually high concentration of cosmic dust in this sample since Au is known to be more abundant in extraterrestrial material.

It should be pointed out that a special effort was made to detect gold by arranging for an early gamma ray count of the irradiated dust samples, since gold has a much shorter half-life than iridium or nickel. Prior to conducting these measurements, I had inferred that gold might be an important component of cosmic dust fallout since Ganapathy and Brownlee (1979) detected elevated amounts of gold in two interplanetary dust particles that they analyzed. As was mentioned in Chapter 8 (Section 8.3), they found gold to be enhanced above C-1 chondritic abundance by 34 ± 11 fold in these particles (~1400 times terrestrial abundance). They attribute the gold enhancement in their particles (which they had sputter coated with paladium) to sample contamination. However, it is also possible that their gold determination could reflect the actual composition of these particles. If so, then this raises the question of whether cosmic dust is gold-enriched relative to meteoritic material. Future measurements of interplanetary dust particles collected from the stratosphere should clear up this question.

As another major discovery, the results of the first irradiation indicated that all of the samples had high levels of iridium. The high Ir levels implied that cosmic dust was being deposited in Late Wisconsin ice at a much faster rate than during the Holocene. This finding, together with the discovery of the gold anomaly, not only constitutes strong evidence in support of the GEH, but also represents a significant scientific discovery in itself.

However, with the completion of the first irradiation, this conclusion could not be drawn without reservation since the possibility existed that the filter **paper** itself could have contained an iridium contaminant. Blanks of the original batch of Millipore filter paper used by Thompson in the Ohio State study had not been irradiated for analysis in this first run. Rather, two blank Millipore filters from a different batch, one obtained in Portland, had been irradiated. Although these blanks showed iridium levels far below those of the measured samples, less than 10^{-14} grams as compared with 10^{-12} to 10^{-11} grams of Ir in the samples, discussions with other investigators revealed that contaminants in Millipore filters could vary markedly from batch to batch. Hence, the blanks that were tested may not have been representative. So to clear up this question, a new sample irradiation was considered to be necessary.

In addition, a second irradiation was deemed necessary to determine whether the Sn in Sample #962-1a was isotopically fractionated. For example, it is known that elements found in meteorites often have isotopic ratios that differ slightly from the ratios found in terrestrial material. These differences, which are normally detected through the use of mass spectrometry techniques, are usually on the order of a few tenths of a percent of terrestrial ratios, although isotopic anomalies as high as 110% have been found in interstellar carbon grains embedded within chondritic meteorites (Swart et al., 1983). Neutron activation analysis may be used to detect the ratios of several isotopes of Sn. However, even with the use of Sn standards, the error inherent in this technique would be on the order of $\pm 5\%$. Still, it was thought that it would be worthwhile to do a second irradiation of the anomalous tin sample along with a few Sn standards for comparison.

Finally, a second irradiation also would have provided an opportunity to analyze ice samples in the vicinity of, or directly adjacent to, Sample #962-1 (1230.5 m), thus allowing a more detailed study to be made of the temporal variation of the elemental concentrations in this critical portion of the ice core. Future geochemical analysis of Camp Century ice core dust samples (1145–1170 meters depth) should provide much needed information of cosmic dust deposition rates during this terminal portion of the Wisconsin Ice Age.

12.1.3 Second Irradiation: Experimental Procedure and Preliminary Findings

Sample Preparation. In the second irradiation, 8 glacial ice dust samples were analyzed. Two were from the mid Holocene section of the Byrd ice core, and the remaining 6 were from the Camp Century ice core. Of the Camp Century ice core samples, 3 were filtered by the author from samples of glacial ice. The remaining Camp Century samples and the Byrd core samples were provided by Dr. Thompson. Most of Sample #962-1, consisting of half of a filter paper, was analyzed in the first irradiation as Subsample #962-1a. However, a small bit remaining from the original sample did not become irradiated. A portion of this remaining filter paper (2 mm \times 2 mm, ~ 0.2 mg in weight) containing glacial dust was coded as Subsample #962-1b and was irradiated along with the other dust samples.

In addition, a few blank 25 mm diameter Millipore filter papers were selected from the same batch of filter papers that Dr. Thompson had used in filtering the other Byrd and Camp Century dust samples in his 1977 study. One of these (weighing 29 mg) was selected as a filter blank. A second filter blank consisted of a clean corner (2 mg piece) of filter paper broken off from Sample #552, a glacial dust sample which Thompson had filtered from Holocene ice of the Byrd core.

Finally, a number of standards were prepared. These included several W-1 standards on the order of 15 mg each, two Sn standards (~ 20 μg each) made from slivers of tin foil, an Sb standard (~ 60 μg) made from a grain of antimony metal, and a gold standard (~ 20 μg) made from a sliver of gold. The weights of the metal standards were determined on a Kahn electrobalance. In addition, a small portion (~ 70 μg) of an 1865 ppm Ir standard (metal powder diluted in silica) was weighed and encapsulated in plastic. However, as in the first irradiation, this Ir standard proved not to be trustworthy due to uneven mixing of the Ir metal powder in the silica base. Therefore, this standard was not used. Sample Ir concentrations, therefore, were determined through the use of a flux calculation procedure; see Appendix G.

Procedure Followed in Filtering Three Glacial Ice Dust Samples. Three samples of glacial ice from core tube numbers 959, 960, and 962 of the Camp Century ice core were shipped to Portland in an insulated ice pack container on November 11, 1981. All samples were half core sections, in cross section. The sample from tube #962 was 5 cm long and came from a portion of that ice core about 1.1 meters below the section sampled in the study

by Thompson (1977b). The sample from tube #960 was 8 cm long and came from a portion of the ice core directly below a section sampled in the study by Cragin, Herron, Langway, and Klouda (1977), and 3 meters above Thompson's sample from core #962. The sample from tube #959 was 5 cm long and was taken from an ice core position that was 1½ meters above the #960 sample.

These ice samples were processed by the author in a clean, dust-free microbiological laboratory at PSU. The surface of each ice sample was washed to remove any external contamination, such as drilling fluid. This was done by three successive washings with acetone followed by a rinse of distilled water prefiltered through 0.45 µ pore size Millipore filter paper. Upon completion of this rinsing, the ice sample was placed in a 500 ml beaker that had been prerinsed with filtered distilled water. The sample was melted in this beaker over a warm hot plate and filtered onto a 25 mm diameter, 0.45 µ pore size Millipore filter. The filtration was carried out by use of a syringe-pressure-type filtering technique. A portion of the meltwater was drawn into a 10 ml syringe and transferred to a filter holder assembly through an inlet to which the conical syringe nozzle adapted. The filtrate was discharged into a 100 ml graduate which was used to determine the liquid volume prior to transferral of the filtrate to a storage beaker. The unfiltered meltwater was agitated periodically with a rubber policeman to keep the particles in suspension.

The syringe-pressured filtration process was then repeated using the same filter paper. This second filtration reduced the possibility of (1) heavy particle loss due to settling in the meltwater beaker, and (2) small particle loss through the filter pores prior to build up of the sample cake on the filter. Both the filtered meltwater and the washwater were bottled and labeled for storage. All glassware and utensils were rinsed with 3N HCl prior to the first and third sample filtrations and with distilled water followed by filtered distilled water prior to each filtration. A control filtration was also performed in which a measured amount of filtered distilled water was passed through a preweighed blank Millipore filter paper. This filter was treated and measured in the same way as the other samples.

All weighings were done on an automatic Kahn electrobalance which was provided for use through the courtesy of Mr. Ken McDonald of the Oregon Department of Environmental Quality. The standard samples for tin, antimony, iridium, and gold metal were also weighed on the Kahn balance. Each filter paper was weighed before and after filtration to determine the net sample weight. Weighings were determined to be accurate to within ± 7 µg, i.e., to within about 1½ % of the net sample weight. Usually at least two determinations were made for each filter weighing to ensure that the filter had stabilized its moisture content with the ambient humidity. Several control filters were also weighed between sample filter weighings to determine the amount of weight increase or decrease caused by humidity change so that the sample filter weighings could be appropriately adjusted. Room humidity was also recorded during the weighing sessions. Care was taken at all times to avoid outside and cross contamination of the samples by using a regimented procedure for handling and storing the samples.

The same procedure used in the first irradiation was used in the second irradiation to carbonize the filters in the quartz vials and to vacuum seal the vials.

Irradiation and Counting. This batch of samples and standards were sent to MURR where they were irradiated for 100 hours at a neutron flux of 2.65×10^{13} n/cm²/s. The irradiation period was terminated on December 7, 1981, and on December 9th the irradiated quartz sample vials were shipped in a lead container to Portland State University. Upon receipt, it was observed that several of the samples were too hot for easy handling and counting due to high sodium activity. In particular, the samples from the Ohio State collection contained a salt residue. The glacial meltwater from which they had been filtered

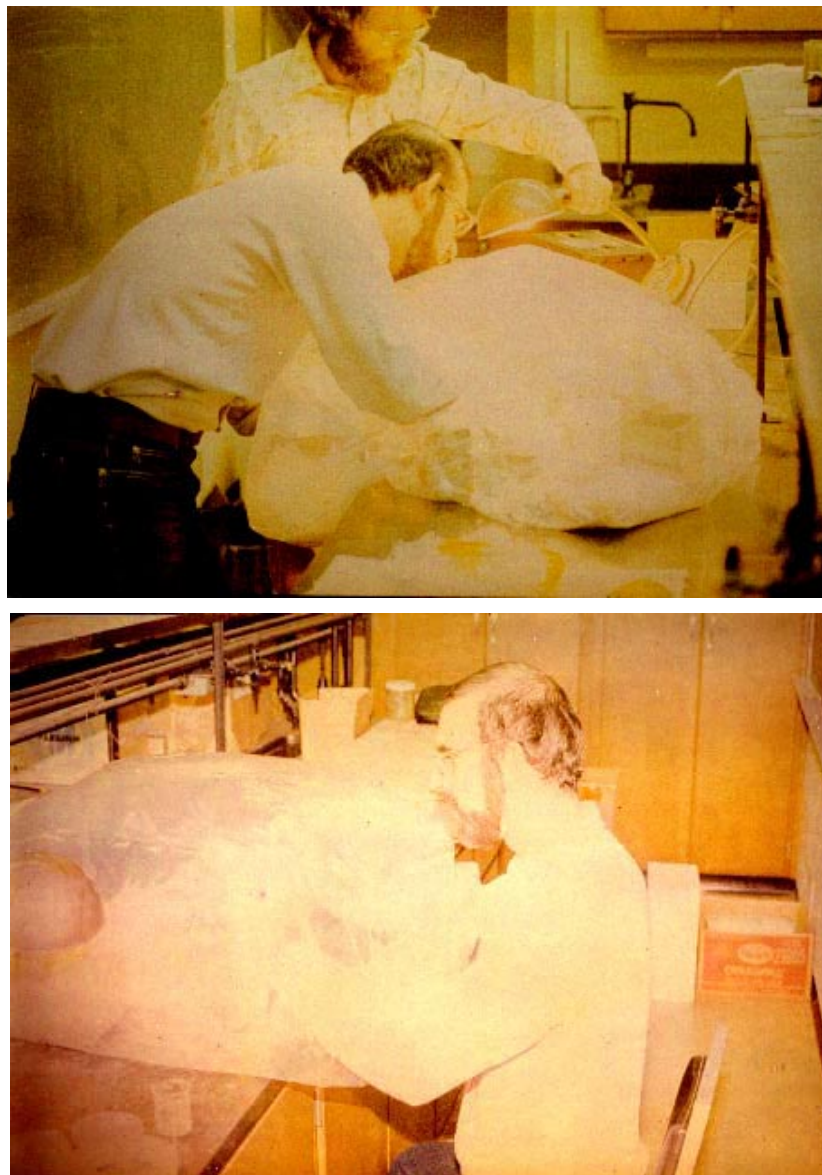


Figure 12-C. Paul LaViolette working inside a glove bag to transfer radioactive samples to plastic vials for gamma ray counting.

in Thompson's 1977 study had been treated with a 2% NaCl solution to prepare the meltwater samples for microparticle counting. Thus it was necessary to delay sample processing for a few days to allow this activity to decay out.

The author prepared the samples for counting by transferring them from their sealed quartz irradiation vials into $\frac{1}{2}$ " diameter plastic polyvials. He did this by working on the quartz vials one at a time inside a glove bag with a lead brick shield installed for radiation protection [see Figure 12-C]. He removed each vial from the lead storage container, broke it open, and transferred its contents to a polyvial. He then rinsed the quartz vial with dilute nitric acid to remove any remaining material and transferred the acid wash to the polyvial. He then heat sealed the polyvial and placed it inside a larger, 2 dram polyvial for counting.

Beginning 7 days after the irradiation, the author counted the samples for 2000 seconds at a distance of 1 cm from the detector face to determine the concentrations of gold and

molybdenum. Counting for iridium and other long lived isotopes was started about 30 days after irradiation. For this, the samples were counted 15 to 25 hours positioned 1 cm from the detector face. In addition, Sample #962-1 and the two tin standards were counted five times over a period of 3 months to look for evidence of any isotopic anomaly.

The detector efficiency for the counter was calibrated with the aid of a standard. With the sample positioned 1 cm from the detector face the efficiency is given by the expression: $\epsilon = 13.5 E^{-0.994}$, for $E > 150$ keV.

Preliminary Findings. Significant preliminary findings from the second irradiation include the following:

1. This second set of measurements confirmed the concentration peaks observed (for Sn, Sb, Ir, Au, Ag, and Ba) in the earlier irradiation of Sample #962-1a. Remeasurement of the unused portion of sample #962-1 (Subsample #962-1b) indicated concentrations which agreed well with elemental concentrations measured in the first irradiation (Subsample #962-1a), so that reproducibility of the overall procedure was confirmed.
2. No isotopic anomaly greater than $\pm 5\%$ was observable for the anomalous glacial dust sample (#962-1b), $\pm 5\%$ being the sensitivity limit characteristic of this NAA technique.
3. Irradiation of the Millipore filter media used in the Ohio State study confirmed the projection that filter contamination by iridium was essentially negligible ($< 4 \times 10^{-14}$ g) compared to the lowest observed iridium content (16×10^{-14} g) in samples prepared on this batch of filter material.

After it had been determined that the filter material was relatively free of Ir contamination, it was realized that the NaCl residue on the Ohio State filter samples could have constituted another potential source of contamination. So, to determine whether this was the case, a 1.3 gram sample of Fisher reagent grade NaCl and an iridium standard was irradiated in the Reed College reactor for 13 hours at a flux of $\sim 10^{12}$ n/cm²/s. About two weeks later (6/28/82), after the sodium activity had died down, the sample was counted on the PSU gamma ray spectrometer for about 3½ hours. The results of this analysis indicate that this brand of NaCl contains less than 0.16 ppb of Ir. If a similar upper limit is characteristic of the NaCl residue on the Ohio State glacial dust samples, then even on samples that had the highest NaCl weight in comparison to the measured Ir weight, the Ir contamination would be less than 10% of this measured iridium weight, hence insignificant.

12.1.4 Overall Results

Camp Century Ice Core. The elemental concentrations (in µg/lit of ice) determined in this study for a Late Wisconsin section of the Camp Century ice core are presented in Figures 12.1(a) and (b). See column (5) of Tables G-I through G-XV in Appendix G for a tabulation of this data. For diagrammatic clarity the elements that are observed to increase in sample #962-1 (relative to adjacent samples 962-2 and 960) have been plotted separately (Figure 12.1(a)) from those that are observed to stay the same or decrease (Figure 12.1(b)), Fe and Co, being two exceptions to this classification. The profile in Figure 12.1(a) marked "total" gives the total weight concentration of dust in the ice for each sample. Arrows pointing downward indicate that the plotted value is an upper limit. Exact weights could not be determined in these cases, either because the filter contributions were large or because the elements were below the threshold of detection; see Appendix G.

The elements Ba, Sn, Ni, Ag, and Ir show peak values in Camp Century samples #949 (~38,650 years b2k), #962-1 (~50,500 years b2k) and #992 (~78,500 years b2k). The Ir and Ni peaks in these samples, which are in the same ratio as are found in C-I chondrites, suggest

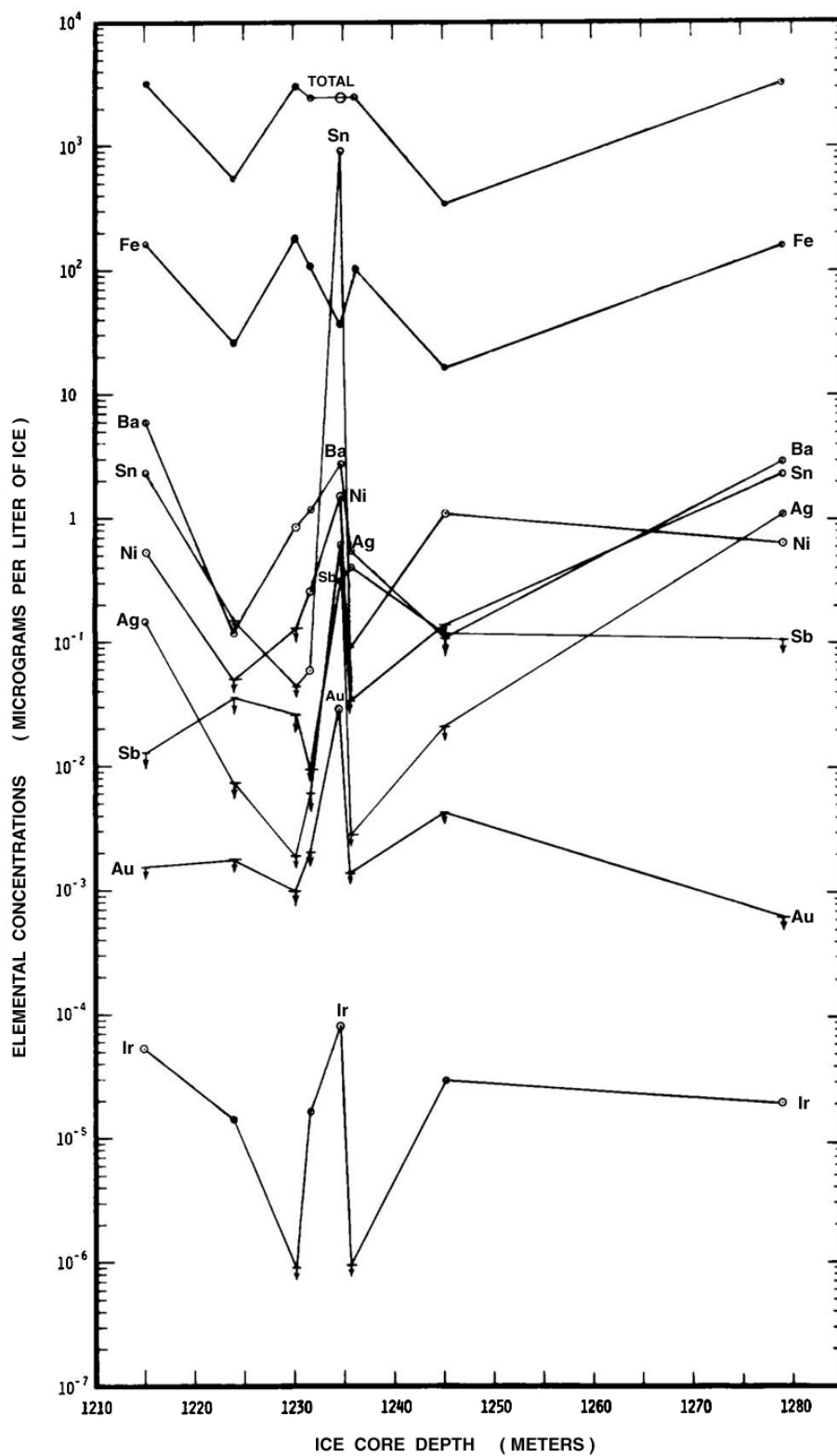


Figure 12.1(a). Elemental concentrations found in the Wisconsin section of the Camp Century ice core, spanning the period 38,650 to 78,500 years b2k. [Depth scale should be moved to the right by 3 meters.]

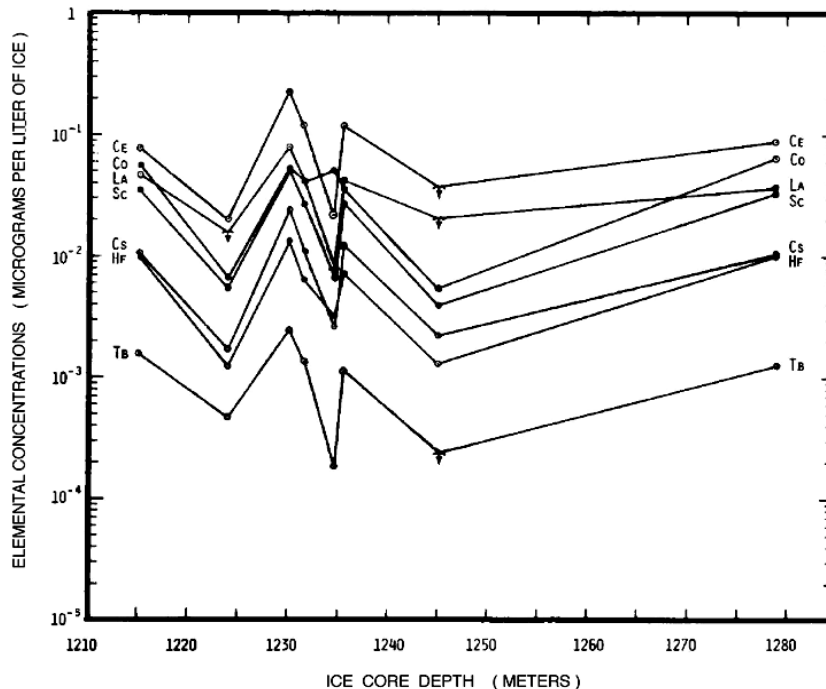


Figure 12.1(b). Elemental concentrations found in Camp Century ice spanning the period 38,650 to 78,500 years b2k. [Depth scale should be moved to the right by 3 meters.]

that Galactic superwaves passed by injecting cosmic dust into the solar system on several previous occasions. In the future, measurements should be made in ice core sections dating from 11,000 to 15,000 years BP to determine the nature of the temporal variation of Ir (cosmic dust) during this key period of ice age termination.

[UPDATE: After I had completed this dissertation, Beer et al. published their ^{10}Be data for the Camp Century ice core record.⁽¹⁾ This showed the presence of a major ^{10}Be peak spanning the period 44,000 to 38,000 years b2k (GICC05 chronology); see **Figure 12-D**. This is also detected in the Byrd and Vostok, Antarctic ice core records; see Chapter 8 update (**pp. 236 - 237**). Moreover following the publication of the accurate Summit, Greenland ice core chronology, which allowed the Camp Century ice core samples of the present study to be accurately dated for the first time, I realized that Sample #949, which contained high concentrations of Ir and Ni and dates at 38,650 years b2k, coincides with the ending of this major ^{10}Be peak. This provided strong confirmation for a key prediction of the Galactic Explosion Hypothesis, namely that cosmic ray volleys periodically pass by transporting cosmic dust into the solar system. There are few other phenomena that could explain the simultaneous increase of ^{10}Be , Ir, and Ni.

In the original dissertation I had assigned erroneously young dates to these Camp Century ice core samples since I had adopted the ice core chronology developed by L. Thompson (1977). Mistakenly dating Sample #949 at 14,200 years BP, I had concluded that the high Ir and Ni concentrations in that sample confirmed the GEH prediction that a superwave had passed through the solar system around 14,200 years ago. In retrospect, with the ice core samples now properly dated and with Be-10 measurements being available for this part of the ice record, we see that this high cosmic dust concentration data point does support the GEH prediction, but it correlates with a ^{10}Be peak registering an earlier superwave that passed us around 44,000 to 38,000 years ago. Confirmatory evidence of extraterrestrial material deposition during the ice age termination phase had to await my later discovery that

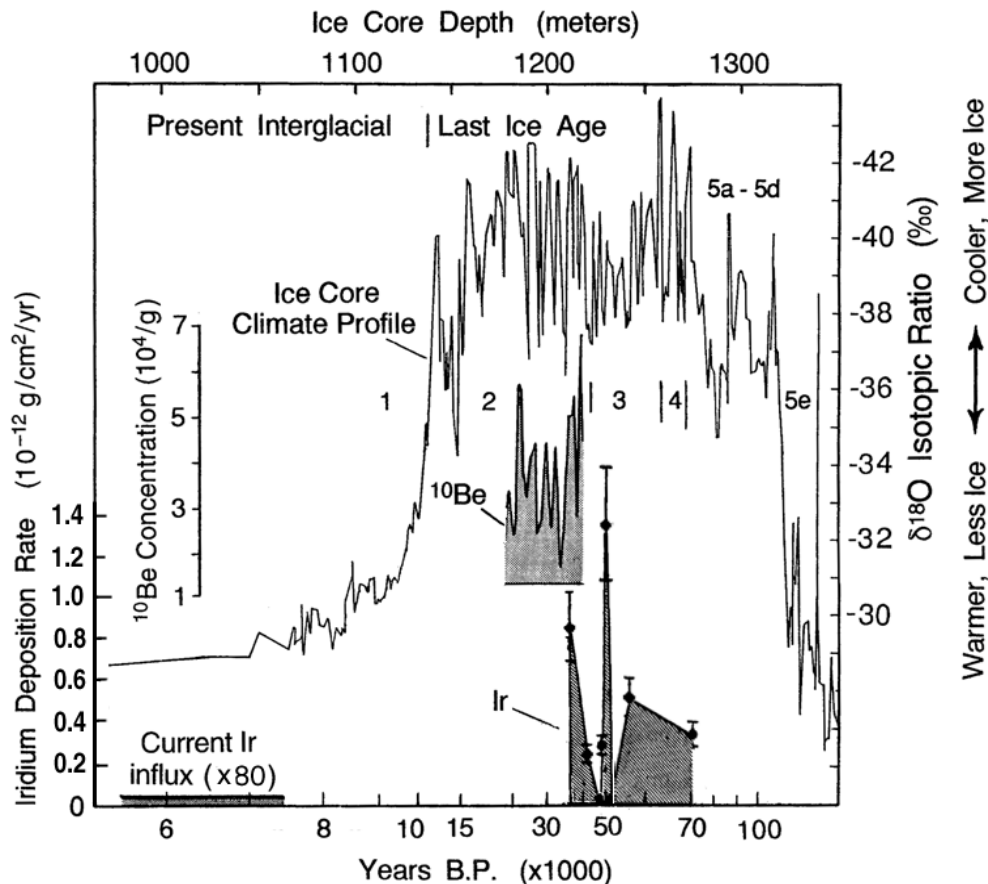


Figure 12-D. Time variation of cosmogenic beryllium and iridium in Camp Century, Greenland ice. Upper curve: the ice core oxygen isotope climatic profile. Middle curve: beryllium-10 concentration (Beer et al., 1992, fig. 3). Lower curve: rate of iridium deposition during the last ice age (this study) and in recent years (Takahashi et al., 1978).

acid residues in 15.85 kyrs b2k Antarctic ice had a solar cycle signature (p. 243) and the announcement in 2007 of the discovery of ET indicators at the AL/YD boundary (p. 360).

Figure 12-E presents a logarithmic plot of iridium concentration against nickel concentration for the eight Camp Century ice core dust samples (filled circles) and for a dust band (Sample #1016B) filtered from the Byrd Station, Antarctica ice core (open circle). Three of the eight Ir-Ni coordinate points are upper thresholds. A linear regression of the five good data points from the Camp Century ice core yields the relation:

$$\log \text{Ni}_{\text{conc.}} = 1.09 \pm 0.23 \log \text{Ir}_{\text{conc.}} + 1.16 \pm 0.33,$$

whose slope and y-intercept lie within 9% (0.4σ) of the slope and y-intercept for the cosmic C1 chondrite ratio:

$$\log \text{Ni}_{\text{conc.}} = 1.00 \log \text{Ir}_{\text{conc.}} + 1.29.$$

If the Byrd Station data point is included, the slope comes slightly closer to the slope for the C1 chondrite ratio, dropping to 1.07. This is quite close considering that there is a 10% variation in the Ni/Ir ratio just in going from a C1 to a C3 chondrite composition. Consequently, the conformance of this ratio is very strong evidence that the Ir and Ni concentrations are reliable indicators of the presence of cosmic dust and are not due to Ir or Ni sample contamination. (end of update)]

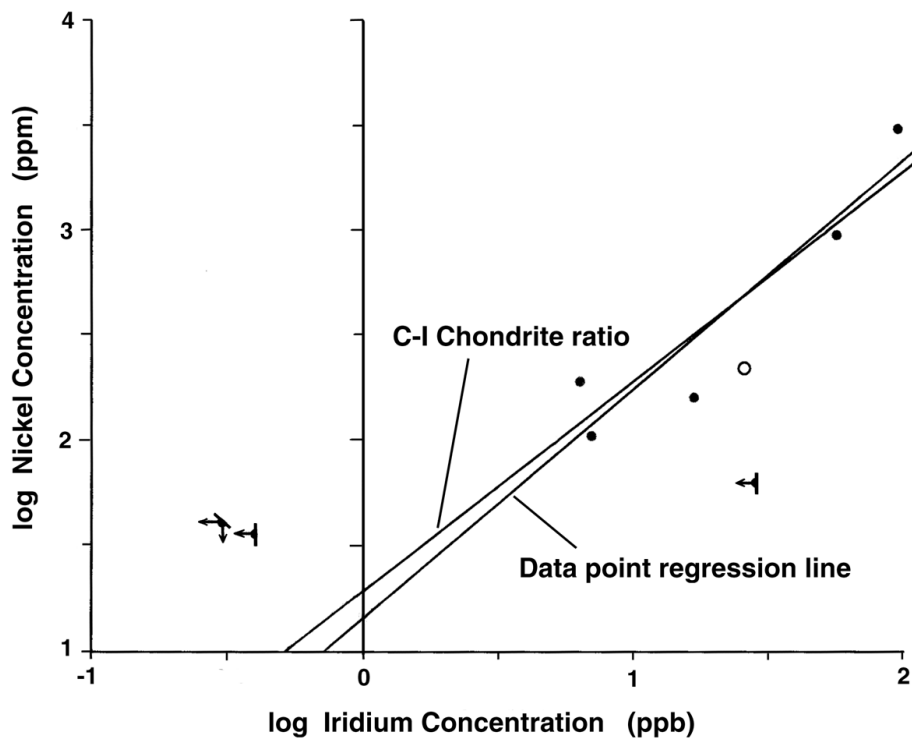


Figure 12-E. Log-log plot of Ir/Ni ratios found in dust from Camp Century, Greenland ice (●) and Byrd Station, Antarctica ice (o) over the period 78,500 - 38,650 years b2k. The slope of the regression line of the five Camp Century data points matches that for C-1 chondrite ratio.

Camp Century ice core sample #962-1 (50,500 years b2k) is of particular interest. Of all the elements that were measured, tin exhibits the most striking change. This element increases at least $4\frac{1}{2}$ orders of magnitude between samples 962-2 and 962-1! Although barium also increases, it is not a spike-like increase like that of Sn and other elements. Rather, after its initial increase, Ba exhibits a gradual decline extending over 10 meters of ice. For some elements, such as Au and Sb, it was not possible to obtain precise values for the majority of the samples due to high filter contribution. In future NAA work, glacial ice dust samples should be filtered on a different brand of filter paper than Millipore®. For example, Nucleopore® filters or Gia® teflon filters contain smaller quantities of the elements analyzed for in this study.

Another way of presenting the Camp Century ice core data is shown in Figure 12.2. The enhancement factors for the various elements have been plotted versus ice core depth; data from column (7) of Tables G-I through G-XV. Elements such as Fe, Sc, Hf, Cs, Ce, La, and Tb which decrease in concentration at a depth of 1230.5 meters (Figure 12.1(b)) are also found to have proportionately decreased enhancement factors at this depth (Figure 12.2). For example, by making a comparison between sample #962-1 and the average of samples #960 and #962-2, it is found that the concentrations in ice and enhancement factors of the rare earths Ce and Tb drop about 6.1 ± 0.6 fold. Cs and Sc decrease by about four fold.

The concentrations of rare earth elements in terrestrial material are enhanced by an order of magnitude or more as compared with their concentrations in chondrites, so such elements should serve as good indicators of the concentration of terrestrially derived material. Moreover, in terrestrial material, rare earth elements having larger ionic radii, such as La and Ce, are enhanced by a greater amount as compared with rare earth elements having small ionic radii, such as Tb. Such a terrestrial signature is found in the rare earths detected in the

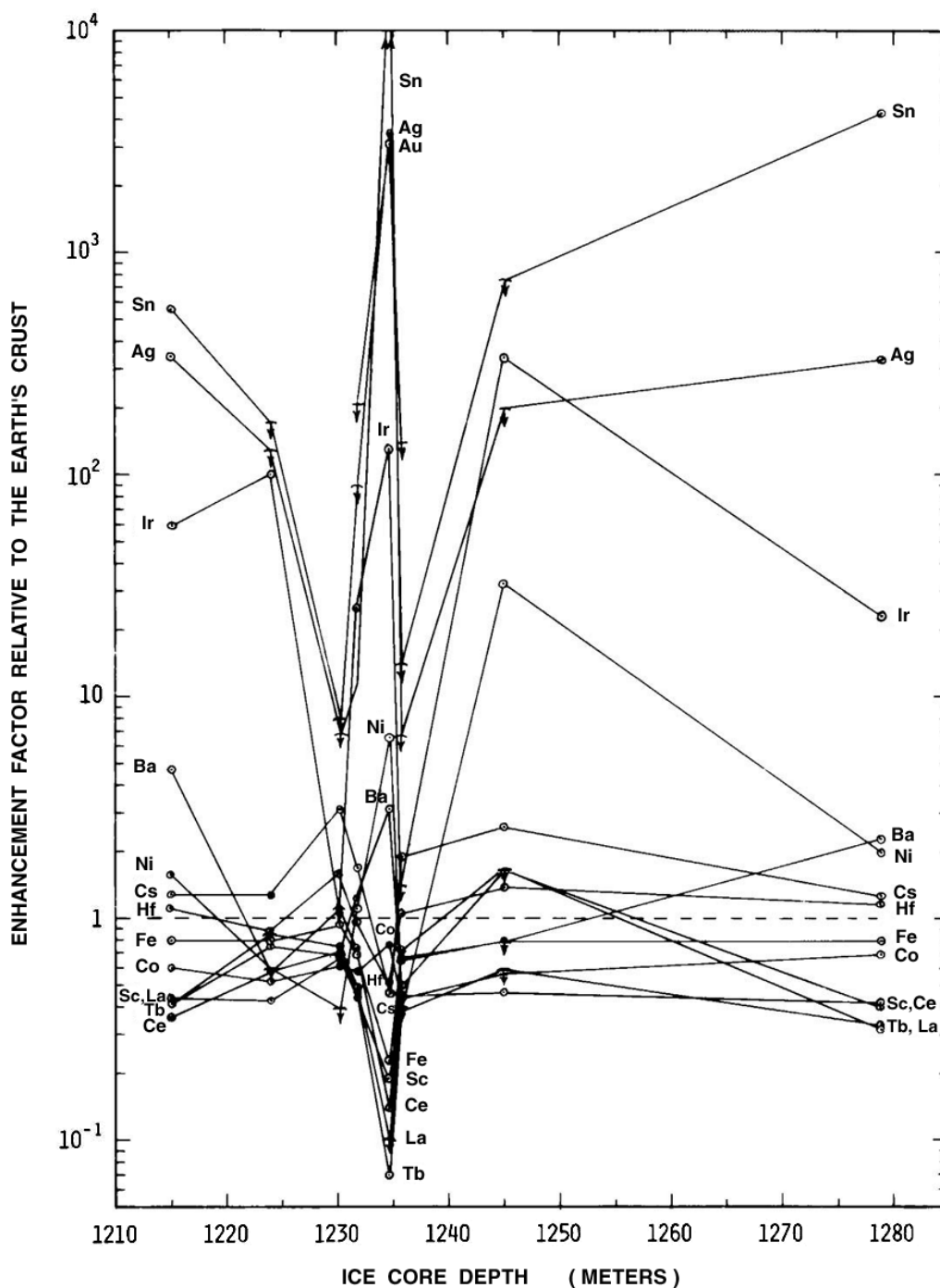


Figure 12.2. Enhancement factors relative to the Earth's crust for various elements found in dust samples filtered from the Wisconsin section of the Camp Century ice core. [Depth scale should be moved to the right by 3 meters.]

glacial ice samples. So, the rare earths La, Ce, and Tb should be good indicators of terrestrially derived material present in glacial dust samples. The dip at sample #962-2, therefore, appears to suggest that at the time when the anomalous sample was formed the accumulation rate of terrestrially derived wind blown dust decreased relative to the ice accumulation rate, and that in so doing this terrestrial dust constituted a smaller fraction of the

total dust sample. If it is assumed that terrestrial dust makes up at most ~100% of the dust in samples #962-2 and #960, and that its concentration dropped by 6.1 ± 0.6 fold, then at most about 410 ± 40 $\mu\text{g}/\text{l}$, or $27 \pm 3\%$ of the dust in sample #962-1 would be of terrestrial origin.

As seen in Figure 12.2, mirroring the elemental decrease in sample #962-1 there is an increase in the enhancement factors of certain other elements. For Ba and Ni the enhancements are not very significant, e.g., 3 and 8 respectively. However, some of the other elements achieve very high enhancement factors, e.g., 130 for Ir, 3200 for Au, 3400 for Ag, 670 for Sb, and 190,000 for Sn. It is reasonable to assume that the same influx of material that was responsible for producing these elemental enhancements was also responsible for causing the reduction in the terrestrial (rare earth) component. On the basis of the extent of the rare earth dilution mentioned above, the extraterrestrial component is estimated to compose about $73 \pm 3\%$ of the sample. This is roughly consistent with the estimate based on the content of Ir, Ni, and Sn found in this sample; see below.

A terrestrial airborne origin for the "*enhanced group*" (i.e., Sn, Sb, Ir, Ni, Au, Ag, and Ba) seems unlikely in view of the high enhancement factors for these elements. Moreover, contamination from the glacial bedrock also seems unlikely; see p. 225. The high levels of Ir and Au seem to suggest that the enhanced elements are of cosmic origin. For example, Ir and Au are normally enhanced by over 10^3 times and 40 times respectively in C-1 chondritic material (see Table XIII, p. 224). However, considering the other elements of the enhanced group, it is noted that Ag, Sn, and Sb are just about as abundant in chondritic material as in crustal material, and Ba is depleted by about 30 fold in chondritic material relative to crustal material. Thus if all 6 of these enhanced elements have a common extraterrestrial origin, the source material cannot be considered to be typical of solar system material. As seen in Figure 12.3, when the dust concentrations of the enhanced group elements for Camp Century ice core sample #962-1 are normalized to abundances found in C-1 chondrites, Sn, Sb, Au, Ag, and Ba are found to be enhanced several orders of magnitude whereas the concentrations of Ir, Fe, Co, and Ni conform to an abundance pattern of about $9 \pm 3\%$ C-1 chondritic material. Thus the dust in #962-1 is best explained as being derived from *two* extraterrestrial sources, one being C-1 chondritic material composing about 9% of the sample, and the other being an anomalous extraterrestrial tin-rich source composing about 60% of the sample. The total extraterrestrial dust content for sample #962-1 is then estimated to be $69 \pm 15\%$ in agreement with the estimate based on the reduction in rare earth content.

Similar element concentration profiles constructed for samples #949 and #992 also indicate a lack of conformity to the C-1 chondritic pattern, with Sn and Ag being more than 4 orders of magnitude over abundant relative to the Ir and Ni. Sample #969 from the Camp Century core, however, does exhibit a C-1 chondrite-like signature for the elements Ir, Ni, and Fe implying that about 20 – 30% of this sample is made up of chondritic material.

In summary, the above evidence suggests that the bulk of the material composing the enhanced group (sample #962-1 dated at 50,500 calendar years b2k) very likely came from an extraterrestrial source, but that such a source was not typical of most material found in the solar system, such as meteorites, asteroids, or chondritic porous interplanetary dust particles. Rather, a source outside of the solar system is more likely. This material may have been derived from a nearby interstellar cloud or from a passing supernova remnant. If this dust were vaporized from cometary bodies originally circulating in the circumsolar cometary cloud, then these bodies must have had compositions differing substantially from the C-1 chondritic compositions inferred for currently observed comets. If this compositional anomaly found in the glacial record is indeed made up of extra-solar system dust, then its presence may be evidence of an earlier superwave passing the Earth 36,000 years prior to the 14,200 years BP superwave (i.e., around 50,500 years BP).

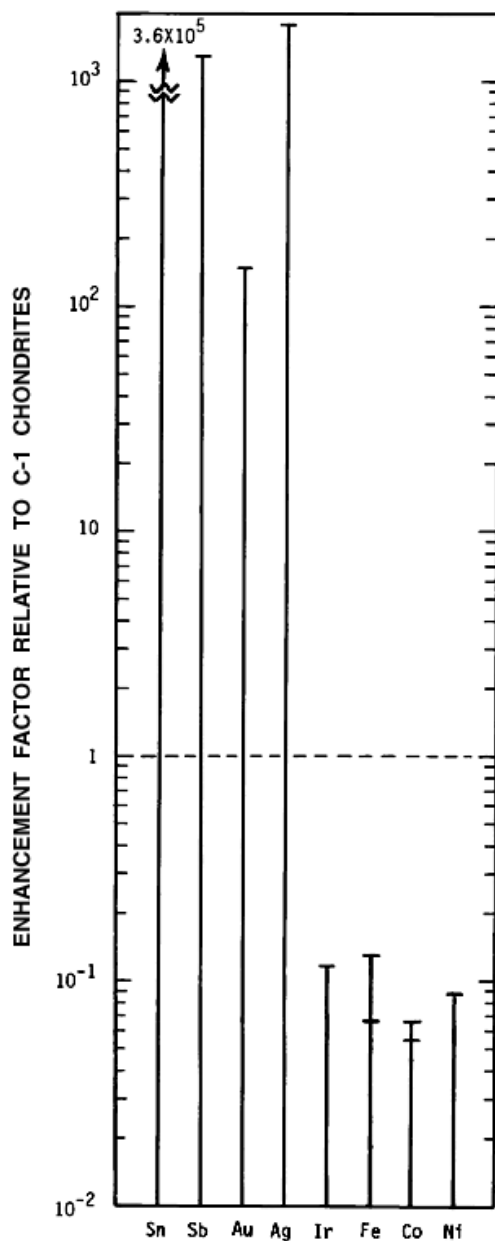


Figure 12.3. Elemental abundances relative to C-1 chondrites in the anomalous Camp Century ice core sample.

Byrd Station Ice Core Dust Band.* The histogram shown in Figure 12.4 (after Thompson, 1977b, p. 110) displays the number of microparticles $>0.62 \mu$ per $\frac{1}{2}$ ml of ice for a section of ice from tube #1016 from the Byrd ice core. The dust band sample that was analyzed (sample #1016-B) was a portion of the filtrate from Thompson's sample assay #28

* In the original version of this dissertation, I had described Sample #1016-B as being an "ash band." However, it should in fact be classified as a *dust band*. Its dust weight concentration in ice is here estimated to be 4.3 mg/l (see Table XVII). This is more characteristic of a dust band for which concentrations normally range <10 mg/l, as compared with ash bands which typically have ash concentrations of 1 gram per liter of ice and much larger dust particles ($\sim 50 \mu$ diameter).

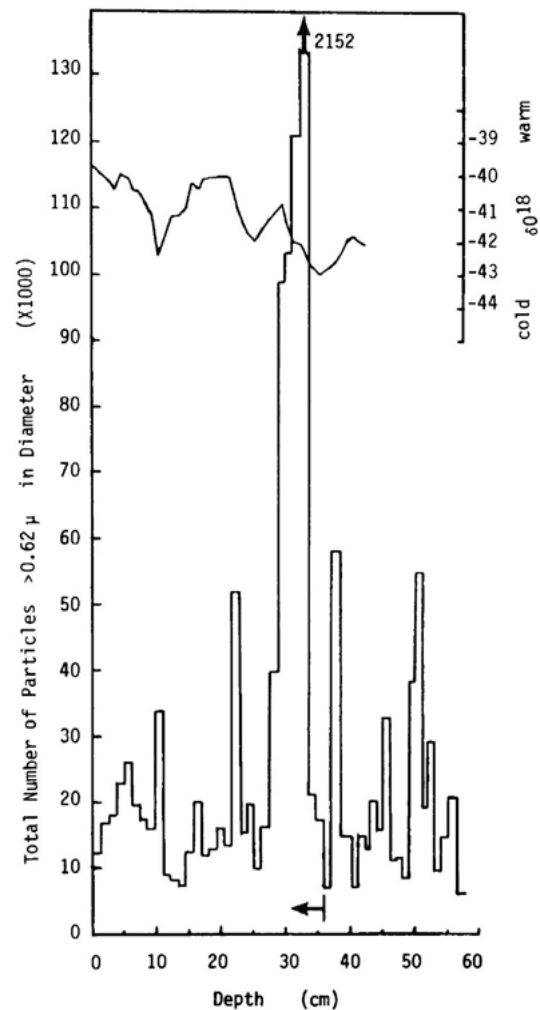


Figure 12.4. Microparticle profile for a section of ice taken from a depth of 1585 meters (core tube #1016) in the Byrd ice core. Vertical scale (left) indicates concentration in number of particles $>0.62 \mu$ in diameter per $\frac{1}{2}$ ml of ice. Vertical scale (right) indicates oxygen isotope ratio in ‰. The horizontal scale indicates depth of the ice sample below the glacier surface. The microparticle concentration for the dust band (vertical arrow) extends off the graph (adapted from Thompson, 1977b, p. 110).

in this succession of increments (marked by vertical arrow). The second dust sample that was analyzed was filtered by Thompson from a combination of sample assays #1 – #30 (0 - 37 cm depth, see horizontal arrow in Figure 12.4), with assay #28 being omitted from this batch. **[UPDATE:** Most of the increase took place within 1.3 cm of ice ($\Delta t < 8$ months) followed by a tailing off period spanning 4 cm of ice (~ 2 years).] Samples #1016 and #1016-B, dated here at about 31,000 calendar years b2k, are compared in Figure 12.5. Elemental concentrations for the dust band (given in Appendix G in $\mu\text{g}/\text{lt}$ of ice) have been individually normalized to the concentrations of corresponding elements found in the immediately surrounding ice (sample #1016), and the resulting relative increases in concentration have been plotted.

Note that the concentration of Ir in ice increased ~ 19 fold in the dust band sample. This increase suggests that the rate of cosmic dust deposition correspondingly increased at this time. A conservative position would be to assume that ice accumulation rate remained

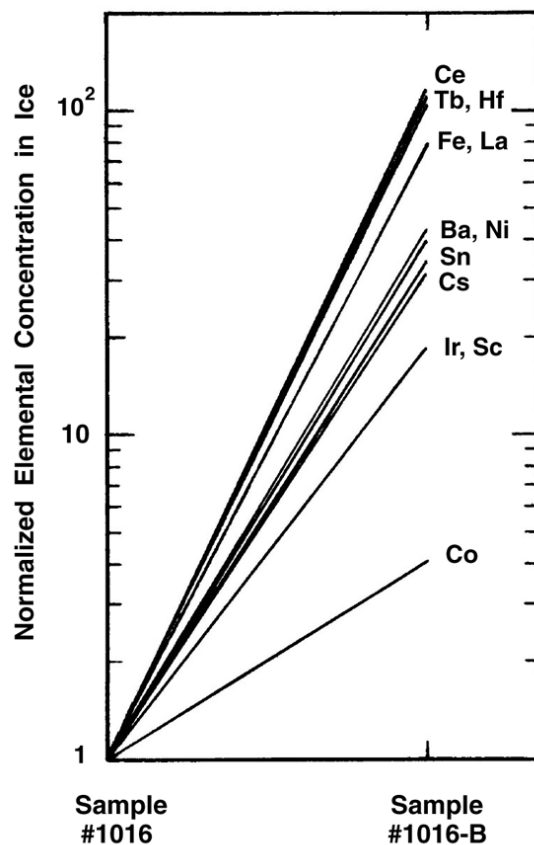


Figure 12.5. Elemental concentrations in ice from the 1585 meter deep Byrd core dust band (right) normalized and compared to elemental concentrations in ice immediately surrounding the dust band (left).

unchanged at the time of dust band formation, in which case the cosmic dust deposition rate would have increased in proportion to the Ir concentration increase. However, it is also possible that the ice accumulation rate increased at the time of dust band formation. In this case the estimated increase in the cosmic dust deposition rate would have to be boosted by an amount comparable to the increase in ice accumulation rate.

On the basis of the data shown in Figure 12.5, it is difficult to argue that the cosmic dust deposition rate remained unchanged in the course of dust band formation since this would require that the rate of ice accumulation had dropped about 19 fold at this time. Also, it is unlikely that the Ir increase was produced through a concentration process, e.g., one involving snow melting and evaporation. Such a process may be ruled out for two reasons. First, if concentration had been involved, all elements would have increased proportionately in the dust band. Instead, there was a wide range of increases ranging from a 4 fold increase for Co to a 117 fold increase for Ce. Second, a detailed stratigraphic analysis of the δO^{18} record reveals the presence of a relatively continuous, unbroken ice accumulation history spanning the dust band; see Figure 12.4.

A comparison of the elemental enhancement factors of sample #1016 and sample #1016-B is shown in Figure 12.6. Note that the enhancement factor for Ir drops by a factor of 6.2. The concentration of Ir drops from 156 ppb (EF = 560) in the dust of the surrounding ice to 26 ppb (EF = 90) in the dust band; see Table G-I. Thus the cosmic dust fraction appears to have become diluted by 6 fold during dust band formation, dropping from a level of about 30% to a level of about 5% in the dust band (assuming a C-1 chondrite-

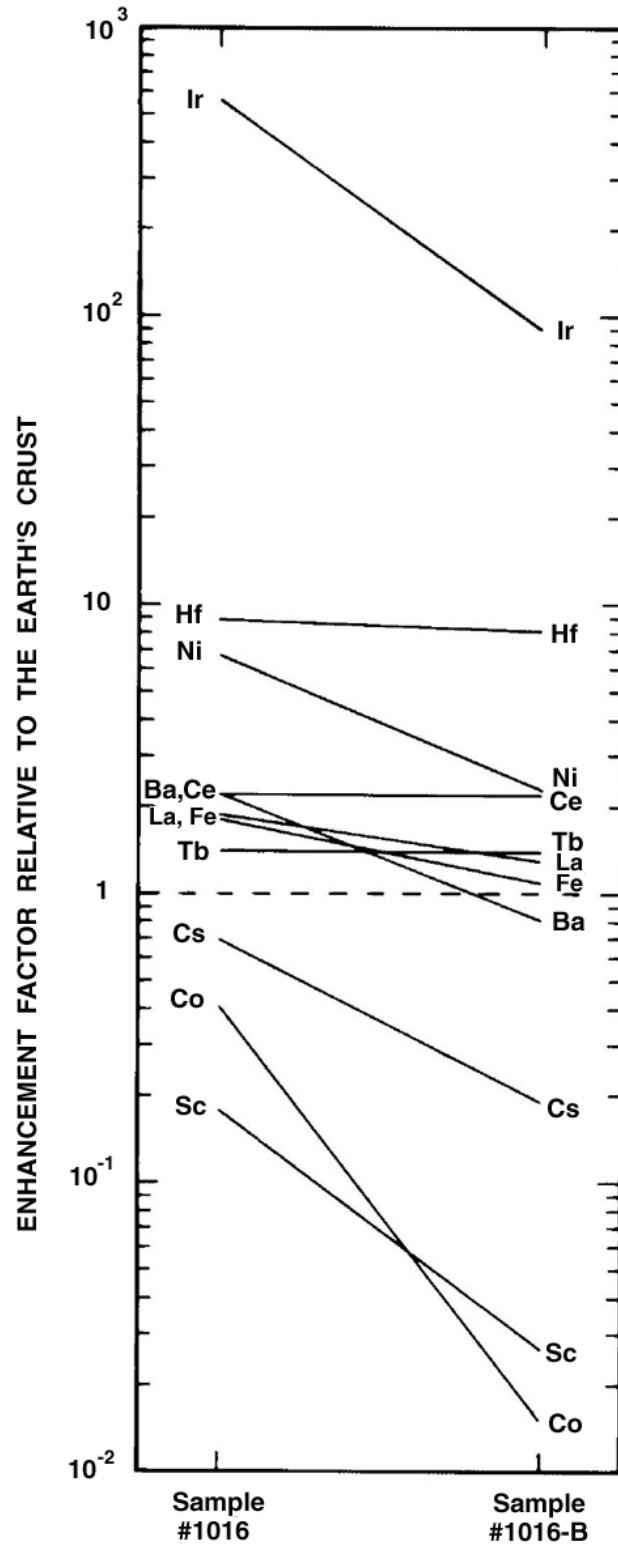


Figure 12.6. Elemental enhancement factors in dust filtered from the analyzed Byrd Station ice core dust band (right) compared to enhancement factors in dust filtered from ice surrounding the dust band (left).

like source material containing 514 ppb of Ir). As will be discussed below, this diluting material is most likely ash that was erupted from a nearby volcano.

The rare earths Ce and Tb present the greatest increase of all the elements shown in Figure 12.5. As mentioned earlier, the rare earths are good indicators of terrestrially derived material. Moreover, rare earths detected in the dust band have a terrestrial signature, in that the C-1 normalized concentrations of La and Ce are enhanced relative to the C-1 normalized concentration of Tb. Thus it is apparent that the bulk of the material composing the dust band is derived from a terrestrial source. A volcanic source is preferred over a continental wind blown source for the dust for the reason that the enhancement factors for cobalt and scandium are very low relative to normal terrestrial abundances for these elements. For example, in most of the other glacial dust samples that were analyzed Co and Sc were present at close to terrestrial abundance levels. On the other hand, it is known that volcanic rocks sometimes contain low amounts of Co and Sc. In particular, peralkaline trachytes such as those composing the recently active Antarctic volcano Mt. Takahe are known to be low in Sc and Co. Thus it is reasonable to conclude that the bulk of the material in sample #1016-B may be dust possibly erupted from Mt. Takahe, a volcano situated about 350 kilometers north-northeast from the Byrd Station ice core site.* Also, Kyle et al. (1982) have shown that glass shards selected from six Byrd core ash bands have a peralkaline trachyte chemical composition similar to an analyzed rock sample from Mt. Takahe.

The question that must now be addressed is whether the iridium and nickel whose concentrations in ice are higher in the 1585 meter dust band, are derived from the same source as the volcanic dust or are these elements of extraterrestrial origin. Consider first iridium. Platinum group metals are normally relatively scarce in most igneous rocks. For example, Columbia River Basalt contains only ~0.004 ppb of Ir; see Table XIII (p. 224). Rankama and Sahama (1950, p. 691) note that platinum group metals have been found at high concentrations in certain types of igneous rocks, e.g., up to 740 ppb in dunite and 290 ppb in peridotite. However, these rocks are associated with nonexplosive-type eruptions and hence widespread dispersal in the form of ash falls would not be expected. Moreover, a platinum-bearing igneous source material may be ruled out in the case of Mt. Takahe, which as stated above has been shown to be peralkaline trachyte in composition. Also, Le Masurier, Kyle, and Rankin, (1976) have analyzed a variety of rock types from volcanoes of the Executive Committee Range which they say include representatives of essentially all rock types present in the entire petrographic province surrounding Byrd Station, and none of the rock types they list fall in the category of a dunite or peridotite. Finally, dunite and peridotite may be ruled out on geochemical grounds since chromium is relatively depleted in the dust band. The NAA results indicate that the 1585 meter dust band has a chromium content below 70 ppm, whereas dunite contains about 3400 ppm of Cr and peridotites average about 500 ppm (Rankama and Sahama, 1950, pp. 151 and 621). Thus it is concluded that the iridium found in the dust band is most likely of extraterrestrial origin.

The high concentration of nickel (224 ppm) found in the dust band dust is also most probably of extraterrestrial origin. Most volcanic rocks are found to have Co:Ni ratios in the range of 0.3 to 4 (Rankama and Sahama, p. 682). Thus even if all of the cobalt in the dust

***Update:** In the original version of this dissertation I had mistakenly concluded that the microparticle concentration in the 1585 meter dust band was comparable to that measured by Phillip Kyle for the 1594 meter ash band whose ash he had geochemically linked to the nearby Mt. Takahe volcano (Kyle et al., 1982). In fact, the 1594 meter ash band contains microparticle concentrations that are two orders of magnitude higher. Consequently, I had mistakenly concluded that the 1585 meter dust band had a Mt. Takahe origin as well. The absence of ash shards in this sample, however, poses a problem. If it is of volcanic origin, it may be associated with a much more distant eruption originating far from Antarctica.

band were of volcanic origin, it would be expected that no more than about 1 ppm of the nickel would be volcanically derived. Consequently, a volcanic origin may be ascribed to only about 0.4% of the nickel in the dust band, leaving an extraterrestrial source as the most likely explanation for the majority of this element.

If the Ir and Ni are of extraterrestrial origin and, hence, if the increased concentration of these elements in dust band ice is indicative of a 20–40 fold increase in cosmic dust deposition rate, the next question that must be answered is what could have caused the deposition rate to increase at a time when the volcano erupted. For cosmic dust particles less than 1 micron in diameter the primary mode of removal from the stratosphere is through coagulation with sulfate aerosols and through aerosol size growth due to the adsorption of sulfur vapors (Turco et al., 1981, p. 1119). A volcanic eruption would on the one hand have accelerated the process of particle growth by increasing the quantity of H₂SO₄ available for adsorption, and on the other hand would have accelerated the coagulation process by increasing by many orders of magnitude the number of available stratospheric particles. Moreover, volcanic ash particles having a size greater than 10 microns would have rapidly settled through the stratosphere, reaching the Earth's surface within a few weeks. Such particles can sometimes be heavily laden with sulfuric acid, as was observed for the Mt. St. Helens eruption (Inn et al., 1982), and consequently would be effective scrubbers of smaller stratospheric aerosols, sweeping them up and trapping them within their acid coating. Thus it is reasonable to suppose that submicron-sized cosmic dust grains which might otherwise take several years to settle out of the stratosphere would become deposited within a few weeks or months during an ash eruption. At such times elements such as Ir and Ni would be expected to be deposited in glacial ice at higher concentrations, as is observed in the 1585 meter dust band.

It should be mentioned that, while the concentrations of Ir and Ni in sample #1016-B conform closely to a C1 chondrite ratio (see **Figure 12-E** -- open circle), cobalt does not. For example, cobalt is depleted by almost two orders of magnitude relative to Ir and Ni. Thus the source for this material must be different from that typically found in meteorites. It might be considered, then, that this material comes from a source outside of the solar system, e.g., cometary bodies differing in composition from that of the primitive solar nebula, or dust from a passing supernova remnant or interstellar cloud.

Elevated Cosmic Dust Deposition Rates During the Late Wisconsin. One of the main objectives of the glacial ice dust tests was to determine whether cosmic dust deposition rates during the Late Wisconsin ice age were abnormally high. A positive finding in this regard would constitute strong evidence in support of the GEH.

The present work is the first study of its kind to determine cosmic dust deposition rates for the Wisconsin ice age from dust deposited in glacial ice. Altogether 8 samples of glacial ice dust from the Late Wisconsin portion of the Camp Century ice core were analyzed using the NAA technique. Also, 4 dust samples from the Byrd core were analyzed, of which 2 were from Holocene ice and 2 were from Wisconsin ice (one sample being a dust band). Estimates of cosmic dust deposition rates based on these analyses are summarized in Tables XV and XVI (**pp. 328 – 329**) and are compared to Holocene period estimates made by several other authors. For the Byrd core, samples #1016 and #1016-B (the dust band) have been averaged together to give an upper limit for the Wisconsin cosmic dust deposition rate. The deposition rate estimated for the dust band alone should be excluded from this assessment since this high value is most likely due to the effects of the stratospheric precipitation induced by the presumed volcanic eruption.

The data from these two tables is displayed in Figures 12.7 and 12.8. Note that during the Late Wisconsin there were times when the rate of cosmic dust deposition was apparently one to two orders of magnitude higher than rates currently observed at these polar locations.

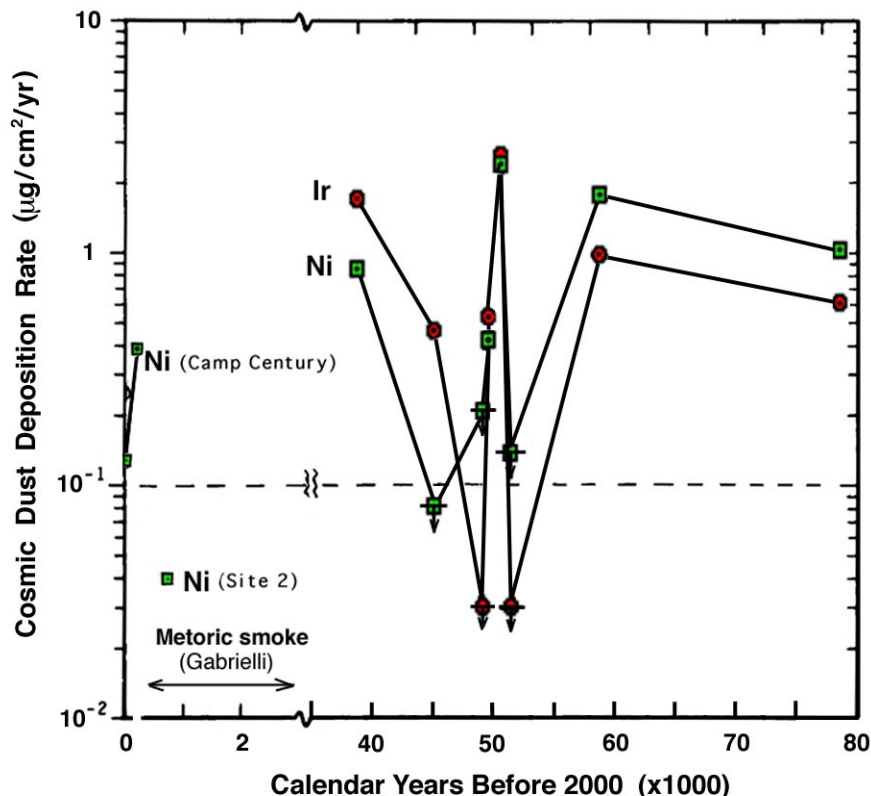


Figure 12.7. Late Wisconsin and Holocene cosmic dust deposition rates at Camp Century, Greenland, determined on the basis of iridium concentration (red circles) and nickel concentration (green squares). See Table XV for data. [UPDATE: Arrow indicates Holocene meteoric smoke deposition rate based on Ir values of Gabrielli et al. (2004).]

This is strong evidence confirming the *a priori* prediction made by the GEH that the rate of cosmic dust influx to the Earth should have increased towards the end of the ice age, given that a sufficient source of interstellar dust was present on the side of the solar system toward the Galactic Center. Note that the 15 fold higher solar system dust concentrations postulated in Subsection 3.3.2 (p. 88) would have produced cosmic dust deposition rates of about 3×10^{-6} g/cm²/yr. Some of the values plotted in Figures 12.7 and 12.8 approach this level.

The results presented here presume: 1) that the abundance of iridium (and nickel) in cosmic dust has remained essentially unchanged since the time of the Wisconsin, and 2) that the rate of snow accumulation has not varied appreciably from present values. In regard to this first assumption, there is some degree of uncertainty. For example, the assumption that Ir and Ni are present in extraterrestrial fallout in C-1 chondritic abundance may be a good assumption for the Late Holocene, but these abundances were probably different during the Late Wisconsin when interstellar dust may have gained entry to the solar system. In addition to C-1 chondritic material, the proposed nebular cloud would have probably contained other non-iridium/nickel-bearing substances, in which case the cosmic dust deposition rates listed in Tables XV and XVI would be underestimated. The second assumption, regarding snow accumulation rates, is a bit conservative since some of the Wisconsin stage glacial dust samples may have come from ice that was accumulated at a very high rate. For example, the 6 fold drop in the concentration of rare earth elements observed in sample #962-1 appears to indicate that there was a 6 fold increase in the ice accumulation rate for this sample; see p. 340. Also, the ice from which dust sample #1016-B was filtered may have accumulated at a

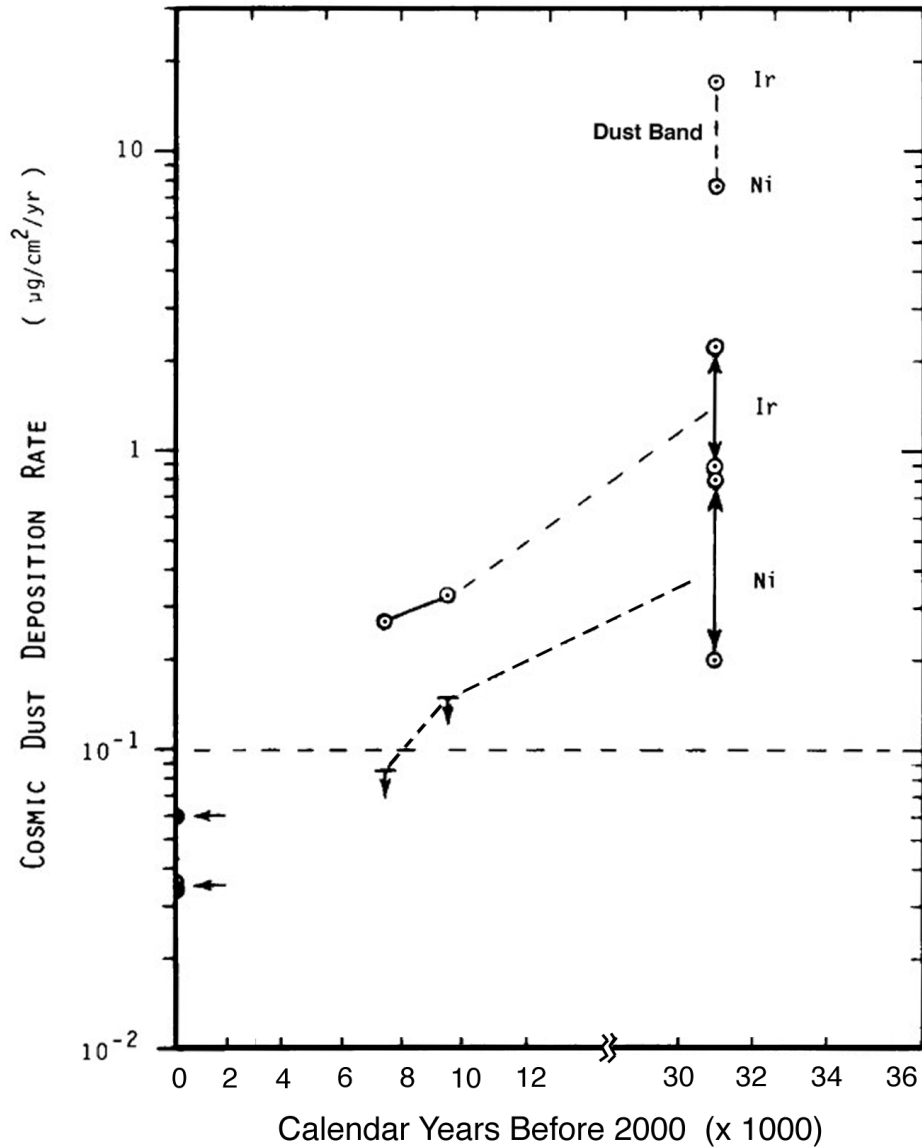


Figure 12.8. Late Wisconsin and Holocene cosmic dust deposition rates at Byrd Station, Antarctica, determined on the basis of iridium and nickel concentration. Range for the 31,000 years b2k sample charts the deposition rate with and without the dust band value included. See Table XVI for data.

higher rate than was assumed in Table XVI.

Of the samples analyzed from the Camp Century ice core, high iridium deposition rates were found at depths dated at 38,650 calendar years b2k, 50,500 calendar years b2k, 58,700 calendar years b2k, and 78,500 calendar years b2k. Note that three of these peaks of "cosmic activity" correlate with dust peaks #4, 5, and 7 shown in Figure 8.1, curve-g. In Chapter 8 (Subsection 8.2), it was suggested that the dust peaks in Wisconsin ice could have been caused by atmospheric winds generated during the passage of a superwave. The observed correlation of iridium deposition rate with dust deposition rate supports this proposal.

12.2 OTHER NEUTRON ACTIVATION ANALYSIS TESTS

12.2.1 Analysis of Dust from the Agassiz Ice Core.

Seven one-liter plastic jugs of glacial meltwater taken from ice core A77 of the Agassiz Ice Cap in Ellesmere Island, Canada (~80°N, 71°W) were received in liquid form at PSU in April of 1981. The meltwater samples were shipped courtesy of Dr. David Fisher and Dr. Richard Koerner of the Polar Continental Shelf Project in Ottawa, Ontario. The samples were not from the ice core itself, but were "bulk samples" of meltwater that had been retrieved from the tubular storage chamber of the thermal drill. At the time of drilling, as the drill tube descended into the ice to drill each core section, the resulting water melted by the drill bit would flow into this storage chamber and refreeze. This refrozen "bulk" meltwater retrieved from each core section was saved along with each ice core section.

Of the bulk samples sent, 6 were from Holocene ice dating between 700 – 800 years b2k, and one was from the second half of the Late Wisconsin (~22,000 – 11,650 calendar years b2k). Vital statistics for these samples are listed in Section C of Table XVII.

Sample Preparation. The meltwater samples were filtered at PSU on April 30, 1981 in a clean dust-free microbiological laboratory. The storage jars were worked on one at a time. First, the jar was shaken vigorously to get all particulate matter in suspension. Then a portion was poured into a 250 ml sample beaker. Water from this beaker was then drawn up with a 30 ml syringe and injected through a preweighed Millipore filter (0.45 μ pore size, 25 mm diameter), as was done in filtering the Camp Century ice samples, refer to **p. 336**. The filtrate was volumetrically measured in a 100 ml graduated cylinder and stored in a reserve flask. When the sample beaker became empty, the storage jar would be shaken up once again and a new portion would be poured. This process was repeated until the storage jar was empty. About 150 ml of filtered meltwater from the reserve flask was then poured into the empty storage jar, shaken vigorously to remove any remaining dust residue, poured into the sample beaker, and filtered onto the same filter paper. This jar rinsing procedure was repeated until all of the filtered meltwater had been recycled in this way.

This procedure was duplicated in filtering all core tube samples. Samples 80, 83, and 84 were filtered into one filter paper labeled "Holocene-A"; samples 85, 86, and 87 were filtered onto a second filter paper labeled "Holocene-B"; and sample 225 was filtered onto a third filter paper labeled "Wisconsin."

To insure complete removal of particulate from the storage jars, the empty jars were each put through a final rinse with 100 – 150 ml of prefiltered 3M HCl solution. The resulting residue was filtered onto a separate filter paper. Thus, corresponding to each of the three filter papers described above, there were three acid rinse filter dust samples. It is estimated that there was better than 95% recovery of the dust sample in the Holocene-A sample and better than 99.5% recovery in the Holocene-B and Wisconsin samples.

All glassware and utensils were rinsed with 3N HCl prior to the first and third sample filtrations and with distilled water followed by filter distilled water prior to each filtration. A control filtration was also performed in which 83 ml of filtered distilled water was passed through a preweighed blank Millipore filter paper. This filter was treated and measured in the same way as the other samples.

As was done in the processing of the Camp Century ice samples, the filter papers were weighed before and after filtration on a Kahn electrobalance to determine their net dust weights; refer to **p. 336**. The 3 dust samples, the 3 acid rinse samples, and the control filter were each rolled up and inserted into a quartz irradiation vial. The vials were heated in a vacuum oven to incinerate the filters and were then vacuum sealed with a gas torch (**p. 332**).

Irradiation and Counting. These 7 vials were sent to MURR where they were irradiated for 1000 hours at a neutron flux of 7.0×10^{13} n/cm²/sec, the irradiation ending on July 29, 1981. The samples were subsequently processed and counted along with the Camp Century and Byrd ice core samples; see **pp. 335 - 338** for details.

Results. Neutron activation analysis results for the Agassiz ice core samples are presented in Tables G-I through G-XV of Appendix G. The "enhanced group" elements found in the Camp Century core were not found in the Agassiz samples in elevated abundance, neither in the Holocene nor in the Wisconsin ice core samples.

Nickel concentrations for the Agassiz ice core imply a cosmic dust deposition rate of ~ 0.11 $\mu\text{g}/\text{cm}^2/\text{yr}$ for the Holocene and ~ 1.6 $\mu\text{g}/\text{cm}^2/\text{yr}$ for the Wisconsin for an ice accumulation rate of 18 g/cm²/yr; i.e., a 15 fold increase. However, the enhancement factor for nickel in these samples relative to average crustal abundance does not exceed 2.2. Thus there may be a question regarding whether the nickel in these samples is primarily of terrestrial or extraterrestrial origin. Nevertheless, the Holocene and Wisconsin cosmic dust deposition rates compare favorably with other deposition rate estimates listed in Tables XV and XVI. However, the nickel results for the Agassiz core are not corroborated by the iridium results. Iridium was not found above the threshold of detection in any of the samples tested. The upper limits for iridium-based cosmic dust deposition rate estimates are: <0.001 and <0.03 $\mu\text{g}/\text{cm}^2/\text{yr}$ for the Holocene (samples A and B) and <0.08 $\mu\text{g}/\text{cm}^2/\text{yr}$ for the Wisconsin. These values are one to two orders of magnitude below the nickel-based cosmic dust deposition rate estimates for the Agassiz core and conflict with other Ir-based deposition rate estimates listed in Tables XV and XVI.

The Agassiz data should be regarded with some reservation since these samples came from ice that was melted at the time of drilling. The extraterrestrial component of glacial dust, being particularly dense, could have settled out during drilling when the meltwater was flowing through the holes in the annular drill bit into the tubular storage chamber surrounding the ice core. During this passage, heavy dust particles in the meltwater would have been free to migrate downward under the force of gravity, and could have been excluded from the bulk sample.

Future tests determining the extraterrestrial dust content of the Agassiz core should be done on ice core samples that have not undergone previous thawing. However, it should be noted that the Wisconsin section of the Agassiz core represents only 4 meters of ice in this 338 meter long core, and begins about 3_ meters above the bedrock surface. At Camp Century, on the other hand, the Wisconsin stage spans about 200 meters of ice and begins about 40 meters above bedrock. It is, therefore, reasonable to conclude that the Wisconsin stage section of the Agassiz Ice Cap has undergone considerably more tectonic deformation and basal melting. Thus, to accurately determine Northern Hemisphere cosmic dust deposition rates for the Wisconsin stage, either the Camp Century or Dye 3 deep ice cores are preferred.

12.2.2 Analysis of Ocean and Lake Bottom Sediments

Supplementary to the glacial ice dust tests, NAA was performed on samples of marine sediment from the northeastern Pacific (off of the Oregon coast), Caribbean, and western Atlantic, and on varved lake bottom sediments from Elk Lake, Minnesota. It was reasoned that if a significant increase in iridium concentration was observed in sediments laid down at the end of the Last Ice Age, this would constitute strong evidence supporting the GEH.

Previously, Alvarez et al. (1980) using the NAA technique detected elevated levels of Ir in sediments spanning the Cretaceous/Tertiary boundary (~ 65 million years BP) and on this

basis proposed an extraterrestrial event (e.g., the impact of a large asteroid) as a cause for the dinosaur extinctions; see Subsection 11.2.2 of Chapter 11. They found levels of Ir peaking at 9.1 ppb in Italian sediments and at 29 ppb in Danish sediments. However, in the present study it was not expected that Ir levels would reach as high as this even if an extraterrestrial event (e.g., Galactic superwave) actually did occur at the end of the ice age. The ice record placed severe constraints on this. For example, even if all of the Late Wisconsin dust increase observed in the Camp Century ice core were due to an influx of extraterrestrial dust of chondritic composition (quite unlikely), then even in the lowest sedimentation rate ocean core that was to be tested (P6304-7 from the Caribbean), an increase of only 4 ppb could be expected.

First Irradiation. During the summer of 1980 a number of samples were obtained from core OSU 6609-7 which came from the Eastern Cascadia Basin off the coast of Oregon (43.2°N, 126.7°W). Climatological work had been previously performed on this core by Duncan, Fowler, and Kulm (1970). Also that same summer, a total of 31 samples were obtained from Elk Lake cores J and K penetrated in Minnesota. These varved lake bottom sediments span the period from 11,100 varve years BP to the present.

On October 3, 1980, 15 samples from the Oregon core and 3 samples from the Elk Lake core (each about 1 gram in weight) were irradiated at the Oregon State University reactor for 8 hours at 3×10^{12} n/cm²/sec. The samples were counted at Portland State University (PSU) beginning on January 26, 1981. No iridium was detected in any of the samples that were counted. The threshold of detection for Ir in these samples ranged between 0.25 – 0.6 ppb.

Second Irradiation. In March of 1981 a total of 13 samples were obtained from core P6304-7 from the Caribbean (15.1°N, 69.6°W). These pelagic sediments came from core depths of 0 – 130 cm, a section of core covering the period from the middle of the Wisconsin ice age to the present, according to the climatological profile published by Emiliani (1972). Also, 3 samples of sediment were obtained from western Atlantic core KN 25-4 (21.5°N, 67.5°W). These 3 samples, coming from a depth of 12.5 – 13.5 meters, span the paleomagnetic boundary marking the initiation of the Blake polarity reversal (Denham, 1976) which occurred at the δO^{18} Stage 5d/5e boundary.

Duplicates of the 13 Caribbean core samples and of the 3 western Atlantic samples, together with 14 of the Elk Lake samples (4 in duplicate) were encapsulated in vacuum sealed quartz irradiation vials. Sample sizes ranged from 0.07 to 0.14 grams. These samples were irradiated together with two USGS PCC-1 standards and two USGS W-1 standards at the Missouri University Research Reactor (MURR) for 100 hours at 3×10^{13} n/cm²/sec. After the irradiation, which ended on July 10, 1981, the samples were transferred to clean plastic polyvials. Counting at MURR was done on July 19 – 24 (half hour per sample) and on October 3 – 10 (2 hours per sample). No iridium was found in any of the samples. Thresholds of detection for Ir were $\sim 1\frac{1}{2}$ ppb for the Caribbean samples, ~ 3 ppb for the western Atlantic core samples, and ~ 0.4 ppb for the Elk Lake samples.

Discussion. The upper limits for Ir of $1\frac{1}{2}$ ppb for the Caribbean core and 0.4 ppb for the Elk Lake core do not conflict with the Late Wisconsin iridium levels found in the Camp Century and Byrd Station ice cores. For example, given a mean cosmic dust deposition rate of ~ 2 $\mu\text{g}/\text{cm}^2/\text{yr}$ for the Late Wisconsin portion of the Camp Century core (see Table XV) and a deposition rate of 11.6 $\text{mg}/\text{cm}^2/\text{yr}$ (16.5 cm/1000 cal. years at a core density of $\rho = 0.7$ g/cm^3) for the Caribbean core P6304-7, an iridium concentration increase of: $C = (2 \times 10^{-6} / 0.012) \times 514$ ppb = 0.09 ppb would be expected to be generated in the Caribbean core sediments. This is about one order of magnitude below the threshold of detection reported above for NAA of this core. On the other hand, if the conventional isotope chronology is

adopted, this core would have a deposition rate of $\sim 2.7 \text{ mg/cm}^2/\text{yr}$, giving an expected Ir concentration of $\sim 0.4 \text{ ppb}$. By comparison, Crocket and Kuo (1979), using a radiochemical separation technique in conjunction with NAA, have measured Ir in a nearby core (P6304-9) at a concentration of $0.26 \pm 0.09 \text{ ppb}$ for a core depth of 87 cm which corresponds to about the beginning of the Late Wisconsin stage.

For the Elk Lake core, given a core sedimentation rate of $50 - 100 \text{ mg/cm}^2/\text{yr}$ ($100 - 200 \text{ cm}/1000 \text{ varve years}$ at a core density of $\rho \sim 0.5 \text{ g/cm}^3$), an iridium concentration increase of:

$$C = (2 \times 10^{-6} / 7.5 \times 10^{-2}) \times 514 \text{ ppb} = 0.01 \text{ ppb}$$

would be expected. This is over an order of magnitude below the threshold of detection reported above for NAA of this core. Finally, for the Oregon coast core, given a core sedimentation rate of $12 \text{ mg/cm}^2/\text{yr}$ ($\sim 17 \text{ cm}/1000 \text{ years}$ at a core density of 0.7 g/cm^3) an iridium concentration increase of:

$$C = (2 \times 10^{-6} / 1.2 \times 10^{-2}) \times 514 \text{ ppb} = 0.09 \text{ ppb}$$

would be expected, which is well below the detection thresholds estimated above (**p. 355**).

In summary, the ocean and lake sediment samples do not indicate the presence of anomalously high iridium at the end of the Wisconsin Ice Age. However, neither of these results conflict with the discovery (Section 12.1 of this chapter) that high iridium levels are recorded in the Late Wisconsin sections of the Camp Century and Byrd ice cores. Future studies of these anomalously high deposition rates of precious metals (and of other "enhanced group" elements) would best be done on glacial ice cores rather than on ocean sediment cores, the rate of influx of terrestrial material being much lower in the former.

UPDATE

Logbook depths that were previously assigned to the Camp Century ice core samples have been changed to corrected depths, the correction amounting to a decrease of about 3 to 4 meters depending on the particular sample depth. Also ages formerly assigned to these samples have been corrected using a time-depth scale that is based on correlations to the accurately dated GISP2 Summit, Greenland ice core record referenced to the GICC05 ice core chronology.⁽¹⁾ The new dates assigned to these samples are listed in Tables XV and XVI.

Tin Abundance of the Sn-rich Dust Sample Determined by Energy Dispersive X-ray Analysis Conducted in 1984 (update to **p. 330**): The tin-rich sample (962-1) was singled out for energy dispersive X-ray analysis. Five locations on an unirradiated fragment of this dust sample were scanned with the electron beam. Four of the scans were centered on individual randomly selected particles that were 20 – 40 microns in size, with the scan covering a $5\mu \times 5\mu$ region. A fifth wide-field scan ($20\mu \times 20\mu$) was made of a filtrate region containing a field of submicron-sized particulate material. To determine the contribution from the filter substrate, two scans were also made of a dust free portion of the filter paper.

The Sn peaks of the spectra were calibrated against spectral peaks obtained for a tin metal standard. The spectra were also corrected for contributions from the filter paper background and the resulting elemental abundances were adjusted to take into account the likely presence of oxygen, which is undetectable by this technique. Elemental weight percents of the principle detected elements (Na, Si, S, Fe and Sn) are listed in Table 12-1 for the four particles (P1 through P4), the wide field (F), and their averages. It was not possible

Table 12-1

Elemental weight percents of particles selected randomly from tin-rich dust sample 962-1

| Element | Element | | Weight | | F | Average P ₁ -P ₄ | Average P ₁ -P ₄ , F |
|-----------|----------------|----------------|----------------|----------------|------|---|---|
| | P ₁ | P ₂ | P ₃ | P ₄ | | | |
| O | 22.1 | 26.5 | 26.5 | 20.7 | 25.0 | 24.0 ± 2.7 | 24.2 ± 2.4 |
| Na | 6.4 | 5.8 | 7.7 | 3.0 | 2.55 | 5.7 ± 1.7 | 5.1 ± 2.0 |
| Si | 3.7 | 7.8 | 10.1 | 2.06 | 7.7 | 5.9 ± 3.2 | 6.3 ± 3.0 |
| S | 1.48 | 2.22 | 0.60 | 1.26 | 1.58 | 1.4 ± 0.6 | 1.4 ± 0.5 |
| Fe | 0.41 | 0.32 | 0.38 | 0.21 | 0.64 | 0.33 ± 0.08 | 0.39 ± 0.14 |
| Sn | 66.0 | 57.3 | 54.8 | 72.7 | 62.5 | 62.7 ± 6.3 | 62.7 ± 6.4 |

to determine the abundance of aluminum due to stray X-ray emission from the aluminum sample mount. The oxygen abundances listed in Table 12-1 are estimates determined by assuming that Sn is present as a 50:50 mixture of Sn₂O₃ and Sn₃O₄ and that Na, Si and S are present as Na₂O, SiO₂ and SO₄. The weight percentage for Sn averages to 62.7 ± 6.4%. Although, I chose a somewhat lower value of 60 ± 15% to represent the true Sn percentage in this sample, since the percentages in Table 12-1 do not take into account the presence of other elements such as Al which could comprise a few percent of the sample's weight.

Since the particles were not removed from the filter when they were analyzed, it is not readily apparent from this data whether the other elements which show up in the particle spectra come from the particles themselves or from the particulate material underlying the particles. Most probably the particles consist mainly of tin, with the elements Na, Si, and SO₄²⁻ being associated with the underlying particulate material which contains dust of terrestrial derivation. When the elemental composition of the submicron particle field F is compared to the average composition of the 4 particles (P₁ - P₄), comparable abundances are found for most of the elements, except for Na, which appears to be half as abundant in field F, and Fe, which appears to be enriched by a factor of two in field F; see Table 12-1. However, further X-ray analyses are needed before these compositional differences can be regarded as being statistically significant.

The relative abundances of Ir, Fe, Co, and Ni conform to a C1 chondrite pattern of 9 ± 3 percent chondritic material. Although the Sn, Sb, Au and Ag components of the enhanced group exceed chondrite abundances by several orders of magnitude, their association with these chondritic pattern elements suggests that all may be of extraterrestrial origin, a conclusion that is further supported by the discovery of isotopic anomalies in the tin component. Consequently, as much as 70 ± 15 percent of the dust in sample #962-1 (50,300 years BP) appears to be of extraterrestrial origin.

An Isotopic Anomaly Discovered in the Tin-rich Camp Century Ice Core Dust Sample: Evidence of an Extraterrestrial Origin (update to p. 338): As mentioned above (pp. 335, 336), efforts were made to see if an isotopic anomaly was present in the Sn-rich sample (962-1). Using the NAA technique, however, I was able to determine only that there were no isotopic anomalies in the tin isotopes greater than 5%. At the time of this research I called around in an attempt to find a mass spectrometrists who would be willing to collaborate to analyze the tin sample. However, I did not find anyone at the time. In September 1983, after this dissertation was completed, I was presenting my findings at the Meteoritical Society meeting in Mainz, Germany and had the occasion of meeting John DeLaeter who at that time was the world's expert on determining the isotopic ratios of tin using mass spectrometry. Just 6 months earlier his group at Curtin University in Australia had succeeded in developing a new sample ionization technique that was able to reduce indium contamination which

previously produced peaks that interfered with the tin determination.⁽²⁾ As it turned out, we were assigned lodging at the same guest house.

DeLaeter agreed to analyze the sample so I sent him a small portion of the 962-1 sample filter paper that had *not* been irradiated which contained a few micrograms of dust filtrate. The actual measurements were done by deLaeter's colleague Robert Loss. By January, they had results to report. These were positive, confirming the conclusions previously published in this dissertation (above) that the tin in the tin-rich sample was of extraterrestrial origin and that it might contain isotopic anomalies. Their measurements indicated that this arctic tin contained a 3.3 ± 0.84 percent isotopic anomaly in the minor isotope ^{115}Sn (4σ increase); see Table 12-2. They also found less significant anomalies in the minor isotopes ^{114}Sn and ^{112}Sn ($+1.7 \pm 1.2\%$ and $+1.0 \pm 1.2\%$) and in the major isotope ^{117}Sn ($-0.51 \pm 0.32\%$). The isotopic ratios for the mean of the four Sn standards matched the ratios previously published by Rosman et al., 1984. The amount of the polar dust sample initially available was sufficient to make only one mass spectrometry determination, which explains why isotopic ratios for the sample have been given higher error limits as compared with those of the standard. The ^{115}Sn anomaly is most interesting, having a significance of 4 standard deviations.

The thermal ionization mass spectrometry procedure they used discriminates against interference by In, Cd, and Te by ionizing them less efficiently than Sn. Rosman et al. (1984) estimate an upper limit of $<0.5\%$ contribution by ^{115}In interference in the absence of a ^{113}In peak. Since no ^{113}In peak was detected, such interference is estimated to account for less than 15% of the observed ^{115}Sn anomaly. Interference from Cd (112, 114, and 116) should also have been minimal since Cd was about 1200 times less abundant than Sn in the sample. These results suggest that the isotopic ratios of Sn in sample 962-1 do not correspond to terrestrial isotopic ratios and that the tin component, therefore, is most probably of extraterrestrial origin. However, additional measurements need to be carried out to improve the accuracy of the measured anomalies.

Prior to the time this analysis had been carried out, Ward and Beer had theorized that extraterrestrial tin should contain a wide variety of isotopic anomalies.⁽³⁾ However, accurate measurements of the abundances of the minor isotopes of Sn in meteorites had not yet been made. Consequently, these results constituted the world's first discovery of an isotopic anomaly in extraterrestrial Sn and also the first time that an isotopic anomaly of any kind had been detected in dust retrieved from ice age polar ice. Publication of the result, however, was regrettably delayed, being reported here for the first time after a lapse of over 17 years! Due to other priorities, DeLaeter and Loss found no time to conduct repeat measurements on the tin-rich dust sample, and did not wish to submit the results of the single measurement for journal publication. It is important to note, however, that their reluctance to publish the 1984 isotopic anomaly results does not make them any less valid.

Table 12-2
Isotopic composition of tin in arctic ice core sample 962-1

| Isotope ratio: | 124/120 | 122/120 | 119/120 | 118/120 | 117/120 | 116/120 | 115/120 | 114/120 | 112/120 |
|--|--------------------------|--------------------------|--------------------------|--------------------------|--|-------------|--------------------------------------|-------------------------------------|---------------------------------------|
| Laboratory Standard | 0.17766 ± 0.00018 | 0.14202 ± 0.00040 | 0.26332 ± 0.00032 | 0.74309 ± 0.00039 | 0.23533 ± 0.00010 | 0.4460 — | 0.01040 ± 0.00001 | 0.02022 ± 0.00002 | 0.02992 ± 0.00005 |
| Sample 962-1 | 0.17791 ± 0.00086 | 0.14253 ± 0.00074 | 0.26345 ± 0.00100 | 0.74335 ± 0.00296 | 0.23413 ± 0.00075 | 0.4460 — | 0.01075 ± 0.00009 | 0.02056 ± 0.00024 | 0.03021 ± 0.00039 |
| Deviation δ Significance: | 0.14 \pm 0.49 | 0.35 \pm 0.59 | 0.05 \pm 0.40 | 0.04 \pm 0.40 | -0.51 \pm 0.32 $\downarrow 3\sigma$ | — | 3.3 \pm 0.84 $\uparrow 8\sigma$ | 1.7 \pm 1.2 $\uparrow 3\sigma$ | 1.0 \pm 1.2 $\uparrow 1.7\sigma$ |

Discovery of Tin in Interplanetary Dust Particles (update to p. 344): Indirect support of the hypothesis that the isotopically anomalous Sn in arctic ice was of extraterrestrial origin came in 1985. At the Lunar and Planetary Science Conference in Houston, cosmochemist F. Rietmeijer announced finding tin oxide grains inside interplanetary dust particles. In a paper published four years later, he reported that the chondritic porous aggregate (CPA) interplanetary dust particle W7029*A contains a substantial number of platy monomineralic tin grains measuring a few tenths of a micron in size.⁽⁴⁾ Note that a similar plate-like particle morphology also characterizes the tin-rich particles found in arctic ice. Rietmeijer's energy dispersive spectrometer measurements indicated that this tin is present in the CPA particle in the form of Sn₂O₃ and Sn₃O₄ and exhibits an abundance 6 times higher than typically found in C1 chondrite meteorites. His finding helps to substantiate my 1983 suggestion that the solar system is surrounded by dust enriched in tin and that this is the source of the tin-rich dust found in polar ice.

Discovery of Cosmic Dust Variations in Ocean Sediments (update to p. 351): A group of cosmochemists who measured helium-3 concentrations in 250,000 to 450,000 year old ocean sediments reported in 1995 their finding that ³He changed by over 3 fold on a 100,000 year cycle. Helium-3 is regarded as an indicator of extraterrestrial dust influx since it is not found in terrestrial material. Although, since ocean sediments are normally subject to homogenization through bioturbation processes, it is likely that these measurements significantly underestimate the magnitude of the cosmic dust variations. Since glacial/interglacial periods also tend to recur on a 100,000 year cycle, this helps to confirm the theory put forth here that cosmic dust influx episodes have had an impact on the Earth's climate.

Discovery of Elevated Iridium and Platinum Concentrations in Ice Age Greenland Ice (update to p. 351): In December 2004 Gabrielli et al. published a study evaluating the concentration of meteoric smoke in Greenland ice using iridium and platinum as cosmic dust indicators.⁽⁵⁾ They measured the abundance of these indicators in 22 samples taken from the present interglacial (11,400 to 680 years BP), in 12 samples from the ice age period (65,400 - 12,800 years BP), and in two samples from the preceding interglacial (96,500 and 128,200 years BP). Five of their samples came from the same ice age interval that investigated in my 1983 cosmic dust study reported here. Their data indicate that iridium and platinum were being deposited two to three times faster in ice age samples as compared with the present interglacial.

Iridium was present in their ice age samples at concentrations 6 to 45 times higher than those found in the Earth's crust, using the crustal abundance values of Shaw et al. To account for this, Gabrielli et al. suggest that dust was being blown onto the ice sheet from an iridium-rich continental source. However, it is also likely that this iridium is of extraterrestrial origin and that its increased flux reflects an increase in the influx of meteoric smoke during the last ice age. The deposition rates projected from the iridium data of Gabrielli et al. are substantially lower than those found in the present study; see black dots in Figure 12.7. This could indicate that they had sampled times of low cosmic dust influx. Also their technique may not have been sensitive to detecting large cosmic dust particles of size > 0.45 μm, the size range analyzed in the present 1983 cosmic dust study. That is, their objective was to assess the influx of much smaller sized meteoric smoke particles which they felt could be adequately ionized and measured in their mass spectrometer. Iridium and platinum rank among the most difficult metals to ionize, hence their technique may have been insensitive to the larger cosmic dust particles which could have comprised the bulk of the extraterrestrial material being deposited during the ice age. The NAA technique used here is not plagued by such a measurement problem.

Discovery of Iridium and Other ET Indicators at the YD Boundary (update to [p. 351](#)).

A key prediction of the superwave theory was that high concentrations of ET material should be found in sediments dating from the period 11,000 to 14,000 b2k (see [p. 6](#)) and particularly around the time of the megafaunal extinction (see [p. 286](#)). Although the superwave theory predicted that there would be an elevated influx into the solar system of meteors and comets (see [pp. 88 - 89](#)), I believe that Firestone et al. are incorrect in attributing the origin of the ET debris at the YD boundary to the impact/explosion of a comet 1 - 500 km in diameter. Nevertheless, the superwave ET material prediction has now been verified by the discovery of iridium and other ET indicators in YD boundary sediments.⁽⁶⁾ These include the following:

- Firestone, et al.^(7,8) report detecting 3.75 ppb of Ir in sediment samples taken from the Allerod/Younger Dryas (AL/YD) boundary at nine Clovis-age sites, with no Ir being detectable above or below this horizon. Magnetic grain microspherules extracted from this boundary were found to contain up to 51 ppb of Ir at North American sites as well as considerable amounts of the cosmic indicators nickel and cobalt. Grains from a site in Belgium were found to contain 117 ppb Ir, equivalent to 25% of the value typical of chondrites.
- Wolbach, et al.⁽⁹⁾ report that sediments at the base of a 12,950 calendar years b2k carbon-rich dark layer coincident with the AL/YD boundary and containing significant amounts of soot contained high concentrations of Ir, magnetic grains, microspherules, and fullerenes abundant in ³He.
- Kobres, et al.⁽¹⁰⁾ report analysis of seven cores penetrated along the long axis of Howard Bay in North Carolina, which is one of the many elliptical depressions known as the "Carolina Bays." They find elevated Ir concentrations, abundant magnetic grains, microspherules, and carbon spherules similar to assemblages found in the YD boundary layer and conclude that these were deposited either immediately before or soon after the bay was formed.
- West, et al.⁽¹¹⁾ report detecting some of the highest AL/YD boundary ET markers in sediments from the Gainey Clovis site in Michigan, which included iridium, magnetic grains, microspherules, carbon spherules, soot, and fullerenes with ET helium. At the Topper Clovis site in South Carolina, they also report finding AL/YD boundary ET markers in a 5 cm thick layer lying immediately above the Clovis artifacts. Also they report finding iridium at 51 ppb (10% chondritic concentrations) inside an extinct horse skull at the Wally's Beach Clovis kill site suggestive of rapid burial following the YD event. They also examined several other sites that date to 12.9 kyrs b2k: glacial Lake Hind in Manitoba, Canada, an ice-aged drumlin at Morley in Alberta, Canada, Daisy Cave on the Channel Islands of California, and Lommel in Belgium. They report that the AL/YD boundary layer, which was evident at all of these sites, contained abundant ET markers.
- Darrah, et al.⁽¹²⁾ report that the Blackwater Draw Clovis site in New Mexico contains metallic iron grains while the Topper site in South Carolina also contains iron spherules, Fe-Ni metallic grains, and Fe-Ni oxides. They also analyzed fullerenes taken from the AL/YD boundary and found that they contained helium with an extraterrestrial isotopic signature. Carbonaceous residues extracted from AL/YD boundary bulk sediments taken from two of the sites contained elevated concentrations of helium-3 (0.3 to 3.5 ncc/g ³He) with an ET isotopic ³He/⁴He ratio of 30 to 220, suggesting substantial exposure to galactic cosmic rays. In particular they report that the residue from Daisy Cave, California contains helium with an isotopic ³He/⁴He ratio of 374 to 800, indicative of a significant galactic cosmic ray

input. They conclude that the increase in ^3He concentrations (5 to 8 ncc/g) with ET $^3\text{He}/^4\text{He}$ isotopic ratios ranging from 10 to 25 near the AL/YD boundary likely reflects an increase in the flux of interstellar dust particles.

These researchers, who referred to themselves as the "YDB group," interpreted the results as evidence that around 12,900 years ago a comet had either impacted the North American ice sheet or exploded in the air. They did not address the prediction I had previously made about the expectation of high iridium concentrations being found in such sediments, nor did they cite their discoveries as evidence in support of the superwave theory. Instead, Firestone and West proposed that these findings be interpreted in terms of the theory they had put forth a few years earlier attributing the megafaunal demise to the impact of a hyper velocity comet traveling around 2200 km/s associated with the passage of a supernova remnant shell.⁽¹³⁻¹⁵⁾ They proposed that this shell originated from a supernova explosion which they suggest occurred 41,000 years ago in the constellation of Gemini and at a distance of about 250 light years.

However, there are many problems with their theory. Twenty-two such problems are described in an eprint I posted on the internet in October 2007, also available on this disc **YD Event.pdf**.⁽¹⁶⁾ In that paper I also raise the concern that the extraterrestrial debris could not exclusively have originated from an impacting comet. The presence of high concentrations of ^3He in YD boundary sediments suggests that much of this debris entered the atmosphere as individual dust particles that were not appreciably heated on entry. Also there is the concern that the high iridium levels are not found just at one horizon, but over a range of depths spanning a period of several hundred years; see Figure 12-F. Such extended deposition favors more the idea of a period of elevated cosmic dust influx as opposed to a discrete comet impact event. Although microspherules and microtektites were found in these sediments, such particles could also have been formed in space. As I had pointed out in this dissertation (p. 222) they are found in the Earth's atmosphere at high altitudes and also on the Moon.⁽¹⁷⁾ Dust particles in the circumterrestrial dust sheath, Earth's "meteoric veil," could have been melted into spherules during an encounter with the plasma ball of a coronal mass ejection and propelled into the Earth's atmosphere as the CME defeated the Earth's magnetic field. So the

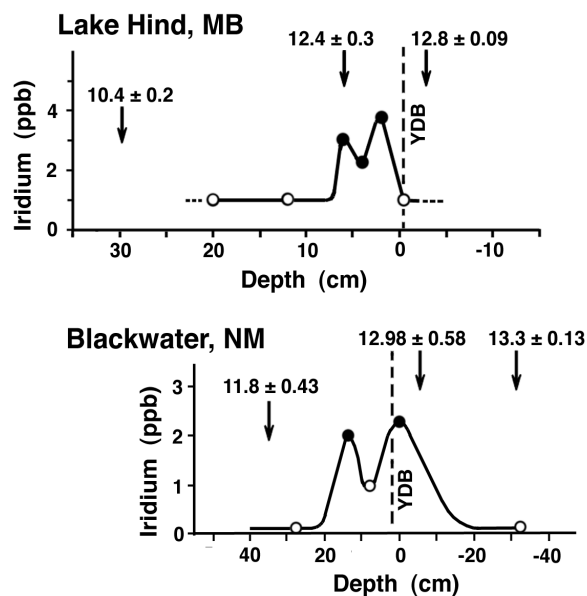


Figure 12-F. Iridium concentration in sediments from Lake Hind, Manitoba (top) and Blackwater Draw, New Mexico (bottom); after Firestone, et al. (2007).⁽⁶⁾

presence of melted particles and double iridium peaks could be indicators of the occurrence of several major solar flare catastrophes. Let us further explore this possibility.

Extraterrestrial dust and the collapse of the circumterrestrial dust cloud. Firestone et al. have suggested that the microspherules found in the YDB stratum underlying the black mat are debris from a cometary impact or aerial cometary explosion.⁽⁶⁾ However, other interpretations are possible. For example, cosmic spherules can be produced in the atmosphere during the high velocity entry of micrometeorite cosmic dust particles having diameters greater than 100 microns. To account for the spherules found on the Moon, Mueller and Hirsch have proposed that dust particles had been melted by an intense outburst of solar radiation (see also Ch. 8, p. 222).⁽¹⁸⁾ Furthermore chondrules (microspheres) are believed to be a component of cometary ice and to be released into the interplanetary medium along with the more friable cosmic dust particles whenever cometary ice vaporizes.

Whereas Pinter and Ishman⁽¹⁹⁾ have suggested that the ET indicators found in the YDB layer could be explained by the normal influx of cosmic dust, the levels reported by Firestone, et al. rule out this possibility since they indicate influx rates at least 10^5 fold higher than current cosmic dust deposition rates. So the presence of high levels of ET material in the YDB layer still needs an explanation.

Assuming that the YDB layer was formed during a period of generally elevated solar activity around the time when the Earth was impacted by a very large magnitude CME, the possibility presents itself that this ET material entered the Earth's atmosphere in connection with this solar event. The most likely cause would have been the CME-induced collapse of the magnetosphere bringing with it the collapse of the circumterrestrial dust cloud. Satellite and rocket observations have shown that the Earth is surrounded by a dust cloud extending radially outward from the Earth for a distance of 10^5 to 10^6 km, or 15 to 150 earth radii.⁽²⁰⁻²³⁾ Sunlight scattered from this dust cloud is believed to account for at least 10% of the light of the zodiacal cloud. Compared with interplanetary space, the number density of dust particles is estimated to be 10^5 fold higher for particles in the radial size range 0.1 to $10 \mu\text{m}$, 3000 fold higher for particles having radii on the order of $100 \mu\text{m}$, and tapering down to essentially no enhancement for 1 cm sized meteoroids. It is estimated that dust particles may have residence times in this cloud for upwards of thousands of years. Having acquired an electrical charge through photoionization by solar UV, they are susceptible to being picked up by the magnetosphere and magnetotail as the Earth sweeps through its orbit around the Sun. The cloud is also stocked by particles blown off the surface of the Moon by the impacting solar wind. The captured particles have very low velocities relative to the Earth and their motions are dominated by the geomagnetic field. For particles in the mass range 10^{-20} g to 10^{-15} g (r from $0.1 \mu\text{m}$ to $5 \mu\text{m}$) the Lorentz force is stronger than gravity.⁽²⁴⁾ Magnetic grains present in the cloud would be particularly susceptible to movement of the geomagnetic field which could explain the abundance of magnetic grains in the YDB layer. With the initial compression and subsequent collapse of the magnetopause, much of the dust in the circumterrestrial cloud would likely have been jettisoned into the Earth's stratosphere leaving its particles to float to the Earth's surface over a period of months to years.

The amount of dust present in the circumterrestrial dust sheath should have been sufficient to account for the ET material found in the YDB layer. Based on the abundances of magnetic grains reported by Firestone et al., it may be surmised that this layer contains about 0.1% ET material by weight within a depth of less than 5 cm, or about 15 mg/cm^2 . Hence if this deposit covers 10% of the Earth's surface, it would contain about 8×10^{15} g of

ET material. Ice core evidence presented here (p.) and elsewhere^(25, 26) suggests that cosmic dust mass concentrations in the interplanetary medium at the end of the last ice age may have reached as high as $5 \times 10^{-20} \text{ g/cm}^3$, or 250 times the present interplanetary mass density. Figuring a 10^5 fold enhancement, the circumterrestrial dust cloud would have contained a dust mass density averaging around 10^{-14} g/cm^3 . The required 8×10^{15} grams of material, then, could have been supplied from the portion of the cloud lying within fifteen earth radii of the Earth's surface, or $r \sim 10^5 \text{ km}$.

The incoming extraterrestrial dust would have served as condensation nuclei for water vapor present in the stratosphere, adding to the condensation nuclei being produced by the impacting solar cosmic rays. Both the formation of stratospheric clouds and the light scattering effects of the dust particles, most of which would have been in the submicron size range, would have dramatically increased the opacity of the stratosphere and reduced light transmission to the Earth's surface. This would explain why the NGRIP ice core oxygen isotope profile shows a sudden two-year cooling immediately after the 12,887 years b2k acidity spike (see Figure 10-G). Along with the light occlusion contributed by the smoke from global wildfires occurring during this time, both effects would have seriously impaired the survival of plant life.

Cosmic spherules could have naturally formed within the circumterrestrial dust cloud by impacting CME cosmic rays heating its trapped cosmic dust particles to their melting point. The most likely region where spherules would form would be between one and four earth radii from the Earth where the cloud's dense inner portion is intersected by the Earth's storm-time radiation belts.

Fullerenes, nanodiamonds, and helium-3, which are reported to be present in the YDB layer should also be expected to be present in the circumterrestrial dust sheath. Fullerenes and nanodiamonds have been found in carbonaceous chondrites and interplanetary dust particle aggregates.⁽²⁷⁾ So their presence in the YDB layer also does not exclusively imply the occurrence of a comet impact. Also helium-3 is a common component of interplanetary dust particles, being implanted during their exposure in space to the solar wind. So if there was a sudden influx of cosmic dust at the time of CME impact, elevated levels of helium-3 would be expected in soil sediments, as is observed.

Discovery of Tin in Association with Ir in YD Boundary Sediments (update to [p. 344](#))
Another very important finding that the YDB group announced at the 2007 Acapulco AGU meeting is their discovery of large concentrations of tin at the YD boundary. Darrah, et al. conducted SEM analysis of magnetic separates taken from the 12,900 years b2k boundary at several C-14 dated Clovis sites across the U.S. and found that these separates contained ET markers such as platinum (Pt) and nickel (Ni), but also in association with volatile metals such as tin (Sn) and copper (Cu).⁽¹²⁾ Metal combinations found included Fe-Ni, Cu-Ni, Fe-Sn-Ni. Abundances ranged from 25 - 28% for Sn, 12 - 90% for Cu, 1 - 11% for Ni, and 5 - 98% for Pt. These grains of extremely unusual composition were found to be in a metallic state and relatively unoxidized.

This provides strong evidence confirming my earlier conclusion that the tin-bearing dust particles found in ice age polar ice were of extraterrestrial origin. As in the polar dust I analyzed, these grains contained tin in combination with high levels of iridium.

References

- 1) J. Beer, et al., "¹⁰Be peaks as time markers in polar ice cores." In *The Last Deglaciation: Absolute and Radiocarbon Chronologies*, Proc. NATO ASI Series, vol. 12, 140–153. Heidelberg: Springer-Verlag, 1992.

- 2) K. J. R. Rosman, R. D. Loss ,and J. R. de Laeter, "The isotopic composition of tin." *Intl. J. Mass Spec. Ion Proc.* **56** (1984): 281 – 291.
- 3) R. A. Ward and H. Beer, *Astonomy and Astrophysics* **103** (1981): 189.
- 4) F. J. Rietmeijer "Tin in a chondritic interplanetary dust particle." *Meteoritics* **24** (1989): 43 – 47.
- 5) P. Gabrielli, "Meteoric smoke fallout over the Holocene epoch revealed by iridium and platinum in Greenland ice," *Nature* **432** (2004):1011-1014.
- 6) R. B. Firestone, et al., "Evidence for an extraterrestrial impact 12,900 years ago that contributed to the megafaunal extinctions and Younger Dryas cooling." *Proceedings of the National Academy of Sciences* **104**, October 9, 2007c, 16016 -16,021.
- 7) R. B. Firestone, et al., "Evidence for an extraterrestrial impact event 12,900 years ago that contributed to megafaunal extinctions and the Younger Dryas cooling." Poster paper PP43A-01, May 2007 AGU Conference, Acapulco, Mexico.
- 8) R. B. Firestone, et al., "Evidence for a massive extraterrestrial airburst over North America 12.9 ka ago." Paper PP41A-01, May 2007 AGU Conference, Acapulco, Mexico.
- 9) W. S. Wolbach, et al., "Is there evidence for impact-triggered fires at the end Pleistocene?" Paper PP43A-03, May 2007 AGU Conference, Acapulco, Mexico.
- 10) R. Kobres, et al., "Formation of the Carolina Bays: ET Impact vs. Wind-and-Water." Poster paper PP43A-10, May 2007 AGU Conference, Acapulco, Mexico.
- 11) A. West, "Extraterrestrial markers found at Clovis sites across North America." Paper PP41A-02, May 2007 AGU Conference, Acapulco, Mexico.
- 12) T. H. Darrah, et al., "Mineralogical and noble gas evidence for an ET impact at the Younger Dryas." Paper PP41A-04, May 2007 AGU Conference, Acapulco, Mexico.
- 13) R. B. Firestone, and W. Topping, "Terrestrial evidence of a nuclear catastrophe in Paleoindian times." *Mammoth Trumpet* **16**(2) March 2001, pp. 9 - 16.
- 14) "Supernova may have caused mammoth extinction." Sept. 23, 2005 Lawrence Berkeley National Laboratory press release, September 23, 2005.
- 15) R. B. Firestone, A. West, and S. Warwick-Smith, *The Cycle of Cosmic Catastrophes*. Rochester, VT, Bear & Co., 2006.
- 16) P. A. LaViolette, "The cause of the megafaunal extinction: Supernova or Galactic core outburst?" Eprint at: <http://www.starburstfound.org/YDextinct/p1.html>.
- 17) D. W. Parkin , R. A. L. Sullivan, and J. N. Andrews, "Cosmic spherules as rounded bodies in space." *Nature* **266** (1977):515-517.
- 18) G. Mueller and G. W. Hinsch, "Glassy particles in lunar fines." *Nature* **228** (1970):254-258.
- 19) N. Pinter and S. E. Ishman, "Impacts, mega-tsunami, and other extraordinary claims." *GSA Today* **18** (2008):37-38.
- 20) N. B. Divari, "Charged dust particles in interplanetary space." *Astronomicheskij Zhurnal***43** (1966):192-197.
- 21) N. B. Divari, "The cosmic dust cloud around the Earth." *Soviet Astronomy* **10** (1967):1017-1030.
- 22) B. A. Tverskoi, "The influence of corpuscular radiation on the circumterrestrial cloud." *Soviet Astronomy* **10** (1967):1031-1033.
- 23) V. N. Senatorov, "On the possible existence of radiation dust belts in near-Earth space." *Cosmic Research* **38** (2000):612-615.
- 24) H. Alfven and G. Arrhenius, *Evolution of the Solar System* (NASA, Washington, 1979).
- 25) P. A. LaViolette, "Evidence of high cosmic dust concentrations in late Pleistocene polar ice." *Meteoritics* **20** (1985):545-558.
- 26) P. A. LaViolette, "Solar cycle variations in ice acidity at the end of the last ice age: Possible marker of a climatically significant interstellar dust incursion." *Planetary and Space Science* **53** (2005):385-393.
- 27) F. J. M. Rietmeijer, "Fullerenes and nanodiamonds in aggregate interplanetary dust and carbonaceous meteorites." in *Natural Fullerenes and Related Structures of Elemental Carbon*, vol. 6. ed. Rietmeijer FJM (Springer, Netherlands, 2006), pp 123-144.

CHAPTER 13

CONCLUSION

I have shown (Chapter 2) that the superwave model offers a consistent theoretical framework for understanding a wide variety of energetic phenomena observed in the nuclei of galaxies. Superwaves may be the cause of:

- a) compact variable continuum emission sources and line emission sources found in active galactic nuclei,
- b) superluminally separating double compact radio sources observed in active galactic nuclei,
- c) the varied optical appearances of both active and normal galaxies,
- d) the formation of double radio emission lobes extending millions of light years away from galaxies,
- e) the formation of spiral arms and ring features in galaxies at distances of up to 10^5 light years from the nucleus.

In our own Galaxy recurrent superwaves could explain the radial motion of gas rings and gas clouds in the Galactic nucleus, and could account for the formation of "supershells" in the interstellar medium of the Galactic disk. Also, superwaves could be the energy source periodically propelling the local interstellar wind.

The present relatively quiescent state of the local interstellar environment is thus misleading. The Galactic Explosion Hypothesis instead suggests that the "calm sea" of space is from time to time interrupted by a "raging storm," i.e., that explosive events generated in the center of the Galaxy have a major impact on the solar system environment. In particular, it is suggested that in the past such recurrent cosmic events have been responsible for triggering abrupt changes in the Earth's climate, for producing geomagnetic excursions and reversals, for causing mass extinctions, and for accelerating the rate of evolution of life.

The proposed passage of a superwave through the solar vicinity beginning about 14,250 years b2k is shown here to be supported by astronomical, planetary, and terrestrial evidence. For example, as was discussed in Chapter 4 (Section 4.1), the asymmetrical distribution of hot dust and ionized gas about the Galactic center suggests that the GC has undergone an explosive outburst within the last 10^4 years. The ellipsoidal event horizon of a recent superwave would be difficult to observe since the radiation emitted by its constituent cosmic rays would be relativistically beamed away from the GC, and hence away from an Earth-based observer. However, some fraction of these cosmic rays, captured into spiral orbits by Galactic magnetic fields, would be expected to beam synchrotron radiation toward the Earth. As is discussed in Chapter 5 (Section 5.1), the observed Galactic nonthermal radio background radiation (synchrotron radiation) may be such evidence of the presence of the 14,250 years b2k superwave. Especially convincing is the conformity of the longitudinal distribution of this background radiation to the distribution predicted by the 14,200 years BP superwave model.

Additionally, the presence of the 14,200 years BP superwave should be revealed wherever its cosmic rays encounter young supernova remnants. As is discussed in Subsection 5.2, the Crab Nebula and Cassiopeia A remnant, the two brightest supernova remnants in the Galaxy, are located on the 14,200 years BP superwave event horizon. Sections 5.3 and 5.4 detail several unusual features of these nebulae which are nicely explained if it is assumed that these remnants are being impacted by an intense volley of cosmic ray electrons propagating

outward through the Galaxy from the GC. It is also suggested there that the supernova explosions forming these and other young remnants in the Galaxy were triggered by the passage of the 14,200 years BP superwave. Moreover, it is noted that the three of the fastest pulsars — the recently discovered Millisecond Pulsar (PSR 1937+21), the Crab Pulsar (PSR 0531+21), and the Binary Pulsar (PSR 1913+16) — coincide approximately with the present position of the 14,200 years BP superwave event horizon. The position of a fourth short period pulsar, the Vela Pulsar, does not presently coincide with this event horizon; however, at the time of this pulsar's birth, about 14,000 years ago, the 14,200 years BP superwave would have been transiting this location. [Read *Decoding the Message of the Pulsars*.⁽¹⁾]

As is described in Subsection 4.7, several unusual features of the planets in our solar system could be explained by a recent exposure to a high temperature environment, as might be created during the passage of a superwave. In particular, very recent heating activity $\sim 10^4$ years ago could explain the perplexing intricately grooved pattern of Saturn's ring system. Also, the solar flare particle track record found in Moon rocks indicates that there was a substantial increase in solar activity between 10,000 – 16,000 years BP. Such an activity increase could have been the Sun's response to the accretion of nebular material brought into the solar system by the hypothesized superwave.

The Earth is able to provide a wealth of information about past changes in its interplanetary environment. Particularly valuable is the glacial ice record, several features of which may be interpreted as evidence of the passage of the 14,200 years BP superwave. First, there is the observation that during the last ice age the deposition rate of cosmogenic beryllium-10 [at times] increased 2 – 3 times above rates typical of the past 10,000 years, indicating an elevation of the local cosmic ray intensity; see Section 8.4. Then there is the observation that around 14,200 years BP there was a one to two orders of magnitude increase in the rate of cosmic dust deposition on the Earth's surface (as indicated by the results of the glacial ice dust tests performed in this study; see Section 8.3 and Subsection 12.1.4).

These elevated cosmic dust deposition rates are best interpreted as evidence that the interplanetary environment was at that time congested with nebular material, possibly vaporized from cometary masses and transported into the solar system by superwaves. As is discussed in Chapter 3 (Subsection 3.3.4), the presence of such dust in the Earth's environment would have produced various climatic effects ranging from climatic cooling and glacial advance to climatic warming and glacial recession.

High deposition rates of extraterrestrial material are also found to be registered at $\sim 50,500$ b2k and $\sim 78,500$ b2k. Since these cosmic episodes tend to correlate with times of high atmospheric dust loading, it may be inferred that other dust peaks present in Wisconsin ice are also associated with increases in cosmic dust deposition rate. Consequently, dust peaks dating prior to 14,200 years BP may be evidence of earlier superwaves. A detailed stratigraphic geochemical analysis of glacial ice should be undertaken to check the results reported here, with particular attention paid to the period 14,200 to 10,000 years BP.

Also noteworthy is the observation that the concentration of dust in glacial ice dating from the Late Wisconsin stage is about an order of magnitude higher than dust concentrations typical of the past 10,000 years; see Subsection 8.2. This unusual dustiness of the Earth's atmosphere may have been caused by increased windiness associated with the presence of thick stratospheric clouds nucleated by cosmic dust particles entering the Earth's atmosphere. While the superwave would have still been passing through the solar system, there was an abrupt climatic warming (the beginning of the Terminal Pleistocene Interstadial) which marked the beginning of the period of glacial recession terminating the Wisconsin Ice Age.

The sedimentary record also provides valuable information about events transpiring on the Earth at the close of the Last Ice Age; see Chapter 9. For example, it is found that from about 14,750 to 14,200 calendar years b2k, while the Earth was still in a glaciated state, there was a period of warm climate during which time the Earth's atmospheric temperature rose by

as much as 10° – 11° C (in high latitude regions). At its hypsithermal peak around 14,400 calendar years b2k, the temperature, particularly in high latitude regions, was either comparable to or higher than levels typical of the current interglacial. Such a major climatic warming occurring at a time when the Earth was in a fully glaciated state could have been brought about by an interplanetary greenhouse effect caused by nebular material in the outer solar system reflecting back sunlight.

It is here concluded that the Terminal Pleistocene Interstadial was most probably the cause of the rapid rate of glacial meltwater discharge which reached a peak around 14,400 calendar years b2k. This accelerated glacial melting in turn appears to have been the cause of the continental flooding which occurred about this time in periglacial regions around the globe. With accelerated surface melting of the ice sheets, it is hypothesized that "glacier waves" could have been produced; i.e., mountainous waves of meltwater propagating forward at speeds of 200 miles per hour or more; see Section 10.3. Such a hydrologic phenomenon is presented here as being a likely candidate for causing the widespread slaughter of large land animals found in alluvial deposits, although other factors associated with this hypsithermal period may have been equally important, e.g., excessive heat exposure or habitat change. It is suggested that this cataclysmic event, referred to here as the "Terminal Pleistocene Extinction Episode," transpired over a relatively short period of time and ended about 12,950 calendar years b2k.

It is here concluded that evidence gathered from the fields of geology, planetology, and extragalactic and Galactic astronomy, is consistent with the Galactic Explosion Hypothesis. Moreover, in the course of this study no data could be found that would specifically refute this hypothesis. It is significant that several predictions of the GEH, made prior to the commencement of this investigation (listed in Table I, **p. 6**), have been subsequently confirmed. In particular the Be-10 data of Raisbeck et al. (1981) and Beer et al. (1982), which have been interpreted here as confirmatory evidence for prediction #2 (Table I), were published after the GEH had been formulated. The positive results of the cosmic tests carried out in the present study (78.5 to 38.7 kyrs b2k) do not necessarily confirm prediction #3 (Table I), but they do strongly suggest that future measurements of the terminal ice age period will confirm this prediction. Moreover, the detection reported here of high concentrations of extraterrestrial material in glacial ice dating from the Late Wisconsin stage represents the first geochemical evidence of its kind indicating that our planet has experienced a cosmic event within recent times, i.e., within the time span of our species. Thus the Terminal Pleistocene may be added to the list of other geologic boundaries, such as the Terminal Cretaceous and Terminal Eocene, in which it is permissible to consider extraterrestrial causes as explanations for past geologic events.

In addition to the predictions listed in Table I, several other predictions have emerged in the course of conducting this research study and these are summarized in Table XVIII. Confirmation of these would provide added strength to the body of evidence already gathered in the present study. [See **predictions.pdf** for confirmation of several predictions.]

It may be concluded that at this time perhaps as many as five superwaves [two major superwaves] are in the process of traveling toward our solar system from the GC. We cannot see them because they are traveling at very close to the speed of light. That is, the radiation which the constituent cosmic rays emit would travel to us about as fast as the superwave itself. Hence the next superwave will arrive without warning. The likelihood that the next superwave would arrive within a given future time frame may be judged on the basis of the arrival times of past events registered in the geologic record. For example, about 6000 years had elapsed between the date of the 6000 years BP event and the end of the 14,200 years BP superwave passage. For the Yarmouthian (Holsteinian) Interglacial, the sedimentary record is consistent with superwaves passing by about every 7000 years; see **p. 248**. So as a conservative estimate, one could conjecture that there is a 90% probability that the next superwave should arrive

TABLE XVIII
Specific Predictions Following from the Galactic Explosion Hypothesis

- A. Extragalactic Predictions Pertaining to the Superwave Model (Chapter 2).
1. Observations made with the Space Telescope, which will have far better optical resolution than existing earth-based telescopes, should result in the following reclassifications of many of the active galaxies: Galaxies formerly classified as blazars and quasars are expected to be seen as N-galaxies, Seyfert galaxies, and giant elliptical galaxies. Also, many galaxies formerly classified as giant ellipticals are expected to display equatorial dust lanes, and hence would be better classified as type S0. Confirmation of this prediction would support the hypothesis that all active galaxies are spiral galaxies (similar to our own) whose nuclei are going through an active phase; see **p. 40**.
[UPDATE: These predictions have now been verified; see the update at the end of this chapter (p. 370).]
 2. Ring galaxies such as 1008-38 and VII Zw466 should be found to have spiral arms; see **pp. 56 and 59**. Such evidence would be consistent with the hypothesis that ring features are a phenomenon characteristic primarily of spiral galaxies, e.g., produced by the outward propagation of superwaves from the galaxy's nucleus.
 3. In addition to radio quasar 3C 179 other radio quasars should be found in which the associated extended radio-emitting lobes are best interpreted as projecting toward the observer. Evidence that such an orientation is typical of the majority of observed radio lobes would support the proposal that such active galaxies emit volleys of relativistic electrons in an isotropic manner and that these cosmic rays penetrate the entire extent of the galaxy.
- B. Predictions Pertaining to Superwaves Presently Propagating through the Galaxy (Chapters 5 and 6).
1. A time sequence of high resolution radio maps made of Cassiopeia A should reveal regions of enhanced radio surface brightness propagating across the remnant at relativistic speeds in a west-to-east direction. Superluminal motion of such radio brightness changes could possibly also be observed; see **p. 186**.
 2. The presence of the 14,200 years BP and 6000 years BP superwaves could be further verified if the locations of unusually energetic stars and interstellar gas clouds are found to preferentially align with the event horizons of these superwaves.
 3. If the martian polar ice cap record date back as far as 20,000 years BP and if a martian ice core spanning this period can be retrieved and analyzed, then it should be found to preserve a record of climatic change, atmospheric dustiness, and cosmic dust deposition similar to the record found in terrestrial polar ice records.
- C. Predictions Regarding the Terrestrial Record (Chapters 7 and 8).
1. A major increase in nitrate concentrations should be observed in glacial ice spanning 16,000 – 12,700 calendar years BP, a period during which the Sun is likely to have engaged in T Tauri-like flare activity.
[UPDATE: Be-10, on the other hand, may not be a good indicator of solar flare activity since solar flare cosmic rays, being less energetic than Galactic cosmic rays, may not have sufficient energy to induce Be-10 production.]

TABLE XVIII (cont.)

2. Geochemical analysis of ice samples from dust peaks Nos. 1, 2, 3, 6, 8, 9, and 10 should show that they contain high concentrations of iridium. A positive finding would constitute strong evidence that there were several previous episodes of interplanetary dustiness suggesting that during the Last Ice Age superwaves may have been passing through the solar system as frequently as once every 10,000 years. Ice samples associated with dust peaks #8 and #10 are of particular interest since they mark boundaries of major climatic change.
 3. Geochemical analysis of dust bands filtered from the Byrd Station ice core should show that in a substantial portion of these the concentration of Ir per unit volume of ice should be higher than in surrounding ice, as was observed in the ash band analyzed in this study.
 4. Geochemical analysis of dust taken from the Dye 3 ice core, at a certain depth in the vicinity of 1899 – 1905 meters, should be found to contain high concentrations of Sn, Au, Ir, Ag, and Sb, as was found in Sample #962-1 taken from the Camp Century ice core; see **p. 227**.
 5. Other climatic boundaries marking the initiation and termination of ice ages during the Pleistocene should be found to exhibit evidence of enhanced concentrations of extraterrestrial dust and cosmogenic beryllium.
[UPDATE: This prediction has now been verified. The Vostok ice core record has been found to contain Be-10 peaks that coincide with climatic boundaries; see the update at the end of chapter 8 (**p. 236**).]
 6. Gold-bearing dust should be found in other glacial ice cores, particularly in Wisconsin stage ice. Such a finding would provide additional evidence supporting the proposal that much of the gold found in Late Pleistocene deposits is of extraterrestrial origin.
-

sometime within the next 4000 years. As a more liberal prediction, it might be estimated that there is a 50:50 chance a superwave might pass through the solar system in the next few hundred years. [See update at the end of this chapter (**p. 371**) for a revised estimate of superwave frequency.]

So, the phenomenon of Galactic superwaves and their effects on the Earth's climate and biosphere should be of concern, not only to the scientific community, but to the international community as a whole. Again, it should be mentioned that mankind's present dependence on electrical and electronic equipment would make modern civilization particularly vulnerable if EMP (electromagnetic pulse) effects are created by a superwave. For example, as mentioned in Subsection 3.3.6, the gamma ray flash of a superwave would travel at the speed of light and would arrive without warning. If such a flash were to produce an EMP in the Earth's atmosphere, in a matter of minutes societies could be paralyzed by widespread failures of electrical power and communication systems. Also, there is the chilling possibility that a superwave EMP might be misinterpreted by the nuclear-armed superpowers as an attack by the "other side" and might result in the triggering of a nuclear world war.

To prepare for such a hazard, steps should be taken both to reduce the threat of nuclear war through disarmament and through the installation of EMP proof "red telephone" communication channels. In addition, measures should be taken to make societies more resistant to the disabling effects of EMP; see **pp. 120–121**. Finally, national and international emergency preparedness plans should be devised for dealing with a superwave disaster should one arise. The climatic consequences of a superwave may be the most difficult of all to

prepare for since the next superwave could very likely trigger the onset of an ice age ending the present 10,000 year period of mild global climate.

In the immediate future, a detailed study of the Earth's glacial and sedimentary records should be undertaken in order to learn as much as possible about past superwave events.

[UPDATE: Dr. LaViolette has attempted to conduct such research; see Appendix K (pp. 470 - 473) and Appendix C of *Earth Under Fire*.⁽²⁾]

In addition, an expanded astronomical program should be undertaken to learn as much as possible about our Galaxy with particular emphasis placed on studying recent superwave event horizons (e.g., 14,200 years BP, 6000 years BP) and with around-the-clock monitoring of the Galactic center to detect possible signs of an impending outburst. The Space Telescope and other satellite telescopes sensitive to infrared, UV, X-ray, and γ -ray wavelengths should be useful in this regard. **[UPDATE:** This situation has since changed somewhat. Astronomers currently make daily observations of the GC (Sgr A*) with the VLA radio telescope.]

Finally, a more serious effort should be made to explore our solar system. At some time in the future it should be possible to land spacecraft on the martian polar ice cap for the purpose of drilling, extracting, and returning to Earth (for analysis) a deep ice core. Comparison of the martian ice record with terrestrial glacial records should provide valuable information on past conditions in the solar system and should allow a definitive test to be made of the Galactic Explosion Hypothesis (GEH).

The GEH should be of considerable value to scientists searching for communication signals from extraterrestrial civilizations. If a major superwave (e.g., the 14,200 years BP superwave) were presently passing through the Galactic disk, then it should be affecting other life-supporting planets and star systems in a manner not too different from the way it appears to have affected our own planet and solar system. Consequently, superwaves would be an obvious topic of conversation for the "Galactic network." [For more about this, read *Decoding the Message of the Pulsars*.⁽¹⁾]

Finally, the GEH should offer valuable insights into the origin of numerous myths and legends describing the past occurrence of unusual astronomical and geological phenomena (e.g., the darkened Sun and Moon, the periods of unending daylight, the Deluge, etc.). [For more about this read *Earth Under Fire*.] Such stories (possibly arising from eyewitness accounts) could provide scientists with valuable assistance in searching for and interpreting geological data. Perhaps even more significant from a humanitarian standpoint, the realization that many of these stories may have a core of truth in them allows us to adopt a radically new perspective in regard to the intelligence of our ancestors. The origin of science, e.g., the art of observing and documenting the occurrence of natural phenomena, may actually have started as far back as "stone age" times.

UPDATE

Hubble Space Telescope Verification of Predictions about the Morphology of Active Galaxies (update to p. 368): As summarized in Table XVIII (A-1), the superwave model predicts that quasars are examples of very intense galactic core explosions, and hence involve essentially the same type of phenomenon that takes place in spiral galaxies. It was suggested that the star-like appearance of quasars arises because of these distant galaxies are not easily resolved with ground based telescopes. As predicted above, observations carried out with the Hubble Space Telescope showed that quasars are highly luminous cores contained within parent galaxies. One example is quasar 1229+204 shown in Figure 13-A. The image to the left shows how it appears with a ground-based telescope and the image to the right shows the

Hubble Space Telescope image which resolves its surrounding spiral arm structure. PG 0052+251, shown in Figure 13-B, is another example of a quasar that has been resolved into a Seyfert-like spiral galaxy. This galaxy's luminous core, which is seven times brighter than its surrounding disc, radiates 100 billion times as much energy as our Sun. In the case of the exceedingly bright quasar 3C273, the Hubble Telescope image shown in Figure 13-C (left) did not resolve its galaxy. However, in 1982 a group of astronomers succeeded in imaging its surrounding galaxy using a charge coupled device detector and a special imaging technique that masks the quasar's light; see Figure 13-C (right).⁽⁴⁾

The prediction that many giant ellipticals should be found to display equatorial dust lanes when imaged with the Hubble Space Telescope is born out by observations of giant elliptical NGC 6251. Figure 13-D compares a ground-based telescope image of this galaxy with an image made with the Hubble Space Telescope which resolves its equatorial dust band. When properly resolved, NGC 6251 has an appearance similar to the nearby active galaxy Centaurus A. Consequently, it may be better classified as an S0 type spiral galaxy which presents an elliptical appearance due to its edge-on inclination and bright nucleus.

Revised Estimate of the Frequency of Minor Superwave Events Inferred from Galactic Core Observations (update to p. 369): The Galactic center may also flare up frequently between major superwave events. Astronomical observation indicates that during the past 5,300 years, the Galactic center has expelled 14 clouds of ionized gas (see p. 131).⁽⁴⁾ The dates estimated for these expulsions are shown on the timeline in Figure 13-E. The age estimates are taken from the data of Lacy et al., decreased by ~70% to correct for the smaller galactocentric distance adopted here, which assumes a distance of 23,000 rather than 30,000 light years. If these minor outbursts were associated with superwave cosmic ray volleys, they apparently were not strong enough to generate beryllium-10 peaks in the ice record visible above background levels. Their associated EMP, however, could have been sufficiently strong that, had one such event occurred today, it could have posed a serious hazard to modern electronics and communications unlike anything thus far witnessed. About 80% of these gas emissions took place within 500 years of one another (Figure 13-F). Yet, it has been 700 years since the last event. So, there is a high probability of another one occurring in the very near future.

References to the Update:

- 1) P. A. LaViolette, *Decoding the Message of the Pulsars*. Rochester, VT: Bear & Co., 2000, 2005.
- 2) P. A. LaViolette, *Earth Under Fire*. Rochester, VT: Bear & Co., 1997, 2005.
- 3) J. N. Bahcall, S. Kirhakos, and D. P. Schneider, "The apparently normal galaxy hosts for two luminous quasars." *Astrophysical Journal* **457** (1996):557 – 564.
- 4) J. A. Tyson, W. A. Baum, and T. Kreidl, "Deep CCD images of 3C 273." *Astrophysical Journal* **257** (1982):L1– L5.
- 5) J. H. Lacy, et al. "Observations of the motion and distribution of the ionized gas in the central parsec of the Galaxy." *Astrophysical Journal* **241** (1980): 132

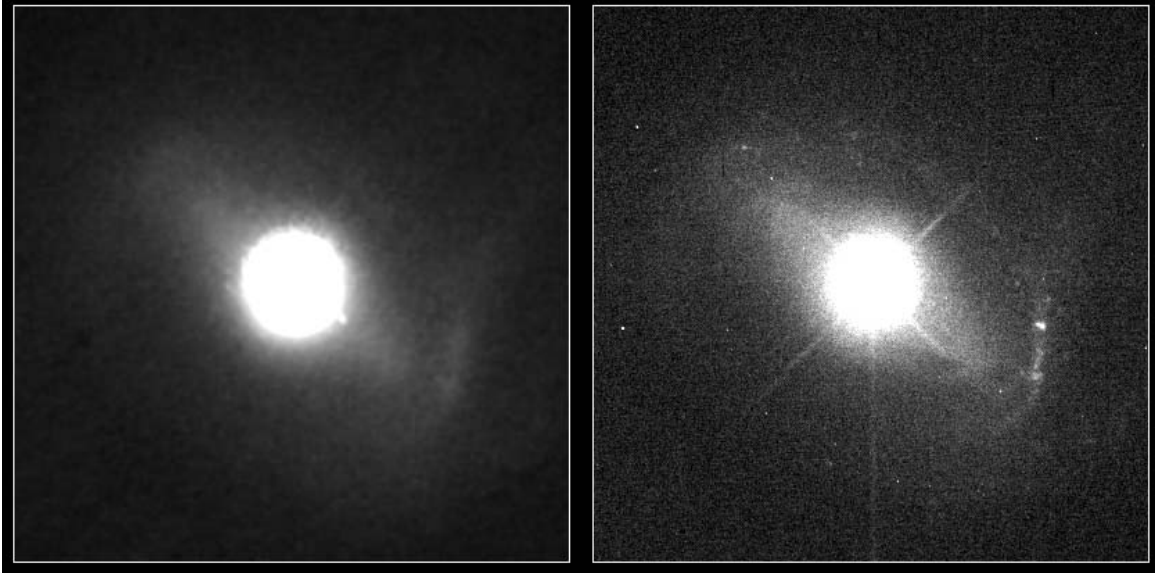


Figure 13-A. Quasar 1229+204, (left) as seen with the Canada-France-Hawaii ground-based telescope, and (right) as seen with the Hubble Space Telescope Wide Field Planetary Camera. The surrounding spiral arm disk is faintly visible (courtesy of J. Hutchings and NASA).

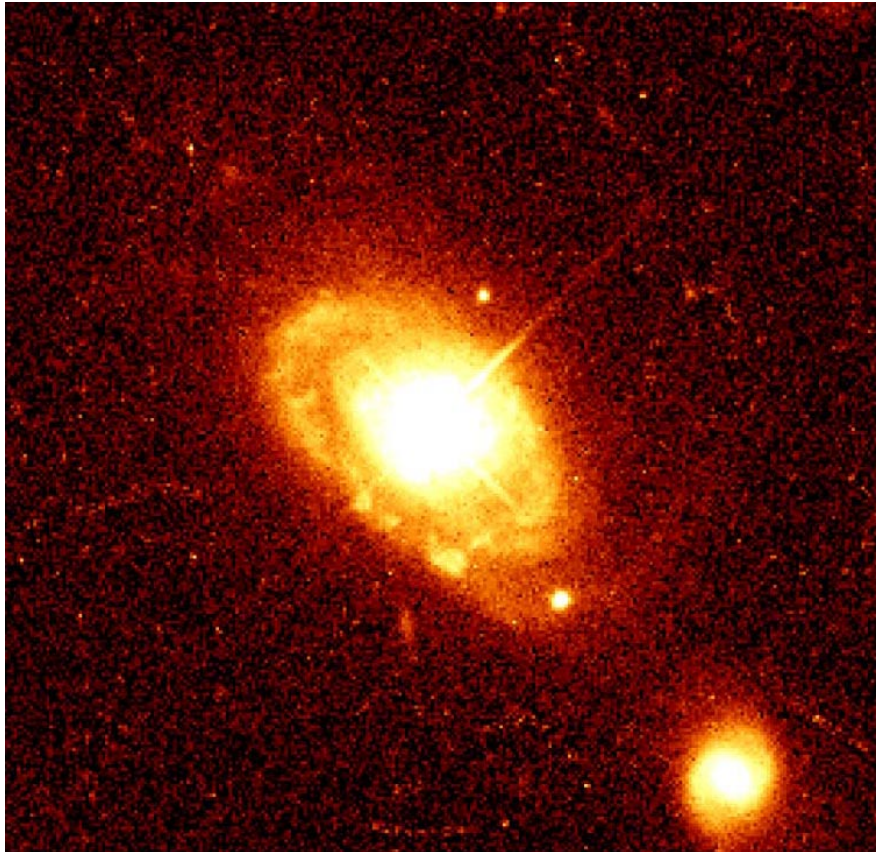


Figure 13-B. Quasar PG 0052+251 as seen with the Hubble Space Telescope. The galaxy's spiral arm structure is clearly visible (courtesy of J. Bahcall and NASA).

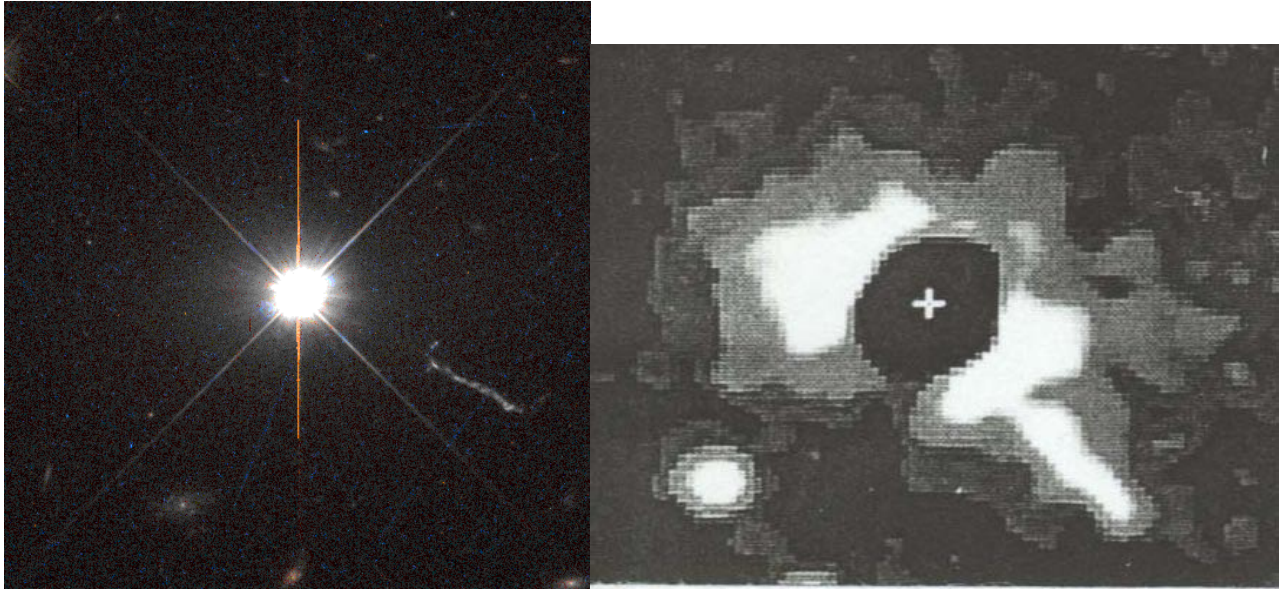


Figure 13-C. Quasar 3C 273 in Virgo (left) as seen with the Hubble Space Telescope and (right) as viewed with a highly sensitive CCD detector with a special imaging technique that resolves the galaxy's disk by masking its bright central core.

(Left: courtesy of J. Bahcall and NASA. Right: courtesy of J. Tyson , W. Baum, and T. Kreidl).

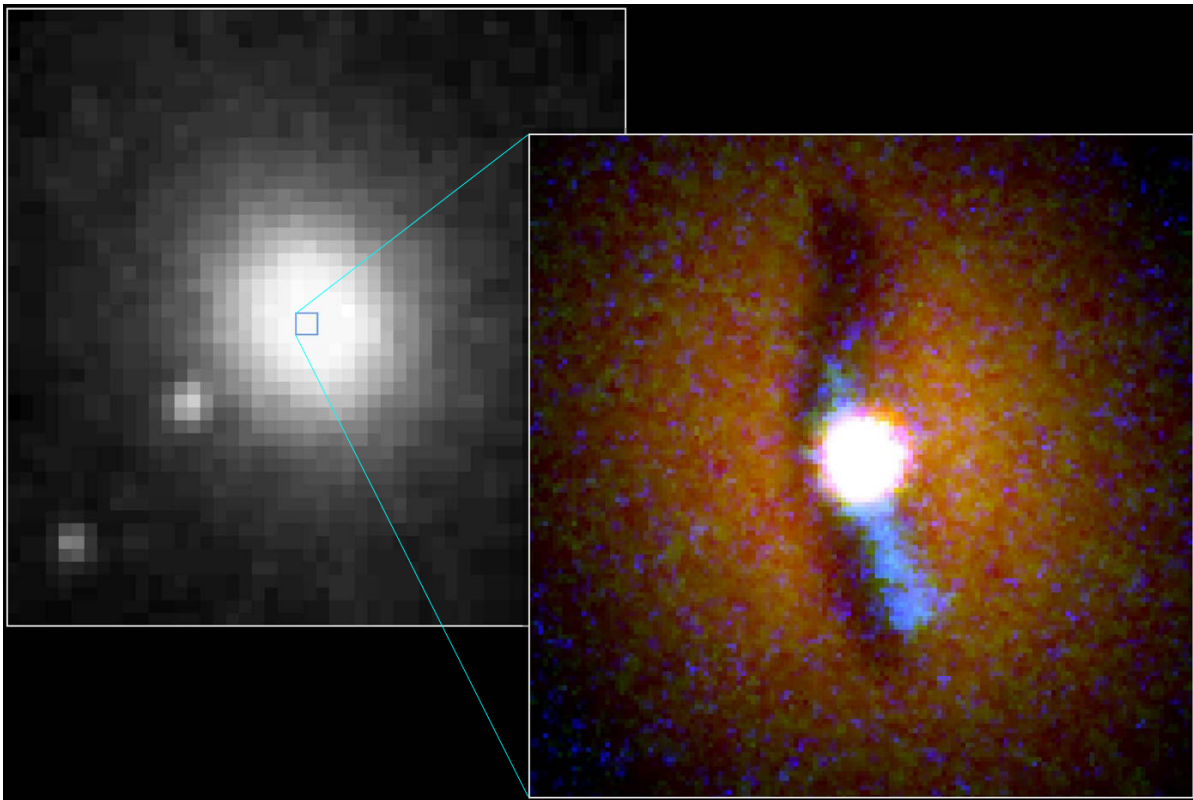


Figure 13-D. Active giant elliptical galaxy NGC 6251 in Ursa Minor, (left) as seen with a ground-based telescope and (right) as seen with the Hubble Telescope Wide Field Planetary Camera (courtesy of P. Crane and NASA). The right image resolves the galaxy's edge-on disc. The blue ridge highlighting the right side of the disk is reflected ultraviolet light imaged with the Hubble Faint Object Camera.

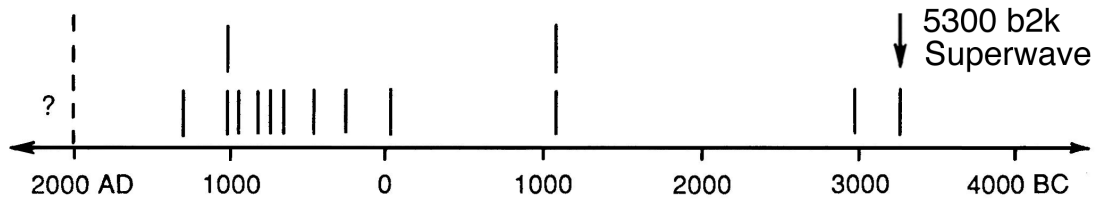


Figure 13-E. History of minor Galactic Center explosions during the past 6000 years; dates approximate times when radiation pulses may have arrived from the Galactic Center.

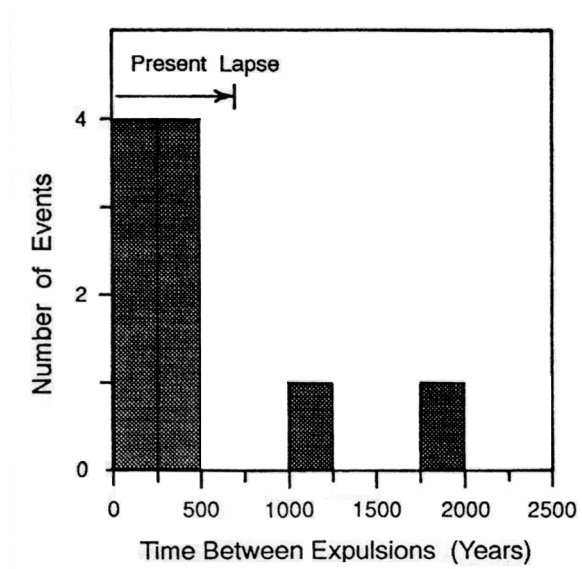


Figure 13-F. Amount of time between successive gas expulsions from the Galactic center, plotted as a frequency histogram.

BIBLIOGRAPHY

- Adams, T. F., and Frisch, P. C. "High-resolution Observations of the Lyman Alpha Sky Background." *Astrophysical Journal* **212** (1977):300.
- Ajello, J. M., Witt, N., and Blum, P. W. "Four UV Observations of the Interstellar Wind by Mariner 10: Analysis with Spherically Symmetric Solar Radiation Models." *Astronomy and Astrophysics* **73**, (1979):260.
- Alexander, J., and Clark, T. A. "Radio Astronomy." In *High Energy Particles and Quanta in Astrophysics*, edited by F. B. McDonald and C. E. Fichtel. Cambridge, Mass.: MIT Press, 1974.
- Allen, D. A. *Infrared: The New Astronomy*. Shaldon, Devon: Keith Reid, 1975.
- "Brighter Than a Million Suns." *Yearbook of Astronomy* (1979):191.
- Allen, R. J., Goss, W. M., Ekers, R. D., and de Bruyn, A. G. "The Giant Spiral Galaxy M101." *Astronomy and Astrophysics* **48** (1976):253.
- Aller, L. H. *Gaseous Nebulae*. New York: John Wiley and Sons, 1956.
- Alvarez, L. W., Alvarez, W., Asaro, F., and Michel, H. V. University of California Lawrence Berkeley Lab., Report # LBL-9666, 1979.
- "Extraterrestrial Cause for the Cretaceous-Tertiary Extinction: Experimental Results and Theoretical Interpretation." *Science* **208** (1980):1095.
- Amaldi, E., Bonifazi, P., Frasca, S., Pallottino, G. V., and Pizzella, G. "Data Analysis for the Gravitational Wave Antennas in Rome and in Frascati." *10th Texas Symposium on Relativistic Astrophysics*, Baltimore, Md., December, 1980 (unpublished).
- Ambartsumian, V. A. *The 11th Solvay Conference*. Brussels: Institute Internationale de Physique Solvay, 1958, p. 241.
- "The Structure and Evolution of Galaxies." *Proceedings of the 13th Solvay Conference, University of Brussels*. New York: Wiley Interscience, 1965.
- Andrillat, Y. "Spectral Variations of the Nucleus of NGC 3516." (Seyfert Galaxy Conference, Paper #15) *Astronomical Journal* **73** (1968): 862.
- Arp, H. C. "The Evolution of Galaxies." *Scientific American* **208** (January 1963):70.
- "Optical Observations of Two Seyfert Galaxies." (Seyfert Galaxy Conference, Paper #4) *Astronomical Journal* **73** (1968):847.
- Atkinson, R. d'E *Proceedings of the Royal Society of London* **272** (1962): 60.

- . "Two General Integrals of $G = 0$." *Astronomical Journal* **70** (1965a):513.
- . "On Light Tracks near a Very Massive Star." *Astronomical Journal* **70** (1965b):517.
- Baade, W. "The Crab Nebula." *Astrophysical Journal* **96** (1942):188.
- Baade, W., and Arp, H. "Positions of Emission Nebulae in M 31." *Astrophysical Journal* **139** (1964):1027.
- Backer, D. C., Kulkarni, S. R., Heiles, C., Davis, M. M., and Goss, W. M. "A Millisecond Pulsar." *Nature* **300** (1982):615.
- Bailey, M. E., and Clube, S. V. M. "Recurrent Activity in Galactic Nuclei." *Nature* **275** (1978):278.
- . "Comets, Planet X and the Orbit of Neptune." *Nature* **302** (1983):399.
- Baker, V. R. "The Spokane Flood Controversy and the Martian Outflow Channels." *Science* **202** (1978):1249.
- Baldwin, J. A. et al. "The Nebulosity Associated with 3C 120." *Astrophysical Journal* **236** (1980):388.
- Baldwin, J. E., Harris, C. S., and Ryle, M. "5 GHz Observations of the Infrared Star MWC 349 and the H II Condensation W 3 (OH)." *Nature* **241** (1973):38.
- Bancroft, H. H. *The Native Races of the Pacific States*. Vol. 3. 1874.
- Barbetti, M., and Flude, K. "Geomagnetic Variation During the Late Pleistocene Period and Changes in the Radiocarbon Time Scale." *Nature* **279** (1979):202.
- Barbetti, M., and McElhinny, M. "Evidence of a Geomagnetic Excursion 30,000 yr B.P." *Nature* **239** (1972):327.
- Barnothy, J. M., and Barnothy, M. F. "Connection Between Seyfert Galaxies, N-Type Radio Galaxies, and Quasistellar Sources." (Seyfert Galaxy Conference, Paper #44) *Astronomical Journal* **73** (1968):912.
- Beard, J. H. "Pleistocene-Holocene Boundary and Wisconsinan Substages, Gulf of Mexico." In *The Wisconsin Stage* (GSA Memoir 136), edited by R. F. Black, R. P. Goldthwait, and H. B. Willman. Boulder: Geological Society of America, 1973.
- Becker, R. H., Szymkowiak, A. E., Boldt, E. A., Holt, S. S., and Serlemitsos, P. J. "Is the Remnant of SN 1006 Crablike?" *Astrophysical Journal* **240** (1980):L33.
- Becklin, E. E., and Westphal, J. A. "Infrared Observations of Comet 1965f." *Astrophysical Journal* **145** (1966):445.
- Becklin, E. E., Matthews, K., Neugebauer, G., and Willner, S. P. "Infrared Observations of the Galactic Center. I. Nature of the Compact Sources." *Astrophysical Journal* **219** (1978):121.

- Beer, J., Andree, M., Oeschger, H., Stauffer, B., Balzer, R., Bonani, G., Stoller, Ch., Suter, M., Wolfli, W., and Finkel, R. C. "Comparison of Be and C Variations." 11th International Radiocarbon Conference, Seattle, 1982.
- Bennett, K. et al. (Caravane Collaboration). *Proceedings of the 12th ESLAB Symposium*, Frascati (ESA SP-124), July 1977, p. 83.
- Berger, A. "Long-Term Variations of the Earth's Orbital Elements." *Celestial Mechanics* **15** (1977):53.
- Berger, W. H., and Killingley, J. S. "Glacial-Holocene Transition in Deep-Sea Carbonates: Selective Dissolution and the Stable Isotope Signal." *Science* **197** (1977):563.
- van den Bergh, S. *Astrophysical Journal Supplement Series* **86** (1964):65.
- . "The Optical Remnant of the Lupus Supernova of 1006." *Astrophysical Journal* **208** (1976):L17.
- van den Bergh, S., and Kamper, K. "The Remnant of Kepler's Supernova." *Astrophysical Journal* **218** (1977):617.
- . "Optical Studies of Cassiopeia A. VI. Observations During the Period 1976-1980." *Astrophysical Journal* **268** (1983):129.
- Berkhuijsen, E. M. "A Radio Continuum Survey of M 31 at 2695 MHz. II. Comparison of Radio and Optical Data." *Astronomy and Astrophysics* **57** (1977):9.
- . "Galactic Continuum Loops and the Diameter-Surface Brightness Relation for Supernova Remnants." *Astronomy and Astrophysics* **24** (1973):143.
- Berman, B. L. "Atlas of Photoneutron Cross Sections Obtained with Monoenergetic Photons." *Atomic Data and Nuclear Data Tables* **15** (1975):319.
- Bertaux, J. L., Blamant, J. E., Mironova, I., Kurt, V. G., and Bourgin, V. G. "Preliminary Results from the H and He Experiment On-board Prognoz-5." Presented at 20th Annual COSPAR Meeting, Tel Aviv, Israel, 1977.
- Bertola, F. "What Shape Are Elliptical Galaxies?" *Sky and Telescope* **61** (1981):380.
- Bertsch, K. *Der Deutsche Wald im Wechsel der Zeiten*. Tübingen, 1935.
- Bhatt, B. Y., et al. In *Effects of Ionizing radiation in Seeds*. Vienna: International Atomic Energy Agency, 1960.
- Bignami, G. F., Caraveo, P. A., Lamb, R. C., Markert, T. H., and Paul, J. A. "Einstein X-ray Identification of the Variable Radio Star LSI + 61 303." *Astrophysical Journal* **247** (1981):L85.
- Billing, K., Kafka, P., Maischberger, K., Meyer, F., and Winckler, W. *Lettre al Nuovo Cimento* **12** (1975):111.

- Blandford, R. D., and Konigl, A. "Relativistic Jets as Compact Radio Sources." *Astrophysical Journal* **232** (1979):34.
- Blandford, R. D., and McKee, C. F. "Fluid Dynamics of Relativistic Blast Waves." *The Physics of Fluids* **19** (1976):1130.
- Blandford, R. D., McKee, C. F., and Rees, M. J. "Superluminal Expansion in Extragalactic Radio Sources." *Nature* **267** (1977):211.
- Blandford, R. D., and Rees, M. J. In *Pittsburgh Conference on BL Lac Objects*, edited by A. M. Wolfe. Pittsburgh: University of Pittsburgh Press, 1978.
- Bloom, A. L. "Glacial-Eustatic and Isostatic Controls of Sea Level Since the Last Glaciation." In *The Late Cenozoic Glacial Ages*, edited by K. K. Turekian. New Haven: Yale University Press, 1971.
- Bodenheimer, P., and Ostriker, J. P. "Do Pulsars Make Supernovae? II. Calculations of Light Curves for Type II Events." *Astrophysical Journal* **191** (1974):465.
- Boley, F., et al. "Optical Identification of A0620-00." *Astrophysical Journal* **203** (1976):L13.
- Bonhommet, N., and Babkine, J. "Sur la Presence d'Aimantations Inversees Dans La Chaines Des Puys." *Comptes Rendus Hebdomadaire des Sceances de L'Academie des Sciences*. **264** (1967):92.
- Bonhommet, N., and Zahringer, J. "Paleomagnetism and Potassium-Argon Age Determinations of the Laschamp Geomagnetic Polarity Event." *Earth and Planetary Science Letters* **6** (1969):43.
- Boriakoff, V., Buccheri, R., and Facui, F. "Discovery of a 6.1-ms Binary Pulsar PSR1953+29." *Nature*, **304** (1983):417.
- Borken, R. J., and Iwan, D. C. "Spatial Structure in the Soft X-ray Background as Observed from OSO-8, and the North Polar Spur as a Reheated Supernova Remnant." *Astrophysical Journal* **218** (1977):511.
- Borns, H. W., Jr. "Late Wisconsin Fluctuations of the Laurentide Ice Sheet in Southern and Eastern New England." In *The Wisconsin Stage* (GSA Memoir 136), edited by R. F. Black, R. P. Goldthwait, and H. B. Willman. Boulder: Geological Society of America, 1973.
- Boughn, S. P., Cheng, E. S., and Wilkinson, D. T. "Dipole and Quadrangle Anisotropy of the 2.7 K Radiation." *Astrophysical Journal* **243** (1981):L113.
- Boughn, S. P., Cheng, E. S., Wilkinson, D. T., and Corey, B. E. "Largescale Anisotropy in the 2.7o K Radiation." *Astrophysical Journal* **232** (1979):L139.
- Boyle, R. W. "The Geochemistry of Gold and Its Deposits." *Geological Survey of Canada, Bulletin* **280**, 1979.

- Bradley, J. P., Brownlee, D. E., and Veblen, D. R. "Pyroxene Whiskers and Platelets in Interplanetary Dust: Evidence of Vapour Phase Growth." *Nature* **301** (1983):473.
- Brandt, J. C. *Introduction to the Solar Wind*. San Francisco: Freeman & Co., 1970.
- Brandt, J. C., Stecher, T. P., Crawford, D. L., and Maran, S. P. "The Gum Nebula: Fossil Stromgren Sphere of the Vela X Supernova." *Astrophysical Journal* **163** (1971):L99.
- Bray, J. R. "Pleistocene Volcanism and Glacial Initiation." *Science* **197** (1977):251.
- Brecher, K., and Wasserman, I. "Dynamical Determination of the Mass Ejected by the Cassiopeia A Supernova." *Astrophysical Journal* **240** (1980):L105.
- Bridle, A. H., Davis, M. M., Fomalont, E. B., Willis, A. G., and Strom. "Structure and Polarization of Jets in the Giant Radio Galaxy NGC 315." *Astrophysical Journal* **228** (1979):L9.
- Broad, W. J. "The Chaos Factor." *Science* **83** January/February (1983):41.
- Broecker, W. S., Ewing, M., and Heezen, B. C. "Evidence for an Abrupt Change in Climate Close to 11,000 Years Ago." *American Journal of Science* **258** (1960):429.
- Broecker, W. S., Kulp, J. L., and Tucek, C. S. "Lamont Natural Radiocarbon Measurements III." *Science* **124** (1956):154.
- Brown, R. L., and Johnston, K. J. "The Gas Density and Distribution within 2 Parsecs of the Galactic Center." *Astrophysical Journal* **268** (1983):L85.
- Brown, R. L. and Marscher, A. P. "Are Supernovae Radio Sources? A Search for Radio Emission from Young Supernova Remnants." *Astrophysical Journal* **220** (1978):467.
- Brownlee, D. E. "Interplanetary Dust." *Reviews of Geophysics and Space Physics* **17** (1979):1735.
- Bruck, M. T. "Photographic Surface Photometry of Nebulae Surrounding V 380 Ori and R Mon." *Monthly Notices of the Royal Astronomical Society* **166** (1974):123.
- Bruhweiler, F. C., and Kondo, Y. "The UV Spectra of Nearby White Dwarfs and the Nature of the Local Interstellar Medium." *Astrophysical Journal* **259** (1982):232.
- de Bruyn, A. G. "A High-Sensitivity Search for Radio Emission from Young Extragalactic Supernova Remnants at 1415 MHz." *Astronomy and Astrophysics* **26** (1973):105.
- Bucha, V. "The Continuous Pattern of Variation of the Geomagnetic Field in the Quaternary and Their Causes." *Studia Geophysica et Geodaetica*. **17** (1973):218.
- Bucha, V., Taylor, R. E., Berger, R., and Haury, E. W. "Geomagnetic Intensity Changes During the Past 3000 Years in the Western Hemisphere." *Science* **168** (1970):111.
- Budyko, M. I. *Climate and Life*. New York: Academic Press, 1974.

- Bullard, E. C. "Dynamo Theory." In *World Magnetic Survey*, edited by J. Zmuda. *IAGA Bulletin* No. 28 (1971):112.
- Burbidge, E. M. "Similarities Between Seyfert Galaxies, N-Type Galaxies, and Quasistellar Objects." (Seyfert Galaxy Conference, Paper #30) *Astronomical Journal* **73** (1968):890.
- "Absorption in the Spectra of Quasi-Stellar Objects." *Physica Scripta* **17** (1978):201.
- Burbidge, E. M., Burbidge, G. R., and Pendergast, K. H. "Motions in NGC 3646, A Strange Spiral Galaxy." *Astrophysical Journal* **134** (1961):237.
- Burbidge, G. R. "A Speculation Concerning the Evolutionary State of Eta Carinae." *Astrophysical Journal* **136** (1962):304.
- "The Nuclei of Galaxies." *Annual Review of Astronomy and Astrophysics* **8** (1970):369.
- Burbidge, G. R., and Burbidge, E. M. "Rotation and Internal Motions in NGC 5128." *Astrophysical Journal* **129** (1959):271.
- Burbidge, G. R., Burbidge, E. M., and Sandage, A. R. "Evidence for the Occurrence of Violent Events in the Nuclei of Galaxies." *Reviews of Modern Physics* **35** (1963):947.
- Burbidge, G. R., Jones, T. W., and O'Dell, S. L. "Physics of Compact Nonthermal Sources. III. Energetic Considerations." *Astrophysical Journal* **193** (1974):43.
- Burnham, R., Jr. *Burnham's Celestial Handbook*. Vols. I, II, III. New York: Dover, 1978.
- Butler, E. J., and Hoyle, F. "On the Effects of a Sudden Change of the Albedo of the Earth." *Astrophysics and Space Science* **60** (1979):505.
- Cameron, A. G. W. "The Origin and Evolution of the Solar System." *Scientific American* **233** (September 1975):15.
- Campbell, M. F., Hoffmann, W. F., Thronson, H. A., and Harvey, P. M. "Far-infrared Survey of Cygnus X." *Astrophysical Journal* **238** (1980):122.
- Canto, J., Rodriguez, L. F., Barral, J. F., and Carral, P. "Carbon Monoxide Observations of R Monocerotis, NGC 2261, and Herbig-Haro 39: The Interstellar Nozzle." *Astrophysical Journal* **244** (1981):102.
- Carr, M. H. "Formation of Martian Flood Features by Release of Water from Confined Aquifers." *Journal of Geophysical Research* **84** (1979):2995.
- "The Geology of Mars." *American Scientist* **68** (1980):631.
- Cash, W., and Charles, P. "Stalking the Cygnus Superbubble." *Sky and Telescope* **59** (1980):455.

- Cash, W., Charles, P., Bowyer, S., Walter, F., Garmire, G., and Riegler, G. "The X-ray Superbubble in Cygnus." *Astrophysical Journal* **238** (1980):L71.
- Cess, Robert D. "Climate Change: An Appraisal of Atmospheric Feedback Mechanisms Employing Zonal Climatology." *Journal of the Atmospheric Sciences* **33** (1976):1831.
- Cheng, E. S., Saulson, P. R., Wilkinson, D. T., and Corey, B. E. "Large-scale Anisotropy in the 2.7 μ K Radiation." *Astrophysical Journal* **232** (1979):L139.
- Chevalier, R. A. "Was SN 1054 a Type II Supernova?" (Preprint Kitt Peak, January 1977).
- Chevalier, R. A., Kirshner, R. P., and Raymond, J. C. The Optical Emission from a Fast Shock Wave with Application to Supernova Remnants." *Astrophysical Journal* **235** (1980):186.
- Christensen, W. N., Frater, R. N., Watkinson, A., O'Sullivan, J. D., and Lockhart, I. A. "Observations of 15 Southern Extragalactic Sources with the Fleurs Synthesis Telescope." *Monthly Notices of the Royal Astronomical Society* **181** (1977):183.
- Ciatti, F., D'Odorico, S., and Mammano, A. "Properties and Evolution of BQ [] Stars." *Astronomy and Astrophysics* **34** (1974):181.
- Clark, H. C., and Kennett, J. P. "Paleomagnetic Excursion Recorded in Latest Pleistocene Deep-Sea Sediments, Gulf of Mexico." *Earth and Planetary Science Letters* **19** (1973):267.
- Clausen, H. B. "Dating of Polar Ice by ^{32}Si ." *Journal of Glaciology* **12** (1973):411.
- Clayton, D. D., and Craddock, W. L. "Radioactivity in Supernova Remnants." *Astrophysical Journal* **142** (1965):189.
- Cleary, M. N., Heiles, C., and Haslam, C. G. T. *Astronomy and Astrophysics Supplement* **36** (1979):95.
- CLIMAP Project Members. "Surface of Ice Age Earth." *Science* **191** (1976):1131.
- Clube, S. V. M. "The Origin of Gravity." *Astrophysics and Space Science* **50** (1977):425.
- . "Does Our Galaxy Have a Violent History?" *Vistas in Astronomy* **22** (1978):77.
- . "The Material Vacuum." *Monthly Notices of the Royal Astronomical Society* **193** (1980):385.
- Clube, S. V. M., and Napier, W. M. "The Role of Episodic Bombardment in Geophysics." *Earth and Planetary Science Letters* **57** (1982):251.
- . "Spiral Arms, Comets and Terrestrial Catastrophism." *Quarterly Journal of the Royal Astronomical Society* **23** (1982):45.
- Cocke, W. J., Disney, M. J., Muncaster, G. W., and Gehrels, T. "Optical Polarization of the Crab Nebula Pulsar." *Nature* **227** (1970): 1327.

- Coe, R. S., Gromme, S., and Mankinen, E. A. "Geomagnetic Paleointensities from Radiocarbon-Dated Lava Flows on Hawaii and the Question of the Pacific Nondipole Law." *Journal of Geophysical Research* **83** (1978):1740.
- Cohen, M. "Infra-Red Observations of Young Stars--IV. Radiative Mechanisms and Interpretations." *Monthly Notices of the Royal Astronomical Society* **164** (1973):395.
- Cohen, M., and Kuhl, L. V. "Observational Studies of Star Formation: Conclusions." *Astrophysical Journal* **227** (1979a):L105.
- . "Observational Studies of Pre-Main-Sequence Evolution." *Astrophysical Journal Supplement Series* **41** (1979b):743.
- Cohen, M., and Schmidt, G. D. "Spectropolarimetry of Herbig-Haro Objects and the Exciting Star of HH 30." *Astronomical Journal* **86** (1981):1228.
- Cohen, M., and Schwartz, R. D. "Infrared Observations of Young Stars--VII. Simultaneous Optical and Infrared Monitoring for Variability." *Monthly Notices of the Royal Astronomical Society* **174** (1976):137.
- Cong, H. Ph.D. dissertation, Columbia University, 1978 (NASA Technical Memorandum 79590).
- Connally, G. G., and Sirkin, L. A. "Wisconsinan History of the Hudson-Champlain Lobe." In *The Wisconsin Stage* (GSA Memoir 136), edited by R. F. Black, R. P. Goldthwait, and H. B. Willman. Boulder: Geological Society of America, 1973.
- Coope, G. R. "Fossil Coleopteran Assemblages as Sensitive Indicators of Climactic Changes During the Devension (Last) Cold Stage." *Philosophical Transactions Royal Society of London* **B 280** (1977):313.
- Coulson, K. L. *Solar and Terrestrial Radiation*. New York: Academic Press, 1975.
- Cox, A. "Geomagnetic Reversals." *Science* **163** (1969):237.
- Cox, D. P., and Smith, B. W. "Large-scale Effects of Supernova Remnants on the Galaxy: Generation and Maintenance of a Hot Network of Tunnels." *Astrophysical Journal* **189** (1974):L105.
- Cragin, J. H., Herron, M. M., Langway, C. C., Jr., and Klouda, G. "Interhemispheric Comparison of Changes in the Composition of Atmospheric Precipitation During the Late Cenozoic Era." (*Proceedings of SCOR/SCAR Polar Oceans Conference, Montreal, Canada, 1974*) In *Polar Oceans*, edited by M. J. Dunbar. Arctic Institute of North America, 1977.
- Craig, H. "Standard for Reporting Concentrations of Deuterium and Oxygen-18 in Natural Waters." *Science* **133** (1961):1833.
- Cram, L. E., Giampapa, M. S., and Imhoff, C. L. "Emission Measures Derived from Far Ultraviolet Spectra of T Tauri Stars." *Astrophysical Journal* **238** (1980):905.

- Creer, K. M., Anderson, T. W., and Lewis, C. F. M. "Late Quaternary Geomagnetic Stratigraphy Recorded in Lake Erie Sediments." *Earth and Planetary Science Letters* **31** (1976):37.
- Crocket, J. H., and Kuo, H. Y. "Sources for Gold, Palladium and Iridium in Deep-sea Sediments." *Geochimica et Cosmochimica Acta* **43** (1979):831.
- Crutcher, R. M. "The Local Interstellar Medium." *Astrophysical Journal* **254** (1982):82.
- Curtis, G. H. "The Problem of Contamination in Obtaining Accurate Dates of Young Geologic Rocks." In *Potassium Argon Dating*, edited by O. A. Schaeffer and J. Zahringer. New York: Springer-Verlag, 1966
- Dana, J. D. "The Flood of the Connecticut River Valley from the Melting of the Quaternary Glacier." *American Journal of Science* **23** (1882): 367.
- . *Manual of Geology*. New York: American Book Co., 1880.
- Dansgaard, W., Clausen, H. B., Gundestrup, N., Hammer, C. U., Johnsen, S. F., Kristinsdottir, P. M., and Reeh, N. "A New Greenland Deep Ice Core." *Science* **218** (1982):1273.
- Dansgaard, W., and Johnsen, S. J. "A Flow Model and a Time Scale for the Ice Core from Camp Century, Greenland." *Journal of Glaciology* **8** (1969):215.
- Dansgaard, W., Johnsen, S. J., Clausen, H. B., and Langway, C. C. "Speculations about the Next Glaciation." *Quaternary Research* **2** (1972):396.
- Dansgaard, W., Johnsen, S. J., Moller, J., and Langway, C. C., Jr. "One Thousand Centuries of Climatic Record from Camp Century on the Greenland Ice Sheet." *Science* **166** (1969):377.
- D'Arcy, R. G., and Colgate, S. A. "Measurements of the Southern Magnetic Conjugate Region of the Fission Debris from the Starfish Nuclear Detonation." *Journal of Geophysical Research* **70** (1965):3147.
- Davidson, C. I., Chu, L., Grimm, T. C., Nasta, M. A., and Qamoos, M. P. "Wet and Dry Deposition of Trace Elements onto the Greenland Ice Sheet." *Atmospheric Environment* **15** (1981):1429.
- Davis, L., and Greenstein, J. L. "The Polarization of Starlight by Aligned Dust Grains." *Astrophysical Journal* **114** (1951):206.
- Denham, C. R. "Blake Polarity Episode in Two Cores from the Greater Antilles Outer Ridge." *Earth and Planetary Science Letters* **29** (1976):422.
- Denham, C. R., and Cox, A. "Evidence that the Laschamp Polarity Event Did Not Occur 13,300-30,400 Years Ago." *Earth and Planetary Science Letters* **13** (1971):181.
- Dennefeld, M., Laustsen, S., and Materne, J. "Structure of a Southern Ring Galaxy." *Astronomy and Astrophysics* **74** (1979):123.

- DeNoyer, L. K., Button, L., Chaffin, D., and Nieznanski, J. "The Distance to Low-latitude Negative-velocity Clouds in the Galactic Anticenter." *Astrophysical Journal* **213** (1977):379.
- Dessler, A. J., and Parker, E. N. "Hydromagnetic Theory of Geomagnetic Storms." *Journal of Geophysical Research* **64** (1959):2239.
- Dicke, R. H. *Evidence for Gravitation Theories*. New York: Academic Press, 1961.
- Dickel, J. R., and Greisen, E. W. "The Evolution of the Radio Emission from Cas A." *Astronomy and Astrophysics* **75** (1979):44.
- Dickel, J. R., and Spangler, S. R. "Measurements of the Radio Flux Density of Tycho's SNR Separated by a 15-year Interval." *Astronomy and Astrophysics* **79** (1979):243.
- Dieter, N. H. "Berkeley Survey of High Velocity Interstellar Neutral Hydrogen: Discussion of Results." *Astronomy and Astrophysics* **12** (1971):59.
- . "A Survey of Interstellar Formaldehyde in Dust Clouds." *Astrophysical Journal* **183** (1973):449.
- Donahue, T. M., Guenther, B., and Blamont, J. E. "Noctilucent Clouds in Daytime: Circumpolar Particulate Layers Near the Summer Mesopause." *Journal of the Atmospheric Sciences* **29** (1972):1205.
- Donn, B., and Sears, G. W. "Planets and Comets: Role of Crystal Growth in Their Formation." *Science* **140** (1963):1208.
- Donnelly, I. *The Destruction of Atlantis (Ragnarok: The Age of Fire and Gravel)*. Blauvelt, New York: Rudolf Steiner Publications, 1971.
- Downes, D., and Maxwell, A. "Radio Observations of the Galactic Center Region." *Astrophysical Journal* **146** (1966):653.
- Dreimanis, A. "Extinction of Mastodons in Eastern North America: Testing a New Climatic-Environmental Hypothesis." *The Ohio Journal of Science* **68** (1968):257.
- Dreimanis, A., and Goldthwait, R. P. "Wisconsin Glaciation in the Huron, Erie, and Ontario Lobes." In *The Wisconsin Stage* (GSA Memoir 136), edited by R. F. Black, R. P. Goldthwait, and H. B. Willman. Boulder: Geological Society of America, 1973.
- Duncan, J. R., Fowler, G. A., and Kulm, L. D. "Planktonic Foraminifera-Radiolarian Ratios and Holocene-Late Pleistocene Deep Sea Stratigraphy off Oregon." *Geological Society of America Bulletin* **81** (1970):561.
- Eakin, H. M. "The Yukon-Koyukuk Region, Alaska." *U.S. Geological Survey* **631** (1916).
- . "The Cosna-Nowitna Region, Alaska." *U. S. Geological Survey* **667** (1918).
- Eardley, A. J., Shuey, R. T., Grosdetsky, W. P., Nash, M., Picard, D., Grey, D. C., and

- Kukla, G. J. "Lake Cycles in the Bonneville Basin." *Geological Society of America Bulletin* **84** (1973):211.
- Edwards, W. E. "The Late-Pleistocene Extinction and Diminution in Size of Many Mammalian Species." In *Pleistocene Extinctions: The Search for a Cause*, edited by P. S. Martin and H. E. Wright, Jr. New Haven: Yale University Press, 1967, p. 141.
- Ehmann, W. D. "New Determinations of Iridium and Tantalum in Meteorite Materials." *Meteorites* **2** (1963):30.
- Einstein, A. *Annals of Physics* **17** (1905):891.
- Ekers, R. D. In *Structure and Evolution of Galaxies*, edited by G. Setti. Dordrecht, Holland: D. Reidel, 1975.
- Elvius, T. "Distribution of Common Stars in Intermediate and High Galactic Latitudes." In *Galactic Structure*, edited by A. Blaauw and M. Schmidt. Chicago: University of Chicago Press, 1965.
- Emerson, D. T. "High-Resolution Observations of Neutral Hydrogen in M31--II Velocity-Field." *Monthly Notices of the Royal Astronomical Society* **176** (1976):321.
- Emery, K. O., Niino, H., and Sullivan, B. "Post-Pleistocene Levels of the East China Sea." In *The Late Cenozoic Glacial Ages*, edited by K. K. Turekian. New Haven: Yale University Press, 1971.
- Emiliani, C. "Isotopic Paleotemperatures." *Science* **154** (1966):851.
- "Quaternary Paleotemperatures and the Duration of the High-Temperature Intervals." *Science* **178** (1972):398.
- Emiliani, C., Gartner, S., Lidz, B., Eldridge, K., Elvey, D. K., Huang, T. C., Stipp, J. J., and Swanson, M. F. "Paleoclimatological Analysis of Late Quaternary Cores from the Northeastern Gulf of Mexico." *Science* **189** (1975):1083.
- Epstein, Samuel, Sharp, R. P., and Gow, A. J. "Antarctic Ice Sheet: Stable Isotope Analysis of Byrd Station Cores and Interhemispheric Climatic Implications." *Science* **168** (1970):1570.
- Erickson, W. C., Kuiper, T. B. H., Clark, T. A., Knowles, S. H., and Broderick, J. J. "Very Long Baseline Interferometer Observations of Taurus A and Other Sources at 121.6 MHz." *Astrophysical Journal* **177** (1972):101.
- Erickson, W. C., and Perley, R. A. "An Anomaly in the Flux of Cassiopeia A at 38 MHz." *Astrophysical Journal* **200** (1975):L83.
- Erman, G. A. *Travels in Siberia*, Vol. II. London: Longman, Brown, Green, and Longmans, 1848.
- Fabbri, R., Guidi, I., Melchiorri, F., and Natale, V. "Measurement of the Cosmic-Background Large-Scale Anisotropy in the Millimetric Region." *Physical Review Letters* **44** (1980):1563.

- Fabian, A. C. "Theories of the Nuclei of Active Galaxies." *Proceedings of the Royal Society of London A* **366** (1979):449.
- Fahr, H. J. "The Extraterrestrial UV-Background and the Nearby Interstellar Medium." *Space Science Reviews* **15** (1974):483.
- Fairbridge, R. W. "Global Climatic Change During the 13,500-B.P. Gothenburg Geomagnetic Excursion." *Nature* **265** (1977):430.
- Farrand, W. R. "Frozen Mammoths and Modern Geology." *Science* **133** (1961):729.
- Fick, E. *Zeitschrift fur Physik* **140** (1955):308.
- Fisher, D. A. "Comparison of 105 Years of Oxygen Isotope and Insoluble Impurity Profiles from the Devon Island and Camp Century Ice Cores." *Quaternary Research* **11** (1979):299.
- Flanagan, F. J. "Descriptions and Analyses of 8 New USGS Rock Standards." *U.S. Geological Survey Professional Paper*, #840, 1976, pp. 171-172.
- Fletcher, J. O. "The Arctic Heat Budget and Atmospheric Circulation." In *Proceedings of the Symposium on the Arctic Heat Budget and Atmospheric Circulation*, edited by J. O. Fletcher. Report RM-5233-NSF. Santa Monica, CA: Rand Corporation, 1966, pp. 23-43.
- Flohn, H. "On Time Scales and Causes of Abrupt Paleoclimatic Events." *Quaternary Research* **12** (1979):135.
- Forman, W., and Visvanathan, N. "Magnetic Field Structure Around the Crab Pulsar." *Nature* **229** (1971):39.
- Freed, W. K., and Healy, N. "Excursions of the Pleistocene Geomagnetic Field Recorded in Gulf of Mexico Sediments." *Earth and Planetary Science Letters* **24** (1974):99.
- Freeman, K. C., and de Vaucouleurs, G. "An Interpretation of Ring Galaxies and the Properties of Intergalactic Gas Clouds." *Astrophysical Journal* **194** (1974):569.
- Frisch, P. C. "The Nearby Interstellar Medium." *Nature* **293** (1981):377.
- Gahm, G. F. "X-Ray Observations of T Tauri Stars." *Astrophysical Journal* **242** (1980):L163.
- Ganapathy, R., and Brownlee, D. E. "Interplanetary Dust: Trace Element Analysis of Individual Particles by Neutron Activation." *Science* **206** (1979):1075.
- Ganapathy, R., Brownlee, D. E., and Hodge, P. W. "Silicate Spherules from Deep-Sea Sediments: Confirmation of Extraterrestrial Origin." *Science* **201** (1978):119.
- Garwin, R. L. "Detection of Gravity Waves Challenged." *Physics Today* **27** (1974):9.
- "More on Gravity Waves." *Physics Today* **28** (1975):13.

- Gatley, I. "Infrared Observations of the Galactic Center." In *The Galactic Center*, edited by G. R. Riegler and R. D. Blandford. New York: American Institute Physics, 1982, p. 25.
- Geisel, S. L. "Infrared Excesses, Low-Excitation Emission Lines, and Mass Loss." *Astrophysical Journal* **161** (1970):L105.
- Geiss, J. "Experimental Evidence on the History of Cosmic Radiation." *Proceedings of the 8th International Conference on Cosmic Rays*, Jaipur **3** (1963):434.
- Genzel, R., Watson, D., Townes, C., Lester, D., Dinerstein, H., Werner, M., and Storey, J. "O I and O III in Sgr A: Neutral and Ionized Gas at the Galactic Center." In *The Galactic Center*, edited by G. R. Riegler and R. D. Blandford. New York, American Institute of Physics, 1982, p. 72.
- Giacconi, R. "The Einstein X-ray Observatory." *Scientific American* **242** (1980):80.
- Gibbons, G. W., and Hawking, S. W. "Theory of the Detection of Short Bursts of Gravitational Radiation." *Physical Review* **D4** (1971):2191.
- Ginzburg, V. L. *Doklady Akademia Nauk SSR* **92** (1953):1133.
- . "The Nature of Cosmic Radio Emission and the Origin of Cosmic Rays." (Ser. X, Suppl.) *Lettre al Nuovo Cimento* **3** (1956):38.
- Ginzburg, V. L., and Syrovatskii, S. I. *The Origin of Cosmic Rays*. New York: Pergamon Press, 1964.
- Glass, B., and Heezen, B. "Tektites and Geomagnetic Reversals." *Scientific American* **217** (1967):33.
- Glass, B. P., and Zwart, M. J. In *Proceedings of the Symposium on Stratigraphic Micropaleontology of the Atlantic Basin and Borderlands*, edited by F. N. Swain. New York: Elsevier, 1977, p. 553.
- Glasstone, and Sesonske. *Nuclear Reactor Engineering*. Princeton, N.J.: Van Nostrand Co., Inc., 1963.
- Gold, T. "Rotating Neutron Stars and the Nature of Pulsars." *Nature* **221** (1969):25.
- . "Apollo II Observations of a Remarkable Glazing Phenomenon on the Lunar Surface." *Science* **165** (1969):1345.
- Goldberg, E. D., Koide, M., Griffin, J. J., and Peterson, M. N. A. "A Geochronological and Sedimentary Profile Across the North Atlantic Ocean." In *Isotopic and Cosmic Chemistry*, edited by H. Craig, S. L. Miller, and G. J. Wasserburg. Amsterdam: North-Holland, 1964.
- Golden, J., Kapetanacos, C. A., Pasour, J. A., and Mahaffey, R. A. "The Generation and Application of Intense Pulsed Ion Beams." *American Scientist* **69** (1981):173.
- Goldschmidt, V. M. *Geochemistry*. London: Oxford University Press, 1951.

- Goldstein, M. L., Ramaty, R., and Fisk, L. A. "Interstellar Cosmic Ray Spectra from the Nonthermal Radio Background from 0.4 to 400 MHz." *Physical Review Letters* **24** (1970):1193.
- Gorenstein, M. V. Ph.D. thesis, University of California, Berkeley, 1978.
- Gorenstein, P., and Tucker, W. "Supernova Remnants." *Scientific American* **225**(1) (1971):74.
- Gottlieb, E. W., and Liller, W. "Photometric Histories of Six Infrared Objects and Three Highly Reddened Blue Supergiants." *Astrophysical Journal* **225** (1978):488.
- Gould, R. J., and Burbidge, G. R. In *Handbuch der Physik*, vol. 46/2, edited by S. Fluge. Berlin: Springer-Verlag, 1967, p. 265.
- Gow, A. J., and Williamson, T. "Volcanic Ash in the Antarctic Ice Sheet and Its Possible Climatic Implications." *Earth and Planetary Science Letters* **13** (1971):210.
- . "Rheological Implications of the Internal Structure and Crystal Fabrics of the West Antarctic Ice Sheet as Revealed by Deep Core Drilling at Byrd Station." *Geological Society of America Bulletin* **87** (1976):1665.
- Grant, V. *The Origin of Adaptations*. New York: Columbia University Press, 1963.
- Grayson, D. K. "Pleistocene Avifaunas and the Overkill Hypothesis." *Science* **196** (1977):691.
- Green, D. A., and Gull, S. F. "Distance to Crab-like Supernova Remnant 3c58." *Nature* **299** (1982):606.
- Greenstein, J. L. "A Possible Energy Source for T Tauri Stars." *Astronomical Society of the Pacific Publication* **62** (1950):156.
- . "MWC 349, An Optical Radio and Infrared Source." *Astrophysical Journal* **184** (1973):L25.
- Griffiths, R. E., Tapia, S., Briel, U., and Chaisson, L. "Optical and X-ray Properties of the Newly Discovered BL Lacertae Object PKS 2155-304 (= H2155-304)." *Astrophysical Journal* **234** (1979):810.
- De Groot, M. "Mass Loss from P Cygni." In *Mass Loss from Stars*, edited by M. Hack. Dordrecht, Holland: D. Reidel, 1969, p. 26.
- Grossman, L. "Refractory Trace Elements in Ca-Al-rich Inclusions in the Allende Meteorite." *Geochimica et Cosmochimica Acta* **37** (1973):1119.
- Guibert, J. "A Neutral Hydrogen Survey of the Andromeda Nebula." *Astronomy and Astrophysics Supplement* **12** (1973):263.
- Guilday, J. E. "Differential Extinction During Late-Pleistocene and Recent Times." In *Pleistocene Extinctions: The Search for a Cause*, edited by P. S. Martin and H. E.

- Wright, Jr. New Haven: Yale University Press, 1967, p. 121.
- Gull, S. F. "Interpretation of Radio Emission from from Supernova Remnants Cas A and 3C 10." *Monthly Notices of the Royal Astronomical Society* **161** (1973):47.
- Gursky, H., and van den Heuvel, E. P. J. "X-ray-Emitting Double Stars." *Scientific American* **232**(3) (1975):24.
- ter Haar, D. *Reviews of Modern Physics* **22** (1950):119.
- Halgren, D. S., and Hemenway, C. L. "Analysis of Impact Craters from the S-149 Skylab Experiment." *Lecture Notes in Physics* **48**. New York: Springer-Verlag, 1976, p. 270.
- Hall, J. S., and Serkowski, K. "Polarization of Starlight." In *Basic Astronomical Data*, edited by K. Aa. Strand. Chicago: University of Chicago Press, 1963.
- Hamilton, P. A., and Haynes, R. F. "A Survey of the Southern Sky at 153 MHz." *Australian Journal of Physics* **22** (1969):839.
- Hammer, C. U., Clausen, H. B., and Dansgaard, W. "Greenland Ice Sheet Evidence of Post-Glacial Volcanism and Its Climatic Impact." *Nature* (1980):230.
- Hammer, C. U., Clausen, H. B., Dansgaard, W. Gundestrup, N., Johnsen, S. J., and Reeh, N. "Dating of Greenland Ice Cores by Flow Models, Isotopes, Volcanic Debris, and Continental Dust." *Journal of Glaciology* **20** (1978):3.
- Hanappe, F., Vosters, M., Picciotto, E., and Deutsch, S. "Chimie des Neiges Antarctiques et Taux de Deposition de Matiere Extraterrestre." *Earth and Planetary Science Letters* **4** (1968):487.
- Harnden, Jr., F. R. "X-Ray Study of the Crab Nebula and the Crab and Vela Pulsars." In *Supernova Remnants and Their X-Ray Emissions*, I. A. U. Symposium No. 101, edited by P. Gorenstein and J. Danziger. Boston: D. E. Reidel Publishing Co., 1983.
- Harper, D. A., Jr., and Low, F. J. "Far-infrared Observations of Galactic Nuclei." *Astrophysical Journal* **182** (1973):L89.
- Harrison, C. G. A. "Evolutionary Processes and Reversals of the Earth's Magnetic Field." *Nature* **217** (1968):46.
- Harrison, C. G. A., and Funnel, B. M. "Relationship of Paleomagnetic Reversals and Micropaleontology in Two Late Cenozoic Cores from the Pacific Ocean." *Nature* **204** (1964):566.
- Hart, L., and Davies, R. D. "Motion of the Local Group of Galaxies and Isotropy of the Universe." *Nature* **297** (1982):191.
- Hartman, L., Jaffe, D., and Huchra, J. P. "On the Nature of MWC 349." *Astrophysical Journal* **239** (1980):905.
- Harvey, P. M., Thronson, H. A., and Gatley, I. "Far-infrared Observations of Optical

- Emission-Line Stars: Evidence for Extensive Cool Dust Clouds." *Astrophysical Journal* **231** (1979):115.
- Hays, J. D. "Faunal Extinctions and Reversals of the Earth's Magnetic Field." *Geological Society of America Bulletin* **82** (1971):2433.
- . "The Stratigraphy and Evolutionary Trends of Radiolaria in North Pacific Deep-sea Sediments." In *Geological Investigations of the North Pacific*, edited by J. D. Hays. *Geological Society of America Memoirs*, No 126 (1970):185.
- Hays, J. D., and Opdyke, N. D. "Antarctic Radiolaria, Magnetic Reversals and Climatic Change." *Science* **158** (1967):1001.
- Hays, J. D., Saito, T., Opdyke, N. D., and Burckle, L. "Pliocene/Pleistocene Sediments of the Equatorial Pacific: Their Paleomagnetic, Biostratigraphic, and Climatic Record." *Geological Society of America Bulletin* **80** (1969):1481.
- Hayward, E. "Photodisintegration of Light Nuclei." *Reviews of Modern Physics* **35** (1963): 324.
- Heiles, C. "The Interstellar Magnetic Field." *Annual Reviews of Astronomy and Astrophysics* **14** (1976):1.
- . "H I Shells and Supershells." *Astrophysical Journal* **229** (1979):533.
- Heiles, C., Chu, Y. H., Reynolds, R. J., Yegingil, I., and Troland, T. H. "A New Look at the North Polar Spur." *Astrophysical Journal* **242** (1980):533.
- Hemenway, C. L. "Collections of Cosmic Dust." In *The Dusty Universe*. Edited by G. B. Field and A. G. W. Cameron. New York: Smithsonian Astrophysical Observatory, 1973, p. 211.
- Hemenway, C. L., Hallgren, D. S., and Schmalberger, D. C. "Stardust." *Nature* **238** (1972):256.
- Herbig, G. H. "Lithium in Main-Sequence Stars." In *Stellar Evolution*, edited by R. F. Stein and A. G. W. Cameron. New York: Plenum Press, 1966.
- . "The Youngest Stars." *Scientific American* **217** (August 1967):30.
- Heusser, C. J., and Flint, R. F. "Quaternary Glaciations and Environments of Northern Isla Chiloe, Chile." *Geology* **5** (1977):305.
- Heusser, C. J., and Streeter, S. S. "A Temperature and Precipitation Record of the Past 16,000 Years in Southern Chile." *Science* **210** (1980):1345.
- Hibbard, C. W., Ray, C. E., Savage, D. E., Taylor, D. W., and Guilday, J. E. "Quaternary Mammals of North America." In *The Quaternary of the United States*, edited by H. E. Wright, Jr. and D. G. Frey. Princeton: Princeton University Press, 1965, p. 509.
- Hibben, F. C. "Evidences of Early Man in Alaska." *American Antiquity* **8** (1943):254.

- Hickey, L. J. "Land Plant Evidence Compatible with Gradual, Not Catastrophic, Change at the End of the Cretaceous." *Nature* **292** (1981): 529.
- Hills, J. G. "Comet Showers and the Steady-State Infall of Comets from the Oort Cloud." *Astronomical Journal* **86** (1981):1730.
- Hirakawa, H., and Narihara, K. "Search for Gravitational Radiation at 145 Hz." *Physical Review Letters* **35** (1975):330.
- Hjellming, R. M., and Smarr, L. L. "The Extended Radio Source in the Center of M 31." *Astrophysical Journal* **257** (1982):L13.
- Hodge, P. W. "Some Optical Properties of Seyfert Galaxies and Related Objects." (Seyfert Galaxy Conference, Paper #22) *Astronomical Journal* **73** (1968):876.
- Holman, G. D., Ionson, J. A., and Scott, J. S. "Particle Streaming: Is the Alfvén Velocity the Ultimate Speed Limit?" *Astrophysical Journal* **228** (1979):576.
- Holmes, A. *Principles of Physical Geology*. London: Nelson, 1965.
- Howorth, H. H. *The Mammoth and the Flood*. London: Sampson Low, Marston, Searle, & Rivington, 1887.
- . *The Glacial Nightmare and the Flood*. (2 vols.) London: Sampson Low, Marston, Searle, & Rivington, 1893.
- Hoyle, F., and Lyttleton, R. A. "Variations in Solar Radiation and the Cause of Ice Ages." *Journal of Glaciology* **1** (1950):453.
- Hoyle, F., and Wickramasinghe, N. C. "Interstellar Grains." *Nature* **223** (1969):459.
- . "Comets, Ice Ages, and Ecological Catastrophes." *Astrophysics and Space Science* **53** (1978):523.
- Hughes, D. W. "Cosmic Dust Influx to the Earth." *Space Research* **15** (1975):34.
- van de Hulst, H. C. *Les Particules Solides dans les Astres* (Mem. Soc. R. Sci. Liege, 4th ser. Vol 15) 1955, pp. 393, 609.
- Humphreys, R. M. "Structure and Motions in the Carina Spiral Feature." *Astronomy and Astrophysics* **20** (1972):29.
- Hyder, C. L. "The Infall-Impact Mechanism and Solar Flares." In *Mass Motions in Solar Flares and Related Phenomena*. Edited by Y. Ohman. New York: Wiley Interscience Division, 1968, p. 57.
- . *Solar Physics* **2** (1967a):49.
- . *Solar Physics* **2** (1967b):267.
- Ilovaisky, S. A., and Bowyer, S. "Soft X-ray Emission from Galactic Radio Spurs." *Nature* **233** (1971):469.

- Ilovaisky, S. A., and Lequeux, J. "A Study of Galactic Supernova Remnants. I. Distances, Radio Luminosity Function and Galactic Distribution." *Astronomy and Astrophysics* **18** (1972a):169.
- . "A Study of Galactic Supernova Remnants. II. Supernova Rate, Galactic Radio Emission and Pulsars." *Astronomy and Astrophysics* **20** (1972b):347.
- Imhoff, C. L., and Giampapa, M. S. "The Ultraviolet Spectrum of the T Tauri Star RW Aurigae." *Astrophysical Journal* **239** (1980):L115.
- Inn, E. C. Y., Farlow, N. H., Russell, P. B., McCormick, M. P., and Chu, W. P. "Observations." In *The Stratospheric Aerosol Layer*, edited by R. C. Whitten. New York: Springer-Verlag, 1982.
- Ising, G. "On the Magnetic Properties of Varved Clay." *Arkiv fur Matematik, Astronomi och Fysik* **29** (1942):1.
- Jameson, R. F., Longmore, A. J., McLinn, J. A., and Woolf, N. J. "Infrared Emission by Dust in NGC 1068 and Three Planetary Nebulae." *Astrophysical Journal* **190** (1974):353.
- Johnsen, S. J., Dansgaard, W., Clausen, H. B., and Langway, C. C., Jr. "Oxygen Istopes Profiles Through the Antarctic and Greenland Ice Sheets." *Nature* **235** (1972):429.
- Johnson, H. M., and MacLeod, J. M. "The Spatial Distribution of Supernovae in Galaxies." *Publication of the Astronomical Society of the Pacific* **75** (1963):123.
- Jones, T. W., O'Dell, S. L., and Stein, W. A. "Physics of Compact Nonthermal Sources. I. Theory of Radiation Processes." *Astrophysical Journal* **188** (1974):353.
- Jones, T. W., and Tobin, W. "Restrictions on Models for Superlight Flux Variations in Radio Sources." *Astrophysical Journal* **215** (1977):474.
- Junge, C. E. *Air Chemistry and Radioactivity*. New York: Academic Press, 1963.
- Kaplan, S. A., and Pikelner, S. B. *The Interstellar Medium*. Cambridge, Mass.: Harvard University Press, 1970.
- Kellermann, K. I. "Detection of a Strong and Possibly Variable Compact Millimeter Wave Component in Centaurus A." *Astrophysical Journal* **194** (1974):Li35.
- . "Structure and Time Variations of Compact Radio Sources in Galaxies and Quasars." *Physica Scripta* **17** (1978):257.
- Kellermann, K. I., Clark, B. G., Niell, A. E., and Shaffer, D. B. "Observations of Compact Radio Nuclei in Cygnus A, Centaurus A, and Other Extended Radio Sources." *Astrophysical Journal* **197** (1975):L13.
- Kellermann, K. I., and Pauliny-Toth, I. I. K. "Variable Radio Sources." *Annual Reviews of Astronomy and Astrophysics* **6** (1968):417.

- . "Compact Radio Sources." *Annual Review of Astronomy and Astrophysics* **19** (1981):373.
- Kennedy, W. J. "Ammonite Evolution." In *Patterns of Evolution, as Illustrated by the Fossil Record*, edited by A. Hallam. Amsterdam: Elsevier, 1977.
- Kennett, J. P., and Huddleston, P. "Abrupt Climatic Change at 90,000 Yr BP; Faunal Evidence from Gulf of Mexico Cores." *Quaternary Research* **2** (1972):384.
- Kennett, J. P., and Shackleton, N. J. "Laurentide Ice Sheet Meltwater Recorded in Gulf of Mexico Deep-Sea Cores." *Science* **188** (1975): 147.
- Khachikian, E. Ye. "Two New Seyfert Galaxies from Markarian's List of Galaxies with Strong UV Continua." (Seyfert Galaxy Conference, Paper #31) *Astronomical Journal* **73** (1968):891.
- Kohoutek, L., and Wehmeyer, R. "Concerning the Nature of the Nebula V-V 1-7 Surrounding BD-18o1967." *Astronomy and Astrophysics* **41** (1975):451.
- Kopper, J. S. "Dating and Interpretation of Archeological Cave Deposits by the Paleomagnetic Method." Columbia University Ph.D. Dissertation, # DAH76-17849 (Section B), 1976.
- Kormendy, J. "A Morphological Survey of Bar, Lens, and Ring Components in Galaxies: Secular Evolution in Galaxy Structure." *Astrophysical Journal* **227** (1979):714.
- Kowalski, K. "The Pleistocene Extinction of Mammals in Europe." In *Pleistocene Extinctions: The Search for a Cause*, edited by P. S. Martin, and H. E. Wright, Jr. New Haven: Yale University Press, 1967, p. 349.
- Krahenbuhl, U., Morgan, J. W., Ganapathy, R., and Anders, E. "Abundance of 17 Trace Elements in Carbonaceous Chondrites." *Geochimica et Cosmochimica Acta* **37** (1973):1353.
- Kraus, J. D. *Radio Astronomy*. New York: McGraw Hill, 1966.
- Kriss, G. A., Canizares, C. R., and Ricker, G. R. "X-ray Observations of Seyfert Galaxies with the Einstein Observatory." *Astrophysical Journal* **242** (1980):492.
- Kristian, J. "Quasars As Events in the Nuclei of Galaxies: The Evidence from Direct Photographs." *Astrophysical Journal* **179** (1973): L61.
- van der Kruit, P. C. "Evidence for a Possible Expulsion of Gas from the Galactic Nucleus." *Astronomy and Astrophysics* **4** (1970):462.
- . "Observation of Core Sources in Seyfert and Normal Galaxies with the Westerbork Synthesis Radio Telescope at 1415 MHz." *Astronomy and Astrophysics* **15** (1971a):110.
- . "Attempt to Explain the Motions of the Gas in the Central Region of the Galaxy by Explosive Events in Its Nucleus." *Astronomy and Astrophysics* **13** (1971b):405.
- . "High-Resolution Radio Continuum Observations of Bright Spiral Galaxies at 1415

- MHz: A General Discussion." *Astronomy and Astrophysics* **29** (1973):263.
- van der Kruit, P. C., and Allen, R. J. "The Radio Continuum Morphology of Spiral Galaxies." *Annual Reviews of Astronomy and Astrophysics* **14** (1976):417.
- Ku, W. H. M., Helfand, D. J., and Lucy, L. B. "X-ray Properties of Quasars." *Nature* **288** (1980):323.
- Kuhi, L. V. "Mass Loss from T Tauri Stars." *Astrophysical Journal* **140** (1964):1409.
- , "T Tauri Mass Ejection." In *Stellar Evolution*. Edited by R. F. Stein and A. G. W. Cameron. New York: Plenum Press, 1966, p. 373.
- Kukla, G. J. "Pleistocene Land--Sea Correlations. I. Europe." *Earth Science Reviews* **13** (1977):307.
- Kukla, G. J., and Koci, A. "End of the Last Interglacial in the Loess Record." *Quaternary Research* **2** (1972):374.
- Kundt, W. "The Wisps in the Crab Nebula: A Cosmic Laser?" *Astronomy and Astrophysics* **60** (1977):L19.
- Kundt, W., and Krotscheck, E. "The Crab Nebula: A Model." *Astronomy and Astrophysics* **83** (1980):1.
- Kundu, I. R., and Velusamy, T. "Brightness and Polarization Structure of Four Supernova Remnants 3C 58, IC443, W 28, and W 44 at 2.8 Centimeter Wavelength." *Astronomy and Astrophysics* **20** (1972):237.
- Kyle, P. R., and Jezek, P. A. "Compositions of Three Tephra Layers from the Byrd Station Ice Core, Antarctica." *Journal of Volcanology and Geothermal Research* **4** (1976):225.
- Kyle, P. R., Jezek, P. A., Mosley-Thompson, B., and Thompson L. G. "Tephra Layers in the Byrd Station Ice Core and the Dome C Ice Core Antarctica and Their Climatic Importance." *Journal of Volcanology and Geothermal Research* **11** (1981):29.
- Kyte, F. T., Zhou, Z., and Wasson, J. T. "Siderophile-Enriched Sediments from the Cretaceous-Tertiary Boundary." *Nature* **288** (1980):651.
- Lacy, J. H., Baas, F., Townes, C. H., and Geballe, T. R. "Observations of the Motion and Distribution of the Ionized Gas in the Central Parsec of the Galaxy." *Astrophysical Journal* **227** (1979):L17.
- Lacy, J. H., Townes, C. H., Geballe, T. R., and Hollenbach, D. J. "Observations of the Motion and Distribution of the Ionized Gas in the Central Parsec of the Galaxy. II." *Astrophysical Journal* **241** (1980):132.
- Landecker, T. L., and Wielebinski, R. "The Galactic Meter Wave Radiation: A Two-Frequency Survey Between Declinations +25° and -25° and the Preparation of a Map of the Whole Sky." *Australian Journal of Physics Astrophysical Supplement* **16** (1970).

- Langway, C. C., Jr. "Stratigraphic Analysis of a Deep Ice Core from Greenland." *The Geological Society of America, Special Paper #125* (1970).
- LaViolette, P. A. "Investigation for Evidence of an Extraterrestrial Event at the Pleistocene-Holocene Boundary." Proposal submitted to the National Science Foundation (1980a).
- . "Historical development of the Galactic Explosion Hypothesis." Appendix I to the proposal for this dissertation topic. Portland State University, Systems Science Ph.D. Program, February 1, 1981 (published for the first time on this CD).
- . "A Nonvelocity Interpretation of the Cosmological Redshift Phenomenon." (1980b).
[Update: This is now published : LaViolette, P. A. "Is the universe really expanding?" *Astrophysical Journal* **301** (1986):544 – 553.]
- . "A Reaction-Diffusion Model of Space-Time." Presented at the Workshop on Instabilities, Bifurcations, and Fluctuations in Chemical Systems, Austin, Texas, March 1980c. [**UPDATE:** Now published as LaViolette, P. A. "An introduction to subquantum kinetics," *International Journal of General Systems (Special Issue on Systems Thinking in Physics)* **11**(4) (1985). Part I "An overview of the methodology," pp. 281 – 293; Part II. "An open system description of particles and fields," pp. 295 – 328; Part III "The cosmology of subquantum kinetics," pp. 329 – 345. Also in: LaViolette, P. A. *Subquantum Kinetics*. (Alexandria, VA, Starlane Publications, 1994).]
- Le Masurier, W. E., Kyle, P. R., and Rankin, P. C. "Rare-Earth Element Geochemistry of Volcanic Rocks from the Executive Committee Range, Marie Byrd Land." *Antarctic Journal* **11** (1976):263.
- Lee, M., Gretz, D., Steppel, S., and Weber, J. "Gravitational Radiation-Detector Observations in 1973 and 1974." *Physical Review D* **14** (1976):893.
- Lequeux, J. "The Radio Continuum of Galaxies. I. Observations." *Astronomy and Astrophysics* **15** (1971a):30.
- . "The Radio Continuum of Galaxies. II. The Origin of the Continuum Emission in Spiral Galaxies." *Astronomy and Astrophysics* **15** (1971b):42.
- Leventhal, M., MacCallum, C. J., Hutters, A. F., and Stang, P. D. "Time-Variable Positron Annihilation Radiation from the Galactic Center Direction." *Astrophysical Journal* **260** (1982):L1.
- Leventhal, M., MacCallum, C. J., and Stang, P. D. "Detection of 511 keV Positron Annihilation Radiation from the Galactic Center Direction." *Astrophysical Journal* **225** (1978):L11.
- Lewis, H. "Catastrophic Selection as a Factor in Speciation." *Evolution* **16** (1962):257.
- . "Speciation in Flowering Plants." *Science* **152** (1966):167.
- Lin, C. C., and Shu, F. H. "On the Spiral Structure of Disk Galaxies." *Astrophysical Journal* **140** (1964):646.

- Linfield, R. "VLBI Observations of Jets in Double Radio Galaxies." *Astrophysical Journal* **244** (1981):436.
- Ling, J. C., Mahoney, W. A., Willett, J. B., and Jacobson, A. S. "A Possible Line Feature at 73 kev from the Crab Nebula." *Astrophysical Journal* **231** (1979):896.
- Lingenfelter, R. E. "Production of Carbon 14 by Cosmic-ray Neutrons." *Reviews of Geophysics and Space Physics* **1** (1963):35.
- Lingenfelter, R. E., and Flamm, E. J. "Production of Carbon 14 by Solar Protons." *The Journal of Atmospheric Sciences* **21** (1964):134.
- Loeblich, A. R., Jr., and Tappan, H. "Foraminiferal Facts, Fallacies, and Frontiers." *Geological Society of America Bulletin* **75** (1964): 367.
- Lorentz, H. A. *Proceedings of the Royal Academy of Amsterdam* **6** (1904): 809.
- Lorius, C., Merlivat, L., Jouzel, J., and Pourchet, M. "A 30,000-yr. Isotope Climatic Record from Antarctic Ice." *Nature* **280** (1979): 644.
- Low, F. J., Johnson, H. L., Kleinmann, D. E., Latham, A. S., and Geisel, S. L. "Photometric and Spectroscopic Observations of Infrared Stars." *Astrophysical Journal* **160** (1970):531.
- Low, F. J., and Kleinmann, D. E. "Infrared Observations of Seyfert Galaxies, Quasistellar Sources, and Planetary Nebulae." (Seyfert Galaxy Conference, Paper #17) *Astronomical Journal* **73** (1968):868.
- Malin, D. F. "A Jet Associated with M 89." *Nature* **277** (1979):279.
- Malin, D. F., and Carter, D. "Giant Shells Around Normal Elliptical Galaxies." *Nature* **285** (1980):643.
- Malmgren, B., and Kennett, J. P. "Principal Component Analysis of Quaternary Planktic Foraminifera in the Gulf of Mexico: Paleoclimatic Applications." *Marine Micropaleontology* **1** (1976):299.
- Manchester, R. N., and Taylor, J. H. "Observed and Derived Parameters for 330 Pulsars." *Astronomical Journal* **86** (1981):1953.
- Margon, B. "The Bizarre Spectrum of SS 433." *Scientific American* **243**(4) (1980):54.
- Markarian, B. E. "On the Nature of Galaxies with UV Continuum Having Broad Emission Lines." *Astronomy and Astrophysics* **58** (1977):139.
- Marscher, A. P. "Relativistic Blast-wave Model for the Rapid Flux Variations of AO 0235+164 and Other Compact Radio Sources." *Astrophysical Journal* **224** (1978):816.
- Marscher, A. P., Marshall, F. E., Mushotzky, R. F., Dent, W. A., Balonek, T. J., and Hartman, M. F. "Search for X-ray Emission from Bursting Radio Sources." *Astrophysical Journal* **233** (1979):498.

- Martin, P. S. "Prehistoric Overkill." In *Pleistocene Extinctions: The Search for a Cause*, edited by P. S. Martin and H. E. Wright, Jr. New Haven: Yale University Press, 1967.
- Mason, B. *Handbook of Elemental Abundances in Meteorites*. New York: Gordon & Breach, 1971.
- Masursky, H., Boyce, J. M., Dial, A. L., Schaber, G. G., and Strobell, M. E. "Classification and Time of Formation of Martian Channels Based on Viking Data." *Journal of Geophysical Research* **82** (1977):4016.
- Mathewson, D. S., and Ford, V. L. "Polarization Observations of 1800 Stars." *Memoirs of the Royal Society* **74** (1970):139.
- Matthews, R. K. "Dynamics of the Ocean Cryosphere System: Barbados Data." *Quaternary Research* **2** (1972):368.
- "Relative Elevation of Late Pleistocene High Sea Level Stands: Barbados Uplift Rates and Their Implications." *Quaternary Research* **3** (1973):147.
- Matthews, T. A., Morgan, W. W., and Schmidt, M. "A Discussion of Galaxies Identified With Radio Sources." *Astrophysical Journal* **140** (1964):35.
- Mayr, E. *Systematics and the Origin of the Species*. Magnolia, Mass.: Peter Smith, 1942.
- "Change of Genetic Environment and Evolution." In *Evolution as a Process*, edited by J. Huxley, A. C. Hardy, and E. B. Ford. London: Allen and Unwin, 1954.
- *Animal Species and Evolution*. Cambridge, Mass.: Harvard University Press, 1963.
- McCarthy, D. W., Low, F. J., Kleinmann, S. G., and Gillett, F. C. "Infrared Speckle Interferometry of the Nucleus of NGC 1068." *Astrophysical Journal* **257** (1982):L7.
- McCorkell, R. H., Fireman, E. L., and Langway, C. C., Jr. "Dissolved Iron, Nickel, and Cobalt in Greenland Ice." *Transactions of the American Geophysical Union* **48** (1967):158.
- McCray, R., and Snow, T. P., Jr. "The Violent Interstellar Medium." *Annual Reviews of Astronomy and Astrophysics* **17** (1979):213.
- McCrea, W. H. "Continual Creation." *Monthly Notices of the Royal Astronomical Society* **128** (1964):335.
- "Ice Ages and the Galaxy." *Nature* **255** (1975):607.
- "Long Time-Scale Fluctuations in the Evolution of the Earth." *Proceedings of the Royal Society of London A* **375** (1981):1.
- McDonald, B. C. "Late Quaternary Stratigraphy and Deglaciation in Eastern Canada." In *The Late Cenozoic Glacial Ages*, edited by K. K. Turekian. New Haven: Yale University Press, 1971.

- McKibben, R. B., Pyle, K. R., and Simpson, J. A. "The Galactic Cosmic-Ray Radial Intensity Gradient and Large-Scale Modulation in the Heliosphere." *Astrophysical Journal* **254** (1982):L23.
- Mehringer, P. J., Jr. "The Environment of Extinction of the Late-Pleistocene Megafauna in the Arid Southwestern United States." In *Pleistocene Extinctions: The Search for a Cause*, edited by P. S. Martin and H. E. Wright, Jr. New Haven: Yale University Press, 1967, p. 247.
- Meltzer, D. J., and Mead, J. I. "The Timing of Late Pleistocene Mammalian Extinctions in North America." *Quaternary Research* **19** (1983):130.
- Mendez, R. H., Lee, P., O'Brien, A., and Liller, W. "The Disappearance of V-V1-7 and the Nature of Its Central Star." *Astronomy and Astrophysics* **91** (1980):331.
- Mendoza, E. E. "Infrared Excesses in T Tauri Stars and Related Objects." *Astrophysical Journal* **151** (1968):977.
- "Infrared Photometry of T Tauri Stars and Related Objects." *Astrophysical Journal* **143** (1966):1010.
- Menzel, D. H., Whipple, F. L., and de Vaucouleurs, G. *Survey of the Universe*. Englewood Cliffs, N.J.: Prentice Hall, 1970.
- Meyer, P. "Cosmic Rays in the Galaxy." *Annual Reviews of Astronomy and Astrophysics* **7** (1969):1.
- Michanowsky, G. *The Once and Future Star*. New York: Barnes and Noble, 1979.
- Milankovitch, M. "Mathematische Klimalehre und Astronomische Theorie der Klimaschwankungen." In *Handbuch der Klimatologie*, Vol. 1A, edited by W. Koppen and R. Geiger. New York: Springer Verlag, 1930.
- Miller, J. S., French, H. B., and Hawley, S. A. "The Spectrum and Magnitude of the Galaxy Associated with BL Lacertae." *Astrophysical Journal* **219** (1978):L85.
- Millman, P. M. "Dust in the Solar System." In *The Dusty Universe*, edited by G. B. Field and A. G. W. Cameron. New York: Smithsonian Astrophysical Observatory, 1973, p. 185.
- Milne, D. K. "Nonthermal Galactic Radio Sources." *Australian Journal of Physics* **23** (1970):425.
- "A New Catalog of Galactic SNRs Corrected for Distance from the Galactic Plane." *Australian Journal of Physics* **32** (1979):83.
- Minkowski, R. "Introductory Remarks." (Seyfert Galaxy Conference, Paper #1) *Astronomical Journal* **73** (1968):842.
- Morgan, J. W., Laul, J. C., Ganapathy, R., and Anders, E. "Glazed Lunar Rocks: Origin by Impact." *Science* **172** (1972):556.
- Morner, N. A. "The Gothenburg Magnetic Excursion." *Quaternary Research* **7** (1977):413.

- . "Annual and Inter-annual Magnetic Variations in Varved Clay." *Journal of Interdisciplinary Cycle Research* **9** (1978):229.
- Morner, N. A., and Lanser, J. P. "Gothenburg Magnetic 'Flip'." *Nature* **251** (1974):408.
- . "Paleomagnetism in Deep-Sea Core A179-15." *Earth and Planetary Science Letters* **26** (1975):121.
- Morrison, D. A., and Zinner, E. "Distribution and Flux of Micrometeoroids." *Philosophical Transactions of the Royal Society of London A* **285** (1977):379.
- Morrison, P. "Resolving the Mystery of the Quasars?" *Physics Today* (March, 1973):23.
- Mosley-Thompson, E., and Thompson, L. G. "Nine Centuries of Microparticle Deposition at the South Pole." *Quaternary Research* **17** (1982):1.
- Mueller, G., and Hinsch, G. W. "Glassy Particles in Lunar Fines." *Nature* **228** (1970):254.
- Muller, H. "Eine pollenanalytische Neubearbeitung des Interglazial- profils von Bilshausen (Unter-Eichsfeld)." *Geologische Jahrbuch* **83** (1965):327.
- . "Pollenanalytische Untersuchungen und Jahresschichtenzahlungen an der Holsteinzeitlichen Kieselgur von Munster Breloh." *Geologische Jahrbuch* **21** (1974):107.
- . "Climatic Changes During the Last Three Interglacials." In *Man's Impact on Climate*, edited by W. Bach. Amsterdam: Elsevier, 1978.
- Mullineaux, D. R. "Age of the Last Major Scabland Flood of the Columbia Plateau in Eastern Washington." *Quaternary Research* **10** (1978):171.
- Munch, G. "Kinematics of the Filaments in the Crab Nebula." *Reviews of Modern Physics* **30** (1958):1042.
- Murray, S. S., Fabbiano, G., Fabian, A. C., Epstein, A., and Giacconi, R. "High-Resolution X-ray Observations of the Cassiopeia A Supernova Remnant with the Einstein Observatory." *Astrophysical Journal* **234** (1979):L69.
- Mutel, R. L., Aller, H. D., and Phillips, R. B. "Milliarcsecond Structure of BL Lac During Outburst." *Nature* **294** (1981):236.
- Nakajima, T., Yaskawa, K., Natsuhara, N., and Kawai, N. "Very Short Period Geomagnetic Excursion 18,000 yr B.P." *Nature Physical Science* **244** (1973):8.
- Napier, W. M., and Clube, S. V. M. "A Theory of Terrestrial Catastrophism." *Nature* **282** (1979):455.
- Ninkovich, D., Opdyke, N. D., Heezen, B. C., and Foster, J. H. *Earth and Planetary Science Letters* **1** (1966):476.
- Noel, M., and Tarling, D. H. "The Laschamp Geomagnetic 'Event'." *Nature* **253** (1975):705.
- Nye, J. F. "Correction Factor for Accumulation Measured by the Thickness of the Annual Layers in an Ice Sheet." *Journal of Glaciology* **4** (1963):785.

- O'Dell, C. R. "Nature of Particulate Matter in Comets as Determined from Infrared Observations." *Astrophysical Journal* **166** (1971):675.
- Oerlemans, J. "Continental Ice Sheets and the Planetary Radiation Budget." *Quaternary Research* **14** (1980):349.
- Oerlemans, J., and Van den Dool, H. M. "Energy Balance Climate Models: Stability Experiments with a Refined Albedo and Updated Coefficients for Infrared Emission." *Journal of the Atmospheric Sciences* **35** (1978):371.
- Oeschger, H., Stauffer, B., Bucher, P., and Moell, M. "Extraction of Trace Components from Large Quantities of Ice in Bore Holes." *Journal of Glaciology* **17** (1976):117.
- Oke, J. B. "Further Spectrophotometry of the Transient X-ray Source A0620-00." *Astrophysical Journal* **217** (1977):181.
- Oke, J. B., and Greenstein, J. L. "Spectrophotometry of the Transient X-ray Source A0620-00." *Astrophysical Journal* **211** (1977):872.
- O'Keefe, J. A. "The Terminal Eocene Event: Formation of a Ring System Around the Earth." *Nature* **285** (1980):309.
- Olsson, I. U. "Dates of C-14/C-12 Variations with Respect to Dendrochronology – Explanation of Plate IV." In *Radiocarbon Variations and Absolute Chronology*, edited by I. Olsson. Stockholm: Almqvist & Wiksell Forlag AB, 1970, p. 625.
- Oort, J. H. "The Structure of the Cloud of Comets Surrounding the Solar System and a Hypothesis Concerning Its Origin." *Bulletin of the Astronomical Institute of Netherlands* **11** No. 408 (1950):91.
- "The Galactic Center." *Annual Reviews of Astronomy & Astrophysics* **15** (1977):295.
- Opdyke, N. D., Glass, B., Hays, J. D., and Foster, J. "A Paleomagnetic Study of Antarctic Deep-sea Cores." *Science* **154** (1966):1349.
- Opdyke, N. D., Ninkovich, D., Lowrie, W., and Hays, J. D. "The Paleomagnetism of Two Aegean Deep-Sea Cores." *Earth and Planetary Science Letters* **14** (1972):145.
- Orth, C. J., Gilmore, J. S., Knight, J. D., Pillmore, C. L., Tschudy, R. H., and Fassett, J. E. "An Iridium Abundance Anomaly at the Palynological Cretaceous-Tertiary Boundary in Northern New Mexico." *Science* **214** (1981):1341.
- Osborne, P. J. "An Insect Assemblage of Early Flandrian Age from Lea Marston, Warwickshire and Its Bearing on the Contemporary Climate and Ecology." *Quaternary Research* **4** (1974):471.
- Owen, F., Balonek, T. J., Dickey, J., Terzian, V., and Gottesman, S. T. "Radio Emission from the X-ray Source A0620-00." *Astrophysical Journal* **203** (1976):L15.
- Pacholczyk, A. G., and Weymann, R. "Proceedings of the Conference on Seyfert Galaxies and Related Objects Held at Steward Observatory, University of Arizona, 14 - 16 February 1968." *Astronomical Journal* **73** (1968):836.

- Parkin, D. W., Sullivan, R. A. L., and Andrews, J. N. "Cosmic Spherules as Rounded Bodies in Space." *Nature* **266** (1977):515.
- Paterson, W. S. B. "Vertical Strain-Rate Measurements in an Arctic Ice Cap and Deductions from Them." *Journal of Glaciology* **17** (1976):3.
- Paterson, W. S. B., Koerner, R. M., Fisher, D., Johnsen, S. J., Clausen, H. B., Dansgaard, W., Bucher, P., and Oeschger, H. "An Oxygen-Isotope Climatic Record from the Devon Island Ice Cap, Arctic Canada." *Nature* **266** (1977):508.
- Penzias, A. A., and Wilson, R. W. "A Measurement of Excess Antenna Temperature at 4080 Mc/s." *Astrophysical Journal* **142** (1965):419.
- Perley, R. A., and Johnston, K. J. "The Arcsecond Structure of Four Compact Radio Sources." *Nature* **84** (1979):1247.
- Petit, J. R., Briat, M., and Royer, A. "Ice Age Aerosol Content from East Antarctic Ice Core Samples and Past Wind Strength." *Nature* **293** (1981):391.
- Pewe, T. L. "Origin of the Upland Silt Near Fairbanks, Alaska." *Bulletin of the Geological Society of America* **67** (1955):699.
- . *Quaternary Geology of Alaska*. Geological Survey Professional Paper 835, 1975a.
- . *Quaternary Stratigraphic Nomenclature in Unglaciated Central Alaska*. Geological Survey Professional Paper 862, 1975b.
- Pewe, T. L., Journaux, A., and Stuckenrath, R. "Radiocarbon Dates and Late-Quaternary Stratigraphy from Mamontova Gora, Unglaciated Central Yakutia, Siberia, U.S.S.R." *Quaternary Research* **8** (1977):51.
- Piddington, J. H. *Cosmic Electrodynamics*. New York: John Wiley & Sons, 1969.
- Pierce, K. A., and Allen, R. G. "The Solar Spectrum between .3 and 10 m." In *The Solar Output and Its Variation*, edited by O. R. White. Boulder, Colorado: Colorado Associated University Press, 1977.
- Pollack, J. B., Toon, O. B., Sagan, C., Summers, A., Baldwin, B., and Van Camp, W. "Volcanic Explosions and Climatic Change: A Theoretical Assessment." *Journal of Geophysical Research* **81** (1976):1071.
- Pooley, G. G. "5c3: A Radio Continuum Survey of M 31 and Its Neighborhood." *Monthly Notices of the Royal Astronomical Society* **144** (1969):101.
- Porcas, R. W. "Superluminal Quasar 3C179 with Double Radio Lobes." *Nature* **294** (1981):47.
- Price, R. M. "Continuum Radio Structure of the Galactic Disk." *Astronomy and Astrophysics* **33** (1974):33.
- Price, S. D., Murdock, T. L., and Marcotte, L. P. "Infrared Observation of the Zodiacal Dust Cloud." *Astronomical Journal* **85** (1980):765.

- Protheroe, R. J., Strong, A. W., and Wolfendale, A. W. "Gamma-Rays from the Cygnus Region and the Nature of CG 78+1." *Monthly Notices of the Royal Astronomical Society* **188** (1979):863.
- Rainey, F. "Archaeological Investigation in Central Alaska." *American Antiquity* **5** (1940):299.
- Raisbeck, G. M., Yiou, F., Fruneau, M., Loiseaux, J. M., Lieuvin, M., Ravel, J. C., and Lorius, C. "Cosmogenic Be Concentrations in Antarctic Ice During the Past 30,000 Years." *Nature* **292** (1981):825.
- Ramaty, Reuven. "Cosmic Electrons." In *High Energy Particles and Quanta in Astrophysics*, edited by F. B. McDonald and C. E. Fichtel. Cambridge, Mass.: MIT Press, 1974.
- Rankama, K., and Sahama, Th. G. *Geochemistry*. Chicago: University of Chicago Press, 1950.
- Raschke, E., Moller, F., and Bandeen, W. "The Radiation Balance of the Earth-Atmosphere System over Both Polar Regions Obtained from Radiation Measurements of the Nimbus II Meteorological Satellite." *Sver. Meteorol. Hydrol. Inst. Medd. Ser. B*, No. 28, 1968.
- Read, P. L. "Measurements of the Flux Density of Cas A and Confirmation of an Anomaly at 38 MHz." *Monthly Notices of the Royal Astronomical Society* **178** (1977):259.
- Rees, M. J. "The Appearance of Relativistically Expanding Radio Sources." *Nature* **211** (1966):468.
- Reich, W., Stute, V., Reif, K., Kaberla, P. M. W., and Kronberg, P. P. "The Discovery of Possible Giant Radio Structure of the Radio Sources 3C 273, 3C 293, 3C 345, and 3C380." *Astrophysical Journal* **236** (1980):L61.
- Reid, P. B., Becker, R. H., and Long, K. S. "An X-ray Image of Tycho's Supernova Remnant." *Astrophysical Journal* **261** (1982):485.
- Richardson, Sir J. *Zoology of the Voyage of the Herald*. London, 1854.
- Richter, G. *Astronomische Nachrichtung* **292** (1971):275.
- Ricker, G. R., Scheepmaker, A., Ryckman, S. G., Ballintine, J. E., Doty, J. P., Downey, P. M., and Lewin, H. W. G. "High-Energy X-Ray Observations of a Lunar Occultation of the Crab Nebula." *Astrophysical Journal* **197** (1975):L83.
- Riehl, H. *Introduction to the Atmosphere*. New York: McGraw-Hill, 1972.
- Rieke, G. H., and Lebofsky, M. J. "Infrared Emission of Extragalactic Sources." *Annual Reviews of Astronomy and Astrophysics* **17** (1979): 477.
- Rieke, G. H., and Low, F. J. "Infrared Photometry of Extragalactic Sources." *Astrophysical Journal* **176** (1972):L95.
- Risbo, T., Clausen, H. B., and Rasmussen, K. L. "Supernovae and Nitrate in the Greenland Ice Sheet." *Nature* **294** (1981):687.

- Roger, R. S., and Pedlar, A. "Atomic and Ionized Hydrogen Associated with NGC 281 (S 184)." *Astronomy and Astrophysics* **94** (1981):238.
- Ronov, A. B., and Yaroshevsky, A. A. "Earth's Crust Geochemistry." In *The Encyclopedia of Geochemistry and Environmental Sciences*, Vol. IV A, edited by F. W. Fairbridge. New York: Van Nostrand Reinhold, 1972.
- Rossi, B. *High-energy Particles*. Englewood Cliffs, N.J.: Prentice-Hall, 1952.
- Rossignol-Strick, M., Nesteroff, W., Olive, P., and Vergnaud-Grazzini, C. "After the Deluge: Mediterranean Stagnation and Sapropel Formation." *Nature* **295** (1982):105.
- Rougoor, G. W., and Oort, J. H. "Distribution and Motion of Interstellar Hydrogen in the Galactic System with Particular Reference to the region within 3 Kiloparsecs of the Center." *Proceedings of the National Academy of Sciences* **46** (1960):1.
- Rubin, V. C., and Ford, W. K., Jr. "Radial Velocities and Line Strengths of Emission Lines across the Nuclear Disk of M 31." *Astrophysical Journal* **170** (1971):25.
- Rubin, V. C., Thonnard, N., Ford, W. K., Jr., and Roberts, M. S. "Motion of the Galaxy and the Local Group Determined from the Velocity Anisotropy of Distant ScI Galaxies. II. The Analysis for the Motion." *Astronomical Journal* **81** (1976):719.
- Ruddiman, W. F., McIntyre, A., Niebler-Hunt, V., and Durazzi, J. T. "Oceanic Evidence for the Mechanism of Rapid Northern Hemisphere Glaciation." *Quaternary Research* **13** (1980):33.
- Ruddiman, W. F., Sancetta, C. D., and McIntyre, A. "Glacial/Interglacial Response Rate of Subpolar North Atlantic Waters to Climatic Change: The Record in Oceanic Sediments." *Philosophical Transactions Royal Society of London* **B 280** (1977):119.
- Ruderman, M. A. "Possible Consequences of Nearby Supernova Explosions for Atmospheric Ozone and Terrestrial Life." *Science* **184** (1974):1079.
- Russell, D. A. "The Mass Extinctions of the Late Mesozoic." *Scientific American* **246**(1) (1982):58.
- Ryle, M., Elsmore, B., and Neville, A. C. "High-Resolution Observations of the Radio Sources in Cygnus and Cassiopeia." *Nature* **205** (1965): 1259.
- Scargle, J. D. "Activity in the Crab Nebula." *Astrophysical Journal* **156** (1969):401.
- Scargle, J. D., and Pacini, F. "On the Mechanism of the Glitches in the Crab Nebula Pulsar." *Nature Physical Science* **232** (1971):144.
- Schendel, J. R. "Are Blazars Quasars?" *Astronomy* (February, 1980):67.
- Scheuer, P. A. G., and Readhead, A. C. S. "Superluminally Expanding Radio Sources and the Radio-Quiet QSOs." *Nature* **277** (1979):182.
- Schmidt, G. D., Angel, J. R. P., and Beaver, E. A. "The Small-Scale Polarization of the Crab Nebula." *Astrophysical Journal* **227** (1979):106.

- Schmidt, T., and Elsasser, H. In *The Zodiacal Light and the Interplanetary Medium*, edited by J. L. Weinberg. Washington, D.C.: NASA SP-150, 1967, p. 301.
- Schove, D. J. (Discussion to paper by N. J. Schackleton) *Philosophical Transactions Royal Society of London* **B 280** (1977):181.
- Schreier, E. J., Feigelson, E., Delvaille, J., Giacconi, R., Grindlay, J., Schwartz, D. A., and Fabian, A. C. "Einstein Observations of the X-ray Structure of Centaurus A: Evidence for the Radio-Lobe Energy Source." *Astrophysical Journal* **234** (1979):L39.
- Schweizer, F. "An Optical Study of the Giant Radio Galaxy NGC 1316 (Fornax A)." *Astrophysical Journal* **237** (1980):303.
- Science editorial "Saturn Redux: The Voyager 2 Mission." *Science* **213** (1981):1236.
- Scott, J. S., and Chevalier, R. A. "Cosmic Ray Production in the Cassiopeia A Supernova Remnant." *Astrophysical Journal* **197** (1975):L5.
- Seargent, D. A. *Comets: Vagabonds of Space*. Garden City, N.Y.: Doubleday, 1982.
- Searle, L., Rodgers, A. W., and Sargent, W. L. W. "Common Features of the Optical Continua Associated with Violent Cosmic Events." *Nature* **208** (1965):1190.
- Sejnowski, T. J. "Sources of Gravity Waves." *Physics Today* (January, 1974):40.
- Seret, G., and Woillard, G. "The Glaciations in the 'Vosges Lor raines'." Fuhrer zur Exkursionstagung des IGCP Projektes 73/1/24. "Quaternary Glaciations in the Northern Hemisphere," 5-13 September 1976, in den Sudvosgesen, im Nordliche Alpenvorland und in Tirol, pp. 1-13.
- Serkowski, K. *Lowell Observatory Bulletin* **4** (1960):296, 301, 317.
- Setti, G., and Woltjer, L. "Density of Galactic Cosmic Ray Electrons." *Astrophysical Letters* **8** (1971):125.
- Seward, F. D., Burginyon, G. A., Grader, R. J., Hill, R. W., Palmieri, T. M., and Stoering, J. P. "X-Rays from Puppis A and the Vicinity of Vela X." *Astrophysical Journal* **169** (1971):515.
- Seward, F. D., Forman, W. R., Giacconi, R., Griffiths, R. E., Harnden, F. R., Jones, C., and Pye, J. P. "X-rays from Eta Carinae and the Surrounding Nebula." *Astrophysical Journal* **234** (1979):L55.
- Shackleton, N. J., and Opdyke, N. D. "Oxygen Isotope and Palaeomagnetic Evidence for Early Northern Hemisphere Glaciation." *Nature* **270** (1977):216.
- "Oxygen Isotope and Paleomagnetic Stratigraphy of Equatorial Pacific Cores V28-238: Oxygen Isotope Temperatures and Ice Volumes on a 105 year -- 106 year Scale." *Quaternary Research* **3** (1973):39.
- Shapiro, P. R. "Relativistic Blast Waves That Accelerate." *Astrophysical Journal* **236** (1980):236.

- Shaw, D. M., Dostal, J., and Keays, R. R. "Additional Estimates of Continental Surface Precambrian Shield Composition in Canada." *Geochimica Cosmochimica Acta* **40** (1976):73.
- Shima, M. "The Distribution of Germanium and Tin in Meteorites." *Geochimica et Cosmochimica Acta* **28** (1964):517.
- Shirkey, R. C. "The Radio Dynamical Evolution of Young Supernova Remnants." *Astrophysical Journal* **224** (1978):477.
- Shklovsky, I. S. *Doklady Akademia Nauk SSSR* **91** (1953):475.
- . *Supernovae*. New York: John Wiley, 1968.
- Silk, J., Smith, H. E., Spinard, H., and Field, G. B. "The Spectrum of the Extranuclear Regions of Ton 256." *Astrophysical Journal* **181** (1973):L25.
- Simard-Normandin, M., and Kronberg, P. P. "Rotation Measures and the Galactic Magnetic Field." *Astrophysical Journal*, **242** (1980):74.
- Simpson, G. G. *Tempo and Mode in Evolution*. New York: Columbia University Press, 1944.
- . *The Major Features of Evolution*. New York: Columbia University Press, 1953.
- Simpson, J. F. "Evolutionary Pulsations and Geomagnetic Polarity." *Geological Society of America Bulletin* **77** (1965):197.
- Singer, S. F. *Transactions of the American Geophysical Union* **38** (1957): 175.
- Skeels, M. A. "The Mastodons and Mammoths of Michigan." *Michigan Academy of Sciences, Arts Letters Papers* **47** (1962):101.
- Slaughter, B. H. "Animal Ranges as a Clue to Late-Pleistocene Extinction." In *Pleistocene Extinctions: The Search for a Cause*, edited by P. S. Martin and H. E. Wright, Jr. New Haven: Yale University Press, 1967, p. 155.
- Smith, D., Adams, N. G., and Khan, H. A. "Flux and Composition of Micrometeoroids in the Diameter Range 1 – 10 μm ." *Nature* **252** (1974):101.
- Smith, J. D., and Foster, J. H. "Geomagnetic Reversal in Brunhes Normal Polarity Epoch." *Science* **163** (1969):565.
- Smoot, G. F., Gorenstein, M. V., and Muller, R. A. "Detection of Anisotropy in the Cosmic Blackbody Radiation." *Physical Review Letters* **39** (1977):898.
- Smoot, G. F., and Lubin, P. M. "Southern Hemisphere Measurements of the Anisotropy in the Cosmic Microwave Background Radiation." *Astrophysical Journal* **234** (1979):L83.
- Souffrin, S. "An Interpretation of the Variations of the Spectrum of NGC 3516." (Seyfert Galaxy Conference, Paper #36) *Astronomical Journal* **73** (1968):897.

- Spencer, J. H., and Burke, B. F. "A Search for Radio Emission from S Andromedae." *Astrophysical Journal* **185** (1973):L83.
- Van Speybroeck, L., Epstein, A., Forman, W., Giacconi, R., Jones, C., Liller, W., and Smarr, L. "Observations of X-ray Sources in M 31." *Astrophysical Journal* **234** (1979):L45.
- Spitzer, L., Jr. "On a Possible Interstellar Galactic Corona." *Astrophysical Journal* **124** (1956):20.
- . *Physics of Fully Ionized Gases*. New York: John Wiley & Sons, 1962.
- Spitzer, L., Jr., and Schatzman, E. *Astrophysical Journal* **54** (1949): 195.
- Spitzer, L., Jr., and Tukey, J. W. *Astrophysical Journal* **114** (1951): 187.
- Spoelstra, T. A. "A Survey of Linear Polarization at 1415 MHz. IV. Discussion of the Results for the Galactic Spurs." *Astronomy and Astrophysics* **21** (1972):61.
- Stanley, S. M. *Macroevolution: Pattern and Process*. San Francisco: Freeman, 1979.
- Stephenson, F. R. "Supernovae in History." *1979 Yearbook of Astronomy*, p. 200.
- Stockton, A., Chesley, D., and Chesley, S. "Spectroscopy of R Monocerotis and NGC 2261." *Astrophysical Journal* **199** (1975):406.
- Street, F. A., and Grove, A. T. "Global Maps of Lake-Level Fluctuations Since 30,000 yr. B.P." *Quaternary Research* **12** (1979):83.
- Strom, R. G., and Duin, R. M. "A High Resolution 21 cm Continuum Study of the Supernova Remnants 3C 10 (Tycho's Supernova Remnant) and 3C461 (Cas A)." *Astronomy and Astrophysics* **25** (1973):351.
- Stuiver, M. "Long-Term C-14 Variations." In *Radiocarbon Variations and Absolute Chronology*, edited by I. V. Olsson. New York: Wiley Interscience Division, 1970.
- . "Evidence for the Variation of Atmospheric C-14 Content in the Late Quaternary." In *The Late Cenozoic Glacial Ages*, edited by K. K. Turekian. New Haven: Yale University Press, 1971, p. 57.
- Suess, H. E. "Secular Variations in the Cosmic-Ray-Produced Carbon 14 in the Atmosphere and Their Interpretation." *Journal of Geophysical Research* **70** (1965):5937.
- Swart, P. K., Grady, M. M., Pillinger, C. T., Lewis, R. S., and Anders, E. "Interstellar Carbon in Meteorites." *Science* **220** (1983):406.
- Taber, S. "Perennially Frozen Ground in Alaska: Its Origin and History." *Bulletin of the Geological Society of America* **54** (1943):1433.
- Takahashi, H., Yokoyama, Y., Fireman, E. L., and Lorus, C. "Iridium Content of Polar Ice and Accretion Rate of Cosmic Matter." *Lunar and Planetary Science* **9**(2) (1978):1131.

- Tananbaum, H., Peters, G., Forman, W., Giacconi, R., Jones, C., and Avni, Y. "UHURU Observations of X-ray Emission from Seyfert Galaxies." *Astrophysical Journal* **223** (1978):74.
- Tauber, H. "The Scandinavian Varve Chronology and C14 Dating." In *Radiocarbon Variations and Absolute Chronology*, edited by Ingrid Olsson. New York: John Wiley & Sons, 1970.
- Teichert, C. "Major Features of Cephalopod Evolution. In *Essays in Paleontology and Stratigraphy*, edited by C. Teichert and E. Yochelson. Lawrence: University of Kansas Press, 1967.
- Telesco, C. M., and Harper, D. A. "Far-infrared Observations of NGC 7027." *Astrophysical Journal* **211** (1977):475.
- Terrell, J. "Size Limits on Fluctuating Astronomical Sources." *Astrophysical Journal* **213** (1977):L93.
- Terry, K. D., and Tucker, W. H. "Biologic Effects of Supernovae." *Science* **159** (1968):421.
- Thiede, J. "Aspects of the Variability of the Glacial and Interglacial North Atlantic Eastern Boundary Current (Last 150,000 years)." "Meteor" Forschungen Ergebnisse C (1977):1.
- Thiel, E., and Schmidt, R. A. "Spherules from the Antarctic Ice Cap." *Journal of Geophysical Research* **69** (1964):307.
- Thieys, J. C., and Spiegel, E. A. "Ring Galaxies I." *Astrophysical Journal* **208** (1976):650.
- Thomas, G. E. "The Interstellar Wind and Its Influence on the Interplanetary Environment." *Annual Reviews of Earth and Planetary Science* **6** (1978):173.
- Thompson, L. G. "Variations in Microparticle Concentration, Size Distribution and Elemental Composition Found in Camp Century, Greenland, and Byrd Station, Antarctica, Deep Ice Cores." In *Isotopes and Impurities in Snow and Ice (Proceedings of the Grenoble Symposium, 1975)*, IAHS Publ. No. 118 (1977a), p. 351.
- "Microparticles, Ice Sheets and Climate." Institute of Polar Studies Report No. 64. Columbus: Ohio State University, 1977b.
- Thompson, L. G., Hamilton, W. L., and Bull, C. "Climatological Implications of Microparticle Concentrations in the Ice Core from "Byrd" Station, Western Antarctica." *Journal of Glaciology* **14** (1975):433.
- Thompson, L. G., and Mosley-Thompson, E. "Microparticle Concentration Variations Linked with Climatic Change: Evidence from Polar Ice Cores." *Science* **212** (1981):812.
- Thompson, R. I., Strittmatter, P. A., Erickson, E. F., Witteborn, F. C., and Strecker, D. W. "Observation of Preplanetary Disks Around MWC 349 and LkH 101." *Astrophysical Journal* **218** (1977):170.

- Thomsen, D. E. "Fast Pulsars: One by Light, Two by Radio." *Science News* **123** (1983):324.
- Thorarinsson, S. "Some New Aspects of the Grimsvotn Problem." *Journal of Glaciology* **2** (1953):267.
- Thunell, R., Federman, A., Sparks, S., and Williams, D. "The Age, Origin, and Volcanological Significance of the Y-5 Ash Layer in the Mediterranean." *Quaternary Research* **12** (1979):241.
- Tolmachoff, I. P. "The Carcasses of the Mammoth and Rhinoceros Found in the Frozen Ground of Siberia." *American Philosophical Society Transactions* **23** (1929):1.
- Toon, O. B., and Pollack, J. B. "Stratospheric Aerosols and Climate." In *The Stratospheric Aerosol Layer*, edited by R. C. Whitten. New York: Springer-Verlag, 1982.
- Toor, A. "X-Ray Characteristics of the Lupus Loop and SN 1006 Supernova Remnants." *Astronomy and Astrophysics* **85** (1980):184.
- Townes, C. H., Lacy, J. H., Geballe, T. R., and Hollenbach, D. J. "The Centre of the Galaxy." *Nature* **301** (1983):661.
- Trimble, V. "Motions and Structure of the Filamentary Envelope of the Crab Nebula." *Astronomical Journal* **73** (1968):535.
- "Ionization and Excitation in the Crab Nebula." *Astronomical Journal* **75** (1970):926.
- Tucker, W. H. "Soft X-rays from the Cygnus Loop: Interpretation." *Science* **172** (1971):372.
- "Supernova in the Sail." *Star and Sky* **1**(7) (1979):11.
- "The X-ray Universe Comes into Focus." *Star and Sky* **2**(1) (1980a):36.
- "The Colossus of Carina." *Star and Sky* **2**(3) (1980b):22.
- Tuohy, I., and Garmire, G. "Discovery of a Compact X-ray Source at the Center of the Supernova Remnant RCW 103." *Astrophysical Journal* **239** (1980):L107.
- Turco, R. P., Toon, O. B., Hamill, P., and Whitten, R. C. "Effects of Meteoric Debris on Stratospheric Aerosols and Gases." *Journal of Geophysical Research* **86** (1981):1113.
- Twomey, S. *Atmospheric Aerosols*. New York: Elsevier Scientific Publishing Co., 1977.
- Tyson, J. S., Baum, W. A., and Kreidl, T. "Deep CCD Images of 3C273." *Astrophysical Journal* **257** (1982):L1.
- Tyson, J. A., and Giffard, R. P. "Gravitational-Wave Astronomy." *Annual Reviews of Astronomy and Astrophysics* **16** (1978):521.

- Uffen, R. J. "Influence of the Earth's Core on the Origin and Evolution of Life." *Nature* **198** (1963):143-144.
- . "Evolution of the Interior of the Earth and Its Effects on Biological Evolution." 22nd International Geological Congress, New Delhi, 1964.
- Ulrich, R. K., and Knapp, G. R. "The Gas Flow Near T Tauri Stars." *Astrophysical Journal* **230** (1979):L99.
- Urch, I. H., and Gleeson, L. J. "Galactic Cosmic-Ray Modulation from 1965 to 1970." *Astrophysics and Space Science* **17** (1972):426.
- Urey, H. C. "Origin of Tektites." *Nature* **179** (1957):556.
- . "Origin of Tektites." *Science* **137** (1962):746.
- . "Cometary Collisions and Tektites." *Nature* **197** (1963):228.
- . "Cometary Collisions and Geological Periods." *Nature* **242** (1973):32.
- de Vaucouleurs, G., and de Vaucouleurs, A. "Photographic, Photometric, and Spectroscopic Observations of Seyfert Galaxies." (Seyfert Galaxy Conference, Paper #12) *Astronomical Journal* **73** (1968):858.
- Vereshchagin, N. K. "Primitive Hunters and Pleistocene Extinction in the Soviet Union." In *Pleistocene Extinctions: The Search for a Cause*, edited by P. S. Martin and H. E. Wright, Jr. New Haven: Yale University Press, 1967, p. 365.
- Verosub, K. L., and Banerjee, S. K. "Geomagnetic Excursions and their Paleomagnetic Record." *Reviews of Geophysics and Space Physics* **15** (1977):145.
- Vidal-Madjar, A., Laurent, C., Bruston, P., and Audouze, J. "Is the Solar System Entering a Nearby Interstellar Cloud?" *Astrophysical Journal* **223** (1978):589.
- Waddington, C. J. "Palaeomagnetic Field Reversals and Cosmic Radiation." *Science* **158** (1967):913.
- Wade, C. M. "Radio Structure of Seyfert Galaxies and Other Spirals." (Seyfert Galaxy Conference, Paper #22) *Astronomical Journal* **73** (1968):876.
- Walborn, N. R. "The Complex Outer Shell of Eta Carinae." *Astrophysical Journal* **204** (1976):L17.
- Waldrop, M. M. "The 0.001557806449023-Second Pulsar." *Science* **219** (1983):831.
- Walker, A. L. "Ultraviolet Excess in T Tauri Stars." In *Stellar Evolution*. Edited by R. F. Stein and A. G. W. Cameron. New York: Plenum Press, 1966, p. 405.
- Wallace, A. L. *The Geographical Distribution of Animals*. Vol. 1. London: MacMillan, 1876.

- . *The World of Life*. New York: Moffat, Yard, 1911.
- Ward, R. *Floods: A Geographical Perspective*. New York: John Wiley & Sons, 1978.
- Warren, H. C. *Buddhism in Translations*. New York: Atheneum, 1979.
- Wasson, J. T., and Kimberlin, J. "The Chemical Classification of Iron Meteorites. II. Irons and Pallasites with Germanium Concentrations between 8 and 100 ppm." *Geochimica et Cosmochimica Acta* **31** (1967): 2065.
- Wdowczyk, J., and Wolfendale, A. W. "Cosmic Rays and Ancient Catastrophes." *Nature* **268** (1977):510.
- Weaver, H., and Williams, D. R. W. "The Berkeley Low-Latitude Survey of Neutral Hydrogen." *Astronomy and Astrophysics Supplement* **8** (1973):1.
- Weber, J. "Anisotropy and Polarization in the Gravitational Radiation Experiments." *Physical Review Letters* **25** (1970):180.
- . "Advances in Gravitational Radiation Detection." *General Relativity and Gravitation* **1** (1972):59.
- . "Detection of Gravity Waves Challenged." *Physics Today* **27** (December, 1974):11.
- . "More on Gravity Waves." *Physics Today* **28** (November, 1975): 13.
- . "Gravitational Radiation Detector Observations in 1973 and 1974." *Nature* **266** (1977a):243.
- . "Gravitational Radiation Experiments." In *Topics in Theoretical and Experimental Gravitation Physics*, edited by V. De Sabbata and J. Weber. New York: Plenum Publishing, 1977b.
- . "The Search for Gravitational Radiation." In *General Relativity and Gravitation*, Vol. 2, edited by A. Held. New York: Plenum Publishing, 1980.
- Weekes, T. C. *High-Energy Astrophysics*. London: Chapman & Hall, 1969.
- Weiler, K. W., and Panagia, N. "Vela X and the Evolution of Plerions." *Astronomy and Astrophysics* **90** (1980):269.
- Weiler, K. W., and Shaver, P. A. "Total Intensity and Polarization Structure of the Supernova Remnant G74.9+1.2 at $\lambda = 6, 21, \text{ and } 49$ Centimeters." *Astronomy and Astrophysics* **70** (1978):389.
- Weller, C. S., and Meier, R. R. "Observations of Helium in the Interplanetary/Interstellar Wind: The Solar-Wake Effect." *Astrophysical Journal* **193** (1974):471.
- Westurlund, B. E., and Wall, J. V. "Photometry of Southern Quasistellar Objects, N Galaxies, and Possibly Related Objects." (Seyfert Galaxy Conference, Paper #26) *Astronomical Journal* **73** (1968):883.

- Weymann, R. "Seyfert Galaxies." *Scientific American* **220**(1) (1969):28.
- Whipple, F. L. "The Theory of Micrometeorites. Part II. In Heterothermal Atmospheres." *Proceedings of the National Academy of Sciences* **37** (1951):19.
- . "Do Comets Play a Role in Galactic Chemistry and γ -ray Bursts?" *Astronomical Journal* **80** (1975):525.
- White, M. J. D., Blackith, R. E., Blackith, R. M., and Cheney, J. *Australian Journal of Zoology* **15** (1967):263.
- Wickramasinghe, N. C. *Light Scattering Functions for Small Particles with Applications in Astronomy*. New York: John Wiley & Son, 1973.
- Wielebinski, R., Smith, D. H., Garzon-Cardenas, X. "A Survey of the Galactic Plane at 85 and 150 MHz." *Australian Journal of Physics* **21** (1968):185.
- Wijmstra, T. A. "Palynology and Paleoclimatology of the Last 100,000 Years." *Proceedings WMO/IAMAP Symposium on Long-Term Climatic Fluctuation, Norwich, 1975*. (World Meteorological Organization, No. 421, 1975, p. 5.)
- Will, C. "Theoretical Tools of Experimental Gravitation." In *Proceedings of Course 56 of the International School of Physics "Enrico Fermi"*, edited by B. Bertotti. New York: Academic Press, 1974.
- Willis, A. G. "The Large Scale Structure of Extra-Galactic Radio Sources (>1 Arcsecond)." *Physica Scripta* **17** (1978):243.
- Willner, S. P. *Compact Infrared Sources: NGC 7538 and the Galactic Center*. Ph.D. thesis, California Institute of Technology, 1976.
- Winkler, P. F., Jr., Hearn, D. R., Richardson, J. A., and Behnken, J. M. "Soft X-ray Emission from the Lupus Loop and SN 1006 Supernova Remnants." *Astrophysical Journal* **229** (1979):L123.
- Woillard, G. M. "Recherches Palynologiques Sur le Pleistocene dans l'Est de la Belgique et dans les Vosges Lorraines." *Acta Geographica Lovaniensia* **14** (1975):1.
- . "Grande Pile Peat Bog: A Continuous Pollen Record for the Last 140,000 Years." *Quaternary Research* **9** (1978):1.
- . "Abrupt End of the Last Interglacial S.S. in North-East France." *Nature* **281** (1979):558.
- Woillard, G. M., and Mook, W. G. "Carbon-14 Dates at Grande Pile: Correlation of Land and Sea Chronologies." *Science* **215** (1982):159.

- Wolfe, A. M. "Properties of BL Lac Objects." *Annals of the New York Academy of Sciences* **336** (1980):12.
- Wollin, G., Ericson, D. B., and Ryan, W. B. F. "Magnetism of the Earth and Climatic Changes." *Earth and Planetary Science Letters* **12** (1971):175.
- Wollman, E. R. "Ne II 12.8 Emission from the Galactic Center and Compact H II Regions. Ph.D. thesis, California Institute of Technology, 1976.
- Wollman, E. R., Geballe, T. R., Lacy, J. H., Townes, C. H., and Rank, D. M. "Ne II 12.8 Micron Emission from the Galactic Center II." *Astrophysical Journal* **218** (1977):L103.
- Woltjer, L. *Bulletin of the Astronomical Institute of the Netherlands* **14** (1958):39.
- ". "Supernova Remnants." *Annual Reviews of Astronomy and Astrophysics* **10** (1972):129.
- Woodwell, G. M. "Radiation and the Pattern of Nature." *Science* **156** (1967):461.
- Woody, D. P., and Richards, P. L. "Spectrum of the Cosmic Background Radiation." *Physical Review Letters* **42** (1979):925.
- Worden, S. P., Schneeberger, T. J., Kuhn, J. R., and Africano, J. L. "Flare Activity on T Tauri Stars." *Astrophysical Journal* **244** (1981):520.
- Wrangell, F. P. *Narrative of an Expedition to Siberia and the Polar Sea*. 1841.
- Wright, H. E., Jr. "Tunnel Valleys, Glacial Surges, and Subglacial Hydrology of the Superior Lobe, Minnesota." In *The Wisconsin Stage (GSA Memoir 136)*, edited by R. F. Black, R. P. Goldthwaite, and H. B. Willman. Boulder: Geological Society of America, 1973, p. 251.
- Wyckoff, S., and Wehinger, P. A. "Are Quasars Luminous Nuclei of Galaxies?" *Sky and Telescope* **61** (1981):200.
- Wyckoff, S., Wehinger, P. A., Gehren, T., Morton, D. C., Boksenberg, A., and Albrecht, R. "Discovery of Nebulosity Associated with the Quasar 3C 273." *Astrophysical Journal* **242** (1980):L59.
- Yabushita, S. "A Statistical Study of the Evolution of the Orbits of Long-Period Comets." *Monthly Notices of the Royal Astronomical Society* **187** (1979):445.
- Zahringer, J. "Isotope Chronology of Meteorites." *Annual Review of Astronomy and Astrophysics* **2** (1964):121.
- Zimmermann, O. *Zeitschrift fur Naturforschung* **12a** (1957):647.

Zook, H. A. "Temporal and Spatial Variations of the Interplanetary Dust Flux." *Space Research* **18** (1978):411.

Zook, H. A., Hartung, J. B., and Storzer, D. "Solar Flare Activity: Evidence for Large-Scale Changes in the Past." *Icarus* **32** (1977):106.

LIST OF SYMBOLS AND ABBREVIATIONS

| | |
|--------------|---|
| Galaxy | The Milky Way |
| GC | Galactic Center |
| GEH | Galactic Explosion Hypothesis |
| VLBI | Very long baseline |
| SNR | Supernova remnant |
| EMP | Electromagnetic pulse |
| HI | Neutral hydrogen |
| HII | Ionized hydrogen |
| l.y. | Light year ($\sim 10^{18}$ cm) |
| pc | Parsec (1 pc = 3.26 l.y.) |
| kpc | Kiloparsec (1000 pc) |
| AU | Astronomical unit (1.55×10^{13} cm) |
| μ | Micron (10^{-4}) cm |
| \AA | Angstrom (10^{-8}) cm |
| RA | Right ascension |
| δ | Declination |
| ℓ | Galactic longitude |
| b | Galactic latitude |
| MHz | Megahertz (10^6 cycles per second) |
| GHz | Gigahertz (10^9 cycles per second) |
| Mev | Million electron volts (1.6×10^{-6} ergs) |
| Gev | Billion electron volts (1.6×10^{-3} ergs) |
| γ | Lorentz factor $\left(\sqrt{1 - v^2 / c^2}\right)^{-1}$ |
| Γ | Spectral index |

| | |
|-------------|---|
| m_0 | Particle rest mass |
| L_{\odot} | Solar luminosity (3.9×10^{33} ergs/s) |
| M_{\odot} | Solar mass (1.99×10^{33} grams) |
| R_{\odot} | Solar radius (6.69×10^{10} cm) |
| c | Speed of light (3.00×10^{10} cm/s) |
| σ | Boltzmann's constant (5.67×10^{-5} erg cm ⁻² (°K ⁻⁴) s ⁻¹) |
| r | Roentgen |
| mr | Milliroentgen (10^{-3} r) |
| μ g | Microgram (10^{-6} g) |
| pg | Picogram (10^{-12} g) |
| ‰ | Parts per thousand |
| ppm | Parts per million |
| ppb | Parts per billion |
| BP | Years before present (0 date = 1950 AD) |
| b2k | Years before year 2000 |
| H | Holocene |
| LW | Late Wisconsin |
| MW | Mid Wisconsin |
| EW | Early Wisconsin |
| S | Sangamon |
| NAA | Neutron activation analysis |

APPENDICES

APPENDIX A

ESTIMATES OF THE QUANTITY OF COSMIC RAY ENERGY THAT MUST IMPACT THE EARTH'S ATMOSPHERE IN ORDER TO DOUBLE THE TERRESTRIAL C-14 RESERVOIR

The size of the present C-14 reservoir may be estimated as follows: The current C-14 to carbon ratio is 5.8×10^{10} C-14 atoms per gram of carbon or, alternatively, 1.35×10^{-12} grams C-14 per gram carbon. Also, the carbon reservoir is estimated to be $\sim 7.85 \text{ g/cm}^2$ which includes the reservoir in the atmosphere, ocean, and humus (Junge, 1963, p. 267). The bulk of the carbon reservoir is contained in the ocean; however, mixing between the ocean and atmospheric reservoirs takes place with a characteristic time of 4 - 5 years (Junge, 1963, p. 30). Thus the total carbon reservoir would contain $7.85 \text{ g/cm}^2 \times 5.1 \times 10^{18} \text{ cm}^2 = 4 \times 10^{19}$ grams of carbon. Of this, about $4 \times 10^{19} \times 1.35 \times 10^{-12} = 5.4 \times 10^7$ grams would consist of C-14.

Cosmic Ray Protons. Cosmic ray proton primaries colliding with nitrogen and oxygen nuclei in the atmosphere produce large numbers of neutrons which are ultimately captured by nitrogen nuclei to produce carbon-14. This capture process is represented by the reaction: $n + {}^{14}\text{N} \rightarrow {}^{14}\text{C} + p$. The current C-14 production rate from cosmic ray protons is estimated to be $2.5 \pm 0.5 \text{ atoms/cm}^2/\text{s}$ (Lingenfelter, 1963). Given a present energy flux of cosmic ray protons of $3 \times 10^{-2} \text{ ergs/cm}^2/\text{s}$, about 100 C-14 atoms should be produced for every erg of proton energy.

A doubling of the terrestrial C-14 reservoir would require an absorption of:

$$U_p = \frac{5.4 \times 10^7 \text{ grams C-14} \times 6 \times 10^{23} \text{ atoms / mole} \times 10^{-2} \text{ ergs / C-14 atom}}{14 \text{ grams / mole}}$$

$$= 2.3 \times 10^{28} \text{ ergs}$$

Given that the Earth presents a cross-sectional area of $1.28 \times 10^{18} \text{ cm}^2$, then a doubling of the C-14 reservoir could be produced by the interception of $1.8 \times 10^{10} \text{ ergs/cm}^2$ of cosmic ray protons. If half of the incident particles are deflected by the geomagnetic field, then this C-14 increase would require an integral flux of $3.6 \times 10^{10} \text{ ergs/cm}^2$. This could be supplied by a blast that elevated the cosmic ray proton background 100 fold above its present level for 400 years. If the Earth were positioned on the inner side of the heliopause sheath, the allowable intensity outside the sheath could be as much as 10 times greater due to the sheath's screening effect (see **p. 73**). If the incident protons were to propagate unattenuated and isotropically from the GC, assumed to be at a distance of 22,800 l.y. from the Sun, then the cosmic ray outburst would comprise a total energy of: $U_p = 6.5 \times 10^{45} \text{ cm}^2 \times 3.6 \times 10^{10} \text{ ergs/cm}^2 = 2.3 \times 10^{56} \text{ ergs}$, or $2.3 \times 10^{57} \text{ ergs}$, if modulation by the heliopause is included.

Cosmic Ray Electrons. Cosmic ray electrons, by themselves, are ineffective in producing C-14. It is the γ -rays which they spawn in atmospheric photon-electron cascades which are mainly responsible for their share of the C-14 production. The C-14 production rate ultimately resulting from the exposure of the Earth's atmosphere to a blast of cosmic ray electrons may be estimated as follows.

Gamma rays eject neutrons from oxygen and nitrogen nuclei in a process called *photoneutron production*. The probability for such ejection is highest for γ -rays in the 25 ± 5 Mev energy range where the cross section is on the order of 6 milli barns (mb) (Hayward, 1963, Berman, 1975, p. 341). Other competing collision processes include *Compton scattering*, in which a photon scatters an orbital or free electron, and *pair production*, in which a photon collides with an atomic nucleus and emerges as an electron and positron pair. The cross section for Compton scattering and pair production is about 500 mb, almost two orders of magnitude greater than for photoneutron production. Thus, the fraction of 25 Mev γ -rays producing neutrons will be equal to the ratio of those cross sections: $6 \text{ mb}/500 \text{ mb} = 0.012$. Since only about half of the resulting photoneutrons would become captured to produce C-14 (see Lingenfelter, 1963, p. 41), the C-14 production rate would be: $0.012 \times \frac{1}{2} = 6 \times 10^{-3}$ C-14 atoms/25 Mev photon. Since a 25 Mev photon comprises an energy of 4×10^{-5} ergs, this rate represents 150 C-14 atoms per erg of 25 Mev photons.

To derive a crude upper limit for C-14 production by cosmic ray electrons it may be assumed that γ -rays make up roughly half of the quanta in a photon-electron cascade (the other half being electrons), and that all of the higher energy γ -ray quanta eventually degrade to the 25 Mev level. This would yield a radiocarbon production rate of 75 C-14 atoms per erg of incident cosmic ray electrons. However, a more realistic value of *~10 C-14 atoms per erg of incident cosmic ray electrons* is adopted here since it is expected that only a fraction of the γ -rays in the photon-electron cascade actually end up in this 10 Mev wide resonance channel where photoneutron production is highest. Besides, if the C-14 production rate from cosmic ray electrons were much higher than this, then theoretical calculations for C-14 production by cosmic ray photons would have to be significantly revised, since cosmic ray electron secondaries make up a considerable fraction of the cosmic ray population of the Earth's atmosphere.

In light of the above it may be concluded that cosmic ray electrons are at most 10% as effective as cosmic ray protons in producing radiocarbon. Consequently, a Galactic explosion would have to be about 10 times more powerful to produce a comparable doubling of the terrestrial C-14 reservoir, i.e., $U_e \sim 2 \times 10^{58}$ ergs with heliopause modulation included. The corresponding cosmic ray electron intensities for the solar vicinity would be: $\sim 10^3$ times the current cosmic ray proton background for 400 years, if the Earth were outside the heliopause sheath, or $\sim 10^4$ times the current cosmic ray proton background, if the Earth were on the inner side of the heliopause sheath.

Solar Flare Protons. The rate of C-14 production due to solar flare protons averaged over one solar cycle is estimated to be in the range of 0.05 – 0.12 C-14 atoms/cm²/s, or about 3 – 6% of the rate due to cosmic ray protons (Lingenfelter and Flamm, 1964). A doubling of the C-14 reservoir could be produced if solar flare activity were to increase by a factor of 10^3 over a 300 year period, or by a factor of 10^4 over a 30 year period. **[UPDATE:** These solar cosmic ray activity estimates may be inflated; e.g., see update at the end of Chapter 10.]

APPENDIX B

THE HELIOPAUSE SHEATH AND THE 3° K COSMIC BACKGROUND RADIATION

As was mentioned in Chapter 3, Section 3.2, somewhere between 50 – 70 A.U. from the Sun the solar wind and interplanetary magnetic field confront the interstellar magnetic field and ambient cosmic ray flux in a shock region called the heliopause sheath. This sheath most probably consists of a plasma of protons and electrons bound together with the interplanetary magnetic field. The solar wind would not only supply particles to the heliopause sheath, but would keep these particles ionized (Brandt, 1970, p. 98).

A variety of different types of waves may become excited in such a magnetized plasma, e.g., electromagnetic waves, hydromagnetic waves, and electrostatic waves. Wave excitation may occur at the boundaries of a plasma through a number of different mechanisms. According to one process, charged particles such as cosmic rays or solar wind ions travelling perpendicular to magnetic field lines would induce hydromagnetic oscillations of these field lines. This might be viewed as being analogous to the plucking of stretched strings. Positive ions bound to these field lines would provide the "loading," or inertia for this oscillation, while magnetic effects would provide the restoring force (cf. Spitzer, 1962, p. 51).

The rate of hydromagnetic energy input into the heliopause would depend primarily on the amount of energy that the cosmic ray background radiation would be capable of transferring to the sheath. The solar wind by comparison would contribute a very small percentage, so its effect may be neglected. The energy density of the unmodulated cosmic ray background is probably in the range of $u_0 = 3 \pm 1 \times 10^{-12}$ ergs/cm³, which is about 3 times higher than the modulated intensity in the Earth's vicinity; cf. McKibben, Pyle, and Simpson (1982). This translates into an energy intensity of: $I_0 = u_0 c = 0.09 \pm 0.03$ ergs/cm²/s.

However, not all of this incident particle energy would go into pumping the heliopause sheath. The energy transferred to the sheath as hydromagnetic oscillations would come mostly from cosmic rays that had become magnetically trapped in the sheath. Cosmic rays that were magnetically deflected from the sheath or that happened to diffuse out of the sheath would not have a chance to impart much of their energy. Moreover, of the fraction of particle kinetic energy that was available for pumping the heliopause, a considerable portion would become lost to synchrotron and bremsstrahlung radiation processes. Thus if I_0 represents the incident cosmic ray energy intensity, only a fraction of this energy,

$$I_{in} = \eta I_0, \quad (B-1)$$

would be expected to become converted into hydromagnetic motion.

Electromagnetic waves radiated by the heliopause sheath plasma as a result of its hydromagnetic motion would constitute the sheath's principle means of energy loss. The intensity of this energy loss I_{out} would depend on the equilibrium temperature T_e of the plasma sheath, and would be given by the relation

$$I_{out} = \epsilon \sigma T_e^4, \quad (B-2)$$

where ϵ is the emissivity of the sheath and where σ is the Stephan-Boltzmann constant.* Here it is assumed that the magnetic field of the heliopause sheath couples together large regions of the plasma allowing any given portion to maintain a state of local thermodynamic equilibrium and permitting the sheath to radiate with a blackbody spectrum.

Under steady-state conditions, relation (B-1) may be set equal to relation (B-2) giving:

$$T_e = \sqrt[4]{\frac{\eta u_o c}{\epsilon \sigma}} \quad (\text{B-3}).$$

Given $I_o = 0.09 \pm 0.03$ ergs/cm²/s and assuming an ideal emissivity of $\epsilon = 1$, the resulting blackbody radiation temperature is estimated to be: $T_e = 6.3 \sqrt[4]{\eta}$ °K, where $0 \leq \eta \leq 1$. Note that this temperature range spans the value 3° K that Penzias and Wilson (1965) observed in connection with their discovery of the cosmic microwave background radiation. Moreover, like the observed microwave background field, the proposed microwave emission from the heliopause sheath would also be isotropically distributed since the sheath would be isotropically pumped by the cosmic ray field. It is interesting to note that the observed 2.96° K microwave temperature could be simulated by the above heliopause model if the excitation efficiency were chosen to be $\eta = 0.05$, a relatively reasonable value.

At the time of its discovery the microwave background radiation was interpreted as being remnant fireball emission from the Big Bang explosion and was assumed to permeate all of space. This is an interpretation that is still in fashion with the majority of the scientific community. However, the question that must be addressed now, is whether it is necessary to invoke the existence of a 3° K radiation field permeating all of space when in fact a reasonable mechanism is already at hand for generating this radiation locally in the heliopause sheath, the scenario I present here. It is my contention that the microwave radiation is actually locally generated and that a big bang interpretation for the 3° K microwave radiation is unnecessary. To support this argument I will point out some difficulties with the cosmogenic interpretation.

To begin with, if one is to adopt a big bang interpretation for the origin of this radiation, one must first accept the premise that the entire universe originated in a big bang explosion. Since we have no direct observational evidence that the universe actually originated in such an explosion, such a premise must be regarded as a tentative assumption. As justification of the big bang scenario, theorists often point to indirect evidence of a central explosion, such as cosmological redshift data. They claim that the observed redshifts of galactic spectra are evidence that the universe is expanding and that these galaxies are receding from one another, as a result of a past explosion. However, this claim itself involves the tacit assumption that the observed redshifts are of Doppler origin. Moreover, when the various expanding universe models that have been proposed are compared to observations on a number of different cosmological tests, it is found that they do not fit the data in a consistent manner (LaViolette, 1980b [1986]). Therefore it is my opinion that even *indirect* evidence of a big bang explosion is lacking.

Second, even if one accepts the expanding universe model, one must make the ad hoc assumption that the fireball was expanding at exactly 99.9% of the speed of light at the time of electron ion recombination. Only in this way could the 4000° K fireball be red shifted by a factor of 1350 down to the observed temperature of 2.96° K. Of course, a similar criticism may be made of the heliopause interpretation which makes the ad hoc assumption

* The sheath temperature calculated here is not the same as the temperature of the ion gas in the plasma, which may be many orders of magnitude higher than this. These two temperatures are at different levels of description (macro vs. micro).

of a 5% excitation efficiency.

A third difficulty with the cosmological interpretation is revealed by the measurements of Woody and Richards (1979). They found that the observed wavelength distribution of the cosmic microwave radiation deviates by more than 5σ from an ideal 2.96° K blackbody curve. Their measurements indicate a 10% excess intensity at the long wavelength end of the spectrum (at ~ 1.7 mm) varying smoothly to a 20% deficiency in intensity at the short wavelength end (at ~ 0.9 mm). They conclude that their data do not fit a simple Planck curve representing a single temperature and point out that any likely modifications of the big bang model would be inadequate in accounting for this distortion. That is, mechanisms likely to cause deviations from the ideal 3 K curve would instead produce departures in a direction *opposite* to the observed deviations.

Finally, a fourth difficulty with the big bang interpretation is that it is not consistent with the observation of Formaldehyde (H_2CO) absorption lines in interstellar dust clouds. Dieter (1973) has observed 381 interstellar dust clouds believed to lie within 100 pc of the Sun. She has detected H_2CO absorption lines indicating a temperature of $\sim 2.5^\circ$ K in three of these clouds and a temperature of $\sim 1.7^\circ$ K in a fourth cloud. If the 3° K cosmic microwave radiation is assumed to pervade all of space, as required by the big bang interpretation, then such cold spots in the interstellar medium are puzzling. As a possible solution, Dieter has proposed that these clouds must be continuously refrigerating themselves through some sort of collisional mechanism. However, she does not go into the details of how such a mechanism would function.

Having enumerated a few of the difficulties associated with the big bang interpretation, consider now the heliopause interpretation. First, the existence of energetic particle radiation (e.g., cosmic rays) is very well established on observational grounds. Also, the existence of an heliopause sheath consisting of a magnetically bound plasma surrounding the Solar System is generally accepted. Accepting the existence of these two components (charged cosmic ray particles and an heliopause sheath) one is naturally led to the conclusion that an isotropic, approximately black body, microwave radiation field must exist. In fact, if there is any difficulty to be encountered it is in proving that this local emission is absent and that the observed 3° K radiation comes from some other source. The fact that the observed microwave radiation spectrum deviates from a pure blackbody curve is no problem for the heliopause interpretation. Such deviations might simply reflect the fact that there are transmission losses in the sheath (e.g., Landau wave damping). Or it may be that there is a radial gradient in the sheath's steady state temperature.

The Origin of the Dipole Anisotropy in the Cosmic Microwave Radiation Field. Further evidence in support of the local generation hypothesis comes from observations of the large-scale, dipole anisotropy in the cosmic microwave background radiation field. It is found that the temperature of the 3° K field has a slight dipole anisotropy which may be modeled by the relation:

$$T(\hat{\theta}) = T_0 + T_1 \cos(\hat{\theta}, \hat{n}), \quad (\text{B-4})$$

where $T(\hat{\theta})$ is the temperature in an arbitrary direction, $T_0 \sim 3^\circ$ K is the magnitude of the isotropic component, T_1 is the magnitude of the anisotropic component, \hat{n} is the direction of maximum temperature, and where $(\hat{\theta}, \hat{n})$ is the angular deviation of vector $\hat{\theta}$ from the \hat{n} direction. Various investigators have made determinations of the magnitude T_1 and direction \hat{n} of the dipole anisotropy. The values they have found are listed in Table B-I.

An average of the T_1 values in the third column indicates that the anisotropy has a magnitude of $T_1 \sim 0.0033^\circ$ K, which is equivalent to a variation of $\pm 0.1\%$ in the mean blackbody temperature, i.e., $T_1 \sim 10^{-3} T_0$. By averaging the six coordinate values in the

TABLE B-I
DETERMINATIONS OF THE MAGNITUDE AND DIRECTION OF THE DIPOLE
ANISOTROPY IN THE COSMIC MICROWAVE BACKGROUND RADIATION

| Reference | Detection frequency (GHz) | T_1 (mK) | \hat{h} (R.A.) (hr) | \hat{h} (δ) (deg arc) |
|-------------------------|---------------------------------|------------------|--------------------------|-------------------------------------|
| 1. Smoot et al (1977) | 33 | 3.5 ± 0.6 | 11.0 ± 0.5 | 6 ± 10 |
| 2. Gorenstein (1978) | 33 | 3.6 ± 0.5 | 11.23 ± 0.46 | 19 ± 7.5 |
| 3. Cheng et al. (1979) | 24.8 | 2.99 ± 0.34 | 12.3 ± 0.4 | -1 ± 6 |
| 4. Smoot & Lubin (1979) | 33 | 3.1 ± 0.4 | 11.4 ± 0.4 | 9.6 ± 6 |
| 5. Fabbri et al. (1980) | 90-600 | $2.9 +1.3, -0.6$ | 11.4 ± 0.7 | 3 ± 10 |
| 6. Boughn et al. (1981) | 19-46 | 3.78 ± 0.3 | 11.6 ± 0.2 | -12 ± 5 |
| Average: | | 3.31 ± 0.36 | 11.49 ± 0.45 | 4.1 ± 10.4 |

fourth and fifth columns it is found that the radiation field is warmest in the direction $RA = 11h 29m \pm 27m$, $\delta = 4.1 \pm 10.4^\circ$ toward the constellation of Leo (see Figure B-1) and coolest in the opposite direction ($23h 29m$, -4.1°) toward Aquarius. In galactic coordinates the warm direction lies toward $\ell = 264^\circ$, $b = +60^\circ$.

The conventional interpretation of this large-scale dipole anisotropy is that it is produced as a result of the Solar System's motion relative to the microwave background "aether," the microwave field being blue-shifted in the direction of travel and redshifted in the opposite direction. A 3.3° mK (milliKelvin) anisotropy, for example, would be interpreted as a solar motion of 336 ± 40 km/s, i.e.,

$$v = (T_1/T_0)c = \frac{0.0033}{2.96} \times 300,000 \text{ km/s} \sim 335 \text{ km/s.}$$

This velocity would be expected to be the vector sum of the velocities of the Sun travelling around the Galaxy and of the Galaxy travelling relative to very distant galaxies. However, when the magnitude and direction of this velocity is compared to cosmological redshift determinations of the Sun's motion relative to distant galaxies, a substantial discrepancy is found. For example, Rubin et al. (1976), measuring the radiation velocities of 96 Sc galaxies some 100 million light years away, found that the Sun is moving at 600 ± 125 km/s in the direction $\ell = 135^\circ$, $b = -8^\circ$ relative to this field. This constitutes a discrepancy of 270 km/s in magnitude and 146° in direction. However, Hart and Davies (1982) have made a different determination of the motion of the Sun and the Local Group of galaxies relative to background galaxies and conclude that the direction and velocity are consistent with the microwave anisotropy findings.

So, what alternative explanation is there to account for the origin of the dipole anisotropy? When the directions of the observed anisotropy are closely examined, two clues

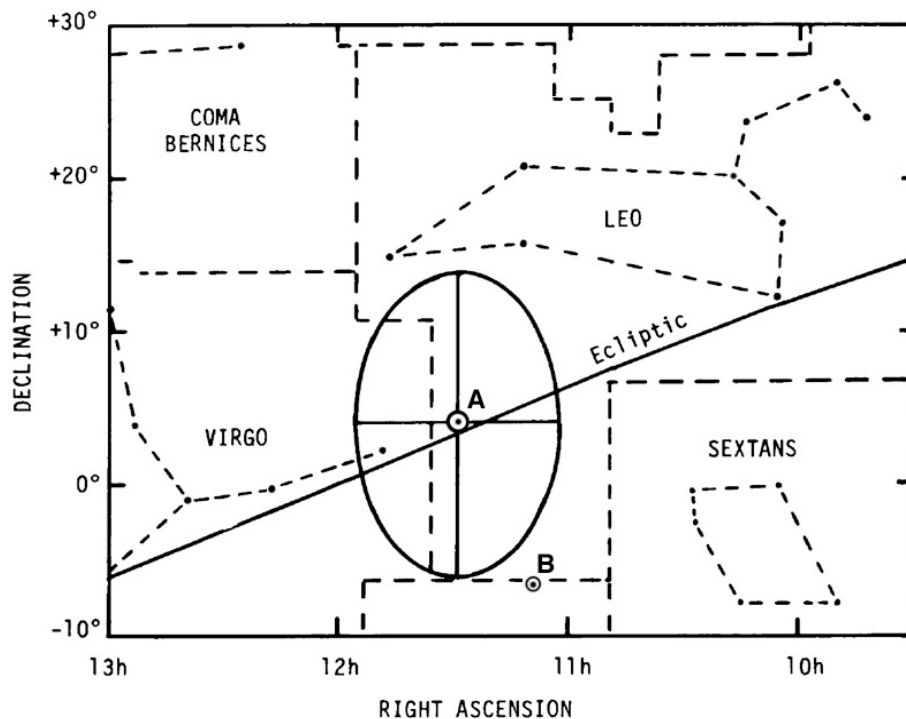


Figure B.1. The location of the hot pole of the 3° K microwave background radiation temperature dipole. A) The direction indicated by the average of the measurements listed in Table B-I (1977 to 1981). The ellipse indicates 1 σ of uncertainty from the central average. [**UPDATE:** B) The direction indicated by the first year observations of WMAP (2003).]

are noticeable, and both point toward the heliopause interpretation. First, the mean declination of \hat{n} is almost exactly coincident with the plane of the ecliptic, to within 1°, or $\sigma/10$. Second, the \hat{n} direction is approximately orthogonal to the direction of the GC. Compare RA = 17h 29m \pm 27m (the coordinate for the orthogonal direction) with RA = 17h 42.5m (the coordinate of the GC); see Figure 4.3 (p. 136). If the 3° K microwave background is assumed to be of extragalactic origin, as is suggested by the big bang hypothesis, then such correspondences would have to be regarded as purely coincidental. However, on the basis of the heliopause interpretation, these alignments become easily accounted for. They imply that the heliopause sheath is being impacted by an additional cosmic ray flux issuing from the general direction of the GC.

This may be demonstrated as follows. Suppose the circle shown in Figure B-2 represents a projection of the heliopause sheath viewed from an orientation in which the plane of the ecliptic appears face-on in the plane of the paper. The dot and cross symbols indicate the field line directions of a uniform magnetic dipole field that is here hypothesized to surround the heliopause. Such a field would be generated if the heliopause carried a net negative charge on its exterior surface and were rotating in a counterclockwise direction; i.e., in the direction of solar rotation. If it is supposed that the Solar System is being impacted by cosmic ray electrons coming from the direction of the GC in about the same direction as the interstellar wind (see (a) and (d) of Figure 4.3), then upon encountering the south-pointing magnetic field lines on the outside of the sheath, they would be made to orbit in a clockwise direction. Consequently, those particles passing the side of the sheath facing the constellation of Leo would be made to turn into field lines of increasingly strong intensity and would eventually become captured in the sheath. Particles passing the side of the

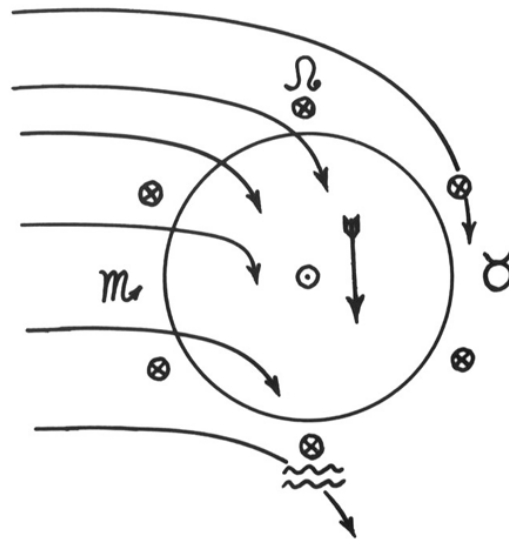


Figure B-2. Hypothetical diffusion trajectories (curved arrows) followed by cosmic ray electrons impacting the heliopause sheath from the direction of the Galactic Center. Ecliptic is viewed face on. The symbols \odot and \otimes indicate the general direction of the interplanetary magnetic field at the periphery of the sheath. The central arrow indicates the net direction of electron diffusion.

sheath facing Aquarius would be made to turn into field lines of weaker intensity and would ultimately be deflected from the sheath. Consequently, the side of the sheath facing Leo, being exposed to a higher particle energy density would become warmer than the side facing Aquarius.

The magnitude of the temperature anisotropy that would be produced by this electron deflection phenomenon may be estimated as follows. The energy intensity of the unmodulated cosmic ray electron flux will be taken as $I_e = u_e c = 9 \pm 3 \times 10^{-4}$ ergs/cm²/s, about 3 times higher than the modulated intensity in the Earth's vicinity. This is consistent with the modulation assumption made earlier. Together with an isotropic cosmic ray energy input of 9×10^{-2} ergs/cm²/s, the total energy flux on the warmer side of the sheath would come to 9.09×10^{-2} ergs/cm²/s. Given an efficiency of $\eta = 5\%$, this would yield a temperature of 2.9922° K as compared with 2.9848° K for just the isotropic component alone. This represents a temperature difference of: $\Delta T = 7.4^\circ$ mK or about $\pm 3.7^\circ$ mK, about the same as the observed anisotropy.

The interpretation of the microwave anisotropy data made here does not require that the entire cosmic ray electron flux originate in the GC. Other sources in the Galactic nucleus might also be responsible. Nevertheless, the possibility that almost all of these electrons may originate from the GC should be left open for consideration.

A direction oriented 90° to \hat{n} and lying in the plane of the ecliptic would fall at RA = 17h 29m, $\delta = +23.3^\circ$ ($\ell = 3.1^\circ$, $b = +5.6^\circ$). It is not certain that the proposed cosmic ray electron wind would be coming specifically from this declination since orientations at points off the ecliptic (but having the same right ascension coordinate) would be expected to produce a dipole anisotropy similar to that observed. However, as seen in Figure 4.3 (p. 136), the ecliptic location falls very close to the direction which Fahr (1974) has proposed for the upwind direction of the interstellar wind. If, as proposed earlier, the interstellar hydrogen wind is propelled by the cosmic ray electron wind (especially during Galactic outbursts), then the ecliptic position for this cosmic ray wind direction appears to be the best choice.

APPENDIX C

THE VELA SUPERNOVA

The close proximity of the Vela Supernova to the Earth would have made it easily visible to prehistoric peoples. In fact, George Michanowsky (1979, Chapter 4) reports that the ancient Sumerians had preserved records of the appearance of a "giant star" in the constellation of Vela, which they identified with the god Ea. He notes that Ea (Lord of the Waters) was connected with the Sumerian flood myth (pp. 45–46), and suggests that gamma rays from the Vela supernova produced a period of major climatic warming, which in turn caused melting of the polar ice caps, a rise of sea level, and flooding of certain islands in the Persian Gulf (pp. 15, 71–73). Also, he infers that γ -ray and X-ray radiation from the supernova could have led to sudden biological mutations and possibly to extinctions. Finally, he postulates (pp. 14, 77) that the Sumerians observed this event around 6000 years BP.

However, it is doubtful that the Vela supernova produced any such effects on the Earth. Astrophysicists estimate that the energy of the gamma ray flash of a supernova is in the range of $10^{48} - 10^{50}$ ergs. At Vela's distance of 1500 l.y. this would amount to $10^5 - 10^7$ ergs/cm². The higher figure is equivalent to the amount of solar energy that the Earth receives per cm² in 3 seconds. So obviously no climatic effects would be expected. Moreover, it is doubtful that serious mutation effects would have been produced. The Earth's upper atmosphere receives 10^6 ergs/cm²/yr from the cosmic ray background. Thus, biological organisms exposed to the Vela supernova would have received no more than what is normally received in 10 years exposure to background radiation, i.e., ~500 milliroentgens. The increase in accumulated mutations would be less than 1%. Finally, 6000 years BP is too recent. The date for the Vela supernova has been established to be 12,000 years b2k, probably to an accuracy of ± 1000 years, on the basis of X-ray observations of the Vela remnant; see Tucker (1979). Thus the Sumerians could not have been the original observers of this event. They must have been handing down knowledge of observations recorded over 6000 years before their time!

Nevertheless, Michanowsky's discovery of the association of the Vela supernova with the god Ea has some important implications when considered in the context of the findings presented here. According to the Sumerian flood myth, it was Ea who warned Ziusudra (Noah) of the impending flood disaster that was to drown the world. As mentioned in Chapter 9 (Section 9.3), major global flooding, possibly associated with the passage of a superwave, took place about 14,250 years b2k. If the flood legend refers to the Terminal Pleistocene Flood, with the implication that it was Ea in the form of the Vela supernova that warned humanity, then a date of ~14,250 years b2k would be implied for the Vela supernova. This date agrees both with the current predictions of the age of Vela X and with the hypothesis that the Vela supernova was triggered by the 14,250 years b2k superwave.

Michanowsky suggests that the Vela supernova so much impressed the Earth's inhabitants that it stimulated the rise of science. Indeed, Ea was regarded by the Sumerians as the god of Wisdom and teacher of the arts of civilization. However, the impression created by the Vela supernova was probably insignificant compared to that created by the Flood, the associated global extinction episode, and the array of cosmic "fireworks" (which would have been produced by the proposed superwave). If anything, it was these other terrestrial and extraterrestrial happenings which prodded humanity into a concerted effort to develop mythology and writing so that knowledge of these events could be passed down to posterity.

It is interesting to note that some of the terrestrial effects which Michanowsky alludes to (e.g., climatic change, flooding due to polar ice cap melting, and radiation-induced biological

mutation and extinction) bear a strong resemblance to effects mentioned in the Galactic Explosion Hypothesis, although the GEH proposes a different cause and different time for these events. Michanowsky's proposed 6000 years BP date, though, does happen to coincide with the passage date for the 6000 years BP superwave.

The ancient records that inspired the formulation of the GEH, mentioned in Chapter 1 (p. 4) [and in the Appendix I to the proposal for this dissertation], are different from those that inspired Michanowsky's work. I became aware of Michanowsky's hypothesis subsequent to formulating the Galactic Explosion Hypothesis.

APPENDIX D

A GRAVITATIONAL MECHANISM FOR TRIGGERING SUPERNOVAE EXPLOSIONS

One possible mechanism by which superwaves could trigger supernovae was suggested in Subsection 5.2.2 (pp. 160–161). In the following Appendix a different mechanism is explored involving a propagating gravitational potential wave.

If a galactic explosion were accompanied by the lateral motion of a considerable amount of mass, it is conceivable that a sizable burst of gravitational quadrupole radiation would be produced. However, it is unlikely that such radiation would be strong enough to produce much of a mechanical effect on stars beyond the Galactic nucleus. It is interesting to note, however, that the Galactic nucleus, which has a mass of $\sim 10^{11} M_{\odot}$, contributes about one-fourth of the gravitational field potential measured at the surface of the Sun, the other three-quarters being due to the Sun's own mass. Consequently, if the *total magnitude* of the Galactic gravity field were to undergo a sudden transitory change as a result of an explosion event at the Galactic center, significant tidal effects could be produced even as far away as the Sun. As is discussed further on, by adopting a Lorentzian space-time framework, rather than the traditional Einsteinian framework, such time-variations of the Galactic gravity field are permissible. However, first it is useful to review evidence suggesting that gravitational disturbances of a very small scale may be presently buffeting the Earth and may be originating from the Galactic center.

D.1 TERRESTRIAL GRAVITY WAVE DETECTIONS

Comparing the 1973 and 1974 data of two gravity wave detectors separated by 1000 kilometers, Joseph Weber and his research team have found extended periods during which statistically significant coincident excitations have been recorded (Lee, Gretz, Steppel, and Weber, 1976; Weber, 1980). The events to which Weber's detectors are sensitive appear to have a duration on the order of 0.1 seconds. By simultaneously monitoring environmental factors such as temperature, seismic disturbances, and high frequency electromagnetic waves, Weber believes that all conceivable causes of such excitations except for gravity waves have been ruled out.

Within a $1\frac{1}{2}$ year observation period, May 1973 to November 1974, the Weber group observed statistically significant coincident events during four intervals: May 20 – June 13, 1973 (24 day period), December 15 – 25, 1973 (10 day period), May 21 – June 25, 1974 (35 day period), and August 3 – October 17, 1974 (75 day period). This amounts to about 25% of the total time period during which their detectors were "on the air." The number of coincident pulses at zero delay exceeded the background noise level by over 3 standard deviations for the first of these intervals, and by over 4 standard deviations for the other three intervals. Moreover, one four day period selected at random from these four intervals was found to have a zero-delay excess of coincident pulses that was 5.6 standard deviations above noise level. Weber (1980) estimates that the pulse rate recorded during the 75 day interval in the fall of 1974 (zero delay excess coincidences at a 4.2σ level) could occur only once every 1232 years if due purely to chance coincidences of background pulses. Yet the observation period being considered here lasted only $1\frac{1}{2}$ years. Therefore the evidence strongly favors the interpretation that the pulses that Weber's antennae detected here were

real gravity wave events.

In his earlier investigations, Weber (1970) had discovered a sidereal correlation to these coincident events, more events being detected when the antennae were aligned in the Galactic center/anticenter direction ($\sim 6\sigma$ if due to chance). He suggested the possibility that these events could be caused by gravity waves radiating from the Galactic center. However, other directions would be possible depending on the relative phase of the detected pulses (Weber, 1981, personal communication). Since the time of the late 60's measurements a sidereal anisotropy has not been observed. Thus, if this directional effect is real it may be intermittent.

Sparked by Weber's first gravity wave discoveries made in the late 60's and early 70's, other investigators built their own gravity wave detectors and began observing in an attempt to confirm Weber's findings. The failure of many of these researchers to record coincident events led them to question Weber's results, and a controversy developed (cf. Garwin, 1974, 1975; Weber, 1974, 1975; Tyson, 1978). In the course of a data exchange initiated by this controversy, an error was discovered in the computer program that Weber used for the recognition of coincidences between his two detectors. Also, there was a minor oversight in determining the relative synchronization of the standard clocks at his two antenna sites. These errors were promptly acknowledged and rectified.

Having made these corrections, Weber's group rechecked their earlier data and verified that gravity waves with a sidereal anisotropy had indeed been observed. To remove any chance of unconscious human bias in the data analysis, Weber's group automatized their data collection operation as of 1972. Moreover, third party checks made on a randomly selected tape recording of their 1973–74 data also verified the existence of a significant number of coincident pulses (Weber, 1977a). This painstaking analysis indicates that the phenomenon being studied has an objective validity. This conclusion is further supported by the fact that other experimenters have sporadically reported positive findings, e.g., Amaldi (1980), Billing et al. (1975), Hirakawa and Narihara (1975). The failure of other groups to detect gravity wave events could be due to a number of factors, e.g., failure to control the temperature of the antenna, use of a different algorithm for computing the amplitude/phase excitations of the antenna, or insufficient observing time (Weber, 1974, 1977b, 1980; Weber, 1981, personal communication).

Lee et al. (1976, p. 904) report that during the 1973–1974 observation period event rates were found to vary from 5.7σ effects to insignificant levels within a period as short as 4 days. This variability suggests that a single source could be responsible for the observed coincident pulses. If the detected zero delay excess events are due to gravity waves, as evidence seems to indicate, then an estimate of the power radiated by this source may be made. It is assumed conservatively that these events are detected by Weber's antennae at the rate of 1 per day, and that the source is located at the Galactic center. By taking into account the detection efficiency of Weber's antennae, it may be estimated that such a source would be radiating energy at the astounding rate of 10^3 – $10^4 M_{\odot} c^2/\text{year}$ (Weber, 1972; Gibbons and Hawking, 1971). If real, such a high mass consumption rate is difficult to explain on the basis of observational considerations. For example, the entire Galactic nucleus, which contains only about $10^{11} M_{\odot}$, at the above rate would have become annihilated within 10^7 – 10^8 years. This is difficult to reconcile with an age for the Galaxy of at least 10^{10} years. Thus, some process other than matter annihilation may be active in producing these fluctuations. Perhaps there is a need to develop a new theory of how gravitational field disturbances are generated. Such a theory might not necessarily be based on general relativity.

D.2 AN ALTERNATIVE VIEW OF GRAVITY

There are two alternative definitions of time and space, one proposed by Einstein (1905) and another proposed by Lorentz (1904), and at present a choice between these two frameworks is a matter of personal preference since no critical test has as yet been performed to distinguish between them. Clube (1977, 1980) has proposed a theory of gravitation which adopts the Lorentzian framework, space-time being considered flat and invariant, and mass m and light velocity c being allowed to vary. He proposes that mass increases and light velocity decreases with increasing gravitational potential ϕ according to the following relations:

$$m = m_0 \exp(3\phi/c_0^2) \quad (D-1)$$

$$c = c_0 \exp(-2\phi/c^2), \quad (D-2)$$

where c_0 and m_0 are the true rest mass of a material particle and the limiting velocity of light in regions of space remote from material bodies. He has shown (1977) that with such a formulation of m and c it is possible to reproduce the standard observational tests of general relativity. Also pertinent in this regard are similar discussions by Dicke (1961) and Atkinson (1962, 1965).

According to relation (D-1), if a single celestial body (or cluster of many bodies) were to undergo gravitational collapse, the net mass of the collapsing system would be expected to increase exponentially. Such a "supermass effect" has been proposed by Clube (1977, 1978, 1980), among other things to account for the residual radial motions of stars in the Galaxy. He suggests that in attaining the supermassive state the nuclear mass of a spiral galaxy might increase from about $10^{11} M_\odot$ to $10^{14} - 10^{16} M_\odot$.

In Clube's scenario these field potential changes would occur gradually over a period of millions of years and would involve an actual change in the dimensions of a galaxy. However, suppose instead that such a collapse involved only the motion of material composing a single dense body and that the collapse were to instead take place over only a few hundred to a thousand years with the supermassive state being reached only momentarily, e.g., for a few days. If this collapse were temporary and the gravitating system were to rebound, e.g., as a result of the release of a large amount of energy, then a gravitational potential pulse could be produced and communicated away from the central mass as a potential wave propagating radially at the speed of light.

The possibility of the occurrence of a brief gravitational potential increase with the release of a great quantity of radiant or particle energy emerges as an astrophysical prediction of a microphysical theory (LaViolette, 1980c) that I had been working on over a period of 6 years prior to the time I first formulated the GEH. Rather than expanding on this subject here, which would require a considerably involved discussion, I would like to leave this to subsequent publication.

Note that the gravity pulse suggested above would have a dipole moment directed radially with respect to the generating source. A quadrupole moment could also be present, but only if the gravitational potential change occurred in an asymmetric fashion about the center of the source. This is quite different from the general relativistic situation, which predicts that dipole radiation cannot be generated due to the restriction of momentum conservation. The Brans-Dicke scalar-tensor theory, on the other hand, permits scalar and dipole gravitational radiation to be generated in addition to quadrupole radiation (Sejnowski, 1974, after Will, 1974). Since the dipole and quadrupole moments would excite different modes of a gravity wave antenna, it might be possible to make a distinction between these two possible types of excitation as a test of alternative theories of gravitation.

D.3 A MODEL OF A GRAVITY PULSE AND ITS EFFECTS ON CELESTIAL BODIES

Galactic Center Generation. I will assume that the condensed object Sagittarius A, postulated earlier to be the source of the outburst of relativistic electrons during a Galactic explosion event, is also the source of a major change in gravitational potential. In this model Sgr A*, which normally has a mass of $M_a \sim 5 \times 10^6 M_\odot$ (Oort, 1977, p. 353), would increase its gravitational mass exponentially by a factor of 2×10^6 in the space of ~ 4 days. This could be expressed as:

$$M_a(t) = M_a \cdot e^{\alpha t} \quad (\text{D-3})$$

where $\alpha = \ln 2 / 1.5 \times 10^4 \text{ seconds} = 4.6 \times 10^{-5} \text{ s}^{-1}$. Thus Sgr A* would double its mass every 1.5×10^4 seconds, reaching its peak value of $10^{13} M_\odot$ after about 21 doubling times, or $\sim 3.15 \times 10^5$ seconds. This rise time is comparable with the time taken for a nova outburst to reach peak light. Also suppose that the decline is equally abrupt.

Since the dimensions of stars and planets would be small compared with the wavelength of a gravitational pulse, the gravitational interaction of the pulse with these objects may be treated classically. That is, a test mass would respond to the potential gradient of the pulse gradient as if it were experiencing a static gravity potential field. During the period of sudden potential drop, the test mass would be centripetally accelerated toward the GC and during the period of gradual potential rise, it would become centrifugally accelerated away from the GC. The velocities accumulated at the end of each acceleration would be equal in magnitude, but opposite in direction. Consequently, the passage of a gravitation potential "superwave" would be expected to induce only a temporary disturbance in the motions of stars orbiting around the center of the Galaxy. So, a test mass would have a motion relative to the GC after the passage of a superwave that was about the same as the motion it had before the superwave had passed.

Tidal Effects Induced on the Earth and on the Sun. During the passage of the initial steep potential drop, substantial tidal effects could be produced in celestial bodies. The magnitude of such effects induced in the solar vicinity by the proposed potential profile may be estimated as follows using a treatment based on classical gravitational field theory.

First I will estimate the gravitational acceleration which the Galactic nucleus currently produces in the solar vicinity, and which would prevail before passage of the pulse. The gravitational potential energy, G_p , of a test mass having mass m in the gravitational field of the Galactic nucleus is given by the formula:

$$G_p = - \frac{m \cdot M_o \cdot G}{r}, \quad (\text{D-4})$$

where M_o represents the mass of the Galactic nucleus before generation of the pulse, G is the gravitational field potential constant, and r is the galactocentric distance. Also, the *gravitational potential field intensity* of the Galactic nucleus (before generation of the superwave) may be written as:

$$\phi_o(r) = \frac{G_p}{m} = - \frac{M_o G}{r} \quad (\text{D-5})$$

and the gravitational acceleration as:

$$g(r) = \nabla \phi_o(r) = \frac{-\phi_o(r)}{r} = \frac{M_o G}{r^2}, \quad (\text{D-6})$$

For $M_0 = 2 \times 10^{44}$ grams ($10^{11} M_\odot$), $G = 6.67 \times 10^{-8}$ dynes cm^2/g^2 , and $r = r_0 = 2.28 \times 10^{22}$ cm (the solar galactocentric distance of 22,800 l.y.), relation (D-5) gives $\phi_0(r_0) = -5.85 \times 10^{14}$ cm^2/s^2 , and relation (D-6) gives $g(r_0) = 2.57 \times 10^{-8}$ cm/s^2 . This represents the gravitational acceleration that the Galactic nucleus currently produces in the solar vicinity.

The gravitational acceleration induced while the event horizon is passing through the solar system may be estimated as follows. Suppose that at time $t = 0$ the gravitational mass of Sgr A* begins to increase from its steady state value of $5 \times 10^6 M_\odot$. As in relation (D-5) the gravitational potential of Sgr A* may be written as:

$$\phi_a(r,t) = -\frac{M_a(t)G}{r}, \quad (\text{D-7})$$

where $M_a(t)$ is given by relation (D-3). Then relation (D-7) may be written as:

$$\phi_a(r,t) = \phi_a(r) \cdot e^{\alpha t}, \quad (\text{D-8})$$

where $\phi_a(r) = -\frac{M_a G}{r}$ is the initial gravitational potential field intensity of Sgr A*. The total gravitational potential field intensity $\phi_n(r,t)$ of the Galactic nucleus would then be given as:

$$\phi_n(r,t) = \phi_0(r) + \phi_a(r) \cdot e^{\alpha t} \quad (\text{D-9}).$$

The doubling time δt for the Sgr A* potential $\phi_a(r,t)$ would be given as: $\delta t = (\ln 2)/\alpha = 1.5 \times 10^4$ seconds. After about $t = 2.2 \times 10^5$ s, the Sgr A* potential would have become comparable to, and begun to exceed, $\phi_0(r)$. At this point the total gravitational potential field intensity generated by the nuclear region, $\phi_n(r,t)$ would exhibit significant change, also doubling every δt seconds. This potential change of the nuclear field would become communicated radially away from the GC at the speed of light. Thus a field potential gradient would be set up in which the field intensity would double over a distance of $\delta r = \delta t \cdot c$, measured radially in the direction of the GC. That is, the field intensity doubling distance would be given as:

$$\delta r = \frac{\ln 2}{\alpha} \cdot c = 0.693 (3 \times 10^{10} \text{ cm/s})/4.6 \times 10^{-5} = 4.5 \times 10^{14} \text{ cm (or 30 AU)}.$$

At a given point P in space located a distance r from the GC, *this radially propagating potential profile would be indistinguishable from a static profile produced by the mass $M_a(t)$ at a distance δr from the GC, where $\delta r \ll r$.* Thus the gravitational acceleration at a distance r would be given as:

$$g(r,t) = \nabla \phi_n(r,t) \sim \nabla \phi_a(r) \cdot e^{\alpha t} \sim -\frac{\phi_a(r)}{\delta r} e^{\alpha t},$$

or

$$g(r,t) = \frac{M_a G}{r \cdot \delta r} \cdot e^{\alpha t} \quad (\text{D-10})$$

So, at a distance $r = r_0 = 2.28 \times 10^{22}$ cm (22,800 l.y., the galactocentric distance of the Sun) the gravitational acceleration would be given as:

$$g(r_0,t) = 6.47 \times 10^{-5} e^{(4.6 \times 10^{-5})t}. \quad (\text{D-11}).$$

The peak acceleration attained at the end of 3.15×10^5 seconds (3.6 days) would be: $g_{\text{final}} =$

$6.5 \times 10^{-5} e^{14.5} = 128 \text{ cm/s}^2$. This is about 10^{10} times greater than the gravitational acceleration presently induced by the Galactic nucleus at this galactocentric distance. Compare with the estimate on **p. 431**. Over a period of $t = 3.15 \times 10^5$ seconds a celestial body accelerated by this field potential profile would be capable of attaining a velocity of:

$$v = \int_0^t g(t) dt = \frac{6.5 \times 10^{-5}}{4.6 \times 10^{-5}} \cdot e^{4.6 \times 10^{-5} t} \sim e^{14.5} = 2.8 \times 10^6 \text{ cm/s} = 28 \text{ km/s},$$

directed radially inward toward the Galactic center. The trailing portion of the potential well would accelerate celestial bodies to a velocity equal in magnitude, but opposite in direction, away from the Galactic center. So, a null residual velocity would result after passage of the superwave. [**UPDATE:** However, this may not necessarily be the case. An electromagnetic shock impulse (triangular shaped wave profile) is known to produce a residual force in the direction of the onset force. The same may be true of gravity waves, in which case gravity potential shock waves emitted by Sgr A* could result in a residual velocity.]

At a distance r the gravitational acceleration $g(r,t)$ would be changing at a rate:

$$\dot{g}(r,t) = \frac{d}{dt} g(r,t) = \frac{M_a G \alpha^2}{(\ln 2) \cdot c \cdot r} e^{\alpha t}. \quad (\text{D-12})$$

So, at $t = 3.15 \times 10^5$ seconds and $r = r_0$, the rate of change of acceleration would be $\dot{g} = 5.28 \times 10^{-3} \text{ cm/s}^3$. A point at the surface of a celestial body on the side facing the GC would have an acceleration slightly greater as compared with a point at the center of the body. This difference in gravitational acceleration, the "tidal acceleration" would be given as:

$$\Delta g(R,r,t) = \dot{g}(r,t) \cdot \Delta t = \dot{g}(r,t) \cdot \frac{R}{c}, \quad (\text{D-13})$$

where $\Delta t = R/c$ is the light travel time across the radius of the body under consideration. Substituting relation (D-12), relation (D-13) becomes:

$$\Delta g(R,r,t) = \frac{M_a G \alpha}{c \cdot \delta r} e^{\alpha t} \frac{R}{r}. \quad (\text{D-14})$$

For the Earth, $R = 6.4 \times 10^8 \text{ cm}$ ($\Delta t \sim 0.02$ seconds) so the tidal acceleration at $t = 3.15 \times 10^5$ seconds would be $\Delta g = 1.26 \times 10^{-4} \text{ cm/s}^2$. This is approximately equivalent to the tidal acceleration induced on the Earth by the Moon.

By comparison, the *steady state* gravitational force field produced by the Galactic nucleus at a galactocentric distance r (before passage of the pulse) would be capable of inducing a tidal acceleration of:

$$g(R,r) \sim M G \frac{2R}{r^3}. \quad (\text{D-15}).$$

For the Earth, $r = r_0$, this would amount only to $\Delta g \sim 1.4 \times 10^{-21} \text{ cm/s}^2$, or about 10^{-17} of the tidal force induced on the Earth by the Moon. Thus the proposed gravity pulse would be able to amplify the $r = r_0$ tidal force generated by the Galactic nucleus by a factor of 10^{17} .

If the gravitational potential of a superwave were to change more rapidly than is estimated above, then even larger tidal accelerations might be induced. For example, suppose that at the end of the initial acceleration period when the GC had reached its maximum negative potential (i.e., after $t = 3.15 \times 10^5$ seconds), the acceleration $g(t)$ were to drop from 128 cm/s^2 to zero over a period of 2000 seconds. Then, the rate of change of gravitational

acceleration would be $g(r_o,t) = 0.64 \text{ cm/s}^3$ and the tidal acceleration would be $\Delta g \sim 1.4 \times 10^{-3} \text{ cm/s}^2$, hence a tidal acceleration 10 times stronger than that induced on the Earth by the Moon. Lunar tides normally reach heights of 2 meters on the open seas. So a tidal force 10 times greater would induce tides reaching as high as 20 meters. Moreover, land tides would be induced by this tidal acceleration which could act as a trigger for seismic and volcanic events. The Sun, which has a radius about 100 times that of the Earth, would experience a tidal accelerating force of $\sim 0.15 \text{ cm/s}^2$, with tides on its surface reaching heights of 200 meters. This is only a small fraction of the solar radius. However, it is conceivable that certain stars operating near a threshold of instability could be thrown into an unstable condition by disturbances of this magnitude with the result that they would shortly thereafter undergo a supernova explosion.

UPDATE

Possible evidence of gravitational torquing of the Earth's polar axis by the Galactic gravity field. A study of ^{10}Be peaks recorded in the Vostok ice core suggests that major Galactic superwaves have impacted about every $25,000 \pm 3000$ years with a half-cycle period of 12,000 years also being present and that at these times the Earth's pole is inclined either maximally toward the Galactic center or maximally away from the Galactic center; see **p. 238**. As discussed in my book *Earth Under Fire*, this cycle period matches the Earth's polar precession period which suggests that the Earth's rotational dynamics may be gravitationally affected by superwaves. Polar precession which is normally due to the tidal force of the Sun and Moon appears to be entrained into the "Galactic heartbeat," becoming timed so that the Earth's equator is maximally inclined at the time of superwave arrival, allowing a maximal torque to be imparted to the Earth's axis. This gravitational effect could also be responsible for producing the Earth's 100,000 year orbital eccentricity cycle. The precessional cycle of other planets such as Mars does not approximate this Galactic period. As a result, the polar axis alignment for other planets would not be expected to be similarly aligned at these times.

Possible evidence of gravity wave triggering of terrestrial seismic events by distant supernova. On December 26, 2004 a magnitude 9.3 earthquake occurred in the Indian Ocean off the coast of Sumatra, causing a powerful tsunami that devastated coastal regions and leaving over 240,000 people either dead or missing. It was the worst tsunami to affect this area since the 1883 explosion of Krakatao. The earthquake that produced it was so strong that it exceeded by a factor of 10 the next most powerful quake to occur anywhere in the past 25 years. Interestingly, just 44.6 hours later gamma ray telescopes orbiting the Earth picked up the arrival of the brightest gamma ray burst ever recorded, 100 times more intense than any previously observed burst. The burst originated from the soft gamma ray repeater star, SGR 1806-20, a neutron star located about 10 degrees northeast of the Galactic center and about 20,000 to 32,000 light years from us, or about as far away as the Galactic center.

One is led to believe that the two events are connected and that the December 2004 earthquake was triggered by a longitudinal gravity wave from the same explosion that produced the gamma ray burst. The gravity wave would have traveled slightly faster than the gamma ray burst since the latter would have suffered some scattering in the course of its journey through the Galaxy. Also laboratory experiments suggest that longitudinal shock waves travel at superluminal speeds, eventually declining to the speed of light as they leave their point of origin. Thus a longitudinal gravity wave would have gained a lead over its gamma ray counterpart. Once it arrived, the gravity wave would have produced a slight tidal force on the Earth and acted as a trigger for the release of seismic stresses. A galactic core explosion could have had a similar effect on the Earth, only much larger. More information on this may be found at: <http://www.etheric.com/GalacticCenter/GRB.html>.

APPENDIX E

CONVERSION OF RADIOCARBON DATES TO CALENDAR DATES

UPDATE

Table I
Scandinavian Climatic Zone Dates

| Climatic Zone | Acronym | Calendar Date (Years b2k) | C-14 Date (Years b2k) |
|--------------------------|---------|------------------------------|--------------------------|
| Preboreal warming | PB | 11,600 – 11,525 | ~10,000 |
| Younger Dryas Stadial | YD | 13,000 – 11,600 | 11,050 – 10,000 |
| Intra Allerod Cold Peak | IACP | 13,350 – 13,180 | 11,550 – 11,330 |
| Alleröd Interstadial | AL | 14,050 – 13,000 | 12,200 – 11,050 |
| Older Dryas Stadial | OD | 14,180 – 14,050 | 12,380 – 12,200 |
| Bölling Interstadial | BO | 14,750 – 14,180 | 12,600 – 12380 |
| Lista Stadial | LI | 15,000 – 14,750 | 12,650 – 12600 |
| Pre-Bölling Interstadial | P-BÖ | 15,850 - 15,000 | 13,150 - 12,650 |

Calendar and radiocarbon dates for these zones are based on dates assigned to corresponding climatic boundaries evident in the Cariaco Basin gray scale varved sediment core of Hughen, et al. (2000).

TABLE II
CONVERSIONS FROM RADIOCARBON TO CALENDAR DATES

| Years b2k Calendar | Years b2k C-14 | Correction (years) |
|-----------------------|-------------------|-----------------------|
| 10,000 | 9,000 | 1000 |
| 10,720 | 9,500 | 1220 |
| 11,300 | 10,000 | 1300 |
| 12,390 | 10,500 | 1890 |
| 12,950 | 11,000 | 1950 |
| 13,300 | 11,500 | 1800 |
| 13,800 | 12,000 | 1800 |
| 14,350 | 12,500 | 1850 |
| 14,950 | 12,600 | 2350 |
| 15,450 | 13,000 | 2450 |
| 16,920 | 13,500 | 3420 |
| 17,170 | 14,000 | 3170 |
| 17,650 | 14,500 | 3150 |
| 17,950 | 15,000 | 2950 |
| 18,050 | 15,500 | 2550 |
| 18,950 | 16,000 | 2950 |
| 19,550 | 16,500 | 3050 |
| 20,050 | 17,000 | 3050 |
| 20,200 | 17,500 | 2700 |
| 20,550 | 18,000 | 2550 |
| 22,100 | 19,000 | 3100 |
| 23,150 | 20,000 | 3150 |
| 28,850 | 25,000 | 3850 |
| 34,550 | 30,000 | 4550 |

The conversions of radiocarbon dates to calendar dates are based on the radiocarbon chronology developed for the Cariaco Basin gray scale varved sediment core (Hughen, et al., 2000, 2004). The conversions for dates earlier than 20,000 ^{14}C yrs b2k are based on Fairbanks, et al. (2005).

APPENDIX F

SYNTHESIS OF HIGH RESOLUTION DUST CONCENTRATION PROFILES FOR THE BYRD STATION AND CAMP CENTURY GLACIAL ICE CORES

The dust concentration curves shown in Figures 8.1(d) and (g) were synthesized from: a) dust weight concentration values I have calculated from data published by Cragin et al. (1977), plotted squares; b) microparticle concentration values published by Thompson (1977b), plotted circles; and c) dust weight concentrations determined in the course of the present study, plotted triangles. This integration of the measurements made by several authors into a single graph greatly improves the resolution of the concentration vs. time profile, and as a result, valuable insights may be gained regarding the rapid variations in dust concentration that occurred during the Last Ice Age.

The dust weight concentration values plotted in Figure 8.1, curves-d and -g, are given in terms of mg/lt, while the microparticle concentration values are given in terms of number of particles (diameter $>0.6\mu$) per 0.5 ml of ice. The two concentration indices were brought into register by assuming the equivalence: $\sim 2 \times 10^5$ particles/0.5 ml = 1.0 mg/lt for the Byrd ice core and 2×10^5 particles/0.5 ml = 1.5 mg/lt for the Camp Century ice core. This equivalence would suggest a mean particle size of 1.2 - 1.4 microns for perfectly spherical particles having a density of $\rho = 2.7 \text{ g/cm}^3$. For irregularly shaped particles a larger mean particle size would be predicted. The relative error involved in meshing the two data sets is estimated to be $\pm 20\%$.

Dust weight concentration values estimated from the data of Cragin et al. are presented in Table F-I (column 6). The related calculations were performed as follows. The concentration values given for silicon (column 2) were divided by 27.7% (the crustal abundance value for Si) to give estimates of the total dust weight concentrations (column 4). Also, the concentration values given for aluminum (column 3) were divided by 8.1% (the crustal abundance value for Al) to give supplementary estimates of the total dust weight concentrations (column 5). These two total dust concentration estimates were then averaged together to produce a mean total dust concentration estimate (column 6).

Microparticle concentration values reported by Thompson (1977b, pp. 34 and 41) have been reproduced in Table F-II. Depths for 8 of Thompson's Byrd core samples (marked by asterisks) have been changed from log book depths (given in Thompson's data) into true depths (i.e., depths corrected for bore hole slanting). The conversion of these particular depth values had apparently been overlooked in the original study.

[**UPDATE:** Log book depths for the Camp Century samples listed in this table still need to be converted to true depths.]

Dust concentrations for 11 ice core dust samples analyzed in the present study are listed in Table F-III. Values for the Camp Century ice core samples taken from depths of 1226.2, 1227.7, and 1231.5 meters have been determined gravimetrically. Values for the other samples have been based on geochemical analysis determinations of Fe and Sn concentrations; see Chapter 12 (Subsection 12.1.1).

TABLE F-1
DUST WEIGHT CONCENTRATIONS IN POLAR ICE

| A. Byrd Station Ice Core | | | | | |
|--------------------------|-----------------------------------|-----------------------------------|--|---------------------------------------|---|
| (1) | (2) | | (4) | | (6) |
| Depth (meters) | Measured Concentration | | Total Dust Concentration Assuming Crustal Ratios: | | Total Dust Concentration: |
| | Si ($\mu\text{g}/\text{lt}$) | Al ($\mu\text{g}/\text{lt}$) | for Si ($\mu\text{g}/\text{lt}$) | for Al ($\mu\text{g}/\text{lt}$) | Average for col. 4 & col. 5 ($\mu\text{g}/\text{lt}$) |
| 450 | 6 \pm 2 | 1.1 \pm .4 | 21.7 | 13.6 | 17.7 \pm 6.0 |
| 502.5 | < 2 | 1.7 \pm .2 | < 7 | 21.0 | 14 \pm 2 |
| 1096 | 10 \pm 2 | 1.7 \pm .2 | 36.1 | 21.0 | 28.6 \pm 8 |
| 1194.3 | 27 \pm 3 | 9.9 \pm 1.2 | 97.5 | 122.2 | 110 \pm 12 |
| 1292.5 | 30 \pm 2 | 7.0 \pm 1.5 | 108.3 | 86.4 | 97.4 \pm 11 |
| 1340 | 44 \pm 7 | 12.5 \pm 2.8 | 158.8 | 154.3 | 156.5 \pm 25 |
| 1392 | 28 \pm 2 | 8.5 \pm 1.7 | 101.1 | 104.9 | 103 \pm 8 |
| 1413.5 | 72 \pm 3 | 16.8 \pm 4.4 | 259.9 | 207.4 | 233.7 \pm 10 |
| 1489 | 48 \pm 5 | 10.2 \pm 1.4 | 173.3 | 125.9 | 149.6 \pm 25 |
| 1524 | 69 \pm 5 | 15.3 \pm 1.7 | 249.1 | 188.9 | 219 \pm 29 |
| 1562 | 68 \pm 9 | 10.8 \pm 2.3 | 245.5 | 133.3 | 189.4 \pm 56 |
| 1710.5 | 12 \pm 3 | 3.8 \pm 1.1 | 43.3 | 46.9 | 45.1 \pm 11 |
| 1783 | 9 \pm 2 | 3.3 \pm .5 | 32.5 | 40.7 | 36.6 \pm 8 |
| 1856.5 | 35 \pm 3 | 6.2 \pm 1.7 | 126.4 | 76.5 | 101.5 \pm 25 |
| 1882 | 23 \pm 2 | 8.0 \pm 1.0 | 83.0 | 98.8 | 91 \pm 9 |
| 1978.5 | 19 \pm 4 | 4.0 \pm 1.8 | 68.6 | 49.4 | 59 \pm 12 |
| 2018 | 37 \pm 2 | 8.4 \pm 1.9 | 133.6 | 103.7 | 118.7 \pm 15 |
| 2135 | 28 \pm 2 | 7.0 \pm 2.1 | 101.1 | 86.4 | 93.8 \pm 7 |
| 2154 | 11 \pm 2 | 1.4 \pm 0.4 | 39.7 | 17.3 | 28.5 \pm 11 |

TABLE F-I (Continued)
DUST WEIGHT CONCENTRATIONS IN POLAR ICE

| B. <u>Camp Century Ice Core</u> | | | | | |
|---------------------------------|-----------------------------------|-----------------------------------|--|---------------------------------------|---|
| (1) | (2) | (3) | (4) | (5) | (6) |
| Log Book Depth * (meters) | Measured Concentration | | Total Dust Concentration Assuming Crustal Ratios: | | Total Dust Concentration: Average for col. 4 & col. 5 ($\mu\text{g}/\text{lt}$) |
| | Si ($\mu\text{g}/\text{lt}$) | Al ($\mu\text{g}/\text{lt}$) | for Si ($\mu\text{g}/\text{lt}$) | for Al ($\mu\text{g}/\text{lt}$) | |
| 560 | 27 \pm 3 | 7.7 \pm 1.5 | 97.5 | 95.1 | 96 \pm 11 |
| 565 | 33 \pm 4 | 12 \pm 2.4 | 119.1 | 148.1 | 134 \pm 16 |
| 679.3 | 51 \pm 11 | 14.8 \pm 2.2 | 184.1 | 182.7 | 183 \pm 40 |
| 898.5 | 31 \pm 9 | 6.1 \pm .8 | 111.9 | 75.3 | 94 \pm 27 |
| 930 | 52 \pm 9 | 9.7 \pm 1.7 | 187.7 | 119.8 | 154 \pm 30 |
| 968 | 23 \pm 2 | 5.0 \pm 1.7 | 83.0 | 61.7 | 72 \pm 11 |
| 993 | 24 \pm 8 | 9.1 \pm 1.0 | 86.6 | 112.3 | 100 \pm 33 |
| 1109 | 38 \pm 2 | 9.3 \pm 2.0 | 137.2 | 114.8 | 126 \pm 12 |
| 1136.5 | 65 \pm 4 | 26 \pm 6 | 234.7 | 321.0 | 278 \pm 43 |
| 1146 | 234 \pm 34 | 82 \pm 8 | 844.8 | 1012.3 | 929 \pm 135 |
| 1152.5 | 208 \pm 20 | 47 \pm 3 | 750.9 | 580.2 | 666 \pm 86 |
| 1170.5 | 224 \pm 42 | (very high) | 808.7 | | 809 \pm 150 |
| 1202 | 325 \pm 32 | 93 \pm 3 | 1173 | 1148 | 1161 \pm 114 |
| 1231.5 | 835 \pm 54 | 173 \pm 12 | 3014 | 2136 | 2575 \pm 439 |
| 1254 | 668 \pm 42 | 153 \pm 5 | 2412 | 1889 | 2151 \pm 262 |
| 1267 | 107 \pm 28 | 43 \pm 6 | 386.3 | 530.9 | 458 \pm 120 |
| 1268.5 | 124 \pm 18 | 48 \pm 5 | 447.7 | 592.6 | 520 \pm 73 |
| 1290 | 76 \pm 11 | 27 \pm 5 | 274.4 | 333.3 | 304 \pm 44 |
| 1300.5 | 395 \pm 32 | 129 \pm 7 | 1426 | 1592.6 | 1509 \pm 122 |
| 1304.5 | 152 \pm 37 | 27 \pm 8 | 548.7 | 333.3 | 441 \pm 108 |
| 1315.5 | 76 \pm 6 | 17 \pm 2 | 274.4 | 209.9 | 242 \pm 32 |
| 1322 | 168 \pm 20 | 50 \pm 2 | 606.5 | 617.3 | 612 \pm 73 |
| 1325.5 | 99 \pm 16 | 35 \pm 5 | 357.4 | 432.1 | 395 \pm 64 |
| 1331.5 | 70 \pm 8 | 10 \pm 4 | 252.7 | 123.5 | 188 \pm 65 |
| 1333.3 | 56 \pm 15 | 21 \pm 3 | 202.2 | 259.3 | 231 \pm 62 |
| 1337.5 | 61 \pm 7 | 15 \pm 2 | 220.2 | 185.2 | 203 \pm 23 |
| 1338 | 61 \pm 22 | 11 \pm 3 | 220.2 | 135.8 | 178 \pm 64 |
| 1341.3 | 78 \pm 7 | 18 \pm 3 | 281.6 | 222.2 | 252 \pm 30 |
| 1345.3 | 89 \pm 17 | 22 \pm 4 | 321.3 | 271.6 | 296 \pm 57 |
| 1348 | 199 \pm 12 | 44 \pm 3 | 718.4 | 543.2 | 631 \pm 88 |
| 1348.5 | 155 \pm 35 | 45 \pm 7 | 559.6 | 555.6 | 558 \pm 126 |
| 1353.5 | 130 \pm 13 | 56 \pm 6 | 469.3 | 691.4 | 580 \pm 60 |
| 1355.5 | 86 \pm 20 | 49 \pm 4 | 310.5 | 604.9 | 458 \pm 148 |

* To get the true depth for ice age period samples (>1100 m), 3 to 4 meters must be subtracted from the log book depth.

TABLE F-II
MICROPARTICLE CONCENTRATIONS IN POLAR ICE

| A. <u>Byrd Core</u> | | B. <u>Camp Century Core</u> | |
|---------------------|--|--------------------------------|--|
| Depth (meters) | No. of particles > 0.62 μ per $\frac{1}{2}$ ml ($\times 10^4$) | Depth [†] (meters) | No. of Particles > 0.62 μ per $\frac{1}{2}$ ml ($\times 10^5$) |
| 199.3 | 0.55 | 1043.7 | 0.317 |
| 298.8 | 1.04 | 1061.0 | 0.650 |
| 401.3 | 1.45 | 1066.0 | 0.089 |
| 896.9 | 1.13 | 1086.6 | 0.546 |
| 949.8* | 0.20 | 1109.0 | 0.223 |
| 1046.8 | 1.74 | 1135.1 | 0.128 |
| 1194.1 | 0.87 | 1155.6 | 0.466 |
| 1217.9* | 1.21 | 1166.0 | 3.74 |
| 1244.2* | 0.86 | 1178.7 | 3.72 |
| 1295.6* | 1.95 | 1186.0 | 5.52 |
| 1342.7 | 3.19 | 1197.7 | 2.03 |
| 1376.5* | 4.23 | 1204.9 | 5.00 |
| 1389.7 | 2.30 | 1215.0 | 2.89 |
| 1547.4 | 4.63 | 1223.9 | 0.641 |
| 1584.8* | 2.54 | 1234.5 | 1.54 |
| 1633.7 | 2.01 | 1245.0 | 0.534 |
| 1731.2* | 1.11 | 1255.1 | 0.506 |
| 1900.0 | 0.75 | 1265.5 | 1.06 |
| 1998.6* | 0.54 | 1278.8 | 2.17 |
| 2139.6 | 0.68 | 1285.5 | 0.385 |
| | | 1295.6 | 0.240 |
| | | 1306.0 | 0.541 |
| | | 1324.8 | 0.548 |
| | | 1334.7 | 0.276 |
| | | 1345.4 | 1.08 |
| | | 1354.9 | 0.599 |

† This column gives log book depths. To convert to actual core depths, 3 - 4 meters must be subtracted from the tabulated values.

TABLE F-III
DUST WEIGHT CONCENTRATIONS IN POLAR ICE

A. Byrd Core

| Depth (meters) | Dust Concentration ($\mu\text{g}/\text{lt}$) |
|-------------------|--|
| 700.8 | 17 ± 5 |
| 897.5 | 66 ± 20 |
| 1585.0 | 370 ± 90 |

B. Camp Century Core

| Log Book Depth (meters) | True Depth (meters) | Dust Concentration ($\mu\text{g}/\text{lt}$) |
|-------------------------------|---------------------------|--|
| 1215.1 | 1212 | 3260 ± 700 |
| 1224.0 | 1221 | 525 ± 100 |
| 1230.2 | 1226.2 | 3090 ± 40 |
| 1231.7 | 1227.7 | 2460 ± 40 |
| 1234.7 | 1230.5 | 1530 ± 380 |
| 1235.7 | 1231.5 | 2510 ± 40 |
| 1245.0 | 1241 | 345 ± 70 |
| 1278.9 | 1275 | 3260 ± 700 |

APPENDIX G

NEUTRON ACTIVATION ANALYSIS RESULTS FOR GLACIAL ICE DUST SAMPLES: BYRD, CAMP CENTURY, AND AGASSIZ ICE CORES

Tables G-1 through G-XV list by element the neutron activation analysis (NAA) results for both irradiations of glacial dust samples. Column (1) lists the samples according to their core tube number. Column (2) gives the ice core depth from which the samples were taken. Column (3) presents the weight of the designated element in each dust sample, as determined from NAA. Column (4) gives the filter contribution, i.e., the ratio (in percent) of the elemental weight found in the filter paper to the elemental weight found in the dust sample. Column (5) gives the weight concentration of that element per unit volume of ice from which the dust was filtered. The values in this column were determined by dividing a given elemental weight listed in column (3) by the corresponding meltwater volume for that sample given in column (8) of Table XVII. Column (6) lists the elemental concentration as a fraction of total dust sample weight. The values in this column were determined by dividing a given elemental weight listed in column (3) by the corresponding sample dust weight given in column (9) of Table XVII. Column (7) gives the enhancement factor (EF) which is derived by dividing the concentration value in column (6) by the average crustal abundance value for that element. Also, for four elements (Ir, Au, Co, and Ni) estimates have been made of the concentration of cosmic dust in the sample (column 8) if a C-1 chondrite composition were to be assumed for this dust.

The majority of elemental sample weights (column 3) were determined through comparison with a measured standard. By consecutively counting a sample and a standard, the weight of an element in a sample could be determined according to the following relation:

$$C = \frac{N}{N'} \cdot \frac{\epsilon^{\odot}}{\epsilon} \cdot \frac{t_a^{\odot}}{t_a} \cdot e^{-\lambda(T \ominus T')} \cdot w \cdot k, \quad (G-1)$$

where

- C = elemental concentration in grams.
- N and N' = counts above background in the photopeaks of the sample and standard.
- ϵ and ϵ' = detector efficiency (at the chosen gamma ray energy)
- t_a and t_a' = detector acquisition livetime (seconds) in counting the sample and standard.
- T and T' = decay time (hours) for the sample and standard.
- w = weight of the standard.
- k = weight fraction concentration of the element in the standard.

In the first irradiation Fe, Co, Ni, Sc, and Hf weights were determined through comparison with a PCC-1 standard. In the second irradiation Sn, Sb, and Au were determined by comparison respectively with Sn, Sb, and Au metal standards. The other 10 elements, except for Ir and Ag, were determined by comparison with a USGS W-1 standard. In the case of Ir this was necessary because the specially prepared Ir standard could not be relied upon. In the case of Ag this was necessary because neither the PCC-1 or W-1 standards contain sufficient amounts of silver. Instead, these two elements were determined in both irradiations by the flux (described below). Besides Ir and Ag, several other elements in the first irradiation (Au, Ba, Sb, Sn, Cs, La, Ce, and Tb) were determined by the flux method since the PCC-1 standard did not have sufficient amounts of these elements to provide detectable photopeaks.

In using the flux method, elemental weights were calculated with the aid of the following relation:

$$C = \frac{N \cdot A}{0.602 \cdot \epsilon \cdot I \cdot t_a \cdot \theta \cdot \phi_{th} (\sigma_{th} + F \cdot R) (1 - e^{-\lambda t}) (e^{-\lambda T})} \quad (G-2)$$

where C = elemental concentration in grams
 N = counts above background in the photopeak
 A = atomic weight of the element
 ϵ = detector efficiency at the energy of the observed γ -ray
 I = γ -ray abundance factor, photons per decay
 t_a = detector acquisition livetime (seconds)
 θ = isotopic abundance of the target nuclide
 ϕ_{th} = thermal neutron flux (n/cm²/s)
 σ_{th} = thermal neutron cross section ((cm²/n) X 10²⁴)
 F = ratio of epithermal-to-thermal flux (3 \pm 0.5%)
 R = resonance integral (cm²/n) X 10²⁴)
 λ = decay constant (ln2/half life)
 t_i = irradiation time (hours)
 T = decay time (hours)

The sample weights for Ir and Au calculated for the first irradiation were increased by 20% and 50% respectively to adjust for sample "burn up" during the 1000 hour long high flux irradiation.

Through the use of flux monitors, the ratio of epithermal-to-thermal flux (F) was determined to be 3 \pm 5%. The error in determining C by equation G-2 is estimated to be \pm 20% due to uncertainties in the values chosen for ϵ , ϕ_{th} , and F and due to statistical fluctuations inherent in the decay and count process which lead to uncertainties in N.

For the values listed in columns (3) and (5) where no error range is given, the error should be assumed to be \pm 20% of the listed number. In cases where the sample weights of Sn, Sb, and Au have been determined with the use of standards, the error ranges are usually less than 20% of the listed value and, in this case, are individually recorded. In some cases errors were greater than 20%, and these have also been individually recorded. These larger errors sometimes arise because of uncertainty in the filter contribution, in cases where the filter makes a substantial contribution to the gross elemental weight being determined. Or large errors may arise in cases where the γ -ray background level is so large in comparison to the photopeak magnitude that substantial errors are introduced in determining the net counts in the photopeak, e.g., as in certain iridium determinations.

In some cases upper limits are given for the elemental sample weights. Exact weights could not be specified either because the γ -ray photopeaks for that element were below the threshold of detection, i.e., were undetectable above the γ -ray background as in the case of Ir, Sn, and Tb in some samples, or because the filter contribution was so large that the sample contribution could not be accurately determined. If the latter was the case, a horizontal line was placed in column (4). Of all elements, Au was most difficult to determine due to filter contribution. Only in Sample #962-1 (a and b) was gold abundant enough to be accurately determined above the filter background.

[**UPDATE:** Based on energy dispersive X-ray analysis of a portion of Camp Century sample 962-1 conducted in 1984, the total dust concentration in ice for samples 962-1a and 962-1b has been revised to 1.53 ± 0.38 $\mu\text{g}/\text{lt}$ which is two-thirds of its previously estimated value; see update at the end of Chapter 8. The values tabulated for these two samples for elemental concentration (in dust), enhancement factor, and cosmic dust percent have been revised accordingly.

Also the log book depths tabulated here for the Camp Century, Greenland ice core samples are not the actual sample depths. The actual depths for these samples are smaller by 3 to 4 meters and are listed in Table XVII of Chapter 12.]

TABLE G-1
NAA RESULTS FOR GLACIAL ICE DUST SAMPLES: BYRD STATION,
CAMP CENTURY, AND AGASSIZ ICE CORES

| (1) Core Tube No. | (2) Log book Depth (m) | (3) Element Weight (grams) | (4) Filter Contribution (%) | (5) Concentration | | (6) in dust (ppb) | (7) E.F. ¹ | (8) Cosmic ² dust (%) | |
|----------------------------|---------------------------------|-------------------------------------|--------------------------------------|---------------------------------------|----------------|-------------------------|--------------------------|---|--------|
| | | | | in ice ($\mu\text{g}/\text{lt}$) | | | | | |
| <u>Byrd Station</u> | | | | | | | | | |
| 422 | 700.8 | 0.76 | (-12) | < 3 | 11.4 | (-6) | 660 | 27,500 | 100 |
| 552 | 897.5 | 0.56 \pm 0.14 | (-12) | < 5 | 13.7 \pm 3.4 | (-6) | 207 | 8600 | 40 |
| 1016 | 1585.0 | 12.5 | (-12) | < 0.7 | 58 | (-6) | 156 | 6500 | 30 |
| 1016-B | 1585.15 | 10.5 | (-12) | < 0.4 | 1105 | (-6) | 26 | 1080 | 5 |
| <u>Camp Century</u> | | | | | | | | | |
| 949 | 1215.1 | 3.9 | (-12) | < 1 | 54 | (-6) | 16.6 | 690 | 3.2 |
| 955 | 1224.0 | 0.65 | (-12) | < 5 | 14.6 | (-6) | 28 | 1170 | 5.4 |
| 959 | 1230.2 | < 0.16 | (-12) | < 20 | < 0.91 | (-6) | < 0.3 | < 13 | < .06 |
| 960 | 1231.7 | 3.1 | (-12) | < 1 | 17.1 | (-6) | 6.9 | 6.9 | 1.3 |
| 962-1-a | 1234.7 | 4.4 | (-12) | < 0.8 | 85 | (-6) | (56) ³ | 2310 | 10.7 |
| 962-1-b | 1234.7 | 0.14 \pm 0.04 | (-12) | < 0.4 | 86 | (-6) | (56) ³ | 2310 | 10.7 |
| 962-2 | 1235.7 | < 0.18 | (-12) | < 19 | < 0.95 | (-6) | < 0.4 | < 17 | < .07 |
| 969 | 1245.0 | 0.64 | (-12) | < 5 | 31 | (-6) | 96 | 4000 | 18.6 |
| 992 | 1278.9 | 0.83 | (-12) | < 5 | 20.5 | (-6) | 6.3 | 260 | 1.2 |
| <u>Agassiz</u> | | | | | | | | | |
| Hol A | 105 | < 0.11 | (-12) | < 35 | < 0.04 | (-6) | < 0.14 | < 6 | < 0.03 |
| Hol B | 110 | < 1.86 | (-12) | < 2 | < 0.77 | (-6) | < 1.04 | < 43 | < 0.2 |
| Wisc. | 314 | < 1.54 | (-12) | < 2 | < 2.2 | (-6) | < 0.54 | < 23 | < 0.1 |

¹ Assume that the crustal abundance of Ir is 0.024 ppb; see Table XIII.

² Assume a C-1 chondrite abundance of 514 ppb; see Table XIII.

³ [Update: Element concentration relative to total sample dust concentration is determined by assuming a dust concentration of 1.53 ± 0.38 mg/lt for this sample.]

TABLE G-II
NAA RESULTS FOR GLACIAL ICE DUST SAMPLES: BYRD STATION,
CAMP CENTURY, AND AGASSIZ ICE CORES

| (1) Core Tube No. | (2) Log book Depth (m) | (3) Element Weight (grams) | (4) Filter Contribution (%) | (5) Concentration | | (6) in dust (ppm) | (7) E.F. ¹ | (8) ² Cosmic dust (%) |
|----------------------------|---------------------------------|-------------------------------------|--------------------------------------|---------------------------------------|--------|-------------------------|--------------------------|---|
| | | | | in ice ($\mu\text{g}/\text{lt}$) | | | | |
| <u>Byrd Station</u> | | | | | | | | |
| 422 | 700.8 | < 0.53 | (-10) | - | < 0.8 | (-4) | < 46 | - |
| 552 | 897.5 | < 0.62 | (-10) | - | < 15 | (-4) | < 23 | - |
| 1016 | 1585.0 | < 1.1 | (-10) | - | < 5.14 | (-4) | < 1.4 | - |
| 1016-B | 1585.15 | < 0.85 | (-10) | - | < 90 | (-4) | < 0.2 | - |
| <u>Camp Century</u> | | | | | | | | |
| 949 | 1215.1 | < 1.1 | (-10) | - | < 15 | (-4) | < 0.47 | - |
| 955 | 1224.0 | < 0.8 | (-10) | - | < 18 | (-4) | < 3.4 | - |
| 959 | 1230.2 | < 1.79 | (-10) | - | < 10 | (-4) | < 0.33 | - |
| 960 | 1231.7 | < 3.7 | (-10) | - | < 20 | (-4) | < 0.82 | - |
| 962-1-a | 1234.7 | 15.1 \pm .8 | (-10) | 4.3 | 290 | (-4) | (19) ³ | 4800 |
| 962-1-b | 1234.7 | 0.44 \pm .02 | (-10) | 2.7 | 278 | (-4) | (18) ³ | 4500 |
| 962-2 | 1235.7 | < 2.6 | (-10) | - | < 14 | (-4) | < 0.56 | - |
| 969 | 1245.0 | < 0.85 | (-10) | - | < 43 | (-4) | < 13 | - |
| 992 | 1278.9 | < 0.26 | (-10) | - | < 6.5 | (-4) | < 0.20 | - |
| <u>Agassiz</u> | | | | | | | | |
| Ho1 A | 105 | < 2.0 | (-10) | - | < 0.82 | (-4) | < 0.26 | - |
| Ho1 B | 110 | < 2.2 | (-10) | - | < 0.91 | (-4) | < 0.12 | - |
| Wisc. | 314 | < 0.16 | (-10) | - | < 0.22 | (-4) | < 0.0056 | - |

¹ Assume that the crustal abundance of Au is 4 ppb (Ronov and Yaroshevsky, 1972).

² Assume a C-1 chondrite abundance of 152 ppb; see Table XIII.

³ [Update: Element concentration relative to total sample dust concentration is determined by assuming a dust concentration of 1.53 \pm 0.38 mg/lt for this sample.]

TABLE G-III
NAA RESULTS FOR GLACIAL ICE DUST SAMPLES: BYRD STATION,
CAMP CENTURY, AND AGASSIZ ICE CORES

| (1) Core Tube No. | (2) Log book Depth (m) | (3) Element Weight (grams) | (4) Filter Contribution (%) | (5) Concentration | | (6) in dust (ppm) | (7) E.F. ¹ |
|----------------------------|---------------------------------|-------------------------------------|--------------------------------------|---------------------------------------|-------|-------------------------|--------------------------|
| | | | | in ice ($\mu\text{g}/\text{lt}$) | | | |
| <u>Byrd Station</u> | | | | | | | |
| 422 | 700.8 | 8.6 | (-10) | 13 | 13 | (-3) | 750 |
| 552 | 897.5 | 12.4 | (-10) | 15 | 30 | (-3) | 460 |
| 1016 | 1585.0 | < 2.8 | (-10) | - | < 1.3 | (-3) | < 3.5 |
| 1016-B | 1585.15 | < 1.7 | (-10) | - | < 18 | (-3) | < 0.4 |
| <u>Camp Century</u> | | | | | | | |
| 949 | 1215.1 | 105 | (-10) | 2.7 | 146 | (-3) | 45 |
| 955 | 1224.0 | < 3.3 | (-10) | - | < 7.5 | (-3) | < 14 |
| 959 | 1230.2 | < 3.4 | (-10) | - | < 2.0 | (-3) | < 0.63 |
| 960 | 1231.7 | < 11.1 | (-10) | - | < 6.1 | (-3) | < 7.1 |
| 962-1-a | 1234.7 | 320 | (-10) | 0.3 | 610 | (-3) | (400) ² |
| 962-1-b | 1234.7 | 8.3 | (-10) | 0.5 | 520 | (-3) | (340) ² |
| 962-2 | 1235.7 | < 5.3 | (-10) | - | < 2.8 | (-3) | < 1.1 |
| 969 | 1245.0 | < 4.1 | (-10) | - | < 21 | (-3) | < 61 |
| 992 | 1278.9 | 450 | (-10) | 0.6 | 1120 | (-3) | 340 |
| <u>Agassiz</u> | | | | | | | |
| Ho1 A | 105 | 4.3 | (-10) | 3 | 0.18 | (-3) | 0.57 |
| Ho1 B | 110 | 2.8 | (-10) | 4.5 | 0.12 | (-3) | 0.16 |
| Wisc. | 314 | 2.8 | (-10) | 4.5 | 0.39 | (-3) | 0.10 |

¹ Assume crustal abundance of Ag is 0.08 ppm (Ronov and Yaroshevsky, 1972).

² [Update: Element concentration relative to total sample dust concentration is determined by assuming a dust concentration of 1.53 \pm 0.38 mg/lt for this sample.]

TABLE G-IV
 NAA RESULTS FOR GLACIAL ICE DUST SAMPLES: BYRD STATION,
 CAMP CENTURY, AND AGASSIZ ICE CORES

| Iron (Fe) | | | | | | |
|---------------------|--------------------------|------------------------------|-------------------------------|--|---------------------------------|-------------------|
| (1) | (2) | (3) | (4) | (5) | (6) | (7) |
| Core Tube No. | Log book Depth (m) | Element Weight (grams) | Filter Contribution (%) | Concentration in ice ($\mu\text{g}/\text{lt}$) | Concentration in dust (%) | E.F. ⁵ |
| <u>Byrd Station</u> | | | | | | |
| 422 | 700.8 | 0.23 (-6) | 33 | 3.4 | 20 \pm 6 ¹ | 3.2 |
| 552 | 897.5 | 0.54 (-6) | 24 | 13.2 | 20 \pm 6 ¹ | 3.2 |
| 1016 | 1585.0 | 8.7 (-6) | 2.8 | 40.7 | 11 \pm 3 ² | 1.8 |
| 1016-B | 1585.15 | 29 (-6) | 0.3 | 3050 | 7 \pm 1 ³ | 1.1 |
| <u>Camp Century</u> | | | | | | |
| 949 | 1215.1 | 11.7 (-6) | 1.0 | 163 | 5 \pm 1 ⁴ | 0.8 |
| 955 | 1224.0 | 1.17 (-6) | 12 | 26.3 | 5 \pm 1 ⁴ | 0.8 |
| 959 | 1230.2 | 32.8 (-6) | 1.0 | 187 | 5.8 \pm .2 | 0.94 |
| 960 | 1231.7 | 20.2 (-6) | 1.5 | 111 | 4.3 \pm .2 | 0.69 |
| 962-1-a | 1234.7 | 1.95 (-6) | 6.7 | 38 | (2.5 \pm 1.0) ⁶ | 0.40 |
| 962-1-b | 1234.7 | 0.058 (-6) | 4.0 | 37 | (2.5 \pm 1.0) ⁶ | 0.40 |
| 962-2 | 1235.7 | 19.0 (-6) | 1.4 | 102 | 4.0 \pm 2 | 0.65 |
| 969 | 1245.0 | 0.33 (-6) | 41 | 16.9 | 5 \pm 1 ⁴ | 0.8 |
| 992 | 1278.9 | 6.6 (-6) | 2.0 | 163 | 5 \pm 1 ⁴ | 0.8 |
| <u>Agassiz</u> | | | | | | |
| Hol A | 105 | 38 (-6) | 0.8 | 15.5 | 5.0 | 0.81 |
| Hol B | 110 | 45 (-6) | 0.6 | 18.6 | 2.5 | 0.40 |
| Wisc. | 314 | 170 (-6) | 0.2 | 240 | 6.0 | 0.97 |

¹ These Fe concentrations have been set at levels that are consistent with Thompson's findings in which he measured individual particles for Fe content using the energy dispersive X-ray analysis technique (1977b, Appendix C). As a double check on the accuracy of these estimates note that the total sample concentration in $\mu\text{g}/\text{lt}$ of ice, predicted from the Fe NAA determinations, match up reasonably well with other dust weight and microparticle number concentrations plotted in Figure 8.1, curve-d.

² This Fe concentration has been set at the level 11 \pm 3% which is consistent with a mixture of 70% terrestrial components containing 6% Fe with 30% extraterrestrial components containing 24% Fe.

³ This Fe concentration has been set at the level 7 \pm 1% which is consistent with the measurements of Kyle et al. (1981) of 6% Fe in glass shards from 6 Byrd core ash bands with an additional 1% added for a 5% cosmic dust contribution.

⁴ These Fe concentrations have been set at the level 5 \pm 1% based on the observations that samples 959, 960, and 962-2, for which direct determinations have been made, fall in this range. Again note that the predicted dust weight concentration values match up well on Figure 8.1, curve-g.

⁵ Assume that the crustal abundance of Fe is 6.2% (Ronov and Yaroshevsky, 1972).

⁶ [Update: Element concentration relative to total sample dust concentration is determined by assuming a dust concentration of 1.53 \pm 0.38 mg/lt for this sample.]

TABLE G-V
NAA RESULTS FOR GLACIAL ICE DUST SAMPLES: BYRD STATION,
CAMP CENTURY, AND AGASSIZ ICE CORES

| Cobalt (Co) | | | | | | | | | |
|----------------------------|---------------------------------|-------------------------------------|--------------------------------------|----------------------|-----------|-------------------------|--------------------------|---|-------|
| (1) Core Tube No. | (2) Log book Depth (m) | (3) Element Weight (grams) | (4) Filter Contribution (%) | (5) Concentration | | (6) in dust (ppm) | (7) E.F. ¹ | (8) ² Cosmic dust (%) | |
| | | | | in ice (µg/lit) | | | | | |
| Byrd Station | | | | | | | | | |
| 422 | 700.8 | 1.4 | (-10) | 65 | 2.1 | (-3) | 122 | 4.2 | 25 |
| 552 | 897.5 | < 1.7 | (-10) | -- | < 4 | (-3) | < 24 | < 0.82 | < 4.9 |
| 1016 | 1585.0 | 9.8 | (-10) | 35 | 4.6 | (-3) | 12.3 | 0.42 | 2.5 |
| 1016-B | 1585.15 | 1.8 ± 5 | (-10) | 95 | 19 ± 5 | (-3) | 0.44 | 0.015 | 0.09 |
| Camp Century | | | | | | | | | |
| 949 | 1215.1 | 41 | (-10) | 4.2 | 57 | (-3) | 17.4 | 0.60 | 3.6 |
| 955 | 1224.0 | 3.5 | (-10) | 48 | 7.9 | (-3) | 15.0 | 0.52 | 3.1 |
| 959 | 1230.2 | 95 | (-10) | 2.4 | 54 | (-3) | 17.6 | 0.61 | 3.6 |
| 960 | 1231.7 | 75 | (-10) | 3.0 | 41 | (-3) | 16.7 | 0.58 | 3.5 |
| 962-1-a | 1234.7 | 26.3 | (-10) | 4.9 | 51 | (-3) | (33) ³ | 1.14 | 6.8 |
| 962-1-b | 1234.7 | 0.62 | (-10) | 4.5 | 39 | (-3) | (25) ³ | 0.86 | 5.2 |
| 962-2 | 1235.7 | 60 | (-10) | 3.8 | 32 | (-3) | 12.9 | 0.44 | 2.7 |
| 969 | 1245.0 | 1.1 ± 5 | (-10) | 150 | 5.6 ± 2.6 | (-3) | 16.4 | 0.57 | 3.4 |
| 992 | 1278.9 | 26.6 | (-10) | 6.4 | 66 | (-3) | 20.2 | 0.69 | 4.2 |
| Agassiz | | | | | | | | | |
| Hol A | 105 | 109 | (-10) | 1.8 | 4.4 | (-3) | 14.3 | 0.49 | 3.0 |
| Hol B | 110 | 128 | (-10) | 1.6 | 5.3 | (-3) | 7.1 | 0.25 | 1.5 |
| Wisc. | 314 | 520 | (-10) | 0.4 | 73 | (-3) | 18.3 | 0.63 | 3.8 |

¹ Assume crustal abundance of Co is 29 ppm (Ronov and Yaroshevsky, 1972).

² Assume a C-1 chondrite abundance of 483 ppm; see Table XIII.

³ [Update: Element concentration relative to total sample dust concentration is determined by assuming a dust concentration of 1.53 ± 0.38 mg/lit for this sample.]

TABLE G-VI
NAA RESULTS FOR GLACIAL ICE DUST SAMPLES: BYRD STATION,
CAMP CENTURY, AND AGASSIZ ICE CORES

| Nickel (Ni) | | | | | | | | | |
|----------------------------|---------------------------------|-------------------------------------|--------------------------------------|----------------------|-------------|-------------------------|--------------------------|---|--------|
| (1) Core Tube No. | (2) Log book Depth (m) | (3) Element Weight (grams) | (4) Filter Contribution (%) | (5) Concentration | | (6) in dust (ppm) | (7) E.F. ¹ | (8) ² Cosmic dust 1% Ni 9% Ni (%) (%) | |
| | | | | in ice (µg/lit) | | | | | |
| Byrd Station | | | | | | | | | |
| 422 | 700.8 | < 4.6 | (-9) | - | < 0.07 | < 4000 | < 40 | < 40 | < 4.4 |
| 552 | 897.5 | < 4.7 | (-9) | - | < 0.12 | < 1740 | < 17.6 | < 17 | < 1.9 |
| 1016 | 1585.0 | 53 | (-9) | 13.5 | 0.25 | 660 | 6.7 | 6.6 | 0.7 |
| 1016-B | 1585.15 | 92 | (-9) | 4 | 9.7 | 224 | 2.3 | 2.2 | 0.25 |
| Camp Century | | | | | | | | | |
| 949 | 1215.1 | 38 | (-9) | 9.4 | 0.53 | 162 | 1.6 | 1.6 | 0.18 |
| 955 | 1224.0 | < 2.3 | (-9) | - | < 0.05 | < 64 | < 0.6 | < 0.6 | < 0.07 |
| 959 | 1230.2 | < 22 | (-9) | - | < 0.13 | < 41 | < 0.4 | < 0.4 | < 0.05 |
| 960 | 1231.7 | 48 ± 12 | (-9) | 50 | 0.26 ± 0.07 | 107 | 1.1 | 1.1 | 0.11 |
| 962-1-a | 1234.7 | 78 | (-9) | 3.6 | 1.50 | (980) ³ | 9.9 | 9.9 | 0.72 |
| 962-1-b | 1234.7 | 1.8 ± 5 | (-9) | 3.3 | 1.14 ± 3 | (745) ³ | 7.5 | 7.5 | 0.83 |
| 962-2 | 1235.7 | < 17 | (-9) | - | < 0.09 | < 36 | < 0.36 | < 0.36 | < 0.04 |
| 969 | 1245.0 | 21.6 | (-9) | 17 | 1.11 | 3220 | 32.6 | 32 | 3.6 |
| 992 | 1278.9 | 25.8 | (-9) | 14 | 0.64 | 195 | 2.0 | 2.0 | 0.22 |
| Agassiz | | | | | | | | | |
| Hol A | 105 | 160 | (-9) | 15 | 0.065 | 210 | 2.1 | 2.1 | 0.23 |
| Hol B | 110 | 140 | (-9) | 17 | 0.058 | 78 | 0.78 | 0.78 | 0.09 |
| Wisc. | 314 | 630 | (-9) | 3.8 | 0.88 | 222 | 2.24 | 2.2 | 0.25 |

¹ Assume crustal abundance of Ni is 99 ppm (Ronov and Yaroshevsky, 1972).

² Assume respectively a C-1 chondrite abundance of 1.0% and an iron meteorite abundance of 9%.

³ [Update: Element concentration relative to total sample dust concentration is determined by assuming a dust concentration of 1.53 ± 0.38 mg/lit for this sample.]

TABLE G-VII
NAA RESULTS FOR ICE DUST SAMPLES: BYRD STATION,
CAMP CENTURY, AND AGASSIZ ICE CORES

| Barium (Ba) | | | | | | | |
|----------------------------|---------------------------------|-------------------------------------|--------------------------------------|---|---|--------------------------|--|
| (1) Core Tube No. | (2) Log book Depth (m) | (3) Element Weight (grams) | (4) Filter Contribution (%) | (5) Concentration in ice ($\mu\text{g}/\text{lt}$) | (6) Concentration in dust (ppm) ¹ | (7) E.F. ² | |
| <u>Byrd Station</u> | | | | | | | |
| 422 | 700.8 | < 1.1 (-9) | - | < 0.017 | < 960 | < 2.5 | |
| 552 | 897.5 | < 1.7 (-9) | - | < 0.042 | < 630 | < 1.6 | |
| 1016 | 1585.0 | 70 (-9) | 7 | 0.33 | 875 | 2.2 | |
| 1016-B | 1585.15 | 131 (-9) | 17 | 13.8 | 320 | 0.82 | |
| <u>Camp Century</u> | | | | | | | |
| 949 | 1215.1 | 430 (-9) | 0.5 | 6.0 | 1830 | 4.7 | |
| 955 | 1224.0 | 5.3 (-9) | 36 | 0.118 | 226 | 0.58 | |
| 959 | 1230.2 | 149 \pm 9 (-9) | 15 | 0.85 | 275 | 0.71 | |
| 960 | 1231.7 | 215 \pm 14 (-9) | 11 | 1.18 \pm .08 | 479 | 1.23 | |
| 962-1-a | 1234.7 | 1.45 (-9) | 1.4 | 2.8 | (1800) ³ | 4.6 | |
| 962-2 | 1235.7 | 121 \pm 8 (-9) | 19 | 0.65 \pm .07 | 260 | 0.67 | |
| 969 | 1245.0 | < 2.1 (-9) | - | < 0.11 | < 310 | < 0.80 | |
| 992 | 1278.9 | 119 (-9) | 1.7 | 2.9 | 900 | 2.3 | |
| <u>Agassiz</u> | | | | | | | |
| Hol A | 105 | 410 (-9) | 1.0 | 0.167 | 540 | 1.4 | |
| Hol B | 110 | 660 (-9) | 0.6 | 0.27 | 370 | 1.0 | |
| Wisc. | 314 | 2000 (-9) | 0.2 | 2.79 | 700 | 1.8 | |

¹ Concentration for some samples is given in percent, as marked.

² Assume crustal abundance of Ba is 390 ppm (Ronov and Yaroshevsky, 1972).

³ [Update: Element concentration relative to total sample dust concentration is determined by assuming a dust concentration of 1.53 \pm 0.38 mg/lt for this sample.]

TABLE G-VIII
NAA RESULTS FOR GLACIAL ICE DUST SAMPLES: BYRD STATION,
CAMP CENTURY, AND AGASSIZ ICE CORES

| Antimony (Sb) | | | | | | | |
|----------------------------|---------------------------------|-------------------------------------|--------------------------------------|---|--|--------------------------|--|
| (1) Core Tube No. | (2) Log book Depth (m) | (3) Element Weight (grams) | (4) Filter Contribution (%) | (5) Concentration in ice ($\mu\text{g}/\text{lt}$) | (6) Concentration in dust (ppm) | (7) E.F. ¹ | |
| <u>Byrd Station</u> | | | | | | | |
| 422 | 700.8 | < 14 (-10) | - | < 2.1 (-2) | < 1220 | - | |
| 552 | 897.5 | < 23 (-10) | - | < 5.5 (-2) | < 850 | - | |
| 1016 | 1585.0 | < 4.4 (-10) | - | < 0.2 (-2) | < 6 | - | |
| 1016-B | 1585.15 | < 9.2 (-10) | - | < 9.7 (-2) | < 2 | - | |
| <u>Camp Century</u> | | | | | | | |
| 949 | 1215.1 | < 9.4 (-10) | - | < 1.3 (-2) | < 4.0 | - | |
| 955 | 1224.0 | < 16 (-10) | - | < 3.6 (-2) | < 68 | - | |
| 959 | 1230.2 | 45 \pm 5 (-10) | 4.7 | 2.6 \pm .3 (-2) | 8.3 | 42 | |
| 960 | 1231.7 | 17.4 \pm 2 (-10) | 12 | 0.95 \pm .1 (-2) | 3.9 | 19 | |
| 962-1-a | 1234.7 | 160 (-10) | 12 | 31 (-2) | (200) ³ | 1000 | |
| 962-1-b | 1234.7 | 3.15 \pm .35 (-10) | 11 | 20 \pm 2 (-2) | (130) ³ | 650 | |
| 962-2 | 1235.7 | 760 \pm 80 (-10) | 0.3 | 41 \pm 4 ² (-2) | 160 ² | 810 | |
| 969 | 1245.0 | < 23 (-10) | - | < 12 (-2) | < 340 | - | |
| 992 | 1278.9 | < 4.4 (-10) | - | < 11 (-2) | < 3.3 | - | |
| <u>Agassiz</u> | | | | | | | |
| Hol A | 105 | 12.8 (-10) | 17 | 0.052 (-2) | 1.7 | 8.5 | |
| Hol B | 110 | 18.7 (-10) | 11 | 0.077 (-2) | 1.0 | 5 | |
| Wisc. | 314 | 45 (-10) | 4.6 | 0.63 (-2) | 1.6 | 8 | |

¹ Assume crustal abundance of Sb is 0.2 ppm (Ronov and Yaroshevsky, 1972).

² Suspect that the high Sb value in this sample was due to contamination by the Sb standard.

³ [Update: Element concentration relative to total sample dust concentration is determined by assuming a dust concentration of 1.53 \pm 0.38 mg/lt for this sample.]

TABLE G-IX

NAA RESULTS FOR GLACIAL ICE DUST SAMPLES: BYRD STATION,
CAMP CENTURY, AND AGASSIZ ICE CORES

Tin (Sn)

| (1) Core Tube No. | (2) Log book Depth (m) | (3) Element Weight (grams) | (4) Filter Contribution (%) | (5) Concentration in ice ($\mu\text{g}/\text{lt}$) | (6) Concentration in dust (ppm) ¹ | (7) E.F. ³ |
|----------------------------|---------------------------------|-------------------------------------|--------------------------------------|---|---|--------------------------|
| <u>Byrd Station</u> | | | | | | |
| 422 | 700.8 | < 0.125 (-8) | - | < 0.019 | < 1090 | < 520 |
| 552 | 897.5 | 0.61 \pm .07 (-8) | 23 | 0.15 \pm .02 | 2260 | 1080 |
| 1016 | 1585.0 | < 0.46 (-8) | - | < 0.021 | < 58 | < 27 |
| 1016-B | 1585.15 | 0.65 \pm .36 (-8) | 28 | 0.68 \pm .39 | 16 | 7.6 |
| <u>Camp Century</u> | | | | | | |
| 949 | 1215.1 | 16.6 (-8) | 0.9 | 2.3 | 710 | 340 |
| 955 | 1224.0 | < 0.65 (-8) | < 22 | < 0.15 | < 280 | < 130 |
| 959 | 1230.2 | < 0.77 (-8) | < 54 | < 0.044 | < 14.2 | < 6.8 |
| 960 | 1231.7 | 1.07 \pm .13 (-8) | 24 | 0.059 \pm .006 | 24 | 11.4 |
| 962-1-a | 1234.7 | 4800 (-8) | < 0.01 | 920 | 60 \pm 15 ² | 286,000 |
| 962-1-b | 1234.7 | 146 (-8) | < 0.01 | 920 | 60 \pm 15 ² | 286,000 |
| 962-2 | 1235.7 | < 0.64 (-8) | < 41 | < 0.034 | < 14 | < 6.7 |
| 969 | 1245.0 | < 0.28 (-8) | < 57 | < 0.14 | < 420 | < 200 |
| 992 | 1278.9 | 9.1 (-8) | 2 | 2.2 | 690 | 330 |
| <u>Agassiz</u> | | | | | | |
| Hol A | 105 | 2.0 (-8) | 12 | 0.0082 | 26 | 12.4 |
| Hol B | 110 | 2.2 (-8) | 11 | 0.0091 | 12 | 5.7 |
| Wisc. | 314 | 6.7 (-8) | 3.6 | 0.094 | 24 | 11.4 |

¹ Concentration values are given in ppm except for samples 962-1-a and 962-1-b which are given in percent.

² Concentration has been set by assuming a total dust weight of 1.53 \pm 0.38 mg. See update at end of Chapter 8 for justification.

³ Assume crustal abundance of Sn is 2.1 ppm (Ronov and Yaroshevsky, 1972).

TABLE G-X

NAA RESULTS FOR GLACIAL ICE DUST SAMPLES: BYRD STATION,
CAMP CENTURY, AND AGASSIZ ICE CORES

Scandium (Sc)

| (1) Core Tube No. | (2) Log book Depth (m) | (3) Element Weight (grams) | (4) Filter Contribution (%) | (5) Concentration in ice ($\mu\text{g}/\text{lt}$) | (6) Concentration in dust (ppm) ¹ | (7) E.F. ¹ |
|----------------------------|---------------------------------|-------------------------------------|--------------------------------------|---|---|--------------------------|
| <u>Byrd Station</u> | | | | | | |
| 422 | 700.8 | 0.057 (-10) | 93 | 0.085 (-3) | 5.0 | 0.20 |
| 552 | 897.5 | 0.109 (-10) | 85 | 0.66 (-3) | 4.0 | 0.16 |
| 1016 | 1585.0 | 3.5 (-10) | 5.4 | 1.62 (-3) | 4.4 | 0.18 |
| 1016-B | 1585.15 | 2.8 (-10) | 3.5 | 30 (-3) | 0.68 | 0.027 |
| <u>Camp Century</u> | | | | | | |
| 949 | 1215.1 | 26 (-10) | 0.4 | 36 (-3) | 11.1 | 0.44 |
| 955 | 1224.0 | 2.5 (-10) | 3.6 | 5.6 (-3) | 10.7 | 0.43 |
| 959 | 1230.2 | 90 (-10) | 0.2 | 51 (-3) | 16.6 | 0.67 |
| 960 | 1231.7 | 49 (-10) | 0.3 | 27 (-3) | 10.9 | 0.44 |
| 962-1-a | 1234.7 | 3.55 (-10) | 2.3 | 6.8 (-3) | (4.4) ² | 0.18 |
| 962-1-b | 1234.7 | 0.122 (-10) | 1.3 | 7.7 (-3) | (5.0) ² | 0.20 |
| 962-2 | 1235.7 | 52 (-10) | 0.3 | 28 (-3) | 11.2 | 0.45 |
| 969 | 1245.0 | 0.79 (-10) | 13 | 4.1 (-3) | 11.8 | 0.47 |
| 992 | 1278.9 | 13.8 (-10) | 0.7 | 34 (-3) | 10.5 | 0.42 |
| <u>Agassiz</u> | | | | | | |
| Hol A | 105 | 85 (-10) | 0.2 | 3.5 (-3) | 11.0 | 0.44 |
| Hol B | 110 | 130 (-10) | 0.14 | 5.4 (-3) | 7.3 | 0.29 |
| Wisc. | 314 | 450 (-10) | 0.04 | 63 (-3) | 15.9 | 0.64 |

¹ Assume crustal abundance of Sc is 25 ppm (Ronov and Yaroshevsky, 1972).

² [Update: Element concentration relative to total sample dust concentration is determined by assuming a dust concentration of 1.53 \pm 0.38 mg/lt for this sample.]

TABLE G-XI
NAA RESULTS FOR GLACIAL ICE DUST SAMPLES: BYRD STATION,
CAMP CENTURY, AND AGASSIZ ICE CORES

| Hafnium (Hf) | | | | | | | | |
|---------------------|--------------------|------------------------|-------|-------------------------|-----------------|------|--------------------|-------------------|
| (1) | (2) | (3) | | (4) | (5) | | (6) | (7) |
| Core Tube No. | Log book Depth (m) | Element Weight (grams) | | Filter Contribution (%) | Concentration | | | E.F. ¹ |
| | | | | | in ice (µg/lit) | | in dust (ppm) | |
| <u>Byrd Station</u> | | | | | | | | |
| 422 | 700.8 | < 0.06 | (-10) | - | < 0.117 | (-3) | < 5.2 | < 1.9 |
| 552 | 897.5 | < 0.08 | (-10) | - | < 0.268 | (-3) | < 3.0 | < 1.1 |
| 1016 | 1585.0 | 20 | (-10) | 0.9 | 9.3 | (-3) | 25 | 8.9 |
| 1016-B | 1585.15 | 93 | (-10) | 0.1 | 980 | (-3) | 22.7 | 8.1 |
| <u>Camp Century</u> | | | | | | | | |
| 949 | 1215.1 | 7.3 | (-10) | 1.2 | 10.1 | (-3) | 3.1 | 1.1 |
| 955 | 1224.0 | 0.57 | (-10) | 13 | 1.28 | (-3) | 2.4 | 0.87 |
| 959 | 1230.2 | 24 | (-10) | 0.7 | 13.7 | (-3) | 4.4 | 1.58 |
| 960 | 1231.7 | 12.1 | (-10) | 1.3 | 6.6 | (-3) | 2.7 | 0.96 |
| 962-1-a | 1234.7 | 1.73 | (-10) | 4.0 | 3.3 | (-3) | (2.2) ² | 0.79 |
| 962-2 | 1234.7 | 13.5 | (-10) | 1.2 | 7.3 | (-3) | 2.9 | 1.03 |
| 969 | 1245.0 | 0.26 | (-10) | 31 | 1.33 | (-3) | 3.9 | 1.39 |
| 992 | 1278.9 | 4.3 | (-10) | 2.1 | 10.6 | (-3) | 3.3 | 1.16 |
| <u>Agassiz</u> | | | | | | | | |
| Ho1 A | 105 | 34 | (-10) | 0.5 | 1.39 | (-3) | 4.5 | 1.6 |
| Ho1 B | 110 | 49 | (-10) | 0.3 | 2.0 | (-3) | 2.7 | 0.98 |
| Wisc. | 314 | 134 | (-10) | 0.1 | 18.7 | (-3) | 4.7 | 1.7 |

¹ Assume crustal abundance of Hf is 2.8 ppm (Ronov and Yaroshevsky, 1972).

² [Update: Element concentration relative to total sample dust concentration is determined by assuming a dust concentration of 1.53±0.38 mg/lit for this sample.]

TABLE G-XII
NAA RESULTS FOR GLACIAL ICE DUST SAMPLES: BYRD STATION,
CAMP CENTURY, AND AGASSIZ ICE CORES

| Cesium (Cs) | | | | | | | | |
|---------------------|--------------------|------------------------|-------|-------------------------|-----------------|------|--------------------|-------------------|
| (1) | (2) | (3) | | (4) | (5) | | (6) | (7) |
| Core Tube No. | Log book Depth (m) | Element Weight (grams) | | Filter Contribution (%) | Concentration | | | E.F. ¹ |
| | | | | | in ice (µg/lit) | | in dust (ppm) | |
| <u>Byrd Station</u> | | | | | | | | |
| 422 | 700.8 | < 0.45 | (-11) | - | < 0.7 | (-4) | < 3.9 | < 1.5 |
| 552 | 897.5 | < 1.2 | (-11) | - | < 3 | (-4) | < 4.4 | < 1.7 |
| 1016 | 1585.0 | 14.4 | (-11) | 16 | 6.7 | (-4) | 1.8 | 0.69 |
| 1016-B | 1585.15 | 20.4 | (-11) | 6 | 215 | (-4) | 0.5 | 0.19 |
| <u>Camp Century</u> | | | | | | | | |
| 949 | 1215.1 | 79 | (-11) | 1.5 | 110 | (-4) | 3.4 | 1.29 |
| 955 | 1224.0 | 7.8 | (-11) | 15 | 17.5 | (-4) | 3.3 | 1.28 |
| 959 | 1230.2 | 430 | (-11) | 0.7 | 246 | (-4) | 7.9 | 3.1 |
| 960 | 1231.7 | 200 | (-11) | 1.5 | 110 | (-4) | 4.5 | 1.7 |
| 962-1-a | 1234.7 | 14.2 | (-11) | 6.5 | 27 | (-4) | (1.8) ² | 0.69 |
| 962-1-b | 1234.7 | 0.73 | (-11) | 2.6 | 46 | (-4) | (3.0) ² | 1.15 |
| 962-2 | 1235.7 | 235 | (-11) | 1.0 | 126 | (-4) | 5.0 | 1.9 |
| 969 | 1245.0 | 4.5 | (-11) | 34 | 23 | (-4) | 6.7 | 2.6 |
| 992 | 1278.9 | 44 | (-11) | 2.7 | 109 | (-4) | 3.3 | 1.28 |
| <u>Agassiz</u> | | | | | | | | |
| Ho1 A | 105 | 270 | (-11) | 1.0 | 11 | (-4) | 3.6 | 1.4 |
| Ho1 B | 110 | 490 | (-11) | 0.6 | 20 | (-4) | 1.5 | 0.58 |
| Wisc. | 314 | 1350 | (-11) | 0.2 | 189 | (-4) | 4.8 | 1.8 |

¹ Assume crustal abundance of Cs is 2.6 ppm (Ronov and Yaroshevsky, 1972).

² [Update: Element concentration relative to total sample dust concentration is determined by assuming a dust concentration of 1.53±0.38 mg/lit for this sample.]

TABLE G-XIII

NAA RESULTS FOR GLACIAL ICE DUST SAMPLES: BYRD STATION,
CAMP CENTURY, AND AGASSIZ ICE CORES

Lanthanum (La)

| (1) Core Tube No. | (2) Log book Depth (m) | (3) Element Weight (grams) | (4) Filter Contribution (%) | (5) Concentration in ice ($\mu\text{g}/\text{lt}$) | (6) Concentration in dust (ppm) | (7) E.F. ¹ |
|----------------------------|---------------------------------|-------------------------------------|--------------------------------------|---|--|--------------------------|
| <u>Byrd Station</u> | | | | | | |
| 422 | 700.8 | < 0.4 | (-9) | - | < 0.6 | < 10 |
| 552 | 897.5 | 4.4 | (-9) | 11.5 | 10.7 | 47 |
| 1016 | 1585.0 | 5.3 | (-9) | 10 | 2.5 | 1.9 |
| 1016-B | 1585.15 | 18.8 | (-9) | 6.0 | 198 | 1.3 |
| <u>Camp Century</u> | | | | | | |
| 949 | 1215.1 | 3.4 | (-9) | 15 | 4.7 | 0.42 |
| 955 | 1224.0 | < 0.7 | (-9) | - | < 1.6 | < 30 |
| 959 | 1230.2 | 14.0 | (-9) | 3.6 | 8.0 | 0.75 |
| 960 | 1231.7 | 7.6 | (-9) | 6.0 | 4.2 | 0.49 |
| 962-1-a | 1234.7 | < 0.4 | (-9) | - | < 0.8 | < (5) ² |
| 962-1-b | 1234.7 | 0.115 | (-9) | 7.8 | 7.3 | (48) ² |
| 962-2 | 1235.7 | 8.0 | (-9) | 6.0 | 4.3 | 17 |
| 969 | 1245.0 | < 0.4 | (-9) | - | < 2.1 | < 60 |
| 992 | 1278.9 | 1.48 | (-9) | 36 | 3.7 | 11 |
| <u>Agassiz</u> | | | | | | |
| Hol A | 105 | 16.8 | (-9) | 3.0 | 0.69 | 22.0 |
| Hol B | 110 | 33.2 | (-9) | 1.5 | 1.37 | 18.5 |
| Wisc. | 314 | 60.5 | (-9) | 0.8 | 8.4 | 21.3 |

¹ Assume crustal abundance of La is 34.6 ppm (Ronov and Yaroshevsky, 1972)

² [Update: Element concentration relative to total sample dust concentration is determined by assuming a dust concentration of 1.53 ± 0.38 mg/lt for this sample.]

TABLE G-XIV

NAA RESULTS FOR GLACIAL ICE SAMPLES: BYRD STATION,
CAMP CENTURY, AND AGASSIZ ICE CORES

Cerium (Ce)

| (1) Core Tube No. | (2) Log book Depth (m) | (3) Element Weight (grams) | (4) Filter Contribution (%) | (5) Concentration in ice ($\mu\text{g}/\text{lt}$) | (6) Concentration in dust (ppm) | (7) E.F. ¹ |
|----------------------------|---------------------------------|-------------------------------------|--------------------------------------|---|--|--------------------------|
| <u>Byrd Station</u> | | | | | | |
| 422 | 700.8 | < 0.24 | (-9) | - | < 0.35 | < 3.1 |
| 552 | 897.5 | 9.2 | (-9) | 6 | 22 | 51 |
| 1016 | 1585.0 | 11.4 | (-9) | 11 | 5.3 | 2.2 |
| 1016-B | 1585.15 | 59 | (-9) | 1 | 620 | 2.2 |
| <u>Camp Century</u> | | | | | | |
| 949 | 1215.1 | 5.6 | (-9) | 11 | 7.8 | 0.36 |
| 955 | 1224.0 | 0.9 \pm .3 | (-9) | 58 | 2.0 \pm .7 | 0.58 |
| 959 | 1230.2 | 40 | (-9) | 3 | 23 | 1.11 |
| 960 | 1231.7 | 22 | (-9) | 5 | 12 | 0.74 |
| 962-1-a | 1234.7 | 0.87 \pm .28 | (-9) | 58 | 1.7 \pm .5 | (1.11) ³ |
| 962-1-b | 1234.7 | 0.30 | (-9) | 3 | 19.2 | (125) ³ |
| 962-1 ² | 1234.7 | 1.17 \pm .28 | (-9) | 43 | 2.2 \pm .5 | (14.4) ³ |
| 962-2 | 1235.7 | 22.5 | (-9) | 5 | 12 | 0.72 |
| 969 | 1245.0 | < 0.74 | (-9) | - | < 3.8 | < 110 |
| 992 | 1278.9 | 3.6 | (-9) | 17 | 8.9 | 27 |
| <u>Agassiz</u> | | | | | | |
| Hol A | 105 | 28 | (-9) | 4.0 | 1.14 | 37 |
| Hol B | 110 | 36 | (-9) | 3.1 | 1.48 | 20 |
| Wisc. | 314 | 113 | (-9) | 1.0 | 15.8 | 40 |

¹ Assume crustal abundance of Ce is 66.4 ppm (Ronov and Yaroshevsky, 1972).

² Average of samples 962-1-a and 962-1-b.

³ [Update: Element concentration relative to total sample dust concentration is determined by assuming a dust concentration of 1.53 ± 0.38 mg/lt for this sample.]

TABLE G-XV
 NAA RESULTS FOR GLACIAL ICE DUST SAMPLES: BYRD STATION,
 CAMP CENTURY, AND AGASSIZ ICE CORES

Terbium (Tb)

| (1) Core Tube No. | (2) Log book Depth (m) | (3) Element Weight (grams) | (4) Filter Contribution (%) | (5) Concentration in ice ($\mu\text{g}/\text{lt}$) | (6) Concentration in dust (ppm) | (7) E.F. ¹ |
|----------------------------|---------------------------------|-------------------------------------|--------------------------------------|---|--|--------------------------|
| <u>Byrd Station</u> | | | | | | |
| 422 | 700.8 | < 0.33 (-11) | > 54 | < 0.49 (-4) | < 2.9 | < 2.4 |
| 552 | 897.5 | < 0.40 (-11) | > 110 | < 0.98 (-4) | < 1.5 | < 1.2 |
| 1016 | 1585.0 | 13.5 (-11) | 3 | 6.3 (-4) | 1.69 | 1.4 |
| 1016-B | 1585.15 | 66.2 (-11) | 0.37 | 697 (-4) | 1.61 | 1.4 |
| <u>Camp Century</u> | | | | | | |
| 949 | 1215.1 | 11.4 (-11) | 1.7 | 15.8 (-4) | 0.49 | 0.41 |
| 955 | 1224.0 | 2.07 (-11) | 11 | 4.7 (-4) | 0.88 | 0.75 |
| 959 | 1230.2 | 43.2 (-11) | 1 | 24.7 (-4) | 0.8 | 0.68 |
| 960 | 1231.7 | 24.6 (-11) | 1.7 | 13.5 (-4) | 0.55 ² | 0.47 |
| 962-1-a | 1234.7 | 0.97 (-11) | 16 | 1.87 (-4) | (0.12) ² | 0.10 |
| 962-2 | 1234.7 | 21.2 (-11) | 1.9 | 11.4 (-4) | (0.75) | 0.64 |
| 969 | 1245.0 | 0.47 (-11) | > 92 | < 2.4 (-4) | < 0.70 | < 0.59 |
| 992 | 1278.9 | 5.2 (-11) | 4 | 12.8 (-4) | 0.39 | 0.33 |
| <u>Agassiz</u> | | | | | | |
| Hol A | 105 | 25 (-11) | 1.6 | 1.0 (-4) | 0.33 | 0.28 |
| Hol B | 110 | 41 (-11) | 1.0 | 1.7 (-4) | 0.23 | 0.19 |
| Wisc. | 314 | 176 (-11) | 0.3 | 24.6 (-4) | 0.62 | 0.53 |

¹ Assume crustal abundance of Tb is 1.18 ppm (Ronov and Yaroshevsky, 1972).

² [Update: Element concentration relative to total sample dust concentration is determined by assuming a dust concentration of 1.53 ± 0.38 mg/lt for this sample.]

APPENDIX H

UPDATE:

DETERMINING THE INTENSITY OF SUPERWAVE COSMIC RAYS IMPACTING THE EARTH

Estimating Cosmic Ray Intensity Based on Vostok Be-10 Concentration Data

The relative cosmic ray intensity profile shown in Figure 8-B of chapter 8 was obtained by converting the ^{10}Be concentration values (C atoms/g) of Raisbeck et al.^(1, 2) into normalized ^{10}Be production rates (Φ atoms/cm²/yr) according to the formula: $\Phi = (C \cdot a \cdot \rho)/k$, where a is the variable ice accumulation rate at Vostok given in column 6 of Table H-I, $\rho = 0.917 \text{ g/cm}^3$ is the density of ice, and $k = 1.7 \times 10^5 \text{ atoms/cm}^2/\text{yr}$ is the Holocene ^{10}Be production rate average used to normalize the product.

Ice accumulation rates for Vostok (Table H-I, column 6) have been estimated throughout the core by the formula $a = \lambda \cdot \tau$, where λ is the estimated annual layer thickness of the ice (column 5) calculated using calendar dates assigned to various core depths (columns 1 & 3) and where τ is the correction for plastic deformation of the ice sheet (column 4). The correction for plastic deformation is calculated according to the nonlinear relation $\tau = (3740/(3740 - d))^{0.6}$, where 3740 is the present meter thickness of the ice sheet minus 17m and d is the sample depth in meters minus 17 m.

Calendar dates listed in column 1 were assigned to the Vostok ice core by correlating specific climatic features in the Vostok deuterium profile to climatic boundaries in the varve dated Cariaco Basin Gray Scale profile and to similar features in the NGRIP isotope profile dated according to the GICC05 ice core chronology.^(3, 4) An accumulation rate of 1.1 cm/yr has been arbitrarily assigned to the ice core depth interval 356 to 450 meters on the assumption that 31 meters of ice are missing from the record in this interval due to melting associated with Heinrich Event 1. If this assumption is not made the accumulation rate calculates to an abnormally low value in this section. Dates for corresponding boundaries in the NGRIP ice core are listed in column (2) up to 85.6 kyrs b2k. For depths 1439 meters and deeper the Vostok GT4 chronology was used with the exception that 1700 years were subtracted in the depth interval 1622 -1910 m which corresponds to the Eemian interglacial (Stage 6). This was done so that the Eemian would have a duration of 15,000 years to be in accordance with the varve count studies of Muller (1974, 1978), the GT4 chronology instead ascribing 16,700 years to this period.

Estimating Cosmic Ray Intensity Based on Byrd Station Be-10 Concentration Data

The ^{10}Be profile shown in Figure 8-C was obtained by converting the ^{10}Be concentration values (C atoms/g) of Beer et al.⁽⁵⁾ into normalized ^{10}Be production rates (Φ atoms/cm²/yr) according to the formula $\Phi = (C \cdot a \cdot \rho)/k$, where a is the variable ice accumulation rate at Byrd Station given in column 7 of Table H-II, and where $k = 1.68 \times 10^5 \text{ atoms/cm}^2/\text{yr}$ is the Holocene ^{10}Be production rate average used to normalize the product. Ice accumulation rates for Byrd Station (Table A-II, column 6) have been estimated throughout the core in the same fashion as for Vostok by the formula $a = \lambda \cdot \tau$, where λ (column 4) is the estimated annual layer thickness of the ice (cm/year) calculated from the calendar dates (column 1) that have been assigned to various core depths (column 3) and where τ is the correction for plastic deformation of the ice sheet (column 5). Calendar dates were assigned to the Byrd ice core by correlating specific climatic features in the Byrd oxygen isotope profile to climatic boundaries in the varve dated Cariaco Basin Gray Scale profile and for dates prior to 15 k yrs b2k to similar features in the NGRIP isotope profile dated according to the GICC05 ice core

Table H-I
 Chronology, Accumulation Rate Adjustments, and
 Climatic Zone Correlations for the Vostok Ice Core

| (1) | (2) | (3) | (4) | (5) | (6) | (7) | (8) | (9) |
|----------------------|------------|--------------|-------------------|---------------|----------------|---|---------------------|------------------------|
| kyrs b2k calendar | GICC 05 | DEPTH (m) | Deform Correc. | Ann. cm/yr | Accum. Rate | CLIMATIC Europe | PHASE N. America | CLIMATIC BOUNDARIES |
| 0 | 0 | | | | | | | |
| | | | | ---- | 2.42 | | | |
| 0.7 | 0 | 30 | | | | | | |
| 10.105 | | 251.5 | 1.02 | 2.36 | 2.40 | | | |
| 11.615 | | 282.5 | 1.042 | 2.05 | 2.14 | | | |
| | | | 1.047 | 1.25 | 1.31 | Y. Dryas ends | | H / LW |
| 13.01 | | 300 | 1.049 | 1.79 | 1.88 | Y. Dryas begins | | |
| 13.35 | | 306 | 1.052 | 2.14 | 2.25 | ACP begins | | |
| 14.75 | | 336 | 1.057 | 1.82 | 1.92 | Bölling begins, Cary/Port Huron Inter. begins | | |
| 15.85 | 17.0 | 356 | 1.07 | 1.03 | 1.1 | Pre-Bölling Inter. begins | | |
| 28.0 | 24.9 | 450 | 1.09 | 1.22 | 1.33 | | | |
| 38.5 | 35.6 | 580 | 1.13 | 1.34 | 1.52 | Denekamp Inter. Plum Pt. Inter. 2/3, LW/MW | | |
| 58.2 | 57.0 | 844 | 1.18 | 1.36 | 1.60 | Moershoofd Inter. Port Talbot Inter. 3/4, MW/EW | | |
| 64.7 | 63.4 | 920 | 1.19 | 1.11 | 1.32 | | | |
| 72.8 | 71.7 | 1010 | 1.23 | 1.44 | 1.77 | Börup Inter. | St. Pierre Inter. | |
| 85.4 | 85.6 | 1191 | 1.29 | 1.42 | 1.83 | | | 4/5, EW/S 5b/a |
| 102.9 | 102.9 | 1439 | 1.36 | 1.33 | 1.81 | | | 5e/d |
| 116.7 | 116.7 | 1622 | 1.43 | 1.89 | 2.71 | | | 6/5e |
| 125.7 | 126.6 | 1792 | 1.49 | 2.1 | 3.12 | | | |
| 129.9 | 131.3 | 1880 | 1.53 | 1.67 | 2.55 | | | |
| 131.7 | 133.4 | 1910 | 1.54 | 1.4 | 2.16 | | | S / I |
| 134.7 | 136.6 | 1945 | 1.58 | 0.96 | 1.52 | | | |
| 147.7 | 150.4 | 2070 | | | | | | |

Table H-II
Chronology, Accumulation Rate Adjustments, and
Climatic Zone Correlations for the Byrd Station Ice Core

| (1) | (2) | (3) | (4) | (5) | (6) | (7) |
|-------------------------------|-----------------------|----------------------|-------------------------------------|-----------------------------|--|---|
| kyrs b2k GICC5 calendar | NGRIP Depth (m) | BYRD Depth (m) | λ (cm yr ⁻¹) | Deform Correc. τ | Accum. Rate (cm yr ⁻¹) | Climatic boundary |
| -0.03 | | 0 | | | | |
| 11.60 | 1491 | 1093 | 9.45 | 1.32 | 12.4 | Younger Dryas Stad. ends |
| 12.10 | 1505 | 1115 | 4.40 | 1.96 | 8.6 | |
| 13.00 | 1527 | 1142 | 3.00 | 2.00 | 6.0 | Younger Dryas Stad. begins |
| 13.35 | 1540 | 1156 | 4.00 | 2.03 | 8.1 | |
| 14.18 | 1573 | 1207 | 6.14 | 2.08 | 12.8 | Intra Allerod Cold Peak begins Allerod |
| 14.75 | 1606 | 1242 | 6.14 | 2.17 | 13.3 | Older Dryas Stad begins |
| 15.00 | 1611 | 1252 | 4.0 | 2.22 | 8.9 | Bölling Inter. begins |
| 15.85 | 1637.5 | 1294 | 4.9 | 2.28 | 11.27 | Lista Stad. begins |
| 38.5 | 2050 | 1706 | 1.82 | 2.97 | 5.4 | Pre-Bölling Inter. begins |
| 45 | | 1854 | 2.28 | 4.79 | 11.2 | Denekamp Inter. (35k in GRIP) |
| 58.2 | | 2012 | 1.20 | 6.86 | 8.2 | Port Talbot-2 Inter. |
| 72.8 | | 2099 | 0.60 | 11.0 | 6.6 | |

chronology.^(3, 4) The depths were taken from the oxygen isotope profile of M. Blunier. Compared to the isotope profile published by Johnsen et al. (1972), and shown in Figure 8.1 (c), Blunier's profile is shifted by up to 12.5 meters toward deeper depths. The Be-10 data published by Beer et al. appear to be referenced to the Blunier isotope profile; see Figure H-1. So we use this as the reference profile for calculating Be-10 flux values.

The correction for plastic deformation of the ice sheet is calculated according to the linear relation $\tau = (2250/(2250 - d))$, where 2250 is the height of the ice sheet on the assumption that during the last ice age the ice sheet was 210 meters thicker than it is at present, and d is the sample depth. For the late Holocene (0 - 1093 m depth), 6 meters have been subtracted to figure the average accumulation rate as $a = 12.4$ cm/yr (for $\lambda = 1087$ m/11,570 years), which approximates the present ice accumulation rate at Byrd Station. The depths given in column 3 are uncorrected log book depths for the Byrd core as given in data of Blunier et al..

Ice Core Chronology and the Assumption of Synchronous Climatic Change

In correlating the Antarctic and Greenland ice core isotope profiles, we have assumed that major changes in climate occur contemporaneously in both the northern and southern hemispheres and hence that distinct climatic change boundaries evident in the NGRIP ice core may be matched up with similar boundaries in the Byrd Station and Vostok ice cores. The

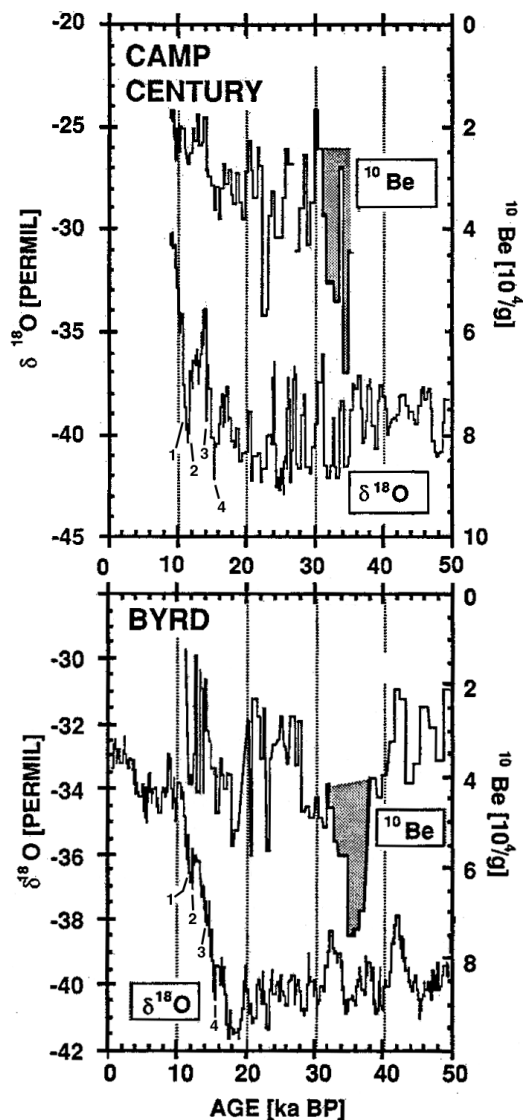


Figure H-1. The Byrd Station, Antarctica and Camp Century, Greenland Climatic profiles correlated by means of their ^{10}Be peaks (Beer et al., 1992). Note that the GICC05 chronology adopted in this update differs from that given above in this earlier diagram.

assumption that the Earth's climate warmed and cooled in a globally synchronous manner at the end of the last ice age is supported by evidence from dated land, sea, and ice climate profiles which show evidence that the Bölling/Alleröd/Younger Dryas oscillation occurred synchronously in both northern and southern latitudes (see chapter 9 of the dissertation (pp. 259 - 263).^(6 - 10)

The chronology adopted here for the Byrd core is consistent with that of Beer et al. which was obtained by correlating distinctive ^{10}Be concentration peaks found in both the Byrd Station, Antarctica and Camp Century, Greenland isotope records, some peaks dating as early as 12 – 20 kyrs BP; see Figure H-1.⁽⁵⁾ The Camp Century isotope profile, in turn, has been accurately dated through correlation with the annual layer dated Summit, Greenland isotope profile.⁽¹¹⁾ The Byrd oxygen isotope profile shows a progressive climatic amelioration beginning at a depth of 1290 meters which correlates with the beginning of the Pre-Bölling

warming (15,850 calendar years b2k) evident in the Summit, Greenland core, and which continues through the Bölling and Alleröd Interstadials. In the Vostok ice core this warming trend begins at a depth of 357 meters. The cooling evident in the Byrd ice core from 1156 to 1093 meters depth and in the Vostok ice core from 309.5 to 281 meters depth is termed the Antarctic Cold Reversal (ACR). This feature correlates with the Intra-Alleröd Cold Peak and Younger Dryas stadials combined together which in the Summit record and spans the period 13,350 to 11,650 calendar years b2k. This cool period is followed by a terminal warming correlative with the beginning of the Holocene PreBoreal in the Northern Hemisphere.

A substantial number of glaciologists hold the different opinion that the warming at the end of the ice age occurred asynchronously, beginning in the Southern Hemisphere 3000 years prior to its commencement in the Northern Hemisphere. They support their view by reference to the study by Blunier et al. which intercorrelated the Byrd and Summit ice core records using the rise in methane concentration at the end of the ice age as a common time marker.^(12, 13) However, there are a number of reasons to doubt the conclusion reached by that study:

- a) There is the substantial number of land and sea climatic data published over the past 20 years which when considered together leads convincingly to the conclusion that the northern and southern hemispheric climatic change was synchronous.
- b) There is also the paper by Beer et al. mentioned earlier which uses Be-10 peaks as common markers to correlate the Byrd Station, Antarctica and Camp Century, Greenland ice core records. With such markers there is no need to make model dependent assumptions about air bubble seal off depth as is necessary to do when using methane as a time marker. Note that in their scheme the ACR in the Byrd ice core aligns with the Younger Dryas stadial in the Greenland (features marked as 1 & 2 in Figure H-1).
- c) The study by Steig et al. used methane as a common time marker for correlating the Taylor Dome and GISP Summit, Greenland ice core chronologies.⁽⁹⁾ Their results indicate that the ACR in the Taylor Dome core was synchronous with the IntraAlleröd cold peak and Younger Dryas in the GISP core, contradicting the puzzling conclusions of Blunier that the ACR occurred 500 years earlier at Byrd Station and 1700 years earlier at Vostok. In an attempt to reconcile their results with those of Blunier, Steig et al. have made the speculative suggestion that the warming at Taylor Dome, although synchronous with Greenland some 35,000 kilometers to the north was delayed with respect to the Byrd and Vostok cores lying just several thousand kilometers away on the same Antarctic ice sheet. Thus we would be asked to believe that climate at Vostok cooled and then warmed up, that 1200 years later climate at Byrd Station (about 4000 km away) cooled and then warmed up in a similar fashion, and that 500 years later climate at Taylor Dome (about 2700 km from Byrd Station) similarly cooled and then warmed up again. This would require us to imagine some sort of exotic refrigeration mechanism proceeding at Vostok while the ice age was in the process of ending at Byrd Station, and cooling Byrd Station while the ice age was in the process of ending at Taylor Dome. Even greater age discrepancies are projected for the Bölling deglacial warming, being professed to begin in Vostok and Byrd Station around 17,000 to 18,000 years b2k and to begin at Taylor Dome about 3000 years later at 14,550 years b2k.

Clearly, such asynchronies in the local Antarctic climate are absurd. Moreover, such a suggestion runs counter to the findings of Mulvaney et al.⁽¹⁴⁾ Using Ca concentration to synchronize the Taylor Dome and Dome C ice core isotope profiles, they argue that at least the ACR feature occurred synchronously at both locations, hence that climate in various parts of Antarctica changed in a synchronous manner. This is supported by the evidence from Greenland, where the various ice core climate records are separated by similar distances yet are agreed to have undergone synchronous climatic change. By making the

Vostok, Dome C, and Byrd Station chronologies progressively younger for the period 14.5-19.5 kyrs BP into alignment with Steig's Taylor Dome chronology, ice would have had to be accumulating over this deglacial warming period at a faster rate than previously been supposed. However, this is entirely expected since ice accumulation rate is known to be high at times of warming (e.g., as seen in Greenland).

d) It should be kept in mind that the technique of using methane concentration for correlating ice cores has the inherent uncertainty that the difference in age between the sampled air bubbles and their surrounding ice matrix (Δ_{age}) is not a known measured quantity. The magnitude of this difference depends on the estimated rate of ice accumulation and on the estimated depth at which air became sealed off into bubbles when the firn compacted to form ice. The estimate of this seal-off depth can vary depending on a number of factors. The calculations, which must be done separately for each ice core, are model dependent and highly assumption laden. The resulting dating error is a greatest for cores such as Vostok which have relatively low ice accumulation rates. Such errors are evident in Blunier's paper which dates the beginning of the ACR at 13.8 kyrs BP at Byrd Station and at 15.0 kyrs BP at Vostok.

References

1. G. M. Raisbeck, et al., "Evidence for two intervals of enhanced ^{10}Be deposition in Antarctic ice during the last glacial period." *Nature* **326** (1987): 273–277.
2. G. M. Raisbeck, et al., " ^{10}Be deposition at Vostok, Antarctica during the last 50,000 years and its relationship to possible cosmogenic production variations during this period." In *The Last Deglaciation: Absolute and Radiocarbon Chronologies* (Proc. NATO ASI, vol. 12), edited by E. Bard and W. Broecker, pp. 127–139. Heidelberg: Springer-Verlag, 1992.
3. K. A. Hughen, et al. "Synchronous radiocarbon and climate shifts during the last deglaciation." *Science* **290** (2000):1951-1954.
4. A. Svensson, et al. "The Greenland ice core chronology, 15-42 ka. Part II. comparison to other records." *Quaternary Science Reviews* **25** (2006): 3258-3267.
5. J. Beer, et al., " ^{10}Be peaks as time markers in polar ice cores." In: E. Bard and W. Broecker (Editors) *The Last Deglaciation: Absolute and Radiocarbon Chronologies* (Proc. NATO ASI Series, vol. 12). Springer-Verlag, Heidelberg, pp. 140–153, 1992.
6. P. A. LaViolette, *Galactic Explosions, Cosmic Dust Invasions and Climatic Change*, Ph.D. dissertation, Portland State University, Portland, Oregon, 763 pp., 1983.
7. P. A. LaViolette, "Cosmic-ray volleys from the Galactic Center and their recent impact on the Earth environment." *Earth Moon Planets* **37** (1987):241–286.
8. P. A. LaViolette, *Earth Under Fire*, Starlane Publications, Alexandria, VA, 1997.
9. E. J. Steig, et al., "Synchronous climatic changes in Antarctica and the North Atlantic," *Science* **282** (1998):92–95.
10. P. A. LaViolette, "Evidence for a global warming at the termination I boundary and its possible cosmic dust cause." 2005); eprint at: arxiv.org/abs/physics/0503158.
11. S. J. Johnsen, et al., "Irregular glacial interstadials recorded in a new Greenland ice core." *Nature* **359** (1992):311–313.
12. T., Blunier, et al., "Asynchrony of Antarctic and Greenland climate change during the last glacial period." *Nature* **394** (1998):739–743.
13. T. Blunier and E.J. Brook, "Timing of millennial-scale climate change in Antarctica and Greenland during the last glacial period." *Science* **291** (2001): 109–112.
14. R. Mulvaney, et al. "The transition from the last glacial period in inland and near-coastal Antarctica." *Geophysical Research Letters* **27** (2000):2673–2676.

APPENDIX J

2005 **UPDATE:**

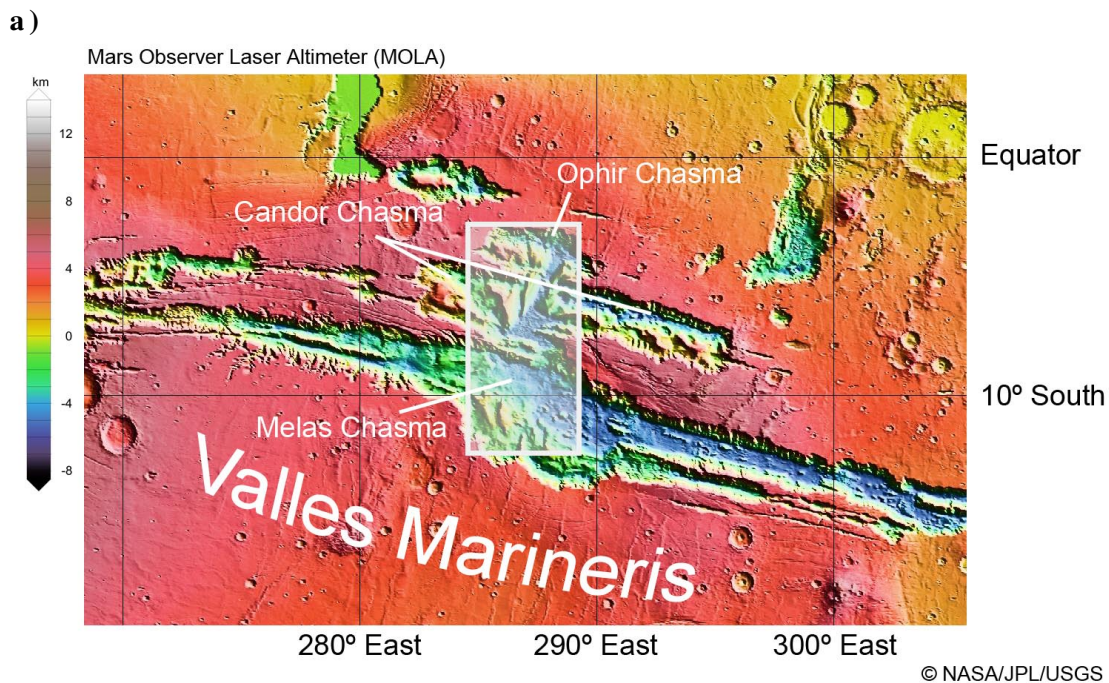
Parts taken from P. LaViolette, *Earth Under Fire* (Rochester, VT: Bear & Co., 2005), ch. 6.

THE CANYONS OF MARS

Giant coronal mass ejections issuing from the Sun during its T Tauri phase would also have impacted Mars as well as the Earth and Moon. The planet's almost negligible magnetic field would have offered it little protection. Upon contacting Mars' surface, this hot coronal plasma would have caused the upper permafrost layer to rapidly melt, releasing floods of water, not in one place, but over much of Mars' surface [see pp. 139 -40]. This could explain the immense outflow channels and canyons seen primarily within 40° of Mars' equator. Studying early photos taken by the Mariner and Viking spacecraft, geologist Victor Baker noted in 1978 that the morphology of these outflow channels resembles land features on Earth which have been cut by catastrophic floods, such as the Missoula glacial meltwater flood that carved out the Channeled Scablands of eastern Washington about 14,500 years B.P.¹ Many of the Martian outflow channels, however, are considerably larger. By one estimate, the floods that formed some of them would have reached as high as one cubic kilometer per second, or ten thousand times the mean discharge rate of the Amazon river.² Baker has concluded that floods on Mars, and the warm climate associated with them, have occurred right up to recent times.³

Missions completed between 1997 and 2005 have provided a wealth of high-definition photographs of Mars' surface. For example Figure J-1 (a) presents an altimeter map of a portion of the 4000 kilometer-long Valles Marineris which is located just south of the equator. This is the largest system of canyons on Mars, three times longer and four times deeper than the North American Grand Canyon. It originates in the Martian highland area to the west (the map's left) and empties into a basin to the east which connects with the large flat lowland region in the north which at one time may have been an ocean during a warmer past. Figure J-1 (b) presents a northward-looking perspective view of the chasm's 300 kilometer-wide central portion (3° - 13°S, 284° - 289°E). The canyon floor seen here lies up to 8 kilometers below the surrounding Martian plateau. Melas Chasma is seen in the foreground, Candor Chasma further to the north; and beyond that Ophir Chasma. Figure J-2 shows an aerial close-up of a precipice outcrop located at the eastern end of Candor Chasma (8°S, 295°E). What appears to be a frozen meltwater river is seen hugging the bottom of the ravine.

Careful study of these photos and of images of other gorges and valleys on Mars has led planetary geologists to the unanimous conclusion that these features have been formed by floods. Still, they have been puzzled by their existence, wondering where the water came from and how was it able to flow on Mars' surface since present conditions on Mars do not permit water to exist in liquid form. During the course of a Martian summer, day temperatures on average vary between -140° to 20° Centigrade. So, on Mars, water should for the most part remain frozen. Windblown salts mixed in with the ice would allow ice to melt at subzero temperatures and solar radiation absorbed by dust covering its surface would provide enough warmth to cause a minimal amount of melting during summer daylight hours. But, space scientists have had difficulty explaining how water could have been produced in sufficient quantities to have carved these features. They also have wondered how it would have stayed liquid long enough to have journeyed the hundreds of kilometers through these gorges. The atmospheric pressure on Mars is only 6 millibars, less than one percent of what it is on Earth, and at such low pressures ice sublimates when heated, bypassing the liquid phase to change directly to vapor. Due to the rapid boiling that would occur at



b)

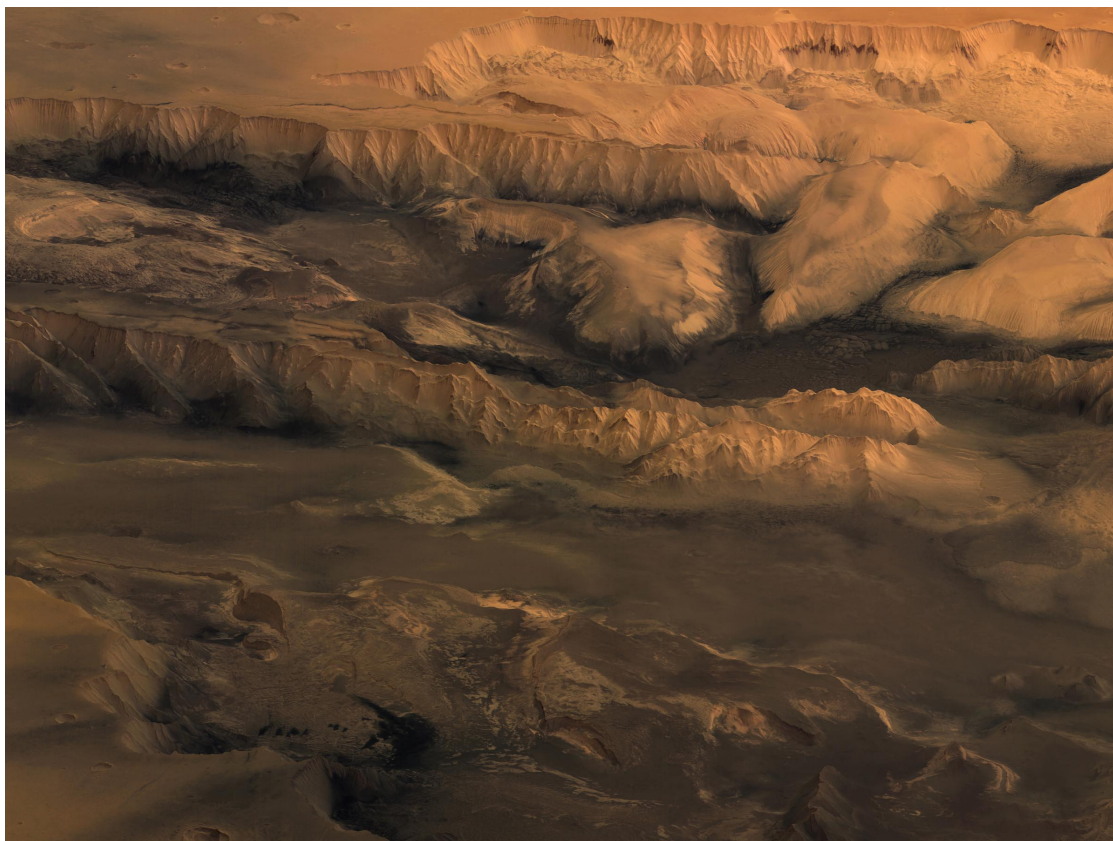


Figure J-1. a) A map showing part of the Valles Marineris generated with the Mars Observer Laser Altimeter (MOLA) (photo courtesy of NASA, JPL, USGS). The rectangle indicates the region imaged in (b) below. b) A 300 kilometer-wide perspective view of the valley's central region from an image taken by the Mars Express spacecraft (photo courtesy of ESA, DLR, FU Berlin, and G. Neukum).

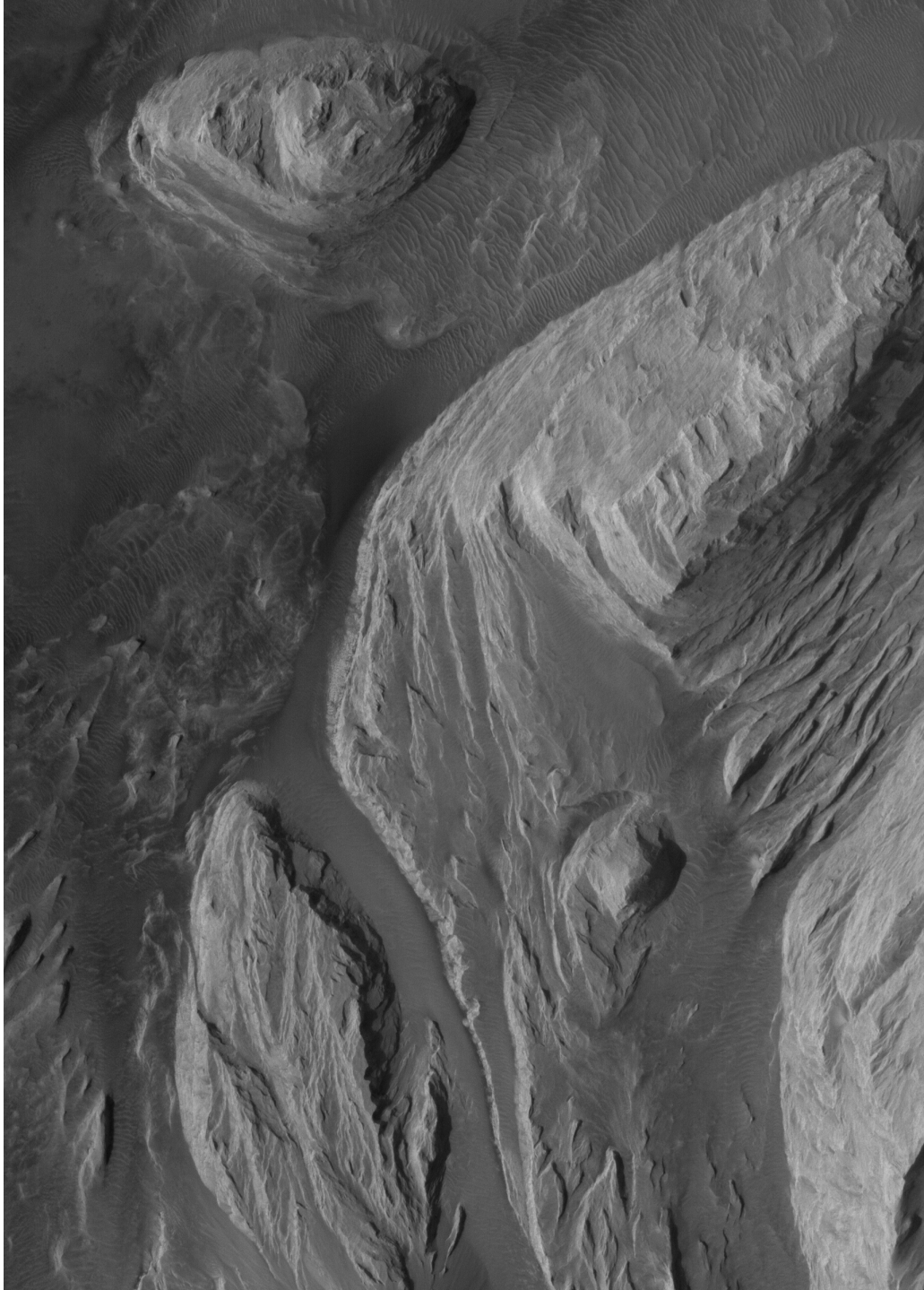


Figure J-2. Canyon outcrop in East Candor Chasma showing what may be a frozen river at the foot of the stratified precipice. Image size is about 3 km by 4 km (photo courtesy of NASA, JPL, and Malin Space Science Systems).

these low pressures, the water surface would cool and freeze over, and as a result, its ability to move would be severely restricted.

In the late 1970's several theories had been put forth to account for the outflow channels evident in the Viking spacecraft photos—icy comets striking the surface of the planet, water kept liquid by geothermal heat, and suddenly bursting to the surface as a gigantic artesian spring, or volcanic melting of surface ice. But, it is highly unlikely that such events would supply water at the required rates or could have recurred so often to account for the hundreds of canyons and channels scattered across most of Mars' surface.

The mystery becomes easily solved when two things are realized. First, the surface of Mars is not arid, as had previously been supposed, but is almost completely covered in water currently locked up in the form of ice sheets and glacial permafrost. Second, the Sun and solar system have not always been as they are today; as recently as 10 to 16 thousand years ago, the Sun was much more luminous and active and the solar system was incubating within a cocoon of interstellar dust injected by a passing superwave. Mars, like the Earth, was then receiving more solar radiation than it does today, both from the increased heat output from the flaring Sun and from the interplanetary hothouse effect produced by the invading dust. This would have softened the upper surface of the Martian permafrost and formed vast subsurface lakes. The surface temperature would have risen especially fast if Mars had been engulfed by a large mass of coronal gas.

This solar radiation theory would explain why there are so many of these outflow features scattered over the surface of Mars with canyons tending to occur most frequently near the equator, the region receiving the greatest insolation. It also would account for the large size of the headwater regions, which are seen to cover tens of thousands of square kilometers, and for the observation that their origins tend to have abrupt beginnings without feeding tributaries. Finally, it would explain why these flood features are relatively young, their youth being indicated by the fact that they cut across older, extensively cratered terrain and are, themselves, virtually crater free.

The elevated temperatures would not only have caused these ice and permafrost sheets to melt, but the large amounts of water vapor released into the atmosphere would have raised the atmospheric pressure sufficiently to keep the resulting meltwater stable in liquid form. For example, if just one meter of ice were to have sublimated or evaporated from the planet's surface and remained in a gaseous state, the atmospheric pressure would have risen to about 0.1 atmospheres which would have allowed surface water to remain liquid anywhere from its freezing point up to a temperature of 65° C. Furthermore, fog banks and clouds formed by the evaporating water would have created a greenhouse effect, retarding night-time heat loss from the planet's surface. This would have acted to increase the planet's temperature and moderate its diurnal temperature extremes. These warmer climatic conditions could explain the presence of lacustrine terraces and Gilbert-type deltas on Mars' surface. Ori et al. have noted that these features could only have been formed if lakes had persisted on Mars' surface for 10^3 to 10^4 years.⁴

Recent spacecraft data has established that water ice covers Mars' North polar cap to a maximum depth of 3 kilometers over an area about 1200 kilometers across, a region about the size of Greenland; see Figure J-3. The ice cap is seen to be dissected by canyons and troughs up to one kilometer deep, suggesting that this relatively young polar ice sheet has been subject to recent melting.

Measurements made remotely by the Odyssey spacecraft to probe the composition of the upper one meter of Mars' surface indicate that Mars is covered with a layer of water-rich permafrost. These measurements suggest that the uppermost few centimeters or so may be dry soil with no ice, transitioning down into a layer several centimeters thick in which ice fills the pore spaces between the soil grains. Finally, beneath that would be a very ice-rich layer. The upper layers are drier because the ice there has sublimated away due to surface heating

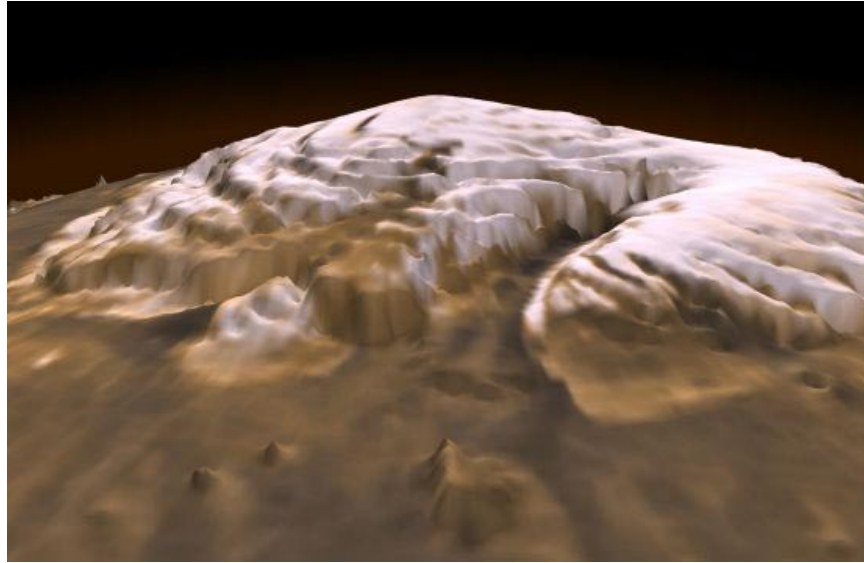


Figure J-3. A perspective view of Mars' North polar ice cap based on altitude measurements made with the Mars Observer Laser Altimeter (MOLA). The vertical dimension has been purposely exaggerated (photo courtesy of the MOLA team, MGS project, NASA, and Greg Shirah (SVS)).

of the soil. The overlying dust blanket that remains acts to insulate and protect the underlying ice from further sublimation. They estimate that for regions lying between 55° latitude and either pole, the uppermost meter contains 60% to nearly 100% water ice, while for regions lying between 55° latitude and the equator the upper meter would be comparatively drier, averaging 2% to 10% water by weight (or $\sim 5\%$ to $\sim 35\%$ water by volume). Since the equatorial region receives more insolation, the upper soil layer here would sublimate water at a faster rate which would explain why it is observed to be drier.

The bulk of the permafrost lying below the upper meter, not directly accessible to observation, would likely exceed 75% water-ice at all latitudes. William Feldman, one of the Odyssey team investigators, has speculated that the depth of the Martian permafrost could range anywhere from one meter to a kilometer or more.⁵ The upper end of this depth estimate may be closer to the truth. Craters over 5 kilometers in diameter have fluidized ejecta which indicates the presence of water or water-ice in the crust, consisting of permafrost possibly to a depth of one kilometer with liquid water below that.

Extrapolating from these observations, we come to realize that the plateau seen in Figure J-1-b is not rock, but ice; it is the upper surface of the permafrost ice sheet that covers much of Mars. The canyons would be places where this ice sheet has been dissected by melting that took place in the past on a grand scale. The outflow that carved this system of canyons did not originate at just one location; it came from the canyon's entire perimeter, generated as its very walls liquefied under the Sun's intense radiation. Meltwater may also have come from the surrounding permafrost plateau to contribute groundwater torrents that would have spilled from beneath the canyon's rim. The same warming event would have carved the canyons that currently transect the polar caps. Also seen from this perspective, perhaps the outcropping shown in Figure J-2 is not composed just of sedimentary rock as some geologists have suggested. It too might be part of the permafrost ice sheet, its low albedo, dust strewn surface camouflaging the dirty ice that lurks within. Raise Mars' daytime temperature some tens of degrees and torrents would pour from its walls into the river below.

In February of 2005 the Mars Express team reported discovering an entire frozen sea

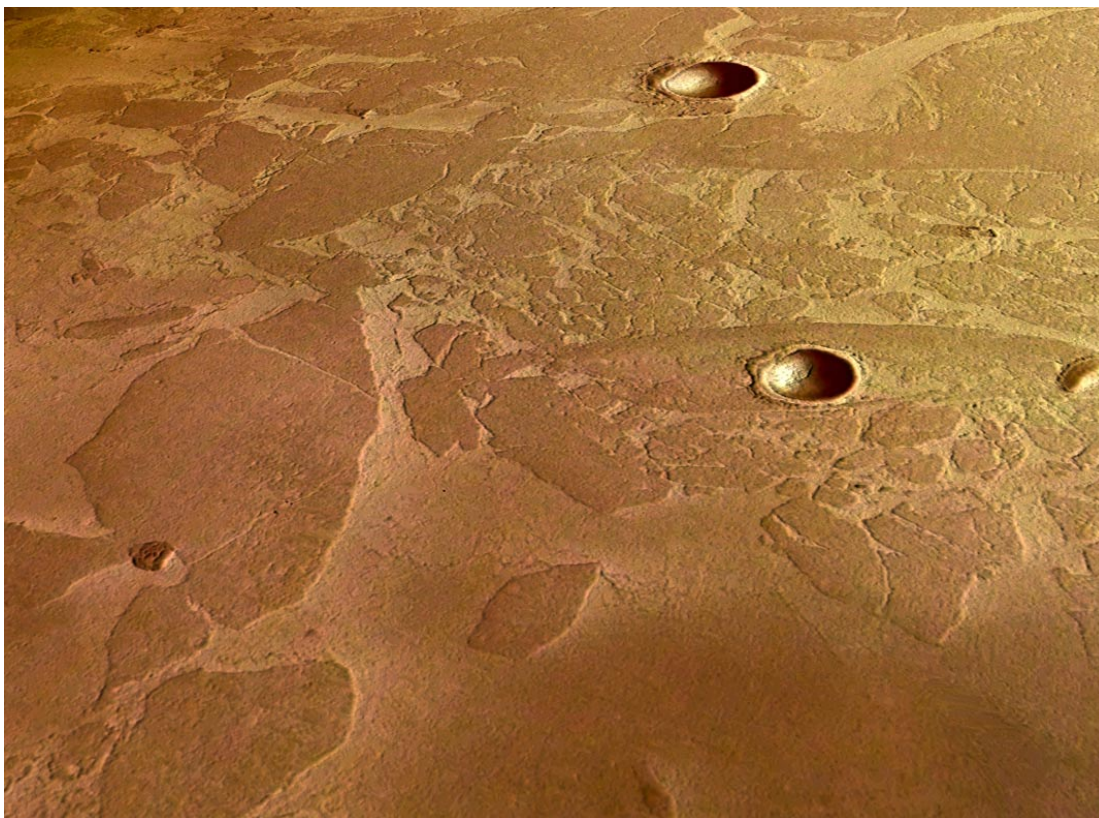


Figure J-4. Part of a frozen sea in Elysium Planitia (5° N, 150° E). Image width is a few tens of kilometers (photo courtesy of ESA, DLR, and FU Berlin/G. Neukum).

near Mars' equator in a region called Elysium Planitia, part of which is imaged in Figure J-4. This body of water ice measures 800 by 900 kilometers in extent and is estimated to be 45 meters deep. Members of the Mars Express mission have concluded that the water entered this sea in a catastrophic flood. The irregular plates seen in Figure J-4 appear to be pack ice or icebergs that at one time had been swept along in this immense outflow and were later immobilized when the surrounding water froze over.

One thing that has puzzled scientists is why water ice is found at such low latitudes on Mars. Their models predict that ice should be found at Mars' poles, but not at its equator. They have come to conclude that Mars' current permafrost distribution reflects a state of disequilibrium, that the planet is in the process of emerging from an ice age and will eventually attain equilibrium as water sublimates from its equator to its poles. Furthermore, they wonder how the ice became deposited in these low latitudes in the first place. Mars' present thin, frigid atmosphere might be able to precipitate thin frost covers, but certainly nothing of the extent required to build ice sheets.

The picture changes entirely when we realize that there was a time some ten thousand years ago, and on numerous other occasions prior to that, when the solar system was filled with light scattering dust particles and when the Sun was in a highly energized, T Tauri state. Mars climate would then have warmed to the point where its surface ice would have begun to rapidly melt and evaporate. Its newly created vaporous atmosphere, and the resulting high winds, would have transported immense amounts of water over the entire planet to precipitate in the form of snow, sleet, and hail during each year-long winter season. The melting that produced Mars' canyons would have most likely occurred during its summer seasons.

The Earth has been in an ice epoch for the past three million years, due to the solar

system's passage through an unusually dusty interstellar environment. The same would apply to Mars. However, whereas the Earth has sometimes been able to experience periods during which its ice sheets receded to its poles, as during the current interglacial, Mars has not been as quick to respond. Once formed, its equatorial permafrost would persist for a very long time. During the respite following a superwave's passage when the Sun has returned to its normal state and swept the solar system clean of invading dust, Mars' climate would cool down and its atmosphere would return to its current low pressure state. But, unlike on Earth such conditions are not favorable to ice sheet recession. So the permafrost sheets that we currently see on Mars are about the same extent that they were ten thousand years ago, and are likely the result of three million years of accumulation. Similarly, its canyons would not have been carved by conflagrations occurring during just one T Tauri interval, but over a hundred or more such intervals occurring over the past three million years.

Spacecraft photos show that the walls of Mars' canyons are currently in the process of melting, but at a relatively subdued rate. For example, Figure J-5 shows a Mars Express image of the north wall of Tithonium Chasma (5.5°S, 280.5° E), a canyon that makes up one branch of the Valles Marinaris complex. The vertical pleats that extend down the face of the scarps are actually large gullies. It is the general consensus that these have been formed by ground water issuing from near the top of the cliff and that they are relatively recent, the erosional process continuing even today. The discharges forming them may be due to sudden releases rather than to a continuous outflow. From the length of the streaks it appears that the resulting meltwater outflow is able to travel downward a distance of several kilometers before totally dissipating either due to evaporation or refreezing.

Judging from the width of the photo which spans 40 kilometers, we see that the apron sloping up the canyon wall has a breadth of about 6 kilometers, and from its grade we may conclude that the canyon floor lies about 4 kilometers below the plateau, i.e., below the upper surface of the permafrost ice sheet. The hummocky terrain covering the canyon floor would most likely be the exposed underlying bedrock which seems to be covered over with a thin layer of permafrost. It is difficult to say whether the adjacent permafrost sheet similarly has a depth of 4 kilometers or whether it overlies several kilometers of drier soil which flood waters had eroded away when they carved the canyon. Similarly, in regard to the central part of the Valles Marinaris shown in Figure J-1 (b) where the canyon floor is seen to lie about 8 kilometers below the surrounding plateau, we cannot say for sure what is the true thickness of the permafrost layer. Such questions hopefully will be answered by radar measurements carried out during the latter half of 2005 by the Mars Express.

Also seen in Figure J-5, the canyon walls begin with a precipitous drop from their upper edge and about 5% of the way down change to a more gradual slope as the erosional apron is encountered. The apron is most likely composed of refrozen meltwater that has accumulated from the dust-laden runoff. Its surface would be protected by a dust layer due to the combined processes of ice sublimation and aerial dust deposition. The cliff edge above the apron appears to be the region where melting is currently active, the permafrost ice there presumably being directly exposed to the Sun. Originally, the precipice would have been positioned close to where the foot of the apron now lies. Then, over the years, it would have progressively receded and the apron would have gradually climbed upward forming an increasingly greater part of the canyon wall. If the most recent floods to pass through this canyon occurred about 10,000 to 16,000 years ago, then this apron forming process would have been proceeding since that time and the cliff wall would have receded approximately 3 kilometers during this time. This suggests that the permafrost surface has melted back at the rate of approximately 30 centimeters per year. By comparison, glaciers in Alaska are known to recede at rates of 10 to 300 meters per year. The recession rates would be lower on Mars due to its cooler average temperature and lower level of insolation.

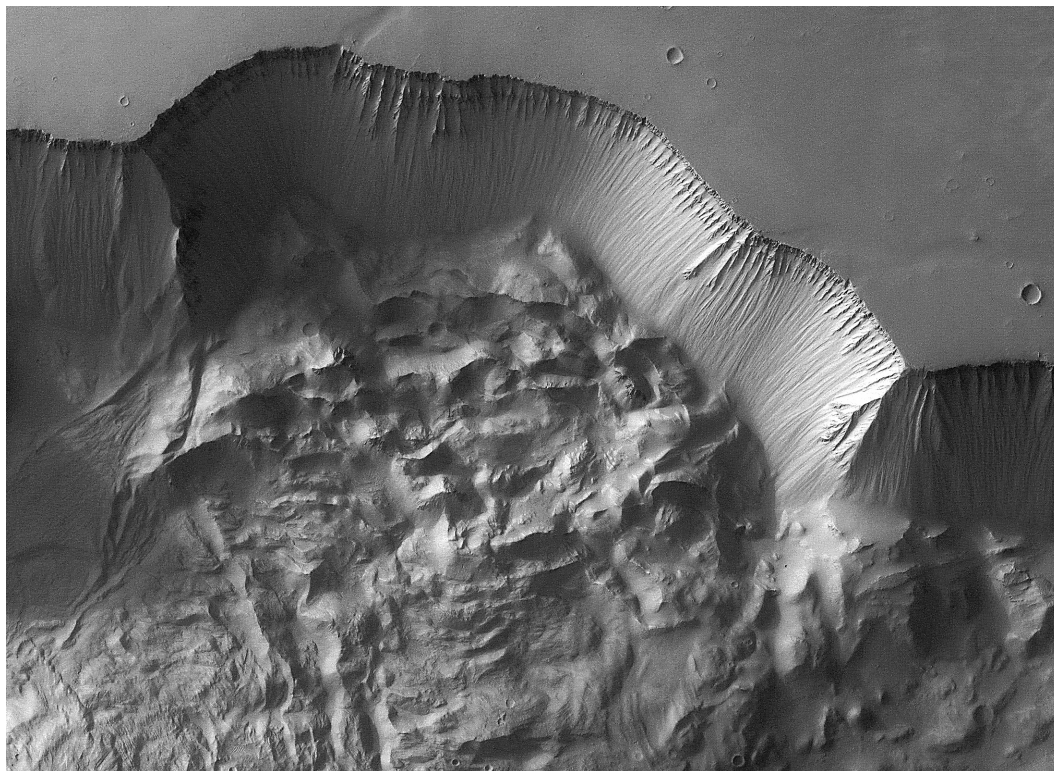


Figure J-5. A view of the North face of Tithonium Chasma taken by the Mars Express. Image width is 40 kilometers (photo courtesy of ESA, DLR, and FU Berlin/G. Neukum).

Closer views of Martian gullies are seen in Figures J-6 and J-7. Figure J-6 is a Mars Global Surveyor photo showing gullies cut in the wall of a Newton Basin crater located in Sirenum Terra (42°S, 202°E). Erosional aprons are seen to have formed on the crater's wall below the point of meltwater discharge. The viscous flows resembling oozing ice cream, which are apparent in the lower part of the photo, may be glaciers formed on the crater's lower slopes. Figure J-7 is a two-kilometer-wide close up view of gullies that are eroding the side of another Sirenum Terra crater located at 39°S, 194°E. The meltwater runoff appears to have accumulated in a thermokarst lake whose surface may likely be frozen over; see lower right of photo. Other images of gullies are shown in Figures J-8 and J-9.

In summary, as data flows in from recent spacecraft missions to Mars, it becomes increasingly apparent that, like the Moon, Mars' surface has undergone very strong heating in the geologic recent past.

References

- 1.. V. R. Baker, "The Spokane Flood controversy and the Martian outflow channels," *Science* **202** (1978): 1249–1256.
2. M. H. Carr, "The geology of Mars," *American Scientist* **68** (1980): 626-635.
3. V. R. Baker, "Water and the martian landscape." *Nature* **412** (2001): 228-236.
4. G. G. Ori, L. Marinangeli, and A. Baliva, "Terraces and Gilbert-type deltas in crater lakes in Ismenius Lacus and Memnonia (Mars)," *Journal of Geophysical Research* **105** (2000):17629-17641.
- 5.. "Mars emerging from ice age, data suggest." space.com/scienceastronomy/mars_ice-age_031208.html.

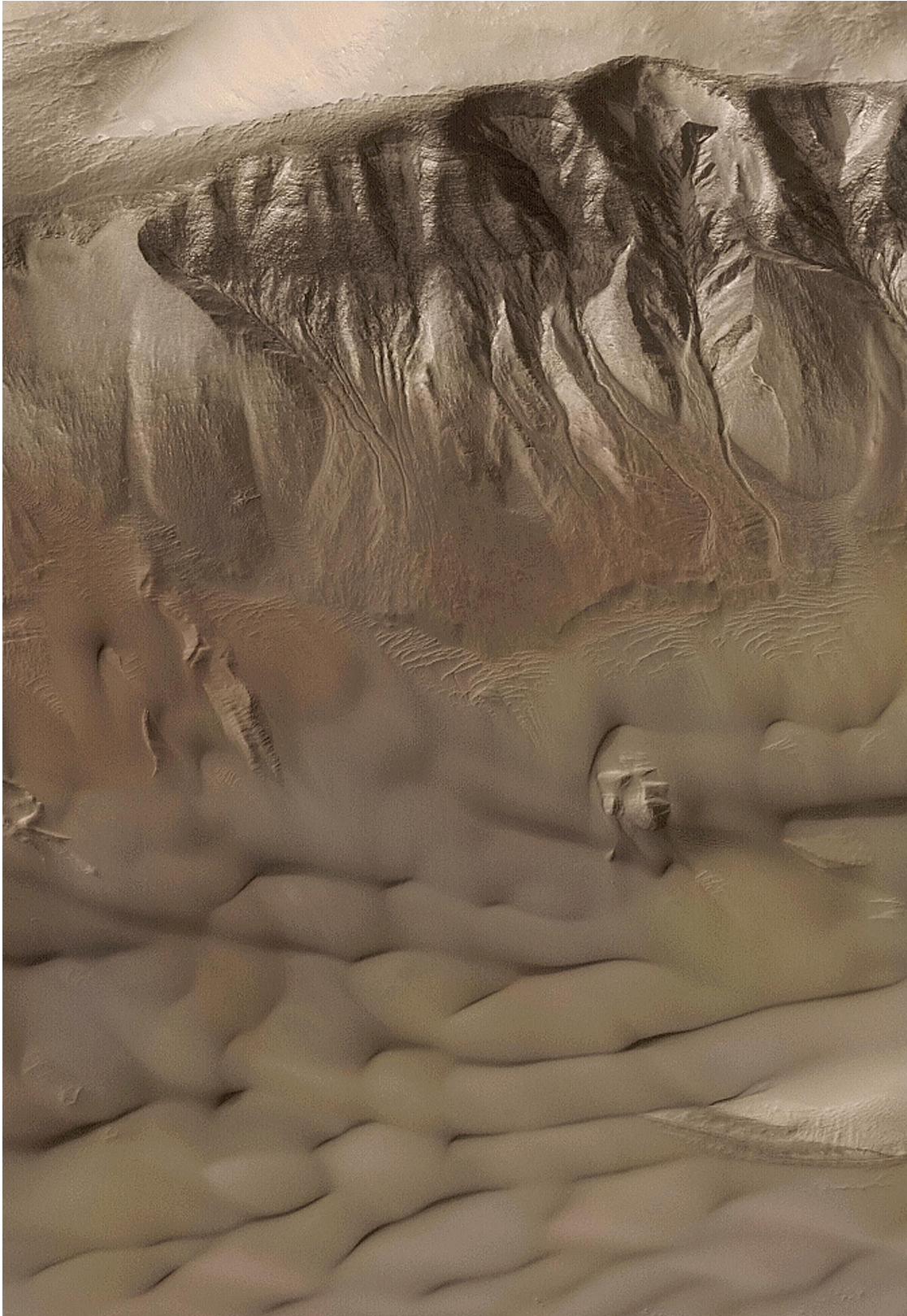


Figure J-6. Thermokarst gullies cut in the wall of a Newton Basin crater located in Sirenum Terra (42.4°S, 201.8°E) (photo courtesy of NASA, JPL, and MSSS).



Figure J-7. Gullies in the wall of another Sirenum Terra crater (39.0°S, 193.9°E) (photo courtesy of NASA, JPL, and MSSS).

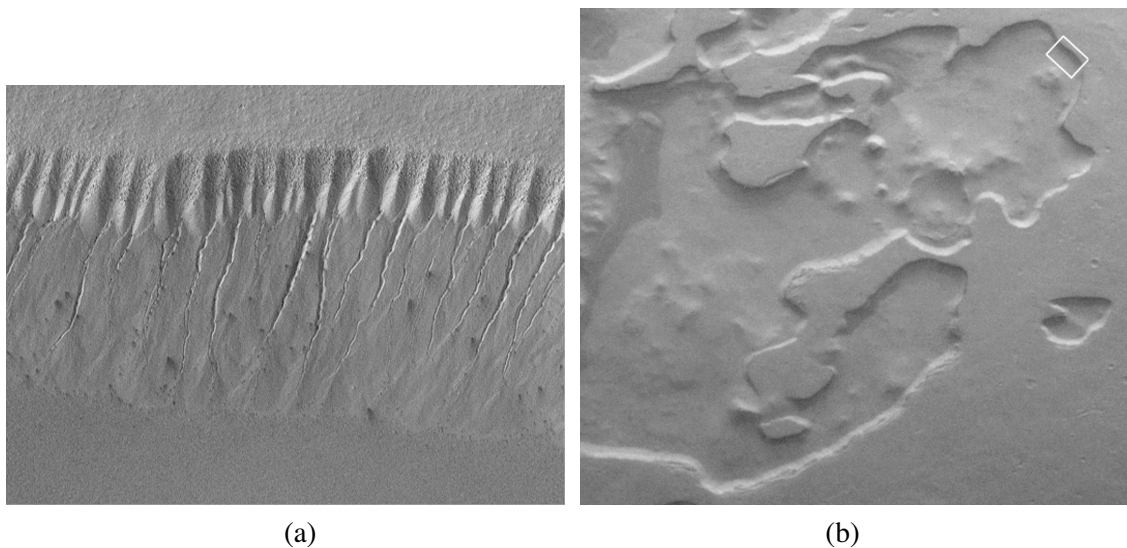


Figure J-8. a) Mars Orbiter Camera showing gullies in an escarpment located in the Southern polar region (70.7° S, 355.7° W). b) Viking 2 orbiter context view of this region. The escarpment image comes from region marked by the white box (photos courtesy of NASA, JPL, and MSSS)



Figure J-9. Cliff gullies in Aram Chaos located near Ares Vallis (photo courtesy of NASA, JPL, and MSSS).

NATIONAL SECURITY COUNCIL
WASHINGTON, D.C. 20506

May 10, 1985

Dear Mr. LaViolette,

Thank you for your letter and enclosure dated May 1, which I received by hand when I was in Portland last week.

I appreciate your bringing to my attention the issue of Galactic Superwaves and their possible EMP effects.

As you may know, President Reagan initiated, in 1981, a major program to improve the command and control (C³I) capability over the strategic forces of the United States with particular attention being given to the matter of EMP effects.

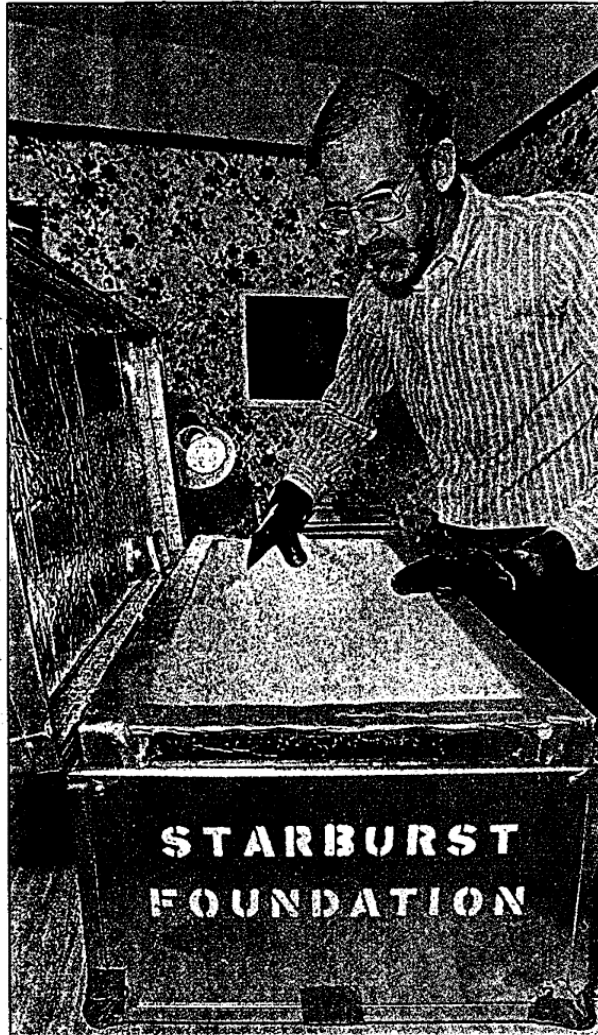
You may be sure I shall share your one-page paper with the appropriate individuals at the National Security Council and at the Department of Defense.

Sincerely,



Christopher M. Lehman
Special Assistant to the
President for National
Security Affairs

Mr. Paul A. LaViolette
2166 N.E. Clackamas Street, #2
Portland, OR 97232



The Oregonian/RANDY WOOD

Paul LaViolette, who is picking up Antarctic ice-core samples in The Netherlands this week, carefully prepares a container in which he planned to transport the samples to Denver.

Scientist to test galaxy theory with Soviet ice

By RICHARD HILL
of The Oregonian staff

A Portland researcher outside the "mainstream" U.S. science community is scoring a coup this week in The Netherlands.

Paul A. LaViolette is in Rotterdam picking up 16 ice-core samples from Vostok, the Soviet Union's year-round base in Antarctica. He is the first American to receive Vostok ice samples directly from the Soviets.

The 40-year-old scientist hopes the samples will help in researching his theory about what he terms "superwaves" from the center of the galaxy and the impact he thinks they could have on Earth.

The Soviets, using a new thermal technique, obtained the core by drilling more than 7,200 feet — the deepest ever drilled into the Antarctic ice. Ice-core samples are especially valuable to scientists because air bubbles and particulates become trapped in the ice, allowing researchers to look at what atmospheric conditions existed in the past — in this case, more than 160,000 years ago through the last Ice Age that ended about 12,000 years ago.

LaViolette received a telegram May 20 requesting that he pick up the samples this week in Rotterdam from the Akademik Fedovov, a Soviet research vessel.

"I was very surprised when I found out that they were going to let me have the samples," said LaViolette, who managed to obtain approval for the ice transfer after writing the scientific attaché with the Soviet Embassy in Washington, D.C. Three previous letters to the Soviet institute in charge of the Antarctic base had gone unanswered, he said.

"It's absolutely amazing that he got these samples, a real coup," said Todd K. Hinkley, a geologist with the U.S. Geological Survey in Denver who plans to analyze the samples in his high-tech government laboratory.

Please turn to
GALAXY, Page E2

SCIENCE

Galaxy: LaViolette requests fellowship to study ice samples

■ Continued from Page E1

LaViolette is scheduled to turn the ice over Saturday to Hinkley, who will store the samples until final arrangements for the analysis can be worked out.

To study the ice-core samples, Hinkley hopes that LaViolette will be able to obtain a national research fellowship from the National Research Council through the USGS. "But it's highly competitive, and it's going to be tough. If he doesn't get the fellowship, then he's going to have to jump through some hoops to get this study financed,"

Soviets stingy

Only one other American has ever received the Vostok core material, "and that was obtained through a third-country collaborator," Hinkley said, referring to Clare Patterson, a geochemist at the California Institute of Technology who received Vostok samples about three years ago through a French science agency.

"I can't emphasize enough the significance of what Paul has done," Hinkley added. "The Soviets have been very tight-fisted with their samples, and here they're turning them over to a rather unrecognized individual who is not connected with an established institution."

Hinkley speculated that LaViolette's superwave theory may have captured the attention of international researchers, including Soviet scientists, although the theory has not been given much credence by the U.S. scientific community.

From Earth to Milky Way

That theory, which LaViolette has been working on for nearly a decade, doesn't begin deep within the ice but about 22,000 light-years away in the center of the Milky Way, the galaxy in which Earth resides. (A light-year is the distance that light travels in one year, about 5.9 trillion miles.)

The main points of his "galactic superwave" theory include these:

- Eruptions that periodically take place in the galaxy's center throw out cosmic rays accompanied by electromagnetic radiation — such as gamma rays, X-rays, radio waves and light waves.

- The explosive outbursts last from several hundred to several thousand years and recur about every 5,000 to 15,000 years.

- Upon entering the solar system, the "superwaves" vaporize comets and push the resulting cosmic dust into the Earth's atmosphere, causing climatic changes. LaViolette proposes that the last Ice Age came abruptly to an end because the dust particles caused a "greenhouse effect," trapping the sun's heat close to the Earth's surface.

- Because the superwaves are traveling at the speed of light, they not only could alter the Earth's climate in the future, but they could create electromagnetic interference similar to the electromagnetic pulse generated by the aerial detonation of a nuclear weapon. The superwave signal possibly could be mistaken for a nuclear explosion, LaViolette says, and could lead to a nation launching missiles in the belief it was under attack.

Tracking superwaves

What LaViolette is looking for in the ice-core samples is evidence of past superwave episodes. That can be determined by analyzing the levels of beryllium 10, an isotope produced in the atmosphere by cosmic ray bombardment, he said.

LaViolette previously studied ice-core samples from Camp Century in northwest Greenland and filtrates from ice core samples taken from the Byrd Station in Antarctica while working on his dissertation about the theory at Portland State University.

In analyzing those samples, he found that greater concentrations of the metallic elements iridium and nickel corresponded with climatic changes during the last Ice Age. He contends that the particles most likely came from the vaporizing of comets rather than from terrestrial sources, such as volcanic eruptions.

He also rules out the possibility that the elements came from an asteroid or comet striking the Earth.

"The problem is that such events would not be expected to occur frequently enough to account for the observed" high levels of iridium, he stated in a paper published in the journal *Meteoritics*.

LaViolette received his doctorate in systems science from PSU in 1983 after working four years on his superwave theory. His résumé lists a bachelor's degree in physics from John Hopkins University and a master's degree in organizational administration from the University of Chicago.

In addition to the ice study, LaViolette is using the 27-antenna Very Large Array radio telescope in Socorro, N.M., to examine CTB 80, a radio-emitting supernova remnant in the Cygnus constellation. He hopes the data he obtains will provide additional evidence to support his theory that cosmic ray volleys travel through space from the Milky Way's center.

"At this point my goal is to present a little more evidence to convince the scientific community that indeed there are high levels of cosmic dust in the ice," the soft-spoken LaViolette said before leaving Portland last week.

"I'd like to see two or three other scientists take a look at my theory and do their own investigations."

Support slow-developing

Getting support for his theory has been difficult, however.

"The problem is that I'm a newcomer to this field, and it's very difficult to become established, especially when you're submitting an entirely new idea," LaViolette said.

In 1984, in an effort to raise money to support his research, LaViolette launched his Starburst Foundation. The foundation's aim, he said, is to serve as a vehicle "through which donors may support research on novel ideas that normally would have a difficult time being funded through most foundation or government channels."

SCIENCE

The Oregonian, Thursday, November 3, 1988

D

Theory waiting 'on ice'

Scientist in search of research funds

By RICHARD L. HILL
of The Oregonian staff

A Portland scientist's theory is on ice in Denver. Paul A. LaViolette, who last summer became the first American to directly receive ice-core samples from the Soviet Union's Vostok station in Antarctica, now is seeking to analyze that ice in hopes that it will provide evidence to support his theory which involves "galactic superwaves" and climatic changes.

To thaw, however, requires cold cash. Most U.S. scientists are familiar with the fund-raising process, perhaps the least glamorous aspect of scientific research. It can take several forms: Tedious grant-writing to compete for public funds, seeking ties with corporations interested in specific research, or searching for noble benefactors who enjoy scientific pursuit for itself rather than a big dividend.

For LaViolette, the funding quest is an especially difficult venture in that he is a self-described "maverick," out of the scientific mainstream where funding usually depends on peer review or belonging to an established research facility.

Five years ago, LaViolette began his non-profit "Starburst Foundation," which he says serves as a way for donors to contribute to research on "novel ideas" that would have a tough time being funded through most foundation or government channels.

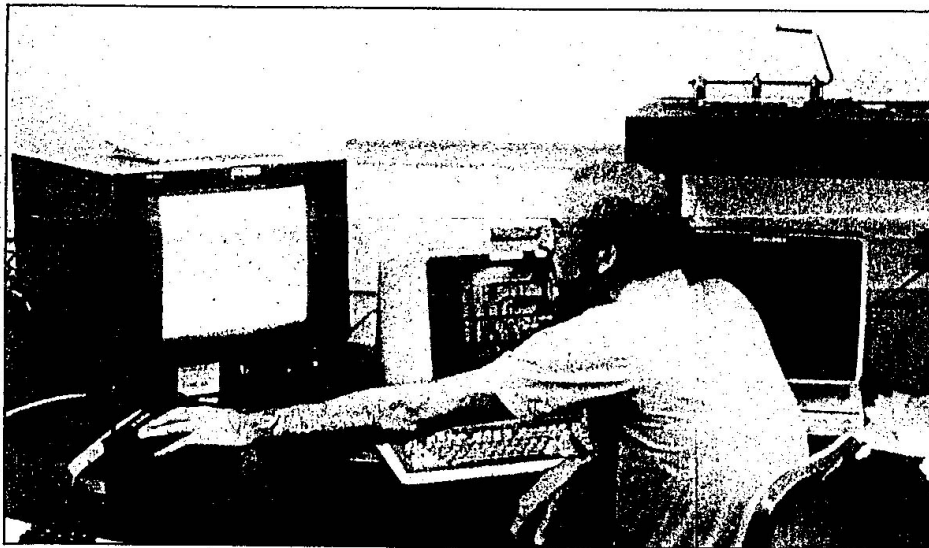
LaViolette says the traditional methods of funding work "against the maverick. One of the reasons Starburst was set up was to avoid the peer-review process, which can sort of be an old-boy's club."

"If reviewers happen to know you and you're part of their group then you stand a much better chance of getting your proposal funded. We're trying to get around those restrictions."

Gathering evidence to support his "superwave" theory is a complex proposition, requiring examining the far reaches of space as well as the deep confines of polar ice. This summer he traveled to Amsterdam to get the Soviet ice and to Socorro, N.M., to use the Very Large Array national radio telescope in examining a distant supernova remnant.

The 40-year-old researcher has met with some success in raising funds. His ice-retrieval trip to Amsterdam was funded by a donation from the Ruth and Vernon Taylor Foundation in Denver and his radio telescope research was aided by a grant from the Sunflower Foundation in New York City.

His theory involves what he calls "galactic superwaves," intense volleys of cosmic rays that are periodically emitted from the center of the Milky Way — which is believed to be a black hole — and travel outward at close to the speed of light. Such eruptions last from several hundred to several thousand years and recur about every 5,000 to 15,000 years, according to his theory.



Paul A. LaViolette examines a computer terminal at the Very Large Array national radio telescope in Socorro, N.M.

Theory: Greenhouse effect ends Ice Age

Continued from Page D1

LaViolette theorizes that upon entering the solar system, the superwaves vaporize comets and push the resulting cosmic dust into the Earth's atmosphere, causing climatic changes. He proposes that the last Ice Age abruptly ended because the dust particles created a "greenhouse effect," trapping the sun's heat close to the Earth's surface.

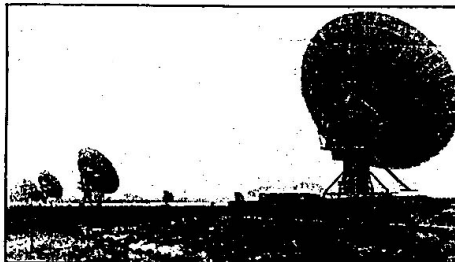
In addition to climatic changes, LaViolette proposes that the waves could cause electromagnetic interference with communication systems. He said the superwave signal could, in a worst-case scenario, be mistaken for a nuclear explosion and possibly lead to a nation launching missiles in the belief it was being attacked.

In the ice-core samples, he hopes to determine how peaks in cosmic dust concentration correlate with cosmic ray intensity, which would be indicated by amount of beryllium-10, an isotope produced in the atmosphere by cosmic ray bombardment.

"It would be quite a thorough study," LaViolette said. "We'd be looking at 30 different elements using two different techniques: nuclear activation analysis and isotope mass spectrometry."

Such analysis "definitely has value beyond my theory," he added. "If the interplanetary dust concentration has changed in the past, that's a major factor that has to be taken into account in our astronomy texts because it means the earth and solar system are somehow affected by some kind of astronomical event."

LaViolette, who received his doctorate in systems science from Portland State University in 1983, picked up the Vostok ice in Amsterdam



Los Angeles Times

These dishes, each 82 feet in diameter, are strung across an ancient New Mexico lakebed as part of the world's most powerful radio telescope. Twenty-seven dishes are linked together, forming a single antenna 21 miles in diameter. Portland scientist Paul A. LaViolette used the telescope to study the supernova remnant CTB 80.

from the Soviet research vessel Akademik Fedorov in June. He obtained approval for the ice transfer after writing the scientific attaché with the Soviet Embassy in Washington, D.C.

The ice samples came in 17 cylindrical pieces, each about 12 centimeters wide and from 5 to 15 centimeters long, he said. The samples were placed in special containers and taken to Denver, where they were placed in a commercial freezer.

Todd K. Hinkley, a geologist with the U.S. Geological Survey in Denver, said he would like to analyze the samples in his high-tech laboratory if funding can be found.

"It would cost about \$75,000 to \$82,000 to do the research," and would take about a year, LaViolette said.

dium and nickel corresponded with climatic changes during the last Ice Age.

He rules out that the elements may have come from comets or asteroids colliding with Earth. In a paper published in the journal *Meteoritics*, he stated that such events "would not be expected to occur frequently enough to account for the observed" high levels of iridium.

In late August, LaViolette spent five hours using the radio telescope in New Mexico to study the radio-emitting CTB 80, a supernova remnant. He hoped that studying the remnant would provide additional evidence to support the theory that cosmic ray volleys originating at the galactic center travel through the galaxy.

He didn't find a bow shock front, shaped like a bow around the radio source, that he was hoping to detect, but he did find that the radio source was "oriented perpendicular to the direction that superwaves would be propagating."

"I think that polarization would justify further investigation, but we don't have the money to do it."

The Portland scientist has received national attention by being mentioned in a recently published book, "Fire in the Crucible: The Alchemy of Creative Genius" by John Briggs. LaViolette is mentioned for developing a model to describe how the brain processes the complexity of emotional theme.

"I haven't given up hope (of finding a funding source)," said LaViolette, who has been slowly gathering evidence for his superwave theory the past 10 years. "I think the ice analysis will provide valuable information about what happened on our planet thousands of years ago."

The Soviets obtained the ice-core samples by drilling about 7,200 feet below the surface — the deepest ever drilled into the Antarctic ice. Ice samples are valuable to scientists because air bubbles and particulates become trapped in the ice, allowing researchers to examine atmospheric conditions that existed thousands of years ago.

According to the journal *Nature*, the Soviets perfected a thermal technique at Vostok whereby the base of the cylindrical sampler is electrically heated, penetrating the ice as it melts without damaging the sample.

LaViolette previously studied ice-core samples from Greenland and filtrates from ice-core samples from the Byrd Station in Antarctica. In analyzing those samples, he found that greater concentrations of iri-

NATIONAL SECURITY COUNCIL
WASHINGTON, D.C. 20506

May 10, 1985

Dear Mr. LaViolette,

Thank you for your letter and enclosure dated May 1, which I received by hand when I was in Portland last week.

I appreciate your bringing to my attention the issue of Galactic Superwaves and their possible EMP effects.

As you may know, President Reagan initiated, in 1981, a major program to improve the command and control (C³I) capability over the strategic forces of the United States with particular attention being given to the matter of EMP effects.

You may be sure I shall share your one-page paper with the appropriate individuals at the National Security Council and at the Department of Defense.

Sincerely,



Christopher M. Lehman
Special Assistant to the
President for National
Security Affairs

Mr. Paul A. LaViolette
2166 N.E. Clackamas Street, #2
Portland, OR 97232

EDWARD M. KENNEDY
MASSACHUSETTS

United States Senate

WASHINGTON, DC 20510

January 19, 1990

Paul A. LaViolette
President
The Starburst Foundation
P.O. Box 5943
Portland, Oregon 97228-5943


Dear Mr. LaViolette:

I am in receipt of your letter of December 28, 1989, and the corresponding materials on the 1983 Gamma Ray Burst. After reviewing the information I have forwarded it to my colleague, Senator Alan J. Dixon, who chairs the Senates Armed Service's Subcommittee on Readiness, Sustainability and Support, where they will be able to give it the attention which it warrants.

It is very helpful hearing from concerned groups like the Starburst Foundation who care about the status of our nation's national security and take the time to put together information which assists the Congress to make the many difficult and perplexing issues which it faces daily. As a member of the Armed Services Committee I can assure you that I will make sure that the other members of the committee are kept abreast of gamma ray bursts or any other items which threaten our nations military preparedness.

Thank you for your assistance in this matter and please continue to keep me informed of any further developments in the study of gamma ray bursts.

Sincerely,


Edward M. Kennedy

UNITED REPUBLIC OF



TANZANIA

PERMANENT MISSION TO THE
UNITED NATIONS
205 EAST 42ND STREET, ROOM 1300
NEW YORK, NEW YORK 10017
(212) 972-9160

5 May, 1989

Dr. Paul A. LaViolette
President
The Starburst Foundation
P.O. Box 5943
Portland, Oregon 97228-5943

Dear Dr. LaViolette,

Thank you for your letter of 15 April, 1989, to which was attached a copy of the Starburst Foundation article entitled "GALACTIC CORE EXPLOSIONS - THE REAL ATOMIC THREAT" which I have personally found of great interest, if not frightening!

I have transmitted copies of your letter and the article attached to the relevant authorities in my country, but in view of the highly technical nature of the issue, we in Tanzania cannot contribute much to the activities which were listed at the end of the article.

With best wishes,

Yours sincerely,

A handwritten signature in dark ink, appearing to read "W.K. Chagula".

Wilbert K. Chagula
Ambassador
Permanent Representative

~~From~~ Sir Crispin Tickell GCMG KCVO



UNITED KINGDOM MISSION
TO THE UNITED NATIONS
845 THIRD AVENUE
NEW YORK, N.Y. 10022

4 May 1989

Dr Paul A LaViolette PhD
President
The Starburst Foundation
PO Box 5943
Portland
Oregon 97228 5943

Dear Dr. LaViolette,

Thank you for your letter of 15 April enclosing your Foundation's paper on cosmic ray events.

I was most interested to read it, not least because I am among those long aware of the dangers which this and other astronomical phenomena, such as asteroid activity, pose to this planet. My own experience in the field of arms control enables me to say that the nuclear weapon states are already well seized of the need not to misinterpret such events. I can assure you that this continues to be a factor in current discussions on nuclear arms control.

Yours sincerely
Crispin Tickell

Crispin Tickell